Advances and New Perspectives in Marine Biotechnology

Volume 2: Marine Microbes & Metagenomes

Edited by

Paul F. Long, Bernie Degnan and Pabulo H. Rampelotto

Printed Edition of the Special Issue Published in *Marine Drugs*

www.mdpi.com/journal/marinedrugs

Paul F. Long, Bernie Degnan and Pabulo H. Rampelotto (Eds.)

Advances and New Perspectives in Marine Biotechnology

Volume 2: Marine Microbes & Metagenomes

MDPI

This book is a reprint of the Special Issue that appeared in the online, open access journal, *Marine Drugs* (ISSN 1660-3397) from 2013–2014 (available at: http://www.mdpi.com/journal/marinedrugs/special_issues/marine-biotechnology).

Guest Editors
Paul F. Long
Institute of Pharmaceutical Science & Department of Chemistry
King's College London
Franklin-Wilkins Building, 150 Stamford Street
London SE1 9NH, United Kingdom

Bernie Degnan
School of Biological Sciences
The University of Queensland
Brisbane, Queensland 4072, Australia

Pabulo H. Rampelotto
Center of Biotechnology and PPGBCM
Federal University of Rio Grande do Sul
Bento Gonçalves Avenue, P.O. Box 15005
91501-970, Porto Alegre—RS, Brazil

Editorial
MDPI AG
Klybeckstrasse 64
Basel, Switzerland

Office Publisher
Shu-Kun Lin

Managing Editor
Alicia Li

1. Edition 2015

MDPI • Basel • Beijing • Wuhan • Barcelona

ISBN 978-3-03842-105-4 Volume 1-2 (Hbk)
ISBN 978-3-03842-108-5 Volume 1-2 (PDF)

ISBN 978-3-03842-106-1 Volume 1 (Hbk) ISBN 978-3-03842-109-2 Volume 1 (PDF)

ISBN 978-3-03842-107-8 Volume 2 (Hbk) ISBN 978-3-03842-110-8 Volume 2 (PDF)

Table of Contents

List of Contributors

Usama Ramadan Abdelmohsen: Department of Botany II, Julius-von-Sachs Institute for Biological Sciences, University of Würzburg, Julius-von-Sachs-Platz 3, Würzburg D-97082, Germany.

Janet Adamson: Cawthron Institute, 98 Halifax Street East, Private Bag 2, Nelson 7042, New Zealand.

Kazuaki Akasaka: Shokei Gakuin University, 4-10-1 Yurigaoka, Natori, Miyagi 981-1295, Japan.

Masahiro Ando: Consolidated Research Institute for Advanced Science and Medical Care, Waseda University, 513, Wasedatsurumaki-cho, Shinjuku-ku, Tokyo 162-0041, Japan.

Paula B. Andrade: REQUIMTE/Laboratory of Pharmacognosy, Department of Chemistry, Faculty of Pharmacy, University of Porto, Rua de Jorge Viterbo Ferreira, no. 228, 4050-313 Porto, Portugal.

Midori A. Arai: Department of Natural Products Chemistry, Graduate School of Pharmaceutical Sciences, Chiba University, 1-8-1 Inohana, Chuo-ku, Chiba 260-8675, Japan.

Munhyung Bae: Natural Products Research Institute, College of Pharmacy, Seoul National University, Seoul 151-742, Korea.

Jean-Pascal Bergé: IFREMER, Laboratoire de Science et Technologie de la Biomasse Marine (STBM), 44311 Nantes cedex 03, France.

Ira Bhatnagar: Nanotheranostics Laboratory, Centre for Cellular and Molecular Biology, Hyderabad 500-007, India.

Doug R. Braun: Pharmaceutical Sciences Division, University of Wisconsin-Madison, 777 Highland Avenue, Madison, WI 53705, USA.

Tim S. Bugni: Pharmaceutical Sciences Division, University of Wisconsin-Madison, 777 Highland Avenue, Madison, WI 53705, USA.

Ricardo Calado: Departamento de Biologia & CESAM, Universidade de Aveiro, Campus Universitário de Santiago, Aveiro 3810-193, Portugal.

Shmuel Carmeli: Raymond and Beverly Sackler School of Chemistry and Faculty of Exact Sciences, Tel Aviv University, Tel Aviv 69978, Israel.

Diana Negrão Cavalcanti : Departamento de Biologia Marinha, Instituto de Biologia, Universidade Federal Fluminense, Outeiro de São João Batista, s/n, Centro, Niterói, 24001-970, RJ, Brazil.

Chao-Yuan Chang : Department of Anatomy, College of Medicine, Kaohsiung Medical University, Kaohsiung 807, Taiwan.

Chen-Tung Arthur Chen: Ocean College, Zhejiang University, Hangzhou 310058, China; Institute of Marine Geology and Chemistry, National Sun Yat-sen University, Kaohsiung 80424, Taiwan.

Huei-Mei Chen: Pingtung Branch of Kaohsiung Veterans General Hospital, Nutrition Branch, Pingtung 912, Taiwan.
Lin Chen: Key Laboratory for Chemical Biology of Fujian Province, School of Pharmaceutical Sciences, Xiamen University, South Xiang-An Road, Xiamen 361102, China.
Yu-Cheng Chen: Graduate Institute of Marine Biotechnology, National Dong Hwa University, Pingtung 944, Taiwan.
Laura de Andrade Moura : Departamento de Biologia Molecular e Celular, Instituto de Biologia, Universidade Federal Fluminense, Outeiro de São João Batista, s/n, Centro, Niterói, 24020-141, RJ, Brazil.
Sueli de Oliveira Silva: Postgraduate Program in Pharmaceutical Sciences, State University of Maringa, Colombo Avenue 5790, Maringa, Parana CEP 87020-900, Brazil; Department of Basic Health Sciences, State University of Maringa, Colombo Avenue 5790, Maringa, Parana CEP 87020-900, Brazil.
Miguel de Salas: Tasmanian Herbarium, Tasmanian Museum and Art Gallery, Private Bag 4, Hobart, Tasmania 7001, Australia.
Victória del Pino: Necton SA, Belamandil s/n, 8700-152 Olhão, Portugal.
Vânia Cristina Desoti: Postgraduate Program in Pharmaceutical Sciences, State University of Maringa, Colombo Avenue 5790, Maringa, Parana CEP 87020-900, Brazil.
Gisela Dionísio: Departamento de Biologia & CESAM, Universidade de Aveiro, Campus Universitário de Santiago, Aveiro 3810-193, Portugal; Laboratório Marítimo da Guia, Centro de Oceanografia, Faculdade de Ciências da Universidade de Lisboa, Av. Nossa Senhora do Cabo, 939, Cascais 2750-374, Portugal.
Alan D.W. Dobson: School of Microbiology, University College Cork, National University of Ireland, Cork, Ireland; Marine Biotechnology Centre, Environmental Research Institute, University College Cork, National University of Ireland, Cork, Ireland.
Lei Feng: Instrumental Analysis Center, Shanghai Jiao Tong University, Shanghai 200240, China.
Thaisa Francielle Souza Domingos: Departamento de Biologia Molecular e Celular, Instituto de Biologia, Universidade Federal Fluminense, Outeiro de São João Batista, s/n, Centro, Niterói, 24020-141, RJ, Brazil; Departamento de Biologia Marinha, Instituto de Biologia, Universidade Federal Fluminense, Outeiro de São João Batista, s/n, Centro, Niterói, 24001-970, RJ, Brazil.
Gregory A. Ellis: Pharmaceutical Sciences Division, University of Wisconsin-Madison, 777 Highland Avenue, Madison, WI 53705, USA.
Mohamed El-Shazly: Department of Pharmacognosy and Natural Products Chemistry, Faculty of Pharmacy, Ain-Shams University, Organization of African Unity Street, Abassia, Cairo 11566, Egypt.
Mei-Juan Fang: Key Laboratory for Chemical Biology of Fujian Province, School of Pharmaceutical Sciences, Xiamen University, South Xiang-An Road, Xiamen 361102, China.

Federico Ferreres: Research Group on Quality, Safety and Bioactivity of Plant Foods, Department of Food Science and Technology, CEBAS (CSIC), P.O. Box 164, Campus University Espinardo, Murcia 30100, Spain.

Christopher Franco: Centre for Marine Bioproducts Development, Flinders University, Adelaide, SA 5042, Australia; Department of Medical Biotechnology, School of Medicine, Flinders University, Adelaide, SA 5042, Australia.

Charles G. Fry: Department of Chemistry, University of Wisconsin-Madison, 1101 University Avenue, Madison, WI 53706, USA.

Masaki J. Fujita: Creative Research Institution, Hokkaido University, 3-1-1 Minato-cho, Hakodate, Hokkaido 041-8611, Japan.

Takao Fukuda: Biotechnology Research Center, Toyama Prefectural University, 5180 Kurokawa, Imizu, Toyama 939-0398, Japan.

André Lopes Fuly: Departamento de Biologia Molecular e Celular, Instituto de Biologia, Universidade Federal Fluminense, Outeiro de São João Batista, s/n, Centro, Niterói, 24020-141, RJ, Brazil.

Guang-Chun Gao: Jiaxing University College of Medicine, Jiaxing 314001, China.

Clara Grosso: REQUIMTE/Laboratory of Pharmacognosy, Department of Chemistry, Faculty of Pharmacy, University of Porto, Rua de Jorge Viterbo Ferreira, no. 228, 4050-313 Porto, Portugal.

Dina Hajjar: Division of Chemical & Life Sciences and Engineering and Division of Applied Mathematics and Computer Science, King Abdullah University of Science and Technology, Thuwal 23955-6900, Saudi Arabia.

Hiro-o Hamaguchi: Consolidated Research Institute for Advanced Science and Medical Care, Waseda University, 513, Wasedatsurumaki-cho, Shinjuku-ku, Tokyo 162-0041, Japan; Institute of Molecular Science and Department of Applied Chemistry, National Chiao Tung University, 1001 To Hsuch Road, Hsinchu 300, Taiwan.

Tie-Sheng Han: State Key Laboratory of Microbial Metabolism and School of Life Science & Biotechnology, State Key Laboratory of Ocean Engineering, Shanghai Jiao Tong University, Shanghai 200240, China.

Catriona Harrington: BIOMERIT Research Centre, School of Microbiology, University College Cork, National University of Ireland, Cork, Ireland.

Enjuro Harunari: Graduate School of Marine Science and Technology, Tokyo University of Marine Science and Technology, 4-5-7 Konan, Minato-ku, Tokyo 108-8477, Japan.

Mian He: Department of Obstetrics and Gynecology, The First Affiliated Hospital, Sun Yat-sen University, Guangzhou 510080, China.

Ute Hentschel: Department of Botany II, Julius-von-Sachs Institute for Biological Sciences, University of Würzburg, Julius-von-Sachs-Platz 3, Würzburg D-97082, Germany.

Hannes Horn: Department of Botany II, Julius-von-Sachs Institute for Biological Sciences, University of Würzburg, Julius-von-Sachs-Platz 3, Würzburg D-97082, Germany.

Masahito Hosokawa: Department of Life Science and Medical Bioscience, Waseda University, 2-2 Wakamatsu-cho, Shinjuku-ku, Tokyo 162-8480, Japan; Consolidated Research Institute for Advanced Science and Medical Care, Waseda University, 513, Wasedatsurumaki-cho, Shinjuku-ku, Tokyo 162-0041, Japan; Core Research for Evolutionary Science and Technology (CREST), Japan Science and Technology Agency (JST), 5, Sanbancho, Chiyoda-ku, Tokyo 102-0075, Japan.
Yaohua Hu: State Key Laboratory of Quality Research in Chinese Medicine, Institute of Chinese Medical Sciences, University of Macau, Macao 999078, China.
Yasuhiro Igarashi: Biotechnology Research Center, Toyama Prefectural University, 5180 Kurokawa, Imizu, Toyama 939-0398, Japan.
Micha Ilan: Department of Zoology, George S. Wise Faculty of Life Sciences, Tel Aviv University, Tel Aviv 69978, Israel.
Chiaki Imada: Graduate School of Marine Science and Technology, Tokyo University of Marine Science and Technology, 4-5-7 Konan, Minato-ku, Tokyo 108-8477, Japan.
Masami Ishibashi: Department of Natural Products Chemistry, Graduate School of Pharmaceutical Sciences, Chiba University, 1-8-1 Inohana, Chuo-ku, Chiba 260-8675, Japan.
Hanako Ito: Department of Natural Products Chemistry, Graduate School of Pharmaceutical Sciences, Chiba University, 1-8-1 Inohana, Chuo-ku, Chiba 260-8675, Japan.
Wei Jiang: Ocean College, Zhejiang University, Hangzhou 310058, China.
Yung-Shun Juan: Department of Urology, Kaohsiung Municipal Hsiao-Kang Hospital, Kaohsiung 812, Taiwan; Department of Urology, College of Medicine, Kaohsiung Medical University, Kaohsiung 807, Taiwan; Department of Urology, Kaohsiung Medical University Hospital, Kaohsiung 807, Taiwan.
Byung-Yong Kim: ChunLab, Inc., Seoul National University, Seoul, 151-742, Korea
Se-Kwon Kim: Marine Bioprocess Research Center, Department of Chemistry, Pukyong National University, Busan 608-737, Korea.
Seong-Hwan Kim: Natural Products Research Institute, College of Pharmacy, Seoul National University, Seoul 151-742, Korea.
Youngju Kim: Biotechnology Research Center and Department of Biotechnology, Toyama Prefectural University, 5180 Kurokawa, Imizu, Toyama 939-0398, Japan.
Takeshi Kobayashi: Graduate School of Marine Science and Technology, Tokyo University of Marine Science and Technology, 4-5-7 Konan, Minato-ku, Tokyo 108-8477, Japan.
Yi-Hsin Kung: Department of Life Science, National Taitung University, 684, Sec. 1, Chunghua Rd., Taitung 95092, Taiwan; Division, Sunway Biotechnology Company Limited, Taipei 11494, Taiwan.
Yun Kwon: Natural Products Research Institute, College of Pharmacy, Seoul National University, Seoul 151-742, Korea.
Teresa Lamela: Necton SA, Belamandil s/n, 8700-152 Olhão, Portugal.
Danielle Lazarin-Bidóia: Postgraduate Program in Pharmaceutical Sciences, State University of Maringa, Colombo Avenue 5790, Maringa, Parana CEP 87020-900, Brazil.

Miguel Costa Leal: Departamento de Biologia & CESAM, Universidade de Aveiro, Campus Universitário de Santiago, Aveiro 3810-193, Portugal; Skidaway Institute of Oceanography, University of Georgia, 10 Ocean Science Circle, Savannah, GA 31411, USA.
Chun-Lin Lee: Department of Life Science, National Taitung University, 684, Sec. 1, Chunghua Rd., Taitung 95092, Taiwan.
Sang Kook Lee: Natural Products Research Institute, College of Pharmacy, Seoul National University, Seoul 151-742, Korea.
Catherine Legrand: Faculty of Health and Life Sciences, Centre for Ecology and Evolution in Microbial Model Systems (EEMiS), Linnæus University, 391 82 Kalmar, Sweden.
Jie Lei: Centre for Marine Bioproducts Development, Flinders University, Adelaide, SA 5042, Australia; Department of Medical Biotechnology, School of Medicine, Flinders University, Adelaide, SA 5042, Australia.
Ning Li: Institute of Oceanology, Chinese Academy of Sciences, Qingdao 266071, China.
Tao Li: Key Laboratory of Tropical Marine Bio-resources and Ecology, South China Sea Institute of Oceanology, Chinese Academy of Sciences, Guangzhou 510301, China.
Xue-Gong Li: College of Marine Life Sciences, Ocean University of China, Qingdao 266003, China; State Key Laboratory of Microbial Metabolism and School of Life Science & Biotechnology, State Key Laboratory of Ocean Engineering, Shanghai Jiao Tong University, Shanghai 200240, China.
Yue Liang: Division of Biotechnology and Life Science, Institute of Engineering, Tokyo University of Agriculture and Technology, 2-24-16, Naka-cho, Koganei, Tokyo 184-8588, Japan.
Hanzhi Lin: Environmental Biophysics and Molecular Ecology Program, Institute of Marine and Coastal Sciences, Rutgers University, 71 Dudley Road, New Brunswick, NJ 08901, USA.
Xiukun Lin: Department of Pharmacology, Capital Medical University, Beijing 100069, China.
Huaide Liu: School of Life Sciences, Nantong University, Seyuan Road 9, Nantong 226019, China.
Jun-Xiu Liu : Department of Obstetrics and Gynecology, The First Affiliated Hospital, Sun Yat-sen University, Guangzhou 510080, China.
Ming Liu: Key Laboratory of Marine Drugs, Ministry of Education, School of Medicine and Pharmacy, Ocean University of China, Qingdao 266003, China.
Xiaohui Liu: Department of Pharmacology, Capital Medical University, Beijing 100069, China.
Lijuan Long: Key Laboratory of Tropical Marine Bio-resources and Ecology, South China Sea Institute of Oceanology, Chinese Academy of Sciences, Guangzhou 510301, China.
Si-Mei Long : Guangdong Key Laboratory for Diagnosis and Treatment of Major Neurological Diseases, Department of Neurology, National Key Clinical Department and Key Discipline of Neurology, The First Affiliated Hospital, Sun Yat-sen University, Guangzhou 510080, China.

Mei-Chin Lu: Graduate Institute of Marine Biotechnology, National Dong Hwa University, Pingtung 944, Taiwan; National Museum of Marine Biology & Aquarium, Pingtung 944, Taiwan.

Tzu-Ying Lung: Department of Life Science, National Taitung University, 684, Sec. 1, Chunghua Rd., Taitung 95092, Taiwan; Stone & Resource Industry R & D Center, Hualien 97356, Taiwan.

Min-Qi Luo : Department of Clinical Laboratory, The Third Affiliated Hospital, Sun Yat-sen University, Guangzhou 510630, China.

Xiong-Ming Luo: CAS Key Laboratory of Tropical Marine Bio-resources and Ecology, South China Sea Institute of Oceanology, Chinese Academy of Sciences, Guangzhou 510301, China.

Guang-Hui Ma: Key Laboratory of Marine Biogenetic Resources, The Third Institute of Oceanography, State Oceanic Administration, Xiamen 361005, China.

Yoshiaki Maeda: Division of Biotechnology and Life Science, Institute of Engineering, Tokyo University of Agriculture and Technology, 2-24-16, Naka-cho, Koganei, Tokyo 184-8588, Japan.

Ana Carolina Marqui de Almeida : Departamento de Biologia Molecular e Celular, Instituto de Biologia, Universidade Federal Fluminense, Outeiro de São João Batista, s/n, Centro, Niterói, 24020-141, RJ, Brazil.

Mitsufumi Matsumoto: Biotechnology Laboratory, Electric Power Development Co., Ltd., 1, Yanagisaki-machi, Wakamatsu-ku, Kitakyusyu 808-0111, Japan; Japan Science and Technology Agency (JST), Core Research for Evolutionary Science and Technology (CREST), 5, Sanbancho, Chiyoda-ku, Tokyo 102-0075, Japan.

Nobuyasu Matsuura: Okayama University of Science, 1-1 Ridai-cho, Okayama, Okayama 700-0005, Japan.

Mohammad Ferdous Mehbub: Centre for Marine Bioproducts Development, Flinders University, Adelaide, SA 5042, Australia; Department of Medical Biotechnology, School of Medicine, Flinders University, Adelaide, SA 5042, Australia; Department of Fisheries Technology, Faculty of Fisheries, Hajee Mohammad Danesh Science and Technology University, Dinajpur 5200, Bangladesh.

Rimi Miyaoka: Department of Life Science and Medical Bioscience, Waseda University, 2-2 Wakamatsu-cho, Shinjuku-ku, Tokyo 162-8480, Japan.

Tetsushi Mori: Department of Life Science and Medical Bioscience, Waseda University, 2-2 Wakamatsu-cho, Shinjuku-ku, Tokyo 162-8480, Japan; Consolidated Research Institute for Advanced Science and Medical Care, Waseda University, 513, Wasedatsurumaki-cho, Shinjuku-ku, Tokyo 162-0041, Japan; Core Research for Evolutionary Science and Technology (CREST), Japan Science and Technology Agency (JST), 5, Sanbancho, Chiyoda-ku, Tokyo 102-0075, Japan.

Celso Vataru Nakamura: Postgraduate Program in Pharmaceutical Sciences, State University of Maringa, Colombo Avenue 5790, Maringa, Parana CEP 87020-900, Brazil; Department of Basic Health Sciences, State University of Maringa, Colombo Avenue 5790, Maringa, Parana CEP 87020-900, Brazil.

Emmelie Nilsson: Faculty of Health and Life Sciences, Centre for Ecology and Evolution in Microbial Model Systems (EEMiS), Linnæus University, 391 82 Kalmar, Sweden.

Fergal O'Gara: BIOMERIT Research Centre, School of Microbiology, University College Cork, National University of Ireland, Cork, Ireland; School of Microbiology, University College Cork, National University of Ireland, Cork, Ireland; Marine Biotechnology Centre, Environmental Research Institute, University College Cork, National University of Ireland, Cork, Ireland; School of Biomedical Sciences, Curtin University, Perth, WA 6102, Australia.

Hiromu Ogura: Biotechnology Research Center and Department of Biotechnology, Toyama Prefectural University, 5180 Kurokawa, Imizu, Toyama 939-0398, Japan.

Dong-Chan Oh: Natural Products Research Institute, College of Pharmacy, Seoul National University, Seoul 151-742, Korea.

Ki-Bong Oh: Department of Agricultural Biotechnology, College of Agriculture and Life Science, Seoul National University, Seoul 151-921, Korea.

Tsutomu Oikawa: School of Nutrition and Dietetics, Kanagawa University of Human Services, 1-10-1 Heisei-cho, Yokosuka, Kanagawa 238-8566, Japan.

Martin Olofsson: Faculty of Health and Life Sciences, Centre for Ecology and Evolution in Microbial Model Systems (EEMiS), Linnæus University, 391 82 Kalmar, Sweden.

Fredy Ortiz-Ramirez: Departamento de Biologia Marinha, Instituto de Biologia, Universidade Federal Fluminense, Outeiro de São João Batista, s/n, Centro, Niterói, 24001-970, RJ, Brazil.

Ronald Osinga: Department of Aquaculture and Fisheries, Wageningen University, P.O. Box 338, 6700 AH Wageningen, The Netherlands; Porifarma BV, Poelbos 3, 6718 HT Ede, The Netherlands.

Tzu-Ming Pan: Department of Biochemical Science and Technology, National Taiwan University, Taipei 10617, Taiwan.

Irina Panizel: Raymond and Beverly Sackler School of Chemistry and Faculty of Exact Sciences, Tel Aviv University, Tel Aviv 69978, Israel; Department of Zoology, George S. Wise Faculty of Life Sciences, Tel Aviv University, Tel Aviv 69978, Israel.

Renato Crespo Pereira: Department of Marine Biology, Federal Fluminense University, P.O. Box 100644, Niteroi, Rio de Janeiro CEP 24001-970, Brazil.

Song Qin: Key Lab of Coastal Biology and Bio-resource Utilization, Yantai Institute of Coastal Zone Research, Chinese Academy of Sciences, 17 Chunhui Road, Yantai 264003, China.

Ying-Kun Qiu: Key Laboratory for Chemical Biology of Fujian Province, School of Pharmaceutical Sciences, Xiamen University, South Xiang-An Road, Xiamen 361102, China.

Timothy Ravasi: Division of Chemical & Life Sciences and Engineering and Division of Applied Mathematics and Computer Science, King Abdullah University of Science and Technology, Thuwal 23955-6900, Saudi Arabia.
Lesley L. Rhodes: Cawthron Institute, 98 Halifax Street East, Private Bag 2, Nelson 7042, New Zealand.
Rui Jorge Miranda Rocha: Departamento de Biologia & CESAM, Universidade de Aveiro, Campus Universitário de Santiago, Aveiro 3810-193, Portugal.
Javier Rocha-Martin: BIOMERIT Research Centre, School of Microbiology, University College Cork, National University of Ireland, Cork, Ireland.
Rui Rosa: Laboratório Marítimo da Guia, Centro de Oceanografia, Faculdade de Ciências da Universidade de Lisboa, Av. Nossa Senhora do Cabo, 939, Cascais 2750-374, Portugal.
Ryuichi Sakai: Faculty of Fisheries Sciences, Hokkaido University, 3-1-1 Minato-cho, Hakodate, Hokkaido 041-8611, Japan.
Ling Shen: Eye Center, The Second Affiliated Hospital, Zhejiang University School of Medicine, Hangzhou 310000, China.
Christopher Sheridan: Biology of Marine Organisms and Biomimetics Laboratory, Research Institute for Biosciences, University of Mons, Pentagone 2B, 6 Avenue du Champ de Mars, Mons 7000, Belgium.
Huei-Chuan Shih: Department of Nursing, Meiho University, Pingtung 912, Taiwan.
Shou-Ping Shih: Graduate Institute of Marine Biotechnology, National Dong Hwa University, Pingtung 944, Taiwan.
Jongheon Shin: Natural Products Research Institute, College of Pharmacy, Seoul National University, Seoul 151-742, Korea.
Yoonho Shin: Natural Products Research Institute, College of Pharmacy, Seoul National University, Seoul 151-742, Korea.
Bruna Silva: Departamento de Biologia & CESAM, Universidade de Aveiro, Campus Universitário de Santiago, Aveiro 3810-193, Portugal.
Kirsty F. Smith: Cawthron Institute, 98 Halifax Street East, Private Bag 2, Nelson 7042, New Zealand.
Huanxing Su: State Key Laboratory of Quality Research in Chinese Medicine, Institute of Chinese Medical Sciences, University of Macau, Macao 999078, China.
Jui-Hsin Su: Graduate Institute of Marine Biotechnology, National Dong Hwa University, Pingtung 944, Taiwan; National Museum of Marine Biology & Aquarium, Pingtung 944, Taiwan.
Daniela Bueno Sudatti: Department of Marine Biology, Federal Fluminense University, P.O. Box 100644, Niteroi, Rio de Janeiro CEP 24001-970, Brazil.
Xiumei Sun: Key Laboratory of Tropical Marine Bio-resources and Ecology, South China Sea Institute of Oceanology, Chinese Academy of Sciences, Guangzhou 510301, China; Graduate School of Chinese Academy of Sciences, Beijing 100049, China.

Yoshihiko Sunaga: Division of Biotechnology and Life Science, Institute of Engineering, Tokyo University of Agriculture and Technology, 2-24-16, Naka-cho, Koganei, Tokyo 184-8588, Japan; Core Research for Evolutionary Science and Technology (CREST), Japan Science and Technology Agency (JST), 5, Sanbancho, Chiyoda-ku, Tokyo 102-0075, Japan.
Haruko Takeyama: Department of Life Science and Medical Bioscience, Waseda University, 2-2 Wakamatsu-cho, Shinjuku-ku, Tokyo 162-8480, Japan; Consolidated Research Institute for Advanced Science and Medical Care, Waseda University, 513, Wasedatsurumaki-cho, Shinjuku-ku, Tokyo 162-0041, Japan; Core Research for Evolutionary Science and Technology (CREST), Japan Science and Technology Agency (JST), 5, Sanbancho, Chiyoda-ku, Tokyo 102-0075, Japan.
Tsuyoshi Tanaka: Division of Biotechnology and Life Science, Institute of Engineering, Tokyo University of Agriculture and Technology, 2-24-16, Naka-cho, Koganei, Tokyo 184-8588, Japan; Japan Science and Technology Agency (JST), Core Research for Evolutionary Science and Technology (CREST), 5, Sanbancho, Chiyoda-ku, Tokyo 102-0075, Japan.
Kaihao Tang: College of Marine Life Sciences, Ocean University of China, Qingdao 266003, China.
Xiao-Min Tang: Key Laboratory of Marine Biogenetic Resources, The Third Institute of Oceanography, State Oceanic Administration, Xiamen 361005, China.
Valéria Laneuville Teixeira: Departamento de Biologia Marinha, Instituto de Biologia, Universidade Federal Fluminense, Outeiro de São João Batista, s/n, Centro, Niterói, 24001-970, RJ, Brazil.
Takeshi Terahara: Graduate School of Marine Science and Technology, Tokyo University of Marine Science and Technology, 4-5-7 Konan, Minato-ku, Tokyo 108-8477, Japan.
Kazufumi Toume: Department of Natural Products Chemistry, Graduate School of Pharmaceutical Sciences, Chiba University, 1-8-1 Inohana, Chuo-ku, Chiba 260-8675, Japan
Tsung-Yu Tsai: Department of Food Science, Fu Jen Catholic University, New Taipei 24205, Taiwan.
Kentaro Tsukahara: Department of Natural Products Chemistry, Graduate School of Pharmaceutical Sciences, Chiba University, 1-8-1 Inohana, Chuo-ku, Chiba 260-8675, Japan.
Tania Ueda-Nakamura: Postgraduate Program in Pharmaceutical Sciences, State University of Maringa, Colombo Avenue 5790, Maringa, Parana CEP 87020-900, Brazil; Department of Basic Health Sciences, State University of Maringa, Colombo Avenue 5790, Maringa, Parana CEP 87020-900, Brazil.
Pauliina Uronen: Neste Oil, Technology Centre, POB 310, 06101 Porvoo, Finland.
Patrícia Valentão: REQUIMTE/Laboratory of Pharmacognosy, Department of Chemistry, Faculty of Pharmacy, University of Porto, Rua de Jorge Viterbo Ferreira, no. 228, 4050-313 Porto, Portugal.
Jayachandran Venkatesan: Marine Bioprocess Research Center, Department of Chemistry, Pukyong National University, Busan 608-737, Korea.
Genzhu Wang: Key Laboratory of Marine Drugs, Ministry of Education, School of Medicine and Pharmacy, Ocean University of China, Qingdao 266003, China.

Jing Wang: Institute of Oceanology, Chinese Academy of Sciences, Qingdao 266071, China; Nantong Branch, Institute of Oceanology, Chinese Academy of Sciences, Nantong, Jiangsu 226006, China; Collaborative Innovation Center for Marine Biomass Fibers, Materials and Textiles of Shandong Province, Qingdao 266071, China.
Jyh-Jye Wang: Department of Nutrition and Health Science, Fooyin University, Kaohsiung 83102, Taiwan.
Kuiwu Wang: Department of Applied Chemistry, Zhejiang Gongshang University, Hangzhou 310058, China.
Li-Chun Wang: Continuing Education School, National Taitung Junior College, Taitung 95045, Taiwan; Department of Food Science, Fu Jen Catholic University, New Taipei 24205, Taiwan.
Ya-Hui Wang: State Key Laboratory of Oncogenes and Related Genes, Shanghai Cancer Institute, Ren Ji Hospital, School of Medicine, Shanghai Jiao Tong University, Shanghai 200240, China.
Bai-Luh Wei: Department of Life Science, National Taitung University, 684, Sec. 1, Chunghua Rd., Taitung 95092, Taiwan.
Bin Wu: Ocean College, Zhejiang University, Hangzhou 310058, China.
Hualian Wu: Key Laboratory of Tropical Marine Bio-resources and Ecology, South China Sea Institute of Oceanology, Chinese Academy of Sciences, Guangzhou 510301, China.
Qi Wu : Guangdong Key Laboratory for Diagnosis and Treatment of Major Neurological Diseases, Department of Neurology, National Key Clinical Department and Key Discipline of Neurology, The First Affiliated Hospital, Sun Yat-sen University, Guangzhou 510080, China.
Xiaodan Wu: Ocean College, Zhejiang University, Hangzhou 310058, China.
Yang-Chang Wu: Natural Medicinal Products Research Center, China Medical University Hospital, Taichung 404, Taiwan; Center for Molecular Medicine, China Medical University Hospital, Taichung 404, Taiwan.
Zhen Wu: Key Laboratory for Chemical Biology of Fujian Province, School of Pharmaceutical Sciences, Xiamen University, South Xiang-An Road, Xiamen 361102, China
Thomas P. Wyche: Pharmaceutical Sciences Division, University of Wisconsin-Madison, 777 Highland Avenue, Madison, WI 53705, USA.
Meng Xia : Department of Obstetrics and Gynecology, The First Affiliated Hospital, Sun Yat-sen University, Guangzhou 510080, China.
Wenzhou Xiang: Key Laboratory of Tropical Marine Bio-resources and Ecology, South China Sea Institute of Oceanology, Chinese Academy of Sciences, Guangzhou 510301, China.
Jing Xiao: Key Laboratory of Marine Biogenetic Resources, The Third Institute of Oceanography, State Oceanic Administration, Xiamen 361005, China.
Lin Xiao: College of Chemistry and Pharmaceutical Sciences, Qingdao Agricultural University, Qingdao 266109, China.

Xiang Xiao: Ministry of Education Key Laboratory of Systems Biomedicine, Shanghai Center for Systems Biomedicine, Shanghai Jiao Tong University, Shanghai 200240, China.
Shu-Jie Xie: Key Laboratory of Marine Biogenetic Resources, The Third Institute of Oceanography, State Oceanic Administration, Xiamen 361005, China.
Jun Xu: State Key Laboratory of Microbial Metabolism and School of Life Science & Biotechnology, State Key Laboratory of Ocean Engineering, Shanghai Jiao Tong University, Shanghai 200240, China.
Li Xu: Key Laboratory of Marine Biogenetic Resources, The Third Institute of Oceanography, State Oceanic Administration, Xiamen 361005, China.
Min-Juan Xu: Ministry of Education Key Laboratory of Systems Biomedicine, Shanghai Center for Systems Biomedicine, Shanghai Jiao Tong University, Shanghai 200240, China.
Pingxiang Xu: Department of Pharmacology, Capital Medical University, Beijing 100069, China.
Xuanli Xu: College of Chemistry and Pharmaceutical Sciences, Qingdao Agricultural University, Qingdao 266109, China.
Xia Yan: Key Laboratory for Chemical Biology of Fujian Province, School of Pharmaceutical Sciences, Xiamen University, South Xiang-An Road, Xiamen 361102, China.
Chen Yang: Division of Chemical & Life Sciences and Engineering and Division of Applied Mathematics and Computer Science, King Abdullah University of Science and Technology, Thuwal 23955-6900, Saudi Arabia.
Fangfang Yang: Key Laboratory of Tropical Marine Bio-resources and Ecology, South China Sea Institute of Oceanology, Chinese Academy of Sciences, Guangzhou 510301, China; Graduate School of Chinese Academy of Sciences, Beijing 100049, China.
Shu-Zhong Yao: Department of Obstetrics and Gynecology, The First Affiliated Hospital, Sun Yat-sen University, Guangzhou 510080, China.
Xiao-Li Yao : Guangdong Key Laboratory for Diagnosis and Treatment of Major Neurological Diseases, Department of Neurology, National Key Clinical Department and Key Discipline of Neurology, The First Affiliated Hospital, Sun Yat-sen University, Guangzhou 510080, China.
Oded Yarden: Department of Plant Pathology and Microbiology, The Robert H. Smith Faculty of Agriculture, Food and Environment, The Hebrew University of Jerusalem, Rehovot 76100, Israel.
Hisato Yasuda: Center for Advanced Marine Core Research, Kochi University, B200 Monobe, Nankoku, Kochi 783-8502, Japan.
Panpan Ye: Eye Center, The Second Affiliated Hospital, Zhejiang University School of Medicine, Hangzhou 310000, China.
Ying Ye: Ocean College, Zhejiang University, Hangzhou 310058, China.
Zhi-Wei Yi: Key Laboratory of Marine Biogenetic Resources, Third Institute of Oceanography State Oceanic Administration, Xiamen 361005, China.

Tomoko Yoshino: Division of Biotechnology and Life Science, Institute of Engineering, Tokyo University of Agriculture and Technology, 2-24-16, Naka-cho, Koganei, Tokyo 184-8588, Japan.
Zhong-Yuan You: State Key Laboratory of Microbial Metabolism and School of Life Science & Biotechnology, State Key Laboratory of Ocean Engineering, Shanghai Jiao Tong University, Shanghai 200240, China.
Hong Zhang: Institute of Oceanology, Chinese Academy of Sciences, Qingdao 266071, China.
Quanbin Zhang: Institute of Oceanology, Chinese Academy of Sciences, Qingdao 266071, China; Nantong Branch, Institute of Oceanology, Chinese Academy of Sciences, Nantong, Jiangsu 226006, China; Collaborative Innovation Center for Marine Biomass Fibers, Materials and Textiles of Shandong Province, Qingdao 266071, China.
Wei Zhang: Centre for Marine Bioproducts Development, Flinders University, Adelaide, SA 5042, Australia; Department of Medical Biotechnology, School of Medicine, Flinders University, Adelaide, SA 5042, Australia.
Xiao-Hua Zhang: College of Marine Life Sciences, Ocean University of China, Qingdao 266003, China.
Zhi-Gang Zhang: State Key Laboratory of Oncogenes and Related Genes, Shanghai Cancer Institute, Ren Ji Hospital, School of Medicine, Shanghai Jiao Tong University, Shanghai 200240, China.

About the Guest Editors

Paul F. Long is a Reader in Pharmacognosy at King's College London. Dr Long has been a Visiting Scientist at the Australian Institute of Marine Science and is currently a Visiting International Research Professor at the University of São Paulo, Brazil. Dr Long's research uses a combination of bioinformatics, laboratory, and field experimental approaches. He is currently interested in understanding the molecular mechanisms underpinning the generation of toxin diversification in cnidarian venoms.

Bernie Degnan is an Australian Laureate Fellow and Professor at the Centre for Marine Sciences and the School of Biological Sciences at The University of Queensland (UQ) in Brisbane, Australia. He jointly heads the Marine Genomics Lab at UQ, which seeks to understand, through the study of a wide range of marine invertebrates, the genomic mechanisms that underpin the formation and evolution of animals. He was the Director and co-Chair of the 10th International Marine Biotechnology Conference, which was held in Brisbane in 2013. Most of the papers in this edited book come from this conference.

Pabulo Henrique Rampelotto is a molecular biologist currently developing his research at the Federal University of Rio Grande do Sul. His work is developed in collaboration with the biotech company, Neoprospecta Microbiome Technologies. Prof. Rampelotto is the founder and Editor-in-Chief of the Springer Book Series “Grand Challenges in Biology and Biotechnology.” He is also an Editor-in-Chief, Associate Editor, Guest Editor, and member of the editorial board of several scientific journals in the field of Life Sciences and Biotechnology. He is best known for his leadership and eminent work as Guest Editor of several successful Special Issues. In his Special Issues, some of the most distinguished team leaders in the field have published their works, ideas, and findings.

Preface

As the Century of Biology begins to bear fruit, through the translation of predictive biological understanding into applications that enhance the human condition and maintain biodiversity, the almost infinite potential of marine biological resources will be unlocked. Although Marine Biotechnology already has delivered products for medicine, food, bioenergy, nanomaterials, and bioremediation, less than 5% of our vast oceanic environment has been explored. Marine Biotechnology is a scientifically and economically expanding enterprise that is poised to harness the enormous but uncharted functional diversity of marine life, with its novel and rich array of biodesigns and biosynthetic capabilities. From this pursuit comes new genes, chemicals, materials, and inspirations for the benefit of industry, nutrition, and medicine, and which enable the sustainable use and management of the world's oceans. This Special Issue in Marine Drugs highlights the cutting-edge developments in Marine Biotechnology with a collection of papers written by authors who are leading experts in the field, including selected papers from the 10th International Marine Biotechnology Conference (IMBC-2013), the premier meeting in marine biotechnology, which is held under the auspices of the International Marine Biotechnology Association.

Paul F. Long, Bernie Degnan, Pabulo H. Rampelotto
Guest Editors

Harnessing the Potential of Halogenated Natural Product Biosynthesis by Mangrove-Derived Actinomycetes

Xue-Gong Li, Xiao-Min Tang, Jing Xiao, Guang-Hui Ma, Li Xu, Shu-Jie Xie, Min-Juan Xu, Xiang Xiao and Jun Xu

Abstract: Mangrove-derived actinomycetes are promising sources of bioactive natural products. In this study, using homologous screening of the biosynthetic genes and anti-microorganism/tumor assaying, 163 strains of actinomycetes isolated from mangrove sediments were investigated for their potential to produce halogenated metabolites. The $FADH_2$-dependent halogenase genes, identified in PCR-screening, were clustered in distinct clades in the phylogenetic analysis. The coexistence of either polyketide synthase (PKS) or nonribosomal peptide synthetase (NRPS) as the backbone synthetases in the strains harboring the halogenase indicated that these strains had the potential to produce structurally diversified antibiotics. As a validation, a new enduracidin producer, *Streptomyces atrovirens* MGR140, was identified and confirmed by gene disruption and HPLC analysis. Moreover, a putative ansamycin biosynthesis gene cluster was detected in *Streptomyces albogriseolus* MGR072. Our results highlight that combined genome mining is an efficient technique to tap promising sources of halogenated natural products synthesized by mangrove-derived actinomycetes.

Reprinted from *Mar. Drugs*. Cite as: Li, X.-G.; Tang, X.-M.; Xiao, J.; Ma, G.-H.; Xu, L.; Xie, S.-J.; Xu, M.-J.; Xiao, X.; Xu, J. Harnessing the Potential of Halogenated Natural Product Biosynthesis by Mangrove-Derived Actinomycetes. *Mar. Drugs* **2013**, *11*, 3875–3890.

1. Introduction

Mangroves, unique habitats in tropical and subtropical tidal areas, are known to be highly productive ecosystems [1]. There is unambiguous evidence that the mangrove ecosystem contains a large diversity of actinomycetes, which have the potential of producing anti-infection and anti-tumor bioactive secondary metabolites [2–4]. Structurally unique bioactive compounds have been obtained from mangrove-derived actinomycetes [4–6], however, how to tap the treasure trove of natural products produced by mangrove-derived actinomycetes is still of interest to drug developers.

The traditional cultivation-dependent approach of screening secondary metabolites was time-consuming and resulted in high labor costs. Additionally, intensive chemical exploitation of natural products always led to the identification of already known compounds [7,8]. These situations greatly hamper the discovery of novel secondary metabolites from microorganisms. Therefore, an effective and rational screening strategy is needed to investigate the biosynthetic potential of a large set of bacterial strains. A sequence-guided screening method is becoming more and more important for strain evaluation [9,10]. Polyketide synthase (PKS) and nonribosomal peptide synthetase (NRPS) are multi-domain enzymes or enzyme complexes that produce pharmaceutic important polyketides and nonribosomal peptides, respectively [11], but only targeting the conservative

domains in either PKS or NRPS will always get more than one hit that belongs to different biosynthesis gene clusters.

The tailing steps, in general, enhance the bioactivity of the compounds, during which glycosyltransferases, methyltransferases, acyltransferases, prenyltransferases, aminotransferases, cyclases, halogenases, ketoreductases, and oxygenases, were involved to further diversify the structures of the natural products [7,12]. Thus, tailoring genes were deemed as unique indicators for hunting natural product biosynthetic genes in actinomycetes [7]. For example, using the cyclase gene that involved in the formation of aromatic ring as indicator, the angucycline-producing potential of actinobacteria was rapidly estimated by a PCR-based approach [13]. Epoxidase were proven to be a good marker for the existence of polyether biosynthetic gene clusters in the case of monensin, nanchangmycin, lasalocid, nigericin, and tetronomycin [14]. Based on polyether-specific epoxidase sequences, a degenerate primer was designed and a salinomycin biosynthesis gene cluster was cloned and characterized successfully [15].

Halogenation is an important feature for the bioactivity of a large number of distinct natural products. Chlorination was the most frequently found modification, followed by bromination, while iodination and fluorination are rare in nature [16]. $FADH_2$-dependent halogenases, which introduced chloride and bromide into natural compounds, is the biggest group of specific halogenating enzymes known to date. Using $FADH_2$-dependent halogenases as indicators, Gao *et al.* [17] describe an effective and rational screen strategy that can rapidly estimate the antibiotic producing potential in a large actinobacterial strain collection. They found that genes adjacent to the halogenase genes show significant identities to genes that involved in the biosynthetic gene clusters for avilamycin, viomycin, and sporolide.

To exploit the potential of halogenated natural products from mangrove-derived actinomycetes, we investigated the diversity of $FADH_2$-dependent halogenases in 163 mangrove-derived actinomycetes and evaluated the potential of these strains to produce halogenated metabolites. A new enduracidin producer, *S. atrovirens* MGR140, was identified, and a putative biosynthetic gene cluster for halogenated ansamycin in *S. albogriseolus* MGR072 was proposed.

2. Results and Discussion

2.1. Potential of Biosynthesis of Halogenated Metabolites in Mangrove-Derived Actinomycetes

Mangrove forests are one of the most productive wetlands on Earth and exhibit unique biodiversity. In this study, 163 strains of mangrove-derived actinomycetes were screened for the presence of halogenase gene sequences by PCR amplification with the primers Hal3A/3B. A total of 26 different halogenase gene fragments were identified. The bioactivities of the strains harboring these halogenase genes were evaluated using anti-microorganism bioassays with five test strains and anti-tumor assays with three cell lines (Figure 1). These results indicated that the mangrove-derived actinomycetes have good potential in producing bioactive secondary metabolites.

Modular polyketide synthases (PKS-I), iterative polyketide synthases (PKS-II), and non-ribosomal peptide synthetases (NRPS) are involved in the biosynthesis of a vast array of structurally diverse natural secondary metabolites in microorganisms [18–20]. Gao *et al.* found that the strains

containing highly homologous halogenase genes tended to produce halometabolites with similar structures [17]. Thus, the coincidence of the halogenase gene with either NRPS, PKS-I, or PKS-II genes, was checked through the specific amplification of the target genes by PCR. In the 26 halogenase-positive strains, PKS-I, PKS-II, and NRPS genes were detected (Supplementary Table S1). The strains that possessed halogenase gene and polyketide synthase genes or nonribosomal peptide synthetase genes displayed good antagonistic activities (Supplementary Table S1).

Figure 1. Antagonistic spectrum of halogenase positive strains. Fermentation broth was centrifuged and filtered, and use the supernatant for anti-microorganism tests or for anti-tumor tests with 50× dilution, respectively.

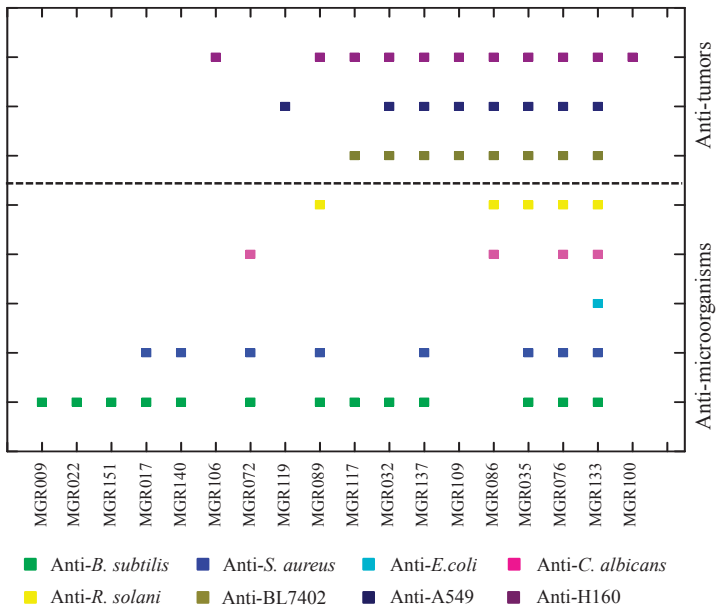

The Hal3A/3B primer pair was deduced from the conserved regions of the $FADH_2$-dependent halogenases, which catalyze the chlorination of phenol- and pyrrole-containing metabolites [7]. All of the obtained sequences belonged to $FADH_2$-dependent halogenases, and these sequences shared a high similarity at the amino acid level to sequences retrieved from GenBank. Phylogenetic analysis showed that these halogenase sequences were clustered into several subgroups (Figure 2a).

Group 1 is most closely related to *Streptomyces fungicidicus* (ATCC 21013), which harbors a biosynthetic gene cluster for the antibiotic enduracidin. Some strains in this clade, such as MGR140, MGR009, MGR017, and MGR151, showed a similar antimicrobial spectrum to that of enduracidin (Figure 2a). The 16S rRNA gene sequences of these strains showed closed similarity to *Streptomyces atrovirens*, suggesting that this species might be a potential producer of enduracidin.

Group 2 consisted of *Streptomyces albogriseolus* MGR072, *Streptomyces* sp. MGR060, and *Streptomyces* sp. CS. Our previous study isolated and identified a novel benzonaphthyridine alkaloid from MGR072 [21]. The clustering of MGR072 with the naphthomycin producer

Streptomyces sp. CS and the presence of PKS-I, PKS-II, and NRPS genes in MGR072 strongly suggest that this strain possesses the potential to produce halogenated ansamycin.

Figure 2. (**a**) Phylogenetic tree constructed using the halogenase sequences that were amplified with the Hal3A/3B primers. Tree topography and evolutionary distances were determined using the neighbor-joining method with 1000 replicates of bootstrapping. Bootstrap values, providing ≥50% support, are indicated. The scale bar indicates 0.2 substitutions per nucleotide position. The heme containing haloperoxidases were used as an outgroup. The numbers in the right of the close brace suggest three promising groups for genome mining; (**b**) Structures of enduracidin A [26], naphthomycin A [27], and xiamenmycin [23].

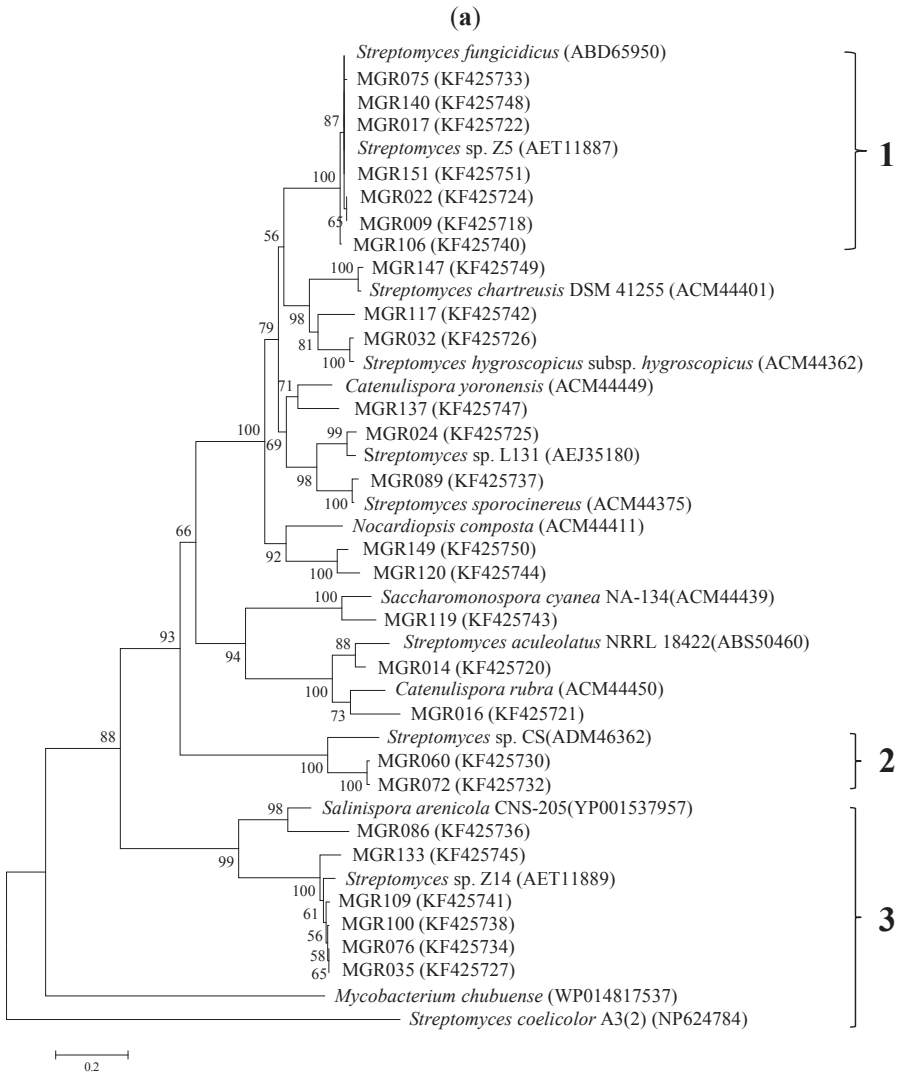

Figure 2. *Cont.*

(b)

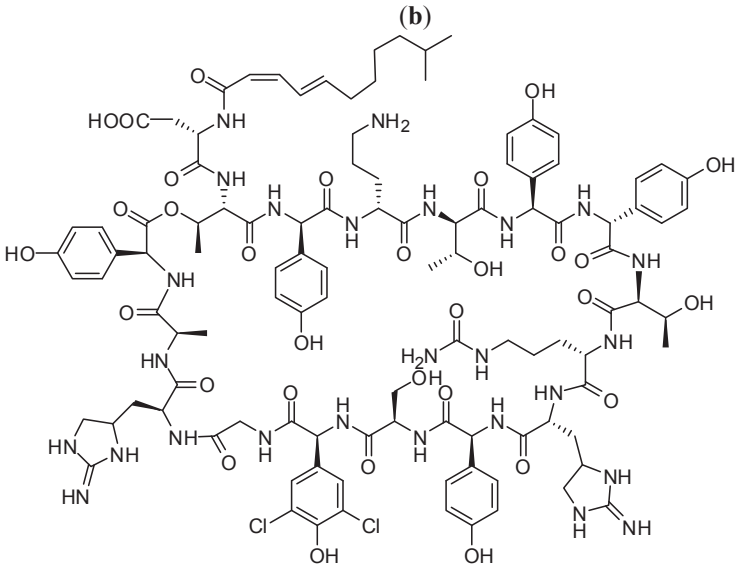

enduracidin A

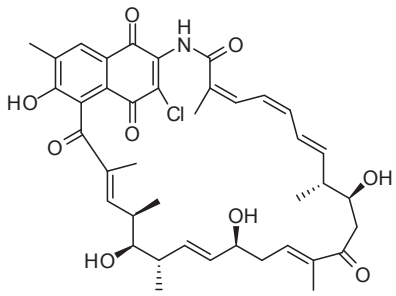

naphthomycin A

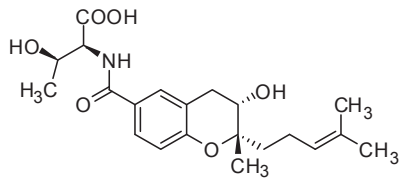

xiamenmycin

Group 3 contained *Salinispora arenicola*, the representative genus of obligate marine Actinomycetales, which can produce anti-tumor compounds. Strains in group 3, except for MGR100, show broad anti-tumor bioactivity (Figure 2a). For example, *Streptomyces xiamenensis* MGR035 was identified as a novel species of mangrove-derived actinomycetes [22], and the crude extract of MGR035 exhibits versatile antagonism bioactivity including anti-bacterial, anti-tumor, anti-fibrotic, and anti-inflammatory bioactivities [23,24]. *S. xiamenensis* was first characterized as a new *Streptomyces* species that was isolated from mangrove sediment. It is interesting to find that *S. xiamenensis* has subsequently been isolated from coral and marine sponges [25], confirming that this species is widespread in the marine environment. The higher similarities in the halogenase genes of group 3 indicated that these strains may produce halogenated natural secondary metabolites due to the marine habitation features.

2.2. A New Enduracidin Producer S. atrovirens MGR140

The halogenase gene in *S. atrovirens* MGR140 showed 100% similarity to the halogenase gene involved in enduracidin biosynthesis in *S. fungicidicus* [26]. To test whether enduracidin was produced, the fermentation broth from *S. atrovirens* MGR140 was extracted and analyzed using high performance liquid chromatography (HPLC), using standard enduracidin as a reference (Figure 3a). The fingerprints of the metabolites showed that the target compounds had the same retention time and similar UV profiles as enduracidin (Figure 3a).

The primer set P4 [28], which targeted the conserved motifs in the NRPS adenylation domains, was used to probe the enduracidin biosynthetic gene cluster in *S. atrovirens* MGR140. A total of seven clones that contained NRPS adenylation domains were found in the genomic library that consisted of 3000 fosmid clones. Further investigations were performed using the primer sets P3 and P5 for *endP* (PLP-dependent aminotransferase) and *endD* (nonribosomal peptide synthetase) amplification, respectively. Primer sets P1 and P2 were used to confirm the boundary regions of the putative enduracidin biosynthetic gene cluster. Eventually, a 116 kb region consisted of four overlapping fosmids was identified, and this region harbored the entire enduracidin biosynthetic gene cluster (Supplementary Figure S1).

To confirm the function of the cluster, the *endA* gene was replaced with the *acc(3)IV* cassette (apramycin resistance) to disrupt the putative enduracidin biosynthetic gene cluster. Regions of approximately 2 kb, flanking the *endA* and the *acc(3)IV* cassette, were cloned, resulting pLXG01 (Figure 3b). This plasmid was introduced into *S. atrovirens* MGR140 through conjugation. The crossover mutant was confirmed by PCR amplification. As expected, the mutant LXG1 strain completely lost the ability to produce enduracidin (Figure 3a). This result proved that the putative gene cluster was responsible for the enduracidin biosynthesis observed in *S. atrovirens* MGR140.

2.3. Identification of a Putative Halogenated Ansamycin Gene-Cluster from S. albogriseolus MGR072

The halogenase gene identified in *S. albogriseolus* MGR072 displayed 64% similarity to the halogenase gene involved in ansamitocin biosynthesis. Further analysis of the flanking regions of the halogenase gene in MGR072 revealed that the gene fragments encoded AHBA (3-amino-5-hydroxybenzoic acid) synthase and PKS. The high similarity between the identified genes and the rifamycin biosynthetic pathway in *Amycolatopsis mediterranei* U32 indicated that *S. albogriseolus* MGR072 may produce ansamycin antibiotics in addition to benzonaphthyridine alkaloids.

Figure 3. A gene cluster in *S. atrovirens* MGR140 presumably governing enduracidin biosynthesis. (**a**) HPLC analysis of enduracidin production at a UV wavelength of 267 nm. I, enduracidin standard (MP Biomedicals); II, extract from wild-type *S. atrovirens* MGR140; III, mutant LXG1 (Δ*endA*); (**b**) Construction of the *endA* mutant strain LXG1 by double-crossover gene replacement.

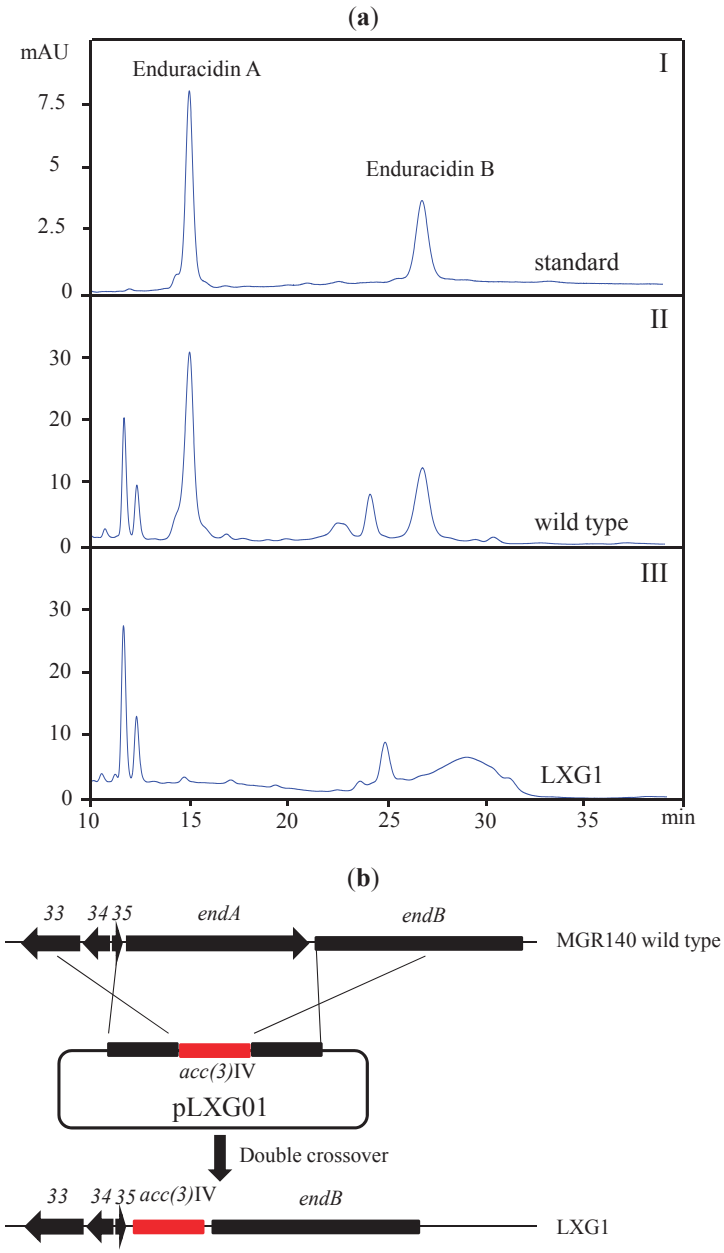

As the AHBA synthase genes were highly conserved in the AHBA-derived antibiotics biosynthetic gene cluster, a special probe for AHBA synthase was used to clone the putative halogenated ansamycin biosynthetic gene cluster in *S. albogriseolus* MGR072. A total of 16 clones that contained the AHBA synthase genes were detected in the genomic library that consisted of 3000 fosmid clones. Three fosmids (5G2, 21A3, and 23G6) that contained the AHBA synthase, PKS, and halogenase were shown to reside in the putative ansamycin biosynthesis pathway. To obtain the complete putative ansamycin gene cluster, the *S. albogriseolus* MGR072 genomic library was further screened using the terminal sequence of 5G2 as a probe. Two more positive clones (26H8 and 29C9) were identified in the genomic library by sequential chromosome walking. The overlapping fosmids (Supplementary Figure S2) that covered a 84.9 kb DNA region were obtained and were tentatively named the *sha*-cluster. The predicted functions of the 41 complete open reading frames (ORFs) (ACC# KF425715) are shown in Figure 4a and Supplementary Table S2.

Figure 4. (**a**) The putative ansamycin biosynthetic gene cluster and gene organization of *S. albogriseolus* MGR072; (**b**) Rifamycin biosynthesis gene cluster from *Amycolatopsis mediterranei* U32 [29]; (**c**) Naphthomycin biosynthetic gene cluster from *Streptomyces* sp. CS [27].

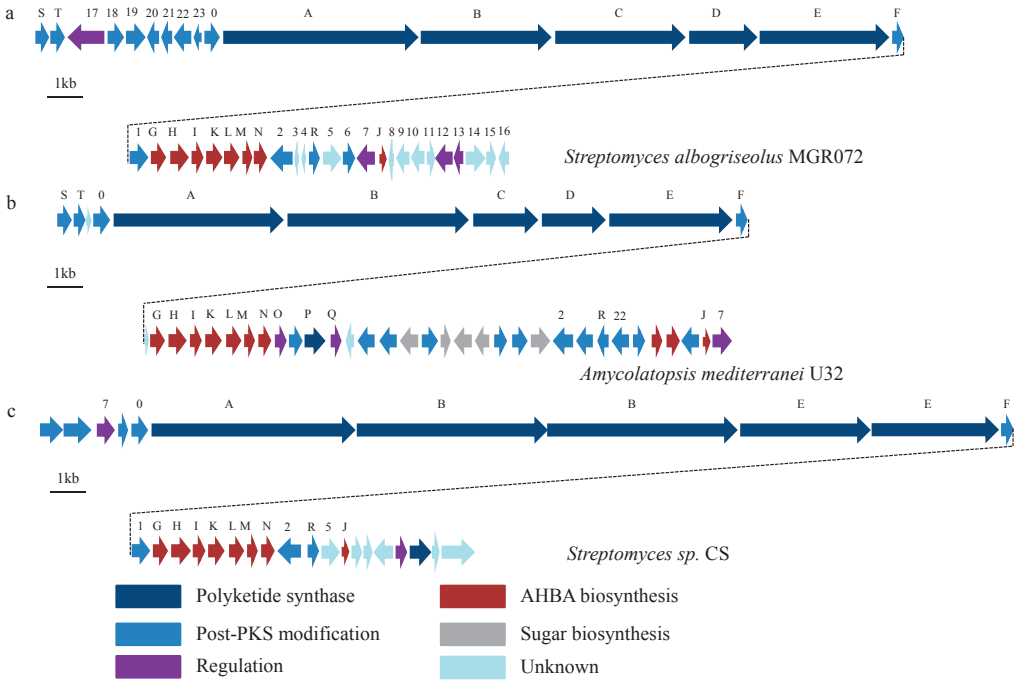

For the common starter unit AHBA, a conserved location and arrangement in the biosynthetic gene cluster of all ansamycin could be observed [30]. As the AHBA biosynthetic genes in rifamycin [31] and naphthomycin [27] (Figure 4b,c), the *shaGHIKLMN* genes form an operon that appears to be responsible for the biosynthesis of AHBA, while the *shaJ* gene is located 7.5 kb downstream of *shaN*. Upstream of the *sha-AHBA* cluster, a large region encoded five modular type I PKS genes

(*shaA–E*) and an amide synthase gene (*shaF*), which showed similar arrangement with that in rifamycin gene cluster from *A. mediterranei* U32, but contrasted in the numbers of modulars to that in napthomycin gene cluster from *Streptomyces* sp. CS. Interestingly, *rifB* contained three KS-AT-DH-KR-ACP domains and *shaB* contained two. However, *shaC* encoding two KS-AT-DH-KR-ACP domains and *rifC* have only one. It is speculated that proteins encoded by *shaA-E* contain one loading module and ten extension modules that are capable of incorporating a total of eight propionate units and two acetate units into the AHBA starter unit. The *shaF* gene, which encodes an amide synthase, showed a high degree of similarity to the *rifF* gene of rifamycin (identity = 64%) and *natF* gene of napthomycin (identity = 57%), may catalyze the release of the completed polyketide chain from PKS, as well as generate the macrocyclic lactam.

Except the core structure biosynthetic gene cluster, the post-synthase modifications are various. Located between the *sha*-PKS cluster and *sha*-AHBA cluster is a *sha1* gene, which encoding $FADH_2$-dependent halogenase, show high similarity to the *nat1* of napthomycin. It is proposed that *sha1* may relate to the halogenated modification of the proansamycin. Downstream of *shaN* is an *orf2*, that may involve in the formation of naphthalene ring. It is predicted that *orf2* catalyzes the oxidation of the tetraketide intermediate. *shaR* encoding a type II thioesterase that is predicted to removing aberrant units from carrier domains. *Orf5*, located on the downstream of *shaN*, has a sequence identity of 66% to *nat4* from naphthomycin gene cluster. *Orf7* encoding a transcriptional regulator is 44% and 48% identical to *AMED_0655* from *A. mediterranei* and *orf5* from *Streptomyces* sp. CS, respectively. Located downstream of *shaJ* is a set of genes (*orf8*, *9*, *10*, *11*, and *12*) that appear to participated in the regulation of transcription. *Orf13* encoding an EmrB/QacA family drug resistance transporter was deduced that to export putative halogenated ansamycin from *S. albogriseolus*. But functions of these genes are still unknown.

3. Discussion

Currently, over 4000 different natural halogen-containing compounds have been found [32]. Many of these compounds are predominately produced by microorganisms that originated in marine environments due to the relatively high halogen ion content [33]. Chloramphenicol, 7-chlorotetracyclin, and vancomycin are representative examples of antibiotics in which halogenation increases the complexity of the structure and enhances its bioactivity [34]. In addition to the enzymes involved in the natural product backbone biosynthesis, tailoring genes in the biosynthesis pathway, such as halogenases, could be used as effective probes to estimate the genetic coding potential of natural products [7,12,35,36].

There are two classes of halogenases including $FADH_2$-dependent halogenases and non-heme Fe^{II}-dependent halogenases that embedded in the biosynthetic gene clusters of natural products [37]. Phylogenetic analyses of $FADH_2$-dependent halogenases showed that strains containing highly homologous halogenases tended to produce halometabolites with related structures [17]. To this day, almost all known $FADH_2$-dependent halogenases, which form the largest class of halogenating enzymes, are involved in the halogenation of aromatic or heteroaromatic ring systems [38]. Two distinct groups of $FADH_2$-dependent halogenases exist, one group that uses tryptophan as a substrate and the other that uses phenol or pyrrol [39]. Using the conserved regions

of $FADH_2$-dependent halogenases as probes, a sequence-guided genetic screening strategy enabled pre-selection of strains from thousands of strain collections and allowed for rapid access to the novel natural products with predetermined structural properties [7]. In addition, the non-heme Fe^{II}-dependent halogenases represent a new subtype of the O_2 and α-ketoglutarate-decarboxylating superfamily, which act on unactivated, aliphatic carbon centers [35,37]. This allows the novel halogenase as special indicator to identify the completely different classes of natural products. In this study, 26 halogenase-positive strains were screened from 163 mangrove-derived actinomycetes strains. Most of the halogenase-positive strains exhibited attractive antagonistic bioactivity, include anti-tumor, and anti-microorganism activity. Additionally, it is worth noting that there is a higher incidence of anti-microorganism bioactivity in the halogenase-positive strains compared to that of the halogenase-negative strains.

Halogenase genes might undergo widespread horizontal gene transfer (HGT) within actinomycetes [17]. Although the phylogenetic analysis of the $FADH_2$-dependent halogenase genes and the 16S rRNA gene in the 26 strains showed poor consistency (Supplementary Figure S3), three promising groups of halometabolite producers could still be observed. *S. atrovirens* MGR140 in Group 1 was shown to produce the antibiotic enduracidin, whereas *S. xiamenensis* MGR035 in Group 3 was subjected to extensive studies due to its broad antagonism bioactivity [23,24]. *S. albogriseolus* MGR072 in Group 2 produced a novel benzonaphthyridine alkaloid [21], and this strain also has potential to produce halogenated ansamycin.

The putative halogenated ansamycin biosynthetic pathway in *S. albogriseolus* MGR072 has a classic core gene structure similar to that of rifamycin, though the post-PKS modifications genes are distinct. *Orf1*, which encodes a $FADH_2$-dependent halogenase, is adjacent to the PKS cluster and AHBA cluster and may be involved in halogenated ansamycin biosynthesis. *Orf1* contains two typical conserved regions of this enzyme group, GxGxxG and WxWxIP (Supplementary Figure S4), and also has a flavin binding site located at the amino terminal end. *Orf1* has a sequence identity of 78% to *nat1*, which is thought to incorporate the chlorine atom at the C-30 position in naphthomycin A. The *Asm12* gene also encodes a $FADH_2$-dependent halogenase and is considered to be responsible for the chlorination of ansamitocin. The well-designed cross-complementation experiment showed that the roles of *nat1* and *asm12* can be effectively taken over by each other [27]. Based on the sequence analysis, *orf1* was considered to be responsible for the chlorination of the putative halogenated ansamycin. The gene from *orf2* encodes a 3-(3-hydroxyphenyl) propionate hydroxylase, and this gene shows highly homology with the *mphA* and *nat2* genes involved in the formation of the naphthalene ring of rifamycin and naphthomycin, respectively [27,29]. *Orf2* contains three conserved regions (GXGXXG (motif I), DGXXSXXR (motif II) and GDXXH (motif III)) of the flavoprotein hydroxylases family (Supplementary Figure S5) and may catalyze the formation of the naphthalene ring of putative halogenated ansamycin. *Orf0* shows sequence similarity to cytochrome P450 hydroxylase, which is located immediately upstream of the PKS genes, and may be involved in the oxidation steps before or during the formation of the core structure of naphthoquinone. In addition, *orf22* also encodes a cytochrome P450 hydroxylase; however, this gene only has a sequence identity of 29.8% to *orf0*. The function of *orf22* could not be deduced by search and comparison with the databases. Located upstream of *orf22* are two

methyltransferases that may be involved in the methylated modifications. The *shaS* and *shaT* genes encode two dehydrogenases that contain oxidoreductase domains, and these proteins are thought to catalyze naphthoquinone ring closure.

4. Experimental Section

4.1. Strain and Culture Conditions

In total, 163 actinomycetes strains were isolated from mangrove surface sediments from the Jiulong River Estuary, China. *Streptomyces* were grown at 30 °C in TSB liquid medium and SFM solid medium. *Escherichia coli* strain DH5α was used for vector construction, and propagation was cultivated in Luria-Bertani (LB) medium at 37 °C. When needed, ampicillin was added to the medium at a concentration of 100 μg/mL.

4.2. Detection of PKS I, PKS II, and NRPS Genes by PCR Amplifications

PCRs were run for 30 cycles. The conditions for each cycle were 1 min at 94 °C, 1 min of touchdown from 55 °C to 40 °C, and 2 min at 72 °C. Each reaction mix contained 5 ng of genomic DNA, 12.5 pmol of each primer, 1 U of Ex Taq DNA polymerase, and 10% dimethyl sulfoxide. The PCR products were purified using OMEGA Gel Extraction kits after agarose gel separation and were cloned into the pMD18-T plasmid vector (Takara Bio Inc., Tokyo, Japan) for sequencing.

The following set of PCR primers was used for the amplification the halogenase genes: Hal3A (5′-TTCCCSCGSTACCASATCGGSGAG-3′) and Hal3B (5′-GS GGGATSWMCCAGWACCA SCC-3′) [7]. Another three sets of PCR primers were used: NRPS2A (5′-GCSTACSYSATSTACAC STCSGG-3′) and NRPS2B (5′-SASGTCVCCSGTSCGGTAS-3′) targeting the NRPS sequences [40]; PKS4A (5′-GCSATGGAYCCSCARCARCGSVT-3′) and PKS4B (5′-GTSCCSGTSCCRT GSSCYTCSAC-3′) targeting the type I PKS sequences [41]; PKS1A (5′-TSGCSTGCTTCGA YGCSATC-3′) and PKS1B (5′-TGGAANCCGCCGAABCCGCT-3′) targeting the type II PKS sequences [42].

4.3. Fosmid Library Construction and Screening

Genomic DNA from *S. albogriseolus* MGR072 and *S. atrovirens* MGR140 was prepared using the standard methods [43]. The DNA was sheared to approximately 40 kb fragments and ligated into the CopyControl pCC2FOS vector. The ligated DNA was then packaged using MaxPlax Lambda Packaging Extracts and plated on EPI300-T1R plating cells (EPICENTRE). To locate the halogenated ansamycin biosynthetic gene cluster, degenerated primers were used to screen the genomic library (AHBAF: 5′-CCSGCCTTCACCTTCATCTCCTC-3′ and AHBAR: 5′-AYCCGGAACATSGCCATGTAGTG-3′ [27]). The entire gene cluster was obtained by subcloning and sequencing the PCR products. The enduracidin cluster from *S. atrovirens* MGR140 was screened using five pairs of primers: P1 (end1F: 5′-AATGCCGACAGCCGGACAA GGT-3′/end1R: 5′-GATCCACGAAGCTCTGGTT-3′), P2 (end2F: 5′-ATCACCGCCGACAACT ACGA-3′/end2R: 5′-CAGGTTCAGCATCAGCCACA-3′), P3 (end28F: 5′-TGTCAGCACAT

GGCGCAACGC-3′/end28R: 5′-TCATCGAGGACACGGGCAAGCT-3′), P4 (end37F: 5′-TTCACGCAGGAACGCAACAAC-3′/end37R: 5′-TGAGCGAAGGACAGCGGCAC-3′), and P5 (end40F: 5′-CTCGACAACCAGGTCAAGCT-3′/end37R: 5′-AGTTCCCGCCCAGTTCCCA-3′).

4.4. Gene Inactivation

Gene inactivation was carried out using standard genetic approaches. A 915 bp fragment of the *aac(3)IV* gene was amplified using the pSET152 plasmid as a template and the following primers containing *Sca*I sites: ApraR-F: 5′-AAAAGTACTTGGTTCATGTGCAGCTCCATC-3′ and ApraR-R: 5′-AAAAGTACTTGAGCTCAGCCAATCGACTG-3′. The PCR product was cloned into the pHZ1358 vector with approximately 2 kb upstream and downstream sequences of the target genes as flanking regions. The pLXG01 plasmid was constructed and introduced into *Streptomyces* sp. through conjugation with *E. coli*. The apramycin-resistant and thiostrepton-sensitive clones were selected for further verification by PCR amplification. The *endA*-deleted mutant was selected and named LXG1.

4.5. DNA Sequencing and Bioinformatic Analysis

DNA sequencing was carried out using Roche's 454 sequencing platform. Approximately 237.5 Mb data, which represented 30.8-fold coverage of the genome, were produced from the Roche 454 GS FLX sequencer. Putative ORFs were predicted using the FramePlot 3.0 beta online program [44], and function annotation was performed using BLAST analysis. The PKS domains were predicted and analyzed by searching the SEARCHPKS database [45].

4.6. Phylogenetic Analysis

Deduced amino acid sequences of the halogenase genes retrieved from the strains were searched in the NCBI database. Related sequences were aligned using the DNAMAN program (version 5.1; Lynnon Biosoft, Quebec, Canada). A phylogenetic tree was constructed from a matrix of pairwise genetic distances using the maximum-parsimony algorithm and the neighbor-joining method in the MEGA 3.0 program, and 1000 trials of bootstrap analyses were used to provide confidence estimates for the phylogenetic tree topologies.

5. Conclusions

The PCR-based genetic screening approach suggests that the mangrove-derived actinomycetes harboring diversified halogenase genes are a rich source of natural products. Of the 163 mangrove-derived actinomycetes, 16% of these strains have the potential to produce various halogenated ($FADH_2$-dependent halogenases) natural products. A new enduracidin producer, *S. atrovirens* MGR140, was identified. Moreover, a putative halogenated ansamycin cluster was revealed in *S. albogriseolus* MGR072. This study has applied a research strategy to screen the mangrove-derived actinomycetes for produce halogenated natural secondary metabolites.

Acknowledgments

This work was supported by grants from the National Science Foundation of China (NSFC 81273404) and the National Basic Research Program of China ("973" 2012CB721001). We are indebted to Yuemao Shen for his generous support and long-standing cooperation.

Conflicts of Interest

The authors declare no conflicts of interest.

References and Notes

1. Costanza, R.; d'Arge, R.; De Groot, R.; Farber, S.; Grasso, M.; Hannon, B.; Limburg, K.; Naeem, S.; O'neill, R.V.; Paruelo, J. The value of the world's ecosystem services and natural capital. *Nature* **1997**, *387*, 253–260.
2. Kathiresan, K.; Bingham, B.L. Biology of mangroves and mangrove ecosystems. *Adv. Mar. Biol.* **2001**, *40*, 81–251.
3. Remya, M.; Vijayakumar, R. Isolation and characterization of marine antagonistic actinomycetes from west coast of India. *Facta Universitatis Ser. Med. Biol.* **2008**, *15*, 13–19.
4. Hong, K.; Gao, A.-H.; Xie, Q.-Y.; Gao, H.G.; Zhuang, L.; Lin, H.-P.; Yu, H.-P.; Li, J.; Yao, X.-S.; Goodfellow, M. Actinomycetes for marine drug discovery isolated from mangrove soils and plants in China. *Mar. Drugs* **2009**, *7*, 24–44.
5. Dias, A.C.; Andreote, F.D.; Dini-Andreote, F.; Lacava, P.T.; Sá, A.L.; Melo, I.S.; Azevedo, J.L.; Araújo, W.L. Diversity and biotechnological potential of culturable bacteria from Brazilian mangrove sediment. *World J. Microbiol. Biotechnol.* **2009**, *25*, 1305–1311.
6. Huang, H.; Lv, J.; Hu, Y.; Fang, Z.; Zhang, K.; Bao, S. *Micromonospora rifamycinica* sp. nov., a novel actinomycete from mangrove sediment. *Int. J. Syst. Evol. Microbiol.* **2008**, *58*, 17–20.
7. Hornung, A.; Bertazzo, M.; Dziarnowski, A.; Schneider, K.; Welzel, K.; Wohlert, S.E.; Holzenkämpfer, M.; Nicholson, G.J.; Bechthold, A.; Süssmuth, R.D. A Genomic Screening Approach to the Structure-Guided Identification of Drug Candidates from Natural Sources. *Chembiochem* **2007**, *8*, 757–766.
8. Wang, G.; Zhang, H.; Sun, G.; Wu, L.; Zhang, J.; Wang, Y. A new method for rapid identification of ansamycin compounds by inactivating KLM gene clusters in potential ansamycin-producing actinomyces. *J. Appl. Microbiol.* **2012**, *112*, 353–362.
9. Zerikly, M.; Challis, G.L. Strategies for the discovery of new natural products by genome mining. *Chembiochem* **2009**, *10*, 625–633.
10. Walsh, C.T.; Fischbach, M.A. Natural products version 2.0: Connecting genes to molecules. *J. Am. Chem. Soc.* **2010**, *132*, 2469–2493.
11. Du, L.; Lou, L. PKS and NRPS release mechanisms. *Nat. Prod. Rep.* **2010**, *27*, 255–278.
12. Olano, C.; Méndez, C.; Salas, J.A. Post-PKS tailoring steps in natural product-producing actinomycetes from the perspective of combinatorial biosynthesis. *Nat. Prod. Rep.* **2010**, *27*, 571–616.

13. Ouyang, Y.; Wu, H.; Xie, L.; Wang, G.; Dai, S.; Chen, M.; Yang, K.; Li, X. A method to type the potential angucycline producers in actinomycetes isolated from marine sponges. *Antonie van Leeuwenhoek* **2011**, *99*, 807–815.
14. Liu, T.; Cane, D.E.; Deng, Z. The enzymology of polyether biosynthesis. *Methods Enzymol.* **2009**, *459*, 187–214.
15. Jiang, C.; Wang, H.; Kang, Q.; Liu, J.; Bai, L. Cloning and Characterization of the Polyether Salinomycin Biosynthesis Gene Cluster of *Streptomyces albus* XM211. *Appl. Environ. Microbiol.* **2012**, *78*, 994–1003.
16. Neumann, C.S.; Fujimori, D.G.; Walsh, C.T. Halogenation strategies in natural product biosynthesis. *Chem. Biol.* **2008**, *15*, 99–109.
17. Gao, P.; Huang, Y. Detection, distribution, and organohalogen compound discovery implications of the reduced flavin adenine dinucleotide-dependent halogenase gene in major filamentous actinomycete taxonomic groups. *Appl. Environ. Microbiol.* **2009**, *75*, 4813–4820.
18. Shen, B. Polyketide biosynthesis beyond the type I, II and III polyketide synthase paradigms. *Curr. Opin. Chem. Biol.* **2003**, *7*, 285–295.
19. Schwarzer, D.; Finking, R.; Marahiel, M.A. Nonribosomal peptides: From genes to products. *Nat. Prod. Rep.* **2003**, *20*, 275–287.
20. González, I.; Ayuso-Sacido, A.; Anderson, A.; Genilloud, O. Actinomycetes isolated from lichens: Evaluation of their diversity and detection of biosynthetic gene sequences. *FEMS Microbiol. Ecol.* **2005**, *54*, 401–415.
21. Li, X.-L.; Xu, M.-J.; Zhao, Y.-L.; Xu, J. A Novel Benzo [f][1,7] Naphthyridine Produced by *Streptomyces Albogriseolus* from Mangrove Sediments. *Molecules* **2010**, *15*, 9298–9307.
22. Xu, J.; Wang, Y.; Xie, S.-J.; Xu, J.; Xiao, J.; Ruan, J.-S. *Streptomyces xiamenensis* sp. nov., isolated from mangrove sediment. *Int. J. Syst. Evol. Microbiol.* **2009**, *59*, 472–476.
23. Xu, M.-J.; Liu, X.-J.; Zhao, Y.-L.; Liu, D.; Xu, Z.-H.; Lang, X.-M.; Ao, P.; Lin, W.-H.; Yang, S.-L.; Zhang, Z.-G. Identification and characterization of an anti-fibrotic benzopyran compound isolated from mangrove-derived *Streptomyces xiamenensis*. *Mar. Drugs* **2012**, *10*, 639–654.
24. Liu, X.-J.; Xu, M.-J.; Fan, S.-T.; Wu, Z.; Li, J.; Yang, X.-M.; Wang, Y.-H.; Xu, J.; Zhang, Z.-G. Xiamenmycin Attenuates Hypertrophic Scars by Suppressing Local Inflammation and the Effects of Mechanical Stress. *J. Invest. Dermatol.* **2013**, *133*, 1351–1360.
25. Zhang, X.; Sun, Y.; Bao, J.; He, F.; Xu, X.; Qi, S. Phylogenetic survey and antimicrobial activity of culturable microorganisms associated with the South China Sea black coral *Antipathes dichotoma*. *FEMS Microbiol. Lett.* **2012**, *336*, 122–130.
26. Yin, X.; Zabriskie, T.M. The enduracidin biosynthetic gene cluster from *Streptomyces fungicidicus*. *Microbiology* **2006**, *152*, 2969–2983.
27. Wu, Y.; Kang, Q.; Shen, Y.; Su, W.; Bai, L. Cloning and functional analysis of the naphthomycin biosynthetic gene cluster in *Streptomyces* sp. CS. *Mol. Biosyst.* **2011**, *7*, 2459–2469.
28. Marahiel, M.A.; Stachelhaus, T.; Mootz, H.D. Modular peptide synthetases involved in nonribosomal peptide synthesis. *Chem. Rev.* **1997**, *97*, 2651–2674.

29. Zhao, W.; Zhong, Y.; Yuan, H.; Wang, J.; Zheng, H.; Wang, Y.; Cen, X.; Xu, F.; Bai, J.; Han, X. Complete genome sequence of the rifamycin SV-producing *Amycolatopsis mediterranei* U32 revealed its genetic characteristics in phylogeny and metabolism. *Cell Res.* **2010**, *20*, 1096–1108.
30. Floss, H.G.; Yu, T.-W.; Arakawa, K. The biosynthesis of 3-amino-5-hydroxybenzoic acid (AHBA), the precursor of mC_7N units in ansamycin and mitomycin antibiotics: A review. *J. Antibiot. (Tokyo)* **2010**, *64*, 35–44.
31. Floss, H.G.; Yu, T.W. Rifamycin-mode of action, resistance, and biosynthesis. *Chem. Rev.* **2005**, *105*, 621–632.
32. Gribble, G.W. The diversity of naturally produced organohalogens. *Chemosphere* **2003**, *52*, 289–297.
33. Gribble, G.W. Naturally occurring organohalogen compounds—a comprehensive survey. *Fortschr. Chem. Org. Naturst.* **1996**, *68*, 1–423.
34. Auffinger, P.; Hays, F.A.; Westhof, E.; Ho, P.S. Halogen bonds in biological molecules. *Proc. Natl. Acad. Sci. USA* **2004**, *101*, 16789–16794.
35. Smith, D.R.; Gruschow, S.; Goss, R.J. Scope and potential of halogenases in biosynthetic applications. *Curr. Opin. Chem. Biol.* **2013**, *17*, 276–283.
36. Pistorius, D.; Muller, R. Discovery of the rhizopodin biosynthetic gene cluster in *Stigmatella aurantiaca Sg a15* by genome mining. *Chembiochem* **2012**, *13*, 416–426.
37. Vaillancourt, F.H.; Vosburg, D.A.; Walsh, C.T. Dichlorination and Bromination of a Threonyl-*S*-Carrier Protein by the Non-heme Fe^{II} Halogenase SyrB2. *Chembiochem* **2006**, *7*, 748–752.
38. Bayer, K.; Scheuermayer, M.; Fieseler, L.; Hentschel, U. Genomic mining for novel FADH2-dependent halogenases in marine sponge-associated microbial consortia. *Mar. Biotechnol.* **2013**, *15*, 63–72.
39. Murphy, C.D. Recent developments in enzymatic chlorination. *Nat. Prod. Rep.* **2006**, *23*, 147–152.
40. Ayuso-Sacido, A.; Genilloud, O. New PCR primers for the screening of NRPS and PKS-I systems in actinomycetes: Detection and distribution of these biosynthetic gene sequences in major taxonomic groups. *Microb. Ecol.* **2005**, *49*, 10–24.
41. Schirmer, A.; Gadkari, R.; Reeves, C.D.; Ibrahim, F.; DeLong, E.F.; Hutchinson, C.R. Metagenomic analysis reveals diverse polyketide synthase gene clusters in microorganisms associated with the marine sponge *Discodermia dissoluta*. *Appl. Environ. Microbiol.* **2005**, *71*, 4840–4849.
42. Metsä-Ketelä, M.; Salo, V.; Halo, L.; Hautala, A.; Hakala, J.; Mäntsälä, P.; Ylihonko, K. An efficient approach for screening minimal PKS genes from Streptomyces. *FEMS Microbiol. Lett.* **1999**, *180*, 1–6.
43. Kieser, T.; Bibb, M.J.; Buttner, M.J.; Chater, K.F.; Hopwood, D.A. *Practical Streptomyces Genetics*; John Innes Foundation Norwich: Norwich, UK, 2000; p. 412.

44. Ishikawa, J.; Hotta, K. FramePlot: A new implementation of the frame analysis for predicting protein-coding regions in bacterial DNA with a high G + C content. *FEMS Microbiol. Lett.* **1999**, *174*, 251–253.
45. Yadav, G.; Gokhale, R.S.; Mohanty, D. SEARCHPKS: A program for detection and analysis of polyketide synthase domains. *Nucleic Acids Res.* **2003**, *31*, 3654–3658.

Enhanced Anti-Obesity Activities of Red Mold Dioscorea When Fermented Using Deep Ocean Water as the Culture Water

Li-Chun Wang, Tzu-Ying Lung, Yi-Hsin Kung, Jyh-Jye Wang, Tsung-Yu Tsai, Bai-Luh Wei, Tzu-Ming Pan and Chun-Lin Lee

Abstract: Deep ocean water (DOW) has, in previous studies, been found to be a novel anti-obesity drink and useful in raising *Monascus*-produced monascin and ankaflavin levels. This may resolve the limited anti-obesity ability of red mold dioscorea (RMD) known as the *Monascus purpureus*-fermented *Disocorea batatas*. This study aims to compare the anti-obesity effect of DOW-cultured RMD (DOW-RMD) and ultra-pure water-cultured RMD (UPW-RMD) in rats fed on a high fat diet. Moreover, the effect of ions composition of DOW and DOW-influenced functional metabolites change of RMD on the differentiation and lipogenesis regulation were investigated using 3T3-L1 pre-adipocytes. In the animal test, compared to UPW-RMD, DOW-RMD possessed better ability to inhibit increases in weight gain, and better feed efficiency, body-fat pad and cross-sectional area of adipocytes. In the cell test, the anti-obesity abilities of DOW-RMD in inhibiting PPARγ and C/EBPα expression in differentiation and lipoprotein lipase activity in lipogenesis were contributed to by the DOW-increased monascin and ankaflavin levels and the ions of DOW, respectively.

Reprinted from *Mar. Drugs*. Cite as: Wang, L.-C.; Lung, T.-Y.; Kung, Y.-H.; Wang, J.-J.; Tsai, T.-Y.; Wei, B.-L.; Pan, T.-M.; Lee, C.-L. Enhanced Anti-Obesity Activities of Red Mold Dioscorea When Fermented Using Deep Ocean Water as the Culture Water. *Mar. Drugs* **2013**, *11*, 3902–3925.

1. Introduction

Obesity is associated with a higher risk of developing diabetes and cardiovascular disease. At the cellular level, enlargement of the adipose tissue mass has been characterized by an increase in the size (hypertrophy) or number (hyperplasia) of adipocytes. The triglyceride (TG) content in adipocytes reflects the balance between lipogenesis and lipolysis, which is largely related to cell volume. When adipocytes reach a critical size threshold, preadipocytes in close proximity to the adipocytes will respond to positive energy balance by proliferating and then differentiating into adipocytes to store the excess energy [1]. Early in life, adipose tissue expansion occurs primarily through hyperplasia. However, humans and rodents have the capacity to form new fat cells from preadipocytes throughout life. Several mechanisms reduce the risk of obesity, including reduced food intake, decreased intestine adsorption, suppressed lipogenesis, enhanced lipolysis and fatty acid oxidation, increased energy expenditure and inhibited preadipocyte proliferation, differentiation, and pharmacological treatment [2–4].

Monascus species has been used as the traditional food fungus in Eastern Asia for several centuries. *Monascus*-fermented products are gradually developed as the popular and important functional food for the prevention of cardiovascular disease. Red mold dioscorea (RMD) known as

the *Monascus purpureus*-fermented *Disocorea batatas* was proven as the strong hypolipidemic functional food in the previous study [5]. However, we found that RMD had only a weak effect on anti-obesity, which limited the development of RMD for the prevention of metabolic syndrome. Monascin and ankaflavin isolated form *Monascus*-fermented product were proven to prevent obesity development via the suppressions of differentiation and lipogenesis in our *in vitro* and *in vivo* studies [5,6]. Therefore, enhancing monascin and ankaflavin levels in RMD may straighten the anti-obesity of RMD.

Deep ocean water (DOW) generally means ocean water from a depth of more than 200 m in depth. The character of DOW includes high purity, cold temperature, abundant nutrients, and minerals [7,8]. Currently, DOW has been applied to food, agriculture, cosmetic and medical field in many countries such as Taiwan, Japan, Korea and America. Due to its high contents of minerals such as magnesium (Mg), calcium (Ca), potassium (K), zinc (Zn), *etc.* [9–13]. A previous study used DOW as the culture water of *Monascus* in order to straighten the hypolipidemic function [14]. DOW-cultured RMD (DOW-RMD) using DOW as the culture water has greater effect on lowering serum total cholesterol (TC), triglyceride (TG), low density lipoprotein cholesterol (LDL-C) levels and raising high density lipoprotein cholesterol (HDL-C) levels than reverse osmosis water-cultured RMD (ROW-RMD). Furthermore, greater anti-atherosclerosis effect, and anti-fatty liver effect are performed by DOW-RMD treatment than ROW-RMD treatment group [14].

According to above-mentioned study, RMD had strong hypolipidemic effect but not anti-obesity effects. RMD cultured in DOW contains substantial amounts of monascin and ankaflavin, and relatively low levels of citrinin. In addition, DOW enhances the production of monascin and ankaflavin. Previous research has shown that monascin and ankaflavin were the effective compounds that perform hypolipidemic and anti-obesity effects. Furthermore, DOW was previously shown to possess anti-obesity capability. Therefore, DOW and the DOW-enhanced functional metabolites in RMD may improve the anti-obesity effect. In this study, animal test was adopted to examine whether DOW-RMD has better anti-obesity effect than ultra-pure water (UPW)-cultured RMD (UPW-RMD) does. Moreover, the effect of ions composition of DOW and DOW-influenced functional metabolites change of RMD on the differentiation and lipogenesis regulation were investigated using 3T3-L1 pre-adipocytes.

2. Results

2.1. Weight Gain, Food Intake and Feed Efficiency

In the animal test, the rats were randomly assigned to one of the following diets for 8 weeks: standard chow (control group, NOR), high-fat (HF) diet (HF group), HF diet plus 27.81 mg/day 100 g bw UPW-RMD powder (UPW-R-1X group), HF diet plus 27.81 mg/day 100 g bw DOW-RMD powder (DOW-R-1X group), HF diet plus 55.62 mg/day 100 g bw DOW-RMD powder (DOW-R-2X, group), HF diet plus 0.152 mg/day 100 g bw monascin (MS group), HF diet plus 0.162 mg/day 100 g bw ankaflavin (AK group). Following a simultaneous feeding of a HF diet and various test substances, the test animals were sacrificed after 8 weeks and subsequently underwent various analyses. The results are shown in Table 1. The weight gain of the HF group

was significantly higher than that of the NOR group ($p < 0.05$), and the weight of the UPW-R1X group did not present significant differences with that of the HF group, indicating that UPW-RMD cannot reduce weight gain. However, the weight gain of the UPW-R1X group was significantly lower than that of the HF group ($p < 0.05$), and the MS group and AK group demonstrated a significant reduction in weight gain ($p < 0.05$).

The study results are tabulated in Table 1. Food intake of the HF group was lower than that of the NOR group ($p < 0.05$), because calorie consumption in the HF diet was higher (HF group: 4.17 kcal/g and NOR group: 3.34 kcal/g), and the homeostasis mechanism in the animals caused a reduction in food intake. Food intake of the MS and AK groups were significantly lower than that of the HF group ($p < 0.05$). This result corresponded to that of previous studies [6]. Monascin and ankaflavin may cause the loss of appetite and subsequently reduce food intake. However, further research is required to examine the mechanism.

Feed efficiency can be regarded as the ability to convert feed mass into increased body mass. According to Table 1, the feed efficiency of the HF group was significantly increased ($p < 0.05$). No significant difference was identified between the feed efficiency of the UPW-R1X group and the HF group ($p > 0.05$). The feed efficiency of the DOW-R1X group substantially decreased because this group was fed with DOW-RMD. Furthermore, the reduction in the feed efficiency of the DOW-R2X group was further enhanced. The feed efficiency of the MS and AK groups also declined significantly ($p < 0.05$).

In summary, the weight gain and feed efficiency of DOW-RMD declined significantly, possibly because DOW-RMD has higher levels of monascin and ankaflavin than UPW-RMD does.

2.2. Fat Pads Weight

The effects of DOW-RMD on the fat pads weight of rats fed with the HF diet are shown in Table 2. The weights for the total fat pads, perirenal fat pads, and epididymal fat pads of the DOW-R1X group were all lower than those of the UPW-R1X group; however, no significant differences were presented between the two groups ($p > 0.05$). The MS and AK groups demonstrated the ability to significantly reduce the weight of the fat pads, suggesting that DOW can further enhance the effect of reducing total fat pad weight by increasing monascin and ankaflavin levels.

Table 1. Effect of ultra-pure water-cultured-red mold dioscorea (UPW-RMD) and deep ocean water (DOW)-RMD on body weight, food intake and feed efficiency in male Sprague Dawley (SD) rats.

Groups	Initial Body Weight (g)	Final Body Weight (g)	Weight Gain (g)	Calorie Intake (kcal/8 weeks)	Food Intake (g)	Feed Efficiency (%)
NOR	463.0 ± 33.9 b	579.0 ± 37.6 bc	116.0 ± 20.9 b	5833.3 ± 125.9 d	1746.5 ± 37.7 d	6.8 ± 1.2 a
HF	430.1 ± 37.4 ab	601.4 ± 42.0 c	171.3 ± 18.0 de	5962.7 ± 203.1 bc	1429.9 ± 48.7 bc	12.0 ± 1.4 de
UPW-R-1X	428.5 ± 28.1 ab	605.4 ± 30.2 c	176.9 ± 22.3 e	6106.1 ± 143.9 c	1464.3 ± 34.5 c	12.7 ± 1.5 e
DOW-R-1X	436.9 ± 18.1 ab	591.9 ± 23.3 bc	155.0 ± 12.6 cd	5858.9 ± 175.1 b	1405.0 ± 42.0 b	10.8 ± 0.9 cd
DOW-R-2X	417.5 ± 12.0 ab	565.8 ± 27.4 b	148.3 ± 20.7 c	5956.4 ± 176.4 bc	1428.4 ± 42.3 bc	9.8 ± 1.4 bc
MS	410.3 ± 20.8 a	514.5 ± 23.1 a	104.3 ± 5.2 ab	5262.5 ± 264.0 a	1262.0 ± 63.3 a	7.9 ± 0.6 ab
AK	413.8 ± 17.0 a	512.1 ± 26.9 a	97.4 ± 11.4 a	5447.3 ± 233.1 a	1306.3 ± 55.9 a	6.3 ± 1.2 a

NOR, normal diet (3.34 kcal/g); HF, high-fat diet (4.17 kcal/g); UPW-R-1X, UPW-RMD powder (1×, 27.81 mg/day 100 g bw) and high-fat diet; DOW-R-1X, DOW-RMD powder (1×, 27.81 mg/day 100 g bw) and high-fat diet; DOW-R-2X, DOW-RMD powder (2×, 55.62 mg/day 100 g bw) and high-fat diet; and high-fat diet; MS, monascin powder (2×, 0.152 mg/day 100 g bw) and high-fat diet; AK, ankaflavin powder (2×, 0.162 mg/day 100 g bw) and high-fat diet. Data are presented as means ± SD (n = 8). Mean values within each column with different superscripts are significant difference ($p < 0.05$).

Table 2. Effect of UPW-RMD and DOW-RMD on total fat pads, perirenal fat pads and epididymal fat pads weight in male SD rats.

Groups	Total fat pads weight (g)	Perirenal fat pads weight (g)	Epididymal fat pads weight (g)
NOR	16.8 ± 2.6 a	10.4 ± 1.4 ab	8.3 ± 1.5 ab
HF	27.6 ± 3.5 c	17.0 ± 3.9 d	13.0 ± 1.5 d
UPW-R-1X	25.4 ± 7.0 bc	14.9 ± 5.4 cd	10.5 ± 1.9 c
DOW-R-1X	22.8 ± 4.1 b	12.8 ± 2.7 bc	9.8 ± 1.3 bc
DOW-R-2X	18.9 ± 2.2 a	10.7 ± 1.5 ab	8.5 ± 1.2 ab
MS	16.5 ± 2.8 a	9.4 ± 1.6 a	6.9 ± 1.2 a
AK	17.5 ± 2.5 a	9.9 ± 1.4 ab	6.9 ± 1.4 a

NOR, normal diet (3.34 kcal/g); HF, high-fat diet (4.17 kcal/g); UPW-R-1X, UPW-RMD powder (1×, 27.81 mg/day 100 g bw) and high-fat diet; DOW-R-1X, DOW-RMD powder (1×, 27.81 mg/day 100 g bw) and high-fat diet; DOW-R-2X, DOW-RMD powder (2×, 55.62 mg/day 100 g bw) and high-fat diet; and high-fat diet; MS, monascin powder (2×, 0.152 mg/day 100 g bw) and high-fat diet; AK, ankaflavin powder (2×, 0.162 mg/day 100 g bw) and high-fat diet. Data are presented as means ± SD (n = 8). Mean values within each column with different superscripts are significant difference ($p < 0.05$).

2.3. Cross-Sectional Area and Cell Number of Adipocytes

As shown in Table 3, compared to the UPW-R1X group, the cross-sectional area of the perirenal and epididymal adipocytes of the DOW-R1X group decreased significantly ($p < 0.05$), meaning that DOW-RMD was able to significantly reduce a larger cross-sectional area of adipocytes than the UPW-RMD. Moreover, DOW-RMD significantly reduced a higher number of adipocytes than the UPW-RMD did. In addition, DOW-RMD contains the effective compounds monascin and ankaflavin; therefore, because DOW-RMD comprises higher levels of monascin and ankaflavin, this RMD was able to inhibit the lipogenesis of adipocytes, thereby decreasing the cross-sectional area of adipocytes.

2.4. Lipase Activity and HR-LPL (Heparin-Releasable Lipoprotein Lipase) Activity of Fat Pads

TG hydrolysis of mature adipocytes produces glycerol and free fatty acids, which are then released into extracellular or intracellular spaces to undergo oxidation for energy production or to be employed as raw materials for TG synthesis. Glycerol kinase in adipocytes is present in extremely low quantities; thus, glycerol cannot be reused. Consequently, the glycerol produced from lipolysis is released into extracellular space [5]. The results in Table 4 showed that because the HF group was fed with a relatively high quantity of HF diet, the large amount of adipocytes resulted in the feedback inhibition of adipogenesis and consequently increased lipase activity. The UPW-R1X group has higher lipase activity than HF group, but this activity is higher in the DOW-R1X group. Monascin and ankaflavin are also capable of enhancing lipase activity. Therefore, using DOW as the culture medium increases the of monascin and ankaflavin levels in RMD, thereby improving the ability of RMD to increase lipase activity.

Table 3. Effect of UPW-RMD and DOW-RMD on cell cross-sectional area and cell number of adipocyte in male SD rats.

Groups	Perirenal		Epididymal	
	Cell cross-sectional area (μm^2)	Cell number ($\times 10^4$)	Cell cross-sectional area (μm^2)	Cell number ($\times 10^4$)
NOR	16,434 ± 2033 b	7.52 ± 0.88 a	14,555 ± 2766 a	7.40 ± 0.95 a
HF	23,453 ± 3397 c	14.85 ± 2.63 d	22,400 ± 3097 b	13.07 ± 1.33 c
UPW-R-1X	19,283 ± 3455 b	12.87±1.57 cd	19,465 ± 2122 b	10.45± 0.89 b
DOW-R-1X	16,023 ± 2745 a	11.45±0.98 c	15,390 ±1983 a	8.44± 1.45 ab
DOW-R-2X	14,005 ± 2409 a	10.44±1.08 b	14,186 ± 2309 a	7.64± 1.04 a
MS	15,093 ± 3011 a	9.50 ± 1.57 ab	15,123 ± 2793 a	7.28 ± 1.37 a
AK	14,302 ± 2320 a	9.90 ± 1.56 ab	14,907 ± 2123 a	7.44± 1.58 a

NOR, normal diet (3.34 kcal/g); HF, high-fat diet (4.17 kcal/g); UPW-R-1X, UPW-RMD powder (1×, 27.81 mg/day 100 g bw) and high-fat diet; DOW-R-1X, DOW-RMD powder (1×, 27.81 mg/day 100 g bw) and high-fat diet; DOW-R-2X, DOW-RMD powder (2×, 55.62 mg/day 100 g bw) and high-fat diet; and high-fat diet; MS, monascin powder (2×, 0.152 mg/day 100 g bw) and high-fat diet; AK, ankaflavin powder (2×, 0.162 mg/day 100 g bw) and high-fat diet. Data are presented as means ± SD (n = 8). Mean values within each column with different superscripts are significant difference ($p < 0.05$).

LPL hydrolyzes the TG in the blood lipoprotein, and the products of hydrolysis are then absorbed by surrounding tissues. Therefore, LPL is crucial to adipocytes in that this enzyme facilitates lipid droplet accumulation [5]. According to Table 4, feeding the test animals with DOW-RMD but not UPW-RMD significantly decreased the HR-LPL activity, as compared with HF group. In addition, monascin and ankaflavin are capable of inhibiting HR-LPL activity. Thus, because DOW-RMD may contain comparatively high levels of monascin and ankaflavin, the ability of this RMD to inhibit the HR-LPL activity was significantly enhanced.

Table 4. Effect of UPW-RMD and DOW-RMD on lipase activity and Heparin-Releasable Lipoprotein Lipase (HR-LPL) activity of fat pads in male SD rats.

Groups	Lipase activity (U/g fat pad)	HR-LPL activity (U/g fat pad)
NOR	100.0 ± 11.7 a	100.0 ± 25.8 a
HF	140.9 ± 15.1 b	194.6 ± 27.1 c
UPW-R-1X	157.7 ± 13.4 bc	182.8 ± 40.3 bc
DOW-R-1X	165.5 ± 9.4 c	148.0 ± 43.9 ab
DOW-R-2X	168.0 ± 11.2 c	136.7 ± 54.3 ab
MS	169.8 ± 12.1 c	128.1 ± 60.2 ab
AK	165.8 ± 15.0 c	141.2 ± 39.4 ab

NOR, normal diet (3.34 kcal/g); HF, high-fat diet (4.17 kcal/g); UPW-R-1X, UPW-RMD powder (1×, 27.81 mg/day 100 g bw) and high-fat diet; DOW-R-1X, DOW-RMD powder (1×, 27.81 mg/day 100 g bw) and high-fat diet; DOW-R-2X, DOW-RMD powder (2×, 55.62 mg/day 100 g bw) and high-fat diet; and high-fat diet; MS, monascin powder (2×, 0.152 mg/day 100 g bw) and high-fat diet; AK, ankaflavin powder (2×, 0.162 mg/day 100 g bw) and high-fat diet. Data are presented as means ± SD (n = 8). Mean values within each column with different superscripts are significant difference ($p < 0.05$).

2.5. Blood Lipid

Obesity frequently causes an increase in blood lipid concentration, which increases the risk of cardiovascular disease. Thus, the TC, TG, HDL-C, and LDL-C concentrations are key factors that control metabolic syndrome. The results are presented in Table 5. Because high fat diet does not contain cholesterol, the TC level of the HF group did not increase significantly. Therefore, the TC levels of each group did not present significant differences ($p > 0.05$). The TG level of the HF group increased substantially because this group was provided a HF diet ($p < 0.05$). Previous studies have shown that RMD has the ability to reduce blood lipid, and monascin and ankaflavin were proven as the effective compounds. The results of this study indicated that the TG levels of the DOW-R1X and UPW-R1X groups were significantly lower than that of the HF group ($p < 0.05$). However, the TG level of the DOW-R1X group was significantly lower than that of the UPW-R1X group ($p < 0.05$), and monascin and ankaflavin were able to considerably reduce the TG level ($p < 0.05$). Regarding the HDL-C and LDL-C concentrations, the results indicated that both DOW-RMD and UPW-RMD reduced the LDL-C concentration but not the HDL-C concentration, which consequently achieves the effect of preventing cardiovascular disease.

2.6. Ketone Body and Creatine Kinase Activity

HF diet intake may increase the supply of fatty acids. Free fatty acids are the main ingredient of ketone body (D-3-hydroxybutyrate) synthesis in the liver. Excessive ketone bodies are excreted along with sodium (Na) salt, causing loss of body fluids (*i.e.*, dehydration). Subsequently, loss of excessive Na salt results in a pH imbalance and blood acidification, which ultimately leads to complications in the physiological functions of the body. Creatine kinase is an enzyme that catalyzes the conversion of creatine phosphate into creatine to produce energy for muscles. Thus, a significant increase in the level of creatine kinase represents the occurrence of muscle disease [15]. The effects of test substances on the concentration of ketone bodies and creatine kinase activity are shown in Table 6. Each substance was able to substantially reduce the concentration of D-3-hydroxybutyrate. The results of this study indicated that both DOW-RMD and UPW-RMD reduce the D-3-hydroxybutyrate concentration in the blood because these RMD reduce the levels of TG consisting of glycerol and fatty acid. Therefore, the D-3-hydroxybutyrate may be decreased by the decrease of free fatty acid levels. Moreover, monascin and ankaflavin are effective compounds that reduce lipase activity. The creatine kinase activity in the serum was not affected, suggesting that all test substances did not induce muscle damage.

Table 5. Effect of UPW-RMD and DOW-RMD on serum lipidic parameters in male SD rat.

Groups	TC (mg/dL)	TG (mg/dL)	HDL-C (mg/dL)	LDL-C (mg/dL)
NOR	63.1 ± 9.3 a	62.6 ± 10.3 ab	28.3 ± 1.9 bc	24.2 ± 6.2 ab
HF	65.1 ± 8.6 a	94.5 ± 17.5 c	22.6 ± 2.4 a	31.5 ± 7.9 b
UPW-R-1X	63.5 ± 6.9 a	69.8 ± 8.4 b	27.3 ± 3.6 bc	27.2 ± 7.3 ab
DOW-R-1X	64.6 ± 7.9 a	52.8 ± 8.5 a	28.8 ± 1.6 c	25.2 ± 6.6 ab
DOW-R-2X	62.9 ± 2.3 a	60.5 ± 20.1 ab	26.3 ± 2.0 bc	22.0 ± 6.6 a
MS	67.0 ± 16.1 a	67.1 ± 14.5 ab	22.5 ± 3.5 a	24.5 ± 13.2 ab
AK	60.2 ± 6.8 a	60.4 ± 4.6 ab	22.2 ± 1.1 a	18.6 ± 5.4 a

NOR, normal diet (3.34 kcal/g); HF, high-fat diet (4.17 kcal/g); UPW-R-1X, UPW-RMD powder (1×, 27.81 mg/day 100 g bw) and high-fat diet; DOW-R-1X, DOW-RMD powder (1×, 27.81 mg/day 100 g bw) and high-fat diet; DOW-R-2X, DOW-RMD powder (2×, 55.62 mg/day 100 g bw) and high-fat diet; and high-fat diet; MS, monascin powder (2×, 0.152 mg/day 100 g bw) and high-fat diet; AK, ankaflavin powder (2×, 0.162 mg/day 100 g bw) and high-fat diet. Data are presented as means ± SD (n = 8). Mean values within each column with different superscripts are significant difference ($p < 0.05$).

Table 6. Effect of UPW-RMD and DOW-RMD on serum D-3-hydroxybutyrate, and creatine kinase in male SD rat.

Groups	D-3-hydroxybutyrate (mmole/L)	Creatine kinase (U/L)
NOR	1.86 ± 0.43 b	111.8 ± 55.7 ab
HF	2.06 ± 0.30 b	108.8 ± 67.6 ab
UPW-R-1X	0.46 ± 0.23 a	76.9 ± 19.4 ab
DOW-R-1X	0.31 ± 0.07 a	75.3 ± 27.4 ab
DOW-R-2X	0.57 ± 0.18 a	69.9 ± 16.4 a
MS	0.14 ± 0.04 a	115.7 ± 32.9 b
AK	0.27 ± 0.09 a	107.3 ± 15.8 b

NOR, normal diet (3.34 kcal/g); HF, high-fat diet (4.17 kcal/g); UPW-R-1X, UPW-RMD powder (1×, 27.81 mg/day 100 g bw) and high-fat diet; DOW-R-1X, DOW-RMD powder (1×, 27.81 mg/day 100 g bw) and high-fat diet; DOW-R-2X, DOW-RMD powder (2×, 55.62 mg/day 100 g bw) and high-fat diet; and high-fat diet; MS, monascin powder (2×, 0.152 mg/day 100 g bw) and high-fat diet; AK, ankaflavin powder (2×, 0.162 mg/day 100 g bw) and high-fat diet. Data are presented as means ± SD (n = 8). Mean values within each column with different superscripts are significant difference ($p < 0.05$).

2.7. Liver and Kidney Function

To determine whether the adoption of test substances to reduce body fat and anti-obesity effect simultaneously causes side effects or complications, we tested the effects of the substances on liver and kidney tissues. The results of relevant index analyses showed that each substance did not significantly influence the liver and kidney (Table 7).

Table 7. Effect of UPW-RMD and DOW-RMD on hepatosomatic and renal index in male SD rat.

Groups	AST (U/L)	ALT (U/L)	Creatinine (mg/dL)	Uric acid (mg/dL)
NOR	113.4 ± 11.5 b	53.8 ± 3.8 ab	0.50 ± 0.00 c	3.1 ± 0.8 a
HF	111.3 ± 14.2 b	52.1 ± 3.9 ab	0.50 ± 0.00 c	4.0 ± 0.8 bc
UPW-R-1X	93.0 ± 10.5 ab	42.8 ± 5.7 b	0.44 ± 0.07 ab	3.6 ± 0.5 ab
DOW-R-1X	85.1 ± 11.0 a	38.6 ± 4.5 a	0.39 ± 0.04 a	3.0 ± 0.5 a
DOW-R-2X	88.8 ± 7.4 a	45.5 ± 2.6 ab	0.43 ± 0.07 ab	3.2 ± 0.3 a
MS	95.9 ± 42.1 ab	63.1 ± 53.1 b	0.44 ± 0.04 ab	4.4 ± 1.0 c
AK	89.3 ± 21.8 ab	51.9 ± 26.0 ab	0.45 ± 0.04 bc	4.5 ± 0.4 c

NOR, normal diet (3.34 kcal/g); HF, high-fat diet (4.17 kcal/g); UPW-R-1X, UPW-RMD powder (1×, 27.81 mg/day 100 g bw) and high-fat diet; DOW-R-1X, DOW-RMD powder (1×, 27.81 mg/day 100 g bw) and high-fat diet; DOW-R-2X, DOW-RMD powder (2×, 55.62 mg/day 100 g bw) and high-fat diet; and high-fat diet; MS, monascin powder (2×, 0.152 mg/day 100 g bw) and high-fat diet; AK, ankaflavin powder (2×, 0.162 mg/day 100 g bw) and high-fat diet. Data are presented as means ± SD (n = 8). Mean values within each column with different superscripts are significant difference ($p < 0.05$).

2.8. Electrolyte Balance

The composition and concentration of electrolytes in the body fluids must be maintained at a certain level to stabilize body pH, osmotic pressure, and water balance, as well as to sustain normal cell growth. Acting as an indicator for electrolyte balance analysis, Na^+ and K^+ are cations that are found in the highest quantity inside and outside of cells, respectively. As shown in Table 8, each test substance does not affect the electrolyte balance.

Table 8. Effect of UPW-RMD and DOW-RMD on electrolyte balance in male SD rat.

Groups	Na (mEq/L)	K (mEq/L)
NOR	146.8 ± 1.5 a	6.7 ± 0.5 bc
HF	149.4 ± 0.4 b	6.7 ± 0.6 bc
UPW-R-1X	148.8 ± 1.3 b	7.0 ± 0.7 bc
DOW-R-1X	149.5 ± 1.3 b	6.5 ± 0.3 ab
DOW-R-2X	149.7 ± 0.8 b	6.4 ± 0.6 ab
MS	148.9 ± 1.1 b	7.2 ± 0.6 c
AK	149.0 ± 1.1 b	7.2 ± 0.3 c

NOR, normal diet (3.34 kcal/g); HF, high-fat diet (4.17 kcal/g); UPW-R-1X, UPW-RMD powder (1×, 27.81 mg/day 100 g bw) and high-fat diet; DOW-R-1X, DOW-RMD powder (1×, 27.81 mg/day 100 g bw) and high-fat diet; DOW-R-2X, DOW-RMD powder (2×, 55.62 mg/day 100 g bw) and high-fat diet; and high-fat diet; MS, monascin powder (2×, 0.152 mg/day 100 g bw) and high-fat diet; AK, ankaflavin powder (2×, 0.162 mg/day 100 g bw) and high-fat diet. Data are presented as means ± SD (n = 8). Mean values within each column with different superscripts are significant difference ($p < 0.05$).

2.9. Monascin and Ankaflavin Production

To determine whether the main ions in the DOW enhance monascin and ankaflavin production and inhibit citrinin formation, this study prepared the synthetic water (SW) according to the

composition and concentration of main ions in DOW, which was then used to culture *Dioscorea batatas* to produce the SW-cultured RMD (SW-RMD). The analytical results for the monascin, ankaflavin, and citrinin levels showed that DOW-RMD and SW-RMD have significantly higher levels of monascin than UPW-RMD, and SW-RMD has a considerably lower level of ankaflavin than DOW-RMD (Table 9). Furthermore, SW significantly reduced the citrinin level in RMD. Based on the above findings, additional ions that possess the ability to boost monascin and ankaflavin productions may be present in DOW. Moreover, other ions are possibly present to antagonize the reduction of citrinin formation, consequently allowing DOW to reduce the level of citrinin (*i.e.*, compared to SW).

Table 9. Effect of UPW, DOW, and synthetic water (SW) on the production of monascin, ankaflavin, citrinin in RMD.

Groups	Monascin concentration (mg/kg)	Ankaflavin concentration (mg/kg)	Citrinin concentration (mg/kg)
UPW-RMD	2146 ± 35 a	2221 ± 4 a	2.864 ± 0.085 b
DOW-RMD	2727 ± 219 b	2912 ± 263 b	2.725 ± 0.090 b
SW-RMD	2614 ± 175 b	2414 ± 176 c	2.312 ± 0.092 a

UPW-RMD, the red mold dioscorea cultured by ultra-pure water; DOW-RMD, the red mold dioscorea cultured by deep ocean water; SW-RMD, the red mold dioscorea cultured by synthetic water; Data are presented as means ± SD (n = 3). Mean values within each column with different superscripts are significant difference ($p < 0.05$).

2.10. Differentiation of Pre-Adipocytes

Based on the above-mentioned results, DOW-RMD possessed a superior ability of reducing weight and body fat. In this study, to understand how DOW-RMD regulates body fats metabolism, the effects of DOW-RE on adipocyte differentiation and lipogenesis were investigated using *in vitro* cell tests. In addition, ions in DOW may possibly influence adipocyte regulation; thus, in a cell model, we simulated an SW containing the ions in DOW. The SW contained Mg^{2+}, Ca^{2+}, Na^{+}, K^{+}, Fe^{2+}, and Zn^{2+}, which are the main ions of DOW, and the concentrations of these ions was identical to those in DOW. The objective was to investigate how the main ions of DOW alter the ability of RMD for adipogenesis regulation, and to elucidate whether these ions are crucial in DOW.

Following the ninth day of induced differentiation, 3T3-L1 pre-adipocyte underwent oil-red O staining, in which the dye combined with neutral oil to form red oil droplets that facilitated the observation of cell differentiation. According to the experimental results (Figure 1), monascin and ankaflavin effectively inhibited the accumulation of lipid droplets in cells. Moreover, 100 μg/mL and 200 μg/mL of UPW-RE, DOW-RE, and SW-RE extracts effectively and significantly inhibited the accumulation of lipid droplets ($p < 0.05$). Particularly, at 100 μg/mL of DOW-RE, the amount of lipid droplets accumulated was significantly lower than that at 100 μg/mL of UPW-RE and 100 μg/mL of SW-RE, respectively. The results suggested that the use of UPW, DOW, and SW to culture RMD effectively inhibited differentiation of pre-adipocytes, and DOW-RE produced better results possibly because DOW has higher levels of monascin and ankaflavin.

Subsequently, we examined whether DOW possesses inhibitory effects (Figure 1). Adding DOW and SW effectively inhibited the accumulation of adipocyte lipid droplets. In addition, DOW demonstrated better inhibitory effect than SW, indicating that DOW may be the primary cause of enabling DOW-RE to inhibit lipid droplet accumulation. Furthermore, the main ions selected from SW may be extremely crucial in facilitating the reduction of lipid droplet formation.

2.11. Transcription Factor Expression during Differentiation

Differentiation agents were added to pre-adipocytes to induce differentiation. Subsequently, key transcription factors were activated to enhance adipocyte maturation, which increased protein expression and consequently stimulates lipid droplet accumulation. On the second day of differentiation, we examined whether the test substances were able to effectively inhibit the protein expression of transcription factor C/EBPβ. Furthermore, on the sixth day of differentiation, changes in the protein expression of transcription factors PPARγ and C/EBPα were investigated. Because C/EBPβ is activated at the initial stage of differentiation, it is expressed briefly, thereby activating the expression of PPARγ and C/EBPα. Thus, protein expressions of the three key transcription factors were analyzed to explore the effects of DOW and the products of RMD on differentiation in this study.

As shown in Figure 2a,c, using monascin and ankaflavin treatment, the C/EBPβ protein expression for the MS and AK groups was significantly reduced ($p < 0.05$). However, significant lowering effects in the UPW-RE, DOW-RE, and SW-RE treatments were not observed. The experimental results showed that each extract solution was unable to significantly reduce C/EBPβ expression, possibly because the monascin level was insufficient to trigger inhibition. Subsequently, we determined whether DOW can effectively enhance effect of RMD on inhibiting PPARγ expression. The results for the PPARγ protein expression on the sixth day of differentiation are shown in Figure 2a,c. Monascin and ankaflavin treatments significantly lowered the PPARγ protein expression ($p < 0.05$). PPARγ protein expression were also reduced to 86.95%, 72.14%, and 35.99% by the treatments of UPW-RE, DOW-RE, and SW-RE, respectively ($p < 0.05$). Furthermore, the presence of monascin and ankaflavin significantly reduced the expression of C/EBPα protein to 57.34% and 59.22%, respectively ($p < 0.05$). Although the UPW-RE extract did not influence C/EBPα expression, the DOW-RE and SW-RE treatments decreased the expression to 74.01% and 48.80%, respectively ($p < 0.05$).

Overall, DOW-RE possessed better ability than UPW-RE to reduce the expression of the transcription factors. Therefore, this study next determined whether DOW and SW affected expression of the transcription factors. The results showed that DOW treatment did not significantly influence the expression of C/EBPβ, PPARγ, and C/EBPα; however, SW treatment was able to inhibit PPARγ, and C/EBPα expressions (Figure 2b,d). Summarizing the above results showed that DOW-RE effectively inhibited the expressions of the transcription factors compared to UPW-RE. Because SW-RE (in contrast to DOW-RE and UPW-RE) was able to substantially inhibit the expressions of the transcription factors, we speculated that besides monascin and ankaflavin, the main ions in DOW enabled DOW-RMD to possess better ability of inhibiting differentiation.

Figure 1. Effects of DOW-RMD ethanol extracts (DOW-RE), UPW-RMD ethanol extracts (UPW-RE), SW-RMD ethanol extracts (SW-RE), monascin (MS), ankaflavin (AK) on 3T3-L1 preadipocyte differentiation. Preadipocytes were differentiated according to the method described in 'Materials and methods.' During differentiation the cells were treated with various samples. On day 8, the cells were fixed and stained with oil-red O.

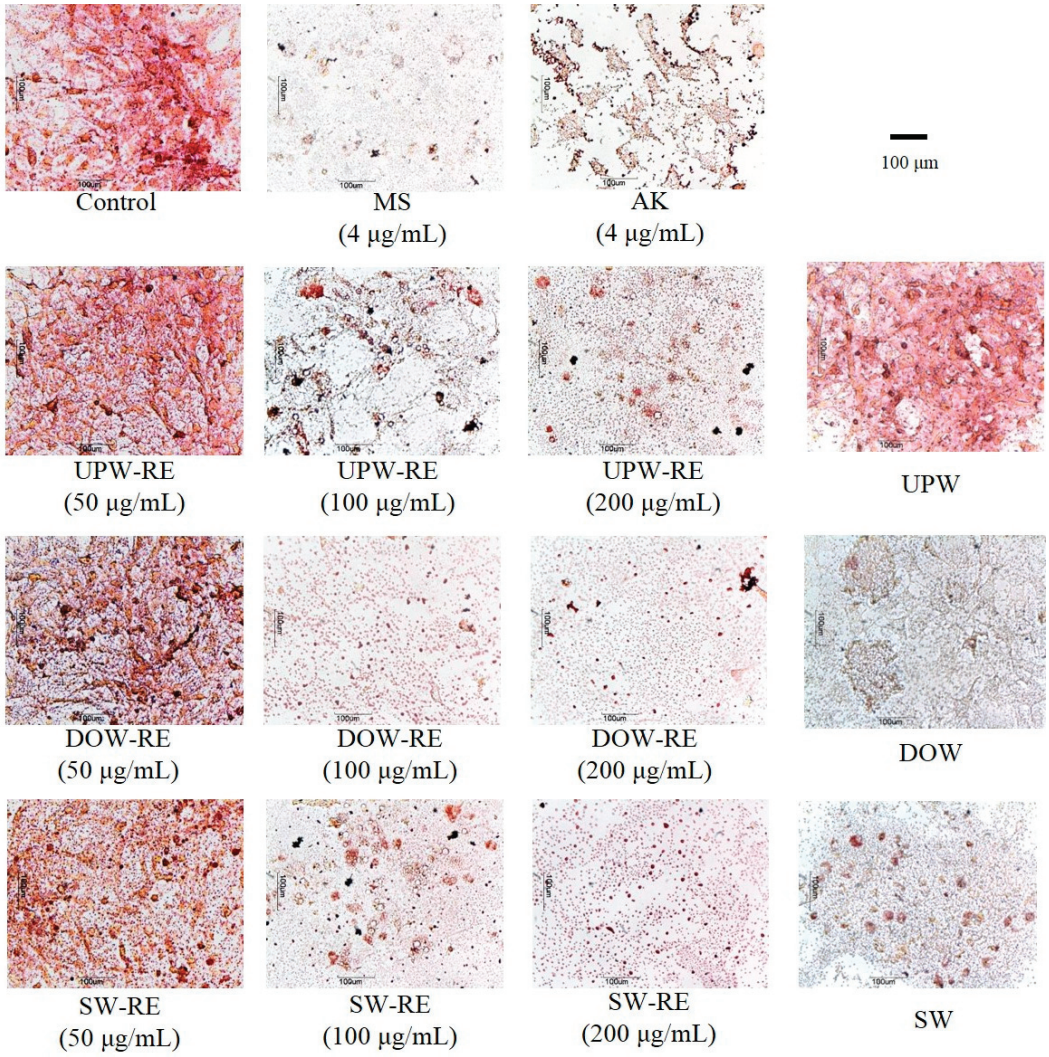

Figure 2. Effect of various substances on C/EBPβ, PPARγ, and C/EBPα protein expressions in 3T3-L1 preadipocyte differentiation. (**a**) Target protein expressions were visualized using immunoblotting in the treatment of DOW-RMD ethanol extracts (DOW-RE), UPW-RMD ethanol extracts (UPW-RE), SW-RMD ethanol extracts (SW-RE), monascin (MS), and ankaflavin (AK); (**b**) Target protein expressions were visualized using immunoblotting in the treatment of UPW, DOW, and SW. (**c**) Quantification of protein expressions in the treatment of DOW-RE, UPW-RE, SW-RE, MS, and AK. (**d**) Quantification of protein expressions in the treatment of UPW, DOW, and SW. Mean values with different superscripts are significant difference ($p < 0.05$).

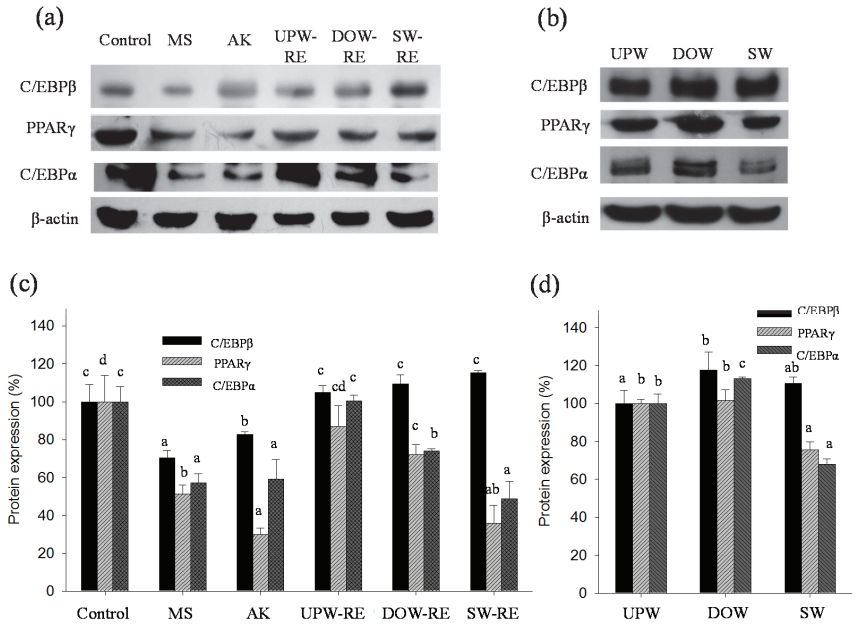

2.12. Lipolysis Effect and HR-LPL Activity in Lipogenesis

After 12 days of differentiation, the majority of 3T3-L1 pre-adipocytes have transformed to mature adipocytes. The lipolysis effect was investigated. As shown in Figure 3a, after monascin and ankaflavin treatments, the lipolysis effect were increased to 110% and 120%, respectively, showing a significant difference ($p < 0.05$); however, the extent of the increase was unsubstantial. The RMDs cultured with three types of water presented a weak lipolysis effect. Furthermore, the lipolysis effect in DOW-RE and SW-RE treatments were increased to 118% and 112%, respectively, but the extent of the increase was not significant ($p > 0.05$). Therefore, both DOW-RE and SW-RE demonstrated a weak lipolysis effect.

Figure 3. Effect of DOW-RMD ethanol extracts (DOW-RE), UPW-RMD ethanol extracts (UPW-RE), SW-RMD ethanol extracts (SW-RE), monascin (MS), ankaflavin (AK), UPW, DOW, SW on lipogenesis in mature 3T3-L1 adipocyte. (**a**) lipase activity (**b**) HR-LPL activity. Mean values with different superscripts are significant difference ($p < 0.05$).

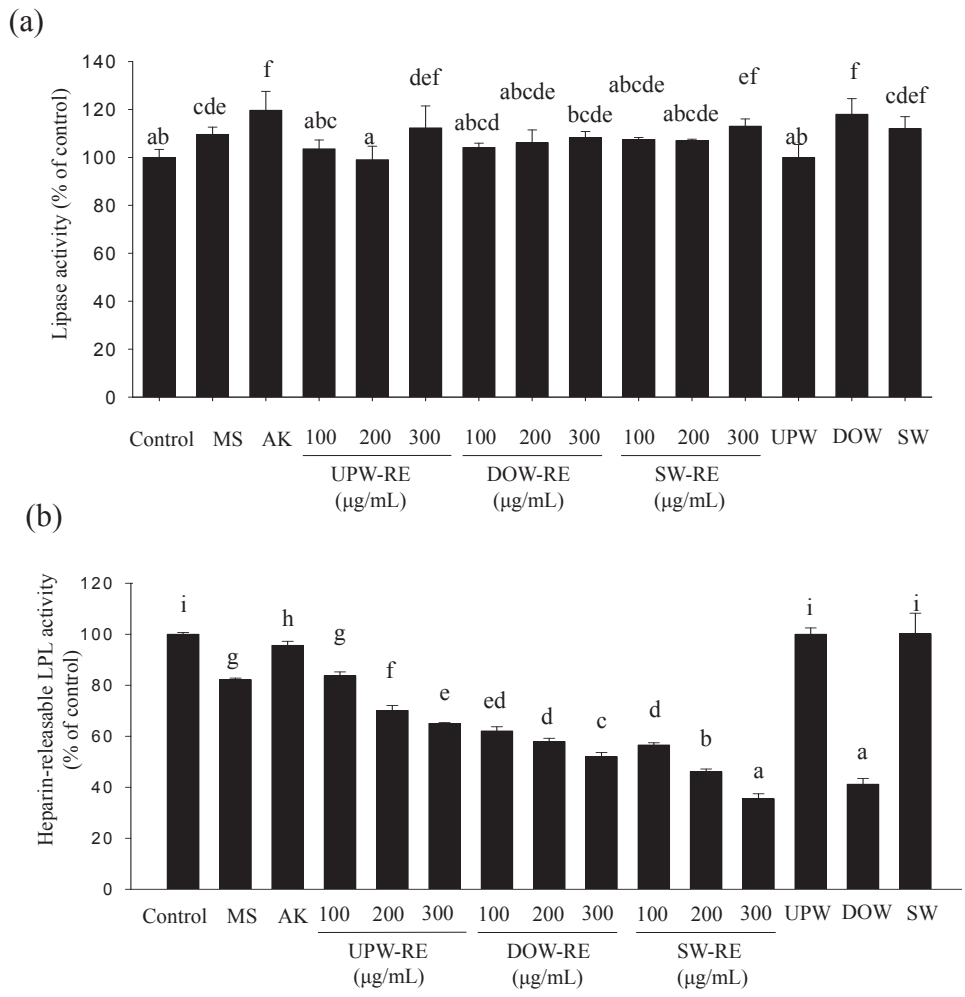

HR-LPL is a crucial enzyme that influences the lipogenesis of mature adipocytes and stimulates the accumulation of fatty acid to form lipid droplets. The effects of the test substances on the activity of HR-LPL are presented in Figure 3b. Monascin treatment was shown to significantly reduce the LPL activity to 82% ($p < 0.05$). Moreover, treatments with 100 μg/mL of UPW-RE, DOW-RE, and SW-RE reduced the HR-LPL activity to 84%, 62%, and 57%, respectively ($p < 0.05$), and significant differences among the three REs were observed ($p < 0.05$). Therefore, DOW-RE and SW-RE all presented better ability in inhibiting HR-LPL activity; particularly, SW-RE has better inhibition ability than DOW-RE. Furthermore, DOW significantly reduced

HR-LPL activity to 41%, whereas SW has no effect on the activity. Based on the results, DOW possessed an inhibitory effect, and DOW-RE demonstrated a better inhibitory effect on the LPL activity. These results indicated that DOW may inhibit lipid droplet formation by employing its functional effects and enhancing monascin production in RMD. However, the main ions in SW do not possess the ability to inhibit LPL activity.

3. Discussion

DOW, enriched with minerals and trace elements, has been applied in the manufacturing of various fermented food products, such as sake, soya sauce, and miso. Moreover, DOW is composed many major elements, Mg^{2+}, Ca^{2+}, K^{+}, Zn^{2+}, Fe^{2+}, *etc*., that enhances the secondary metabolite production of *Monascus purpureus* [14]. In this study, DOW and UPW were used to culture RMD. The analytical results indicated that DOW-cultured RMD contains a relatively high level of monascin and comparatively low amount of citrinin. Monascin yield increased by 22%, and citrinin yield was reduced by 33%, suggesting that certain minerals or trace elements in DOW may enhance *Monascus* to produce higher amounts of monascin and inhibit the production of citrinin [14]. However, these salts such as NaCl, $MgCl_2$, KCl, and *etc.* in DOW may also induce stress due to decreased water availability (water activity). The previous studies indicated that the growth and secondary metabolites formation of fungus were stimulated by the stress [16,17]. Furthermore, the previous studies indicated that salts have a major impact on the nature and extent of the biosphere, because solutes radically influence water activity and exert other activities that also affect biological systems (e.g., ionic, kosmotropic, chaotropic and those that affect cell turgor), and as a consequence can be major stressors of cellular systems. $MgCl_2$ known as a chaotropic agent disrupts the structure of macromolecules such as proteins and nucleic acids. The extreme chaotropicity of $MgCl_2$ at high concentrations not only denatures macromolecules, but also preserves the more stable ones: such indicator molecules, hitherto regarded as evidence of life, may thus be misleading signatures in chaotropic environments [18–20]. Compared to DOW, UPW has a high water activity that is supra-optimal and stressful for growth and metabolism of fungus [16,21]. Therefore, DOW including salts may act a stressor with lower water activity that may cause up-regulation of growth, secondary metabolites production, and pharmaceutical activities [21–23].

Regarding the reduction of body-fats, compared to UPW-RMD, DOW-RMD possessed better ability of lowering weight gain, food intake, feed efficiency, body-fat pad, cross-sectional area of adipocytes, serum TG level, and liver TC level. Previous research has confirmed that *Monascus* was able to reduce body-fats; however, the ability of RMD to reduce body-fat was not significant [24]. In this study, DOW-RMD, but not UPW-RMD, demonstrated the ability to significantly reduce weight gain, body-fat pad, and the cross-sectional area of adipocytes. This result suggested that DOW use in RMD fermentation can enhance the anti-obesity effect of RMD.

Numerous factors explain the reason that DOW contributed higher anti-obesity to DOW-RMD, one of which is that the water absorbed during the fermentation is retained in RMD, which therefore improved the anti-obesity function in DOW-RMD. According to a previous study, drinking DOW reduces the PPAR-γ expression in adipocytes [12]. Furthermore, in an *in vitro* cell test, Hwang *et al.* (2009) [25] investigated the mechanism of how DOW influences 3T3-L1

pre-adipocytes. The results verified that DOW effectively inhibited the proliferation of pre-adipocytes and significantly reduced the accumulation of lipid droplets. Moreover, DOW was able to reduce the regulation of adipocyte transcription factors; consequently, differentiation of pre-adipocytes was inhibited.

The other factor may be attributed to the DOW-stimulated functional metabolites production in the RMD. In the previous study, monascin and ankaflavin were observed to inhibit differentiation of 3T3-L1 pre-adipocytes. Specifically, the expressions of C/EBPα, C/EBPβ, C/EBPδ, and PPARγ proteins were inhibited, which also reduced the accumulation of intracellular TG. Moreover, monascin and ankaflavin enhanced the decomposition of intracellular lipid droplets in mature adipocytes lipogenesis to release glycerol and reduce extracellular LPL activity, which subsequently reduces intracellular TG synthesis [5]. In addition to inhibiting mature adipocyte lipogenesis by lowering HR-LPL activity and increasing the lipolysis effect, monascin and ankaflavin were also observed to inhibit pre-adipocyte differentiation in animals by inhibiting the expression of C/EBPα, C/EBPβ, and PPARγ proteins [5].

In the *in vivo* animal test, the results showed that DOW-RMD demonstrated better anti-obesity ability. The ions in DOW may influence the regulation of adipocytes. Therefore, we further simulated SW that contains the major ions in a DOW. In metabolite production, DOW-RMD and SW-RMD are RMDs cultured in DOW and SW. The two products contained similar amount of monascin, but the ankaflavin level in SW-RMD was less than that in DOW-RMD. Thus, the ions in SW are crucial to enhancing monascin production; however, other effective ions in DOW may be present to facilitate an increase in ankaflavin. The levels of monascin and ankaflavin may influence the anti-obesity ability such as differentiation and lipogenesis. The *in vitro* results showed that the inhibitory effect of DOW-RE and SW-RE on PPARγ and C/EBPα protein expressions was substantially better than that of UPW-RE. The inhibitory effect of monascin and ankaflavin on PPARγ and C/EBPα expressions was also evident. Therefore, DOW-RE and SW-RE, compared to UPW-RE, were able to significantly inhibit differentiation possibly because of the relatively high levels of monascin and ankaflavin. Although previous studies have shown that DOW inhibited the expression of C/EBPβ, PPARγ, and C/EBPα [25], the inhibitory effect of DOW on transcription factor expressions was not identified in this study. However, the six ions in SW possessed the ability to inhibit PPARγ and C/EBPα expressions, indicating that these ions are effective in inhibiting differentiation. Besides the six ions contained in DOW, additional ions may exist in small quantities. These additional ions may stimulate PPARγ and C/EBPα expressions. Consequently, although SW-RE contains fewer amounts of monascin and ankaflavin than DOW-RE, its ability to inhibit PPARγ and C/EBPα expressions is superior to DOW-RE. This phenomenon suggests that SW-RMD may have absorbed the ions in SW, which subsequently increased the inhibitory effect on PPARγ and C/EBPα expressions.

In the process of forming lipid droplets in mature adipocytes, the results showed that the lipolysis effect of RMD extract improves with increasing concentration to inhibit lipogenesis. The lipolysis effect of UPW-RE, DOW-RE, and SW-RE demonstrated no significant differences. This result was similar to that obtained in animal testing, where no significant differences were observed between the lipolysis effect of DOW-RMD and UPW-RMD. This observation showed that DOW

cannot significantly enhance the lipolysis effect in RMD. This research and previous studies have verified that the lipolysis ability of monascin and ankaflavin [6]. However, increases in monascin and ankaflavin cannot reflect the enhancement of the lipolysis effect in DOW-RMD in this study, possibly because insufficient amounts of monascin and ankaflavin were available to perform lipolysis effect or because monascin and ankaflavin have reached maximum utility that increasing the level does not significantly influence the lipolysis effect. In this study, we identified that significant lipolysis effect was performed by DOW treatment but not DOW-RMD because the amount of DOW absorbed in DOW-RMD may be not more enough to achieve the lipolysis effect.

In this study, as the concentration increased, the RMD extract effectively inhibited LPL activity, thereby inhibiting lipid droplet formation. Compared to the UPW-RE, the DOW-RE was shown to perform a better inhibitory effect on LPL activity. This result corresponded to that of the animal testing, in which DOW-RMD presented a better inhibitory effect on LPL activity. LPL expression is mediated by the activation of PPARγ by cognate ligands, as LPL is a downstream gene of PPARγ. The PPARγ/RXR complex binds to the PPRE present in the promoter region of the LPL gene and increases LPL gene expression [26]. The induction of lipoprotein lipase synthesis by PPARγ is mainly in the mature adipocytes in order to increase local generation of free fatty acids [27,28]. However, monascin is proven to inhibit PPARγ expression and HR-LPL activity in this study and our previous study [6]. Therefore, this could be one of the primary factors of monascin- and ankaflavin-mediated inhibition of lipogenesis. According to the *in vivo* and *in vitro* tests results, more potent LPL activity may be contributed from the higher monascin levels, as well as the absorption of DOW in DOW-RMD. Furthermore, SW-RE but not SW demonstrated an inhibitory effect on LPL activity, suggesting that the LPL activity-lowering effect of SW-RE should be contributed form the increased monascin levels or other compound but not the ions of SW. However, besides the six ions in SW, additional ions in DOW may be the functional ions for the LPL activity-lowering effect.

SW contains Mg^{2+}, Ca^{2+}, Na^{+}, K^{+}, Fe^{2+}, and Zn^{2+}, all of which are the main ions in DOW. In addition, the concentrations of these ions in SW were adjusted to that in DOW. Although SW contains fewer types of ions than DOW (which comprises more than ten types of ions), it still enhanced the rate of monascin and ankaflavin production in RMD. However, the ability of SW to increase the ankaflavin level is less effective than that of DOW. Despite having several similarities with DOW in monascin production, the ability of DOW and SW in the regulation of adipogenesis exhibits numerous differences. SW is able to inhibit PPARγ and C/EBPα expressions and is able to slightly increase lipolysis effect but not inhibit the HR-LPL activity. Conversely, DOW cannot inhibit PPARγ and C/EBPα expressions but is able to enhance the lipolysis effect and inhibit HR-LPL activity. However, both DOW-RMD and SW-RMD are able to inhibit PPARγ and C/EBPα expressions and improve HR-LPL activity because of the different reason as follow: DOW-RMD contains higher monascin and ankaflavin levels as well as DOW accumulation; and SW-RMD contains higher level of monascin and accumulates six types of effective ions.

Regarding the reduction of blood lipids, in comparison to UPW-RMD, DOW-RMD was able to reduce the level of TC and LDL-C in the serum. This result corresponded to that obtained in our previous results [14]. DOW-RMD performed better blood lipid-reduction effect because it

contained higher levels of blood lipid-reducing substances monascin and ankaflavin. Furthermore, DOW comprised minerals and trace elements such as Mg^{2+}, Ca^{2+}, and K^{+}. Numerous studies have indicated that a higher Mg/Ca ratio facilitates the prevention of cardiovascular disease [29]. Cohen *et al.* (2002) showed that an intake of 8.3 g Mg salt per day significantly reduced TC and TG levels in the blood [29]. Shahkhalili *et al.* (2001) [30] identified that supplementing participants with 0.9 mg/day Ca reduced the level of LDL-C in the blood. DOW-RMD was used as the test substance in this study. DOW including Mg^{2+}, Ca^{2+}, Zn^{2+}, Fe^{2+}, K^{+}, and *etc.* was supplemented daily to culture RMD, accumulated gradually in DOW-RMD; thus, the hypolipidemic effect of was enhanced.

4. Experimental Section

4.1. Chemicals

LC grade acetonitrile, chloroform, methanol, and dimethyl sulfoxide (DMSO) were purchased from Merck Co. (Darmstadat, Germany). Tryptone, yeast extract, peptone, malt extract, potato dextrose agar (PDA), and Bacto-agar were purchased from Difco Co. (Detroit, MI, USA). Monoclonal C/EBPα antibody was purchased from GeneTex Co (Irvine, CA, USA). Monoclonal C/EBPβ antibody and polyclonal PPARγ antibody were purchased from Novus Biological (Littleton, CO, USA). Dulbecco's modified Eagle's medium and fetal bovine serum were purchased from Invitrogen Life Technologies (Carlsbad, CA, USA). Dexamethasone, isobutylmethylxanthine, insulin, oil-red O, heparin, *p*-nitrophenyl butyrate were purchased from Sigma Chemical Co. (St Louis, MO, USA). Trypan blue stain was purchased from Gibco BRL Life Technologies Inc. (Gaithersburg, MD, USA).

4.2. The Source of DOW and the Preparation of SW

The DOW purchased from the Taiwan Yes Deep Ocean Water Co. (Hualien, Taiwan) was pumped from a depth of 670 m in the Pacific Ocean near the Eastern Taiwan and processed though the electrodeionization. The concentrations of the trace elements and minerals in DOW including Al, Cu, Zn, As, Ba, Cd, Cr, Pb, Hg, Se, Ag, Ca, Mg, K, Na, Sb, Tl, Be, Fluoride, Nitrate, Sulfate, Chloramines, and Chlorine have been measured and published in our previous study [14]. SW was prepared by mixing the main ions of DOW including 20.65 mg/L Mg, 5.02 mg/L Ca, 7.71 mg/L Na, 0.22 mg/L K, 0.0062 mg/L Fe, and 0.019 mg/L Zn ion with equal concentrations to that in DOW.

4.3. Preparation of UPW-RMD, DOW-RMD, and SW-RMD

Monascus purpureus NTU 568 fermented product has been proven to perform a potent hypolipidemic effect in our previous study [31,32]. The culture strain was maintained on PDA slant at 10 °C and transferred monthly. The *Dioscorea* root (*Dioscorea batatas* Dence) purchased from a local supermarket in Taiwan was used to produce RMD using the method of solid-state culture. UPW, DOW, and SW were used as all of the water used in the production of UPW-RMD,

DOW-RMD, and SW-RMD, respectively. Five hundred grams *Dioscorea* substrates were, respectively, soaked in distilled water for 8 and 1 h. After that, excess water was removed with a sieve. The substrate was autoclaved for 20 min at 121 °C in a "koji-dish" (the koji-dish is made of wood with the dimension of 30 × 20 × 5 cm). After being cooled, the substrate was inoculated with a 5% (v/w) spore suspension (10^7 spores/mL). The inoculated substrate was cultured at 28 °C for 10 days. In addition, during the culturing stage, 100 mL of water is added once every 12 h at a total of three times and the addition of water starts on the fifth day of culture. After fermentation, the crushed and dried product with the mold was used for the experiments [14,33].

4.4. Animal Experiments

Animal experiments protocol is refer to our previous study involved the anti-obesity evaluation of RMR [6]. Male Sprague Dawley (SD) rats at 6–8 weeks of age were purchased from the BioLasco Co. (Taipei, Taiwan). The animals were housed individually and allowed free access to a standard laboratory chow (Ralston Purina, St Louis, MO, USA) and water. Three weeks later, the rats were randomly assigned to one of the following diets for 8 weeks: standard chow (control group, NOR; 4.5% fat, 3.34 kcal/g), high-fat (HF) diet consisting of 26.7% butter powder (Gene Asia Biotech Co., Ltd., Nang-Tou, Taiwan) in standard chow (HF group; 30% fat, 4.17 kcal/g), HF diet plus 27.81 mg/day 100 g bw UPW-RMD powder (UPW-R-1X group), HF diet plus 27.81 mg/day 100 g bw DOW-RMD powder (DOW-R-1X group), HF diet plus 55.62 mg/day 100 g bw DOW-RMD powder (DOW-R-2X, group), HF diet plus 0.152 mg/day mg/day 100 g bw monascin (MS group), HF diet plus 0.162 mg/day 100 g bw ankaflavin (AK group), The recommendation dosage of DOW-RMD or UPW-RMD for anti-obesity effect is suggested as 2 g/day for human in our previous study [24]. The dosage of monascin and ankaflavin in the MS and AK groups were equal to that in the DOW-R-1X group. The doses of the test substances used in this study were calculated according to Boyd's formula for body surface area for adult humans (weight: 65 kg; height: 170 cm). Each sample was orally administrated to the rats by stomach tube in each group [24].

Food consumption and body weight were recorded weekly. At the end of the study, the rats were deprived of food for 16 h before being scarified by CO_2 asphyxiation. Blood samples were collected from the posterior vena cava and centrifuged at 700× *g* for 10 min; the serum was stored at −20 °C until analyzed. Perirenal and epididymal fat pads were removed and weighed. Portions of the adipose tissue were immersed in 10% formaldehyde for histological inspection; other portions were frozen immediately in liquid nitrogen and stored at −80 °C for analysis of lipolysis and HR-LPL activity. Liver was excised and stored at −20 °C for the measurement of lipids. The experiment was reviewed and approved by the Animal Care and Research Ethics Committee of the National Taitung University.

4.5. Biochemical Analyse

The serum total cholesterol (TC), triglyceride (TG), low density lipoprotein cholesterol (LDL-C), high density lipoprotein cholesterol (HDL-C), creatinine, uric acid, Na, K, ketone body

(hydroxybutyrate) concentrations, and aspartate aminotransferase (AST), alanine aminotransferase (ALT), and creatine kinase (CK) activities were measured using the commercial kits (Randox Laboratories Ltd., Antrim, UK). Lipolysis effect and HR-LPL activity assay followed the method of our previous studies [6].

4.6. Adipose Tissue Histology

The adipose tissue samples were fixed in formaldehyde, embedded in paraffin, cut into 5-mm sections and stained with hematoxylin and eosin. Cross-sectional areas of the adipocytes were calculated from the histogram according to Chen and Farese [34]. For the estimation of fat pads cell number, the lipid content of 0.3 g of fat tissue was extracted by using the method of Folch *et al.* [35]. The total cell number in the fat pads was calculated by dividing the lipid content of the fat pad by the mean weight of cell lipids. The lipid weight of the average fat cell was calculated from the mean cell volume, assuming a lipid density of 0.915 (density of triolein).

4.7. Cell Culture

3T3-L1 preadipocytes purchased from the Bioresource Collection and Research Center (Hsinchu, Taiwan) were cultured in Dulbecco's modified Eagle's medium (DMEM) containing 10% fetal bovine serum) at 37 °C in 5% CO_2. To induce differentiation, 2-day postconfluent 3T3-L1 preadipocytes (day 0) were stimulated for 48 h with 0.5 mM isobutylmethylxanthine, 1 mM dexamethasone and 10 mg/mL insulin (MDI) added to basal medium. On day 2, the MDI medium was replaced with basal medium containing insulin only. On day 4 and thereafter, the cells were cultured in basal medium, which was freshly changed every 2 days until the cells were analyzed.

DOW-RE, SW-RE, and UPW-RE were prepared using the extraction of DOW-RMD, SW-RMD, and UPW-RMD with 10-fold volume of 95% ethanol at 37 °C for 24 h, respectively. DOW-RE, SW-RE, and UPW-RE were diluted to various concentrations with DMEM medium, and further used as the treatment medium in the cell experiments. The vehicle control was 0.3% ethanol in culture medium, which was equal to the ethanol concentration in all RMD extract treatments.

4.8. Oil-Red O Staining

Differentiated 3T3-L1 cells on day 8 were fixed with 10% formaldehyde and then stained with oil-red O. Pictures were taken using a microscope (ECLIPSE TS100; Nikon Co., Tokyo, Japan) [36].

4.9. Lipolysis Assay

The fully differentiated 3T3-L1 adipocytes (days 8–12 after differentiation induction) were treated with test substances in Krebs Ringer bicarbonate (KRB) buffer (20 mM NaCl, 4.7 mM KCl, 2.2 mM $CaCl_2$, 1.2 mM $MgSO_4$ $7H_2O$, 1.2 mM KH_2PO_4, 25 mM $NaHCO_3$ and 2% BSA; pH 7.4) for 24 h. Adipose explants (0.1 g) of perirenal and epididymal fat pads from experimental rats were

incubated in 1 mL of KRB buffer at 37 °C for 1 h [37]. Glycerol was determined enzymatically from the supernatant by using a Randox kit.

4.10. Heparin-Releasable Lipoprotein Lipase (HR-LPL) Activity Assay

After incubation of the 3T3-L1 mature adipocytes with the experimental medium for 24 h, the medium was discarded. The cells were rinsed with KRB buffer and then cultured in heparin-KRB (10 U/mL heparin) at 37 °C for 1 h. The conditioned heparin-KRB was collected from each well for the assay of HR-LPL activity. In the animal study, a sample of perirenal and epididymal adipose tissue weighing 0.1 g was placed in 1 ml of KRB buffer supplemented with 10 U/mL heparin at 37 °C for 1 h. LPL activity was measured according to the previous study on the basis of its esterase property using *p*-nitrophenyl butyrate as a substrate [36].

The TG hydrolase activity of LPL with synthetic TG substrates is inhibited by molar sodium chloride, and this property has been used to distinguish LPL activity from the activities of other lipases in plasma. Thus, HR-LPL activity was calculated from the productivity of *p*-nitrophenol using the following equation [36].

$$C\ (\mu M) = [A_{400}\ (0.15\ M\ NaCl) - A_{400}\ (1\ M\ NaCl)]/0.012$$

where A_{400} (0.15 M NaCl) and A_{400} (1 M NaCl) were the absorbances of released *p*-nitrophenol at 400 nm in 0.15 M and in 1 M NaCl assay buffer, respectively, and 0.012 is the micromolar extinction coefficient of *p*-nitrophenol.

4.11. Immunoblotting

Protein concentration was determined by bicinchoninic acid (BCA) method. A total of 40 μg of total protein from each sample was applied for Western blot representative of three independent experiments according to the previous studies [38,39]. The samples were separated on 10% SDS-PAGE gels and transferred to polyvinylidene fluoride membranes. After blocking in a gelatin-NET solution, blots were incubated with monoclonal C/EBPα antibody (1:5000), monoclonal C/EBPβ antibody (1:2000), polyclonal PPARγ antibody (1:1000), polyclonal PPARγ antibody (1:1000) at room temperature for 1 h. Then, bands were incubated with specific horse radish peroxidase (HRP)-conjugated secondary antibodies (1:100,000) at room temperature for 1 h and visualized by enhanced chemiluminescence (ECL) substrate with UVP AutoChemi Image system (UVP Inc., Upland, CA, USA). Protein loading was evaluated by anti-actin antibody (1:5000).

4.12. Statistics

Data are expressed as means ± standard deviation. Analysis of variance by Duncan's test and Pearson's product-moment correlation coefficient test were determined using SPSS version 10.0 software (SPSS Institute, Inc., Chicago, IL, USA). Differences with $p < 0.05$ were considered statistically significant.

5. Conclusions

Combining each of the above test results, in the animal testing, RMD cultured with DOW demonstrated better effects in reducing weight gain, body-fat pads, and the cross-sectional area of adipocytes because, according to the *in vitro* test results, DOW-RMD possessed better ability to inhibit differentiation and LPL activity. Furthermore, DOW-RMD demonstrated better inhibitory effect on differentiation because DOW enhances the rate of monascin and ankaflavin production in RMD, which subsequently increases the ability of RMD to inhibit PPARγ and C/EBPα protein expressions. Moreover, monascin, ankaflavin, and DOW were able to inhibit LPL activity. Thus, DOW-RMD possessed both DOW and relatively high levels of monascin and ankaflavin, all of which facilitated lipogenesis inhibition and consequently prevented the accumulation of lipid droplets. In addition, SW was able to provide SW-RMD with similar anti-obesity effects as that of DOW-RMD, but they resulted from a different mechanism of regulation of differentiation and lipogenesis because of different ion composition. In this study, we simultaneously confirmed that the anti-obesity abilities of DOW-RMD in inhibiting PPARγ and C/EBPα expression in differentiation and lipoprotein lipase activity in lipogenesis were contributed to by the DOW-increased monascin and ankaflavin levels and the ions of DOW, respectively.

Acknowledgments

This study was supported by a grant from the National Science Council, Taiwan (NSC-98-2313-B-143-002-MY3; NSC 101-2313-B-143-003-MY3) and Ministry of Economic Affairs, Taiwan (102-EC-17-A-32-S1-230).

References

1. Marques, B.G.; Hausman, D.B.; Martin, R.J. Association of fat cell size and paracrine growth factors in development of hyperplastic obesity. *Am. J. Physiol*. **1998**, *275*, R1898–R1908.
2. Kirkland, J.L.; Hollenberg, C.H.; Kindler, S.; Gillon, W.S. Effects of age and anatomic site on preadipocyte number in rat fat depots. *J. Gerontol.* **1994**, *49*, B31–B35.
3. Chumlea, W.C.; Roche, A.F.; Siervogel, R.M.; Knittle, J.L.; Webb, P. Adipocytes and adiposity in adults. *Am. J. Clin. Nutr.* **1981**, *34*, 1798–1803.
4. Mastinu, A.; Pira, M.; Pinna, G.A.; Pisu, C.; Casu, M.A.; Reali, R.; Marcello, S.; Murineddu, G.; Lazzari, P. NESS06SM reduces body weight with an improved profile relative to SR141716A. *Pharmacol. Res.* **2013**, *74*, 94–108.
5. Jou, P.C.; Ho, B.Y.; Hsu, Y.W.; Pan, T.M. The effect of *Monascus* secondary polyketide metabolites, monascin and ankaflavin, on adipogenesis and lipolysis activity in 3T3-L1. *J. Agric. Food Chem.* **2010**, *58*, 12703–12709.
6. Lee, C.L.; Wen, J.Y.; Hsu, Y.W.; Pan, T.M. Monascus-Fermented yellow pigments monascin and ankaflavin showed antiobesity effect via the suppression of differentiation and lipogenesis in obese rats fed a high-fat diet. *J. Agric. Food Chem.* **2013**, *61*, 1493–1500.
7. Othmer, D.F.; Roels, O.A. Power, fresh water, and food from cold, deep sea water. *Science* **1973**, *182*, 121–125.

8. Fujita, D. Deep ocean water. *Shokuhin Eiseigaku Zasshi* **2001**, *42*, J340−J342.
9. Kimata, H.; Tai, H.; Nakagawa, K.; Yokoyama, Y.; Nakajima, H.; Ikegami, Y. Improvement of skin symptoms and mineral imbalance by drinking deep sea water in patients with atopic eczema/dermatitis syndrome (AEDS). *Acta Medica (Hradec Kralove)* **2002**, *45*, 83–84.
10. Kuwayama, H.; Nagasaki, A. Desalted deep sea water increases transformation and homologous recombination efficiencies in *Dictyostelium discoideum*. *J. Mol. Microbiol. Biotechnol.* **2008**, *14*, 157–162.
11. Hataguchi, Y.; Tai, H.; Nakajima, H.; Kimata, H. Drinking deep-sea water restores mineral imbalance in atopic eczema/dermatitis syndrome. *Eur. J. Clin. Nutr.* **2005**, *59*, 1093–1096.
12. Hwang, H.S.; Kim, H.A.; Lee, S.H.; Yun, J.W. Anti-Obesity and antidiabetic effects of deep sea water on ob/ob mice. *Mar. Biotechnol.* **2009**, *11*, 531–539.
13. Katsuda, S.; Yasukawa, T.; Nakagawa, K.; Miyake, M.; Yamasaki, M.; Katahira, K.; Mohri, M.; Shimizu, T.; Hazama, A. Deep-sea water improves cardiovascular hemodynamics in Kurosawa and Kusanagi-Hypercholesterolemic (KHC) rabbits. *Biol. Pharm. Bull.* **2008**, *31*, 38–44.
14. Lee, C.L.; Kung, Y.H.; Wang, J.J.; Lung, T.Y.; Pan, T.M. Enhanced hypolipidemic effect and safety of red mold dioscorea cultured in deep ocean water. *J. Agric. Food Chem.* **2011**, *59*, 8199–8207.
15. Vandenberghe, K.; Goris, M.; van Hecke, P.; van Leemputte, M.; Vangerven, L.; Hespel, P. Long-Term creatine intake is beneficial to muscle performance during resistance training. *J. Appl. Physiol.* **1997**, *83*, 2055–2063.
16. Hallsworth, J.E.; Nomura, Y.; Iwahara, M. Ethanol-Induced water stress and fungal growth. *J. Ferment. Bioeng.* **1998**, *86*, 451–456.
17. Giorni, P.; Magan, N.; Pietri, A.; Battilani, P. Growth and aflatoxin production of an Italian strain of *Aspergillus flavus*: Influence of ecological factors and nutritional substrates. *World Mycot. J.* **2011**, *4*, 425–432.
18. Duda, V.I.; Danilevich, V.N.; Suzina, N.F.; Shorokhova, A.P.; Dmitriev, V.V.; Mokhova, O.N.; Akimov, V.N. Changes in the fine structure of microbial cells induced by chaotropic salts. *Mikrobiologiia* **2004**, *73*, 406–415.
19. Cray, J.A.; Russell, J.T.; Timson, D.J.; Singhal, R.S.; Hallsworth, J.E. A universal measure of chaotropicity and kosmotropicity. *Environ Microbiol* **2013**, *15*, 287–296.
20. Hallsworth, J.E.; Yakimov, M.M.; Golyshin, P.N.; Gillion, J.L.; D'Auria, G.; de Lima Alves, F.; La Cono, V.; Genovese, M.; McKew, B.A.; Hayes, S.L.; Harris, G.; Giuliano, L.; Timmis, K.N.; McGenity, T.J. Limits of life in $MgCl_2$-containing environments: Chaotropicity defines the window. *Environ. Microbiol.* **2007**, *9*, 801–813.
21. Lasram, S.; Oueslati, S.; Valero, A.; Marin, S.; Ghorbel, A.; Sanchis, V. Water activity and temperature effects on fungal growth and ochratoxin A production by ochratoxigenic *Aspergillus carbonarius* isolated from Tunisian grapes. *J. Food Sci.* **2010**, *75*, M89–M97.
22. Cray, J.A.; Bell, A.N.; Bhaganna, P.; Mswaka, A.Y.; Timson, D.J.; Hallsworth, J.E. The biology of habitat dominance; Can microbes behave as weeds? *Microb. Biotechnol.* **2013**, *6*, 453–492.

23. Sepcic, K.; Zalar, P.; Gunde-Cimerman, N. Low water activity induces the production of bioactive metabolites in halophilic and halotolerant fungi. *Mar. Drugs* **2011**, *9*, 43–58.
24. Chen, W.P.; Ho, B.Y.; Lee, C.L.; Lee, C.H.; Pan, T.M. Red mold rice prevents the development of obesity, dyslipidemia and hyperinsulinemia induced by high-fat diet. *Int. J. Obes. (Lond)* **2008**, *32*, 1694–1704.
25. Hwang, H.S.; Kim, S.H.; Yoo, Y.G.; Chu, Y.S.; Shon, Y.H.; Nam, K.S.; Yun, J.W., Inhibitory effect of deep-sea water on differentiation of 3T3-L1 adipocytes. *Mar. Biotechnol.* **2009**, *11*, 161–168.
26. Kota, B.P.; Huang, T.H.; Roufogalis, B.D. An overview on biological mechanisms of PPARs. *Pharmacol. Res.* **2005**, *51*, 85–94.
27. Rangwala, S.M.; Lazar, M.A. Peroxisome proliferator-activated receptor gamma in diabetes and metabolism. *Trends Pharmacol. Sci.* **2004**, *25*, 331–336.
28. Yoke Yin, C.; So Ha, T.; Abdul Kadir, K. Effects of glycyrrhizic acid on peroxisome proliferator-activated receptor gamma (PPARgamma), lipoprotein lipase (LPL), serum lipid and HOMA-IR in rats. *PPAR Res.* **2010**, doi:10.1155/2010/530265.
29. Cohen, H.; Sherer, Y.; Shaish, A.; Shoenfeld, Y.; Levkovitz, H.; Bitzur, R.; Harats, D. Atherogenesis inhibition induced by magnesium-chloride fortification of drinking water. *Biol. Trace Elem. Res.* **2002**, *90*, 251–259.
30. Shahkhalili, Y.; Murset, C.; Meirim, I.; Duruz, E.; Guinchard, S.; Cavadini, C.; Acheson, K. Calcium supplementation of chocolate: effect on cocoa butter digestibility and blood lipids in humans. *Am. J. Clin. Nutr.* **2001**, *73*, 246–252.
31. Lee, C.L.; Hung, H.K.; Wang, J.J.; Pan, T.M. Red mold dioscorea has greater hypolipidemic and antiatherosclerotic effect than traditional red mold rice and unfermented dioscorea in hamsters. *J. Agric. Food Chem.* **2007**, *55*, 7162–7169.
32. Lee, C.L.; Tsai, T.Y.; Wang, J.J.; Pan, T.M. *In vivo* hypolipidemic effects and safety of low dosage *Monascus* powder in a hamster model of hyperlipidemia. *Appl. Microbiol. Biotechnol.* **2006**, *70*, 533–540.
33. Lee, C.L.; Hung, H.K.; Wang, J.J.; Pan, T.M. Improving the ratio of monacolin K to citrinin production of *Monascus purpureus* NTU 568 under dioscorea medium through the mediation of pH value and ethanol addition. *J. Agric. Food Chem.* **2007**, *55*, 6493–6502.
34. Chen, H.C.; Farese, R.V., Jr. Determination of adipocyte size by computer image analysis. *J. Lipid Res.* **2002**, *43*, 986–989.
35. Folch, J.; Lees, M.; Sloane Stanley, G.H. A simple method for the isolation and purification of total lipides from animal tissues. *J. Biol. Chem.* **1957**, *226*, 497–509.
36. Kusunoki, M.; Hara, T.; Tsutsumi, K.; Nakamura, T.; Miyata, T.; Sakakibara, F.; Sakamoto, S.; Ogawa, H.; Nakaya, Y.; Storlien, L.H. The lipoprotein lipase activator, NO-1886, suppresses fat accumulation and insulin resistance in rats fed a high-fat diet. *Diabetologia* **2000**, *43*, 875–880.
37. Berger, J.J.; Barnard, R.J. Effect of diet on fat cell size and hormone-sensitive lipase activity. *J. Appl. Physiol.* **1999**, *87*, 227–232.

38. Bihaqi, S.W.; Singh, A.P.; Tiwari, M. Supplementation of Convolvulus pluricaulis attenuates scopolamine-induced increased tau and Amyloid precursor protein (AbetaPP) expression in rat brain. *Indian J. Pharmacol.* **2012**, *44*, 593–598.
39. Lee, C.L.; Kuo, T.F.; Wu, C.L.; Wang, J.J.; Pan, T.M. Red mold rice promotes neuroprotective sAPPalpha secretion instead of Alzheimer's risk factors and amyloid beta expression in hyperlipidemic Abeta40-infused rats. *J. Agric. Food Chem.* **2010**, *58*, 2230–2238.

Identification of Two Novel Anti-Fibrotic Benzopyran Compounds Produced by Engineered Strains Derived from *Streptomyces xiamenensis* M1-94P that Originated from Deep-Sea Sediments

Zhong-Yuan You, Ya-Hui Wang, Zhi-Gang Zhang, Min-Juan Xu, Shu-Jie Xie, Tie-Sheng Han, Lei Feng, Xue-Gong Li and Jun Xu

Abstract: The benzopyran compound obtained by cultivating a mangrove-derived strain, *Streptomyces xiamenensis* strain 318, shows multiple biological effects, including anti-fibrotic and anti-hypertrophic scar properties. To increase the diversity in the structures of the available benzopyrans, by means of biosynthesis, the strain was screened for spontaneous rifampicin resistance (Rif), and a mutated *rpsL* gene to confer streptomycin resistance (Str), was introduced into the *S. xiamenensis* strain M1-94P that originated from deep-sea sediments. Two new benzopyran derivatives, named xiamenmycin C (**1**) and D (**2**), were isolated from the crude extracts of a selected Str-Rif double mutant (M6) of M1-94P. The structures of **1** and **2** were identified by analyzing extensive spectroscopic data. Compounds **1** and **2** both inhibit the proliferation of human lung fibroblasts (WI26), and **1** exhibits better anti-fibrotic activity than xiamenmycin. Our study presents the novel bioactive compounds isolated from *S. xiamenensis* mutant strain M6 constructed by ribosome engineering, which could be a useful approach in the discovery of new anti-fibrotic compounds.

Reprinted from *Mar. Drugs*. Cite as: You, Z.-Y.; Wang, Y.-H.; Zhang, Z.-G.; Xu, M.-J.; Xie, S.-J.; Han, T.-S.; Feng, L.; Li, X.-G.; Xu, J. Identification of Two Novel Anti-Fibrotic Benzopyran Compounds Produced by Engineered Strains Derived from *Streptomyces xiamenensis* M1-94P that Originated from Deep-Sea Sediments. *Mar. Drugs* **2013**, *11*, 4035–4049.

1. Introduction

During daily urban life, a causal relationship between the elevated urban air pollution and an increased severity of airway diseases, including lung fibrosis and lung cancers, has been supported by epidemiological and toxicological research [1,2]. Fibrosis, a result of chronic inflammatory reactions induced by a variety of stimuli, has recently garnered increasing attention [3]. Fibrotic diseases such as idiopathic pulmonary fibrosis, liver cirrhosis, systemic sclerosis, progressive kidney disease, and cardiovascular fibrosis are threatening the public health [3]. However, successful methods for treating fibrosis have been limited, and the lack of effective small-molecule medicines is one of the serious issues [4,5]. Therefore, the search for bioactive compounds from natural resources represents an emerging pharmacological and therapeutic area in the fight against excessive fibrotic diseases.

Benzopyran derivatives have been demonstrated to have considerable bioactivities, including anti-oxidative, anti-hypertensive, anti-microorganism, and anti-inflammatory properties [6–9]. In our previous studies, it was shown that xiamenmycin, a benzopyran compound with the structure of

N-((3,4-dihydro-3*S*-hydroxy-2*S*-methyl-2-(4′*R*-methyl-3′*S*-pentenyl)-2*H*-1-benzopyran-6-yl)carbonyl)-threonine, was obtained by cultivating the mangrove-derived strain *Streptomyces xiamenensis* 318, and it was found to have multiple biological effects toward inhibiting fibrosis, *i.e.*, the inhibition of excessive lung fibrosis *in vitro* and the attenuation of hypertrophic scars by the suppression of local inflammation, and by the reduction of the effects of mechanical stress [10–12]. The possible mechanism could be the inhibition of the mechanical stress-induced pro-fibrotic effects by suppressing proliferation, activation, and contraction of fibroblast, and inactivating focal adhesion kinase (FAK), p38, and Rho guanosine triphosphatase signaling [10–12]. During excessive fibrogenesis, the existence of self-perpetuating loops for inflammation and extracellular matrix (ECM) accumulation, which results from the inflammatory response and the mechanical forces, is closely related to formation of fibrotic diseases [13]. Xiamenmycin, aimed at the loops, has inhibitory effects on both inflammation and mechanotransduction; therefore, it may be a potential candidate for the development of new anti-fibrotic drugs. Thus, in our ongoing study, it is worthwhile to continue the chemical and pharmaceutical investigations of new benzopyran compounds.

Streptomyces are known as versatile producers of novel secondary metabolites from various biosynthetic pathways. The same species of *Streptomyces* strains even if the strains originate from different ecological niches can be used to hunt for novel bioactive compounds. Not surprisingly, an affined strain of *S. xiamenensis* 318, namely the strain M1-94P isolated from deep-sea sediments, can produce small amounts of potentially novel benzopyrans. As the secondary metabolic pathways in the microorganisms isolated from the deep sea normally remained dormant or weakly expressed under laboratory conditions, rational strain development was critical prior to extensive chemical investigation. Ribosomal engineering is a simple but practical approach for strain breeding by targeting the microbial ribosomal proteins or the subunits of RNA polymerase and has been widely used for strain improvement [14–17]. This strategy was therefore adopted to either increase the production of the benzopyran compound or stimulate the biosynthesis of novel benzopyrans by activating dormant or weakly expressed secondary metabolite biosynthetic genes in the strain *S. xiamenensis* M1-94P.

First, we introduced a spontaneous rifampicin resistant (Rif) mutation in strain M1-94P, and we then conferred streptomycin resistance (Str) to the Rif mutant by introducing a mutated *rpsL* gene. From the HPLC fingerprints of the constructed drug resistant mutants (M1-5R22, M5, and M6), the profiles of the metabolites were found to be altered, and the production of the benzopyran compounds improved. Two novel benzopyran compounds, xiamenmycin C (**1**) and D (**2**), were isolated from the crude extracts of M6, the strain with the highest productivity of benzopyran derivatives. The structures of **1** and **2** were identified through the analysis of extensive spectroscopic data. In this study, we showed that secondary metabolite production potential in the deep-sea derivatized *Streptomyces* strain *S. xiamenensis* M1-94P was awoken by ribosomal engineering. Our results also showed that **1** and **2** have anti-fibrotic activities, and **2** is even better than xiamenmycin, due to its lower concentration and higher inhibitory effect against WI26. Our work provided unique structures for use in the study of structure-bioactivity relationships, aimed at the development of anti-fibrotic compounds for the therapeutic treatment of excessive fibrotic diseases.

2. Results

2.1. Construction of the Mutants

Based on the methodology of ribosomal engineering, the combination of rifampicin and streptomycin is the most popular pair of drugs to screen for potential high producers of bioactive compounds among drug-resistant mutants. We first screened for spontaneously occurring Rif mutants from strain M1-94P by plating the spores on a GYM (glucose 4 g/L, yeast extract 4 g/L, malt extract 10 g/L, and agar 1.5% at pH = 7.2–7.4) plate containing 10 μg/mL of rifampicin (five times minimal inhibitory concentration (MIC)). The amplified *rpoB* gene fragments from nine candidates of Rif mutation strains were sequenced to check whether the Rif mutation was targeted at RNAP or not. The mutant strain M1-5R22 was chosen for use in further strain improvements due to its altered HPLC profile and its confirmed point mutation in the *rpoB* gene (see Table 1).

A combined resistance to streptomycin in the strain M1-5R22 was obtained by introducing two types of mutated *rpsL* genes into its genome through plasmid conjugation and integration. As summarized in Table 1, all three of the mutants that showed resistance to rifampicin contained a mutation within the *rpoB* gene, in which an altered nucleotide (from G to A) was found at position 1319, which resulted in an amino acid alteration of Arg-440 to His. The generated double mutants, namely M5 and M6, contained an additional mutation in the *rpsL* gene that changed nucleotides A-262 to G or C-268 to A and T-269 to A, resulting in amino acid alterations in the ribosome protein S12 from Lys-88 to Glu or Leu-90 to Lys.

Table 1. Mutations in the *rpsL* and *rpoB* genes that resulted in amino acid exchanges in *S. xiamenensis* M1-94P.

Strain	Resistance *	Position in *rpoB* gene	Amino acid position (exchange)	Position in *rpsL* gene	Amino acid position (exchange)
M1-94P	-	-	-	-	-
M1-5R22	Rif	G-1319 → A	440 (Arg → His)	-	-
M5	Rif + Str	G-1319 → A	440 (Arg → His)	A-262 → G	88 (Lys → Glu)
M6	Rif + Str	G-1319 → A	440 (Arg → His)	C-268 → A T-269 → A	90 (Leu → Lys)

***** Rifampicin resistance = 10 μg/mL, streptomycin resistance = 20 μg/mL.

2.2. HPLC Analysis of Wild-Type M1-94P and Its Mutants

To compare the profiles of the secondary metabolites in the wild-type M1-94P and its three mutants, HPLC analysis was performed. There are six main metabolites from M1-94P and its mutants, and these are marked by arrows A through F in the HPLC spectra (Figure 1). The peak areas of the metabolites were increased in three mutants compared with M1-94P. The double mutant strains, M5 and M6, produced several compounds (e.g., peaks A, C, and E) that were barely detected in the wild type strain M1-94P. According to the characteristics of UV absorbance and the retention time of xiamenmycin, the production of xiamenmycin, labeled as peak F, was gradually

improved in the three mutants. The results suggested that mutant M6 was best suited for use in large-scale fermentations to prepare an extract containing benzopyran derivatives. Compounds **1** and **2** were isolated from the peak F with close retention time after repeatedly chromatography.

Figure 1. HPLC profiles of wild type M1-94P and its three mutants. The arrows (A–F) indicate the six main peaks, and arrow F indicates xiamenmycin as a standard reference.

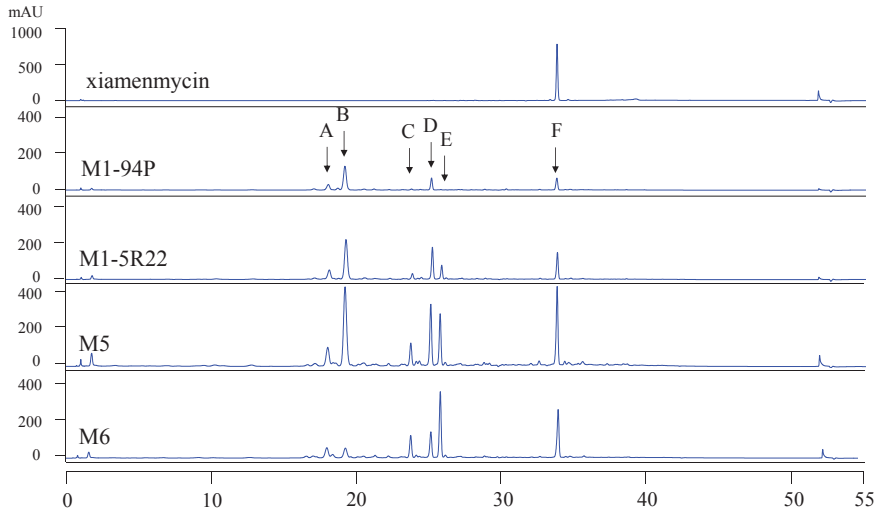

2.3. Structural Elucidation of Compounds **1** *and* **2**

The mutant M6 was selected to perform large-scale liquid fermentations under the same conditions as the small-scale fermentation. Total liquid cultures of M6 were extracted with organic solvent. Two novel benzopyran compounds **1** and **2**, as well as xiamenmycin (Figure 2), were isolated from peak F (Figure 1) after semi-preparative HPLC purification. The retention times of **1** and **2** are quite close to that of xiamenmycin during the HPLC analysis; thus, it was difficult to detect these two compounds from the crude extract initially.

Figure 2. Structures of the anti-fibrotic benzopyran compounds **1**, **2**, and xiamenmycin.

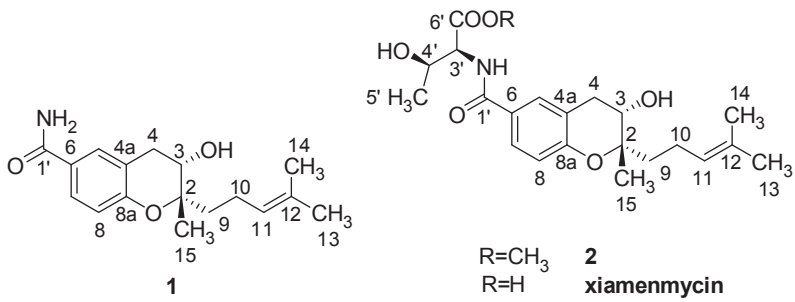

The molecular formula of **1** was determined to be $C_{17}H_{23}NO_3$ by HRESIMS (*m/z* = 290.1768 $[M + H]^+$, positive ion mode and *m/z* = 288.1610 $[M - H]^-$, negative ion mode). Based on similar

UV characteristics, compound **1** was considered to be a derivative of xiamenmycin. The ^{1}H and ^{13}C NMR data, in combination with the HMBC and the HMQC correlations, resulted in the identification of benzopyran as the main structural feature. The HMBC correlations between H_2-9 (δ_H 1.59, m), C-2 (δ_C 79.7), and C-3 (δ_C 66.3) confirmed the isoprenyl side chain to be located at C-2. The substituent position of the carboxamide was determined to be C-6 in the benzopyran skeleton based on the HMBC correlation between H-5 (δ_H 7.63, d, 1.8), H-6 (δ_H 7.60, dd, 8.4, 1.8) and C-1′ (δ_C 168). The main difference in the NMR data between **1** and xiamenmycin was found in the amino acid moieties and was due to the missing signal related to the 1′–6′ positions in the ^{1}H and the ^{13}C NMR spectra (Table 2). From biosynthetic reasoning and the similarity of the CD data compared with xiamenmycin, we assumed that compound **1** has the identical absolute configuration as xiamenmycin in the benzopyran portion of the molecule. Accordingly, the structure of **1** was identified as (2*S*,3*S*)-3-hydroxy-2-methyl-2-(4-methylpent-3-enyl)chroman-6-carboxamide and was named xiamenmycin C.

Table 2. ^{1}H and ^{13}C NMR spectroscopic data of the novel benzopyran compounds **1** and **2** [a].

Position	1			2		
	δ_H (*J* in Hz)	**δ_C, type**	**HMBC**	**δ_H (*J* in Hz)**	**δ_C, type**	**HMBC**
1	-	-	-	-	-	-
2	-	79.7, C	-	-	79.8, C	-
3	3.74, dd (7.4, 5.2)	66.3, CH	4a, 2, 9, 15	3.76, dd (7.4, 5.2)	66.3, CH	4a, 2, 9, 15
4	2.66, dd (17.3, 7.4) 2.93, dd (17.3, 5.2)	31.3, CH_2	8a, 5, 4a, 2, 3, 6	2.71, dd (17.3, 7.4) 2.97, dd (17.3, 5.2)	31.2, CH_2	8a, 5, 4a, 2, 3
4a	-	120.4, C	-	-	120.6, C	-
5	7.63, d (1.8)	130.2, CH	7, 8a, 4, 1′	7.69, d (1.8)	130.0, CH	7, 8a, 4, 1′
6	-	126.3, C	-	-	125.7, C	-
7	7.60, dd (8.4, 1.8)	127.4, CH	5, 8a, 1′	7.64, dd (8.4, 1.8)	127.4, CH	5, 8a, 1′
8	6.74, d (8.4)	116.5, CH	4a, 8a, 6	6.80, d (8.4)	116.7, CH	4a, 8a, 6
8a	-	156.0, C	-	-	156.2, C	-
9	1.59, m	38.0, CH_2	11, 12, 2, 3, 10	1.60, m	37.9, CH_2	11, 10, 12, 2, 3
10	2.10, m	21.6, CH_2	11, 12, 2, 9	2.11, m	21.6, CH_2	11, 12, 2, 9
11	5.10, t (7.3)	124.8, CH	13, 10, 14, 9	5.11, t (7.2)	124.8, CH	13, 10, 14
12	-	131.3, C	-	-	131.3, C	-
13	1.56, s	18.0, CH_3	11, 12, 14	1.57, s	17.9, CH_3	11, 12, 14
14	1.63, s	25.9, CH_3	11, 12, 13	1.64, s	25.9, CH_3	11, 12, 13
15	1.16, s	18.8, CH_3	2, 3, 9	1.18, s	18.8, CH_3	2, 3, 9
1′	-	168.0, C	-	-	166.9, C	-
2′	-	-	-	8.02, d (8.2)	-	1′, 3′, 4′
3′	-	-	-	4.47, dd (8.1, 4.1)	59.4, CH	1′, 4′, 5′, 6′
4′	-	-	-	4.17, dq (6.3, 4.1)	66.9, CH	5′, 6′
5′	-	-	-	1.14, d (6.3)	20.7, CH_3	3′, 4′
6′	-	-	-	-	171.8, C	-
7′	-	-	-	3.65, s	52.3, CH_3	6′
CO–NH_2	8.38, brs	-	-	-	-	-

[a] Measured in DMSO-d_6, chemical shifts (δ) in ppm.

Compound **2** gave a *pseudo*-molecular ions $[M + H]^+$ peak at m/z = 406.2210 by HRESIMS, consistent with an elemental composition of $C_{22}H_{31}NO_6$, which was 15 amu more than the molecular weight of xiamenmycin. The ^1H and ^{13}C NMR data showed an additional methyl group due to the presence of signals at δ_H 3.65 (3H, s) and δ_C 52.3 (CH_3). The HMBC correlations between CH_3-7′ and CO-6′ (δ_C 171.8) confirmed the methyl esterification. The good agreement of the respective NMR data of **2** with those of xiamenmycin, together with ROESY data and proton coupling constants indicated that both compounds shared the same relative configurations of pyran-ring and the amino acid portion. Compound **2** possessed the same stereo-configurations as xiamenmycin, confirmed by the similar CD spectrum. Therefore, the structure of **2** was determined as (2*R*,3*S*)-methyl 3-hydroxy-2-((2*S*,3*S*)-3-hydroxy-2-methyl-2-(4-methylpent-3-enyl)chroman-6-carboxamido)butanoate, named xiamenmycin D.

2.4. Inhibition of the Proliferation of Human Diploid Lung Fibroblast (WI26) Cells by Compounds **1** *and* **2**

Fibroblasts play pivotal roles in establishing and maintaining the self-perpetuating inflammatory circuits and are, in fact, the main ECM generating cells in fibrotic diseases [18]. Thus, finding a small molecule that can slow the rapid fibrotic response would be a reasonable way to develop an anti-fibrotic drug. We investigated the anti-proliferative activities of **1** and **2** against human lung fibroblast. WI26 cells were exposed to **1** at a concentration of 15 μg/mL, **2** at a concentration of 30 μg/mL, and xiamenmycin at a concentration of 30 μg/mL, respectively, for 0, 1, 2, 3, 4, 5, and 6 days, and the optical density (OD) at λ = 450 nm was monitored as a function of time. As illustrated in Figure 3, compound **1** significantly inhibited the proliferation of the WI26 cells at lower concentration, compared with both **2** and xiamenmycin. The extent of this inhibition of **1** increased with time, from a decrease of 13.8% at day one to a decrease of 38% at day six at a concentration of 15 μg/mL, compared with a control sample that was only treated with solvent (Figure 3A, Table S1). Therefore, compound **1** does indeed exhibit better anti-proliferative effects on human lung fibroblast. Compared with xiamenmycin, **2** showed similar anti-fibrotic bioactivity, which can inhibit the proliferation from a decrease of 12.8% at day one to a decrease of 38% at day six at a concentration of 30 μg/mL (Figure 3B, Table S1).

3. Discussion

The wild-type *S. xiamenensis* strain M1-94P, an affined strain of *S. xiamenensis* 318, was isolated from deep-sea sediments and used as a biosource in the search for new benzopyran compounds. The possibility of discovering novel chemical structures may be higher when shifting to an alien niche, such as deep-sea derived microbial strains, from the view of chemical ecology, but the production of secondary metabolites in the deep-sea derived microbes is normally quite low, due to physiological stress, when they are cultivated under the usual laboratory conditions. Therefore, the use of a rational strain development approach such as ribosomal engineering may be useful to increase the production of secondary metabolites in the laboratory.

Figure 3. Inhibitory effects of compounds **1** and **2** on the proliferation of WI26 cells. The WI26 cells were exposed to 15 μg/mL of **1** and 30 μg/mL of **2** at day 0, 1, 2, 3, 4, 5 and 6. The surviving fraction was determined by Cell Counting Kit-8 assay. As illustrated below, the proliferation of the WI26 cells was significantly inhibited by **1** (**A**) and **2** (**B**) in a time-dependent manner. The data are given as the means of triplicate values ± SD of three independent experiments. Significant differences from the value of the control sample treated with only 0.1% DMSO solvent are marked. ** $p < 0.01$, *** $p < 0.001$.

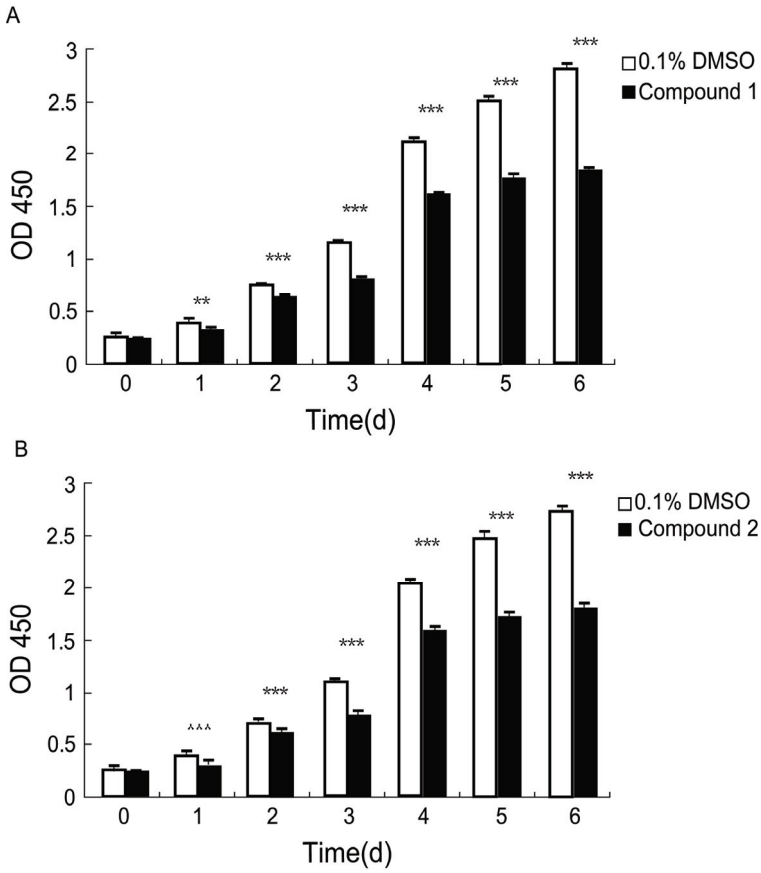

Improving the production of the secondary metabolites by bacteria by modulating the ribosome components as well as other translating factors or RNAP [15] has several advantages, including the ability to screen for drug-resistant mutations by simple selection on drug-containing plates and without prior genetic mutagenesis [19]. It was reported that the introduction of multiple drug resistant mutations had the cumulative effect of increasing the production of secondary metabolites, which led to a dramatic increase in the production of the bioactive compounds. Rifampicin and streptomycin is a pair of drugs widely used in ribosomal engineering to screen potential high producers among drug-resistant mutants. In our case, the introduction of combined drug resistance to rifampicin and streptomycin in *S. xiamenensis* M1-94P was a successful method to improve the

production of benzopyran compounds for chemical isolation, although the detailed mechanism of the enhancement of the specific natural product compound remains unknown.

Because spontaneous rifampicin resistance mutants always have point mutations clustered in the so-called Rif domain on the *rpoB* gene (encoding the β-subunit of RNA polymerase) and could mimic the ppGpp binding effect on the mutated RNAP [20], we decided to screen for a Rif resistant mutant as the first step in the strain development. We have sequenced the *rpoB* gene fragment of nine Rif mutants including six Rif mutants from 5 × MIC and 3 Rif mutants from 10 × MIC. All of the mutants have a point mutation in the Rif domain in the *rpoB* gene.

There are two types of streptomycin resistance that could effectively alter ribosomal function. Determination of the mutation in the ribosomal RNA that engenders a low level of streptomycin resistance is not easy, but the introduction of a mutation into the highly conserved ribosomal protein S12 is conveniently achieved by site-directed mutagenesis using PCR (polymerase chain reaction). Furthermore, certain *rpsL* mutations, resulting in the amino acid substitution of either K88E or L90K, that confer resistance to Str can increase the production of secondary metabolites in *Streptomyces* [21–25]. Thus, it is more rational to engineer ribosomal protein S12 as the second step in the strain development; thus, we introduced a mutated *rpsL* gene to confer streptomycin resistance to the Rif mutant M1-5R22 and to interfere with its ribosomal function. As shown in the HPLC profiles, the production of the target compounds, xiamenmycin increased drastically in the Rif-Str double resistance strains M5 and M6.

Xiamenmycin, xiamenmycin C (**1**) and D (**2**), with highly similar chemical structures, were all isolated from mutant M6 of deep-sea derived *S. xiamenensis* M1-94P. Compared with xiamenmycin, obtained from our previous study [11], xiamenmycin C had the same benzopyran skeleton and isoprene side chain. The only difference in the structures is in the amino acid moiety (on position 1′). Compound **1** is the possible precursor of xiamenmycin during biosynthesis. Compound **2** is methyl ester of xiamenmycin, which may be synthesized in the tailing step of the biosynthetic pathway. From the view of combinatorial biosynthesis, more “unnatural” natural products may be produced by the elucidation of the biosynthetic pathway for the synthesis of benzopyran compounds.

Xiamenmycin C (**1**) was found to exhibit better inhibitory effects on the cell proliferation of human lung fibroblasts (WI26) using lower doses compared with xiamenmycin. It seems that the benzopyran skeleton is crucial for the anti-fibrotic activity. Xiamenmycin is an antifibrotic small molecule that targets the inflammatory and mechanical stress responses, the two pivotal pathological processes that occur during excessive fibrogenesis [12]. Xiamenmycin D (**2**) showed similar anti-fibrotic activity, compared with xiamenmycin. It indicated the methylation on position 6′ may not affect the bioactivity significantly. As a type of potential anti-fibrotic drug, more diverse benzopyran structures are needed for the investigation of the structure-activity relationship (SAR). For example, compounds with distinct substituent groups on the benzopyran skeleton are expected from natural sources, or a variation in the benzopyran configuration could be achieved by total or partial synthesis.

In summary, our results showed that xiamenmycin C and D, two new benzopyran structures, can be isolated from the deep-sea derived *S. xiamenensis* M1-94P. Ribosomal engineering, *i.e.*, the introduction of a spontaneous rifampicin resistance mutation combined with the introduction of a

streptomycin resistant mutation, was performed to generate mutant M6 with enhanced secondary metabolite production. As a promising candidate for treating excessive fibrotic diseases, the effects of xiamenmycin and its derivatives on mechanical stress and inflammation in association with various fibroblast cellular behaviors will be examined in the next stage of research.

4. Experimental Section

4.1. General

^{1}H and ^{13}C NMR spectra were recorded with Bruker DRX-500 and Advance Ⅲ-600 NMR spectrometers using the solvent as an internal standard (DMSO-d_6 δ = 2.51 and 40.0 ppm, respectively). Coupling constants (*J*) are reported in Hertz (Hz) and chemical shifts (δ) are expressed in parts per million (ppm). Optical rotation was measured by a JASCO P-2000 polarimeter, and CD spectra were recorded on a J-815 spectropolarimeter (JASCO, Gross-Umstadt, Germany) at room temperature. UPLC-HRMS was measured on a Waters ACQUITY UPLC system equipped with a binary solvent delivery manager and a sample manager coupled with a Waters Micromass Q-TOF Premier Mass Spectrometer equipped with an electrospray interface (Waters Corporation, Milford, MA, USA). HPLC was performed on Agilent Technologies 1200 series instrument (Agilent Technologies, Wadbronn, Germany). Column chromatography was carried out with Sephadex LH-20 (40–70 μm, Amersham Pharmacia Biotech AB, Uppsala, Sweden), silica gel (200–300 mesh, Qingdao Marine Chemical, Inc., Qingdao, China), Lichroprep reversed-phase RP-18 silica gel (40–63 μm, Merck, Darmstadt, Germany) and silica gel H (10–40 μm, Qingdao, China). Analytical HPLC was carried out on an Agilent XDB-C18 column (4.6 × 150 mm, 5 μm) with a flow rate of 1 mL/min. Organic solvents for HPLC were analytical grade and were purchased from Merck KGaA (Darmstadt, Germany).

4.2. The Original Strain Materials

The *Streptomyces xiamenensis* strain M1-94P was isolated from a deep-sea sediment sample collected at the depth of 2628 m in the Eastern Pacific (12.7115′N, 103.9071′W). This strain M1-94P was determined to be *S. xiamenensis* by 16S rRNA gene sequence analysis.

4.3. Construction of Mutants by the Screening for Spontaneous Rifampicin Resistance

Fresh spores of wild strain M1-94P formed by cultivation on SFM (soy flour 20 g/L, D-mannitol 20 g/L, agar 1.5%, pH = 7.2) plates were incubated at 30 °C for 7 days and were then harvested and suspended in the appropriate amount of sterilized and distilled water. They were filtered to remove medium fragments and were then preserved in the 20% (v/v) glycerol tube (2 mL).

The M1-94P spore suspension was spread on GYM agar medium (glucose 4 g/L, yeast extract 4 g/L, malt extract 4 g/L, and agar 1.5% at pH = 7.2–7.4) containing various rifampicin concentrations. The MIC of rifampicin against M1-94P was determined through a two day incubation period at 30 °C on GYM agar medium. Spontaneous Rif mutants were obtained from the colonies that grew within 7–10 days after the spores of M1-94P were spread on the GYM agar medium containing

different rifampicin concentrations (5 × MIC, 10 × MIC, 50 × MIC). Spontaneous drug resistant mutants were selected for further characterization.

4.4. Introduction of Streptomycin Resistance by Site Directed Mutagenesis

The *rpsL* gene fragment was amplified by PCR using the M1-94P genomic DNA as the template and was subjected to site-directed mutagenesis using PCR. The sequences of the forward primers were (mutagenic positions underlined): K88E-F (5′-GGCCGTGTGGAGGACCTGCCGGGTG-3′) and L90K-F (5′-GTGTGAAGGACAAGCCGGGTGTCCG-3′). The utilized reverse primers, K88E-R and L90K-R, were complementary to the forward primers. Primer pairs XJ1F (5′-CATATGGTGCCAACGATCCAGCA-3′) and XJ1R (5′-GATATCTTACTTCTCCTTCTTGGCGC-3′) were designed to introduce *Nde*I and *Eco*RV sites (underlined below) at the translation start and stop codon of the *rpsL* gene and combined with the primers K88E-F/R and L90K-F/R to generate point mutations in the mutagenesis PCR amplification.

The entire length of the mutated *rpsL* gene was amplified by PCR and inserted into the pMD 18-T vector to check for site directed mutagenesis by sequencing, which generated plasmids p822 (K88E) and p827 (L90K). The *Nde*I-*Eco*RV fragments containing mutated *rpsL* genes were excised and inserted into the same sites of pIB139, an integrative expression vector in *Streptomyces* [26], generating pIB139-822 (K88E) and pIB139-827 (L90K). These two plasmids were transformed into *E. coli* ET12567: pUZ8002 separately and used as the donor strains for two parental *E. coli—Streptomyces* conjugations. Exoconjugants derived from the wild type *S. xiamenensis* M1-5R22 were selected by rifampicin and apramycin on the SFM solid medium plates [27]. The mutants harboring pIB139-822 and pIB139-827 were named M5 and M6, respectively.

4.5. Mutation Analysis of the rpsL and rpoB Genes

The primers for the PCR amplification of the *rpoB* and the *rpsL* genes were designed using the sequence information of the draft genome of *S. xiamenensis* (unpublished data). The partial *rpoB* gene fragments (nucleotides 374–1582, 1.2 kb) of the wild strain M1-94P and its Rif-resistant mutants (M1-5R22, M5 and M6) were obtained by PCR using their genomic DNA as templates and the synthetic oligonucleotide primers (forward: 5′-CCGAGTTCACCAACAACGAGACC-3′, reverse: 5′-CGATGACGAAGCGGTCCTCC-3′). The complete *rpsL* gene was amplified from the wild strain M1-94P and its drug-resistant mutants (M1-5R22, M5 and M6) by primer pairs (forward: 5′-TGTCCTCGGGTATCGGTCTG-3′ and reverse: 5′-TTACTTCTCCTTCTT GGCGCCGTAG-3′). The PCR products were directly sequenced by Sangon Biotech (Shanghai, China) Co., Ltd.

4.6. HPLC Analysis

Spore suspensions of the wild type strain M1-94P and its three mutants were inoculated in test tubes (15 × 150 mm) with 5 mL of Tryptone Soy Broth (TSB) (Oxoid, Hampshire, UK) and were pre-cultured at 30 °C for 1 day on a rotary shaker at 280 rpm. The TSB broth was then transferred into a 500 mL flask containing 100 mL of yeast extract-malt extract broth (GYM medium) and was

cultured at 30 °C for 7 days on a rotary shaker at 280 rpm. Each culture was centrifuged at 9000 rpm for 10 min, and the supernatant was then extracted three times at room temperature overnight with equal volumes of the solvent ethyl acetate. The supernatant was combined and concentrated under vacuum at 37 °C to remove the organic phase. Each crude extract was subsequently dissolved in the same volume of HPLC grade methanol.

The samples were analyzed by HPLC using an Agilent XDB-C18 column (4.6 × 150 mm, 5 μm) and monitored by UV detection at 254 nm. The solvent system of methanol (A) and H_2O (B) was used as the mobile phase in the following linear gradient: 0 min 10% B, 10 min 10% B, 40 min 100% B, 50 min 100% B, 51 min 10% B, 55 min 10% B, at a flow rate of 1 mL/min. The xiamenmycin obtained by our group was used as the standard reference.

4.7. Fermentation, Extraction, and Isolation

Mutant M6 was selected to perform a large-scale fermentation (33 L) in yeast extract-malt extract broth. The liquid culture was centrifuged at 9000 rpm for 10 min, and the supernatant was extracted at room temperature by ethyl acetate. The residue was extracted at room temperature overnight by a solvent mixture of ethyl acetate:methanol:acetic acid (80:5:5, v:v:v). The second supernatant was then filtered, and the residue was extracted twice more as described above. All the supernatants were combined and concentrated under vacuum at 37 °C to remove the organic phase. The crude extract (13.4 g) was obtained and was then subjected to silica gel column chromatography with elution by a mixture of dichloromethane (CH_2Cl_2) and methanol (MeOH) (gradient from CH_2Cl_2 (300 mL), 70:1 (v:v, 300 mL), 60:1 (v:v, 300 mL), 50:1 (v:v, 1.5 L), 30:1 (v:v, 800 mL), 10:1 (v:v, 1.5 L), 5:1 (v:v, 1 L), 2:1 (v:v, 1 L), 1:1 (v:v, 600 mL) to MeOH (600 mL)) and ten fractions (Fr.A–Fr.J) were obtained. Guided by HPLC fingerprinting, two fractions, Fr.F (3.09 g) eluted by CH_2Cl_2:MeOH = 15:1 to 10:1 and Fr.H (1.17 g) eluted by CH_2Cl_2:MeOH = 2:1, were collected and further subjected to Sephadex LH-20 column chromatography with elution by 100% methanol.

Fr.F-2 (0.478 g) was a subfraction of Fr.F, which was identified as the target fraction according to the HPLC fingerprints. Fr.F-2 was subsequently subjected to silica gel column chromatography and was eluted with CH_2Cl_2:MeOH. Fr.F-2-4 (eluted with CH_2Cl_2:MeOH (40:1, v:v)) showed the target peaks of the xiamenmycin derivatives from UV characterization at λ_{max} = 206 and 260 nm. Fr.F-2-4 (18 mg) was further purified again by semi-preparative HPLC (Agilent ZOBRAX-C18 column, 5 μm, 9.4 × 250 mm), with the following gradient: CH_3CN (A)/H_2O (B): 0 min 42% A, 8 min 42% A, 33 min 72% A, 34 min 100% A, 50 min 100% A, at a flow rate of 1.5 mL/min. One sub-fraction Fr.F-2-4-2 contained compound **2** (1.5 mg). Fr.F-2-2 (8 mg) was subsequently purified by semi-preparative HPLC (Agilent ZOBRAX-C18 column, 5 μm, 9.4 × 250 mm), with the following gradient: CH_3CN (A)/H_2O (B): 0 min 45% A, 5 min 45% A, 35 min 55% A, 36 min 100% A, 50 min 100% A, at the flow rate of 1.5 mL/min. One sub fraction Fr.F-2-2-3 was collected as compound **1** (1.5 mg).

Compound **1**: Yellow amorphous powder (MeOH); $[\alpha]^{26}_D$ +28.45° (*c* 0.0034, MeOH); UV (MeOH) λ_{max} = 206, 260 nm; CD (*c* 0.0024, MeOH) $\Delta\varepsilon_{201}$ +12.3, $\Delta\varepsilon_{202}$ +9.6, $\Delta\varepsilon_{205}$ +8.0, $\Delta\varepsilon_{207.4}$ +7.1, $\Delta\varepsilon_{213.6}$ +0.14, $\Delta\varepsilon_{217}$ −1.2, $\Delta\varepsilon_{245.2}$ +2.0, $\Delta\varepsilon_{259.8}$ +3.14, $\Delta\varepsilon_{283}$ +0.03; ^{1}H and ^{13}C NMR data,

see Table 2; HRESIMS *m*/*z* 290.1768 $[M + H]^+$, (calcd. for $C_{17}H_{24}NO_3$, *m*/*z* 290.1756), 288.1610 $[M - H]^-$, (calcd. for $C_{17}H_{22}NO_3$, *m*/*z* 288.2073).

Compound **2**: Yellow amorphous powder (MeOH); $[\alpha]^{30}_D$ +6.52° (*c* 0.0024, MeOH); UV (MeOH) λ_{max} 206, 260 nm; CD (*c* 0.0034, MeOH) $\Delta\varepsilon_{205.6}$ +6.7, $\Delta\varepsilon_{206.9}$ +5.5, $\Delta\varepsilon_{213}$ +20.1, $\Delta\varepsilon_{223.4}$ +0.85, $\Delta\varepsilon_{260}$ +9.23, $\Delta\varepsilon_{296.8}$ +1.0; ^1H and ^{13}C NMR data, see Table 2; HRESIMS *m*/*z* 406.2210 $[M + H]^+$, (cacld. for $C_{22}H_{32}NO_6$, *m*/*z* 406.2230).

4.8. Cell Proliferation Assay

The effects of compounds **1** and **2**, as well as xiamenmycin on cell proliferation were determined using a standard Cell Counting Kit-8 (CCK-8, Dojindo, Kumamoto, Japan) assay according to the manufacturers instructions. WI26 cells at 70%–80% confluency were treated with a 0.25% trypsin and 0.02% EDTA solution, centrifuged and resuspended in DMEM supplemented with 10% FBS and antibiotics. The cells were then seeded in 96-well plates (100 µL/well) at an initial density of 2.5×10^4 cells/mL. The medium was replaced 24 h later by fresh DMEM with 10% FBS and antibiotics containing 15 µg/mL of compound **1**, 30 µg/mL of compound **2**, 30 µg/mL of xiamenmycin, or 0.1% DMSO (AppliChem, Darmstadt, Germany). Subsequently, the medium was refreshed and the viabilities of the cells were measured by using a CCK-8 solution at day 0, 1, 2, 3, 4, 5, and 6, respectively. A proliferation measurement was performed by adding 10 µL of CCK-8 solution to each well and incubating the solutions at 37 °C for 1 h. The OD values of each well were measured at the primary wavelength λ = 450 nm using a Microplate Spectrophotometer (PowerWaveXS, BioTek, Seattle, WA, USA). The data are shown as the means ± standard deviations (SD) of three independent experiments, each performed in triplicate.

4.9. Statistical Analysis

Statistical differences were calculated using student's paired *t*-test at significance levels of $p < 0.05$ to 0.001.

5. Conclusions

The benzopyran compound xiamenmycin can be obtained through the cultivation of a mangrove-derived strain of *Streptomyces xiamenensis*, strain 318, and it has multiple anti-fibrotic effects. The deep sea-derived *S. xiamenensis* strain M1-94P was selected for further chemical and pharmaceutical studies of benzopyran compounds. The introduction of spontaneous rifampicin resistance combined with streptomycin resistance by introducing a mutated *rpsL* gene into M1-94P was performed to increase the production of its secondary metabolites. Two new benzopyran derivatives, xiamenmycin C (**1**) and D (**2**), were isolated from one of the Rif-Str double mutants, M6. The structures of **1** and **2** were identified through extensive spectroscopic data analysis. The isolation of the novel compounds increased the structural diversity of known benzopyran compounds, and the anti-proliferation bioactivities of **1** and **2** on human lung fibroblast behavior were investigated. Compared with xiamenmycin, the bioactivity of **1** is increased when the amino acid moiety was removed and compound **2** showed similar anti-fibrotic activity. Our work may be

useful for a structure-activity relationship study of anti-fibrotic benzopyran compounds to develop leading drugs for medical treatment of excessive fibrotic disease from marine natural product.

Acknowledgments

We are grateful to Jieli Wu for technical support in the NMR measurements and to Ruibin Wang for the CD measurements in the Instrumental Analysis Center of Shanghai Jiao Tong University. This work was supported by the National Natural Science Foundation of China (NSFC 81273404) and the National Basic Research Program of China "973" 2012CB721001.

Conflicts of Interest

The authors declare no conflict of interest.

References

1. Vlietinck, A.J.; de Bruyne, T.; Apers, S.; Pieters, L.A. Plant-derived leading compounds for chemotherapy of human immunodeficiency virus (HIV) infection. *Planta Med.* **1998**, *64*, 97–109.
2. Borm, P. Toxicity of Selected: Toxicology of Fibers and Particles. In Proceedings of Toxicology and Risk Assessment, Heerlen, The Netherland, 14–17 April 2008; Greim, H., Snyder, R., Eds.; John Wiley & Sons Ltd.: Chichester, UK, 2008; pp. 565–583.
3. Wynn, T.A. Cellular and molecular mechanisms of fibrosis. *J. Pathol.* **2008**, *214*, 199–210.
4. Friedman, S.L.; Sheppard, D.; Duffield, J.S.; Violette, S. Therapy for fibrotic diseases: Nearing the starting line. *Sci. Transl. Med.* **2013**, *5*, 1–17.
5. Wynn, T.A.; Ramalingam, T.R. Mechanisms of fibrosis: Therapeutic translation for fibrotic disease. *Nat. Med.* **2012**, *18*, 1028–1040.
6. Machado, N.F.L.; Marques, M.P.M. Bioactive chromone derivatives—Structural diversity. *Curr. Bioact. Compd.* **2010**, *6*, 76–89.
7. Evans, J.M.; Fake, C.S.; Hamilton, T.C.; Poyser, R.H.; Watts, E.A. Synthesis and antihypertensive activity of substituted *trans*-4-amino-3,4-dihydro-2,2-dimethyl-2*H*-1-benzopyran-3-ols. *J. Med. Chem.* **1983**, *26*, 1582–1589.
8. Göker, H.; Boykin, D.W.; Yıldız, S. Synthesis and potent antimicrobial activity of some novel 2-phenyl or methyl-4*H*-1-benzopyran-4-ones carrying amidinobenzimidazoles. *Bioorg. Med. Chem.* **2005**, *13*, 1707–1714.
9. Kawamura, N.; Tsuji, E.; Watanabe, Y.; Tsuchihashi, K.; Takako, T. Benzopyran Derivatives, Their Manufacture with *Streptomyces* Species, and Their Use for Treatment of Asthma and Rheumatoid Arthritis. Jpn. Patent P2000-726766A, 7 March 2000.
10. Xu, J.; Wang, Y.; Xie, S.J.; Xiao, J.; Ruan, J.S. *Streptomyces xiamenensis* sp. nov., isolated from mangrove sediment. *Int. J. Syst. Evol. Microbiol.* **2009**, *59*, 472–476.

11. Xu, M.J.; Liu, X.J.; Zhao, Y.L.; Liu, D.; Xu, Z.H.; Lang, X.M.; Ao, P.; Lin, W.H.; Yang, S.L.; Zhang, Z.G.; *et al*. Identification and characterization of an anti-fibrotic benzopyran compound isolated from mangrove-derived *Streptomyces xiamenensis*. *Mar. Drugs* **2012**, *10*, 639–654.
12. Liu, X.J.; Xu, M.J.; Fan, S.T.; Wu, Z.; Li, J.; Yang, X.M.; Wang, Y.H.; Xu, J.; Zhang, Z.G. Xiamenmycin attenuates hypertrophic scars by suppressing local inflammation and the effects of mechanical stress. *J. Invest. Dermatol.* **2013**, *133*, 1351–1360.
13. Nathan, C.; Ding, A.H. Nonresolving inflammation. *Cell* **2010**, *140*, 871–882.
14. Ochi, K. From microbial differentiation to ribosome engineering. *Biosci. Biotechnol. Biochem.* **2007**, *71*, 1373–1386.
15. Ochi, K.; Okamoto, S.; Tozawa, Y.; Inaoka, T.; Hosaka, T.; Xu, J.; Kurosawa, K. Ribosome engineering and secondary metabolite production. *Adv. Appl. Microbiol.* **2004**, *56*, 155–184.
16. Tanaka, Y.; Kasahara, K.; Hirose, Y.; Murakami, K.; Kugimiya, R.; Ochi, K. Activation and products of the cryptic secondary metabolite biosynthetic gene clusters by rifampin resistance (rpoB) mutations in actinomycetes. *J. Bacteriol.* **2013**, *195*, 2959–2570.
17. Ochi, K.; Hosaka, T. New strategies for drug discovery: Activation of silent or weakly expressed microbial gene clusters. *Appl. Microbiol. Biotechnol.* **2013**, *97*, 87–98.
18. Eckes, B.; Nischt, R.; Krieg, T. Cell-matrix interactions in dermal repair and scarring. *Fibrogenesis Tissue Repair* **2010**, *3*, doi:10.1186/1755-1536-3-4.
19. Wang, G.; Hosaka, T.; Ochi, K. Dramatic activation of antibiotic production in *Streptomyces coelicolor* by cumulative drug resistance mutations. *Appl. Environ. Microbiol.* **2008**, *74*, 2834–2340.
20. Xu, J.; Tozawa, Y.; Lai, C.; Hayashi, H.; Ochi, K. A rifampicin resistance mutation in the *rpoB* gene confers ppGpp-independent antibiotic production in *Streptomyces coelicolor* A3(2). *Mol. Genet. Genomics* **2002**, *268*, 179–189.
21. Okamoto-Hosoya, Y.; Okamoto, S.; Ochi, K. Development of antibiotic-overproducing strains by site-directed mutagenesis of the *rpsL* gene in *Streptomyces lividans*. *Appl. Environ. Microbiol.* **2003**, *69*, 4256–4259.
22. Hu, H.; Ochi, K. Novel approach for improving the productivity of antibiotic-producing strains by inducing combined resistant mutations. *Appl. Environ. Microbiol.* **2001**, *67*, 1885–1892.
23. Hesketh, A.; Ochi, K. A novel method for improving *Streptomyces coelicolor* A3(2) for production of actinorhodin by introduction of *rpsL* (encoding ribosomal protein S12) mutations conferring resistance to streptomycin. *J. Antibiot. (Tokyo)* **1997**, *50*, 532–535.
24. Okamoto-Hosoya, Y.; Sato, T.A.; Ochi, K. Resistance to paromomycin is conferred by *rpsL* mutations, accompanied by an enhanced antibiotic production in *Streptomyces coelicolor* A3(2). *J. Antibiot. (Tokyo)* **2000**, *53*, 1424–1427.
25. Shima, J.; Hesketh, A.; Okamoto, S.; Kawamoto, S.; Ochi, K. Induction of actinorhodin production by *rpsL* (encoding ribosomal protein S12) mutations that confer streptomycin resistance in *Streptomyces lividans* and *Streptomyces coelicolor* A3(2). *J. Bacteriol.* **1996**, *178*, 7276–7284.

26. Wilkinson, C.J.; Hughes-Thomas, Z.A.; Martin, C.J.; Bohm, I.; Mironenko, T.; Deacon, M.; Wheatcroft, M.; Wirtz, G.; Staunton, J.; Leadlay, P.F. Increasing the efficiency of heterologous promoters in actinomycetes. *J. Mol. Microbiol. Biotechnol.* **2002**, *4*, 417–426.
27. Kieser, T.; Bibb, M.J.; Buttner, M.J.; Chater, K.F.; Hopwood, D.A. *Practical Streptomyces Genetics*; John Innes Foundation: Norwich, UK, 2000.

Eight New Peptaibols from Sponge-Associated *Trichoderma atroviride*

Irina Panizel, Oded Yarden, Micha Ilan and Shmuel Carmeli

Abstract: Eight new and four known peptaibols were isolated from a strain of the fungus, *Trichoderma atroviride* (NF16), which was cultured from an Axinellid sponge collected from the East Mediterranean coast of Israel. The structures of the pure compounds were determined using HRMS, MS/MS and one- and two-dimensional NMR measurements. The isolated compounds belong to the trichorzianines, a family of 19-residue linear hydrophobic peptides containing a high proportion of α-aminoisobutyric acid (Aib), an acetylated *N*-terminus and a *C*-terminal amino alcohol. These new peptaibols exhibited antimicrobial activity against environmental bacteria isolated from the Mediterranean coast of Israel.

Reprinted from *Mar. Drugs*. Cite as: Panizel, I.; Yarden, O.; Ilan, M.; Carmeli, S. Eight New Peptaibols from Sponge-Associated *Trichoderma atroviride*. *Mar. Drugs* **2013**, *11*, 4937–4960.

1. Introduction

Peptaibols are linear peptides of 5–20 residues, characterized by an acetate or acyl group in the *N*-terminus, *C*-terminal amino alcohol, a high proportion of α-aminoisobutyric acid (Aib) and other dialkylamino acids, such as isovaline (Iva). Most peptaibols were isolated from *Trichoderma* spp. or other closely related genera of fungi [1,2]. Peptaibols are produced by nonribosomal peptide synthetases [3]. To date, more than 300 peptaibols have been described, and their properties are summarized in the Peptaibol Database [4]. Peptaibols exhibit antimicrobial activity against fungi and Gram-positive bacteria and have an important role in biocontrol by *Trichoderma* spp. They act synergistically with cell wall degrading enzymes to inhibit the growth of fungal pathogens [5]. Trichorzianines are a subgroup of 19-residue peptaibols, initially isolated from *Trichoderma harzianum* [6–8]. They have similar amino acids sequences, except for differences in residues 5 (Aib or Iva), 14 (Leu or Val), 16 (Ile or Leu), 18 (Gln or Glu) and 19 (Pheol or Trpol) (Table S1 in the supporting material). A study, in which a trichorzianine type A (neutral trichorzianines) mixture was analyzed by MS/MS, revealed that in addition to the above-mentioned variable residues, other residues might be changed. In position 2, Ala might be substituted with Gly, in position 3 Ala with Gly or Aib, in position 5 Aib with Iva or Val, in positions 7, 8 and 9 Aib with Ala and in position 14 Val or Ile or Leu with Ala [9]. Recent investigation of five marine-derived *T. atroviride* strains afforded a new class of 17 residue-long peptaibols along with 19-residue peptaibols [10]. Peptaibols initially isolated from *Trichoderma atroviride* are termed atroviridins [11] and neoatroviridins [12]. LC-MS/MS study of *T. atroviride* peptaibols [2,13] revealed trichorzianines isolated from *T. harzianum* [7,8], as well.

In the current research, eight new and four known trichorzianines were isolated from the extract of *T. atroviride* (strain NF16), which was cultivated from an Axinellid sponge, collected by SCUBA diving from the Mediterranean Sea near Akhziv, Israel, as a part of a study on the

chemical ecology of sponge-associated fungi. In re-isolation and culture trials, *T. atroviride* was re-isolated from both *Axinella polypoides* and *A. verrucosa* specimens (from 75% to 90% of the specimens; $n = 4$ and $n = 11$, respectively).

2. Results and Discussion

The culture medium was treated with Amberlite XAD-7 HP, and the compounds absorbed to the resin were washed from it with acetone. The crude acetone extract was subject to a Sephadex LH-20 column, and the active fraction was repeatedly separated on a preparative reversed phase HPLC column. The twelve peptaibols isolated in this study vary in four of 19 positions: position 5 was occupied by Aib or Iva, position 9 by Ala or Aib, position 14 by Leu or Val and position 17 by Glu, Glu-OMe or Gln (Table 1).

2.1. Structure Elucidation of Trichorzianine 1938 (TA1938) (**1**)

Trichorzianine 1938 (TA1938) (**1**) was isolated as an amorphous white solid. In the ESI^+ TOF MS of **1**, the quasi-molecular ions *m/z* 1939.1 ($[M + H]^+$), *m/z* 1961.2 ($[M + Na]^+$), *m/z* 981.1 ($[M + H + Na]^{2+}$), *m/z* 992.0 ($[M + 2Na]^{2+}$), and *m/z* 669.0 ($[M + 3Na]^{3+}$) were observed. High-resolution mass measurement established its molecular formula, $C_{91}H_{151}N_{21}O_{25}$, for the $[M + Na]^+$ ion of **1**, at *m/z* 1961.1099. In addition to the molecular ions, some prominent fragment ions were also present in the ESI^+ spectrum; including the two complementary fragments, *m/z* 1122.7 and *m/z* 817.5, derived from the cleavage between the proline nitrogen and carboxyl group of the adjacent amino acid, characteristic of the peptaibols [14]. These two fragments were advantageous in the structural elucidation of **1** by MS/MS (Figure 1).

Table 1. Trichorzianines (TA) **1–12** isolated from *Trichoderma atroviride* (NF16). Positions marked in grey differ between compounds. TA1938, trichorzianine 1938. Aib, α-amino-isobutyric acid.

Compound name	New/known	1	2	3	4	5	6	7	8	9	10	11	12	13	14	15	16	17	18	19
TA1938 (**1**)	**new**	AcAib	Ala	Ala	Aib	Iva	Gln	Aib	Aib	Aib	Ser	Leu	Aib	Pro	Leu	Aib	Ile	Glu	Gln	Pheol
TA1909 (**2**)	**new**	AcAib	Ala	Ala	Aib	Aib	Gln	Aib	Aib	Ala	Ser	Leu	Aib	Pro	Leu	Aib	Ile	Gln	Gln	Pheol
TA1895 (**3**)	**new**	AcAib	Ala	Ala	Aib	Aib	Gln	Aib	Aib	Ala	Ser	Leu	Aib	Pro	Val	Aib	Ile	Gln	Gln	Pheol
TA1896 (**4**)	**new**	AcAib	Ala	Ala	Aib	Aib	Gln	Aib	Aib	Ala	Ser	Leu	Aib	Pro	Val	Aib	Ile	Glu-OMe	Gln	Pheol
TA1924 (**5**)	**new**	AcAib	Ala	Ala	Aib	Iva	Gln	Aib	Aib	Aib	Ser	Leu	Aib	Pro	Val	Aib	Ile	Glu-OMe	Gln	Pheol
TA1910 (**6**)	**new**	AcAib	Ala	Ala	Aib	Iva	Gln	Aib	Aib	Ala	Ser	Leu	Aib	Pro	Val	Aib	Ile	Glu-OMe	Gln	Pheol
TA1924a (**7**)	**new**	AcAib	Ala	Ala	Aib	Aib	Gln	Aib	Aib	Aib	Ser	Leu	Aib	Pro	Leu	Aib	Ile	Glu-OMe	Gln	Pheol
TA1909a (**8**)	**new**	AcAib	Ala	Ala	Aib	Iva	Gln	Aib	Aib	Ala	Ser	Leu	Aib	Pro	Val	Aib	Ile	Gln	Gln	Pheol
TA.VIb (**9**)	known	AcAib	Ala	Ala	Aib	Aib	Gln	Aib	Aib	Aib	Ser	Leu	Aib	Pro	Val	Aib	Ile	Gln	Gln	Pheol
TA.VIa (**10**)	known	AcAib	Ala	Ala	Aib	Iva	Gln	Aib	Aib	Aib	Ser	Leu	Aib	Pro	Leu	Aib	Ile	Gln	Gln	Pheol
TA.VII (**11**)	known	AcAib	Ala	Ala	Aib	Iva	Gln	Aib	Aib	Aib	Ser	Leu	Aib	Pro	Val	Aib	Ile	Gln	Gln	Pheol
TA.Vb (**12**)	known	AcAib	Ala	Ala	Aib	Aib	Gln	Aib	Aib	Aib	Ser	Leu	Aib	Pro	Leu	Aib	Ile	Gln	Gln	Pheol

Figure 1. Secondary MS fragmentation of trichorzianine 1938 (**1**) ions at *m/z* 1122.5, $\mathbf{b_{12}}$-ion (**A**); and *m/z* 839.5, $\mathbf{y_7}$-ion (**B**).

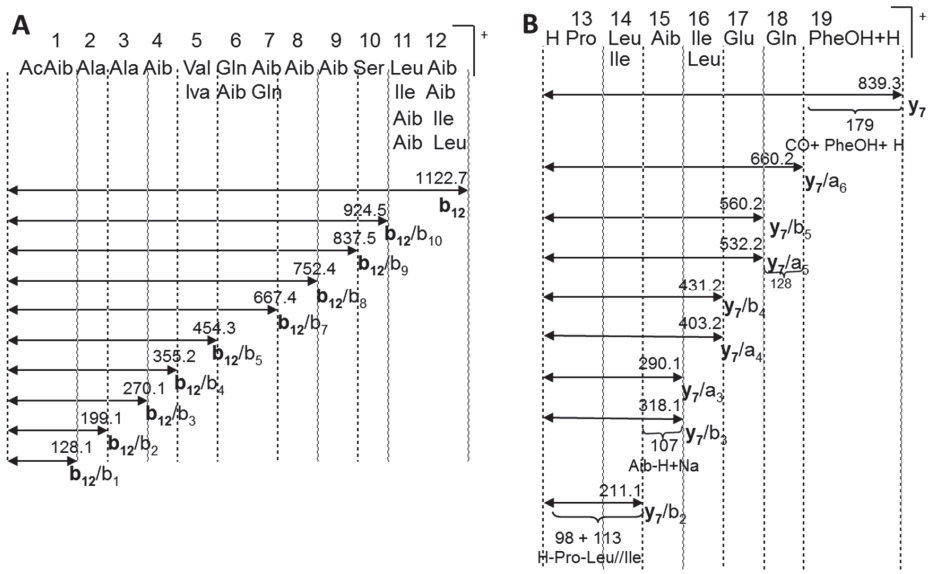

The ^{1}H and ^{13}C NMR spectra (Table 2 and Supplementary Figures S1 and S2) revealed that **1** is composed of the amino alcohol, phenylalaninol (Pheol), acetate, the non-proteinogenic amino acids, α-amino-isobutyric acid (Aib) and isovaline, and the proteinogenic amino acids, leucine, isoleucine, serine, glutamine, glutamic acid, proline and alanine. According to the MS/MS data (Figure 1), Aib appeared seven times in the molecule. The presence of the amino alcohol and isovaline and a high proportion of Aib indicated that the compound belonged to the peptaibol family. The amino acid sequence of the peptide, which was partially determined by the MS/MS, was confirmed and completed by analysis of the 2D NMR data (Table 2 and Supplementary Figures S3–S6). Initially, the structure of the amino acids were determined through interpretation of the COSY, TOCSY, HSQC and HMBC correlations, followed by their connection into the complete planar peptide structure through the HMBC and ROESY correlations and MS/MS data.

According to the MS/MS spectra (Figure 1), the difference of 85 mass units appears seven times, in the positions 1, 4, 7 (or 6), 8, 9, 12 (or 11) and 15. The difference of 213 mass units in positions 6–7, which was explained by a couple of amino acids, glutamine (128) and Aib (85), could also be explained by the amino acids, valine or isovaline (99) and asparagine (114). The difference of 198 mass units in positions 11–12, which was explained by the amino acids, leucine (123) and Aib (85), could also be explained by the presence of two Vxx (valine or isovaline). However, according to the NMR data, valine and asparagine were not present in the molecule, and the only isovaline was assigned to position 5 according to the MS/MS and NMR data analysis. In the NMR spectra, signals typical of α-amino-isobutyric acid (Aib) were observed, including eight singlet amide signals resonating at δ_H 7.47 (assigned to the isovaline), 7.89, 8.56, 7.55, 7.64, 7.77, 7.86 and 7.87 ppm, multiple carbon signals resonating at δ_C 55.8–56.3, typical of carbons α to carboxyl; all of them, except one, (δ_C 56.0, assigned to ^{6}glutamine) are quaternary according to the

HSQC spectrum and multiple overlapping singlet methyl signals in the region of 1.30–1.49 ppm of the ^{1}H NMR spectrum. According to the HSQC map, some of the protons of these methyl signals were bound to carbons resonating between 22.6 and 23.4 or between 25.8 and 26.7 ppm, while one to a carbon at 24.2 ppm. In addition to the Aib methyls, a proton signal of a single methyl of isovaline, one of the methylene protons of the isoleucine and methyl signals of ^{2}alanine and ^{3}alanine, resonate in the region of 1.30–1.49 ppm. Four methyl carbons, resonating between 22.6 and 23.4 ppm, were assigned to ^{11}leucine, ^{14}leucine, acetate and ^{5}isovaline, in addition to the seven Aib methyls. In the region of 25.8–26.7 ppm, three methylene carbons of ^{13}proline, ^{6}glutamine and ^{17}glutamic acid resonate beside the Aib methyl groups. Due to signal overlap, some geminal methyl groups and carbon α to carboxyls of Aib could not be distinguished unambiguously and remain interchangeable. Carboxyamides and amide protons were assigned according to HMBC correlations with amide protons and carboxyamide carbons of the neighboring amino acids, when the amino acids were connected to the full peptide chain.

Table 2. NMR data of trichorzianine 1938 [a] in DMSO-d_6.

Position		δ_C, mult. [b]	δ_H, mult., *J* (Hz)	LR C–H correlations [c]	NOE correlations [d]
Ac	1	171.1 s		Ac-2, ^{1}Aib-NH,4	
	2	23.1 q	1.93 s		^{1}Aib-NH,3,4
^{1}Aib	1	175.7 [e] s		^{2}Ala-NH, ^{1}Aib-NH,3,4	
	2	55.8 s		^{1}Aib-NH,3,4	
	3	26.2 [g] q	1.35 s	^{1}Aib-NH	^{1}Aib-NH
	4	24.0 [h] q	1.32 s	^{1}Aib-3	^{1}Aib-NH
	NH		8.56 s		Ac-2, ^{1}Aib-3,4
^{2}Ala	1	174.5 s		^{3}Ala-NH, ^{2}Ala-2,3	
	2	50.9 d	4.02 m	^{2}Ala-NH,3	^{2}Ala-NH,3
	3	16.8 q	1.31 d	^{2}Ala-NH,2	^{2}Ala-NH,2
	NH		8.25 d (5.2)		^{3}Ala-NH, ^{2}Ala-2,3
^{3}Ala	1	174.5 s		^{4}Aib-NH, ^{3}Ala-2,3	
	2	51.0 d	3.99 m	^{3}Ala-NH,3	^{3}Ala-NH,3, ^{4}Aib-NH
	3	16.2 q	1.33 d	^{3}Ala-NH,2	^{3}Ala-NH,2
	NH		7.68 d (5.6)		^{4}Aib-NH, ^{3}Ala-2,3, ^{2}Ala-NH
^{4}Aib	1	175.0 s		^{5}Iva-NH	
	2	56.0 [f] s		^{4}Aib-NH,3,4	
	3	26.1 [g] q	1.43 [k] s	^{4}Aib-NH,4	^{4}Aib-NH
	4	23.2 [h] q	1.35 [l] s	^{4}Aib-NH,3	^{4}Aib-NH
	NH		7.87 s		^{4}Aib-2,3, ^{3}Ala-NH,2
^{5}Iva	1	176.4 s		^{6}Gln-NH, ^{5}Iva-3,NH	
	2	58.6 s		^{5}Iva-NH,3a,3b,4,5	
	3a	25.6 t	2.20 m	^{5}Iva-4	^{5}Iva-4,3b
	3b		1.62 m		^{5}Iva-4,3a
	4	7.4 q	0.74 t	^{5}Iva-3a,3b	^{5}Iva-NH,3a,3b
	5	22.7 q	1.35 [l] s	^{5}Iva-NH,3a	^{5}Iva-NH,
	NH		7.47 s		^{5}Iva-4,5
^{6}Gln	1	174.0 s		^{7}Aib-NH, ^{6}Gln-2	

Table 2. *Cont*.

	2	56.0 d	3.78 m	^{6}Gln-NH,3,4a,4b	^{7}Aib-NH, ^{6}Gln-NH,3,4a,4b
	3	26.2 t	1.97 m	^{6}Gln-2,4a,4b,NH	^{6}Gln-2,4a,4b,NH, ^{7}Aib-NH
	4a	31.6 [i] t	2.15 m	^{6}Gln-3,NH_2b	^{6}Gln-2,3,4b,NH,NH_2a
	4b		2.23 m		^{6}Gln-2,3,4a
	5	173.6 s		^{6}Gln-3,4a,4b,NH_2a,b	
	NH_2a		7.17 s		^{6}Gln-4a,NH_2b
	NH_2b		6.76 s		^{6}Gln-NH_2a
	NH		7.74 m		^{6}Gln-2,3,4a
^{7}Aib	1	175.8 [e] s		^{8}Aib-NH, ^{7}Aib-NH,3,4	
	2	56.1 [f] s		^{7}Aib-NH,3,4	
	3	25.8 [g] q	1.42 [k] s	^{7}Aib-NH,4	^{7}Aib-NH
	4	22.6 [h] q	1.34 s	^{7}Aib-NH	^{7}Aib-NH
	NH		7.86 s		^{6}Gln-2,3, ^{7}Aib-3,4, ^{8}Aib-NH
^{8}Aib	1	175.9 [e] s		^{9}Aib-NH, ^{8}Aib-3,4	
	2	56.1 [f] s		^{8}Aib-NH,3,4	
	3	26.3 [g] q	1.42 [k] s	^{8}Aib-NH,4	^{8}Aib-NH
	4	23.3 [h] q	1.39 [l] s	^{8}Aib-3	^{8}Aib-NH
	NH		7.55		^{8}Aib-3,4, ^{7}Aib-NH, ^{9}Aib-NH
^{9}Aib	1	176.4 s		^{10}Ser-NH, ^{9}Aib-3,4	
	2	56.1 [f] s		^{9}Aib-NH,3,4	
	3	26.5 [g] q	1.46 [k] s	^{9}Aib-NH,4	
	4	23.0 [h] q	1.42 [l] s	^{9}Aib-3	^{9}Aib-NH
	NH		7.77		^{9}Aib-4, ^{8}Aib-NH
^{10}Ser	1	170.6 s		^{11}Leu-NH, ^{10}Ser-2,3a	-
	2	58.9 d	4.02 m		^{10}Ser-NH,3a,3b, ^{11}Leu -NH
	3a	61.2 t	3.73 m	^{10}Ser-NH,2	^{10}Ser-NH,2
	3b		3.78 m		^{10}Ser-NH,2
	OH				
	NH		7.74 m		^{10}Ser-2,3a,3b
^{11}Leu	1	173.7 [j] s		^{12}Aib-NH, ^{11}Leu-2	
	2	51.5 d	4.27 m	^{11}Leu-NH,4	^{12}Aib-NH, ^{11}Leu-NH,3a,3b,5, ^{13}Pro-5a
	3a	39.2 t	1.56 m	^{11}Leu-2,5,6	^{11}Leu-2,3b,5
	3b		1.70 m		^{11}Leu-NH,2,3a,5
	4	23.9 d	1.73 m	^{11}Leu-5,6	^{11}Leu-NH,6
	5	20.5 q	0.76 d	^{11}Leu-6,3b	^{11}Leu-2,3a,3b
	6	23.0 q	0.82 d	^{11}Leu-5,3b	^{11}Leu-4
	NH		7.59 d (8.0)		^{10}Ser-2, ^{11}Leu-2,3b,4
^{12}Aib	1	173.0 s		^{12}Aib-NH,3,4	
	2	56.2 [f] s		^{12}Aib-NH,3,4	
	3	25.8 [g] q	1.39 s	^{12}Aib-NH	^{12}Aib-NH
	4	23.2 [h] q	1.49 s	^{12}Aib-NH	^{12}Aib-NH, ^{13}Pro-5b
	NH		7.89 s		^{13}Pro-5a,5b, ^{11}Leu-2, ^{12}Aib-3,4
^{13}Pro	1	173.4 s		^{14}Leu-NH, ^{13}Pro-2,3a	

Table 2. *Cont.*

	2	63.1 d	4.21 t (8.0)	^{13}Pro-3a,4	^{14}Leu-NH,5, ^{13}Pro-3b,4
	3a	28.7 t	1.59 m	^{13}Pro-2,5b	^{13}Pro-3b,5a
	3b		2.22 m		^{13}Pro-3a,2,4,5b
	4	26.2 t	1.86 m	^{13}Pro-2	^{13}Pro-2,3b,5a,5b
	5a	48.7 t	3.44 m	^{13}Pro-3b	^{13}Pro-2,3a,4,5b, ^{11}Leu-2, ^{14}Leu-NH, ^{12}Aib-NH
	5b		3.69 m		^{13}Pro-4,5a, ^{12}Aib-NH,3
^{14}Leu	1	173.7 [j] s		^{15}Aib-NH, ^{14}Leu-2	
	2	53.4 d	3.91 m	^{14}Leu-NH,4	^{14}Leu-3a,3b,4,5,6,NH, ^{15}Aib-NH
	3a	38.7 t	1.51 m	^{14}Leu-2,5,6	^{14}Leu-2,3b,6,NH
	3b		1.78 m		^{14}Leu-2,3a,6,NH
	4	24.8 d	1.68 m	^{14}Leu-5,6	^{14}Leu-2,5,NH
	5	23.0 q	0.92 d (6.0)	^{14}Leu-6	^{14}Leu-2,4, ^{13}Pro-2
	6	21.0 q	0.82 m	^{14}Leu-5	^{14}Leu-2,3a,3b
	NH		7.72 m		^{14}Leu-2,3a,3b,4, ^{13}Pro-2,5a
^{15}Aib	1	175.4 s		^{16}Ile-NH, ^{15}Aib-NH,3,4	
	2	56.3 [f] s		^{15}Aib-NH,3,4	
	3	26.1 [g] q	1.44 [k] s	^{15}Aib-4	^{15}Aib -NH
	4	23.4 [h] q	1.37 [l] s	^{15}Aib-NH,3	^{15}Aib-NH
	NH		7.64 s		^{16}Ile-NH, ^{15}Aib-3,4, ^{14}Leu-2
^{16}Ile	1	172.0 s		^{17}Glu-NH, ^{16}Ile-2	-
	2	58.9 d	3.93 m	^{16}Ile-NH,4b,6	^{16}Ile-NH,3,4b,6
	3	35.6 d	1.88 m	^{16}Ile-2,4a,4b,5,6	^{16}Ile-NH,2,6
	4a	25.0 t	1.20 m	^{16}Ile-2,3,5,6	^{16}Ile-NH,4b
	4b		1.47 m		^{16}Ile-NH,2,4a,5
	5	11.5 q	0.82 m	^{16}Ile-4a	^{16}Ile-4b
	6	15.6 q	0.86 d	^{16}Ile-4a,2	^{16}Ile-NH,2,3
	NH		6.96 s		^{16}Ile-2,3,4a,4b,6, ^{15}Aib-NH
^{17}Glu	1	171.3 s		^{18}Gln-NH, ^{17}Glu-2,3a,3b	
	2	53.6 d	4.06 m	^{17}Glu-NH,4a,4b	^{18}Gln-NH, ^{17}Glu-NH,3a,3b,4a,4b
	3a	26.5 t	1.87 m	^{17}Glu-2,4a,4b	^{17}Glu-NH,2,4b
	3b		1.97 m		^{17}Glu-NH,2.4a
	4a	30.4 t	2.25 m	^{17}Glu-2,3a,3b	^{17}Glu-NH,2,3b
	4b		2.37 m		^{17}Glu-NH,2,3a
	5	173.8 [j] s		^{17}Glu-4b	
	NH		7.68 d (5.6)		^{17}Glu-2,3a,3b,4a,4b
^{18}Gln	1	170.8 s		^{19}PheOH-NH, ^{18}Gln-2,3a,3b	
	2	53.1 d	4.06 m	^{18}Gln-NH,3a,3b,4a,4b	^{19}PheOH-NH, ^{18}Gln-NH,3a,3b,,4b
	3a	27.7 d	1.83 m	^{18}Gln-2,4a,4b,NH	^{18}Gln-NH,2,3b,4a
	3b		1.70 m		^{18}Gln-NH,2,3a,4b
	4a	31.7 [i] t	2.05 m	^{18}Gln-NH$_2$a,2,3a,3b	^{18}Gln-3a
	4b		1.97 m		^{18}Gln-NH,NH$_2$b,2,3b

Table 2. *Cont.*

	5	173.6		^{18}Gln-NH_2a,b,3a,3b,4a,4b	
	NH_2a		6.65 s		^{18}Gln-NH_2b
	NH_2b		7.10 s		^{18}Gln-NH_2a,4b
	NH		7.46 d		^{19}PheOH-NH, ^{18}Gln-2,3a,3b,4b
^{19}PheOH	1a	62.7 t	3.29 m	^{19}PheOH-2,3a,3b	^{19}PheOH-NH,2,3a,3b,5
	1b		3.32 m		^{19}PheOH-NH,2,3a,3b
	2	52.5 d	3.86 m	^{19}PheOH-1a,1b,3a,3b,NH	^{19}PheOH-NH,1a,1b,3a,3b,5
	3a	36.6 t	2.61 dd (13.4, 8.2)	^{19}PheOH-1a,1b,2,5	^{19}PheOH-NH,1a,1b,2,5
	3b		2.84 dd (13.2,4.8)		^{19}PheOH-1a,1b,2,5
	4	139.2 s		^{19}PheOH-2,3a,3b,5	
	5	129.4 d	7.21 m	^{19}PheOH-3a,3b,6,7	^{19}PheOH-1a,2,3a,3b,7,NH
	6	128.2 d	7.19 m	^{19}PheOH-5,7	
	7	126.0 d	7.12 m	^{19}PheOH-5,6	^{19}PheOH-5,NH
	OH				
	NH		7.27 d (8)		^{18}Gln-NH,2, ^{19}PheOH-1a,1b,2,3a,5,7

[a] Carried out on an AVANCE-400 Bruker instrument; [b] multiplicity and assignment are from HSQC experiment; [c] values determined from HMBC experiment; $^{n}J_{CH}$ = 8 Hz, recycle time 1 s; [d] selected NOE's from a ROESY experiment; [e,f,g,h,i,j,k,l] these signals may interchange.

The structure determination of acetyl-^{1}Aib started with the methyl protons (δ_H 1.93, s, δ_C 23.1) that exhibited an HMBC correlation with the carboxyamide (δ_C 171.1), which, in turn, was connected to a singlet amide proton resonating at δ_H 8.56. The amide proton and two singlet methyl groups (δ_H 1.32 and 1.35) exhibited HMBC correlations with a carboxyamide (one of the three carbons resonating at δ_C 175.7–175.9) and to a quaternary carbon α to a carboxyamide, resonating at δ_C 55.8), assigning the amino acid as ^{1}Aib. The amide proton exhibited ROESY correlations to the methyl signals (δ_H 1.35, δ_C 26.5 and δ_H 1.32, δ_C 24.1). The carbon of the second methyl group exhibited an HMBC correlation with the protons of the first methyl (δ_H 1.35). These correlations allowed the assignment of the acetyl-^{1}Aib sub-structure.

The assignment of the structure of ^{2}alanine and ^{3}alanine started with COSY correlations of the protons of two doublet methyl groups (δ_H 1.31, δ_H 1.33) with the α-protons resonating at δ_H 4.02 and 3.99, respectively, which, in turn, were connected to amide protons resonating at 8.25 and 7.68 ppm, respectively. This structure was reinforced by HMBC correlations (see Table 2). HMBC correlations connected the methyl groups and α-protons (δ_H 1.31, 1.33, 4.02, 3.99) to carboxyamide carbons resonating at δ_C 174.5, culminating in the structure of the two alanine residues.

A singlet amide proton resonating at δ_H 7.87 exhibited an HMBC correlation with the quaternary carbon resonating at δ_C 56.0 ppm and ROESY and HMBC correlations with two singlet methyl residues (δ_H 1.35, δ_C 23.2 and δ_H 1.43, δ_C 26.1), assigning the signals, except for the carboxyamide carbon of ^{4}Aib. The other Aib residues in positions 7, 8, 9, 12 and 15 were assigned in a similar way.

The methyl protons (δ_H 0.74 t, δ_C 7.4) exhibited COSY correlation to methylene protons (δ_H 2.20 and 1.62) and HMBC correlation to the methylene carbon (δ_C 25.6). HMBC correlations of a quaternary carbon at δ_C 58.6, typical of a carbon α to carboxyamide, with the methyl and the methylene protons, established it as the isovaline C-2 carbon, which, in turn, was coupled by HMBC correlations to an amide proton (δ_H 7.47) and with a single methyl group (δ_H 1.35). Several singlet methyl groups, most belonging to Aib residues, resonated at 1.35 ppm, interfering with the assignment of this methyl carbon by HSQC. However, this carbon was assigned by HMBC correlation of the amide proton (δ_H 7.47) with a carbon resonating at 22.7 ppm. HMBC correlations of the amide (δ_H 7.47), one of the methylene protons (δ_H 2.20), and amide proton of the neighboring amino acid, ^{6}glutamine with a carboxyamide carbon resonating at δ_C 174.6 ppm, established it as the ^{5}isovaline carboxyamide.

The structure determination of ^{6}glutamine and ^{18}glutamine was initiated through COSY correlations of the two pairs of singlet amide protons resonating at 7.17 and 6.76 ppm and at 7.10 and 6.65 ppm, respectively. These amide protons exhibited HMBC correlations to two carbonyl signals resonating at δ_C 173.6, thus establishing two primary amides. These amides were connected through HMBC correlations of the amide protons resonating at 6.65 ppm and 6.76 ppm to two methylene carbons resonating at 31.7–31.6 ppm (^{6}C-4 and ^{18}C-4, δ_H 2.15, 2.23 and 2.05, 1.97, respectively), which, in turn, exhibited HMBC correlations with two pairs of methylene protons, (^{6}Gln-3, δ_H 1.97, 2H, δ_C 26.2) and (^{18}Gln-3, δ_H 1.70, 1.83 ppm, δ_C 27.7). One of the C-3 carbons (26.2 ppm) exhibited HMBC correlations to the pair of methylene-4 protons resonating at 2.15 and 2.23 ppm, while the second C-3 carbon (27.7 ppm) exhibited HMBC correlation with the methylene protons at 1.97 ppm and 2.05 ppm (H-4a, H-4b), allowing the differentiation between the two spin systems. HMBC correlations of C-3 carbons at 26.2 and 27.7 ppm with the methine protons resonating at δ_H 3.78 (δ_C 56.0) and δ_H 4.06 (δ_C 53.1), respectively, established the methines at position 2 of these amino acids. This assignment was further supported by the COSY correlations of H_2-3 with H-2 of both spin systems. The α-amide protons were assigned through the COSY correlation of the α-proton, resonating at 3.78 ppm with the amide proton resonating at 7.74 ppm, and that at 4.06 ppm with that at 7.47 ppm, and reinforced by the HMBC correlations of C-2 carbons with these amide protons. HMBC correlations of the carbon resonating at 174.0 ppm with the proton resonating at 3.78 ppm, and of the carbon resonating at 170.8 ppm with protons resonating at 4.06 ppm, 1.70 ppm and 1.83 ppm, established those carbons as the carboxyamides of the glutamine residues.

The structure elucidation of ^{10}serine was based on COSY correlations of the oxymethylene protons (δ_H 3.73, 3.78; δ_C 61.2) with a proton resonating at 4.02 ppm (δ_C 58.9), which, in turn, was connected to an amide proton resonating at δ_H 7.74. HMBC correlations of the protons resonating at δ_H 4.02 and 3.73 with the carbon resonating at δ_C 170.6 established the latter as a serine carboxyamide. The hydroxyl proton was not observed in the NMR spectrum of TA1938, but was observed at chemical shifts of 4.70–4.85 ppm in some of the other peptaibols (TA1895, TA1909, TA1909A, TA1896 and TA.Vb).

Two methyl groups, H_3-5 and H_3-6 (δ_H 0.76 d, 0.82 d), were coupled to the same methine proton (H-4, δ_H 1.73, C-4: δ_C 23.9) through COSY correlations. In the HMBC spectrum, the two methyl

groups exhibit correlations to C-4 (23.9 ppm) and to a methylene carbon (δ_C 39.2, C-3, δ_H 1.56 and 1.70). COSY correlations coupled H-3b and H-3a through H-2 (δ_H 4.27) to an amide resonating at δ_H 7.59 and HMBC correlation to one of the three carbons resonating at δ_C 173.7–173.8, establishing the structure of [11]leucine.

The structure elucidation of the [13]proline was initiated with COSY correlation of the aminomethylene protons resonating at δ_H 3.44 and 3.69 (H-5a and H-5b) with methylene protons resonating at δ_H 1.86 (H-4a and -4b). The later protons were coupled through COSY correlations to protons of additional methylene δ_H 1.59 and 2.22 (H-3a and H-3b), which, in turn, exhibited COSY correlations with a methine proton (δ_H 4.21, t). The chemical shifts of this proton and the carbon to which it was attached (δ_C 63.1, established through HSQC experiment) indicated their location α to a carboxyamide and amine. HMBC correlations between the methine carbon (δ_C 63.1 d, C-2) and H-3b (δ_H 2.22), C-3 (δ_C 28.7, CH_2) and H-2, C-5 (δ_C 48.7) and H-3b reinforced this structure. H-2 (δ_H 4.21) was connected through HMBC correlation to a carbon that resonated at δ_C 173.4, which was assigned as C-1 of this residue. No HMBC or ROESY correlations were present, which could prove the ring closure. However, the chemical shifts of the H-5a, H-5b and C-5 (δ_H 3.44 and 3.69, δ_C 48.7) indicated their vicinity to a nitrogen atom. Besides, none of the carbons or protons of this residue exhibited correlations with any of the amide protons, indicating a tertiary amide. In addition, the chemical shifts of the carbons and protons were similar to those of proline in TA1909 (**2**), in which a ^3J HMBC correlation between C-2 (δ_C 63.0) and H-5b (δ_H 3.71) was observed, indicating the closure of a pyrrolidine ring. Based on the above evidences, the structure of this amino acid was established as proline.

The structure elucidation of [14]leucine started with COSY correlations of two methyl groups resonating at δ_H 0.92 and 0.82 (H_3-5 and H_3-6, respectively) with the same methine proton that resonated at δ_H 1.68 (H-4). In the HMBC spectrum, H_3-5 and -6 exhibited correlations with a methine carbon (δ_C 24.8, C-4) and a methylene carbon, (δ_C 38.7, C-3, δ_H 1.51 and 1.78, H-3a and H-3b, respectively). H-3a and H-3b exhibited COSY correlations with a proton resonating at δ_H 3.91 (H-2), which, in turn, was correlated with the amide proton resonating at δ_H 7.72. HMBC correlation connected H-2 and one of three carbons resonating at δ_C 173.7–173.8. This HMBC correlation was weak, but the connectivity was reinforced by the HMBC correlation of this carbon with the amide proton δ_H 7.64 of the adjacent amino acid, [15]Aib.

The structure elucidation of [16]isoleucine started with COSY correlation of protons of a doublet methyl, (H_3-6, resonating at δ_H 0.86, δ_C 15.7) with a methine proton, H-3 (δ_H 1.88). Methine-3 carbon (δ_C 35.6) exhibited HMBC correlations with the protons of CH_3-6, the protons of an additional triplet methyl group (δ_H 0.82) and protons of a methylene (δ_H 1.20 and 1.47, δ_C 25.0 by HSQC). COSY correlations of the methylene protons with the methyl protons at δ_H 0.82 determined the ethyl segment. COSY correlations coupled the ethyl moiety through the methine proton at 1.88 ppm to a downfield shifted methine (H-2, δ_H 3.93, C-2, δ_C 58.9) and the later to an amide proton resonating at δ_H 6.96. H-2 presented an HMBC correlation to a carbon resonating at δ_C 170.6 that was assigned as the carboxyamide carbon of the isoleucine residue. In the ^{13}C NMR spectrum, three carbons resonate at 173.7–173.8 ppm. Two of them were attributed to [11]leucine and [14]leucine. The third one exhibited an HMBC correlation to a proton that resonated at 2.37 ppm

(H-4b, δ_C 30.4, $\delta_{H\text{-}4a}$ 2.25). The protons of the later methylene were coupled through COSY correlations to protons that resonated at δ_H 1.97 and 1.87 (H-3a and H-3b, δ_C 26.5), which, in turn, were connected to an α-proton resonating at 4.06 ppm and to an amide proton (δ_H 7.68). HMBC correlations of the carbon resonating at δ_C 171.3 with the protons at δ_H 4.06, 1.97 and 1.87 established it as the glutamic acid carboxamide, establishing the structure of ^{17}glutamic acid.

The four aromatic carbons presented in the ^{13}C spectrum were assigned to ^{19}phenylalaninol. The carbon at δ_C 139.2 was identified as a quaternary carbon and the other three carried protons (δ_C 126.0, δ_H 7.12), (δ_C 128.2, δ_H 7.18) and (δ_C 129.4, δ_H 7.21). The signal intensity of the carbons and integration of the protons indicated that two pairs of symmetric aromatic protons resonate at 7.18 and 7.21 ppm and one proton resonates at δ_H 7.12 ppm, in accordance with a mono-substituted phenyl ring. COSY correlations coupled the later proton with the protons resonating at δ_H 7.18 (H-6,6′, δ_C 128.2) and to those resonating at δ_H 7.21 (H-5,5′, δ_C 129.4). This was reinforced by HMBC correlations (see Table 2). The assignment of the aliphatic part of the amino alcohol was based on HMBC correlations of the aromatic carbons, C-4 and C-5, with the two methylene protons, δ_H 2.84 and 2.61 ppm (H-3a, H-3b), which were coupled by COSY correlations to a methine proton resonating at δ_H 3.86 (H-2). This methine proton was connected to an amide proton (δ_H 7.27 ppm) and to the protons of an oxymethylene resonating at δ_H 3.29 and 3.32 (H-1a and H-1b, δ_C 62.7). The hydroxyl proton of the phenylalaninol did not appear in the NMR spectra of **1**, but was present in other trichorzianine: TA1895, TA1909, TA1909A, TA1896 and TA.Vb.

The assembling of the amino acids to the planar peptide structure was based on HMBC correlations from the carboxyamide carbon of an amino acid to the amide protons of the adjacent amino acid, by NOE correlations (from ROESY experiment) of the α- or amide proton of an amino acid with the α- or amide proton of the adjacent amino acid and by interpretation of MS/MS data. The structure of the peptide with the most significant HMBC and NOE correlations that led to the structure elucidation are summarized in Figure 2. The sequence Ac-^{1}Aib-^{2}Ala-^{3}Ala-^{4}Aib-^{5}Iva/Val was inferred from MS/MS data. ^{1}Aib carboxyamide carbon resonated (δ_C 175.7–175.9) closely with those of ^{7}Aib and ^{8}Aib, excluding an unequivocal proof of the HMBC correlation of ^{2}Ala-NH with ^{1}Aib-C-1.

The carboxyamides carbons of ^{2}Ala and ^{3}Ala resonated at the same chemical shift (δ_C 174.5), not allowing the confirmation of their connection by HMBC correlation, but NOE correlation of ^{2}Ala-NH with ^{3}Ala-NH confirmed their vicinity. NOE correlation of ^{3}Ala-H-2 with ^{4}Aib-NH and HMBC correlation of ^{4}Aib-C-1 with ^{5}Iva-NH established the ^{3}Ala-^{4}Aib-^{5}Iva partial structure. The connection of ^{5}Iva with ^{6}Gln could not be proven either by HMBC or NOE correlations, since the carboxyamides of ^{5}Iva and ^{9}Aib (δ_C 174.6) and the doublet amide protons of ^{6}Gln and ^{10}Ser (δ_H 7.74) resonated at the same chemical shifts. The correlation of these chemical shifts (δ_C 174.6 with δ_H 7.74) in the HMBC map remained unequivocal, while no correlations between ^{5}Iva and ^{6}Gln were observed in the ROESY map. The MS/MS data suggested that ^{5}Iva was connected either to Gln or Aib. HMBC and especially NOE correlations (Table 2) confirmed the ^{6}Gln-^{7}Aib-^{8}Aib-^{9}Aib substructure, and in conjugation, with the MS/MS data, the ^{5}Iva-^{6}Gln-^{7}Aib-^{8}Aib-^{9}Aib-^{10}Ser sequence could be secured. ^{10}Ser was connected to ^{11}Leu based on the HMBC correlation of ^{10}Ser-carboxyamide with ^{11}Leu-NH. ^{11}Leu- and ^{14}Leu- carboxyamides resonated close one to the

other (δ_C 173.7–173.8), not allowing unambiguous assignment of their neighboring amino acid residues. However, NOE correlations of ^{12}Aib-NH with ^{11}Leu-NH and ^{13}Pro-5-Ha and 5-Hb established the ^{11}Leu-^{12}Aib-^{13}Pro sequence. HMBC correlation of ^{13}Pro-C-1 with ^{14}Leu-NH established the connectivity of the latter two amino acids. NOE correlations of ^{15}Aib-NH with ^{14}Leu-H-2 and ^{16}Ile-NH determined the ^{14}Leu-^{15}Aib-^{16}Ile fragment. The rest of the sequence, ^{16}Ile-^{17}Glu-^{18}Gln-^{19}Pheol, could be secured with correlations from the HMBC map, resulting in the full planar structure of **1**.

Figure 2. Structure of trichorzianine 1938 (**1**) with HMBC ( ) and ROESY ( ) correlations.

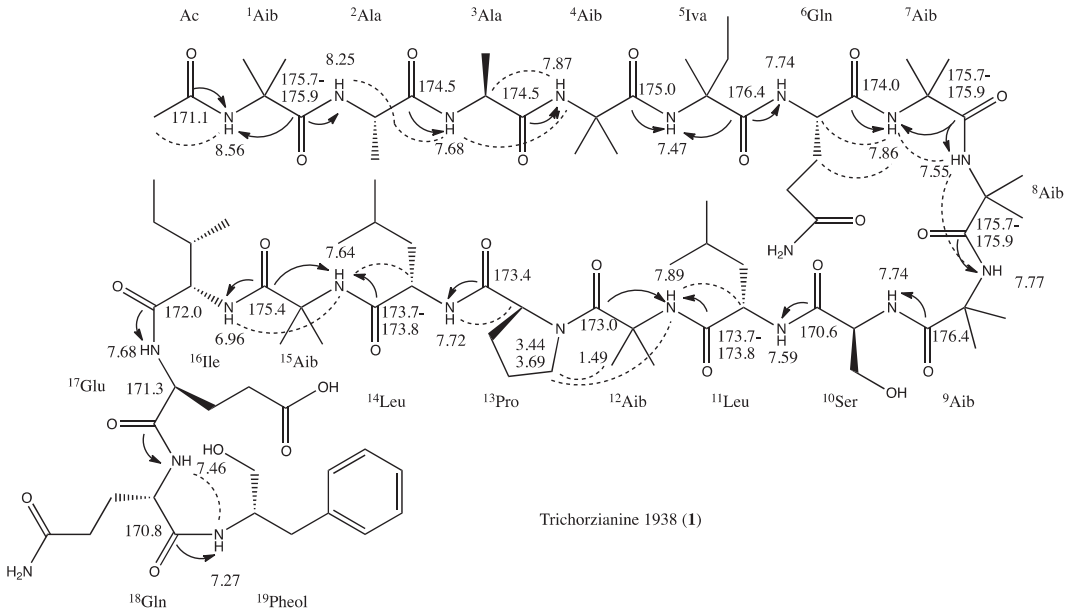

2.2. Structure Elucidation of **2**–**12**

The structures of compounds **2**–**12** were determined in a similar manner to that of TA1938 (**1**). Compounds **2**–**12** vary from **1** in the amino acid residues of positions 5, 9, 14 and 17. ^{1}H- and ^{13}C-NMR data of the new trichorzianines are summarized in Tables 3 and 4. Schemes of the secondary fragmentation in the MS/MS (Supplementary Figures S7–S15), complete NMR data (Supplementary Tables S2–S12 and Figures S16–S29) and the assemblage of the amino acids to the planar peptide structures (Supplementary Figures S30–S40) of compounds **2**–**12** are displayed in the supplementary material. The presence of Glu-OMe in compounds **4**–**7** was supported by the direct connectivity of the OMe-proton signal with the side-chain carboxyl carbon of Glu.

Table 3. ^{1}H NMR chemical shifts of trichorzianines **2**–**8** in DMSO-d_6.

Position		TA1909 (2) [a]	TA1895 (3) [a]	TA1896 (4) [b]	TA1924 (5) [b]	TA1910 (6) [a]	TA1924a (7) [a]	TA1909a (8) [a]
Ac	2	1.93 s	1.92 s	1.92 s	1.92 s	1.92 s	1.93 s	1.93 s
^{1}Aib	3	1.35 s	1.35 s	1.35 s	1.35 s	1.35 s	1.36 s	1.36 s
	4	1.32 s	1.32 s	1.32 s	1.32 s	1.33 s	1.32 s	1.33 s
	NH	8.57 s	8.57 s	8.58 s	8.54 s	8.57 s	8.57 s	8.56 s
^{2}Ala	2	3.99 m	3.98 m	3.98 m	4.00 m	4.01 m	4.01 m	4.01 m
	3	1.31 d	1.31 d	1.31 d	1.30 d	1.31 d	1.31 d	1.31 d
	NH	8.27 d	8.27 d	8.27 d	8.24 d	8.26 d	8.27 d	8.25 d
^{3}Ala	2	3.99 m	3.99 m	3.98 m	4.02 m	4.01 m	4.01 m	4.01 m
	3	1.33 d	1.33 d	1.33 d	1.33 d	1.33 d	1.33 d	1.33 d
	NH	7.69 d	7.69 d	7.70 d	7.68 d	7.68 d	7.71 m	7.68 d
^{4}Aib	3	1.41 [d] s	1.39 [c] s	1.43 [c] s	1.43 s	1.45 [c] s	1.45 s	1.46 s
	4	1.36 [c] s	1.38 s	1.38 [d] s	1.35 s	1.35 [d] s	1.38 [c] s	1.35 [c] s
	NH	7.81 s	7.81 s	7.82 s	7.86 s	7.87 s	7.83 s	7.87 s
^{5}Iva/^{5}Aib	3a	1.44 s	1.42 [e] s	1.43 [c] s	2.20 m	2.21 m	1.44 s	2.21 m
	3b				1.62 m	1.62 m		1.62 m
	4	1.39 s	1.37 [d] s	1.35 s	0.73 t	0.73 m	1.36 [c] s	0.73 t
	5				1.35 [c] s	1.35 s		1.36 s
	NH	7.54 s	7.53 s	7.53 s	7.46 s	7.47 s	7.55 s	7.47 s
^{6}Gln	2	3.74 m	3.73 m	3.74 m	3.78 m	3.78 m	3.77 m	3.78 m
	3	1.98 m	1.99 m	1.99 m	1.95 m	1.97 m	1.97 m	1.97 m
	4a	2.13 m	2.13 m	2.13 m	2.14 m	2.14 m	2.15 m	2.14 m
	4b	2.23 m	2.23 m	2.23 m	2.23 m	2.23 m	2.23 m	2.23 m
	NH_2a	7.13 s	7.13 s	7.17 s	7.16 s	7.16 s	7.16 s	7.16 s
	NH_2b	6.75 s	6.75 s	6.75 s	6.74 s	6.77 s	6.76 s	6.76 s
	NH	7.74 m	7.74 m	7.74 m	7.72 m	7.73 m	7.77 m	7.73 m
^{7}Aib	3	1.41 [d] s	1.41 [c] s	1.44 s	1.42 [d] s	1.43 [c] s	1.45 [d] s	1.43 [d] s
	4	1.34 [c] s	1.37 [d] s	1.39 [d] s	1.35 [c] s	1.36 [d] s	1.35 [c] s	1.36 [c] s
	NH	7.90 s	7.89 s	7.89 s	7.84 s	7.90 s	7.86 s	7.90 s
^{8}Aib	3	1.46 [c] s	1.45 s	1.46 s	1.42 [d] s	1.45 [c] s	1.43 [d] s	1.43 [d] s
	4	1.38 [d] s	1.35 [d] s	1.39 [d] s	1.38 [c] s	1.35 [d] s	1.35 [c] s	1.39 [c] s
	NH	7.59	7.58 s	7.58 s	7.54 s	7.55 s	7.59 s	7.55 s
^{9}Ala/^{9}Aib	2	3.94 m	3.93 m	3.93 m		3.96 m		3.96 m
	3	1.40 d	1.40 d	1.40 d	1.46 s	1.40 d	1.48 s	1.40 d
	4				1.42 s		1.43 s	
	NH	7.73 m	7.73 m	7.73 m	7.75 s	7.72 s	7.79 s	7.72 s

Table 3. *Cont.*

[10]Ser	2	4.09 m	4.09 m	4.09 m	4.02 m	4.10 m	4.03 m	4.11 m
	3a	3.72 m	3.72 m	3.73 m	3.76 m	3.73 m	3.75 m	3.72 m
	3b	3.77 m	3.77 m	3.77 m	3.78 m	3.76 m	3.79 m	3.76
	OH	4.86 t	4.85 t	4.85 t	-	-	-	4.87 t
	NH	7.77 m	7.77 m	7.76 m	7.73 m	7.76 d	7.74 m	7.76 m
[11]Leu	2	4.27 m	4.27 m	4.27 m	4.28 m	4.28 m	4.27 m	4.28 m
	3a	1.54 m	1.52 m	1.53 m	1.55 m	1.55 m	1.56 m	1.55 m
	3b	1.67 m	1.65 m	1.66 m	1.68 m	1.67 m	1.70 m	1.67 m
	4	1.73 m	1.68 m	1.69 m	1.69 m	1.69 m	1.73 m	1.69 m
	5	0.76 d	0.77 d	0.77 m	0.76 d	0.78 d	0.76 m	0.78 d
	6	0.81 d	0.83 d	0.83 d	0.83 d	0.84 d	0.82 d	0.84 d
	NH	7.43 d	7.44 d	7.43 m	7.59 d	7.44 d	7.59 d	7.44 m
[12]Aib	3	1.40 s	1.38 [e] s	1.36 s	1.38 s	1.39 s	1.37 s	1.40 s
	4	1.46 s	1.45 s	1.47 s	1.48 s	1.46 s	1.49 s	1.49 s
	NH	7.78 s	7.91 s	7.89 s	7.93 s	7.91 s	7.92 s	7.93 s
[13]Pro	2	4.21 t	4.23 t	4.21 t	4.22 t	4.22 t	4.21 t	4.24 t
	3a	1.58 m	1.64 m	1.64 m	1.65 m	1.65 m	1.60 m	1.65 m
	3b	2.22 m	2.22 m	2.22 m	2.22 m	2.22 m	2.24 m	2.22 m
	4	1.84 m	1.84 m	1.84 m	1.86 m	1.86 m	1.86 m	1.86 m
	5a	3.38 m	3.47 m	3.47 m	3.52 m	3.48 m	3.45 m	3.48 m
	5b	3.71 m	3.69 m	3.69 m	3.67 m	3.70 m	3.70 m	3.70 m
[14]Leu/[14]Val	2	3.94 m	3.76 m	3.68 m	3.72 m	3.68 m	3.90 m	3.77 m
	3a	1.51 m	2.22 m	2.22 m	2.21 m	2.21 m	1.52 m	2.21 m
	3b	1.78 m					1.78 m	
	4	1.67 m	0.93 d	0.93 d	0.93 d	0.94 d	1.68 m	0.94 d
	5	0.91 d	0.86 d	0.86 d	0.87 d	0.89 d	0.92 d	0.88 d
	6	0.82 d					0.82 d	
	NH	7.74 m	7.59 m	7.59 m	7.58 m	7.59 d	7.72 m	7.60 d
[15]Aib	3	1.42 [d] s	1.43 s	1.42 [c] s	1.42 [d] s	1.43 [c] s	1.42 [d] s	1.45 [d] s
	4	1.35 [c] s	1.37 [d] s	1.35 s	1.35 [c] s	1.38 [d] s	1.36 [c] s	1.39 [c] s
	NH	7.63 s	7.48 s	7.45 s	7.43 s	7.43 s	7.63 s	7.43 s
[16]Ile	2	3.91 m	3.84 t	3.87 t	3.88 m	3.88 m	3.93 m	3.87 m
	3	1.87 m	1.88 m	1.88 m	1.88 m	1.88 m	1.88 m	1.88 m
	4a	1.20 m	1.20 m	1.20 m	1.20 m	1.20 m	1.20 m	1.20 m
	4b	1.47 m	1.47 m	1.47 m	1.50 m	1.50 m	1.47 m	1.50 m
	5	0.81 t	0.81 t	0.80 t	0.80 t	0.81 t	0.82 t	0.81 t
	6	0.85 d	0.85 d	0.85 d	0.84 d	0.85 d	0.86 d	0.86 d
	NH	6.96 d	7.22 m	7.20 m	7.20 m	7.21 m	6.94 d	7.22 m
[17]Gln/[17]Glu	2	4.03 m	3.95 m	4.01 m	4.01 m	4.02 m	4.06 m	3.97 m
	3a	1.85 m	1.90 m	1.98 m	1.95 m	1.95 m	1.87 m	1.90 m
	3b	1.94 m					1.97 m	
	4a	2.08 m	2.13 m	2.41 m	2.40 m	2.49 m	2.37 m	2.13 m
	4b	2.18 m	2.23 m	2.47 m	2.30 m	2.40 m	2.44 m	2.23 m
	NH	7.69 d	7.69 d	7.67 d	7.68 d	7.68 d	7.68 m	7.69 d
	OMe			3.55 s	3.55 s	3.55 s	3.54 s	
	NH_2a	6.72 s	6.72 s					6.72 s
	NH_2b	7.13 s	7.13 s					7.13 s

Table 3. *Cont*.

[18]Gln	2	4.04 m	4.00 m	4.01 m	4.03 m	4.03 m	4.06 m	4.03 m
	3a	1.83 m	1.81 m	1.83 m	1.81 m	1.83 m	1.83 m	1.85 m
	3b	1.70 m	1.70 m	1.70 m	1.70 m	1.72 m	1.70 m	1.72 m
	4a	2.03 m	2.04 m	2.05 m	2.05 m	2.05 m	2.05 m	2.05 m
	4b	1.97 m	1.97 m	1.97 m	1.97 m	1.98 m	1.97 m	1.98 m
	5							
	NH_2a	6.64 s	6.62 s	6.51 s	6.61 s	6.63 s	6.65 s	6.63 s
	NH_2b	7.10 s	7.07 s	7.05 s	7.04 s	7.07 s	7.10 s	7.07 s
	NH	7.47 d	7.44 d	7.45 d	7.44 d	7.46 d	7.48 d	7.46 d
[19]Pheol	1a	3.28 m	3.30 m	3.30 m	3.30 m	3.30 m	3.28 m	3.30 m
	1b	3.32 m	3.32 m	3.33 m	3.33 m	3.33 m	3.32 m	3.33 m
	2	3.86 m	3.84 t	3.86 m	3.86 m	3.86 m	3.87 m	3.86 m
	3a	2.61 dd	2.61 dd	2.61 dd	2.61 dd	2.62 dd	2.61 dd	2.63 dd
	3b	2.83 dd	2.83 dd	2.83 dd	2.84 dd	2.84 dd	2.84 dd	2.84 dd
	5	7.20 m	7.22 m	7.21 m	7.21 m	7.22 m	7.21 m	7.22 m
	6	7.19 m	7.18 m	7.19 m	7.19 m	7.20 m	7.19 m	7.20 m
	7	7.11 m	7.11 m	7.11 m	7.11 m	7.12 m	7.13 m	7.12 m
	OH	4.70 t	4.69 t	4.67 t				4.69 t
	NH	7.27 d	7.15 m	7.18 m	7.18 m	7.19 m	7.30 d	7.18 m

[a] Instrument ^{1}H frequency 400 MHz; [b] Instrument ^{1}H frequency 500 MHz; [c,d,e] These signals may interchange in columns.

Table 4. ^{13}C NMR data of new trichorzianines in DMSO-d_6.

Position		**TA1909 (2) [a]**	**TA1895 (3) [a]**	**TA1896 (4) [b]**	**TA1924 (5) [b]**	**TA1910 (6) [a]**	**TA1924a (7) [a]**	**TA1909a (8) [a]**
Ac	1	171.1 s	171.2 s	171.1s	171.0 s	171.1 s	171.1 s	171.1 s
	2	23.1 q	23.3 q	23.2 q	23.0 q	23.0 q	23.1 q	23.1 q
[1]Aib	1	176.0 [e] s	176.0 [e] s	175.9 [e] s	175.6 [e] s	175.8 s	175.9 [e] s	175.8 [e] s
	2	55.7 [d] s	55.8 [d] s	55.8 s	55.8 s	55.8 s	55.7 [d] s	55.8 [d] s
	3	26.5 [g] q	26.8 q	26.5 [g] q	26.5 q	26.5 q	26.5 q	26.3 q
	4	24.1 q	24.2 q	24.1 q	24.1 q	24.1 q	24.1 q	23.7 q
[2]Ala	1	174.8 s	174.6 s	174.6 s	174.5 s	174.6 s		174.6 s
	2	51.0 d	51.0 d	51.0 d	50.8 d	50.9 d	50.9 d	50.9 d
	3	16.8 q	16.8 q	16.8 q	16.8 q	16.9 q	16.8 q	16.9 q
[3]Ala	1	174.8 s	174.8 s	174.8 s	174.5 s	174.6 s	174.7 s	174.6 s
	2	51.4 d	51.3 d	51.3 d	51.0 d	51.1 d	51.2 d	51.1 d
	3	16.1 q	16.1 q	16.1 q	16.2 q	16.2 q	16.1 q	16.2 q
[4]Aib	1	175.0 s	175.0 s	175.0 s	175.0 s	175.0 s	175.0 s	175.0 s
	2	56.0 s	56.0 s	55.7 [d] s	55.9 [d] s	56.4 s	56.0 [d] s	56.4 s
	3	26.2q	25.8 [j] q	26.2 [g] q	26.5 q	26.0 [g] q	26.1 q	26.3 [g] q
	4	23.3 [f] q	22.6 [f] q	23.4 [h] q	22.9 [h] q	23.1 [f] q	22.5 [f] q	23.3 [f] q
[5]Aib/[5]Iva	1	176.0 [e] s	176.0 [e] s	175.9 [e] s	176.4 s	176.2 s	176.0 [e] s	176.2 s
	2	55.8 [d] s	55.7 [d] s	55.8 [d] s	58.6 s	58.5 s	55.8 [d] s	58.5 s
	3	26.7 [g] q	26.7 [g] s	26.5 [g] q	25.6 t	25.8 t	26.6 q	25.9 t
	4	22.6 q	22.8 [f] q	22.6 [h] q	7.4 q	7.4 q	22.7 [f] q	7.4 q
	5				22.7 [h] q	22.7 q		22.6 q

Table 4. *Cont.*

^{6}Gln	1	174.1 s	174.1 s	174.1 s	173.8 s	174.1 s	173.8 s	174.1 s
	2	56.2 ^{d} d	56.4 d	56.4 d	56.0 d	56.0 d	56.0 d	56.0 d
	3	26.2 t	26.5 t	26.2 t	26.2 t	26.2 t	26.2 t	26.2 t
	4	31.5 ^{c} t	31.5 ^{c} t	31.5 ^{c} t	31.6 ^{c} t	31.6 ^{c} t	31.5 ^{c} t	31.7 ^{c} t
	5	173.6 s	173.6 ^{k} s	173.6 ^{f} s	173.8 s	173.6 s	173.7 s	173.6 ^{f} s
^{7}Aib	1	176.0 ^{e} s	176.0 ^{e} s	176.0 ^{e} s	175.7 ^{e} s	176.0 ^{e} s	176.0 ^{e} s	176.0 ^{e} s
	2	56.0 s	56.0 s	55.9 ^{d} s	55.9 ^{d} s	56.4 ^{d} s	55.9 ^{d} s	56.2 ^{d} s
	3	26.4 ^{g} q	26.2 ^{j} q	26.5 ^{g} q	26.2 ^{g} q	26.3 ^{g} q	26.2 q	26.2 ^{g} q
	4	23.0 q	23.0 ^{f} q	22.9 ^{h} q	22.6 ^{h} q	22.7 ^{e} q	22.8 ^{f} q	22.9 ^{f} q
^{8}Aib	1	176.3 s	176.2 s	176.2 s	175.9 ^{e} s	176.4 s	175.6 s	176.4 s
	2	56.0 s	56.0 s	56.0 ^{d} s	56.1 ^{d} s	56.0 s	56.0 ^{d} s	56.1 ^{d} s
	3	26.8 ^{h} q	26.8 q	26.8 ^{g} q	25.8 ^{g} q	26.8 ^{g} q	26.6 ^{g} q	26.4 ^{g} q
	4	22.7 q	23.2 ^{h} q	23.3 ^{h} q	23.0 ^{h} q	22.9 ^{e} q	22.8 ^{f} q	23.2 ^{e} q
^{9}Ala/^{9}Aib	1	174.7 s	174.6 s	174.6 s	176.5 s	174.6 s	176.4 s	174.6 s
	2	51.9 d	51.8 d	51.8 d	56.0 ^{d} s	51.7 d	56.1 ^{d} s	51.7 d
	3	16.5 q	16.5 q	16.5 q	26.2 ^{g} q	16.5 q	26.5 ^{g} q	16.5 q
	4				23.2 ^{h} q		22.9 ^{f} q	
^{10}Ser	1	170.7 s	170.7 s	170.7 s	170.6 s	170.6 s	170.6 s	170.6 s
	2	58.3 d	58.2 d	58.2 d	58.8 d	58.1 d	58.9 d	58.1 d
	3	61.1 t	61.1 t	61.1 t	61.0 t	61.1 t	61.2 t	61.0 ^{h} t
^{11}Leu	1	173.5 s	173.3 s	173.3 s	173.5 s	173.3 s	173.7 s	173.3 s
	2	51.6 d	51.5 d	51.5 d	51.4 d	51.4 d	51.6 d	51.4 d
	3	39.5 t	39.5 t	39.5 t	39.8 t	39.8 t	39.2 t	39.8 t
	4	24.0 d	24.2 d	24.2 d	24.1 d	24.2 d	23.9 d	24.0 d
	5	20.6 q	21.0 q	20.8 q	20.8 q	20.9 q	20.5 q	21.0 q
	6	23.0 q	23.1 q	23.1 q	23.4 q	22.9 q	23.0 q	22.9 q
^{12}Aib	1	173.0 s	172.7 s	172.8 s	172.8 s	172.8 s	173.0 s	172.7 s
	2	55.9 s	56.4 s	56.1 ^{d} s	56.1 ^{d} s	56.2 ^{d} s	56.3 ^{d} s	56.1 ^{d} s
	3	25.6 q	26.3 ^{g} q	26.4 ^{g} q	26.4 ^{g} q	26.4 q	25.8 q	25.5 q
	4	23.4 ^{f} q	23.1 q	23.2 ^{h} q	22.6 q	23.0 q	23.1 q	22.9 q
^{13}Pro	1	173.4 s	173.8 s	173.8 s	173.7 s	173.8 s	173.3 s	173.8 s
	2	63.0 d	63.0 d	63.0 d	63.0 d	63.0 d	63.0 d	63.0 d
	3	28.8 t	28.8 t	28.8 t	28.7 t	28.7–28.8 t	28.7 t	29.1 t
	4	25.9 t	25.8 t	25.8 t	26.0 t	25.9 t	26.1 t	26.0 t
	5	48.7 t	48.6 t	48.6 t	48.5 t	48.6 t	48.7 t	48.6 t
^{14}Leu/^{14}Val	1	173.7	172.7	172.6	172.7 s	172.7 s	173.8 s	172.7 s
	2	53.1 d	61.0 d	61.1 d	61.1 d	61.1 d	53.6 d	61.1 ^{h} d
	3	38.7 t	28.8 d	28.8 d	28.8 d	28.7–28.8 d	38.7 t	28.8 d
	4	24.8 d	19.1 q	19.1 ^{k} q	19.1 q	19.2 q	24.8 d	19.2 q
	5	23.0 q	19.1 q	19.2 ^{k} q	19.2 q	19.1 q	23.0 q	19.2 q
	6	21.1 q					20.9 q	
^{15}Aib	1	175.4 s	175.7 s	175.6 s	175.6 s	175.7 s	175.3 s	175.7 s
	2	56.3 s	56.4 s	56.2 ^{d} s	55.9 ^{d} s	56.1 ^{d} s	56.2 ^{d} s	56.1 ^{d} s
	3	26.3 ^{g} q	26.4 ^{g} q	26.2 ^{g} q	26.6 ^{g} q	26.5 ^{g} q	26.1 ^{g} q	26.3 ^{g} q
	4	23.4 ^{f} q	23.4 ^{f} q	22.9 ^{h} q	23.3 ^{h} q	23.3 ^{f} q	23.4 ^{f} q	23.2 ^{f} q

Table 4. *Cont.*

[16]Ile	1	172.0 s	172.4 s	172.3 s	172.2 s	172.3 s	171.9 s	172.4 s
	2	58.9 d	59.6 d	59.5 d	59.5 d	59.5 d	58.9 d	59.6 d
	3	35.6 d	35.5 d	35.5 d	35.5 d	35.5 d	35.6 d	35.5 d
	4	25.0 t	25.4 t	25.3 t	25.4 t	25.4 t	25.0 t	25.4 t
	5	11.4 q	11.4 q	11.4 q	11.4 q	11.4 q	11.5 q	11.4 q
	6	15.7 q	15.7 q	15.7 q	15.7 q	15.7 q	15.7 q	15.7 q
[17]Glu/[17]Gln	1	171.5 s	171.8 s	171.4 s	171.6 s	171.4 s	171.1 s	171.8 s
	2	53.8 d	54.3 d	53.7 d	53.8 d	53.7 d	53.1 d	54.3 d
	3	27.1 t	26.8 t	26.0 t	26.3 t	26.3 t	26.5 t	26.8 t
	4	31.7 [c] t	31.8 [c] t	30.2 t	30.5 t	30.2 t	30.1 t	31.7 [c] t
	5	173.7 s	173.7 [k] s	173.0 s	172.9 s	173.0 s	172.9 s	173.7 [f] s
	OMe			51.4 q	51.4 q	51.4 q	51.4 q	
[18]Gln	1	170.9 s	171.0 s	170.9 s	170.9 s	170.9 s	170.8 s	171.0 s
	2	53.1 d	53.4 d	53.3 d	53.3 d	53.3 d	53.0 d	53.4 d
	3	27.7 t	27.5 t	27.5 t	27.5 t	27.5 t	27.7 t	27.4 t
	4	31.7 [c] t	31.7 [c] t	31.7 [c] t	31.7 [c] t	31.7 [c] t	31.6 [c] t	31.5 [c] t
	5	173.7	173.8 [k] s	173.5 [f] s	173.6 s	173.6	173.6 s	173.8 [f] s
[19]PheOH	1	62.7 t	62.9 t	62.8 t	62.8 t	62.8 t	62.7 t	62.9 t
	2	52.6 d	52.6 d	52.6 d	52.6 d	52.6 d	52.5 d	52.6 d
	3	36.7 t	36.7 t	36.7 t	36.7 t	36.7 t	36.6 t	36.7 t
	4	139.2 s	139.3 s	139.3 s	139.3 s	139.3 s	139.2 s	139.3 s
	5	129.4 d	129.4 d	129.4 d	129.4 d	129.4 d	129.4 d	129.4 d
	6	128.2 d	128.1 d	128.1 d	128.1 d	128.1 d	128.1 d	128.1 d
	7	126.0 d	126.0 d	125.9 d	126.0 d	126.0 d	126.0 d	126.0 d

[a] Instrument ^{13}C frequency 100 MHz; [b] Instrument ^{13}C frequency 125 MHz; [c,d,e,f,g,h,k] These signals may interchange in columns.

2.3. Determination of the Absolute Stereochemistry

Marfey's analysis [15] of TA1938 (**1**) using L-FDAA as derivatizing reagent established the L-configuration of Ile, Leu × 2, Glu × 3 (one from glutamic acid, two from glutamine), Pro and Ser. Advanced Marfey analysis [16] of TA1938 using L-FDAA and D-FDAA as derivatizing agents and analysis by LC/MS established the L-configuration of Ala × 2. Iva configuration was not established, and Aib is not chiral. Configuration of phenylalaninol was established as L in TA1909 (**2**) by Marfey's analysis preceded by Jones oxidation [17] and comparison to the Phe standard and assumed as L in other compounds, due to the similarity of their structures. Marfey's analysis of TA1910 (**6**) using L-FDAA as derivatizing reagent established the L-configuration of Ile, Leu, Glu × 3 (one from glutamic acid, two from glutamine), Pro, Ser and Val. Marfey's analysis of TA1895 (**5**) using L-FDAA as derivatizing reagent established the L-configuration of Val. The configurations of other amino acids were established by comparison of Marfey's chromatograms to those of TA1938 (**1**). Retention times were found similar, meaning that absolute configurations of amino acids are as in TA1938 (**1**). Marfey's analysis of TA1909 (**2**), TA1896 (**4**), TA1924 (**5**), TA1924A (**7**) and TA1909A (**8**) using L-FDAA was performed by comparison to Marfey's chromatograms of TA1938 (**1**) and other peptaibols.

2.4. Antibacterial Bioassay

The antibacterial activity of the isolated trichorzianines (**1**–**12**) was tested against five environmental bacteria and three laboratory bacterial strains (detailed in the Experimental Section). MIC (minimal inhibitory concentration) was designated as the lowest concentration in which bacterial growth was inhibited to 0%–10% and MEC (minimal effective concentration) as the lowest concentration in which bacterial growth was inhibited to 70%. The results that were obtained after 48 h of incubation are summarized in Figure 3.

Figure 3. Antibacterial activity of trichorzianines after 48 h (**A**) Minimal inhibitory concentration (MIC) (µg/mL); (**B**) minimal effective concentration (MEC) (µg/mL). + represents Gram-positive bacteria; −, Gram-negative bacteria. Value of 250 µg/mL means no activity (MIC > 200 µg/mL).

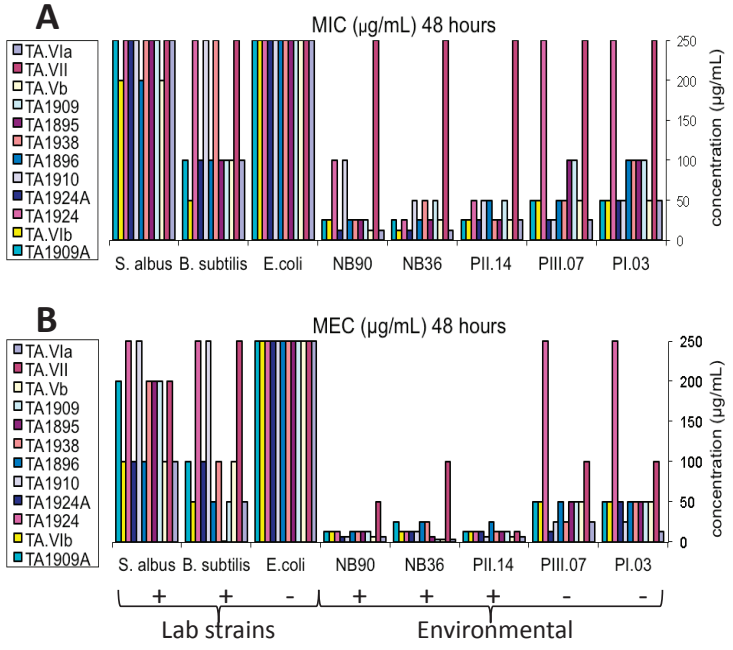

Examination of the trichorzianines activity (Figure 3) shows a general pattern. The tested trichorzianines exhibited stronger activity against environmental bacteria than against the laboratory strains. When compared within each group (environmental/laboratory), Gram-positive bacteria were more sensitive than Gram-negative bacteria (*E. coli* was resistant to all the tested compounds at all concentrations). Upon comparison of pairs of compounds differing in a single amino acid, no correlation was found between change in the amino acid sequence and activity.

3. Experimental Section

3.1. General Experimental Procedures

MS data were acquired using MALDI-Synapt Waters mass spectrometer using positive ES ionization. UV spectra were recorded on an Agilent 8453 spectrophotometer. Optical rotation values were obtained on a Jasco P-1010 polarimeter. IR spectra were recorded on a Bruker Vector 22 spectrophotometer. ^{1}H- and ^{13}C-NMR and 2D NMR data were recorded on spectrometers: Bruker ARX 500 (500.13 MHz for ^{1}H, 125.8 MHz for ^{13}C), Bruker AVANCE 400 (400.13 MHz for ^{1}H, 100.62 MHz for ^{13}C) and Bruker AVANCE 400 (400.17 MHz for ^{1}H, 100.63 MHz for ^{13}C), at room temperature, in 5 mm NMR tubes, with tetramethylsilane (TMS, δ 0.0 ppm) as the internal standard. COSY-45, gTOCSY, gROESY, gHSQC and gHMBC spectra were recorded using standard Bruker pulse sequences. HPLC chromatography rations were performed on Jasco (model PU-2080 plus intelligent pump, model LG-2080-04 plus quaternary gradient unit), Merck-Hitachi (model L-6200A intelligent pump, model L-4200 UV-Vis detector) and Agilent 1100 series HPLC system.

3.2. Biological Material

The sponge, *Axinella* sp., was collected by SCUBA diving at a depth of 19 m in the Mediterranean Sea, Akhziv, Israel. The sponge sample was sealed underwater in a bag with seawater and brought, cooled, to the laboratory for isolation and culturing of fungi. A pure fungal strain was obtained by inoculating slices of the sponge (initially rinsed with sterile Ca^{2+}- and Mg^{2+}-free artificial seawater) in potato dextrose agar (PDA, Difco) tubes containing chloramphenicol (0.25 g/L) and subsequent re-inoculations on PDA plates. Fungal genomic DNA was extracted from 15–20 mg of ground lyophilized mycelia grown in Potato Dextrose Broth (PDB, Difco), as described in [18]. The fungus was identified as *Trichoderma atroviride* based on its PCR-amplified ITS region, using primers ITS1 and ITS4 [19] and cycling parameters as in [20], followed by sequencing and comparison to the GenBank database (Trichokey [21], BLAST [22]). The strain was maintained on PDA. To determine the abundance of *T. atroviride* in the sponges, 25 new *Axinella* spp. specimens were collected. Pure fungal strains were isolated by dispersing 100 µL of the liquid obtained from a sponge sample ground by pestle and mortar on PDA plates containing chloramphenicol (0.25 g/L) and subsequent re-inoculations on PDA plates. Other details of fungal isolation were as described above. DNA was extracted by a protocol based on [23] using SDS–lysozyme-proteinase K lysis.

3.3. Culture Procedure

For the initial screening, a culture of 1 L of the fungus was grown. The culture was incubated for three weeks, at room temperature, in the horizontal position in 850-mL tissue culture flasks containing 200 mL of PDB. For the isolation of the active compounds, 15 L of the fungus were cultured in the same manner.

3.4. Isolation Procedure

The medium was filtered through glass wool to separate it from the mycelium and adsorbed on Amberlite XAD7HP, followed by washing of the organic compounds from the resin with acetone (method based on [24]). Briefly, after adding 20 g of Amberlite XAD-7-HP resin for each liter of medium, the medium was stirred for two h on a magnetic stirrer, followed by decanting the liquid. Then, the resin was washed with two small portions of acetone in order to remove water, extracted twice with acetone and washed with distilled water. The acetone was filtered and evaporated. The 15-L medium yielded 8.3 g of the crude extract. During initial separation, the fractionation was guided by ^{1}H-NMR and anti-bacterial assays. At the later stages of the separation, while according to NMR and MS spectra, it became clear that there was a mixture of peptaibols, it was determined by MS and MS/MS whether the fraction was pure or required further purification. The crude extract was separated on a Sephadex LH-20 column using MeOH–$CHCl_3$ (1:1). Fractions 1–6 from this separation (5.8 g) were further separated on a Sephadex LH-20 column using MeOH–$CHCl_3$ (2:1). Fractions 1–6 from this separation (4.2 g) were separated on an open column C_{18}-reversed phase column and eluted with solvent of decreasing polarity from water to methanol (10% steps of methanol each fraction). Fractions 8–11 and column wash in methanol (total weight 3.0 g) were separated on a Sephadex LH-20 using MeOH–$CHCl_3$ (1:1). Fractions 1–13 (2.7 g) were separated again on a Sephadex LH20, using MeOH–H_2O (7:3). Fractions 4–8 from this separation (2.36 g) were separated on an HPLC column (Hibar, Lichrospher 60 RP-Select B, 5 µm, 250 × 20 mm, flow rate 5 mL/min, UV detection, eluent 55–50:45–50 acetonitrile/water), to give 14 fractions, four of which (fractions 6 to 9) were found to be active. Fraction 7 (236 mg) was separated by HPLC (Hibar, Lichrospher 60 RP-Select B, 5 µm, 250 × 20 mm, flow rate 5 mL/min, UV detection, eluent 53:47 acetonitrile/aq. TFA (0.1%)) followed by HPLC separation (Cosmosil, 5C-8 MS Waters, 250 × 20 mm, UV detection, eluent with 81.5–83:18.5–17 methanol/aq. TFA (0.1%)) were used to afford TA1909 (t_R 92 min, 5.2 mg) and TA1895 (t_R 99 min, 3.7 mg). Fraction 6 (391.5 mg) was separated by HPLC (Hibar, Lichrospher 60 RP-Select B, 5 µm, 250 × 20 mm, flow rate 5 mL/min, UV detection, eluent 53:47 acetonitrile/aq. TFA (0.1%)) to two fractions: one yielded TA1896 (4.8 mg) and the second yielded, again, TA1909 (6.2 mg), as well as TA1895 (2.4 mg), by following HPLC separations. Fraction 8 (291.3 mg) was separated by repeated HPLC separations, resulting in TA1909a (2.2 mg), TA.VIb (5.2 mg), TA.Vb (9.7 mg), TA.VIa (1.8 mg), TA1924a (2.2 mg), TA.VII (1.9 mg) and TA1910 (4.0 mg). HPLC separations of Fraction 9 yielded TA1938 (7.8 mg), TA1924 (2.8 mg), TA.VIa (8.3 mg) and TA.VII (6.7 mg).

Trichorzianine 1938 (**1**): amorphous white solid; $[\alpha]_D^{29}$ −25 (*c* 0.68, MeOH); UV (MeOH) λ_{max} (log ε) 203 (4.61); IR (KBr) ν_{max} 3320, 2960, 2360, 1661, 1541, 1204 cm^{-1}; ^{1}H and ^{13}C NMR (see Table 2); HR TOF-MS-ES^{+} *m*/*z* 1961.1099 $[M + Na]^{+}$ (calcd for $C_{91}H_{151}N_{21}NaO_{25}$, 1961.1088). Retention time of amino acid (AA) Marfey's derivatives: L-Ile 44.5 min (D-Ile 47.1 min), L-Leu 45.3 min (D-Leu 47.7 min), L-Pro 35.8 min (D-Pro 36.4 min), L-Glu 32.7 min (D-Glu 33.6 min) and L-Ser 29.7 min (D-Ser 33.2 min). Advanced Marfey: L-Ala (L-Ala-L-FDAA, 3.40 min; L-Ala-D-FDAA, 3.99 min). Iva, not determined; Pheol, (L as in TA1909).

Trichorzianine 1909 (**2**): amorphous white solid; $[\alpha]_D^{29}$ −23 (*c* 0.4, MeOH); UV (MeOH) λ_{max} (log ε) 203 (4.46); IR (ATR probe) ν_{max} 3309, 1647, 1541, 1201 cm^{-1}; ^1H and ^{13}C NMR (see Tables 3 and 4 and Supplementary Table S3); HR TOF-MS-ES$^+$ *m/z* 1932.0946 $[M + Na]^+$ (calcd for $C_{89}H_{148}N_{22}NaO_{24}$, 1932.0935). Retention time of amino acid (AA) Marfey's derivatives: L-Ile 44.2 min (D-Ile 47.8 min), L-Leu 45.0 min (D-Leu 47.7 min), L-Pro 35.5 min (D-Pro 36.4 min), L-Glu 32.7 min (D-Glu 33.6 min), L-Pheol: as L-Phe 45.6 min (D-Phe 47.7 min), L-Ser 29.4 min (D-Ser 33.2 min) and Ala, (L as in TA1938).

Trichorzianine 1895 (**3**): white powder; $[\alpha]_D^{29}$ −32 (*c* 0.26, MeOH); UV (MeOH) λ_{max} (log ε) 203 (4.48); IR (ATR probe) ν_{max} 3308, 2936, 1638, 1537, 1202, 1047 cm^{-1}; ^1H and ^{13}C NMR (see Tables 3 and 4 and Supplementary Table S4); HR TOF-MS-ES$^+$ *m/z* 1918.0864 $[M + Na]^+$ (calcd for $C_{88}H_{146}N_{22}NaO_{24}$, 1918.0778). Retention time of amino acid (AA) Marfey's derivatives: L-Ile 44.3 min (D-Ile 47.8 min), L-Leu 45.0 min (D-Leu 47.7 min), L-Pro 35.6 min (D-Pro 36.4 min), L-Glu 32.7 min (D-Glu 33.6 min), L-Ser 29.5 min (D-Ser 33.2 min) and L-Val 40.9 min (D-Val 43.7 min). Pheol, (L as in TA1909); Ala, (L as in TA1938).

Trichorzianine 1896 (**4**): amorphous, white solid; $[\alpha]_D^{29}$ −18 (*c* 0.48, MeOH); UV (MeOH) λ_{max} (log ε) 203 (4.56); IR (ATR probe) ν_{max} 3312, 1653, 1540, 1201 cm^{-1}; ^1H and ^{13}C NMR (see Tables 3 and 4 and Supplementary Table S5); HR TOF-MS-ES$^+$ *m/z* 1933.0819 $[M + Na]^+$ (calcd for $C_{89}H_{147}N_{21}NaO_{25}$, 1933.0775). Retention time of amino acid (AA) Marfey's derivatives: L-Ile 44.3 min (D-Ile 47.8 min), L-Leu 45.1 min (D-Leu 47.7 min), L-Pro 35.7 min (D-Pro 36.4 min), L-Glu 32.7 min (D-Glu 33.6 min), L-Ser 29.6 min (D-Ser 33.2 min), L-Val 41.0 min (D-Val 43.7 min), Pheol, (L as in TA1909) and Ala, (L as in TA1938).

Trichorzianine 1924 (**5**): amorphous, white solid; $[\alpha]_D^{29}$ −17 (*c* 0.26, MeOH); UV (MeOH) λ_{max} (log ε) 203 (4.48); IR (KBr) ν_{max} 3335, 2966, 2363, 1663, 1541, 1207 cm^{-1}; ^1H and ^{13}C NMR (see Tables 3 and 4 and Supplementary Table S6); HR TOF-MS-ES$^+$ *m/z* 1961.1240 $[M + Na]^+$ (calcd for $C_{91}H_{151}N_{21}NaO_{25}$, 1961.1088). Retention time of amino acid (AA) Marfey's derivatives: L-Ile 44.4 min (D-Ile 47.8 min), L-Leu 45.1 min (D-Leu 47.7 min), L-Val 41.0 min (D-Val 43.7 min), L-Pro 35.7 min (D-Pro 36.4 min), L-Glu 32.7 min (D-Glu 33.6 min) and L-Ser 29.3 min (D-Ser 33.2 min). Iva, not determined; Pheol, (L as in TA1909); Ala, (L as in TA1938).

Trichorzianine 1910 (**6**): amorphous, white solid; $[\alpha]_D^{29}$ −36 (*c* 0.39, MeOH); UV (MeOH) λ_{max} (log ε) 203 (4.60); IR (ATR probe) ν_{max} 3310, 1654, 1541, 1217 cm^{-1}; ^1H and ^{13}C NMR (see Tables 3 and 4 and Supplementary Table S7); HR TOF-MS-ES$^+$ *m/z* 1947.0995 $[M + Na]^+$ (calcd for $C_{90}H_{149}N_{21}NaO_{25}$, 1947.0931). Retention time of amino acid (AA) Marfey's derivatives: L-Ile 44.5 min (D-Ile 47.8 min), L-Leu 45.3 min (D-Leu 48.1 min), L-Pro 35.8 min (D-Pro 37.0 min), L-Glu 33.4 min (D-Glu 34.1 min), L-Ser 29.8 min (D-Ser 33.6 min) and L-Val 41.2 min (D-Val 44.1 min). Iva, not determined; Pheol, (L as in TA1909); Ala, (L as in TA1938).

Trichorzianine 1924A (**7**): amorphous, white solid; $[\alpha]_D^{29}$ −30 (*c* 0.21, MeOH); UV (MeOH) λ_{max} (log ε) 203 (4.67); IR (ATR probe) ν_{max} 3310, 1655, 1541, 1204 cm^{-1}; ^1H and ^{13}C NMR (see Tables 3 and 4 and Supplementary Table S8); HR TOF-MS-ES$^+$ *m/z* 1961.1086 $[M + Na]^+$ (calcd for $C_{90}H_{149}N_{21}NaO_{25}$, 1961.1088). Retention time of amino acid (AA) Marfey's derivatives: L-Ile

44.4 min (D-Ile 47.8 min), L-Leu 45.2 min (D-Leu 48.1 min), L-Pro 35.7 min (D-Pro 37.0 min), L-Glu 32.7 min (D-Glu 34.1 min) and L-Ser 29.7 min (D-Ser 33.6 min), Pheol, (L as in TA1909); Ala, (L as in TA1938).

Trichorzianine 1909A (**8**): amorphous, white solid; $[\alpha]_D^{29}$ −49 (*c* 0.20, MeOH); UV (MeOH) λ_{max} (log ε) 203 (4.60); IR (ATR probe) ν_{max} 3312, 2292, 1661, 1541, 1204 cm^{-1}; ^1H and ^{13}C NMR (see Tables 3 and 4 and Supplementary Table S9); HR TOF-MS-ES$^+$ *m*/*z* 1932.1022 $[M + Na]^+$ (calcd for $C_{89}H_{148}N_{22}NaO_{24}$, 1,932.0935). Retention time of amino acid (AA) Marfey's derivatives: L-Ile 44.5 min (D-Ile 47.8 min), L-Leu 45.2 min (D-Leu 48.1 min), L-Val 41.1 min (D-Val 44.1 min), L-Pro 35.9 min (D-Pro 37.0 min), L-Glu 32.7 min (D-Glu 34.1 min) and L-Ser 29.7 min (D-Ser 33.6 min). Iva, not determined; Pheol, (L as in TA1909); Ala, (L as in TA1938).

3.5. Antibacterial Bioassay

Antibacterial activity of the fractions was tested against 3 environmental bacteria: 2 Bacilli from the same sponge from which the fungus was isolated (NB70, NB36) and *Sporosarcina* sp. from the sediment (NB90). Bacteria were cultured in 5 mL liquid media (Marine broth or Lennox broth) on a shaker. According to OD measurement at 620 nm, bacterial cultures were diluted with growth medium to a concentration giving OD absorbance of 0.4 at 620 nm, followed by an additional 1000-fold dilution. Tested fractions were diluted in DMSO to a concentration of 10 mg/mL, followed by further dilutions to 1, 0.5 and 0.25 mg/mL, 10% DMSO in purified water. The test was performed in 96 well plates, in three replicates for each concentration, each replicate on a different plate. The arrangement of the compounds on the plates was random. Into each well, 60 µL of growth media, 40 µL of the compound, and 100 µL of the diluted bacteria were added, to give a final concentrations of 0.2, 0.1 and 0.05 mg/mL, 2% DMSO. Plates were incubated on a shaker at 25 °C. OD was read at the beginning of the experiment (subtracted from later measurements) and after 24 and 48 h. The percentage of growth was calculated relatively to the positive control: a well containing the same bacteria in 2% DMSO without the compounds.

Antibacterial activity of the pure trichorzianines was tested on five environmental bacteria: from the sediment, *Sporosarcina* sp. (NB90), from the same sponge, *Bacillus* sp. (NB36), from *Axinella polypoides Microbacterium* sp. (PII.14), Rhodobacteraceae (PI.03), *Shewanella* sp. (PIII.07) and 3 laboratory strains (*S. albus*, *B. subtilis and E. coli*). Bacterial stocks were prepared as described above. Compounds were prepared in DMSO at a concentration of 20 mg/mL and diluted with purified water to 2 mg/mL, 10% DMSO. The test was performed in 96 well plates in liquid medium for bacterial growth (Lennox Broth or Marine Broth) with DMSO at a final concentration of 1% and a series of dilutions of the tested compound, the highest of which was 0.2 mg/mL (for some of the compounds two of the three replicates were prepared at lower concentrations). Into the well containing the highest concentration, 160 µL of medium and 40 µL of the sample (2 mg/mL, 10% DMSO) were added, to give a final concentration of 0.4 mg/mL, 2% DMSO. Into the other wells, 100 µL of the growth medium containing 2% DMSO were inserted, followed by the addition of 100 µL from the previous well. In this manner, a series of 2-fold dilutions was prepared in 2% DMSO, the highest concentration being 0.4 mg/mL. Subsequently, 100 µL of the bacteria were

added to each well, diluting their contents to 0.2 mg/mL at the highest concentration, 1% DMSO. OD at 620 nm was measured at the beginning of the experiment (subtracted from later measurements) and after 24 and 48 h of growth. The percentage of growth was calculated relative to the positive control: a well containing the same bacteria in 1% DMSO without the compounds.

4. Conclusions

The *Trichoderma atroviride* strain isolated from Axinellid sponge yielded 12 trichorzianines, eight of which are new and four known. The isolated peptaibols belong to the trichorzianine family. This family was previously isolated from *T. harzianum*, as well as *T. atroviride*. The profile of the peptaibols described here differs from previous reports on these compounds in *T. atroviride*: some of the new compounds include glutamic acid as the seventeenth residue, which contains only glutamine in all known trichorzianines. In contrast, not all of the known compounds were isolated here. For example, none of the isolated compounds contained glutamic acid as the eighteenth residue or tryptophanol as the nineteenth residue. In fact, some fractions contained Trpol, but further purification was impossible, due to the small available quantity of the material.

All isolated trichorzianines exhibited moderate antibacterial activity (MIC 12.5–200 µg/mL) against tested environmental bacteria, except for TA.VII, which showed no activity and TA1924 which did not inhibit Gram-negative bacteria. The absence of activity in tests as seen for TA.VII is not unusual and could indicate either activity on a narrow range of microorganisms or on antibacterial activity that is not expressed in the lab or in liquid medium. Laboratory bacterial strains were much more resistant to the peptaibols: *E. coli* exhibited no inhibition, and *S. albus* and *B. subtilis* were inhibited by some of the peptaibols (MIC 50–200 µg/mL).

Acknowledgments

We thank Noam Tal, The Mass Spectrometry Laboratory of The School of Chemistry, Tel Aviv University, for the mass spectra measurements. We thank Zahi Paz for help with fungal identification. We thank Markus Haber, Pierre Sauleau, Boaz Mayzel and Amir Gur from Micha Ilan's group, for the collection of the sponge samples. This study was supported by the Israel Science Foundation grant (ISF 996/06).

Conflicts of Interest

The authors declare no conflict of interest.

References

1. Chugh, K.J.; Wallace, B.A. Peptaibols: Models for ion channels. *Biochem. Soc. Trans*. **2001**, *29*, 565–570.

2. Schuhmacher, R.; Stoppacher, N.; Zeilinger, S. Peptaibols of *Trichoderma atroviride*: Screening, Identification, and Structure Elucidation by Liquid Chromatography-Tandem Mass Spectrometry. In *Communicating Current Research and Education Topics and Trends in Applied Microbiology*; Méndez-Vilas, A., Ed.; Formatex: Badajoz, Spain, 2007; pp. 609–617.
3. Kleinkauf, H.; Dohren, H. Nonribosomal biosynthesis of peptide antibiotics. *Eur. J. Biochem.* **1990**, *192*, 1–15.
4. Peptaibol Database. Available online: http://www.cryst.bbk.ac.uk/peptaibol (accessed on 14 May 2012).
5. Benitez, T.; Rincon, A.M.; Limon, M.C.; Codon, A.C. Biocontrol mechanisms of *Trichoderma* strains. *Int. Microbiol.* **2004**, *7*, 249–260.
6. Bodo, B.; Rebuffat, S.; El Hajii, M.; Davoust, D. Structure of Trichorzianine A IIIC, an antifungal peptide from *Trichoderma harzianum*. *J. Am. Chem. Soc.* **1985**, *107*, 6011–6017.
7. El Hajii, M.; Rebuffat, S.; Lecommandeur, D.; Bodo, B. Isolation and sequence determination of trichorzianines A antifungal peptides from *Trichoderma harzianum*. *Int. J. Peptide Prot. Res.* **1987**, *29*, 207–215.
8. Rebuffat, S.; El Hajii, M.; Hennig, P.; Davoust, D.; Bodo, B. Isolation, sequence and conformation of seven trichorzianines B from *Trichoderma harzianum*. *Int. J. Peptide. Prot. Res.* **1989**, *34*, 200–210.
9. Pocsfalvi, G.; Scala, F.; Lorito, M.; Ritieni, A.; Randazzo, G.; Ferranti, P.; Vekey, K.; Malorni, A. Microheterogeneity characterization of a trichorzianine-A mixture from *Trichoderma harzianum*. *J. Mass. Spectrom.* **1998**, *33*, 154–163.
10. Carroux, A.; van Bohemen, A.-I.; Roullier, C.; du Pont, T.R.; Vansteelandt, M.; Bondon, A.; Zalouk-Vergnoux, A.; Pouchus, Y.F.; Ruiz, N. Unprecedented 17-residue peptaibiotics produced by marine-derived *Trichoderma atroviride*. *Chem. Biodivers.* **2013**, *10*, 772–786.
11. Oh, S.U.; Lee, S.J.; Kim, J.H.; Yoo, I.D. Structural elucidation of new antibiotic peptides, atroviridins A, B and C from *Trichoderma atroviride*. *Tetrahedron Lett.* **2000**, *41*, 61–64.
12. Oh, S.U.; Yun, B.S.; Lee, S.J.; Kim, J.H.; Yoo, I.D. Atroviridins A–C and neoatroviridins A–D, novel peptaibol antibiotics produced by *Trichoderma atroviride* F80317. I. Taxonomy, fermentation, isolation and biological activity. *J. Antibiot.* **2002**, *55*, 557–564.
13. Stoppacher, N.; Reithner, B.; Omann, M.; Zeilinger, S.; Krska, R.; Schuhmacher, R. Profiling of trichorzianines in culture samples of *Trichoderma atroviride* by liquid chromatography/tandem mass spectrometry. *Rapid Commun. Mass Spectrom.* **2007**, *21*, 3963–3970.
14. Sabareesh, V.; Balaram, P. Tandem electrospray mass spectrometric studies of proton and sodium ion adducts of neutral peptides with modified *N*- and *C*-termini: Synthetic model peptides and microheterogeneous peptaibol antibiotics. *Rapid Commun. Mass Spectrom.* **2006**, *20*, 618–628.
15. Marfey, P. Determination of D-amino acids. II. Use of a bifunctional reagent, 1,5-fluoro-2,4-dinitrobenzene. *Carlsberg Res. Commun.* **1987**, *49*, 591–596.

16. Fujii, K.; Shimoya, T.; Ikai, Y.; Oka, H.; Harada, K. Further application of Advanced Marfey's method for determination of absolute configuration of primary amino compound. *Tetrahedron Lett*. **1998**, *39*, 2579–2582.
17. Bowden, K.; Heilbron, I.M.; Jones, E.R.H.; Weedon, B.C.L. Researches on acetylenic compounds. Part I. The preparation of acetylenic ketones by oxidation of acetylenic carbinols and glycols. *J. Chem. Soc*. **1946**, 39–45.
18. Gal-Hemed, I.; Atanasova, L.; Komon-Zelazowska, M.; Druzhinina, I.S.; Viterbo, A.; Yarden, O. Marine isolates of *Trichoderma* as potential halotolerant agents of biological control for arid-zone agriculture. *Appl. Environ. Microbiol*. **2011**, *77*, 5100–5109.
19. White, T.J.; Bruns, T.; Lee, S.; Taylor, J. Amplification and Direct Sequencing of Fungal Ribosomal RNA Genes for Phylogenetics. In *PCR Protocol: A Guide to Methods and Applications*; Innis, M.A., Gellfand, D.H., Sninisky, J.J., White, T.J., Eds.; Academic Press: New York, NY, USA, 1990; pp. 315–322.
20. Paz, Z.; Komon-Zelazowska, M.; Druzhinina, I.S.; Aveskamp, M.M.; Shnaiderman, A.; Aluma, Y.; Carmeli, S.; Ilan, M.; Yarden, O. Diversity and potential antifungal properties of fungi associated with a Mediterranean sponge. *Fungal Divers*. **2010**, *42*, 17–26.
21. International Subcommission on *Trichderma* and *Hypocrea* Taxonomy. Available online: http://www.isth.info (accessed on 11 August 2011).
22. National Center for Biotechnology Information. Available online: http://www.ncbi.nlm.nih.gov (accessed on 20 September 2012).
23. Pitcher, D.J.; Saunders, N.A.; Owen, R.J. Rapid extraction of bacterial genomic DNA with guanidinium thiocyanate. *Lett. Appl. Microbiol*. **1989**, *8*, 151–156.
24. Oh, D.C.; Jensen, P.R.; Fenical, W. Zygosporamide, a cytotoxic cyclic depsipeptide from the marine-derived fungus *Zygosporium masonii*. *Tetrahedron Lett*. **2006**, *47*, 8625–8628.

Chitosan-Alginate Biocomposite Containing Fucoidan for Bone Tissue Engineering

Jayachandran Venkatesan, Ira Bhatnagar and Se-Kwon Kim

Abstract: Over the last few years, significant research has been conducted in the construction of artificial bone scaffolds. In the present study, different types of polymer scaffolds, such as chitosan-alginate (Chi-Alg) and chitosan-alginate with fucoidan (Chi-Alg-fucoidan), were developed by a freeze-drying method, and each was characterized as a bone graft substitute. The porosity, water uptake and retention ability of the prepared scaffolds showed similar efficacy. The pore size of the Chi-Alg and Chi-Alg-fucoidan scaffolds were measured from scanning electron microscopy and found to be 62–490 and 56–437 μm, respectively. *In vitro* studies using the MG-63 cell line revealed profound cytocompatibility, increased cell proliferation and enhanced alkaline phosphatase secretion in the Chi-Alg-fucoidan scaffold compared to the Chi-Alg scaffold. Further, protein adsorption and mineralization were about two times greater in the Chi-Alg-fucoidan scaffold than the Chi-Alg scaffold. Hence, we suggest that Chi-Alg-fucoidan will be a promising biomaterial for bone tissue regeneration.

Reprinted from *Mar. Drugs*. Cite as: Venkatesan, J.; Bhatnagar, I.; Kim, S.-K. Chitosan-Alginate Biocomposite Containing Fucoidan for Bone Tissue Engineering. *Mar. Drugs* **2014**, *12*, 300–316.

1. Introduction

Bone, a complex and hierarchical tissue with a major portion made up of hydroxyapatite (HA) and collagen, plays a major role in the structural framework, mineral deposition, pH regulation and mechanical support. Bone defects or damages are possible in a number of ways, including motor accidents, birth defects and chronic diseases. Over 2.2 million-bone graft procedures are performed annually worldwide [1,2]. Several materials or treatment options are available to reconstruct bone defects, such as autograft, allograft, xenograft and synthetic graft. Autograft and allograft techniques are ideal bone graft procedures; however, a few concerns (such as problems of donor site morbidity, the availability of bone grafts for use with the autograft technique and the associated risk of transmissible diseases, for example, acquired immune deficiency syndrome (AIDS) or hepatitis in the allograft) exist. Recently, considerable attention has been given to synthetic tissue engineering scaffolds for the construction of artificial bone. Such synthetic bone grafts should be biocompatible, biodegradable, osteoconductive, osteoinductive and structurally similar to bone, with excellent mechanical strength, easy to handle and cost effective [2,3].

Chitin is a natural polysaccharide, and it is the most important polymer after cellulose. It occurs in the exoskeleton of arthropods or in the cells walls of fungi and yeast. An important derivative of chitin is chitosan. It is obtained by partial deacetylation of chitin using a chemical method (concentrated NaOH) or by enzymatic hydrolysis [4]. Chitosan (Chi) is composed of repeating units of D-glucosamine and *N*-acetyl glucosamine linked in a β (1-4) manner. Chitosan possesses excellent biocompatibility, biodegradation, antimicrobial activity and low immunogenicity. It can

be molded into various forms (gels, membranes, sponges, beads and scaffolds) and has an exceptional pore forming ability for potential applications in tissue engineering, drug delivery and wound healing [4,5]. Chitosan has been combined with a variety of biopolymers and bioceramic systems, such as alginate, hyaluronic acid, amylopectin, carbon nanotubes, poly(methyl methacrylate), polylactic acid, growth factors, HA and calcium phosphate [6–13]. Alginate (Alg) is an anionic linear copolymer that is made up of homopolymeric blocks of both (1-4)-linked β-D-mannuronate and α-L-guluronate residues. These homopolymeric blocks are covalently linked together in sequences that include blocks of alternating α-L-guluronate-β-D-mannuronate copolymer. Alginate is commonly isolated from marine seaweed. Similar to chitosan, alginate is also an exceptional biomaterial for bone tissue engineering, due to its biocompatibility, biodegradability, non-antigenicity, encapsulation capacity, chelating ability and ability to be cast in different forms, such as gels, microspheres, foams, fibers and sponges. Alginate scaffolds are often used for delivering materials, such as bone morphogenetic protein-2 (BMP-2) and mesenchymal stem cells (MSC) to the defective area for repairing the tissues [14,15]. Chi-Alg composites have been widely used for drug delivery and protein delivery [16–22], wound healing [23–25], tendon and ligament tissue engineering [26] and intervertebral tissue engineering [27]. In fact, a few reports are also available on a calcium-based composite using Alg-*N*-succinyl-chitosan for bone tissue regeneration [28]. Apart from this, Chi-Alg-MSC-BMP-2 composite was used to generate new bone [29].

Fucoidan is a sulfated polysaccharide that contains L-fucose and sulfate. It is commonly found in marine brown seaweeds. Fucoidan can increase the level of alkaline phosphatase (ALP), type-1 collagen expression, osteocalcin and BMP-2 and even helps in mineral deposition associated with bone mineralization [30,31]. In addition, fucoidan treatment enhanced the expression of ALP, type-1 collagen, Runt-related transcription factor 2 (Runx-2), osteopontin and osteocalcin in human adipose-derived stem cells. It also promoted osteogenic differentiation in human amniotic fluid stem cells, which suggested that it is a potential candidate for bone tissue regeneration [32]. Composite containing polycaprolactone-fucoidan showed excellent cellular proliferation and mineralization [33,34]. Around 30% enhanced mineral deposition was observed in fucoidan containing composite. This is mainly because of the presence of fucoidan in the composite scaffold. [31]. Moreover, Chi-fucoidan composite film showed significant wound dressing ability *in vitro* and *in vivo* [35].

Hence, considering the biocompatibility, biodegradation, antibacterial nature, film-forming ability and induction of osteogenic differentiation by fucoidan, Chi and Alg, we aimed to report the synthesis and characterization of the newly developed Chi-Alg biocomposite containing fucoidan for bone tissue engineering.

2. Results and Discussion

2.1. General Observation

In this study, scaffolds were fabricated by a freeze-drying method. The Chi-Alg and Chi-Alg-fucoidan scaffolds were found to be stiff and inelastic. Chi-Alg scaffolds were observed in

a colorless state, whereas Chi-Alg-fucoidan scaffolds obtained a pale brown color, which is due to the dispersion of fucoidan in the composites. By the visual observation (Figure 1), fucoidan was uniformly dispersed in the Chi-Alg composite, and no agglomeration was observed. The preparation procedure is graphically sketched and shown in Figure 1.

2.2. Fourier Transform-Infrared Spectroscopy

Alginate is an anionic polymer that possesses the ability to form strong electrostatic interaction with cationic polymers. In this case, the cationic charged amine group of the chitosan unit interacted electrostatically with the negatively charged alginate to form a polyelectrolyte mixture. The addition of fucoidan in the Chi-Alg may make more complex ionic interactions possible. Several studies suggested that hydrogen bonding or ion-ion pair interaction between the components usually increases the uniform dispersion [36]. These molecular chemical interactions between Chi-Alg and Chi-Alg-fucoidan were studied by FT-IR. FT-IR spectra were used to confirm the functional groups and interactions of chitosan, alginate, fucoidan, Chi-Alg and Chi-Alg-fucoidan scaffolds, and the spectra are depicted in Figure 2.

The alginate spectrum shows the characteristic peak at 1623 cm^{-1}, which corresponds to the carboxylate group (C=O). In addition, a strong intense peak was observed at 3446 cm^{-1}, corresponding to the –OH group. The symmetric stretching frequency of the carboxyl group was observed at 1418 cm^{-1}, whereas 1098–1026 cm^{-1} shows the asymmetric stretching frequency. Chitosan shows vibration at 3433 cm^{-1} (–OH and N-H stretching vibrations), 2855 cm^{-1} (C-H stretch), 1640 cm^{-1} (amide I), 1575 cm^{-1} (N-H bending of amine) and 1029 cm^{-1} (skeletal vibration of C-O stretching frequency).

On the other hand, in the case of Chi-Alg, an intense peak was observed at 1613 cm^{-1}, corresponding to the superposition of the bands assigned to the carboxylate group of alginate and the amine group of chitosan. The interaction from electrostatic interaction between the carboxylate group of alginate and the amine group of chitosan forms a polyelectrolyte complex. The results are consistent with previous studies [37]. The lower stretching frequency in –OH was observed from 3433 cm^{-1} to 3420 cm^{-1}. This suggests that intermolecular hydrogen bonds exist in the chitosan-alginate system [36].

Fucoidan exhibits its characteristic bands at 1210–1280 cm^{-1} assigned to the (S=O) group and a sharp band at 842 cm^{-1} assigned to the sulfate group in fucoidan [38]. The peaks at 3491 cm^{-1} corresponded to the –OH group on the fucoidan moiety. The corresponding stretching frequency of fucoidan is not clearly visible in the Chi-Alg-fucoidan composite. This may be due to the fact that the level of fucoidan in the Chi-Alg-fucoidan scaffold was too small to be detected.

Figure 1. Graphical representation of the chemical interaction of fucoidan incorporated alginate (Alg)-chitosan (Chi) composite scaffolds.

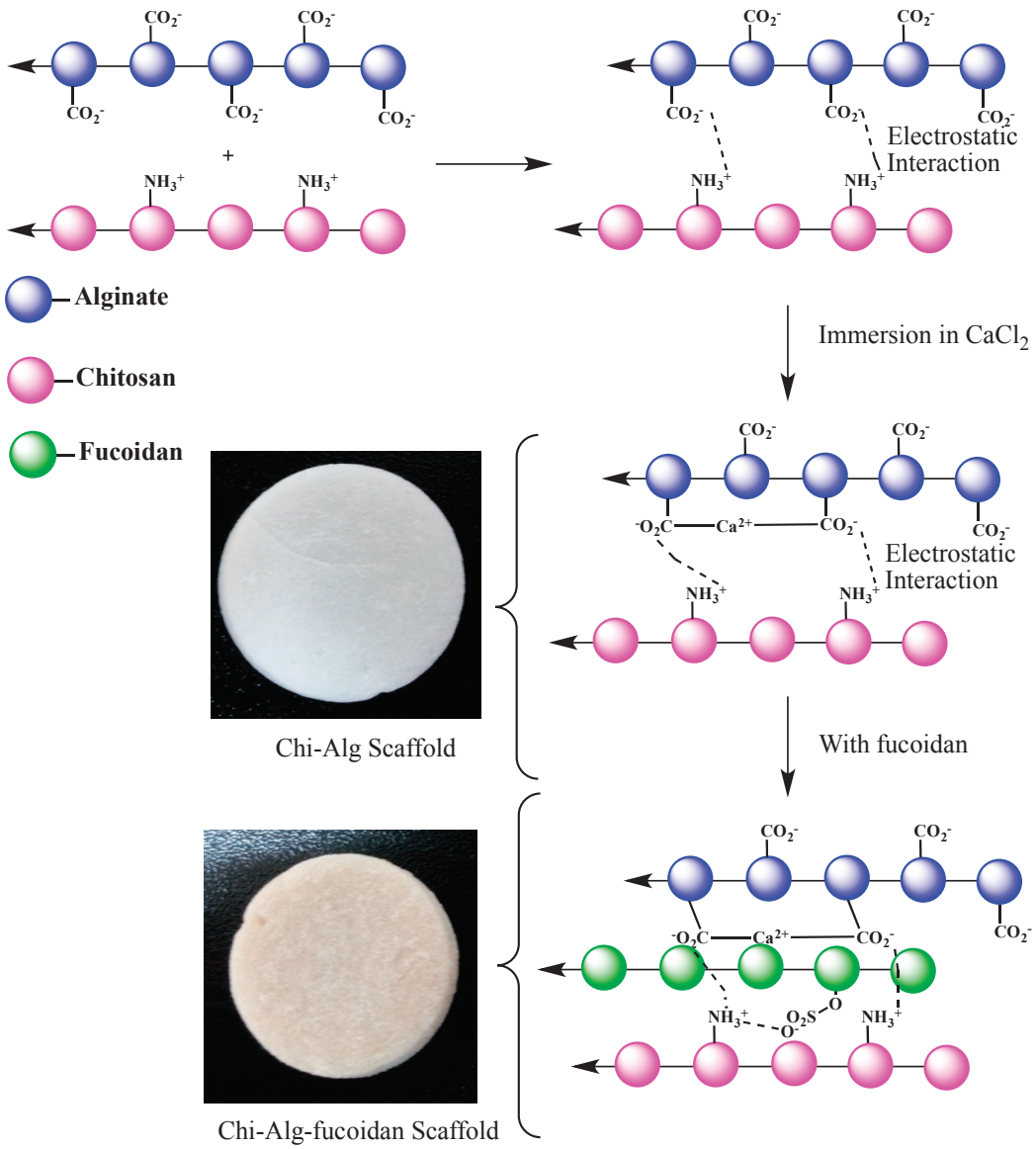

Figure 2. Fourier transform infrared spectrum of (**A**) chitosan, (**B**) alginate, (**C**) fucoidan, (**D**) Chi-Alg and (**E**) Chi-Alg-fucoidan.

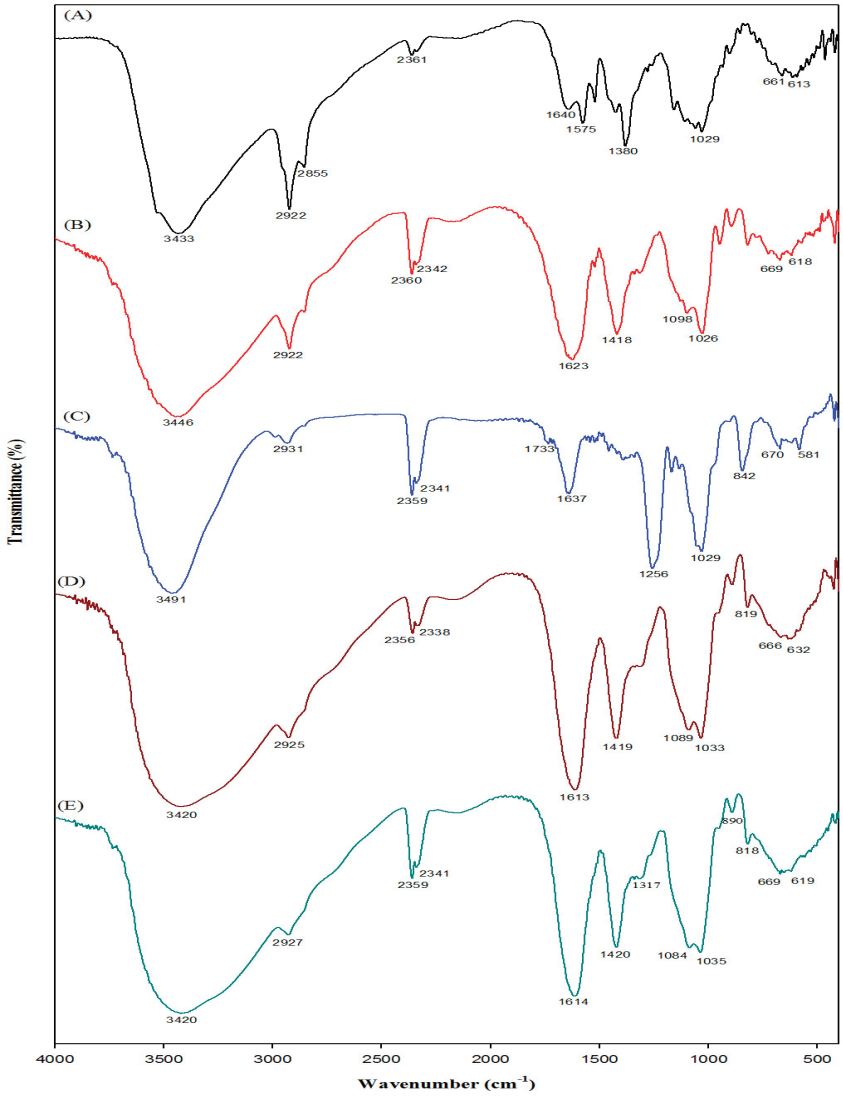

2.3. Porosity of the Scaffolds

The porosity of the prepared scaffolds was measured through the liquid displacement method using ethanol. The results suggest that the porosity of the scaffolds are >90%. The porosity of the Chi-Alg and Chi-Alg-fucoidan scaffolds were measured as 94.5% ± 0.5% and 94.9% ± 0.2%, respectively. Greater than 90% total porosity was observed for the polymeric scaffold, which could be an added advantage for tissue engineering purposes [39]. This high degree of porosity would allow cells to migrate into and populate within the scaffold.

2.4. Water Uptake and Retention Ability of the Scaffolds

The water uptake ability of the scaffolds is measured by the swelling behavior of the scaffold in phosphate buffer saline (PBS) solution. The water uptake and retention ability of the Chi-Alg and Chi-Alg-fucoidan were studied by immersing these scaffolds in 1× PBS solution (Figure 3a). The results showed that there are differences in the swelling behavior among the scaffolds, where the water uptake ability of the Chi-Alg-fucoidan scaffold was higher when compared to Chi-Alg. It has been reported earlier that alginate absorbs water quickly and holds 200–300 times its own weight of water [3]. The addition of negatively charged fucoidan increases the availability of free functional groups in the Chi-Alg-fucoidan system. Hence, the swelling behavior of Chi-Alg-fucoidan is higher compared to the Chi-Alg scaffold. The surface generally increases upon swelling of the scaffold, which is suitable for more cell adhesion and infiltration. Hence, as the Chi-Alg-fucoidan scaffolds exhibited increased swelling, the presence of fucoidan in the scaffolds would exhibit more surface area. The water retention ability of the Chi-Alg-fucoidan scaffold was comparatively less than the Chi-Alg scaffold. This may be due to the fact that unbound water molecules are easily removed from the surface of Chi-Alg-fucoidan scaffold.

2.5. Protein Adsorption Efficiency

The study of the protein adsorption of the prepared scaffold plays a significant role in *in vivo* study. Proteins, including fibronectin, vitronectin and other signaling molecules, can be adsorbed by the scaffolds from the circulating body fluids, which facilitate cell adhesion, proliferation and differentiation. The amount of adsorbed protein on the Chi-Alg and Chi-Alg-fucoidan scaffolds was measured with respect to time. The scaffolds were incubated with Dulbecco's Modified Eagle's Medium (DMEM) containing 10% Fetal Bovine Serum (FBS), and as shown in Figure 3b, Chi-Alg-fucoidan showed increased protein adsorption from the initial period of incubation. Increasing the incubation period further enhanced the protein adsorption, and the Chi-Alg-fucoidan scaffold showed three times more protein adsorption when compared to the Chi-Alg scaffold (Figure 3b). The negatively charged sulfate group in fucoidan might be electrostatically attracted to the positively charged amino acid in the FBS solution [40].

2.6. In Vitro Biodegradation Behavior

In vitro biodegradation is a crucial parameter to be considered in bone tissue engineering. The biodegradation of scaffolds provides space for tissue growth and matrix deposition. In the present study, no difference was observed in the biodegradation in Chi-Alg (15%) and Chi-Alg-fucoidan (15%) at 24 h. However, higher degradation was observed in the Chi-Alg-fucoidan scaffold (40%) compared to Chi-Alg (15.7%) at 72 h. This might be because of the electrostatic interactions between chitosan and fucoidan, as well as the weak ionic bonding forces between fucoidan and calcium in PBS.

Figure 3. (**a**) Water uptake and retention of Chi-Alg and Chi-Alg-fucoidan composite scaffolds after 24 h. (**b**) Protein adsorption studies of the Chi-Alg and Chi-Alg-fucoidan scaffolds in DMEM containing FBS at 37 °C at different intervals of 3 h, 12 h and 24 h. The values are the mean ± SD of a minimum of three replicates.

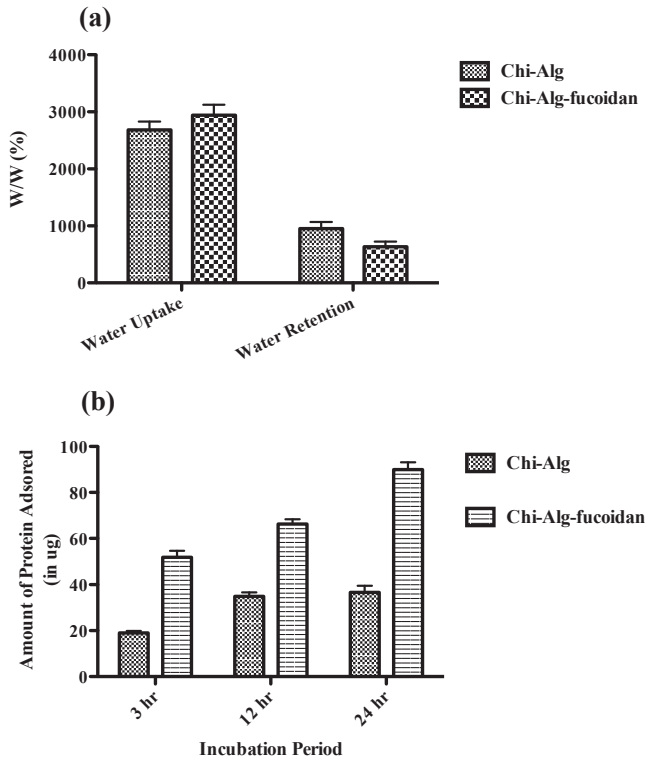

2.7. Scanning Electron Microscopy and Optical Microscopy Analysis

The surface morphology, pore distribution and pore size of Chi-Alg and Chi-Alg-fucoidan were examined using scanning electron microscopy analysis (Figure 4). The pore sizes of the scaffolds were directly measured in a scanning electron micrograph, and all the prepared scaffolds were found to be highly porous with a pore size of 62–490 µm and 56–437 µm for the Chi-Alg and Chi-Alg-fucoidan scaffolds, respectively. Negatively charged anionic fucoidan polymer interacted with chitosan and alginate. As a result, the pore size seemed to be decreased. Chi-Alg scaffolds showed well defined and interconnected pore structure, whereas the addition of fucoidan to the Chi-Alg composite resulted in reduced pore structure. The optimum pore size for bone tissue engineering remains unclear; however, investigations that sought to identify the optimum pore size for bone tissue engineering found pore sizes ranging from 80 to 500 µm to be viable [41]. The depicted pore size enables the scaffolds to allow for cell adhesion, proliferation and also nutrient supply, which will enable proper bone tissue growth. The optical microscopic images inferred that the dispersion of the components is uniform within the scaffolding network for both the Chi-Alg and Chi-Alg-fucoidan scaffolds.

Figure 4. High and low magnification SEM micrographs of (**a**, **b**) Chi-Alg and (**c**, **d**) Chi-Alg-fucoidan; and optical microscopy images of (**e**) Chi-Alg and (**f**) Chi-Alg-fucoidan.

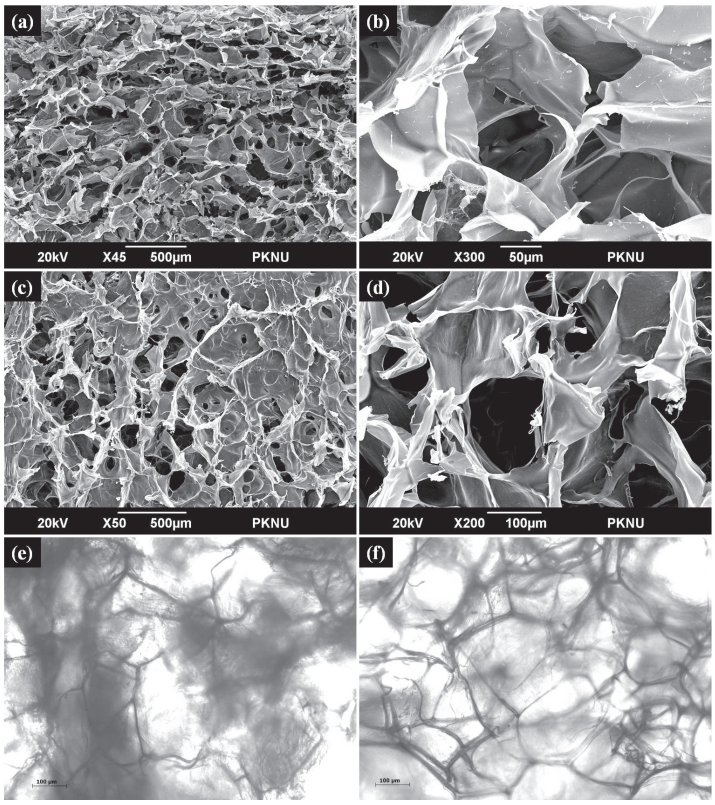

Pukyong National University (PKNU).

2.8. Biocompatibility of the Scaffolds

The toxicity and biocompatibility of the prepared scaffolds are important concerns before proceeding to the *in vivo* study. An ample number of assays are available to measure the cytotoxicity of the scaffolds, such as the MTT (3-(4,5-dimethylthiazole-2-yl)-2,5-diphenyl tetrazolium), WSTs (Water Soluble Tetrazolium salts) and LDH (Lactate dehydrogenase) assays. In the present study, we have used the MTT assay to measure the biocompatibility of the prepared scaffolds. This assay is based on the ability of cellular mitochondrial dehydrogenase to reduce the yellow-colored tetrazolium salt to blue-colored formazan crystals. Human osteoblast-like cells (MG-63) were used in the experiment to measure the toxicity level of the prepared scaffolds. Cell viability on the fabricated scaffolds (Chi-Alg and Chi-Alg-fucoidan) at different time intervals is shown in Figure 5. The prepared scaffolds are shown to be biocompatible and non-cytotoxic in nature. There is no difference in the viability and cell proliferation between Chi-Alg and Chi-Alg-fucoidan scaffolds after 48 h, confirming that the addition of fucoidan in the Chi-Alg composite shows no cytotoxicity.

Figure 5. Cell viability of the Chi-Alg and Chi-Alg-fucoidan composite scaffolds with the MG-63 cell line.

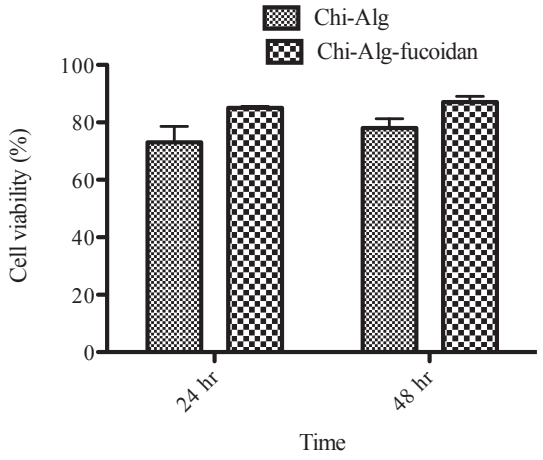

2.9. Alkaline Phosphatase Activity

The measured ALP activity of the scaffolds are shown in Figure 6. Significantly, very little difference was observed in the ALP level among the composite scaffolds (the Chi-Alg and Chi-Alg-fucoidan scaffolds). It is known that fucoidan can significantly enhance the expression of osteogenesis-specific marker genes alkaline phosphatase and osteocalcin [31,32]. Korean researcher, Cho *et al.* (2009) reported that *Undaria pinnatifida*-derived fucoidan significantly induced the osteoblastic differentiation required for bone formation, by increasing the activity of the phenotypic markers, alkaline phosphatase and osteocalcin [30]. The understanding of the actual role of fucoidan in ALP is apprehensive; this might be due to the presence of a sulfated group in fucoidan.

Figure 6. Alkaline phosphatase activity of the Chi-Alg and Chi-Alg-fucoidan scaffolds.

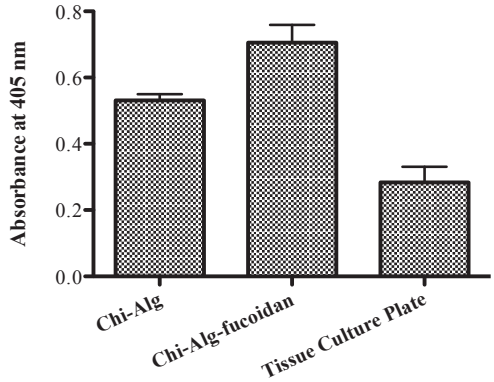

2.10. Mineralization Results

The low molecular weight of fucoidan suggested that it has the capacity to promote osteoblast proliferation, increase fibrillar collagen content and induce mineralization, which is essential for bone tissue growth [31]. One hundred micrograms per milliliter of fucoidan increased the amount of HA in cells, which was detected by alizarin red S staining. The mineralization increased dose-dependently with fucoidan [30]. The mineralization effect of the Chi-Alg and Chi-Alg-fucoidan scaffolds on MG-63 cells is shown in Figure 7. Mineralization was increased by the presence of fucoidan in the Alg-Chi-fucoidan scaffolds as compared to the Chi-Alg scaffolds. According to our previous study, an increased ALP level and HA deposition were observed by the addition of fucoidan (100 µg/mL) in the osteoblast-like cells, which is an important process for bone tissue regeneration *in vivo* [30].

Figure 7. Quantitative measurement of minerals by the cetylpyridinium chloride (CPC) method: (**a**) Chi-Alg and (**b**) Chi-Alg-fucoidan.

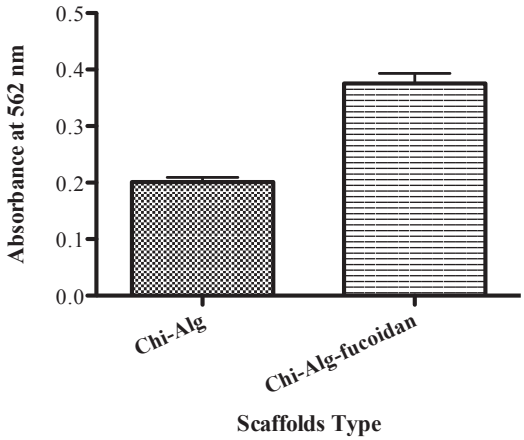

3. Experimental Section

3.1. Preparation of the Chitosan-Alginate (Chi-Alg) Scaffold

Alginate (3% w/v) was dissolved in 100 mL of water by using a mechanical stirrer (RW 20.n Lobortechik, Wasserburg, Germany) for 1 h to make a homogeneous solution. Secondly, chitosan (1% w/v, 310 kDa and 90%) was dissolved in 50 mL of 2% acetic acid solution and was carefully added into the alginate solution, with the help of a dropper. The homogeneous gel solution was stirred at 500 rpm for 1–2 h at room temperature. This gel solution was transferred into the tissue culture dish (35 × 10 mm^2) and frozen at −24 °C for 1 day and freeze dried to form scaffolds. These scaffolds were immersed or cross-linked with 10% $CaCl_2$ solution for 30 min, followed by soaking in absolute ethyl alcohol for 10 min. Finally, scaffolds were washed with an excess amount of water and freeze dried again for experimentation. In the present study, we have used Chi and Alg in a 3:1 weight ratio for the Chi-Alg scaffold fabrication.

3.2. Chitosan-Alginate-Fucoidan (Chi-Alg-Fucoidan) Scaffold

One hundred milligrams of fucoidan were added into the alginate solution, as prepared above, with the help of a dropper. This solution was mechanically stirred for 1 h to dissolve the entire fucoidan in the alginate solution to form a homogenous solution. Finally, chitosan (1% w/v) was dissolved in 50 mL of 2% acetic acid solution and was carefully added into the alginate-fucoidan solution, with the help of a dropper. This chitosan-alginate-fucoidan gel solution was transferred into the tissue culture dish, and the rest of the procedure was followed as described for the chitosan-alginate scaffold preparation. Ratios of Chi, Alg and Fucoidan of 3:1:0.1 weight were used in the construction of the Chi-Alg-fucoidan system.

3.3. Physicochemical Characterization

3.3.1. Fourier Transform-Infrared (FT-IR) Spectroscopy

FT-IR was used to characterize and to know the chemical interactions between the Chi-Alg and Chi-Alg-fucoidan scaffolds. The spectra of the chitosan, alginate, fucoidan, Chi-Alg and Chi-Alg-fucoidan composite scaffolds were recorded using the KBr pellet method in an FT-IR spectrophotometer (Perkin Elmer, Waltham, MA, USA) with the range of 4000 cm^{-1} to 400 cm^{-1}.

3.3.2. Porosity Measurement

The total porosity was determined by the liquid displacement method. Initially, the volume of the ethanol and the dry weight of the scaffolds were measured. Then, the scaffold was immersed into the dehydrated alcohol for 48 h until absorbing the alcohol saturated it, and the scaffold was weighed again. Finally, the porosity of the sample was calculated based on the following formula:

$$\text{Porosity} = (V_2 - V_1 - V_3)/(V_2 - V_3) \times 100 \quad (1)$$

where V_1 = the initial known weight of the scaffold, V_2 = the sum of the weights of ethanol and the submerged scaffold and V_3 = the weight of ethanol after the removal of the scaffold.

Three parallel sets were analyzed for every scaffold, and the mean value of the porosities of different scaffolds was achieved.

3.3.3. Water Uptake and Retention Abilities

The water uptake and retention ability of scaffold were studied, as described in our previous study [8,42]. Dry scaffolds were weighed (W_{dry}) and immersed in 1× PBS solution for 24 h. Then, the scaffolds were gently removed from the beaker after 24 h and placed on a wire mesh rack. Excessive water was drained, and the scaffolds were weighed (W_{wet}) after 5 min to determine the water uptake. To measure the water retention ability, the wet scaffolds were transferred to centrifuge tubes containing filter paper at the bottom, centrifuged (Combi 514-Hanil Science) at 500 rpm for 3 min and weighed immediately (W'_{wet}). The percentages of water absorption (EA) and water retention (ER) of the scaffolds at equilibrium were calculated using the following equations:

$$EA = [(W_{wet} - W_{dry})/W_{dry}] \times 100 \quad (2)$$

$$ER = [(W'_{wet} - W_{dry})/W_{dry}] \times 100 \quad (3)$$

3.3.4. Protein Adsorption Study

The protein adsorption ability of the Chi-Alg and Chi-Alg-fucoidan scaffolds was measured, as per a previous report [3]. Briefly, the scaffolds were equally cut into small pieces and placed in 24-well plates. The scaffolds were immersed in 100% ethanol for 1 h, and the ethanol was changed to 1× PBS for 30 min. After 30 min, the PBS was removed, and 500 µL of DMEM (Containing 10% FBS solution) were added to 24-well plates for 3 h, 12 h and 24 h to evaluate the protein adsorption amount corresponding to the different time periods. After a predetermined time, the scaffolds were blot dried and washed with 1× PBS 3 times to remove loosely adsorbed proteins. Proteins were agitated by incubating them in radioimmunoprecipitation (RIPA) buffer for 2 h. The eluted protein was measured by the absorbance at 570 nm using the bicinchoninic acid (BCA) protein assay method.

3.3.5. *In Vitro* Biodegradation Behavior

The rate of degradation of the biocomposite scaffolds was studied according to the previous method [3]. The Chi-Alg and Chi-Alg-fucoidan scaffolds were equally weighed, and the initial weight was recorded as W_I, followed by immersion in 1× PBS containing lysozyme (1000 U/L) and incubated at 37 °C at different intervals (24 and 72 h). After completion of the incubation period, the scaffolds were washed with deionized water to remove ions and blot dried with filter paper. The dry weights of the scaffolds were noted as (W_t). The degradation was calculated by using the following formula:

$$Degradation = (W_I - W_t)/W_I \times 100 \quad (4)$$

3.3.6. Scanning Electron Microscopy (SEM) and Optical Microscopy

The pore size and surface morphology of the biocomposite scaffolds were studied using scanning electron microscopy (SEM JSM-6490LV, JEOL, Tokyo, Japan). Briefly, scaffold samples were cut into small pieces and fixed on carbon tape, then dried under vacuum and gold coated before examining under SEM. In addition, optical microscopy was also performed with the prepared scaffolds using an optical microscope (CTR 6000; Leica, Wetzlar, Germany).

3.4. Cell Culture Studies

3.4.1. Cytotoxic Studies

The scaffolds (Chi-Alg and Chi-Alg-fucoidan) were cut into small pieces and placed in 24-well plates and incubated with cell culture media (DMEM) for 4 h at 37 °C in an incubator with 5% CO_2 and 95% air. The MTT assay was used to measure the cytotoxicity of the prepared scaffolds. Osteosarcoma MG-63 cells with the concentration of 1×10^5 cells/100 µL were seeded dropwise on

the small pieces of scaffold and incubated at 37 °C. The cell culture media was removed on the respective days and incubated with fresh medium containing 200 µL of MTT (3-(4,5-dimethyl thiazole-2-yl)-2,5-diphenyl tetrazolium) for 4 h in darkness. After the incubation period, the MTT dye was removed, followed by the addition of 200 µL DMSO to solubilize the formazan crystals, and optical densities (OD) were determined at 570 nm using a spectrophotometer (GENios R microplate reader; Tecan Austria GmbH, Grodig, Austria).

3.4.2. Alkaline Phosphatase Activity

For ALP activity, scaffolds were immersed in 500 µL of osteogenic differentiation medium (ODM) in 24-well culture plate for 3 h, and 5×10^4 cells/mL of MG-63 cells were seeded on the plate and kept for 7 days in the incubator. The ODM was replaced every 2 days. After the incubation, cells were rinsed with PBS, and 100 µL of 25 mM carbonate buffer (pH 10.3) containing 0.2% Tritox X-100 were added. Each well of the plate was transferred with 50 µL of 250 mM carbonate buffer (pH 10.3) containing 2.5 mM $MgCl_2$ and 15 mM *p*-nitro phenyl phosphate (*p*-NPP). The plate was incubated for 30 min at 37 °C, and the absorbance was measured at 405 nm in a spectrophotometer (Tecan Austria GmbH, Grodig, Austria).

3.4.3. Mineralization Assay

The mineralization assay was performed by alizarin red S stain. Briefly, scaffolds were immersed in ODM in a 24-well plate for 3 h. After 3 h, MG-63 cells were seeded dropwise into the plate (5×10^3 cells/100 µL). The media were changed every 2 days until 14 days, then the media were removed. The cells were washed twice by PBS and fixed in 70% ethyl alcohol for 1 h at room temperature. The ethyl alcohol-fixed cells and scaffolds were stained with 40 mM alizarin red S (pH 4.1) for 10 min. Cells were washed with deionized water five times and with PBS two times, then the cells were incubated in 10 mM of sodium phosphate buffer (pH 7.0) containing 10% of cetylpyridium chloride for 15 min. The optical density was measured at 562 nm using a GENios R microplate reader (Tecan Austria GmbH, Grodig, Austria).

3.5. Statistical Analysis

All the data are expressed as means ± the standard deviation of a minimum of three replicates for each scaffold in each experiment, using Graphpad Prism 5.0.

4. Conclusions

In this study, we prepared two different types of composite scaffolds. Chemical ionic interactions were observed between chitosan, alginate and fucoidan, which led to the improved bioactivity of the scaffolds. The addition of negatively charged and sulfated fucoidan in Chi-Alg showed a better activity towards bone tissue regeneration. Owing to the great water uptake ability, sufficient porosity, enhanced protein adsorption and increased mineralization effects, the Chi-Alg-fucoidan scaffolds would be promising biomaterials for bone tissue engineering.

Acknowledgments

This work was supported by a grant from the Marine Bioprocess Research Centre of the Marine Bio 21 Center funded by the Ministry of Land, Transport and Maritime, Korea.

Conflicts of Interest

The authors declare no conflict of interest.

References

1. American Academy of Orthopaedic Surgeons Home Page. Available online: http://www.aaos.org/news/aaosnow/jan08/reimbursement2.asp (accessed on 21 December 2013).
2. Giannoudis, P.V.; Dinopoulos, H.; Tsiridis, E. Bone substitutes: An update. *Injury* **2005**, *36*, S20–S27.
3. Sowjanya, J.; Singh, J.; Mohita, T.; Sarvanan, S.; Moorthi, A.; Srinivasan, N.; Selvamurugan, N. Biocomposite scaffolds containing chitosan/alginate/nano-silica for bone tissue engineering. *Colloids Surf. B Biointerfaces* **2013**, *109*, 294–300.
4. Jayakumar, R.; Menon, D.; Manzoor, K.; Nair, S.; Tamura, H. Biomedical applications of chitin and chitosan based nanomaterials—A short review. *Carbohydr. Polym.* **2010**, *82*, 227–232.
5. Muzzarelli, R.A. Chitins and chitosans for the repair of wounded skin, nerve, cartilage and bone. *Carbohydr. Polym.* **2009**, *76*, 167–182.
6. Di Martino, A.; Sittinger, M.; Risbud, M.V. Chitosan: A versatile biopolymer for orthopaedic tissue-engineering. *Biomaterials* **2005**, *26*, 5983–5990.
7. Pallela, R.; Venkatesan, J.; Janapala, V.R.; Kim, S.K. Biophysicochemical evaluation of chitosan-hydroxyapatite-marine sponge collagen composite for bone tissue engineering. *J. Biomed. Mater. Res. A* **2012**, *100*, 486–495.
8. Thein-Han, W.W.; Misra, R.D.K. Biomimetic chitosan–nanohydroxyapatite composite scaffolds for bone tissue engineering. *Acta Biomater.* **2009**, *5*, 1182–1197.
9. Venkatesan, J.; Pallela, R.; Bhatnagar, I.; Kim, S.-K. Chitosan–amylopectin/hydroxyapatite and chitosan–chondroitin sulphate/hydroxyapatite composite scaffolds for bone tissue engineering. *Int. J. Biol. Macromol.* **2012**, *51*, 1033–1042.
10. Zhang, Y.; Zhang, M. Synthesis and characterization of macroporous chitosan/calcium phosphate composite scaffolds for tissue engineering. *J. Biomed. Mater. Res.* **2001**, *55*, 304–312.
11. Croisier, F.; Jérôme, C. Chitosan-based biomaterials for tissue engineering. *Eur. Polym. J.* **2013**, *49*, 780–792.
12. Dash, M.; Chiellini, F.; Ottenbrite, R.; Chiellini, E. Chitosan—A versatile semi-synthetic polymer in biomedical applications. *Prog. Polym. Sci.* **2011**, *36*, 981–1014.
13. Venkatesan, J.; Kim, S.-K. Chitosan composites for bone tissue engineering—An overview. *Mar. Drugs* **2010**, *8*, 2252–2266.

14. Sun, J.; Tan, H. Alginate-based biomaterials for regenerative medicine applications. *Materials* **2013**, *6*, 1285–1309.
15. Lee, K.Y.; Mooney, D.J. Alginate: properties and biomedical applications. *Prog. Polym. Sci.* **2012**, *37*, 106–126.
16. Anal, A.K.; Stevens, W.F. Chitosan–alginate multilayer beads for controlled release of ampicillin. *Int. J. Pharm.* **2005**, *290*, 45–54.
17. Hamman, J.H. Chitosan based polyelectrolyte complexes as potential carrier materials in drug delivery systems. *Mar. Drugs* **2010**, *8*, 1305–1322.
18. Lai, H.L.; Abu'Khalil, A.; Craig, D.Q. The preparation and characterisation of drug-loaded alginate and chitosan sponges. *Int. J. Pharm.* **2003**, *251*, 175–181.
19. Lee, M.; Li, W.; Siu, R.K.; Whang, J.; Zhang, X.; Soo, C.; Ting, K.; Wu, B.M. Biomimetic apatite-coated alginate/chitosan microparticles as osteogenic protein carriers. *Biomaterials* **2009**, *30*, 6094–6101.
20. Mi, F.-L.; Sung, H.-W.; Shyu, S.-S. Drug release from chitosan–alginate complex beads reinforced by a naturally occurring cross-linking agent. *Carbohydr. Polym.* **2002**, *48*, 61–72.
21. Ribeiro, A.J.; Silva, C.; Ferreira, D.; Veiga, F. Chitosan-reinforced alginate microspheres obtained through the emulsification/internal gelation technique. *Eur. J. Pharm. Sci.* **2005**, *25*, 31–40.
22. Xu, Y.; Zhan, C.; Fan, L.; Wang, L.; Zheng, H. Preparation of dual crosslinked alginate–chitosan blend gel beads and *in vitro* controlled release in oral site-specific drug delivery system. *Int. J. Pharm.* **2007**, *336*, 329–337.
23. Hong, H.-J.; Jin, S.-E.; Park, J.-S.; Ahn, W.S.; Kim, C.-K. Accelerated wound healing by smad3 antisense oligonucleotides-impregnated chitosan/alginate polyelectrolyte complex. *Biomaterials* **2008**, *29*, 4831–4837.
24. Murakami, K.; Aoki, H.; Nakamura, S.; Nakamura, S.-I.; Takikawa, M.; Hanzawa, M.; Kishimoto, S.; Hattori, H.; Tanaka, Y.; Kiyosawa, T.; *et al.* Hydrogel blends of chitin/chitosan, fucoidan and alginate as healing-impaired wound dressings. *Biomaterials* **2010**, *31*, 83–90.
25. Wang, L.; Khor, E.; Wee, A.; Lim, L.Y. Chitosan-alginate PEC membrane as a wound dressing: Assessment of incisional wound healing. *J. Biomed. Mater. Res.* **2002**, *63*, 610–618.
26. Majima, T.; Funakosi, T.; Iwasaki, N.; Yamane, S.-T.; Harada, K.; Nonaka, S.; Minami, A.; Nishimura, S.-I. Alginate and chitosan polyion complex hybrid fibers for scaffolds in ligament and tendon tissue engineering. *J. Orthop. Sci.* **2005**, *10*, 302–307.
27. Shao, X.; Hunter, C.J. Developing an alginate/chitosan hybrid fiber scaffold for annulus fibrosus cells. *J. Biomed. Mater. Res. A* **2007**, *82*, 701–710.
28. Gomez d'Ayala, G.; De Rosa, A.; Laurienzo, P.; Malinconico, M. Development of a new calcium sulphate-based composite using alginate and chemically modified chitosan for bone regeneration. *J. Biomed. Mater. Res. A* **2007**, *81*, 811–820.
29. Park, D.J.; Choi, B.H.; Zhu, S.J.; Huh, J.Y.; Kim, B.Y.; Lee, S.H. Injectable bone using chitosan-alginate gel/mesenchymal stem cells/BMP-2 composites. *J. Cranio-Maxillofac. Surg.* **2005**, *33*, 50–54.

30. Cho, Y.-S.; Jung, W.-K.; Kim, J.; Choi, I.-W.; Kim, S.-K. Beneficial effects of fucoidan on osteoblastic MG-63 cell differentiation. *Food Chem.* **2009**, *116*, 990–994.
31. Changotade, S.; Korb, G.; Bassil, J.; Barroukh, B.; Willig, C.; Colliec-Jouault, S.; Durand, P.; Godeau, G.; Senni, K. Potential effects of a low-molecular-weight fucoidan extracted from brown algae on bone biomaterial osteoconductive properties. *J. Biomed. Mater. Res. A* **2008**, *87*, 666–675.
32. Park, S.-J.; Lee, K.W.; Lim, D.-S.; Lee, S. The sulfated polysaccharide fucoidan stimulates osteogenic differentiation of human adipose-derived stem cells. *Stem Cells Dev.* **2012**, *21*, 2204–2211.
33. Jin, G.; Kim, G.H. Rapid-prototyped PCL/fucoidan composite scaffolds for bone tissue regeneration: design, fabrication, and physical/biological properties. *J. Mater. Chem.* **2011**, *21*, 17710–17718.
34. Lee, J.S.; Jin, G.H.; Yeo, M.G.; Jang, C.H.; Lee, H.; Kim, G.H. Fabrication of electrospun biocomposites comprising polycaprolactone/fucoidan for tissue regeneration. *Carbohydr. Polym.* **2012**, *90*, 181–188.
35. Sezer, A.; Hatipoglu, F.; Cevher, E.; Oğurtan, Z.; Bas, A.; Akbuğa, J. Chitosan film containing fucoidan as a wound dressing for dermal burn healing: Preparation and *in vitro*/in vivo evaluation. *AAPS PharmSciTech* **2007**, *8*, E94–E101.
36. Zhang, L.; Guo, J.; Zhou, J.; Yang, G.; Du, Y. Blend membranes from carboxymethylated chitosan/alginate in aqueous solution. *J. Appl. Polym. Sci.* **2000**, *77*, 610–616.
37. Ho, Y.-C.; Mi, F.-L.; Sung, H.-W.; Kuo, P.-L. Heparin-functionalized chitosan–alginate scaffolds for controlled release of growth factor. *Int. J. Pharm.* **2009**, *376*, 69–75.
38. Rodriguez-Jasso, R.M.; Mussatto, S.I.; Pastrana, L.; Aguilar, C.N.; Teixeira, J.A. Microwave-assisted extraction of sulfated polysaccharides (fucoidan) from brown seaweed. *Carbohydr. Polym.* **2011**, *86*, 1137–1144.
39. Levene, H.B.; Lhommeau, C.M.; Kohn, J.B. Porous polymer scaffolds for tissue engineering. U.S. Patent 6103255 A, 15 August 2000.
40. Kim, S.; Pyo, H.-B.; Ko, S.H.; Ah, C.S.; Kim, A.; Kim, W.-J. Fabrication of anionic sulfate-functionalized nanoparticles as an immunosensor by protein immobilization. *Langmuir* **2010**, *26*, 7355–7364.
41. Fisher, J.; Reddi, A. Functional tissue engineering of bone: Signals and scaffolds. In *Topics in Tissue Engineering*; Ashammakhi, N., Ferretti, P., Eds.; University of Oulu: Oulu, Finland, 2003.
42. Venkatesan, J.; Qian, Z.-J.; Ryu, B.; Ashok Kumar, N.; Kim, S.-K. Preparation and characterization of carbon nanotube-grafted-chitosan—Natural hydroxyapatite composite for bone tissue engineering. *Carbohydr. Polym.* **2011**, *83*, 569–577.

Hyaluromycin, a New Hyaluronidase Inhibitor of Polyketide Origin from Marine *Streptomyces* sp.

Enjuro Harunari, Chiaki Imada, Yasuhiro Igarashi, Takao Fukuda, Takeshi Terahara and Takeshi Kobayashi

Abstract: Hyaluromycin (**1**), a new member of the rubromycin family of antibiotics, was isolated from the culture extract of a marine-derived *Streptomyces* sp. as a HAase inhibitor on the basis of HAase activity screening. The structure of **1** was elucidated through the interpretation of NMR data for the compound and its 3″-*O*-methyl derivative in combination with an incorporation experiment with [1,2-$^{13}C_2$]acetate. The compound's absolute configuration was determined by the comparison of its circular dichroism (CD) spectrum with those of other rubromycins. Hyaluromycin (**1**) consists of a γ-rubromycin core structure possessing a 2-amino-3-hydroxycyclopent-2-enone (C_5N) unit as an amide substituent of the carboxyl function; both structural units have been reported only from actinomycetes. Hyaluromycin (**1**) displayed approximately 25-fold more potent hyaluronidase inhibitory activity against hyaluronidase than did glycyrrhizin, a known inhibitor of plant origin.

Reprinted from *Mar. Drugs*. Cite as: Harunari, E.; Imada, C.; Igarashi, Y.; Fukuda, T.; Terahara, T.; Kobayashi, T. Hyaluromycin, a New Hyaluronidase Inhibitor of Polyketide Origin from Marine *Streptomyces* sp. *Mar. Drugs* **2014**, *12*, 491–507.

1. Introduction

Hyaluronidase (HAase)—an endoglycosidase—hydrolyzes hyaluronic acid (HA), the only non-sulfated glycosaminoglycan that is not attached to a core protein, which consists of a repeating unit of D-glucuronic acid and *N*-acetyl glucosamine. HA was synthesized by HA synthases which polymerize HA on the intracellular membrane surface. The HA polymers are extruded onto the glycocalyx or into the extra cellular matrix (ECM). HA exists mainly in the skin, primarily in the dermis, of mammalians and is degraded by various different HAases in the somatic cells in a step-by-step manner. HAase is found in a number of organisms, including mammals, bacteria (*Streptomyces* [1], *Streptococcus* [2]) and bacteriophages [3], as well as in the venom of terrestrial (bees [4], hornets [5], scorpions [6], snakes [7], lizards [8]) and marine (krill [9], lobster [10], fishes [11]) animals. One HAase is an acid-active enzyme in the mammalian circulatory system. Three types of eukaryotic HAase exist: Neutral-active endo-β-*N*-glucosaminidase, acidic-active endo-β-*N*-glucosaminidase, and endo-β-glucuronidase.

HAs have several functions in inflammation [12,13], immunity oncogenesis, *etc*., largely depending on the molecular size of the polymer. Low-molecular weight HAs stimulate angiogenesis [14] and the induction of chemokines [15] and cytokines [16–18], while high-molecular weight HAs suppress these phenomena [13,15,19]. Recently, extremely high-molecular weight HAs (6–12 MDa) were found in naked mole-rat (*Heterocephalus glaber*) fibroblasts [20]; these compounds were more than five times larger than human and mouse HAs (0.5–3 MDa) [21]. Although the naked mole rat is known as an exceptionally long-lived rat (40/86, many of which

were alive after 24 years) [22], surprisingly, neoplasms have never been found in the rat [22,23]. However, in the rats with HA synthase knockdown or HAase overexpression, tumor formation was observed [21].

HAase is some molecular target of anti-inflammatory and anti-allergic drugs. For example, anti-allergic agents such as disodium cromoglycate (DSCG) and tranilast and anti-inflammatory agents, like glycyrrhizin, demonstrate HAase inhibitory activity [24–26]. Further, the compound 48/80, a well-known histamine-releasing agent [27], also activates HAase [27]. Therefore, HAase inhibitors may become candidate compounds for anti-inflammatory drugs. In a previous study, various types of HAase inhibitors were reported: Proteins, glycosaminoglycans, polysaccharides, fatty acids, alkaloids, flavonoids, terpenoids, antioxidants, polyphenols, antibiotics, antinematodes, lanostanoids, synthetic organic compounds, glycosides and saponins [28]. However, very few studies have been reported on a screening of HAase inhibitor from microbial and marine-derived compounds. Also, the screening from actinomycetes has not been reported to the best of our knowledge.

The rubromycin family of antibiotics consists of reddish polyketide pigments produced by some groups of actinomycetes (*Streptomyces*, *Dactylosporangium* and *Actinoplanes*). These compounds possess a naphthoquinone ring and an isocoumarin ring connected through a 5,6-spiroketal system. The rubromycins α (**3**), β (**4**), γ (**5**) [29,30], δ and 3′-hydroxy-β-rubromycin [31]; the griseorhodins A (**6**), C (**7**) and G [32]; the DK-7814s A (**8**), B and C [33]; purpuromycin (**9**) [34] and heliquinomycin (**10**) [35] are compounds that are structurally related to the rubromycin family (Figure 1). Rubromycins show inhibitory activity against human telomerase and the reverse transcriptase of human immunodeficiency virus-1 [36]. α-Rubromycin (**3**) is the only compound in this family that lacks the spiroketal structure, and it displays much lower activity against telomerase and HIV reverse transcriptase-1 than its spiroketal congeners [36]; this suggests that the spiroketal system acts as a pharmacophore for telomerase and HIV inhibition. Further, several structurally related analogues of rubromycins also inhibit telomerase [37]. Heliquinomycin, a glycosylated derivative of the rubromycins, bears a cymarose moiety, and exhibits a DNA helicase inhibitory activity against a wide range of cancer cells [35].

The 2-amino-3-hydroxycyclopent-2-enone (C_5N unit) has been found to be a partial structure of polyketides from actinomycetes (Figure 2). Most of the C_5N unit-containing metabolites were isolated from *Streptomyces* and the others were isolated from *Micromonospora* (micromonospolide [38], R176502 [39]), *Kitasatospora* (bafilomycin B1 (**14**) [40], Sch 725424 [41]) and *Amycolatopsis* (ECO-0501 [42]). Compounds containing the C_5N unit include diverse structural types such as manumycins [43], moenomycins [44], bafilomycins [40], enopeptins [45], senacarcins [46], limocrocin (**17**) [47], reductiline [48], reductiomycins [49], virustomycins [50], ECO-02301 [51], ECO-0501 [42], and 2880-II [52]. The molecular weights of these compounds range from 300 to 1500 daltons. Although 2-acetamino-3-hydroxycyclopent-2-enone itself developed no microbial activity, in the case of manymycin A (**11**), acetylation of 3″-OH (**18**) and 2″-NH (**19**) in the C_5N unit led to a decrease of the biological activity [53]. Nisamycin (**20**), **11** that lacks the C_5N unit, displayed six-fold more active antimicrobial activity than alisamycin (**21**), the analog that contains the C_5N unit [54]. For the bafilomycins (**14**, **22** and **23**) and enopeptins (**16**, **25**, **26** and **27**), no significant differences were observed in the microbial activity of compounds

containing or lacking the C_5N unit [40,55]. Three bafilomycins compounds, bafilomycin A1 (**22**) (lacking the C_5N unit), **14** (containing the C_5N unit) and R176502 (**24**) (**14** analog) exhibited similar potency for the inhibition of tumor cell proliferation [39]. These results suggest that the 2-amino-3-hydroxycyclopent-2-enone sub-structure is not related to the biological activity of these compounds (Figure 3).

Figure 1. Natural rubromycins.

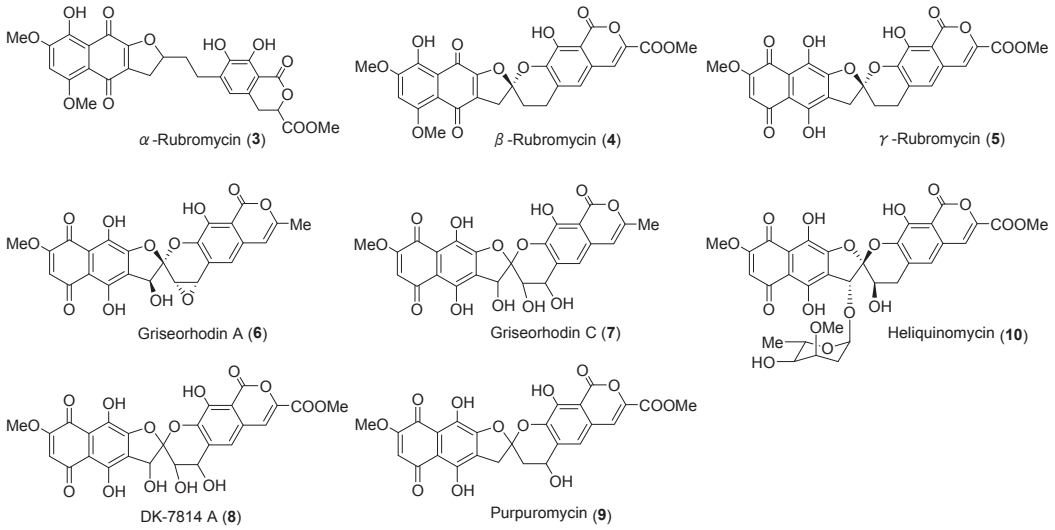

Figure 2. Natural products containing the C_5N substructure.

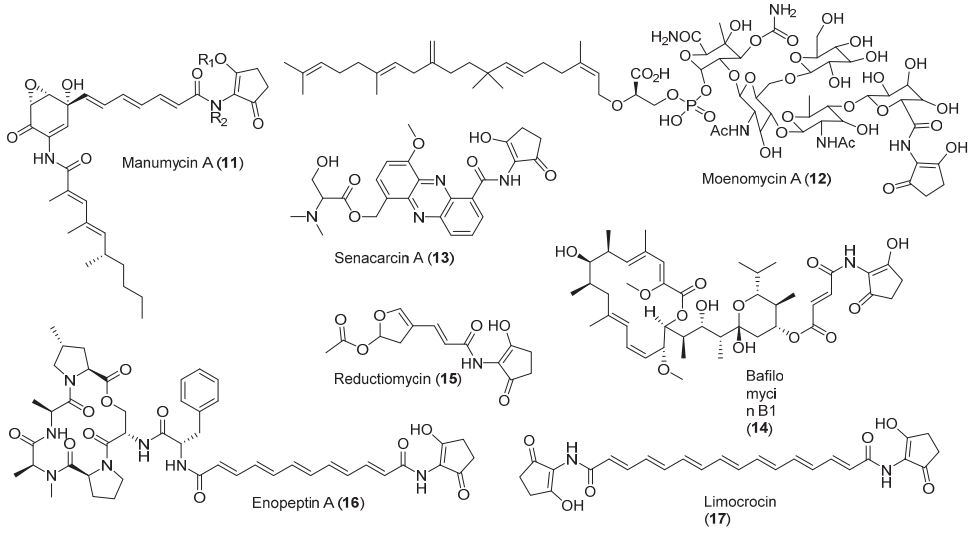

Figure 3. Families of compounds containing the C_5N substructure.

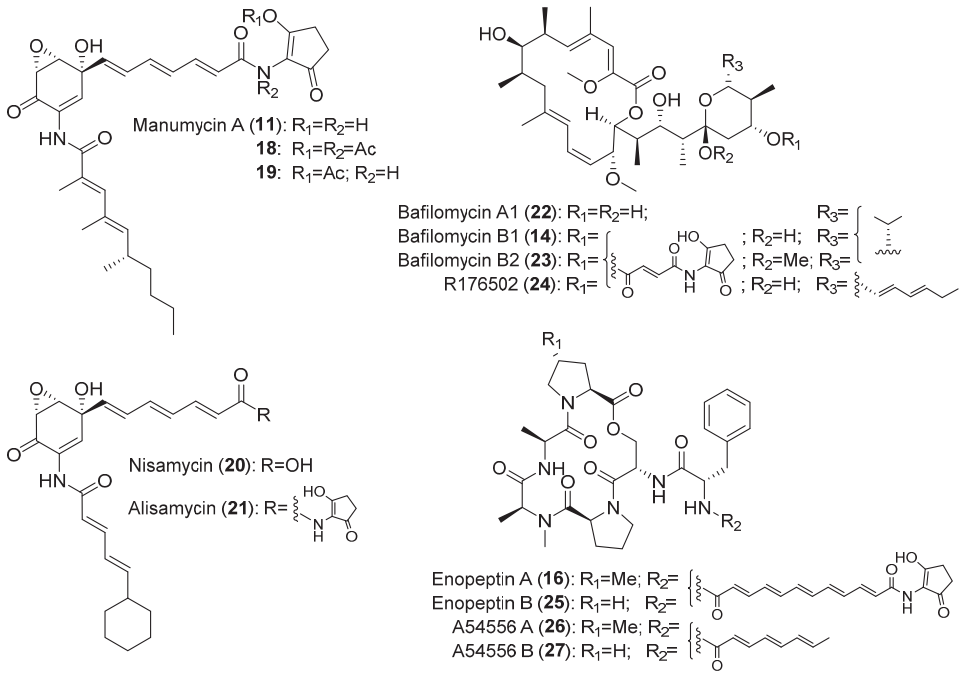

The objective of this study is to obtain a new type of HAase inhibitor as an anti-inflammatory candidate compound from marine derived-actinomycetes. In this paper, we report the isolation, structural elucidation and bioactivity of hyaluromycin (**1**) (Figure 4), a new member of rubromycin family, from the culture extract of the *Streptomyces* sp. strain MB-PO13 isolated from marine sea squirt (*Molgula manhattensis*). This strain was selected from approximately 1,000 marine organism-derived actinomycete strains through the screening of anti-inflammatory compounds on the basis of HAase inhibitory activity. In the last section of this paper, we report the results of the assays on the HAase inhibition of **1**, derivative **1**, rubromycins and glycyrrhizin, a known HAase inhibitor.

Figure 4. Structure of hyaluromycin (**1**).

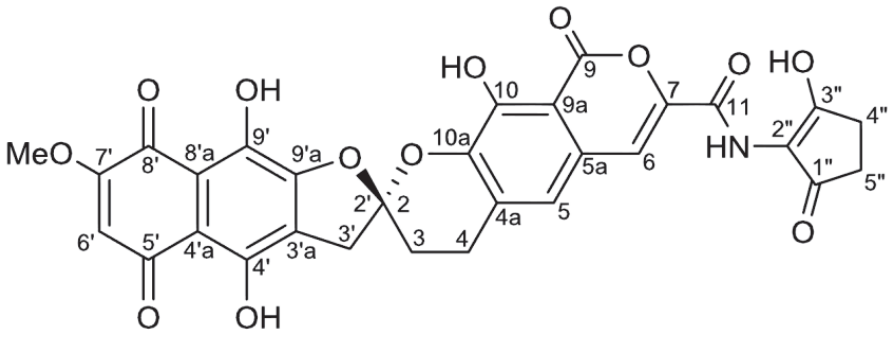

2. Results and Discussion

The producing strain MB-PO13 was cultured in A-3M medium at 30 °C for seven days, and the entire culture broth was extracted with EtOAc at pH 3. The extract was fractionated by reversed-phase column chromatography, followed by HPLC purification on a C18 column, to yield (**1**) as an optically active, red amorphous powder ($[\alpha]^{25}_{D}$ −168, DMSO). The molecular formula of $C_{30}H_{21}NO_{13}$ was confirmed by high-resolution ESITOFMS data showing a pseudomolecular ion $[M + H]^+$ at *m/z* 604.1091. The IR spectrum indicated the presence of hydroxyl (3357 cm^{-1}) and carbonyl (1693 cm^{-1}) functional groups. The UV spectrum showed absorption maxima at 307, 352, 368 and 506 nm similar to those of the rubromycin class of antibiotics [29–35].

The ^{1}H NMR spectrum of **1** measured in DMSO-d_6 indicated the presence of one methoxy (δ_H 3.89), three methine (δ_H 6.41, 7.25 and 7.52) and four exchangeable (δ_H 9.44, 10.67, 11.90 and 13.14) protons. In the ^{13}C NMR spectrum, all of the 25 carbons assignable to γ-rubromycin core were detected. Comparison with the MS data showed that five carbon atoms were lacking [31,56,57]. The ^{1}H-^{1}H COSY spectrum established only one H-3/H-4 spin system. Further HSQC and HMBC analysis allowed the assignment most of the ^{13}C signals except for C-9, C-8′a and C-9′ (Figure 5). An exchangeable proton at δ_H 9.44 showed a correlation with C-11, suggesting that this proton could be an amide proton.

Figure 5. ^{1}H-^{1}H COSY and HMBC correlations of compound **1**.

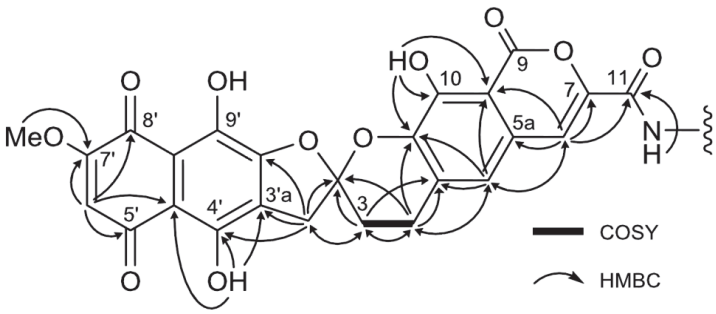

The NMR data and UV spectrum of **1** strongly indicated the presence of a γ-rubromycin (5) skeleton, but three carbons remained unassigned. Additionally, five further carbons were not detected in the ^{13}C NMR spectrum. To establish the aromatic polyketide structure, a feeding experiment was conducted using [1,2-$^{13}C_2$]acetate to obtain ^{13}C-enriched **1** for a 2D-INADEQUATE experiment. However, in the INADEQUATE spectrum, cross peaks were not observed because of the low concentration of **1** in NMR solvents. To improve its solubility, an *O*-methylation reaction of ^{13}C-labeled **1** was carried out using an excess of methyl iodide and 1,8-diazabicyclo[5,4,0]-7-undecene (DBU) in MeCN/acetone. The reaction proceeded smoothly at 50 °C, and the starting material (**1**) was consumed within 1 h. The crude extract contained a mixture of three *O*-methylated adducts, whose structures were deduced from LC/MS analysis, to be in order of elution, the mono-, di- and trimethyl derivatives of **1** (Figure 6). The monomethyl derivative (**2**) was purified by preparative HPLC, and its structure was determined as follows.

Figure 6. HPLC chromatogram of methylated derivatives of **1**.

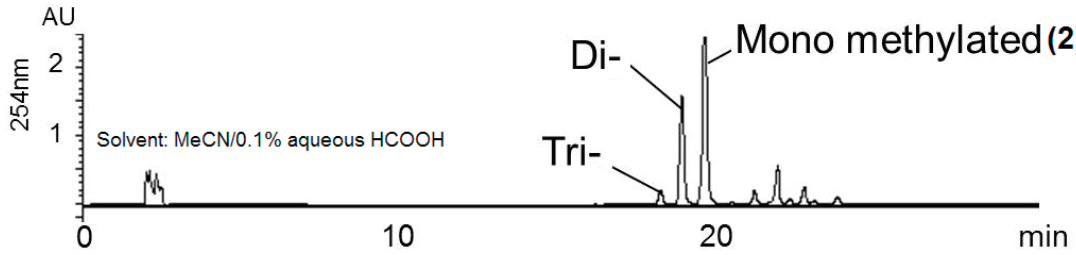

The solubility of [1,2-$^{13}C_2$]acetate-labeled **2** in DMSO-d_6 was much improved, allowing a high-quality ^{13}C NMR spectrum to be obtained in which 31 discrete resonances could be observed (Figure 7). Of these resonances, 25 carbons were readily assigned to the rubromycin core on the basis of HMBC correlations (Figure 8, Table 1). The three carbons C-9, C-8′a and C-9′ had no HMBC correlations but were assigned on the basis of the INADEQUATE experiments. In the 2D-INADEQUATE spectrum of [1,2-$^{13}C_2$]acetate-labeled **2**, with the parameters optimized for $^1J_{CC}$ 50 Hz, cross peaks were observed for all of the carbons of the rubromycin core structure: C-4a/C-5, C-5a/C-6, C-7/C-11, C-9/C-9a, C-10/C-10a, C-2′/C-3′, C-3′a/C-4′, C-4′a/C-5′, C-6′/C-7′, C-8′/C-8′a and C-9′/C-9′a, with the exception of C-3/C-4 (Figure 9a). Because the coupling constant for C-3/C-4 read from the ^{13}C NMR spectrum (Figure 7) was smaller (31.1 Hz), the INADEQUATE spectrum was measured with a parameter set optimized for $^1J_{CC}$ 35 Hz, which indicated a cross peak between C-3 and C-4 (Figure 9b), establishing the complete ^{13}C NMR assignment for the rubromycin core of **2** (Figure 9d). Although cross peaks were not observed for C-1″, C-2″, C-3″, C-4″, and C-5″, the coupling constants $^1J_{CC}$ for C-1″/C-5″ (38.3 Hz) and C-3″/C-4″ (40.2 Hz) established these carbons as belong to two separate acetate units (Figure 9c). The incorporation patterns of [1,2-$^{13}C_2$]acetate in the C_5N unit were consistent with those obtained for manumycin and asukamycin [58].

Figure 7. ^{13}C NMR spectrum of [1,2-$^{13}C_2$]acetate-labeled **2**.

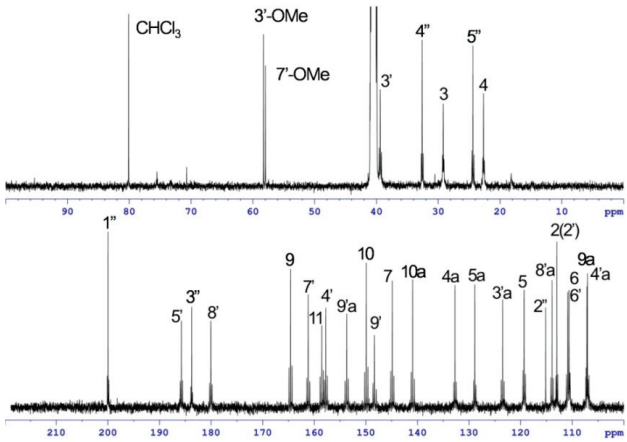

Figure 8. ^{1}H-^{1}H COSY and HMBC correlations of [1,2-$^{13}C_2$]acetate-labeled **2**.

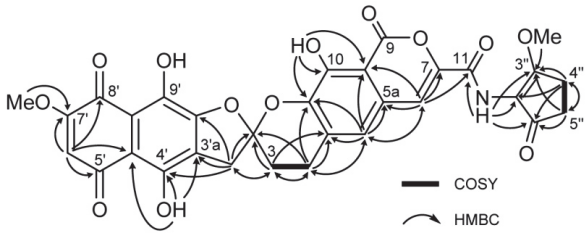

Figure 9. ^{13}C-^{13}C couplings observed in 2D INADEQUATE (**a**,**b**) and ^{13}C (**c**) NMR spectra of [1,2-$^{13}C_2$]acetate-labeled **2**. The coupling of C-1″/C-5″ and C-3″/C-4″ were only observed in the ^{13}C NMR spectrum (**c**). (**a**) Optimized for $^{1}J_{cc}$ = 50 Hz; (**b**) Optimized for $^{1}J_{cc}$ = 35 Hz; (**c**) ^{13}C NMR spectra; (**d**) Observed in 2D INADEQUATE.

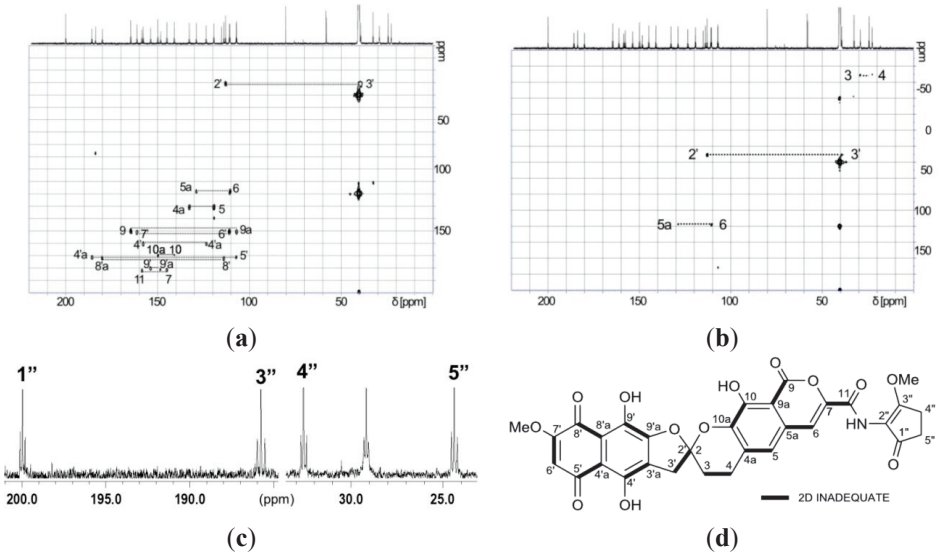

The remaining six carbons were attributed to the methoxycyclopentenone moiety based on the 2D-NMR analytical data. A COSY cross peak between H-4″ and H-5″ established a two-carbon fragment consisting of two methylene groups. H-4″ was correlated with the three sp^2 trisubstituted carbons C-1″ (δ_C 200.0), C-2″ (δ_C 115.1), and C-3″ (δ_C 183.8) and H-5″ to C-1″. An HMBC correlation between the protons of OMe-3″ and the carbon C-3″ and the chemical shifts of the aforementioned three carbons established the presence of a cyclopent-2-enone bearing a methoxy substitution at the 3-position. This six-carbon unit was connected to C-11 through an amide linkage on the basis of the HMBC correlations of an amide proton (δ_H 9.44) with C-1″, C-2″, and C-3″, finally providing the full planar structure of **2**. ^{1}H and ^{13}C NMR resonances for the 3-hydroxycyclopent-2-enone subunit of **1** were not detected. This result could be attributed to the keto-enol tautomerization of the 1,3-diketone structure. All carbons for the cyclopentenone unit were detected in the methylated derivative **2**, in which tautomerization does not occur. Similar

observations have been reported for several other compounds containing the same 1,3-diketo substructure [40,59,60].

Table 1. NMR data for hyaluromycin (**1**) and [1,2-$^{13}C_2$]acetate-labeled **2** in DMSO-d_6.

Position	1			[1,2-$^{13}C_2$]Acetate-labeled 2			
	δ_C [a], Type	δ_H, Mult. (*J* in Hz) [b]	HMBC [c]	δ_C [a], Type	$^1J_{CC}$ (Hz), Mult.	δ_H, Mult. (*J* in Hz) [b]	HMBC [c]
2 (2′)	113.0, qC			113.0, qC	42.4, dd		
3	29.1, CH_2	2.37, m; 2.56, m	2, 4a	29.2, CH_2	30.8, dd	2.38–2.60, m	2, 4a
4	22.7, CH_2	3.06, m; 3.17, m	2, 3, 4a, 5, 10a,	22.7, CH_2	31.4, dd	3.07, m; 3.19, m	2, 3, 4a, 5, 10a
4a	132.8, qC			132.7, qC	59.8, dd		
5	119.5, CH	7.25, s	4a, 5a, 6, 9a, 10a	119.3, CH	59.9, dd	7.24, s	4a, 5a, 6, 9a, 10a
5a	128.9, qC			128.9, qC	54.6, dd		
6	110.9, CH	7.52, s	5, 5a, 7, 9a, 11	110.6, CH	56.0, dd	7.50, s	5, 5a, 7, 9a, 11
7	144.7, qC			144.9, qC	78.6, dd		
9	164.4, qC			164.6, qC	72.5, dd		
9a	107.0, qC			106.9, qC	76.3, dd		
10	150.0, qC			149.9, qC	79.1, dd		
10a	141.1, qC			140.9, qC	78.9, dd		
11	158.8, qC			158.5, qC	78.4, dd		
2′ (2)	113.0, qC			113.0, qC	42.4, dd		
3′	39.4, CH_2	3.55, d (18.0)	3, 2′, 3′a, 4′, 9′a	39.4, CH_2	42.8, dd	3.49, d (17.9)	3, 2′, 3′a, 4′, 9′a
		3.48, d (18.0)				3.63, d (17.9)	
3′a	123.6, qC			123.5, qC	71.6, dd		
4′	157.8, qC			157.8, qC	71.4, dd		
4′a	107.2, qC			107.2, qC	56.5, dd		
5′	185.9, qC			185.8, qC	38.4, dd		
6′	110.9, CH	6.41, s	4′a, 5′, 7′, 8′	110.9, CH	65.5, dd	6.42, s	4′a, 5′, 7′, 8′
7′	161.2, qC			161.2, qC	71.3, dd		
8′	180.2, qC			180.1, qC	59.1, dd		
8′a	114.0, qC			113.9, qC	59.1, dd		
9′	148.3, qC			148.3, qC	73.9, dd		
9′a	153.7, qC			153.7, qC	74.8, dd		
7′-OMe	58.0, CH_3	3.89, s	7′	58.0, CH_3		3.91, s	7′
1″	n.d. [d]			200.0, qC	38.4, dd		
2″	113.9, qC			115.1, qC			
3″	n.d. [d]			183.8, qC	39.8, dd		
4″	n.d. [d]			32.6, CH_2	40.5, dd	2.41, m	1″, 3″, 4″
5″	n.d. [d]			24.4, CH_2	38.3, dd	2.83, dd (3.7, 3.7)	1″, 2″, 3″, 5″
3″-OMe				58.3, CH_3		4.01, s	3″
10-OH		10.67, s	9a, 10, 10a			10.71, s	9a, 10, 10a
4′-OH		13.14, s	3′a, 4′, 4′a			11.88, s	3′a, 4′, 4′a
9′-OH		11.90, s				13.15, s	
11-NH		9.44, s	11			9.44, s	11, 1″, 2″, 3″

[a] Recorded at 125 MHz; [b] Recorded at 500 MHz; [c] Correlation are from proton(s) to carbon; [d] Not detected.

The absolute configuration of the spiro carbon C-2 (C-2′) of **2** was determined from circular dichroism (CD) data. In the CD spectrum of **2**, two characteristic Cotton effects were observed (Figure 9), a positive one at 224 nm ($\Delta\varepsilon = +25.7$) and a negative one at 262 nm ($\Delta\varepsilon = -10.0$). These results are in agreement with those previously obtained for β-rubromycin (**4**), γ-rubromycin (**5**) and griseorhodin A (**6**) [61,62]. Therefore, the absolute configuration of **2** was determined to be *S* (Figure 10). To our knowledge, the only member of this family of compounds possessing an *R* configuration of the spiro center is heliquinomycin (**10**), whose absolute configuration was deduced from X-ray analysis and which possesses Cotton effects opposite to those of the above molecules [34].

Figure 10. CD spectrum and absolute configuration of **2**.

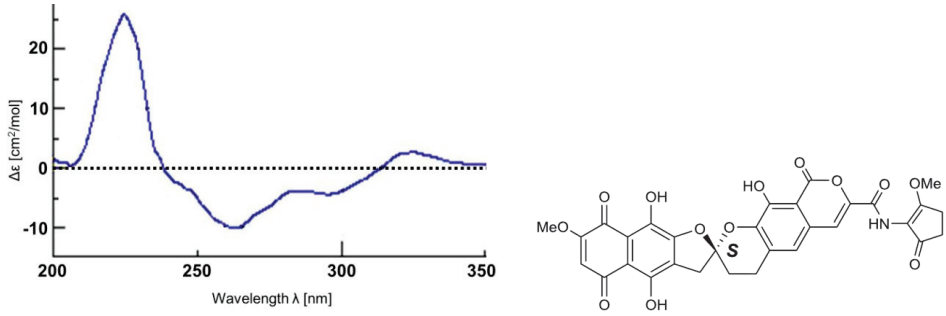

Hyaluromycin (**1**) displayed 25-fold more potent inhibitory activity against HAase from bovine testes with an IC_{50} value of 14 μM, than did glycyrrhizin (IC_{50} = 340 μM), a well-known plant terpenoid [26]. Interestingly, β-rubromycin (**4**) and γ-rubromycin (**5**), which lacks the aminocylopentenone unit, showed no inhibitory activity in the concentration range from 0.013% to 0.5%. More noteworthy is that the derivative **2**, in which the enol hydroxyl group in the cyclopentane unit is protected as a methyl ether, showed no inhibitory activity in the concentration range from 0.013% to 0.5%. These results suggest that the 2-amino-3-hydroxycyclopent-2-enone subunit, and possibly its tautomeric structure, play an essential role in hyaluronidase inhibition (Table 2).

Table 2. HAase inhibition (%) of **1**, **2**, β-rubromycin (**4**), γ-rubromycin (**5**) and glycyrrhizin.

Compound	0.0031	0.0063	0.013	0.025	0.050	0.10	0.25	0.50	1.0	2.0	(%)
1	7.1	33.5	70.5	94.2	94.9	96.7					
2			0	0	0	0	0	0			
β-Rubromycin (**4**)			0	0	0	0	0	0			
γ-Rubromycin (**5**)			0	0	0	0	0	0			
Glycyrrhizin					10.6	20.0	37.9	87.6	99.1	99.2	

3. Experimental Section

3.1. General Experimental Procedures

Sodium [1,2-$^{13}C_2$]acetate was purchased from Sigma-Aldrich Co. LLC (St. Louis, MO, USA). Optical rotations were measured using a JASCO DIP-3000 polarimeter. UV spectra were recorded on a Hitachi U-3210 spectrophotometer. IR spectra were measured by a Perkin-Elmer 100 spectrometer. NMR spectra were obtained on a Bruker AVANCE 500 spectrometer in DMSO-d_6 and referenced to the residual solvent signals (δ_H 3.36, δ_C 40.6). HRESITOFMS were recorded on a Bruker microTOF apparatus. Cosmosil 75C18-PREP (Nacalai Tesque, Inc., Nakagyo-ku, Kyoto, Japan, 75 μm) was used for ODS column chromatography. HPLC separation was performed using COSMOSIL 5C18-AR-II Packed Column (Nacalai Tesque, Inc., Nakagyo-ku, Kyoto, Japan, 10 × 250 mm) with a photodiode array detector.

3.2. Microorganism

Strain MB-PO13 was selected by screening the HAase inhibitory activity of approximately 1000 strains of marine organisms-derived actinomycetes. The strain was isolated from a sea squirt specimem (*Molgula manhattensis*) collected at a harbor near Minato-ku, Tokyo. The strain was identified as a member of genus *Streptomyces* on the basis of 99.2% 16S rRNA gene sequence identity (1429 nucleotides; DDBJ accession number AB840588) with *Streptomyces misawanensis* strain NBRC 13855 (accession number AB184533).

3.3. Fermentation

Strain MB-PO13 growing on a yeast-starch agar medium consisting of soluble starch (Wako Pure Chemical Industries, Ltd., Chuo-ku, Osaka, Japan) 1.0%, yeast extract (Becton, Dickinson and Company, Sparks, MD, USA) 0.2%, and agar 1.5% (pH 7.2) was inoculated into 500 mL K-1 flasks each containing 100 mL of the V-22 seed medium consisting of soluble starch 1.0%, glucose 0.5%, NZ-case (Wako Pure Chemical Industries, Ltd., Chuo-ku, Osaka, Japan) 0.3%, yeast extract (Difco Laboratories) 0.2%, tryptone (Difco Laboratories) 0.5%, K_2HPO_4 0.1%, $MgSO_4$ $7H_2O$ 0.05%, and $CaCO_3$ 0.3% (pH 7.0). The flasks were placed on a rotary shaker (200 rpm) at 30 °C for four days. Then, the seed culture (3 mL) was transferred into 500 mL K-1 flasks each containing 100 mL of the A-3 M production medium consisting of soluble starch 2.0%, glycerol 2.0%, glucose 0.5%, Pharmamedia 1.5%, yeast extract 0.3%, and Diaion HP-20 resin (Mitsubishi Chemical Co., Chiyoda-ku, Tokyo, Japan) 1%. The pH of the medium was adjusted to 7.0 before sterilization. The inoculated flasks were placed on a rotary shaker (200 rpm) at 30 °C for seven days.

3.4. Extraction and Isolation

After incubation, 100 mL of ethyl acetate was added to each flask, and the flasks were allowed to shake for one hour. The mixture was centrifuged at 6000 rpm for 10 min and the organic layer was separated from the aqueous layer containing the mycelium and evaporated to give 450 mg of

crude extract from 1 L of culture. This extract was subjected to reversed-phase ODS column chromatography with a gradient of MeCN/0.1% aqueous HCO_2H (2:8, 3:7, 4:6, 5:5, 6:4, 7:3, and 8:2 v/v). The fraction eluted with 70% MeCN was pooled and evaporated *in vacuo*, and the major part of the solvent evaporated in vacuum. The remaining aqueous phase was extracted twice with EtOAc concentrated to give a red solid (46 mg). The final purification was achieved by preparative HPLC using a linear gradient of MeCN/0.1% aqueous HCO_2H (MeCN concentration: 15%–85% for 0–30 min) at 4 mL/min, yielding hyaluromycin (20 mg) with a retention time of 22.5 min.

*3.5. Hyaluromycin (***1***)*

Red powder; $[\alpha]^{25}_D$ −168 (*c* 0.005, DMSO); UV (1% DMSO in MeOH) λ_{max} (log ε) 257 (4.74), 307 (sh, 4.30), 352 (4.40), 368 (sh, 3.98), 472 (sh, 3.80), 506 (3.78), 544 (sh, 3.62); (1% DMSO in 0.01 N methanolic HCl) 250 (4.60), 307 (sh, 4.22), 354 (4.02), 366 (sh, 3.68), 474 (sh, 3.66), 504 (3.69), 545 (sh, 3.43); (1% DMSO in 0.01 N methanolic NaOH) 236 (4.60), 259 (4.50), 333 (sh, 3.92), 392 (3.94), 503 (sh, 3.77), 539 (3.98), 570 (3.95); IR (ATR) ν_{max} 3357, 2935, 1981, 1693, 1599, 1537, 1440, 1331, 1221 cm^{-1}; ^1H and ^{13}C NMR data, see Table 1 and Supplementary Information; HRESITOFMS $[M + H]^+$ 604.1091 (calcd for $C_{30}H_{22}NO_{13}$, 604.1086).

3.6. Feeding Experiment

[1,2-$^{13}C_2$]Acetate-labeled hyaluromycin (**1**) was prepared by culturing the producing strain in a liquid medium containing sodium [1,2-$^{13}C_2$]acetate. The inoculation, cultivation, extraction and purification were conducted in the same manner as described above. Sodium [1,2-$^{13}C_2$]acetate (20 mg/mL in distilled water) was added at 48 h after inoculation, then every 24 h four times. After further incubation for two days, the culture broth was extracted with EtOAc. From 1 L culture, 20 mg of [1,2-$^{13}C_2$]acetate-labeled **1** was obtained.

*3.7. Methylation of [1,2-$^{13}C_2$]Acetate-Labeled Hyaluromycin (***1***)*

3″-*O*-Methylhyaluromycin (**2**) labeled with [1,2-$^{13}C_2$]acetate: DBU (40 μL, 0.27 μmol) and CH_3I (400 μL, 6.43 μmol) were added to a stirred solution of [1,2-$^{13}C_2$]acetate-labeled **1** (20.0 mg, 0.83 μmol) in Me_2CO/MeCN (400 μL each). After heating at 50 °C for 1 h, the reaction mixture was diluted with water and EtOAc (500 μL each), and the organic layer was separated and evaporated *in vacuo*. The residue was purified by ODS column chromatography by a gradient of MeCN/0.1% aqueous HCO_2H (2:8, 3:7, 4:6, 5:5, 6:4, 7:3, and 8:2 v/v). Final purification was achieved by preparative HPLC using a linear gradient of MeCN/0.1% aqueous HCO_2H (MeCN concentration: 15%–85% for 0–30 min) at 4 mL/min to give 3″-*O*-methyl [1,2-$^{13}C_2$]acetate-labeled hyaluromycin (**2**, 7.2 mg, 36% yield, t_R = 18.8 min) as a red powder. For physico-chemical properties, see the data for non-labeled **2** described below. ^1H and ^{13}C NMR data, see Table 1 and Supplementary Information.

*3.8. Methylation of Hyaluromycin (**1**)*

For the measurement of physico-chemical properties and biological evaluation, a small portion of non-labeled **1** was methylated to give non-labeled **2** in the same manner as described above. 3″-*O*-methylhyaluromycin (**2**): Red powder; $[\alpha]^{25}_{D}$ −77 (*c* 0.005, DMSO); UV (1% DMSO in MeOH) λ_{max} (log ε) 249 (4.82), 314 (sh, 4.02), 350 (4.10), 366 (sh, 3.77), 498 (3.88); (1% DMSO in 0.01 N methanolic HCl) 248 (4.75), 315 (sh, 4.30), 356 (4.15), 491 (3.87), 520 (3.77); (1% DMSO in 0.01 N methanolic NaOH) 254 (4.50), 392 (3.81), 538 (3.90), 560 (3.89); IR (ATR) ν_{max} 3348, 2934, 1677, 1604, 1514, 1439, 1331, 1228 cm^{-1}; ^{1}H and ^{13}C NMR data, see Supplementary Information; HRESITOFMS $[M + Na]^{+}$ 640.1057 (calcd for $C_{31}H_{24}NO_{13}Na$, 640.1062).

3.9. Hyaluronidase Inhibitory Activity

HAase inhibitory activity was measured by the turbidimetric assay described by Ferrante [63] with slight modifications. HAase (EC 3.2.1.35) from the bovine testes type I-S (Sigma-Aldrich Co. LCC, St. Louis, MO, USA) and HA sodium salt from rooster comb (Wako Pure Chemical Industries, Ltd., Chuo-ku, Osaka, Japan) were dissolved in acetate buffer (0.2 M sodium acetate, 0.15 M NaCl, pH 5.0). The mixtures contained 100 µL of 0.01% HAase and 20 µL of either 0.0031%–0.10% **1**, 0.013%–0.50% **2**, 0.013%–0.50% β-rubromycin (isolated from *Streptomyces*), 0.013%–0.50% γ-rubromycin (BioViotica Naturstoffe GmbH, Dransfelder Weg, Dransfeld, Germany) or 0.050%–2.0% glycyrrhizin (Tokyo Chemical Industry Co., Ltd., Chuo-ku, Tokyo, Japan) in DMSO (Table 2). The mixtures were incubated at 37 °C for 20 min. After incubation, 100 µL of 0.1% HA was added and the mixtures were further incubated at 37 °C for 60 min. After incubation, the enzymatic reaction was terminated by the addition of 1 mL of 2.5% cetyltrimethylammonium bromide (CTAB) in 2% aqueous NaOH. The turbidity at 400 nm was measured after 30 min. All incubations were performed in triplicate.

4. Conclusions

Hyaluromycin (**1**), a new member of rubromycin family of antibiotics, was isolated from a marine-derived *Streptomyces* sp. as a HAase inhibitor on the basis of HAase activity screening. Hyaluromycin (**1**) consists of rubromycin common structure and 2-amino-3-hydroxycyclopent-2-enone (C_5N) structure; both structures units have been reported only from actinomycetes. Hyaluromycin (**1**) displayed approximately 25-fold more potent inhibitory activity against HAase than did glycyrrhizin, a well-known plant terpenoid. Interestingly, β-rubromycin (**4**) and γ-rubromycin (**5**), lacking the C_5N unit, showed no inhibitory activity. More noteworthy is that the derivative **2** in which the enol hydroxyl group in the cyclopentane unit is protected as a methyl ether showed no inhibitory activity. These results suggest that the C_5N unit plays an essential role in the observed hyaluronidase inhibition. The present study may provide new insight for developing new, promising anti-inflammation molecules.

Acknowledgments

The authors would like to thank Naoya Oku, Toyama Prefectural University, for assistance with NMR measurements.

Conflicts of Interest

The authors declare no conflict of interest.

References

1. Ohya, T.; Kaneko, Y. Novel hyaluronidase from streptomyces. *Biochim. Biophys. Acta* **1970**, *198*, 607–609.
2. Hamai, A.; Morikawa, K.; Horei, K.; Tokuyasu, K. Purification and characterization of hyaluronidase from *Streptococcus dysgalactiae*. *Agric. Biol. Chem.* **1989**, *53*, 2163–2168.
3. Baker, J.R.; Dong, S.; Pritchard, D.G. The hyaluronan lyase of *Streptococcus pyogenes* bacteriophage H4489A. *Biochem. J.* **2002**, *365*, 317–322.
4. Kemeny, D.M.; Dalton, N.; Lawrence, A.J.; Pearce, F.L.; Vernon, C.A. The purification and characterisation of hyaluronidase from the venom of the honey bee, *Apis mellifera*. *Eur. J. Biochem.* **1984**, *139*, 217–223.
5. Kolarich, D.; Léonard, R.; Hemmer, W.; Altmann, F. The *N*-glycans of yellow jacket venom hyaluronidases and the protein sequence of its major isoform in *Vespula vulgaris*. *FEBS J.* **2005**, *272*, 5182–5190.
6. Pessini, A.C.; Takao, T.T.; Cavalheiro, E.C.; Vichnewski, W.; Sampaio, S.V.; Giglio, J.R.; Arantes, E.C. A hyaluronidase from *Tityus serrulatus* scorpion venom: Isolation, characterization and inhibition by flavonoids. *Toxicon* **2001**, *39*, 1495–1504.
7. Girish, K.S.; Kemparaju, K. Inhibition of *Naja naja* venom hyaluronidase: Role in the management of poisonous bite. *Life Sci.* **2006**, *78*, 1433–1440.
8. Tu, A.T.; Hendon, R.R. Characterization of lizard venom hyaluronidase and evidence for its action as a spreading factor. *Comp. Biochem. Physiol. B* **1983**, *76*, 377–383.
9. Karlstam, B.; Ljungloef, A. Purification and partial characterization of a novel hyaluronic acid-degrading enzyme from Antarctic krill (*Euphausia superba*). *Polar Biol.* **1991**, *11*, 501–507.
10. Krishnapillai, A.M.; Taylor, K.D.A.; Morris, A.E.J.; Quantick, P.C. Characterisation of Norway lobster (*Nephrops norvegicus*) hyaluronidase and comparison with sheep and bovine testicular hyaluronidase. *Food Chem.* **1999**, *65*, 515–521.
11. Hopkins, B.J.; Hodgson, W.C. Enzyme and biochemical studies of stonefish (*Synacneja trachynis*) and solidfish (*Gymnapistes marmoratus*). *Toxicon* **1998**, *36*, 791–793.
12. Noble, P.W.; McKee, C.M.; Cowman, M.; Shin, H.S. Hyaluronan fragments activate an NF-kappa B/I-kappa B alpha autoregulatory loop in murine macrophages. *J. Exp. Med.* **1996**, 183, 2373–2378.
13. Termei, R.; Laschinger, C.; Lee, W.; McCulloch, C.A. Intercellular interactions between mast cells and fibroblasts promote pro-inflammatory signaling. *Exp. Cell Res.* **2013**, *319*, 1839–1851.

14. Feinberg, R.N.; Beebe, D.C. Hyaluronate in vasculogenesis. *Science* **1983**, *220*, 1177–1179.
15. McKee, C.M.; Penno, M.B.; Cowman, M.; Burdick, M.D.; Strieter, R.M.; Bao, C.; Noble, P.W. Hyaluronan (HA) fragments induce chemokine gene expression in alveolar macrophages. The role of HA size and CD44. *J. Clin. Investig.* **1996**, *98*, 2403–2413.
16. Kobayashi, H.; Terao, T. Hyaluronic acid-specific regulation of cytokines by human uterine fibroblasts. *Am. J. Physiol.* **1997**, *273*, 1151–1159.
17. Nakamura, K.; Yokohama, S.; Yoneda, M.; Okamoto, S.; Tamaki, Y.; Ito, T.; Okada, M.; Aso, K.; Makino, I. High, but not low, molecular weight hyaluronan prevents T-cell-mediated liver injury by reducing proinflammatory cytokines in mice. *J. Gastroenterol.* **2004**, *39*, 346–354.
18. Asari, A.; Kanemitsu, T.; Kurihara, H. Oral administration of high molecular weight hyaluronan (900 kDa) controls immune system via toll-like receptor 4 in the intestinal epithelium. *J. Biol. Chem.* **2010**, *285*, 24751–24758.
19. Delmage, J.M.; Powars, D.R.; Jaynes, P.K.; Allerton, S.E. The selective suppression of immunogenicity by hyaluronic acid. *Ann. Clin. Lab. Sci.* **1986**, *16*, 303–310.
20. Tian, X.; Azpurua, J.; Hine, C.; Vaidya, A.; Myakishev-Rempel, M.; Ablaeva, J.; Mao. Z.; Nevo, E.; Gorbunova, V.; Seluanov, A. High-molecular-mass hyaluronan mediates the cancer resistance of the naked mole rat. *Nature* **2013**, *499*, 346–349.
21. Holmes, M.W.; Bayliss, M.T.; Muir, H. Hyaluronic acid in human articular cartilage. Age-related changes in content and size. *Biochem. J.* **1988**, *250*, 435–441.
22. Sherman, P.W.; Javis, J.U.M. Extraordinary life spans of naked mole-rats (*Heterocephalus glaber*). *J. Zool.* **2002**, *258*, 307–311.
23. Buffenstein, R. Negligible senescence in the longest living rodent, the naked mole-rat: Insights from a successfully aging species. *J. Comp. Physiol. B* **2008**, *178*, 439–445.
24. Sakamoto, K.; Nagai, H.; Koda, A. Role of hyaluronidase in immediate hypersensitivity reaction. *Immunopharmacology* **1980**, *2*, 139–146.
25. Kakegawa, H.; Mitsuo, N.; Matsumoto, H.; Satoh, H.; Akagi, M.; Tasaka, K. Hyaluronidase-inhibitory and anti-allergic activities of the photo-irradiated products of tranilast. *Chem. Pharm. Bull.* **1983**, *33*, 3738–3744.
26. Furuya, T.; Yamagata, S.; Shimoyama, Y.; Fujihara, M.; Morishita, N.; Ohtsuki, K. Biochemical characterization of glycyrrhizin as an effective inhibitor for hyaluronidase from bovine testis. *Biol. Pharm. Bull.* **1997**, *20*, 973–977.
27. Kakegawa, H.; Matsumoto, H.; Satoh, T. Activation of hyaluronidase by metallic salts and compound 48/80, and inhibitory effect of anti-allergic agents on hyaluronidase. *Chem. Pharm. Bull.* **1985**, *33*, 642–646.
28. Girish, K.S.; Kemparaju, K.; Nagaraju, S.; Vishwanath, B.S. Hyaluronidase inhibitors: A biological and therapeutic perspective. *Curr. Med. Chem.* **2009**, *16*, 2261–2288.
29. Brockmann, H.; Lenk, W.; Schwantje, G.; Zeeck, A. Rubromycin II. *Chem. Ber.* **1969**, *102*, 126–151.
30. Brockmann, H.; Zeeck, A. Rubromycins. 3. The constitution of alpha-rubromycin, beta-rubromycin, gamma-rubromycin, and gamma-iso-rubromycin. *Chem. Ber.* **1970**, *103*, 1709–1726.

31. Yan, J.X.; Fan, S.X.; Pei, H.S.; Zhu, B.Q.; Xu, W.S.; Naganawa, H.; Hamada, M.; Takeuchi, T. 8-Methoxygriseorhodin C, a new member of griseorhodin antibiotic. *J. Antibiot.* **1991**, *44*, 1277–1279.
32. Eckardt, K.; Tresselt, D.; Ihn, W. The structure of the antibiotic griseorhodin C. *J. Antibiot.* **1978**, *31*, 970–973.
33. Ohshima, M.; Ishizaki, N.; Horiuchi, T.; Marumoto, Y.; Sugiyama, N. Novel antibiotics substance DK-7814. Jpn. Patent 57,032,286, 20 February 1982.
34. Coronelli, C.; Pagani, H.; Bardone, M.R.; Lancini, G.C. Purpuromycin, a new antibiotic isolated from *Actinoplanes ianthinogenes* N. sp. *J. Antibiot.* **1974**, *27*, 161–168.
35. Chino, M.; Nishikawa, K.; Umekita, M.; Hayashi, C.; Yamazaki, T.; Tsuchida, T.; Sawa, T.; Hamada, M.; Takeuchi, T. Heliquinomycin, a new inhibitor of DNA helicase, produced by *Streptomyces* sp. MJ929-SF2 I. Taxonomy, production, isolation, physico-chemical properties and biological activities. *J. Antibiot.* **1996**, *49*, 752–757.
36. Ueno, T.; Takahashi, H.; Oda, M.; Yokoyama, A.; Goto, Y.; Mizushima, Y.; Sakaguchi, K.; Hayashi, H. Inhibition of human telomerase by rubromycins: Implication of spiroketal system of the compounds as an active moiety. *Biochemisrty* **2000**, *39*, 5995–6002.
37. Yuen, T.Y.; Ng, Y.P.; Ip, F.C.F.; Chen, J.L.Y.; Atkinson, D.J.; Sperry, J.; Ip, N.Y.; Brimble, M.A. Telomerase inhibition studies of novel spiroketal-containing rubromycin derivatives. *Aust. J. Chem.* **2013**, *66*, 530–533.
38. Ohta, E.; Ohta, S.; Kubota, N.K.; Suzuki, M.; Ogawa, T.; Yamasaki, A.; Ikegami, S. Micromonospolide A, a new macrolide from *Micromonospora* sp. *Tetrahedron Lett.* **2001**, *42*, 4179–4181.
39. Laakso, J.A.; Mocek, U.M.; Van, D.J.; Wouters, W.; Janicot, M. R176502, a new bafilolide metabolite with potent antiproliferative activity from a novel *Micromonospora* species. *J. Antibiot.* **2003**, *56*, 909–916.
40. Werner, G.; Hagenmaier, H.; Albert, K.; Kohlshorn, H. The structure of the bafilomycins, a new group of macrolide antibiotics. *Tetrahedron Lett.* **1983**, *24*, 5193–5196.
41. Yan, S.W.; Chan, T.M.; Terracciano, J.; Patel, R.; Loebenberg, D.; Chen, G.; Patel, M.; Gullo, V.; Pramanik, B.; Chu, M. New antibiotic Sch 725424 and its dehydration product Sch 725428 from *Kitasatospora* sp. *J. Antibiot.* **2005**, *58*, 192–195.
42. Banskota, A.H.; McAlpine, J.B.; Sørensen, D.; Ibrahim, A.; Aouidate, M.; Piraee, M.; Alarco, A.M.; Farnet, C.M.; Zazopoulos, E. Genomic analyses lead to novel secondary metabolites part 3. ECO-0501, a novel antibacterial of a new class. *J. Antibiot.* **2006**, *59*, 533–542.
43. Zeeck, A.; Schröder, K.; Frobel, K.; Grote, R.; Thiericke, R. The structure of manumycin. I. Characterization, structure elucidation and biological activity. *J. Antibiot.* **1987**, *40*, 1530–1540.
44. Huger, G. Moenomycin and related phosphorus-containing. *Antibiotics* **1979**, *5*, 135–153.
45. Koshino, H.; Osada, H.; Yano, T.; Uzawa, J.; Isono, K. The structure of enopeptins A and B, novel depsipeptide antibiotics. *Tetrahedron Lett.* **1991**, *32*, 7707–7710.

46. Nakano, H.; Yoshida, M.; Shirahata, K.; Ishii, S.; Arai, Y.; Morimoto, M.; Tomita, F. Senacarcin A, a new antitumor antibiotic produced by *Streptomyces endus* subsp. *aureus*. *J. Antibiot.* **1982**, *35*, 760–762.
47. Brockmann, H.; Grothe, G. Über Actinomycetenfarbstoffe, II. mitteil.: Limocrocin, ein gelber actinomycetenfarbstoff. *Chem. Ber.* **1953**, *36*, 1110–1115.
48. Ojika, M.; Shizuri, Y.; Niwa, H.; Yamada, K.; Iwadare, S. Structure and synthesis of reductiline, a novel metabolite from a variant of *Streptomyces orientalis*. *Tetrahedron Lett.* **1982**, *23*, 4977–4980.
49. Simizu, K.; Tamura, G. Reductiomycin, a new antibiotic. I. Taxonomy, fermentation, isolation, characterization and biological activities. *J. Antibiot.* **1981**, *34*, 649–653.
50. Omura, S.; Shimizu, H.; Iwai, Y.; Hinotozawa, K.; Otoguro, K.; Hashimoto, H.; Nakagawa, A. AM-2604 A, a new antiviral antibiotic produced by a strain of *Streptomyces*. *J. Antibiot.* **1982**, *35*, 1632–1637.
51. McAlpine, J.B.; Backmann, B.O.; Piraee, M.; Tremblay, S.; Alarco, A.M.; Zazopoudos, E.; Farnet, C.M. Microbial genomics as a guide to drug discovery and structural elucidation: ECO-02301, a novel antifungal agent, as an example. *J. Nat. Prod.* **2005**, *68*, 493–496.
52. Grote, R.; Zeek, A.; Drautz, H.; Zähner, H. Metabolic products of microorganisms. 246. 2880-II, a metabolite related to ferulic acid from *Streptomyces griseoflavus*. *J. Antibiot.* **1988**, *41*, 1275–1276.
53. Zeeck, A.; Frobel, K.; Heusel, C.; Schröder, K.; Thiericke, R. The structure of manumycin. II. Derivatives. *J. Antibiot.* **1987**, *40*, 1541–1548.
54. Hayashi, K.; Nakagawa, M.; Fujita, T.; Tanimori, S.; Nakayama, M. Nisamycin, a new manumycin group antibiotic from *Streptomyces* Sp K106 .2. Structure determination and structure-activity-relationships. *J. Antibiot.* **1994**, *47*, 1110–1115.
55. Hinzen, B.; Raddatz, S.; Paulsen, H.; Lampe, T.; Schumacher, A.; Häbich, D.; Hellwig, V.; Benet, B.J.; Endermann, R.; Labischinski, H.; *et al*. Medicinal chemistry optimization of acyldepsipeptides of the enopeptin class antibiotics. *ChemMedChem* **2006**, *1*, 689–693.
56. Puder, C.; Loya, S.; Hizi, A.; Zeeck, A. Structural and biosynthetic investigations of the rubromycins. *Eur. J. Org. Chem.* **2000**, *5*, 729–735.
57. Suetsuna, K.; Osajima, Y. Isolation of structure of dideoxygriseorhodin C produced by a *Streptomyces* sp. *Agric. Biol. Chem.* **1989**, *53*, 241–242.
58. Thiericke, R.; Zeeck, A.; Nakagawa, A.; Omura, S.; Herrold, R.E.; Wu, S.T.S.; Beale, J.M.; Floss, H.G. Biosynthesis of the manumycin group antibiotics. *J. Am. Chem. Soc.* **1990**, *112*, 3979–3987.
59. He, H.; Shen, B.; Korshalla, J.; Siegel, M.M.; Carter, G.T. Isolation and structural elucidation of AC326-α, a new member of the moenomycin group. *J. Antibiot.* **2000**, *53*, 191–195.
60. Li, F.; Maskey, R.P.; Qin, S.; Sattler, I.; Fiebig, H.H.; Maier, A.; Zeeck, A.; Laatsch, H. Chinikomycins A and B: Isolation, structure elucidation, and biological activity of novel antibiotics from a marine *Streptomyces* sp. isolate M045. *J. Nat. Prod.* **2005**, *68*, 349–353.

61. Bringmann, G.; Kraus, J.; Schmitt, U.; Puder, C.; Zeeck, A. Determination of the absolute configurations of γ-rubromycin and related spiro compounds by quantum chemical CD calculations. *Eur*. *J*. *Org*. *Chem*. **2000**, *15*, 2729–2734.
62. Yunt, Z.; Reinhardt, K.; Li, A.; Engeser, M.; Dahse, H.M.; Götschow, M.; Bruhn, T.; Bringmann, G.; Piel, J. Cleavage of four carbon-carbon bonds during biosynthesis of the griseorhodin A spiroketal pharmacophore. *J*. *Am*. *Chem*. *Soc*. **2009**, *131*, 2297–2305.
63. Ferrante, N.D. Turbidimetric measurement of acid mucopolysaccharides and hyaluronidase activity. *J*. *Biol*. *Chem*. **1956**, *220*, 303–306.

Solwaric Acids A and B, Antibacterial Aromatic Acids from a Marine *Solwaraspora* sp.

Gregory A. Ellis, Thomas P. Wyche, Charles G. Fry, Doug R. Braun and Tim S. Bugni

Abstract: Two novel trialkyl-substituted aromatic acids, solwaric acids A and B, were isolated from a marine *Solwaraspora* sp. cultivated from the ascidian *Trididemnum orbiculatum*. Solwaric acids A and B were isotopically labeled with U-^{13}C glucose, and analysis of a ^{13}C–^{13}C COSY allowed for unambiguous determination of the location of the phenyl methyl group. The two novel compounds demonstrated antibacterial activity against methicillin-resistant *Staphylococcus aureus* (MRSA) and methicillin-sensitive *Staphylococcus aureus* (MSSA).

Reprinted from *Mar. Drugs*. Cite as: Ellis, G.A.; Wyche, T.P.; Fry, C.G.; Braun, D.R.; Bugni, T.S. Solwaric Acids A and B, Antibacterial Aromatic Acids from a Marine *Solwaraspora* sp. *Mar. Drugs* **2014**, *12*, 1013–1022.

1. Introduction

Infectious disease continues to be a major issue, as it is the second leading cause of death worldwide [1]. Complicating the treatment of infectious disease is antibiotic resistance, which results in about $20 billion in health service costs and at least 23,000 deaths in the United States per year [2,3]. Among antibiotic resistant bacteria, methicillin-resistant *Staphylococcus aureus* (MRSA) has become a major concern for human health [4–8]. While the mortality percentages in methicillin-susceptible *Staphylococcus aureus* (MSSA) patients range from 5% to 28%, the mortality percentages for MRSA patients tend to be even higher, ranging from 10% to 64% [5–8]. Although ranging between studies, one study encompassing data from different European countries found an additional 80% excess mortality rate at day 30 after infection was contributed by methicillin resistance in *S. aureus* [5,6,8]. Therefore, antibiotic resistance escalates the importance for discovering new and effective antibiotics in an efficient manner.

In our pursuit of novel antibacterial compounds, we isolated two novel aromatic acids that were named solwaric acids A (**1**) and B (**2**) and the known 2,4,6-triphenyl-1-hexene (**3**) [9–11], from a marine *Solwaraspora* sp. (Strain WMMB329) cultivated from the ascidian *Trididemnum orbiculatum* (Van Name, 1902) [12]. To our knowledge, these are the first novel compounds reported from a *Solwaraspora* sp., although strain WMMB329 also showed 99% 16S rDNA sequence similarity to some *Micromonospora* spp. Solwaric acids A (**1**) and B (**2**) demonstrated antibacterial activity against methicillin-resistant *Staphylococcus aureus* (MRSA) and methicillin-sensitive *Staphylococcus aureus* (MSSA). Aromatic acids are somewhat rare in natural products, with most being produced by actinomycetes [13–16].

Although the solwaric acids did not present elucidation challenges typical of some natural products, such as few protons, the aromatic ring was substituted only with carbon-based substituents. As a result, the chemical shifts of the protons presented challenges with respect to unambiguously determining the location of the methyl group. HMBC correlations were not

conclusive and ^{13}C calculations using density functional theory were questionable due to the small differences between two potential structures. Therefore, solwaric acids A (**1**) and B (**2**) were isotopically enriched with U-^{13}C glucose, which allowed for acquisition of a ^{13}C–^{13}C COSY and unambiguous assignment of the aromatic methyl group location. While the gCOSY requires isotopic enrichment, the method is still economically feasible, and can be made even more so by the use of ^{13}C-optimized cryoprobes, which drastically reduce the amount of compound needed and therefore the amount of U-^{13}C glucose required. We have more broadly explored the ^{13}C gCOSY as a rapid route for establishing carbon connectivity, and it appears broadly useful for a broad range of bacterially produced natural products. Overall, we have found this method to be highly promising.

2. Results and Discussion

2.1. Bacterial Strain Selection and Structure Elucidation

Strain WMMB329 was investigated due to the lack of chemistry described in the literature from *Solwaraspora* spp. as well as antibacterial activity from initial screening of a crude extract. After fermentation and isolation of the bioactive compounds, WMMB329 was found to produce solwaric acids A (**1**) and B (**2**), as well as the known 2,4,6-triphenyl-1-hexene (**3**) (Figure 1).

Figure 1. Structures of **1**–**3**.

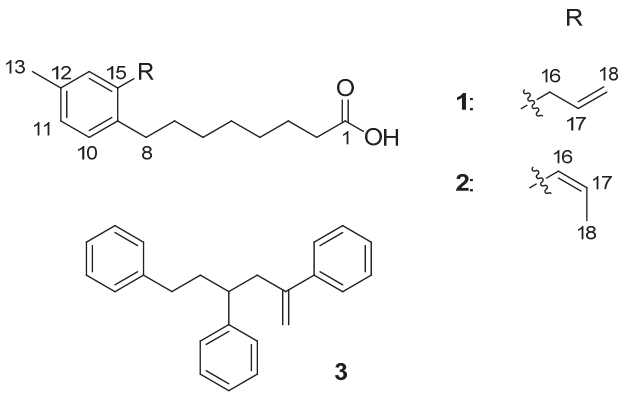

HRMS supported the molecular formula of $C_{18}H_{26}O_2$ for both solwaric acid A (**1**) and B (**2**). The structures of solwaric acids A (**1**) and B (**2**) were determined by analysis of ^{1}H and ^{13}C NMR data (Table 1, Supplementary Figures S1–S16). Since the assignment of solwaric acid A (**1**) and B (**2**) was confirmed by direct ^{13}C–^{13}C correlation experiments, the discussion of elucidation has been eliminated with the exception of the olefin at C-16 and C-17 in solwaric acid B (**2**), which was determined to be *Z* based on the vicinal coupling constant ($^{3}J_{H}$ 11.4) [17]. The presence of a methyl group (C-13) attached to the phenyl ring was indicated by HMBC correlations to three aromatic carbon atoms, but it could not be determined unambiguously relative to the other aromatic carbons. The major problem was that two protons in the aromatic ring (H-11 and H-14) were at nearly identical chemical shifts. Additionally, C-9 and C-15 were at nearly identical chemical shifts.

Therefore, the HMBC correlations supported two possible arrangements for C-10 through C-14 relative to positions 9 and 15. To further complicate matters, the close chemical shifts of H-11 and H-14 made it difficult to justify assignment based on NOE. Finally, DFT calculations showed differences in the calculated ^{13}C shifts that were within what we have observed as typical experimental error (*i.e.*, not overly conclusive). Direct ^{13}C–^{13}C correlations, however, would solve the problem. Consequently, we evaluated the use of ^{13}C-labeling of the two compounds using U-^{13}C glucose and subsequent acquisition of a ^{13}C–^{13}C gCOSY to address this issue.

Table 1. ^{1}H and ^{13}C NMR data for **1** and **2** (600 MHz for ^{1}H, 150 MHz for ^{13}C, $CDCl_3$).

Position	1		2		COSY	HMBC
	δ_C, mult.	δ_H (*J* in Hz)	δ_C, mult.	δ_H (*J* in Hz)		
1	180.1, C		180.5, C			
1-OH				9.34, s		
2	34.4, CH_2	2.33, t (6.6)	34.8, CH_2	2.29, t (6.6)	3	3, 4
3	24.9, CH_2	1.60, m	25.0, CH_2	1.59, m	2, 4	2, 4
4	29.2, CH_2	1.30, m	29.3, CH_2	1.30, m	3	
5	29.4, CH_2	1.30, m	29.4, CH_2	1.30, m		
6	29.9, CH_2	1.30, m	29.6, CH_2	1.30, m	7	
7	31.3, CH_2	1.51, m	30.9, CH_2	1.48, m	8	9
8	32.5, CH_2	2.52, t (7.6)	33.2, CH_2	2.50, t (7.6)	7	6, 9, 10
9	137.9, C		138.1, C			
10	129.4, CH	7.02, d (7.2)	129.0, CH	7.04, d (7.2)	11	8, 12
11	127.2, CH	6.95, d (7.2)	127.6, CH	6.96, d (7.2)	10	14
12	135.5, C		134.7, C			
13	21.2, CH_3	2.27, s	21.2, CH_3	2.30, s		11, 12, 14
14	130.4, CH	6.94, s	130.3, CH	6.97, s		9, 13
15	137.5, C		136.1, C			
16	37.2, CH_2	3.33, br d (6.4)	129.1, CH	6.47, br d (11.4)	17	12, 14, 18
17	137.7, CH	5.93, tdd (6.4, 10.1, 16.9)	126.9, CH	5.77, dq (11.4, 7.0)	16, 18	18
18	115.7, CH_2	5.04, tdd (1.7, 1.7, 10.1) 5.00, tdd (1.7, 1.7, 16.9)	14.6, CH_3	1.71, dd (1.8, 7.0)	17	16, 17

2.2. ^{13}C–^{13}C gCOSY

NMR experiments, such as the 2D INADEQUATE, have been used for direct determination of carbon-carbon connectivity within natural products [18,19]. Even with cryoprobes, the INADEQUATE can present difficulties due to sample solubility since it requires a fairly concentrated sample. Therefore, we decided to evaluate a ^{13}C–^{13}C gCOSY, which would require a shorter minimum phase cycle than the INADEQUATE, could be easily implemented, and could be easily interpreted. In particular, calculations suggested that the standard two-pulse gCOSY implemented on NMR spectrometers for ^{1}H experiments could be used for ^{13}C–^{13}C with no

modifications to the pulse program. In fact, after adjusting for ^{13}C and spectral widths, a theoretical sampling of coupling constants in the range 30 to 60 Hz would produce maximum polarization transfer at 33 to 17 ms, respectively. Additionally, S/N for J_{CC} = 60 Hz would be maximized with 450 increments—though smaller values (e.g., 256) could be used without much loss in sensitivity—resulting in the 2D resolution of 0.55 ppm (Supplementary Figure S17). The combination of easily optimizing for a range of ^{13}C–^{13}C coupling constants combined with the fact that the gCOSY does not require ^{13}C inversion pulses and that the experiment could be immediately implemented by others with no requirement for pulse programming made the simple gCOSY an encouraging prospect (Supplementary Figures S18 and S19). The only drawback was that the ^{13}C–^{13}C COSY experiment requires isotopic enrichment. To address this problem, we tested the feasibility of ^{13}C incorporation of microbial-derived natural products in conjunction with evaluating the feasibility of the ^{13}C–^{13}C gCOSY.

To increase the ^{13}C abundance, fermentation of WMMB329 in 1 L ASW-A using uniformly ^{13}C-labeled glucose (10 g/L ASW-A) and subsequent purification yielded solwaric acids A (**1**) and B (**2**) with about 35% ^{13}C incorporation (as evidenced by MS isotopic distribution). The ^{13}C–^{13}C gCOSY (Figure 2) was acquired in two hours on 18 μmoles (105 μM) solwaric acid A (**1**) and allowed for the methyl group (C-13) to be unambiguously assigned as attached to C-12; likewise, ^{13}C–^{13}C COSY correlations were seen between C-12 and C-14, as well as C-14 and C-15. Analysis of the ^{13}C–^{13}C COSY also confirmed the carbon connectivity throughout the rest of the structure (Supplementary Figure S20). While the ^{13}C–^{13}C gCOSY was acquired on 5 mg of solwaric acid A (**1**), the experiment can be effectively acquired at considerably lower concentrations. The exact concentration is dependent on the level of ^{13}C incorporation and the spectrometer used, but our initial studies suggest that a ^{13}C–^{13}C gCOSY can be effectively acquired on low μM concentrations in less than 24 h.

Figure 2. ^{13}C–^{13}C COSY of ^{13}C-labeled **1**.

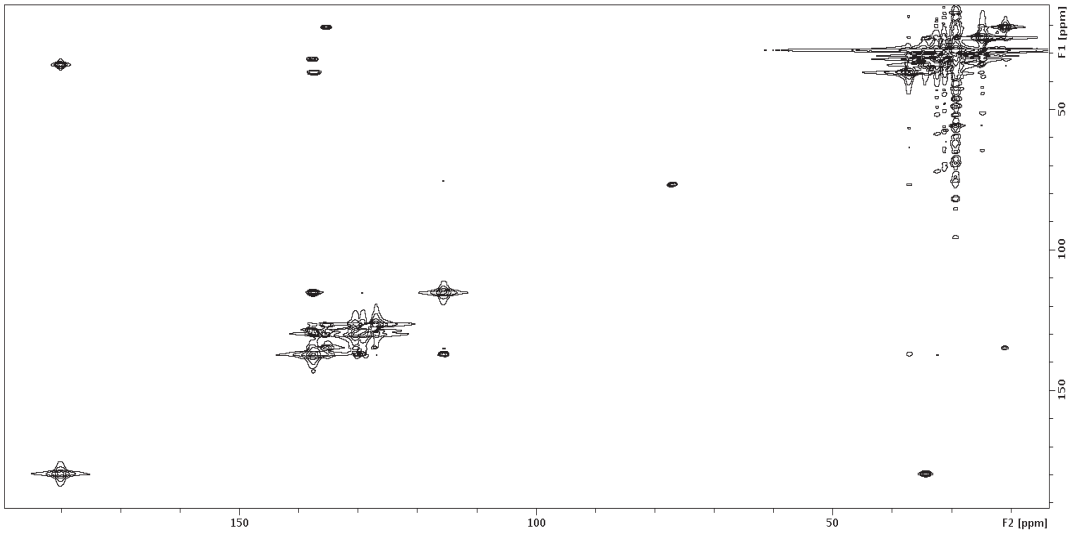

We have also tested to see if this approach would be more broadly applicable to other types of natural products. For example, we have produced two novel ^{13}C-labeled peptides from marine-derived bacteria, the structures of which will be reported in a subsequent publication. For complicated structures, this method will drastically reduce elucidation time, which is currently a bottleneck in natural products discovery. Also, recent work by Williamson and Martin has shown that ^{13}C–^{13}C coupling constants can aid in establishing configuration [20]. Even modest levels of ^{13}C incorporation would be helpful to apply ^{13}C–^{13}C coupling constants for help in structure elucidation.

Additionally, ^{13}C-labeling and acquisition of a ^{13}C–^{13}C COSY can be useful for analyzing crude extracts or mixtures of compounds. We have demonstrated this approach by acquiring a ^{13}C–^{13}C COSY on the extract from the $CHCl_3$ partition of WMMB329 (Supplementary Figure S21). The $CHCl_3$ partition was the first step of purification of the crude extract, and therefore, contained a mixture of compounds. Acquisition of the ^{13}C–^{13}C COSY on ^{13}C-labeled extract allows for separation of the chemistry on a large sweep width (~200 ppm) and elimination of most media components—which are unlabeled—from the spectrum. Although there may still be a mixture of several labeled compounds, this method could rapidly provide carbon-carbon connectivity for portions of the structures, which could be helpful for dereplication. Therefore, ^{13}C-labeling of natural products can be a valuable tool for structure elucidation, as well as other areas of natural product research.

2.3. Biological Activity

Solwaric acids A (**1**) and B (**2**) showed antibacterial activity and were more potent against gram positive bacteria (Table 2). Vancomycin and gentamicin were used as a positive control in assays with gram positive and gram negative bacteria, respectively. The known 2,4,6-triphenyl-1-hexene (**3**) (Supplementary Figures S22–S24) demonstrated no antibacterial activity.

Table 2. Minimum Inhibitory Concentration (μg/mL) of **1**–**3**.

	MRSA	**MSSA**	***E. coli***	***P. aeruginosa***
1	32	64	128	128
2	32	64	128	128
3	>128	>128	>128	>128

3. Experimental Section

3.1. General Experimental Procedures

Optical rotations were measured on a Perkin–Elmer 241 Polarimeter. UV spectra were recorded on an Aminco/OLIS UV-Vis spectrophotometer. IR spectra were measured with a Bruker Equinox 55/S FT–IR spectrophotometer. NMR spectra were obtained in $CDCl_3$ with a Bruker Avance 600 MHz spectrometer equipped with a 1.7 mm $^{1}H\{^{13}C/^{15}N\}$ cryoprobe, a Bruker Avance 500 MHz spectrometer equipped with a $^{13}C/^{15}N\{^{1}H\}$ cryoprobe, and a Varian Unity-Inova 500 MHz spectrometer. HRMS data were acquired with a Bruker MaXis™ 4G QTOF mass spectrometer. RP HPLC was performed using a Shimadzu Prominence HPLC system and a Phenomenex Luna

C18 column (250 × 10 mm, 5 µm), as well as a Gilson Preparative HPLC and Phenomenex Gemini C18 column (250 × 30 mm, 5 µm).

3.2. Biological Material

Ascidian specimens were collected on 11 October 2010, in the Florida Keys (24°37.4873′, 81°27.443′). Identification was confirmed by Shirley Parker-Nance. A voucher specimen (FLK10-5-1) for *Trididemnum orbiculatum* (Van Name, 1902) [12] is housed at the University of Wisconsin-Madison. For cultivation, a sample of ascidian (1 cm^3) was rinsed with sterile seawater, macerated using a sterile pestle in a micro-centrifuge tube, and dilutions were made in sterile seawater, with vortexing between steps to separate bacteria from heavier tissues. Dilutions were separately plated on three media: ISP2 supplemented with artificial seawater [21], R2A [22], and M4 [23]. Each medium was supplemented with 50 µg/mL cycloheximide and 25 µg/mL nalidixic acid. Plates were incubated at 28 °C for at least 28 days, and strain WMMB329 was purified from an M4 isolation plate.

3.3. Sequencing

16S rDNA sequencing was conducted as previously described [24]. WMMB329 was identified as a *Solwaraspora* sp. and demonstrated 99% sequence similarity to *Solwaraspora* sp. UMM486 (accession number AY552774) and 99% sequence similarity to *Micromonospora* sp. S3-1 (accession number AB645957). The 16S sequence for WMMB329 was deposited in GenBank (accession number KC856821).

3.4. Fermentation, Extraction, and Isolation

One 10 mL seed culture (25 × 150 mm tube) in medium modified ASW-A (5 g soluble starch, 10 g glucose, 5 g peptone, 5 g yeast extract per liter of 50%/50% artificial seawater/diH_2O) were inoculated with strain WMMB329 and shaken (200 RPM, 28 °C) for fifteen days. For fermentation, 500 mL baffled flasks (2 × 100 mL) containing ASW-A (20 g soluble starch, 10 g glucose, 5 g peptone, 5 g yeast extract, 5 g $CaCO_3$ per liter of artificial seawater) were inoculated with 4 mL seed culture and were incubated (200 RPM, 28 °C) for fourteen days. Two-liter flasks (15 × 500 mL) containing medium ASW-A with Diaion HP20 (7% by weight) were inoculated with 5 mL from the 100 mL culture and shaken (200 RPM, 28 °C) for ten days. Filtered HP20 and cells were washed with H_2O and extracted with acetone. The acetone extract (7.1 g) was subjected to liquid-liquid partitioning using 90%/10% MeOH/H_2O and hexanes (1:1) followed by liquid-liquid partitioning of the previous aqueous layer using 70%/30% MeOH/H_2O and $CHCl_3$ (1:1). The hexanes partition (287 mg) was fractionated by Sephadex LH20 column chromatography (2.5 × 40 cm, $CHCl_3$:MeOH, 1:1). Fractions containing 1–3 were subjected to RP HPLC (70/30% to 90/10% ACN/H_2O with H_2O containing 0.1% acetic acid, 25 min, 25 mL/min followed by 90/10% to 100/0% of same solvents, 3 min, 25 mL/min, and a hold at 100/0% of same solvents) using a Phenomenex Gemini C18 column (250 × 30 mm, 5 µm), yielding 1 (15.4 mg, t_R 18.0 min), 2 (13.8 mg, t_R 19.5 min), and 3 (4.9 mg, t_R 31.5 min). For ^{13}C incorporation, the same procedure

was used with two-liter flasks (2 × 500 mL) containing medium ASW-A (U-^{13}C-glucose substituted for unlabeled glucose). Yields for solwaric acids A (**1**) and (**2**) were approximately the same during fermentation with U-^{13}C glucose as with unlabeled glucose.

Solwaric acid A (**1**). colorless solid; UV (MeOH) λ_{max} (log ε) 204 (2.77), 218 (2.49), 271 (1.27) nm; IR (ATR) ν_{max} 2928, 2856, 1707, 1412, 1217, 994, 911, 819, 755 cm^{-1}; ^{1}H and ^{13}C NMR (Table 1); HRMS $[M + Na]^+$ *m/z* 297.1836 (calcd. for $C_{18}H_{26}O_2Na^+$, 297.1825).

Solwaric acid B (**2**). colorless solid; UV (MeOH) λ_{max} (log ε) 208 (2.79), 238 (2.48), 281 (1.29) nm; IR (ATR) ν_{max} 2928, 2856, 1708, 1410, 1217, 820, 755, 707, 667 cm^{-1}; ^{1}H and ^{13}C NMR (Table 1); HRMS $[M + Na]^+$ *m/z* 297.1838 (calcd. for $C_{18}H_{26}O_2Na^+$, 297.1825).

3.5. Antibacterial Assay

Solwaric acid A (**1**) and B (**2**) and 2,4,6-triphenyl-1-hexene (**3**) were tested for antibacterial activity against MSSA (ATCC #29213), MRSA (ATCC #33591), *E. coli* (ATCC #25922), and *P. aeruginosa* (ATCC #27853), and MICs were determined using a dilution antimicrobial susceptibility test for aerobic bacteria [25]. Solwaric acids A (**1**) and B (**2**) and 2,4,6-triphenyl-1-hexene (**3**) were dissolved in DMSO, serially diluted to 10 concentrations (0.25–128 µg/mL), and tested in a 96-well plate. Vancomycin was used as a control and exhibited an MIC of 1 µg/mL against MSSA and 1 µg/mL against MRSA. Gentamicin was used as a control and exhibited an MIC of 4 µg/mL against *E. coli* and 4 µg/mL against *P. aeruginosa*. Solwaric acids A (**1**) and B (**2**) and 2,4,6-triphenyl-1-hexene (**3**) were tested in triplicate, and vancomycin and gentamicin was tested in triplicate. Six untreated media controls were included on each plate. The plates were incubated at 33 °C for 18 h. The MIC was determined as the lowest concentration that inhibited visible growth of bacteria.

4. Conclusions

We reported the isolation and structure elucidation of two novel trialkyl-substitued aromatic acids, solwaric acids A (**1**) and B (**2**), and the known 2,4,6-triphenyl-1-hexene (**3**). The novel compounds demonstrated antibacterial activity against methicillin-resistant *Staphylococcus aureus* (MRSA) and methicillin-sensitive *Staphylococcus aureus* (MSSA). Solwaric acid A (**1**) and B (**2**) were enriched with ^{13}C-labeled glucose that allowed for the acquisition of a ^{13}C–^{13}C COSY and unambiguous assignment of the methyl group location on the phenyl ring. While this example utilized ^{13}C-labeling to determine carbon connectivity for one challenging portion of the structure, this method could be valuable for molecules with multiple tetrasubstituted centers, which make structure elucidation by standard NMR experiments more challenging. Hence, ^{13}C incorporation and subsequent acquisition of a ^{13}C–^{13}C COSY—aided by the increasing sensitivity of NMR spectrometers—could drastically reduce the time for structure determination of microbial-derived natural products, including peptides and terpenes. Compared to the cost and time involved with other methods such as computer assisted structure determination, labeling microbial natural products offers a cost effective solution while providing high confidence in the proposed structure.

Acknowledgments

This work was supported by funding from the University of Wisconsin-Madison School of Pharmacy, the Graduate School at the University of Wisconsin, and the UW College of Agriculture and Life Sciences. This work was also funded by the NIH, NIGMS Grant R01 GM092009 and by R01 GM104192. We would like to thank the Analytical Instrumentation Center at the University of Wisconsin-Madison for the facilities to acquire spectroscopic data, as well as the University of Wisconsin-Madison Chemistry Instrument Center (The purchase of the Waters (Micromass) Autospec® in 1994 was partially funded by NSF Award #CHE-9304546 to the Department of Chemistry). This study made use of the National Magnetic Resonance Facility at Madison, which is supported by NIH grants P41RR02301 (BRTP/NCRR) and P41GM66326 (NIGMS). Additional equipment was purchased with funds from the University of Wisconsin, the NIH (RR02781, RR08438), the NSF (DMB-8415048, OIA-9977486, BIR-9214394), and the USDA. We would like to thank Don Demaria for assistance with collection and Shirley Parker-Nance for taxonomy.

Conflicts of Interest

The authors declare no conflict of interest.

References

1. World Health Organization. *Deaths by Cause, Sex, and Mortality Stratum in WHO Regions, Estimates for 2002: World Health Report—2004*; World Health Organization: Geneva, Switzerland, 2004; p. 1.
2. Smith, R.; Coast, J. The true cost of antimicrobial resistance. *Br. Med. J.* **2013**, *346*, doi:10.1136/bmj.f1493.
3. Center for Disease Control and Prevention. Available online: http://www.cdc.gov/drugresistance/threat-report-2013/ (accessed on 13 December 2013).
4. Boucher, H.W.; Talbot, G.H.; Bradley, J.S.; Edwards, J.E., Jr.; Gilbert, D.; Rice, L.B.; Scheld, M.; Spellberg, B.; Bartlett, J. Bad bugs, no drugs: No ESKAPE! An update from the Infectious Diseases Society of America. *Clin. Infect. Dis.* **2009**, *48*, 1–12.
5. Stefani, S.; Chung, D.R.; Lindsay, J.A.; Friedrich, A.W.; Kearns, A.M.; Westh, H.; MacKenzie, F.M. Meticillin-Resistant *Staphylococcus aureus* (MRSA): Global epidemiology and harmonisation of typing methods. *Int. J. Antimicrob. Agents* **2012**, *39*, 273–282.
6. Köck, R.; Becker, K.; Cookson, B.; van Gemert-Pijnen, J.E.; Harbarth, S.; Kluytmans, J.; Mielke, M.; Peters, G.; Skov, R.L.; Struelens, M.J.; *et al*. Methicillin-Resistant *Staphylococcus aureus* (MRSA): Burden of disease and control challenges in Europe. *Euro Surveill.* **2010**, *15*, 19688–19696.
7. Klevens, R.M.; Morrison, M.A.; Nadle, J.; Petit, S.; Gershman, K.; Ray, S.; Harrison, L.H.; Lynfield, R.; Dumyati, G.; Townes, J.M.; *et al*. Invasive methicillin-resistant *Staphylococcus aureus* infections in the United States. *JAMA* **2007**, *298*, 1763–1771.

8. de Kraker, M.E.A.; Wolkewitz, M.; Davey, P.G.; Koller, W.; Berger, J.; Nagler, J.; Icket, C.; Kalenic, S.; Horvatic, J.; Seifert, H.; *et al*. Clinical impact of antimicrobial resistance in European hospitals: Excess mortality and length of hospital stay related to methicillin-resistant *Staphylococcus aureus* bloodstream infections. *Antimicrob. Agents Chemother.* **2011**, *55*, 1598–1605.
9. Staudinger, H.; Steinhofer, A. Über hochpolymere verbindungen. 107. Mitteilung. Beiträge zur kenntnis der polystyrole. *Justus Liebigs Ann. Chem.* **1935**, *517*, 35–53.
10. Mayo, F.R. The dimerization of styrene. *J. Am. Chem. Soc.* **1968**, *90*, 1289–1295.
11. Ayer, W.A.; Muir, D.J.; Chakravarty, P. Phenolic and other metabolites of *Phellinus pini*, a fungus pathogenic to pine. *Phytochemistry* **1996**, *42*, 1321–1324.
12. Van Name, W.G. The ascidians of the Bermuda Islands. *Trans. Connecticut Acad. Sci*. **1902**, *11*, 325–412.
13. Iwata, F.; Sato, S.; Mukai, T.; Yamada, S.; Takeo, J.; Abe, A.; Okita, T.; Kawahara, H. Lorneic acids, trialkyl-substituted aromatic acids from a marine-derived actinomycete. *J. Nat. Prod.* **2009**, *72*, 2046–2048.
14. Wenzel, S.C.; Bode, H.B. Novel polyene carboxylic acids from *Streptomyces*. *J. Nat. Prod.* **2004**, *67*, 1631–1633.
15. Mehnaz, S.; Saleem, R.S.; Yameen, B.; Pianet, I.; Schnakenbur, G.; Pietraszkiewicz, H.; Valeriote, F.; Josten, M.; Sahl, H.G.; Franzblau, S.G.; *et al*. Lahorenoic acids A–C, *ortho*-dialkyl-substituted aromatic acids from the biocontrol strain *Pseudomonas aurantiaca* PB-St2. *J. Nat. Prod.* **2013**, *76*, 135–141.
16. Raju, R.; Gromyko, O.; Fedorenko, V.; Luzhetskyy, A.; Müller, R. Lorneic acids C and D, new trialkyl-substituted aromatic acids isolated from a terrestrial *Streptomyces* sp. *J. Antibiot.* **2013**, *66*, 347–349.
17. Williams, D.H.; Fleming, I. *Spectroscopic Methods in Organic Chemistry*, 4th ed.; McGraw-Hill Book Company Limited: London, UK, 1987; pp. 143–146.
18. Bugni, T.S.; Bernan, V.S.; Greenstein, M.; Janso, J.E.; Maiese, W.M.; Mayne, C.L.; Ireland, C.M. Brocaenols A–C: Novel polyketides from a marine-derived *Penicillium brocae*. *J. Org. Chem.* **2003**, *68*, 2014–2017.
19. Meyer, S.W.; Köck, M. NMR studies of phakellins and isophakellins. *J. Nat. Prod.* **2008**, *71*, 1524–1529.
20. Bifulco, G.; Riccio, R.; Martin, G.E.; Buevich, A.V.; Williamson, R.T. Quantum chemical calculations of $^{1}J_{CC}$ coupling constants for the stereochemical determination of organic compounds. *Org. Lett.* **2013**, *15*, 654–657.
21. Harrison, P.J.; Waters, R.E.; Taylor, F.J.R. A broad spectrum artificial seawater medium for coastal and open ocean phytoplankton. *J. Phycol.* **1980**, *16*, 28–35.
22. Reasoner, D.J.; Geldreich, E.E. A new medium for the enumeration and subculture of bacteria from potable water. *Appl. Environ. Microbiol.* **1985**, *49*, 1–7.
23. Maldonado, L.A.; Fragoso-Yáñez, D.; Pérez-García, A.; Rosellón-Druker, J.; Quintana, E.T. Antinobacterial diversity from marine sediments collected in Mexico. *Antonie Van Leeuwenhoek* **2009**, *95*, 111–120.

24. Wyche, T.P.; Hou, Y.; Braun, D.; Cohen, H.C.; Xiong, M.P.; Bugni, T.S. First natural analogs of the cytotoxic thiodepsipeptide thiocoraline A from a marine *Verrucosispora* sp. *J. Org. Chem.* **2011**, *76*, 6542–6547.
25. National Committee for Clinical Laboratory Standards. *Methods for Dilution Antimicrobial Susceptibility Tests for Bacteria that Grow Aerobically*, 7th ed.; NCCLS: Villanova, PA, USA, 2006; Approved standard M7-A7.

Optimization of Medium Using Response Surface Methodology for Lipid Production by *Scenedesmus* sp.

Fangfang Yang, Lijuan Long, Xiumei Sun, Hualian Wu, Tao Li and Wenzhou Xiang

Abstract: Lipid production is an important indicator for assessing microalgal species for biodiesel production. In this work, the effects of medium composition on lipid production by *Scenedesmus* sp. were investigated using the response surface methodology. The results of a Plackett–Burman design experiment revealed that $NaHCO_3$, $NaH_2PO_4 \cdot 2H_2O$ and $NaNO_3$ were three factors significantly influencing lipid production, which were further optimized by a Box–Behnken design. The optimal medium was found to contain 3.07 g L^{-1} $NaHCO_3$, 15.49 mg L^{-1} $NaH_2PO_4 \cdot 2H_2O$ and 803.21 mg L^{-1} $NaNO_3$. Using the optimal conditions previously determined, the lipid production (304.02 mg·L^{-1}) increased 54.64% more than that using the initial medium, which agreed well with the predicted value 309.50 mg L^{-1}. Additionally, lipid analysis found that palmitic acid (C16:0) and oleic acid (C18:1) dominantly constituted the algal fatty acids (about 60% of the total fatty acids) and a much higher content of neutral lipid accounted for 82.32% of total lipids, which strongly proved that *Scenedesmus* sp. is a very promising feedstock for biodiesel production.

Reprinted from *Forests*. Cite as: Fangfang Yang, Lijuan Long, Xiumei Sun, Hualian Wu, Tao Li and Wenzhou Xiang. Optimization of Medium Using Response Surface Methodology for Lipid Production by *Scenedesmus* sp. *Mar. Drugs* **2014**, *12*, 1245–1257.

1. Introduction

In recent years, since the energy crisis and climate change have been major challenges we are facing, it is essential to develop novel energy forms, which are sustainable and friendly to the environment [1,2]. As an ideal and effective alternative fuel, biofuel has drawn more and more attention of researchers. To date, three generations of biofuel feedstocks have been developed [3]. Compared to the first and second generation (food crops, non-food crops), microalgae, a third generation biofuel feedstock, have been indicated as a superior replacement, because of their capability to grow rapidly and produce abundant triacylglycerols (TAG). Moreover, microalgae can survive over a wide range of environmental conditions, even non-arable land and saline water. Therefore, producing oils by microalgae does not result in a discord between food and fuel [4–6].

Based upon these advantages of microalgae, the annual lipid yield can achieve 200 barrels per hectare of land in theory [7]. So far, producing biodiesel by microalgae has obtained significant advances in small-scale laboratory experiments and field testing stages [7,8]. However, due to the high cost and low lipid yield, microalgae-based biodiesel production still lacks economic viability at a large-scale. Therefore, optimization of lipid production is important for biodiesel production from microalgae. Extensive research revealed that environmental conditions can modify the lipid metabolism of microalgae efficiently [9–11]. In particular, nutritional factors (e.g., nitrogen, phosphorus, carbon and iron) are recognized as one of the most crucial factors influencing the lipid accumulation and the yield of biomass [12–16]. Generally, nutrient starvation, such as nitrogen and

phosphorus deficiency, can stimulate lipid accumulation for several microalgae species [17,18]. For instance, the lipid content of *Nannochloris* sp. UTEX LB1999 had an 83.08% increase with the nitrogen concentration decreasing to 0.9 mM [19]. However, the deficiencies in a few nutrients have been also observed to severely limit the growth of microalgae. As a result, the overall lipid production, which is the product of the growth rate multiplied by the lipid content, may be lower [13,20]. Moreover, these studies have been carried out to investigate single-factor optimization. It is obvious that the classical method of optimization may bring about unsatisfactory or incorrect results, due to the ignoring of the interaction between factors.

The response surface methodology (RSM) is an effective and convenient method for screening key factors rapidly from multiple factors and optimizing culture conditions, which can avoid the defects brought by single-factor optimization [21,22]. The method has already been successfully utilized in many fields, such as the chemical industry, engineering, biology, *etc*. [23–25]. However, only a few reports related the application of RSM in the optimizing of autotrophic microalgal medium for lipid production, where RSM had been shown to enhance lipid production by a two-step strategy with initial optimization of microalgal growth and final optimization of lipid accumulation [26,27]. To our knowledge, the research using directly RSM for improving the value of lipid production by one-stage culture in the autotrophic microalgae has been scarcely reported till now. Additionally, differences among species exist and, sometimes, even among strains of the same species. Therefore, for each individual microalga, systematic studies are needed to optimize the medium in order to obtain its maximum lipid production.

In this study, a green microalga identified as *Scenedesmus* sp. was isolated. Due to its strong tolerance to high alkalinity and salinity, this species could be resistant to contamination by other organisms. In our previous experiment, the feasibility of *Scenedesmus* sp. culture has been demonstrated in an outdoor raceway system of up to 66 m^3. However, the lipid production needed to be improved further. To maximize its lipid production, a Plackett–Burman design was used to evaluate the significance of nine nutrient factors of the medium towards lipid production, and then, a Box–Behnken design was also utilized to identify the best culture strategy. Furthermore, the extracted lipids were investigated to further assess the potential of *Scenedesmus* sp. in producing biodiesel.

2. Results and Discussion

2.1. Evaluating the Significant Nutrient Factors Using Plackett–Burman Design

The Plackett–Burman design with two coded levels for all twelve runs was employed to analyze comprehensively the influence of nine nutrient components on the response value-lipid production. The lipid production was the product of lipid content and biomass, the importance of which is above the lipid content and growth rate individually. Therefore, lipid production was a reliable indicator for evaluating algal species for biodiesel production [20]. The experimental data, illustrated in Table 1 and Supplementary Table S1, were calculated by the Design-Expert software, and the results of variance analysis and the estimation of parameters are listed in Table 2. The *p*-value was used to evaluate the significance of the variable. When the *p*-value of the variable was less than 5%, it

represented that the variable had significant effects on the response value. To further assess the effect of the variable, coefficient estimate was applied. Lipid production could grow with increasing concentrations of the variable if the coefficient estimate were positive; conversely, the value was negative, indicating that lipid production was negatively correlated with the variable levels [28]. As shown in Table 2, A_5 solution, soil extract and $NaH_2PO_4 \cdot 2H_2O$ had a negative effect, whereas the other factors displayed a positive effect on lipid production. $NaH_2PO_4 \cdot 2H_2O$ was the most important variable impacting lipid production and growth, with *p*-value less than 0.0001. With decreasing phosphate concentrations from 100 mg L^{-1} to 25 mg L^{-1}, the cellular lipid content in microalgae *Scenedesmus* sp. increased evidently, where the *p*-value was less than 0.001. Furthermore, low phosphate had a positive effect on biomass associated with inducing a higher lipid accumulation in cells. Therefore, lipid production was observed to be more with the low phosphate medium than with the high phosphate medium (Table 2).

So far, various studies have been carried out to demonstrate that the nitrogen source was the important nutrition in the medium affecting the growth and lipid accumulation [13]. There was evidence to suggest that nitrogen deficiency could stimulate lipid accumulation [29,30]. However, under the applied experimental conditions, this phenomenon was not observed; instead, $NaNO_3$ had a positive effect on lipid production (Table 2). The reason might be that the $NaNO_3$ concentration did not reach the limiting level for *Scenedesmus* sp. In fact, these experiments were limited to nine days of culture, and the nitrogen level was set in the range of 250 and 1,000 mg·L^{-1}, which was higher than that previously reported [29]. In a short period of time, the $NaNO_3$ may not be depleted and reach the limiting level. Additionally, although the lipid production was increased with the increasing nitrogen level, the contribution of $NaNO_3$ was low, with 4.47%.

Table 1. Results and experimental layout of *Scenedesmus* sp. in a Plackett–Burman design.

Run	X_1	X_2	X_3	X_4	X_5	X_6	X_7	X_8	X_9	Lipid production (mg·L^{-1})
1	4	200	25	1000	40	100	0.5	0.5	0.5	230.38
2	1	200	100	250	40	100	2	0.5	0.5	174.27
3	4	50	100	1000	10	100	2	2	0.5	188.56
4	1	200	25	1000	40	20	2	2	2	208.85
5	1	50	100	250	40	100	0.5	2	2	152.85
6	1	50	25	1000	10	100	2	0.5	2	199.58
7	4	50	25	250	40	20	2	2	0.5	215.37
8	4	200	25	250	10	100	0.5	2	2	214.41
9	4	200	100	250	10	20	2	0.5	2	173.23
10	1	200	100	1000	10	20	0.5	2	0.5	166.16
11	4	50	100	1000	40	20	0.5	0.5	2	188.82
12	1	50	25	250	10	20	0.5	0.5	0.5	196.58

X_1, $NaHCO_3$ (g·L^{-1}); X_2, KCl (mg·L^{-1}); X_3, $NaH_2PO_4 \cdot 2H_2O$ (mg·L^{-1}); X_4, $NaNO_3$ (mg·L^{-1}); X_5, $CaCl_2$ (mg·L^{-1}); X_6, $MgSO_4 \cdot 7H_2O$ (mg·L^{-1}); X_7, EDTA-Fe^{3+} (mL·L^{-1}); X_8, A_5 solution (mL·L^{-1}); X_9, soil extract (mL·L^{-1}).

In this study, $NaHCO_3$ was also identified as a significant factor for lipid production. It was obvious that increasing the concentration of carbon could dramatically promote the growth rate of *Scenedesmus* sp. (*p*-value lower than 0.0001). The lipid production was improved considerably with increasing carbon concentration, which accounted for 18.27% of the total contribution (Table 2). This was in agreement with previous reports [16,31,32]. For instance, the lipid production was significantly increased when supplemented with 2 $g \cdot L^{-1}$ bicarbonate, compared with zero and 1 $g \cdot L^{-1}$ bicarbonate in microalga *Tetraselmis suecica* and *Nannochlorpsis salina* [16]. Besides, growing well in a high level of $NaHCO_3$ (3 $g \cdot L^{-1}$) implied that *Scenedesmus* sp. had a high tolerance for alkalinity.

Table 2. Statistical analysis of the Plackett–Burman experiment design.

Factor	Level		Effect	Sum of Squares	Contribution %	Coefficient Estimate	*t*-value	*p*-value	Effect
	−1	+1							
$NaHCO_3$	1	4	18.7476	1,054.3100	18.2703	9.37	0.0034	0.0015 [a]	
KCl	50	200	4.2567	54.3576	0.9420	1.9608	0.1537	—	
$NaH_2PO_4 \cdot 2H_2O$	25	100	−36.8800	4080.4000	70.7096	−18.6075	0.0006	<0.0001 [a]	
$NaNO_3$	250	1000	9.2733	257.9840	4.4706	4.4692	0.0582	0.0477 [a]	
$CaCl_2$	10	40	5.3367	85.4400	1.4806	2.8358	0.1306	—	
$MgSO_4 \cdot 7H_2O$	20	100	1.8400	10.1568	0.1760	1.0875	0.3203	—	
EDTA-Fe^{3+}	0.5	2	1.7767	9.4696	0.1641	1.0558	0.2877	—	
A_5	0.5	2	−2.7767	23.1296	0.4008	−1.5558	0.1907	—	
Soil extract	0.5	2	−5.5967	93.9680	1.6284	−2.6308	0.1046	—	

[a] Significance level at a *p*-value less than 5%; —, significance level at a *p*-value of more than 5%, $R^2 = 0.9345$; $R_{adj}^2 = 0.9099$; $R_{pred}^2 = 0.8526$; coefficient of variation (CV) = 3.57.

In conclusion, $NaH_2PO_4 \cdot 2H_2O$, $NaHCO_3$ and $NaNO_3$ were the important variables impacting lipid production, whereas other factors were insignificant, suggesting that they were not limiting in the process of lipid production. Therefore, $NaH_2PO_4 \cdot 2H_2O$, $NaHCO_3$ and $NaNO_3$ were chosen to make further optimization by the Box–Behnken design.

In order to check the fit of the model, R^2 and *F*-value were calculated. Here, R^2 was 0.9345, indicating that 93.45% of the data in Plackett–Burman design could be explained by the model; that is, the proposed model was reasonable. Moreover, the model *F*-value of 38.05 demonstrated that the model was significant, as revealed by a *p*-value lower than 0.0001, which further supported that the model was fit to these data. From the analysis of R_{adj}^2 and R_{pred}^2, the R_{pred}^2 of 0.8526 was in good agreement with the R_{adj}^2 of 0.9099 (Table 2). In conclusion, the model was used to explain the data well.

2.2. Identifying the Best Culture Conditions for Lipid Production Using Box–Behnken Design

Based on the results of the previous experiments, the Box–Behnken design was used to further confirm the optimum concentrations of $NaH_2PO_4 \cdot 2H_2O$, $NaHCO_3$ and $NaNO_3$, to maximize lipid production. In this experiment, five replicates of the center points and twelve star points were required, resulting in a total number of seventeen experiments. Table 3 presented the experimental

project and the experimental and predicted values of response. Among the seventeen experiments, experiment seventeen ($NaHCO_3$, $NaH_2PO_4{\cdot}2H_2O$ and $NaNO_3$ concentrations of 3 g L^{-1}, 15 mg L^{-1}, 750 mg L^{-1}) offered the highest lipid production (315.74 mg L^{-1}), while experiment five ($NaHCO_3$, $NaH_2PO_4{\cdot}2H_2O$ and $NaNO_3$ concentrations of 2 g L^{-1}, 15 mg L^{-1}, 500 mg L^{-1}) provided the lowest total lipid production (171.96 mg L^{-1}).

Table 3. Experimental design and lipid production in the Box–Behnken design.

Run	$NaHCO_3$ (g L^{-1})	$NaH_2PO_4{\cdot}2H_2O$ (mg L^{-1})	$NaNO_3$ (mg L^{-1})	Lipid production (mg L^{-1})	
				Experimental	Predicted
1	2	10	750	207.53	207.77
2	4	10	750	211.29	209.08
3	2	20	750	186.23	188.44
4	4	20	750	229.44	229.20
5	2	15	500	171.96	166.17
6	4	15	500	201.35	198.01
7	2	15	1000	203.78	207.12
8	4	15	1000	211.58	217.37
9	3	10	500	240.55	246.1
10	3	20	500	200.97	204.55
11	3	10	1000	237.89	234.31
12	3	20	1000	282.19	276.64
13	3	15	750	304.86	307.51
14	3	15	750	305.22	307.51
15	3	15	750	310.39	307.51
16	3	15	750	301.35	307.51
17	3	15	750	315.74	307.51

By applying multiple regression analysis on the data above, the equation for lipid production was established as follows:

Lipid production = $-784.5075 + 423.4910NaHCO_3 + 14.9340NaH_2PO_4{\cdot}2H_2O + 0.8162NaNO_3 + 1.9725NaHCO_3{*}NaH_2PO_4{\cdot}2H_2O - 0.0216NaHCO_3{*}NaNO_3 + 0.0168NaH_2PO_4{\cdot}2H_2O{*}NaNO_3 - 71.0610NaHCO_3^2 - 1.1131\ NaH_2PO_4{\cdot}2H_2O^2 - 0.0006NaNO_3^2$.

In order to investigate the adequacy of the model, multiple regression analyses on the data were applied. The results are listed in Table 4, which were mainly the individual effects of all variables and their interactions on lipid production. The multiple correlation coefficient R^2 of 0.992 suggested that the quadratic polynomial model was suitable for revealing the mutual relationship of factors and predicting the response values in the study (Table 4).

As shown in Table 4, $NaHCO_3$ and $NaNO_3$ exerted significant individual and quadratic effects, respectively (p-value less than 0.05). $NaH_2PO_4{\cdot}2H_2O$, varying from 10 mg L^{-1} to 20 mg L^{-1}, was not significant (p-value more than 0.05), yet with significant quadratic effects for the response value (p-value less than 0.05).

The interactions between three parameters ($NaHCO_3$, $NaH_2PO_4{\cdot}2H_2O$ and $NaNO_3$) and lipid production were revealed by response surface plots and contour plots, as shown in Figure 1. Figure 1A

represents the effects of $NaHCO_3$ and $NaH_2PO_4{\cdot}2H_2O$ levels individually and their mutual interaction on the lipid production. Varying $NaHCO_3$ and $NaH_2PO_4{\cdot}2H_2O$ concentration mutual interactions had a significant effect on the total lipid production value. The increase in $NaHCO_3$ and $NaH_2PO_4{\cdot}2H_2O$ concentrations enhanced the production of lipid initially, but then, with increasing their concentrations further, which exceed 3.07 and 15.49 mg L^{-1}, respectively, the lipid production could decrease. The highest response value was observed at 3.07 g L^{-1} $NaHCO_3$ and 15.48 mg L^{-1} $NaH_2PO_4{\cdot}2H_2O$ (Figure 1A). A similar phenomenon was observed in Figure 1B with $NaH_2PO_4{\cdot}2H_2O$ and $NaNO_3$ while maintaining other variables constant. However, the lipid production was almost constant when $NaHCO_3$ and $NaNO_3$ concentrations were increased at a fixed $NaH_2PO_4{\cdot}2H_2O$ concentration (Figure 1C). This implied that the interaction between $NaHCO_3$ and $NaNO_3$ did not have a significant effect on lipid production under nitrogen sufficiency.

Table 4. Statistical analysis of the Box−Behnken experiment design.

Factor	Sum of squares	Degree of Freedom	Mean square	Coefficient Estimate	*F*-value	*p*-value
Model	38,929.9101	9	4,325.5456	307.5120	96.8736	<0.0001
$NaHCO_3$	885.3632	1	885.3632	10.5200	19.8283	0.0030
$NaH_2PO_4{\cdot}2H_2O$	0.3081	1	0.3081	0.1963	0.0069	0.9361
$NaNO_3$	1,818.3465	1	1,818.3465	15.0763	40.7231	0.0004
$NaHCO_3$*$NaH_2PO_4{\cdot}2H_2O$	389.0756	1	389.0756	9.8625	8.7136	0.0213
$NaHCO_3$*$NaNO_3$	116.5320	1	116.5320	−5.3975	2.6098	0.1502
$NaH_2PO_4{\cdot}2H_2O$*$NaNO_3$	1,758.9636	1	1,758.9396	20.9700	39.3932	0.0004
$NaHCO_3^2$	21,261.7504	1	21,261.7504	−71.0610	476.1715	<0.0001
$NaH_2PO_4{\cdot}2H_2O^2$	3,260.7386	1	3,260.7386	−27.8285	73.0265	<0.0001
$NaNO_3^2$	6,497.6563	1	6,497.6563	−39.2835	145.5195	<0.0001
Residual	312.5602	7	44.6515			
Lack of fit	186.3207	3	62.1069		1.9679	0.2609
Pure error	126.2395	4	31.5599			
Corr. total	39,242.4703	16				
Model	38,929.9101	9	4,325.5456	307.5120	96.8736	<0.0001

R^2 = 0.9920; R_{adj}^2 = 0.9818; R_{pred}^2 = 0.9190; coefficient of variation (CV) = 2.76.

According to the attained results and the equation, the model predicted the maximum lipid production of 309.50 mg L^{-1} in the concentration of 3.07 g L^{-1} $NaHCO_3$, 15.49 mg L^{-1} $NaH_2PO_4{\cdot}2H_2O$ and 803.21 mg L^{-1} $NaNO_3$. The final optimum condition was as follows: $NaHCO_3$, 3.07 g L^{-1}; $NaH_2PO_4{\cdot}2H_2O$, 0.01549 g L^{-1}; $NaNO_3$, 0.80321 g L^{-1}; $CaCl_2$, 0.02 g L^{-1}; $MgSO_4{\cdot}7H_2O$, 0.05 g L^{-1}; KCl, 0.1 g L^{-1}; A_5, 1 mL L^{-1}; EDTA-Fe^{3+}, 1 mL L^{-1}; soil extract, 1 mL L^{-1}. Under the optimum condition, the biomass and lipid content were 0.93 g·L^{-1} and 32.69% dry weight (dw), which were increased 13.41% and 36.32% more than those of the original condition, respectively. The observed lipid production was 304.02 mg·L^{-1}, agreeing well with the predicted value, indicating that the model was valid. Compared with that under the original culture condition, lipid production increased 54.64%.

2.3. Lipid Analysis and Fatty Acid Composition

The lipid profiles and fatty acid composition of *Scenedesmus* sp. were studied to evaluate the optimum medium in terms of lipid quality. As shown in Table 5, whatever the culture conditions applied, the fatty acid composition of *Scenedesmus* sp. was similar. The dominant fatty acids included palmitic acid (C16:0), oleic acid (C18:1), linoleic acid (C18:2) and linolenic acid (C18:3), accounting for about 90% of the total fatty acids. Demirbas and Demirbas [33] reported that C16:0 and C18:1 were the most important fatty acids, which were considered as the indicators for the quality of biodiesel. In the study, we observed that the C16:0 and C18:1 presented in major quantities (about 60% of the total fatty acids), implying that *Scenedesmus* sp. was suitable for biodiesel production. Similar results were reported by Chen *et al*. [34].

Figure 1. Three-dimensional response surface plots for lipid production showing the interactions effects of (**A**) $NaHCO_3$ and $NaH_2PO_4{\cdot}2H_2O$; (**B**) $NaH_2PO_4{\cdot}2H_2O$ and $NaNO_3$; and (**C**) $NaHCO_3$ and $NaNO_3$.

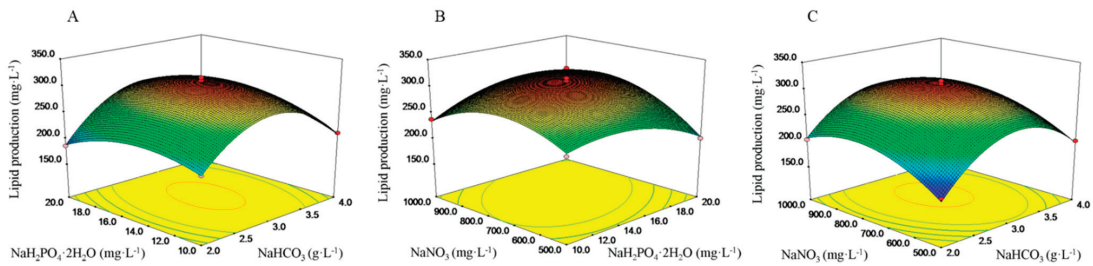

Table 5. Fatty acid composition of *Scenedesmus* sp. (a) in the original medium; (b) in the optimized medium. Values were given as the means of total FAME percentage ± standard deviation.

Fatty acid (%)	C16:0	C16:1	C16:2	C18:0	C18:1	C18:2	C18:3
a	29.43 ± 1.75	1.99 ± 0.69	2.42 ± 0.24	7.33 ± 0.13	30.04 ± 1.02	13.60 ± 0.45	12.76 ± 0.26
b	30.77 ± 0.76	1.96 ± 0.54	1.37 ± 0.02	3.41 ± 0.09	36.27 ± 0.78	11.55 ± 0.12	12.52 ± 0.39

In the study, although no significant differences in fatty acid composition were observed, it was obvious that the exact amount of some fatty acids could alter according to different culture conditions, which was similar to that presented by Miao and Wu [35]. It is worthwhile to note that C18:1 increased from 30.04% to 36.27% in the optimized medium, which improved the feasibility for producing biodiesels by *Scenedesmus* sp. Additionally, it is observed that the microalga, *Scenedesmus* sp., had a high percentage of α-linolenic acid (12.52% of the total fatty acid), which played an important role in human health [36].

The exact amount of each lipid class was detected under the original and optimized conditions. As shown in Table 6, regardless of whether the medium was optimized, the neutral lipid was a major class (over 80% of total lipids), which was known as the most significant component of biodiesel production. The content of the neutral lipid was remarkably higher than that examined in most of the algal strains [7,12]. Guckert and Cooksey [37] have detailed high pH-induced TAG accumulation in

a *Chlorella* species. Depending on this, Gardner *et al*. [32] further proposed that the addition of bicarbonate may be a trigger to promote TAG accumulation. In this study, the value of the pH measured by a pH meter exceeded 11 after cultivation for 9 d, which could resulted in the accumulation of the neutral lipid. Additionally, when the pH value of the growing medium was maintained at 9, the content of the neutral lipid was significantly reduced in the preliminary trial. Therefore, we speculated that high pH stress may result in neutral lipid accumulation in *Scenedesmus* sp. For *Scenedesmus* sp., further experimentation is required to clearly understand if high pH and bicarbonate addition are involved in TAG accumulation.

Table 6. Lipid class analysis of *Scenedesmus* sp. (a) in the original medium; (b) in the optimized medium.

Lipid class	Composition (wt% of total lipids)	
	a	b
Neutral lipid	81.29 ± 0.65	82.32 ± 0.89
Glycolipid	12.56 ± 0.53	10.93 ± 0.47
Phospholipid	6.14 ± 0.35	6.74 ± 0.76

3. Experimental Section

3.1. Strain and Culture Conditions

The *Scenedesmus* sp. was found as a contaminant in an outdoor cyanobacterium *Plectonema* sp. culture with a highly alkaline environment, then was isolated and purified by the streak plate method. The alga was cultured in a modified soil extract (SE) medium composed of the following components: $NaHCO_3$, 2 g L^{-1}; $NaH_2PO_4{\cdot}2H_2O$, 0.05 g L^{-1}; $NaNO_3$, 0.5 g L^{-1}; $CaCl_2$, 0.02 g L^{-1}; $MgSO_4{\cdot}7H_2O$, 0.05 g L^{-1}; KCl, 0.1 g L^{-1}; A_5 solution, 1 mL L^{-1}; EDTA-Fe^{3+}, 1 mL L^{-1}; soil extract, 1 mL L^{-1}. The A_5 solution was composed of the following compositions (g L^{-1}): H_3BO_3 2.86, $MnCl_2{\cdot}4H_2O$ 1.80, $ZnSO_4{\cdot}7H_2O$ 0.22, $CuSO_4{\cdot}5H_2O$ 0.08 and $Na_2MoO_4{\cdot}2H_2O$ 0.39. The cultures were incubated in 500-mL Erlenmeyer flasks with 300 mL of culture media at 24 ± 1 °C and illuminated by fluorescent lamps for 24 h (120 μmol $m^{-2}s^{-1}$). In all experiments, triplicate batch cultures were set up for each treatment. After cultivation for 9 d, cells were harvested by centrifugation (3000× *g*, 5 min).

3.2. RSM Experimental Design

In order to obtain the maximization of lipid production by *Scenedesmus* sp., the optimization of medium components were divided into the following two parts.

3.2.1. Plackett–Burman Design

The Plackett–Burman design is a mathematical approach for identifying the critical factors that influence the response [38]. In the experiment, Plackett–Burman design was utilized to evaluate the significance of each medium component towards lipid production. The chosen variables were $NaHCO_3$, $NaH_2PO_4{\cdot}2H_2O$, $NaNO_3$, $CaCl_2$, $MgSO_4{\cdot}7H_2O$, KCl, A_5, EDTA-Fe^{3+} and soil extract.

Each independent variable was set at two levels: −1 for a low level and +1 for a high level, according to the Plackett–Burman design and preliminary trials. For estimating the experimental error, two dummy variables, whose effects were negligible under high and low concentrations, were employed and twelve experiments run in all. The actual factor levels corresponding to the coded factor levels, together with the experimental data, were given in Table 1. The lipid production, which was the average of the triplicates in each trial, respectively, was considered as the response variable.

3.2.2. Box–Behnken Design

The optimum levels of variables, having significant effects on lipid production, were identified using the RSM based on the Box–Behnken design [39]. The chosen variables were as follows: $NaHCO_3$, $NaH_2PO_4 \cdot 2H_2O$ and $NaNO_3$. For this procedure, seventeen experiments, including five replicates of the center points and twelve star points, were required. The levels of $NaHCO_3$, $NaH_2PO_4 \cdot 2H_2O$ and $NaNO_3$ were varied as shown in Table 3, while the concentrations of other components were constant, as described above. The predicted value of optimum lipid production and culture conditions were obtained. According to experimental results, the second-degree polynomial equation was as follows, which could calculate the predicted value of lipid production:

$$Y = a_0 + a_1A + a_2B + a_3C + a_4AB + a_5AC + a_6BC + a_7A^2 + a_8B^2 + a_9C^2$$

where A, B and C stand for three variables having significant effects on lipid production, Y represents the value of lipid production, a_0 is the intercept and a_1–a_9 are the estimated coefficients. The Design-Expert program (8.05 version) was utilized to analyze the data obtained. According to the determination coefficient (R^2) and F-test, the adequacy of the model was evaluated.

To verify the model of the response surface, the experimental value, obtained under the optimum condition, was compared with the predicted value of the lipid production.

3.3. Biomass Determination and Lipid Extraction

In all experiments, three series of batch cultures were set up in parallel for each treatment. Algal biomass was measured by dry weight. Aliquots of 20-mL microalgal suspension were filtered by preweighed GF/C filter paper (Whatman, Poole, UK). The filter paper with biomass was then dried at 105 °C to a constant weight. After cooling down to room temperature, the filter paper was weighed. After cultivation for 9 d, cells were harvested by centrifugation (3000× *g*, 5 min). Intracellular lipid was extracted, as previously reported by Khozin-Goldberg *et al*. [40]. A mixture of methanol-dimethyl sulphoxide, diethyl ether and hexane (1:1:1, v/v/v) were used to extract the lipids. When the algae debris was removed, water was added into the organic solvent loaded with lipids, forming a liquid-liquid separation state. Finally, the upper layer, including diethyl ether and lipids, was transferred into the weighed vial and dried by a stream of N_2. Lipid production was calculated from the relation: $Y = m_t \times L_t$ (Y, lipid production/g·L^{-1}; m_t, biomass concentration/g·L^{-1}; L_t, lipid content/% dw). The extracted lipids were stored at 4 °C to further analyses.

3.4. Lipid Analysis and Fatty Acid Composition

The fatty acid composition of the lipids was analyzed by GC-MS with an Omegawax 250 polyethylene glycol capillary column (length, 30 m; diameter, 0.25 mm; 0.25-μm film thickness) using the method reported by Khozin-Glodberg *et al*. [40]. One microliter samples were injected into the capillary column with a split ratio of 5:1. Helium was employed as the carrier gas with a flow rate of 1.5 mL/min. The temperatures of the injector and detector were both maintained at 250 °C. The column temperature was programmed from a 130 °C at 5 °C/min ramp rate to 250 °C maintained for 5 min. The content of each component was determined according to the area normalization method.

Lipid class separation was performed by silica gel column chromatography, according to the method illustrated by Christie [41]. Typically, the samples of lipids re-suspended in chloroform were loaded onto a silica gel column (Agela, Tianjin, China). Neutral lipid, phospholipid and glycolipid were successively eluted using chloroform, acetone and methanol, respectively. Each component was dried by a stream of N_2 and then weighed.

4. Conclusions

The response surface methodology was employed to optimize the medium compositions for maximal lipid production. The medium containing 3.07 g L^{-1} $NaHCO_3$, 15.49 mg L^{-1} $NaH_2PO_4 \cdot 2H_2O$ and 803.21 mg L^{-1} $NaNO_3$ was considered as the optimal medium, which improved lipid production by 54.64% more than that obtained in the initial medium. Profiling of lipids achieved in the optimum medium showed that neutral lipid was the major lipid (over 80% of the total lipid), and the dominant components of the fatty acids were C16:0 and C18:1, suggesting that *Scenedesmus* sp. can be suitable for biodiesel production. Moreover, these results proved that the response surface methodology was useful for enhancing the lipid production of the microalga, *Scenedesmus* sp.

Acknowledgments

This research was supported by the Ocean Public Welfare Scientific Research Project (201305018-3), Funds for Marine Renewable Energy (GHME2011SW04), the Main Direction Program of Chinese Academy of Sciences (KSCX2-YW-R-093) and the Guangdong Ocean Innovative Demonstration Area of Economic Development Project (GD2012-D01-002).

Conflicts of Interest

The authors declare no conflict of interest.

References

1. Rodolfi, L.; Zittelli, G.C.; Bassi, N.; Padovan, G.; Biondi, N.; Bonini, G.; Tredici, M.R. Microalgae for oil: Strain selection, induction of lipid synthesis and outdoor mass cultivation in a low-cost photobioreactor. *Biotechnol. Bioeng.* **2009**, *102*, 100–112.

2. Mata, T.M.; Martins, A.A.; Caetano, N.S. Microalgae for biodiesel production and other applications: A review. *Renew. Sustain. Energy Rev.* **2010**, *14*, 217–232.
3. Rawat, I.; Kumar, R.R.; Mutanda, T.; Bux, F. Biodiesel from microalgae: A critical evaluation from laboratory to large scale production. *Appl. Energy* **2013**, *103*, 444–467.
4. Chisti, Y. Biodiesel from microalgae. *Biotechnol. Adv.* **2007**, *25*, 294–306.
5. Helena, M.A.; Catarina, G.A.; Xavier, M.F. Advances and perspectives in using microalgae to produce biodiesel. *Appl. Energy* **2011**, *88*, 3401–3410.
6. Huang, G.; Chen, F.; Wei, D.; Zhang, X.; Chen, G. Biodiesel production by microalgal biotechnology. *Appl. Energy* **2010**, *87*, 38–46.
7. Hu, Q.; Sommerfeld, M.; Jarvis, E.; Ghirardi, M.; Posewitz, M.; Seibert, M.; Darzins, A. Microalgal triacylglycerols as feedstocks for biofuel production: Perspectives and advances. *Plant J.* **2008**, *54*, 621–639.
8. Feng, D.A.; Chen, Z.A.; Xue, S.; Zhang, W. Increased lipid production of the marine oleaginous microalgae *Isochrysis zhangjiangensis* (Chrysophyta) by nitrogen supplement. *Bioresour. Technol.* **2011**, *102*, 6710–6716.
9. Roessler, P.G. Environmental control of glycerol lipid metabolism in microalgae: Commercial implications and future research directions. *J. Phycol.* **1990**, *26*, 3933–3939.
10. Guschina, I.A.; Harwood, J.L. Lipids and lipid metabolism in eukaryotic algae. *Prog. Lipid Res.* **2006**, *45*, 160–186.
11. Sharma, K.K.; Schuhmann, H.; Schenk, P.M. High lipid induction in microalgae for biodiesel production. *Energies* **2012**, *5*, 1532–1553.
12. Khozin-Goldberg, I.; Cohen, Z. The effect of phosphate starvation on the lipid and fatty acid composition of the fresh water eustigmatophyte *Monodus subterraneus*. *Phytochemistry* **2006**, *7*, 696–701.
13. Li, Y.Q.; Horsman, M.; Wang, B.; Wu, N.; Lan, C.Q. Effects of nitrogen sources on cell growth and lipid accumulation of green alga *Neochloris oleoabundans*. *Appl. Microbiol. Biotechnol.* **2008**, *81*, 629–636.
14. Liu, Z.Y.; Wang, G.C.; Zhou, B.C. Effect of iron on growth and lipid accumulation in *Chlorella vulgaris*. *Bioresour. Technol.* **2008**, *11*, 4717–4722.
15. Yeesang, C.; Cheirsilp, B. Effect of nitrogen, salt, and iron content in the growth medium and light intensity on lipid production by microalgae isolated from freshwater sources in Thailand. *Bioresour. Technol.* **2011**, *3*, 3034–3040.
16. White, D.A.; Pagarette, A.; Rooks, P.; Ali, S.T. The effect of sodium bicarbonate supplementation on growth and biochemical composition of marine microalgae cultures. *J. Appl. Phycol.* **2013**, *25*, 153–165.
17. Reitan, K.I.; Rainuzzo, J.R.; Olsen, Y. Effect of nutrient limitation on fatty acid and lipid content of marine microalgae. *J. Phycol.* **1994**, *30*, 972–979.
18. Dean, A.P.; Sigee, D.C.; Estrada, B.; Pittman, J.K. Using FTIR spectroscopy for rapid determination of lipid accumulation in response to nitrogen limitation in freshwater microalgae. *Bioresour. Technol.* **2010**, *101*, 4499–4507.

19. Takagi, M.; Watanabe, K.; Yamaberi, K.; Yoshida, T. Limited feeding of potassium nitrate for intracellular lipid and triglyceride accumulation of *Nannochloris* sp. UTEX LB1999. *Appl. Microbiol. Biotechnol.* **2002**, *54*, 112–117.
20. Griffiths, M.J.; Harrison, S.T.L. Lipid productivity as a key characteristic for choosing algal species for biodiesel production. *J. Appl. Phycol.* **2009**, *21*, 493–507.
21. Zhang, J.; Fu, D.; Xu, Y.; Liu, C. Optimization of parameters on photocatalytic degradation of chloramphenicol using TiO_2 as photocatalyist by response surface methodology. *J. Environ. Sci.* **2012**, *22*, 1281–1289.
22. Qin, J.Z.; Song, F.F.; Qiu, Y.F.; Li, X.X.; Guan, X. Optimization of the medium composition of a biphasic production system for mycelial growth and spore production of *Aschersonia placenta* using response surface methodology. *J. Invertebr. Pathol.* **2013**, *112*, 108–115.
23. Aybastier, O.; Demir, C. Optimization of immobilization conditions of *Thermomyces lanuginosus* lipase on styrene-divinylbenzene copolymer using response surface methodology. *J. Mol. Catal. B Enzym.* **2010**, *63*, 170–178.
24. Pandian, M.; Sivapirakasam, S.P.; Udayakumar, M. Investigation on the effect of injection system parameters on performance and emission characteristics of a twin cylinder compression ignition direct injection engine fuelled with pongamia biodiesel–diesel blend using response surface methodology. *Appl. Energy* **2011**, *88*, 2663–2676.
25. Yücel, Y.S. Optimization of biocatalytic biodiesel production from pomace oil using response surface methodology. *Fuel Process. Technol.* **2012**, *99*, 97–102.
26. Cheng, K.C.; Ren, M.; Ogden, K.L. Statistical optimization of culture media for growth and lipid production of *Chlorella protothecoides* UTEX 250. *Bioresour. Technol.* **2013**, *128*, 44–48.
27. Karemore, A.; Pal, R.; Sen, R. Strategic enhancement of algal biomass and lipid in *Chlorococcum infusionum* as bioenergy feedstock. *Algal Res.* **2013**, *2*, 113–121.
28. Jiang, P.; Zhang, Y.; Shan, Z.X.; Zheng, Q.H. Optimizing the extraction yield of polyprenols from needles of *Cunninghamia Ianceolata* (Lamb.) hook using response surface methodology and its antioxidative activities. *BioResources* **2013**, *1*, 545–556.
29. Mandal, S.; Mallick, N. Microalga *Scenedesmus obliquus* as a potential source for biodiesel production. *Appl. Microbiol. Biotechnol.* **2009**, *84*, 281–291.
30. Welter, C.; Schwenk, J.; Kanani, B.; Blargan, J.V.; Belovicha, J.M. Minimal Medium for Optimal Growth and Lipid Production of the Microalgae *Scenedesmus dimorphus*. *Environ. Prog. Sustain. Energy* **2013**, *4*, 937–945.
31. Yeh, K.L.; Chang, J.S.; Chen, W.M. Effect of light supply and carbon source on cell growth and cellular composition of a newly isolated microalga *Chlorella vulgaris* ESP-31. *Eng. Life Sci.* **2010**, *10*, 201–208.
32. Gardner, R.D.; Cooksey, K.E.; Mus, F.; Macur, R.; Moll, K.; Eustance, E.; Carlson, R.P.; Gerlach, R.; Fields, M.W.; Peyton, B.M. Use of sodium bicarbonate to stimulate triacylglycerol accumulation in the chlorophyte *Scenedesmus* sp. and the diatom *Phaeodactylum tricornutum*. *J. Appl. Phycol.* **2012**, *24*, 1311–1320.
33. Demirbas, A.; Demirbas, M.F. Importance of algal oil as a source of biodiesel. *Energy Convers Manag.* **2011**, *52*, 163–170.

34. Chen, Z.; Gong, Y.M.; Fang, X.T.; Hu, H.H. *Scenedesmus* sp. NJ-1 isolated from Antarctica: A suitable renewable lipid source for biodiesel production. *World J. Microbiol. Biotechnol.* **2012**, *28*, 3219–3225.
35. Miao, X.; Wu, Q. Biodiesel production from heterotrophic microalgal oil. *Bioresour. Technol.* **2006**, *6*, 841–846.
36. Hugo, P.; Luisa, B.; Filipe, F.; Luisa, C.; Catarina, V.D.; Cristina, P.; Eva, R.; Aschwin, E.; Joao, V. Polyunsaturated fatty acids of marine macroalgae: Potential for nutritional and pharmaceutical applications. *Mar. Drugs* **2012**, *10*, 1920–1935.
37. Guckert, J.B.; Cooksey, K.E. Triglyceride accumulation and fatty acid profile changes in *Chlorella* (Chlorophyta) during high pH-induced cell cycle inhibition. *J. Phycol.* **1990**, *26*, 72–79.
38. Plackett, R.L.; Burman, J.P. The design of optimum multifactorial experiments. *Biometrika* **1946**, *33*, 305–325.
39. Box, G.E.P.; Behnken, D.W. Some new three level designs for the study of quantitative variables. *Technometrices* **1960**, *2*, 455–475.
40. Khozin-Goldberg, I.; Shrestha, P.; Cohen, Z. Mobilization of arachidonyl moieties from triacylglycerols into chloroplastic lipids following recovery from nitrogen starvation of the microalga *parietochloris incisa*. *BBA-Mol. Cell Biol. Lipids* **2005**, *1738*, 63–71.
41. Christie, W.W. *Lipid Analysis: Isolation, Separation, Identification and Structural Analysis of Lipids*, 3rd ed.; The Oily Press: Bridgewater, UK, 2003; pp. 373–387.

A Novel Lipid Extraction Method from Wet Microalga *Picochlorum* sp. at Room Temperature

Fangfang Yang, Wenzhou Xiang, Xiumei Sun, Hualian Wu, Tao Li and Lijuan Long

Abstract: A novel method using ethanol was proposed for extracting lipids from wet microalga *Picochlorum* sp. at room temperature and pressure. In this study, Central Composite design (CCD) was applied to investigate the optimum conditions of lipid extraction. The results revealed that the solvent to biomass ratio had the largest effect on lipid extraction efficiency, followed by extraction time and temperature. A high lipid extraction yield (33.04% of the dry weight) was obtained under the following extraction conditions: 5 mL solvents per gram of wet biomass for 37 min with gentle stirring at room temperature. The extraction yield was comparable to that obtained by the widely used Bligh-Dyer method. Furthermore, no significant differences in the distribution of lipid classes and fatty acid composition were observed according to different extraction methods. In conclusion, these results indicated that the proposed procedure using ethanol could extract lipids from wet biomass efficiently and had giant potential for lipid extraction at large scale.

Reprinted from *Mar. Drugs*. Cite as: Yang, F.; Xiang, W.; Sun, X.; Wu, H.; Li, T.; Long, L. A Novel Lipid Extraction Method from Wet Microalga *Picochlorum* sp. at Room Temperature. *Mar. Drugs* **2014**, *12*, 1258–1270.

1. Introduction

Due to the serious energy crisis and environmental pollution associated with the using of fossil fuels, biofuel derived from microalgae has been advocated in recent years. Compared to other feedstocks like plant oils, animal fats, *etc.*, microalgae have outstanding advantages: they are capable of growing rapidly and converting CO_2 into substantial amounts of lipids [1–3]. Some microalgae species can absorb essential nutrients including the carbon, nitrogen and phosphorus from exhaust gas and waste water [4,5]. Additionally, many microalgae can grow well in unfavorable lands and saline water. That is, microalgae do not compete for the land required for producing food and overcome the discord between food and fuel [6–8].

Extracting lipids is one of the most key and limited processes for biofuel production based on microalgae at large scale. The conventional methods for lipid extraction generally involve dewatering before extracting lipids since residual water in wet microalgal biomass hindered mass transfer of the lipids from the cell and then lead to a decrease in the efficiency of lipids extraction. Lardon *et al.* [9] and Patil *et al.* [10] reported that the consumption energy of the drying accounted for the majority of the total process energy (84.9%). In addition, the organic solvents used in the conventional methods are regarded as highly-toxic, being environmentally unfriendly. These shortcomings hinder the application of conventional methods in industrial lipid extraction, despite of the high extraction efficiency. Therefore, it is essential to develop novel approach of lipid extraction, which is an effective eco-friendly process.

Compared to the traditional methods involving drying, extracting lipids from wet biomass is a more economic method, which requires no energy to dry the biomass. Various researchers have investigated the wet lipid extraction methods, including ultrasound-assisted extraction [11], simultaneous distillation and extraction process [12], microwave-assisted extraction [13] and supercritical fluid extraction [14]. Unfortunately, the most cases still require high temperature, long times or high energy inputs. Therefore, the technologies of lipid extraction are only limited to laboratory scale. The ideal method being suitable for industrial-scale extraction has not yet been settled.

The aim of the present study is to develop an eco-friendly solvent technique that will make it possible to extract lipid from wet microalgal biomass efficiently at large scale. Ethanol is considered as a cheap and safe solvent; additionally, ethanol has a strong affinity to the lipid complex, which implies that lipids can be extracted efficiently. Fajardo *et al.* [15] used ethanol, following by hexane, to extract and purify lipids from drying microalga *Phaeodactylum tricornutum* efficiently. Chen *et al.* [16] extracted lipids from wet microalga *Nannochloropsis* sp. at high temperature and pressure. However, no investigation about the application of ethanol in extracting lipids from wet microalgal biomass at room temperature and pressure has been reported.

In this study, we adopted a novel method using ethanol with gentle stirring for lipid extraction from wet microalga *Picochlorum* sp. directly. Then the effects of parameters including time, temperature, and the ratio of solvent to biomass on the lipid extraction yield were investigated by Central Composite design (CCD) to identify the optimum extraction conditions. Finally, the proposed methods were compared with the conventional Bligh-Dyer method in terms of lipid extraction yield, lipids quality.

2. Results and Discussion

2.1. Examine Ethanol for Lipid Extraction from Wet Biomass

A novel method, extracting lipids from wet biomass using ethanol at room temperature (27 °C) for 30 min, was proposed. The ratio of ethanol to wet biomass was 4:1 (mL/g). To examine the feasibility of the method, the lipid extraction yield was determined as described in Section 3.3. The lipids arising from microalgal biomass by ethanol, referred to as crude lipids, frequently contain several non-lipids (proteins bonding to lipids strongly and carbohydrates). To avoid the interference of non-lipid complex, the crude lipids were purified. Hexane was a low-toxicity solvent and employed to remove non-lipids complex from crude lipids. The purified lipids were quantified and used to calculate the lipid extraction yield. The extraction yield by ethanol was close to that of Bligh-Dyer's method, namely, 31.89% and 33.18% of the dry weight, respectively. That is, the extraction rate of lipids was 96.1%. The result implied that ethanol had potential for extracting lipids from wet microalgae at room temperature.

2.2. Investigating the Optimum Procedure of Extracting Lipids Using Ethanol

In the experiment, Central Composite design (CCD) was employed to analyze comprehensively the influences of three extraction parameters on the lipid extraction yield and determine the optimum

extraction conditions. Table 1 shown the actual factor levels corresponding to the coded factor levels. In total, 20 experiments were designated.

Table 1. Levels and variables involved in Central Composite design.

Variables	Levels				
	−α	**−1**	**0**	**1**	**α**
Extraction time (min)	2.5	10	25	40	47.5
Extraction temperature (°C)	20	25	35	45	50
the ratio of solvent to biomass (mL/g)	1	2	4	6	7

The corresponding response value obtained from each run were illustrated in Table 2. By analyzing these data in Table 2, the following second order polynomial equation expressed in terms of coded values fitted to the results from the optimization experiments was obtained.

$$Y = +30.98 + 1.27\,X_1 + 0.042X_2 + 4.06X_3 + 0.14X_1X_2 - 0.24X_1X_3 - 0.25X_2X_3 - 0.66X_1^2 + 0.37X_2^2 - 2.71X_3^2$$

where, Y stood for lipid extraction yield (% of the dry weight); X_1, X_2 and X_3 were extracting time (min), extracting temperature (°C) and the ratio of solvent to biomass (mL/g), respectively.

Table 2. Results and experimental layout in Central Composite design.

NO.	Extraction time (min)	Extraction temperature (°C)	Solvent to biomass ratio (mL/g)	Extraction yield (of the dry weight)	
				Experimental	**Predicted**
1	10.00	25.00	2.00	22.62	22.26
2	40.00	25.00	2.00	25.20	25.01
3	10.00	45.00	2.00	22.77	22.57
4	40.00	45.00	2.00	26.26	25.87
5	10.00	25.00	6.00	30.84	31.36
6	40.00	25.00	6.00	32.81	33.14
7	10.00	45.00	6.00	30.35	30.67
8	40.00	45.00	6.00	32.51	33.00
9	2.50	35.00	4.00	27.73	27.60
10	47.50	35.00	4.00	31.51	31.41
11	25.00	20.00	4.00	31.90	31.76
12	25.00	50.00	4.00	31.96	31.88
13	25.00	35.00	1.00	17.97	18.79
14	25.00	35.00	7.00	32.01	30.96
15	25.00	35.00	4.00	31.29	30.98
16	25.00	35.00	4.00	30.11	30.98
17	25.00	35.00	4.00	30.56	30.98
18	25.00	35.00	4.00	31.28	30.98
19	25.00	35.00	4.00	31.64	30.98
20	25.00	35.00	4.00	30.83	30.98

To check the adequacy of the quadratic polynomial model, the statistical significance of the above equation was calculated, illustrated in Table 3. Here, R^2 was 0.9857, indicating that 98.57% of the data in CCD could be explained by the response surface model, that is, the model can be carried out

to reveal the effects of variables on the response value and predict the maximum response value in subsequent optimization experiments. In addition, the *F*-value of 76.57 demonstrated that the model was significant, as indicated by the *p*-value less than 0.0001, which further supported the fitness of the proposed model. From the analysis of R_{adj}^2 and R_{pred}^2, there was a high degree of agreement between them. In conclusion, these results clearly indicated that the model could be used to explain these data well.

As shown in Table 3, the linear coefficient indicated that the ratio of solvent to biomass (X_3) was the most significant independent variable impacting on extraction yield with *p*-value less than 0.01. The higher ratio of solvent to biomass was, the more the extraction yield could be. The extraction time (X_1) also exerted a positive individual influence on the extraction yield. That implied that an increase in the extraction time improved the lipid extraction amounts. In addition, the ratio of solvent to biomass and extraction time exerted the significant quadratic effects (Table 3). However, other terms (X_2, X_2^2, X_1X_2, X_1X_3, X_2X_3) were insignificant (Table 3). In particular, extraction temperature in the range of 20–50 °C had litter effect on extraction yield and the lipids could be extracted effectively at room temperature. It was therefore possible that *Picochlorum* sp. was cracked during the extracting process and ethanol get into the cell easily without the cell wall resistance. Additionally, gentle stirring could accelerate cells lysis and elevate extraction efficiencies.

Table 3. Statistical analysis for experimental results of Central Composite design.

Source	Sum of squares	Df	Mean square	*F* value	*p*-Value
Model	308.98	9	34.33	76.57	< 0.0001
Linear					
X_1	20.16	1	20.16	44.97	< 0.0001
X_2	0.022	1	0.022	0.049	0.8301
X_3	205.72	1	205.72	458.83	< 0.0001
Quadratic					
X_1^2	0.15	1	0.15	0.34	0.0105
X_2^2	0.47	1	0.47	1.05	0.1041
X_3^2	0.50	1	0.50	1.12	< 0.0001
Interaction					
X_1X_2	4.43	1	4.43	9.87	0.5714
X_1X_3	1.43	1	1.43	3.20	0.3301
X_2X_3	75.84	1	75.84	169.16	0.3148
Residual	4.48	10	0.45		
Lack of fit	2.91	5	0.58	1.85	0.2578
Pure error	1.57	5	0.31		
Cor total	313.47	19			

$R^2 = 0.9857$; $R_{Adj}^2 = 0.9728$; $R_{Pred}^2 = 0.9223$.

To understand the interaction of the corresponding parameters, the regression model was represented in terms of response surface plots, as shown in Figure 1. Figure 1a represented the mutual effect of the extraction time and temperature on the extraction yield. It was apparent that the interaction between the two selected variables had litter influence on the extraction yield. As seen in Figure 1b, it could be observed that the extraction yield increased significantly with an increase in the ratio of solvent to biomass at a given extraction time. However, excess solvent amount would not improve further the extraction yield. In addition, as extraction time elevating, the extraction

efficiency enhanced, resulting in a higher lipid extraction yield. However, the interaction terms of the two variables possessed litter role as indicated by its *p*-value of 0.3301. Similarly, the interaction between extraction temperature and the ratio of solvent to biomass had insignificant effects on extraction yield, as illustrated in Figure 1c.

2.3. The Validation of the Model

According to the above results, the optimum extraction conditions were obtained as following: the ratio of solvent to biomass was 5:1 (mL/g) at room temperature (26 °C) for 37 min of extraction time. The extraction yield obtained from *Picochlorum* sp. was predicted to be 33.10% of the dry weight. In order to confirm these conclusions, extraction experiments based on the optimal extraction parameters were performed and the extraction yield was determined. The experimental value was 33.04% of the dry weight, which was agreement well with the predicted value calculated by the model equation, demonstrating the adequacy of the regression equation. The results also revealed that ethanol could employed successfully to extract lipids from wet microalga *Picochlorum* sp. However, the particular reason for this is not well understood and requires further research. Halim *et al*. [17] proposed a probable mechanism for lipid extraction from microalgae by solvent. The solvent penetrated through the cell membrane into the cytoplasm. Then the solvent interacted with the lipid complex and formed a complex. Finally, the solvent-lipids complex diffused out the cell and lipids were extracted. Ranjan *et al*. [18] revealed that the prominent mechanism of lipid extraction by organic solvent was diffusion across a cell wall. The extent of diffusion was attributed to the selectivity of the solvent. In the study, ethanol was used as extractant. Since ethanol had both polar and non-polar properties, it could interact with non-poplar and poplar lipids after entering into cells. This meant that ethanol could pull out neutral and polar lipids from cell efficiently [15,19]. Additionally, the gentler stirring in the extraction process could sweep away the extracted lipids from the microalgal cell surface and maintain a continuous diffusion of lipids from the cells. On the other hand, the disruption of microalgal cells was also a mechanism of lipid extraction [18]. The disruption depended greatly on cell morphology and the probability of interaction of the cell with cavitation bubbles [18,20]. The cell wall of *Picochlorum* sp. used in this study could be disrupted in the extracting procedure and cellular contents were probably released. Therefore, ethanol could extract lipids from wet microalga efficiently. However, the special mechanism requires further research.

2.4. Lipid Analysis and Fatty Acid Composition Comparisons

To evaluate the efficiency of our proposed method, extracting lipids from wet biomass using ethanol, the conventional Bligh-Dyer method was employed as a reference, due to its high lipid extraction efficiency. The moisture content of wet biomass was 90.02% wet weight.

Table 4 presented the lipid extraction yield for two extraction methods. When using ethanol as extractant, a high extraction yield of lipids (33.04% of the dry weight), which was similar with that of Bligh-Dyer method (33.18% of the dry weight), was obtained. This implied extraction rate of the proposed method was up to 99.6%. Additionally, we investigated the lipid extraction ratio

of the fresh microalga. The results revealed that there were no significant changes in the extraction efficiency.

Figure 1. Response surfaces and contour plots showing the mutual effect of (**a**) extraction temperature and time; (**b**) the ratio of solvent to biomass and extraction time; (**c**) the ratio of solvent to biomass and extraction temperature on the lipid extraction yield.

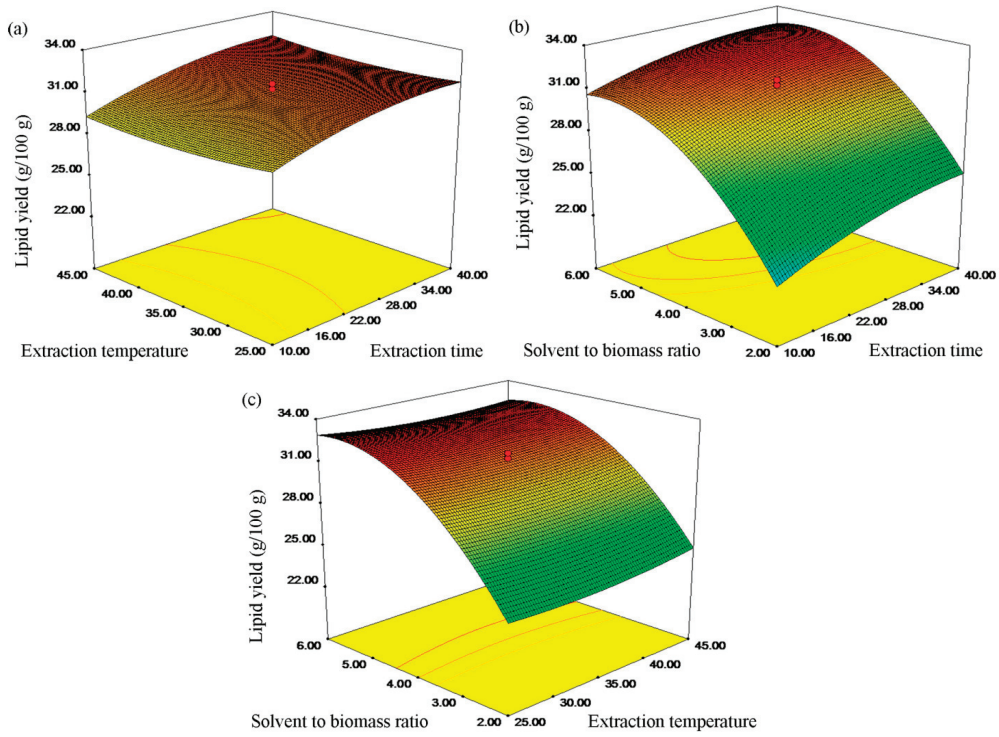

Table 4. Fatty acid profile comparison between different extraction methods.

	Extraction method	
	Bligh-Dyer	**Ethanol**
Lipid extraction yield (% of the dry weight)	33.18 ± 0.24	33.04 ± 0.16
Fatty acid composition (% of FAME)		
Saturated		
C16:0	32.49 ± 1.54	29.48 ± 3.12
C18:0	2.82 ± 0.43	6.00 ± 1.89
Unsaturated		
C16:1	2.57 ± 0.62	2.05 ± 0.38
C16:2	5.76 ± 0.16	5.65 ± 0.58
C16:3	6.62 ± 0.54	6.09 ± 0.11
C18:1	8.42 ± 0.01	9.06 ± 0.28
C18:2	22.25 ± 0.21	22.47 ± 2.63
C18:3	17.37 ± 0.65	17.04 ± 0.93
Others	1.71 ± 0.35	2.16 ± 0.40

The major fatty acid composition of lipids was determined by gas chromatography coupled to mass spectrometry (GC-MS). As shown in Table 4, no significant differences in fatty acid composition were observed between different extraction methods. The dominant fatty acids were palmitic acid (C16:0), oleic acid (C18:1), linoleic acid (C18:2) and linolenic acid (C18:3), which accounted for approximately 80% of total fatty acids. Other fatty acids, such as palmitolenic (C16:1), palmitolenic (C16:2), palmitoleidic (C16:3) and stearic (C18:0), were also present in smaller quantities. The fatty acid composition of *Picochlorum* sp. was similar with the profile presented by Tanzi *et al.* [12]. In generally, C16:0, C18:0, C18:1 and C18:2 were known to the most common components in biodiesel [14,21]. Therefore, the extracted lipids of *Picochlorum* sp. were suitable for biodiesel production.

The content of each fatty acid had no significant difference between two methods according to statistical analysis ($P > 0.05$). However, the ratio of some fatty profiles, especially C18:0, represented slight variation according to different extraction methods. When using ethanol as solvent, the lower proportion of C16:0, C16:1 and C16:3, with corresponding increasing in C18:0 and C18:1, compared to the Bligh-Dyer method (Table 4). The probable reason was that the change of extraction conditions resulted in the fatty acid profile of the extracted lipids [14]. The results revealed that ethanol could extract most of fatty acids efficiently. In addition, it must be highlighted that the microalga *Picochlorum* sp. had a high percentage of linolenic acid (around 17%), which was an essential and important fatty acid to human health [22].

The lipid class was determined and presented as % of lipid class in total lipids as shown in Table 5. The lipids were consisted mainly of neutral lipid, glycolipid and phospholipid. By statistical analysis, no significant difference in the content of each lipid class was observed ($P > 0.05$), although the content of phospholipid was higher than that obtained using Bligh-Dyer method. Additionally, the percentage of neutral lipid was highest (about 50% of total lipids) using the two extraction methods, suggesting the microalga *Picochlorum* sp. was a promising feedstock for biodiesel production. As a conclusion, most of essential lipids for biodiesel production could be extracted from wet biomass effectively using ethanol.

Table 5. The lipid class comparison between different extraction methods. Values were given as means of total lipids percentage ± standard deviation.

Lipid class	Extraction method	
	Bligh-Dyer	**Ethanol**
Neutral lipid	54.73 ± 1.47	53.49 ± 2.11
Glycolipid	16.46 ± 0.76	15.62 ± 0.54
Phospholipid	28.81 ± 0.71	30.89 ± 1.57

2.5. Lipid Extraction at Larger Scale and Ethanol Recycling

To validate the applicability of the optimal method in lipid extraction at enlarged scale, 250 g wet biomass was employed to extract lipids. A summary of the protocol was shown in Figure 2. A high extraction ratio of 99.4% was obtained, implying that the optimum method was effective for extracting lipids at larger scale. Additionally, ethanol was recovered by using distillation tower in

order to decrease the consumption of ethanol. The results revealed that the recovery of ethanol reached a yield of 95.24% with the purity of 93%. Furthermore, the experiments confirmed that the recycled ethanol had high efficiency for extracting lipids from wet biomass. Therefore, the extraction method with ethanol was suitable for extracting lipids from microalgae at large scale, with a high extraction efficiency and low environment pollution.

Figure 2. A scheme illustration of lipid extraction procedure from wet microalga using ethanol.

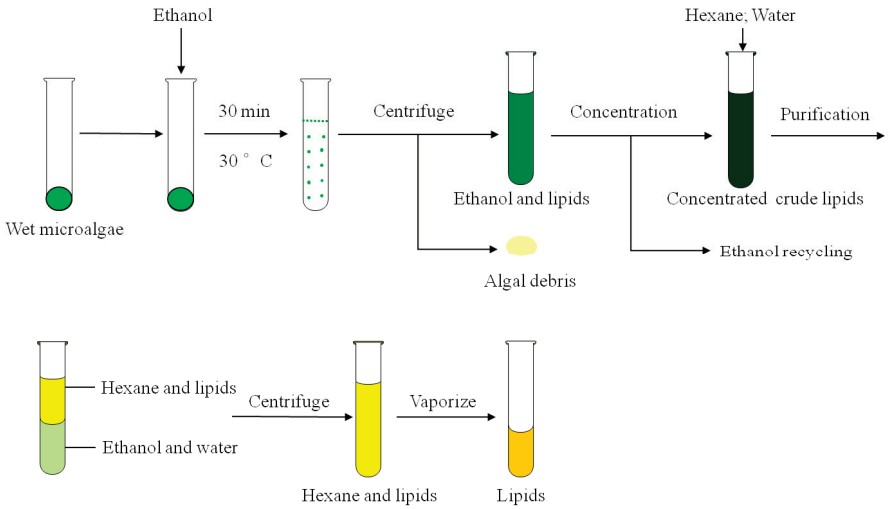

2.6. Lipid Extraction Methods Comparison

The lipid extraction method using ethanol was evaluated in terms of extraction yield and lipid quality. There was no significant difference compared to the conventional Bligh-Dyer method, that is, ethanol could extract lipids from wet microalga effectively.

Comparing to the Bligh-Dyer method, the method, because it used ethanol, was environmentally friendly. Moreover, since the debris contained high contents of proteins, the debris would be reused for producing bait after extracting lipids. Conversely, the debris would be toxic and be not reused if the Bligh-Dyer method was employed to extract lipids. Therefore, the method was considered safe and suitable for the lipid extraction in the industrial scale.

So far, there have been a few reports related to the application of ethanol in extracting lipids [15,16]. However, in these cases, dewatering or high temperature still be required. In the study, ethanol was employed successfully to extract lipids from high-moisture microalgae at room temperature and pressure. It was probable that the *Picochlorum* sp. used in this study had different bio-characteristics and the cell wall was cracked easily. Hence, there was slight cell wall resistance and the ethanol could enter into cells for extracting lipids quickly. This was consistent with Prommuak *et al.* [20] which revealed that the extraction efficiency depended greatly on cell morphology. Compared to the conventional Bligh-Dyer method, the method did not require dewatering and heating, which implied the method was easier to operate at large scale.

In conclusion, the method based on ethanol possessed important advantages over Bligh-Dyer method, such as shorter treatment time, less environment pollution, high extraction efficiency, which was more applicable for lipid extraction at large scale than the conventional methods.

Despite this, the effectiveness of the method will be further evaluated using different types of microalgae at large scale to test the practical application of this method. Otherwise, it would be necessary to further investigate the applications of the residual biomass and linolenic acid as byproduct, to improve the overall economics of microalgal biofuel production.

3. Materials and Methods

3.1. Strain, Culture Conditions and Harvesting Method

Picochlorum sp., isolated from the India Ocean, was cultured in the modified f/2 media composed of sea water with an addition of phosphorus and nitrogen sources. The cultures were cultivated in an outdoor raceway system of up to 500 m^2. Temperature and illumination intensity depended on the daily weather. Daily microscopic analysis revealed that *Picochlorum* sp. was not contaminated. At the same time, microalgal cultures were harvested and concentrated by the floatation method. A dilute aqueous suspension with water content of 90.02% wet weight was obtained and stored at 4 °C for subsequent analysis. In the experiments involving dried microalgae, the concentrated microalgal cultures were frozen-dried completely in a lyophilizer. In the experiments where wet microalgae were used, the concentrated microalgal cultures were used to extract lipid directly without further treatment.

3.2. Conventional Lipid Extraction Method

The lipids of drying biomass were extracted by Bligh-Dyer's method with chloroform and methanol mixture [23]. The method was used as standard to evaluate our proposed method of extracting lipids from wet biomass. The chloroform and methanol mixture was added to 100 mg of drying biomass at 50 °C for 1 h. The extracted lipids were quantified and analyzed.

3.3. Lipid Extraction using Ethanol as Extractant

Ethanol was performed to extract lipids from wet biomass (approximately 1 g). The lipids arising from microalgal biomass by ethanol, referred to as total lipids or crude lipids, frequently contain several non-lipids (proteins bonding to lipids strongly and carbohydrates). Then the biomass residue was removed and the crude lipids obtained were later purified.

The lipid extraction ratio obtained by hexane was low since hexane preferably extracted non-polar lipids in the microalga. However, hexane was a low-toxicity solvent and could remove non-lipids from crude lipids efficiently [20]. In the study, to purify the crude lipids, the water and hexane were added into the crude lipids to form a liquid-liquid separation state according to the method illustrated by Fajardo *et al*. [15]. The upper phase (hexane and some ethanol) was loaded with most of the lipids while the lower phase (most ethanol with water) contained most non-lipids. The upper phase that contained lipids was transferred to a weighted tube and dried by stream of N_2. The purified lipids

were quantified and were later analyzed by gas chromatography and silica gel column chromatography. In all experiments, three parallels were set up for each treatment.

3.4. Experimental Design and Data Analysis

In order to investigate the optimum extraction conditions, a mathematical model-Central Composite design (CCD) was utilized when ethanol was used as extractant. By applying the CCD, the effect of each parameter, such as extraction time, extraction temperature and the ratio of solvent to biomass, on extraction yield were evaluated quickly and effectively. Table 1 illustrated the actual factor levels corresponding to the coded factor levels. In the experiment, the low and high levels of all variables, that is, star points were set up first. Depending on the number of parameters involved and desire of the design, the value of α, which expressed distance between star points and center points, was determined. In all, twenty experiments were employed with fifteen being the different combinations of three parameters and five being replications of center points. Each trial was performed in triplicate and lipid extraction yield was the mean values. According to the experimental results obtained, the second-degree polynomial equation was given below, which could calculate the predicted value of lipid extraction yield.

$$Y = \alpha_0 + \alpha_1 X_1 + \alpha_2 X_2 + \alpha_3 X_3 + \alpha_4 X_1 X_2 + \alpha_5 X_1 X_3 + \alpha_6 X_2 X_3 + \alpha_7 X_1^2 + \alpha_8 X_2^2 + \alpha_9 X_3^2$$

where, Y represents the predicted value of extraction yield (% of the dry weight); X_1, X_2, X_3 are the code values of extraction time (min), extraction temperature (°C) and the ratio of solvent to wet biomass (mL/g), respectively; α_0 is quantity; α_1–α_9 stand for coefficient estimate.

The software (Design Expert, version 8.05) was conducted to analyze and calculate these results. Under the optimum conditions, the lipids were extracted. By comparing the experimental and predicted values, the model was verified.

3.5. Esterification and Analysis of Fatty Acids

The lipids were converted to fatty acid methyl ester (FAME) for gas chromatography. 1 mL of chloroform containing 0.2 mg of heptadecanoic acid (C17:0) was added to each of the purified lipid samples as an internal standard. Then 1 mL of NaOH-CH_3OH was added at 75 °C for 10 min and 2 mL of BF_3-CH_3OH was added for transesterification reaction at 75 °C for 10 min. After the reaction, 3 mL of hexane and 1 mL of deionized water were added to the above samples. Finally, the samples were centrifuged and upper layer was separated for GC-MS analysis. Fatty acid compositions of the lipids were analyzed by GC-MS with an Omegawax 250 polyethylene glycol capillary column (length 30 m, diameter 0.25 mm and 0.25 μm film thickness) using the method reported by Goldberg *et al.* [24]. Samples of 1 μL were injected into the capillary column with a split ratio of 5:1. Helium was employed as the carrier gas with a flow rate of 1.5 mL/min. The temperatures of injector and detector both maintained at 250 °C. The column temperature was programmed from 130 °C at 5 °C/min ramp rate to 250 °C maintained for 5 min. Each component was identified by comparing retention time and fragmentation with standards using the GC-MS library. The fatty acid content was expressed as percentage of total fatty acids.

3.6. Lipid Analysis Using Silica Gel Column Chromatography

Lipid class separation was performed by silica gel column chromatography according to the method illustrated by Christie [25]. Typically, the samples of lipids re-suspended in chloroform were loaded onto silica gel column chromatography (Agela, Tianjin, China). Neutral lipid, phospholipid and glycolipid were successively eluted using chloroform, acetone and methanol, respectively. Each component was dried by stream of N_2 and then weighed.

3.7. Lipid Extraction at Larger Scale and Ethanol Recycling

Ethanol was added to wet microalgal biomass (250 g) in an approximately 5:1 mass ratio. Under the optimum conditions, lipids were extracted. After extraction, the supernatant, loading with lipids and ethanol, was separated and then ethanol was recycled using distillation tower. The purity of ethanol was measured by the alcohol detector. The recycled ethanol was once again employed to extract lipids from wet biomass in order to evaluate its ability of extracting lipids. A summary of the protocol was shown in Figure 2.

4. Conclusions

This study demonstrated that the novel method using ethanol could be used to extract lipids from high-moisture microalgae at room temperature, with an extraction yield of 33.04% of the dry weight. The extraction yield was comparable to that of the conventional Bligh-Dyer method. Additionally, only minor variations in lipid profiles and fatty acid composition were observed according to different methods, suggesting that ethanol extracted the main components for biodiesel production effectively. Further research revealed that a high lipid extraction ratio of 99.4% was obtained using the proposed method at larger scale. Taken together, the results suggested that the method with ethanol was an easy, less environmentally polluting and high efficiency extraction process.

Acknowledgements

This research was supported by the Ocean Public Welfare Scientific Research Project (201305018-3), Funds for Marine Renewable Energy (GHME2011SW04), Main Direction Program of Chinese Academy of Sciences (KSCX2-YW-R-093).

Conflict of Interest

The authors declare no conflict of interest.

References

1. Chisti, Y. Biodiesel from microalgae. *Biotechnol. Adv.* **2007**, *25*, 294–306.
2. Liam, B.; Philip, O. Biofuels from microalgae-a review of technologies for production, processing, and extractions of biofuels and co-products. *Renew. Sustain. Energy Rev.* **2010**, *2*, 557–577.

3. Mairet, F.; Bernard, O.; Masci, P.; Lacour, T.; Sciandra, A. Modelling neutral lipid production by the microalga *Isochrysis aff. galbana* under nitrogen limitation. *Bioresour. Technol.* **2011**, *1*, 142–149.
4. Rawat, I.; Ranjith, K.R.; Mutanda, T.; Bux, F. Dual role of microalgae: Phycoremediation of domestic wasterwater and biomass production for sustainable biofuels production. *Appl. Energy* **2011**, *88*, 3411–3424.
5. Hende, S.V.D.; Vervaeren, H.; Boon, N. Flue gas compounds and microalgae: (Bio-) chemical interactions leading to biotechnological opportunities. *Biotechnol. Adv.* **2012**, *30*, 1405–1424.
6. Hu, Q.; Sommerfeld, M.; Jarvis, E.; Ghirardi, M.; Posewitz, M.; Seibert, M.; Darzins, A. Microalgal triacylglycerols as feedstocks for biofuel production: Perspectives and advances. *Plant J.* **2008**, *54*, 621–639.
7. Schenk, P.M.; Thomas-Hall, S.R.; Stephens, E.; Marx, U.C.; Mussgnug, J.H.; Posten, C.; Kruse, O.; Hankamer, B. Second generation biofuels: High-Efficiency microalgae for biodiesel production. *BioEnergy Res.* **2008**, *1*, 20–43.
8. Singh, J.; Gu, S. Commercialization potential of microalgae for biofuels production. *Renew. Sustain. Energy Rev.* **2010**, *9*, 2596–2610.
9. Lardon, L.; Helias, A.; Sialve, B.; Steyer, J.P.; Bernard, O. Life-Cycle assessment of biodiesel production from microalgae. *Sci. Technol.* **2009**, *17*, 6475–6481.
10. Patil, P.D.; Gude, V.G.; Mannarswamy, A.; Cooke, P.; Nirmalakhandan, N.; Lammers, P.; Deng, S.G. Comparison of direct transesterification of algal biomass under supercritical methanol and microwave irradiation conditions. *Fuel* **2012**, *97*, 822–831.
11. Adam, F.; Vian, M.A.; Peltier, G.; Chemat, F. "Solvent-Free" ultrasound assisted extraction of lipids from fresh microalgae cells: A green, clean and scalable process. *Bioresour. Technol.* **2012**, *114*, 457–465.
12. Tanzi, C.D.; Vian, M.A.; Chemat, F. New procedure for extraction of algal lipids from wet biomass: A green clean and scalable process. *Bioresour. Technol.* **2013**, *134*, 271–275.
13. Cheng, J.; Yu, T.; Li, T.; Zhou, J.H.; Cen, K.F. Using wet microalgae for direct biodiesel production via microwave irradiation. *Bioresour. Technol.* **2013**, *131*, 531–535.
14. Halim, R.; Gladman, B.; Danquah, M.K.; Webley, P.A. Oil extraction from microalgae for biodiesel production. *Bioresour. Technol.* **2011**, *1*, 178–185.
15. Fajardo, A.R.; Cerdán, L.E.; Medina, A.R.; Fernández, F.G.A.; Moreno, P.A.G.; Grima, E.M. Lipid extraction from the microalga *Phaeodactylum tricornutum*. *Eur. J. Lipid Sci. Technol.* **2007**, *2*, 120–126.
16. Chen, M.; Chen, X.L.; Liu, T.Z.; Zhang, W. Subcritical ethanol extraction of lipid from wet microalgae paste of *Nannochloropsis* sp. *J. Biobased Mater. Bioenergy* **2011**, *5*, 385–389.
17. Halim, R.; Danquah, M.K.; Webley, P.A. Extraction of oil from microalgae for biodiesel production: A review. *Biotechnol. Adv.* **2012**, *30*, 709–732.
18. Ranjan, A.; Patil, C.; Moholkar, V.S. Mechanistic assessment of microalgal lipid extraction. *Ind. Eng. Chem. Res* **2010**, *49*, 2979–2985.
19. Brian, M.C. *Kinetics of Lipid Extraction from Microalgae*; University of New Hampshire, University of New Hampshire Scholars' Repository: Durham, NC, USA, 2013.

20. Prommuak, C.; Pavasant, P.; Quitain, A.T.; Goto, M.; Shotipruk, A. Microalgal lipid extraction and evaluation of single-step biodiesel production. *Eng. J.* **2012**, *5*, 157–166.
21. Knothe, G. Dependence of biodiesel fuel properties on the structure of fatty acid alkyl esters. *Fuel Process Technol.* **2005**, *86*, 1059–1070.
22. Hugo, P.; Luisa, B.; Filipe, F.; Luisa, C.; Catarina, V.D.; Cristina, P.; Eva, R.; Aschwin, E.; Joao, V. Polyunsaturated fatty acids of marine macroalgae: Potential for nutritional and pharmaceutical applications. *Mar. Drugs* **2012**, *10*, 1920–1935.
23. Bligh, E.G.; Dyer, W.J. A rapid method of total lipid extraction and purification. *Can. J. Biochem. Physiol.* **1959**, *37*, 913–917.
24. Goldberg, K.I.; Shrestha, P.; Cohen, Z. Mobilization of arachidonyl moieties from triacylglycerols into chloroplastic lipids following recovery from nitrogen starvation of the microalga *Parietochloris incisa*. *BBA Mol. Cell Biol. Lipids* **2005**, *1738*, 63–71.
25. Christie, W.W. *Lipid Analysis: Isolation, Separation, Identification and Structural Analysis of Lipids*, 3rd ed.; The Oily Press: Bridgewater, UK, 2003; pp. 373–387.

Rapid and Accurate Identification by Real-Time PCR of Biotoxin-Producing Dinoflagellates from the Family Gymnodiniaceae

Kirsty F. Smith, Miguel de Salas, Janet Adamson and Lesley L. Rhodes

Abstract: The identification of toxin-producing dinoflagellates for monitoring programmes and bio-compound discovery requires considerable taxonomic expertise. It can also be difficult to morphologically differentiate toxic and non-toxic species or strains. Various molecular methods have been used for dinoflagellate identification and detection, and this study describes the development of eight real-time polymerase chain reaction (PCR) assays targeting the large subunit ribosomal RNA (LSU rRNA) gene of species from the genera *Gymnodinium*, *Karenia*, *Karlodinium*, and *Takayama.* Assays proved to be highly specific and sensitive, and the assay for *G. catenatum* was further developed for quantification in response to a bloom in Manukau Harbour, New Zealand. The assay estimated cell densities from environmental samples as low as 0.07 cells per PCR reaction, which equated to three cells per litre. This assay not only enabled conclusive species identification but also detected the presence of cells below the limit of detection for light microscopy. This study demonstrates the usefulness of real-time PCR as a sensitive and rapid molecular technique for the detection and quantification of micro-algae from environmental samples.

Reprinted from *Mar. Drugs*. Cite as: Smith, K.F.; de Salas, M.; Adamson, J.; Rhodes, L.L. Rapid and Accurate Identification by Real-Time PCR of Biotoxin-Producing Dinoflagellates from the Family Gymnodiniaceae. *Mar. Drugs* **2014**, *12*, 1361–1376.

1. Introduction

The dinoflagellate family Gymnodiniaceae includes the genera *Gymnodinium*, *Karenia*, *Karlodinium*, and *Takayama* [1,2]. Species from the genera *Gymnodinium* and *Karenia* have been responsible for fish kills and shellfish contamination events worldwide [3,4] including New Zealand [5–8]. The only toxic *Gymnodinium* species, *G. catenatum* was first recorded along the northwest coastline of New Zealand following the detection of paralytic shellfish poisons (PSP) in shellfish in May 2000. During that bloom event, PSP toxicity reached 4027 μg saxitoxin equivalents/100 g in Greenshell™ mussels (*Perna canaliculus*) [7]. A number of species in the *Karenia* genus have been reported to cause severe blooms including *K. brevis*, *K. mikimotoi*, *K. brevisulcata*, *K. selliformis*, *K. longicanalis*, and *K. digitata* [6,9–11]. The first recorded major bloom of a *Karenia* species in New Zealand occurred in 1992/93 along the coast of Northland. At that time 180 cases of illness that fitted the symptoms of neurotoxic shellfish poisoning (NSP) were reported [5,12,13]. The identity of the causative organism was not definitely determined, but later confirmed as *K. mikimotoi* [13]. Brevetoxins and brevetoxin analogues were detected in shellfish samples causing the total closure of all bivalve industries in New Zealand [12]. In addition to brevetoxins, *Karenia* species are known to produce gymnodimines [11,14], *Karenia brevisulcata* toxins (KBTs) and brevisulcatic acids (BSXs) [15], the ichthyotoxic gymnocins A and B [16,17],

and haemolytic glycolipids that cause gill damage in fish and have been linked to fish kills in Japan and Norway [11]. Additionally, species from the genera *Karlodinium* and *Takayama* have been implicated in fish kills worldwide [18].

Aside from their negative impacts on food safety, the biotoxins and compounds produced by Gymnodiniaceae species are of interest for commercial exploitation and potential medical applications [19]. For example, compounds (karlotoxins) produced by *Karlodinium veneficum* have been investigated for application as non-toxic cholesterol pharmacophores [20]. Due to their molecular complexity the main method for obtaining these compounds from dinoflagellates is still extraction and purification from laboratory cultures of cells isolated from environmental samples [21] and, in some cases, via contaminated shellfish tissue [22]. Because of the large variability in the type of compounds produced even within a species, accurate identification of biotoxin-producing species from both cultures and environmental samples is crucial.

Routine phytoplankton monitoring of seawater is carried out weekly at approximately 100 sites around New Zealand to inform shellfish harvesters of the potential for toxins in shellfish [23,24]. Analyses are currently carried out at the Cawthron Institute (Nelson, New Zealand), with results expected within 24 h. This monitoring data is critical for shellfish harvesting management decisions in New Zealand. Species in the genus *Karenia* can be difficult to distinguish from each other under the light microscope [11] and are identified as *Karenia* cf. *mikimotoi* for the New Zealand Non-Commercial Marine Biotoxin Monitoring Programme [25]. This term encompasses the following species: *K. mikimotoi*, *K. bidigitata*, *K. brevisulcata*, *K. papilionacea*, *K. selliformis*, *Karlodinium veneficum* and *Gymnodinium impudicum*. Efforts to differentiate *G. catenatum* from look-alike, non-toxic species, e.g., *G. impudicum*, using light microscopy can also be difficult and the morphology of *G. catenatum* cells are often variable [26].

The rapid and accurate identification of toxin-producing dinoflagellate species is essential to assess the risk of bloom formation that can negatively impact human health, marine ecosystems, and aquaculture activities [27–30], and to aid with isolation of the valuable bioactive compounds produced by these species [19]. Monitoring programmes typically involve microscopic examination of water samples, which requires considerable taxonomic experience [31]. Additionally, the species of interest may only occur as a minor component of the community and it can be difficult to morphologically differentiate between toxic and non-toxic species or even strains, e.g., the *Alexandrium tamarense* species complex [32]. In recent years the application of molecular methods for the detection of dinoflagellate species has increased, as these methods are generally rapid, species-specific and do not require specialised expertise [33]. Various molecular methods have been utilised for dinoflagellate detection each with its own advantages and disadvantages [31,33,34], including most commonly: fluorescence *in situ* hybridisation assay (FISH) [26,35,36], sandwich hybridisation assay (SHA) [26,37,38], and traditional or real-time polymerase chain reaction (PCR) [39–47]. Several types of real-time PCR assays with differing levels of specificity have been developed and positive reactions are detected either with a fluorescent reporter probe (e.g., hydrolysis probes, molecular beacons, locked-nucleic acid bases (LNA)) or a double-stranded DNA-binding dye (e.g., SYBR green). More recently, microarray technologies have demonstrated the ability to detect numerous species simultaneously [48,49].

This study describes the development and optimisation of eight real-time PCR assays, all targeting the large subunit ribosomal RNA (LSU rRNA) gene, for the detection of a range of toxic and morphologically similar non-toxic *Karenia*, *Gymnodinium*, *Karlodinium*, and *Takayama* species to assist with toxic dinoflagellate monitoring programmes [24] as well as chemical and ecological research.

2. Results and Discussion

In this study eight real-time PCR assays were developed for the dinoflagellate species *Gymnodinium aureolum*, *G. catenatum*, *Karenia brevisulcata*, *K. mikimotoi*, *K. papilionacea*, *K. umbella*, *Karlodinium veneficum*, and *Takayama tasmanica*, all targeting the D1-D3 region of LSU rRNA gene. Designed assays ranged from 93 to 232 bp in length (Table 1). All of the assays, except for the *G. aureolum* assay, amplified only the target species as determined via cross-reactivity testing with strains listed in Table 2. The *in silico* analysis using NCBI blast also showed that primers and probes did not match with other species. Positive results for the *G. aureolum* assay were obtained for the strains *Gymnodinium* sp. (CAWD71), *G. chlorophorum* (CAWD62) and *G.* cf. *microreticulatum* (CAWD191). However, the assay did not cross-react with *K. mikimotoi*. The assay was primarily developed to differentiate the non-toxic *G. aureolum* from the morphologically similar toxic *K. mikimotoi* and so is still useful for this purpose.

Table 1. Sequences of primers and probes designed in this study including optimised final concentrations for real-time PCR assays.

Target Species	Primer Name and Sequence	Product Size (bp)	Final Concentration
Gymnodinium aureolum	GA519-F: GGACATGGTAGCCTGCC		500 nM
	GA683-R: GTCAGGAAGGTGCTCAGC	153	500 nM
	GA560-P: 6FAM-CAGAACTCACTGTCATATTGCTCCTCC-BHQ-1		50 nM
Gymnodinium catenatum	GC397-F: CTTGGTGAGATTGTCGCAC		500 nM
	GC471-R: GCAAGAAACATCACACCGA	93	1000 nM
	GC426-P: 6FAM-TGATCACCTTCTATTCCAGCGAAAGC-BHQ-1		80 nM
Karenia brevisulcata	KBS460-F: GATCTGGATGCGATACTGAAT		300 nM
	KBS585-R: AGCACTGCTACAAGACATATAA	153	900 nM
	KBS544-P: 6FAM-TGACTGAATGTCCCTAGTTGAACTC-BHQ-1		50 nM
Karenia mikimotoi	KM541-F: CGAGTGACTGAATGTCCTCA		500 nM
	KM645-R: CCAACAACCTTCATGCAGAG	112	250 nM
	KM578-P: 6FAM-CTACCAGACACACAGAGAGCAG-BHQ-1		50 nM
Karenia papilionacea	KP449-F: TCTGGATGCGATACTGGTTG		1000 nM
	KP682-R: TACTTATGTCAAGGATGTGTTC	232	750 nM
	KP630-P: 6FAM-CTTGTTAGTTACCTGGCATGAGAC-BHQ-1		125 nM
Karenia umbella	KU480-F: ATGTCAACGTCAGTTCACAAT		750 nM
	KU623-R: GCACGAGACGAGGCTTA	161	250 nM
	KU542-P: 6FAM-TTCGACTAGGCACATTCAGTCAC-BHQ-1		50 nM
Karlodinium veneficum	KV590-F: TGCCTGGTAGAACTCATGTC		1000 nM
	KV672-R: ACGAGTAACAGAAGCTACAAG	100	1000 nM
	KDV640-P: 6FAM-TGTTCTCATTACCTGCGTCTGGG-BHQ-1		50 nM
Takayama tasmanica	TT533-F: ACTTCTGGGTGACTGAACGT		100 nM
	TT665-R: CCACGTCCTGTCCCATGC	134	1000 nM
	TT616-P: 6FAM-CTGGGCTTTGTTCACTGCTCTTAA-BHQ-1		125 nM

Table 2. The dinoflagellate strains with corresponding Cawthron Institute Culture Collection of Micro-algae (CICCM) codes used in this study. Accession numbers included are for sequences from the target species used to design the real-time PCR assays.

Species Name	CICCM Code	Accession Number
Gymnodinium aureolum	CAWD59, 87	AY947659
Gymnodinium catenatum	CAWD102, 101, 109, 126	AY036128
Gymnodinium cf. *impudicum*	CAWD139	
Gymnodinium cf. *microreticulatum*	CAWD191	
Gymnodinium chlorophorum	CAWD62	
Gymnodinium impudicum	CAWD03	
Gymnodinium instriatum	CAWD137	
Gymnodinium simplex	CAWD86	
Gymnodinium sp.	CAWD172	
Karenia bidigitata	CAWD80	
Karenia brevis	CAWD08	
Karenia brevisulcata	CAWD82	AY243032
Karenia mikimotoi	CAWD63, 117, 133, 134, 192	U92249
Karenia papilionacea	CAWD91	U92252
Karenia selliformis	CAWD79	
Karenia umbella	CAWD131, 65	AY947664
Karlodinium veneficum	CAWD84	AY947665
Takayama helix	CAWD128	
Takayama tasmanica	CAWD115	AY947669

Figure 1. Mean A260/A280 ratios and cycle threshold (C*t*) values for replicate DNA extractions of *Karenia mikimotoi*. Error bars are ± standard error of three replicate DNA extractions.

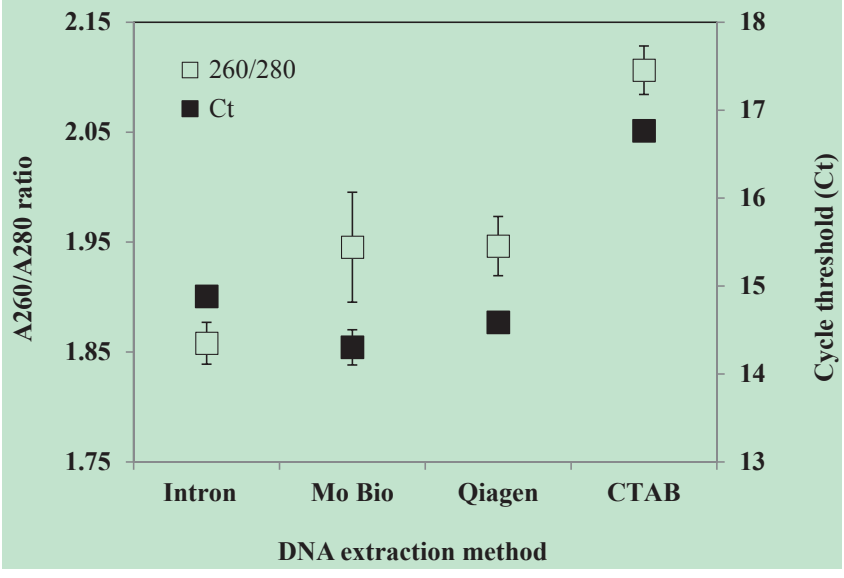

The assays all had various optimised primer and probe concentrations (Table 1). The DNA extraction method that gave the best A260/A280 ratios and lowest Ct values was the PowerSoil® DNA isolation kit (Mo Bio, Carlsbad, CA, USA) (Figure 1). The PowerSoil® DNA isolation kit was also selected as these kits are optimised for the removal of environmental PCR inhibitors and environmental samples showed no evidence of PCR inhibition.

The real-time PCR assays had a linear range of detection six to eight orders of magnitude with a limit of detection (LOD) well below one cell for all assays (Table 3). This is similar to the LOD reported for other real-time PCR assays for Gymnodiniaceae species [50,51]. The amplification efficiency of all assays was between 93% and 106% (Table 3).

Table 3. Range of detection, amplification efficiency and R^2 values.

Target Species	Lower Limit of Detection (Cells/Reaction, 1 s.f.)	Amplification Efficiency	R^2 Value
K. mikimotoi	0.007	101%	1.00
K. umbella	0.09	105%	0.99
K. papilionacea	0.2	95%	0.99
K. brevisulcata	0.2	102%	0.99
K. veneficum	0.3	93%	0.98
G. catenatum	0.006	106%	1.00
G. aureolum	0.006	105%	0.99
T. tasmanica	0.09	102%	1.00

For the last two decades, species belonging to the family Gymnodiniaceae have caused a number of toxic events along the New Zealand coastline. Additionally, blooms of these species have caused major damage to marine ecosystems and aquaculture internationally during the past 60 years [15]. All assays developed in this study are regularly utilised by the micro-algae laboratory at the Cawthron Institute for confirmation of species identification during routine examination of samples as part of the New Zealand Marine Phytoplankton Monitoring Programme [24]. The identification of *Karenia* species by LM is particularly difficult and thus cells in field samples are often identified as *K.* cf. *mikimotoi*. The conclusive identification of a potentially toxic species is most difficult when cell concentrations are low or the species is rarely encountered in routine monitoring. For example, in 1998 the southern coast of the North Island of New Zealand experienced a severe HAB, which devastated almost all the marine life in Wellington Harbour [52]. A new *Karenia* species was isolated from the bloom and named *Karenia brevisulcata*. This species is similar in morphology to other *Karenia* species and has never been reported since. If this species were to bloom again it could have devastating impacts on marine ecosystems, aquaculture activities and human health. Additionally, the toxins produced by this and other *Karenia* species are novel bioactive compounds of great interest [15]. Accurate and early identification is vital and the assays designed in this study enable the conclusive identification of species from environmental samples with results available the same day as sample receipt. This is an important consideration for routine monitoring programmes that require a 24-h turn-around for results, but also for the mining of environmental samples for specific bioactive compound producers.

The copy number of the LSU rRNA gene per cell was determined for *G. catenatum*. The standard curve of serially diluted PCR product had a regression equation of $y = -3.17 + 19.60x$, $R^2 = 1.0$ and an amplification efficiency of 107%. This is similar to the regression curve and amplification efficiency of the standard curve generated by cell number (Table 3). The mean copy number of the cultured strain was 20,800 ± 1566 copies per cell cell. This is comparable to values calculated for other dinoflagellate species [43,46,53]. The estimated LSU rRNA gene copy number calculated in this study also corresponds to the finding from Godhe *et al.* [54] that found the number of rDNA copies per cell is significantly correlated to the biovolume of dinoflagellate cells ($y = -0.61 + 1.22x$, $R^2 = 0.75$; x = log rDNA molecules cell^{-1}, y = log biovolume μm^3 cell^{-1}). The average biovolume of *G. catenatum* cells from the culture used to calculate copy number was 38,438 μm^3, which equates to 23,335 copies of rDNA molecules cell^{-1} from the regression equation in Godhe *et al.* [54].

The *G. catenatum* assay was further developed for quantification to demonstrate the potential for the analysis of environmental samples and in response to the detection of naturally occurring cells in Manukau Harbour, New Zealand. The saxitoxin producing species *G. catenatum* was first detected in New Zealand in 2000 [7], although there is some evidence that this species may have been present in New Zealand prior to this, with a large range expansion in 2000 [8]. *Gymnodinium catenatum* has increased its geographic range around the entire North Island coastline of New Zealand over the last 12 years, and regular blooms are common in some areas (New Zealand Food Safety Authority, [55]). The ability to differentiate *G. catenatum* from morphologically similar, non-toxic species (e.g., *G. impudicum*) during routine monitoring using LM can be difficult, particularly at the onset of blooms when only a few individual cells per litre are present in seawater samples. Additionally, the morphology of *G. catenatum* cells can also be variable and be present as either single cells or chains [26].

Estimates of *G. catenatum* cells per litre determined by the real-time PCR assay were generally similar to or slightly fewer than LM estimates, except at low levels below the limit of detection for LM (Figures 2 and 3). Real-time PCR cell estimates ranged between 70% and 108% of LM cell estimates. This is comparable to what has been found for other real-time PCR assays [50] and has been proposed to be due to factors such as DNA recovery, PCR inhibitors and the exponential nature of PCR [46]. To test for PCR inhibition, the DNA extracts were diluted 1:10 and re-amplified. This did not alter the results and the assay successfully detected cell numbers ranging from below 10 cells per reaction to over 5000 cells per reaction in the spiked samples, which equated to 700 to over 600,000 cells per litre. For natural samples the assay detected a range of cell estimates from 0.07 to 16 cells per reaction, which equated to 3 to 1528 cells per litre. The sample size analysed by the two methods was very different (*i.e.*, 10 mL *versus* 300 mL) and as *G. catenatum* can occur as both single cells and chains of variable length (more than 60 cells/chain) [7] reliable subsampling can be difficult. LM analysis did not detect *G. catenatum* from samples collected in Manukau Harbour on the 23 September 2012, but the real-time PCR assay detected approximately three cells per litre (Figure 3). All positive environmental samples from Manukau Harbour were sequenced and sequences were identical. Using blastn searches, the highest homology found was with *G. catenatum* (e.g., GenBank acc. no. AY036128, coordinates 395-487: query coverage = 100%,

E-value = 5×10^{-15}, percent identity = 100%). Due to the difficulties in thoroughly testing all assays for specificity, we recommend DNA sequencing to confirm species identification especially during the initial stages of assay development.

Figure 2. *Gymnodinium catenatum* cell number estimates by real-time PCR and light microscopy (LM) from natural phytoplankton samples spiked with cultured *G. catenatum* cells. Error bars are ±standard error from triplicate LM analyses and real-time PCR assays.

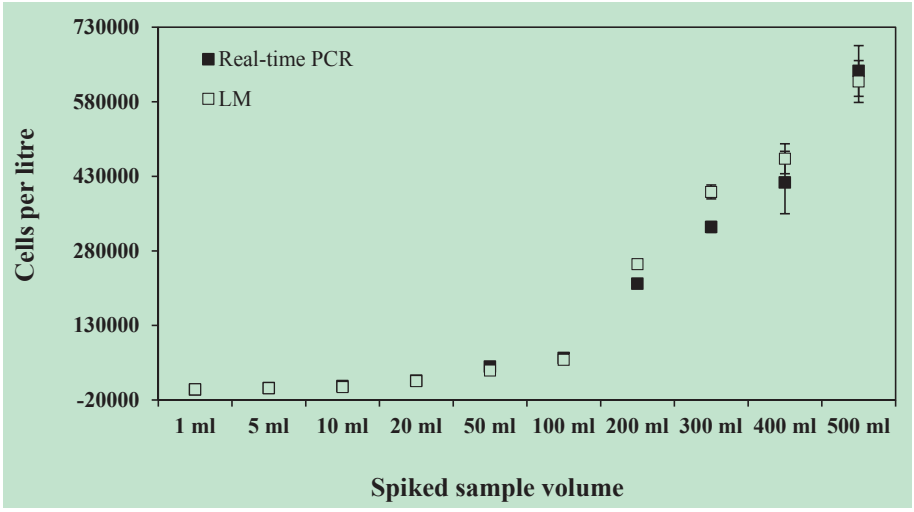

Figure 3. *Gymnodinium catenatum* cell number estimates by real-time PCR and light microscopy (LM) from samples collected at Manukau Bay, New Zealand. Error bars are ±standard error from replicate real-time PCR assays.

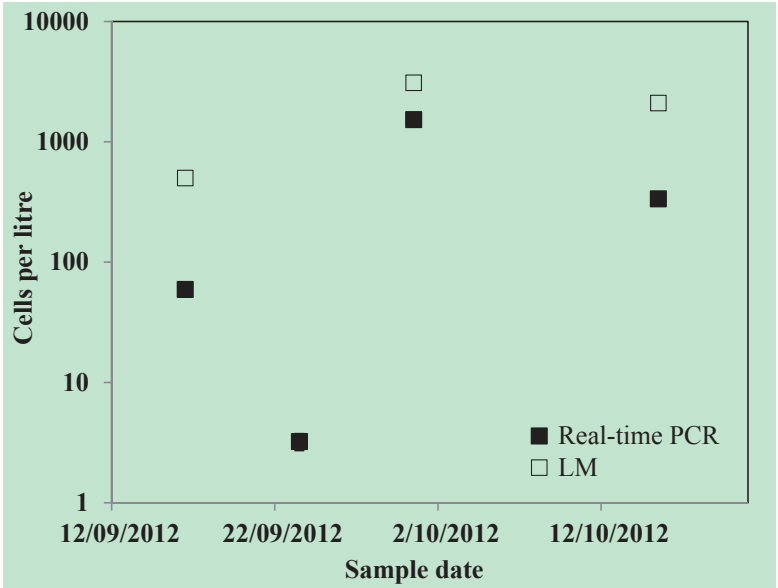

The *G. catenatum* quantitative real-time PCR assay not only enabled conclusive identification but also detected the presence of cells at the LOD for LM. In this study the analysis of samples by LM and Utermöhl chambers has a lower LOD of 100 cells per litre [31]. This is at the threshold for triggering toxin testing in shellfish. As the real-time PCR assay has a LOD of less than one cell, *G. catenatum* could be reliably detected in field samples that were negative using LM. This lower LOD allows far greater forewarning of potentially toxic blooms for shellfish harvesters.

3. Experimental Section

3.1. Culture Maintenance

Dinoflagellate cultures (Table 2) were maintained in GP, 50% GP [56], or F/2 [57] medium at 100 µmol photons m^{-2} s^{-1} (14:10 h light:dark), 19 °C (±1 °C). The Cawthron Institute Culture Collection of Micro-algae (CICCM) provided the strains used in this study (Table 2). Cultures were harvested during exponential growth phase for assay optimisation or cross-reactivity testing.

3.2. DNA Extraction

Exponentially growing cultures of *Karenia mikimotoi* (CAWD63, CAWD117, CAWD133, CAWD134, CAWD192) were pooled and twelve 30 mL subsamples were filtered (Durapore membrane filters, 0.45 µm, Millipore, Billerica, MA, USA) and frozen overnight (−20 °C). DNA extraction was assessed using four methods (three replicates of each); (i-genomic CTB DNA extraction mini kits (Intron, Gyeonggi-do, South Korea), PowerSoil® DNA isolation kit (Mo Bio, Carlsbad, CA, USA), DNeasy mini plant kit (Qiagen, Alameda, CA, USA), and a cetyltrimethylammonium bromide (CTAB) method [58]. All DNA extractions were eluted into 50 µL and quantified using a NanoPhotometer (Implen, Munich, Germany) to check for DNA quantity and quality (A260/A280 ratio). Each DNA extraction was assessed using 10 ng of *K. mikimotoi* genomic DNA with the real-time PCR conditions described above.

3.3. Primers and Probe Design for Real-Time PCR Assays

The target positions for forward and reverse primers and the hydrolysis probes were designed using a multiple LSU rRNA gene (D1-D3 region) alignments (ClustalW) [59] of the target species and sequences from closely related species obtained from GenBank. Separate assays were designed for the detection of eight species including *Gymnodinium aureolum*, *G. catenatum*, *Karenia brevisulcata*, *K. mikimotoi*, *K. papilionacea*, *K. umbella*, *Karlodinium veneficum*, and *Takayama tasmanica*. The specificity of the primer sequences was then confirmed using BLAST (Basic Local Alignment Search Tool) at NCBI (National Centre for Biotechnology Information). The hydrolysis probes were synthesized (GeneWorks, Adelaide, Australia) with 6-FAM reporter dye at the 5′-end and Black Hole Quencher 1 at the 3′-end (Table 1).

3.4. Real-Time PCR Assay Optimisation, Specificity and Sensitivity

Real-time PCR assays were optimised on a Rotor-Gene 6000 (Corbett, Sydney, NSW, Australia), using genomic DNA extracted from an exponentially growing culture of the target species. The optimised assays consisted of a 20 μL reaction containing 10 μL of Platinum® Quantitative PCR SuperMix-UDG (Invitrogen, Carlsbad, CA, USA), 0.8 μg non-acetylated bovine serum albumin (BSA; Sigma-Aldrich, Auckland, New Zealand), and 10 ng of DNA template. Optimised primer and probe concentrations for each assay are shown in Table 1. All PCR reactions in this study were set up manually and all included no template control reactions. Assays were run in clear 0.2 mL thin-wall PCR tubes (Axygen, Union City, CA, USA). All assays had an optimised annealing temperature of 60 °C and PCR cycling conditions were: 50 °C for 2 min, 95 °C for 2 min and 45 cycles of 95 °C for 15 s and 60 °C for 45 s.

The specificity of each assay was verified using DNA from closely related species (Table 2). DNA from each species (10 ng) was used in the real-time PCR assays as described above. The sensitivity of each assay was evaluated with genomic DNA extracted using PowerSoil® DNA isolation kits from known cell concentrations of the target species. The amplification efficiency of the assay was determined by using serially diluted genomic DNA samples (analysed in duplicate) ranging from approximately 100,000 to 1×10^{-4} cells per reaction and the corresponding cycle threshold (C*t*) data.

3.5. Determination of Copy Number and Quantification of the Gymnodinium catenatum *Assay*

The assay specific for *G. catenatum* was further developed in order to demonstrate the potential for quantification of field samples. DNA was extracted from replicate samples of known numbers of cells of the CAWD126 strain of *G. catenatum*. Cell concentrations of culture were estimated during exponential growth phase using the Utermöhl technique [60]. Replicates samples consisting of 150,000 cells were were filtered (Durapore membrane filters, 0.45 μm, Millipore, Billerica, MA, USA), frozen overnight (−20 °C) and transferred to the first tube of a PowerSoil® DNA isolation kit. These extractions were serially diluted and used to generate a standard curve of known cell number per reaction *versus* Ct data.

To estimate the LSU rRNA gene copy number per cell a dilution series of a known concentration of LSU rRNA gene PCR product, ranging from 1 to 0.001 ng was analysed together with extractions of known cell number from above. The number of molecules of PCR product was then determined by the formula: $(A \times 6.022 \times 10^{23}) \times (660 \times B)^{-1}$, with A being the concentration of the PCR product and B the length of the PCR product. The number of molecules in the extractions with known cell number was determined using the PCR product standard curve to obtain the copy number of the LSU rRNA gene per cell. The average biovolume of cells from the culture used was also calculated to determine the relationship between cell size and gene copy number following Godhe *et al.* [54].

3.6. Spiked Environmental and Natural Sample Testing

The effectiveness of the real-time PCR assay for the identification and discrimination of *G. catenatum* from phytoplankton samples was examined using samples spiked with cultured cells. A surface seawater sample (10 L) was collected from Nelson Marina (Nelson, South Island, New Zealand). Different volumes (1, 5, 10, 20, 50, 100, 200, 300, 400 and 500 mL) of *G. catenatum* culture (mix of CAWD101, CAWD102, CAWD109 and CAWD126) were made up to one litre volume with the natural phytoplankton sample to create ten contrived samples. From the one litre samples triplicate 10 mL aliquots were preserved in Lugol's solution analysed by Light Microscopy (LM) and triplicate 300 mL aliquots were analysed using the real-time PCR assay. For real-time PCR analyses samples were filtered and genomic DNA extracted with PowerSoil® DNA isolation kits (Mo Bio, Carlsbad, CA, USA) as described above. To estimate the abundance of *G. catenatum* in environmental samples C*t* values were used to calculate cell number per reaction based on the standard curve generated with the serial dilution of DNA extracts of known cell number (ranging from 6000 to 0.006 cells per reaction). The real-time PCR assays all included standard curves, positive controls, negative controls and blank extraction controls. DNA samples were also diluted 1:10 to determine evidence of PCR inhibition.

Samples were collected from Manukau Harbour (Auckland, North Island, New Zealand) as part of the New Zealand Marine Phytoplankton Monitoring Programme (by the New Zealand Food Safety Authority, Ministry for Primary Industries, Wellington, New Zealand). Unpreserved and preserved (Lugol's solution [60]) replicate samples were received within 24 h of collection. Grab samples (100 mL) from three depths (0, 3 and 6 m) were pooled (total 300 mL). *G. catenatum* cells were identified by LM and cell number estimates estimated using the Utermöhl technique [61] by the micro-algae laboratory at the Cawthron Institute, New Zealand (International Accreditation New Zealand: ISO 17025). One 10 mL subsample, from the pooled 300 mL, was analysed by LM for each environmental sample. For real-time PCR analysis the unpreserved grab samples filtered and genomic DNA extracted with PowerSoil® DNA isolation kits (Mo Bio, Carlsbad, CA, USA) as described above. The abundance of *G. catenatum* in environmental samples was calculated as above. Environmental samples were also PCR amplified for DNA sequencing (Sanger sequencing) to confirm positive results. PCR amplifications were carried out in 50 μL reaction volumes containing i-Taq 26 PCR master mix (25 μL; Intron, Gyeonggi-do, Korea), both forward and reverse primers (0.4 mM) and template (*ca.* 50–150 ng of DNA). Thermocycling conditions were the same as for real-time PCR. Amplification products were purified (AxyPrep PCR cleanup kits, Axygen, Union City, CA, USA) and sequenced in both directions using the primers from real-time PCR assay by an external contractor (University of Waikato DNA Sequencing Facility, Hamilton, New Zealand). The resulting sequences were compared to existing sequences in GenBank using the BLAST online software.

4. Conclusions

At present real-time PCR is the most cost-effective, sensitive, and rapid molecular technique for the detection and quantification of dinoflagellates from environmental samples [62]. The assays

developed in this study demonstrate great potential for aiding in monitoring programmes for both food safety purposes and rapid screening of samples for species of interest. These assays are all utilised regularly as part of the New Zealand Marine Phytoplankton Monitoring Programme [24], as support for LM analyses by confirming the identification of toxic species in water samples. However, as multiplexing techniques, sequencing technologies, genomic and bioinformatic resources all improve, it is likely that molecular techniques will be increasingly utilised for routine phytoplankton monitoring programmes [34,45,62].

Acknowledgements

We would like to thank K. Ponikla (Cawthron Institute) for technical support, L. MacKenzie for *Gymnodinium catenatum* measurements, and the Ministry of Primary Industries for kindly supplying the environmental samples. This work was supported by funding from the New Zealand Ministry of Science and Innovation, contract CAW0703.

Author Contributions

K.F.S., L.L.R. and M.d.S. designed the experiments. M.d.S. designed the primers. K.F.S. collected the field samples except for samples collected by the New Zealand Food Safety Authority. K.F.S., M.d.S. and J.A. performed the laboratory work. K.F.S., L.L.R. and M.d.S. wrote the manuscript.

Conflicts of Interest

The authors declare no conflict of interest.

References

1. Daugbjerg, N.; Hansen, G.; Larsen, J.; Moestrup, O. Phylogeny of some of the major genera of dinoflagellates based on ultrastructure and partial LSU rDNA sequence data, including the erection of three new genera of unarmoured dinoflagellates. *Phycologia* **2000**, *39*, 302–317.
2. de Salas, M.F.; Bolch, C.J.S.; Botes, L.; Nash, G.; Wright, S.W.; Hallegraeff, G.M. *Takayama* gen. nov (Gymnodiniales, Dinophyceae), a new genus of unarmored dinoflagellates with sigmoid apical grooves, including the description of two new species. *J. Phycol.* **2003**, *39*, 1233–1246.
3. Brand, L.E.; Campbell, L.; Bresnan, E. *Karenia*: the biology and ecology of a toxic genus. *Harmful Algae* **2012**, *14*, 156–178.
4. Taylor, F.J.R.; Fukuyo, Y.; Larsen, J.; Hallegraeff, G.M. Taxonomy of Harmful Dinoflagellates. In *Manual on Harmful Marine Microalgae*; Hallegraeff, G.M., Anderson, D.M., Cembella, A.D., Eds.; UNESCO Intergovernmental Oceanographic Commission: Pairs, France, 2003; pp. 389–432.

5. Rhodes, L.L.; Haywood, A.J.; Ballantine, W.J.; MacKenzie, A.L. Algal blooms and climate anomalies in north-east New Zealand, August–December 1992. *N. Z. J. Mar. Freshw. Res.* **1993**, *27*, 419–430.
6. Wear, R.G.; Gardner, J.P.A. Biological effects of the toxic algal bloom of February and March 1998 on the benthos of Wellington Harbour, New Zealand. *Mar. Ecol. Prog. Ser.* **2001**, *218*, 63–76.
7. MacKenzie, L.A.; Beauchamp, T. Gymnodinium catenatum *in New Zealand: A New Problem for Public Health and the Shellfish Industry*; Cawthron Institute: Nelson, New Zealand, 2002.
8. Irwin, A.; Hallegraeff, G.M.; McMinn, A.; Harrison, J.; Heijnis, H. Cyst and radionuclide evidence demonstrate historic *Gymnodinium catenatum* dinoflagellate populations in Manukau and Hokianga Harbours, New Zealand. *Harmful Algae* **2003**, *2*, 61–74.
9. Yang, Z.B.; Takayama, H.; Matsuoka, K.; Hodgkiss, I.J. *Karenia digitata* sp nov. (Gymnodiniales, Dinophyceae), a new harmful algal bloom species from the coastal waters of west Japan and Hong Kong. *Phycologia* **2000**, *39*, 463–470.
10. Yang, Z.B.; Hodgkiss, I.J.; Hansen, G. *Karenia longicanalis* sp nov. (Dinophyceae): A new bloom-forming species isolated from Hong Kong, May 1998. *Bot. Mar.* **2001**, *44*, 67–74.
11. Haywood, A.J.; Steidinger, K.A.; Truby, E.W.; Bergquist, P.R.; Bergquist, P.L.; Adamson, J.; MacKenzie, L. Comparative morphology and molecular phylogenetic analysis of three new species of the genus *Karenia* (Dinophyceae) from New Zealand. *J. Phycol.* **2004**, *40*, 165–179.
12. Jasperse, J.A. *Marine Toxins and New Zealand Shellfish: Proceedings of a Workshop on Research Issues, 10–11 June 1993*; Royal Society of New Zealand: Wellington, New Zealand, 1993.
13. Todd, K. *A Review of NSP Monitoring in New Zealand in Support of a New Programme*; Cawthron Report No. 660; Marine Biotoxin Technical Committee: Nelson, New Zealand, 2003.
14. MacKenzie, L.A.; Haywood, A.J.; Adamson, J.; Truman, P.; Till, D.; Seki, T.; Satake, M.; Yasumoto, T. Gymnodimine Contamination of Shellfish in New Zealand. In *Harmful and Toxic Algal Blooms*; Yasumoto, T., Oshima, Y., Fukuyo, Y., Eds.; Intergovernmental Oceanographic Commission of UNESCO: Paris, France, 1996; pp. 97–100.
15. Holland, P.T.; Shi, F.; Satake, M.; Hamamoto, Y.; Ito, E.; Beuzenberg, V.; McNabb, P.; Munday, R.; Briggs, L.; Truman, P.; *et al.* Novel toxins produced by the dinoflagellate *Karenia brevisulcata*. *Harmful Algae* **2012**, *13*, 47–57.
16. Satake, M.; Shoji, M.; Oshima, Y.; Naoki, H.; Fujita, T.; Yasumoto, T. Gymnocin-A, a cytotoxic polyether from the notorious red tide dinoflagellate, *Gymnodinium mikimotoi*. *Tetrahedron Lett.* **2002**, *43*, 5829–5832.
17. Satake, M.; Tanaka, Y.; Ishikura, Y.; Oshima, Y.; Naoki, H.; Yasumoto, T. Gymnocin-B with the largest contiguous polyether rings from the red tide dinoflagellate, *Karenia* (formerly *Gymnodinium*) *mikimotoi*. *Tetrahedron Lett.* **2005**, *46*, 3537–3540.
18. de Salas, M.F.; Bolch, C.J.S.; Hallegraeff, G.M. *Karlodinium australe* sp. nov. (Gymnodiniales, Dinophyceae), a new potentially ichthyotoxic unarmoured dinoflagellate from lagoonal habitats of south-eastern Australia. *Phycologia* **2005**, *44*, 640–650.

19. García Camacho, F.; Gallardo Rodríguez, J.; Sánchez Mirón, A.; Cerón García, M.C.; Belarbi, E.H.; Chisti, Y.; Molina Grima, E. Biotechnological significance of toxic marine dinoflagellates. *Biotechnol. Adv.* **2007**, *25*, 176–194.
20. Waters, A.L.; Hill, R.T.; Place, A.R.; Hamann, M.T. The expanding role of marine microbes in pharmaceutical development. *Curr. Opin. Biotechnol.* **2010**, *21*, 780–786.
21. Beuzenberg, V.; Mountfort, D.; Holland, P.; Shi, F.; MacKenzie, L. Optimization of growth and production of toxins by three dinoflagellates in photobioreactor cultures. *J. Appl. Phycol.* **2012**, *24*, 1023–1033.
22. Selwood, A.I.; van Ginkel, R.; Wilkins, A.L.; Munday, R.; Ramsdell, J.S.; Jensen, D.J.; Cooney, J.M.; Miles, C.O. Semisynthesis of *S*-Desoxybrevetoxin-B2 and Brevetoxin-B2, and assessment of their acute toxicities. *Chem. Res. Toxicol.* **2008**, *21*, 944–950.
23. Rhodes, L.L.; Scholin, C.; Tyrrell, J.; Adamson, J.; Todd, K. The integration of DNA probes into New Zealand's routine phytoplankton monitoring programmes. In *Harmful Algal Blooms*; Hallegraeff, G.M., Blackburn, S.I., Bolch, C.J., Lewis, R.J., Eds.; Intergovernmental Oceanographic Commission of UNESCO: Paris, France, 2001; pp. 429–432.
24. Rhodes, L.L.; Smith, K.F.; Moisan, C. Shifts and stasis in marine HAB monitoring in New Zealand. *Environ. Sci. Pollut. Res.* **2013**, *20*, 6872–6877.
25. NZFSA. *Non-Commercial Marine Biotoxin Monitoring Programme: NZFSA VA Operating and Response Manual*; New Zealand Food Safety Authority (NZFSA): Wellington, New Zealand, 2010; p. 39.
26. Rhodes, L.L.; Smith, K.F.; de Salas, M. DNA probes, targeting large sub-unit rRNA, for the rapid identification of the paralytic shellfish poison producing dinoflagellate, *Gymnodinium catenatum*. *N. Z. J. Mar. Freshw. Res.* **2007**, *41*, 385–390.
27. Burkholder, J.M. Implications of harmful microalgae and heterotrophic dinoflagellates in management of sustainable marine fisheries. *Ecol. Appl.* **1998**, *8*, S37–S62.
28. Van Dolah, F.M. Marine algal toxins: origins, health effects, and their increased occurrence. *Environ. Health Perspect.* **2000**, *108*, 133–141.
29. Landsberg, J.H. The effects of harmful algal blooms on aquatic organisms. *Rev. Fish. Sci.* **2002**, *10*, 113–390.
30. Hallegraeff, G.M. Ocean climate change, phytoplankton community responses, and harmful algal blooms: a formidable predictive challenge. *J. Phycol.* **2010**, *46*, 220–235.
31. Godhe, A.; Cusack, C.; Pedersen, J.; Anderson, P.; Anderson, D.M.; Breasnan, E.; Cembella, A.; Dahl, E.; Diercks, S.; Elbrachter, M.; *et al.* Intercalibration of classical and molecular techniques for identification of *Alexandrium fundyense* (Dinophyceae) and estimation of cell densities. *Harmful Algae* **2007**, *6*, 56–72.
32. John, U.; Medlin, L.K.; Groben, R. Development of specific rRNA probes to distinguish between geographic clades of the *Alexandrium tamarense* species complex. *J. Plankton Res.* **2005**, *27*, 199–204.
33. Penna, A.; Bertozzini, E.; Battocchi, C.; Galluzzi, L.; Giacobbe, M.G.; Vila, M.; Garces, E.; Luglie, A.; Magnani, M. Monitoring of HAB species in the Mediterranean Sea through molecular methods. *J. Plankton Res.* **2007**, *29*, 19–38.

34. Wood, S.A.; Smith, K.F.; Banks, J.C.; Tremblay, L.A.; Rhodes, L.L.; Mountfort, D.; Cary, S.C.; Pochon, X. Molecular genetic tools for environmental monitoring of New Zealand's aquatic habitats, past, present and the future. *N. Z. J. Mar. Freshw. Res.* **2013**, *47*, 90–119.
35. Miller, P.E.; Scholin, C.A. Identification and enumeration of cultured and wild *Pseudo-nitzschia* (Bacillariophyceae) using species-specific LSU rRNA-targeted fluorescent probes and filter-based whole cell hybridization. *J. Phycol.* **1998**, *34*, 371–382.
36. Rhodes, L.L.; Scholin, C.; Garthwaite, I. *Pseudo-nitzschia* in New Zealand and the role of DNA probes and immunoassays in refining marine biotoxin monitoring programmes. *Nat. Toxins* **1998**, *6*, 105–111.
37. Ayers, K.; Rhodes, L.L.; Tyrrell, J.V.; Gladstone, M.; Scholin, C.A. International accreditation of sandwich hybridisation assay format DNA probes for micro-algae. *N. Z. J. Mar. Freshw. Res.* **2005**, *39*, 1225–1231.
38. Haywood, A.J.; Scholin, C.A.; Marin, R., III.; Steidinger, K.A.; Heil, C.; Ray, J. Molecular detection of the brevetoxin-producing dinoflagellate *Karenia brevis* and closely related species using rRNA-targeted probes and a semiautomated sandwich hybridization assay. *J. Phycol.* **2007**, *43*, 1271–1286.
39. Bowers, H.A.; Tengs, T.; Goto, S.; Tomas, C.; Ono, C.; Yoshimatsu, S.; Oldach, D.; Steidinger, K.A.; Landsberg, J.H.; Tomas, C.R.; *et al.* Development of real-time PCR assays for the detection of *Chattonella* species in culture and environmental samples. In *Harmful Algae 2002*; Steidinger, K.A., Landsberg, J.H., Tomas, C.R., Vargo, G.A., Eds.; Florida Institute of Oceanography, and Intergovernmental Oceanographic Commission of UNESCO: Pairs, France, 2004; pp. 231–233.
40. Coyne, K.J.; Handy, S.M.; Demir, E.; Whereat, E.B.; Hutchins, D.A.; Portune, K.J.; Doblin, M.A.; Cary, S.C. Improved quantitative real-time PCR assays for enumeration of harmful algal species in field samples using an exogenous DNA reference standard. *Limnol. Oceanogr.* **2005**, *3*, 381–391.
41. Patil, J.; Gunasekera, R.; Deagle, B.; Bax, N.; Blackburn, S. Development and evaluation of a PCR based assay for detection of the toxic dinoflagellate, *Gymnodinium catenatum* (Graham) in ballast water and environmental samples. *Biol. Invasions* **2005**, *7*, 983–994.
42. Dyhrman, S.T.; Erdner, D.L.; La Du, J.; Galac, M.; Anderson, D.M. Molecular quantification of toxic *Alexandrium fundyense* in the Gulf of Maine using real-time PCR. *Harmful Algae* **2006**, *5*, 242–250.
43. Murray, S.A.; Wiese, M.; Stüken, A.; Brett, S.; Kellmann, R.; Hallegraeff, G.; Neilan, B.A. sxtA-based quantitative molecular assay to identify saxitoxin-producing harmful algal blooms in marine waters. *Appl. Environ. Microb.* **2011**, *77*, 7050–7057.
44. Perini, F.; Casabianca, A.; Battocchi, C.; Accoroni, S.; Totti, C.; Penna, A. New approach using the real-time PCR method for estimation of the toxic marine dinoflagellate *Ostreopsis* cf. *ovata* in marine environment. *PLoS One* **2011**, *6*, e17699.
45. Penna, A.; Galluzzi, L. The quantitative real-time PCR applications in the monitoring of marine harmful algal bloom (HAB) species. *Environ. Sci. Pollut. Res.* **2013**, *20*, 6851–6862.

46. Vandersea, M.W.; Kibler, S.R.; Holland, W.C.; Tester, P.A.; Schultz, T.F.; Faust, M.A.; Holmes, M.J.; Chinain, M.; Litaker, R.W. Development of semi-quantitative PCR assays for the detection and enumeration of *Gambierdiscus* species (Gonyaulacales, Dinophyceae). *J. Phycol.* **2012**, *48*, 902–915.
47. Hariganeya, N.; Tanimoto, Y.; Yamaguchi, H.; Nishimura, T.; Tawong, W.; Sakanari, H.; Yoshimatsu, T.; Sato, S.; Preston, C.M.; Adachi, M. Quantitative PCR method for enumeration of cells of cryptic species of the toxic marine dinoflagellate *Ostreopsis* spp. in coastal waters of Japan. *PLoS One* **2013**, *8*, e57627.
48. Gescher, C.; Metfies, K.; Medlin, L.K. The ALEX CHIP—Development of a DNA chip for identification and monitoring of *Alexandrium*. *Harmful Algae* **2008**, *7*, 485–494.
49. Galluzzi, L.; Cegna, A.; Casabianca, S.; Penna, A.; Saunders, N.; Magnani, M. Development of an oligonucleotide microarray for the detection and monitoring of marine dinoflagellates. *J. Microbiol. Methods* **2011**, *84*, 234–242.
50. Zamor, R.M.; Glenn, K.L.; Hambright, K.D. Incorporating molecular tools into routine HAB monitoring programs: using qPCR to track invasive *Prymnesium*. *Harmful Algae* **2012**, *15*, 1–7.
51. Yuan, J.; Mi, T.; Zhen, Y.; Yu, Z. Development of a rapid detection and quantification method of *Karenia mikimotoi* by real-time quantitative PCR. *Harmful Algae* **2012**, *17*, 83–91.
52. Chang, F.H. *Gymnodinium brevisulcatum* sp nov (Gymnodiniales, Dinophyceae), a new species isolated from the 1998 summer toxic bloom in Wellington Harbour, New Zealand. *Phycologia* **1999**, *38*, 377–384.
53. Galluzzi, L.; Bertozzini, E.; Penna, A.; Perini, F.; Garces, E.; Magnani, M. Analysis of rRNA gene content in the Mediterranean dinoflagellate *Alexandrium catenella* and *Alexandrium taylori*: Implications for the quantitative real-time PCR-based monitoring methods. *J. Appl. Phycol.* **2010**, *22*, 1–9.
54. Godhe, A.; Asplund, M.E.; Härnström, K.; Saravanan, V.; Tyagi, A.; Karunasagar, I. Quantification of diatom and dinoflagellate biomasses in coastal marine seawater samples by real-time PCR. *Appl. Environ. Microb.* **2008**, *74*, 7174–7182.
55. New Zealand Food Safety Authority, Ministry for Primary Industries. Wellington, New Zealand. Unpublished data, 2013.
56. Loeblich, A.R.; Smith, V.E. Chloroplast pigments of the marine dinoflagellate *Gyrodinium resplendens*. *Lipids* **1968**, *3*, 5–13.
57. Keller, M.D.; Selvin, R.C.; Claus, W.; Guillard, R.R.L. Media for the culture of oceanic ultraphytoplankton. *J. Phycol.* **1987**, *23*, 633–638.
58. Doyle, J.J.; Doyle, J.L. A rapid DNA isolation procedure for small quantities of fresh leaf tissue. *Phytochem. Bull.* **1987**, *19*, 11–15.
59. Thompson, J.D.; Higgins, D.G.; Gibson, T.J. CLUSTAL W: Improving the sensitivity of progressive multiple sequence alignment through sequence weighting, position-specific gap penalties and weight matrix choice. *Nucleic Acids Res.* **1994**, *22*, 4673–4680.

60. Throndsen, J. Preservation and storage. In *Phytoplankton Manual*; Sournia, A., Ed.; United Nations Educational, Scientific and Cultural Organization (UNESCO): Paris, France, 1978; pp. 69–74.
61. Utermöhl, H. Zur vervollkommung der quantitativen phytoplankton methodik (Towards a perfection of quantitative phytoplankton methodology). *Mitt. Int. Ver. Theor. Angew. Limnol.* **1958**, *9*, 1–38.
62. Ebenezer, V.; Medlin, L.K.; Ki, J.S. Molecular detection, quantification, and diversity evaluation of microalgae. *Mar. Biotechnol.* **2012**, *14*, 129–142.

Combined Effects of Nitrogen Concentration and Seasonal Changes on the Production of Lipids in *Nannochloropsis oculata*

Martin Olofsson, Teresa Lamela, Emmelie Nilsson, Jean-Pascal Bergé, Victória del Pino, Pauliina Uronen and Catherine Legrand

Abstract: Instead of sole nutrient starvation to boost algal lipid production, we addressed nutrient limitation at two different seasons (autumn and spring) during outdoor cultivation in flat panel photobioreactors. Lipid accumulation, biomass and lipid productivity and changes in fatty acid composition of *Nannochloropsis oculata* were investigated under nitrogen (N) limitation (nitrate:phosphate N:P 5, N:P 2.5 molar ratio). *N. oculata* was able to maintain a high biomass productivity under N-limitation compared to N-sufficiency (N:P 20) at both seasons, which in spring resulted in nearly double lipid productivity under N-limited conditions (0.21 g L^{-1} day^{-1}) compared to N-sufficiency (0.11 g L^{-1} day^{-1}). Saturated and monounsaturated fatty acids increased from 76% to nearly 90% of total fatty acids in N-limited cultures. Higher biomass and lipid productivity in spring could, partly, be explained by higher irradiance, partly by greater harvesting rate (~30%). Our results indicate the potential for the production of algal high value products (*i.e.*, polyunsaturated fatty acids) during both N-sufficiency and N-limitation. To meet the sustainability challenges of algal biomass production, we propose a dual-system process: Closed photobioreactors producing biomass for high value products and inoculum for larger raceway ponds recycling waste/exhaust streams to produce bulk chemicals for fuel, feed and industrial material.

Reprinted from *Mar. Drugs*. Cite as: Olofsson, M.; Lamela, T.; Nilsson, E.; Bergé, J.-P.; del Pino, V.; Uronen, P.; Legrand, C. Combined Effects of Nitrogen Concentration and Seasonal Changes on the Production of Lipids in *Nannochloropsis oculata*. *Mar. Drugs* **2014**, *12*, 1891–1910.

1. Introduction

Microalgae have been proposed as feedstock for biodiesel due to their rapid growth and high lipid content [1–3]. The advantages with microalgae derived biodiesel may be (1) higher biomass productivity compared to land grown crops, (2) possibility to grow on marginal or non-arable land, (3) utilization of seawater and waste water, therefore reducing fresh water use, (4) both CO_2 neutral fuel manufacture and CO_2 sequestration (5) non-toxic, biodegradable and renewable fuel [1,2,4,5]. However, Tredici [6] argues that microalgae are not superior to land grown agro crops in terms of photosynthetic efficiency and biomass productivity. The main advantage would rather be the ability of microalgae to alter their cellular composition as a response to distinctive culture conditions (*i.e.*, nutrient deficiency). Thus, the potential lipid production of microalgae is much greater than agro crops.

Few microalgal species accumulate large quantities of lipids during exponential phase and the lipids are primarily present as structural polar lipids, typically polyunsaturated fatty acids (PUFA), which can be commercially valuable as food supplement [7] and for nutritional enrichment in

aquaculture industry [8–10]. In particular, the genus *Nannochloropsis* contains high amounts of eicosapentaenoic acid (20:5 ω3, EPA) [11–13]. EPA can serve as a marine drug since it has a well documented positive effect on human health [14]. At stationary phase microalgae can accumulate substantial amounts of neutral storage lipids in the form of triglycerides (TAGs), which are considered as the best substrate for biodiesel [15,16]. TAGs consist principally of saturated fatty acids (SAFA) and monounsaturated fatty acids (MUFA). Biodiesel is manufactured using a transesterification process where vegetable or animal TAGs are reacting with an alcohol (typically methanol) to produce an ester then referred to as a fatty acid methyl ester (FAME) and glycerol [1]. Distinct from biodiesel is renewable diesel, such as hydrotreated vegetable oil (HVO) that is chemically similar to petrodiesel, but is derived from a wide range of vegetable sources, although waste animal fats and other waste and residue streams can be used. In the process hydrogen is used to remove oxygen from TAGs, which produces a pure hydrocarbon chain (paraffin) containing no oxygen but small amounts of water, CO_2 and propane as by-products [17].

Nutrient stress, mainly nitrogen (N) limitation or deprivation, is well known to enhance lipid accumulation in microalgal cells with generally higher degrees of SAFA and MUFA [18–22]. Other growth conditions affecting lipid content and composition are CO_2 concentration [23,24], light [8,11,12,25,26], temperature [25–30], salinity [31,32] and growth phase [33,34]. Increased lipid content in microalgal cells due to nutrient stress induction may not always yield a net gain in algal oil since biomass production usually is reduced. There are examples though, of net gain in lipid productivity in large-scale cultures [21,35] exposed to complete nutrient starvation during high productive seasons. Whether this net gain in lipid production can be sustainable over the entire production season is unknown. Thus, we investigated the combined effect of nutrient limitation and seasonal variation (autumn and spring) on algal lipid production using *Nannochloropsis oculata*.

In contrast to the numerous laboratory-based experiments, nutrient stress induced algal oil production needs to be demonstrated in scaled-up conditions outdoors. Thus, outdoor large-scale cultures of *N. oculata* grown in flat panel photobioreactors (PBRs) were nutrient manipulated at steady-state to maximize algal lipid production in *N. oculata*. Total lipids (TL), fatty acid (FA) profiles, biomass productivity (BP) and lipid productivity (LP) were determined during the study. The aim was to increase lipid content and change FA composition through nutrient limitation without substantial loss of biomass resulting in a total net gain in lipid productivity. The study was conducted with N-manipulation experiments in autumn 2008 and in spring 2009. Seasonal conditions can be specific to geographical location and may vary among years. As seasonal variations cannot be manipulated, it is important to include their impact in combination with nitrogen stress on algal productivity to improve estimates of lipid productivity over an entire year.

2. Results and Discussion

Ambient daily average temperatures ranged 19–21 °C during autumn 2008 and 17–20 °C during spring 2009. Total global radiation (TGR) in autumn 2008 varied between 15 and 20 MJ m^{-2} day^{-1} with a dip as low as 5 MJ m^{-2} day^{-1} on day 4 during the first experiment. TGR in spring 2009 was higher and ranged 23–31 MJ m^{-2} day^{-1}.

2.1. Optical Density (OD) and Dry Weight (DW)

Both in autumn and spring, algal biomass followed a similar pattern in control (N:P 20, molar ratio) and N-limited cultures (N:P 5, N:P 2.5), regardless of N-limitation level (Figure 1). Significantly lower biomass (DW) was found in N-limited cultures compared to control in both autumn and spring at N:P 5(ANOVA, $p = 0.00732$). At N:P 2.5 in spring, there was no difference between treatment and control indicating very little effect of the level of N stress(Fisher test, $p = 0.5993$). DW showed no lag phase in response to N-limitation compared to OD. This trend was clearer in the autumn experiment as the study period was 9 days instead of 5 days (spring).

Figure 1. Biomass of *N. oculata* illustrated by optical density at 540 nm (OD_{540}) and dry weight (DW) at different N-limitations. Autumn: (**a**) N:P 5. Spring: (**b**) N:P 5; (**c**) N:P 2.5. DW shows mean values ± SD of 3 technical triplicates.

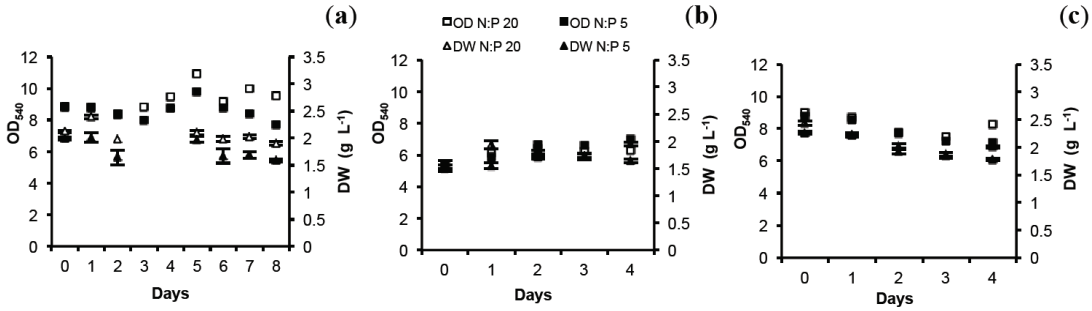

2.2. Total Lipids (TL) and Total Protein (TP)

There was a significant effect of treatment (ANCOVA, $p = 8.89 \times 10^{-7}$), season (ANCOVA, $p = 7.92 \times 10^{-8}$) and an interaction effect of time and treatment on TL (ANCOVA $p = 0.0121$). N-limited cultures accumulated more lipids compared to control and the slope (the rate of increase in lipid accumulation) was higher in autumn. TL concentrations in % of DW for *N. oculata* showed an increase with 10–15 percentage points compared to control in 48 to 96 h by N-stress (Figure 2d–f). The TL reached 40% in both autumn (N:P 5) and spring (N:P 2.5). Lipid accumulation for microalgae at N-deficiency or N-limitation has been reported by several studies [18–22,35–37] and the conditions applied by these studies vary widely, making comparison difficult. Moreover, the actual increase in TL may be species and strain specific. [21,35,38–42]. Our results of TL were in consent with literature, although the increase was not as drastic as for outdoor studies of *Nannochloropsis* sp. F&M-M24 strain [21,35] and *Neochloris oleoabundans* [22]. Both species doubled the TL content up to 50%–60% of DW after N-starvation. The N-stress level in spring (N:P 2.5 *vs.* N:P 5) did not have a major effect on the amount of lipids accumulated and the differences in percentage points between treatment and control were similar (16%). However, a significant interaction effect of both N:P 5 and N:P 2.5 and time on lipid accumulation was found (ANCOVA, $p = 0.0011$ and $p = 0.00174$, respectively).

Figure 2. Total lipids (TL) and protein (TP) total in % of dry weight for *N. oculata* at different N-limitations. (**a**) TL at N:P 5 in autumn; (**b**) TL at N:P 5 in spring; (**c**) TL at N:P 2.5 in spring; (**d**) TP at N:P 5 in autumn; (**e**) TP at N:P 5 in spring; **(f)** TP at N:P 2.5 in spring. White bars represent control (N:P 20) for both TL and TP, light grey bars represent N:P 5 values for both TL and TP, and dark grey bars represent N:P 2.5 for both TL and TP.TL and TP show mean values ± SD of 5 and 3 technical replicates, respectively.

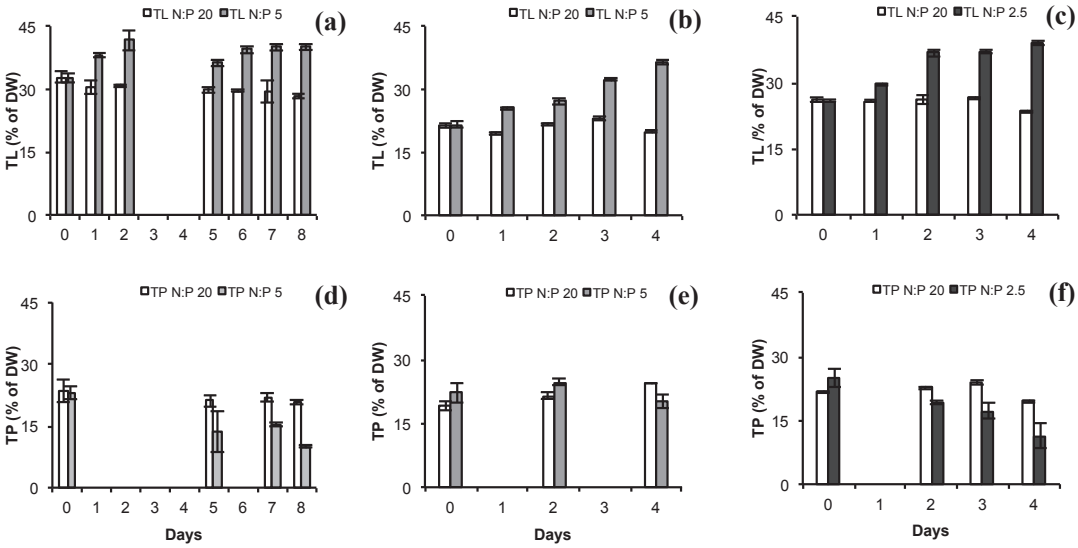

Nitrogen is essential for protein synthesis [43]. Hence protein content may be reduced at nitrogen limitation [36,44], which also was a trend for *N. oculata* in the N-limited treatments compared to the controls (Figure 2a–c). A significant interaction effect of time and treatment was found (ANCOVA, $p = 0.0065$) and a seasonal effect (ANCOVA, $p = 0.0305$). The TP content decreased from approximately 20% of DW at N-sufficient growth to nearly half the protein content observed at N-limitation (N:P 5 in autumn and N:P 2.5 in spring). The use of co-products in algal biofuels production must take into account the lower protein content at N-limitation or N-deprivation. TP content for control cultures was similar among autumn and spring experiments (20% of DW).

The trend for the total lipid to total protein (TL/TP) ratio implied an increase at N-stress with average ratios of 2 at N-limitation compared to 1.2 for control cultures (data not shown). Killham *et al.* [45] reported similar relative values for the freshwater green algae *Ankistrodesmus falcatus*. However, the values in spring at N:P 5 were similar to the control as shown by only minor decrease in TP (Figure 2b).

2.3. Fatty Acid (FA) Profiles

Fatty acid (FA) profiles of *N. oculata* were comparable to those of other *Nannochloropsis* strains [8,11,12,21,22,26,35,46–48]. In this study, FA profiles of *N. oculata* under N-limitation

differed mainly in respect of C16:0, C18:1 and C20:5. N-stressed cells accumulated more C16:0 and C18:1 but less C20:5 compared to control (Table 1). Minor differences could also be observed for C14:0, C18:2 (spring) and C20:4. The level of N-stress (N:P 2.5 *vs.* N:P 5) seemed to have a stronger influence on the profile compared to the length of the N-stress. In spring, the difference in C16:0 was as much as 15 percentage points and the discrepancy in C20:5 was 10 percentage points at the most severe N-stress (N:P 2.5) compared to 10 and 8 percentage points (N:P 5), respectively. The profile after 8 days of N-stress was similar to the profile after 4–5 days (N:P 5).

Accordingly, saturated fatty acids (SAFAs) increased during N-limited growth and together with monounsaturated fatty acids (MUFAs) constituted nearly 90% of total FA compared to 76% for the N:P 20 grown cultures (Figure 3). However, the SAFAs and MUFAs fraction during N-limitation was slightly higher in spring compared to autumn (Table 1). Similar levels for SAFAs and MUFAs were also shown by Rodolfi *et al.* [21] for *Nannochloropsis* sp. F&M-M24 strain at N-starvation. For this strain, Bondioli *et al.* [35] found more than 75% of SAFAs and MUFAs in N-starved culture and 70% of TL consisted of neutral lipids compared to 25% for control. SAFAs and MUFAs are mainly associated with neutral storage lipids in the form of triglycerides (TAGs), highly desirable in algal biofuels production [2,15,16]. Suen *et al.* [19] found 79% TAGs in N-deficient *Nannochloropsis* sp. QII. The fatty acids C16:0 and C16:1 were suggested to be the main storage lipids in *Nannochloropsis* sp. [11,29]. In the present study C16: 0, mainly, and C18:1 increased as a response to N-stress. Both these FA made up a large part of the SAFAs-MUFAs fraction (>86%). Previous studies [19,21,35] suggested that under nutrient stress some microalgae are able to store neutral oil compounds from *de novo* synthesized lipids without compromising the fraction or function of other lipid classes. Hence, the increase in SAFAs and MUFAs under N-limitation in our study was possibly allocated to the neutral lipid fraction.

Microalgae are also known to be a source of significant amount of polyunsaturated fatty acids (PUFAs) and *N. oculata* contained 11%–24% PUFAs of total FA. C20:5 (EPA) made up 6%–19% of total FA and decreased at N-limitation. High PUFAs content is not desirable according to the European standard for biodiesel [49] but can be mixed with other oils, hydrogenated or separated through fractional distillation. The average EPA content in the present study was approximately 13% at N-replete conditions and 8% at N-limited conditions and a rough estimation of the EPA productivity would then be around 13 mg L^{-1} day^{-1} for both strategies. EPA is a high value nutritional supplement (omega-3) for human and animal health benefits. Since EPA production can take place at both nutrient sufficient and nutrient limited growth, and if separated in an algal biorefinery, EPA should be considered as a major commercial co-product in algal biofuels production.

Table 1. The major fatty acids (FAs) of the FA profiles (% of total FA) of *N. oculata* grown under nitrogen sufficiency (N:P 20) and nitrogen limitation (N:P 5 and N:P 2.5) in autumn 2008 and spring 2009. Profiles are shown for control and treatment at corresponding days: 0, 2, 5, 7, 8 in autumn 2008; 2, 4 during the first experiment in spring 2009; 4 during the second experiment in spring 2009.

Autumn 2008										
Days	**0**		**2**		**5**		**7**		**8**	
FA	N:P 20	N:P 5	N:P 20	N:P 5	N:P 20	N:P 5	N:P 20	N:P 5	N:P 20	N:P 5
C14:0	7.90	7.75	7.4	7.25	7.00	6.80	7.40	5.85	7.45	5.90
C16:0	39.80	39.40	36.75	43.30	31.00	39.75	40.50	43.30	39.80	43.95
C16:1	29.10	27.75	31.35	27.65	32.65	29.50	28.5	28.65	28.35	28.40
C18:1	5.35	7.20	5.20	7.15	4.50	8.30	5.20	8.45	3.80	8.80
C18:2	1.95	1.75	1.90	1.60	2.60	1.65	1.70	1.40	1.90	1.35
C20:4	4.30	3.60	4.75	2.95	6.60	3.65	4.35	3.10	5.00	2.90
C20:5	9.15	8.95	10.55	7.65	13.40	7.80	9.85	6.90	11.15	6.30

Spring 2009					**Spring 2009**	
Days	**2**		**4**		**4**	
FA	N:P 20	N:P 5	N:P 20	N:P 5	N:P 20	N:P 2.5
C14:0	7.10	5.90	7.0	5.40	6.70	5.30
C16:0	31.20	37.80	35.80	45.10	29.80	45.40
C16:1	26.50	27.40	27.20	27.90	30.40	27.00
C18:1	4.90	6.30	4.90	8.60	4.60	9.10
C18:2	3.50	2.40	2.90	1.30	3.50	1.40
C20:4	5.20	4.10	4.30	2.60	4.70	2.50
C20:5	18.70	14.00	15.60	7.00	17.50	7.40

Figure 3. Fractions of saturated fatty acids (SAFAs), monounsaturated fatty acids (MUFAs) and polyunsaturated fatty acids (PUFAs) for *N. oculata* during nitrogen sufficient growth (N:P 20) and nitrogen limited growth (N:P 5 and N:P 2.5) after 4–5 days of N-limitation. N:P 20 shows mean value ± SD (n = 3), N:P 5 shows mean value ± SD (n = 2) and N:P 2.5 shows one value.

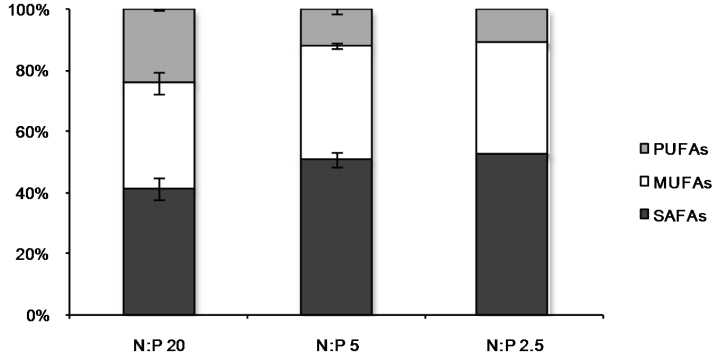

2.4. Biomass Productivity (BP) and Lipid Productivity (LP)

The BP and LP over time for *N. oculata* during the different experiments are shown in Figure 4. Average values of BP and LP are presented in Table 2. The BP ranged 0.24–0.43 g L^{-1} day^{-1} for N-limited cultures and 0.34–0.48g L^{-1} day^{-1} for control cultures, with higher values in spring compared to autumn. No significant differences were found between N-limited cultures and controls (ANOVA, $p = 0.7420$) but with a minor significant seasonal effect (ANOVA, $p = 0.0464$). The level of N-stress in spring had no significant effect (ANOVA, $p = 0.6145$).

Figure 4. Biomass productivity (BP) and lipid productivity (LP), respectively, for *N. oculata* at; (**a**, **b**) N:P 5 in autumn; (**c**, **d**) N:P 5 in spring; and (**e**, **f**) N:P 2.5 in spring. BP is represented by white bars for controls (BP N:P 20) and medium grey bars for N-limitation (BP N:P 5, N:P 2.5). White bars represent control (N:P 20) for both BP and LP, light grey bars represent N:P 5 values for both BP and LP, and dark grey bars represent N:P 2.5 for both BP and LP. Temperature (open diamonds, dashed line) and total global radiation, TGR, (closed triangles, solid line).

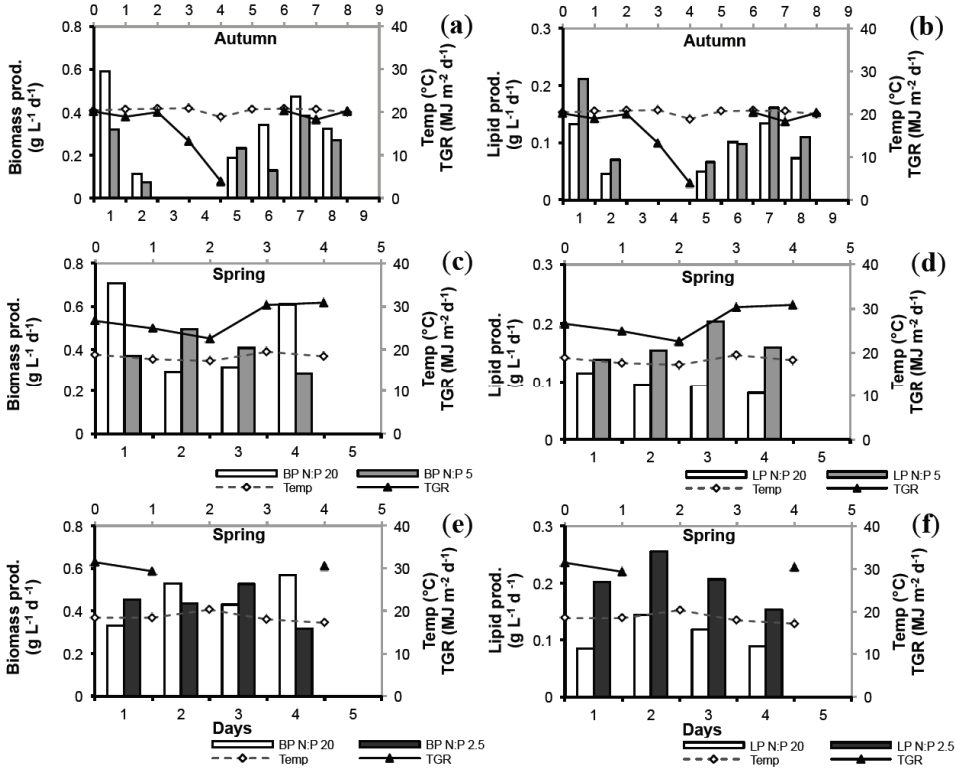

Table 2. Average biomass production (BP) and lipid production (LP) compared between N:P 20 (control) and treatments(N:P 5, N:P 2.5).

Nutrient Stress	Average BP (g L^{-1} day^{-1})		Average LP (g L^{-1} day^{-1})	
	Control	Treatment	Control	Treatment
N:P 5 autumn	0.34	0.24	0.09	0.12
N:P 5 spring	0.48	0.39	0.10	0.16
N:P 2.5 spring	0.47	0.43	0.11	0.21

For all three experiments the N-limited cultures produced significantly more lipids compared to control (ANOVA, N:P 5 autumn and spring: $p = 0.0264$; N:P 2.5 spring: $p = 0.0051$). At 15%–22% harvesting rate in autumn (Table 3) LP of the N:P 5 treatment (0.12 g L^{-1} day^{-1}) was only slightly higher compared to N:P 20 (0.09 g L^{-1} day^{-1}). In spring at 22% harvesting rate LP was 60% higher at N:P 5 (0.16 g L^{-1} day^{-1}) compared to control (0.10 g L^{-1} day^{-1}). More severe N-stress in spring (N:P 2.5) at 22%–33% harvesting rate resulted in 90% higher LP, 0.21 g L^{-1} day^{-1} compared to 0.11 g L^{-1} day^{-1} for the control. However, no significant seasonal effect was found (ANOVA, $p = 0.1898$).

Table 3. Nutrient ratios, concentrations and harvesting rate of the *N. oculata* cultures for treatments and control during autumn 2008 and spring 2009.

Parameter	N-sufficiency (control)	N-limitation	
N:P	20	5	2.5
Season	Autumn, Spring	Autumn, Spring	Spring
N	2000 µM	500 µM	250 µM
P	100 µM	100 µM	100 µM
Harvesting rate	15%–22%, 22%, 22%–33%	15%–22%, 22%	22%–33%

Clearly, nitrate limitation resulted in an increase of intracellular lipid content in *N. oculata* cultures. The present work also demonstrated a net gain in LP (up to 90%) for N-limited *N. oculata* cultures since relatively high biomass productivity (BP) was recorded for nutrient stressed cultures (N:P 2.5, during 5 days). Different ways to express productivity (volumetric and areal—illuminated surface or occupied ground) makes comparison among studies difficult, especially due to different PBR design. Two previous studies at up-scaled conditions expressing either volumetric or illuminated surface areal productivity [21,35] were compared to our result (Table 4). In these two studies, *Nannochloropsis* sp. F&M-M24 strain was grown in Green Wall Panel (GWP) PBRs (110 L and 590 L), applying N-starvation at 40% and 44% daily dilution rate, respectively. Normalizing productivity values to volumetric productivity, Table 4 shows that BP and LP in the present study, equated well to these previous studies using *Nannochloropsis* at up-scaled conditions [21,35].

Differences in lipid contents and productivities may be due to strain specificity but could also be an effect of cultivation approach (N-starvation or N-limitation) and dilution rate. In order to optimize lipid production in large-scale cultures of microalgae, further fine-tuning of growth conditions and nutrient stress level is required. Possibly the higher harvesting rate during N:P 2.5 growth (22%–30%) compared to N:P 5 growth (22%) also had an effect on the productivity

attributed to a more diluted culture with higher light capturing efficiency. On the other hand, if the harvesting rate is too great the culture will be too diluted to maintain a stable productivity. Empirical evidence suggested that maximum culture productivity is attained at dilution rates approximately half the maximum specific growth rate [50]. Applying a harvesting rate of at least 30% but probably not more than 40% would then yield in a net gain in LP of approximately 30%–100% compared to N-sufficiently grown cultures. For this particular strain a similar cultivation approach to that suggested by Rodolfi *et al.* [21], where cultures are grown in sufficient growth medium to high cell density before N-limitation is induced, can be proposed.

Table 4. A comparison among the present study, Rodolfi *et al.* [21] and Bondioli *et al.* [35] concerning the variables biomass productivity (BP) and lipid productivity (LP) expressed as volumetric productivity (g L^{-1} day^{-1}) at N-sufficiency, N-limitation and N-starvation (n.a. = not available). * The values from Bondioli *et al.* [35], originally given as g m^{-2} of illuminated reactor surface day^{-1}, were normalized to volumetric productivity.

Study	Dilution Rate	PBR Volume (L)	Variable	N-sufficiency (g L^{-1} day^{-1})	N-limitation (g L^{-1} day^{-1})	N-starvation (g L^{-1} day^{-1})
Present study	30%–33%	1374	BP	0.48	0.43	n.a.
			LP	0.11	0.21	n.a.
Rodolfi *et al.* [21]	40%	110	BP	0.36	0.22	0.30
			LP	0.12	0.11	0.20
Bondioli *et al.* [33]	44%	590	BP	n.a.	n.a.	0.33 *
			LP	n.a.	n.a.	0.22 *

Table 5 shows projections of biomass and lipid yields. Based on our results, LP of 0.21 g L^{-1} day^{-1}, considered as a best-case scenario, would at a full growth season (350 days) eventuate a total lipid yield of 13 t ha^{-1} $year^{-1}$. A more cautious calculation based on an annual average LP of 0.10–0.15 g L^{-1} day^{-1} would project an annual lipid yield of 8.0–10 t ha^{-1} $year^{-1}$ at N-limitation (Table 4). Maintaining LP of 0.21 g L^{-1} day^{-1} on annual basis will be difficult. Hence, the cautious scenario may be a more realistic baseline but with potential of attaining higher yield from optimization and extensive R&D.

Table 5. Biomass productivity (BP), lipid productivity (LP), biomass and lipid yield predictions for a flow-through flat panel PBR system cultivating *N. oculata* in the south of Portugal. Projections are based on experimental data (this study, Olofsson *et al.* [26]), a PBR volume of 1374 L, an occupied ground area of 75 m^2 per PBR and a growth season of 350 days.

Treatment	Cautious Scenario		Best-Case Scenario	
	Volumetric (g L^{-1} day^{-1})	Annual Yield (t ha^{-1} $year^{-1}$)	Volumetric (g L^{-1} day^{-1})	Annual Yield (t ha^{-1} $year^{-1}$)
		BP		
N-sufficiency	0.30–0.40	19–26	0.40–0.50	26–32
N-limitation	0.25–0.35	16–22	0.35–0.45	22–29
		LP		
N-sufficiency	0.05–0.10	3.0–6.0	0.10–0.12	6.0–8.0
N-limitation	0.12–0.15	8.0–10	0.15–0.20	10–13

2.5. Lab vs. Large Scale

Numerous lab-based studies reported BP and LP of different *Nannochloropsis* strains ranging 0.2–2.9 g L^{-1} day^{-1} [13,34,41,42,47,51] and 0.02–0.48 g L^{-1} day^{-1} [24,34,41,42,52–54], respectively. Our results are in the lower range regarding BP (0.24–0.47 g L^{-1} day^{-1}) and in the middle range concerning LP (0.08–0.21 g L^{-1} day^{-1}). Different culture conditions within these studies complicate comparison. Furthermore, few studies documented BP and LP from outdoor large-scale experiments. Zittelli *et al.* [12] investigated eicosapentaenoic acid (EPA) production of *Nannochloropsis* sp. in outdoor tubular reactors (610 L) in Florence, Italy. In September, BP ranged 0.57–0.73 g L^{-1} day^{-1} during two consecutive years was, while in May BP reached 0.76 g L^{-1} day^{-1}. Considering the FA content (13%–21%), LP ranging 0.07–0.16 g L^{-1} day^{-1} would be possible, with average EPA productivity (5 months) of 24 mg L^{-1} day^{-1} [12] to compare with 13 mg L^{-1} day^{-1} for our experiments. The present study would end up in the lower range concerning BP, both spring and autumn, but in the same range concerning LP but with less EPA productivity. As shown in Table 4, our results are in the same range for both BP and LP of other outdoor up-scaled studies with *Nannochloropsis*.

High LP was reported for other species at lab scale under different culture conditions, ranging 0.04–0.46 g L^{-1} day^{-1} [37,41,42,55–59]. More relevant and interesting for future studies would be long-term results on annual basis from outdoor large-scale operated plants monitoring BP and LP from applied nutrient manipulation. As a rare report, Moheimani and Borowitzka [60] found the haptophyte *Pleurochrysis carterae* to attain a decent annual average BP of 22 g m^{-2} day^{-1} in outdoor raceway ponds at nutrient replete conditions. At an outdoor algae production facility (total capacity 174,000 L) consisting of panel photobioreactors submerged in water basins, Quinn *et al.* [61] reported annual average biomass productivity for *N. oculata* from May 2008 to June 2009 and *N. salina* from April 2009 to January 2011 (0.15–0.16 g L^{-1} day^{-1}) with peak values of 0.37 g L^{-1} day^{-1}. Average lipid yield reached approximately 7–13 m^3 ha^{-1} $year^{-1}$ (approximately 6.5–10 t ha^{-1} $year^{-1}$) with peak values of 36 m^3 ha^{-1} $year^{-1}$ (33 t ha^{-1} $year^{-1}$).

Extrapolations of lab-based, indoor or small-scale data to outdoor mass-cultivation of microalgal oil yield up to 80–130 t ha^{-1} $year^{-1}$ [1,2,62] seem unrealistic. Weyer *et al.* [63] estimated the annual oil yield for a best-case scenario to be 37–49 t ha^{-1}. However, Rodolfi *et al.* [21], obtaining the same lipid productivity as in our experiment, estimated oil yield, at a best-case scenario, to be about 20 t ha^{-1} $year^{-1}$ for a production plant constructed of cheap plastic green wall panels (GWP) in Tuscany, Italy and up to 30 t ha^{-1} $year^{-1}$was suggested for tropical regions. Table 5 depicts both a cautious and a best-case scenario based on our results. The present work was conducted with flow-through flat panel PBRs in the south of Portugal, receiving slightly higher annual solar radiation than Tuscany. Higher BP compensated the lower lipid content in the *N. oculata* strain used in the present study. Our results demonstrated that different PBR design and formation of algae production units might result in different volume to areal footprint efficiency and thus different areal oil yield (Table 5), even though volumetric productivity is similar. Nevertheless, it also shows the potential for the Necton *N. oculata* strain, in the south of Portugal at a best-case scenario, to attain oil yields of 20 t ha^{-1} $year^{-1}$. Our scenarios (Table 5) show that seasonal variation

may result in lower estimates of the annual lipid productivity compared to the literature, and emphasize the importance of including seasonal variation in annual economic projections.

2.6. Seasonal Variation

Lipid content and composition have previously been shown to vary with season in this *N. oculata* strain [26]. In the present study, the initial lipid content was higher in autumn than in spring in accordance to Olofsson *et al.* [26]. A positive significant relationship was also found between TL (all experiments) and temperature explaining 19% of the variation (simple regression, $p = 0.0104$) as shown in Figure 5. Even though the differences in lipid content between treatment and control seemed not to be affected by the degree of N-limitation, applying N:P 2.5 stress in summer-autumn when lipid content in general is high, could possibly lead to a pronounced increase in TL and consequently also boost LP. On the other hand, TP values were similar comparing autumn and spring experiments.

Figure 5. (**a**) Total lipids (TL) as a function of temperature for all nutrient manipulation experiments; (**b**) biomass productivity; and (**c**) lipid productivity as a function of total global radiation (TGR) for all nutrient manipulation experiments. Regression lines disclose the relationship of the complete datasets for respective variable (simple regressions, TL: $p = 0.0104$, BP: $p = 0.0164$ and LP: $p = 0.0264$).

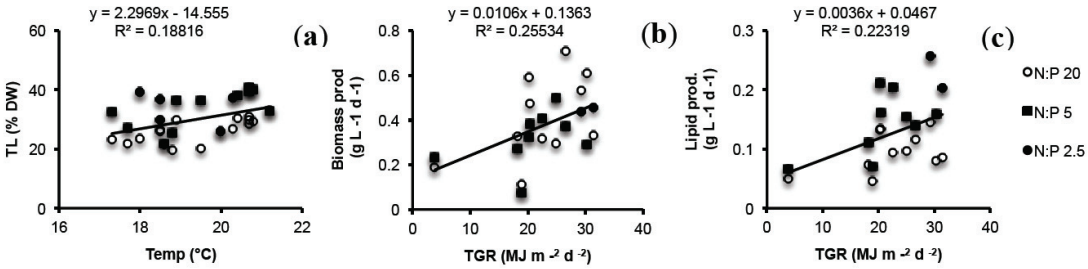

Although temperature explained 19% of the variation in TL, no significant effects of temperature on BP and LP was found (simple regressions, $p > 0.05$). Positive significant relationships were found between both BP and LP and TGR explaining 26% and 22% (simple regressions, $p = 0.0164$ and $p = 0.0264$) of the variation, respectively (Figure 5). Consequently, slightly higher BP was observed in spring compared to autumn in both treatments and controls. The higher BP in spring also resulted in enhanced LP in spite of lower TL content. Therefore, seasonal variations of light and temperature need to be considered, in combination with nutrient manipulation, when projecting oil yield of microalgae. Nonetheless, the results suggested a major role for N-stress as such.

Lipid composition of *N. oculata* changed with N-stress. Increasing the stress from N:P 5 to N:P 2.5 did not further change lipid quality. No major change in lipid composition for the N-limited cultures could be found when comparing autumn *vs.* spring experiments. However, for control

cultures especially C16:0 was higher and C20:5 was lower in autumn compared to spring, which was suggested to be an effect of changing light and temperature [26].

Our results may also have implications for molecular engineering. Starchless mutant strains of the freshwater green algae *Chlamydomonas* was found to accumulate up to 65% lipids under N-deficiency compared to 13% for wild type strains [64]. Typically, the vast majority of engineered efforts have been done on *Chlamydomonas*. However, the more widely available molecular techniques may in a near future facilitate metabolic engineering of other wild type algal strains that accumulate oil as a natural response to N-limitation. In addition, recent improvements of multispecies microbial cell factories represent an interesting approach [65]. Genetically engineered *Nannochloropsis*-bacteria mutualistic relationships providing carbon and nutrient recycling could possibly enhance lipid production and other high value products even more.

3. Experimental Section

3.1. Photobioreactors (PBRs) and Experimental Set Up

N. oculata (commercial strain, Necton) was inoculated and grown in batch mode outdoors in two adjacent closed flow-through vertical flat panel PBRs (1374 L) at Necton's facility in Algarve (Olhão, Portugal). The water used for cultivation was pumped from ground seawater (salinity 35‰), filtered first through a 5 μm cartridge filter followed by hypochlorite addition in a disinfection tank. Before a second cartridge filtration (1 μm) hypochlorite was neutralized with tiosulphate.). Nutrients were added as NutriBloom medium (Necton's commercial and industrial culture medium recipe) to reach nitrate levels of 2 mM and phosphate levels of 0.1 mM (final concentration in circulating cultures, N:P = 20). Original NutriBloom medium contains 2 M $NaNO_3$, 100 mM KH2PO_4, 20 mM $FeCl_3$, 20 mM EDTA-Na, 1 mM $ZnCl_2$, 1 mM $ZnSO_4$-H_2O, 1 mM $MnCl_2 \cdot 4H_2O$, 0.1 mM $Na_2MoO_4 \cdot 2H_2O$ 0.1 mM $CoCl_2 \cdot 6H_2O$, 0.1 mM $CuSO_4 \cdot 5H_2O$, 6.4 mM EDTA-Na, 2 mM $MgSO_4$-$7H_2O$. Nitrate concentrations were monitored daily (data not shown) and fresh NutriBloom medium was added to maintain nitrate concentration at 2 ± 0.2 mM and constant N:P = 20 to ensure sufficient nutrient availability. When the online pH set point reached 8.5, CO_2 was injected into the system at 2 bar pressure. The pH ranged 7.5–9.5 during the day but could drop to as low as 6.0 at night. When culture temperature in the PBRs reached 25 °C the reactor panels were cooled with water sprinklers. The temperature varied from 10 °C at night to 30 °C during the day despite cooling of the panels.

In autumn 2008 (24 September–2 October) and spring 2009 (11–15 May and 18–22 May) nitrogen levels were manipulated in large-scale cultures of *N. oculata* in the south of Portugal (Olhaõ). *N. oculata* was grown in semi-continuous mode under nutrient repletion (N:P 20) and nitrogen limitation (N:P 5, N:P 2.5) according to Table 3. PBRs were operated with a daily harvesting rate of 22%–33% and replacement of the culture volume with fresh medium at different N-levels (Table 3). Each N-level treatment was run concurrently with a control (N:P 20). The experiments were run for 9 days (autumn) and 5 days (spring) as the autumn experiment showed a rapid response (24 h) to N-stress. Daily sampling included nitrate concentrations in the N-limited

treatments (N:P 5, N:P 2.5), OD, DW and TL. Samples for TP and FA profiles were collected every second day.

3.2. Analyses Methods

Samples for nitrate analysis were collected before harvest and before replenishment of new medium. Nitrate concentrations were determined according to Eaton *et al.* [66], by centrifuging 8 mL of *N. oculata* culture (2000× *g*) and adding 1 mL of the supernatant to 8.8 mL of NaCl solution (35 g L^{-1}) followed by addition of 0.2 mL of 1 M HCl and measuring the absorbance at 220 nm and corrected for organic matter at 275 nm in the spectrophotometer. OD was measured in the spectrophotometer at 540 nm as a proxy for biomass. DW was determined by filtering 5–10 mL of algal culture onto pre-weighed 45 mm glass fiber filters, rinsed with 10 mL ammonium formiate (0.5 M) and dried in the oven at 70 °C until constant weight.

TL was determined according to Bligh & Dyer [67], modified as following: 30–50 mL of culture were centrifuged for 15 min (2000× *g*), the supernatant was removed and the algal pellet dissolved in chloroform:methanol (1:2 v/v) mixture followed by sonication for 5 min. Samples were put in the fridge over night followed by centrifugation for 5 min (2000× *g*) and collection of the supernatant. This extraction procedure was repeated 2–3 times for full extraction since *Nannochloropsis* cells have a rigid cell wall difficult to rupture. To the collected supernatant chloroform and distilled H_2O were added to a final ratio of 2:2:1 chloroform:methanol:H_2O v/v and centrifuged for 5 min (2000× *g*) to separate the lipid phase in chloroform from the water-methanol phase. The latter phase was discarded and the chloroform-lipid phase was transferred to pre-weighed glass tubes. Chloroform was evaporated in the oven at 55 °C until constant weight.

TP were determined according to the method of Lowry *et al.* [68] modified by Herbert *et al.* [69]. In brief, 10 mL of algal culture were centrifuged (2000× *g*), the supernatant discarded and the pellet resuspended in 2 mL 1 N NaOH and put in a water bath at 95–100 °C for 60 min. Samples were cooled down in room temperature and centrifuged (2000× *g*) for 10 min. 100 µL of the supernatant was transferred to a new glass tube and mixed with 300 µL dH_2O and 400 µL 1 N NaOH. 2 mL of freshly prepared Reagent A (50 mL 5% $NaCO_3$ + 2 mL (0.5% $CuSO_4 \cdot H_2O$ + 1% potassium sodium tartrate)) was added to the samples and agitated. After 10 min in room temperature 400 µL of freshly prepared Reagent B (1:1 Folin-Ciocalteau:dH_2O) was added to the samples and mixed. The samples were incubated for 30 min in room temperature. Absorbance was measured at 750 nm in the spectrophotometer and compared to a standard curve prepared from bovine serum albumin (20–300 µg mL^{-1}).

For FA 1 L of algal culture was centrifuged for 15 min at 7520× *g* (Beckman Avanti™ J-25, Beckman Coulter, Inc., Brea, CA, USA), and algal paste frozen at −20° C. Rests of seawater salt was removed from the paste according to Olofsson *et al.* [26]. Algal paste was stored frozen (−20 °C) prior to freeze-drying. FA profiles were determined using gas chromatography (GC) at Ifremer, Nantes, France [70]. An aliquot of lipid was evaporated under nitrogen and trans-methylated by contact with methanol-sulfuric acid (98:2, v/v) in excess at 50 °C overnight. After cooling, 2 mL of hexane and 1 mL of water were added and vortexed. The upper organic phase containing fatty acid methyl esters (FAMEs) was collected and assayed by gas chromatography using a PerkinElmer

Auto system equipped with an FID detector. Separation was done using helium as carrier gas on a fused-silica column (BPX-70, 60 m long, 0.25 mm i.d., 0.25 μm film thickness, SGE Analytical Science Pty Ltd., Ringwood, Australia) programmed from 55 °C (for 2 min) to 150 °C at 20 °C min^{-1} then to 230 °C at 1.5 °C min^{-1}. Sample was injected with a programmable split/splitless inlet and large-volume injection system (PSS) using the following temperature program: 55 °C (for 2 min) to 350 °C at 200 °C min^{-1}. FAMEs were identified by comparison of their equivalent chain length with those of authentic standards. Quantification was done using margaric acid (C17:0) as internal standard.

Biomass and lipid productivity were determined from the difference in DW or TL, both in g L^{-1}, between two sampling days taking into account the remaining biomass or lipid content after harvest. Biomass productivity:

$$BP = DW_{t2} - (\text{Remaining Biomass } (\%) \times DW_{t1}) \quad (1)$$

where BP is biomass productivity, DW_{t2} is the dry weight at a specific day, $DW_{t1}$is the dry weight at the previous day and Remaining Biomass is the percentage of biomass remaining after harvest (e.g., 80% at a harvesting rate of 20%).

Lipid productivity:

$$LP = TL_{t2} - (\text{Remaining Biomass } (\%) \times TL_{t1}) \quad (2)$$

where LP is lipid productivity, TL_{t2} is the total lipids (g L^{-1}) at a specific day, TL_{t1} is the total lipids at the previous day and Remaining Biomass is the percentage of biomass remaining after harvest (e.g., 80% at a harvesting rate of 20%). Biomass and lipid productivity are expressed in g L^{-1} day^{-1}.

Projections of biomass and lipid yields in Table 4 were based on the PBR volume (1374 L) and the occupied ground area, including ancillary equipment (75 m^2).

Temperature data was obtained from the meteorology portal Clima Tiempo Meteored [71] and light in the form of total global radiation (TGR) was obtained from the Meteorological Institute of Portugal (Instituto Português do Mar e da Atmosfera).

To test the effect of N-limitation and season on the response variables (DW, TL, TP, BP, LP), we started with a linear model including the time effect as a continuous covariate (ANCOVA). By backward stepwise procedure in R (version 3.0.2, R Foundation for Statistical Computing, Vienna, Austria) the simplest model with the highest explanatory power was applied to each variable. The same procedure was used to test the effects of three different levels of N-limitation (N:P 20, N:P 5, N:P 2.5) on the response variables in spring. Assumptions of normality and homogeneity of variances were checked by plotting residuals *versus* predicted values. Simple regressions between TL, BP and LP as the dependent variables and temperature and TGR as the independent variables were performed using GraphPad Prism 6 (GraphPad Software Inc., La Jolla, CA, USA).

4. Conclusions

The present study shows under commercially realistic conditions (outdoor, different seasons) that *N. oculata* is a suitable candidate in biofuel production since BP was maintained at a high level under N-limitation resulting in a total net gain in LP. Dilution rate optimization during nutrient

manipulation needs to account for seasonal variation of biomass and lipid productivity and adjusted accordingly. Despite the 50-year-old concept of algae based biofuel, no commercially viable production is yet in use. In terms of production capacity, to meet promising predictions based on lab work, the only solution would be scaling up, producing biomass and algae oil on annual basis, utilizing cheap nutrients and CO_2 from exhaust/waste streams. Sustainability challenges must be met by recycling of water and nutrients. Industrial waste products have to be seen as resources in order to produce a wide range of high value components from microalgae including sustainable fuel production. Closed PBRs may be used to produce fine chemicals (PUFAs, peptides, pigments, *etc.*) with high revenue potential to finance R&D efforts into algae based biofuels. As shown in the present study, EPA production may be feasible at both N-sufficiency and serve as a valuable co-product in biofuel production at N-limitation. The PBRs also produce large enough inoculum for open raceways where algal cultures convert cheap waste streams and exhaust gases to bulk chemicals for fuel and industrial material with the aid of N-stress to boost lipid production.

Acknowledgments

The authors acknowledge funding from Neste Oil (Finland), the French Research Institute for Exploration of the Sea (Ifremer), the Faculty of Health and Life Sciences, Linnæus University (Sweden), and the Strategic funding from the Swedish Research Council (Formas), "Ecosystem dynamics in the Baltic Sea in a changing climate perspective—ECOCHANGE". We wish to thank Alice Newton for providing workplace at the University of Algarve, Portugal, Bruno Fragoso for practical arrangements, the staff at Necton for help and assistance during the experiments and Alexis Avril at the Faculty of Health and Life Sciences, Linnæus University, for help with statistical analyses. This is a contribution to the LnU Centre for Ecology and Evolution using Microbial models Systems (EEMiS).

Author Contributions

Martin Olofsson designed, planned and performed research, analyzed data and wrote the paper. Teresa Lamela contributed to photobioreactors operation and performed research. Emmelie Nilsson planned and performed research. Jean-Pascal Bergé contributed to analytic tools and analyzed fatty acids data. Victória del Pino contributed to photobioreactors operation. Pauliina Uronen contributed to conception of research. Catherine Legrand conceived and designed research, analyzed data and wrote the paper.

Conflicts of Interest

The authors declare no conflict of interest.

References

1. Chisti, Y. Biodiesel from microalgae. *Biotechnol. Adv.* **2007**, *25*, 294–306.

2. Schenk, P.M.; Thomas-Hall, S.R.; Stephens, E.; Marx, U.C.; Mussgnug, J.H.; Posten, C.; Kruse, O.; Hankamer, B. Second generation biofuels: High-efficiency microalgae for biodiesel production. *BioEnergy Res.* **2008**, *1*, 20–43.
3. Meng, X.; Yang, J.; Xu, X.; Zhang, L.; Nie, Q.; Xian, M. Biodiesel production from oleaginous microorganisms. *Renewable Energy* **2009**, *34*, 1–5.
4. Dismukes, G.C.; Carrieri, D.; Bennette, N.; Ananyev, G.M.; Posewitz, M.C. Aquatic phototrophs: efficient alternatives to land-based crops for biofuels. *Curr. Opin. Biotechnol.* **2008**, *19*, 235–240.
5. Mata, T.M.; Martins, A.A.; Caetano, N.S. Microalgae for biodiesel production and other applications: A review. *Renew. Sust. Energ. Rev.* **2010**, *14*, 217–232.
6. Tredici, M. Photobiology of microalgae mass cultures: Understanding the tools for the next green revolution. *Biofuels* **2010**, *1*, 143–162.
7. Becker, W. 18 Microalgae in Human and Animal Nutrition. In *Handbook of Microalgal Culture: Biotechnology and Applied Phycology*; Richmond, A., Ed.; Blackwell Science Ltd.: Oxford, UK, 2004; pp. 312–352.
8. Renaud, S.M.; Parry, D.L.; Thinh, L.V.; Kuo, C.; Padovan, A.; Sammy, N. Effect of light-intensity on the proximate biochemical and fatty-acid composition of *Isochrysis* sp. and *Nannochloropsis oculata* for use in tropical aquaculture. *J. Appl. Phycol.* **1991**, *3*, 43–53.
9. Dhert, P.; Rombaut, G.; Suantika, G.; Sorgeloos, P. Advancement of rotifer culture and manipulation techniques in Europe. *Aquaculture* **2001**, *200*, 129–146.
10. Ferreira, M.; Coutinho, P.; Seixas, P.; Fabregas, J.; Otero, A. Enriching Rotifers with "Premium" Microalgae. *Nannochloropsis gaditana*. *Mar. Biotechnol.* **2009**, *11*, 585–595.
11. Sukenik, A.; Carmeli, Y.; Berner, T. Regulation of fatty-acid composition by irradiance level in the eustigmatophyte *Nannochloropsis* sp. *J. Phycol.* **1989**, *25*, 686–692.
12. Zittelli, G.C.; Lavista, F.; Bastianini, A.; Rodolfi, L.; Vincenzini, M.; Tredici, M.R. Production of eicosapentaenoic acid by *Nannochloropsis* sp. cultures in outdoor tubular photobioreactors. *J. Biotechnol.* **1999**, *70*, 299–312.
13. Zou, N.; Richmond, A. Effect of light-path length in outdoor flat plate reactors on output rate of cell mass and of EPA in *Nannochloropsis* sp. *J. Biotechnol.* **1999**, *70*, 351–356.
14. Pulz, O.; Gross, W. Valuable products from biotechnology of microalgae. *Appl. Microbiol. Biotechnol.* **2004**, *65*, 635–648.
15. Hu, Q.; Sommerfeld, M.; Jarvis, E.; Ghirardi, M.; Posewitz, M.; Seibert, M.; Darzins, A. Microalgal triacylglycerols as feedstocks for biofuel production: Perspectives and advances. *Plant J. Cell Mol. Biol.* **2008**, *54*, 621–639.
16. Yu, E.T.; Zendejas, F.J.; Lane, P.D.; Gaucher, S.; Simmons, B.A.; Lane, T.W. Triacylglycerol accumulation and profiling in the model diatoms *Thalassiosira pseudonana* and *Phaeodactylum tricornutum* (Bacilariophyceae) during starvation. *J. App. Phycol.* **2009**, *21*, 669–681.
17. Aatola, H.; Larmi, M.; Sarjovaara, T. Hydrotreated vegetable oil (HVO) as a renewable diesel fuel: trade-off between NO_x, particulate emission, and fuel consumption of a heavy duty engine. *SAE Int. J. Engines* **2009**, *1*, 1251–1262.

18. Shifrin, N.S.; Chisholm, S.W. Phytoplankton lipids—Interspecific differences and effects of nitrate, silicate and light-dark cycles. *J. Phycol.* **1981**, *17*, 374–384.
19. Suen, Y.; Hubbard, J.S.; Holzer, G.; Tornabene, T.G. Total lipid production of the green-alga *Nannochloropsis* sp. QII under different nitrogen regimes. *J. Phycol.* **1987**, *23*, 289–296.
20. Takagi, M.; Watanabe, K.; Yamaberi, K.; Yoshida, T. Limited feeding of potassium nitrate for intracellular lipid and triglyceride accumulation of *Nannochloris* sp. UTEX LB1999. *Appl. Microbiol. Biotechnol.* **2000**, *54*, 112–117.
21. Rodolfi, L.; Chini Zittelli, G.; Bassi, N.; Padovani, G.; Biondi, N.; Bonini, G.; Tredici, M.R. Microalgae for oil: strain selection, induction of lipid synthesis and outdoor mass cultivation in a low-cost photobioreactor. *Biotechnol. Bioeng.* **2009**, *102*, 100–112.
22. Gouveia, L.; Oliveira, A.C. Microalgae as a raw material for biofuels production. *J. Ind. Microbiol. Biotechnol.* **2009**, *36*, 269–274.
23. Roncarati, A.; Meluzzi, A.; Acciarri, S.; Tallarico, N.; Melotti, P. Fatty acid composition of different microalgae strains (*Nannochloropsis* sp., *Nannochloropsis oculata* (Droop) Hibberd, *Nannochloris atomus* Butcher and *Isochrysis* sp.) according to the culture phase and the carbon dioxide concentration. *J. World Aquacult. Soc.* **2004**, *3*, 401–411.
24. Chiu, S.Y.; Kao, C.Y.; Tsai, M.T.; Ong, S.C.; Chen, C.H.; Lin, C.S. Lipid accumulation and CO_2 utilization of *Nannochloropsis oculata* in response to CO2 aeration. *Bioresour. Technol.* **2009**, *100*, 833–838.
25. Hu, C.; Li, M.; Li, J.; Zhu, Q.; Liu, Z. Variation of lipid and fatty acid compositions of the marine microalga *Pavlova viridis* (Prymnesiophyceae) under laboratory and outdoor culture conditions. *World J. Microbiol. Biotechnol.* **2007**, *24*, 1209–1214.
26. Olofsson, M.; Lamela, T.; Nilsson, E.; Berge, J.P.; del Pino, V.; Uronen, P.; Legrand, C. Seasonal variation of lipids and fatty acids of the microalgae *Nannochloropsis oculata* grown in outdoor large-scale photobioreactors. *Energies* **2012**, *5*, 1577–1592.
27. Lynch, D.V.; Thompson, G.A. Low Temperature-induced alterations in the chloroplast and microsomal-membranes of *Dunaliella salina*. *Plant Physiol.* **1982**, *69*, 1369–1375.
28. Thompson, P.A.; Guo, M.X.; Harrison, P.J.; Whyte, J.N.C. Effects of variation in temperature. II. on the fatty-acid composition of 8 species of marine-phytoplankton. *J. Phycol.* **1992**, *28*, 488–497.
29. Sukenik, A.; Yamaguchi, Y.; Livne, A. Alterations in lipid molecular-species of the marine eustigmatophyte *Nannochloropsis* sp. *J. Phycol.* **1993**, *29*, 620–626.
30. Renaud, S.M.; Thinh, L.V.; Lambrinidis, G.; Parry, D.L. Effect of temperature on growth, chemical composition and fatty acid composition of tropical Australian microalgae grown in batch cultures. *Aquaculture* **2002**, *211*, 195–214.
31. Takagi, M.; Karseno; Yoshida, T. Effect of salt concentration on intracellular accumulation of lipids and triacylglyceride in marine microalgae *Dunaliella* cells. *J. Biosci. Bioeng.* **2006**, *101*, 223–226.
32. Bartley, M.L.; Boeing, W.J.; Corcoran, A.A.; Holguin, F.O.; Schaub, T. Effects of salinity on growth and lipid accumulation of biofuel microalga *Nannochloropsis salina* and invading organisms. *Biomass Bioenerg.* **2013**, *54*, 83–88.

33. Xu, Z.B.; Yan, X.J.; Pei, L.Q.; Luo, Q.J.; Xu, J.L. Changes in fatty acids and sterols during batch growth of *Pavlova viridis* in photobioreactor. *J. Appl. Phycol.* **2008**, *20*, 237–243.
34. Huerlimann, R.; de Nys, R.; Heimann, K. Growth, lipid content, productivity, and fatty acid composition of tropical microalgae for scale-up production. *Biotechnol. Bioeng.* **2010**, *107*, 245–257.
35. Bondioli, P.; Della Bella, L.; Rivolta, G.; Chini Zittelli, G.; Bassi, N.; Rodolfi, L.; Casini, D.; Prussi, M.; Chiaramonti, D.; Tredici, M.R. Oil production by the marine microalgae *Nannochloropsis* sp. F&M-M24 and *Tetraselmis suecica* F&M-M33. *Bioresour. Technol.* **2012**, *114*, 567–572.
36. Li, M.; Gong, R.M.; Rao, X.J.; Liu, Z.L.; Wang, X.M. Effects of nitrate concentration on growth and fatty acid composition of the marine microalga *Pavlova viridis* (Prymnesiophyceae). *Ann. Microbiol.* **2005**, *55*, 51–55.
37. Weldy, C.S.; Huesemann, M. Lipid production by *Dunaliella salina* in batch culture: Effects of nitrogen limitation and light intensity. *US Dep. Energy J. Undergrad. Res.* **2007**, *7*, 115–122.
38. Gordillo, F.J.L.; Goutx, M.; Figueroa, F.L.; Niell, F.X. Effects of light intensity, CO_2 and nitrogen supply on lipid class composition of *Dunaliella viridis*. *J. Appl. Phycol.* **1998**, *10*, 135–144.
39. Simionato, D.; Block, M.A.; La Rocca, N.; Jouhet, J.; Marechal, E.; Finazzi, G.; Morosinotto, T. The response of *Nannochloropsis gaditana* to nitrogen starvation includes de novo biosynthesis of triacylglycerols, a decrease of chloroplast galactolipids, and reorganization of the photosynthetic apparatus. *Eukaryot. Cell* **2013**, *12*, 665–676.
40. El-Baky, H.H.A.; El-Baz, F.K.; El-Baroty, G.S. Production of lipids rich in omega 3 fatty acids from the halotolerant alga *Dunaliella salina*. *Biotechnology* **2004**, *3*, 102–108.
41. Su, C.-H.; Chien, L.-J.; Gomes, J.; Lin, Y.-S.; Yu, Y.-K.; Liou, J.-S.; Syu, R.-J. Factors affecting lipid accumulation by *Nannochloropsis oculata* in a two-stage cultivation process. *J. Appl. Phycol.* **2010**, *23*, 903–908.
42. Pal, D.; Khozin-Goldberg, I.; Cohen, Z.; Boussiba, S. The effect of light, salinity, and nitrogen availability on lipid production by *Nannochloropsis* sp. *Appl. Microbiol. Biotechnol.* **2011**, *90*, 1429–1441.
43. Fabregas, J.; Abalde, J.; Cabezas, B.; Herrero, C. Changes in protein, carbohydrates and gross energy in the marine microalga *Dunaliella tertiolecta* (Butcher) by nitrogen concentrations as nitrate, nitrite and urea. *Aquacult. Eng.* **1989**, *8*, 223–239.
44. Harrison, P.; Thompson, P.; Calderwood, G. Effects of nutrient and light limitation on the biochemical composition of phytoplankton. *J. Appl. Phycol.* **1990**, *2*, 45–56.
45. Kilham, S.S.; Kreeger, D.A.; Goulden, C.E.; Lynn, S.G. Effects of nutrient limitation on biochemical constituents of *Ankistrodesmus falcatus*. *Freshwater Biol.* **1997**, *38*, 591–596.
46. Dunstan, G.A.; Volkman, J.K.; Barrett, S.M.; Garland, C.D. Changes in the lipid-composition and maximization of the polyunsaturated fatty-acid content of 3 microalgae grown in mass-culture. *J. Appl. Phycol.* **1993**, *5*, 71–83.

47. Hu, H.H.; Gao, K.S. Optimization of growth and fatty acid composition of a unicellular marine picoplankton, *Nannochloropsis* sp., with enriched carbon sources. *Biotechnol. Lett.* **2003**, *25*, 421–425.
48. Fabregas, J.; Maseda, A.; Dominguez, A.; Otero, A. The cell composition of *Nannochloropsis* sp. changes under different irradiances in semicontinuous culture. *World J. Microbiol. Biotechnol.* **2004**, *20*, 31–35.
49. European Standard. *Automotive Fuels—Fatty Acid Methyl Esters (FAME) for Diesel Engines—Requirements and Test Methods*; EN 14214; Standardiserings-Kommissionen I Sverige Publications: Paramus, NJ, USA, 2008.
50. Richmond, A. Biological Principles of Mass Cultivation. In *Handbook of Microalgal Culture: Biotechnology and Applied Phycology*; Blackwell Publishing Ltd.: Oxford, UK, 2004; pp. 125–177.
51. Fisher, T.; Minnaard, J.; Dubinsky, Z. Photoacclimation in the marine alga *Nannochloropsis* sp. (Eustigmatophyte): A kinetic study. *J. Plankton Res.* **1996**, *18*, 1797–1818.
52. Zou, N.; Zhang, C.W.; Cohen, Z.; Richmond, A. Production of cell mass and eicosapentaenoic acid (EPA) in ultrahigh cell density cultures of *Nannochloropsis* sp. (Eustigmatophyceae). *Eur. J. Phycol.* **2000**, *35*, 127–133.
53. Griffiths, M.J.; Hille, R.P.; Harrison, S.T.L. Lipid productivity, settling potential and fatty acid profile of 11 microalgal species grown under nitrogen replete and limited conditions. *J. Appl. Phycol.* **2011**, *24*, 989–1001.
54. Sheehan, J.; Dunahay, T.; Benemann, J.; Roessler, P. *A Look Back at the US Department of Energy's Aquatic Species Program: Biodiesel from Algae*; Close-Out Report NREL/TP-580-24190; National Renewable Energy Laboratory: Golden, CO, USA, 1998.
55. Li, Y.; Horsman, M.; Wang, B.; Wu, N.; Lan, C.Q. Effects of nitrogen sources on cell growth and lipid accumulation of green alga *Neochloris oleoabundans*. *Appl. Microbiol. Biotechnol.* **2008**, *81*, 629–636.
56. Yamaberi, K.; Takagi, M.; Yoshida, T. Nitrogen depletion for intracellular triglyceride accumulation to enhance liquefaction yield of marine microalgal cells into a fuel oil. *J. Mar. Biotechnol.* **1998**, *6*, 44–48.
57. Illman, A.M.; Scragg, A.H.; Shales, S.W. Increase in *Chlorella* strains calorific values when grown in low nitrogen medium. *Enzyme Microb. Technol.* **2000**, *27*, 631–635.
58. Matsukawa, R.; Hotta, M.; Masuda, Y.; Chihara, M.; Karube, I. Antioxidants from carbon dioxide fixing *Chlorella sorokiniana*. *J. Appl. Phycol.* **2000**, *12*, 263–267.
59. Feng, Y.J.; Li, C.; Zhang, D.W. Lipid production of *Chlorella vulgaris* cultured in artificial wastewater medium. *Bioresource Technol.* **2011**, *102*, 101–105.
60. Moheimani, N.R.; Borowitzka, M.A. The long-term culture of the coccolithophore *Pleurochrysis carterae* (Haptophyta) in outdoor raceway ponds. *J. Appl. Phycol.* **2006**, *18*, 703–712.
61. Quinn, J.C.; Yates, T.; Douglas, N.; Weyer, K.; Butler, J.; Bradley, T.H.; Lammers, P.J. *Nannochloropsis* production metrics in a scalable outdoor photobioreactor for commercial applications. *Bioresource Technol.* **2012**, *117*, 164–171.

62. Moazami, N.; Ashori, A.; Ranjbar, R.; Tangestani, M.; Eghtesadi, R.; Nejad, A.S. Large-scale biodiesel production using microalgae biomass of *Nannochloropsis*. *Biomass Bioenerg.* **2012**, *39*, 449–453.
63. Weyer, K.M.; Bush, D.R.; Darzins, A.; Willson, B.D. Theoretical maximum algal oil production. *BioEnergy Res.* **2010**, *3*, 204–213.
64. James, G.O.; Hocart, C.H.; Hillier, W.; Chen, H.C.; Kordbacheh, F.; Price, G.D.; Djordjevic, M.A. Fatty acid profiling of *Chlamydomonas reinhardtii* under nitrogen deprivation. *Bioresource Technol.* **2011**, *102*, 3343–3351.
65. Ortiz-Marquez, J.C.F.; Do Nascimento, M.; Zehr, J.P.; Curatti, L. Genetic engineering of multispecies microbial cell factories as an alternative for bioenergy production. *Trends Biotechnol.* **2013**, *31*, 521–529.
66. Eaton, A.; Clesceri, L.; Rice, R.; Greenberg, A.; Franson, M. *Standard Methods for the Examination of Water and Wastewate*; American Public Health Association (APHA), American Water Works Association (AWWA) and Water Environment Federation (WEF): Washington, DC, USA, 2005.
67. Bligh, E.G.; Dyer, W.J. A rapid method of total lipid extraction and purification. *Can. J. Biochem. Phys.* **1959**, *37*, 911–917.
68. Lowry, O.H.; Rosebrough, N.J.; Farr, A.L.; Randall, R.J. Protein measurement with the folin phenol reagent. *J. Biol. Chem.***1951**, *193*, 265–275.
69. Herbert, B.N.; Gould, H.J.; Chain, E.B. Crystal protein of *Bacillus thuringiensis* var. *tolworthi*—subunit sttructure and toxicity to *Pieris brassicae*. *Eur. J. Biochem.* **1971**, *24*, 366–375.
70. Dumay, J.; Barthomeuf, C.; Bergé, J. How enzymes may be helpful for upgrading fish by-products: Enhancement of fat extraction. *J. Aquat. Food Prod. Technol.* **2004**, *13*, 69–84.
71. Clima Tiempo Meteored. Meteorology portal by Alpred SL. Available online: http://clima.meteored.com/clima-en-faro+aeropuerto-085540.html (accessed on 22 February 2011).

Two New Cytotoxic Indole Alkaloids from a Deep-Sea Sediment Derived Metagenomic Clone

Xia Yan, Xi-Xiang Tang, Lin Chen, Zhi-Wei Yi, Mei-Juan Fang, Zhen Wu and Ying-Kun Qiu

Abstract: Two new indole alkaloids, metagenetriindole A (**1**) and metagenebiindole A (**2**), were identified from deep-sea sediment metagenomic clone derived *Escherichia coli* fermentation broth. The structures of new compounds were elucidated by spectroscopic methods. The two new indole alkaloids demonstrated moderately cytotoxic activity against CNE2, Bel7402 and HT1080 cancer cell lines *in vitro*.

Reprinted from *Mar. Drugs*. Cite as: Yan, X.; Tang, X.-X.; Chen, L.; Yi, Z.-W.; Fang, M.-J.; Wu, Z.; Qiu, Y.-K. Two New Cytotoxic Indole Alkaloids from a Deep-Sea Sediment Derived Metagenomic Clone. *Mar. Drugs* **2014**, *12*, 2156–2163.

1. Introduction

Deep marine subsurface sediments are one of the most extensive microbial habitats on Earth. The deep sea is usually characterized by extremely high salinity, darkness, high pressure, and high/low temperature [1]. Due to the particularity of the marine environment, marine microorganisms have unique metabolic properties, producing many novel chemical structures with great complexity and diversity. This untapped potential has resulted in the recent acceleration in interest in the study of marine microorganisms. However, the dilemma is that the vast majority of the microorganisms cannot be cultivated at present [2].

Metagenomics, which utilizes culture-independent methods to access the collective genomes of natural bacterial populations, provides a means of exploring the secondary metabolites produced by the large collections of bacteria that are known to be present in the environment but remain recalcitrant to culturing. The foundation of all metagenomic approaches is the isolation and subsequent examination of DNA extracted directly from naturally occurring microbial populations (environmental DNA, eDNA). The eDNA libraries can be examined in simple high-throughput assays designed to identify clones that associated with the production of bioactive small molecules [3,4].

We previously reported isolation of a new compound, which showed potent analgesic activity on fatty-acid amide hydrolase (FAAH) and monoacylglycerol lipase (MGL), from a deep-sea sediment metagenomic clone [5]. In the continuing studies on deap-sea sediment eDNA libraries, we screen the metagenomic library and found a clone coded QD15 exhibited cytotoxic activity. This paper deals with the isolation, structural elucidation, as well as cytotoxic activities of two new indole alkaloids from the QD15 metagenomic clone derived *E. coli* fermentation broth.

2. Results and Discussion

Metagenetriindole A (**1**) was isolated as pink powder and its molecular formula was established as $C_{26}H_{19}N_3O$ from a sodiated ion at *m/z* 412 in the ESIMS and further supported by the HRESIMS at 412.1420 (calcd. For $C_{26}H_{19}N_3ONa$, 412.1420) and implying 19 degrees of unsaturation. The presence of amide groups in **1** was evidenced by IR absorption bands at 3270, 1630 cm^{-1}. The ^{13}C spectrum of **1** showed 26 carbon signals (Table 1), which were assigned by the assistance of DEPT spectrum to 15 sp^2 methines, one sp^3 methine and 10 sp^2 quaternary carbons. The ^1H NMR spectrum displayed an olefinic proton at δ_H 8.74 (1H, d, *J* = 3.2 Hz), a set of four-spin proton system signals at δ_H 7.43 (1H, br. d, *J* = 7.3 Hz), 8.19 (1H, br. d, *J* = 7.3 Hz), 7.13 (1H, td, *J* = 7.1, 1.2 Hz) and 7.17 (1H, td, *J* = 7.1, 1.2 Hz), as well as a down field labile proton singlet at δ_H 11.95 (1H, br. d, *J* = 2.5 Hz), suggested that **1** might have a 3-substituted indole moiety. Another set of proton signals belonging to two symmetrical *mono*-substituted indole moieties could also be found in ^1H NMR spectrum at δ_H 7.24 (2H, d, *J* = 2.2 Hz), 7.65 (2 H, br. d, *J* = 8.1 Hz), 7.31 (2H, br. d, *J* = 8.1 Hz), 6.90 (2H, td, *J* = 8.1, 1.0 Hz), 7.02 (2H, td, *J* = 7.1, 1.0 Hz) and 10.86 (2H, br. d, *J* = 1.7 Hz). The ^{13}C NMR spectrum also revealed the presence of the three indole rings, at δ_C 133.8 (C), 126.0 (C), 115.6 (CH), 112.0 (CH), 121.6 (CH), 122.7 (CH), 121.5 (CH), 136.6 (C) and δ_C 124.0 (2CH), 114.3 (2C), 126.7 (2C), 119.3 (2CH), 118.2 (2CH), 120.8 (2CH), 111.3 (2CH), 136.1 (2C). Other signals in the ^1H and ^{13}C NMR spectra indicated the presence of a methane in high field at δ_H 6.41 (1 H, s) and δ_C 42.7 (CH), as well as a carbonyl in low field at δ_C 193.9 (C). The attachment of carbonyl to a double bond sp^2 carbon and an sp^3 carbon, could be deduced from the chemical shift at δ_C 193.9 (C). Hence, the 3-C of an indole ring, together with the unique sp^3 methine, was linking to the carbonyl.

From the ^1H-^1H COSY spectrum of **1**, the separate spin systems of H-1′/H-2′, H-1″, 1‴/H-2″, 2‴, H-4′/H-5′/H-6′/H-7′, and H-4″, 4‴/H-5″, 5‴/H-6″, 6‴/H-7″, 7‴ were differentiated. These data, together with the HMBC correlations among H-2′/C-3a′, C-7a′ and H-2″, 2‴/C-3a″, 3a‴, C-7a″, 7a‴, confirmed the structure fragments of the three indole rings. However, the molecular framework was finally established by the HMBC correlations between H-2 (δ_H 6.41) and C-1, C-3′, C-3″, 3‴, C-4″, 4″, as shown in Figure 1. Up till now, the structure of **1** was elucidated as 1,2,2-tri-1*H*-indol-3-ylethanone, named metagenetriindole A. Similar tri-indole type compounds have also been reported previously, especially from metagenomic clones. Gillespie *et al.* isolated turbomycin A from clones P57G4, *E. coli* with DNA extracted directly from soil, in which the three indole rings are connected to a methyl instead of ethanone [6]. To the best of our knowledge, this is the first report of the isolation of a tri-indole type new compound from metagenomic library derived from deep-sea sediment [7].

Metagenediindole A (**2**) was isolated as a yellow powder and ESI-MS gave its quasi-molecular ion peak at *m/z* 263 $[M + H]^+$, 285 $[M + Na]^+$. The molecular formula was established as $C_{17}H_{14}N_2O$ by the HRESIMS at 285.0995 (calcd. For $C_{17}H_{14}N_2ONa$, 285.0998). The ^1H and ^{13}C NMR spectra indicated that **2** was also an indole type compound. In the ^1H NMR spectrum, an entire set of 3′-substituted indole proton signals, including a set of four-spin proton system signals at δ_H [7.10 (1H, br.d, *J* = 8.1 Hz), 6.80 (1H, td, *J* = 8.1, 1.0 Hz), 7.01 (1H, td, *J* = 7.1, 1.0 Hz), 7.32

(1H, br.d, J = 8.1 Hz)], a down field labile proton singlet at δ_H 11.03 (1H, br. s), as well as an olefinic proton at δ_H 7.37 (1H, d, J = 2.4 Hz), could be observed. Another *ortho*-substituted benzene ring proton signal at δ_H 7.44 (1H, br.d, J = 7.3 Hz), 6.73 (1H, td, J = 7.1, 0.5 Hz), 7.50 (1H, td, J = 8.3, 1.3 Hz) and 6.90 (1H, br.d, J = 8.3 Hz), could also be found, showing the existence of another indole ring. However, the olefinic proton signal at H-2 position of the indole ring was absent, and the amine labile proton singlet was high-field shifted to δ_H 7.73 (1H, br. s), suggesting that the C-2, 3 double bond in this indole ring was substituted by other functional groups. The carbon signals of the complete 3′-substituted indole ring and the *ortho*-substituted benzene ring, could be observed in the ^{13}C spectrum of **2**. A carbonyl signal at δ_C 203.3 (C) and an sp^3 quaternary carbon signal at δ_C 65.0 (C), were attributed to the C-3 and C-2 carbon of the other indole ring. Otherwise, a methyl signal at δ_H 1.62 (3H, s) and δ_C 65.0 (C) was furnished in the ^{1}H and ^{13}C spectrum, respectively.

Table 1. ^{1}H (400 MHz, DMSO-d_6) and ^{13}C (100 MHz, DMSO-d_6) NMR data, ^{1}H-^{1}H COSY and HMBC correlations for **1**.

Position	δ_H (J in Hz)	δ_C, Multiple		^{1}H-^{1}H COSY	HMBC
1		193.9	C		
2	6.41 s	42.7	CH		C-1, 3′, 3″, 3‴, 4″, 4‴
1′	11.95 br.d (2.5)			H-2′	n.o. [a]
2′	8.74 d (3.2)	133.8	CH	H-1′	C-3′, 3a′, 7a′
3′		126	C		
3a′		115.6	C		
4′	7.43 br.d (7.3)	112	CH	H-5′	C-3′, 6′, 7a′
5′	7.13 td (7.1, 1.2)	121.6	CH	H-4′, H-6′	C-3a′, 7′
6′	7.17 td (7.1, 1.2)	122.7	CH	H-5′, H-7′	C4′, 7a′
7′	8.19 br.d (7.3)	121.5	CH	H-6′	C-3a′, 6′, 7a′
7a′		136.6	C		
1″, 1‴	10.86 br.d (1.7)			H-2″, 2‴	
2″, 2‴	7.24 br.d (2.2)	124	CH	H-1″, 1‴	C-3″, 3a″, 7a″, C-3‴, 3a‴, 7a‴
3″, 3‴		114.3	C		
3a″, 3a‴		126.7	C		
4″, 4‴	7.65 br.d (8.1)	119.3	CH	H-5″, 5‴	C-3″, 6″, 7a″, C-3‴, 6‴, 7a‴
5″, 5‴	6.90 td (8.1, 1.0)	118.2	CH	H-4″, 4‴, H-6″, 6‴	C-3a″, 7″, C-3a‴, 7‴
6″, 6‴	7.02 td (7.1, 1.0)	120.8	CH	H-5″, 5‴, H-7″, 7‴	C4″, 7a″, C4‴, 7a‴
7″, 7‴	7.31 br.d (8.1)	111.3	CH	H-6″, 6‴	C-3a″, 6″, 7a″, C-3a‴, 6‴, 7a‴
7a″, 7a‴		136.1	C		

[a] n.o. is not observed.

From the ^{1}H-^{1}H COSY spectrum of **2**, the separate spin systems of H-1′/H-2′, H-4′/H-5′/H-6′/H-7′, and H-4/H-5/H-6/H-7 were differentiated, which confirmed the structure fragments of the two indole rings. The molecular framework was finally established by the HMBC correlations between methyl proton signal (δ_H 1.62) and C-2, C-3, C-3′, as shown in Figure 2. Up till now, the structure of **2** was elucidated as 2-methyl-1,2-dihydro-1′*H*,3*H*-2,3′-biindol-3-one, named metagenediindole A, as a new di-indole type compound from deep-sea sediment metagenomic library. Although the

chiral center at C-2 suggested the optical activity of the compound, measured optical rotation value was nearly zero, indicating that compound **2** was isolated as a pair of externally compensated compounds. Similar compound has also been found from metagenome. Abe *et al.* constructed a metagenomic library from the marine sponge *Halichondria okadai* and screened for colored clones then separated a novel compound halichrome A (1), which was different from metagenediindole A (**2**) with C-2 substituted by ethyl [8].

Figure 1. Structure and key ^{1}H-^{1}H COSY, HMBC correlations of metagenetriindole A (**1**).

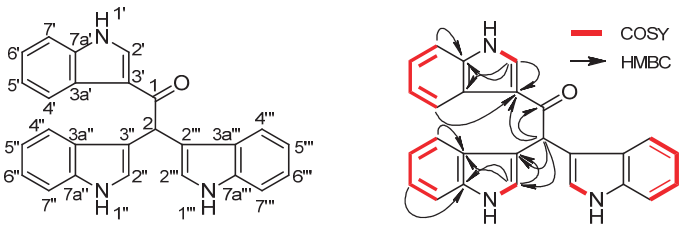

Figure 2. Structure and key ^{1}H-^{1}H COSY, HMBC correlations of metagenediindole A (**2**).

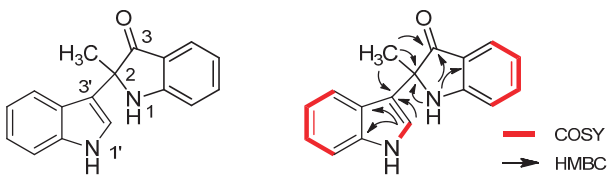

The cytotoxic activities of these compounds were preliminarily evaluated using CNE2, Bel7402 and HT1080 cell lines by the CCK 8 method [9]. The results revealed that the two new indole alkaloids, exhibited moderately cytotoxic activities against CNE2, Bel7402 and HT1080 cell lines with IC_{50} values 47.70, 50.55, 44.58 μg/mL (**1**) and 34.25, 43.62, 35.80 μg/mL (**2**) respectively.

3. Experimental Section

3.1. General Experimental Procedures

UV spectra were recorded on a Shimadzu UV-260 spectrometer (Shimadzu, Tokyo, Japan). IR spectra were determined on a Perkin-Elmer 683 (Perkin-Elmer, Norwalk, CT, USA) infrared spectrometer in KBr pellets. NMR spectra were taken with TMS as internal standard on a Bruker Avance 400 FT-NMR spectrometer (Bruker, Bremen, Germany). ESI-MS were measured on an AB MD-SCIEX Advantage spectrometer (Applied Biosystems, Foster, CA, USA) and HR-ESI-MS on a Bruker FT-MS Apex III spectrometer (Bruker, Bremen, Germany). Column chromatography was performed on silica gel (Yantai Chemical Industry Research Institute, Yantai, China) and Cosmosil 75 C_{18}-OPN (75 μm, Nakalai Tesque Co. Ltd., Kyoto, Japan). TLC was conducted on Silica GF254 (Yantai Chemical Industry Research Institute, Yantai, China) and RP-18 F254 (Merck, Scandici, Germany) plates. Detection was done by spraying 10% H_2SO_4/ethanol, followed

by heating. HPLC was performed with a Varian preparative apparatus using an ODS column (Shimadzu C_{18}, 20 × 250 mm, Kyoto, Japan).

3.2. Fermentation

Sediment samples for DNA extraction were collected from the subsurface sediments at water depths of 3006 m (102.612575°E, 2.022449°N) in Southwestern Indian Ocean by the Third Institute of Oceanography of China. The samples were maintained at 4 °C before being processed. Sediment samples were precultured in 2216E medium for three days, then, the DNA of enrichment product were extracted and purified, and the size-separated DNAs of 30–40 kb were pooled and end-repaired to blunt end and cloned into fosmid vector. The ligation mixture was packed, and the packaged DNA was transformed into *E. coli*, generating a library of 3500 clones, followed by cytotoxic activity screening. The clone QD15 producing light green pigment was selected and characterized. Finally, QD15 was vaccinated into 100 L fermentation tank and fermented for 36 h at 37 °C, 200 rpm, pH 7.0. Fermentation broth supernatant fluid was collected by continuous flow centrifuge at 60 L/min throughput. A voucher specimen (QD15) has been deposited at the Third Institute of Oceanography, State Oceanic Administration of China.

3.3. Extraction and Isolation

AB-8 macroporous adsorption resin (5 L) was used to handle the fermentation broth (80 L). After eluted with 15 L water, the 95% ethanol eluents (15 L) were collected, followed by evaporating the solvent under reduced pressure to give the total extract (108.7 g). The total extract was extracted with ethyl acetate (EtOAc). The EtOAc extract left after removal of the solvent (18.5 g) was separated by silica gel and eluted using a mixture of chloroform/methanol in a stepwise fashion from 100:1—pure methanol to yield 20 fractions. Fraction 10 was chromatographed on ODS column and eluted using a mixture of methanol and water (10:90, 30:70, 50:50, 70:30, 90:10, pure methanol) to yield 18 subfractions. Fraction 10-10 was purified by RP-HPLC, using a mixture of methanol and water in a stepwise manner from 40:60 to 60:40, to yield **1** (2.0 mg) and **2** (1.5 mg).

Metagenetriindole A (**1**): Pink powder; ^{13}C NMR (100 MHz, DMSO-d_6) and ^{1}H NMR (400 MHz, DMSO-d_6) spectral data were listed in Table 1; ESIMS: *m*/*z* 389 $[M + H]^+$, 412 $[M + Na]^+$; HR-ESI-MS: *m*/*z* 412.1420 (calcd. For $C_{26}H_{19}N_3ONa$, 412.1420) (Supplementary Information, Figures S1, S2, S4, S6 and S7).

Metagenediindole A (**2**): Yellow powder; ^{13}C NMR (100 MHz, DMSO-d_6) and ^{1}H NMR (400 MHz, DMSO-d_6) spectral data were listed in Table 2; ESIMS: *m/z* 263 $[M + H]^+$, 285 $[M + Na]^+$; HR-ESI-MS: *m*/*z* 285.0995 (calcd. For $C_{17}H_{14}N_2ONa$, 285.0998) (Supplementary Information, Figures S3, S5 and S8–S14).

Table 2. ^{1}H (400 MHz, DMSO-d_6) and ^{13}C (100 MHz, DMSO-d_6) NMR data, ^{1}H-^{1}H COSY and HMBC correlations for **2**.

Position	δ_H (*J* in Hz)	δ_C, Multiple		^{1}H-^{1}H COSY	HMBC
1	7.73 br.s				C-2, 3, 3a
2		65.0	C		
3		203.3	C		
3a		117.7	C		
4	7.44 br.d (7.3)	124.3	CH	H-5	C-6, 7a
5	6.73 td (7.1, 0.5)	117.1	CH	H-4, H-6	C-7
6	7.50 td (8.3, 1.3)	137.5	CH	H-5, H-7	C-4, 7a
7	6.90 br.d (8.3)	111.9	CH	H-6	C-5
7a		160.5	C		
1′	11.03 br.s.			H-2′	n.o.
2′	7.37 d (2.4)	123.5	CH	H-1′	C-2′, 3a′, 7a′
3′		114.4	C		
3a′		124.8	C		
4′	7.10 br.d (8.1)	119.5	CH	H-5′	C-7a′
5′	6.80 td (8.1, 1.0)	118.5	CH	H-4′, H-6′	C-3a′, 7′
6′	7.01 td (7.1, 1.0)	121.0	CH	H-5′, H-7′	C-5′, 7a′
7′	7.32 br.d (8.1)	111.6	CH	H-6′	C-3a′
7a′		136.6	C		
2-CH_3	1.62 s	38.0	CH		C-2, 3, 3′

[a] n.o. is not observed.

3.4. Cytotoxic Activity

The cytotoxic activities of these compounds were preliminarily evaluated using CNE2, Bel7402 and HT1080 cell lines by the CCK8 method [9]. Human nasopharyngeal cells CNE2, hepatoma cells BEL7402 and osteosarcoma cells HT1080 (all purchased from CCTCC, Wuhan, China) grown in DMEM (Dulbecco Modified Eagle Medium) supplemented with 10% fetal bovine serum and 1% (w/v) penicillin/strepto-mycin were seeded as 100 μL aliquots into a sterile 96 well microtiter plate at a titer of approximately 1000 cells per plate and incubated (24 h, 37 °C, 5% CO2). Compounds **1** and **2** resuspended in DMSO and a compound-free DMSO control were diluted in fresh medium and added to the appropriate wells at final concentrations of 100, 50, 25, 13, 6.3, 3.1, 1.6, 0.78, 0.39 and 0.20 μg/mL. These plates were then cultured for an additional 72 h. A cell counting kit 8 (CCK8) assay was used to assess the cytotoxicity of compound 1 and 2 to the cells. Briefly, 10 μL CCK8 solution (Dojindo Laboratories, Kumamoto, Japan) was added to each well and the 96-well plate was continuously incubated at 37 °C for 2 h. The OD value for each well was read at a 450 nm wavelength to determine the cell survival rate on a microplate reader (Epoch; Biotek, Winooski, VT, USA). The assay was repeated three times. An IC50 value was calculated using Origin 7.5 software (OriginLab, Northampton, MA, USA).

4. Conclusions

Metagenomics provides a means of exploring the secondary metabolites produced by the large collections of bacteria that are present in such extreme environment as deep sea, which are remain recalcitrant to culturing. Novel bioactive small molecules have been identified using metagenomic approaches in recent studies [10,11]. We screened a 3500 clones including deep sea origin eDNA library and found a cytotoxic activity clone, QD15. Further investigation on the chemical constituents of QD15 clone, lead to the identification of two new indole alkaloids, metagenetriindole A (**1**) and metagenediindole A (**2**), which were found to exhibited moderately cytotoxic activities against CNE2, Bel7402 and HT1080 cell lines. To the best of our knowledge, the two novel compounds is the first reported cytotoxic compound derived from deep sea metagenomic.

Acknowledgments

The project was supported by the National Natural Science Foundation of China (No. 81102333 and No. 81273400), as well as Fujian Natural Science Foundation for Distinguished Young Scholars (No. 2012J06020). The authors would also like to acknowledge the financial supports from R&D Special Fund for Public Welfare Industry (Oceanography) (201005022-1, 201005032-1), China Ocean Mineral Resources R&D Association (COMRA DY125-15-T-07) and Xiamen South Marine Center project (13GZP002NF08), and Fundamental Research Funds for the Central Universities (No. 2010121108).

Author Contributions

X.X.T. conceived the deap-sea metagenomic strategies. Z.W. and Y.-K.Q. supervised the project. X.Y. and L.C. isolated the two new compounds. Z.W.Y. performed the cytotoxic activities assay. M.J.F. was responsible for structural elucidation.

Conflicts of Interest

The authors declare no conflict of interest.

References

1. Deming, J.W. Deep ocean environmental biotechnology. *Curr. Opin. Microbiol*. **1998**, *9*, 283–287.
2. Lim, H.K.; Chung, E.J.; Kim, J.C.; Choi, G.J.; Jang, K.S.; Chung, Y.R.; Cho, K.Y.; Lee, S.W. Characterization of a forest soil metagenome clone that confers indirubin and indigo production on *Escherichia coli*. *Appl. Environ. Microbiol.* **2005**, *71*, 7768–7777.
3. Handelsman, J.; Rondon, M.R.; Brady, S.F.; Clardy, J.; Goodman, R.M. Molecular biological access to the chemistry of unknown soil microbes: A new frontier for natural products. *Chem. Biol.* **1998**, *5*, R245–R249.

4. Banik, J.J.; Brady, S. Recent application of metagenomic approaches toward the discovery of antimicrobials and other bioactive small molecules. *Curr. Opin. Microbiol*. **2010**, *13*, 603–609.
5. Chen, L.; Tang, X.X.; Zheng, M.; Yi, Z.W.; Xiao, X.; Qiu, Y.K.; Wu, Z. A novel indole alkaloid from deep-sea sediment metagenomic clone-derived *Escherichia coli* fermentation broth. *J. Asian Nat. Prod. Res.* **2011**, *13*, 444–448.
6. Gillespie, D.E.; Brady, S.F; Bettermann, A.D.; Cianciotto, N.P. Isolation of antibiotics turbomycins A and B from a metagenomic library of soil microbial DNA. *Appl. Environ. Microb*. **2002**, *68*, 4301–4306.
7. Wu, Z.; Xiao, X.; Qiu, Y.K.; Tang, X.X.; Chen, L.; Yi, Z.W.; Zhao, H.Y.; Zhao, M. A Tri-Indole Compound, Preparation Method and Application Thereof. *CN 102070507 A*, 25 May 2011.
8. Abe, T.; Kukita, A.; Akiyama, K. Isolation and structure of a novel biindole pigment substituted with an ethyl group from a metagenomic library derived from the marine sponge *Halichondria okadai*. *Chem. Lett*. **2012**, *41*, 728–729.
9. Zhuang, P.; Tang, X.X.; Yi, Z.W.; Qiu, Y.K.; Wu, Z. Two new compounds from marinederived fungus *Penicillium* sp. F11. *J. Asian Nat. Prod. Res.* **2012**, *14*, 197–203.
10. Brady, S.F.; Clardy, J. Cloning and heterologous expression of isocyanide biosynthetic genes from environmental DNA. *Angew. Chem. Int. Ed. Engl.* **2005**, *44*, 7063–7065.
11. Craig, J.W.; Chang, F.Y.; Brady, S.F. Natural products from environmental DNA hosted in *Ralstonia metallidurans*. *ACS Chem. Biol.* **2009**, *4*, 23–28.

A New Benzofuran Glycoside and Indole Alkaloids from a Sponge-Associated Rare Actinomycete, *Amycolatopsis* sp.

Yun Kwon, Seong-Hwan Kim, Yoonho Shin, Munhyung Bae, Byung-Yong Kim, Sang Kook Lee, Ki-Bong Oh, Jongheon Shin and Dong-Chan Oh

Abstract: Three new secondary metabolites, amycofuran (**1**), amycocyclopiazonic acid (**2**), and amycolactam (**3**), were isolated from the sponge-associated rare actinomycete *Amycolatopsis* sp. Based on combined spectroscopic analyses, the structures of **1**–**3** were determined to be a new benzofuran glycoside and new indole alkaloids related to cyclopiazonic acids, a class that has previously only been reported in fungi. The absolute configurations of **1** and **3** were deduced by ECD calculations, whereas that of **2** was determined using the modified Mosher method. Amycolactam (**3**) displayed significant cytotoxicity against the gastric cancer cell line SNU638 and the colon cancer cell line HCT116.

Reprinted from *Mar. Drugs*. Cite as: Kwon, Y.; Kim, S.-H.; Shin, Y.; Bae, M.; Kim, B.-Y.; Lee, S.K.; Oh, K.-B.; Shin, J.; Oh, D.-C. A New Benzofuran Glycoside and Indole Alkaloids from a Sponge-Associated Rare Actinomycete, *Amycolatopsis* sp. *Mar. Drugs* **2014**, *12*, 2326–2340.

1. Introduction

Natural products from marine organisms have been proposed as "a new wave of drugs" because of their great potential for supplying structurally and biologically novel compounds for drug discovery [1]. As of 2013, several drugs derived from marine natural products are in clinical use. These drugs include the anticancer drug cytarabine and the antiviral agent vidarabine from the sponge *Tethya crypta*; Prialt from the cone snail *Conus magnus*, which is used for chronic pain treatment; the anticancer drug Yondelis from the marine tunicate *Ecteinascidia turbinata*; and Halaven from the sponge *Halichondria okadai*, a compound used to treat breast cancer [2]. During drug development, compound supply was one of the most challenging problems to overcome, as these drugs originate from marine invertebrates, which are difficult to cultivate [1]. The recent advent of the genomic era and the development of microbial biotechnology have revealed that the majority of secondary metabolites from marine invertebrates are actually produced by symbiotic microorganisms in invertebrate tissues, indicating that the microbial fermentation of useful marine invertebrate-derived compounds may resolve the supply problem [3]. For example, a recent study determined that didemnin anticancer agents, originally discovered from the tunicate *Tridemnum solidum*, were produced by the symbiotic bacteria *Tistrella mobilis* and *Tistrella bauzanensis* [4]. The sponge-derived metabolites swinholide A [5,6], onnamide A [7], and psymberin [8] were also shown to be bacterially produced natural products. These results have spurred the study of the chemistry and phylogenetic diversity of symbiotic microbial communities in marine invertebrates [9,10].

Actinomycetes, belonging to the phylum Actinobacteria, are prolific chemical synthesizers, providing 40% of the 33,500 microbial bioactive compounds reported as of 2010, including numerous drugs in clinical use [11]. Actinomycetes are one of the major phylogenetic groups in

symbiosis with sponges by accounting for ~15% of all symbiotic communities associated with sponges [9]. Given that actinomycetes are chemically prolific and that sponge-associated actinomycetes have not been thoroughly studied, chemical investigations of sponge-associated actinomycetes should lead to the discovery of a novel chemical hemisphere [12]. However, compared to the phylogenetic analysis of sponge-associated microbial communities, the chemical investigation of sponge-associated actinomycetes is only just beginning, as demonstrated by a few recent examples, including new nucleoside analogs discovered from *Streptomyces microflavus* in association with the sponge *Hymeniacidon perlevis* [13] and new lobophorin derivatives isolated from a sponge-associated actinomycete, *Streptomyces carnosus* [14]. Therefore, we selectively isolated actinomycete strains associated with marine sponges to search for new bioactive compounds. Then, we chemically analyzed the production of secondary metabolites from sponge-associated actinomycetes by LC/MS (Liquid Chromatography/Mass Spectrometry). During our chemical screening, we found that a rare actinomycete strain (Cra33g) belonging to *Amycolatopsis* sp., produced a new benzofuran glycoside, as well as two new indole alkaloids, which are quite rare as bacterial metabolites. Here, we report the structural elucidation and biological activity of these three new compounds from the *Amycolatopsis* strain: amycofuran (**1**), amycocyclopiazonic acid (**2**), and amycolactam (**3**) (Figure 1).

Figure 1. The structures of amycofuran (**1**), amycocyclopiazonic acid (**2**), and amycolactam (**3**).

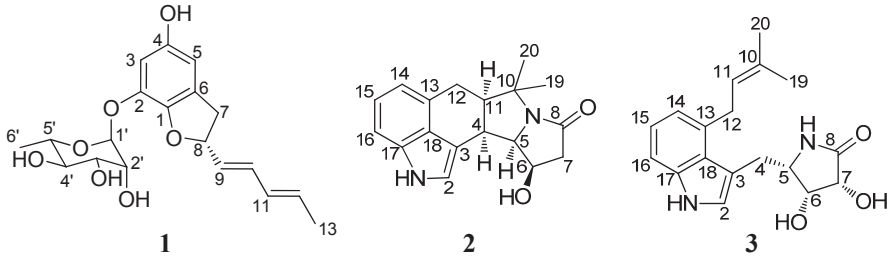

2. Results and Discussion

2.1. Structural Elucidation

Amycofuran (**1**) was isolated as a white powder, and the molecular formula was established as $C_{19}H_{24}O_7$ by HR-ESI (High Resolution-Electrospray Ionization) mass (obsd $[M + Na]^+$ *m*/*z* 387.1407; calcd $[M + Na]^+$ 387.1420) and ^1H and ^{13}C NMR spectroscopic data (Table 1). The ^1H and HSQC (Heteronuclear Single Quantum Coherence) NMR spectra of **1** showed a *meta*-coupled pair of aromatic protons (δ_H 7.25 and 6.83), four olefinic protons (δ_H 6.37, 6.04, 5.78, and 5.67), one proton attached to a dioxygenated carbon (δ_H 6.30), five protons connected to oxygen-bearing carbons (δ_H 5.26, 4.82, 4.75, 4.52, and 4.35), two aliphatic protons (δ_H 3.27 and 2.95), and two methyl signals (δ_H 1.63 and 1.56) along with four hydroxy protons (δ_H 11.07, 7.07, 6.70, and 6.87). The ^{13}C NMR spectrum revealed ten double-bond carbons, including four quaternary carbons between 154.1 and 130.7 ppm, one dioxygenated carbon at δ_C 101.5, five oxygenated sp^3 carbons

from 84.5 to 71.4 ppm, an aliphatic carbon at δ_C 37.8, and two methyl carbons (δ_C 18.9 and 18.5). Further analysis of the ^{1}H-^{1}H COSY (Correlation Spectroscopy) NMR spectrum was useful for the construction of two separate spin systems. First, a diene-bearing system was elucidated by the consecutive COSY correlations from H_2-7 (δ_C 3.27 and 2.95) to H_3-13 (δ_C 1.63) through H-8, H-9, H-10, H-11, and H-12 (Figure 2). The geometries of the diene were established as 9*E* and 11*E* based on the *trans*-coupling constants (15.0 Hz each) of the double-bond ^{1}H peaks corresponding to H-9, H-10, H-11, and H-12. The second spin system indicated the presence of a hexose. The proton bound to a dioxygenated carbon (H-1′; δ_H 6.30-δ_C 101.5) was correlated with the carbinol proton H-2′ (δ_H 4.82) in the COSY spectrum, revealing C-1′-C-2′ connectivity. H-2′ displayed a homonuclear coupling with H-3′ (δ_H 4.75), placing C-3′ next to C-2′. The COSY correlation between H-3′ and H-4′ (δ_H 4.35) connected C-3′ and C-4′. Further extension of the spin system was accomplished using the COSY correlations between H-4′ and H-5′ (δ_H 4.52) and between H-5′ and H_3-6′ (δ_H 1.56), suggesting a hexose. The hydroxy protons (δ_H 7.07, 6.70, and 6.87) belonging to the hexose were assigned based on COSY correlations.

Table 1. NMR data for amycofuran (**1**) in pyridine-d_5.

C/H	δ_H [a]	Mult (*J* in Hz)	δ_C [b]	Type
1			143.2	C
2			141.5	C
3	7.25	d (1.5)	106.9	CH
4			154.1	C
4-OH	11.07			OH
5	6.83	d (1.5)	107.7	CH
6			130.7	C
7a	3.27	dd (16.0, 8.0)	37.8	CH_2
7b	2.95	dd (16.0, 8.0)		
8	5.26	ddd (8.0, 8.0, 8.0)	84.5	CH
9	5.78	dd (15.0, 8.0)	130.8	CH
10	6.37	dd (15.0, 10.5)	133.1	CH
11	6.04	dd (15.0, 10.5)	131.7	CH
12	5.67	dq (15.0, 7.0)	131.4	CH
13	1.63	d (7.0)	18.5	CH_3
1′	6.30	d (1.0)	101.5	CH
2′	4.82	br m	72.5	CH
2′-OH	7.07	br s		OH
3′	4.75	br d (9.0)	72.9	CH
3′-OH	6.70	br s		OH
4′	4.35	br m	74.2	CH
4′-OH	6.87	br s		OH
5′	4.52	m	71.4	CH
6′	1.56	d (6.0)	18.9	CH_3

[a] 600 MHz; [b] 125 MHz.

Figure 2. Key ^{1}H–^{1}H COSY and HMBC correlations of **1**–**3**.

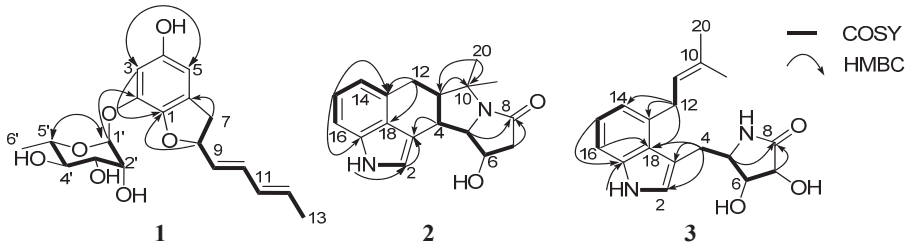

The analysis of the HMBC (Heteronuclear Multiple Bond Correlation) correlations allowed complete elucidation of the planar structure of amycofuran (**1**). The long-range heteronuclear coupling from H-5' to the dioxygenated carbon at 101.5 ppm confirmed the identity of the sugar unit as a six-membered ring. The HMBC correlations from the *meta*-coupled aromatic protons (H-3 at δ_H 7.25; H-5 at δ_H 6.83) to the aromatic carbons C-1 to C-6 established a six-membered aromatic ring. The connectivity of the diene-bearing spin system to the aromatic ring was confirmed by the HMBC correlations from H_2-7 to C-1, C-5, and C-6. An additional long-range coupling from H-8 to C-1 indicated that the dihydrofuran ring was attached to the aromatic ring. The HMBC correlation from H-1′ to C-2 connected the sugar moiety to C-2, completing the planar structure of amycofuran (**1**) and indicating a new benzofuran.

The relative configuration of the hexose was examined using the $^{1}J_{CH}$ value of the anomeric proton and the $^{3}J_{HH}$ values and ROESY (Rotating-frame Overhauser Effect Spectroscopy) correlations of the protons in the six-membered ring. The magnitude of the $^{1}J_{CH}$ value (171 Hz) clearly revealed the α-configuration [15], placing the anomeric proton in an equatorial position. The equatorial position of H-2′ was assigned by the ROESY correlation between H-2′ and H-3′. The large ^{1}H-^{1}H coupling constant (9.0 Hz) between H-3′ and H-4′ established their *anti*-relationship. The 1,3-ROESY correlation between H-3′ and H-5′ established the axial position of H-5′ (Figure 3). The analysis of the relative configuration of the sugar showed that it was a rhamnose moiety, which exists solely in the L-form in nature.

Figure 3. Key ROESY correlations of the hexose of **1**.

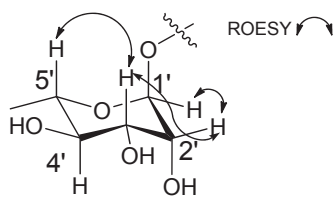

We tried to determine the absolute configuration of C-8 in amycofuran (**1**) comparing the experimental CD (Circular Dichroism) spectrum with the calculated ECD (Electronic Circular Dichroism) spectra. Initially, because of the glycosidic bond between rhamnose and benzofuran in **1**, which can cause various changes in conformation during energy-minimized structure calculation, we carefully analyzed ROESY correlations between the sugar and aglycone to obtain a most

probable conformation (see Supplementary Information). After the calculation of the energy-minimized structure from the conformation based on the ROESY correlation, we calculated ECD spectra [16,17]. The ECD spectra based on the conformation were calculated for the 8*S* and 8*R* configurations. The ECD spectrum for 8*R* turned out to be consistent with the observed CD spectrum, proposing the 8*R* configuration in amycofuran (Figure 4). In literature, a fungal metabolite asperfuran, which is aglycone of **1**, also displayed a very similar CD spectrum to that of **1**, also supporting the 8*R* configuration (see Supplementary Information) [18].

Figure 4. Measured CD and calculated ECD spectra of **1**.

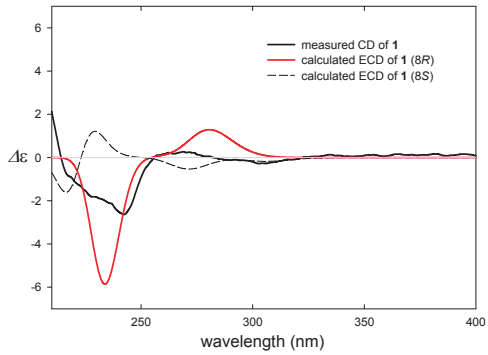

Amycocyclopiazonic acid (**2**) was purified as a white powder. Its molecular formula was determined to be $C_{18}H_{20}N_2O_2$ based on high-resolution mass spectrometry data as well as ^1H and ^{13}C NMR spectroscopic data (Table 2). The UV spectrum of **2** displayed characteristic indole UV absorption maxima at 222 and 280 nm. The ^1H NMR spectrum showed one downfield singlet proton (δ_H 11.79) attached to a heteroatom and four aromatic resonances between 7.46 and 7.08 ppm. Two protons bound to heteroatom-bearing carbons were observed at δ_H 4.83 and 4.18. In addition, the ^1H NMR spectrum displayed six aliphatic protons between 3.76 and 2.47 ppm and two methyl singlets in the upfield region (δ_H 1.74 and 1.65). The ^{13}C and HSQC NMR spectra exhibited one carbonyl carbon (δ_C 170.4); eight double-bond signals from 134.5 to 109.0 ppm, including four methines and four quaternary carbons; two heteroatom-bearing sp^3 methine carbons at δ_H 73.9 and 73.6; one quaternary carbon at δ_C 60.6; two aliphatic methines at δ_C 53.2 and 39.7; two aliphatic methylenes at δ_C 46.8 and 27.0; and two methyl groups at 26.4 and 22.4 ppm.

An analysis of the COSY and HMBC correlations established the expected indole moiety. Next, the COSY correlations and ^1H-^1H coupling constants (7.5–8.0 Hz) of the double-bond protons H-14 (δ_H 7.08), H-15 (δ_H 7.34), and H-16 (δ_H 7.43) connected the three consecutive carbons (C-14, C-15, and C-16) in a six-membered aromatic ring. The HMBC correlations from the three aromatic protons (H-14, H-15, and H-16) and an additional aromatic singlet proton to aromatic carbons revealed an indole substructure (Figure 2). The C-12–C-11 connectivity was determined from the COSY correlations between H_2-12 (δ_H 3.13 and 3.03) and H-11 (δ_H 2.47). C-11 was then connected to C-4 by the homonuclear coupling between H-11 and H-4 (δ_H 3.76). The spin system was further extended to C-5, C-6, and C-7 by an array of COSY correlations involving H-5, H-6, and H_2-7. The HMBC correlation from H_2-7 to C-8 (δ_C 170.4) extended the connection to the carbonyl carbon,

which was verified as an amide carbon based on the IR absorption at 1671 cm^{-1}. HMBC cross peaks from the methyl groups (δ_H 1.65 and 1.74) to C-10, C-11, C-19, and C-20 indicated a *gem*-dimethyl moiety connected to C-11. The carbon chemical shift of C-10 (δ_C 60.6) indicated that this carbon bears a nitrogen atom, placing the nitrogen atom of the amide functional group next to C-10. Finally, the connectivity from C-5 to the amide nitrogen atom was deduced by the carbon chemical shift of C-5 (δ_C 73.6) and the degree of unsaturation. Therefore, the planar structure of **2** was elucidated, and it was determined to be a new member of the indole alkaloid cyclopiazonic acid class.

Table 2. NMR data for amycocyclopiazonic acid (**2**) in pyridine-d_5.

C/H	δ_H [a]	Mult (*J* in Hz)	δ_C [b]	Type
1	11.79			NH
2	7.46	d (2.0)	120.8	CH
3			111.1	C
4	3.76	dd (10.0, 6.0)	39.7	CH
5	4.18	dd (10.0, 7.0)	73.6	CH
6	4.83	ddd (7.0, 7.0, 6.0)	73.9	CH
7	2.99	m	46.8	CH_2
8			170.4	C
9				N
10			60.6	C
11	2.47	m	53.2	CH
12a	3.13	dd (12.0, 6.0)	27.0	CH_2
12b	3.03	dd (12.0, 6.0)		
13			129.7	C
14	7.08	d (7.5)	116.1	CH
15	7.34	dd (8.0, 7.5)	122.4	CH
16	7.43	d (8.0)	109.0	CH
17			134.5	C
18			126.9	C
19	1.65	s	22.4	CH_3
20	1.74	s	26.4	CH_3

[a] 600 MHz; [b] 125 MHz.

The relative stereochemistry of **2** was readily assigned by ROESY NMR spectroscopic analysis. Strong ROESY correlations among H-4, H-5, and H-6 revealed that these protons are on the same side. The ROESY correlation between H-4 and H-11 established their *syn*-relationship, thus determining the entire relative configuration of **2**. The absolute configuration of amycocyclopiazonic acid was assigned by the modified Mosher method [19]. The esterification of **2** with *R*- and *S*-MTPA-Cl (α-methoxy-α-(trifluoromethyl) phenylacetyl chloride) yielded the *S*- and *R*-MTPA esters of **2** (**4** and **5**, respectively). The analysis of the ^{1}H NMR $\Delta\delta_{S-R}$ values revealed a clearly consistent sign distribution, thus confirming the absolute configuration of **2** as 4*R*, 5*R*, 6*R,* and 11*R* (Figure 5).

Figure 5. $\Delta\delta_{S-R}$ values of **4** and **5** in pyridine-d_5.

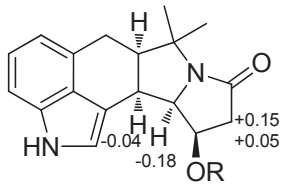

Amycolactam (**3**) was obtained as a white powder with a molecular formula of $C_{18}H_{22}N_2O_3$, as determined by HR-ESI-MS and ^{1}H and ^{13}C NMR spectroscopic data (Table 3). The UV spectrum of **3** was very similar to that of **2**, indicating that this compound also possesses an indole substructure. The ^{1}H NMR spectrum showed three downfield protons attached to a heteroatom (δ_H 12.04, 8.87, and 6.78), four aromatic protons from 7.61 to 7.13 ppm, one olefinic proton at δ_H 5.56, three protons bound to carbons bearing a nitrogen or oxygen atom (δ_H 4.76, 4.73, and 4.26), four aliphatic protons (δ_H 4.02 (2H), 3.93, and 3.78), and two methyl groups (δ_H 1.70 and 1.67). The ^{13}C and HSQC NMR spectra enabled the identification of one quaternary carbonyl carbon (δ_C 176.8); ten sp^2 carbons, including five methines and five quaternary carbons between 138.7 and 110.6; two oxygen-bearing methines (δ_C 74.2 and 71.4); one nitrogen-bound methine (δ_C 57.1); two aliphatic methylenes (δ_C 32.7 and 27.9); and two methyl groups (δ_C 25.8 and 18.0).

Three partial structures were identified on the basis of the analysis of the COSY and HMBC NMR spectra. In accordance with the UV spectrum, an indole moiety was readily assigned in a manner analogous to that used for amycocyclopiazonic acid (**2**). A dihydroxy γ-lactam ring was indicated by the COSY correlation from H-6 (δ_H 4.73) to H-5 (δ_H 4.26) and H-7 (δ_H 4.76) as well as the long-range heteronuclear coupling from H-5 and H-7 to the amide carbon C-8 (δ_C 176.8). An additional COSY correlation between H-5 and H_2-4 (δ_H 3.93 and 3.78) connected the lactam ring to the C-4 methylene. The HMBC correlation from the methyl group protons H_3-19 (δ_H 1.67) and H_3-20 (δ_H 1.70) to C-10 (δ_C 131.9) and C-11 (δ_C 125.1) constructed a dimethyl group bonded to an alkene carbon. The double bond was connected to an aliphatic methylene C-12 (δ_C 32.7) by the ^{1}H-^{1}H coupling between H-11 (δ_H 5.56) and H_2-12 (δ_H 4.02), allowing the assignment of an isoprene unit. These three partial structures were assembled by heteronuclear correlations. The HMBC coupling from H_2-4 to C-3 (δ_C 112.6) connected the dihydroxy γ-lactam ring to the indole ring. Furthermore, the two-bond heteronuclear correlation from H_2-12 to C-13 placed the isoprene unit next to C-13 (δ_C 134.8), finalizing the planar structure of amycolactam (**3**) and indicating that it is a new indole alkaloid bearing an isoprene unit and a dihydroxy γ-lactam (Figure 2).

The relative configuration of the dihydroxy γ-lactam ring was firstly deduced from the ROESY correlations and ^{1}H–^{1}H coupling constants. A clear correlation between H-5 and H-7 led to the well supported assignment of a *syn*-relationship between these two protons. However, the chemical shifts of H-6 (δ_H 4.73) and H-7 (δ_H 4.76) were too close to allow the definitive assignment of the relative configuration of C-6 from the ROESY correlation. Thus, we analyzed the ^{1}H–^{1}H coupling constants in the dihydroxy γ-lactam ring by comparing them with literature values (Figure 6). The coupling constants $^3J_{H5H6}$ and $^3J_{H6H7}$ in **3** were 5.0 and 3.5 Hz, respectively. These values are consistent with the coupling constants of a dihydroxy γ-lactam ring with the *S**, *R**, and *R**

configurations, whereas an alternative isomer with the *S**, *S**, and *R** configurations showed significantly different coupling constants [20–22].

Table 3. NMR data for amycolactam (**3**) in pyridine-d_5.

C/H	δ_H [a]	Mult (*J* in Hz)	δ_C [b]	Type
1	12.04	s		NH
2	7.61	d (2.0)	124.9	CH
3			112.6	C
4a	3.93	dd(15.0, 7.5)	27.9	CH_2
4b	3.78	dd(15.0, 7.5)		
5	4.26	m	57.1	CH
6	4.73	dd (5.0, 3.5)	71.4	CH
6-OH	6.78			OH
7	4.76	d (5.0)	74.2	CH
7-OH	8.87			OH
8			176.8	C
9	ND [c]			NH
10			131.9	C
11	5.56	dd (6.0, 6.0)	125.1	CH
12	4.02	m	32.7	CH_2
13			134.8	C
14	7.13	d (7.0)	120.1	CH
15	7.29	dd (8.0, 7.0)	122.4	CH
16	7.53	d (8.0)	110.6	CH
17			138.7	C
18			126.4	C
19	1.67	s	25.8	CH_3
20	1.70	s	18.0	CH_3

[a] 600 MHz; [b] 125 MHz; [c] Not detected.

Figure 6. (**a**) ^{1}H-^{1}H coupling constants of the dihydroxy γ-lactam ring observed in **3**. ^{1}H-^{1}H coupling constants of (**b1**) the dihydroxy γ-lactam ring possessing 1*S**, 2*R**, and 3*R**, and (**b2**) 1*S**, 2*S**, and 3*R** found in literature.

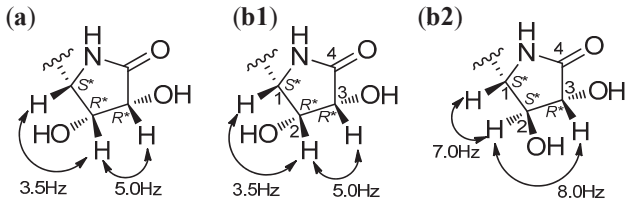

To determine the absolute configuration, we first attempted to use the modified Mosher method, but amycolactam (**3**) decomposed during MTPA esterification, even under mild conditions. Therefore, ECD calculation was utilized to determine the absolute configuration of **3**. When we performed the ECD calculation for **3**, we found that the existence of two or more conformations.

Then, we optimized the conformers of **3** using the basis set def-SV(P) for all atoms and the functional B3LYP/DFT level and considered the conformers when calculating the ECD spectra with TDDFT using the basis set def2-TZVPP for all atoms and the functional B3LYP/DFT level. The calculated ECD spectra of (5*S*, 6*R*, 7*R*)-amycolactam (**3**) displayed negative Cotton effects at 242 nm, consistent with the experimental CD spectrum (see the Supplementary Information).

The structure of amycofuran (**1**), which is a benzofuran glycoside, is interesting. To the best of our knowledge, no benzofuran substituted together with a diene moiety and a rhamnose sugar has been previously reported. A comprehensive literature search indicated that benzofurans are very rare as bacterial secondary metabolites, although a few examples, such as actiketal [23] and isoaurostatin [24], have been reported from actinomycetes whereas benzofurans are relatively common in fungi [18,25]. Amycocylopiazonic acid (**2**) is a new member of the cyclopiazonic acid class, which was previously reported to be produced by fungi belonging to the genus *Penicillium* [26]. Interestingly, this class has not been discovered from a bacterium. Therefore, amycocyclopiazonic acid (**2**) is the first bacterially produced member of the cyclopiazonic acid class. Based on the carbon backbone structure of amycolactam (**3**), this new alkaloid may be considered as an acyclic version of amycocyclopiazonic acid (**2**) generated during cyclopiazonic acid biosynthesis [27]. The biological activities of **1**–**3** were evaluated in antibacterial and antifungal assays against various pathogenic microbes, but the compounds did not exhibit significant inhibitory activities. The cytotoxicities of **1**–**3** were tested against human carcinoma cell lines, including A549 (lung cancer), HCT116 (colon cancer), SNU638 (gastric cancer), K562 (leukemia), SK-HEP1 (liver cancer), and MDA-MB231 (breast cancer). Amycolactam (**3**) significantly inhibited the proliferation of SNU638 and HCT116, with IC_{50} values of 0.8 and 2.0 μM, respectively. The cytotoxic effects of **3** against A546, K562, and SK-HEP1 were moderate (IC_{50} = 13.7, 9.6, and 8.3 μM, respectively), whereas virtually no cytotoxicity was observed against MDA-MB231. However, amycofuran (**1**) and amycocyclopiazonic acid (**2**) did not exhibit significant cytotoxicity against the cancer cells tested.

3. Experimental Section

3.1. General Experimental Procedures

Optical rotations were obtained in a 1 cm cell with a Jasco P-1020 polarimeter. UV spectra were measured with a Perkin Elmer Lambda 35 UV/VIS spectrometer. IR spectra were recorded with a Thermo N1COLET iS10 spectrometer. A Bruker Avance 600 MHz spectrometer at NCIRF (National Center for Inter-University Research Facilities, Seoul National University, Seoul, Korea) was used to obtain ^{1}H, ^{13}C, and 2D NMR spectra. Electrospray ionization (ESI) low-resolution LC/MS data were collected on an Agilent Technologies 6130 Quadrupole mass spectrometer attached to an Agilent Technologies 1200 series HPLC using a reversed-phase C_{18} column (Phenomenex Luna, 100 × 4.6 mm, Torrance, CA, USA). High-resolution electrospray ionization (HR-ESI) mass spectra were acquired with a Thermo Finnigan LCQ high-resolution mass spectrometer at NICEM (National Instrumentation Center for Environmental Management, Seoul

National University, Seoul, Korea). Circular Dichroism was measured with an Applied Photophysics Chirascan plus (Surrey, UK) with a 0.2 cm cell at NICEM.

3.2. Isolation of Bacteria, Cultivation, and Extraction

A sponge sample was gathered from Micronesia. One gram of unidentified sponge sample was extracted with 3 mL of sterilized artificial seawater at a 1:3 dilution ratio and shaken at 180 rpm for 1 h. A total of 150 µL of the resulting solution was spread on Gause1 agar (20 g soluble starch, 1 g KNO_3, 0.5 g K_2HPO_4, 0.01 g $FeSO_4 \cdot 7H_2O$), M2 agar (6 mL glycerol, 1 g arginine, 1 g KH_2PO_4, 0.5 g $MgSO_4 \cdot 7H_2O$, 16.0 g agar), SC agar (10.0 g starch, 0.3 g casein, 2.0 g KNO_3, 2.0 g K_2HPO_4, 0.05 g $MgSO_4 \cdot 7H_2O$, 0.02 g $CaCO_3$, 0.01 g $FeSO_4 \cdot 7H_2O$), IM6 agar (0.5 g glycerol, 0.5 g starch, 0.5 g sodium propionate, 0.1 g KNO_3, 0.1 g asparagine, 0.3 g casein, 0.5 g K_2HPO_4, 1 mg $FeSO_4 \cdot 7H_2O$, 16.0 g agar, 1 mg vitamin B), and K agar (25 g soluble starch, 15 g soy peptone, 2 g dry yeast, 4 g $CaCO_3$). The strain Cra33g was isolated on Gause1 agar. An analysis of the 16S rDNA sequence (Figure S23 in the Supplementary Information) indicated that Cra33g is most similar to *Amycolatopsis saalfeldensis*. The strain Cra33g was cultivated in 60 mL S medium (25 g soluble starch, 15 g soy peptone, 2 g dry yeast, 4 g calcium carbonate in 1 L artificial seawater) in a 150 mL Erlenmeyer flask. After cultivation for 70 h on a rotary shaker at 180 rpm at 27 °C, a 5 mL aliquot of the culture was transferred into 250 mL Diaion LH-20 (1 g/L) with GSS medium (10 g soluble starch, 20 g glucose, 25 g soy peptone, 1 g beef extract, 4 g yeast extract, 2 g NaCl, 0.25 g KH_2PO_4, and 2 g $CaCO_3$ in 1 L artificial seawater) in 500 mL Erlenmeyer flasks (20 ea × 250 mL; total volume 5 L). After 10 days of cultivation, 18 L of ethyl acetate was added to the whole culture (5 L) and shaken for extraction. Anhydrous sodium sulfate was added to the separated organic layer, which was then filtered and dried. In total, the ethyl acetate extract yielded 4.5 g (a rotary evaporator was used to concentrate the extracts *in vacuo*). This procedure was performed 10 times (50 L culture; total amount of extract: 45 g) to acquire quantities of **1**–**3** sufficient for structure elucidation and bioassays.

*3.3. Isolation of **1**–**3***

The dried ethyl acetate crude extract was adsorbed on Celite and then loaded on a 6 g Sep-Pak C_{18} open column and fractionated with 100 mL each of 20%, 40%, 60%, 80%, and 100% MeOH in water and 1:1 MeOH/dichloromethane. The 40%, 60%, and 80% MeOH/water fractions contained **1**–**3**. The combined 40%, 60%, and 80% MeOH/water fractions were eluted on silica gel and a Sephadex LH-20 column to remove the fatty acids, which would have HPLC (high-performance liquid chromatography) retention times similar to **1**–**3** in the subsequent HPLC purification. Reversed-phase HPLC (Kromasil C_{18} (2): 250 × 10 mm; 5 µm) under isocratic conditions in 4:6 acetonitrile/water (UV 220 nm detection; flow rate: 2 mL/min) was used to purify **1**–**3** from the three fractions. Finally, amycofuran (**1**) (20 mg), amycocyclopiazonic acid (**2**) (18 mg), and amycolactam (**3**) (10 mg) were obtained at the retention times of 12 min, 13 min, and 15 min, respectively.

3.3.1. Amycofuran (**1**)

[α]$_D$ −2 (c 0.10, MeOH); UV (MeOH) λ_{max} (log ε) 214 (3.76), 227 (3.89), 297 (2.96) nm; CD (MeOH) (Δε) 243 (−2.61), 257 (0.10), 269 (0.27), 283 (−0.09) nm; IR (neat) ν_{max} 2980, 2971, 1605, 1455, 1346, 1032 cm^{-1}; for ^{1}H and ^{13}C NMR data, see Table 1; HRESIMS at *m/z* 387.1407 [M + Na]$^+$ (calcd for $C_{19}H_{24}O_7Na$ 387.1420).

3.3.2. Amycocyclopiazonic acid (**2**)

[α]$_D$ −16 (c 0.10, MeOH); UV (MeOH) λ_{max} (log ε) 207 (2.84), 222 (3.02), 280 (2.29) nm; IR (neat) ν_{max} 3309, 2980, 1671, 1413 cm^{-1}; for ^{1}H and ^{13}C NMR data, see Table 2; HRESIMS at *m/z* 297.1591 [M + H]$^+$ (calcd for $C_{18}H_{21}N_2O_2$ 297.1603).

3.3.3. Amycolactam (**3**)

[α]$_D$ −3 (c 0.05, MeOH); UV (MeOH) λ_{max} (log ε) 214 (3.07), 221 (3.08), 275 (2.49) nm; CD (MeOH) (Δε) 211 (0.51), 267 (−1.56) nm; IR (neat) ν_{max} 3402, 2971, 2921, 1687, 1032 cm^{-1}; for ^{1}H and ^{13}C NMR data, see Table 3; HRESIMS at *m/z* 315.1694 [M + H]$^+$ (calcd for $C_{18}H_{23}N_2O_3$ 315.1709).

3.4. MTPA Esterification of Amycocyclopiazonic Acid (2)

Two 40 mL vials containing **2** (1 mg sample in each vial) were completely dried under high vacuum for 10 h. Freshly distilled anhydrous pyridine (1 mL) and catalytic amounts of crystalline dimethylaminopyridine (DMAP) were added to each reaction vial in that order under argon gas. Then, *R*- and *S*-α-methoxy trifluoromethyl-phenylacetic acid (MTPA) chloride (20 µL of *R*-MTPA-Cl and 60 µL of *S*-MTPA-Cl) were separately added. Whereas the reaction with *R*-MTPA chloride was completed at room temperature after 90 min, the reaction with *S*-MTPA chloride required 2 h at 50 °C. The reactions were quenched by the addition of 50 µL of MeOH. The products were purified using reversed-phase HPLC (Kromasil C_{18} (2): 250 × 10 mm; 5 µm) with a gradient (40% to 100% aqueous acetonitrile for 30 min and followed by 100% acetonitrile under isocratic conditions for 30 min). The *S*- and *R*-MTPA esters (**4** and **5**, respectively) of **2** eluted at 45.5 and 50.4 min, respectively. The $\Delta\delta_{S-R}$ values around the stereogenic centers of the MTPA esters were assigned based on the ^{1}H and ^{1}H-^{1}H COSY NMR spectra.

3.4.1. *S*-MTPA Ester (**4**) of Amycocyclopiazonic Acid (**2**)

^{1}H NMR (600 MHz, pyridine-d_5) δ 11.95 (s, 1H), 7.46 (d, *J* = 8.0, 1H), 7.38–7.31 (m, 5H), 7.09–7.05 (m, 3H), 6.04 (ddd, *J* =17.0, 8.5, 7.0, 1H), 3.99 (dd, *J* = 10.5, 7.0, 1H), 3.77 (dd, *J* = 10.5, 6.5, 1H), 3.54 (s, 3H), 3.15 (dd, *J* = 17.0, 8.5, 1H), 2.98–2.93 (m, 3H), 2.41 (dq, *J* = 12.0, 6.5, 1H), 1.67 (s, 3H), 1.60 (s, 3H). The molecular formula of **4** was confirmed as $C_{28}H_{27}N_2O_4F_3$ ([M + H]$^+$ at *m/z* 513).

3.4.2. *R*-MTPA Ester (**5**) of Amycocyclopiazonic Acid (**2**)

^{1}H NMR (600 MHz, pyridine-d_5) δ 11.90 (s, 1H), 7.53 (d, *J* = 8.0, 1H), 7.46 (d, *J* = 8.0, 2H), 7.37 (d, *J* = 4.5, 1H), 7.27 (dd, *J* = 15.0, 8.0, 3H), 7.10 (d, *J* = 7.0, 1H), 7.05 (s, 1H), 6.10 (ddd, *J* = 16.0, 9.0, 7.0, 1H), 4.16 (dd, *J* = 10.5, 7.0, 1H), 3.81 (dd, *J* = 10.5, 5.5, 1H), 3.38 (s, 3H), 3.10 (m, 1H), 3.07 (dd, *J* = 16.0, 8.0, 1H), 2.99 (dd, *J* = 16.0, 8.0, 1H), 2.81 (dd, *J* = 16.0, 9.0, 1H), 2.44 (dq, *J* = 16.0, 6.5, 1H), 1.70 (s, 3H), 1.67 (s, 3H). The molecular formula of **5** was confirmed as $C_{28}H_{27}N_2O_4F_3$ ($[M + H]^+$ at *m/z* 513).

3.5. ECD Computational Calculation

The theoretical calculations of compound **1**, the aglycone of compound **1**, and **3** were performed using Turbomole 6.5. The optimized conformation geometries and energy levels are provided in the Supplementary Information (Tables S1–S3). The theoretical calculation of ECD was performed using TDDFT using the basis set def2-TZVPP for all atoms and the functional B3LYP/DFT level. The ECD spectra are obtained by Gaussian functions for each transition.

$$\Delta\epsilon(E) = \frac{1}{2.297 \times 10^{-39}} \frac{1}{\sqrt{2\pi\sigma}} \sum_{i}^{A} \Delta E_i \, R_i e^{[-(E-\Delta E_i)^2/(2\sigma)^2]} \quad (1)$$

where σ represents the width of the band at 1/*e* height and ΔE_i and R_i are the excitation energies and rotational strengths for transition *i*, respectively. $\sigma = 0.10$ eV and R^{velocity} were used in this work.

3.6. Evaluation of Anti-Proliferative Activity

Cell proliferation was measured using the sulforhodamine B (SRB) assay. Briefly, six human cancer cell lines (A549, HCT116, SNU638, K562, SK-HEP1, and MDA-MB231) (3×10^5 cells/mL) were seeded in 96-well plates with various concentrations of **1**–**3** and incubated at 37 °C in a humidified atmosphere with 5% CO_2. After 72 h of treatment with amycofuran (**1**), amycocyclopiazonic acid (**2**), and amycolactam (**3**), the cells were fixed with a 10% TCA solution for 1 h, and cellular proteins were stained with 0.4% SRB in a 1% acetic acid solution. The stained cells were dissolved in 10 mM Tris buffer (pH 10.0). The effect of **1**–**3** on cell proliferation was calculated as the percentage relative to a solvent-treated control, and the IC_{50} values were determined using nonlinear regression analysis (percent survival *versus* concentration).

4. Conclusions

Investigation of the secondary metabolites produced by a sponge-associated rare actinomycete, *Amycolatopsis* sp., led to the discovery of amycofuran (**1**), amycocyclopiazonic acid (**2**), and amycolactam (**3**). Amycofuran (**1**) is a structurally new benzofuran bearing a rhamnose sugar. Amycocyclopiazonic acid (**2**) and amycolactam (**3**) are the first bacterial indole alkaloids related to the cyclopiazonic acid class, which has previously only been found in fungi. Amycolactam showed significant cytotoxicity against gastric carcinoma cells (SNU638) and colon cancer cells (HCT116).

Our findings indicate that the relatively underinvestigated sponge-associated rare actinomycetes have great potential for the discovery of bioactive small molecules.

Acknowledgments

This work was supported by a National Research Foundation of Korea (NRF) grant funded by the Korean government (Ministry of Science, ICT and Future Planning) (M1A5A1-2010-0020429).

Author Contributions

Y. Kwon and D.-C. Oh designed the experiment, analyzed the data, and wrote the manuscript. Y. Kwon also performed most of the experiments. S.-H. Kim calculated ECD spectra and determined the absolute configurations of **1** and **3**. Y. Shin and S. K. Lee evaluated the cytotoxicity of **1**–**3**. M. Bae contributed to the determination of the absolute configuration of **2**. B.-Y. Kim performed the phylogenetic analysis of the bacterial strain. K.-B. Oh and J. Shin collected the sponge sample and contributed to writing the manuscript.

References

1. Monster, R.; Luesch, H. Marine natural products: A new wave of drugs? *Future Med. Chem*. **2011**, *3*, 1475–1489.
2. Liu, Y. Renaissance of marine natural product drug discovery and development. *J. Mar. Sci. Res. Dev.* **2012**, *2*, e106.
3. Hentschel, U.; Piel, J.; Degnan, S.M.; Taylor, M.W. Genomic insights into the marine sponge microbiome. *Nat. Rev. Microbiol*. **2012**, *10*, 641–654.
4. Xu, Y.; Kersten, R.D.; Nam, S.-J.; Lu, L.; Al-Suwailem, A.M.; Zheng, H.; Fenical, W.; Dorrestein, P.C.; Moore, B.S.; Qian, P.-Y. Bacterial biosynthesis and maturation of the didemnin anti-cancer agents. *J. Am. Chem. Soc.* **2012**, *134*, 8625–8632.
5. Bewley, C.A.; Holland, N.D.; Faulkner, D.J. Two classes of metabolites from *Theonella swinhoei* are localized in distinct populations of bacterial symbionts. *Experientia* **1996**, *52*, 716–722.
6. Andrianasolo, E.H.; Groos, H.; Goeger, D.; Musafija-Girt, M.; McPhail, K.; Leal, R.M.; Mooberry, S.L.; Gerwick, W.H. Isolation of swinholide A and related glycosylated derivatives from two field collections of marine cyanobacteria. *Org. Lett*. **2005**, *7*, 1375–1378.
7. Piel, J.; Hui, D.; Wen, G.; Butzke, D.; Platzer, M.; Fusetani, N.; Matsunaga, S. Antitumor polyketide biosynthesis by an uncultivated bacterial symbiont of the marine sponge *Theonella swinhoei. Proc. Natl. Acad. Sci. USA* **2004**, *101*, 16222–16227.
8. Fischbach, M.A.; Walsh, C.T. Assembly-line enzymology for polyketide and nonribosomal peptide antibiotics: logic machinery, and mechanisms. *Chem. Rev.* **2006**, *106*, 3468–3496.
9. Webster, N.S.; Taylor, M.W. Marine sponges and their microbial symbionts: Love and other relationships. *Environ. Microbiol*. **2012**, *14*, 335–346.

10. Wilson, M.C.; Mori, T.; Ruckert, C.; Uria, A.R.; Helf, M.J.; Takada, K.; Gernert, C.; Steffens, U.A.E.; Heycke, N.; Schmitt, S.; *et al*. An environmental bacterial taxon with a large and distinct metabolic repertoire. *Nature* **2014**, *506*, 58–62.
11. Bérdy, J. Thoughts and facts about antibiotics: Where we are now and where we are heading. *J. Antibiot.* **2012**, *65*, 385–395.
12. Vincente, J.; Stewart, A.; Song, B.; Hill, R.T.; Wright, J.L. Biodiversity of actinomycetes associated with Caribbean sponges and their potential for natural product discovery. *Mar. Biotechnol.* **2013**, *15*, 413–424.
13. Li, K.; Li, Q.-L.; Ji, N.-Y.; Liu, B.; Zhang, W.; Cao, X.-P. Deoxyuridines from the marine sponge associated actinomycete *Streptomyces microflavus*. *Mar. Drugs* **2011**, *9*, 690–695.
14. Wei, R.-B.; Xi, T.; Li, J.; Wang, P.; Li, F.-C.; Lin, Y.-C.; Qin, S. Lobophorin C and D, new kijanimicin derivatives from a marine sponge-associated actinomycetal strain AZS17. *Mar. Drugs* **2011**, *9*, 359–368.
15. Pretsch, E.; Bühlmann, P.; Affolter, C. *Structure Determination of Organic Compounds—Tables of Spectral Data*; Springer: New York, NY, USA, 2000; p. 153.
16. Berova, N.; Di Bari, L.; Pescitelli, G. Application of electronic circular dichroism in configurational and conformational analysis of organic compounds. *Chem. Soc. Rev.* **2007**, *36*, 914–931.
17. Shi, Y.-M.; Wang, L.-Y.; Zou, X.-S.; Li, X.-N.; Shang, S.-Z.; Gao, Z.-H.; Liang, C.-Q.; Luo, H.-R.; Li, H.-L.; Xiao, W.-L.; *et al*. Nortriterpenoids from *Schisandra chinensis* and their absolute configurational assignments by electronic circular dichroism study. *Tetrahedron* **2014**, *70*, 859–868.
18. Pfefferle, W.; Anke, H.; Bross, M.; Steffan, B.; Vianden, R.; Steglich, W. Asperfuran, a novel antifungal metabolite from *Aspergillus oryzae*. *J. Antibiot.* **1990**, *43*, 648–654.
19. Felix, F.; Manuel, S.J.; Emilio, Q.; Riguera, R. Determining the absolute stereochemistry of secondary/secondary diols by ^{1}H NMR: Basis and applications. *J. Org. Chem.* **2005**, *70*, 3778–3790.
20. Pabba, J.; Rempel, B.P.; Withers, S.G.; Vasella, A. Synthesis of glycaro-1,5-lactams and tetrahydrotetrazolopyridine-5-carboxylates: Inhibitors of β-D-glucuronidase and α-L-iduronidase. *Helv. Chim. Acta* **2006**, *89*, 635–666.
21. Prasad, K.R.; Pawar, A.B. Enantiospecific total synthesis of (+)-lentiginosine. *ARKIVOC* **2010**, *6*, 39–46.
22. Huang, Y.; Dalton, D.R.; Carroll, P.J. The efficient, enantioselective synthesis of aza sugars from amino acids. 1. The polyhydroxylated pyrrolidines. *J. Org. Chem*. **1997**, *62*, 372–376.
23. Sonoda, T.; Osada, H.; Uzawa, J.; Isono, K. Actiketal, a new member of the glutarimide antibiotics. *J. Antibiot*. **1991**, *44*, 160–163.
24. Suzuki, K.; Yahara, S.; Maehata, K.; Uyeda, M. Isoaurostatin, a novel topoisomerase inhibitor produced by *Thermomonospora alba*. *J. Nat. Prod*. **2001**, *64*, 204–207.
25. Simonetti, S.O.; Larghi, E.L.; Bracca, A.B.J.; Kaufman, T.S. Angular tricyclic benzofurans and related natural products of fungal origin. Isolation, biological activity and synthesis. *Nat. Prod. Rep.* **2013**, *30*, 941–969.

26. Holzapfel, C.W. Isolation and structure of cyclopiazonic acid, a toxic metabolite of *Penicillium cyclopium*. *Tetrahedron* **1968**, *24*, 2101–2119.
27. Liu, X.; Walsh, C.T. Characterization of cyclo-acetoacetyl-L-tryptophan dimethylallytransferase in cyclopiazonic acid biosynthesis: Substrate promiscuity and site directed mutagenesis studies. *Biochemistry* **2009**, *48*, 11032–11044.

Antiplatelet and Anticoagulant Effects of Diterpenes Isolated from the Marine Alga, *Dictyota menstrualis*

Laura de Andrade Moura, Ana Carolina Marqui de Almeida, Thaisa Francielle Souza Domingos, Fredy Ortiz-Ramirez, Diana Negrão Cavalcanti, Valéria Laneuville Teixeira and André Lopes Fuly

Abstract: Cardiovascular diseases represent a major cause of disability and death worldwide. Therapeutics are available, but they often have unsatisfactory results and may produce side effects. Alternative treatments based on the use of natural products have been extensively investigated, because of their low toxicity and side effects. Marine organisms are prime candidates for such products, as they are sources of numerous and complex substances with ecological and pharmacological effects. In this work, we investigated, through *in vitro* experiments, the effects of three diterpenes (pachydictyol A, isopachydictyol A and dichotomanol) from the Brazilian marine alga, *Dictyota menstrualis*, on platelet aggregation and plasma coagulation. Results showed that dichotomanol inhibited ADP- or collagen-induced aggregation of platelet-rich plasma (PRP), but failed to inhibit washed platelets (WP). In contrast, pachydictyol A and isopachydictyol A failed to inhibit the aggregation of PRP, but inhibited WP aggregation induced by collagen or thrombin. These diterpenes also inhibited coagulation analyzed by the prothrombin time and activated partial thromboplastin time and on commercial fibrinogen. Moreover, diterpenes inhibited the catalytic activity of thrombin. Theoretical studies using the Osiris Property Explorer software showed that diterpenes have low theoretical toxicity profiles and a drug-score similar to commercial anticoagulant drugs. In conclusion, these diterpenes are promising candidates for use in anticoagulant therapy, and this study also highlights the biotechnological potential of oceans and the importance of bioprospecting to develop medicines.

Reprinted from *Mar. Drugs*. Cite as: de Andrade Moura, L.; de Almeida, A.C.M.; Domingos, T.F.S.; Ortiz-Ramirez, F.; Cavalcanti, D.N.; Teixeira, V.L.; Fuly, A.L. Antiplatelet and Anticoagulant Effects of Diterpenes Isolated from the Marine Alga, *Dictyota menstrualis*. *Mar. Drugs* **2014**, *12*, 2471–2484.

1. Introduction

Nowadays, cardiovascular diseases (thrombosis, venous thromboembolism, stroke and pulmonary embolism) represent the leading cause of disability and mortality worldwide. Such pathologies may occur due to dysfunctions in the hemostatic system, involving the platelets and blood coagulation components [1]. The hemostasis system consists of a complex process to maintain blood flow, but also causes bleeding to stop. Hemostasis is divided into primary and secondary hemostasis, where a platelet plug formation (primary hemostasis) occurs, and the secondary one is the coagulation system, which is composed of a series of enzymes and co-factors (Ca^{+2}, platelet phospholipids, vitamin K) to activate thrombin to form a stable fibrin clot. Moreover, thrombin also has a positive feedback function, promoting the activation of specific

coagulation factors (factor XI and co-factors V and VIII), stabilizing the fibrin clot, and it also induces platelet aggregation, thereby influencing the formation of plug formation. After a vessel injury, hemostasis has three steps: (1) vasoconstriction; (2) temporary blockage by the platelet plug; and (3) blood coagulation by the forming of a clot that seals the hole until the tissues are repaired. Traditionally, the coagulation cascade is divided into intrinsic and extrinsic coagulation pathways; but nowadays, this model is only useful for *in vitro* diagnostic purposes [2].

The current antithrombotic therapies include vitamin K antagonists, direct thrombin inhibitors, pentasaccharide oral anticoagulants and/or antiplatelet drugs [3]. These therapies have some benefits, but they also have limitations, such as narrow therapeutic windows and indices, resulting in dietary or drug interactions, so that they require monitoring and may produce serious side effects, including gastric disorders, bleeding and thrombocytopenia [4]. Heparin and its analogues are also included among such drugs associated with medication risks [5]. Therefore, alternative antithrombotic therapies are under extensive investigation, and many substances from natural sources are being isolated and studied to counteract these side effects [6].

Marine organisms produce numerous and chemically complex products, identified as secondary metabolites, which display ecological functions, such as defense against herbivores and predators, prevention of biofouling and mediation of symbiosis and reproduction [7]. Apart from these ecological actions, some molecules also exhibit a range of pharmacological effects [8,9], including anti-inflammatory [10], antiviral [11], antiophidic [12], antilonomic [13] or anticoagulant properties [14]. In addition, other natural products have been isolated with antithrombotic activities, such as sulfated galactans from the red alga, *Botryocladia occidentalis* [15], heterofucans from the brown alga, *Canistrocarpus cervicornis* [16], a triterpene saponin from the fruits of *Ilex paraguariensis* [17] and a peptide from the Australian sponge, *Lamellodysidea chlorea* [18]. However, the inhibitory mechanisms of these molecules are still under investigation, with some speculation that they bind directly to thrombin, factor Xa, antithrombin and/or a heparin cofactor II [19].

It has already been shown that crude extracts of the marine brown alga, *Dictyota menstrualis*, collected in different areas of the Brazilian coast and prepared in different polarity solvents, exhibited antiplatelet and anticoagulant properties [20,21]. Previous results have shown that the diterpenes, (6*R*)-6-hydroxydichotoma-3,14-diene-1,17-dial, called pachydictyol A (**1**), and its acetate derivative, isopachydictyol A (**2**), as well as 6-Hydroxy-dichotomano-3,14-dieno-1,17-dial (called dichotomanol) (**3**), isolated form *D. menstrualis*, inhibit the human immunodeficiency virus type-1 (HIV-1) replication *in vitro* [22,23]. Moreover, their mechanisms of action and toxicity have been studied, and the results showed that such diterpenes do not induce any cytotoxicity or lethality in mice. Now, the objective of the present study was to evaluate the effects of the diterpenes, pachydictyol A (**1**), isopachydictyol A (**2**) and dichotomanol (**3**) (Figure 1), on platelet aggregation and plasma coagulation.

Figure 1. The chemical structure of the diterpenes. **1**, **2** and **3** represent the structure of pachydictyol A, isopachydictyol A and dichotomanol, respectively.

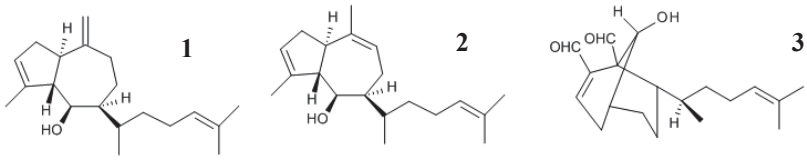

2. Results and Discussion

Hemostasis is a physiologically dynamic process that involves platelet aggregation and blood coagulation and has a major function in the formation of a thrombus, as well as in the prevention of hemorrhage in the case of a vessel injury [24]. The coagulation system is divided into three phases, called initiation, amplification and propagation, which lead to an activation of thrombin, which is a pivotal enzyme generating a fibrin net and activating platelet aggregation. Platelets are equally important to the formation of the thrombus, and after their activation by an agonist (such as collagen, ADP and thrombin), they contribute to the amplification of the blood coagulation system [25,26]. Once uncontrolled, thrombus generation may lead to vascular disturbances and death. Blood disorders represent a global public health problem, and there is not yet a drug sufficiently active, efficient and safe for managing thrombotic disorders [1]. As a result of these problems, new, safer and more effective antithrombotic molecules need to be discovered or designed, but without any, or at least low, side effects.

2.1. Effect of Diterpenes on Platelet Aggregation

Dichotomanol (0.18 mM–1.38 mM) inhibited platelet aggregation in platelet-rich plasma (PRP) induced by ADP (15 µM) or collagen (16 µg/mL), in a concentration-dependent manner, with IC_{50} values of 0.31 mM and 1.06 mM, respectively (Figure 2A). In contrast, at the highest tested concentration of pachydictyol A/isopachydictyol A (1.38 mM), inhibitions of only 15% and 20% were achieved for collagen- and ADP-induced aggregation in PRP, respectively [27]. Therefore, IC_{50} values could not be determined for the pachydictyol A/isopachydictyol A with PRP. However, when tested on washed platelets (WP), pachydictyol A/isopachydictyol A (0.18 mM–0.7 mM) inhibited aggregation induced by collagen (IC_{50} 0.12 mM) or thrombin (IC_{50} 0.25 mM) (Figure 2B); while dichotomanol (0.32 mM) inhibited only 15% and 30% aggregation induced by collagen or thrombin, respectively [27]. Thus, IC_{50} could not be achieved for dichotomanol on WP. Thrombin was only tested on WP, because it also triggers plasma coagulation and aggregation cannot be monitored. In this way, PRP experiments cannot be performed using thrombin.

ADP, collagen and thrombin bind to different receptors located at the platelet membrane and trigger platelet aggregation through different intracellular pathways [28]. Thus, diterpenes may differentially interact with these receptors, resulting in varying inhibitory profiles in platelet aggregation induced by each agonist. Other factors in the plasma, such as fibrinogen and the Von Willebrand factor, which also participate in platelet aggregation [29], may also have interfered

with the inhibitory effect of the diterpenes upon aggregation either with PRP or WP. When testing an effect of any molecules on aggregation, it is mandatory to test them on PRP and WP in order to evaluate if any component of plasma (proteins, lipids, sugars, metals) will interfere on the effect of such molecules, as well as making possible the investigation of a mechanism of action of a molecule on platelets. Pachydictyol A/isopachydictyol A or dichotomanol did not induce the aggregation of platelets, even when tested at the highest concentration (1.38 mM, [27]).

Figure 2. The effect of diterpenes on platelet aggregation. (**A**) Platelet-rich plasma (PRP) was incubated with different concentrations of dichotomanol for 2 min, while stirring, at 37 °C. Then, 16 µg/mL collagen (●) or 15 µM ADP (○) were added to induce platelet aggregation. (**B**) Different concentrations of pachydictyol A/isopachydictyol A were incubated with washed platelets (WP) for 2 min, while stirring, at 37 °C, and then 16 µg/mL collagen (■) or 10 nM thrombin (○) were added to induce aggregation. For both panels, one hundred percent of the platelet aggregation was obtained with supramaximal (able to give a platelet aggregation 70%–80%) concentrations of the agonists in the presence of dimethylsulfoxide (DMSO) after 6 min of reaction. Data are expressed as the means ± SEM of two individual experiments (n = 3).

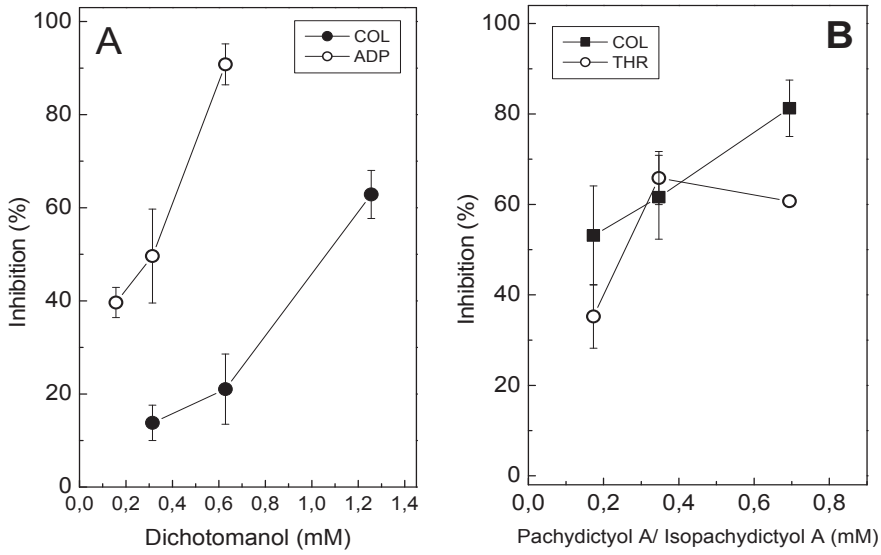

Figures 3 and 4 show typical patterns of platelet aggregation on PRP (Figure 3) or WP (Figure 4) in the presence of increasing concentrations of diterpenes. Although diterpenes have inhibited aggregation, shape-change reactions (indicated by the initial decrease in light transmission) were not prevented (Figures 3 and 4). Shape-change is not the second wave of aggregation, as well as it is not a prerequisite for platelet aggregation. Platelet aggregation occurs independently of shape-change, and that shape change is not necessarily followed by aggregation. Some authors hypothesize that the initial changes in light transmission could be due to the microaggregation of the platelets.

Figure 3. Typical patterns of platelet aggregation with PRP. (**A**,**B**) PRP was incubated for 2 min at 37 °C while stirring with 0.69 mM (Line b) or with 1.38 mM (Line c) of pachydictyol A/isopachydictyol A, then 16 µg/mL of collagen (upper panel) or 15 µM of ADP (lower panel) were added to induce aggregation. (**C**,**D**) PRP was incubated as above, with 0.31 mM (Line b), 0.62 mM (Line c) or with 1.25 mM (Line d) of dichotomanol, and then collagen (upper panel) or ADP (lower panel) was added to the medium. For all panels, Lines a represent PRP incubated with 1% DMSO (v/v, final concentration). The arrows mark the addition of agonists.

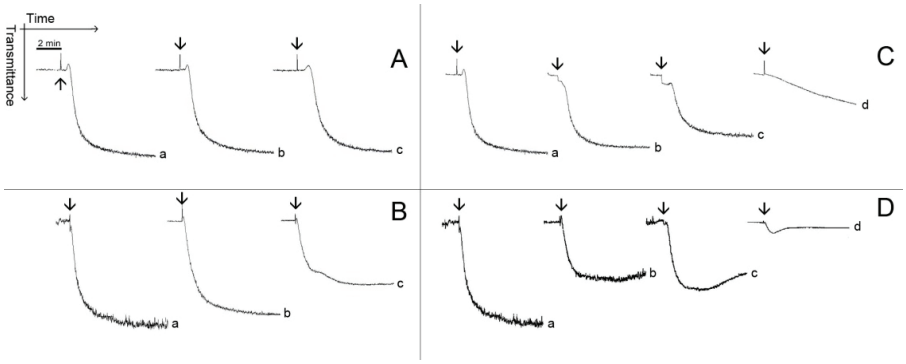

2.2. Effect of Diterpenes on Coagulation

None of diterpenes exerted a pro-coagulant activity on plasma or on commercial fibrinogen, but they did inhibit coagulation. The pachydictyol A/isopachydictyol A did not prevent coagulation in the prothrombin time test (PT) and moderately delayed coagulation in the activated partial thromboplastin time test (aPTT); while dichotomanol moderately delayed coagulation in the PT and more significantly in the aPTT test (Table 1). All the diterpenes inhibited the coagulation of fibrinogen (FC) induced by thrombin (Table 1).

2.3. Effect of Diterpenes on Thrombin Activity

Pachydictyol A/isopachydictyol A and Dichotomanol alone inhibited platelet aggregation (Figures 2–4) and coagulation (Table 1). This inhibitory effect of diterpenes may be due to their ability to inhibit the catalytic activity of thrombin. Therefore, the effect of diterpenes on the enzymatic activity of thrombin was performed using a commercial chromogenic substrate, S-2238, that is specific for the thrombin enzyme and regularly used to evaluate its catalytic activity. As seen in Figure 5A, diterpenes inhibited the enzymatic activity of thrombin, since the hydrolysis of S-2238 by thrombin was diminished. At 0.35 mM, pachydictyol A/isopachydictyol A failed to inhibit hydrolysis, while dichotomanol had 50% inhibition (Figure 5A). However, at higher concentrations (0.68 mM), all diterpenes recorded over 50% inhibition.

Figure 4. Typical patterns of aggregation with washed platelets. (**A**,**B**) Washed platelets (WP) were incubated for 2 min at 37 °C while stirring with 0.173 mM (Line b), 0.347 (Line c) and 0.694 (Line d) of Pachydictyol A/isopachydictyol A, then 16 µg/mL collagen (upper panel) or 10 nM thrombin (lower panel) was added to induce aggregation. (**C**,**D**) WP were incubated as above with dichotomanol (0.34 mM), and then collagen (upper panel) or thrombin (lower panel) was added to the medium. For all panels, Lines a represent WP incubated with 1% DMSO (v/v, final concentration). The arrows mark the addition of agonists.

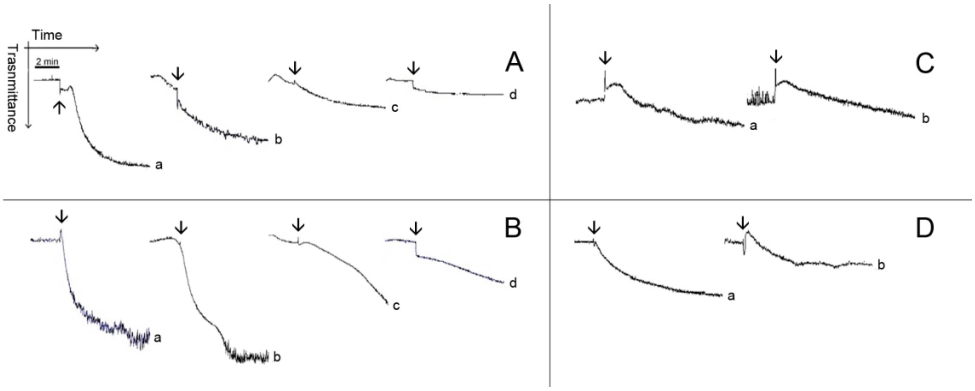

Table 1. The effect of diterpenes on coagulation time analyzed by different methods. For prothrombin time (PT), diterpenes were incubated with plasma for 10 min at 37 °C, and then thromboplastin was added to induce coagulation. For the activated partial thromboplastin time (aPTT), diterpenes were incubated with plasma plus cephalin for 10 min at 37 °C, and then, $CaCl_2$ (8.3 mM) was added to induce coagulation. For fibrinogen coagulation (FC), diterpenes were incubated for 10 min at 37 °C with fibrinogen (2 mg/mL), and then, thrombin (10 nM) was added to induce coagulation. Results are expressed as the means ± SEM of two individual experiments (n = 8). PAC/ISO, pachydictyol A/isopachydictyol A; DIC, dichotomanol. * $p < 0.05$ when compared with NaCl or DMSO.

Samples	Concentration	Coagulation time (s)		
		PT	aPTT	FC
NaCl	150 mM	21.6 ± 0.5	62.90 ± 1.3	26.4 ± 0.5
DMSO	1% (v/v)	23.3 ± 0.3	65.75 ± 1.0	34.1 ± 1.4
	2% (v/v)	26.7 ± 0.4	73.6 ± 1.8	40.8 ± 1.3
PAC/ISO	0.7 mM	23.9 ± 1.0	72.8 ± 1.5 *	65.3 ± 3.5 *
	1.4 mM	26.9 ± 0.7	87.6 ± 0.9 *	66.7 ± 0.8 *
DIC	0.7 mM	32.4 ± 1.8 *	101.8 ± 4.9 *	47.3 ± 1.6 *
	1.3 mM	41.0 ± 2.6 *	139.9 ± 5.8 *	86.4 ± 2.6 *

Figure 5. (**A**) Pachydictyol A/isopachydictyol A (Group 1) and dichotomanol (Group 2) were incubated with thrombin (40 nM) for 10 min at 37 °C. After, S-2238 (0.5 mM) was added to the medium, and the reaction was monitored at A 405 nm during 1200 s. One hundred percent of the activity was determined as the difference between values at Absorbance 405 nm obtained at the end and at the beginning of the reaction. Data are expressed as means ± SEM of two individual experiments (n = 4); (**B**) The theoretical toxicity risk was evaluated for pachydictyol A/isopachydictyol A (Column 1), for dichotomanol (Column 2), acetyl salicylic acid (Column 3) and warfarin (Column 4). The risks of mutagenicity (black columns), tumorigenicity (white columns), irritability (gray columns) and reproductive negative effects (striped columns) are shown on the Y-axes as numbers and represent one for low, two for medium and three for high.

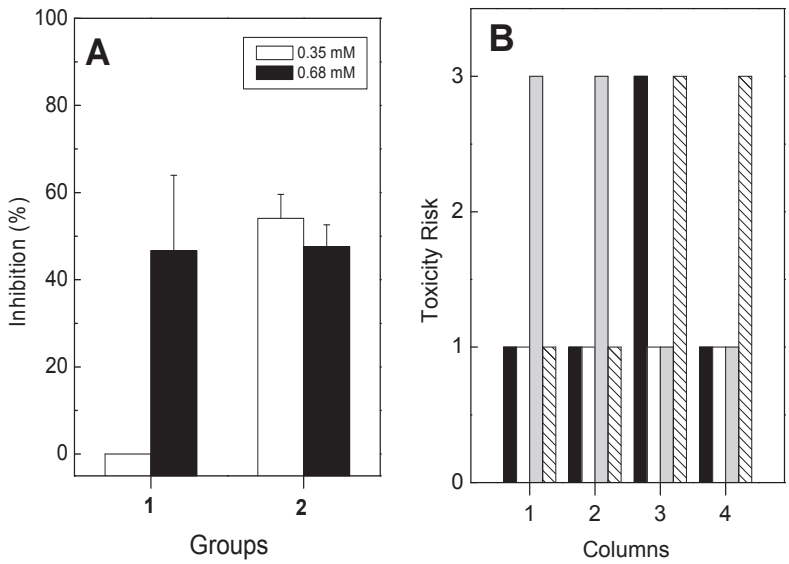

The anticoagulant effect of diterpenes suggests that pachydictyol A/isopachydictyol A interferes only in the amplification pathway of the coagulation system, while dichotomanol acts in both, the initiation and the augmentation processes. Moreover, the diterpenes also inhibited the enzymatic activity of thrombin that is a serine protease involved in blood coagulation and platelet aggregation [24]. Thrombin is also responsible for converting fibrinogen into insoluble fibrin, as well as activating other blood coagulation factors (factors XI, VIII and V), thus reducing blood loss. Besides acting on hemostasis, thrombin has a pro-inflammatory action, stimulating the proliferation and migration of smooth muscle cells and apoptosis [30,31]. However, all of those effects are not entirely dependent on the active site of thrombin, since two positively charged domains, called Exosites 1 and 2, participate, as well. The former binds to fibrinogen, platelet receptor PAR-1 and factors V and Va, and the latter is referred to as the heparin-binding site [32]. The interaction of some anticoagulant molecules, such as hirudin, with the thrombin exosites does not inhibit its catalytic activity [33]. The pachydictyol A/isopachydictyol A mixture and dichotomanol inhibited coagulation and platelet aggregation induced by thrombin, and it could be speculated that this inhibitory effect

may be due to their ability to inhibit the catalytic activity of thrombin, measured by using a specific chromogenic substrate, S-2238, for such an enzyme [34]. In some cases, a substance with high anticoagulant activity, but a low antiplatelet effect, or the opposite, or even a molecule that does not inhibit all the signaling pathway of platelet aggregation or the coagulation cascade, would be interesting, because the hemorrhagic risk can be diminished. Hemorrhage is one of the most dangerous side effects of current antithrombotic drugs [35].

A candidate molecule to be used as a drug should be safe and not have any toxicity to humans. The theoretical toxicity study is an *in silico* evaluation to predict the toxicity risks of molecules based on their chemical structure. Moreover, it describes the disposition of a pharmaceutical compound within an organism. Four criteria are taken into account—absorption, distribution, metabolism and excretion—because they all influence drug levels and the kinetics of the drug exposure to tissues and, hence, the influence of the action or performance of the molecule as a drug. The theoretical toxicity risks of the diterpenes (pachydictyol A/isopachydictyol A (PAC/ISO) and dichotomanol (DIC)) revealed no theoretical toxicity risks for all the parameters (mutagenicity, tumorigenicity and reproductive negative effects) except for a high irritant profile (Figure 5B). Some commercial antithrombotic drugs, such as acetyl salicylic acid (Figure 5B, column 3) and warfarin (Figure 5B, column 4), had high theoretical mutagenic or reproductive effects, but lacked tumorigenic or irritant activity. The drug-score is a multi-parameter theoretical and structure based value, ranging from zero to one, that may be used to judge the compound's overall potential to qualify as a drug. Moreover, such theoretical approaches are important tools as a first step to drug discovery, because they may reduce the number of test animals required. The drug-score of the diterpenes were also compared with two commercial antithrombotic drugs, acetyl salicylic acid and warfarin, and such theoretical evaluation of diterpenes regarding toxicity and drug-score showed a low toxicity profile and drug-score values similar or better than acetyl salicylic acid and warfarin [27]. In this way, the theoretical results reinforce the potential use of these diterpenes as antithrombotic compounds.

3. Experimental Section

3.1. Algae Collection and Isolation of Diterpenes

Specimens of *Dictyota menstrualis* (Dictyotaceae, Phaeophyta) were collected by snorkeling during July, 2010, at Praia do Forno, in the city of Armação de Búzios, located to the north of Rio de Janeiro State, Brazil (22°45′42″ S and 41°52′27″ W), at depths ranging from 0.3 to 2 m. The algae were washed with local sea water and separated from sediments, epiphytes and other associated organisms. The air-dried algal material (95 g) was extracted in 100% dichloromethane (CH_2Cl_2) exhaustively at room temperature, yielding 5 g of CH_2Cl_2 crude extract. The mixture of the diterpenes, pachydictyol A (**1**)/isopachydictyol A (**2**) (45 mg) and the 6-hydroxy-dichotomano-3,14-diene-1,17-dial (also called dichotomanol) (**3**) (21 mg) were obtained and identified according to [36], with some modifications. The crude extract of alga (5 g) was subjected to silica gel (0.015–0.045 mm), eluted with CH_2Cl_2:AcOEt (8:2), CH_2Cl_2:AcOEt (1:1), AcOEt and acetone. The Fractions **2** and **3** (165 mg) containing a mixture (55 mg) of pachydictyol A/isopachydictyol A

were further purified by silica gel-column chromatography (eluent: *n*-hexane) obtaining pachydictyol A/isopachydictyol A (45 mg). Fraction **4** (300 mg), enriched in dichotomanol, was subjected to a reverse-phase (C18) chromatography eluted with CH_3CN, yielding an impure dichotomanol (41 mg), which was further purified by washing with petroleum ether (21 mg). Their structures were analyzed by NMR spectroscopy and are shown in Figure 1. Finally, the diterpenes were dissolved in dimethylsulfoxide (DMSO, 30% v/v) to perform the biological assays.

3.2. Platelet Aggregation Assays

The platelet aggregation assays were carried out according to Fuly *et al.* [37], with some modifications, using platelet-rich plasma (PRP) or washed platelets (WP) from healthy volunteer donors. PRP was prepared by the centrifugation of citrated (0.31%, v/v) human whole blood (340 g for 12 min) at room temperature. For WP, blood was collected in EDTA (5 mM) and centrifuged (340 g for 12 min). Then, PRP was further centrifuged at 1300× *g* for 15 min. The pelleted platelets were then resuspended in a calcium-free Tyrode's solution containing 0.35% w/v BSA and 0.1 mM EGTA (final concentrations), pH 6.5, and washed twice by centrifugation. The final pellet was resuspended in Tyrode-BSA, pH 7.5, without EGTA (TG) and was adjusted to give 3–4 × 10^5 platelets/μL. Platelet aggregation was measured turbidimetrically (the increasing light transmission of the platelet suspension) using a Whole Blood Lumi-Aggregometer (Chrono-Log Corporation, Havertown, Pennsylvania, USA). Assays were performed at 37 °C in siliconized glass cuvettes using 300 μL of PRP or WP, while stirring, and aggregation was triggered after incubation for 2 min. One hundred percent (100%) of aggregation was taken as the full platelet response obtained with a supramaximal concentration of agonists, ADP, collagen (purchased from Chrono-Log Corporation, Havertown, Pennsylvania, USA) or human alpha-thrombin (from Haematologic Technologies Inc., Vermont, USA), determined 6 min after their addition, and 0% (base line) platelet aggregation was the light transmittance recorded in the presence of PRP or WP alone or after addition of TG or vehicle (1% v/v DMSO). Different concentrations of diterpenes were incubated with PRP or WP for 2 min at 37 °C while stirring, and then, platelet aggregation was triggered by adding agonists, ADP (15 μM), collagen (16 μg/mL) or thrombin (10 nM). Inhibitory effects on platelet aggregation were expressed as the percentual difference in the maximal responses obtained from the platelet in the presence or in the absence of diterpenes, challenged with agonists. The inhibitory concentration (IC_{50}) was designed as the concentration of diterpenes able to inhibit 50% of the platelet aggregation. Control experiments were performed in the presence or the absence of DMSO (1% v/v, final concentration).

3.3. Coagulation Assays

Prothrombin time (PT) and activated partial thromboplastin time (aPTT) assays were performed according to the manufacturer's instructions (Wiener laboratories, Rosario, Argentina). For the PT test, diterpenes were incubated with plasma (50 μL) during 10 min at 37 °C, and then, 100 μL of pre-warmed thromboplastin with calcium were added to initiate coagulation. For the aPTT test, diterpenes were incubated with plasma plus 100 μL of the aPTT reagent, cephalin plus kaolin, for

10 min at 37 °C, with a final volume of 200 µL, and the reaction was started by adding $CaCl_2$ (8.3 mM, final concentration). For fibrinogen coagulation (FC), diterpenes were incubated for 10 min at 37 °C with commercial fibrinogen (2 mg/mL) in a final volume of 100 µL, and coagulation was then triggered by adding thrombin (10 nM). Coagulation assays were performed on a Multichannel Coagulometer (Amelung, model KC4A, Labcon, Germany), and coagulation time was recorded in seconds. Plasma was obtained from a pool of citrated healthy volunteer donators (diluted with an equal volume of saline) kindly donated from the public blood bank of the University Hospital Antônio Pedro of the Federal Fluminense University. The collection of blood has been approved by the ethics committee of the hospital. Control experiments were performed by mixing DMSO with plasma or fibrinogen, instead of diterpenes.

3.4. Hydrolytic Assay

Hydrolysis of the chromogenic substrate, H-D-Phe-pipecolyl-Arg-pNA.2HCl (S-2238), bought from Chromogenix (Milan, Italy), was monitored using a microplate reader (Thermomax, Molecular Devices, Menlo Park, CA, USA) at A405 nm. The diterpenes were incubated with thrombin (40 nM, final concentration) for 10 min at 37 °C, and then, the reaction was triggered by adding S-2238 (0.1 mM, final concentration). The reaction was monitored during 20 min at 37 °C. Control experiments were performed by incubating thrombin with either DMSO (1% v/v) or saline.

3.5. Theoretical Toxicity Study

The theoretical studies of toxicity and drug-score were performed using the software, Osiris Property Explorer [38], and four theoretical toxicity risks were calculated: mutagenicity, tumorigenicity, irritability and reproductive negative effects. They were calculated based on the structure of molecules and were compared with known structures obtained from a databank. The theoretical parameter drug-score was calculated, as well. The drug-score is a multi-parameter value that combines drug likeness, molecular weight and toxicity risks in one handy value in order to be used to judge the molecule's overall potential to qualify as a drug.

3.6. Statistical Analysis

The results were expressed as the means ± standard error (SEM) obtained with the number of experiments performed indicated. The statistical significance of differences among experimental groups was evaluated using the Student *t*-test. *p*-values of <0.05 were considered statistically significant.

4. Conclusions

Taken together, these algal diterpenes have revealed antithrombotic properties, and the results have shown the value of bioprospecting research for discovering novel products with promising pharmacological effects for drug development. However, it is important to state that the theoretical or *in vivo* toxicity is not fully reliable, nor does it guarantee that diterpenes are completely free of any toxic effect, but rather should be used as a base to guide the selection of compounds for future

assays. Natural products, such as diterpenes, could also be used to help to design structure-based anticoagulant or antiplatelet drugs in order to improve antithrombotic therapies, since diterpenes have low or no toxicity and do not promote side effects. Moreover, agents from non-mammalian sources may diminish the risk of contamination with a foreign body or pathogenic substances. On the other hand, commercial therapeutic drugs usually promote side effects, such as hemorrhage, hypotension and thrombocytopenia.

Acknowledgments

This work was supported by grants from the International Foundation for Science (IFS) (Grant F/4571-1) and Brazilian funding agencies: Fundação de Amparo à Pesquisa do Estado do Rio de Janeiro Carlos Chagas Filho (FAPERJ), Conselho Nacional de Desenvolvimento Científico e Tecnológico (CNPq), Coordenação de Aperfeiçoamento de Pessoal de Nível Superior (CAPES) and Universidade Federal Fluminense/Pró-reitoria de Pós-graduação, Pesquisa e Inovação (UFF/PROPPI). The authors want to thank Norman Ratcliffe, from Swansea University (Swansea, UK), for kindly revising the manuscript.

Author Contributions

Laura de Andrade Moura performed platelet and coagulation experiments as well as theoretical toxicity studies and helped writing the paper. Ana Carolina Marqui de Almeida performed hydrolytic assays and helped in the theoretical toxicity studies. Thaisa Francielle Souza Domingos, Fredy Ortiz-Ramirez, Diana Negrão Cavalcanti and Valéria Laneuville Teixeira performed algae collection and identification and isolation of diterpenes. André Lopes Fuly wrote of the paper, supervised experiments and students and was the mentor of paper.

Conflicts of Interest

The authors declare no conflict of interest.

References

1. Agnelli, G. Current issues in Anticoagulation. *Pathophysiol. Haemost. Thromb.* **2005**, *34*, 2–9.
2. Sattari, M.; Lowenthal, D.T. Novel oral anticoagulant in development: Dabigatran, Rivaroxaban and Apixaban. *Am. J. Ther.* **2011**, *18*, 332–338.
3. Steven, K.A. Haemostasis. *Medicine* **2013**, *41*, 208–211.
4. Lopes, R.D. Antiplatelet agents in cardiovascular disease. *J. Thromb. Thrombol.* **2011**, *31*, 306–309.
5. Reis, A.M.M.; Marques, T.C.; Opitz, S.P.; Silva, A.E.B.C.; Gimenes, F.R.E.; Teixeira, T.C.A.; Lima, R.E.F.; Cassiani, S.H.B. Errors in medicine administration—Profile of medicines: Knowing and preventing. *Acta Paul. Enferm.* **2010**, *23*, 181–186.
6. Nutescu, E.A.; Shapiro, N.L.; Chevalier, A.; Amin, A.N. A pharmacological overview of current and emerging anticoagulants. *Clev. Clin. J. Med.* **2005**, *72*, 2–6.

7. Teixeira, V.L. Produtos naturais marinhos. In *Biologia Marinha*, 2nd ed.; Pereira, R.C., Soares-Gomes, A., Eds.; Editora Interciência: Rio de Janeiro, Brasil, 2009; pp. 443–472.
8. Mayer, A.M.S.; Rodrígez, A.D.; Berlink, R.G.S.; Hamann, M.T. Marine compounds with anthelmintic, antibacterial, anticoagulant, antifungal, antiinflammatory, antimalarial, antiprotozoal, antituberculosis, and antiviral activities; affecting the cardiovascular, immune and nervous systems, and other miscellaneous mechanisms of action. *Biochim. Biophys. Acta* **2009**, *1790*, 283–308.
9. Molinski, T.F.; Dalisay, D.S.; Lievens, S.L.; Saludes, J.P. Drug development from marine natural products. *Nat. Rev. Drug Discov.* **2009**, *8*, 69–85.
10. Cumashi, A.; Ushakova, N.A.; Preobrazhenskaya, M.E.; D'Incecco, A.; Piccoli, A.; Totani, L.; Tirani, N.; Morozevich, G.E.; Berman, A.E.; Bilan, M.I.; *et al.* A comparative study of the anti-inflammatory, anticoagulant, antiangiogenic and antiadhesive activities of nine different fucoidans from brown seaweeds. *Glycobiology* **2007**, *17*, 541–552.
11. Souza, T.M.; Abrantes, J.L.; Epifanio, R.A.; Leite Fontes, C.F.; Frugulhetti, I.C.P.P. The alkaloid 4-methylaaptamine isolated from the sponge *Aaptos aaptos* impairs Herpes simplex virus type 1 penetration and immediate-early protein synthesis. *Planta Med.* **2007**, *73*, 200–205.
12. Domingos, T.F.S.; Vallim, M.A.; Carvalho, C.; Sanchez, E.F.; Teixeira, V.L.; Fuly, A.L. Anti-snake venom effect of secodolastane diterpenes isolated from Brazilian marine brown alga *Canistrocarpus cervicornis* against *Lachesis mut*a venom. *Rev. Bras. Farmacogn.* **2011**, *21*, 234–238.
13. Domingos, T.F.S.; Carvalho, C.; Moura, L.A.; Teixeira, V.L.; Pereira, R.C.; Bianco, E.M.; Ferreira, W.J.; Ramos, C.J.B.; de Miranda, A.L.P.; Melo, P.A.; *et al.* Antilonomic effects of brazilian brown seaweeds extracts. *Nat. Prod. Commun.* **2009**, *4*, 1075–1078.
14. Moura, L.A.; Bianco, E.M.; Pereira, R.C.; Teixeira, V.L.; Fuly, A.L. Anticoagulation and antiplatelet effects of a dolastane diterpene isolated from the marine brown alga *Canistrocarpus cervicornis*. *J. Thromb. Thrombol.* **2011**, *31*, 235–240.
15. Melo, F.R.; Mourão, P.A. An algal sulfated galactan has unusual dual effect on venous thrombosis due to activation of factor XII and inhibition of the coagulation proteases. *Thromb. Haemost.* **2008**, *99*, 531–538.
16. Camara, R.B.G.; Costa, L.S.; Fidelis, G.P.; Nobre, L.T.D.B.; Dantas-Santo, N.; Cordeiro, S.L.; Costa, M.S.S.P.; Alves, L.G.; Rocha, H.A.O. Heterofucans from the brown seaweed *Canistrocarpus cervicornis* with anticoagulant and antioxidant activities. *Mar. Drugs* **2011**, *9*, 124–138.
17. Dahmer, T.; Berger, M.; Barlette, A.G.; Reck, J., Jr.; Segalin, J.; Verza, S.; Ortega, G.G.; Gnoatto, S.C.B.; Guimarães, J.A.; Verli, H.; *et al.* Antithrombotic effect of Chikusetsusaponin Iva isolated from *Ilex paraguariensis* (Maté). *J. Med. Food* **2012**, *15*, 1–8.
18. Carroll, A.R.; Buchanan, M.S.; Edser, A.; Hyde, E.; Simpson, M.; Quinn, R.J. Dysinosins B–D, inhibitors of factor VIIa and thrombin from the Australian sponge *Lamellodysidea chlorea*. *J. Nat. Prod.* **2004**, *67*, 1291–1294.

19. Melo, F.R.; Pereira, M.S.; Foguel, D.; Mourao, P.A. Antithrombin-mediated anticoagulant activity of sulfated polysaccharides: Different mechanisms for heparin and sulfated galactans. *J. Biol. Chem.* **2004**, *279*, 20824–20835.
20. Ortiz-Ramirez, F.A.; Cavalcanti, D.N.; Villaça, R.C.; de Paula, J.C.; Valentin, Y.Y.; Teixeira, V.L. Chemical variations in the diterpenes from the Brazilian brown alga *Dictyota menstrualis* (Dictyotaceae, Phaeophyta). *Nat. Prod. Commun.* **2008**, *11*, 1879–1884.
21. Moura, L.A.; Ortiz-Ramirez, F.A.; Cavalcanti, D.N.; Ribeiro, S.M.; Muricy, G.; Teixeira, V.L.; Fuly, A.L. Evaluation of marine brown algae and sponges from Brazil as anticoagulant and antiplatelet products. *Mar. Drugs* **2011**, *9*, 1346–1358.
22. Pereira, H.S.; Leão-Ferreira, L.R.; Moussatché, N.; Teixeira, V.L.; Cavalcanti, D.N.; Costa, L.J.; Diaz, R.; Frugulhetti, I.C. Antiviral activity of diterpenes isolated from the Brazilian marine alga *Dictyota menstrualis* against human immunodeficiency virus type 1 (HIV-1). *Antivir. Res.* **2004**, *64*, 69–76.
23. Pereira, H.S.; Leão-Ferreira, L.R.; Moussatché, N.; Teixeira, V.L.; Cavalcanti, D.N.; Costa, L.J.; Diaz, R.; Frugulhetti, I.C.P. Effects of diterpenes isolated from the Brazilian marine alga *Dictyota menstrualis* on HIV-1 reverse trancriptase. *Planta* **2005**, *2*, 1019–1024.
24. Esmon, C.T. Regulation of blood coagulation. *Biochim. Biophys. Acta* **2000**, *7*, 349–360.
25. Andrews, R.K.; Berndt, M.C. Platelet physiology and thrombosis. *Thromb. Res.* **2004**, *114*, 447–453.
26. Costello, M.J.; Coll, M.; Danovaro, R.; Halpin, P.; Ojaveer, H.; Milolasvich, P. A census of marine biodiversity knowledge, resources, and future challenges. *PLoS One* **2010**, *5*, e12110.
27. Moura, L.A.; Fuly, A.L. Departamento de Biologia Molecular e Celular, Instituto de Biologia, Universidade Federal Fluminense, Niterói, RJ, Brazil. Antiplatelet and anticoagulant Effects of Diterpenes Isolated from the Marine Alga, *Dictyota menstrualis*. Unpublished work, 2014.
28. Surin, W.R.; Barthwal, M.K.; Dikshit, M. Platelet collagen receptors, signaling and antagonism: Emerging approaches for the prevention of intravascular thrombosis. *Thromb. Res.* **2008**, *122*, 786–803.
29. Rivera, J.; Lozano, M.L.; Navarro-Núñez, L.; Vicente, V. Platelet receptors and signaling in the dynamics of thrombus formation. *Haematologica* **2009**, *94*, 700–711.
30. Borissoff, J.I.; Spronk, H.M.; Heeneman, S.; Ten-Cate, H. Is thrombin a key player in the 'coagulation-atherogenesis' maze? *Cardiovasc. Res.* **2009**, *82*, 392–403.
31. Borissoff, J.I.; Spronk, H.M.; Ten-Cate, H. The hemostatic system as a modulator of atherosclerosis. *N. Engl. J. Med.* **2011**, *364*, 1746–1760.
32. Sheehan, J.P.; Sadler, J.E. Molecular mapping of the heparin binding exosite of thrombin. *Proc. Natl. Acad. Sci. USA* **1994**, *91*, 5518–5522.
33. Liu, L.W.; Vu, T.K.H.; Esmon, C.T.; Coughlin, S.R. The region of the thrombin receptor resembling hirudin binds to thrombin and alters enzyme specificity. *J. Biol. Chem.* **1991**, *266*, 16977–16980.
34. Axelsson, G.; Korsan-Bengtsen, K.; Waldenström, J. Prothrombin determination by means of chromogenic peptide substrate. *Thromb. Haemost.* **1976**, *36*, 517–524.

35. Guerrouij, M.; Uppal, C.S.; Alklabi, A.; Douketis, J.D. The clinical impact of bleeding during oral anticoagulant therapy. *J. Thromb. Thrombolysis* **2011**, *31*, 419–423.
36. Teixeira, V.L.; Cavalcanti, D.N.; Pereira, R.C. Chemotaxonomic studies of the diterpenes from the brown algae. *Dictyota menstrualis. Biochem. Syst. Ecol.* **2001**, *29*, 313–316.
37. Fuly, A.L.; de Miranda, A.L.; Zingali, R.B.; Guimarães, J.A. Purification and characterization of a phospholipase A_2 isoenzyme isolated from *Lachesis muta* snake venom. *Biochem. Pharmacol.* **2002**, *63*, 1589–1597.
38. OSIRIS Property Explorer. Available online: http://www.organic-chemistry.org/prog/peo/ (accessed on 14 April 2014).

Bioactive Marine Drugs and Marine Biomaterials for Brain Diseases

Clara Grosso, Patrícia Valentão, Federico Ferreres and Paula B. Andrade

Abstract: Marine invertebrates produce a plethora of bioactive compounds, which serve as inspiration for marine biotechnology, particularly in drug discovery programs and biomaterials development. This review aims to summarize the potential of drugs derived from marine invertebrates in the field of neuroscience. Therefore, some examples of neuroprotective drugs and neurotoxins will be discussed. Their role in neuroscience research and development of new therapies targeting the central nervous system will be addressed, with particular focus on neuroinflammation and neurodegeneration. In addition, the neuronal growth promoted by marine drugs, as well as the recent advances in neural tissue engineering, will be highlighted.

Reprinted from *Mar. Drugs*. Cite as: Grosso, C.; Valentão, P.; Ferreres, F.; Andrade, P.B. Bioactive Marine Drugs and Marine Biomaterials for Brain Diseases. *Mar. Drugs* **2014**, *12*, 2539–2589.

1. Introduction

Along with the increase of average life expectancy, the prevalence of neurological/neurodegenerative diseases is rising, prompting the recent research focused on developing novel drugs targeting the central nervous system (CNS) [1]. Inspired by the vastness and biodiversity richness of the marine environment, researchers have pursued the pharmacological potential of marine metabolites [2].

Pharmacological studies with marine compounds affecting the CNS involve areas of neuropharmacology, such as those of stimulation of neurogenesis, modulation of receptors and voltage-dependent ion channels and enzymes inhibition [3]. For instance, conotoxins peptides are currently being used as standard research tools in neuroscience, since they can interfere with receptors and channels, allowing a better understanding of how antagonist/agonist drugs bind to the binding sites [4]. These researches have already culminated with Food and Drug Administration (FDA) approval of Ziconitide (Prialt®), a synthetic equivalent of the ω-conotoxin MVIIA (isolated from *Conus magus* L.), for pain and stroke treatment [4,5]. Moreover, several other marine compounds are being evaluated in preclinical trials, such as the α-conotoxin Vc1.1 (isolated from *Conus victoriae* Reeve) and the χ-conotoxin MrIA/B (from *Conus marmoreus* L.), for the treatment of neuropathic pain, and the anti-epileptic conantokin-G, isolated from *Conus geographus* L. Currently undergoing a more advanced evaluation, *i.e.*, phase II trials, are ω-conotoxin CVID (from *Conus catus* Hwass in Bruguière) for neuropathic pain treatment, and contulakin-G (from *C. geographus*) for neuropathic and chronic inflammatory pain treatments [5], as well as 3-(2,4-dimethoxybenzylidene)-anabaseine (DMXBA), the synthetic derivative produced from the alkaloid anabaseine (isolated from nemertines), to treat schizophrenia [6] and Alzheimer's disease (AD) [7].

This review covers the studies performed with marine invertebrate drugs from the year 2000 until the present, focusing on their role in fighting neuroinflammation states and neurodegeneration. One hundred and eighty-four examples of marine drugs affecting neuronal growth and synaptic

functions, neuroinflammation, CNS enzymes and CNS voltage and ligand-gated ion channels will be given. Towards the conclusion of this paper, the usefulness of marine skeletons in neural tissue engineering will be discussed. Recently, some review papers have been published focusing on some of the aspects considered in this review. The modulation of receptors, voltage-dependent channels and enzymes by conopeptides is, by far, the most extensively reviewed subject [4,8–10]. Sakai and Swanson [11] presented a broad spectrum of marine drugs affecting those targets. Arias *et al.* [12] focused their attention on marine drugs affecting ion channels, and Al-Sabi *et al.* [13] reviewed data about marine toxins that target voltage-gated sodium channels. Kochanowska-Karamyan and Hamann [14] covered the role of marine indole alkaloids as potential new antidepressant and anti-anxiety drug leads. Bharate *et al.* [15] and Skropeta *et al.* [16] gathered information concerning sponge drugs with protein kinase inhibitory activity. A broader spectrum of enzyme inhibited by marine drugs was covered by Nakao and Fusetani [17]. Senthilkumar and Kim [18] compiled information concerning marine invertebrate natural drugs for inflammatory and chronic diseases, including AD. Finally, information regarding preclinical and clinical candidates in the field of neurology was published by Martínez [19], Twede *et al.* [10] and Bharate *et al.* [15].

2. The Nervous System

The nervous system is the network of specialized cells that conduct nerve impulses between parts of the body. The central nervous system (CNS) is responsible for driving and interpreting signals and for supplying excitatory stimuli to the peripheral nervous system (PNS); PNS nerves innervate muscle tissue, conducting sensory and excitatory stimuli to and from the spinal cord [20].

Besides neurons, whose function is to propagate nerve impulses, CNS and PNS also contain another type of cells called glial cells or neuroglia. Neuroglia comprises four types of cells, namely, astrocytes, oligodendrocytes, microglia cells in the CNS and Schwann cells in the PNS. Astrocytes are a very heterogeneous population of cells and they can interfere in axon guidance, synaptic support, control of the blood–brain barrier (BBB) and blood flow [21]. These are excitable cells like neurons, but they communicate by spontaneous or evoked cytosolic Ca^{2+} variations, instead of membrane electrical signals [22]. Oligodendrocytes and Schwann cells are responsible for the production of myelin [21,23]. Microglia cells are the immune cells of the CNS, contributing to CNS homeostasis during development, adulthood and ageing [24]. They protect the brain from damage and infection, by engulfing dead cells and debris. They are also implicated in synaptic remodelling during the development of the nervous system and they are activated in many neurodegenerative diseases [21,23]. In the nervous system, glial cells are more abundant than neurons and have some capacity for cell division. Conversely, neurons have no capacity for mitotic division, but can regenerate portions under certain conditions [20].

3. Regeneration of the CNS: Drawbacks and Challenges

Complete recovery from a CNS injury or neurological disorders has not yet been made possible [25]. This is because an injury is a continuous process, with a primary damage triggering a cascade of deleterious events, such as blood–brain barrier disruption, excitotoxicity, inflammation,

oedema, ischemia, increase of free radicals and altered cell signalling and gene expression [26,27]. Therefore, a massive death of neuronal and glial cells may occur along with the loss of both the 3D spatial organization and the connectivity of neuronal networks [28].

Although neurite growth inhibitors are present in both CNS and PNS, the capacity for CNS nerves to regenerate is lower than that of peripheral nerves for several reasons. First, because astrocytes become "reactive astrocytes," which produce glial scars that constitute a physical barrier to growth and up-regulate several extracellular-matrix-associated inhibitors of regeneration, such as chondroitin sulfate proteoglycans [29]. Second, conversely to a PNS injury, in the case of a CNS injury, BBB and blood–spine barrier function as constrainers to the recruitment of macrophages from the blood circulation to remove myelin and axonal debris and resident microglia can only give a delayed and slow response [24,30,31]. Moreover, in contrast to PNS, the up-regulation of regeneration-associated proteins (RAGs), which play a positive role in neurite outgrowth and axon regeneration, is relatively modest in the CNS after injury [32,33].

In order to counteract this low regenerating environment after a CNS injury, clinical trials have taken advantage of the recent progress in regenerative medicine, and new approaches for the treatment of CNS injuries have been explored, such as (i) cellular replacement with stem cells, (ii) delivery of brain-derived neurotrophic factor (BDNF), (iii) axon guidance with cell adhesion molecules and removal of growth inhibition molecules, (iv) manipulation of intracellular signalling with transcription factors, (v) bridging with a peripheral nerve bridge or foetal tissue or use of artificial substrates to guide axons across the scar, and (vi) modulation of the immune response [25,34]. Even though transplantation is a promising approach, therapeutic effects are currently limited due to the high level of donor cell death and lack of integration with the host brain tissue [27]. Conversely, PNS injuries are usually treated surgically by reconnection of the damaged nerve ends (78%) or by using an autograft (15%) or conduit (4%) [35–37]. Approximately 50% of surgical cases achieve normal to good function restoration [35].

4. Marine Drugs: Neuritogenic Activity, Neurotrophin-Mimic and Neurotrophin-Enhancer Agents

Compounds inducing neuronal growth are expected to become a new lead for medical treatment of CNS disorders, such as ischemic stroke and neurodegenerative diseases. Dysideamine (Figure 1), a sesquiterpene aminoquinone from the marine sponge *Dysidea* sp. 05C33, was shown to induce neurite outgrowth in mouse neuroblastoma Neuro 2A cells [38]. More than 40% of the cells treated with 3 μM of this compound presented neurite outgrowth but, at 10 μM, slight cytotoxic effects were observed [38]. Using the same cell system, as well as rat pheochromocytoma PC12 cells, Aoki *et al.* [39] studied the neuritogenic activity of four pyridoacridine alkaloids (Figure 1) isolated from the marine sponge *Biemna fortis* Topsent. None of these compounds were able to induce neurite outgrowth in rat pheochromocytoma PC12 cells. On the other hand, neurite outgrowth was induced in more than 50% of the Neuro 2A cells treated with compound 3 (0.01 μM), but at concentrations higher than 0.3 μM it was cytotoxic. Compounds 1 (labuanine A), 2 and 4 were less active. Taking into account the structure of these pyridoacridine alkaloids and the displayed activity, the authors suggested that the wide difference in neuritogenic activity between compounds 2 and 3

should be due to the presence of the amino group at C-9 in 3. Moreover, compound 3 provoked a four-fold increase of acetylcholinesterase (AChE) activity at 0.03 μM compared with the control, indicating that it induced both morphological and functional neuronal differentiation. Since neuronal differentiation closely relates to the cell cycle, the effect of the pyridoacridine alkaloids on the cell cycle of Neuro 2A cells was evaluated, revealing that, like topoisomerase II inhibitors, they arrested the cell cycle at G2/M phase. Thus, a possible mechanism suggested by the authors was that the induced neuronal differentiation could be related with inhibition of topoisomerase II.

Figure 1. Potent marine drugs affecting neuronal growth and synaptic functions.

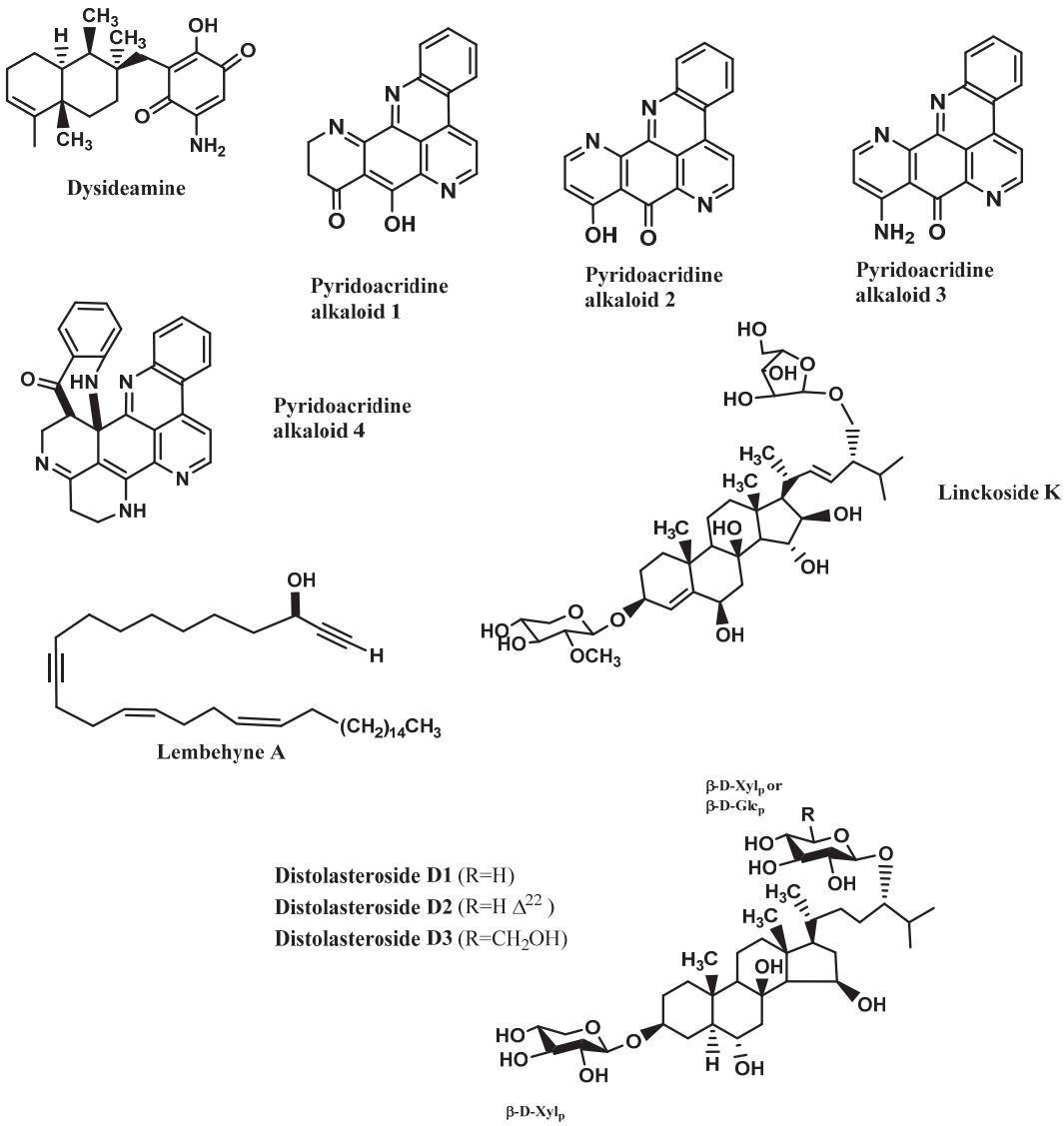

Figure 1. *Cont.*

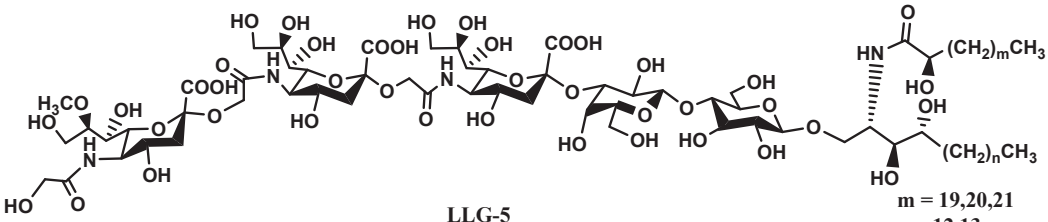

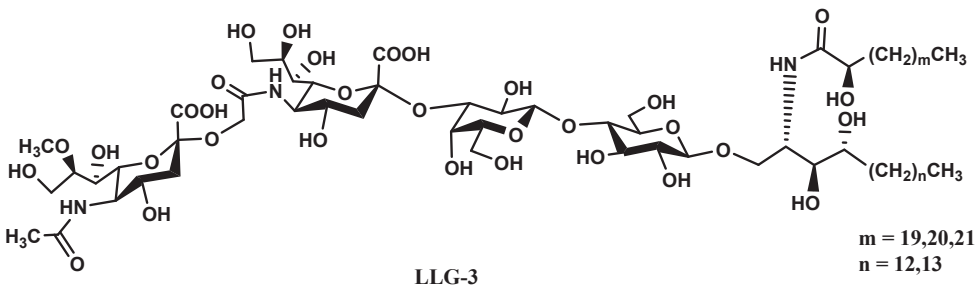

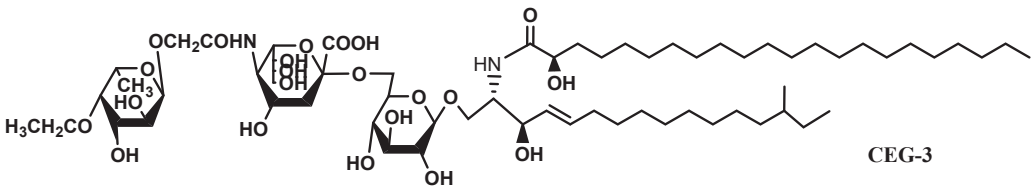

In a similar study, lembehyne A (Figure 1), a linear polyacetylene isolated from the sponge *Haliclona* sp., induced neuritogenesis in both PC12 and Neuro 2A cell lines, at 2 and 0.1 μg/mL, respectively. Since treatment with an inhibitor of actin polymerization (cytochalasin B) or with an inhibitor of protein synthesis in eukaryotes (cycloheximide) inhibited the effect of lembehyne A, a mechanism dependent on actin polymerization and *de novo* protein synthesis was suggested for this compound [40,41]. Aditionally, lembehyne A (1 and 3 μg/mL) arrested the cell cycle at the G1 phase, a response also known to be induced by nerve growth factor (NGF), and induced a two- and four-fold increase of AChE activity at 1 and 3 μg/mL, respectively [41]. Later, the same research group investigated the structure–activity relationship among lembehynes A–C and five analogs using Neuro 2A cell system. They concluded that the features contributing to the activity were the carbon-chain length, since analogs with shorter carbon-chain were more active than lembehynes A–C, and that the presence of a hydroxyl group at C-3 was essential [42].

NGF and BDNF are essential for neuronal differentiation, growth, survival, function maintenance and prevention of ageing in the CNS and PNS [43,44].

Although NGF and BDNF are expected to have therapeutic potential in the treatment of neuronal injuries, they do not cross the BBB due to their size. Therefore, low molecular weight compounds mimicking their activity should be interesting as promising therapeutic agents to treat traumatic or ischemic brain injuries and neurodegenerative diseases [44]. In recent years, several low molecular weight substances from various natural sources have been shown to possess

neurotrophic ability. Several marine drugs have proved to mimic and/or enhance NGF or BDNF activities.

Palyanova *et al.* [44] evaluated the neurotrophic potential of six sterols from *Asterina pectinifera* Muller and Troschel (starfish) using C1300-NB cell line. C1300-NB, in contrast to PC12 cells, have the capacity to spontaneously differentiate; a residual differentiation of 14%–25% was thus observed. This differentiation was increased by distolasterosides D_1–D_3 (>5 nM; Figure 1) more efficiently than by asterosaponin P1 (>50 nM), (25*S*)-5α-cholestane-3β,4β,6α,7α,8,15α,16β,26-octaol (>10 nM), and (25*S*)-5α-cholestane-3β,6α,7α,8,15α,16β,26-heptaol (>50 nM). These compounds also synergistically enhanced NGF and BDNF activities.

Tables 1 and 2 report the neurotrophin mimic and neurotrophin-enhancement effects of several marine drugs in PC12 cells [43,45–50].

Table 1. Marine drugs with neurotrophin mimic activity in PC12 cell line.

Compound/organism	Concentration tested (μM)	Neurites longer than soma diameter (%)
Linckoside A/blue starfish *Linckia laevigata* L.	40	25.0 [47]
Linckoside B/blue starfish *L. laevigata* L.	40	76.0 [47]
Linckoside F/blue starfish *L. laevigata* L.	40	30.0 [43]
Linckoside G/blue starfish *L. laevigata* L.	40	<10.0 [43]
Linckoside H/blue starfish *L. laevigata* L.	40	<10.0 [43]
Linckoside I/blue starfish *L. laevigata* L.	40	40.0 [43]
Linckoside J/blue starfish *L. laevigata* L.	40	<10.0 [43]
Linckoside K/blue starfish *L. laevigata* L.	40	50.0 [43]
NGF	10 *	45.0 [47]

* ng/mL.

Some of the studies allowed establishing structure-activity relationships. Han *et al.* [43] tested six steroid glycosides (Linckosides F–K) from the blue starfish *Linckia laevigata* L. and concluded that the carbon branch modified by a pentose at the side chain (present only in linckoside K; Figure 1) and the 2′-*O*-methyl ether group of xylose at C-3 (present in linckosides F and K) were the most important structures for the NGF-mimic activity. 2′-*O*-Methyl ether group of xylose at C-3 plays a role for the significant NGF-enhancing activity. Another steroid glycoside, granulatoside A [45], and two gangliosides, LLG-3 (Figure 1) and LLG-5 (Figure 1) [46], isolated from the same blue starfish, were also very promising.

Kisa *et al.* [50] evaluated the NGF-mimic activity of five monosialo-gangliosides from the sea cucumber *Cucumaria echinata* Von Marenzeller, SJG-1, CG-1, CEG-3, CEG-4 and CEG-5. The most active one was CEG-3 (Figure 1), which possesses an acetyl group at the terminal fucose unit. Among the disialogangliosides (HLG-3 and CEG-6) and trisialogangliosides (CEG-8 and CEG-9) isolated from the same sea cucumber [49], those displaying highest activity were CEG-6, HLG-3 and CEG-8, although lower than that of CEG-3. This was in accordance with the previous assumption made by the same authors, since CEG-6 and HLG-3 possess a terminal fucose without acetyl group and CEG-8 does not contain a terminal fucose. Despite their structural similarity, the

different NGF-enhancement effect of linckosides A and B suggests that the sugar moiety at C-29 of the aglycon plays an important role for the activity of these steroid glycosides [47].

Table 2. Synergistic effect between NGF and marine drugs in PC12 cells.

Compound/organism	[NGF] ng/mL	Effect of NGF alone (%)	[Drug] μM	Effect of NGF + marine drug (%)
Linckoside A/blue starfish *Linckia laevigata* L.	2.5	5.0	40	62.0 [47]
Linckoside B/blue starfish *L. laevigata* L.	2.5	5.0	40	87.0 [47]
Linckoside F/blue starfish *L. laevigata* L.	1.5	6.0	40	90.0 [43]
Linckoside G/blue starfish *L. laevigata* L.	1.5	6.0	40	40.0 [43]
Linckoside H/blue starfish *L. laevigata* L.	1.5	6.0	40	46.0 [43]
Linckoside I/blue starfish *L. laevigata* L.	1.5	6.0	40	95.0 [43]
Linckoside J/blue starfish *L. laevigata* L.	1.5	6.0	40	46.0 [43]
Linckoside K/blue starfish *L. laevigata* L.	1.5	6.0	40	98.0 [43]
LLG-5/blue starfish *L. laevigata* L.	5.0	20.6	10	59.3 [46]
LLG-3/blue starfish *L. laevigata* L.	5.0	20.6	10	63.1 [46]
Granulatoside A/blue starfish *L. laevigata* L.	1.5	<10.0	40	95.0 [45]
GP-3/starfish *A. pectinifera* Muller and Troschel	5.0	20.6	10	38.2 [48]
CEG-6/sea cucumber *Cucumaria echinata* Von Marenzeller	5.0	7.5	10	43.0 [49]
HLG-3/sea cucumber *C. echinata* Von Marenzeller	5.0	7.5	10	42.0 [49]
CEG-8/sea cucumber *C. echinata* Von Marenzeller	5.0	7.5	10	40.2 [49]
CEG-9/sea cucumber *C. echinata* Von Marenzeller	5.0	7.5	10	35.1 [49]
SJG-1/sea cucumber *C. echinata* Von Marenzeller	5.0	7.5	10	39.1 [50]
SJG-2/sea cucumber *Stichopus japonicus* Selenka	5.0	20.6	10	64.8 [50]
CG-1/sea cucumber *C. echinata* Von Marenzeller	5.0	7.5	10	43.0 [50]
CEG-3/sea cucumber *C. echinata* Von Marenzeller	5.0	7.5	10	50.8 [50]
CEG-4/sea cucumber *C. echinata* Von Marenzeller	5.0	7.5	10	34.0 [50]
CEG-5/sea cucumber *C. echinata* Von Marenzeller	5.0	7.5	10	35.7 [50]

5. Marine Drugs Affecting Enzymes Involved in Neurodegeneration

Neurodegenerative diseases, such as AD and Parkinson's disease (PD), are characterized by the loss of particular neuronal populations and by intraneuronal and extracellular accumulation of fibrillary materials [51]. AD is the most common form of dementia. It is an age-related neurodegenerative disorder characterized by extracellular deposition of plaques of aggregated β-amyloid protein (Aβ), intracellular deposition of neurofibrillary tangles that contain hyperphosphorylated tau (τ) protein, and a profound loss of basal forebrain cholinergic neurons that innervate the hippocampus and the neocortex [52]. Current AD treatment consists of the administration of inhibitors of AChE and butyrylcholinesterase (BuChE) enzymes in order to counteract brain's acetylcholine deficiency [53]. However, other enzymes could be considered a target for future drug development, such as the proteases β-secretase (BACE1) and presenilin-dependent γ-secretase [54–56] involved in the cleavage of amyloid-β precursor protein (APP) into Aβ fragments, and protein

kinases that hyperphosphorylate τ protein making up paired helical filaments (PHFs) and straight filaments of neurofibrillary tangles (NFTs) in the brain [57–59].

Protein kinases also display a pivotal role in other neurodegenerative disorders, such as in PD. Hyperphosphorylated α-synuclein, the major constituent of Lewy bodies, is one of the most important hallmarks of PD [60,61]. Several post-translational modifications to α-synuclein occur in PD, phosphorylation at serine (Ser)-129 residue being among them [61,62].

In the next sections, examples of marine compounds with inhibitory activity against cholinesterases (AChE and BuChE), BACE1 and protein kinases will be given.

5.1. Inhibition of Cholinesterases (ChEs) Activity

Beedessee *et al.* [53] evaluated the anticholinesterase effect of 134 extracts from 45 species of marine sponges and two of them showed strong AChE inhibition, namely the ethyl acetate extracts of *Pericharax heteroraphis* Poléjaeff (90% inhibition at 0.1 mg/mL) and of *Amphimedon navalis* Pulitzer-Finali (96% inhibition at 0.1 mg/mL). These extracts were rich in terpenoid compounds. Two other extracts obtained from the sponges *Latrunculia lendenfeldi* Hentschel and *Latrunculia bocagei* Ridley and Dendy displayed IC_{50} = 1.3 and 9 ng/mL, respectively [63].

Some examples of AChE inhibitors isolated from sponges, corals and molluscs are shown in Table 3. The kinetics analysis of AChE inhibition promoted by the stigmastane-type steroidal alkaloid 4-acetoxy-plakinamine B (Figure 2) suggested a mixed-competitive mode of inhibition [64].

Table 3. Marine drugs as AChE inhibitors.

Compound/Organism	IC_{50} (μM)
4-acetoxy-plakinamine B/sponge *Corticium* sp.	3.75 [64]
2-Bromoamphimedine/sponge *Petrosia n.* sp.	300 [65]
Petrosamine/sponge *Petrosia n.* sp.	91 [65]
Cladidiol/soft coral *Cladiella* sp.	67 [66]
Turbotoxin A/mollusc *Turbo marmoratus* L.	28 [67]

5.2. Inhibition of BACE1

Williams *et al.* [68] screened 130 pre-fractionated extracts from marine invertebrates and cyanobacteria against BACE1 activity, resulting in 7% of the extracts with outstanding inhibition (>90%) and 11% with activity between 70% and 89%. One group of submicromolar BACE1 inhibitors revealed by this study was the bastadins, a family of highly modified tetrapeptides occurring in some species of sponges, from which bastadin 9 is an example. Several metabolites isolated from sponges [69–74] showed BACE1 inhibitory activity (Table 4). The most promising ones are dictyodendrins F and H–J (Figure 2) [74] and topsentinol K trisulfate (Figure 2) [70].

Dai *et al.* [69] tested several xestosaprols and concluded that the β-orientation of the C-3 alcohol (only present in xestosaprol H) was an important feature for the activity. Structure-activity relationships were also established for topsentinols. Topsentinol K trisulfate was the only active sterol isolated from the sponge *Topsentia* sp., while topsentinols K and L were inactive. These results demonstrated that the presence of sulfate esters contribute to BACE1 activity [70].

Table 4. BACE1 inhibitors.

Compound/organism	IC_{50} (μM)
Xestosaprol D/sponge *Xestospongia* sp.	93.2 [72]
Xestosaprol F/sponge *Xestospongia* sp.	135.0 [69]
Xestosaprol G/sponge *Xestospongia* sp.	155.0 [69]
Xestosaprol H/sponge *Xestospongia* sp.	82.0 [69]
Xestosaprol I/sponge *Xestospongia* sp.	163.0 [69]
Xestosaprol J/sponge *Xestospongia* sp.	90.0 [69]
Xestosaprol K/sponge *Xestospongia* sp.	93.0 [69]
Xestosaprol L/sponge *Xestospongia* sp.	98.0 [69]
Xestosaprol M/sponge *Xestospongia* sp.	104.0 [69]
Dictyodendrin F/sponge *Ianthella* sp.	1.5 [74]
Dictyodendrin H/sponge *Ianthella* sp.	1.0 [74]
Dictyodendrin I/sponge *Ianthella* sp.	2.0 [74]
Dictyodendrin J/sponge *Ianthella* sp.	2.0 [74]
Dictazole A/sponge *Smenospongia cerebriformis* Duchassaing and Michelotti	135.0 [71]
Topsentinol K trisulfate/sponge *Topsentia* sp.	1.2 [70]
Lamellarin O/sponge *Ianthella* sp.	40% (at 10 μM) [73]
Lamellarin O1/sponge *Ianthella* sp.	60% (at 10 μM) [73]
Lamellarin O2/sponge *Ianthella* sp.	40% (at 10 μM) [73]
Ianthellidone F/sponge *Ianthella* sp.	40% (at 10 μM) [73]

5.3. Inhibition of Protein Kinases

The human kinome codifies nearly 500 different protein kinases, which have serine/threonine (Ser/Thr) or tyrosine (Tyr) specificity. They catalyse phosphorylation pathways that regulate most of the biological processes, but abnormal phosphorylation is, normally, a cause or a consequence of disease [61]. As stated above, inhibitors of these protein kinases can be useful to alleviate the symptoms of neurodegenerative disorders, such as AD and PD. In the next sections, a brief description on the involvement of protein kinases in neurodegeneration will be given, as well as some examples of marine protein kinases inhibitors and, when available, data about their inhibition mode.

5.3.1. Glycogen Synthase Kinase 3 (GSK-3)

GSK-3, also known as τ phosphorylating kinase I, is a multifunctional Ser/Thr kinase that is involved in glycogen metabolism, insulin signalling, cell proliferation, neuronal function, oncogenesis and embryonic development. There are two isoforms (α and β) with 98% homology and similar biological functions, but most of the research has been dedicated to the isoform β. GSK-3 is highly expressed in the brain and is associated with several CNS disorders, such as AD, bipolar disorder, Huntington's disease and other neurodegenerative diseases [75,76].

GSK-3β phosphorylates transcription factors and cytoskeletal proteins, such as τ [77]. There are, at least *in vitro*, 40 different Ser and Thr residues in τ that can be phosphorylated by GSK-3 [78–81].

Figure 2. AChE and BACE1 inhibitors isolated from marine invertebrates.

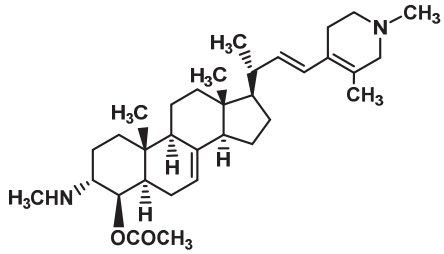

4-Acetoxy-plakinamine B

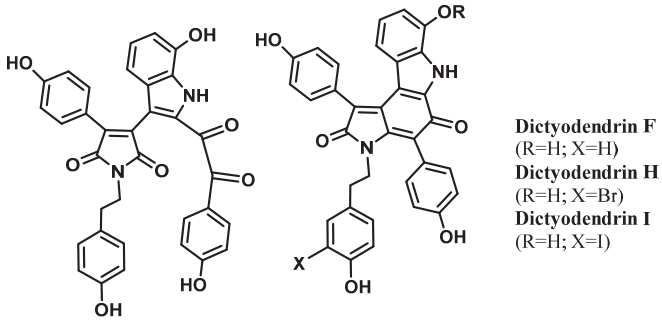

Dictyodendrin J

Dictyodendrin F (R=H; X=H)
Dictyodendrin H (R=H; X=Br)
Dictyodendrin I (R=H; X=I)

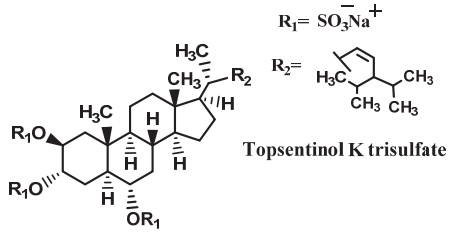

Topsentinol K trisulfate

The human τ gene suffers extensive alternative splicing, giving rise to the expression of multiple spliced exons, exon 10 being one of them. The presence of exon 10 results in τ with four repeat microtubule-binding sequences (4R), while isoforms without exon 10 have only three (3R). Normally, the ratio of 3R and 4R tau transcripts is close to one. Although mutations in splicing regulatory elements are common in inherited tauopathies, in sporadic AD the ratio 4R/3R is also increased [82]. In addition to hyperphosphorylate τ, GSK-3 can also induce τ splicing, because it phosphorylates the splicing factor SC35, an enhancer of splicing elements that regulate exon 10 splicing in τ [79]. Hernández *et al.* [83] demonstrated that GSK-3 inhibition in cultured neurons affected τ splicing, resulting in increased τ mRNA containing exon 10.

Moreover, GSK-3β has been reported to play a role in the toxic effect mediated by Aβ since, in cultured cells, Aβ activates GSK-3, leading to the phosphorylation of SC35 [79] and exposure of cortical and hippocampal primary neuronal cultures to Aβ induces activation of GSK-3β, τ

hyperphosphorylation and cell death [78]. Thus, inhibition of GSK-3 can contribute to the reduced formation of both Aβ plaques and neurofibrillary tangles [84].

Marine compounds [76,78,80,81,85–90] able to inhibit both isoforms of GSK-3 are shown in Table 5 and Figure 3. As it can be seen, hymenialdisine (Figure 3), lamellarins (Figure 3) and meridianins (Figure 3) are the most active ones.

Few studies explored the mode of inhibition and the structural features contributing to high inhibitory activity of GSK-3 inhibitors. Concerning the first aspect, it is known that the alkaloid hymenialdisine and meridianins are competitive inhibitors at the ATP-binding site [81,91], while the alkaloid manzamine A [80] and the furanoterpenoids tricantin [89] and palinurin [76] are non-ATP competitive. According to Eldar-Finkelman and Martinez [91], ATP non-competitive GSK-3 inhibitors should be more selective than ATP-competitive ones, since they bind to unique regions within GSK-3, leading to a more subtle modulation of the kinase activity than by simply ATP entrance blockade.

Table 5. GSK-3 inhibitors from marine organisms.

Compound/organism	Isoform	IC_{50} (μM)
Carteriosulfonic acid A/sponge *Carteriospongia* sp.	GSK-3β	12.5 [88]
Carteriosulfonic acid B/sponge *Carteriospongia* sp.	GSK-3β	6.8 [88]
Carteriosulfonic acid C/sponge *Carteriospongia* sp.	GSK-3β	6.8 [88]
Hymenialdisine/sponge *Axinella verrucosa* Esper	GSK-3β	10.0* [81]
Tricantin/sponge *Ircinia* sp.	GSK-3β	7.5 [89]
Lamellarin α/ascidian *Didemnum obscurum* F. Monniot	GSK-3α/β	1.4 [86]
Lamellarin D/prosobranch mollusc *Lamellaria* sp.	GSK-3α/β	0.3 [86]
Lamellarin H/ascidian *Didemnum chartaceum* Sluiter	GSK-3α/β	9.5 [86]
Lamellarin L/ascidian *Didemnum* sp.	GSK-3α/β	40.0 * [86]
Lamellarin N/ascidian *Didemnum* sp.	GSK-3α/β	5.0 * [86]
Leucettamine B/sponge *Leucetta microraphis* Haeckel	GSK-3α	7.7 [85]
Leucettamine B/sponge *L. microraphis* Haeckel	GSK-3β	>10.0 [85]
Leucettamine B/sponge *L. microraphis* Haeckel	GSK-3α/β	2.9 [85], 15.0 [90]
Manzamine A/sponge *Acanthostrongylophora* sp.	GSK-3β	10.2 [80], 12.30 [78]
Meridianin A/ascidian *Aplidium meridianum* Sluiter	GSK-3β	1.3 [87]
Meridianin B/ascidian *A. meridianum* Sluiter	GSK-3β	0.5 [87]
Meridianin C/ascidian *A. meridianum* Sluiter	GSK-3β	2.0 [87]
Meridianin D/ascidian *A. meridianum* Sluiter	GSK-3β	2.5 [87]
Meridianin E/ascidian *A. meridianum* Sluiter	GSK-3β	2.5 [87]
Meridianin F/ascidian *A. meridianum* Sluiter	GSK-3β	2.0 [87]
Meridianin G/ascidian *A. meridianum* Sluiter	GSK-3β	350.0 [87]
Palinurin/sponge *Ircinia dendroides* Schmidt	GSK-3β	2.6 [76]
(*Z*)-5-(4-Hydroxybenzylidene)-hydantoin/sponge *Hemimycale arabica* Ilan, Gugel and van Soest	GSK-3β	13.70 [78]

* nM.

Figure 3. Most potent protein kinases inhibitors from marine organisms.

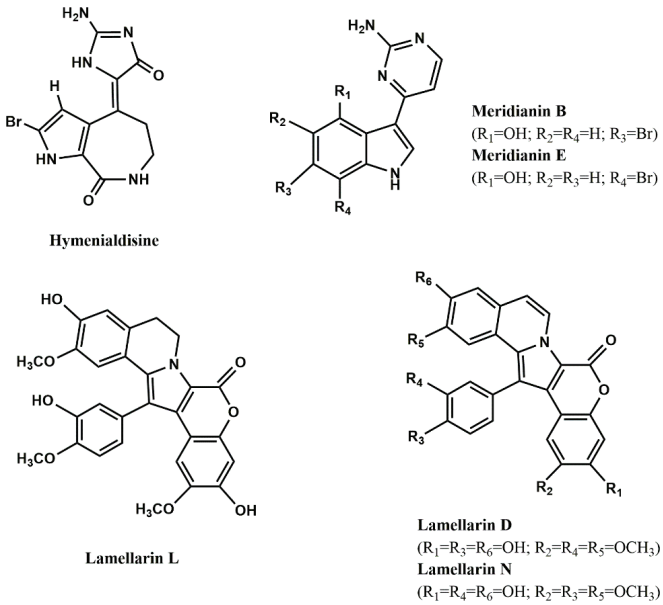

Regarding the second issue, Hamann *et al.* [80] synthetized several manzamine A analogs to study the influence of several substituents on GSK-3 inhibition. They concluded that the entire molecule (carboline moiety and aliphatic heterocyclic system) contributed for the inhibitory activity. Concerning the carboline moiety, the substitution of nitrogen 9 by large groups, such as isobutyl, dodecyl or methylcarboxybutyl, produced non-active compounds, while shorter groups (methyl and ethyl) did not cause activity reduction. Changes in the aliphatic heterocyclic system also influence GSK-3 inhibition, because if conformational restriction is increased, compounds are more active.

Baunbæk *et al.* [86] evaluated the ability of several lamellarins (Figure 3) and their analogs to inhibit not only GSK-3, but also other kinases (see next sections). Structure-activity studies led them to conclude that complex, but specific, interactions between lamellarins' substituents and their kinase targets may exist, since different substituents influenced the inhibitory activity against different kinases.

Other protein kinases function as activators for τ phosphorylations by GSK-3, such as casein kinase 1 (CK1) e 2 (CK2), dual specificity tyrosine phosphorylation-regulated kinase 1 A (DYRK1A), AMP-dependent protein kinase (PKA) and cyclin-dependent kinase-5 (CDK5) [61,79]. For instance, when CDK-5 phosphorylates τ at Ser-235 and Ser-404 residues, it promotes the subsequent τ phosphorylation by GSK-3 at Thr-231 and Ser-400, respectively. On the other hand, if PKA phosphorylates τ at Ser-214, it will activate τ phosphorylation by GSK-3 at Ser-210, Thr-205, Ser-199 and Ser-195 residues. However, some τ residues, such as Ser-396 and Ser-404, can be directly phosphorylated by GSK-3 without prior activity of other kinases [77,79].

5.3.2. DYRK1A

DIRK1A is located in chromosome 21 and codifies a protein kinase responsible for the phosphorylation of τ at Thr-212, Ser-202 and Ser-404 residues *in vitro* and *in vivo*. Studies indicate that overexpression of DYRK1A in the brains of Down's syndrome patients may contribute to early onset of AD pathology through hyperphosphorylation of τ [59].

Moreover, DYRK1A also phosphorylates other AD-related proteins, *in vitro* and *in vivo*. Phosphorylation of APP at Thr-668 residue leads to APP cleavage by BACE1 and γ-secretase and consequently to increased production of Aβ peptide [92]. In a similar way, phosphorylation at Thr-354 residue of presenilin 1 (PS1), a key component of the γ-secretase complex, also induced an increased γ-secretase activity [93]. Phosphorylation of septin-4 (SEPT-4) at Ser-68 and Ser-107 residues by DYRK1A may regulate specific protein–protein interactions, since septins are a family of filament-forming guanine nucleotide-binding proteins involved in cytokinesis, exocytosis and other cellular processes, such as synapse functions. It was shown that a complex formed by SEPT4, DYRK1A and α-synuclein may contribute to the development of α-synuclein-positive cytoplasmic aggregates characteristic of PD and, since SEPT4 has been found in neurofibrillary tangles, SEPT4/DIRK1A is also involved in the pathology of AD [94–96]. Finally, DIRK1A also phosphorylates the regulator of calcineurin 1 (RCAN) at Ser-112 and Thr-192 residues, the latter enhancing τ phosphorylation [97] and phosphorylating Munc18–1 at Thr-479 residue, stimulating its binding to Syntaxin 1 and X11α, two proteins involved in synaptic vesicle exocytosis and APP processing, respectively [98]. Examples of marine compounds [85,86] that inhibit DYRK1A are shown in Table 6 and Figure 3.

Table 6. DYRK1A inhibitors from marine organisms.

Compound/organism	IC_{50} (μM)
Lamellarin α/ascidian *Didemnum obscurum* F. Monniot	5.0 [86]
Lamellarin D/prosobranch mollusc *Lamellaria* sp.	0.5 [86]
Leucettamine B/sponge *Leucetta microraphis* Haeckel	0.6–1.0 [85]
Lamellarin L/ascidian *Didemnum* sp.	0.1 [86]
Lamellarin N/ascidian *Didemnum* sp.	40.0 * [86]

* nM.

5.3.3. CK1 and CK2

In mammals, the CK1 family of protein kinases consist of monomeric enzymes assembled from seven isoforms (α, β, γ1, γ2, γ3, δ, and ε). They are responsible for the phosphorylation of cytoskeletal proteins, such as spectrin, troponin, myosin, ankyrin, τ and α-synuclein, but also of non-cytoskeletal proteins (SV40 T antigen, p53, and β-catenin). These phosphorylations modulate important physiological functions like vesicular trafficking, DNA repair, cell cycle kinetics and cell division [99].

In AD patients' brains, CK1α and CK1δ are co-localized with neurofibrillary lesions and granulovacuolar degeneration bodies. Furthermore, CK1α, CK1ε and CK1δ levels are increased in CA1 region of hippocampus, with a predominance of CK1δ. This CK1δ isoform phosphorylates τ

at Ser-202, Thr-205, Ser-396 and Ser-404 residues and a combination of CK1δ and GSK-3 activities induce more than three-quarters of the Ser/Thr phosphorylations identified in τ-PHF, indicating that both protein kinases are involved in the pathogenesis of AD [61]. Additionally, APP, BACE1 and γ-secretase contain multiple CK1 phosphorylation sites and CK1ε leads to an increase of Aβ peptide production. On the other hand, Aβ stimulates CK1 activity [79,100].

CK1 is also involved in PD pathology. It has been demonstrated that α-synuclein is phosphorylated at Ser-129 by CK1 [61].

The CK2 holoenzyme forms a heterotetrameric complex with two catalytic (CK2α and CK2α′) and two regulatory (CK2β) subunits. Overexpression of CK2 leads to several pathological conditions, ranging from cardiovascular pathologies and cancer progression to infectious diseases and neurodegeneration. CK2 activity increases due to the presence of Aβ peptide and, thus, may accelerate τ phosphorylation. Besides CK2's role in AD progression, CK2β subunits are present in Lewy bodies and phosphorylate α-synuclein at Ser-129 residue [61].

Table 7 and Figure 3 report some examples of marine compounds [81,86,87] that display inhibitory activity against CK1 and CK2.

Hymenialdisine is a competitive inhibitor at the ATP-binding site [81].

5.3.4. Cyclin-Dependent Kinase 5 (CDK5)

CDKs are a group of protein kinases that regulate cell-cycle control (CDK1–4, 6 and 7), thymocyte apoptosis (CDK2), neuronal functions (CDK5) and transcriptional control (CDK7–9). CDK5, initially known as brain proline-directed protein kinase or neuronal cdc2-like protein kinase, has been considered a major τ kinase that contributes to tauopathies. Interaction of CDK5 with either p35 or p39, two activator proteins, is necessary for its activation [101]. CDK5/p35 is involved in several processes critical to CNS function during development and throughout maturity [102]. CDK5/p35 is known to phosphorylate τ (at Ser-235, Ser-396 and Ser-404) and MAP-1B, Pak1 kinase and neurofilament subunits [81] and its activity is promoted by Aβ peptide. Indeed, CDK5/p35 phosphorylates τ at Ser-396 and Ser-404 residues in response to Aβ25–35 [103].

Table 7. CK1 and CK2 inhibitors from marine organisms.

Compound/organism	Enzyme	IC_{50} (μM)
Hymenialdisine/sponge *Axinella verrucosa* Esper	CK1	35.0 * [81]
Hymenialdisine/sponge *A. verrucosa* Esper	CK2	7.0 [81]
Lamellarin α/ascidian *Didemnum obscurum* F. Monniot	CK1	7.9 [86]
Lamellarin D/prosobranch mollusc *Lamellaria* sp.	CK1	13.0 [86]
Lamellarin K/ascidian *Didemnum* sp.	CK1	6.0 [86]
Lamellarin H/ascidian *Didemnum chartaceum* Sluiter	CK1	5.3 [86]
Meridianin B/ascidian *Aplidium meridianum* Sluiter	CK1	1.0 [87]
Meridianin C/ascidian *A. meridianum* Sluiter	CK1	30.0 [87]
Meridianin D/ascidian *A. meridianum* Sluiter	CK1	100.0 [87]
Meridianin E/ascidian *A. meridianum* Sluiter	CK1	0.4 [87]

* nM.

Aberrant CDK5 activity is induced by the conversion of p35 to p25 by calpain, a Ca^{2+}-dependent cysteine protease. CDK5/p25 plays a role in the pathogenesis of neurodegenerative diseases since it induces the formation of τ-PHF, τ aggregation and neuronal loss [102,104]. Other evidence from the involvement of Aβ peptide in τ hyperphosphorylation comes from the ability of Aβ to directly promote an increase of the levels of intracellular Ca^{2+} ($[Ca^{2+}]i$) in neurons, this increment leading to calpain activation, which, in turn, cleaves p35 into p25 [105].

Table 8 and Figure 3 show some examples of CDK5 inhibitors isolated from marine organisms [80,86,87,106].

Table 8. CDK5 inhibitors from marine organisms.

Compound/organism	Enzyme	IC_{50} (μM)
Lamellarin α/ascidian *Didemnum obscurum* F. Monniot	CDK5/p25	>10.0 [86]
Lamellarin D/prosobranch mollusc *Lamellaria* sp.	CDK5/p25	0.6 [86]
Lamellarin L/ascidian *Didemnum* sp.	CDK5/p25	0.1 [86]
Lamellarin N/ascidian *Didemnum* sp.	CDK5/p25	25.0 * [86]
Fascaplysin/sponge *Fascaplysinopsis* sp.	CDK5/p35	20.0 [106]
Manzamine A/sponge *Acanthostrongylophora* sp.	CDK5/p35	1.5 [80]
Meridianin A/ascidian *Aplidium meridianum* Sluiter	CDK5/p25	3.0 [87]
Meridianin B/ascidian *A. meridianum* Sluiter	CDK5/p25	1.0 [87]
Meridianin C/ascidian *A. meridianum* Sluiter	CDK5/p25	6.0 [87]
Meridianin D/ascidian *A. meridianum* Sluiter	CDK5/p25	5.5 [87]
Meridianin E/ascidian *A. meridianum* Sluiter	CDK5/p25	0.2 [87]
Meridianin F/ascidian *A. meridianum* Sluiter	CDK5/p25	20.0 [87]
Meridianin G/ascidian *A. meridianum* Sluiter	CDK5/p25	140.0 [87]

* nM.

5.3.5. PKA Inhibitors

PKA is the first element of cAMP signal transduction cascade, one of the several second messenger-dependent pathways that generate intracellular responses to extracellular signals. PKA mediates most of cAMP actions by phosphorylation [107].

Phosphorylation of τ at Ser-214 residue by PKA affects the interaction between τ and microtubules by reducing the tau's affinity for them. This phenomenon also occurs with the phosphorylation caused by GSK-3β and CDK5 [108].

Examples of marine PKA inhibitors [87] are shown in Table 9 and Figure 3.

Table 9. PKA inhibitors from marine organisms.

Compound/organism	IC_{50} (μM)
Meridianin A/ascidian *Aplidium meridianum* Sluiter	11.0 [87]
Meridianin B/ascidian *A. meridianum* Sluiter	0.2 [87]
Meridianin C/ascidian *A. meridianum* Sluiter	0.7 [87]
Meridianin D/ascidian *A. meridianum* Sluiter	1.0 [87]
Meridianin E/ascidian *A. meridianum* Sluiter	90.0 * [87]
Meridianin F/ascidian *A. meridianum* Sluiter	3.2 [87]
Meridianin G/ascidian *A. meridianum* Sluiter	120.0 [87]

* nM.

6. Marine Drugs Modulating CNS Voltage-Dependent Ion Channels and CNS Receptors

Voltage-dependent ion channels are intrinsic membrane proteins that play a pivotal role in fast communication in excitable cells. The pore region determines cation selectivity and is the binding site for many channel blockers. Toxins that interact with the pore can be used to understand its spatial organisation and may also be useful to design drugs that modify the function of ion channels in pathological conditions, such as stroke, pain, or epilepsy [109]. Calcium, sodium and potassium channels are voltage-dependent ion channels.

6.1. Calcium Channels

At least four distinct types of high-voltage-activated Ca^{2+} channels (L-, N-, P/Q- and R-type) are expressed in cultured hippocampal neurons and are sensitive to different blockers, such as ω-conotoxin GVIA (N-type Cav2.2 channels), spider ω-Aga-IVA (P/Q-type Cav2.1 channels) and nimodipine (L-type Cav1.1–1.4 channels) [110,111]. Several types may contribute to neurotransmitter release, mainly P/Q- and R-type. Selective modulators may, therefore, allow the selective treatment of conditions, such as pain and stroke [109].

Many of the ischemia-induced pathophysiologic cascades that destroy the CA1 pyramidal neurons in hippocampus are triggered by pre- and post-synaptic Ca^{2+} influx. Therefore, many Ca^{2+} channels blockers, such as ω-conotoxins, have been shown to be neuroprotective in global models of ischemia [112,113].

Favreau *et al.* [114] injected ω-conotoxin CNVIIA intracerebroventricularly to mice, which caused shaking activity. At 1.5 pmol/g, the toxin produced mild tremors in mice that became more intense as the amount injected increased. This behaviour is characteristic of ω-conotoxins blockers of N-type voltage-sensitive Ca^{2+} channels and, consequently, the authors tested the selectivity of CNVIIA for different subtypes of Ca^{2+} channels. Binding of ^{125}I-ω-Ctx CNVIIA to rat brain synaptosome indicated its reversibility. Moreover, CNVIIA exhibited a clear selectivity for N-type voltage-sensitive Ca^{2+} channels *vs.* P/Q-type, since it displaced ^{125}I-ω-CNVIIA and ^{125}I-ω-GVIA with the same affinity, but was not so efficient at inhibiting ^{125}I- ω-MVIIC binding. Similarly, the ω-conotoxin SO-3 inhibited high-voltage-activated N-type Ca^{2+} currents in primary cultures of hippocampal cells in a dose-dependent way, displaying an IC_{50} value (0.16 μM) in the same order as that of MVIIA (IC_{50} = 0.20 μM). The blockade effects of SO-3 and MVIIA on N-type calcium channels were both reversible. P/Q- and R- types were not inhibited [111].

ω-Conotoxin TxVII is a L-type Ca^{2+} channel antagonist and ω-conotoxin MVIIC, besides producing a complete N-type channel blockade, also blocks P-type channels in cerebellar Purkinje cells [115].

6.2. Sodium Channels

Sodium channels consist of three protein subunits (α, β-1 and β-2) in a 1:1:1 stoichiometry. There are three different types of brain Na^+ channel α-subunits (I, II, and III) [109]. Based on their susceptibility to be blocked by tetrodotoxin, Na^+ channels can be divided into tetrodotoxin-sensitive and tetrodotoxin-resistant ones. The first class includes the neuronal type I/Nav1.1, type II/Nav1.2,

type III/Nav1.3, PN1/Nav1.7 and PN4/Nav1.6, all of them present in the CNS [116]. Some of these subtypes have been implicated in clinical conditions, such as neuropathic pain [117–119], stroke [120] and epilepsy [121].

δ-Conotoxins are known to inhibit the fast inactivation of voltage-gated sodium channels [113]. δ-Conotoxin SVIE (from *Conus striatus* L.) is a strong excitotoxin when injected intracranial on mice [122]. It induced twitching of hind limbs at 12 pmol/g and at higher concentrations (70 pmol/g); SVIE induced more severe excitatory symptoms (running in circles and spastic paralysis). This toxin is more potent than δ-conotoxins PVIA and TxVIA, which did not cause any behaviour changes at 20 pmol/g and 1000 pmol/g, respectively. SVIE (IC_{50} = 12 nM), as well as δ-conotoxins PVIA and TxVIA, was able to displace ^{125}I-δ-conotoxin TxVIA in sagittal sections of rat brain.

Sea anemones possess specialized structures, called tentacles, containing a wide variety of toxins that are used in the capture of prey, as well as for defence against predators [123]. APE 1–1 and APE 1–2 (5 μg/mL, each), polypeptides present in the venom of the sea anemone *Anthopleura elegantissima* Brandt, did not affect Na^+ current activation, but provoked delayed and incomplete inactivation of the current passing through fast Na^+ channels in mouse neuroblastoma N1E-115 cells [124].

Microinjection of granulitoxin (8 μg), a neurotoxin from sea anemone *Bunodosoma granulifera* Lesueur, into the dorsal hippocampus (CA1–CA3 areas) of rats induced seizure activity and the rats presented behavioural alterations similar to the pilocarpine model of temporal lobe epilepsy: akinesia, facial automatisms, head tremor, salivation, rearing, jumping, barrel-rolling, wet dog shakes and forelimb clonic movements [125].

On the other hand, μ-conotoxins are peptide inhibitors of voltage-sensitive Na^+ channels. They act selectively to occlude the pore of the channel by competing with tetrodotoxin and saxitoxin [116]. μ-Conotoxin PIIIA, from *Conus purpurascens* G. B. Sowerby II, reduced tetrodotoxin-sensitive voltage-dependent Na^+ current in rat peripheral and CA1 neurons. In the radioligand binding studies, PIIIA showed the highest potency at rat and human brain voltage-sensitive Na^+ channels, GIIIB (from *Conus geographus*) exhibited intermediate potency, and GIIIA and GIIIC (from *Conus geographus*) were the less active. However, none of them were able to fully displace [^{3}H]saxitoxin from rat or human brain, compared with the displacement induced by tetrodotoxin [116].

6.3. Potassium Channels

The human genome encodes 40 voltage-gated K^+ channels (KV), which are involved in several physiological processes, namely repolarization of neuronal and cardiac action potentials, regulation of Ca^{2+} signalling and cell volume, cellular proliferation and migration. The subtypes present in the CNS are Kv1.1–Kv1.8, Kv2.1, Kv2.2, Kv3.1- Kv3.4, Kv4.1–4.3, Kv7.2, Kv7.3, Kv7.5, Kv10.1, Kv10.2 and Kv11.2 [126].

κ-Conotoxins are antagonists of potassium-gated channels [113]. A κ-conotoxin from *Conus virgo* L., ViTx, inhibited homomeric vertebrate K^+ channels Kv1.1 (rat; IC_{50} = 1.59 μM) and Kv1.3 (human; IC_{50} = 2.09 μM), but not Kv1.2 (rat) expressed in *Xenopus* oocytes, whereas the

κ-conotoxin PVIIA, which blocks the Shaker K^+ channel, was effective at nanomolar concentration (IC_{50} about 70 nM) [127].

κM-conotoxin RIIIK from *Conus radiatus* Gmelin (4 nmol) administered by intracerebrovascular route into mice caused seizures. However, when the peptide was injected intraperitoneally, there were no visible effects. RIIIK was also shown to inhibit the Shaker K^+ channel expressed in *Xenopus* oocytes (IC_{50} = 1.21 μM), leading to the hypothesis that RIIIK targets a K^+ channel subtype in peripheral axons and in combination with other excitatory peptides (such as the δ-conotoxins that inhibit Na^+ channel inactivation) causes a massive depolarization of peripheral axons near the venom injection site. This elicits bidirectional propagated action potentials, which allow the toxins to cross the BBB and the effect is equivalent to a tonic/clonic seizure, resulting in a very rapid tetanic paralysis of the prey [128].

Marine drugs also modulate ligand-gated ion channels, such as ACh, glutamate, serotonin, histamine, GABA, glycine and norepinephrine receptors.

6.4. ACh Receptors

ACh acts on the nervous system through two types of receptors: muscarinic (mAChRs) and nicotinic (nAChRs). Five mAChR subtypes (m1–m5) have been identified, all of them present in the brain. They belong to the superfamily of G-protein-coupled receptors and they trigger second messenger cascades. nAChRs are ligand-gated ion channels that modulate the fast synaptic transmission of ACh and have been implicated in attention, memory, learning, development, antinociception, nicotine addiction, PD, AD, Tourette's syndrome, certain forms of epilepsy and schizophrenia. nAChRs are mainly located pre-synaptically, but also post-synaptically throughout the CNS [129–131]. Pre-synaptic nAChRs regulate the synaptic release of ACh and also of other important neurotransmitters, such as dopamine (DA), norepinephrine (NE), serotonin (5-HT), glutamate (Glu), and γ-aminobutyric acid (GABA), being important targets for the treatment of pain, epilepsy and of a wide range of neurodegenerative and psychiatric disorders. There are 17 identifed genetically distinct subunits of nAChRs, from which 5 are muscle-type (α1, β1, δ, γ and ε) and 12 are neuronal-type (α2–α10 and β2–β4). A functional nAChR comprises five homopentamer or heteropentamer subunits placed symmetrically around a central cation-channel pore. α7 and α4β2 are the most abundant combinations in CNS [129,132–134]. The distribution of nAChRs types in CNS was reviewed by Gotti *et al.* [135].

Anabaseine (Figure 4), an alkaloid isolated from carnivorous marine worms of the phylum Nemertea, is a non-selective nicotinic agonist. It is a full agonist of *Xenopus* oocyte-expressed rat nAChR α7 receptor, but only a very weak agonist of the α4β2 subtype [136].

On the other hand, several marine drugs have demonstrated inhibition of ACh-elicited current nAChRs (Table 10) expressed in *Xenopus* oocytes [132,134,137–141].

ACh (1 μM)-elicited currents through α4β2 subtype and ACh (100 μM)-elicited currents through α7 subtype were blocked by (−)-pictamine (Figure 4) and (−)-lepadin B (Figure 4), two alkaloids from the ascidians *Clavelina picta* Verrill and *Clavelina lepadiformis* Müller, respectively [132].

Table 10. Marine drugs as nAChR antagonists.

Compound/Organism	nAChR subtype	IC_{50} (nM)
(−)-Lepadin B/ascidian *Clavelina lepadiformis* Müller	α7	0.7 * [132]
(−)-Pictamine/ascidian *Clavelina picta* Verrill	α7	1.3 * [132]
α-conotoxin GID/*Conus geographus* L.	α7	4.5 [137]
α-Conotoxin ImII/*Conus imperialis* L.	α7	441.0 [138]
α-Conotoxin ImI/*Conus imperialis* L.	α7	191.0 [138]
αD-contoxin VxXIIB/*Conus vexillum* Gmelin	α7	0.4 [134]
α-conotoxin Qc1.2/*Conus quercinus* Lightfoot	α3β2	<10.0 * [139]
α-conotoxin GID/*Conus geographus* L.	α3β2	3.1 [137]
α-conotoxin Qc1.2/*C. quercinus* Lightfoot	α3β4	>10.0 * [139]
(−)-Lepadin B/ascidian *C. lepadiformis* Müller	α4β2	0.9 * [132]
(−)-Pictamine/ascidian *C. picta* Verrill	α4β2	1.5 * [132]
α-conotoxin GID/*C. geographus* L.	α4β2	152.0 [137]
αD-conotoxin VxXIIB/*C. vexillum* Gmelin	α3β2	8.4 [134]
αD-conotoxin VxXIIB/*C. vexillum* Gmelin	α4β2	228.0 [134]
αD-conotoxin VxXIIA/*C. vexillum* Gmelin	α3β2	370.0 [134]
Phycotoxins found in marine invertebrate glands		
13-Desmethyl spirolide C	α7	0.4 [140]
Gymnodiamine	α7	2.0 [140]
13-Desmethyl spirolide C	α4β2	0.7 [140]–3.9 [141]
Gymnodimine	α4β2	0.5 [140]–0.9 [141]

* μM.

α-Conotoxins are a class of nAChRs antagonists [142]. Several works have been conducted with rat or mouse nAChRs expressed in *Xenopus* oocytes. Peng *et al.* [139] showed that the α-conotoxin Qc1.2, from *Conus quercinus* Lightfoot, had little effect on rat neuronal α7 subtype at 1 μM and at 10 μM it blocked ACh (100 μM)-elicited currents in α3β2 and α3β4 nAChR subtypes, but not in α4β2 subtype. Similarly, other α-conotoxin, GID, from *C. geographus* L., strongly inhibited rat α7 and α3β2, was less active as α4β2 antagonist, but was at least 1000-fold less potent at α3β4 and α4β4 receptors [137]. α-Conotoxins ImII and ImI from *Conus imperialis* L. were less active than GID against rat α7 nAChR. Using crude rat brain membranes, only ImI (EC_{50} = 1.56 nM) was able to displace 3–^{125}I-α-bungarotoxin (4 nM), a snake toxin that is a classical reversible competitive inhibitor of some nAChR subtypes, such as α7 subtype [138].

αD-contoxin VxXIIB was more potent against α7, α3β2 and α4β2 receptors than VxXIIA and VxXIIC, all of them found in the venom of *Conus vexillum* Gmelin [134].

Despite not being produced by marine invertebrates, some phycotoxins are accumulated in phytoplankton and mollusc digestive glands. Examples are the macrocyclic imines spirolines and gymnodimines, which caused fast neurotoxic death when administered to mice. Indeed, four spirolides, A, B, C, and 20-methyl spirolide G, were toxic to mice by intraperitonneal injection, with LD_{50} values of 37.0, 99.0, 8.0 and 8.0 μg/kg BW, respectively [143]. Spirolines function as brain mAChR and nAChR antagonists, while gymnodimines target muscle and neuronal nAChR [141,143]. Besides inhibiting ACh (25 or 150 μM)-evoked currents in neuronal nAChRs, gymnodimine and

13-desmethyl spirolide C from the dinoflagellate *A. ostenfeldii* were also able to inhibit the nicotine (10 μM)-mediated dopamine release from rat striatal synaptosomes containing both α4β2 and α6* receptors, displaying IC_{50} values of 0.3 and 0.2 nM, respectively [140].

6.5. Glutamate Receptors

Glutamate (L-Glu) and aspartate are excitatory neurotransmitters in the CNS. They cause excitotoxicity by hyperactivating post-synaptic glutamate receptors, which is observed in ischemia, hypoglycemia, epileptic seizures and in neurodegenerative diseases, such as AD, Parkinsonism, amyotrophic lateral sclerosis and Huntington's disease. Additionally, pre-synaptic glutamate receptors can modulate neurotransmitter release. There are two types of receptors: ionotropic (ligand-gated cation channels) and metabotropic (G-protein coupled) receptors. Within ionotropic receptors, the three major types are *N*-methyl-D-aspartate (NMDA) receptors (NR1, NR2A-D and NR3A-B), α-amino-3-hydroxy-5-methyl-4-isoazolepropionic acid (AMPA) receptors (GluR1–4) and 2-carboxy-3-carboxymethyl-4-isopropenylpyrrolidine (kainate) receptors (GluR5–7 and KA1–2) [144–147]. The excitotoxic effect of the receptor agonists is associated with the massive entry of Ca^{2+} into the cells, inducing multiple cytotoxic damage to the neurons, such as perturbation of cytoskeletal proteins and activation of proteases and phospholipases [144,145,148]. However, under physiological conditions, glutamate offers a beneficial effect on the regulation of neuronal function, growth and differentiation [145].

Neodysiherbaine (Figure 4; 50 μM), isolated from the marine sponge *Dysidea herbacea* Keller, is an agonist of AMPA (GluR4) and of kainate (GluR5, GluR6, KA2) receptors [146] and an extract obtained from the marine sponge *Suberites domuncula* Olivi containing quinolinic acid (Figure 4) is an agonist of NMDA receptors [149].

Two important marine toxins that also bind KA and AMPA receptors and provoke excitotoxicity are kainic and domoic acids, algae-derived metabolites that can accumulate in shellfish. Both acids are potent agonists of kainate and AMPA subclasses of Glu-receptors [150]. Doucette *et al.* [151] tested the toxicity of these two toxins in neonatal rats. Domoic acid proved to be more toxic than kainic acid (ED_{50} = 0.08 and 0.43 mg/kg at postnatal day 8 and ED_{50} = 0.19 and 1.19 mg/kg at postnatal day 14).

On the other hand, several antagonists of glutamate were isolated from marine invertebrate organisms. Aiello *et al.* [152] incubated rat primary cortical cells with 200 μM of L-Glu and 2.4 mM $CaCl_2$, which resulted in a strong rise in $[Ca^{2+}]i$. However, incubation of daminin (Figure 4; 0.5, 1.0 and 3.0 μg/mL), a bioactive pyrrole alkaloid from the sponge *Axinella damicornis* Esper, resulted in a significant decrease of $[Ca^{2+}]i$. Moreover, this alkaloid (1.0 μg/mL) also reverted the increase of $[Ca^{2+}]i$ induced by 200 μM of NMDA and 2.4 mM $CaCl_2$. A similar neuroprotective effect was found for four bromopyrrole alkaloids (Figure 4) characteristic of the sponge *Axinella verrucosa* Esper [145]. Pre-incubation of rat neurons with 10 μg/mL of these compounds counteracted the increase in $[Ca^{2+}]i$ provoked by 200 μM L-Glu and 2.5 mM $CaCl_2$. Moreover, they also decreased the rise of free $[Ca^{2+}]i$ induced by 200 μM quisqualic acid (QUIS), a selective agonist of the metabotropic glutamate receptors, and by 2.5 mM $CaCl_2$.

Figure 4. Potent marine modulators of voltage-dependent and ligand-gated ion channels.

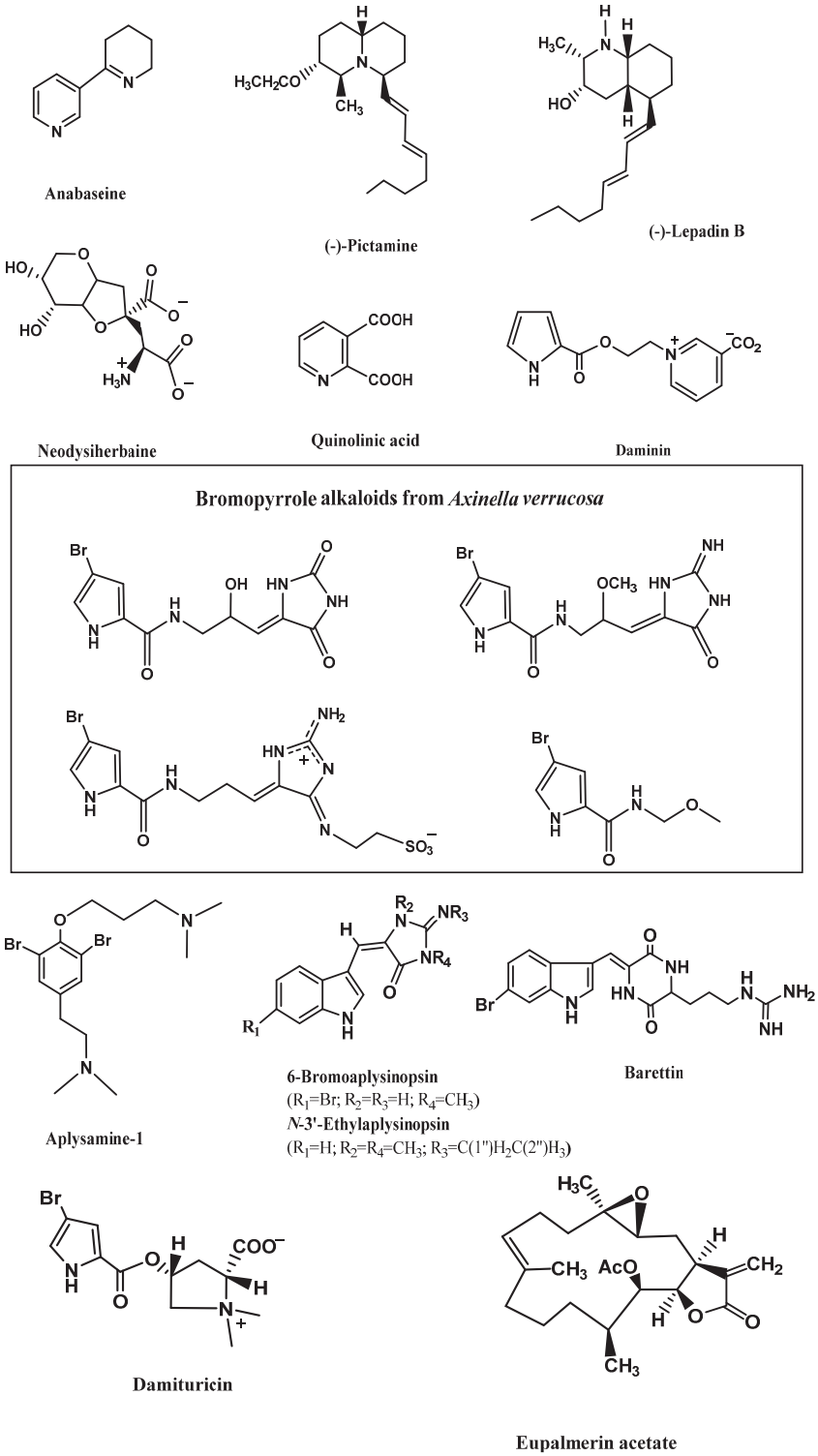

The peptides conantokins are NMDA receptor antagonists present in *Conus* venoms and are currently being tested as potential anticonvulsants. Jimenez *et al.* [153] showed that, although conantokin-L appears to be almost as potent as conantokin-R in NMDA receptor binding assays, the last is a more potent anticonvulsant compound, with a protective index of 17.5 (*vs.* 1.2 for conantokin-L) when tested in the audiogenic mouse model of epilepsy. Furthermore, conantokin-R was 2–5 times more effective (IC_{50} = 93 nM) than conantokin-G or conantokin-T as NMDA receptor antagonist, in the assay involving inhibition of binding of the non-competitive antagonist of the NMDA receptor, [^{3}H]MK-801, to the NMDA receptors in rat brain membranes [154]. Anyway, conantokin-G showed neuroprotection in a rat model of focal cerebral ischemia, when delivered intrathecally, and its protection lasted for 8 h [155].

6.6. Serotonin Receptors

Serotonin (5-HT) is a neurotransmitter that plays an important role in normal brain function and modulation of sleep, mood, appetite, sexual function, memory, among others. This neurotransmitter binds to different subtypes of serotonin receptors ($5HT_1$–$5HT_7$). $5HT_3$ receptor is the only class of ligand-gate ion channels, while the others are G protein-coupled receptors [14].

Hu *et al.* [156] isolated twelve compounds from the sponge *Smenospongia aurea* Pulitzer-Finali, which included the sesquiterpenes aureol, 6′-chloroaureol and aureol acetate, and the alkaloids 3-carboxylindole, *N*,*N*-dimethyltryptamine, isoplysin A, 2′-de-*N*-methyl-aplysinopsin, 6-bromo-2′-de-*N*-methylaplysinopsin, 6-bromoaplysinopsin (Figure 4), *N*-3′-methylaplysinopsin and *N*-3′-ethylaplysinopsin (Figure 4). In the radioligand binding assays of crude membranes, only 6-bromo-2′-de-*N*-methylaplysinopsin (*Ki* = 2.3 μM), 6-bromoaplysinopsin (*Ki* = 0.3 μM) and *N*-3′-ethylaplysinopsin (*Ki* = 3.5 μM) displaced high-affinity [^{3}H]mesulergine binding from cloned human $5\text{-}HT_{2C}$ receptors. The last two compounds also displaced [^{3}H]methylspiperone from $5\text{-}HT_{2A}$ subtype (*Ki* = 2.0 and 1.7 μM, respectively). Structure–activity analysis of these aplysinopsins revealed the importance of the functional groups at positions 6, 2′ and 3′ to bind to the receptors. The length of the alkyl chain at 3′ is a key factor, since the active *N*-3′-ethylaplysinopsin differs in one CH_3 group in relation to the inactive *N*-3′-methylaplysinopsin. When ethylation is not present, 6-bromination contributes to the binding activity and is also important for selective binding to the $5\text{-}HT_{2C}$ receptor subtype. Moreover, methylation in position 2' contributes for the selectivity towards $5\text{-}HT_{2A}$ receptors.

Hedner *et al.* [157] tested two brominated cyclodipeptides from the sponge *Geodia barrette* Bowerbank for binding different subtypes of 5-HT receptors expressed in HEK-293 cell membranes ($5\text{-}HT_{1A}$, $5\text{-}HT_{1D}$, $5\text{-}HT_{2A}$, $5\text{-}HT_{2C}$, $5\text{-}HT_{3A}$, $5\text{-}HT_4$, $5\text{-}HT_{5A}$, $5\text{-}HT_6$ and $5\text{-}HT_{7A}$). 8,9-Dihydrobarettin had affinity only for $5\text{-}HT_{2C}$ (*Ki* = 4.63 μM), while barettin binded to $5\text{-}HT_{2A}$ (*Ki* = 1.93 μM), $5\text{-}HT_{2C}$ (*Ki* = 0.34 μM) and $5\text{-}HT_4$ (*Ki* = 1.91 μM). Barettin (Figure 4) clearly has its advantages at the $5\text{-}HT_{2C}$ receptor, with a selectivity ratio of 5.68 ($5\text{-}HT_{2A}$/$5\text{-}HT_{2C}$) between the two $5\text{-}HT_2$ receptor subtypes. The small difference between barettin and 8,9-dihydrobarettin, which differ in one double bond in the tryptophan residue, greatly affected the affinity.

Two bromopyrrole alkaloids, damipipecolin and damituricin (Figure 4), from the sponge *Axinella damicornis* Esper, displayed a modulating effect of serotonin receptor activity *in vitro*.

The marked increase of $[Ca^{2+}]i$ observed in primary neural cells under the effect of 200 μM 5-HT and 2.5 mM $CaCl_2$ was strongly reduced by damipipecolin (0.1 μg/mL) or damituricin (0.1 μg/mL). However, only damituricin displayed the same behaviour in PC12 cells, revealing that it is a strong 5-HT_3 antagonist [158].

6.7. Histamine (H_3) Receptor

There are four types of histamine receptors, namely H_1, H_2, H_3 and H_4. H_3 receptor is an attractive G protein-coupled receptor drug target that modulates neurotransmission in the CNS and plays a role in cognitive and homeostatic functions. H_3 receptors are located pre-synaptically and their antagonists regulate sleep, food intake and obesity, memory, spatial recognition, attention, impulsivity, psychosis, seizures and depression, since they have a direct effect on neurotransmitters' release, particularly acetylcholine, noradrenaline and dopamine. Therefore, this receptor is an attractive CNS drug target [159,160].

Aplysamine-1 (Figure 4), a bromotyrosine derived metabolite isolated from the sponge *Aplysina* sp., was found to possess a high binding affinity for the human H_3 receptor (Ki = 30 ± 4 nM). The human and rat binding affinities were determined for aplysamine-1 and a series of analogs. Structure–activity relationship analysis examined three regions, the bromo-substituent effect, the alkoxy and alkyl amine chain lengths and the size of the two amine groups. Increases are observed when the removal of the aryl bromines or the replacement of the dimethylamine on the alkoxy chain with a piperidine occurs [160].

6.8. $GABA_A$ Receptor

The ionotropic γ-aminobutyric acid receptors ($GABA_AR$) are a member of the superfamily of ligand-gated ion channels sharing many structural and functional features with the nicotinic receptor. The $GABA_AR$ mediates the major component of fast inhibitory transmission in the CNS, and potentiators of the $GABA_AR$ can act as anxiolytics, anticonvulsants, hypnotics, tranquillizers or anaesthetics [161]. $GABA_AR$ are pentameric heteromers assembled from 5 of 19 subunits (six α, four β, three γ, one δ, one ε, one π, and three ρ subunits), each encoded by different genes [162].

Eupalmerin acetate (Figure 4) is a marine diterpene compound isolated from the gorgonian octocorals *Eunicea succinea* Pallas and *Eunicea mammosa* Lamouroux. This compound dose-dependently (3 or 30 μM) potentiated macroscopic currents elicited by GABA (5 μM) or pentobarbital (100 μM) in HEK cells expressing α1β2γ2L, displaying an EC_{50} of 17.4 μM. This potentiation was reduced when 1 mM of GABA was applied. Single-channel experiments were conducted with GABA (50 μM) and eupalmerin acetate (40 μM) and revealed that the diterpene was mechanistically similar to neurosteroids and probably interacts with the steroid-binding site. Indeed, (3α,5α)-17-phenylandrost-16-en-3-ol, an antagonist of neurosteroids potentiation, but not of barbiturates and benzodiazepines, reduced the effect of eupalmerin acetate in HEK cells [161].

6.9. Glycine Receptors

Glycine-gated chloride channel receptors (GlyRs) are members of ligand-gated ion channels family comprising subunits α1–α4 and β. As $GABA_AR$, they are key modulators of inhibitory neurotransmission in CNS. GlyRs are formed either as pentameric homomers or as αβ heteromers [163]. Potentiators and antagonists of glycine receptors are listed in Table 11 [163–165].

Table 11. Marine drugs as GlyR modulators.

Compounds/Organisms	GlyR subtype	Inhibition (IC_{50}), μM	Potentiation (EC_{50}), μM
8-Hydroxyircinialactam B/sponge *Sarcotragus* sp.	α1	0.5 [164]	-
8*E*-3′-Deimino-3′-oxoaplysinopsin + 8*Z*-3′-deimino-3′-oxoaplysinopsin/sponge *Lanthella flabelliformis* Pallas	α1	>200 [163]	-
Tubastrindole B/sponge *L. flabelliformis* Pallas	α1	25.9 [163]	-
(−)-Ircinianin sulfate/sponge *Psammocinia* sp.	α1	38.4 [165]	-
(12*E*,20*Z*,18*S*)-8-Hydroxyvariabilin/sponge *Ircinia variabilis*	α1	-	1.2 [164]
8*E*-3′-Deimino-3′-oxoaplysinopsin + 8*Z*-3′-deimino-3′-oxoaplysinopsin/sponge *L. flabelliformis* Pallas	α3	67 [163]	-
(12*E*,20*Z*,18S)-8-hydroxyvariabilin/sponge *I. variabilis*	α3	7.0 [164]	-
(−)-Ircinianin sulfate/sponge *Psammocinia* sp.	α3	3.2 [165]	-
Ircinialactam A/sponge *Sarcotragus* sp.	α3	30–100 [164]	-
Ircinialactam C/sponge *Sarcotragus* sp.	α3	30–100 [164]	-
Ent-ircinialactam C/sponge *Sarcotragus* sp.	α3	30–100 [164]	-
Ircinialactam D/sponge *Sarcotragus* sp.	α3	30–100 [164]	-
Tubastrindole B/sponge *L. flabelliformis* Pallas	α3	>300 [163]	-
Ircinianin lactam A/sponge *Psammocinia* sp.	α3	-	8.5 [165]

Balansa *et al.* [163] isolated two new sesquiterpene glycinyl lactams, ianthellalactams A and B, the sesquiterpene dictyodendrillin and its ethanolysis artifact ethyl dictyodendrillin, and five indole alkaloids, aplysinopsin, 8*E*-3′-deimino-3′-oxoaplysinopsin, 8*Z*-3′-deimino-3′-oxoaplysinopsin, dihydroaplysinopsin and tubastrindole B. They also synthetized alkaloid analogs to establish a relationship between the structure and the inhibitory activity towards GlyR. They concluded that conversion of 3′-imino to 3′-oxo moiety and the increase of *N*-methylations led to an increase of inhibition.

6.10. Norepinephrine Transporter (NET)

χ-Conopeptide MrIA and MrIB from *Conus marmoreus* L. inhibited the norepinephrine transporter [166,167]. χ-MrIA inhibited the binding of [^{3}H]nisoxetine to the membranes of cells expressing the rat and human NET. The IC_{50} for inhibition was 500 nM for the rat NET and 1.7 μM for the human NET. [^{3}H]mazindol binding to the expressed transporters was also sensitive to χ-MrIA, exhibiting IC_{50} values of 1.9 μM at the rat NET and of 4.0 μM at the human NET. In cells

transfected with the human NET, MrIA became a less effective blocker of [^{3}H]norepinephrine under reduced extracellular Na^+ conditions [166].

7. Protective Effect of Marine Drugs Using Cell Models for Neurodegenerative Disorders

Although some cnidarian venoms, such as those isolated from the nematocysts of the jellyfish *Pelagia noctiluca* Slabber, induce oxidative stress on neuronal-like cells derived from human neuroblastoma SH-SY5Y, by disrupting mitochondrial membrane potential [168], several marine drugs have shown protective effect on several cell models for neurodegenerative diseases.

7.1. Protection against Aβ-Induced Neurotoxicity

Aβ peptide induces protein oxidation, lipid peroxidation and reactive oxygen species (ROS) formation in AD patients' brains [54]. Neuronal dysfunction in AD may occur before the deposition of insoluble fibrillar Aβ and seems to be mediated by soluble Aβ oligomers [56,169]. Peptides with shorter sequences, such as Aβ25–35, can also result from certain forms of Aβ1–40. This short peptide has been reported to be more soluble and easier to inject *in vivo* than Aβ1–40, as it is more toxic and causes more oxidative damage [56,84].

The steroids (3β,4α,5α,8β,11β)-4-methylergost-24(28)-ene-3,8,11-triol (Figure 5) and ergost-4,24 (28)-diene-3-one (Figure 5), from the soft coral *Sinularia depressa* Tixier-Durivault, at 10 μM, displayed neuroprotective effects against Aβ25–35 (10 μM)-induced cellular injuries in SH-SY5Y cells and induced the increase of cell viability by 20.1% and 16.6%, respectively [170].

7.2. Protection against 6-Hydroxydopamine (6-OHDA)-Induced Neurotoxicity

The neurotoxin 6-OHDA is a hydroxylated analog of dopamine, commonly used to study dopaminergic degeneration, both *in vitro* and *in vivo*. Like DA, 6-OHDA quickly oxidizes to form ROS, including hydrogen peroxide (H_2O_2), superoxide ($O_2^{\bullet-}$) and hydroxyl radicals (•OH) [61,171,172]. This neurotoxin also reduces striatal glutathione (GSH) and superoxide dismutase (SOD) enzyme activities and increases the level of malondialdehyde [173,174]. Besides causing oxidative stress, 6-OHDA also leads to respiratory inhibition, as it is toxic to the mitochondrial complex I [175]. Both mechanisms are not necessarily linked, but appear to act synergistically during neuron degeneration. However, 6-OHDA model does not mimic all pathological and clinical features of human Parkinsonism, because it induces dopaminergic neuron death with preservation of non-dopaminergic neurons, without formation of cytoplasmic inclusions (Lewy bodies). Moreover, 6-OHDA does not affect other brain areas involved in PD, and Parkinsonian-like tremor is rare in studies of 6-OHDA-lesioned rodents [60].

11-Dehydrosinulariolide (Figure 5), a terpenoid obtained from the marine soft coral *Sinularia flexibilis* Quoy and Gaimard, displayed protective effects against 6-OHDA (20 μM)-induced cytotoxicity in SH-SY5Y cells, at concentrations ranging from 1 nM to 1 μM. Moreover, pre-treatment with 11-dehydrosinulariolide (10 nM) also inhibited the down-regulation of phospho-Akt protein expression induced by 6-OHDA, as well as inhibited 6-OHDA-induced caspase-3/7 activation and 6-OHDA-induced translocation of NF-κB to the nucleus. 11-Dehydrosinulariolide (10 nM)

inhibited the down-regulation of p-ERK induced by 6-OHDA [176]. The PI3K–Akt and ERK (p42/p44 mitogen-activated protein kinase) pathways are important factors in neuronal cell survival. Their activation was suggested to have neuroprotective effects in PD [176]. AKT, a Ser/Thr protein kinase, regulates a variety of cellular processes, including cell survival, proliferation, protein translation and metabolism [177]. PI3K pathway can activate the kinase Akt, which is also implicated in cell survival, proliferation and growth, as well as in glycogen metabolism [178]. NF-κB is an inducible transcription factor that plays an important role in human inflammatory processes and various neurodegenerative diseases [179,180]. Moreover, the same authors [176] verified the *in vivo* effects of 11-dehydrosinulariolide, which was able to significantly attenuate the 6-OHDA-induced reduction of mean swimming velocity and total swimming distance in zebrafish.

A similar result was found for the sulfur-containing biscembranolide thioflexibilolide A (Figure 5), isolated from the same soft coral. Thioflexibilolide A exhibited neuroprotective activity against 6-OHDA in SH-SY5Y cells between 0.001 and 10 μM, displaying relative neuroprotective effect of 37.2 (at 0.001 μM) and 73.2% (at 0.01 μM), though it decreased for higher concentrations [181].

In a study developed by Ikeda *et al.* [172], the treatment with 6-OHDA (100 μM) markedly induced apoptosis in SH-SY5Y cells by 2.8-fold, but a pre-treatment with astaxanthin (Figure 5; 1–20 μM) significantly suppressed apoptosis in a dose-dependent manner (6%–54% inhibition). Astaxanthin (5–20 μM) also dose-dependently suppressed the cleavage of caspase 3 and of poly(ADP-ribose) polymerase (PARP) induced by 6-OHDA (100 μM), indicating that this compound inhibited caspase-3 activation, as well as caspase 3 activity by 14% (5 μM), 40% (10 μM), and 49% (20 μM). Astaxanthin (20 μM) also displayed protective effect against 6-OHDA (100 μM)-induced mitochondrial dysfunctions, since it significantly increased membrane potential ($\Delta\Psi m$), protected cytochrome c and inhibited caspase 9 cleavage, which is triggered by mitochondrial dysfunction. In addition, 6-OHDA (100 μM) induced both p38 MAPK and ERK1/2 activation, whereas astaxanthin (20 μM) blocked the activation of p38 MAPK, but not of JNK1/2 or ERK1/2. Like astaxanthin, pre-treatment with SB203580 (20 μM), a specific inhibitor of p38 MAPK, also displayed the same protective effects against mitochondrial dysfunction. Finally, a pre-treatment with astaxanthin (5–20 μM) also significantly decreased 6-OHDA-induced ROS generation in a dose-dependent manner (11, 41 and 55% inhibition at 5, 10, and 20 μM, respectively) [172].

7.3. Protection against 1-Methyl-4-Phenyl-Pyridine Ion (MPP^+)-Induced Neurotoxicity

The model using the dopaminergic neurotoxin 1-methyl-4-phenyl-1,2,3,6-tetrahydropyridine (MPTP), an analog of the narcotic meperidine, causes intoxication of dopaminergic structures and induces symptoms resembling PD in humans. MPTP is highly lipophilic and after systemic administration rapidly crosses the BBB. Afterwards, this toxin is converted to 1-methyl-4-phenyl-2, 3-dihydropyridium (MPDP) in non-dopaminergic cells (mainly in astrocytes and serotonergic neurons) by the enzyme monoamine oxidase B (MAO-B) and then spontaneously oxidizes to MPP^+. This polar molecule enters dopaminergic cells through carrier systems and causes oxidative stress. MPP^+ inhibits the mitochondrial complex I, causing abnormal energy metabolism and increased ROS ($O_2^{\bullet-}$, H_2O_2 and •OH) production, resulting in lipid peroxidation, DNA

fragmentation, mitochondrial impairment, LDH leakage, GSH depletion, reduction of Na^+/K^+-ATPase and catalase activities, increased caspase-3 activity and cell death [60,182].

Figure 5. Marine compounds with protective effects against Aβ, 6-OHDA, MPP^+ and IAA.

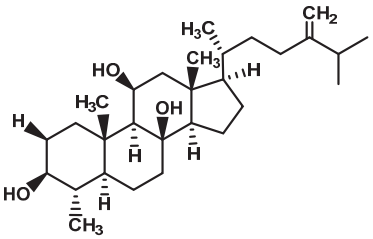

(3β,4α,5α,8β,11β)-4-Methylergost-24(28)-ene-3,8,11-triol

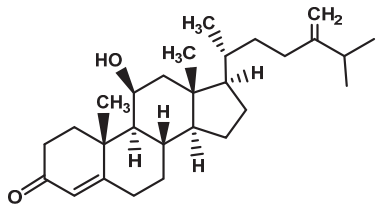

Ergost-4,24(28)-diene-3-one

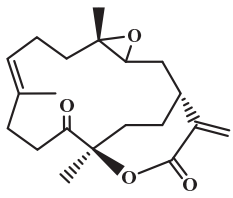

11-Dehydrosinulariolide

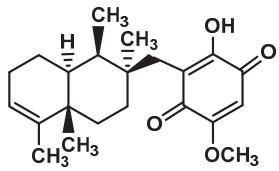

Bolinaquinone

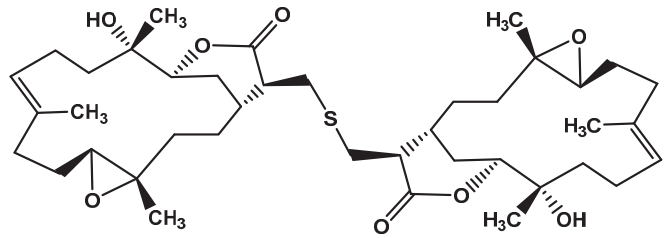

Thioflexibilolide A

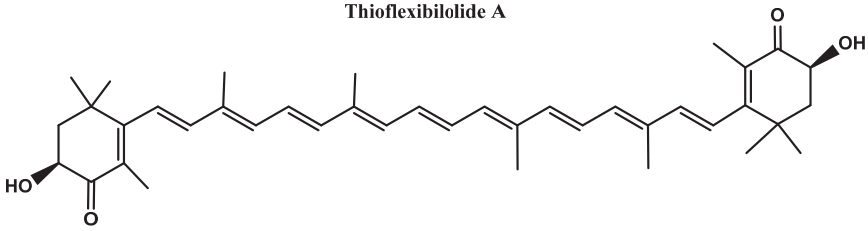

Astaxanthin

Astaxanthin (Figure 5; 10 and 20 μM) showed neuroprotective effects against the neurotoxin MPP^+ (500 μM) in PC12 cells, increasing cell viability by 3.46%. Moreover, mithramycin A (0.36 μM), a specific SP1-DNA binding inhibitor, increased viability by 34.94%, and a co-treatment with mithramycin A (0.36 μM) plus astaxanthin (10 μM) increased cell survival by 26.77%. During oxidative stress, the transcription activator Sp1 is up-regulated, leading to up-regulation of NMDA

receptor subunit 1 (NR1), which initiates neuronal cell death. Expression of Sp1 and NR1 protein levels in the MPP^+ group increases and Sp1 is transferred from nuclei to cytoplasm, but this effect is also reverted by mithramycin A and/or astaxanthin. MPP^+ (500 μM) treatment led to an increase of ROS activity by 26.14%, but astaxanthin induced ROS activity to decrease by 4.75% at 5 μM, 9.36% at 10 μM, 14.60% at 20 μM. Mithramycin A (0.36 μM) only provoked a decrease of 8.79% [182].

7.4. Protection against Iodoacetic acid (IAA) Neurotoxicity

IAA induces cell death following depletion of intracellular ATP, mitochondrial dysfunction and production of ROS. Since these observations are similar to those of *in vivo* ischemic stroke, this is a good cell model to study this disease [38].

The neuroprotective effects of dysideamine (Figure 1) and bolinaquinone (Figure 5), sesquiterpene quinones isolated from the marine sponge *Dysidea* sp. 05C33, against IAA-induced cell death were examined. At 10 μM, both compounds exhibited neuroprotective effect against IAA-induced cell death (43 and 57% of cell survival for dysideamine and bolinaquinone, respectively). The IAA (10 or 20 μM)-treated mouse hippocampal neuronal cells HT22 showed depletion of intracellular ATP, mitochondrial dysfunction and increase of ROS production, which was inhibited by dysideamine (10 μM) [38].

8. Anti-Neuroinflammatory Activity of Marine Drugs

Neuroinflammation is a complex process involved in the pathology of several CNS diseases, such as AD, PD, multiple sclerosis and ischemic stroke, and involves activated microglia [183,184]. Activated microglial cells activate inflammatory mediators, such as proteolytic enzymes [185], ROS and reactive nitrogen species [183–186], eicosanoids [186,187], pro-inflammatory cytokines [185,186,188] and chemokines [185,186,189], which can promote nociceptive transmission by causing activation of dorsal horn neurons. Many studies have indicated that inhibition of microglial activation attenuates the development of neuropathy [183].

Two COX isozymes, COX-1 and COX-2, catalyse the rate-limiting steps of eicosanoids (prostaglandin (PG) and thromboxane) synthesis, by converting arachidonic acid into PGG2 and PGH2 and then into PGE2, PGF2α, PGD2, PGI2 and tromboxanes (TXB2) [187]. Prostaglandins are critically involved in peripheral and spinal nociceptive sensitization. In general, COX1 is considered to be constitutive, while COX2 is considered as inducible, especially under inflammatory conditions. In the brain, COX2 is constitutively expressed only by specific neuronal populations, particularly in the hippocampus, being necessary for synaptic plasticity and memory acquisition. Inhibition of COX-2, but not of COX-1, by selective inhibitors attenuates hyperalgesia in neuropathic rats [190]. Moreover, although nitric oxide (•NO) acts as cellular messenger and modulates neurotransmition, its overproduction has been associated with neuropathological disorders, such as stroke, AD and PD [191]. Therefore, COX 1 and COX 2, as well as the enzyme neuronal nitric oxide synthase (nNOS), responsible for the synthesis of •NO, represent important therapeutic targets for the development of novel anti-neuroinflammatory drugs.

Sinularin (Figure 6), a cembranolide diterpene isolated from the soft coral *Sinularia querciformis* Pratt, displayed *in vitro* anti-inflammatory activity by significantly inhibiting up-regulation of pro-inflammatory proteins (inducible NOS (iNOS) and COX-2) in LPS-stimulated murine macrophage RAW 264.7 cells. Sinularin (0.1–20 μM) dose-dependently reduced the levels of iNOS and increased those of TGF-β, while COX-2 levels were only reduced at 10 and 20 μM. *In vivo*, subcutaneous administration of sinularin (80 mg/kg, intraplantar) to rats had analgesic effects and inhibited carrageenan-induced spinal neuroinflammation, up-regulation of microglial and astrocyte activation and up-regulation of iNOS in the dorsal horn of the lumbar spinal cord. Furthermore, treatment with sinularin (80 mg/kg) clearly inhibited carrageenan-induced leukocyte infiltration and up-regulated TGF-β1, demonstrating its analgesic effect [192]. Nanolobatolide (Figure 6), a C_{18} terpene from the soft coral *Sinularia nanolobata* Verseveldt, at 10 μM, also reduced the accumulation of iNOS in microglial cells stimulated with INFγ to 45.5% [193].

Δ9(12)-Capnellene-8β,10α-diol (Figure 6; GB9), a sesquiterpene isolated from the soft coral *Capnella imbricata* Quoy and Gaimard, was able to down-regulate the expression of pro-inflammatory iNOS (IC_{50} = 17.1 μM) and COX-2 (IC_{50} = 6.21 μM) in INFγ-stimulated mouse microglial cells (BV2). Moreover, GB9 revealed an analgesic effect *in vivo*. GB9 (10 mg/kg, intraperitoneal) significantly inhibited chronic constriction injury (CCI)-induced thermal hyperalgesia behaviour in rats, as well as inhibited CCI-induced elevation of microglial and neuronal COX-2 in the spinal cord [183].

Diterpene isocyanides isolated from marine sponge *Hymeniacidon* sp. (7-isocyano-11(20)-15 (16)-amphilectadiene, (−)-8,15-diisocyano-11(20)-amphilectene (Figure 6), 7,15-diisocyano-11 (20)-amphilectene (Figure 6), 8-isocyano-11(20)-ene-15-amphilectaformamide and monamphilectine A) were screened for anti-neuroinflammatory activity in LPS-activated rat brain microglia. They inhibited TXB2 generation (IC_{50} = 0.20–4.69 μM), (−)-8,15-diisocyano-11(20)-amphilectene (IC_{50} = 0.23 μM) and 7,15-diisocyano-11(20)-amphilectene (IC_{50} = 0.20 μM) being the most active ones. However, all demonstrated minimal effect on $O_2^{\bullet-}$ release (IC_{50} > 10 μM) [184]. Using the same system, Rodriguéz *et al.* [194] and Shi *et al.* [195] tested the anti-inflammatory activity of diterpenoid compounds isolated from the gorgonian *Pseudopterogorgia elisabethae* Bayer. The most promising ones were pseudopterosin Q (Figure 6) (IC_{50} = 4.7 μM against TXB2 and IC_{50} = 11.2 μM against $O_2^{\bullet-}$ [194] and elisabethin H (Figure 6; IC_{50} = 7.0 μM against $O_2^{\bullet-}$) [195]. However, due to its cytotoxicity (LDH release > 50% at 3.4 μM), the inhibition of TXB2 by pseudopterosin Q could result, at least in part, from a toxic rather than a pharmacological effect [194].

Finally, the brominated tryptophan-derived eusynstyelamides A, B, and C (Figure 6), isolated from the ascidian *Eusynstyela latericius* Sluiter, exhibited inhibitory activity against nNOS in rat cerebella, with IC_{50} values of 41.7, 4.3 and 5.8 μM, respectively [191].

Figure 6. Anti-neuroinflammatory marine compounds.

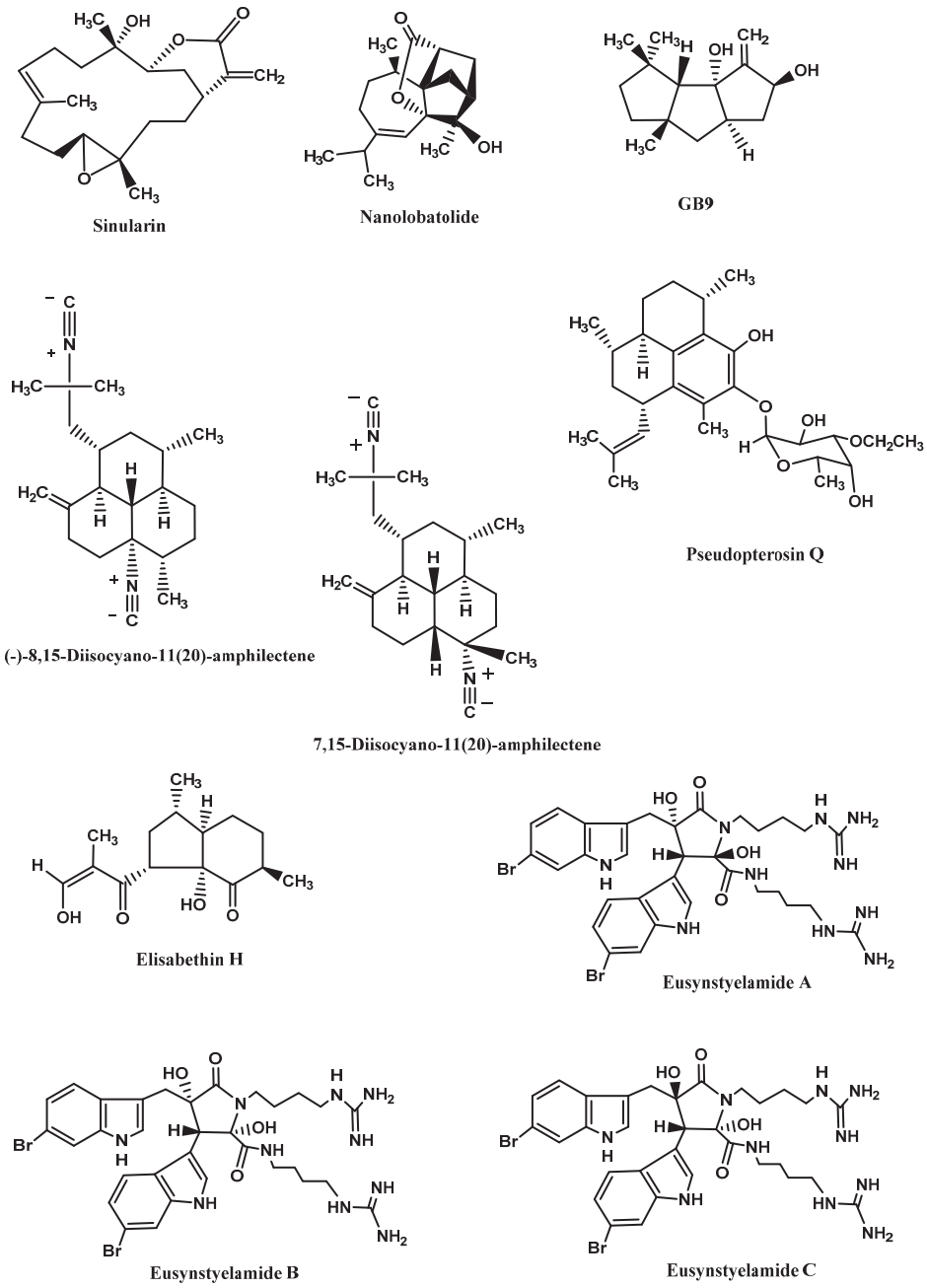

9. Marine Skeletons as Scaffolds for Neural Tissue Engineering

When large tissue volume is lost due to an injury, tissue implantation is advantageous over cell therapy because it enables controlled organization of neurons into intricate networks before

implantation [28]. Thus, the aim of bioengineering is to deliver cells and signalling factors to a target tissue in combination with a non-cellular scaffolding material, which is an immobilization matrix that facilitates tissue ingrowth and regeneration [196]. This three-dimensional (3D) cell cultures mimic the cytoarchitecture of *in situ* tissue to a higher degree than cells grown on non-physiological hard surfaces (2D) and, therefore, 3D cultures have been shown to result in longer neurite outgrowth, higher levels of survival and distinct patterns of differentiation as compared to 2D monolayers [197]. An ideal 3D scaffold must not only facilitate the adherence, spread and outgrowth of neurons and neuronal process, but also possess a large number of pores to allow cell expansion and diffusion transport of nutrients and waste molecules to and from the cells. Naturally derived scaffolds (e.g., gels of collagen and chitosan, polysaccharide fibres and aragonite) and synthetic polymers, such as methyl cellulose, poly(α-hydroxyacids), poly(glycolic acid), poly(L-lactic acid) and poly(lactic-co-glycolic acid) are being tested [198–201].

One of the most efficient scaffolds for neural development is the biodegradable and biocompatible aragonite, a needle-like crystalline form of calcium carbonate ($CaCO_3$) present in the exoskeleton of foraminiferans, sponges, corals, hydrozoans, molluscs (gastropods, bivalves, cephalopods), worms, arthropods (ostracods, barnacles). In invertebrates, this skeleton provides mechanical support for the soft tissues and act as a storage system withdrawing ions during times of special physiological demand [196,202,203]. This scaffold presents several advantages over other templates, like hydrogels, not only because its pores are much larger than those of the hydrogels (160 mm *vs.* few microns), allowing many more cells to accumulate, but also because it can release Ca^{2+} to the medium, promoting cell adhesion, cell–cell contact and survival. Moreover, it also provides higher mechanical strength than hydrogels and the absence of a gel covering the cells may facilitate the explant–tissue interactions [202].

Shanny *et al.* [198] grew rat hippocampal primary neurons on aragonite skeleton of the coral *Porites lutea* Link and observed that the neurons usually grew on a sheet of glial cells and acquired the morphology of hippocampal pyramidal and granule neurons. Moreover, dendrites were branched and long, sometimes extending more than 100 μm away from the cell body, and axons were thinner than dendrites and grew up to hundreds of μm in length in all directions, covering the entire surface of the aragonite support. Synaptic connections were active in these neurons, since the presynaptic sites expressed the synaptic vesicle protein 2 (SV2) and post-synaptic spines contained the glutamate receptors GluR1. Peretz *et al.* [202] proved that *P. lutea* aragonite matrix not only was a good support to cell growth *in vitro*, but also *in vivo*. They implanted the scaffolds in cortical regions of postnatal rat brains and observed that the implants did not cause any severe inflammation or rejection response and did not have significant influence on animal survival or behaviour. The implants were invaded by neural tissue and, besides supporting the survival of neurons in the cortex, they induced their invasion into the injured area.

Using a different marine scaffold, Baranes *et al.* [28] grew co-cultures of primary neurons and glia from rat hippocampi on aragonite matrices from the hydrozoan *Millepora dichotoma* Forsskål. Conversely to the *P. lutea* matrix, this scaffold supported ganglion-like cell spheres, rather than multi-layer cells, which included both astrocytes and mature neurons with active synaptic processes. The spheres were interconnected through fibres of neuronal and astrocytic processes and

most of the cells had only cell–cell and no cell–matrix interactions. This cell organization resembles more the *in vivo* situation, where neurons do not exhibit substrate contact. Moreover, it has also several advantages for neural tissue engineering, because most cells in the spheres are in contact with other cells, instead of with the matrix surface, and it is easier to detach cells from the scaffold since they are connected to the surface through a neck [28].

M. dichotoma-derived aragonite matrix was also used to study the Ca^{2+} uptake by neuronal and glial cells [199]. The authors found that hippocampal cells growing on $^{45}Ca^{2+}$ or calcein-labelled aragonite took up aragonite-derived Ca^{2+} and enhanced this uptake when extracellular Ca^{2+} ions were chelated by EGTA. These ions activate Ca^{2+}-dependent adhesion molecules, like cadherins, which play important roles in cell migration, cell rearrangement and maintenance of tissue integrity.

10. The Supply Problem

Despite the long research on marine drugs, few of them will be successfully marketed with the current technologies available [204]. This occurs because a sustainable supply of marine organisms is necessary to conduct preclinical and clinical trials. Indeed, the continuous supply problem is the major challenge to be overcome in programs of marine natural product drug discovery and development, in order to move on in the pipeline [205,206]. This problem is reflected in the few number of neuroprotective drugs approved by FDA (see Introduction section), as well as the few studies conducted *in vivo* cited in this review.

Several strategies to overcome the supply problem are being under development, such as sampling strategies, nanoscale NMR for structure elucidation, total chemical synthesis, semi-synthetic production, fermentation, and biotechnology [204,205]. Total synthesis may be the best approach to solve the problem. However, despite all efforts, until now few neuroprotective drugs can be obtained this way. As an example, of 184 compounds reffered to in this review, only a few were already obtained in laboratory. These compounds are listed in Table 12 by the order of appearance in the text.

Table 12. Compounds with their total synthesis described.

Compound	Class of compounds	Pharmacologic activity	Ref.
Lembehyne	Linear polyacetylene	Neuritogenic agent	[207]
Turbotoxin A	Diiodotyramine derivative	AChE inhibitor	[67]
Lamellarin O	Alkaloid	BACE1 inhibitor	[208]
Hymenialdisine and analogs	Diterpene isocyanide	Kinase inhibitor	[209–212]
Lamellarin D and analogs	Alkaloid	Kinase inhibitor	[213–216]
Lamellarin H	Alkaloid	Kinase inhibitor	[213]
Lamellarin L	Alkaloid	Kinase inhibitor	[215,217]
Lamellarin N	Alkaloid	Kinase inhibitor	[215]
Leucettamine B and analogs	Alkaloid	Kinase inhibitor	[90,218]
Manzamine A	Alkaloid	Kinase inhibitor	[219,220]
Palinurin	Furanoterpenoid	Kinase inhibitor	[221]
Fascaplysin	Alkaloid	Kinase inhibitor	[222,223]

Table 12. *Cont.*

ω-SO-3	ω-Conotoxin	Calcium channels modulator	[224]
δ-SVIE	δ-Conotoxin	Sodium channels modulator	[122]
μ-PIIIA	μ-Conotoxin	Sodium channels modulator	[116]
κM-RIIIK	κM-Conotoxin	Potassium channels modulator	[128]
Anabaseine	Alkaloid	AChR modulator	[225]
(−)-Pictamine	Alkaloid	AChR modulator	[226,227]
(−)-Lepadin B	Alkaloid	AChR modulator	[228–230]
α-Qc1.2	α-Conotoxin	AChR modulator	[139]
α-ImI	α-Conotoxin	AChR modulator	[138,231]
α-ImII	α-Conotoxin	AChR modulator	[138]
Spirolide C	Macrocyclic imine	AChR modulator	[232]
Gymnodimine	Macrocyclic imine	AChR modulator	[233]
Neodysiherbaine	Amino acid	Glu receptor modulator	[234–237]
Daminin	Alkaloid	Glu receptor modulator	[152]
Kainic acid	Amino acid	Glu receptor modulator	[238–241]
Domoic acid	Amino acid	Glu receptor modulator	[242]
Conatokin-L	Conantokin	Glu receptor modulator	[153,243]
Conatokin-R	Conantokin	Glu receptor modulator	[157]
Aureol	Sesquiterpene	5-HT receptor modulator	[244–246]
N,N-Dimethyltryptamine	Alkaloid	5-HT receptor modulator	[247]
Barettin	Brominated cyclodipeptide	5-HT receptor modulator	[248]
Damipipecolin	Bromopyrrole alkaloid	5-HT receptor modulator	[249]
Damituricin	Bromopyrrole alkaloid	5-HT receptor modulator	[249]
Aplysamine-1 and analogs	Bromotyrosine derived metabolite	histamine receptor modulator	[160,250]
Aplysinopsin and analogs	Indole alkaloid	Glycine receptor modulator	[251]
χ-MrIA	χ-Conotoxin	Norepinephrine transporter modulator	[166]
Astaxanthin	Carotenoid	Neuroprotection against 6-OHDA or MPP^+ treatments	[252]
Nanolobatolide	C_{18}-terpene	Anti-neuroinflammatory activity	[253]
Δ9(12)-Capnellene-8β, 10α-diol	Sesquiterpene	Anti-neuroinflammatory activity	[254,255]
(−)-8,15-Diisocyano-11 (20)-amphilectene	Diterpene isocyanide	Anti-neuroinflammatory activity	[256]
Monamphilectine A	Diterpene isocyanide	Anti-neuroinflammatory activity	[257]
Pseudopterosin	Diterpene	Anti-neuroinflammatory activity	[258–261]
Eusynstyelamide A	Brominated tryptophan-derivative	Anti-neuroinflammatory activity	[262]

11. Conclusions

Complete recovery from a CNS injury or disorder is not yet a reality. Regeneration of parts of the brain, where loss of large amount of neurons occurred, is very difficult. Drugs only alleviate the symptoms and/or delay the progression of the injury or disease, and cell and tissue implantation are still in their infancy. Therefore, the search for new neuroprotective drugs is still an urgent matter,

and natural products isolated from marine invertebrates are excellent candidates for drug development programs. This review intended to update the state of the art on this subject and to show how marine invertebrates neuroactive drugs affect neuronal growth and synaptic functions, neurodegeneration and neuroinflammation. We should continue to be optimistic about the future of therapy development for CNS disorders and continue to explore the marine environment, which is an inexhaustible source of neuroactive drugs.

Acknowledgments

The authors are grateful to the financial support from the European Union (FEDER funds through COMPETE) and National Funds (FCT, Fundação para a Ciência e Tecnologia) through project Pest-C/EQB/LA0006/2013 and from the European Union (FEDER funds) under the framework of QREN through Project NORTE-07–0124-FEDER-000069, to CYTED Programme (Ref. 112RT0460) CORNUCOPIA Thematic Network and project AGL2011–23690 (CICYT). Clara Grosso thanks FCT for the Post-Doc fellowship (SFRH/BPD/63922/2009).

Author Contributions

All authors contributed as the same for the manuscript preparation and design.

Conflicts of Interest

The authors declare no conflict of interest.

References

1. Kanwar, J.R.; Sriramoju, B.; Kanwar, R.K. Neurological disorders and therapeutics targeted to surmount the blood-brain barrier. *Int. J. Nanomedicine* **2012**, *7*, 3259–3278.
2. Glaser, K.B.; Mayer, A.M.S. A renaissance in marine pharmacology: From preclinical curiosity to clinical reality. *Biochem. Pharmacol.* **2009**, *78*, 440–448.
3. Mayer, A.M.S.; Rodríguez, A.D.; Berlinck, R.G.S.; Fusetani, N. Marine pharmacology in 2007–8: Marine compounds with antibacterial, anticoagulant, antifungal, anti-inflammatory, antimalarial, antiprotozoal, antituberculosis, and antiviral activities; affecting the immune and nervous system, and other miscellaneous mechanisms of action. *Comp. Biochem. Physiol. C Pharmacol. Toxicol. Endocrinol.* **2011**, *153*, 191–222.
4. Essack, M.; Bajic, V.B.; Archer, J.A.C. Conotoxins that confer therapeutic possibilities. *Mar. Drugs* **2012**, *10*, 1244–1265.
5. Mortari, M.R.; Cunha, A.O.S.; Ferreira, L.B.; dos Santos, W.F. Neurotoxins from invertebrates as anticonvulsants: From basic research to therapeutic application. *Pharmacol. Ther.* **2007**, *114*, 171–183.
6. Mayer, A.M.S.; Glaser, K.B.; Cuevas, C.; Jacobs, R.S.; Kem, W.; Little, R.D.; McIntosh, J.M.; Newman, D.J.; Potts, B.C.; Shuster, D.E. The odyssey of marine pharmaceuticals: A current pipeline perspective. *Trends Pharmacol. Sci.* **2010**, *31*, 255–265.

7. Kem, W. Alzheimer's drug design based upon an invertebrate toxin (anabaseine) which is a potent nicotinic receptor agonist. *Invertebr. Neurosci.* **1997**, *3*, 251–259.
8. Livett, B.G.; Gayler, K.R.; Khalil, Z. Drugs from the Sea: Conopeptides as potential therapeutics. *Curr. Med. Chem.* **2004**, *11*, 1715–1723.
9. Layer, R.T.; McIntosh, J.M. Conotoxins: Therapeutic potential and application. *Mar. Drugs* **2006**, *4*, 119–142.
10. Twede, V.D.; Miljanich, G.; Olivera, B.M.; Bulaj, G. Neuroprotective and cardioprotective conopeptides: An emerging class of drug leads. *Curr. Opin. Drug Discov. Devel*. **2009**, *12*, 231–239.
11. Sakai, R.; Swanson, G.T. Recent progress in neuroactive marine natural products. *Nat. Prod. Rep.* **2014**, *31*, 273–309.
12. Arias, H.R. Marine toxins targeting ion channels. *Mar. Drugs* **2006**, *4*, 37–69.
13. Al-Sabi, A.; McArthur, J.; Ostroumov, V.; French, R.J. Marine toxins that target voltage-gated sodium channels. *Mar. Drugs* **2006**, *4*, 157–192.
14. Kochanowska-Karamyan, A.; Hamann, M.T. Marine indole alkaloids: Potential new drug leads for the control of depression and anxiety. *Chem. Rev.* **2010**, *110*, 4489–4497.
15. Bharate, S.B.; Sawant, S.D.; Singh, P.P.; Vishwakarma, R.A. Kinase inhibitors of marine origin. *Chem. Rev.* **2013**, *113*, 6761−6815.
16. Skropeta, D.; Pastro, N.; Zivanovic, A. Kinase inhibitors from marine sponges. *Mar. Drugs* **2001**, *9*, 2131–2154.
17. Nakao, Y.; Fusetani, N. Enzyme inhibitors from marine invertebrates. *J. Nat. Prod.* **2007**, *70*, 689–710.
18. Senthilkumar, K.; Kim, S.-K. Marine invertebrate natural products for anti-inflammatory and chronic diseases. *Evid. Based Complement. Alternat. Med.* **2013**, *2013*, 572859:1–572859:10.
19. Martínez, A. Marine-derived drugs in neurology. *Curr. Opin. Invest. Drugs* **2007**, *8*, 525–530.
20. Schmidt, C.E.; Leach, J.B. Neural tissue engineering: strategies for repair and regeneration. *Annu. Rev. Biomed. Eng.* **2003**, *5*, 293–347.
21. Kettenmann, H.; Verkhratsky, A. Neuroglia, der lebende Nervenkitt. *Fortschr. Neurol. Psychiatr.* **2011**, *79*, 588–597.
22. Giugliano, M. Calcium waves in astrocyte networks: Theory and experiments. *Front. Neurosci.* **2009**, *3*, 160–161.
23. Allen, N.J.; Barres, B.A. Neuroscience: Glia—More than just brain glue. *Nature* **2009**, *457*, 675–677.
24. Dowding, A.J.; Scholes, J. Lymphocytes and macrophages outnumber oligodendroglia in normal fish spinal cord. *Proc. Natl. Acad. Sci. USA* **1993**, *90*, 10183–10187.
25. Horner, P.J.; Gage, F.H. Regenerating the damaged central nervous system. *Nature* **2000**, *407*, 963–970.
26. Shoichet, M.S.; Tate, C.C.; Baumann, M.D.; LaPlaca, M.C. *Indwelling Neural Implants: Strategies for Contending with the in Vivo Environment*; Reichert, W.M., Ed.; CRC Press: Boca Raton, FL, USA, 2008.

27. Cullen, D.K.; Stabenfeldt, S.E.; Simon, C.M.; Tate, C.C.; LaPlaca, M.C. *In vitro* neural injury model for optimization of tissue-engineered constructs. *J. Neurosci. Res.* **2007**, *85*, 3642–3651.
28. Baranes, D.; Cove, J.; Blinder, P.; Shany, B.; Peretz, H.; Vago, R. Interconnected network of ganglion-like neural cell spheres formed on hydrozoan skeleton. *Tissue Eng*. **2007**, *13*, 473–482.
29. Yiu, G.; He, Z. Glial inhibition of CNS axon regeneration. *Nat. Rev. Neurosci.* **2006**, *7*, 617–627.
30. Avellino, A.M.; Hart, D.; Dailey, A.T.; Mackinnon, M.; Ellegala, D.; Kliot, M. Differential macrophage responses in the peripheral and central nervous system during wallerian degeneration of axons. *Exp. Neurol.* **1995**, *136*, 183–198.
31. Kuhlmann, T.; Wendling, U.; Nolte, C.; Zipp, F.; Maruschak, B.; Stadelmann, C.; Siebert, H.; Brück, W. Differential regulation of myelin phagocytosis by macrophages/microglia, involvement of target myelin, Fc receptors and activation by intravenous immunoglobulins. *J. Neurosci. Res.* **2002**, *67*, 185–190.
32. Huebner, E.; Strittmatter, S. *Cell Biology of the Axon*; Koenig, E., Ed.; Springer: Berlin Heidelberg, Germany, 2009; Volume 48, pp. 305–360.
33. Plunet, W.; Kwon, B.K.; Tetzlaff, W. Promoting axonal regeneration in the central nervous system by enhancing the cell body response to axotomy. *J. Neurosci. Res.* **2002**, *68*, 1–6.
34. Di Giovanni, S. Regeneration following spinal cord injury, from experimental models to humans: where are we? *Expert Opin. Ther. Targets* **2006**, *10*, 363–376.
35. Pfister, B.J.; Gordon, T.; Loverde, J.R.; Kochar, A.S.; Mackinnon, S.E.; Cullen, D.K. Biomedical engineering strategies for peripheral nerve repair: Surgical applications, state of the art, and future challenges. *Crit. Rev. Biomed. Eng.* **2011**, *39*, 81–124.
36. Scholz, T.; Krichevsky, A.; Sumarto, A.; Jaffurs, D.; Wirth, G.A.; Paydar, K.; Evans, G.R.D. Peripheral nerve injuries: An international survey of current treatments and future perspectives. *J. Reconstr. Microsurg.* **2009**, *25*, 339–344.
37. Moore, A.; Kasukurthi, R.; Magill, C.; Farhadi, H.F.; Borschel, G.; Mackinnon, S. Limitations of conduits in peripheral nerve repairs. *Hand* **2009**, *4*, 180–186.
38. Suna, H.; Arai, M.; Tsubotani, Y.; Hayashi, A.; Setiawan, A.; Kobayashi, M. Dysideamine, a new sesquiterpene aminoquinone, protects hippocampal neuronal cells against iodoacetic acid-induced cell death. *Bioorg. Med. Chem.* **2009**, *17*, 3968–3972.
39. Aoki, S.; Wei, H.; Matsui, K.; Rachmat, R.; Kobayashi, M. Pyridoacridine alkaloids inducing neuronal differentiation in a neuroblastoma cell line, from marine sponge *Biemna fortis*. *Bioorg. Med. Chem.* **2003**, 1969–1973.
40. Aoki, S.; Matsui, K.; Tanaka, K.; Satari, R.; Kobayashi, M. Lembehyne A, a novel neuritogenic polyacetylene, from a marine sponge of *Haliclona* sp. *Tetrahedron* **2000**, *56*, 9945–9948.
41. Aoki, S.; Matsui, K.; Takata, T.; Hong, W.; Kobayashi, M. Lembehyne A, a spongean polyacetylene, induces neuronal differentiation in neuroblastoma cell. *Biochem. Biophys. Res. Commun*. **2001**, *289*, 558–563.

42. Aoki, S.; Matsui, K.; Wei, H.; Murakami, N.; Kobayashi, M. Structure-activity of neuritogenic spongean acetylene alcohols, lembehynes. *Tetrahedron* **2002**, *58*, 5417–5422.
43. Han, C.; Qi, J.; Ojika, M. Structure-activity relationships of novel neuritogenic steroid glycosides from the Okinawan starfish *Linckia laevigata*. *Bioorg. Med. Chem.* **2006**, *14*, 4458–4465.
44. Palyanova, N.V.; Pankova, T.M.; Starostina, M.V.; Kicha, A.A.; Ivanchina, N.V.; Stonik, V.A. Neuritogenic and neuroprotective effects of polar steroids from the far east starfishes *Patiria pectinifera* and *Distolasterias nipon*. *Mar. Drugs* **2013**, *11*, 1440–1455.
45. Qi, J.; Han, C.; Sasayama, Y.; Nakahara, H.; Shibata, T.; Uchida, K.; Ojika, M. Granulatoside A, a starfish steroid glycoside, enhances PC12 cell neuritogenesis induced by nerve growth factor through an activation of MAP kinase. *Chem. Med. Chem*. **2006**, *1*, 1351–1354.
46. Inagaki, M.; Miyamoto, T.; Isobe, R.; Higuchi, R. Biologically active glycosides from Asteroidea, 43. Isolation and structure of a new neuritogenic-active ganglioside molecular species from the starfish *Linckia laevigata*. *Chem. Pharm. Bull.* **2005**, *53*, 1551–1554.
47. Qi, J.; Ojika, M.; Sakagami, Y. Linckosides A and B, two new neuritogenic steroid glycosides from the Okinawan starfish *Linckia laevigata*. *Bioorg. Med. Chem.* **2002**, *10*, 1961–1966.
48. Higuchi, R.; Inoue, S.; Inagaki, K.; Sakai, M.; Miyamoto, T.; Komori, T.; Inagaki, M.; Isobe, R. Biologically active glycosides from Asteroidea, 42. Isolation and structure of a new biologically active ganglioside molecular species from the starfish *Asterina pectinifera*. *Chem. Pharm. Bull.* **2006**, *54*, 287–291.
49. Kisa, F.; Yamada, K.; Miyamoto, T.; Inagaki, M.; Higuchi, R. Constituents of Holothuroidea, 18. Isolation and structure of biologically active disialo- and trisialo-gangliosides from the sea cucumber *Cucumaria echinata*. *Chem. Pharm. Bull.* **2006**, *54*, 1293–1298.
50. Kisa, F.; Yamada, K.; Miyamoto, T.; Inagaki, M.; Higuchi, R. Constituents of Holothuroidea, 17. Isolation and structure of biologically active monosialo-gangliosides from the sea cucumber *Cucumaria echinata*. *Chem. Pharm. Bull.* **2006**, *54*, 982–987.
51. Buée, L.; Bussière, T.; Buée-Scherrer, V.; Delacourte, A.; Hof, P.R. Tau protein isoforms, phosphorylation and role in neurodegenerative disorders. *Brain Res Rev*. **2000**, *33*, 95–130.
52. Kar, S.; Slowikowski, S.P.M.; Westaway, D.; Mount, H.T.J. Interactions between β-amyloid and central cholinergic neurons: Implications for Alzheimer's disease. *J. Psychiatry Neurosci.* **2004**, *29*, 427–441.
53. Beedessee, G.; Ramanjooloo, A.; Surnam-Boodhun, R.; van Soest, R.W.M.; Marie, D.E.P. Acetylcholinesterase-inhibitory activities of the extracts from sponges collected in Mauritius waters. *Chem. Biodivers.* **2013**, *10*, 442–451.
54. Dai, X.-L.; Sun, Y.-X.; Jiang, Z.-F. Attenuated cytotoxicity but enhanced βfibril of a mutant amyloid β-peptide with a methionine to cysteine substitution. *FEBS Lett.* **2007**, *581*, 1269–1274.
55. Kubo, T.; Nishimura, S.; Kumagae, Y.; Kaneko, I. *In vivo* conversion of racemized β-amyloid ([D-Ser26]Aβ1–40) to truncated and toxic fragments ([D-Ser26]Aβ25–35/40) and fragment presence in the brains of Alzheimer's patients. *J. Neurosci. Res*. **2002**, *70*, 474–483.

56. Peña, F.; Ordaz, B.; Balleza-Tapia, H.; Bernal-Pedraza, R.; Márquez-Ramos, A.; Carmona-Aparicio, L.; Giordano, M. Beta-amyloid protein (25–35) disrupts hippocampal network activity: Role of Fyn-kinase. *Hippocampus* **2010**, *20*, 78–96.
57. Wang, J.; Gao, Q.-S.; Wang, Y.; Lafyatis, R.; Stamm, S.; Andreadis, A. Tau exon 10, whose missplicing causes frontotemporal dementia, is regulated by an intricate interplay of *cis* elements and *trans* factors. *J. Neurochem*. **2004**, *88*, 1078–1090.
58. Hanger, D.P.; Byers, H.L.; Wray, S.; Leung, K.-Y.; Saxton, M.J.; Seereeram, A.; Reynolds, C.H.; Ward, M.A.; Anderton, B.H. Novel phosphorylation sites in tau from Alzheimer brain support a role for casein kinase 1 in disease pathogenesis. *J. Biol. Chem.* **2007**, *282*, 23645–23654.
59. Ryoo, S.-R.; Jeong, H.K.; Radnaabazar, C.; Yoo, J.-J.; Cho, H.-J.; Lee, H.-W.; Kim, I.-S.; Cheon, Y.-H.; Ahn, Y.S.; Chung, S.-H.; Song, W.-J. DYRK1A-mediated hyperphosphorylation of tau: A functional link between Down syndrome and Alzheimer disease. *J. Biol. Chem.* **2007**, *282*, 34850–34857.
60. Schober, A. Classic toxin-induced animal models of Parkinson's disease: 6-OHDA and MPTP. *Cell Tissue Res.* **2004**, *318*, 215–224.
61. Perez, D.I.; Gil, C.; Martinez, A. Protein kinases CK1 and CK2 as new targets for neurodegenerative diseases. *Med. Res. Rev.* **2011**, *31*, 924–954.
62. Wang, Y.; Shi, M.; Chung, K.A.; Zabetian, C.P.; Leverenz, J.B.; Berg, D.; Srulijes, K.; Trojanowski, J.Q.; Lee, V.M.; Siderowf, A.D.; *et al*. Phosphorylated α-synuclein in Parkinson's disease. *Sci. Transl. Med.* **2012**, *4*, 121ra20.
63. Turk,T.; Avguštin, J.A.; Batista, U.; Strugar, G.; Kosmina, R.; Čivović, S.; Janussen, D.; Kauferstein, S.; Mebs, D.; Sepčić, K. Biological activities of ethanolic extracts from deep-sea antarctic marine sponges. *Mar. Drugs* **2013**, *11*, 1126–1139.
64. Langjae, R.; Bussarawit, S.; Yuenyongsawad, S.; Ingkaninan, K.; Plubrukarn, A. Acetylcholinesterase-inhibiting steroidal alkaloid from the sponge *Corticium* sp. *Steroids* **2007**, *72*, 682–685.
65. Nukoolkarn, V.S.; Saen-oon, S.; Rungrotmongkol, T.; Hannongbua, S.; Ingkaninan, K.; Suwanborirux, K. Petrosamine, a potent anticholinesterase pyridoacridine alkaloid from a Thai marine sponge *Petrosia* n. sp. *Bioorg. Med. Chem.* **2008**, *16*, 6560–6567.
66. Ata, A.; Ackerman, J.; Bayoud, A.; Radhika, P. Bioactive Chemical constituents of *Cladiella* species. *Helv. Chim. Acta.* **2004**, *87*, 592–597.
67. Kigoshi, H.; Kanematsu, K.; Yokota, K.; Uemura, D. Turbotoxins A and B, novel diiodotyramine derivatives from the Japanese gastropod *Turbo marmorata*. *Tetrahedron* **2000**, *56*, 9063–9070.
68. Williams, P.; Sorribas, A.; Liang, Z. New methods to explore marine resources for Alzheimer's therapeutics. *Curr. Alzheimer Res.* **2000**, *7*, 210–213.
69. Dai, J.; Sorribas, A.; Yoshida, W.Y.; Kelly, M.; Williams, P.G. Xestosaprols from the Indonesian marine sponge *Xestospongi*a sp. *J. Nat. Prod*. **2010**, *73*, 1188–1191.
70. Dai, J.; Sorribas, A.; Yoshida, W.Y.; Kelly, M.; Williams, P.G. Topsentinols, 24-isopropyl steroids from the marine sponge *Topsentia* sp. *J. Nat. Prod*. **2010**, *73*, 1597–1600.

71. Dai. J.; Jiménez, J.I.; Kelly, M.; Williams, P.G. Dictazoles: Potential vinyl cyclobutane biosynthetic precursors to the dictazolines. *J. Org. Chem*. **2010**, *75*, 2399–2402.
72. Millán-Aguiñaga, N.; Soria-Mercado, I.E.; Williams, P. Xestosaprol D and E from the Indonesian marine sponge *Xestospongia* sp. *Tetrahedron Lett*. **2000**, *51*, 751–753.
73. Zhang, H.; Conte, M.M.; Huang, X.C.; Khalil, Z.; Capon, R.J. A search for BACE inhibitors reveals new biosynthetically related pyrrolidones, furanones and pyrroles from a southern Australian marine sponge, *Ianthella* sp. *Org. Biomol. Chem*. **2012**, *10*, 2656–2663.
74. Zhang, H.; Conte, M.M.; Khalil, Z.; Huang, X.-C.; Capon, R.J. New dictyodendrins as BACE inhibitors from a southern Australian marine sponge, *Ianthella* sp. *RSC Adv*. **2012**, *2*, 4209–4214.
75. Rayasam, G.V.; Tulasi, V.K.; Sodhi, R.; Davis, J.A.; Ray, A. Glycogen synthase kinase 3: More than a namesake. *Br. J. Pharmacol.* **2009**, *156*, 885–898.
76. Bidon-Chanal, A.; Fuertes, A.; Alonso, D.; Pérez, D.I.; Martínez, A.; Luque, F.J.; Medina, M. Evidence for a new binding mode to GSK-3: Allosteric regulation by the marine compound palinurin. *Eur. J. Med. Chem.* **2013**, *60*, 479–489.
77. Cho, J.-H.; Johnson, G.V.W. Glycogen synthase kinase 3β phosphorylates tau at both primed and unprimed sites: Differential impact on microtubule binding. *J. Biol. Chem.* **2003**, *278*, 187–193.
78. Khanfar, M.A.; Asal, B.A.; Mudit, M.; Kaddoumi, A.; El Sayed, K.A. The marine natural-derived inhibitors of glycogen synthase kinase-3β phenylmethylene hydantoins: *In vitro* and *in vivo* activities and pharmacophore modeling. *Bioorg. Med. Chem.* **2009**, *17*, 6032–6039.
79. Hanger, D.P.; Noble, W. Functional implications of glycogen synthase kinase-3-mediated tau phosphorylation. *Int. J. Alzheimers Dis.* **2011**, *2011*, 352805:1–352805:11.
80. Hamann, M.; Alonso, D.; Martín-Aparicio, E.; Fuertes, A.; Pérez-Puerto, M.J.; Castro, A.; Morales, S.; Navarro, M.L.; del Monte-Millán, M.; Medina, M.; *et al*. Glycogen synthase kinase-3 (GSK-3) inhibitory activity and structure–activity relationship (SAR) studies of the manzamine alkaloids. Potential for Alzheimer's disease. *J. Nat. Prod.* **2007**, *70*, 1397–1405.
81. Meijer, L.; Thunnissen, A.M.; White, A.W.; Garnier, M.; Nikolic, M.; Tsai, L.H.; Walter, J.; Cleverley, K.E.; Salinas, P.C.; Wu, Y.Z.; *et al*. Inhibition of cyclin-dependent kinases, GSK-3β and CK1 by hymenialdisine, a marine sponge constituent. *Chem. Biol.* **2000**, *7*, 51–63.
82. Glatz, D.C.; Rujescu, D.; Tang, Y.; Berendt, F.J.; Hartmann, A.M.; Faltraco, F.; Rosenberg, C.; Hulette, C.; Jellinger, K.; Hampel, H.; *et al*. The alternative splicing of tau exon 10 and its regulatory proteins CLK2 and TRA2-BETA1 changes in sporadic Alzheimer's disease. *J. Neurochem.* **2006**, *96*, 635–644.
83. Hernández, F.; Pérez, M.; Lucas, J.J.; Mata, A.M.; Bhat, R.; Avila, J. Glycogen synthase kinase-3 plays a crucial role in tau exon 10 splicing and intranuclear distribution of SC35: Implications for Alzheimer's disease. *J. Biol. Chem.* **2004**, *279*, 3801–3806.
84. Phiel, C.J.; Wilson, C.A.; Lee, V.M.-Y.; Klein, P.S. GSK-3α regulates production of Alzheimer's disease amyloid-β peptides. *Nature* **2003**, *423*, 435–439.

85. Tahtouh, T.; Elkins, J.M.; Filippakopoulos, P.; Soundararajan, M.; Burgy, G.; Durieu, E.; Cochet, C.; Schmid, R.S.; Lo, D.C.; Delhommel, F.; *et al*. Selectivity, cocrystal structures, and neuroprotective properties of leucettines, a family of protein kinase inhibitors derived from the marine sponge alkaloid leucettamine B. *J. Med. Chem.* **2012**, *55*, 9312–9330.
86. Baunbæk, D.; Trinkler, N.; Ferandin, Y.; Lozach, O.; Ploypradith, P.; Rucirawat, S.; Ishibashi, F.; Iwao, M.; Meijer, L. Anticancer alkaloid lamellarins inhibit protein kinases. *Mar. Drugs* **2008**, *6*, 514–527.
87. Gompel, M.; Leost, M.; de Kier Joffe, E.B.; Puricelli, L.; Franco, L.H.; Palermo, J.; Meijer, L. Meridianins, a new family of protein kinase inhibitors isolated from the ascidian *Aplidium meridianum*. *Bioorg. Med. Chem. Lett.* **2004**, *14*, 1703–1707.
88. McCulloch, M.W.B.; Bugni, T.S.; Concepcion, G.P.; Coombs, G.S.; Harper, M.K.; Kaur, S.; Mangalindan, G.C.; Mutizwa, M.M.; Veltri, C.A.; Virshup, D.M.; *et al*. Carteriosulfonic acids A–C, GSK-3β inhibitors from a *Carteriospongia* sp. *J. Nat. Prod.* **2009**, *72*, 1651–1656.
89. Gordillo, D.; Diaz, I.; Martinez-Gil, A.; Pliego, G.; Huerta, A.; Puerto, M.J.; Aparicio, E.; Navarro, D.; Padilla, M. Gsk-3 Inhibitors Isolated from Marine Organisms. U.S. Patent 20070088080 A1, 19 April 2007.
90. Debdab, M.; Renault, S.; Lozach, O.; Meijer, L.; Paquin, L.; Carreaux, F.; Bazureau, J.-P. Synthesis and preliminary biological evaluation of new derivatives of the marine alkaloid leucettamine B as kinase inhibitors. *Eur. J. Med. Chem.* **2010**, *45*, 805–810.
91. Eldar-Finkelman, H.; Martinez, A. GSK-3 inhibitors: Preclinical and clinical focus on CNS. *Front. Mol. Neurosci.* **2011**, *4*, 32.
92. Ryoo, S.-R.; Cho, H.-J.; Lee, H.-W.; Jeong, H.K.; Radnaabazar, C.; Kim, Y.-S.; Kim, M.-J.; Son, M.-Y.; Seo, H.; Chung, S.-H.; *et al*. Dual-specificity tyrosine(Y)-phosphorylation regulated kinase 1A-mediated phosphorylation of amyloid precursor protein: Evidence for a functional link between Down syndrome and Alzheimer's disease. *J. Neurochem.* **2008**, *104*, 1333–1344.
93. Ryu, Y.S.; Park, S.Y.; Jung, M.-S.; Yoon, S.-H.; Kwen, M.-Y.; Lee, S.-Y.; Choi, S.-H.; Radnaabazar, C.; Kim, M.-K.; Kim, H.; *et al*. Dyrk1A-mediated phosphorylation of presenilin 1: A functional link between Down syndrome and Alzheimer's disease. *J. Neurochem.* **2010**, *115*, 574–584.
94. Sitz, J.H.; Baumgärtel, K.; Hämmerle, B.; Papadopoulos, C.; Hekerman, P.; Tejedor, F.J.; Becker, W.; Lutz, B. The Down syndrome candidate dual-specificity tyrosine phosphorylation-regulated kinase 1A phosphorylates the neurodegeneration-related septin 4. *Neuroscience* **2008**, *157*, 596–605.
95. Ihara, M.; Tomimoto, H.; Kitayama, H.; Morioka, Y.; Akiguchi, I.; Shibasaki, H.; Noda, M.; Kinoshita, M. Association of the cytoskeletal GTP-binding protein Sept4/H5 with cytoplasmic inclusions found in Parkinson's disease and other synucleinopathies. *J. Biol. Chem.* **2003**, *278*, 24095–24102.
96. Kinoshita, A.; Kinoshita, M.; Akiyama, H.; Tomimoto, H.; Akiguchi, I.; Kumar, S.; Noda, M.; Kimura, J. Identification of septins in neurofibrillary tangles in Alzheimer's disease. *Am. J. Pathol.* **1998**, *153*, 1551–1560.

97. Jung, M.-S.; Park, J.-H.; Ryu, Y.S.; Choi, S.-H.; Yoon, S.-H.; Kwen, M.-Y.; Oh, J.Y.; Song, W.-J.; Chung, S.-H. Regulation of RCAN1 protein activity by Dyrk1A protein-mediated phosphorylation. *J. Biol. Chem.* **2011**, *286*, 40401–40412.
98. Park, J.-H.; Jung, M.-S.; Kim, Y.-S.; Song, W.-J.; Chung, S.-H. Phosphorylation of Munc18–1 by Dyrk1A regulates its interaction with Syntaxin 1 and X11α. *J. Neurochem.* **2012**, *122*, 1081–1091.
99. Li, G.; Yin, H.; Kuret, J. Casein kinase 1 delta phosphorylates tau and disrupts its binding to microtubules. *J. Biol. Chem.* **2004**, *279*, 15938–15945.
100. Flajolet, M.; He, G.; Heiman, M.; Lin, A.; Nairn, A.C.; Greengard, P. Regulation of Alzheimer's disease amyloid-β formation by casein kinase I. *Proc. Natl. Acad. Sci. USA* **2007**, *104*, 4159–4164.
101. Piedrahita, D.; Hernández, I.; López-Tobón, A.; Fedorov, D.; Obara, B.; Manjunath, B.S.; Boudreau, R.L.; Davidson, B.; LaFerla, F.; Gallego-Gómez, J.C.; *et al*. Silencing of CDK5 reduces neurofibrillary tangles in transgenic Alzheimer's mice. *J. Neurochem.* **2010**, *30*, 13966–13976.
102. Kamei, H.; Saito, T.; Ozawa, M.; Fujita, Y.; Asada, A.; Bibb, J.A.; Saido, T.C.; Sorimachi, H.; Hisanaga, S.-I. Suppression of calpain-dependent cleavage of the CDK5 activator p35 to p25 by site-specific phosphorylation. *J. Biol. Chem.* **2007**, *282*, 1687–1694.
103. Hernandez, P.; Lee, G.; Sjoberg, M.; Maccioni, R.B. Tau phosphorylation by cdk5 and Fyn in response to amyloid peptide $A\beta_{25-35}$: Involvement of lipid rafts. *J. Alzheimers Dis.* **2009**, *16*, 149–156.
104. Zheng, Y.-L.; Kesavapany, S.; Gravell, M.; Hamilton, R.S.; Schubert, M.; Amin, N.; Albers, W.; Grant, P.; Pant, H.C. A Cdk5 inhibitory peptide reduces tau hyperphosphorylation and apoptosis in neurons. *EMBO J.* **2005**, *24*, 209–220.
105. Town, T.; Zolton, J.; Shaffner, R.; Schnell, B.; Crescentini, R.; Wu, Y.; Zeng, J.; DelleDonne, A.; Obregon, D.; Tan, J.; *et al.* p35/Cdk5 pathway mediates soluble amyloid-β peptide-induced tau phosphorylation *in vitro*. *J. Neurosci. Res.* **2002**, *69*, 362–372.
106. Soni, R.; Muller, L.; Furet, P.; Schoepfer, J.; Stephan, C.; Zumstein-Mecker, S.; Fretz, H.; Chaudhuri, B. Inhibition of cyclin-dependent kinase 4 (Cdk4) by fascaplysin, a marine natural product. *Biochem. Biophys. Res. Commun.* **2000**, *275*, 877–884.
107. Beebe, S.J. The cAMP-dependent protein kinases and cAMP signal transduction. *Semin. Cancer Biol.* **1994**, *5*, 285–294.
108. Dolan, P.J.; Johnson, G.V.W. The role of tau kinases in Alzheimer's disease. *Curr. Opin. Drug Discov. Devel.* **2010**, *13*, 595–603.
109. Adams, D.J.; Alewood, P.F.; Craik, D.J.; Drinkwater, R.D.; Lewis, R.J. Conotoxins and their potential pharmaceutical applications. *Drug Develop. Res.* **1999**, *46*, 219–234.
110. McDonough, S.; Swartz, K.; Mintz, I.; Boland, L.; Bean, B. Inhibition of calcium channels in rat central and peripheral neurons by ω-conotoxin MVIIC. *J. Neurosci.* **1996**, *16*, 2612–2623.
111. Wen, L.; Yang, S.; Qiao, H.; Liu, Z.; Zhou, W.; Zhang, Y.; Huang, P. SO-3, a new O-superfamily conopeptide derived from *Conus striatus*, selectively inhibits N-type calcium currents in cultured hippocampal neurons. *Br. J. Pharmacol.* **2005**, *145*, 728–739.

112. Valentino, K.; Newcomb, R.; Gadbois, T.; Singh, T.; Bowersox, S.; Bitner, S.; Justice, A.; Yamashiro, D.; Hoffman, B.B.; Ciaranello, R. A selective N-type calcium channel antagonist protects against neuronal loss after global cerebral ischemia. *Proc. Natl. Acad. Sci. USA* **1993**, *90*, 7894–7897.
113. Anderson, P.D.; Bokor, G. Conotoxins: Potential weapons from the sea. *J. Bioterror. Biodef.* **2012**, *3*, 1–4.
114. Favreau, P.; Gilles, N.; Lamthanh, H.; Bournaud, R.; Shimahara, T.; Bouet, F.; Laboute, P.; Letourneux, Y.; Ménez, A.; Molgó, J.; *et al*. A new ω-conotoxin that targets N-type voltage-sensitive calcium channels with unusual specificity. *Biochemistry* **2001**, *40*, 14567–14575.
115. McDonough, S.I.; Boland, L.M.; Mintz, I.M.; Bean, B.P. Interactions among toxins that inhibit N-type and P-type calcium channels. *J. Gen. Physiol*. **2002**, *119*, 313–328.
116. Nielsen, K.J.; Watson, M.; Adams, D.J.; Hammarström, A.K.; Gage, P.W.; Hill, J.M.; Craik, D.J.; Thomas, L.; Adams, D.; Alewood, P.F.; *et al*. Solution structure of μ-Conotoxin PIIIA, a preferential inhibitor of persistent tetrodotoxin-sensitive sodium channels. *J. Biol. Chem.* **2002**, *277*, 27247–27255.
117. Theile, J.W.; Cummins, T.R. Recent developments regarding voltage-gated sodium channel blockers for the treatment of inherited and acquired neuropathic pain syndromes. *Front. Pharmacol.* **2011**, *2*, 54.
118. Dray, A. Neuropathic pain: emerging treatments. *Br. J. Anaesth.* **2008**, *101*, 48–58.
119. Hains, B.C.; Klein, J.P.; Saab, C.Y.; Craner, M.J.; Black, J.A.; Waxman, S.G. Upregulation of sodium channel Nav1.3 and functional involvement in neuronal hyperexcitability associated with central neuropathic pain after spinal cord injury. *J. Neurosci.* **2003**, *23*, 8881–8892.
120. Carter, A.J. The importance of voltage-dependent sodium channels in cerebral ischaemia. *Amino Acids* **1998**, *14*, 159–169.
121. Ragsdale, D.S.; Avoli, M. Sodium channels as molecular targets for antiepileptic drugs. *Brain Res. Rev.* **1998**, *26*, 16–28.
122. Bulaj, G.; DeLaCruz, R.; Azimi-Zonooz, A.; West, P.; Watkins, M.; Yoshikami, D.; Olivera, B.M. δ-Conotoxin structure/function through a cladistic analysis. *Biochemistry* **2001**, *40*, 13201–13208.
123. Santana, A.N.C.; Trindade-Filho, E.M.; Cunha, R.B.; Sousa, M.V.; Cavalheiro, E.A.; Carvalho, K.M. Behavioral and electroencephalographic analysis of seizures induced by intrahippocampal injection of granulitoxin, a neurotoxic peptide from the sea anemone *Bunodosoma granulifera*. *Braz. J. Med. Biol. Res.* **2001**, *34*, 797–801.
124. Bruhn, T.; Schaller, C.; Schulze, C.; Sanchez-Rodriguez, J.; Dannmeier, C.; Ravens, U.; Heubach, J.F.; Eckhardt, K.; Schmidtmayer, J.; Schmidt, H.; *et al*. Isolation and characterisation of five neurotoxic and cardiotoxic polypeptides from the sea anemone *Anthopleura elegantissima*. *Toxicon* **2001**, *39*, 693–702.

125. Santana, A.N.C.; Leite, A.B.; França, M.S.F.; França, L.; Vale, O.C.; Cunha, R.B.; Ricart, C.A.O.; Sousa, M.V.; Carvalho, K.M. Partial sequence and toxic effects of granulitoxin, a neurotoxic peptide from the sea anemone *Bunodosoma granulifera*. *Braz. J. Med. Biol. Res.* **1998**, *31*, 1335–1338.
126. Wulff, H.; Castle, N.A.; Pardo, L.A. Voltage-gated potassium channels as therapeutic targets. *Nat. Rev. Drug Discov.* **2009**, *8*, 982–1001.
127. Kauferstein, S.; Huys, I.; Lamthanh, H.; Stöcklin, R.; Sotto, F.; Menez, A.; Tytgat, J.; Mebs, D. A novel conotoxin inhibiting vertebrate voltage-sensitive potassium channels. *Toxicon* **2003**, *42*, 43–52.
128. Ferber, M.; Sporning, A.; Jeserich, G.; DeLaCruz, R.; Watkins, M.; Olivera, B.M.; Terlau, H. A novel *Conus* peptide ligand for K^+ channels. *J. Biol. Chem.* **2003**, *278*, 2177–2183.
129. Jensen, A.A.; Frølund, B.; Liljefors, T.; Krogsgaard-Larsen, P. Neuronal nicotinic acetylcholine receptors: Structural revelations, target identifications, and therapeutic inspirations. *J. Med. Chem.* **2005**, *48*, 4705–4745.
130. Paterson, D.; Nordberg, A. Neuronal nicotinic receptors in the human brain. *Prog. Neurobiol.* **2000**, *61*, 75–111.
131. Gotti, C.; Clementi, F. Neuronal nicotinic receptors: From structure to pathology. *Prog. Neurobiol.* **2004**, *74*, 363–396.
132. Tsuneki, H.; You, Y.; Toyooka, N.; Sasaoka, T.; Nemoto, H.; Dani, J.A.; Kimura, I. Marine alkaloids (−)-pictamine and (−)-lepadin B block neuronal nicotinic acetylcholine receptors. *Biol. Pharm. Bull.* **2005**, *28*, 611–614.
133. Green, B.T.; Welch, K.D.; Panter, K.E.; Lee, S.T. Plant toxins that affect nicotinic acetylcholine receptors: A review. *Chem. Res. Toxicol.* **2013**, *26*, 1129–1138.
134. Loughnan, M.; Nicke, A.; Jones, A.; Schroeder, C.I.; Nevin, S.T.; Adams, D.J.; Alewood, P.F.; Lewis, R.J. Identification of a novel class of nicotinic receptor antagonists: Dimeric conotoxins VxXIIA, VxXIIB, and VxXIIC from *Conus vexillum*. *J. Biol. Chem.* **2006**, *281*, 24745–24755.
135. Gotti, C.; Zoli, M.; Clementi, F. Brain nicotinic acetylcholine receptors: native subtypes and their relevance. *Trends Pharmacol. Sci.* **2006**, *27*, 482–491.
136. Kem, W.; Soti, F.; Wildeboer, K.; Le Francois, S.; MacDougall, K.; Wei, D.-Q.; Chou, K.-C.; Arias, H. The nemertine toxin anabaseine and its derivative DMXBA (GTS-21): Chemical and pharmacological properties. *Mar. Drugs* **2006**, *4*, 255–273.
137. Nicke, A.; Loughnan, M.L.; Millard, E.L.; Alewood, P.F.; Adams, D.J.; Daly, N.L.; Craik, D.J.; Lewis, R.J. Isolation, structure, and activity of GID, a novel α4/7-conotoxin with an extended *N*-terminal sequence. *J. Biol. Chem.* **2003**, *278*, 3137–3144.
138. Ellison, M.; McIntosh, J.M.; Olivera, B.M. α-Conotoxins ImI and ImII: Similar α7 nicotinic receptor antagonists act at different sites. *J. Biol. Chem.* **2003**, *278*, 757–764.
139. Peng, C.; Chen, W.; Han, Y.; Sanders, T.; Chew, G.; Liu, J.; Hawrot, E.; Chi, C.; Wang, C. Characterization of a novel α4/4-conotoxin, Qc1.2, from vermivorous *Conus quercinus*. *Biochim. Biophys. Acta* **2009**, *41*, 854–868.

140. Hauser, T.A.; Hepler, C.D.; Kombo, D.C.; Grinevich, V.P.; Kiser, M.N.; Hooker, D.N.; Zhang, J.; Mountfort, D.; Selwood, A.; Akireddy, S.R.; *et al*. Comparison of acetylcholine receptor interactions of the marine toxins, 13-desmethylspirolide C and gymnodimine. *Neuropharmacology* **2012**, *62*, 2239–2250.
141. Bourne, Y.; Radic, Z; Aráoz, R.; Talley, T.T.; Benoit, E.; Servent, D.; Taylor, P.; Molgó, J.; Marchot, P. Structural determinants in phycotoxins and AChBP conferring high affinity binding and nicotinic AChR antagonism. *Proc. Natl. Acad. Sci. USA* **2010**, *107*, 6076–6081.
142. Hogg, R.C.; Miranda, L.P.; Craik, D.J.; Lewis, R.J.; Alewood, P.F.; Adams, D.J. Single amino acid substitutions in α-conotoxin PnIA shift selectivity for subtypes of the mammalian neuronal nicotinic acetylcholine receptor. *J. Biol. Chem.* **1999**, *274*, 36559–36564.
143. Munday, R.; Quilliam, M.A.; LeBlanc, P.; Lewis, N.; Gallant, P.; Sperker, S.A.; Ewart, H.S.; MacKinnon, S.L. Investigations into the toxicology of spirolides, a group of marine phycotoxins. *Toxins* **2012**, *4*, 1–14.
144. Kew, J.C.; Kemp, J. Ionotropic and metabotropic glutamate receptor structure and pharmacology. *Psychopharmacology* **2005**, *179*, 4–29.
145. Aiello, A.; D'Esposito, M.; Fattorusso, E.; Menna, M.; Müller, W.E.G.; Perović-Ottstadt, S.; Schröder, H.C. Novel bioactive bromopyrrole alkaloids from the mediterranean sponge *Axinella verrucosa*. *Bioorg. Med. Chem.* **2006**, *14*, 17–24.
146. Sanders, J.M.; Ito, K.; Settimo, L.; Pentikäinen, O.T.; Shoji, M.; Sasaki, M.; Johnson, M.S.; Sakai, R.; Swanson, G.T. Divergent pharmacological activity of novel marine-derived excitatory amino acids on glutamate receptors. *J. Pharmacol. Exp. Ther.* **2005**, *314*, 1068–1078.
147. Pinheiro, P.S.; Mulle, C. Presynaptic glutamate receptors: Physiological functions and mechanisms of action. *Nat. Rev. Neurosci.* **2008**, *9*, 423–436.
148. Fan, M.M.Y.; Raymond, L.A. *N*-Methyl-D-aspartate (NMDA) receptor function and excitotoxicity in Huntington's disease. *Prog. Neurobiol.* **2007**, *81*, 272–293.
149. Schröder, H.-C.; Sudek, S.; Caro, S.; Rosa, S.; Perovic, S.; Steffen, R.; Müller, I.M.; Müller, W.E.G. Synthesis of the neurotoxin quinolinic acid in apoptotic tissue from *Suberites domuncula*: Cell biological, molecular biological, and chemical analyses. *Mar. Biotechnol.* **2002**, *4*, 546–558.
150. Hampson, D.R.; Manalo, J.L. The activation of glutamate receptors by kainic acid and domoic acid. *Nat. Toxins* **1998**, *6*, 153–158.
151. Doucette, T.A.; Strain, S.M.; Allen, G.V.; Ryan, C.L.; Tasker, R.A. Comparative behavioural toxicity of domoic acid and kainic acid in neonatal rats. *Neurotoxicol. Teratol*. **2000**, *22*, 863–869.
152. Aiello, A.; D'Esposito, M.; Fattorusso, E.; Menna, M.; Müller, W.E.G.; Perović-Ottstadt, S.; Tsuruta, H.; Gulder, T.A.M.; Bringmann, G. Daminin, a bioactive pyrrole alkaloid from the mediterranean sponge *Axinella damicornis*. *Tetrahedron* **2005**, *61*, 7266–7270.
153. Jimenez, E.C.; Donevan, S.; Walker, C.; Zhou, L.-M.; Nielsen, J.; Cruz, L.J.; Armstrong, H.; White, H.S.; Olivera, B.M. Conantokin-L, a new NMDA receptor antagonist: Determinants for anticonvulsant potency. *Epilepsy Res.* **2002**, *51*, 73–80.

154. Blandl, T.; Warder, S.E.; Prorok, M.; Castellino, F.J. Structure-function relationships of the NMDA receptor antagonist peptide, conantokin-R. *FEBS Lett.* **2000**, *470*, 139–146.
155. Williams, A.J.; Ling, G.; McCabe, R.T.; Tortella, F.C. Intrathecal CGX-1007 is neuroprotective in a rat model of focal cerebral ischemia. *Neuroreport* **2002**, *13*, 821–824.
156. Hu, J.F.; Schetz, J.A.; Kelly, M.; Peng, J.N.; Ang, K.K.; Flotow, H.; Leong, C.Y.; Ng, S.B.; Buss, A.D.; Wilkins, S.P.; *et al*. New antiinfective and human 5-HT_2 receptor binding natural and semisynthetic compounds from the Jamaican sponge *Smenospongia aurea*. *J. Nat. Prod*. **2002**, *65*, 476–80.
157. Hedner, E.; Sjögren, M.; Frändberg, P.A.; Johansson, T.; Göransson, U.; Dahlström, M.; Jonsson, P.; Nyberg, F.; Bohlin, L. Brominated cyclodipeptides from the marine sponge *Geodia barretti* as selective 5-HT ligands. *J. Nat. Prod*. **2006**, *69*, 1421–1424.
158. Aiello, A.; Fattorusso, E.; Giordano, A.; Menna, M.; Müller, W.E.; Perović-Ottstadt, S.; Schröder, H.C. Damipipecolin and damituricin, novel bioactive bromopyrrole alkaloids from the mediterranean sponge *Axinella damicornis*. *Bioorg. Med. Chem*. **2007**, *15*, 5877–5887.
159. Esbenshade, T.A.; Browman, K.E.; Bitner, R.S.; Strakhova, M.; Cowart, M.D.; Brioni, J.D. The histamine H_3 receptor: an attractive target for the treatment of cognitive disorders. *Br. J. Pharmacol.* **2008**, *154*, 1166–1681.
160. Swanson, D.M.; Wilson, S.J.; Boggs, J.D.; Xiao, W.; Apodaca, R.; Barbier, A.J.; Lovenberg, T.W.; Carruthers, N.I. Aplysamine-1 and related analogs as histamine H_3 receptor antagonists. *Bioorg. Med. Chem. Lett.* **2006**, *16*, 897–900.
161. Li, P.; Reichert, D.E.; Rodríguez, A.D.; Manion, B.D.; Evers, A.S.; Eterović, V.A.; Steinbach, J.H.; Akk, G. Mechanisms of potentiation of the mammalian $GABA_A$ receptor by the marine cembranoid eupalmerin acetate. *Br. J. Pharmacol*. **2008**, *153*, 598–608.
162. Treiman, D.M. GABAergic mechanisms in epilepsy. *Epilepsia* **2001**, *42*, 8–12.
163. Balansa, W.; Islam, R.; Gilbert, D.F.; Fontaine, F.; Xiao, X.; Zhang, H.; Piggott, A.M.; Lynch, J.W.; Capon, R.J. Australian marine sponge alkaloids as a new class of glycine-gated chloride channel receptor modulator. *Bioorg. Med. Chem*. **2013**, *21*, 4420–4425.
164. Balansa, W.; Islam, R.; Fontaine, F.; Piggott, A.M.; Zhang, H.; Webb, T.I.; Gilbert, D.F.; Lynch, J.W.; Capon, R.J. Ircinialactams: Subunit-selective glycine receptor modulators from Australian sponges of the family Irciniidae. *Bioorg. Med. Chem*. **2010**, *18*, 2912–2919.
165. Balansa, W.; Islam, R.; Fontaine, F.; Piggott, A.M.; Zhang, H.; Xiao, X.; Webb, T.I.; Gilbert, D.F.; Lynch, J.W.; Capon, R.J. Sesterterpene glycinyl-lactams: A new class of glycine receptor modulator from Australian marine sponges of the genus *Psammocinia*. *Org. Biomol. Chem*. **2013**, *11*, 4695–4701.
166. Sharpe, I.A.; Palant, E.; Schroeder, C.I.; Kaye, D.M.; Adams, D.J.; Alewood, P.F.; Lewis, R.J. Inhibition of the norepinephrine transporter by the venom peptide χ-MrIA: Site of action, Na^+ dependence, and structure-activity relationship. *J. Biol. Chem.* **2003**, *278*, 40317–40323.
167. Sharpe, I.A.; Gehrmann, J.; Loughnan, M.L.; Thomas, L.; Adams, D.A.; Atkins, A.; Palant, E.; Craik, D.; Adams, D.J.; Alewood, P.F.; *et al*. Two new classes of conopeptides inhibit the α1-adrenoceptor and noradrenaline transporter. *Nat. Neurosci.* **2001**, *4*, 902–907.

168. Morabito, R.; Condello, S.; Currò, M.; Marino, A.; Ientile, R.; La Spada, G. Oxidative stress induced by crude venom from the jellyfish *Pelagia noctiluca* in neuronal-like differentiated SH-SY5Y cells. *Toxicol. In Vitro* **2012**, *26*, 694–699.
169. Sondag, C.; Dhawan, G.; Combs, C. Beta amyloid oligomers and fibrils stimulate differential activation of primary microglia. *J. Neuroinflammation* **2009**, *6*, 1.
170. Liang, L.-F.; Wang, X.-J.; Zhang, H.-Y.; Liu, H.-L.; Li, J.; Lan, L.-F.; Zhang, W.; Guo, Y.-W. Bioactive polyhydroxylated steroids from the Hainan soft coral *Sinularia depressa* Tixier-Durivault. *Bioorg. Med. Chem. Lett.* **2013**, *23*, 1334–1337.
171. Bernstein, A.; Garrison, S.; Zambetti, G.; O'Malley, K. 6-OHDA generated ROS induces DNA damage and p53- and PUMA-dependent cell death. *Mol. Neurodegener.* **2011**, *6*, 2.
172. Ikeda, Y.; Tsuji, S.; Satoh, A.; Ishikura, M.; Shirasawa, T.; Shimizu, T. Protective effects of astaxanthin on 6-hydroxydopamine-induced apoptosis in human neuroblastoma SH-SY5Y cells. *J. Neurochem.* **2008**, *107*, 1730–1740.
173. Perumal, A.S.; Gopal, V.B.; Tordzro, W.K.; Cooper, T.B.; Cadet, J.L. Vitamin E attenuates the toxic effects of 6-hydroxydopamine on free radical scavenging systems in rat brain. *Brain Res. Bull.* **1992**, *29*, 699–701.
174. Sriraksa, N.; Wattanathorn, J.; Muchimapura, S.; Tiamkao, S.; Brown, K.; Chaisiwamongkol, K. Cognitive-enhancing effect of quercetin in a rat model of Parkinson's disease induced by 6-hydroxydopamine. *Evid. Based Complement. Alternat. Med.* **2012**, *2012*, 823206.
175. Tobón-Velasco, J.C.; Limón-Pacheco, J.H.; Orozco-Ibarra, M.; Macías-Silva, M.; Vázquez-Victorio, G.; Cuevas, E.; Ali, S.F.; Cuadrado, A.; Pedraza-Chaverrí, J.; Santamaría, A. 6-OHDA-induced apoptosis and mitochondrial dysfunction are mediated by early modulation of intracellular signals and interaction of Nrf2 and NF-κB factors. *Toxicology* **2013**, *304*, 109–119.
176. Chen, W.-F.; Chakraborty, C.; Sung, C.-S.; Feng, C.-W.; Jean, Y.-H.; Lin, Y.-Y.; Hung, H.-C.; Huang, T.-Y.; Huang, S.-Y.; Su, T.-M.; *et al*. Neuroprotection by marine-derived compound, 11-dehydrosinulariolide, in an *in vitro* Parkinson's model: A promising candidate for the treatment of Parkinson's disease. *Naunyn-Schmiedeberg's Arch. Pharmacol.* **2012**, *385*, 265–275.
177. Yung, H.W.; Charnock-Jones, D.S.; Burton, G.J. Regulation of AKT phosphorylation at Ser473 and Thr308 by endoplasmic reticulum stress modulates substrate specificity in a severity dependent manner. *PLoS One* **2011**, *6*, e17894.
178. Dai, R.; Xia, Y.; Mao, L.; Mei, Y.; Xue, Y.; Hu, B. Involvement of PI3K/Akt pathway in the neuroprotective effect of sonic hedgehog on cortical neurons under oxidative stress. *J. Huazhong Univ. Sci. Technol. Med. Sci.* **2012**, *32*, 856–860.
179. Hayden, M.S.; Ghosh, S. Signaling to NF-κB. *Genes Dev.* **2004**, *18*, 2195–2224.
180. Flood, P.M.; Qian, L.; Peterson, L.J.; Zhang, F.; Shi, J.-S.; Gao, H.-M.; Hong, J.-S. Transcriptional factor NF-κB as a target for therapy in Parkinson's disease. *Parkinsons Dis.* **2011**, *2011*, doi:10.4061/2011/216298.

181. Chen, B.-W.; Chao, C.-H.; Su, J.-H.; Huang, C.-Y.; Dai, C.-F.; Wen, Z.-H.; Sheu, J.-H. A novel symmetric sulfur-containing biscembranoid from the Formosan soft coral *Sinularia flexibilis*. *Tetrahedron Lett.* **2010**, *51*, 5764–5766.
182. Ye, Q.; Zhang, X.; Huang, B.; Zhu, Y.; Chen, X. Astaxanthin suppresses MPP^+-induced oxidative damage in PC12 cells through a Sp1/NR1 signaling pathway. *Mar. Drugs* **2013**, *11*, 1019–1034.
183. Jean, Y.-H.; Chen, W.-F.; Sung, C.-S.; Duh, C.-Y.; Huang, S.-Y.; Lin, C.-S.; Tai, M.-H.; Tzeng, S.-F.; Wen, Z.-H. Capnellene, a natural marine compound derived from soft coral, attenuates chronic constriction injury-induced neuropathic pain in rats. *Br. J. Pharmacol.* **2009**, *158*, 713–725.
184. Mayer, A.M.S.; Avilés, E.; Rodríguez, A.D. Marine sponge *Hymeniacidon* sp. amphilectane metabolites potently inhibit rat brain microglia thromboxane B2 generation. *Bioorg. Med. Chem.* **2012**, *20*, 279–282.
185. Ceulemans, A.-G.; Zgavc, T.; Kooijman, R.; Hachimi-Idrissi, S.; Sarre, S.; Michotte, Y. The dual role of the neuroinflammatory response after ischemic stroke: Modulatory effects of hypothermia. *J. Neuroinflammation* **2010**, *7*, 74.
186. Bitzer-Quintero, O.K.; González-Burgos, I. Immune system in the brain: A modulatory role on dendritic spine morphophysiology? *Neural Plast.* **2012**, *2012*, ID 348642.
187. Aïd, S.; Bosetti, F. Targeting cyclooxygenases-1 and -2 in neuroinflammation: Therapeutic implications. *Biochimie* **2011**, *93*, 46–51.
188. Cacquevel, M.; Lebeurrier, N.; Cheenne, S.; Vivien, D. Cytokines in neuroinflammation and Alzheimer's disease. *Curr. Drug Targets* **2004**, *5*, 529–534.
189. Mennicken, F.; Maki, R.; de Souza, E.B.; Quirion, R. Chemokines and chemokine receptors in the CNS: A possible role in neuroinflammation and patterning. *Trends Pharmacol. Sci*. **1999**, *20*, 73–78.
190. Ryan, J.C.; Cross, C.A.; Van Dolah, F.M. Effects of COX inhibitors on neurodegeneration and survival in mice exposed to the marine neurotoxin domoic acid. *Neurosci. Lett.* **2011**, *487*, 83–87.
191. Tapiolas, D.M.; Bowden, B.F.; Abou-Mansour, E.; Willis, R.H.; Doyle, J.R.; Muirhead, A.N.; Liptrot, C.; Llewellyn, L.E.; Wolff, C.W.W.; Wright, A.D.; *et al*. Eusynstyelamides A, B, and C, nNOS Inhibitors, from the ascidian *Eusynstyela latericius*. *J. Nat. Prod.* **2009**, *72*, 1115–1120.
192. Huang, S.-Y.; Chen, N.-F.; Chen, W.-F.; Hung, H.-C.; Lee, H.-P.; Lin, Y.-Y.; Wang, H.-M.; Sung, P.-J.; Sheu, J.-H.; Wen, Z.-H. Sinularin from indigenous soft coral attenuates nociceptive responses and spinal neuroinflammation in carrageenan-induced inflammatory rat model. *Mar. Drugs* **2012**, *10*, 1899–1919.
193. Tseng, Y.-J.; Wen, Z.-H.; Dai, C.-F.; Chiang, M.Y.; Sheu, J.-H. Nanolobatolide, a new C18 metabolite from the Formosan soft coral *Sinularia nanolobata*. *Org. Lett.* **2009**, *11*, 5030–5032.

194. Rodríguez, I.I.; Shi, Y.-P.; García, O.J.; Rodríguez, A.D.; Mayer, A.M.S.; Sánchez, J.A.; Ortega-Barria, E.; González, J. New pseudopterosin and seco-pseudopterosin diterpene glycosides from two Colombian isolates of *Pseudopterogorgia elisabethae* and their diverse biological activities. *J. Nat. Prod.* **2004**, *67*, 1672–1680.
195. Shi, Y.-P.; Wei, X.; Rodríguez, I.I.; Rodríguez, A.D.; Mayer, A.M.S. New terpenoid constituents of the southwestern Caribbean sea whip *Pseudopterogorgia elisabethae* (Bayer), including a unique pentanorditerpene. *Eur. J. Org. Chem.* **2009**, *2009*, 493–502.
196. Vago, R. Beyond the skeleton: Cnidarian biomaterials as bioactive extracellular microenvironments for tissue engineering. *Organogenesis* **2008**, *4*, 18–22.
197. LaPlaca, M.C.; Vernekar, V.N.; Shoemaker, J.T.; Cullen, D.K. *Methods in Bioengineering: 3D Tissue Engineering*; Berthiaume, F.; Morgan, J.R., Eds.; Artech House Publishers: Norwood, MA, USA, 2010; pp. 187–204.
198. Shanny, B.; Vago, R.; Baranes, D. Growth of primary hippocampal neuronal tissue on an aragonite crystalline biomatrix. *Tissue Eng.* **2005**, *11*, 585–596.
199. Peretz, H.; Blinder, P.; Segal, L.; Baranes, D.; Vago, R. Aragonite crystalline matrix as an instructive microenvironment for neural development. *J. Tissue Eng. Regen. Med.* **2008**, *2*, 463–471.
200. Gautier, S.E.; Oudega, M.; Fragoso, M.; Chapon, P.; Plant, G.W.; Bunge, M.B.; Parel, J.-M. Poly(α-hydroxyacids) for application in the spinal cord: Resorbability and biocompatibility with adult rat Schwann cells and spinal cord. *J. Biomed. Mater. Res.* **1998**, *42*, 642–654.
201. Tibbitt, M.W.; Anseth, K.S. Hydrogels as extracellular matrix mimics for 3D cell culture. *Biotechnol. Bioeng.* **2009**, *103*, 655–663.
202. Peretz, H.; Talpalar, A.E.; Vago, R.; Baranes, D. Superior survival and durability of neurons and astrocytes on 3-dimensional aragonite biomatrices. *Tissue Eng.* **2007**, *13*, 461–472.
203. Seibold, E.; Berger, W.H. *The Sea Floor: An Introduction to Marine Geology*; Springer: Heidelberg, Germany, 1996.
204. Burgess, J.G. New and emerging analytical techniques for marine biotechnology. *Curr. Opin. Biotechnol.* **2012**, *23*, 29–33
205. Liu, Y. Renaissance of marine natural product drug discovery and development. *J. Mar. Sci. Res. Dev.* **2012**, *2*, 2.
206. Montaser, R.; Luesch, H. Marine natural products: A new wave of drugs? *Future Med. Chem*. **2011**, *3*, 1475–1489.
207. Murakami, N.; Nakajima, T.; Kobayashi, M. Total synthesis of lembehyne A, a neuritogenic spongean polyacetylene. *Tetrahedron Lett.* **2001**, *42*, 1941–1943.
208. Boger, D.L.; Boyce, C.W.; Labroli, M.A.; Sehon, C.A.; Jin, Q. Total syntheses of ningalin A, lamellarin O, lukianol A, and permethyl storniamide A utilizing heterocyclic azadiene Diels-Alder reactions. *J. Am. Chem. Soc*. **1998**, *121*, 54–62.
209. Xu, Y.-Z.; Yakushijin, K.; Horne, D.A. Synthesis of C11N5 marine sponge alkaloids: (±)-Hymenin, stevensine, hymenialdisine, and debromohymenialdisine. *J. Org. Chem*. **1997**, *62*, 456–464.

210. Tepe, J. Preparation of hymenialdisine derivatives and use thereof. U.S. Patent 7,732,436, 8 June 2010.
211. Wan, Y.; Hur, W.; Cho, C.Y.; Liu, Y.; Adrian, F.J.; Lozach, O.; Bach, S.; Mayer, T.; Fabbro, D.; Meijer, L.; *et al*. Synthesis and target identification of hymenialdisine analogs. *Chem. Biol.* **2004**, *11*, 247–259.
212. Nguyen, T.N.; Tepe, J.J. Preparation of hymenialdisine, analogues and their evaluation as kinase inhibitors. *Curr. Med. Chem.* **2009**, *16*, 3122–3143.
213. Ishibashi, F.; Miyazaki, Y.; Iwao, M. Total syntheses of lamellarin D and H. The first synthesis of lamellarin-class marine alkaloids. *Tetrahedron* **1997**, *53*, 5951–5962.
214. Pla, D.; Marchal, A.; Olsen, C.A.; Albericio, F.; Álvarez, M. Modular total synthesis of lamellarin D. *J. Org. Chem*. **2005**, *70*, 8231–8234.
215. Fujikawa, N.; Ohta, T.; Yamaguchi, T.; Fukuda, T.; Ishibashi, F.; Iwao, M. Total synthesis of lamellarins D, L, and N. *Tetrahedron* **2006**, *62*, 594–604.
216. Pla, D.; Marchal, A.; Olsen, C.A.; Francesch, A.; Cuevas, C.; Albericio, F.; Álvarez, M. Synthesis and structure–activity relationship study of potent cytotoxic analogues of the marine alkaloid lamellarin D. *J. Med. Chem.* **2006**, *49*, 3257–3268.
217. Cironi, P.; Manzanares, I.; Albericio, F.; Álvarez, M. Solid-phase total synthesis of the pentacyclic system lamellarins U and L. *Org. Lett.* **2003**, *5*, 2959–2962.
218. Roué, N.; Bergman, J. Synthesis of the marine alkaloid leucettamine B. *Tetrahedron* **1999**, *55*, 14729–14738.
219. Toma, T.; Kita, Y.; Fukuyama, T. Total synthesis of (+)-manzamine A. *J. Am. Chem. Soc.* **2010**, *132*, 10233–10235.
220. Jakubec, P.; Hawkins, A.; Felzmann, W.; Dixon, D.J. Total synthesis of manzamine A and related alkaloids. *J. Am. Chem. Soc.* **2012**, *134*, 17482–17485.
221. Perez, M.; Perez, D.I.; Martinez, A.; Castro, A.; Gomez, G.; Fall, Y. The first enantioselective synthesis of palinurin. *Chem. Commun.* **2009**, *2009*, 3252–3254.
222. Zhidkov, M.E.; Baranova, O.V.; Kravchenko, N.S.; Dubovitskii, S.V. A new method for the synthesis of the marine alkaloid fascaplysin. *Tetrahedron Lett*. **2010**, *51*, 6498–6499.
223. Bharate, S.B.; Manda, S.; Joshi, P.; Singh, B.; Vishwakarma, R.A. Total synthesis and anti-cholinesterase activity of marine-derived bis-indole alkaloid fascaplysin. *Med. Chem. Commun.* **2012**, *3*, 1098–1103.
224. Dai, Q.; Liu, F.; Zhou, Y.; Lu, B.; Yu, F.; Huang, P. The synthesis of SO-3, a conopeptide with high analgesic activity derived from *Conus striatus*. *J. Nat. Prod.* **2003**, *66*, 1276–1279.
225. Sobarzo-Sánchez, E.; Castedo, L.; De la Fuente, J.R. Synthesis of anabaseine and anabasine derivatives: Structural modifications of possible nicotinic agonists. *Synth. Commun.* **2007**, *37*, 1331–1338.
226. Toyooka, N.; Yotsui, Y.; Yoshida, Y.; Momose, T.; Nemoto, H. Highly stereoselective construction of 4,6-*cis*-substituted quinolizidine ring core: an application to enantioselective total synthesis of the marine alkaloid clavepictines A, B and pictamine. *Tetrahedron* **1999**, *55*, 15209–15224.

227. Yu, S.; Pu, X.; Cheng, T.; Wang, R.; Ma, D. Total synthesis of clavepictines A and B and pictamine. *Org. Lett.* **2006**, *8*, 3179–3182.
228. Toyooka, N.; Okumura, M.; Takahata, H.; Nemoto, H. Construction of 4a,8a-*cis*-octahydroquinolin-7-one core using an intramolecular aldol type of cyclization: An application to enantioselective total synthesis of lepadin B. *Tetrahedron* **1999**, *55*, 10673–10684.
229. Ozawa, T.; Aoyagi, S.; Kibayashi, C. Total synthesis of the marine alkaloid (−)-lepadin B. *Org. Lett.* **2000**, *2*, 2955–2958.
230. Barbe, G.; Charette, A.B. Total synthesis of (+)-lepadin B: Stereoselective synthesis of nonracemic polysubstituted hydroquinolines using an RC-ROM Process. *J. Am. Chem. Soc.* **2008**, *130*, 13873–13875.
231. McIntosh, J.M.; Yoshikami, D.; Mahe, E.; Nielsen, D.B.; Rivier, J.E.; Gray, W.R.; Olivera, B.M. A nicotinic acetylcholine receptor ligand of unique specificity, alpha-conotoxin ImI. *J. Biol.Chem.* **1994**, *269*, 16733–16739.
232. Stivala, C.E.; Gu, Z.; Smith, L.L.; Zakarian, A. Studies toward the synthesis of spirolide C: Exploration into the formation of the 23-membered all-carbon macrocyclic framework. *Org. Lett*. **2012**, *14*, 804–807.
233. Kong, K.; Romo, D.; Lee, C. Enantioselective total synthesis of the marine toxin (−)-gymnodimine employing a barbier-type macrocyclization. **2011**, *121*, 7538–7541.
234. Sakai, R.; Koike, T.; Sasaki, M.; Shimamoto, K.; Oiwa, C.; Yano, A.; Suzuki, K.; Tachibana, K.; Kamiya, H. Isolation, structure determination and synthesis of neodysiherbaine A, a new excitatory amino acid from a marine sponge. *Org. Lett*. **2001**, *3*, 1479–1482.
235. Lygo, B.; Slack, D.; Wilson, C. Synthesis of neodysiherbaine. *Tetrahedron Lett*. **2005**, *46*, 6629–6632.
236. Takahashi, K.; Matsumura, T.; Corbin, G.R.; Ishihara, J.; Hatakeyama, S. A highly stereocontrolled total synthesis of (−)-neodysiherbaine A. *J. Org. Chem.* **2006**, *71*, 4227–4231.
237. Donohoe, T.J.; Winship, P.C.M.; Tatton, M.R.; Szeto, P. A short and efficient synthesis of neodysiherbaine A by using catalytic oxidative cyclization. *Angew. Chem. Int. Ed*. **2011**, *50*, 7604–7606.
238. Takita, S.; Yokoshima, S.; Fukuyama, T. A practical synthesis of (−)-kainic Acid. *Org. Lett.* **2011**, *13*, 2068–2070.
239. Orellana, A.; Pandey, S.K.; Carret, S.; Greene, A.E.; Poisson, J.-F. A Diels–Alder-based total synthesis of (−)-kainic acid. *J. Org. Chem.* **2012**, *77*, 5286–5296.
240. Stathakis, C.I.; Yioti, E.G.; Gallos, J.K. Total syntheses of (−)-α-kainic Acid. *Eur. J. Org. Chem.* **2012**, *2012*, 4661–4673.
241. Kesava Reddy, N.; Chandrasekhar, S. Total synthesis of (−)-α-kainic acid via chirality transfer through Ireland–Claisen rearrangement. *J. Org. Chem.* **2013**, *78*, 3355–3360.
242. Ohfune, Y.; Tomita, M. Total synthesis of (−)-domoic acid. A revision of the original structure. *J. Am. Chem. Soc.* **1982**, *104*, 3511–3513.
243. Rivier, J.; Galyean, R.; Simon, L.; Cruz, L.J.; Olivera, B.M.; Gray, W.R. Total synthesis and further characterization of the γ-carboxyglutamate-containing "sleeper" peptide from *Conus geographus* venom. *Biochemistry* **1987**, *26*, 8508–8512.

244. Nakamura, M.; Suzuki, A.; Nakatani, M.; Fuchikami, T.; Inoue, M.; Katoh, T. An efficient synthesis of (+)-aureol via boron trifluoride etherate-promoted rearrangement of (+)-arenarol. *Tetrahedron Lett.* **2002**, *43*, 6929–6932.
245. Nakatani, M.; Nakamura, M.; Suzuki, A.; Fuchikami, T.; Inoue, M.; Katoh, T. Enantioselective total synthesis of (+)-aureol via a $BF3{\cdot}Et_2O$-promoted rearrangement/cyclization reaction of (+)-arenarol. *Arch. Org. Chem.* **2003**, *8*, 45–57.
246. Kuan, K.K.W.; Pepper, H.P.; Bloch, W.M.; George, J.H. Total synthesis of (+)-aureol. *Org. Lett.* **2012**, *14*, 4710–4713.
247. Brandt, S.D.; Moore, S.A.; Freeman, S.; Kanu, A.B. Characterization of the synthesis of *N*,*N*-dimethyltryptamine by reductive amination using gas chromatography ion trap mass spectrometry. *Drug Test. Anal.* **2010**, *2*, 330–338.
248. Johnson, A.-L.; Bergman, J.; Sjögren, M.; Bohlin, L. Synthesis of barettin. *Tetrahedron* **2004**, *60*, 961–965.
249. Aiello, A.; Giordano, A.; Fattorusso, E.; Menna, M.; Schroeder, H.C.; Mueller, W.E.G. Isolation, Structure Determination, Synthesis and Bioactivity of Damipipecolin and Damituricin. EP Patent 2007107319 A1, 27 September 2007.
250. Yoshida, M.; Yamaguchi, K. Total synthesis of dispyrin, purpurealidin E, and aplysamine-1. *Chem. Pharm. Bull.* **2008**, *56*, 1362–1363.
251. Gulati, D.; Chauhan, P.M.S.; Pratap, R.; Bhakuni, D.S. A new synthesis of aplysinopsin, a marine alkaloid and its analogues and their biological antivities. *Indian J. Chem.* **1994**, *33B*, 4–9.
252. Leftwick, A.P.; Weedon, B.C.L. Total synthesis of astaxanthin and hydroxyechinenone. *Chem. Commun. (Lond.)* **1967**, 49–50.
253. Cheng, H.M.; Tian, W.; Peixoto, P.A.; Dhudshia, B.; Chen, D.Y.K. Synthesis of ent-nanolobatolide. *Angew. Chem. Int. Ed*. **2011**, *50*, 4165–4168.
254. Ladlow, M.; Pattenden, G.; Teague, S.J. Synthesis of Δ9(12)-capnellene-8β,10α-diol from soft coral *Capnella imbricata*. *Tetrahedron Lett.* **1986**, *27*, 3279–3280.
255. Pattenden, G.; Teague, S.J. Total synthesis of (±)-Δ9(12)-capnellene-8β,10α-diol. *J. Chem. Soc. Perkin Trans. 1* **1988**, *1988*, 1077–1083.
256. Piers, E.; Llinas-Brunet, M. Total synthesis of (±)-8,15-diisocyano-11(20)-amphilectene. *J. Org. Chem.* **1989**, *54*, 1483–1484.
257. Avilés, E.; Rodríguez, A.D. Monamphilectine A, a potent antimalarial β-lactam from marine sponge *Hymeniacidon* sp: Isolation, structure, semisynthesis, and Bioactivity. *Org. Lett*. **2010**, *12*, 5290–5293.
258. Broka, C.A.; Chan, S.; Peterson, B. Total synthesis of (−)-pseudopterosin A. *J. Org. Chem.* **1988**, *53*, 1584–1586.
259. Buszek, K.R.; Bixby, D.L. Total synthesis of pseudopterosin A and E aglycon. *Tetrahedron Lett.* **1995**, *36*, 9129–9132.
260. Kocienski, P.J.; Pontiroli, A.; Qun, L. Enantiospecific syntheses of pseudopterosin aglycones. Part 2. Synthesis of pseudopterosin K–L aglycone and pseudopterosin A–F aglycone via a B→BA→BAC annulation strategy. *J. Chem. Soc. Perkin Trans. 1* **2001**, *2001*, 2356–2366.

261. Harrowven, D.C.; Tyte, M.J. Total synthesis of (±)-pseudopterosin A–F and K–L aglycone. *Tetrahedron Lett.* **2004**, *45*, 2089–2091.
262. Barykina, O.V.; Snider, B.B. Synthesis of (±)-eusynstyelamide A. *Org. Lett.* **2010**, *12*, 2664–2667.

Actinomycetes from Red Sea Sponges: Sources for Chemical and Phylogenetic Diversity

Usama Ramadan Abdelmohsen, Chen Yang, Hannes Horn, Dina Hajjar, Timothy Ravasi and Ute Hentschel

Abstract: The diversity of actinomycetes associated with marine sponges collected off Fsar Reef (Saudi Arabia) was investigated in the present study. Forty-seven actinomycetes were cultivated and phylogenetically identified based on 16S rRNA gene sequencing and were assigned to 10 different actinomycete genera. Eight putatively novel species belonging to genera *Kocuria*, *Mycobacterium*, *Nocardia*, and *Rhodococcus* were identified based on sequence similarity values below 98.2% to other 16S rRNA gene sequences available in the NCBI database. PCR-based screening for biosynthetic genes including type I and type II polyketide synthases (PKS-I, PKS-II) as well as nonribosomal peptide synthetases (NRPS) showed that 20 actinomycete isolates encoded each at least one type of biosynthetic gene. The organic extracts of nine isolates displayed bioactivity against at least one of the test pathogens, which were Gram-positive and Gram-negative bacteria, fungi, human parasites, as well as in a West Nile Virus protease enzymatic assay. These results emphasize that marine sponges are a prolific resource for novel bioactive actinomycetes with potential for drug discovery.

Reprinted from *Mar. Drugs*. Cite as: Abdelmohsen, U.R.; Yang, C.; Horn, H.; Hajjar, D.; Ravasi, T.; Hentschel, U. Actinomycetes from Red Sea Sponges: Sources for Chemical and Phylogenetic Diversity. *Mar. Drugs* **2014**, *12*, 2771–2789.

1. Introduction

Sponges (*Porifera*) are the oldest, evolutionarily ancient multicellular phylum with a fossil record dating back to Precambrian times [1]. The phylum *Porifera* consists of three major classes, Hexactinellida (glass sponges), Calcarea (calcareous sponges) and Demospongiae (demosponges), with the last group representing 85% of all living sponges [2]. Sponges populate tropical reefs in great abundance but also the polar latitudes as well as fresh water lakes and rivers [3,4]. Sponges have developed intimate contact with diverse microorganisms such as viruses, bacteria, archaea, fungi, protozoa, and single-celled algae and the nature of the sponge-microbe interaction is manifold [5]. The microbial distribution in most sponges follows a general pattern with the photosynthetically active microorganisms such as *Cyanobacteria* located in the outer light exposed layers while heterotrophic and possibly autotrophic bacteria inhabiting the inner core [6]. So far, at least 32 bacterial phyla and candidate phyla were described from marine sponges by both cultivation-dependent and cultivation-independent techniques; with the most common phyla being *Acidobacteria*, *Actinobacteria*, *Chloroflexi*, *Cyanobacteria*, *Gemmatimonadetes*, *Nitrospira*, Planctomycetes, *Proteobacteria*, (*Alpha*, *Delta*, *Gamma* subclasses) and Spirochaetes [1,3].

The phylum *Actinobacteria* represents one of the largest taxonomic units among the 18 major lineages currently recognized within the domain bacteria [7]. The subclass Actinobacteridae

includes the order Actinomycetales, members of which are commonly referred to as actinomycetes. These are Gram positive bacteria characterized by their ability to form branching hyphae at some stages of their development [8]. Within the order Actinomycetales, approximately 49 families have been recognized with the most common ones being *Actinomycetaceae*, *Actinoplanaceae*, *Dermatophilaceae*, *Frankiaceae*, *Mycobacteriaceae*, *Micromonosporaceae*, *Nocardiaceae*, and *Streptomycetaceae*, comprising altogether 147 genera [9,10]. Actinobacteria are widespread in nature and have been recovered from a wide variety of terrestrial habitats, where they exist as saprophytes, symbionts or pathogens [11–13]. Actinomycetes have been cultivated from the marine environment including sea water [14], marine snow, and marine sediments [15]. Actinomycetes have also been cultivated from different marine invertebrates [16–18], with the majority being isolated from sponges [19,20]. Marine actinomycetes produced a multitude of novel lead compounds with medicinal and pharmaceutical applications. Figure 1 shows the percentage distribution of compounds obtained from marine sponge-associated bacteria. Here, actinomycetes account for approximately half of the natural products (MarinLit database 2013 (John Blunt, MarinLit, University of Canterbury, New Zealand) [21,22]), (Figure 1). Biological activities such as antibacterial, antifungal, antiparasitic, antimalarial, immunomodulatory, anti-inflammatory, antioxidant, and anticancer activities were reported from sponge-associated actinomycetes [23–26]. These bioactivities are represented by diverse leads of secondary metabolites including polyketides, alkaloids, peptides, and terpenes [24,25,27–30].

Figure 1. Percentage distribution of compounds produced by sponge-associated bacteria (data collected from MarinLit 2013 and literature).

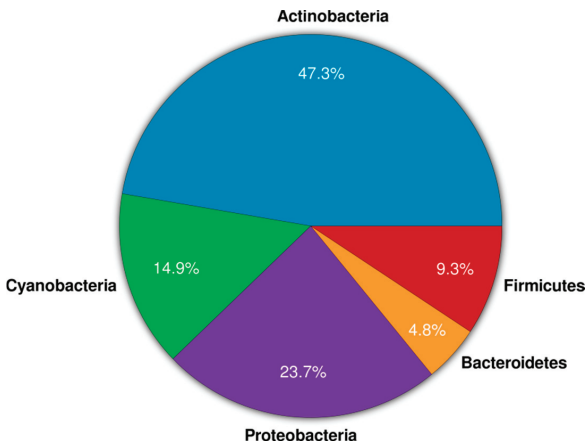

Polyketide synthases (PKS) and nonribosomal peptide synthetases (NRPS) are multi-domain megasynthases that are involved in the biosynthesis of a large fraction of diverse microbial natural products known as polyketides and nonribosomal peptides, respectively [31]. These enzymes are widely distributed among the actinomycetes, cyanobacteria, myxobacteria, and fungi [32]. Structurally, both PKS and NRPS are complex polypeptides organized in a modular fashion for assembling carboxylic acid and amino acid building blocks into their final products [33]. Each PKS module encodes three basic domains including ketosynthase (KS), acyltransferase (AT), and acyl

carrier protein (ACP), which are involved in the selection and condensation of the correct extender unit. Similarly, NRPS modules consist of condensation, adenylation, and thiolation domains for recognition and condensation of the starter substrate [31]. In this study, actinomycetes were cultivated from marine sponge species collected from the Red Sea. The obtained actinomycetes were phylogenetically characterized based on 16S rRNA gene sequencing and their genomic potential for natural products biosynthesis as well as their biological activities in an infection context are reported.

2. Results and Discussion

The Red Sea is one of the most biodiverse marine environments worldwide. It is characterized by high temperature (about 24 °C in spring and up to 35 °C in summer) and high salinity (*ca.* 40.0 psu), rendering this environment physically and chemically different from most other marine ecosystems [34]. About 240 demosponges have been formally recorded from the Red Sea so far and still many more await discovery [35]. Ngugi *et al.* reported a high bacterial diversity in the Red Sea in comparison to other tropical seas [36]. However, few studies have been carried out so far to investigate actinobacterial communities from Red Sea sponges. One such example is the study by Radwan *et al.* [37] who explored the microbial diversity of two Red Sea sponges, *Hyrtios erectus* and *Amphimedon* sp., using cultivation and cultivation-independent analyses.

2.1. Actinomycete Isolation and Phylogenetic Identification

Twenty-five isolates were selected out of cultivated 47 isolates based on their characteristic colony morphology. The 16S rRNA genes as taxonomic markers were sequenced and sequences were blasted against the NCBI GenBank database. The results showed that the isolates belonged to 10 different genera representing six families (*Dietziaceae*, *Micrococcaceae*, *Micromonosporaceae*, *Mycobacteriaceae*, *Nocardiaceae*, *Pseudonocardiaceae*) and four suborders (Corynebacterineae, Micrococcineae, Micromonosporineae, Pseudonocardineae). Eight putatively new species were identified based on sequence similarities <98.2%, which belonged to the genera *Kocuria*, *Mycobacterium*, *Nocardia* and *Rhodococcus* (Table 1). From a taxonomic perspective, sequence similarities after BlAST analysis against type strains may even be lower. As one example, the isolate SA8 showed 96% sequence similarity to the closest type strain (*Rhodococcus trifolii*^{T}). However, as type strains are not available for all obtained isolates, this taxonomically meaningful comparison remains restricted.

The recoverability of actinomycetes varied between different sponge sources; for example, *Amphimedon* aff. *chloros* yielded 17 actinomycetes (six genera), while *A. ochracea* yielded only four isolates from three different genera. These numbers compare to the recovery of four actinomycetes (two genera) from *Amphimedon* sp. from Ras Mohamed (Egypt) [17], 16 actinomycete (four genera) from *Amphimedon* sp. collected from Hurghada (Egypt) [37], and zero actinomycetes from *A. complanata* collected from Puerto Rico [38]. Similarly, while Radwan *et al.* [37] isolated 18 actinomycetes (four genera) from *Hyrtios erectos*, we obtained only three actinomycetes from this sponge species, albeit collected at a different location. Contrary to previous reports [39], we did

not succeed in isolating actinomycetes from *Xestospongia* aff. *testudinaria*. This sporadic isolation of actinomycetes could be explained by environmental factors that would influence the diversity, abundance and recoverability of actinomycetes from sponges. The observed differences also highlight the importance of using a wide range of media to increase the isolation efficiency of marine sponge-associated actinomycetes.

M1, ISP2 and OLIGO media were chosen for actinomycete cultivation based on previous experience and literature reports [17,40]. M1 medium produced the highest number of actinobacterial colonies (25), followed by ISP2 (16), while only six isolates were recovered on OLIGO (Figure 2B). Zhang *et al.* demonstrated that the lack of free amino acids resulted in low recovery of marine actinobacteria [19]. Accordingly, peptone was added to M1 medium which resulted in both, a higher number of actinomycetes and recovery of more genera. Consistent with previous studies [38,41], the genera *Rhodococcus*, *Micromonospora*, and *Nocardia* were cultivated preferentially on ISP2, while *Salinispora* grew better on oligotrophic media [42,43].

Table 1. 16S rRNA gene taxonomic affiliation of cultivated strains.

Isolate Code	Isolation Medium	Sponge Source	Sequence Length (bp)	Closest Relative by BLAST	% Sequence Similarity
SA1	M1	*Amphimedon ochracea*	1379	*Micrococcus* sp. PN13 (KF554087)	99.4
SA2	ISP2	*Amphimedon* aff. *chloros*	1435	*Micrococcus luteus* strain DAG I (KC470045)	99.7
SA3	ISP2	*Amphimedon* aff. *chloros*	1360	*Micrococcus* sp. X2Bc2 (KF465977)	99.5
SA4	ISP2	*Hyrtios erectus*	1423	*Micromonospora* sp. S6 (HF674982)	99.7
SA5	OLIGO	*Chalinula* sp.	1395	*Salinispora arenicola* CNS-205 (NR_074612)	99.9
SA6	OLIGO	*Chalinula* sp.	1372	*Salinispora arenicola* strain SCSIOZ-SH19 (KC747487)	100.0
* SA7	ISP2	*Chalinula* sp.	1338	*Nocardia* sp. W9912 (GU992878)	98.2
* SA8	ISP2	*Chalinula* sp.	1461	*Rhodococcus* equi (AB738794)	97.4
* SA9	ISP2	*Monanchora* sp.	1378	*Rhodococcus* sp. L-15 (JN006270)	97.9
SA10	M1	*Chalinula* sp.	1397	*Micrococcus* sp. PA-E028 (FJ233852)	99.8
* SA11	M1	*Monanchora* sp.	1416	*Mycobacterium* sp. CNJ879 PL04 (DQ448780)	97.6
* SA12	ISP2	*Chalinula* sp.	1374	*Rhodococcus* sp. HL-3 (JF734314)	97.9

Table 1. *Cont.*

* SA13	M1	*Monanchora* sp.	1419	*Mycobacterium* sp. CNJ879 PL04 (DQ448780)	97.8
* SA14	M1	*Amphimedon ochracea*	1341	*Kocuria* sp. PN5 (KF554079)	97.5
* SA15	M1	*Amphimedon* aff. *chloros*	1347	*Kocuria* sp. SS263-23 (JX429815)	97.3
SA16	M1	*Amphimedon* aff. *chloros*	1395	*Rothia terrae* strain F77052 (HQ908743)	99.7
SA17	ISP2	*Crella cyathophora*	1401	*Micrococcus* sp. X-48(JX997909)	99.9
SA18	M1	*Amphimedon* aff. *chloros*	1413	*Dietzia maris* strain KMGL1309-AS3 (KF740541)	100.0
SA19	OLIGO	*Chalinula* sp.	1325	*Salinispora pacifica* strain AMS365 (HQ873949)	99.9
SA20	M1	*Subera* sp.	1330	*Salinispora arenicola* strain SCSIOZ-SH19 (KC747487)	100.0
SA21	ISP2	*Subera* sp.	1443	*Saccharomonospora azurea* strain RR1 (KC855265)	99.2
SA22	OLIGO	*Subera* sp.	1337	*Salinispora pacifica* strain S34 (JX007964)	99.7
SA23	ISP2	*Amphimedon* aff. *chloros*	1396	*Saccharomonospora* sp. G2Z21 (JF806667)	99.8
SA24	M1	*Dactylospongia* aff. *elegans*	1494	*Kocuria palustris* strain LJ27 (KF515677)	99.1
SA25	OLIGO	*Hyrtios erectus*	1453	*Salinispora arenicola* strain SCSIOZ-SH11 (KC747479)	99.9

* Putatively new species.

The genus *Micrococcus* was represented by the highest number of isolates (14) which is likely due to their fast growing nature, rendering them easy to isolate. The second most abundant genus (7) was *Salinispora* which is frequently isolated from sea water, sediments, as well as sponges [43,44]. The other genera belonged to *Rhodococcus* (6), *Kocuria* (5), *Micromonospora* (4), *Dietzia* (3), *Saccharomonospora* (3), *Mycobacterium* (2), *Nocardia* (2), and *Rothia* (1).

A maximum-likelihood tree was calculated for the 25 isolates with the nearest sequence relatives from a Blast run included (Figure 3). The *Rhodococcus* isolates sp. SA8, SA9 and SA12 formed a distinct cluster. The high similarity and high bootstrap value (100) along with a multifurcation in the tree suggests that the isolates represent the same species. The isolates SA11, SA13, SA14, and SA15 form distinct clades in the genera *Mycobacterium* and *Kocuria*.

Interestingly, isolate SA7 falls within the genus *Nocardia* and also shows the lowest level of similarity (98.2%). In this case, further phenotypic and genotypic characterization may be needed to validate the exact taxonomic position of this isolate which might be a novel species within the genus *Nocardia*.

Figure 2. Number of actinomycete isolates (**A**) per sponge species, (**B**) per isolation media.

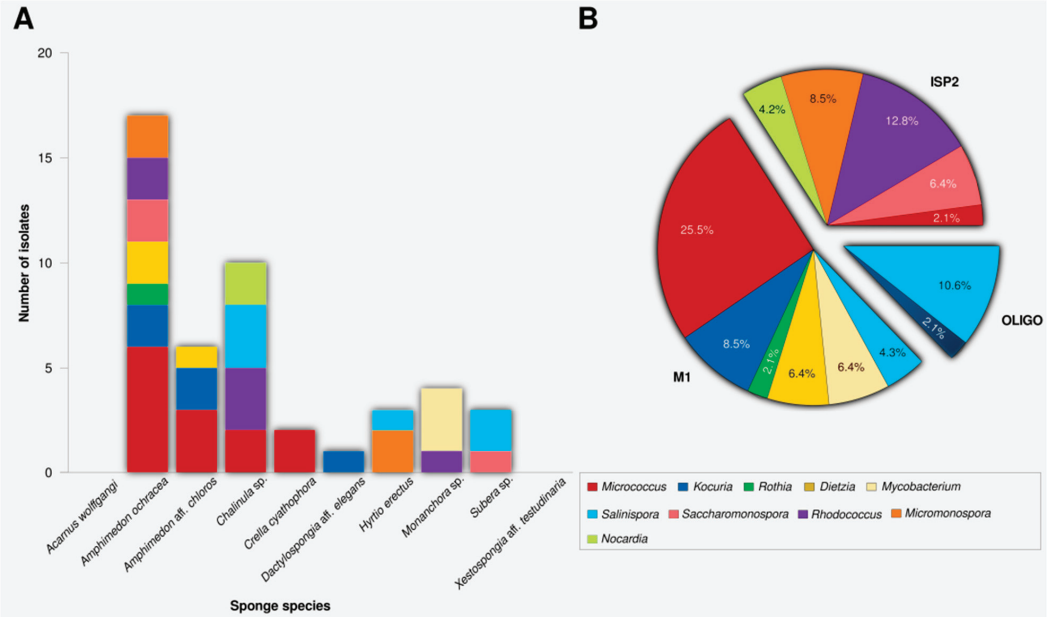

2.2. PCR-Screening for PKS and NRPS Domains

Twenty-five actinomycetes were tested using degenerate PCR primers for the presence of polyketide synthases Type I and II (PKS-I and PKS-II) and nonribosomal peptide synthetases (NRPS). At least one type of biosynthetic gene sequence was recovered from 20 actinomycete isolates (80%), (Table 2). All three types of biosynthetic genes were found in the actinomycetes (7) belonging to genera *Micromonospora* and *Salinispora*. This is unsurprising since *Micromonospora* and *Salinispora* are well known for their natural product diversity encompassing different metabolite classes [25,27,45]. NRPS biosynthetic genes were identified in 19 isolates (76%), while PKS-I genes were detected in 12 strains (48%), and PKS-II genes in eight strains (32%). NRPS and PKS sequence diversity have been reported in marine actinomycetes isolated from different marine environments including marine caves, marine sediments, and marine sponges, where these sequences were detected in up to 90% of the tested strains [46,47].

Figure 3. Maximum-likelihood tree of the actinomycete isolates SA1-SA25 (in bold) and their closest phylogenetic relatives based on the 16S rRNA gene marker. Brackets indicate genus-level assignment. Bootstrap values (1000 resamples) are given in percent at the nodes of the tree (greater than 50). The arrow points to the outgroup (*Escherichia coli* KTCT 2441^T).

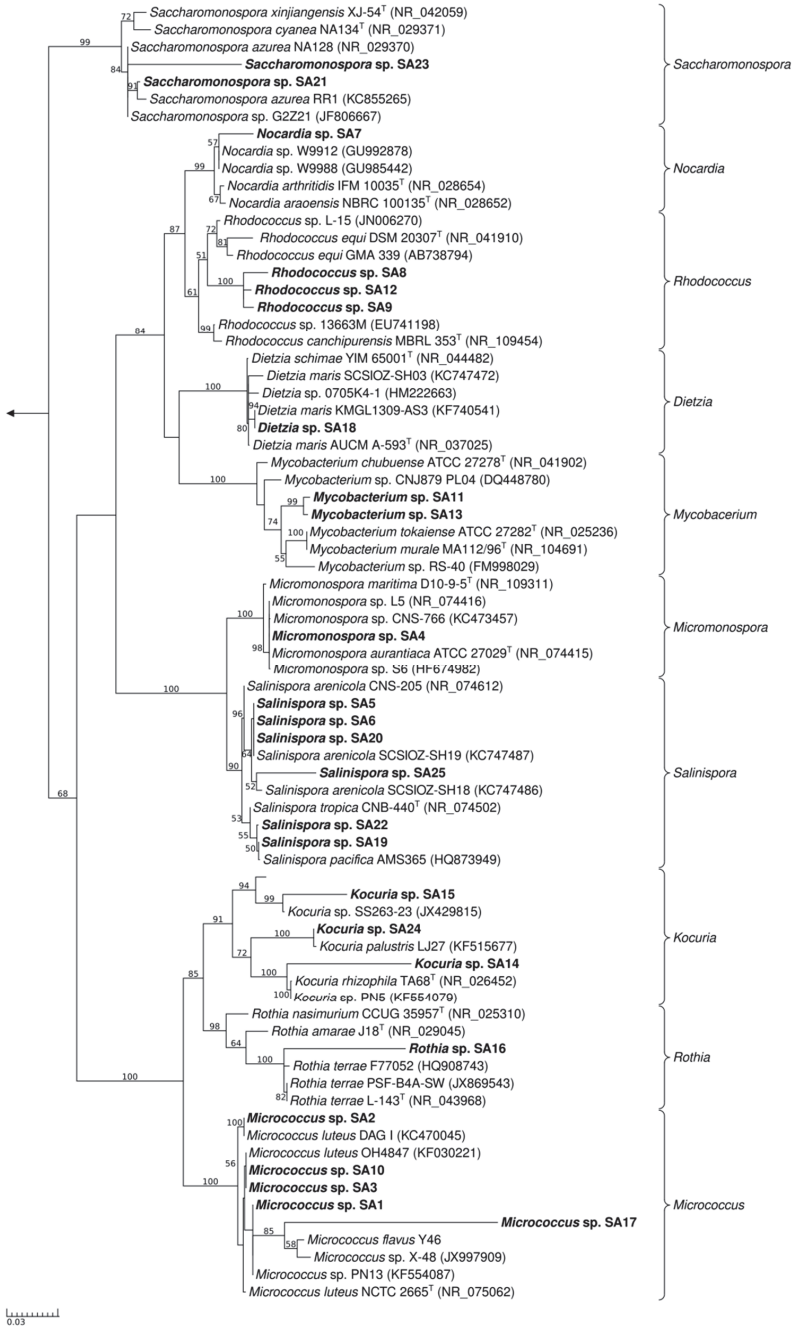

Table 2. NRPS and PKS results of cultivated strains.

Isolate Code	Closest Relative by BLASTX (Sequence Length bp, % Sequence Similarity)		
	NRPS	**PKS I**	**PKS II**
SA1	Amino acid adenylation domain-containing protein [*Micrococcus luteus* (CP001628)] (347, 51)	-	-
SA2	Non-ribosomal peptide synthetase [*Micrococcus luteus* (EFD52022)] (417, 56)	-	-
SA3	Amino acid adenylation domain-containing protein [*Micrococcus luteus* (CP001628)] (511, 62)	-	-
SA4	Amino acid adenylation domain-containing protein [*Micromonospora aurantiaca* (WP_013285021)] (501, 79)	Polyketide synthase [*Micromonospora* sp. CNB394 (WP_018787726)] (473, 67)	Type II PKS ketosynthase, partial [*Micromonospora* sp. SCSIO11524 (AHB18630)] (541, 63)
SA5	Amino acid adenylation domain-containing protein [*Salinispora arenicola* (WP_012184557)] (521, 72)	Polyketide synthase [*Salinispora arenicola* (WP_018795623)] (541, 64)	Beta-ACP synthase, partial [*Salinispora arenicola* (WP_020608853)] (573, 70)
SA6	Amino acid adenylation domain-containing protein [*Salinispora arenicola* (YP_001535283)] (513, 77)	Polyketide synthase [*Salinispora arenicola* (WP_018795623)] (516, 71)	KAS II [*Salinispora arenicola* (WP_020608853)] (581, 67)
* SA7	-	-	Polyketide synthase [*Nocardia nova* SH22a (AHH16328)] (614, 85)

Table 2. *Cont.*

* SA8	Non-ribosomal peptide synthetase [*Rhodococcus equi* (CBH48735)] (570, 69)	Putative polyketide synthase [*Rhodococcus equi* (WP_022593366)] (518, 65)	-
* SA9	Non-ribosomal peptide synthetase, partial [*Rhodococcus qingshengii* (WP_007730195)] (609, 68)	Putative polyketide synthase [*Rhodococcus opacus* B4 (BAH55256)] (428, 75)	-
SA10	-	-	-
* SA11	-	-	-
* SA12	Non-ribosomal peptide synthetase [*Rhodococcus opacus* (WP_005253470)] (622, 58)	Putative polyketide synthase [*Rhodococcus opacus* (BAH55256)] (428, 75)	-
* SA13	-	-	-
* SA14	Non-ribosomal peptide synthetase [*Kocuria rhizophila* (BAG29492)] (532, 74)	-	-
*SA15	Non-ribosomal peptide synthetase [*Kocuria rhizophila* (BAG29492)] (462, 68)	-	-
SA16	-	-	-
SA17	Non-ribosomal peptide synthetase [*Micrococcus luteus* (EFD52022) (423, 66)	-	-
SA18	-	-	-
SA19	Adenylation domain of nonribosomal peptide synthetase [*Salinispora pacifica* (WP_018724218)] (465, 58)	Polyketide synthase [*Salinispora pacifica* (WP_018824659)] (421, 59)	Beta-ACP synthase [*Salinispora pacifica (*WP_018720155)] (541, 61)
SA20	Amino acid adenylation domain-containing protein [*Salinispora arenicola* (WP_012184557)] (465, 58)	Polyketide synthase [*Salinispora arenicola* (WP_019032802)] (506, 61)	KAS II [*Salinispora arenicola* (WP_020608853)] (529, 57)
SA21	Nonribosomal peptide synthetase [*Saccharopolyspora spinosa* (WP_010314019)] (665, 74)	Polyketide synthase [*Saccharopolyspora spinosa* (WP_010311945)] (565, 69)	-
SA22	Amino acid adenylation domain of nonribosomal peptide synthetase [*Salinispora pacifica* (WP_018724218)] (476, 59)	Polyketide synthase [*Salinispora pacifica* (WP_018824659)] (501, 63)	Beta-ACP synthase [*Salinispora pacifica* (WP_018823591)] (531, 71)

Table 2. *Cont.*

SA23	Amino acid adenylation domain-containing protein [*Saccharopolyspora spinosa* (WP_010694383)] (643, 71)	Polyketide synthase [*Saccharopolyspora erythraea* (WP_011873765)] (533, 61)	-
SA24	Nonribosomal peptide synthetase [*Kocuria rhizophila* (WP_019309050)] (592, 73)	-	-
SA25	Amino acid adenylation domain-containing protein [*Salinispora arenicola* (YP_001539321)] (453, 68)	Rifamycin polyketide synthase [*Salinispora arenicola* (WP_020217874)] (578, 71)	Ketosynthase, partial [*Salinispora arenicola* AFO70123] (548, 63)

2.3. Anti-Infective Screening

Twenty-five actinomycete isolates were fermented in the medium, from which they were originally isolated, and ethyl acetate and methanol were used for extraction of secondary metabolites. The ethyl acetate and methanolic extracts were then screened against *Bacillus* sp. P25, *Escherichia coli* K12, *Fusarium* sp. P21, *Trypanosoma brucei* TC 221, *Leishmania major* and NS3 protease of West Nile Virus (Table 3). Nine actinobacterial extracts were active against at least one test pathogen. No activities were documented against *L. major*. Two isolates were active against *Bacillus* sp. and *E. coli* K12 while antifungal activities were reported for six extracts and anti-trypanosomal activity was documented for five extracts.

Two *Micrococcus* isolates were bioactive. Members of the genus *Micrococcus* were cultivated from diverse terrestrial and marine environments, however they are not well known for production of secondary metabolites. The antibiotic 2,4,4′-trichloro-2′-hydroxydiphenylether from sponge-associated *Micrococcus luteus* [48] and recently the thiazolyl peptide kocurin against methicillin-resistant *Staphylococcus aureus* [49]. Although the two *Micrococcus* isolates SA1 and SA3 are phylogenetically related (identical 16S rRNA sequences, Figure 2), their ethyl acetate extracts exhibited different biological profiles. This means that 16S rRNA gene as phylogenetic marker alone was not sufficient to distinguish genomic differences between actinomycete isolates sharing identical 16S rRNA gene sequence homologies and display different biosynthetic gene expression that could result in the production of different natural products [50].

The ethyl acetate extracts of *Salinispora* sp. SA6 and SA22 were active against almost all test pathogens, except *L. major*. The obligate marine *Salinispora* strains are prolific producers of structurally diverse natural products such as salinosporamide A from *S. tropica*, a potent proteasome inhibitor that has reached phase I clinical trials as an anticancer agent [51]. Other examples of bioactive compounds from various *Salinispora* species include arenimycin, rifamycins [52], cyanosporaside A, [53] saliniketals A and B [54], salinipyrones, and pacificanones [55]. The results highlight the high chemical potential of *Salinispora* isolates.

Table 3. Bioactivity results of the actinomycete isolates.

Isolate Code	Inhibition Zone Diameter (mm)			IC_{50} (µg/mL, 72 h)	Growth Inhibition (%)
	***Bacillus* sp. P25**	***Escherichia coli* K12**	***Fusarium* sp. P21**	***Trypanosoma brucei* TC 221**	**West Nile Virus Protease**
Micrococcus sp. SA1E	8	12	-	<10	-
Micrococcus sp. SA3E	-	-	14	-	-
Salinispora sp. SA6E	20	7	22	<10	84
Salinispora sp. SA22E	18	9	15	<10	79
* *Rhodococcus* sp. SA9E	-	-	13	-	-
* *Rhodococcus* sp. SA12E	-	-	16	-	93
Mycobacterium sp. SA11E	14	-	-	<10	-
Saccharomonospora sp. SA21 E	10	12	-	-	-
Saccharomonospora sp. SA23 E	11	13	17	<10	-

* Putatively new species.

Two extracts of the novel isolates *Rhodococcus* sp. SA9 and SA12 exhibited antifungal activity against *Fusarium* sp. P21 with *Rhodococcus* sp. SA12 showing additional activity against West Nile Virus NS3 protease. One isolate of the genus *Mycobacterium* showed activity against *Bacillus* sp. P25 as well as *Trypanosoma brucei* TC 221. The ethyl acetate extract of *Saccharomonospora* sp. SA21 was active against *Bacillus* sp. P25 and *Escherichia coli* K12 while *Saccharomonospora* sp. SA23 showed more broad activities against *Bacillus* sp. P25, *Escherichia coli* K12, *Fusarium* sp. P21, and *Trypanosoma brucei* TC 221.West Nile Virus (WNV) is a zoonotic virus which is widespread and endemic in Africa, the Middle East and western Asia as well as other parts of the world including United States, Europe and Australia [56]. There are commercially available animal vaccines, however up to date, no vaccines or treatments have been approved for human WNV infections [57]. This illustrates the urgent need to develop effective vaccines and antiviral drugs to prevent WNV infection in humans. The WNV protease NS3 is a prime target for antiviral drugs and has become the focus of considerable research efforts [57,58]. Interestingly, three ethyl acetate extracts (SA 6E, 22E, 12E) showed activity against WNV protease NS3 in the present study. Bioactivities were documented for ethyl acetate, but not methanolic extracts, which was consistent with literature reports showing that the majority of microbial natural products are secreted into the medium [59,60].

3. Experimental Section

3.1. Sponge Collection

Ten sponge species (*Amphimedon ochracea*, *Amphimedon* aff. *chloros*, *Acarnus wolffgangi*, *Chalinula* sp., *Crella cyathophora*, *Dactylospongia* aff. *elegans*, *Hyrtios erectus*, *Monanchora* sp., *Subera* sp., *Xestospongia* aff. *testudinaria*) were collected by SCUBA diving at depths of 8–12 m in the Red Sea (Saudi Arabia, Thuwal, Fsar Reef, GPS: 22°23′ N; 39°03′ E) in June 2012. Taxonomic identification was performed by Nicole de Voogd (Naturalis Biodiversity Center,

Leiden, The Netherlands). Sponges were transferred to plastic bags containing sea water and transported to the laboratory. Sponge specimens were rinsed in sterile sea water, cut into pieces of *ca.* 1 cm^3, and thoroughly homogenized in a sterile mortar with 10 volumes of sterile sea water. The supernatant was diluted in 10-fold series (10^{-1}, 10^{-2}, 10^{-3}) and subsequently plated out on agar plates. Processing was equivalent among samples.

3.2. Actinomycete Isolation and Identification

M1, ISP medium 2 and Oligotrophic media (OLIGO) were used for actinomycete isolation as described previously [17]. All media were prepared in artificial sea water and were supplemented with cycloheximide (100 μg/mL) and nalidixic acid (25 μg/mL) to inhibit fungal growth and fast-growing Gram-negative bacteria, respectively. Actinomycetes were picked based on their morphological characteristics and re-streaked several times to obtain pure colonies. The isolates were maintained on plates for short-term storage and long-term strain collections were set up in medium supplemented with 30% glycerol at −80 °C. The isolates were abbreviated as "SA".

DNA was extracted using the AllPrep DNA/RNA mini kit (QIAGEN, Hilden, Germany) following manufacturer's instructions. 16S rRNA gene amplification and sequencing were performed using the universal primers 27F and 1492R. Chimeric sequences were identified using the Pintail program [61]. Raw sequences were processed on the software Sequencher 4.9 (Genecodes Coorperation, Ann Arbor, MI, USA). After ambiguous bases were trimmed to a quality over 99%, forward and reverse strands were assembled into a contig with the length of more than 1300 bases. Nearest related and described sequences were searched with an initial Blast run against the NCBI database. The genus-level identification of all the sequences was done with RDP Classifier (-g 16srrna, -f allrank) [62] and validated with the SILVA Incremental Aligner (SINA) (search and classify option) [63]. An alignment was calculated again using the SINA web aligner (variability profile: bacteria). Gap-only position were removed with trimAL (-noallgaps) [64]. For phylogenetic tree construction, the best fitting model was estimated initially with Model Generator [65]. RAxML (-f a -m GTRGAMMA –x 12345 –p 12345 -# 1000) [66] and the estimated model was used with 1000 bootstrap resamples to generate the maximum-likelihood tree. Visualization was done with TreeGraph2 [67]. The 16S rRNA gene sequences of the putatively novel isolates were deposited in GenBank under the accession numbers showed in parentheses: SA7 (KJ599861), SA8 (KJ599862), SA9 (KJ599863), SA11 (KJ599864), SA12 (KJ599865), SA13 (KJ599866), SA14 (KJ599867), and SA15 (KJ599868).

3.3. PCR Screening of NRPS and PKS-II Gene Fragments

Ketosynthase (KS) domains of type I polyketide synthase (PKS) gene were PCR amplified from genomic DNA using the primers K1F (5′-TSAAGTCSAACATCGGBCA-3′) and M6R (5′-CGCAGGTTSCSGTACCAGTA-3′). Type II PKS sequences were amplified using KSαF (5′-TSGRCTACRTCAACGCSCACGG-3′) and KSβR (5′-TACSAGTCSWTCGCCTGGTTC-3′). In order to target adenylation domains of NRPS genes, the degenerate PCR primers A3F (5′-GCSTACSYSATSTACACSTCSGG-3′) and A7R (5′-SASGTCVCCSGTSCGGTAS-3′) were

used [68]. Sequences of the corresponding PCR products (KS domains, 1250–1400 bp; KSα and KSβ, 800–900 bp; adenylation domains, 700 bp) [69] were compared with NRPS and PKS sequences in the NCBI database by using the Basic Local Alignment Search Tool X (BLASTX).

3.4. Secondary Metabolites Extraction and Bioactivity Testing

Twenty-five strains were cultured in 500 mL Erlenmeyer flasks containing 250 mL of the appropriate cultivation medium for each isolate. The liquid cultures were grown for 7–10 days depending on their growth rate at 30 °C while shaking at 150 rpm. After cultivation and filtration, the supernatant was extracted with ethyl acetate (2 × 150 mL). The cells were macerated in 100 mL methanol and shaken for 3 h (150 rpm) then filtered. The extracts (ethyl acetate and methanol) were concentrated under vacuum and stored at 4 °C.

3.4.1. Antibacterial and Antifungal Activities Testing

Antimicrobial activity was tested using the standard disk diffusion assay against *Bacillus* sp. P25, *Escherichia coli* K12 and *Fusarium* sp. P21. Sterile filter disks (6 mm) loaded 3 times with the test extracts (25 µL, 20 mg/mL in methanol) were placed on agar plates that had been inoculated with the test microorganism. After incubation (24 h for *Bacillus*, *Escherichia coli* K12 and 48 h for *Fusarium* sp.) at 37 °C (*Bacillus*, *Escherichia coli* K12) and 30 °C (*Fusarium* sp.), the antimicrobial potential was quantitatively assessed as diameter of the inhibition zone ($n = 2$).

3.4.2. Anti-Trypanosomal Activity

Anti-trypanosomal activity was tested following the protocol of Huber and Koella [70]. 10^4 trypanosomes per mL of *Trypanosoma brucei brucei* strain TC 221 were cultivated in Complete Baltz Medium. Trypanosomes were tested in 96-well plate chambers against different concentrations of test extracts at 10–200 µg/mL in 1% DMSO to a final volume of 200 µL. For controls, 1% DMSO as well as parasites without any test extracts were used simultaneously in each plate to show no effect of 1% DMSO. The plates were then incubated at 37 °C in an atmosphere of 5% CO_2 for 24 h. After addition of 20 µL of Alamar Blue, the activity was measured after 48 and 72 h by light absorption using an MR 700 Microplate Reader (Dynatech Engineering Ltd., Willenhall, UK) at a wavelength of 550 nm with a reference wavelength of 650 nm. The IC_{50} values of the test extracts were quantified by linear interpolation of three independent measurements.

3.4.3. Anti-Leishmanial Activity

Anti-leishmanial activity was tested following the method of Ponte-Sucre *et al.* [71]. 10^7 cells/mL *Leishmania major* promastigotes were incubated in complete medium for 24 h at 26 °C, 5% CO_2, and 95% humidity in the absence or presence of different concentrations of the test extracts (10–200 µg/mL, 1% DMSO) to a final volume of 200 µL. Following the addition of Alamar Blue, the plates were incubated again and the optical densities were determined after 48 h with a Multiskan Ascent enzyme-linked immunosorbent assay (ELISA) reader (Multiskan Ascent, Thermo Electron

Corporation, Dreieich, Germany). The effects of cell density, incubation time and the concentration of DMSO were examined in control experiments. The results were expressed in IC_{50} values by linear interpolation of three independent experiments.

3.4.4. West Nile Virus NS3 Protease Inhibition Assay

The West Nile Virus NS3 protease inhibition assay was carried out using the commercial kit SensoLyte® 440 West Nile Virus Protease Assay Kit (AnaSep, San Jose, CA, USA) [58]. The quantification of protease activity was measured by using the fluorogenic peptide Pyr-RTKR-AMC which produces free AMC (7-amino-4-methylcoumarin) fluorophore upon NS3 protease cleavage. The extracts and protease solution were applied to 384-well plates and the total reaction mixture in each well was 40 µL. All extracts and controls were performed with three replicates and were generated according to the manufacturer's instructions. Briefly, the test extracts and protease solution were mixed and incubated at 37 °C for 10 min before adding the fluorogenic substrate. After substrate addition, the reagents were completely mixed and incubated at 37 °C for one hour. The fluorescence intensities were measured using a SpectraMax® Paradigm® Multi-mode Microplate Detection Platform (Molecular Devices, Sunnyvale, CA, USA) at 354 nm (excitation) and 442 nm (emission).

4. Conclusions

Marine actinomycetes, such as those associated with marine sponges, are a rich source of bioactive natural products. In the present study, we isolated 47 actinomycetes representing 10 different genera and including eight putatively novel phylotypes. The isolates were obtained from sponges which were collected offshore Fsar reef, Saudi Arabia, a largely uncharted territory with respect to bioprospecting. Although 80% of actinomycetes contained at least one class of NRPS or PKS gene, antimicrobial activity was detected only for 36% of the isolates. This suggests that genomic mining is a worthwhile future endeavour. Bioactivities against bacteria, fungi, human parasites as well as West Nile Virus protease were reported for nine of the isolates. These results underscore the potential of Red Sea sponges as a source of novel actinomycetes with underexplored potential for drug discovery. The combination of PCR-based screening, phylogenetic analysis as well as bioactivity assays is a useful strategy to prioritize actinomycetes for further bioassay-guided isolation work.

Acknowledgments

The authors wish to acknowledge funding from DFG (SFB 630 TP A5) to U. H. We thank H. Bruhn (SFB 630 TP Z1, Würzburg, Germany) for supervising the anti-infective assays platform and for her continued interest. We thank C. Voolstra, S. Kremb, U. Stingl (KAUST, Saudi Arabia) for the laboratory facilities. We thank the students J. Wiezoreck and D. Schmidt (Würzburg, Germany) for their assistance in the laboratory. This publication was funded by the German Research Foundation (DFG) and the University of Wuerzburg in the funding programme Open Access Publishing.

Author Contributions

Usama Ramadan Abdelmohsen (isolation and characterization of actinomycetes, manuscript preparation), Chen Yang (isolation and characterization of actinomycetes, bioactivity testing), Hannes Horn (phylogenetic tree construction, manuscript preparation), Dina Hajjar (West Nile Virus protease testing), Timothy Ravasi (organisation of sponge collection, project supervision), Ute Hentschel (manuscript preparation, project design and supervision).

Conflicts of Interest

The authors state no conflict of interest.

References

1. Hentschel, U.; Piel, J.; Degnan, S.M.; Taylor, M.W. Genomic insights into the marine sponge microbiome. *Nature* **2012**, *10*, 641–654.
2. Van Soest, R.W.; Boury-Esnault, N.; Vacelet, J.; Dohrmann, M.; Erpenbeck, D.; de Voogd, N.J.; Santodomingo, N.; Vanhoorne, B.; Kelly, M.; Hooper, J.N. Global diversity of sponges (*Porifera*). *PLoS One* **2012**, *7*, e35105.
3. Schmitt, S.; Tsai, P.; Bell, J.; Fromont, J.; Ilan, M.; Lindquist, N.; Perez, T.; Rodrigo, A.; Schupp, P.J.; Vacelet, J.; *et al.* Assessing the complex sponge microbiota: Core, variable and species-specific bacterial communities in marine sponges. *ISME J.* **2012**, *6*, 564–576.
4. Belarbi el, H.; Contreras Gomez, A.; Chisti, Y.; Garcia Camacho, F.; Molina Grima, E. Producing drugs from marine sponges. *Biotechnol. Adv.* **2003**, *21*, 585–598.
5. Webster, N.S.; Taylor, M.W. Marine sponges and their microbial symbionts: Love and other relationships. *Environ. Microbiol.* **2012**, *14*, 335–346.
6. Hentschel, U.; Fieseler, L.; Wehrl, A.; Gernert, C.; Steinert, M.; Hacker, J.; Horn, M. Microbial diversity of marine sponges. In *Sponges (Porifera)*; Müller, W.E.G., Ed.; Springer: Berlin, Germany, 2003; pp. 59–88.
7. Ventura, M.; Canchaya, C.; Tauch, A.; Chandra, G.; Fitzgerald, G.F.; Chater, K.F.; van Sinderen, D.; Genomics of Actinobacteria: Tracing the evolutionary history of an ancient phylum. *Microbiol. Mol. Biol. Rev.* **2007**, *71*, 495–548.
8. Goodfellow, M.; Williams, S.T. Ecology of actinomycetes. *Annu. Rev. Microbiol.* **1983**, 37, 189–216.
9. Garrity, G.M.; Bell, J.A.; Lilburn, T.G. Taxonomic outline of the prokaryotes. In *Bergey's Manual of Systematic Bacteriology*; Gray, M.W., Burger, G., Lang, B.F., Eds.; Springer: New York, NY, USA, 2004; pp. 204–301.
10. Adegboye, M.F.; Babalola, O.O. Taxonomy and ecology of antibiotic producing actinomycetes *Afr. J. Agric. Res.* **2012**, *15*, 2255–2261.
11. Andrade, M.R.M.; Amaral, E.P.; Ribeiro, S.C.M.; Almeida, F.M.; Peres, T.V.; Lanes, V.; D'Imperio-Lima, M.R.; Lasunskaia, E.B. Pathogenic *Mycobacterium bovis* strains differ in their ability to modulate the proinflammatory activation phenotype of macrophages. *BMC Microbiol.* **2012**, *12*, 166; doi:10.1186/1471-2180-12-166.

12. Salem, H.; Kreutzer, E.; Sudakaran, S.; Kaltenpoth, M. Actinobacteria as essential symbionts in firebugs and cotton stainers (Hemiptera, Pyrrhocoridae). *Environ. Microbiol.* **2013**, *15*, 1956–1968.
13. Sun, W.; Dai, S.; Jiang, S.; Wang, G.; Liu, G.; Wu, H.; Li, X. Culture-dependent and culture-independent diversity of Actinobacteria associated with the marine sponge *Hymeniacidon perleve* from the South China Sea. *Anton Van Leeuwenhoek* **2010**, *98*, 65–75.
14. Zhang, L.M.; Xi, L.J.; Ruan, J.S.; Huang, Y. *Microbacterium marinum* sp nov., isolated from deep-sea water. *Syst. Appl. Microbiol.* **2012**, *35*, 81–85.
15. Becerril-Espinosa, A.; Freel, K.C.; Jensen, P.R.; Soria-Mercado, I.E. Marine actinobacteria from the Gulf of California: Diversity, abundance and secondary metabolite biosynthetic potential. *Antonie Van Leeuwenhoek* **2013**, *103*, 809–819.
16. Sun, W.; Peng, C.S.; Zhao, Y.Y.; Li, Z.Y. Functional gene-guided discovery of type II polyketides from culturable actinomycetes associated with soft coral *Scleronephthya* sp. *PLoS One* **2012**, *7*, e42847.
17. Abdelmohsen, U.R.; Pimentel-Elardo, S.M.; Hanora, A.; Radwan, M.; Abou-El-Ela, S.H.; Ahmed, S.; Hentschel, U. Isolation, phylogenetic analysis and anti-infective activity screening of marine sponge-associated actinomycetes. *Mar. Drugs* **2010**, *8*, 399–412.
18. Wyche, T.P.; Hou, Y.P.; Vazquez-Rivera, E.; Braun, D.; Bugni, T.S. Peptidolipins B–F, antibacterial lipopeptides from an ascidian-derived *Nocardia* sp. *J. Nat. Prod.* **2012**, *75*, 735–740.
19. Zhang, H.; Lee, Y.K.; Zhang, W.; Lee, H.K. Culturable actinobacteria from the marine sponge *Hymeniacidon perleve*: Isolation and phylogenetic diversity by 16S rRNA gene-RFLP analysis. *Anton Van Leeuwenhoek* **2006**, *90*, 159–169.
20. Xi, L.; Ruan, J.; Huang, Y. Diversity and biosynthetic potential of culturable actinomycetes associated with marine sponges in the china seas. *Int. J. Mol. Sci.* **2012**, *13*, 5917–5932.
21. Lam, K.S. Discovery of novel metabolites from marine actinomycetes. *Curr. Opin. Microbiol.* **2006**, *9*, 245–251.
22. Thomas, T.R.A.; Kavlekar, D.P.; LokaBharathi, P.A. Marine drugs from sponge-microbe association-A Review. *Mar. Drugs* **2010**, *8*, 1417–1468.
23. Pimentel-Elardo, S.M.; Kozytska, S.; Bugni, T.S.; Ireland, C.M.; Moll, H.; Hentschel, U. Anti-parasitic compounds from *Streptomyces* sp. strains isolated from Mediterranean sponges. *Mar. Drugs* **2010**, *8*, 373–380.
24. Blunt, J.W.; Copp, B.R.; Keyzers, R.A.; Munro, M.H.; Prinsep, M.R. Marine natural products. *Nat. Prod. Rep.* **2013**, *30*, 237–323.
25. Abdelmohsen, U.R.; Szesny, M.; Othman, E.M.; Schirmeister, T.; Grond, S.; Stopper, H.; Hentschel, U. Antioxidant and anti-Protease activities of diazepinomicin from the sponge-associated *Micromonospora* strain RV115. *Mar. Drugs* **2012**, *10*, 2208–2221.
26. Bull, A.T.; Stach, J.E. Marine actinobacteria: New opportunities for natural product search and discovery. *Trends Microbiol.* **2007**, *15*, 491–499.
27. Solanki, R.; Khanna, M.; Lal, R. Bioactive compounds from marine actinomycetes. *Indian J. Microbiol.* **2008**, *48*, 410–431.

28. Subramani, R.; Aalbersberg, W. Marine actinomycetes: An ongoing source of novel bioactive metabolites. *Microbiol. Res.* **2012**, *167*, 571–580.
29. Fenical, W.; Jensen, P.R. Developing a new resource for drug discovery: Marine actinomycete bacteria. *Nat. Chem. Biol.* **2006**, *2*, 666–673.
30. Tiwari, K.; Gupta, R.K. Rare actinomycetes: A potential storehouse for novel antibiotics. *Crit. Rev. Biotechnol.* **2012**, *32*, 108–132.
31. Donadio, S.; Monciardini, P.; Sosio, M. Polyketide synthases and nonribosomal peptide synthetases: The emerging view from bacterial genomics. *Nat. Prod. Rep.* **2007**, *24*, 1073–1109.
32. Fieseler, L.; Hentschel, U.; Grozdanov, L.; Schirmer, A.; Wen, G.; Platzer, M.; Hrvatin, S.; Butzke, D.; Zimmermann, K.; Piel, J. Widespread occurrence and genomic context of unusually small polyketide synthase genes in microbial consortia associated with marine sponges. *Appl. Environ. Microbiol.* **2007**, *73*, 2144–2155.
33. Chen, Y.Q.; Ntai, I.; Ju, K.S.; Unger, M.; Zamdborg, L.; Robinson, S.J.; Doroghazi, J.R.; Labeda, D.P.; Metcalf, W.W.; Kelleher, N.L. A proteomic survey of nonribosomal peptide and polyketide biosynthesis in Actinobacteria. *J. Proteome Res.* **2012**, *11*, 85–94.
34. Plahn, O.; Baschek, B.; Badewien, T.H.; Walter, M.; Rhein, M. Importance of the Gulf of Aqaba for the formation of bottom water in the Red Sea. *J. Geophys. Res. Ocean.* **2002**, *107*, 22/1–22/18.
35. Ilan, M.; Gugel, J.; van Soest, R.W.M. Taxonomy, reproduction and ecology of new and known Red Sea sponges. *Sarsia* **2004**, *89*, 388–410.
36. Ngugi, D.K.; Antunes, A.; Brune, A.; Stingl, U. Biogeography of pelagic bacterioplankton across an antagonistic temperature-salinity gradient in the Red Sea. *Mol. Ecol.* **2012**, *21*, 388–405.
37. Radwan, M.; Hanora, A.; Zan, J.; Mohamed, N.M.; Abo-Elmatty, D.M.; Abou-El-Ela, S.H.; Hill, R.T. Bacterial community analyses of two Red Sea sponges. *Mar. Biotechnol.* **2010**, *12*, 350–360.
38. Vicente, J.; Stewart, A.; Song, B.; Hill, R.; Wright, J. Biodiversity of actinomycetes associated with Caribbean sponges and their potential for natural product discovery. *Mar. Biotechnol.* (*N. Y.*) **2013**, *15*, 413–424.
39. Montalvo, N.F.; Mohamed, N.M.; Enticknap, J.J.; Hill, R.T. Novel actinobacteria from marine sponges. *Antonie Van Leeuwenhoek* **2005**, *87*, 29–36.
40. Xin, Y.; Wu, P.; Deng, M.; Zhang, W. Phylogenetic diversity of the culturable rare actinomycetes in marine sponge *Hymeniacidon perlevis* by improved isolation media. *Wei Sheng Wu Xue Bao* **2009**, *49*, 859–866.
41. Abdelmohsen, U.R.; Bayer, K.; Hentschel, U. Diversity, abundance and natural products of marine sponge-associated actinomycetes. *Nat. Prod. Rep.* **2014**, *31*, 381–399.
42. Webster, N.S.; Wilson, K.J.; Blackall, L.L.; Hill, R.T. Phylogenetic diversity of bacteria associated with the marine sponge *Rhopaloeides odorabile*. *Appl. Environ. Microbiol.* **2001**, 67, 434–444.

43. Mincer, T.J.; Fenical, W.; Jensen, P.R. Culture-dependent and culture-independent diversity within the obligate marine actinomycete genus *Salinispora*. *Appl. Environ. Microbiol.* **2005**, *71*, 7019–7028.
44. Prieto-Davo, A.; Villarreal-Gomez, L.J.; Forschner-Dancause, S.; Bull, A.T.; Stach, J.E.; Smith, D.C.; Rowley, D.C.; Jensen, P.R. Targeted search for actinomycetes from near-shore and deep-sea marine sediments. *FEMS Microbiol. Ecol.* **2013**, *84*, 510–518.
45. Asolkar, R.N.; Kirkland, T.N.; Jensen, P.R.; Fenical, W. Arenimycin, an antibiotic effective against rifampin- and methicillin-resistant *Staphylococcus aureus* from the marine actinomycete *Salinispora arenicola*. *J. Antibiot. (Tokyo)* **2010**, *63*, 37–39.
46. Hodges, T.W.; Slattery, M.; Olson, J.B. Unique actinomycetes from marine caves and coral reef sediments provide novel PKS and NRPS biosynthetic gene clusters. *Mar. Biotechnol.* **2012**, *14*, 270–280.
47. Schneemann, I.; Nagel, K.; Kajahn, I.; Labes, A.; Wiese, J.; Imhoff, J.F. Comprehensive investigation of marine actinobacteria associated with the sponge *Halichondria panicea*. *Appl. Environ. Microbiol.* **2010**, *76*, 3702–3714.
48. Bultel-Ponce, V.V.; Debitus, C.; Berge, J.P.; Cerceau, C.; Guyot, M. Metabolites from the sponge-associated bacterium *Micrococcus luteus*. *J. Mar. Biotechnol.* **1998**, *6*, 233–236.
49. Palomo, S.; Gonzalez, I.; de la Cruz, M.; Martin, J.; Tormo, J.R.; Anderson, M.; Hill, R.T.; Vicente, F.; Reyes, F.; Genilloud, O. Sponge-derived *Kocuria* and *Micrococcus* spp. as sources of the new thiazolyl peptide antibiotic kocurin. *Mar. Drugs* **2013**, *11*, 1071–1086.
50. Forner, D.; Berrue, F.; Correa, H.; Duncan, K.; Kerr, R.G. Chemical dereplication of marine actinomycetes by liquid chromatography-high resolution mass spectrometry profiling and statistical analysis. *Anal. Chim. Acta* **2013**, *805*, 70–79.
51. Chauhan, D.; Catley, L.; Li, G.; Podar, K.; Hideshima, T.; Velankar, M.; Mitsiades, C.; Mitsiades, N.; Yasui, H.; Letai, A.; *et al.* A novel orally active proteasome inhibitor induces apoptosis in multiple myeloma cells with mechanisms distinct from Bortezomib. *Cancer Cell* **2005**, *8*, 407–419.
52. Kim, T.K.; Hewavitharana, A.K.; Shaw, P.N.; Fuerst, J.A. Discovery of a new source of rifamycin antibiotics in marine sponge actinobacteria by phylogenetic prediction. *Appl. Environ. Microbiol.* **2006**, *72*, 2118–2125.
53. Jensen, P.R.; Williams, P.G.; Oh, D.C.; Zeigler, L.; Fenical, W. Species-specific secondary metabolite production in marine actinomycetes of the genus *Salinispora*. *Appl. Environ. Microbiol.* **2007**, *73*, 1146–1152.
54. Williams, P.G.; Asolkar, R.N.; Kondratyuk, T.; Pezzuto, J.M.; Jensen, P.R.; Fenical, W. Saliniketals A and B, bicyclic polyketides from the marine actinomycete *Salinispora arenicola*. *J. Nat. Prod.* **2007**, *70*, 83–88.
55. Oh, D.C.; Gontang, E.A.; Kauffman, C.A.; Jensen, P.R.; Fenical, W. Salinipyrones and pacificanones, mixed-precursor polyketides from the marine actinomycete *Salinispora pacifica*. *J. Nat. Prod.* **2008**, *71*, 570–575.

56. May, F.J.; Davis, C.T.; Tesh, R.B.; Barrett, A.D. Phylogeography of West Nile virus: From the cradle of evolution in Africa to Eurasia, Australia, and the Americas. *J. Virol.* **2011**, *85*, 2964–2974.
57. De Filette, M.; Soehle, S.; Ulbert, S.; Richner, J.; Diamond, M.S.; Sinigaglia, A.; Barzon, L.; Roels, S.; Lisziewicz, J.; Lorincz, O.; Sanders, N.N. Vaccination of mice using the West Nile Virus E-Protein in a DNA prime-protein boost strategy stimulates cell-mediated immunity and protects mice against a lethal challenge. *PLoS One* **2014**, *9*, e87837.
58. Samanta, S.; Cui, T.; Lam, Y. Discovery, synthesis, and *in vitro in vitro* evaluation of West Nile virus protease inhibitors based on the 9,10-dihydro-3H,4aH-1,3,9,10a-tetraazaphenanthren-4-one scaffold. *ChemMedChem* **2012**, *7*, 1210–1216.
59. Bode, H.B.; Bethe, B.; Hofs, R.; Zeeck, A. Big effects from small changes: Possible ways to explore nature's chemical diversity. *ChemBioChem* **2002**, *3*, 619–627.
60. Abdelmohsen, U.R.; Zhang, G.L.; Philippe, A.; Schmitz, W.; Pimentel-Elardo, S.M.; Hertlein-Amslinger, B.; Hentschel, U.; Bringmann, G. Cyclodysidins A–D, cyclic lipopeptides from the marine sponge-derived *Streptomyces* strain RV15. *Tetrahedron Lett.* **2012**, *53*, 23–29.
61. Ashelford, K.E.; Chuzhanova, N.A.; Fry, J.C.; Jones, A.J.; Weightman, A.J. At least 1 in 20 16S rRNA sequence records currently held in public repositories is estimated to contain substantial anomalies. *Appl. Environ. Microbiol.* **2005**, *71*, 7724–7736.
62. Wang, Q.; Garrity, G.M.; Tiedje, J.M.; Cole, J.R. Naive Bayesian classifier for rapid assignment of rRNA sequences into the new bacterial taxonomy. *Appl. Environ. Microbiol.* **2007**, *73*, 5261–5267.
63. Pruesse, E.; Peplies, J.; Glockner, F.O. SINA: Accurate high-throughput multiple sequence alignment of ribosomal RNA genes. *Bioinformatics* **2012**, *28*, 1823–1829.
64. Capella-Gutierrez, S.; Silla-Martinez, J.M.; Gabaldon, T. trimAl: A tool for automated alignment trimming in large-scale phylogenetic analyses. *Bioinformatics* **2009**, 25, 1972–1973.
65. Keane, T.M.; Creevey, C.J.; Pentony, M.M.; Naughton, T.J.; McLnerney, J.O. Assessment of methods for amino acid matrix selection and their use on empirical data shows that ad hoc assumptions for choice of matrix are not justified. *BMC Evol. Biol.* **2006**, *6*, 29.
66. Stamatakis, A. RAxML-VI-HPC: Maximum likelihood-based phylogenetic analyses with thousands of taxa and mixed models. *Bioinformatics* **2006**, *22*, 2688–2690.
67. Stover, B.C.; Muller, K.F. TreeGraph 2: Combining and visualizing evidence from different phylogenetic analyses. *BMC Bioinform.* **2010**, *11*, 7.
68. Ayuso-Sacido, A. Genilloud, O. New PCR primers for the screening of NRPS and PKS-I systems in actinomycetes: Detection and distribution of these biosynthetic gene sequences in major taxonomic groups. *Microb. Ecol.* **2005**, *49*, 10–24.
69. Ayuso, A.; Clark, D.; Gonzalez, I.; Salazar, O.; Anderson, A.; Genilloud, O. A novel actinomycete strain de-replication approach based on the diversity of polyketide synthase and nonribosomal peptide synthetase biosynthetic pathways. *Appl. Microbiol. Biotechnol.* **2005**, *67*, 795–806.

70. Huber, W.; Koella, J.C. A comparison of three methods of estimating EC_{50} in studies of drug resistance of malaria parasites. *Acta Trop.* **1993**, *55*, 257–261.
71. Ponte-Sucre, A.; Vicik, R.; Schultheis, M.; Schirmeister, T.; Moll, H. Aziridine-2,3-dicarboxylates, peptidomimetic cysteine protease inhibitors with antileishmanial activity. *Antimicrob. Agents Chemother.* **2006**, *50*, 2439–2447.

Marine Compound Catunaregin Inhibits Angiogenesis through the Modulation of Phosphorylation of Akt and eNOS *in vivo* and *in vitro*

Jun-Xiu Liu, Min-Qi Luo, Meng Xia, Qi Wu, Si-Mei Long, Yaohua Hu, Guang-Chun Gao, Xiao-Li Yao, Mian He, Huanxing Su, Xiong-Ming Luo and Shu-Zhong Yao

Abstract: Angiogenesis is the formation of blood vessels from pre-existing vasculature. Excessive or uncontrolled angiogenesis is a major contributor to many pathological conditions whereas inhibition of aberrant angiogenesis is beneficial to patients with pathological angiogenesis. Catunaregin is a core of novel marine compound isolated from mangrove associate. The potential anti-angiogenesis of catunaregin was investigated in human umbilical vein endothelial cells (HUVECs) and zebrafish. HUVECs were treated with different concentrations of catunaregin in the presence or absence of VEGF. The angiogenic phenotypes including cell invasion cell migration and tube formation were evaluated following catunaregin treatment in HUVECs. The possible involvement of AKT, eNOS and ERK1/2 in catunaregin-induced anti-angiogenesis was explored using Western blotting. The anti-angiogenesis of catunaregin was further tested in the zebrafish embryo neovascularization and caudal fin regeneration assays. We found that catunaregin dose-dependently inhibited angiogenesis in both HUVECs and zebrafish embryo neovascularization and zebrafish caudal fin regeneration assays. In addition, catunaregin significantly decreased the phosphorylation of Akt and eNOS, but not the phosphorylation of ERK1/2. The present work demonstrates that catunaregin exerts the anti-angiogenic activity at least in part through the regulation of the Akt and eNOS signaling pathways.

Reprinted from *Mar. Drugs*. Cite as: Liu, J.-X.; Luo, M.-Q.; Xia, M.; Wu, Q.; Long, S.-M.; Hu, Y.; Gao, G.-C.; Yao, X.-L.; He, M.; Su, H.; *et al*. Marine Compound Catunaregin Inhibits Angiogenesis through the Modulation of Phosphorylation of Akt and eNOS *in vivo* and *in vitro*. *Mar. Drugs* **2014**, *12*, 2790–2801.

1. Introduction

Angiogenesis is the formation of blood vessels from pre-existing vasculature. The process of angiogenesis is very complex and tightly controlled under physiological conditions. Excessive or uncontrolled angiogenesis is associated with various pathological conditions including cancer, diabetic retinopathy, and rheumatoid arthritis [1]. Thus, development of novel anti-angiogenesis could greatly benefit human health. For example, cancer is one of the most devastating diseases, and can be a great burden on modern society, while anti-angiogenic therapy is becoming a powerful treatment approach in cancer therapy.

Traditionally, great efforts have been placed on developing drugs that attack and kill cancer cells. During past years, chemotherapy based on cytotoxic agents has been the main treatment for most cancer patients. Although cytotoxic agents have significantly improved cancer survival, these

conventional anti-cancer drugs often cause serious side effects, chemo- and radio-resistance, disease relapse and metastases. Therefore, the alternative chemotherapeutic regimens with minimal side effects are currently the priority consideration for the development of cancer treatment. Angiogenesis plays a critical role in the progression of cancer. Through stimulating blood vessel growth from nearby pre-existing capillaries, tumors achieve sufficient blood supply for cancer cell progression and metastasis [2]. It has been shown that increased angiogenesis is associated with poor prognosis and relapse of cancer whereas blocking the formation of new blood vessels prevents the growth of cancer. Thus, the development of inhibitors of angiogenesis is increasingly receiving attention in the field of cancer. In the U.S., there are currently thirteen approved anti-angiogenesis therapies in oncology. However, as current anti-angiogenesis therapy is still in the infant stage of the drug development, there are lots of limitations of anti-angiogenesis therapy such as low efficacy, and development of resistance during the long term use of these therapeutic agents. Therefore, intensive efforts are needed to develop novel anti-angiogenic agents, especially small molecule targeting the tumor vasculature [3].

Vascular endothelial growth factor (VEGF) is a very important stimulator for tumor angiogenesis. VEGF is regarded as the prognostic indicator in cancers because of its significant association with tumor size and progress in several cancers. Thus, VEGF signaling pathway is an attractive target for the development of anti-angiogenesis inhibitors.

The marine environment is a rich source of novel and unusual secondary metabolites for drug discovery. Catunaregin was first isolated from the stem bark of *catunaregam spinosa*, a Chinese mangrove associate and the extraction and isolation of catunaregin was described in the literature [4]. Our previous study demonstrated that catunaregin may have anti-cancer property. In this study, we investigated the potential inhibitory action of catunaregin on angiogenesis in human umbilical vein endothelial cells (HUVECs) and transgenic zebrafish (Danio rerio; fli1:EGFP). We further explored the mechanism by which catunaregin inhibited angiogenesis in HUVECs. We found that catunaregin exerted anti-angiogenic activity in both HUVECs and zebrafish. In addition, catunaregin significantly reduced the phosphorylation of Akt and eNOS and the inhibition was in parallel to its anti-angiogenic effect, suggesting that catunaregin inhibited angiogenesis possibly through the modulation of the Akt and eNOS signaling pathways. Since angiogenesis plays an important pathological role in the progress of a wide range of diseases, our findings provide a rationale for future development of this compound as a potential drug or chemopreventive supplement to target diseases with excessive angiogenesis.

2. Results and Discussion

2.1. The Isolation and Preparation of Catunaregin

Catunaregin was first isolated from the stem bark of *Catunaregam spinosa*, a Chinese mangrove associate and the extraction and isolation of catunaregin was described in the experimental part of the literature [4]. In continuation of our studies on the chemical diversity of mangrove plants in Hainan Island, the plant *Micromelum falcatum* (Lour.) Tan was investigated, and the novel norneolignan, catunaregin was isolated again from this plant. The air-dried material *Micromelum falcatum* (Lour.)

Tan (10.0 kg), which was collected in Wenchang, Hainan Province, was extracted with 95% EtOH three times. The aq. residue was subjected to extraction with *n*-hexane and EtOAc (each 3×). The EtOAc extract (102 g) was separated on silica gel (1300 g, 200–300 mesh) with solvents of increasing polarity: 10%–70% acetone in n-hexane and gained 20 fractions. Fr.3 (1.1 g, eluted with *n*-hexane–acetone 7:3) was fractionated on silica gel with chloroform–acetone (19:1), then purified by Semi-preparation HPLC (250 × 10 mm i.d. 5 μm, MeOH/H_2O, 60:40) to 12.0 mg of catunaregin (Chart 1).

Chart 1. Chemical structure of catunaregin.

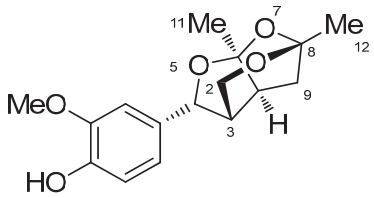

2.2. Inhibitory Effect of Catunaregin on VEGF-induced HUVEC Invasion, Migration, and Tube Formation

Angiogenesis is the process of forming blood vessels from preexisting vessels. In response to VEGF, endothelial cells migrate into the surrounding extracellular matrix where they form blood capillaries, and thus, cell migration is a crucial step in angiogenesis and invasion. In this study, the anti-angiogenesis of catunaregin was first examined using the wound-healing method. Wound-healing assays was performed on HUVECs treated with catunaregin at concentrations of 10, 50, and 100 μM. As shown in Figure 1, treatment of HUVECs with catunaregin at these concentrations significantly prevented cell migration. The percentage decreases were 6.7%, 16.6% and 65.4% at 100 ng/mL VEGF plus catunaregin at 10, 50, and 100 μM, respectively. To further assess the anti-angiogenesis of catunaregin, a transwell invasion assay, the most popular *in vitro* test of angiogenesis [5]. During this assay, cells were seeded onto the upper surface of an 8 mm pore size membrane separating upper and lower chambers. The upper chamber contained catunaregin in 0.1% endothelial basal medium (EBM), and cellular invasion through the membrane was induced when VEGF was present in the lower chamber. The invasion assay showed that catunaregin significantly reduced VEGF-induced invasion of HUVECs. The percentage decrease were 6.4%, 16% and 61.3% at 100 ng/mL VEGF plus catunaregin at 10, 50 and 100 μM, respectively (Figure 2). The anti-angiogenesis of catunaregin was further examined using tube formation assay. In the tube formation assay, HUVECs were seeded on VEGF-reduced two-dimensional Matrigel. Consistent with previous reports, robust tubular structures were formed in the presence of VEGF whereas preincubation with catunaregin markedly and dose-dependently abolished VEGF-induced tube formation (Figure 3).

Figure 1. Anti-angiogenic effect of catunaregin in migration of human umbilical vein endothelial cells (HUVECs). Representative fluorescence microscopy images. The bar chart shows quantitative data for HUVECs migration with different treatments (* VEGF *vs.* catunaregin plus VEGF, $p < 0.01$).

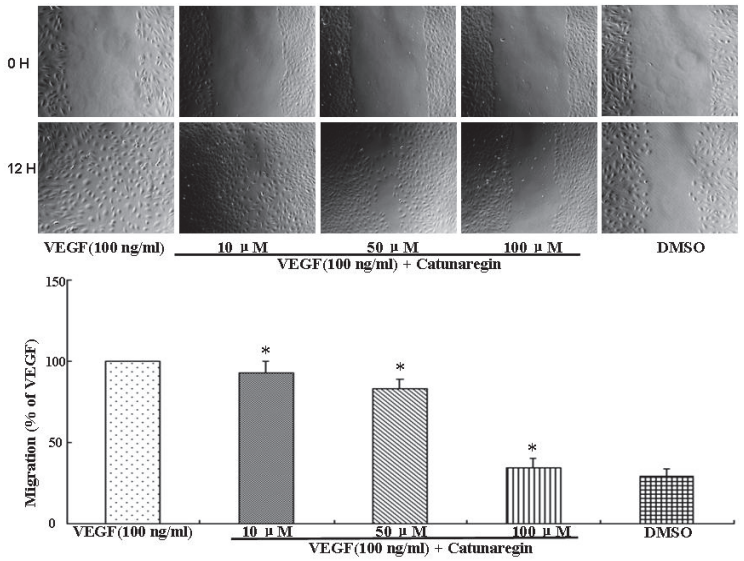

Figure 2. Anti-angiogenic effect of catunaregin in invasion of HUVECs. Representative fluorescence microscopy images. The bar chart shows quantitative data for HUVECs invasion with different treatments (* VEGF *vs.* catunaregin plus VEGF, $p < 0.01$).

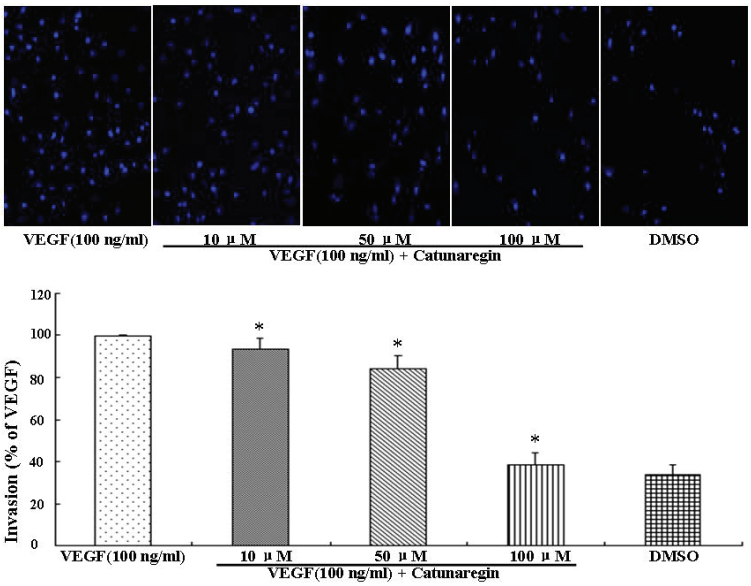

Figure 3. Anti-angiogenic effect of catunaregin in tube formation of HUVECs. Representative fluorescence microscopy images. The bar chart shows quantitative data for HUVECs tube formation with different treatments. (* VEGF *vs.* catunaregin plus VEGF, $p < 0.05$; # VEGF *vs.* catunaregin plus VEGF, $p < 0.01$).

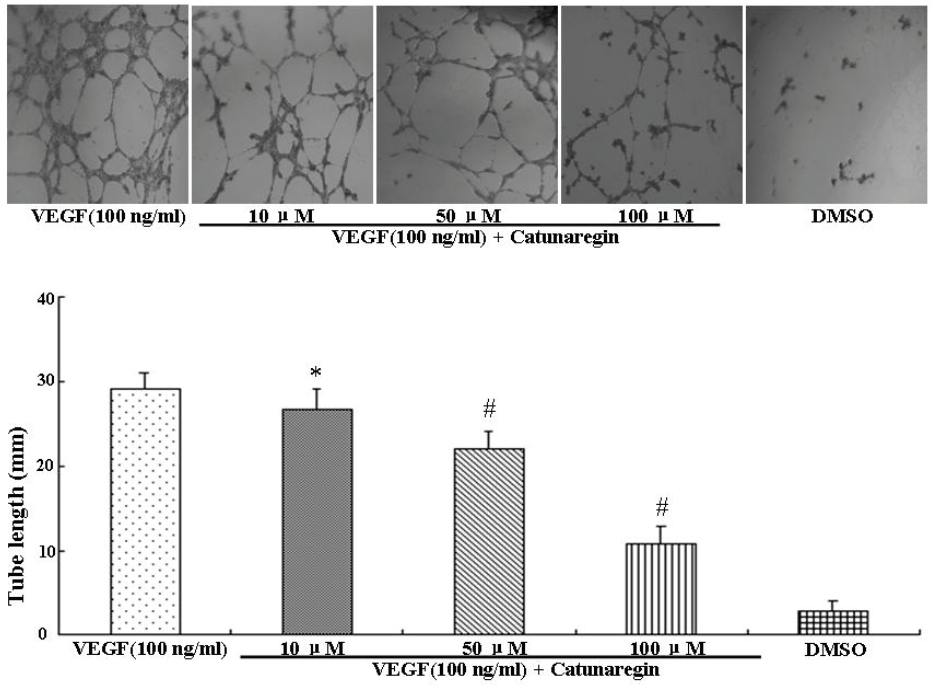

2.3. Catunaregin Inhibited Angiogenesis through Modulation of AKT and eNOS Signaling Pathways

Activation of Akt/eNOS and phosphorylation of ERK 1/2 are two most important mediators in VEGF-induced angiogenesis. To elucidate the mechanisms that underlie the anti-angiogenic effect of catunaregin, we examined these two signaling pathways using Western blotting. As shown in Figure 4, catunaregin significantly and concentration-dependently suppressed the VEGF-triggered phosphorylations of AKT (Ser473) and eNOS (Ser1172), whereas only mildly inhibited VEGF-induced phosphorylation of ERK 1/2 in HUVECs. Therefore, we believe that catunaregin inhibits angiogenesis possibly by modulating the AKT and eNOS signaling pathways.

Figure 4. Catunaregin decreases phosphorylation of AKT and eNOS expression in HUVECs. Catunaregin significantly and concentration-dependently suppressed the VEGF-triggered phosphorylations of AKT and eNOS, whereas only mildly inhibited VEGF-induced phosphorylation of ERK 1/2 in HUVECs (* VEGF *vs.* catunaregin plus VEGF, $p < 0.01$).

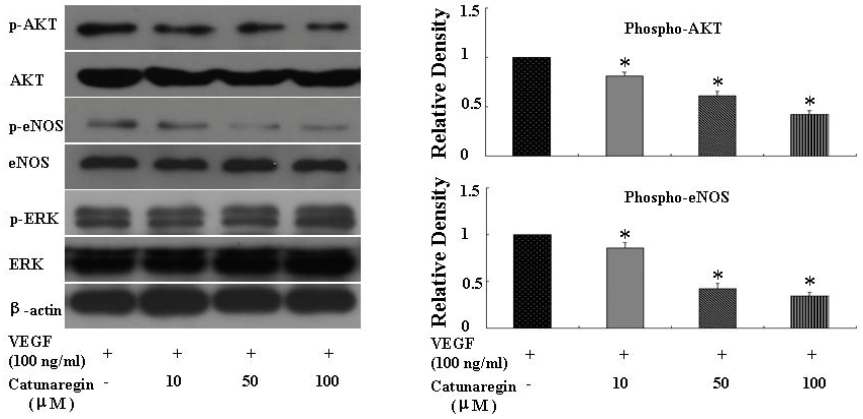

2.4. Catunaregin Inhibited Angiogenesis in Zebrafish Embryo and Caudal Fin Regeneration Assays

To test whether the results obtained from *in vitro* studies is reproducible *in vivo*, we examined the anti-angiogenesis of catunaregin in zebrafish embryo and caudal fin regeneration assays in transgenic TG (fli1:EGFP) zebrafish. In these transgenic animals, enhanced EGFP are expressed in all endothelial cells which allow observation of bright blood vessels at all stages of embryogenesis. We first examined the anti-angiogenesis of catunaregin on the development of caudal intersegmental vessels at late tail bud stages of TG (fli1:EGFP) transgenic zebrafish embryos. In agreement with the results obtained from *in vitro* experiments, catunaregin significantly reduced the number of caudal intersegmental vessels in a dose-dependent manner. We further tested the specificity of anti-angiogenesis of catunaregin in zebrafish caudal fin regeneration assay because this assay can separate regenerative angiogenesis from tissue regrowth [6]. In caudal fin regeneration experiments, zebrafish caudal fins were amputated at mid-fin level, and then allowed to recover. Amputated blood vessels healed their ends by one day post amputation (dpa) and then reconnect arteries and veins via anastomosis, to resume blood flow at wound sites by 2 dpa. By 3 dpa, networks of endothelial cells in the regenerated tissue formed a vascular plexus that extended to the fin tip. When 100 μM catunaregin was added to water, new vessel formation was prevented and fin regeneration was arrested as evidenced by the absence of fin blastema. Although angiogenesis is essential for the regeneration of a complete fin, we found that limited fin tissue could still be formed in the absence of new blood vessels. Within the new formed tissue, skin and pigment cells appeared intact by visual inspection, indicating that catunaregin may specifically inhibited regenerative angiogenesis (Figure 5).

Figure 5. Inhibition of the zebrafish neovascularization by catunaregin. (**A**) Live fluorescent zebrafish embryo assay. Transgenic TG (fli1:EGFP) zebrafish embryos, which show green fluorescent protein (GFP) expression in endothelial cells, were incubated for 72 h without or with 100 μM catunaregin. (**B**) Caudal fin regrowth is limited by angiogenesis. The same fins are shown in bright field (top panels) and with the corresponding endothelial-eGFP signal (bottom panels). Zebrafish tail fins were clipped, then allowed to recover normally or treated with catunaregin as indicated. (**C**) Quantitative comparison of vessel and fin regeneration in control and catunaregin-treated fish. Black bars, nonvascularized fin tissue; white bars, vascularized tissue. Average values are plotted for fin and vessel growth (n = 15) (* catunaregin *vs.* control, $p < 0.01$).

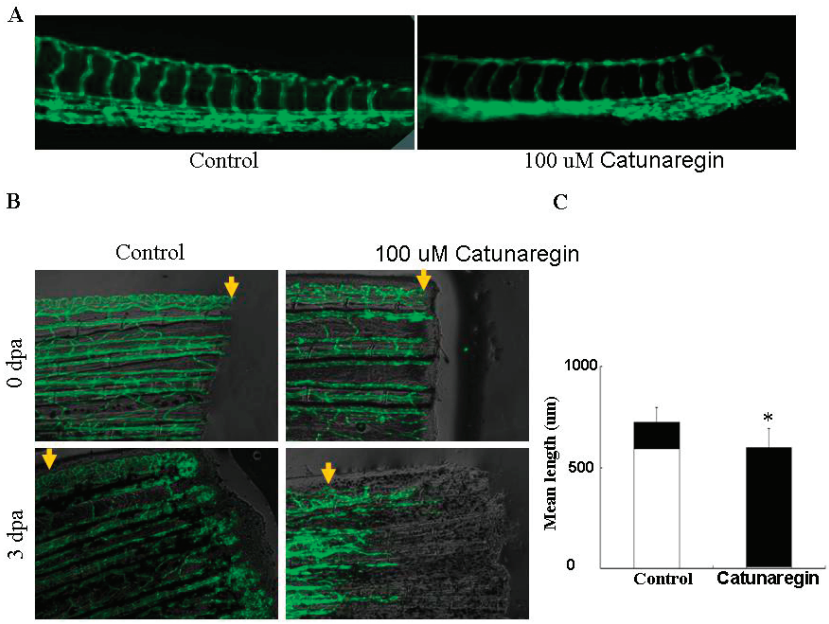

3. Experimental Section

3.1. Preparation of Catunaregin

Reagents and solvents were commercial quality and used without further purification, except for re-purified methanol used in HPLC system. NMR spectra were recorded on Bruker DRX-500 spectrometer (Bruker, Bremen, Germany) with SiMe4 (Cambridge Isctope Laboratories, Tewksbury, MA, USA) as internal standard. HRESI-MS was recorded on VG Auto Spec-3000 MS spectrometer (Bruker, Bremen, Germany). Thin layer chromatography (TLC) was carried out on precoated silica gel G plates (Qingdao Haiyang Chemical Plant, Qingdao, China) and spots were visualized by spraying the plates with 50% H_2SO_4 solution, followed by heating. Semi-preparative RP-HPLC was carried out on ODS columns (YMC-Pack ODS-5-A, 250 × 10 mm, 5 μm, YMC, Kyoto, Japan) with the CH_3OH–H_2O solvent system as eluents. Waters 600 HPLC system (Waters, Voorhees, NJ, USA)

was equipped with a Waters 996 photodiode array detector (Waters, Voorhees, NJ, USA) to check the fraction and purity of target compound.

3.2. The Isolation of Catunaregin

Catunaregin was isolated and purified by CAS Key Laboratory of Tropical Marine Bio-resources and Ecology, South China Sea Institute of Oceanology, Chinese Academy of Sciences, Guangzhou, China. The purity of the compound was >98%. Catunaregin was dissolved in dimethyl sufoxide (DMSO) and stored at −20 °C until use. The solution form of catunaregin was then diluted by PBS to the concentration needed. All reagents were purchased from Sigma (Sigma, Shanghai, China) unless otherwise stated.

3.3. Preparation of Reagents and Cell Culture

Human umbilical vein endothelial cells (HUVECs) were obtained from Sciencell, Carlsbad, NM, USA. HUVECs (Passages 4 to 7) were cultured at 37 °C in M199 media (Invitrogen, Carlsbad, NM, USA) supplemented with 10% FBS. Cells were maintained in a humidified atmosphere of 5% CO_2. The anti-angiogenic effect of catunaregin on HUVECs was evaluated using a stock solution of catunaregin (1 mg/mL) prepared in PBS containing 10% DMSO (GIBCO, Langley, VA, USA). The anti-angiogenic effect on zebrafish was evaluated using a stock solution of catunaregin (1 mg/mL) prepared in sterilized Milli-Q water containing 0.5% DMSO. Vascular endothelial growth factor (VEGF) was obtained from Sigma, St. Louis, MO, USA and prepared as a stock solution of 100 μg/mL in sterilized Milli-Q water.

3.4. Cell Invasion, Migration and Tube Formation

HUVEC migration assay was performed using the wound healing method as previously described [7,8]. The HUVECs (3×10^5 cells) were seeded into each well of a 24-well plate and incubated with complete medium at 37 °C and 5% CO_2. After 24 h of incubation, cells were starved for additional 24 h by low serum (0.5% FBS) medium. The HUVECs were then scraped away horizontally in each well using a P100 pipette tip (Axygen, Union city, CA, USA). Three randomly selected views along the scraped line were photographed on each well using a fluorescent inverted microscope (Olympus, Tokyo, Japan) and the CCD camera (Olympus, Tokyo, Japan) attached to the microscope at 50× magnification. The medium was then changed to fresh low serum (1% FBS) medium containing DMSO with or without vascular endothelial growth factor (VEGF; 100 ng/mL) and the indicated concentration of the compound of catunaregin. The final concentration of DMSO was 0.1% in all experimental groups. After 12 h of incubation, another set of images were taken by the same method. Image analysis for signs of migration was performed by Metamorph Imaging Series (Molecular Devices, Tokyo, Japan). The average scraped area of each well under each condition was measured and subtracted from that of the before-treatment condition. Data are expressed as percentage wound closure relative to the wound closure area in the control medium. The wound closure area of the control cells was set at 100%.

HUVEC invasion was investigated as described [5,9]. Briefly, the effect of catunaregin on HUVEC invasion was measured using the 10 mm tissue culture insert (transwell) with polycarbonate membrane (8 mm pores) and 24-well companion plate. The upper side and lower side of the membrane were pre-coated with 1:30 (v/v) and 1:100 (v/v) of Matrigel, respectively. The HUVECs were resuspended in low serum (1% FBS) medium and seeded onto the culture inserts at 5×10^4 cells per insert in triplicate. They were then deposited into the 24-well companion plate with 500 μL of low serum (1% FBS) medium containing DMSO with or without vascular endothelial growth factor (VEGF; 100 ng/mL) and the indicated concentration of the compound of catunaregin. The final concentration of DMSO was 0.1% in all experimental groups. The inserts were removed after 8 h of incubation and were then washed with PBS. Non-invasive cells on the upper surface of the membrane were removed by wiping with cotton swabs. The inserts were fixed in paraformaldehyde, stained with DAPI and mounted on microscope slides. Images of the invasive cells were captured at 100× magnification using a fluorescent inverted microscope and a CCD camera. Following this, HUVEC invasion was quantified by counting the number of cells per insert with the software Metamorph Imaging Series (Molecular Devices, Tokyo, Japan).

Endothelial tube formation was assessed in 24-well plates using growth factor-reduced Matrigel™ as described previously [10,11]. Briefly, growth factor-reduced Matrigel (250 μL) was pipetted onto 24-well culture plates and polymerized for 30 min at 37 °C. HUVECs were seeded on Matrigel-coated plates at a density of 5×10^4 in low serum (1% FBS) medium containing DMSO with or without vascular endothelial growth factor (VEGF; 100 ng/mL) and the indicated concentration of the compound of catunaregin. The final concentration of DMSO was 0.1% in all experimental groups, then incubated at 37 °C for 8 h. The network-like structures were examined under an inverted microscope (at 50× magnification). Tube-like structures were defined as endothelial cord formations that were connected at both ends. The tube length was quantified using the software NIH Image (NIH, Bethesda, MD, USA) as reported earlier [10,11].

3.5. Western Immunoblot Analysis

HUVECs were plated in 60-mm dishes (16,700 cells per centimeter square) and cultured for 2 days. The culture medium was then replaced with fresh medium containing 2% FBS, and the cells were treated with indicated concentration of the compound of catunaregin for 24 h. Whole-cell protein extracts (20 μg) were separated on 10%–12.5% sodium dodecylsulfate polyacrylamide gels, and transferred to nitrocellulose membranes (Amersham, Pittsburgh, PA, USA). The blotted membranes were incubated with antibodies against Akt, phosphorylated Akt (Ser473), endothelial nitric oxide synthase (eNOS), phosphorylated eNOS (Ser1177) and β-actin. Densitometrical results were calculated by NIH image software. The primary antibodies used were antiphospho-ERK1/2 (Cell Signaling Technology, Danvers, MA, USA), antibody to total ERK1/2 (Cell Signaling), anti-eNOS (Santa Cruz Biotechnology, Santa Cruz, CA, USA), anti-phosphorylation of eNOS at S1177 (P-eNOS S1177) (Cell Signaling), anti-phospho-Akt (Cell Signaling), anti-Akt (Cell Signaling), and anti-β-actin (Biosynthesis Biotechnology, Beijing, China).

3.6. Zebrafish Embryo Assay

The transgenic zebrafish cell line TG (fli1:EGFP), in which endothelial cells expressed eGFP, was kindly provided by ZFIN (Eugene, OR, USA) and maintained as described [11,12]. Zebrafish embryos were generated by natural pair-wise mating of fish that were between 3 and 12 months old. Embryos were collected as described. Healthy embryos were harvested at the 1–4 cell stage, plated in a 96-well microplate and incubated with 100 μL of the indicated concentrations of the tested compounds at 28 °C for 24 h. DMSO was used as both carrier of drugs and control. After incubation, fish embryos were anesthetized with tricaine (0.02%), placed on slides and examined under an OLYMPUS IX71 fluorescence inverted microscope (Olympus, Tokyo, Japan). Phenotypic changes were evaluated by two different observers.

3.7. Zebrafish Caudal Fin Regeneration Assay

Adult TG (Fli-EGFP) transgenic fishes were anesthetized with tricaine (0.02%), and their caudal fin was partially amputated. Then, fishes were maintained for 3 days at 28 °C in 100 μL water containing the indicated concentration of the compound. After three days, fishes were anesthetized and examined and photographed under an OLYMPUS IX71 fluorescence inverted microscope.

3.8. Statistical Analysis

All data were presented as mean ± SEM. Differences among test groups were analyzed by ANOVA, using Newman-Keuls multiple comparison test (Prism 4.0, GraphPad Software, Inc., San Diego, CA, USA). A p value < 0.05 was considered statistically significant.

4. Conclusions

This is the first study concerning the anti-angiogenic action of catunaregin. Our experimental results demonstrated that the catunaregin could significantly inhibit VEGF-induced different angiogenic phenotypes of HUVECs *in vitro* and the vessel formation in transgenic zebrafish. To further investigate the underlying mechanisms behind the anti-angiogenic property of catunaregin, we examined angiogenesis-related signaling pathways in HUVECs. Our results demonstrated that catunaregin inhibited the phosphorylation of Akt and eNOS in HUVECs, indicating a new mode of biological activity for catunaregin. Interestingly, catunaregin inhibited regenerative angiogenesis without severely affecting tissue regrowth. Thus, catunaregin may primarily inhibit the formation of new blood vessels through blockade of angiogenic process of endothelial cells. Given the critical role of Akt and eNOS signaling pathways in tumorigenesis and tumor metastasis, our results provide an impetus for further investigation and development of catunaregin as a novel anti-angiogenesis candidate for the treatment of diseases with increased angiogenesis.

Catunaregin is a novel norneolignan with a unique O-bridged furopyran ring. It can produce hemiacetal compound when 7-position is cleaved via hydrolysis. Moreover, hemiacetal compound can be open loop at 1-position and 5-position through acetal hydrolysis, thereby affording diketone

intermediate. Thus, unsubstituted hydroxyl group or easily activating hydroxyl group like hemiacetal at 6-position and 8-position of compound may be important for its anti-angiogenic action.

Acknowledgments

Grants from the National Key Clinical Department, National Key Discipline and Guangdong Key Laboratory for Diagnosis and Treatment of Major Neurological Diseases. This study was supported by National Natural Science Foundation of China (No. 81371255, 81100936), Doctoral Program of Higher Education of China (No. 20110171110058), the Young Scientists Fund of the National Natural Science. Foundation of China (No. 41006091), Guangdong Technological grant (No. 2010B050700024, 2011B050400031, 2012B031800107), the Natural Science Foundation of Guangdong Province (No. S2011010004860), Sun Yat-sen University 5010 Clinical Research Program (No. 2007010). This study was also supported by multi-year research grant, university of Macau, MYRG122 (Y1-L3)-ICMS12-SHX.

Author Contributions

Conceived and designed the experiments: JX L, XM L, SZ Y; Performed the experiments: JX L, SZ Y, MQ L, M X, Q W, SM L, Y H, GC G, XL Y, M H, H S; Analyzed the data: JX L, SZ Y, M X; Wrote the paper: JX L, SZ Y, XM L, H S.

Conflicts of Interest

The authors declare no conflict of interest.

References

1. Munoz-Chapuli, R.; Quesada, A.; Angel Medina, M. Angiogenesis and signal transduction in endothelial cells. *Cell. Mol. Life. Sci*. **2004**, *61*, 2224–2243.
2. Folkman, J. Tumor angiogenesis: Therapeutic implications. *N. Eng. J. Med*. **1971**, *285*, 1182–1186.
3. Jeong, S.; Koh, W.; Lee, E.; Lee, H.; Bae, H.; Lü, J.; Kim, S. Antiangiogenic phytochemicals and medicinal herbs. *Phytother. Res*. **2011**, *25*, 1–10.
4. Gao, G.; Luo, X.; Wei, X.; Qi, S.; Yin, H.; Xiao, Z.; Zhang, S. Catunaregin and epicatunaregin, two norneolignans possessing an unprecedented skeleton from *Catunaregam spinosa*. *Helv. Chim. Acta*. **2010**, *93*, 339–344.
5. Lu, X.; Xu, Z.; Yao, X.; Su, F.; Ye, C.; Li, J.; Lin, Y.; Wang, G.; Zeng, J.; Huang, R.; *et al.* Marine cyclotripeptide X-13 promotes angiogenesis in zebrafish and human endothelial cells via PI3K/Akt/eNOS signaling pathways. *Mar. Drugs*. **2012**, *10*, 1307–1320.
6. Bayliss, P.; Bellavance, K.; Whitehead, G.; Abrams, J.; Aegerter, S.; Robbins, H.; Cowan, D.; Keating, M.; O'Reilly, T.; Wood, J.; *et al.* Chemical modulation of receptor signaling inhibits regenerative angiogenesis in adult zebrafish. *Nat. Chem. Biol*. **2006**, *2*, 265–273.

7. Lu, X.; Luo, D.; Yao, X.; Wang, G.; Liu, Z.; Li, Z.; Li, W.; Chang, F.; Wen, L.; Lee, S.; *et al.* DL-3*n*-butylphthalide promotes angiogenesis via the extracellular signal-regulated kinase 1/2 and phosphatidylinositol 3-kinase/Akt-endothelial nitric oxide synthase signaling pathways. *J. Cardiovasc. Pharmacol*. **2012**, *59*, 352–362.
8. Lam, H.W.; Lin, H.; Lao, S.; Gao, J.; Hong, S.; Leong, C.; Yue, P.; Kwan, Y.; Leung, A.; Wang, Y.; *et al.* The angiogenic effects of angelica sinensis extract on HUVEC *in vitro* and zebrafish *in vivo*. *J. Cell. Biochem*. **2008**, *103*, 195–211.
9. Raghunath, M.; Wong, Y.; Muhamma, F.; Ge, R. Pharmacologically induced angiogenesis in transgenic zebrafish. *Biochem. Biophys. Res. Commun*. **2009**, *378*, 766–771.
10. Abdel-Malak, N.; Mofarrahi, M.; Mayaki, D.; Khachigian, L.; Hussain, S. Early growth response-1 regulates angiopoietin-1-induced endothelial cell proliferation, migration, and differentiation. *Arterioscler. Thromb. Vasc. Biol*. **2009**, *29*, 209–216.
11. Lam, K.H.; Alex, D.; Lam, I.K.; Tsui, S.K.; Yang, Z.F.; Lee, S.M. Nobiletin, a polymethoxylated flavonoid from citrus, shows anti-angiogenic activity in a zebrafish *in vivo* model and HUVEC *in vitro* model. *J. Cell. Biochem*. **2011**, *112*, 3313–3321.
12. Hong, S.; Wan, J.; Zhang, Y.; Hu, G.; Lin, H.; Seto, S.; Kwan, Y.; Lin, Z.; Wang, Y.; Lee, S. Angiogenic effect of saponin extract from *Panax notoginseng* on HUVECs *in vitro* and zebrafish *in vivo*. *Phytother. Res*. **2009**, *23*, 677–686.

In Situ Detection of Antibiotic Amphotericin B Produced in *Streptomyces nodosus* Using Raman Microspectroscopy

Rimi Miyaoka, Masahito Hosokawa, Masahiro Ando, Tetsushi Mori, Hiro-o Hamaguchi and Haruko Takeyama

Abstract: The study of spatial distribution of secondary metabolites within microbial cells facilitates the screening of candidate strains from marine environments for functional metabolites and allows for the subsequent assessment of the production of metabolites, such as antibiotics. This paper demonstrates the first application of Raman microspectroscopy for *in situ* detection of the antifungal antibiotic amphotericin B (AmB) produced by actinomycetes—*Streptomyces nodosus*. Raman spectra measured from hyphae of *S. nodosus* show the specific Raman bands, caused by resonance enhancement, corresponding to the polyene chain of AmB. In addition, Raman microspectroscopy enabled us to monitor the time-dependent change of AmB production corresponding to the growth of mycelia. The Raman images of *S. nodosus* reveal the heterogeneous distribution of AmB within the mycelia and individual hyphae. Moreover, the molecular association state of AmB in the mycelia was directly identified by observed Raman spectral shifts. These findings suggest that Raman microspectroscopy could be used for *in situ* monitoring of antibiotic production directly in marine microorganisms with a method that is non-destructive and does not require labeling.

Reprinted from *Mar. Drugs*. Cite as: Miyaoka, R.; Hosokawa, M.; Ando, M.; Mori, T.; Hamaguchi, H.; Takeyama, H. *In Situ* Detection of Antibiotic Amphotericin B Produced in *Streptomyces nodosus* Using Raman Microspectroscopy. *Mar. Drugs* **2014**, *12*, 2827–2839.

1. Introduction

Various secondary metabolites, which have broad functions—antibacterial, antifungal, antiviral, antitumor, and antiprotozoal—have been isolated from different microbes found in terrestrial soils and marine sediments [1–3]. One third of the 22,500 known microbial metabolites are the secondary metabolites of actinomycetes, particularly *Streptomyces* species [4]. *Streptomyces* fermentation products are rich sources of antibiotics, such as antibacterial streptomycin (*Streptomyces griseus*) [5], kanamycin (*Streptomyces kanamyceticus*) [6], tetracycline (*Streptomyces rimosus*) [7], antifungal amphotericin B (*Streptomyces nodosus*) [8], antitumor actinomycin (*Streptomyces antibioticus*) [9], and doxorubicin (*Streptomyces peucetius)* [10].

Currently, a large variety of antibiotics are produced in microbial fermentation processes or derived by chemical modification of microbial products. Because of continued demand for their cost-effective production, rapid and efficient assessments of the fermentation product are required for the screening of microbial culture conditions. In general, the metabolite contents within microbial cells are invasively analyzed by solvent extraction-based methods. The purified microbial extracts are subsequently analyzed by GC-MS or NMR to determine their chemical formula and abundance. These processes are invasive, time-consuming, laborious, and require a

substantial amount of microbe cultures. Moreover, the conventional methods cannot provide real-time information for assessment and improvement of the fermentation parameters.

Meanwhile, chemical screening of microbial metabolites is a starting point for discovery of new drug candidates from environmental microbes. For example, marine sponges are known to harbor a massive consortium of uncultivated bacteria, which produce medically important natural products [11,12]. To explore the metabolic potential of these microbes, we have applied metagenomic and single-cell-based approaches to identify target metabolite producers [13,14]. However, because of the lack of appropriate probes that enable *in situ* identification of microbial metabolites, identification of new drug candidates is dependent on the analysis of whole sponge extracts by a solvent extraction-based method. Therefore, in conjunction with the demand for novel drugs from environmental sources and cost-effective production, a non-destructive technique for compositional analysis of microbial secondary metabolites is required.

Raman spectroscopy provides characteristic information on the molecular structure of metabolites and does not require any sample pretreatment such as dye labeling or genetic manipulation, thus allowing for rapid and low-invasive observations. Raman spectroscopy can be used to investigate biological samples—plants [15], animals [16] or human tissues [17]. Indeed, Raman spectroscopy has been utilized to quantify the level of penicillin from fermentation broths for in-line analysis [18]. Moreover, in combination with optical microscopy, Raman microspectroscopy provides high space-resolved information of human cells [19], fungi [20], or bacteria, including *Streptomyces* species [21]. Our research group has carried out time- and space-resolved Raman imaging of living yeast cells using confocal Raman microspectroscopy [22–24]. The Raman images of cells show that the distribution of lipids and proteins vary during cell division cycles. Because of these capabilities, recent reports reveal the distribution of secondary metabolites—pigment in plants [25] and green macroalgae [26]—using FT-Raman microspectroscopy. Since secondary metabolites such as antibiotics generally have diverse and distinctive chemical structures, we postulated that Raman imaging has the potential to distinguish antibiotics from other biomolecules in living cells without labeling or extraction.

Here, we report the first demonstration of Raman imaging for *in situ* detection of microbially derived antibiotics in living microbial cells. In this study, *S. nodosus*—known to produce Amphotericin B (AmB)—was analyzed as a model for antibiotic-producing actinomycetes. AmB belongs to polyene antibiotics, has a broad spectrum of activity, and has shown efficacy against candidiasis, cryptococcosis, aspergillosis, histoplasmosis, blastomycosis, coccidioidomycosis, zygomycosis, sporotrichosis, fusariosis, and phaeohyphomycosis [27]. The Raman spectra of AmB has a strong band, due to the phenomenon of resonance enhancement, at 1559 cm^{-1} that corresponds to the C=C symmetric vibration of the polyene chain [28]. The Raman intensities of this specific band correlate with the antifungal activity and the abundance of antibiotic. To evaluate antibiotic production, we applied Raman imaging of AmB to live *S. nodosus* cells. Here, we demonstrate the ability to detect and image *in situ* distribution of antibiotics within mycelia and individual hyphae with high spatial resolution using Raman microspectroscopy. This study demonstrates the capability of Raman imaging for non-destructive screening of antibiotic producers

and the potential of Raman microspectroscopy, as an in-line monitoring technique, to be a tool for use in antibiotic production from industrial scale fermentation cultures.

2. Results and Discussion

2.1. Raman Spectra of AmB Produced in S. nodosus

In this study, *in situ* detection of AmB produced within the actinomycetes *S. nodosus* was conducted using a laboratory-built confocal Raman microspectrometer. To analyze Raman spectra at single-cell resolution, the Raman microspectrometer was equipped with a 532-nm laser, an inverted microscope with a 100 × 1.4 NA lens, a spectrometer, and a charge-coupled device (CCD) detector [24]. The lateral and depth spatial resolutions of the Raman imaging system were 0.3 and 2.6 μm, respectively.

AmB is an elongated, cyclic molecule consisting of hydrophilic polyhydroxyl and hydrophobic polyene domains (Figure 1 inset). The hydrophobic polyene domain promotes binding to and insertion into fungal, lipid bilayer membranes. As shown in Figure 1, the Raman spectrum of standard AmB (30 mg/mL) shows the specific bands due to the hydrophobic polyene domain at 1559 cm^{-1}, corresponding to the C=C stretch, and 1157 cm^{-1}, corresponding to the C-C stretch due to resonance Raman scattering [29].

Figure 1. Raman spectrum of standard amphotericin B in dimethyl sulfoxide (30 mg/mL).

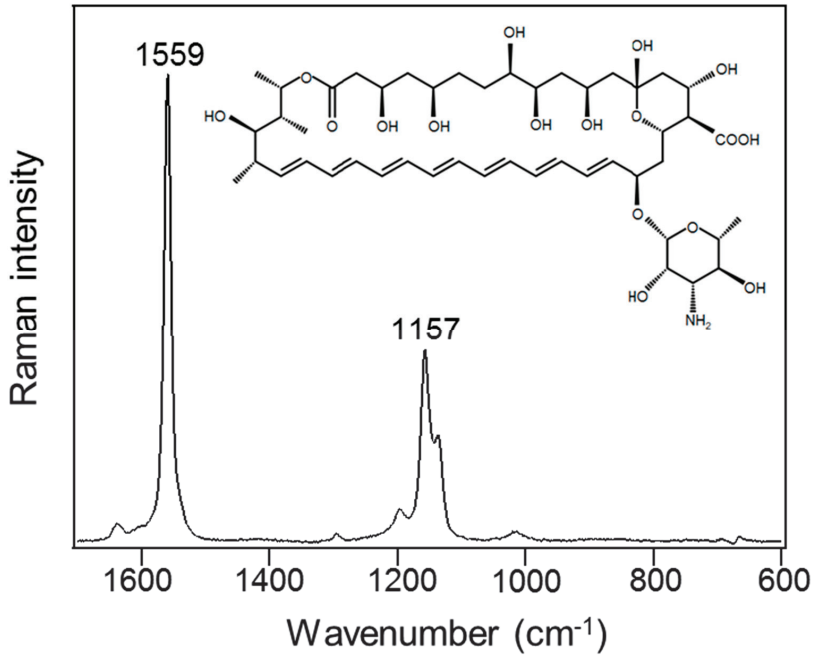

After cultivation of *S. nodosus* under AmB production-inducing or -non-inducing conditions, the mycelia derived from single spores were recovered from the culture media. The synthesis of AmB was also confirmed by a paper disc assay (Figure 2A). Antifungal activity against *Candida albicans* was successfully confirmed in the cell extract obtained from AmB-inducing medium, analysis, the same cell samples while no activity was observed from AmB-non-inducing medium. In the Raman microspectroscopic were analyzed without cell destruction. As shown in Figure 2B, the mycelia were approximately 1.5 mm in size after cultivation. The centers of the mycelia (900 μm^2; indicated by red boxes in Figure 2B) were selected for Raman microspectroscopic analysis. Since the depth resolution of confocal Raman microspectroscopy is smaller than the mycelia, the Raman intensity depends on constituent molecules within focal points. In the Raman spectra of *S. nodosus* (Figure 2C), three notable bands (747, 1129, and 1585 cm^{-1}) of cytochrome b and c can be found, as described previously in resonance Raman spectra [30]. In addition, protein can be found at 1003 cm^{-1}, corresponding to phenylalanine ring breathing. Cytochrome and protein are commonly analyzed by Raman microspectroscopy to identify cell shapes and to evaluate respiration bioactivity [24,30]. Based on the Raman spectra obtained from the cells cultivated under AmB-inducing conditions (Figure 2C (a)), we determined that two bands at 1556 and 1154 cm^{-1} could be assigned to AmB. To confirm the assignments, we further compared the Raman spectra obtained from the AmB-inducing and AmB-non-inducing conditions (Figure 2C (b)). The difference spectrum (Figure 2C (c)) suggests that these bands—1556 and 1154 cm^{-1}—could be observed only in the cells cultivated under AmB-inducing conditions, even though the peaks shifted toward lower frequencies as compared with the spectrum of standard AmB. Moreover, no obvious changes of other cellular components were observed between AmB production-inducing and -non-inducing conditions. On the basis of these results, we assigned these two bands at 1556 and 1154 cm^{-1} to AmB within live cells for the subsequent experiments.

2.2. Prediction of the Molecular State of AmB from Raman Peak Shift

Since polyene antibiotics are poorly soluble in aqueous solvents with water solubility of <1 mg/L at physiological pH (pH 6–7) [31], AmB self-associates and aggregates in water, owing to its amphipathic nature [32]. The molecular aggregation of AmB, which is induced by various physical and chemical factors—concentration, solvent, temperature, and pH—has influence on the spectral shift [33]. The Raman band corresponding to the C=C stretch shows sensitivity to structural changes, resulting in an intensity decrease and a slight shift of the predominant band [28]. Gagos *et al.* reported that aggregated AmB at pH 7 exhibits a Raman peak shift to lower frequencies by 2 cm^{-1}, compared to that of monomeric AmB at pH 12 [28]. In accordance with these findings, the specific bands of AmB at 1556 cm^{-1} obtained from the mycelia (Figure 2) have a spectral shift of 3 cm^{-1} toward lower frequencies, as compared to the standard AmB band, which was solubilized in DMSO in a dimeric state (Figure 1). Therefore, we speculate that AmB accumulates in the molecular aggregate state, which results in the peak shifts visible on the Raman spectra.

Figure 2. Raman microspectroscopic analysis of *S. nodosus* mycelia. (**A**) Evaluation of antifungal activity by the paper disc assay. The paper discs soaked with the extracts of *S. nodosus* mycelia cultivated under amphotericin B (AmB)-inducing (the left disk) and -non-inducing (the right disk) conditions were placed on an agar plate with *Candida albicans*; (**B**) Bright field images of *S. nodosus* mycelia cultivated in AmB-inducing medium and AmB-non-inducing medium. The Raman spectra were acquired from the areas indicated in the red boxes (30 μm × 30 μm). Scale bar = 200 μm; (**C**) Raman spectra were obtained from the centers of mycelia. Difference spectrum (**c**) between inducing (**a**) and non-inducing (**b**) conditions was obtained. Dashed lines indicate the AmB-specific bands at 1154 and 1556 cm^{-1}.

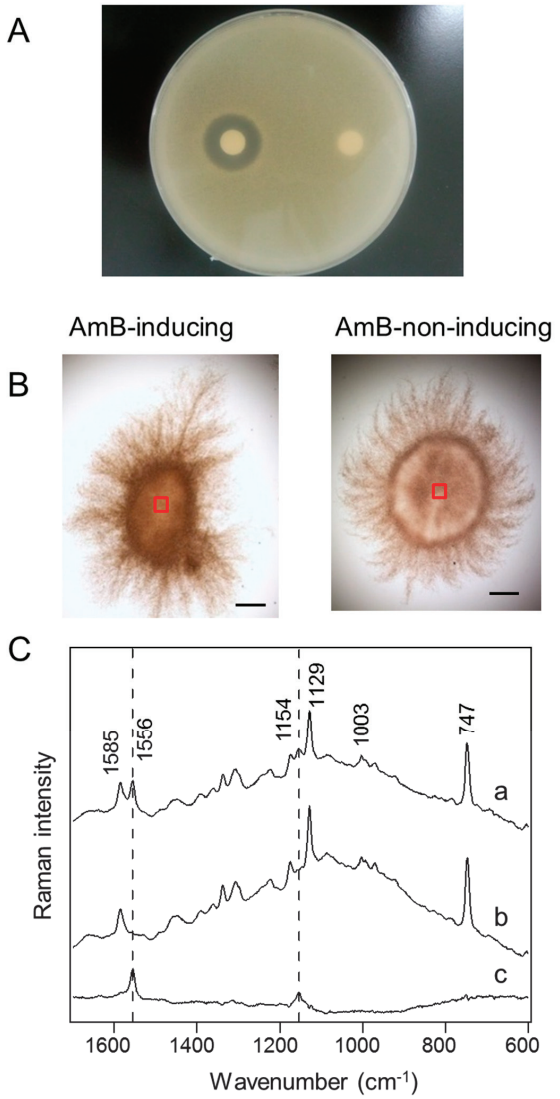

Figure 3. *In situ* time-course analysis of amphotericin B (AmB) production in *S. nodosus* mycelia. (**A**) Bright field images of *S. nodosus* mycelia cultivated for 5 days. Scale bar = 500 μm; (**B**) Magnified images of the center and edge areas of the mycelia at day 5 used for Raman spectroscopy measurements. The Raman spectra were acquired from the areas indicated in the red boxes (10 μm × 10 μm). Scale bar = 20 μm; (**C**) Time-dependent changes of averaged Raman spectra obtained from the center and edge areas of mycelia. Ten mycelia were analyzed at each time point. Dashed lines indicate the AmB-specific bands at 1154 and 1556 cm^{-1}. Insets show the changes of AmB-specific band intensities, which are normalized by the Raman band that corresponds to biomass (1454 cm^{-1}).

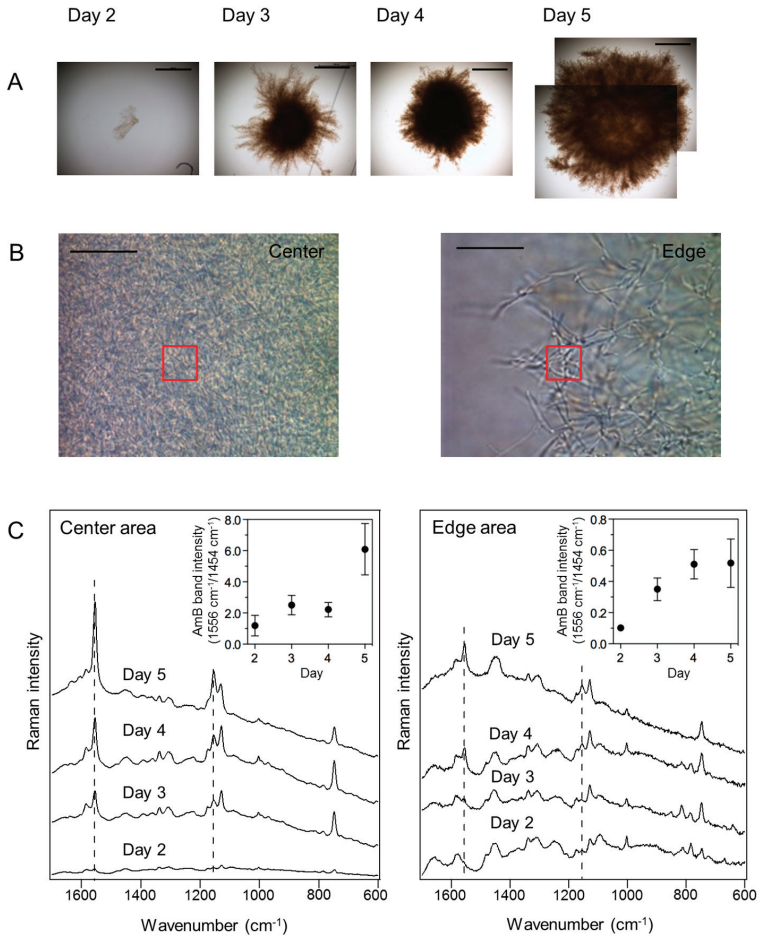

2.3. In Situ Time-Course Analysis of AmB Production in S. nodosus Using Raman Microspectroscopy

To monitor time-dependent changes in AmB production, the Raman spectra of center and edge areas of mycelia were measured on days 2–5 (Figure 3A). In each time point, 10 mycelia were sampled from culture medium and then analyzed by Raman microspectroscopy. The averaged Raman spectra were obtained from the fixed volume of 10 μm × 10 μm × 2.6 μm for the *x*, *y*, and *z* axes at each time point, during a period of mycelia growth (Figure 3B). Hence, the changes of the Raman intensities correlate with the fluctuation of constituent molecular numbers within fixed focal planes. The averaged spectrum obtained from the center area of 10 mycelia shows the AmB-specific Raman bands from day three, and the band intensity of AmB increased as a function of cultivation time (Figure 3C). As compared to the averaged Raman spectra of the edge areas, those of the center areas show significant changes of Raman intensity corresponding to AmB. These results indicate that AmB accumulates predominantly in the center of the mycelium, which is dense with cells, as a function of cultivation time. Therefore, Raman microspectroscopy could be employed for non-destructive monitoring of antibiotic production during microbial fermentation processes.

2.4. In Situ Localization of AmB Production

To elucidate the *in situ* distribution of AmB in *S. nodosus*, Raman images of cytochrome groups (747 cm^{-1}), protein (1003 cm^{-1}), and AmB (1556 cm^{-1}) were constructed (Figure 4). In the center of the mycelia grown in liquid media (Figure 4a,b), proteins and cytochromes were distributed throughout the entire cell area, as seen in the bright field images. The cellular morphology is indistinguishable in the center of mycelia, because hyphae were closely-packed. In contrast, AmB was present only under the AmB-inducing conditions and shows local distribution within the measured area. There is no correlation between the localization of AmB and other biomolecules. To identify AmB production in single cells, the hyphae that expanded from mycelia grown in solid media were also analyzed by Raman imaging (Figure 4c). In these images, although the distribution of protein and cytochrome corresponds to regions that appear to be individual cells, AmB was heterogeneously distributed in the hyphae. These results suggest that AmB production is enhanced locally in the hyphae of mycelium, while the other biomolecules required for cell growth and structure are maintained and distributed over the entire area of the hyphae.

In general, antibiotic biosynthesis correlates with morphological development, cell density and growth phase in *Streptomycetes* [34,35]. Based on this phenomenon, we considered that the cells in the cell crowding center area accumulate much more AmB than those in edge area due to quorum sensing effect. In *S. nodosus*, the biosynthetic gene cluster for AmB (113 kbp) includes six large polyketide synthase genes, two cytochrome P450 enzyme genes, two ABC transporter genes, and genes involved in the biosynthesis and attachment of mycosamine. It was thought that the ABC transporters (AmphG and AmphH) formed a heterodimer that exported AmB from the cell for self-protection and resistance [8]. Nevertheless, the Raman images of mycelia and individual hyphae indicate that AmB is distributed inside mycelia and along hyphae, while they might contain

both intracellular AmB precursors and accumulated AmB within the cells. Thus, we established that Raman imaging could provide intact and real-time localization of AmB production within cells. Since our Raman imaging technique allows us to obtain spatially resolved molecular information in living cells, this technique will be helpful to elucidate the mechanism of antibiotic biosynthesis associated with morphological development. Moreover, the ability to detect antibiotic synthesis *in situ* and at single-cell resolution could be useful for screening antibiotic-producing bacteria from environmental samples.

Figure 4. Raman images of mycelia and individual hyphae of *S. nodosus*. The images were obtained from the center of mycelia under amphotericin B (AmB)-inducing (**a**) and AmB-non-inducing (**b**) conditions. Magnified Raman images were obtained from a hypha in the edge area of a mycelium cultured under AmB-inducing conditions (**c**). Scale bar = 10 μm.

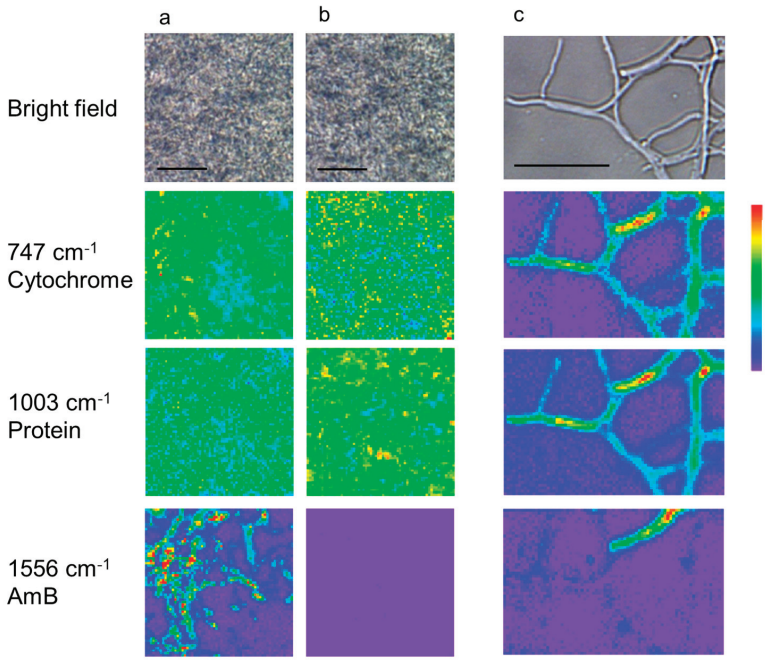

3. Experimental Section

3.1. Sample Preparation for Raman Microspectroscopy

In this study, *S. nodosus* (NBRC 12895) was used for Raman microspectroscopic analyses of AmB production. Yeast extract starch medium (0.2% yeast extract, 1% soluble starch) and 1/10 tryptic soy medium (0.3% Bacto Tryptic Soy Broth (Becton Dickinson, Franklin Lakes, NJ, USA)) were used as AmB production-inducing and -non-inducing liquid media, respectively. Spore suspensions were inoculated into 3 mL of each medium and then cultivated at 28 °C on a 180 rpm shaker for 5 days. Every 24 h after 2 days of cultivation, mycelia were recovered from the culture

media and then washed with PBS to eliminate components from the medium that might obscure Raman signals. To image individual hyphae, streak culture from the glycerol stock was conducted on a 1/10 tryptic soy agar plate. After cultivation at 28 °C for 5 days, a coverslip was stamped on the colony and removed so that the hyphae were transferred to the coverslip. The mycelia were observed in wet conditions to keep them from drying out during measurement. The hyphae were examined by microscopy, and the individual hyphae were selected for Raman imaging based on the bright field image. As a standard of AmB, commercially available AmB powder (Sigma Aldrich, St. Louis, MO, USA) was dissolved in DMSO.

3.2. Raman Microspectroscopy and Imaging

All Raman spectroscopic measurements were carried out with a laboratory-built confocal Raman microspectrometer. A 532 nm line of an Nd:YAG laser (Compass 315M; Coherent Inc., Santa Clara, CA, USA) was used as the Raman excitation line. The laser beam was focused by a 100 × 1.4 NA objective lens (Plan Apo VC; Nikon Corporation, Tokyo, Japan) onto the sample placed on the stage of an inverted microscope (ECLIPSE Ti; Nikon Corporation, Tokyo, Japan). The back-scattered Raman light was collected by the same objective lens and measured with a spectrometer (MS3504i, 1200 lines/mm; SOL Instruments, Ltd., Minsk, Republic of Belarus) and a CCD detector (Newton DU920-M; Andor Technology Plc., Antrim, UK) according to previous report [24]. The lateral and depth spatial resolutions of the Raman imaging system were 0.3 and 2.6 μm, respectively. The laser power was set to 4–20 mW at the sample point. For the measurement of *S. nodosus* in suspension, 10 μL of cell samples were placed on a clean coverslip and sealed with nail polish. To image hyphae with high spatial resolution, the mycelia of *S. nodosus* were immobilized on a coverslip, as described in section 3.1, and the measurement field was determined by microscopic observation. To image mycelia and individual hyphae, the sample area was scanned at 0.5 and 0.3 μm pitch, respectively, using a piezoelectric stage (custom-made; Physik Instrumente GmbH & Co. KG, Karlsruhe, Germany). The exposure times were 1 s per point for the mycelia and 0.5 s per point for the individual hyphae.

3.3. Data Analysis

Raman spectra were acquired and processed by IGOR Pro software (WaveMetrics, Inc., Lake Oswego, OR, USA). After wavelength calibration using the Raman spectrum of indene, all spectra acquired by the Raman mapping experiment were processed by a singular value decomposition analysis for noise reduction, as described in previous reports [19,36]. After the data pre-processing, for measurement of area intensity of the Raman band, the fitted spectrum was processed by gauss fitting method in the spectral region containing the Raman markers associated with cytochrome, protein, and AmB (726–762 cm^{-1}, 997–1009 cm^{-1}, 1533–1568 cm^{-1}, respectively). Their area intensities were calculated as peak area of each Raman band. Raman images were constructed as pseudocolor images from the area intensities of three Raman bands: 1003 cm^{-1} (protein), 747 cm^{-1} (cytochrome), and 1556 cm^{-1} (AmB).

3.4. Antifungal Activity Test

Culture medium (1 mL) was centrifuged at 2400× *g* for 5 min, and the supernatant was removed. Cell pellets were vortexed with ethanol to extract the bacterial components, including AmB. Paper discs (8 mm) were soaked with 70 μL of bacterial extract. The soaked discs were placed in Sabouraud Dextrose Agar plates seeded with 1-day broth culture of *Candida albicans* (NBRC 1594). The plates were incubated at 30 °C for 1 day. The antifungal activity was evaluated by the presence of an inhibition zone.

4. Conclusions

In summary, we were able to detect AmB in small volumes of *S. nodosus* cultures using Raman microspectroscopy *in situ*. Raman images reveal the heterogeneous distribution of AmB within the mycelia at single-cell resolution. Our results suggest that Raman microspectroscopy can provide information about intact antibiotic molecules that are produced by live cells, because the analysis does not require cell destruction. Additionally, Raman imaging can be useful to study the time-dependent change and cellular localization of antibiotic biosynthesis as well as the distribution and secretion of antibiotics from producer cells. Therefore, this technique could allow for routine assessments of microbial culture conditions and antibiotic production to facilitate more efficient antibiotic production. Moreover, Raman imaging could be employed to screen novel antibiotic candidates from marine samples.

Acknowledgments

The authors would like to thank Hisayuki Komaki (National Institution of Technology and Evaluation) for providing materials used in this study and his helpful comments. This study was supported by Japan Science and Technology Agency (JST), Core Research for Evolutionary Science and Technology (CREST), Grant-in-Aid for Challenging Exploratory Research Number 26630436, and MEXT-Supported Program for the Strategic Research Foundation at Private Universities.

Author Contributions

Conceived and designed the experiments: RM, MH, MA, TM and HT. Performed the experiments and analyzed the data: RM and MH. Contributed to the analytic tools: MA and HH. Wrote the paper: RM, MH and HT.

Conflicts of Interest

The authors declare no conflict of interest.

References

1. Stone, M.J.; Williams, D.H. On the evolution of functional secondary metabolites (natural products). *Mol. Microbiol.* **1992**, *6*, 29–34.
2. Penesyan, A.; Kjelleberg, S.; Egan, S. Development of novel drugs from marine surface associated microorganisms. *Mar. Drugs* **2010**, *8*, 438–459.
3. Fenical, W.; Jensen, P.R. Developing a new resource for drug discovery: Marine actinomycete bacteria. *Nat. Chem. Biol.* **2006**, *2*, 666–673.
4. Berdy, J. Bioactive microbial metabolites. *J. Antibiot. (Tokyo)* **2005**, *58*, 1–26.
5. Ohnishi, Y.; Ishikawa, J.; Hara, H.; Suzuki, H.; Ikenoya, M.; Ikeda, H.; Yamashita, A.; Hattori, M.; Horinouchi, S. Genome sequence of the streptomycin-producing microorganism *Streptomyces griseus* IFO 13350. *J. Bacteriol.* **2008**, *190*, 4050–4060.
6. Kharel, M.K.; Subba, B.; Basnet, D.B.; Woo, J.S.; Lee, H.C.; Liou, K.; Sohng, J.K. A gene cluster for biosynthesis of kanamycin from *Streptomyces kanamyceticus*: comparison with gentamicin biosynthetic gene cluster. *Arch. Biochem. Biophys.* **2004**, *429*, 204–214.
7. Darken, M.A.; Berenson, H.; Shirk, R.J.; Sjolander, N.O. Production of tetracycline by *Streptomyces aureofaciens* in synthetic media. *Appl. Microbiol.* **1960**, *8*, 46–51.
8. Caffrey, P.; Lynch, S.; Flood, E.; Finnan, S.; Oliynyk, M. Amphotericin biosynthesis in *Streptomyces nodosus*: Deductions from analysis of polyketide synthase and late genes. *Chem. Biol.* **2001**, *8*, 713–723.
9. Goss, W.A.; Katz, E. Actinomycin formation by *Streptomyces* cultures. *Appl. Microbiol.* **1957**, *5*, 95–102.
10. Crespi-Perellino, N.; Grein, A.; Merli, S.; Minghetti, A.; Spalla, C. Biosynthetic relationships among daunorubicin, doxorubicin and 13-dihydrodaunorubicin in *Streptomyces peucetius*. *Experientia* **1982**, *38*, 1455–1456.
11. Hentschel, U.; Hopke, J.; Horn, M.; Friedrich, A.B.; Wagner, M.; Hacker, J.; Moore, B.S. Molecular evidence for a uniform microbial community in sponges from different oceans. *Appl. Environ. Microbiol.* **2002**, *68*, 4431–4440.
12. Hentschel, U.; Piel, J.; Degnan, S.M.; Taylor, M.W. Genomic insights into the marine sponge microbiome. *Nat. Rev. Microbiol.* **2012**, *10*, 641–654.
13. Okamura, Y.; Kimura, T.; Yokouchi, H.; Meneses-Osorio, M.; Katoh, M.; Matsunaga, T.; Takeyama, H. Isolation and characterization of a GDSL esterase from the metagenome of a marine sponge-associated bacteria. *Mar. Biotechnol.* **2010**, *12*, 395–402.
14. Wilson, M.C.; Mori, T.; Ruckert, C.; Uria, A.R.; Helf, M.J.; Takada, K.; Gernert, C.; Steffens, U.A.; Heycke, N.; Schmitt, S.; *et al.* An environmental bacterial taxon with a large and distinct metabolic repertoire. *Nature* **2014**, *506*, 58–62.
15. Petry, R.; Schmitt, M.; Popp, J. Raman spectroscopy—A prospective tool in the life sciences. *Chemphyschem* **2003**, *4*, 14–30.
16. Zavaleta, C.; de la Zerda, A.; Liu, Z.; Keren, S.; Cheng, Z.; Schipper, M.; Chen, X.; Dai, H.; Gambhir, S.S. Noninvasive Raman spectroscopy in living mice for evaluation of tumor targeting with carbon nanotubes. *Nano Lett.* **2008**, *8*, 2800–2805.

17. Hanlon, E.B.; Manoharan, R.; Koo, T.W.; Shafer, K.E.; Motz, J.T.; Fitzmaurice, M.; Kramer, J.R.; Itzkan, I.; Dasari, R.R.; Feld, M.S. Prospects for *in vivo* Raman spectroscopy. *Phys. Med. Biol.* **2000**, *45*, R1–R59.
18. Clarke, S.J.; Littleford, R.E.; Smith, W.E.; Goodacre, R. Rapid monitoring of antibiotics using Raman and surface enhanced Raman spectroscopy. *Analyst* **2005**, *130*, 1019–1026.
19. Uzunbajakava, N.; Lenferink, A.; Kraan, Y.; Volokhina, E.; Vrensen, G.; Greve, J.; Otto, C. Nonresonant confocal Raman imaging of DNA and protein distribution in apoptotic cells. *Biophys. J.* **2003**, *84*, 3968–3981.
20. Munchberg, U.; Wagner, L.; Spielberg, E.T.; Voigt, K.; Rosch, P.; Popp, J. Spatially resolved investigation of the oil composition in single intact hyphae of *Mortierella* spp. with micro-Raman spectroscopy. *Biochim. Biophys. Acta* **2013**, *1831*, 341–349.
21. Walter, A.; Schumacher, W.; Bocklitz, T.; Reinicke, M.; Rosch, P.; Kothe, E.; Popp, J. From bulk to single-cell classification of the filamentous growing *Streptomyces* bacteria by means of Raman spectroscopy. *Appl. Spectrosc.* **2011**, *65*, 1116–1125.
22. Huang, Y.S.; Karashima, T.; Yamamoto, M.; Hamaguchi, H.O. Molecular-level pursuit of yeast mitosis by time-and space-resolved Raman spectroscopy. *J. Raman Spectrosc.* **2003**, *34*, 1–3.
23. Huang, Y.S.; Karashima, T.; Yamamoto, M.; Hamaguchi, H.O. Molecular-level investigation of the structure, transformation, and bioactivity of single living fission yeast cells by time- and space-resolved Raman spectroscopy. *Biochemistry* **2005**, *44*, 10009–10019.
24. Huang, C.K.; Ando, M.; Hamaguchi, H.O.; Shigeto, S. Disentangling dynamic changes of multiple cellular components during the yeast cell cycle by *in vivo* multivariate Raman imaging. *Anal. Chem.* **2012**, *84*, 5661–5668.
25. Baranska, M.; Schulz, H.; Rosch, P.; Strehle, M.A.; Popp, J. Identification of secondary metabolites in medicinal and spice plants by NIR-FT-Raman microspectroscopic mapping. *Analyst* **2004**, *129*, 926–930.
26. Weissflog, I.A.; Grosser, K.; Brautigam, M.; Dietzek, B.; Pohnert, G.; Popp, J. Raman spectroscopic insights into the chemical gradients within the wound plug of the green alga *Caulerpa taxifolia*. *Chembiochem* **2013**, *14*, 727–732.
27. Ellis, D. Amphotericin B: Spectrum and resistance. *J. Antimicrob. Chemother.* **2002**, *49*, 7–10.
28. Gagos, M.; Arczewska, M.; Gruszecki, W.I. Raman spectroscopic study of aggregation process of antibiotic amphotericin B induced by H^+, Na^+, and K^+ ions. *J. Phys. Chem. B* **2011**, *115*, 5032–5036.
29. Bunow, M.R.; Levin, I.W. Vibrational Raman spectra of lipid systems containing amphotericin B. *Biochim. Biophys. Acta* **1977**, *464*, 202–216.
30. Kakita, M.; Kaliaperumal, V.; Hamaguchi, H.O. Resonance Raman quantification of the redox state of cytochromes b and c *in vivo* and *in vitro*. *J. Biophotonics* **2012**, *5*, 20–24.
31. Lemke, A.; Kiderlen, A.F.; Kayser, O. Amphotericin B. *Appl. Microbiol. Biotechnol.* **2005**, *68*, 151–162.

32. Milhaud, J.; Ponsinet, V.; Takashi, M.; Michels, B. Interactions of the drug amphotericin B with phospholipid membranes containing or not ergosterol: New insight into the role of ergosterol. *Biochim. Biophys. Acta* **2002**, *1558*, 95–108.
33. Torrado, J.J.; Espada, R.; Ballesteros, M.P.; Torrado-Santiago, S. Amphotericin B formulations and drug targeting. *J. Pharm. Sci.* **2008**, *97*, 2405–2425.
34. Folcher, M.; Gaillard, H.; Nguyen, L.T.; Nguyen, K.T.; Lacroix, P.; Bamas-Jacques, N.; Rinkel, M.; Thompson, C.J. Pleiotropic functions of a *Streptomyces pristinaespiralis* autoregulator receptor in development, antibiotic biosynthesis, and expression of a superoxide dismutase. *J. Biol. Chem.* **2001**, *276*, 44297–44306.
35. Takano, E.; Gramajo, H.C.; Strauch, E.; Andres, N.; White, J.; Bibb, M.J. Transcriptional regulation of the redD transcriptional activator gene accounts for growth-phase-dependent production of the antibiotic undecylprodigiosin in *Streptomyces coelicolor* A3(2). *Mol. Microbiol.* **1992**, *6*, 2797–2804.
36. Huang, C.K.; Hamaguchi, H.O.; Shigeto, S. *In vivo* multimode Raman imaging reveals concerted molecular composition and distribution changes during yeast cell cycle. *Chem. Commun. (Camb.)* **2011**, *47*, 9423–9425.

Tipping Points in Seaweed Genetic Engineering: Scaling Up Opportunities in the Next Decade

Hanzhi Lin and Song Qin

Abstract: Seaweed genetic engineering is a transgenic expression system with unique features compared with those of heterotrophic prokaryotes and higher plants. This study discusses several newly sequenced seaweed nuclear genomes and the necessity that research on vector design should consider endogenous promoters, codon optimization, and gene copy number. Seaweed viruses and artificial transposons can be applied as transformation methods after acquiring a comprehensive understanding of the mechanism of viral infections in seaweeds and transposon patterns in seaweed genomes. After cultivating transgenic algal cells and tissues in a photobioreactor, a biosafety assessment of genetically modified (GM) seaweeds must be conducted before open-sea application. We propose a set of programs for the evaluation of gene flow from GM seaweeds to local/geographical environments. The effective implementation of such programs requires fundamentally systematic and interdisciplinary studies on algal physiology and genetics, marine hydrology, reproductive biology, and ecology.

Reprinted from *Mar. Drugs*. Cite as: Lin, H.; Qin, S. Tipping Points in Seaweed Genetic Engineering: Scaling Up Opportunities in the Next Decade. *Mar. Drugs* **2014**, *12*, 3025–3045.

1. Introduction

Seaweeds (marine macroalgae) are plant-like organisms encompassing macroscopic, multicellular, benthic marine algae. The term comprises red, brown and green algae, which are classified according to the thallus color derived from their dominant pigments (phycoerythrin and phycocyanin in red algae, *Chlorophyll* a and b in green algae, and fucoxanthin in brown algae). They generally live attached to hard substrates (such as rocks) in coastal areas, although some brown algae in Laminariales and red algae in Corallinales can live at depths of several or occasionally nearly a hundred meters below the sea surface [1]. A number of species/populations have adapted to be free-floating (*Sargassum* and *Ulva*) via changes of their intercellular gas sacs to maintain their favored depth in the water. There are approximately 10,000 species of seaweed throughout the world; however, seaweeds are generally regarded as a polyphyletic group that does not have a genetically common multicellular ancestor. They originated through multiple endosymbiotic events during the course of geological time. Generally speaking, green and red algae originated from a primary endosymbiosis when a eukaryotic host cell acquired an ancestral cyanobacterium as its plastid to form a primary symbiotic oxygenic eukaryote [2]. Brown algae derived from a secondary endosymbiosis, whose ancestor historically possessed a cryptic green algal endosymbiont that was subsequently replaced by a red algal chloroplast [3]. Due to their genetically polyphyletic origin, they are now classified in different kingdoms (brown algae are in the Kingdom Chromista, green algae and red algae are in the Kingdom Plantae) [4,5], although all are referred to as seaweed in assemblage.

Unlike higher plants, seaweeds, most of which display alternation of generation, have far more complicated life histories due to the flexible relationship among morphological phases, cytological events, and genetic behaviors than generally realized [6]. Many red algae have three generations, two sporophyte (diploid) generations, the carposporophyte and tetrasporophyte, in addition to a gametophyte (haploid) [6], most of which are morphologically macroscopic (e.g., adult thallus in *Porphyra*). The gametophyte and tetrasporophyte phases are usually morphologically similar [7], although they have markedly different physiological behaviors [8]. In some species, the carposporophyte is absent in sexual life history and the male and female gametophytes are vegetatively dimorphic [9] (Figure 1A). The life histories in brown algae may include heteromorphic (*Saccorhiza polyschides*, *Laminaria*), monophasic (*Compsonema saxicola*), and isomorphic types (*Ectocarpus siliculosus*), showing great variability between different groups [10]. In genus *Laminaria*, it consists of a macroscopic diploid generation, producing sporangium in which the cells then divide into haploid zoospores by meiosis prior to being released and growing to microscopic dissimilar male and female gametophytes [11] (Figure 1C). The sexual reproduction in the life history of green algae can be isogamous, anisogamous, or oogamous [12]. *Ulva* undertakes an alternation between macroscopic isomorphic diploid and haploid phases, however, in some species there can be twelve morphologically identical phases that differ in cytological and reproductive details [13] (Figure 1B). One of the most fundamental features of seaweeds is their great variety of life histories, running the entire gamut from haploid dominance to diploid dominance [14].

The traditional seaweed industry includes alginate production from brown algae and agar and carrageenan production from red algae. Approximately 1 million tons of seaweed can produce approximately 55,000 tons of these hydrocolloids with a value of US $ 585 million [17]. Currently, with the rise of world energy demands and depletion of fossil fuel resources, seaweed is receiving increasing attention as an attractive renewable feedstock for producing fuels and chemicals [18–20]. The global farming production of seaweed in 2010 was 19 million tons, with a total value estimated at US $5.7 billion, which is an increase of 30 percent from 2008 [21]. Countries in East and Southeast Asia are leaders in seaweed farming and European countries are using seaweed as a raw natural resource [22]. However, the global scale of seaweed cultivation is still small compared with its increased demand as an alternative renewable fuel [19].

The rapid development of seaweed genetic engineering and the establishment of seaweed expression systems are needed because of the agricultural demands on breeding, the production demands of the industrial and biomedical fields, and the environmental demands for bioremediation [23–26]. Additionally, the use of seaweed genetic engineering could be used as a genome editing method to help scientists decipher the connection between genotype and phenotype, and as a *de novo* genome design tool in synthetic biology from modules to systems [27]. Nevertheless, this field is not fully developed and there currently is not an established seaweed gene expression system, although several transformation methods in seaweeds have been developed [23,28]. The primary purpose of this paper is not to review recent literature in the field of seaweed genetic engineering [23,26–29], but to highlight gaps in knowledge; especially the rapid development of genome engineering and seaweed genomic research, the necessity of new promoter sequence

identification and new transformation methods, as well as, engineering design and biosafety assessments for seaweed expression system establishment.

Figure 1. Life histories of main three groups of seaweeds. (**A**) Life history of *Porphyra*, redrew and based on [6]. (**B**) Life history of *Ulva*, redrew and based on [15]. (**C**) Life history of *Laminara*, adapted from [16], with permission from openstax of Rice University.

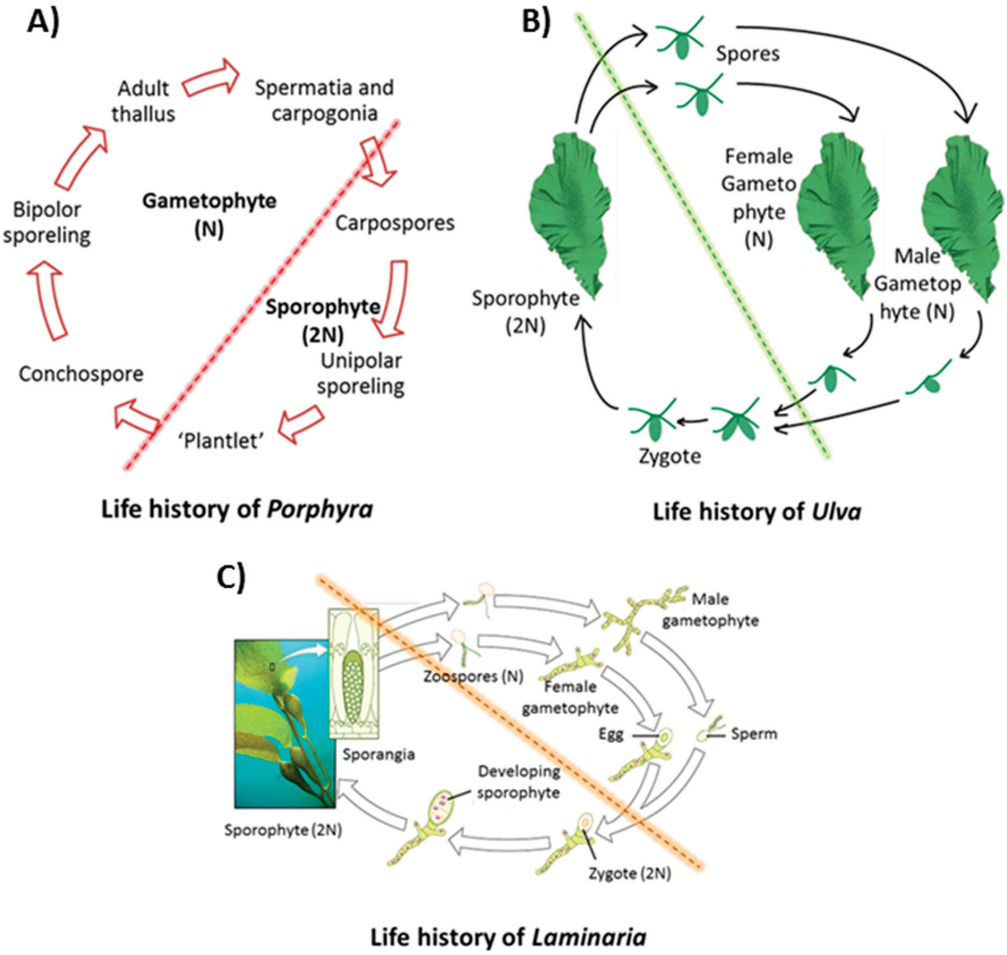

2. Seaweed Genomics and Model Organism Selection in Seaweeds

There is plentiful and complete genomic information for microalgae, whereas the genomic knowledge of seaweed is very limited. The genome of *Ectocarpus siliculosus*, which is highly related to the commercial brown seaweed *Laminaria* spp., sheds light on the physiology and evolution of multicellularity in brown algae. In this genome, extended sets of light harvesting and pigment biosynthesis genes and new halide metabolic processes have been discovered [30]. For carbon storage, the central pathways of carbohydrate and protein glycosylation are well conserved,

while a complicated laminarin metabolism replaces glycogen and starch metabolism from the secondary endosymbiont [31]. The first complete nuclear genome of red seaweed *Chondrus crispus* is a compact genome despite its large size (105 megabase pairs [Mbp]) and possesses rare large-scale gene duplications. Similar to the *Ectocarpus* genome, the *Chondrus* genome possesses halogen metabolism mechanisms for adaptation to the tidal coastal environment. The carbohydrate metabolism of *Chondrus* suggests the polyphyly of cellulose synthesis and the mannosylglycerate synthase in red algae potentially originates from a marine bacterium. In evolutionary history, red algae genomes have undergone loss and expansion including; the loss of genes, introns, and intergenic DNA by ecological forces, followed by an expansion of genome size resulting from the activities of transposable elements [32]. The genome of *Pyropia yezoensis*, one of the most commercialized and well-cultivated seaweeds, has also been sequenced. In its 43 Mbp genome, 35% of the genes are functionally uncharacterized, and a second homolog of the phycobilisome-degradation gene, which had been assumed to be chloroplast derived, was found in the nuclear genome. This newly discovered gene may be involved either in phycobilisome photobleaching or in *P. yezoensis* nitrate metabolism [33]. With the significant development in Next-Generation Sequencing (NGS) technologies, the cost, efficiency has decreased and volume of genome sequencing has increased [34,35]. Recently, it has been reported that the whole genome sequencing of the commercially cultivated seaweed, *Saccharina japonica*, whose genome size is 580–720 Mbp [36], has been completed and the total number of genes is estimated to be up to 35,725; larger than any other eukaryotic algae [37]. In addition to providing basic genomic information for seaweeds that have genomes that are usually large [30,32] and have noise from symbiotic bacteria [33], the decreased cost and increased sequencing efficiency and quality of NGS make it possible to examine species or different strains besides the typical model organisms; providing a new opportunity for comparative genomics within the same phylogenetic seaweed group. Transcriptomic analysis in *Macrocystis pyrifera* assessed gene expression under different abiotic factors such as, light, temperature and nutrients and revealed novel gene families in brown algae. The assembly of the 228 Mbp sequence revealed high genetic similarity between *Macrocystis pyrifera* and its brown seaweed relatives *Ectocarpus* and *Laminaria* [38]. These breakthroughs may produce complete seaweed genomes that could shed light on physiology, ecology, reproduction, evolution, *etc.*, which are essential in genetic engineering.

One bottleneck in seaweed genetic engineering is the diversity of genetic backgrounds and physiological activities (life history) among different seaweed strains. Both transient and stable genetic transformations have been accomplished in only a few strains of red, green, and brown seaweeds [23,28]. At present, only a few genii of seaweeds (well-commercialized ones or ones with long research histories) have been cultivated in the laboratory. Some materials for seaweed genetic engineering are directly field-isolated. A small change in genome or life history could lead to alterations in the parameters of genetic engineering experiments. To some extent, this prevents the spread of established genetic transformation methods to other seaweeds. It also hampers research into the fundamental mechanisms and principles of seaweed genetic transformation; thus some techniques remain at the technological level. With the successful assembly and analysis of the complete genomes stated in last paragraph, it is possible to establish several model organisms in

seaweeds. *Ectocarpus* is regarded as the first promising candidate for consideration since its 214 Mbp genome has been assembled and analyzed [30] and several other genetic datasets or methodologies are available [39,40]. The *Ectocarpus* genome is much smaller than its brown relatives Laminariales (580–720 Mbp) [34] and Fucales (1095–1271 Mbp) [41]; thus it should be more amenable to genome screening and manipulation. In addition, there are ~1800 well-maintained *Ectocarpus* strains in several collection centers and a barcode system for those strains is under construction [42]. In the future, we can expect the ability to conduct comparative genomic studies among these genetic resources, due to the decrease in cost and increase in efficiency brought by NGS. A set of laboratory protocols ranging from high-quality DNA extraction to seaweed cultivation [42–47] for *Ectocarpus* have also recently been published. In red seaweed, *Pyropia yezoensis* and other *Porphyra* spp. have been proposed as model organisms in red seaweed research of life history and ecophysiology [33,48].

3. Genome Engineering

Genome engineering is focused on the development of methods to precisely manipulate nucleic acids in living cells. Targeted genome modification in plants has been regarded as an elusive goal [49]. However, recent advances in sequence-specific genome engineering technologies have enabled the control of genetic material via targeted genome modifications [50] in model plant organisms. These tools can be grouped into two categories: protein-directed and nucleotide-directed specificities [51]. zinc finger nucleases (ZFN) have been successfully applied in *Chlamydomonas* [52], however, ZFN technology suffers from difficulties in design, construction, cost and uncertain success rates [53,54]. Here we are going to focus on two newly developed targeted genome modification tools. The first is protein directed transcription activator-like effectors (TALEs or TALs), the second is RNA-directed type II prokaryotic clustered regularly interspaced short palindromic repeats (CRISPR). For other target genomic engineering tools such as ZFN, readers may refer to several excellent and comprehensive reviews summarizing recent advances in precise genome editing technology [50,51,55,56].

TALs [57] have rapidly developed and have been utilized to create site-specific gene-editing [58] (Figure 2A). TALs are proteins produced by the pathogenic plant bacteria, *Xanthomonas*, when they infect plants through the type III secretion pathway [59]. These proteins can activate the expression of plant genes by binding effector-specific DNA sequences through their central tandem repeat region where the 12th and 13th amino acid diresidue corresponds to a specific nucleotide sequence [60] and transcriptionally activates gene expression. The TAL technique is more cost effective, has simpler design requirements and lower off-target activities than ZFN [61]. Due to the convenience of engineering new DNA binding specificities compared with ZFN [62], it has been applied in model plants to alter reporter-gene expression in tobacco [54,63], insertions and deletions in *Arabidopsis thaliana*, gene knockouts in rice [64], and the generation of disease-resistant rice [58]. There also have been calls for this technology to be applied to microalgae homologous recombination [65]. Several in-house methods of synthesizing TAL proteins to target specific DNA sequences in *Chlamydomonas* have been established, fused with *Fok*I nuclease, this technology could be utilized to create specific modifications in the *Chlamydomonas* genome [66,67].

Figure 2. Schematic diagram comparing TALE and CRISPR genome editing technologies, adapted from [86] with the permission from Journal of Experimental Botany. (**A**) TALE. (**B**) CRISPR, the genome breaks led by CRISPER will generate three possibilities: (1) cell death when dsDNA break are not moved, (2) undefinded indels by NHEJ, (3) homology-directed repair [70].

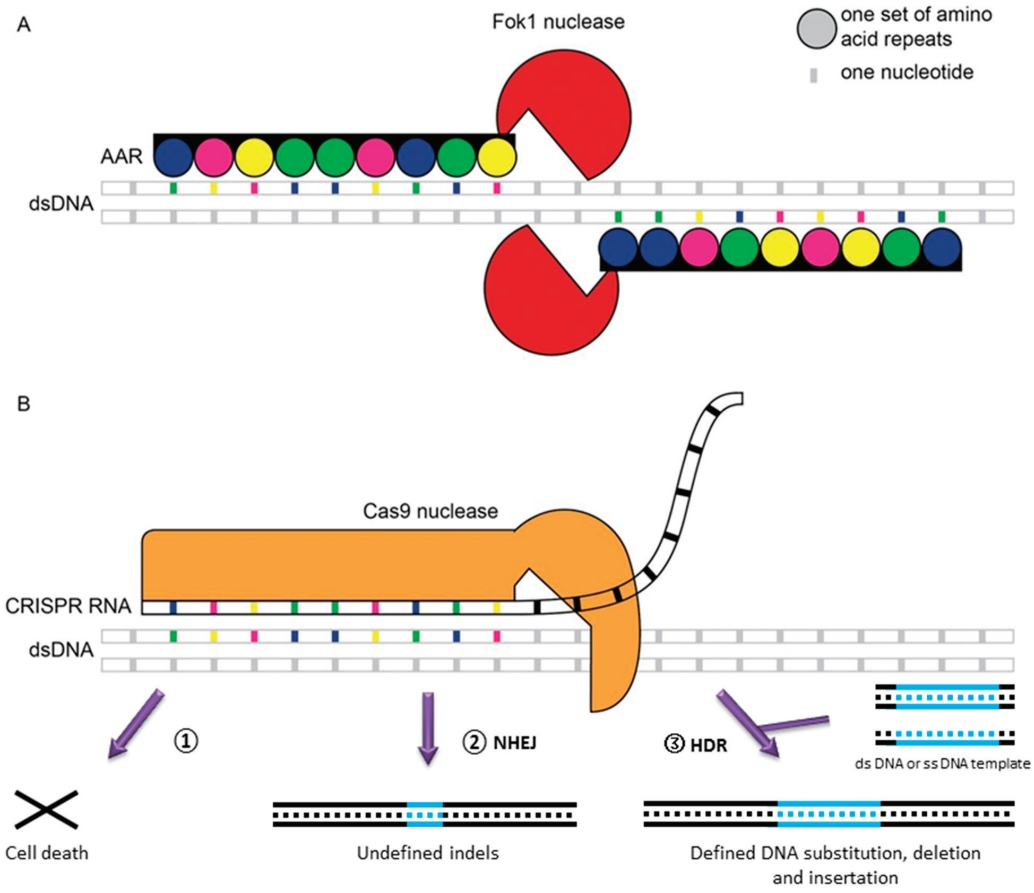

CRISPR has been hailed as a revolution in genomic engineering [68] (Figure 2B). It is a bacterial and archaeal immune system that exists in 40% of eubacteria and 90% of archaea [69] and consists of three core components: RNA guided CRISPR associate protein (Cas9) nuclease, CRISPR RNA (crRNA) and trans-acting crRNA (tracrRNA) [70], although occasionally the latter two components can be fused into a single guide RNA (sgRNA) [71]. CRISPR can directly edit the genome by either Non-Homologous Ending Joining (NHEJ), producing undefined indels, or template-dependent Homology-Directed Repair (HDR), which leads to a defined DNA substitution, deletion and insertion [70]. In *Arabidopsis*, the efficiency of HDR-mediated insertion is higher than NHEJ-mediated insertions [72]. When CRISPR fuses with effectors or transcriptional repressor domains, it generates stable and efficient transcriptional repression or activation, or robustly silences multiple endogenous gene expression in human and yeast cells [73]. This system has been

successfully used in plant organisms to perform gene modification and mutagenesis [74,75], multiplex gene editing [72,76], genome-scale screening [77,78], transcriptional control (up-regulated and down-regulated) [73], dynamic imaging of chromosome activity [79], and even multiplexed RNA-guided transcriptional activation, repression and gene editing simultaneously [80]. Presently, the majority of studies using CRISPR engineering that have been related to genome screening and transcriptional regulation have been performed in bacterial or animal cells [51,70].

Realistically, both the TAL and CRISPR techniques are not mature enough to be applied universally. Efforts must be made to resolve many fundamental problems in both methods; for example, the molecular structure and catalytic mechanism of CRISPR complex [70] and the pathway of TALs delivery into cells by lentiviruses [55]. Additionally, studies need to be performed for these targeted genome editing tools to determine their safety and specificity to decrease off-target possibilities [81,82] and to compare their efficiencies [55]. However, it is not too soon to begin genome editing studies in seaweed, although the aforementioned pioneering works in algae have primarily been performed in the model microalga *Chlamydomonas*. Based on the assumption that closely phylogenetically related species may share similar genetic, biochemical and physiological and morphological features [83]; the establishment of genome editing systems may derive from research in unicellular microalgae such as, *Porphyridium purpureum* [84] in Rhodophyta and *Thalassiosira pseudonana* [85] in Heterokontophyta.

4. Natural Promoter Identification and Promoter Engineering

Eukaryotic promoters are generally described as having a core promoter near the site of transcription initiation and one or more enhancer elements that may be located more distantly [87]. Promoters have guided evolution for millions of years as the primary mechanism responsible for the integration of different mutations favorable for the environmental conditions [88]. Because promoters are in non-coding regions, they are subject to less stringent evolutionary selection than protein-coding regions and have greater probability of nucleotide substitution [89]. The best characterized core promoter element is the TATA box, discovered in 1979 in *Drosophila* [90], which also exists in most promoters used in seaweed genetic engineering [28]. Nevertheless, TATA boxes are not present in all promoter regions—only approximately 10%–20% of metazoan core promoters [91] and only 29% *Arabidopsis* promoters have TATA boxes [92]. It seems that the organization of core promoters is phylogenetically different among different organisms [88], and sometimes significantly different between animals and plants [92]. When compared with higher model plants and animals, it is obvious that many core promoter elements remain undiscovered in marine algae.

The traditional viral promoters CaMV35S and SV40, commonly used in plant and animal genetic engineering, have been broadly applied in seaweed genetic engineering when there is sparse genetic information available [74,93–95]. These two promoters are typical eukaryotic class II promoters with a TATA box. However, exogenous proteins are often difficult to express when they do not originate from the target organism. In unicellular green algae models, some heterologous promoters allow transient gene expression, but the efficiency of the reporter and marker genes is low [96,97]. The same low efficiency of expression is observed in red seaweed. A

considerably low activity of the CaMV35S promoter is observed in *P. yezoensis* cells [98]. Some algal endogenous promoters, such as the diatom-originated fucoxanthin-chlorophyll a/c binding protein gene (*fcp*) and the endogenous 5′ upstream region of the actin 1 gene from *P. yezoensis* (PyAct1), have shown efficient activity when used to construct expression vectors. The former has been applied in *L. japonica* [99], whereas the latter has been found effective in 12 red seaweed species [100,101]. The successful application of the PyAct1 promoter indicates that extensive study should be devoted to the search for and design of endogenous promoters within seaweed genomes. This necessity arises because exogenous promoters usually have different structures of DNA sequence and apply different transcriptional regulation of protein-coding genes. Promoter trapping is one of the methods used for novel promoter isolation and characterization in plants [102], and it has been successfully applied in modeling the green alga, *Chlamydomonas reinhardtii* [103]. Increasing numbers of assembled marine algal genome sequences are now available due to the high sequencing throughput brought about by NGS technologies. Presently, there are approximately 19 marine eukaryotic algae genomes that are finished being sequenced or are in the process of being sequenced [33,37,84,104]. Natural promoter sequence identifications have not been comprehensively conducted in marine algae, but with the help of NGS and bioinformatic technologies the situation is improving. The completion of the algal genomic assemblies will provide a foundation for the comparative analysis of gene regulation networks to determine the *cis*-regulatory code [105], which will allow the discovery of additional endogenous promoters and viral or phage-derived heterologous promoters.

Natural promoters for use in seaweed genetic engineering can either be isolated from endogenous algal sequences or isolated from a heterologous viral promoter. Occasionally, heterologous viral or phage-derived promoters cannot regulate transcription levels, meanwhile, isolated endogenous promoters are commonly unable to maximize the transcriptional capacity of the host [106]. These shortcomings do not allow for fine-tuned control of transcription, which prevents their use in complex metabolic and genomic engineering applications. Promoter engineering may overcome these difficulties and possibly will allow the optimization of metabolic pathways in cooperation with other methods including; synthetic ribosome-binding sites design [107], mRNA stability improvement [108], RNase III activity modulation [109], codon usage [110], *etc.* At present, there are four prevailing strategies in rational promoter design; introducing random mutations into the promoter sequence by error-prone PCR, mutating non-consensus spacer nucleotide regions within a promoter via saturation mutagenesis, assembling different tandem upstream activation sequences to tune the core promoter and altering the structure of transcription factor-binding site sequences [106]. Schlabach and colleagues have established a library of possible 10-mer DNA sequences in tandem from the upstream activation sequence of one promoter to generate stronger enhancement activity for this promoter using a synthetic biology approach [87]. All of these methods make it possible for *de novo* tunable promoter synthesis in seaweed genetic engineering, while more rational strategies will still rely on the increasing understanding of promoter sequence structure diversity from marine algae uncovered by NGS technologies.

Codon usage is another barrier to the transport of exogenous protein-coding genes into seaweeds. Exogenous proteins usually contain codons which are rarely used in the desired host, in addition to

transcriptional regulation elements within their own coding sequence [111]. Codon bias is sometimes regarded as the single most important determinant of exogenous protein expression [112,113]. Optimizing the codon usage of algae-destined transgenes may increase the expression efficiency of proteins and decrease their susceptibility to gene silencing [114]; such optimizations may be necessary for high-level protein expression for commercial purposes [115]. The vectors containing artificially optimized GUS coding sequences with CaMV35S, GAPDH, or PyAct1 promoters show higher expression efficiencies than those of each promoter and the original GUS gene [98]. A cyan fluorescent protein modified according to the codon usage of *P. tenera* and *P. yezoensis* has been successfully used in transgenic research; this fluorescent protein uses short emission wavelengths to diminish the background fluorescence interference from chlorophyll molecules in algal cells [116]. Aside from its original use in gene amplification, *de novo* gene synthesis has become another powerful tool to express heterologous genes in host organisms. Designing an optimal gene requires a comprehensive inspection of codon usage, mRNA secondary structure, cryptic ribosome binding sites [117], and the interaction of the target gene with the cellular environment of the host. A rational way to optimize the criteria and algorithms for heterologous gene expression has recently been proposed [118]. These optimized algorithms are essential in the development of synthetic biology for use in seaweed biotechnology [20].

5. Transformation Methods

Particle bombardment, electroporation, and glass beads are the three primary transformation methods applied in seaweed due to their mature technologies and their successful application in many phylums and classes of seaweeds (red, green, and brown seaweeds) [28,74,100,119–121] (Figure 3). Details on these methods are available in the literature [23]. In some higher plants, the *Agrobacterium*-mediated method yields high proportions of transformants that combine low copy number with the expression of the non-selected reporter gene, and bombardment particles with minimal cassettes yield high absolute transformation efficiencies [122]. However, the scarcity of studies on the *Agrobacterium*-mediated method [123] in seaweed and the limited understanding of the *Agrobacterium* mechanism within the algal nuclear genome constrain the application of the Agrobacterium-mediated method in seaweed [23].

Large dsDNA viruses known to infect eukaryotic algae are categorized into two groups: viruses in the unicellular microalgae *Chlorella* system and viruses in the brown seaweed system [22]. Nearly twenty years ago, virus-mediated transformation was successfully applied in filamentous brown seaweed [124]. However, there are few follow-up studies on this transformation method. Viruses that infect brown algae have different sizes, diameters, and host specificities [125]. When considering a rational and quantitative virus-infected seaweed genetic transformation, at least three factors need to be considered in advance. The first factor is the minimum threshold abundance at which seaweed could be infected by a virus. This minimum infection threshold universally exits in nature [126]. The transport of a virus into a small aquatic organism can be described quantitatively as the diffusive transport from solution [127]. Thus, the viral infection process (transport of virus and host-virus interaction) in the gametophyte of seaweeds can be mathematically modeled. Most of the aquatic host-virus interaction dynamic models introduce a parameter of host cell death rate

due to lysis [128,129], but the viruses that infect brown algae are usually benign and nonlethal [130]. The second factor is the search for a universal nonlethal virus that targets seaweeds. The brown algae is the only class of eukaryotic algae whose species can be infected by an algal virus; in contrast to other cases in which one virus specifically infects a single host species, more than one species of the brown algae can be infected [130]. The virus in the brown algal system is generally benign, but other algal viruses might lead to algal lysis and cause death, which is not expected in genetic engineering. The third and last factor is the infection mechanism. Studies have confirmed that some brown algal viruses maintain the amplification of their DNA, along with algal cellular mitotic divisions, in unicellular gametes or spores and do not form viral particles until the cells develop into a mature organ (gametangia or sporangia) [131]. Details on the mechanism of viral DNA combination and modification to algal genome may be elucidated with the development of genomic tools from genome to phenome.

Figure 3. Workflow of seaweed genetic engineering. (**A**) General workflow; (**B**) Workflow in brown seaweed *Laminaria japonica* (adapted from [24] with permission of Trends in Biotechnology).

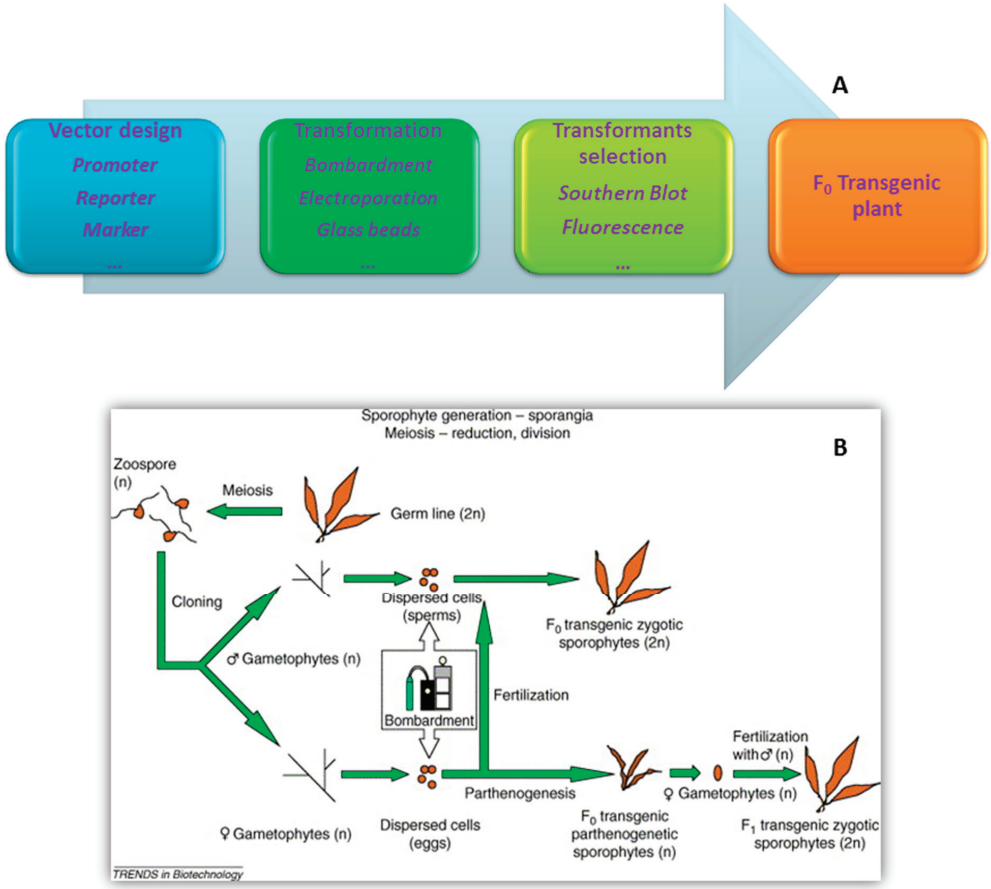

Transposons, a group of mobile DNA first discovered in maize, have been developed as powerful tools for genetic engineering in some microalgae [132,133]. The high transgenic efficiency of transposons can, to a certain extent, avoid the silencing of exogenous genes in host cells. The recently completed seaweed genomes discussed in Section 2, especially the genome of *C. crispus*, implies the existence of many transposon elements. The transposon component of this genome is quite complicated because of their huge number and significant divergence [32]. Transposons were also detected and identified in the *Pyropia yezoensis* genome [33]. These potential endogenous elements will "open a new window" because seaweed genomes are essentially expanded or shrunk to some extent via several endosymbiotic events in evolutionary history [2,134] as a partial consequence of transposable elements [32].

6. Biosafety Assessments of Transgenic Seaweeds

The initial debate about the risks from transgenic organisms emerged with the birth of the first genetically modified (GM) organism in the 1970s [135]. The threat to biodiversity, gene flow, and resistance risk are the main concerns revolving around transgenic plants, including GM seaweeds. We cannot be less cautious when GM organisms are modified by precise editing, replacement or insertion of genes without the use of any selectable markers and to specifically select the targeted genomic region [136]. Some scientists have predicted that most target GM microalgal traits (here, microalgae are morphologically similar to spores from seaweeds) are hard to maintain in nature and would rapidly diminish; they have also emphasized the need for a rigorous evaluation of such traits at the mesocosms scale to monitor their continuous gene flow from GM algae to the environment [137]. In addition, risk analysis should be straightforward at the species level to evaluate its impact on indigenous species [138] or even at the population level when the wild variety of GM seaweed is taken from the local environment. Lessons on scientific risk evaluation and management could be learned from higher plants [139–141]. However, unlike land plants, GM seaweeds cannot avoid escaping to the environment because of constant water flow. This condition leads to gene flow, especially when GM seaweeds become sexually mature and release their spores.

We propose a set of rational assessment programs for evaluating gene flow from GM seaweeds to local or large-scale environment based on the assessment of gene flow probability from transgenic plants [140]. However, necessary modifications are added considering the different fluid features of aquatic environments compared with terrestrial environments and the complex biological and ecological characteristics of seaweeds. This set of programs includes the following. (1) Biology of target seaweed: Fundamental information of genetic structure (endogenous plasmids, reproduction-related genes, *etc.*), life cycle, and maximum growth conditions will have a primary effect on the probability and degree of the gene flow from GM seaweeds; (2) Distribution medium of other aquatic organisms: The life cycle of seaweeds is so complex that any organism, including marine invertebrates, vertebrates, or even other algae and sea grasses, can assist GM seaweeds in the distribution of GM spores; (3) Hydrological structure of the local aquatic environment: The trial area should be a relatively stable environment; however, monthly or seasonal changes should be considered, and daily or weekly hydrological fluctuations must be noted to understand the time of the release of spores; (4) Genetic information exchanges with other related population or species:

Seaweeds can "compare notes" on their respective genetic information by various sexual or asexual reproductive processes according to the degree of their genetic compatibility to other species or populations; (5) Life cycle and reproductive strategies of GM seaweeds: Close attention should be given to any genetic, physiological, or morphological changes in the life history of GM seaweeds, especially during their release of spores to the adjacent aquatic environment; (6) Survivability of algal propagules from GM seaweed: The fitness of any escaped vegetative fragments or sporangia of GM seaweeds to the environment outside the cultivation area must be determined; (7) Semi-quantification of gene flow: Several mathematical models specific to each GM species or population are required because the life cycles of seaweeds are extremely diverse; even within a genus, the life cycle can significantly differ under various conditions [142]. In the present work, we use the term "semi-quantification" instead of "quantification" as mentioned in the study of Chandler [140] because this process is more complex within aquatic systems than within land systems [143,144]; (8) Post-release mechanism of gene dispersal from GM seaweed: Although this program would only be effective after obtaining permission to cultivate GM seaweed in the open sea, it can never be overemphasized because local cultivation may lead to geographical gene flows along the hydrological structure of the sea or the GM seaweed could randomly be water ballasted to other seas similar to the mechanism of other aquatic invasive organisms.

Another necessary step is to construct "complete marine algae-derived" vectors, *i.e.*, endogenous promoters, reverse mutation as a selective marker, and the replacement of any non-algal viral DNA sequence with algal virus nucleotides [23]. Basing on the extensively studied theory of "paradox of the plankton" put forward by Hutchinson [145], Gressel emphasized the "gene mitigation" strategy originating from transgenic higher plants and introduced several mutation strategies to cause GM algae to be unfit to reproduce in nature and become incapable of adapting to local ecosystems [146].

7. Conclusions

Seaweed genetic engineering could bridge the gap between fundamental and applied studies in seaweed research. The decreasing cost of sequencing provides us with many opportunities to investigate the fine genetic structure of seaweeds and consequently identify innovative genetic transformation elements (promoters, transformation methods, selective markers, *etc.*). The final biosafety assessment of a GM seaweed demands multi-disciplinary research on algal genetics, physiology, reproductive biology, and ecology from the molecular to at least the local aquatic ecosystem level through mathematics, biology, chemistry, physics, and even sociology when considering environmental issues. These innovations will bring unlimited possibilities in seaweed genetic engineering, which is still in its infancy. Combining these innovations with the rapidly developing fields of systems biology and metabolic engineering will satisfy the demands related to energy, environment, and human health.

Acknowledgments

This work is funded by the postdoctoral fellowship granted by the Institute of Marine and Coastal Sciences at Rutgers University to Hanzhi Lin, the State Oceanic Administration of China,

through Grant 200905021-3; the NSF of Shandong Province, China, through Grant JQ200914; and the NSF of China through Grant 41176144 to Song Qin.

Conflicts of Interest

The authors declare no conflict of interest.

References

1. Luning, K. *Seaweeds. Their Environment, Biogeography, and Ecophysiology*; John Wiley & Sons, Inc.: Toronto, Canada, 1990.
2. Falkowski, P.G.; Katz, M.E.; Knoll, A.H.; Quigg, A.; Raven, J.A.; Schofield, O.; Taylor, F.J.R. The evolution of modern eukaryotic phytoplankton. *Science* **2004**, *305*, 354–360.
3. Dorrell, R.G.; Smith, A.G. Do red and green make brown?: Perspectives on plastid acquisitions within chromalveolates. *Eukaryot. Cell* **2011**, *10*, 856–868.
4. Cavalier-Smith, T. Eukaryote kingdoms: Seven or nine? *BioSystems* **1981**, *14*, 461–481.
5. Simpson, A.G.B.; Roger, A.J. The real "kingdoms" of eukaryotes. *Curr. Biol.* **2004**, *14*, R693–R696.
6. West, J.A.; Hommersand, M.H. Rhodophyta: Life histories. In *The Biology of Seaweeds*; Lobban, C.S., Wynne, M., Eds.; University of California Press: Berkeley, CA, USA, 1981; pp. 133–193.
7. Kohlmeyer, J. New clues to the possible origin of ascomycetes. *BioScience* **1975**, *25*, 86–93.
8. von Stosch, H.A. The sporophyte of *Liagora farinosa* Lamour. *Br. Phycol. Bull.* **1965**, *2*, 486–496.
9. van derMeer, J.P.; Todd, E.R. The life history of *Palmaria palmata* in culture. A new type for the Rhodophyta. *Can. J. Bot.* **1980**, *58*, 1250–1256.
10. Pedersen, P.M. Phaeophyta: Life histories. In *The Biology of Seaweeds*; Lobban, C.S., Ed.; University of California Press: Berkeley, CA, USA, 1981; pp. 194–217.
11. Tseng, C.K. *Laminaria* mariculture in China. In *Case Studies of Seven Commercial Seaweed Resources*; Doty, M.S., Caddy, J.F., Santelices, B., Eds.; Food and Agriculture Organization of the United Nations: Rome, Italy, 1987; p. 311.
12. Lee, R.E. *Phycology*; Cambridge University Press: Cambridge, UK, 2008; p. 194.
13. Tanner, C.E. Chlorophyta: Life histories. In *The Biology of Seaweeds*; Lobban, C.S., Wynne, M., Eds.; University of California Press: Berkeley, CA, USA, 1981; pp. 218–247.
14. Otto, S.P.; Gerstein, A.C. The evolution of haploidy and diploidy. *Curr. Biol.* **2008**, *18*, R1121–R1124.
15. Institute, M.B.A.R. *Ulva* Life History. Available online: http://www.mbari.org/staff/conn/botany/greens/anna/frontpages/lifecyc.htm (accessed on 25 March 2014).
16. College, O. Groups of Protists. Available online: http://cnx.org/content/m44617/1.7/ (accessed on 25 March 2014).
17. McHugh, D.J. *A Guide to the Seaweed Industry*; Food and Agriculture Organization of the United Nations: Rome, Italy, 2003; Volume 441.

18. Hughes, A.; Kelly, M.; Black, K.; Stanley, M. Biogas from macroalgae: Is it time to revisit the idea? *Biotechnol. Biofuels* **2012**, *5*, doi:10.1186/1754-6834-5-86.
19. Roesijadi, G.; Jones, S.B.; Snowden-Swan, L.J.; Zhu, Y. *Macroalgae as A Biomass Feedstock: A Preliminary Analysis*; Pacific Northwest National Laboratory, U.S. Department of Energy: Washington, DC, USA, 2010.
20. Wei, N.; Quarterman, J.; Jin, Y.S. Marine macroalgae: An untapped resource for producing fuels and chemicals. *Trends Biotechnol.* **2013**, *31*, 70–77.
21. FAO. *Fishery and Aquaculture Statistics 2010*; Food and Agriculture Organization of the United Nations: Rome, Italy, 2012.
22. Murty, U.S.; Banerjee, A.K. Seaweeds: The wealth of oceans. In *Handbook of Marine Macroalgae*; Kim, S.-K., Ed.; John Wiley & Sons, Ltd.: West Sussex, UK, 2012; pp. 36–44.
23. Qin, S.; Lin, H.Z.; Jiang, P. Advances in genetic engineering of marine algae. *Biotechnol. Adv.* **2012**, *30*, 1602–1613.
24. Qin, S.; Jiang, P.; Tseng, C. Transforming kelp into a marine bioreactor. *Trends Biotechnol.* **2005**, *23*, 264–268.
25. Lin, H.; Qin, S.; Jiang, P. Biotechnology of seaweeds: Facing the coming decade. In *Handbook of Marine Macroalgae*; John Wiley & Sons, Ltd.: West Sussex, UK, 2011; pp. 424–430.
26. Walker, T.L.; Collet, C.; Purton, S. Algal transgenics in the genomic era. *J. Phycol.* **2005**, *41*, 1077–1093.
27. Purnick, P.E.M.; Weiss, R. The second wave of synthetic biology: From modules to systems. *Nat. Rev. Mol. Cell Biol.* **2009**, *10*, 410–422.
28. Mikami, K. Current advances in seaweed transformation. In *An Integrated View of the Molecular Recognition and Toxinology—From Analytical Procedures to Biomedical Applications*; Baptista, G.R., Ed.; InTech: Rijeka, Croatia, 2013; pp. 323–347.
29. Hallmann, A. Algal transgenics and biotechnology. *Transgenic Plant J.* **2007**, *1*, 81–98.
30. Cock, J.M.; Sterck, L.; Rouze, P.; Scornet, D.; Allen, A.E.; Amoutzias, G.; Anthouard, V.; Artiguenave, F.; Aury, J.M.; Badger, J.H.; *et al.* The *Ectocarpus* genome and the independent evolution of multicellularity in brown algae. *Nature* **2010**, *465*, 617–621.
31. Michel, G.; Tonon, T.; Scornet, D.; Cock, J.M.; Kloareg, B. The cell wall polysaccharide metabolism of the brown alga *Ectocarpus siliculosus*. Insights into the evolution of extracellular matrix polysaccharides in eukaryotes. *New Phytol.* **2010**, *188*, 82–97.
32. Collen, J.; Porcel, B.; Carre, W.; Ball, S.G.; Chaparro, C.; Tonon, T.; Barbeyron, T.; Michel, G.; Noel, B.; Valentin, K.; *et al.* Genome structure and metabolic features in the red seaweed *Chondrus crispus* shed light on evolution of the Archaeplastida. *Proc. Natl. Acad. Sci. USA* **2013**, *110*, 5247–5252.
33. Nakamura, Y.; Sasaki, N.; Kobayashi, M.; Ojima, N.; Yasuike, M.; Shigenobu, Y.; Satomi, M.; Fukuma, Y.; Shiwaku, K.; Tsujimoto, A.; *et al.* The first symbiont-free genome sequence of marine red alga, Susabi-nori (*Pyropia yezoensis*). *PLoS One* **2013**, *8*, e57122.
34. Mardis, E.R. A decade's perspective on DNA sequencing technology. *Nature* **2011**, *470*, 198–203.

35. Mardis, E.R. Next-generation sequencing platforms. *Annu. Rev. Anal. Chem.* **2013**, *6*, 287–303.
36. Legall, Y.; Brown, S.; Marie, D.; Mejjad, M.; Kloareg, B. Quantification of nuclear-DNA and G-C content in marine macroalgae by flow-cytometry of isolated-nuclei. *Protoplasma* **1993**, *173*, 123–132.
37. Yao, C.; Jun, L. Chinese scientists sequence genome of kelp, seafood species. Available online: http://english.peopledaily.com.cn/202936/8442860.html (accessed on 25 March 2014).
38. Konotchick, T.; Dupont, C.L.; Valas, R.E.; Badger, J.H.; Allen, A.E. Transcriptomic analysis of metabolic function in the giant kelp, *Macrocystis pyrifera*, across depth and season. *New Phytol.* **2013**, *198*, 398–407.
39. Dittami, S.M.; Scornet, D.; Petit, J.L.; Segurens, B.; Da Silva, C.; Corre, E.; Dondrup, M.; Glatting, K.H.; Konig, R.; Sterck, L.; *et al.* Global expression analysis of the brown alga *Ectocarpus siliculosus* (Phaeophyceae) reveals large-scale reprogramming of the transcriptome in response to abiotic stress. *Genome Biol.* **2009**, *10*, R66.
40. Heesch, S.; Cho, G.Y.; Peters, A.F.; Le Corguille, G.; Falentin, C.; Boutet, G.; Coedel, S.; Jubin, C.; Samson, G.; Corre, E.; *et al.* A sequence-tagged genetic map for the brown alga *Ectocarpus siliculosus* provides large-scale assembly of the genome sequence. *New Phytol.* **2010**, *188*, 42–51.
41. Peters, A.F.; Marie, D.; Scornet, D.; Kloareg, B.; Cock, J.M. Proposal of *Ectocarpus siliculosus* (Ectocarpales, Phaeophyceae) as a model organism for brown algal genetics and genomics. *J. Phycol.* **2004**, *40*, 1079–1088.
42. Coelho, S.M.; Scornet, D.; Rousvoal, S.; Peters, N.T.; Dartevelle, L.; Peters, A.F.; Cock, J.M. *Ectocarpus*: A model organism for the brown algae. *Cold Spring Harb. Protoc.* **2012**, *2012*, 193–198.
43. Coelho, S.M.; Scornet, D.; Rousvoal, S.; Peters, N.; Dartevelle, L.; Peters, A.F.; Cock, J.M. Genetic crosses between *Ectocarpus* strains. *Cold Spring Harb. Protoc.* **2012**, *2012*, 262–265.
44. Coelho, S.M.; Scornet, D.; Rousvoal, S.; Peters, N.; Dartevelle, L.; Peters, A.F.; Cock, J.M. Extraction of high-quality genomic DNA from *Ectocarpus*. *Cold Spring Harb. Protoc.* **2012**, *2012*, 365–368.
45. Coelho, S.M.; Scornet, D.; Rousvoal, S.; Peters, N.; Dartevelle, L.; Peters, A.F.; Cock, J.M. Immunostaining of *Ectocarpus* cells. *Cold Spring Harb. Protoc.* **2012**, *2012*, 369–372.
46. Coelho, S.M.; Scornet, D.; Rousvoal, S.; Peters, N.; Dartevelle, L.; Peters, A.F.; Cock, J.M. Isolation and regeneration of protoplasts from *Ectocarpus*. *Cold Spring Harb. Protoc.* **2012**, *2012*, 361–364.
47. Coelho, S.M.; Scornet, D.; Rousvoal, S.; Peters, N.T.; Dartevelle, L.; Peters, A.F.; Cock, J.M. How to cultivate *Ectocarpus*. *Cold Spring Harb. Protoc.* **2012**, *2012*, 258–261.
48. Blouin, N.A.; Brodie, J.A.; Grossman, A.C.; Xu, P.; Brawley, S.H. *Porphyra*: A marine crop shaped by stress. *Trends Plant Sci.* **2011**, *16*, 29–37.

49. Shukla, V.K.; Doyon, Y.; Miller, J.C.; DeKelver, R.C.; Moehle, E.A.; Worden, S.E.; Mitchell, J.C.; Arnold, N.L.; Gopalan, S.; Meng, X.D.; *et al.* Precise genome modification in the crop species *Zea mays* using zinc-finger nucleases. *Nature* **2009**, *459*, 437–441.
50. Voytas, D.F. Plant genome engineering with sequence-specific nucleases. *Annu. Rev. Plant Biol.* **2013**, *64*, 327–350.
51. Esvelt, K.M.; Wang, H.H. Genome-scale engineering for systems and synthetic biology. *Mol. Syst. Biol.* **2013**, *9*, 641.
52. Sizova, I.; Greiner, A.; Awasthi, M.; Kateriya, S.; Hegemann, P. Nuclear gene targeting in *Chlamydomonas* using engineered zinc-finger nucleases. *Plant J.* **2013**, *73*, 873–882.
53. Jiang, W.Z.; Zhou, H.B.; Bi, H.H.; Fromm, M.; Yang, B.; Weeks, D.P. Demonstration of crispr/cas9/sgrna-mediated targeted gene modification in Arabidopsis, tobacco, sorghum and rice. *Nucleic Acids Res.* **2013**, *41*, e188.
54. Mahfouz, M.M.; Li, L.X.; Shamimuzzaman, M.; Wibowo, A.; Fang, X.Y.; Zhu, J.K. De novo-engineered transcription activator-like effector (TALE) hybrid nuclease with novel DNA binding specificity creates double-strand breaks. *Proc. Natl. Acad. Sci. USA* **2011**, *108*, 2623–2628.
55. Gaj, T.; Gersbach, C.A.; Barbas, C.F. ZFN, TALEN, and CRISPR/cas-based methods for genome engineering. *Trends Biotechnol.* **2013**, *31*, 397–405.
56. Liu, W.S.; Yuan, J.S.; Stewart, C.N. Advanced genetic tools for plant biotechnology. *Nat. Rev. Genet.* **2013**, *14*, 781–793.
57. Moscou, M.J.; Bogdanove, A.J. A simple cipher governs DNA recognition by TAL effectors. *Science* **2009**, *326*, 1501.
58. Li, T.; Liu, B.; Spalding, M.H.; Weeks, D.P.; Yang, B. High-efficiency TALEN-based gene editing produces disease-resistant rice. *Nat. Biotechnol.* **2012**, *30*, 390–392.
59. Bogdanove, A.J.; Schornack, S.; Lahaye, T. TAL effectors: Finding plant genes for disease and defense. *Curr. Opin. Plant Biol.* **2010**, *13*, 394–401.
60. Bogdanove, A.J.; Voytas, D.F. TAL effectors: Customizable proteins for DNA targeting. *Science* **2011**, *333*, 1843–1846.
61. Mussolino, C.; Morbitzer, R.; Lutge, F.; Dannemann, N.; Lahaye, T.; Cathomen, T. A novel tale nuclease scaffold enables high genome editing activity in combination with low toxicity. *Nucleic Acids Res.* **2011**, *39*, 9283–9293.
62. Christian, M.; Cermak, T.; Doyle, E.L.; Schmidt, C.; Zhang, F.; Hummel, A.; Bogdanove, A.J.; Voytas, D.F. Targeting DNA double-strand breaks with TAL effector nucleases. *Genetics* **2010**, *186*, 757–761.
63. Zhang, Y.; Zhang, F.; Li, X.H.; Baller, J.A.; Qi, Y.P.; Starker, C.G.; Bogdanove, A.J.; Voytas, D.F. Transcription activator-like effector nucleases enable efficient plant genome engineering. *Plant Physiol.* **2013**, *161*, 20–27.
64. Cermak, T.; Doyle, E.L.; Christian, M.; Wang, L.; Zhang, Y.; Schmidt, C.; Baller, J.A.; Somia, N.V.; Bogdanove, A.J.; Voytas, D.F. Efficient design and assembly of custom TALEN and other TAL effector-based constructs for DNA targeting. *Nucleic Acids Res.* **2011**, *39*, 7879.

65. Weeks, D.P. Homologous recombination in *Nannochloropsis*: A powerful tool in an industrially relevant alga. *Proc. Natl. Acad. Sci. USA* **2011**, *108*, 20859–20860.
66. Borchers, A.; Wright, D.; Spalding, M.H. Development of tal nucleases for genome modification in *Chlamydomonas*. Available online: http://www.cbirc.iastate.edu/files/2012/09/Development-of-TAL-Nucleases-for-Genome-Modification-in-Chlamydomonas.pdf (accessed on 25 March 2014).
67. Brueggeman, A.J. Transcriptomic Analyses of the CO_2-Concentrating Mechanisms and Development of Molecular Tools for *Chlamydomonas Reinhardtii*. Ph.D. Thesis, University of Nebraska, Lincoln, NE, USA, 2013.
68. Rusk, N. CRISPRs and epigenome editing. *Nat. Methods* **2014**, *11*, 28–28.
69. Horvath, P.; Barrangou, R. CRISPR/cas, the immune system of bacteria and archaea. *Science* **2010**, *327*, 167–170.
70. Xu, T.; Li, Y.; Van Nostrand, J.D.; He, Z.; Zhou, J. Cas9-based tools for targeted genome editing and transcriptional control. *Appl. Environ. Microbiol.* **2014**, *80*, 1544–1552.
71. Jinek, M.; Chylinski, K.; Fonfara, I.; Hauer, M.; Doudna, J.A.; Charpentier, E. A programmable dual-RNA-guided DNA endonuclease in adaptive bacterial immunity. *Science* **2012**, *337*, 816–821.
72. Li, J.F.; Norville, J.E.; Aach, J.; McCormack, M.; Zhang, D.D.; Bush, J.; Church, G.M.; Sheen, J. Multiplex and homologous recombination-mediated genome editing in *Arabidopsis* and *Nicotiana benthamiana* using guide RNA and Cas9. *Nat. Biotechnol.* **2013**, *31*, 688–691.
73. Gilbert, L.A.; Larson, M.H.; Morsut, L.; Liu, Z.R.; Brar, G.A.; Torres, S.E.; Stern-Ginossar, N.; Brandman, O.; Whitehead, E.H.; Doudna, J.A.; *et al.* CRISPR-mediated modular RNA-guided regulation of transcription in eukaryotes. *Cell* **2013**, *154*, 442–451.
74. Jiang, P.; Qin, S.; Tseng, C.K. Expression of the *lacZ* reporter gene in sporophytes of the seaweed *Laminaria japonica* (Phaeophyceae) by gametophyte-targeted transformation. *Plant Cell Rep.* **2003**, *21*, 1211–1216.
75. Nekrasov, V.; Staskawicz, B.; Weigel, D.; Jones, J.D.G.; Kamoun, S. Targeted mutagenesis in the model plant *Nicotiana benthamiana* using Cas9 RNA-guided endonuclease. *Nat. Biotechnol.* **2013**, *31*, 691–693.
76. Shan, Q.W.; Wang, Y.P.; Li, J.; Zhang, Y.; Chen, K.L.; Liang, Z.; Zhang, K.; Liu, J.X.; Xi, J.J.; Qiu, J.L.; *et al.* Targeted genome modification of crop plants using a CRISPR-cas system. *Nat. Biotechnol.* **2013**, *31*, 686–688.
77. Shalem, O.; Sanjana, N.E.; Hartenian, E.; Shi, X.; Scott, D.A.; Mikkelsen, T.S.; Heckl, D.; Ebert, B.L.; Root, D.E.; Doench, J.G.; *et al.* Genome-scale CRISPR-Cas9 knockout screening in human cells. *Science* **2014**, *343*, 84–87.
78. Wang, T.; Wei, J.J.; Sabatini, D.M.; Lander, E.S. Genetic screens in human cells using the CRISPR-cas9 system. *Science* **2014**, *343*, 80–84.
79. Chen, B.; Gilbert, L.A.; Cimini, B.A.; Schnitzbauer, J.; Zhang, W.; Li, G.-W.; Park, J.; Blackburn, E.H.; Weissman, J.S.; Qi, L.S.; *et al.* Dynamic imaging of genomic loci in living human cells by an optimized CRISPR/Cas system. *Cell* **2013**, *155*, 1479–1491.

80. Esvelt, K.M.; Mali, P.; Braff, J.L.; Moosburner, M.; Yaung, S.J.; Church, G.M. Orthogonal Cas9 proteins for RNA-guided gene regulation and editing. *Nat. Methods* **2013**, *10*, 1116–1121.
81. Fu, Y.F.; Foden, J.A.; Khayter, C.; Maeder, M.L.; Reyon, D.; Joung, J.K.; Sander, J.D. High-frequency off-target mutagenesis induced by CRISPR-cas nucleases in human cells. *Nat. Biotechnol.* **2013**, *31*, 822–826.
82. Podevin, N.; Devos, Y.; Davies, H.V.; Nielsen, K.M. Transgenic or not? No simple answer! *EMBO Rep.* **2012**, *13*, 1057–1061.
83. Keeling, P.J.; Burger, G.; Durnford, D.G.; Lang, B.F.; Lee, R.W.; Pearlman, R.E.; Roger, A.J.; Gray, M.W. The tree of eukaryotes. *Trends Ecol. Evol.* **2005**, *20*, 670–676.
84. Bhattacharya, D.; Price, D.C.; Chan, C.X.; Qiu, H.; Rose, N.; Ball, S.; Weber, A.P.M.; Arias, M.C.; Henrissat, B.; Coutinho, P.M.; *et al.* Genome of the red alga *Porphyridium purpureum*. *Nat. Commun.* **2013**, *4*, 1941.
85. Armbrust, E.V.; Berges, J.A.; Bowler, C.; Green, B.R.; Martinez, D.; Putnam, N.H.; Zhou, S.G.; Allen, A.E.; Apt, K.E.; Bechner, M.; *et al.* The genome of the diatom *Thalassiosira pseudonana*: Ecology, evolution, and metabolism. *Science* **2004**, *306*, 79–86.
86. Cook, C.; Martin, L.; Bastow, R. Opportunities in plant synthetic biology. *J. Exp. Bot.* **2014**, *65*, doi:10.1093/jxb/eru013.
87. Schlabach, M.R.; Hu, J.K.; Li, M.; Elledge, S.J. Synthetic design of strong promoters. *Proc. Natl. Acad. Sci. USA* **2010**, *107*, 2538–2543.
88. Gagniuc, P.; Ionescu-Tirgoviste, C. Eukaryotic genomes may exhibit up to 10 generic classes of gene promoters. *BMC Genomics* **2012**, *13*, 512.
89. Huang, W.; Nevins, J.R.; Ohler, U. Phylogenetic simulation of promoter evolution: Estimation and modeling of binding site turnover events and assessment of their impact on alignment tools. *Genome Biol.* **2007**, *8*, R225.
90. Smale, S.T.; Kadonaga, J.T. The RNA polymerase II core promoter. *Annu. Rev. Biochem.* **2003**, *72*, 449–479.
91. Kadonaga, J.T. Perspectives on the RNA polymerase II core promoter. *Wiley Interdiscip. Rev. Dev. Biol.* **2012**, *1*, 40–51.
92. Molina, C.; Grotewold, E. Genome wide analysis of *Arabidopsis* core promoters. *BMC Genomics* **2005**, *6*, 25.
93. Kuang, M.; Wang, S.; Li, Y.; Shen, D.; Zeng, C. Transient expression of exogenous GUS gene in *Porphyra yezoensis* (Rhodophyta). *Chin. J. Oceanol. Limnol.* **1998**, *16*, 56–61.
94. Liu, H.; Yu, W.; Dai, J.; Gong, Q.; Yang, K.; Zhang, Y. Increasing the transient expression of GUS gene in *Porphyra yezoensis* by 18s rDNA targeted homologous recombination. *J. Appl. Phycol.* **2003**, *15*, 371–377.
95. Qin, S.; Jiang, P.; Tseng, C.K. Molecular biotechnology of marine algae in China. *Hydrobiologia* **2004**, *512*, 21–26.
96. Feng, S.Y.; Xue, L.X.; Liu, H.T.; Lu, P.J. Improvement of efficiency of genetic transformation for *Dunaliella salina* by glass beads method. *Mol. Biol. Rep.* **2009**, *36*, 1433–1439.

97. Kim, D.H.; Kim, Y.T.; Cho, J.J.; Bae, J.H.; Hur, S.B.; Hwang, I.; Choi, T.J. Stable integration and functional expression of flounder growth hormone gene in transformed microalga, *Chlorella ellipsoidea*. *Mar. Biotechnol.* **2002**, *4*, 63–73.
98. Mikami, K.; Hirata, R.; Takahashi, M.; Uji, T.; Saga, N. Transient transformation of red algal cells: Breakthrough toward genetic transformation of marine crop *Porphyra* species. In *Genetic Transformation*; Alvarez, M., Ed.; InTech: Rijeka, Croatia, 2011; pp. 241–258.
99. Li, F.C.; Qin, S.; Jiang, P.; Wu, Y.; Zhang, W. The integrative expression of GUS gene driven by FCP promoter in the seaweed *Laminaria japonica* (Phaeophyta). *J. Appl. Phycol.* **2009**, *21*, 287–293.
100. Hirata, R.; Takahashi, M.; Saga, N.; Mikami, K. Transient gene expression system established in *Porphyra yezoensis* is widely applicable in Bangiophycean algae. *Mar. Biotechnol.* **2011**, *13*, 1038–1047.
101. Takahashi, M.; Uji, T.; Saga, N.; Mikami, K. Isolation and regeneration of transiently transformed protoplasts from gametophytic blades of the marine red alga *Porphyra yezoensis*. *Electron. J. Biotechnol.* **2010**, *13*, doi:10.2225/vol13-issue2-fulltext-7.
102. Blanvillain, R.; Gallois, P. Promoter trapping system to study embryogenesis. In *Methods in Molecular Biology*; Suarez, M.F., Bozhkov, P.V., Eds.; Humana Press: Totowa, NJ, USA, 2008; Volume 427, pp. 121–135.
103. Vila, M.; Diaz-Santos, E.; de la Vega, M.; Rodriguez, H.; Vargas, A.; Leon, R. Promoter trapping in microalgae using the antibiotic paromomycin as selective agent. *Mar. Drugs* **2012**, *10*, 2749–2765.
104. Coelho, S.M.; Simon, N.; Ahmed, S.; Cock, J.M.; Partensky, F. Ecological and evolutionary genomics of marine photosynthetic organisms. *Mol. Ecol.* **2013**, *22*, 867–907.
105. Levine, M.; Tjian, R. Transcription regulation and animal diversity. *Nature* **2003**, *424*, 147–151.
106. Blazeck, J.; Alper, H.S. Promoter engineering: Recent advances in controlling transcription at the most fundamental level. *Biotechnol. J.* **2013**, *8*, 46–58.
107. Salis, H.M.; Mirsky, E.A.; Voigt, C.A. Automated design of synthetic ribosome binding sites to control protein expression. *Nat. Biotechnol.* **2009**, *27*, 946–950.
108. Dorokhov, Y.L.; Skulachev, M.V.; Ivanov, P.A.; Zvereva, S.D.; Tjulkina, L.G.; Merits, A.; Gleba, Y.Y.; Hohn, T.; Atabekov, J.G. Polypurine (A)-rich sequences promote cross-kingdom conservation of internal ribosome entry. *Proc. Natl. Acad. Sci. USA* **2002**, *99*, 5301–5306.
109. Babiskin, A.H.; Smolke, C.D. Synthetic RNA modules for fine-tuning gene expression levels in yeast by modulating RNase III activity. *Nucleic Acids Res.* **2011**, *39*, 8651–8664.
110. Puigbo, P.; Guzman, E.; Romeu, A.; Garcia-Vallve, S. Optimizer: A web server for optimizing the codon usage of DNA sequences. *Nucleic Acids Res.* **2007**, *35*, W126–W131.
111. Gustafsson, C.; Govindarajan, S.; Minshull, J. Codon bias and heterologous protein expression. *Trends Biotechnol.* **2004**, *22*, 346–353.
112. Lithwick, G.; Margalit, H. Hierarchy of sequence-dependent features associated with prokaryotic translation. *Genome Res.* **2003**, *13*, 2665–2673.

113. Surzycki, R.; Greenham, K.; Kitayama, K.; Dibal, F.; Wagner, R.; Rochaix, J.D.; Ajam, T.; Surzycki, S. Factors effecting expression of vaccines in microalgae. *Biologicals* **2009**, *37*, 133–138.
114. Potvin, G.; Zhang, Z.S. Strategies for high-level recombinant protein expression in transgenic microalgae: A review. *Biotechnol. Adv.* **2010**, *28*, 910–918.
115. Mayfield, S.P.; Schultz, J. Development of a luciferase reporter gene, luxCt, for *Chlamydomonas reinhardtii* chloroplast. *Plant J.* **2004**, *37*, 449–458.
116. Lim, J.-M.; Ahn, J.-W.; Hwangbo, K.; Choi, D.-W.; Park, E.-J.; Hwang, M.S.; Liu, J.R.; Jeong, W.-J. Development of cyan fluorescent protein (CFP) reporter system in green alga *Chlamydomonas reinhardtii* and macroalgae *Pyropia* sp. *Plant Biotechnol. Rep.* **2013**, *7*, 407–414.
117. Norholm, M.H.H.; Toddo, S.; Virkki, M.T.I.; Light, S.; von Heijne, G.; Daley, D.O. Improved production of membrane proteins in *Escherichia coli* by selective codon substitutions. *Febs Lett.* **2013**, *587*, 2352–2358.
118. Welch, M.; Villalobos, A.; Gustafsson, C.; Minshull, J. You're one in a googol: Optimizing genes for protein expression. *J. R. Soc. Interface* **2009**, *6*, S467–S476.
119. Mizukami, Y.; Hado, M.; Kito, H.; Kunimoto, M.; Murase, N. Reporter gene introduction and transient expression in protoplasts of *Porphyra yezoensis*. *J. Appl. Phycol.* **2004**, *16*, 23–29.
120. Huang, X.; Weber, J.C.; Hinson, T.K.; Mathieson, A.C.; Minocha, S.C. Transient expression of the GUS reporter gene in the protoplasts and partially digested cells of *Ulva lactuca* L (Chlorophyta). *Bot. Mar.* **1996**, *39*, 467–474.
121. Wang, J.F.; Jiang, P.; Cui, Y.L.; Guan, X.Y.; Qin, S. Gene transfer into conchospores of *Porphyra haitanensis* (Bangiales, Rhodophyta) by glass bead agitation. *Phycologia* **2010**, *49*, 355–360.
122. Jackson, M.A.; Anderson, D.J.; Birch, R.G. Comparison of Agrobacterium and particle bombardment using whole plasmid or minimal cassette for production of high-expressing, low-copy transgenic plants. *Transgenic Res.* **2013**, *22*, 143–151.
123. Cheney, D.; Metz, B.; Stiller, J. Agrobacterium-mediated genetic transformation in the macroscopic marine red alga *Porphyra yezoensis*. *J. Phycol.* **2001**, *37*, doi:10.1111/j.1529-8817.2001.jpy37303-22.x.
124. Henry, E.C.; Meints, R.H. Recombinant viruses as transformation vectors of marine macroalgae. *J. Appl. Phycol.* **1994**, *6*, 247–253.
125. Muller, D.G.; Kapp, M.; Knippers, R. Viruses in marine brown algae. *Adv. Virus Res.* **1998**, *50*, 49–67.
126. Wommack, K.E.; Colwell, R.R. Virioplankton: Viruses in aquatic ecosystems. *Microbiol. Mol. Biol. Rev.* **2000**, *64*, 69–114.
127. Murray, A.G.; Jackson, G.A. Viral dynamics—A model of the effects of size, shape, motion and abundance of single-celled planktonic organisms and other particles. *Mar. Ecol. Prog. Ser.* **1992**, *89*, 103–116.
128. Fuhrman, K.M.; Pinter, G.A.; Berges, J.A. Dynamics of a virus-host model with an intrinsic quota. *Math. Comput. Model.* **2011**, *53*, 716–730.

129. Middelboe, M. Bacterial growth rate and marine virus-host dynamics. *Microb. Ecol.* **2000**, *40*, 114–124.
130. Short, S.M. The ecology of viruses that infect eukaryotic algae. *Environ. Microbiol.* **2012**, *14*, 2253–2271.
131. Charrier, B.; Coelho, S.M.; Le Bail, A.; Tonon, T.; Michel, G.; Potin, P.; Kloareg, B.; Boyen, C.; Peters, A.F.; Cock, J.M. Development and physiology of the brown alga *Ectocarpus siliculosus*: Two centuries of research. *New Phytol.* **2008**, *177*, 319–332.
132. Kawata, Y.; Yano, S.; Kojima, H.; Toyomizu, M. Transformation of spirulina platensis strain c1 (*Arthrospira* sp PCC9438) with Tn5 transposase-transposon DNA-cation liposome complex. *Mar. Biotechnol.* **2004**, *6*, 355–363.
133. Taton, A.; Lis, E.; Adin, D.M.; Dong, G.; Cookson, S.; Kay, S.A.; Golden, S.S.; Golden, J.W. Gene transfer in *Leptolyngbya* sp. strain BL0902, a cyanobacterium suitable for production of biomass and bioproducts. *PLoS One* **2012**, *7*, e30901.
134. Hohmann-Marriott, M.F.; Blankenship, R.E. Evolution of photosynthesis. In *Annual Review of Plant Biology*; Merchant, S.S., Briggs, W.R., Ort, D., Eds.; Annual Reviews: Palo Alto, CA, USA, 2011; Volume 62, pp. 515–548.
135. Andow, D.A.; Zwahlen, C. Assessing environmental risks of transgenic plants. *Ecol. Lett.* **2006**, *9*, 196–214.
136. Pauwels, K.; Podevin, N.; Breyer, D.; Carroll, D.; Herman, P. Engineering nucleases for gene targeting: Safety and regulatory considerations. *New Biotechnol.* **2014**, *31*, 18–27.
137. Henley, W.J.; Litaker, R.W.; Noyoyeska, L.; Duke, C.S.; Quemada, H.D.; Sayre, R.T. Initial risk assessment of genetically modified (GM) microalgae for commodity-scale biofuel cultivation. *Algal Res. Biomass Biofuels Bioprod.* **2013**, *2*, 66–77.
138. Gressel, J.; van der Vlugt, C.J.B.; Bergmans, H.E.N. Environmental risks of large scale cultivation of microalgae: Mitigation of spills. *Algal Res. Biomass Biofuels Bioprod.* **2013**, *2*, 286–298.
139. Bennett, A.B.; Chi-Ham, C.; Barrows, G.; Sexton, S.; Zilberman, D. Agricultural biotechnology: Economics, environment, ethics, and the future. *Annu. Rev. Env. Res.* **2013**, *38*, 249–279.
140. Chandler, S.; Dunwell, J.M. Gene flow, risk assessment and the environmental release of transgenic plants. *Crit. Rev. Plant Sci.* **2008**, *27*, 25–49.
141. Rieben, S.; Kalinina, O.; Schmid, B.; Zeller, S.L. Gene flow in genetically modified wheat. *PLoS One* **2011**, *6*, e29730.
142. Lin, A.; Shen, S.; Wang, J.; Yan, B. Reproduction diversity of *Enteromorpha prolifera*. *J. Integr. Plant Biol.* **2008**, *50*, 622–629.
143. Colbach, N.; Clermont-Dauphin, C.; Meynard, J.M. GENESYS: A model of the influence of cropping system on gene escape from herbicide tolerant rapeseed crops to rape volunteers—II. Genetic exchanges among volunteer and cropped populations in a small region. *Agric. Ecosyst. Environ.* **2001**, *83*, 255–270.

144. Colbach, N.; Clermont-Dauphin, C.; Meynard, J.M. GENESYS: A model of the influence of cropping system on gene escape from herbicide tolerant rapeseed crops to rape volunteers—I. Temporal evolution of a population of rapeseed volunteers in a field. *Agric. Ecosyst. Environ.* **2001**, *83*, 235–253.
145. Hutchinson, G.E. The paradox of the plankton. *Am. Nat.* **1961**, *95*, 137–145.
146. Gressel, J.; van der Vlugt, C.J.B.; Bergmans, H.E.N. Cultivated microalgae spills: Hard to predict/easier to mitigate risks. *Trends Biotechnol.* **2014**, *32*, 65–69.

Cracking the Cytotoxicity Code: Apoptotic Induction of 10-Acetylirciformonin B is Mediated through ROS Generation and Mitochondrial Dysfunction

Huei-Chuan Shih, Mohamed El-Shazly, Yung-Shun Juan, Chao-Yuan Chang, Jui-Hsin Su, Yu-Cheng Chen, Shou-Ping Shih, Huei-Mei Chen, Yang-Chang Wu and Mei-Chin Lu

Abstract: A marine furanoterpenoid derivative, 10-acetylirciformonin B (10AB), was found to inhibit the proliferation of leukemia, hepatoma, and colon cancer cell lines, with selective and significant potency against leukemia cells. It induced DNA damage and apoptosis in leukemia HL 60 cells. To fully understand the mechanism behind the 10AB apoptotic induction against HL 60 cells, we extended our previous findings and further explored the precise molecular targets of 10AB. We found that the use of 10AB increased apoptosis by 8.9%–87.6% and caused disruption of mitochondrial membrane potential (MMP) by 15.2%–95.2% in a dose-dependent manner, as demonstrated by annexin-V/PI and JC-1 staining assays, respectively. Moreover, our findings indicated that the pretreatment of HL 60 cells with *N*-acetyl-L-cysteine (NAC), a reactive oxygen species (ROS) scavenger, diminished MMP disruption and apoptosis induced by 10AB, suggesting that ROS overproduction plays a crucial rule in the cytotoxic activity of 10AB. The results of a cell-free system assay indicated that 10AB could act as a topoisomerase catalytic inhibitor through the inhibition of topoisomerase IIα. On the protein level, the expression of the anti-apoptotic proteins *Bcl-xL* and *Bcl-2*, caspase inhibitors XIAP and survivin, as well as hexokinase II were inhibited by the use of 10AB. On the other hand, the expression of the pro-apoptotic protein Bax was increased after 10AB treatment. Taken together, our results suggest that 10AB-induced apoptosis is mediated through the overproduction of ROS and the disruption of mitochondrial metabolism.

Reprinted from *Mar. Drugs*. Cite as: Shih, H.-C.; El-Shazly, M.; Juan, Y.-S.; Chang, C.-Y.; Su, J.S; Chen, Y.-C.; Shih, S.-P.; Chen, H.-M.; Wu, Y.-C.; Lu, M.-C. Cracking the Cytotoxicity Code: Apoptotic Induction of 10-Acetylirciformonin B is Mediated through ROS Generation and Mitochondrial Dysfunction. *Mar. Drugs* **2014**, *12*, 3072–3090.

1. Introduction

The oncogene revolution in the last three decades has rekindled interest in studying survival-related pathways in cancer cells with the ultimate goal of developing efficient anticancer therapeutics targeting these pathways [1]. Much focus has been directed on studying mitochondria and their role in cancer cell survival-related pathways. Mitochondria are the principal energy factories in living cells, which play crucial roles in the cellular survival pathway. Thus, they have become major targets in chemotherapy-induced apoptosis against cancer cells [2–4]. One of the most vital functions of mitochondria is energy production in the form of ATP. In normal differentiated cells, the bulk of ATP is produced in mitochondria through the process of oxidative phosphorylation (OXPHOS) [5]. However under stressful conditions, OXPHOS is usually

suppressed. Cancer cells need to evade any process limiting energy supply, especially in the tight abnormal tumor microenvironment and thus they shift from OXPHOS to glycolysis, aiming to produce sufficient ATP. This effect is one of the cancer phenotype hallmarks and known as "Warburg effect" [6]. It allows cancer cells to produce ATP at a faster rate compared with OXPHOS, despite the overall lower efficiency. Recent studies have suggested that hexokinase is a key enzyme that catalyzes the first step in the glycolysis pathway. This enzyme transfers a phosphate group from ATP to glucose to form glucose-6-phosphate [7]. In cancer tissues, the high glycolytic activity requires an up-regulation of the key glycolytic enzymes, including hexokinase. Interestingly, the percentage of hexokinase binding to mitochondria significantly increases in cancer cells [8–10]. Targeting the interplay between mitochondrial hexokinase and cancer cells can provide potential opportunities for the development of new anticancer drugs [11].

Another molecular mechanism that has recently caught significant attention in the continuous war on cancer is the relationship between the accumulation of reactive oxygen species (ROS) and mitochondrial dysfunction [12]. Accumulating evidence suggested that ROS-regulated apoptosis is a promising target for anticancer drugs [13,14]. The manipulation of ROS can influence cancer cell survival, growth, and differentiation. Therefore, targeting the associated pathways can act as an attractive therapeutic strategy against cancer. Recent findings have suggested that the overproduction of ROS can induce apoptosis in cancer cells [15,16]. Moreover, it was found that the anti-apoptotic effect of Bcl-2, which can be related to certain cases of anticancer drug resistance, acts by decreasing the overall cellular oxidative stress through the suppression of the NADPH oxidase complex [17,18]. This protein plays a pivotal role in maintaining mitochondrial integrity and function, as well as in regulating the oxidative metabolic machinery [19]. Additionally, it has been observed that the tumor suppressor gene p53 might induce apoptosis through the induction of ROS production and the upregulation of Bax and PUMA [20]. Thus, inducing ROS generation is expected to increase the sensitivity of cancer cells to apoptotic stimuli in cancer therapy. With these targets in mind, our group has implemented an ambitious plan to explore and elaborate the detailed mechanism of action for some newly isolated cytotoxic compounds from marine organisms. Defining the molecular targets for biologically active compounds is a crucial step in developing any pharmaceutical drug, because it provides the necessary information for the development of highly specialized *in vivo* models and accurate future clinical trials [21,22].

In our previous report, we identified a series of cytotoxic C_{21} and C_{22} terpenoid-derived metabolites in the ethyl acetate (EtOAc) extract from the marine sponge, *Ircinia* sp. [23]. Among the isolates, 10-acetylirciformonin B (10AB) exhibited the highest cytotoxic activity [23]. The potent activity of 10AB encouraged us to investigate the underlying mechanism of action. The cytotoxic evaluation of 10AB against several cancer cell lines revealed that the most vulnerable cell line was HL 60 [24]. Our preliminary results suggested that the 10AB cytotoxic effect against HL 60 cells is mediated through DNA damage and apoptotic induction [24]. Aiming to further investigate the cytotoxic mechanism of 10AB, we examined the effect of 10AB on topoisomerase IIα, mitochondrial stability, and ROS generation in the HL 60 cancer cell line.

2. Results

2.1. The Apoptotic Induction Effect of 10AB in HL 60 Cells

The anti-proliferative and apoptotic induction effects of 10AB in HL 60 cells were demonstrated in our previous report [24]. However, to set the stage for a deeper investigation of the 10AB apoptotic mechanism, it was necessary to further confirm this effect in the current study. The effect of 10AB on nuclear morphology was evaluated utilizing DAPI staining. As shown in Figure 1A, the control group cell nuclei were large and round; however, the nuclei of the treated cells were fragmented and condensed, suggesting that the cells suffered from apoptotic induction. We also analyzed how increasing 10AB concentrations affected the HL 60 apoptotic population utilizing flow cytometric assessment. As shown in Figure 1B, the use of 10AB (1.5, 3.0 and 6.0 μM) resulted in a remarkable increase in the percentage of apoptotic cells (8.9% ± 1.2%, 35.6% ± 2.1%, 87.6% ± 3.47%, respectively) in comparison with the control group (2.5% ± 0.2%). These results confirmed that 10AB suppressed cancer cell growth through apoptotic induction. In our previous study, we demonstrated that the pretreatment of HL 60 cells with caspase 8 or 9 inhibitors attenuated the effect of 10AB by 13% and 27%, respectively [24]. In the current work, we further examined the relationship between caspases and the apoptotic effect induced by 10AB. Caspases 3 and 9 activation was significantly diminished with the pretreatment of a pan caspase inhibitor, Z-VAD-FMK, as confirmed by Western blotting. Additionally, pretreatment with the pan caspase inhibitor slightly diminished γH2AX induction by 10AB (Figure 1C). These results suggested that the apoptotic effect of 10AB is partially mediated through the caspase pathway. To determine whether the cytotoxic effect of 10AB is specific for cancer cells, we examined the effect of 10AB on the viability of rat alveolar macrophage NR8383 cells. Even at the highest dose (6.0 μM), 10AB treatment caused only 18.3% suppression in the viability of NR8383 cells (Figure 1D). Thus, it may be concluded that 10AB's cytotoxic effect is more specific towards HL 60 cells compared to normal macrophage NR8383 cells.

2.2. The Effect of 10AB on Topoisomerase IIα Activity

Our previous work showed that 10AB treatment could induce DNA damage in HL 60 cells as deduced from the abnormal tail size in the comet assay and the increase in H2AX phosphorylation (γH2AX) [24]. To further determine if the DNA damaging effect is associated with the interruption of topoisomerase II (topo II) activity, we utilized cell-free DNA cleavage assay using an enzyme-mediated negatively supercoiled pHOT1 plasmid DNA (Figure 2A). Lane 1 shows a linear DNA strand, which was also observed upon treating the supercoiled pHOT1 plasmid DNA with etoposide, a standard topo II poison (Lane 5) [25,26]. The use of 10AB in increasing concentrations (0, 1.5, 3.0, 6.0 and 12.0 μM) inhibited DNA relaxation and resulted in the formation of supercoiled DNA products in the presence of topo IIα (Lanes 6–9). Moreover, we observed an inhibitory effect of 10AB on topo IIα protein expression, which plays a critical role in DNA replication, transcription and chromosomal segregation [27]. Western blotting indicated that the use of 10AB (3.0 μM) significantly diminished topo IIα protein expression (Figure 2B). These results

suggested that one of 10AB's targets as a DNA damaging agent is to interfere with certain steps of the topo IIα catalytic cycle.

Figure 1. A furanoterpenoid derivative, 10AB, induces apoptosis in HL 60 cells. The cells were treated with different doses of 10AB (0, 1.5, 3.0, and 6.0 μM) for 24 h. (**A**) The treated cells were stained with DAPI. The morphological changes were examined with fluorescence microscopy; (**B**) The treated cells were stained with annexin-V/PI and examined with flow cytometry. The results are presented as means ± SD of three independent experiments and ** $p < 0.001$ indicats statistically significant differences compared with the control group (DMSO treatment); (**C**) Cells were pretreated with or without 25 μM of Z-VAD-FMK and then treated with 6.0 μM of 10AB for 24 h. Cell lysates were analyzed via immunoblotting with specific antibodies; (**D**) The viability of normal rat alveolar macrophage NR8383 cells was determined with different doses of 10AB (0, 1.5, 3.0, and 6.0 μM).

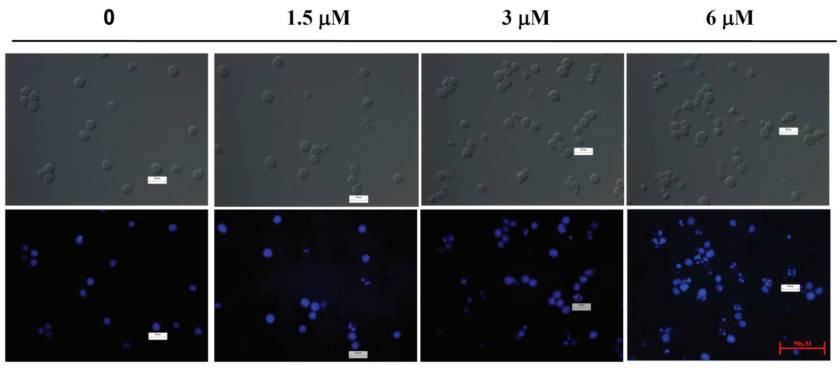

(**A**)

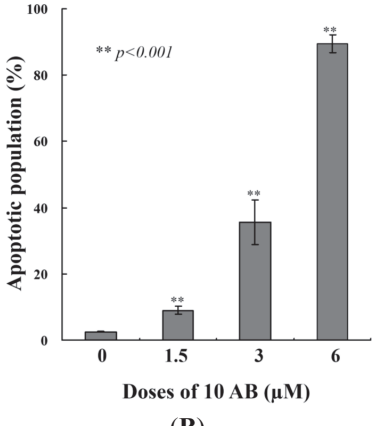

(**B**)

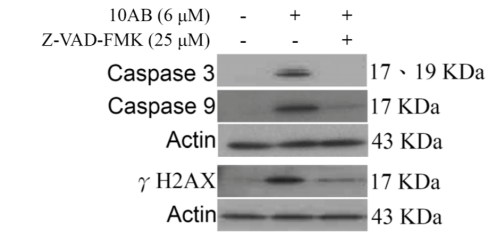

(**C**)

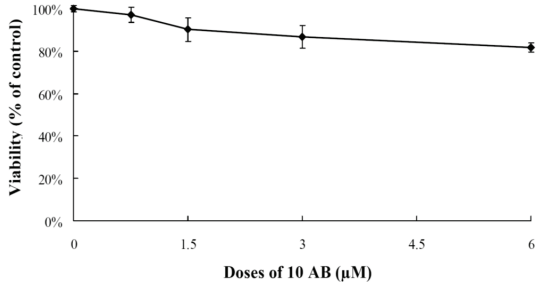

(**D**)

Figure 2. The effect of 10AB on topo IIα function. (**A**) The effect of 10AB on topo IIα mediated supercoiled pHOT1 plasmid DNA relaxation with cell-free system; (**B**) 10AB decreased the expression of topo IIα protein in HL 60 cells. HL 60 cells were treated with 10AB (0, 1.5, 3.0 and 6.0 μM) for 24 h. The protein expression of topo IIα was analyzed via Western blotting. The bands were quantified via densitometry and normalized relative to β-actin levels.

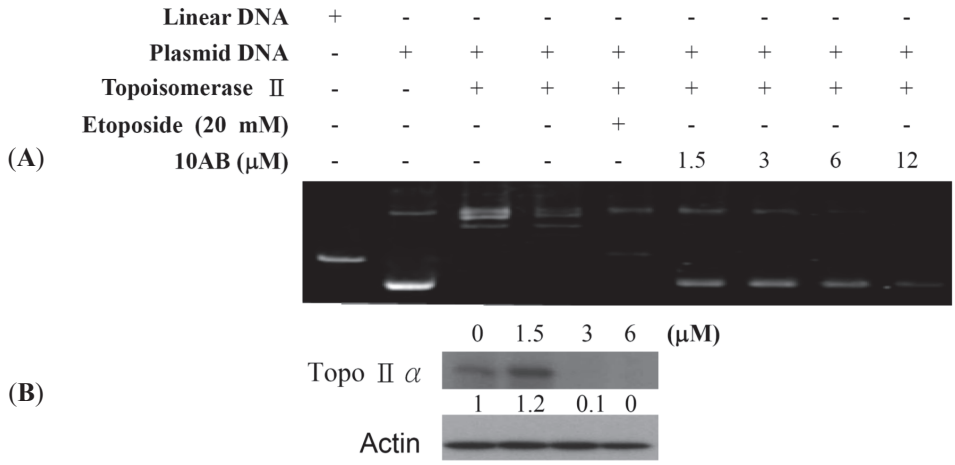

2.3. The Relationship between 10AB-Induced Apoptosis in HL 60 Cells and the Disruption in Mitochondrial Membrane Potential as well as Mitochondrial Metabolism-Related Proteins

After confirming the apoptotic effect of 10AB on HL 60 cells, it was necessary to determine the apoptotic inducer within these cells. We previously demonstrated that treating HL 60 cells with 10AB resulted in caspases 3 and 9 activation [24]. In the current work, we examined if the dysfunction in proteins related to mitochondrial membrane potential and mitochondrial metabolism is involved in 10AB apoptotic induction. JC-1 cationic dye was used to evaluate whether 10AB treatment influenced the mitochondrial membrane potential (MMP) in HL 60 cells. As shown in Figure 3A,B, the use of 10AB (1.5 μM) increased the population of HL 60 cells with disrupted membrane potential from 3.6% to 15.2%. This effect was dramatically increased upon treatment with 10AB at 3.0 and 6.0 μM, which resulted in 80.0% ± 3.0% and 95.2% ± 1.8% cells with disturbed MMP, respectively (** $p < 0.001$). To further explore the mechanism of 10AB-induced apoptosis, the effect of 10AB on apoptotic- and mitochondrial metabolism-related proteins was evaluated. As shown in Figure 3C, 10AB treatment suppressed the anti-apoptotic proteins (Bcl-2 and Bcl-xL), caspase inhibitor (XIAP), and survivin. Concomitantly, 10AB treatment increased the dysfunction of DNA repair genes (PARP cleavage), cytochrome *c* concentration, and the pro-apoptotic protein Bax. Moreover, treatment of leukemia HL 60 cells with different concentrations of 10AB diminished the expression of p-Akt (Ser^{473}), p-PTEN (Ser^{380}), Src, hexokinase II, and PKM 2, but enhanced the expression of p-ERK, p-38, p-JNK, and p-GSK 3β(Ser^{9}) (Figure 3D). In agreement with the results of Western blotting experiments, images

from confocal scanning laser microscopy demonstrated that treatment with 10AB (1.5 or 3.0 μM) was able to enhance the fluorescence of cytochrome *c*. When HL 60 cells were treated with DMSO for 24 h, cytochrome *c* was largely localized in the mitochondria, as revealed by the yellow-orange staining in the overlay. This indicated that green fluorescence (MitoTracker Green) derived from mitochondria and the cytochrome *c*-associated red fluorescence co-localized. Treatment with 10AB (1.5 or 3.0 μM) resulted in the release of cytochrome *c* from the mitochondria into the cytosol, as demonstrated by the appearance of the red fluorescence in the cytoplasm (Figure 3E). This cytochrome *c*-associated red fluorescence was considerably more discernible in HL 60 cells treated with 3.0 μM 10AB than in the control group. These results indicated that 10AB treatment could release cytochrome *c* in HL 60 cells. To further elucidate the apoptotic induction mechanism, we examined the effect of 10AB treatment on Bax conformational change. Previous studies indicated that conformational change of Bax could be induced by several types of apoptotic stimuli [28]. This conformational change can be detected with anti-Bax6A7, which recognizes only the activation/pro-apoptotic form of Bax [29]. We conducted an immunoprecipitation experiment to determine if 10AB treatment could enhance the expression of the active form of Bax. As shown in Figure 3F, 10AB treatment increased the active form of Bax, suggesting that apoptosis induced by 10AB involves Bax activation.

Figure 3. Apoptotic induction induced by 10AB involves mitochondrial dysfunction. The effect of 10AB treatment on the mitochondrial membrane potential (MMP) in HL 60 cells was evaluated. (**A**,**B**) Cells were treated with 10AB (1.5, 3.0, and 6.0 μM) for 24 h. Quantitative results showed a significant increase in HL 60 cells with disturbed MMP in response to the use of 10AB. Results are presented as means ± SD of three independent experiments (** $p < 0.01$; *** $p < 0.001$). The effect of 10AB on the expression of apoptotic; (**C**) and mitochondrial metabolism; (**D**) related proteins in HL 60 cells. The bands were quantified via densitometry and normalized to β-actin levels; (**E**) Merged images of Mitotracker with cytochrome *c* immunofluorescence suggested that the increase in cytochrome *c* was the direct effect of 10AB treatment at 1.5 of 3 μM; (**F**) Cell lysates were subjected to immunoprecipitation with anti-Bax6A7 antibody and analyzed by immunoblotting with anti-Bax antibody.

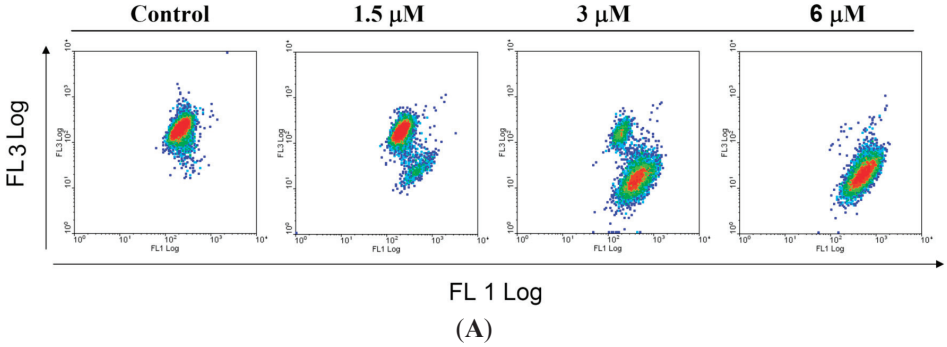

(**A**)

Figure 3. *Cont.*

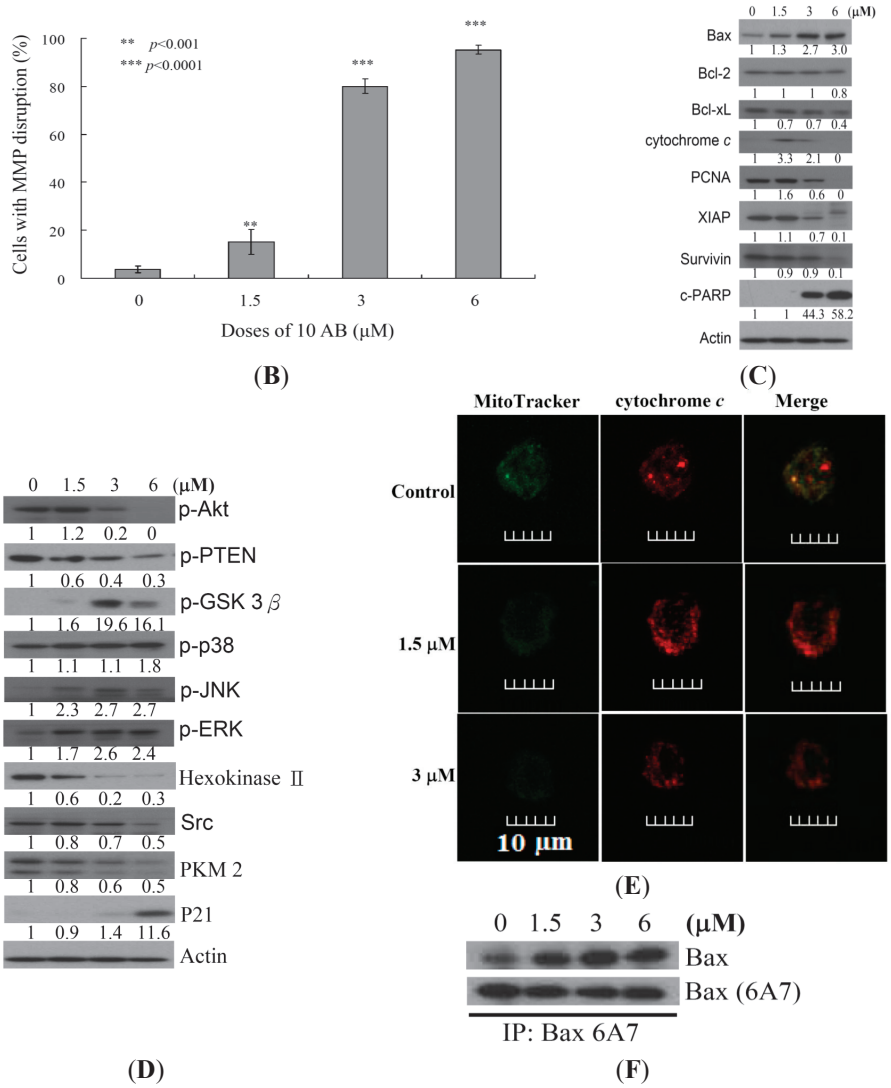

2.4. The Relationship between 10AB-Induced Apoptosis and ROS Generation

To examine whether the 10AB-induced apoptosis in HL 60 cells involves the overproduction of ROS, we determined the levels of ROS at different times following 10AB treatment. A time-dependent increase in ROS generation was monitored using the carboxy derivative of fluorescein, carboxy-H_2DCFDA dye. As shown in Figure 4A,10AB treatment (3.0 μM) for 15, 30, 60, 120 and 180 min resulted in 1.60-, 1.67-, 1.77-, 1.89- and 2.1-fold increase in the ROS levels, respectively, as compared with the mean fluorescence index (MFI) of the control. To clarify whether ROS generation is the major regulator in 10AB-induced apoptosis, HL 60 cells were pretreated with NAC, a ROS scavenger, aiming to suppress the intracellular oxidative stress. The

apoptotic population was measured via annexin V/PI staining following 10AB treatment. As shown in Figure 4B, the result of NAC treatment is similar to the negative control group showing less than 5% of the apoptotic population. In addition, NAC pretreatment diminished the apoptotic cell population from 35.6% and 89.5% to 9.3% and 25% in response to the use of 3.0 and 6.0 μM of 10AB, respectively. These results indicated that blocking oxidative stress by NAC resulted in saving HL 60 from apoptosis induced by 10AB. To further confirm if MMP disruption induced by 10AB is initiated by ROS overproduction, we determined the population of cells with disturbed MMP in response to 10AB treatment with or without NAC pretreatment. The determination of the cell population with disturbed MMP was achieved utilizing a cationic dye, JC-1 (Figure 4C).Cells were divided into four groups, in which two groups were only treated with 3.0 and 6.0 μM of 10AB,whereas the other two groups were treated with NAC (3.0 mM) followed by 3.0 or 6.0 μM of 10AB. After 24 h, the change in the population of cells with disturbed MMP was analyzed in the four groups. The NAC pretreatment diminished the population of cells with disturbed MMP from 80.0% and 95.3% to 17.4% and 20.7% in response to the treatment with 3 and 6 μM of 10AB, respectively. In agreement with the preceding results of annexin V/PI staining, these findings indicate that the cytotoxic effect of 10AB in HL 60 is mediated through apoptotic induction as well as mitochondrial dysfunction and this effect is highly influenced by ROS production.

Figure 4. The apoptotic induction of 10AB in HL 60 cells involves ROS production. We evaluated the effect of the 10AB treatment on ROS generation in HL 60 cells. (**A**) Cells were treated with 10AB (6.0 μM) for the indicated times. Quantitative results showed a gradual increase in the ROS production in response to the 10AB treatment when compared with the control group. We also evaluated the effect of ROS generation on the 10AB-induced apoptosis in HL 60 cells. Cells were pretreated with 3.0 mM NAC for 2 h, then treated with 3.0 or 6.0 μM of 10AB; The apoptotic populations (**B**) and the disruption of MMP (**C**) were examined with annexin-V/PI and JC-1 staining assay. Results are presented as mean ± SD of three independent experiments (** $p < 0.001$).

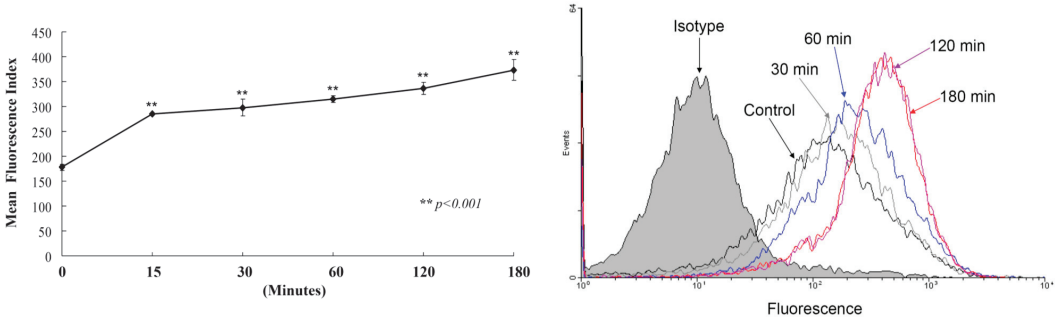

(**A**)

Figure 4. *Cont.*

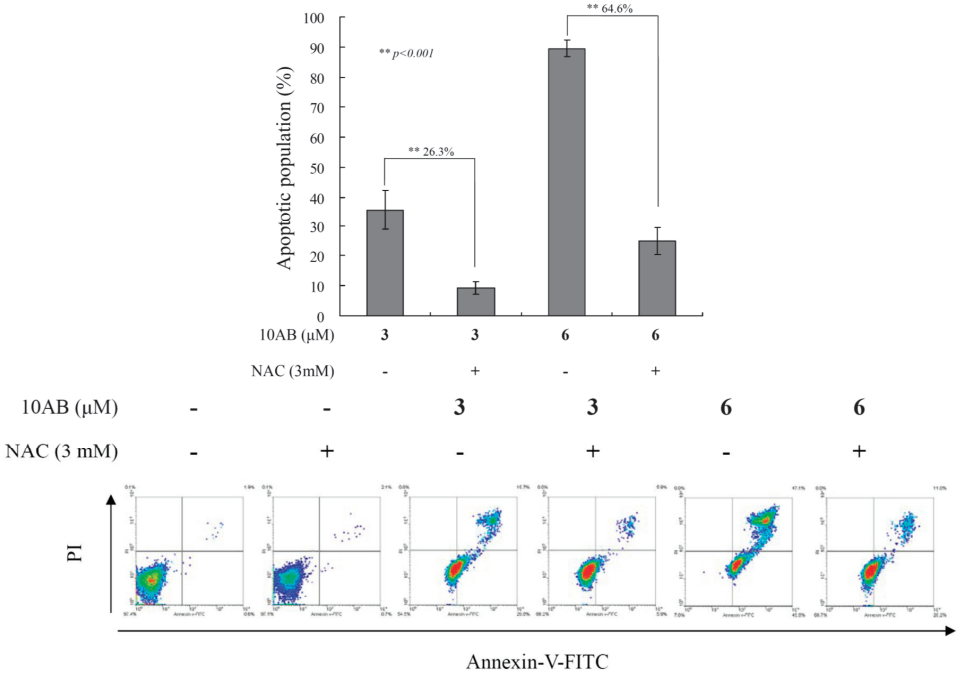

(B)

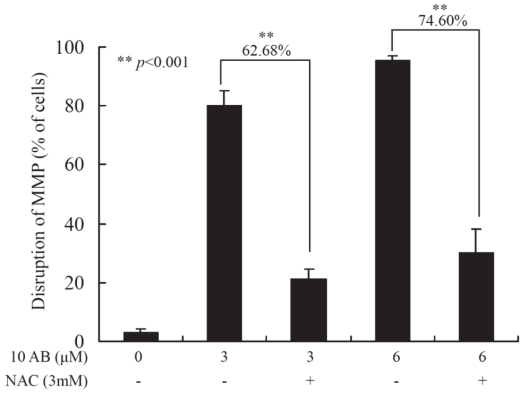

(C)

3. Discussion

Our previous work suggested that the natural marine furanoterpenoid derivative, 10AB, exhibited potent cytotoxic activity in several cancer cell lines, including DLD-1, Hep G2 and 3B, and K 562 cells [23,24]. It was found that the antiproliferative activity of 10AB was mediated through the induction of DNA damage and apoptosis in leukemia HL 60 cells [24]. The DNA damaging effect of 10AB was demonstrated by the induction of H2AX phosphorylation (γH2AX) and the increase of tail movement in the comet assay, suggesting increased DSBs [24]. In the

current study, we tried to uncover other regulatory mechanisms involved in 10AB-induced apoptosis. Our results indicated that the induction of γH2AX caused by 10AB was slightly diminished by the pretreatment with a pan caspase inhibitor, Z-VAD-FMK (Figure 1C). These findings suggested that the apoptotic effect of 10AB was partially mediated through the caspase pathway. This effect was also observed in certain cytotoxic drugs that induce apoptosis, partially through the caspase-mediated pathway [30]. Furthermore, we studied the effect of 10AB on DNA topoisomerase II, ROS generation, MMP, and apoptotic- and mitochondrial metabolism-related proteins. DNA topoisomerase II inhibitors have emerged as a promising class of cancer chemotherapeutics, targeting cancer cells through the induction of DSBs [31]. Etoposide, doxorubicin, and mitoxantrone are clinically approved anticancer drugs, which are known as the first class of DNA topoisomerase II inhibitors. It was found that these drugs can stabilize a cleavage complex in DNA, leading to topo II mediated chromosome DNA breakage [27,32]. Because these agents generate a "lesion" that includes DNA strand breaks and proteins covalently bound to DNA, they have been known as topo II poisons. Unfortunately, in certain cases, the use of these agents has resulted in serious drawbacks, including the induction of secondary malignancies [33–36]. On the other hand, the second class of DNA topo II inhibitors only diminished the enzymatic activity of topo II proteins [27]. To study the effect of 10AB on topo II, we utilized a cell-free DNA cleavage assay. It was found that even at the lowest concentration, 10AB completely inhibited the formation of DNA relaxation (Figure 2A). These results were further confirmed through the elimination of topo II protein expression in response to 10AB (3.0 and 6.0 μM) treatment, as shown in Figure 2B. These findings indicated that the apoptotic effect of 10AB was partially mediated through the inhibition of topo II activity in human acute promyelocytic leukemia HL 60 cells. Unlike etoposide, 10AB can be developed as a topo II catalytic inhibitor, avoiding the side effects of topo II poisons.

Another factor in the cellular survival mechanism that has recently attracted attention is the proliferating cell nuclear antigen (PCNA). It is a nuclear factor protein and a proliferation marker involved in the repair of proliferating cells, DNA replication, and in the regulation of cellular survival pathways [37]. PCNA and other proteins, including p21, cdc/cyclin B1, and MAPKs, are stress response kinases, which are involved in cell cycle regulation. Recent studies have suggested that Gadd45 proteins, which act as stress sensors, are mediated by a complex interplay of physical interactions with stress response kinases [38,39]. Cells that are deficient in Gadd45 proteins are more sensitive to radio- and chemotherapy (ultraviolet radiation, VP-16, and daunorubicin) induced apoptosis compared to wild-type (wt) cells [39]. Interaction of Gadd45 with PCNA or histone or both might play a role in epigenetic gene activation through DNA repair-mediated demethylation [40]. Although cancer cells have the capability to repair DNA damage, extensive fragmentation can lead to the activation of apoptotic triggers [41]. Our results suggested that the elimination of PCNA expression and the induction of PARP dysfunction were the major contributors to 10AB-induced DNA damage in HL 60 cells (Figure 3C).

Moving to another target in the apoptotic pathway, we investigated the interplay between mitochondria and apoptosis [42]. Previous reports have indicated that chemotherapeutic induction of mitochondrial oxidative stress results in the activation of GSK and Bax, phosphorylation of its

chaperone cyclophilin D, and in the facilitation of permeability transition poreopening [43]. Furthermore, a conformational change as a consequence of the exposure of 6A7 epitope in the *N*-terminus (amino acids 13–19) has been suggested to activate the pro-apoptotic function of Bax [44]. The active form of Bax (Bax mutant with the 6A7 epitope conformational change) can be inserted efficiently into the mitochondrial membrane, resulting in cytochrome *c* release, which is one of the key steps in the apoptotic induction mediated by caspase activation in mammalian cells. A previous investigation has suggested that intracellular ROS production is an upstream factor for Bax activation and cytochrome *c* release [45]. In 2011, McCubrey *et al*. [46] proposed that the Ras/Raf/mitogen-activated protein kinase (MEK)/extracellular signal-regulated kinase (ERK) pathway contributes to the sensitivity and resistance of leukemia cells in response to chemotherapy. It was found that the Ras/Raf/MEK/ERK pathway can be activated by chemotherapeutic drugs commonly used in leukemia therapy. The potent cytotoxic activity of 10AB against leukemia cancer cells has encouraged us to investigate its effect on the Ras/Raf/MEK/ERK pathway. We found that 10AB at 3.0 and 6.0 μM resulted in an increase in the percentage of apoptotic cells with perturbed MMP reaching 80.0% and 95.2%, respectively. As shown in Figure 3C,D, 10AB treatment up-regulated Bax activation and cytochrome *c* release as well as ERK, p-38, JNK, and GSK 3β. Concomitantly, 10AB down-regulated the phosphorylation of PTEN and Akt. Based on these findings, it is clear that 10AB targets the Ras/Raf/MEK/ERK and PI3K/PTEN/Akt/mTOR pathways, which implies a potential to block the survival pathways and induce the apoptotic pathways.

Our results were in agreement with previous reports suggesting that the increase in the release of cytochrome *c*, GSK phosphorylation at Ser 9, and the induction of Bax conformational change are the major contributors to the mitochondrial collapse in cancer cells induced by 10AB [42–46]. As outlined above, 10AB treatment elevated intracellular oxidative stress, which interrupted mitochondrial metabolism and triggered apoptosis in HL 60 cells. Based on the Warburg effect, cancer cells entirely reprogram their metabolism to sustain hyperproliferation and mostly rely on glycolysis rather than oxidative phosphorylation for ATP production [47]. Hexokinases (HK) are over-expressed in many tumor cells, contributing to the enhanced tumor capacity for oxidative glycolysis and apoptosis suppression [48,49]. Notably, these proteins are the rate-limiting glycolytic enzymes in the irreversible first step of the glycolysis [49–51]. Gall *et al.* proposed that the loss of mitochondrial HK II is clearly associated with mitochondrial Bax accumulation, AIF release, and caspase 3 activation, resulting in apoptotic cell death [3]. Our findings were consistent with previous reports suggesting that the elimination of proteins related to mitochondrial metabolism, such as HK II, PKM 2, and Src, participates in the 10AB-induced mitochondrial dysfunction via oxidative stress.

Our work suggests that 10AB is a potent cytotoxic agent against acute myelocytic leukemia, which is one of the most common and progressive malignancies among malignant hematopoiesis. Several chemotherapeutic agents have been developed that target this aggressive disease with mediocre results. The need for additional chemotherapeutics is becoming increasingly vital; however, the number of the newly developed candidates has been on the wane. Recently, the clinical application of all-*trans* retinoic acid in acute promyelocytic leukemia, which targets the effect of peroxiredoxins as a defensive mechanism in cancer cells against oxidative stress, has

offered mixed results [52]. We think that the activity of 10AB against specific molecular targets in HL 60 cells offers a promising alternative to be further developed and optimized as a potential candidate for the treatment of acute myelocytic leukemia.

4. Experimental Section

4.1. Bioassays Materials

HL 60 (human promyelocytic leukemia) cells were obtained from the American Type Culture Collection (ATCC, Manassas, VA, USA). Cells were maintained in RPMI 1640 medium supplemented with 10% fetal calf serum, 2 mM glutamine, and antibiotics (100 units/mL penicillin and 100 μg/mL streptomycin) at 37 °C in a humidified atmosphere of 5% CO_2. RPMI 1640 medium, fetal calf serum (FCS), trypan blue, penicillin G, and streptomycin were obtained from Gibco BRL (Gaithersburg, MD, USA). Dimethyl sulfoxide (DMSO), 3-(4,5-dimethylthiazol-2-yl)-2,5-diphenyl-tetrazolium bromide (MTT), and all other chemicals were purchased from Sigma-Aldrich (St. Louis, MO, USA). Antibodies against c-PARP, p-PTEN (Ser^{380}), p-GSK 3β (Ser^{9}), p-Akt (Ser^{473}), hexokinase, p-ERK, p-p38, p-JNK, PCNA, PKM2, and Src were purchased from Cell Signaling Technologies (Beverly, MA, USA). Antibodies for Bax, Bcl-2, Bcl-xL, cytochrome *c*, survivin, topoisomerase IIα, and XIAP were obtained from Santa Cruz Biotechnology (Santa Cruz, CA, USA). JC-1 cationic dye and the carboxy derivative of fluorescein (carboxy-H_2DCFDA) were purchased from Molecular Probes and Invitrogen technologies (Carlsbad, CA, USA). Anti-mouse and rabbit IgG peroxidase-conjugated secondary antibody were purchased from Pierce (Rockford, IL, USA). The annexin V-FITC/PI (propidium iodide) kit was from Strong Biotech Corporation (Taipei, Taiwan). Hybond ECL transfer membrane and ECL Western blotting detection kits were obtained from Amersham Life Sciences (Amersham, UK).

4.2. Preparation of 10-Acetylirciformonin B (10AB) Stock Solution

10-Acetylirciformonin B was isolated and purified from the marine sponge, *Ircinia* sp. and its chemical structure was identified by the interpretation of its spectral data (1H-NMR, 13C-NMR, and 2D NMR), as previously described [23]. This compound was dissolved in DMSO at a concentration of 6 μM and diluted before used.

4.3. MTT Proliferation Assay

Cells were seeded at 4×10^4 per well in 96-well culture plates before treatment with different concentrations of the tested compound [26]. After treatment for 24, 48, or 72 h, the cytotoxicity of the tested compound was determined using the MTT cell proliferation assay (thiazolyl blue tetrazolium bromide, Sigma-M2128). Light absorbance values ($OD = OD_{570} - OD_{620}$) were recorded at 570 and 620 nm using an ELISA reader (AnthosLabtec Instrument, Salzburg, Austria)for calculating the concentration that caused 50% inhibition (IC_{50}), *i.e.*, the cell concentration at which the light absorbance value of the experimental group is half that of the

control group. These results were expressed as a percentage of the control ± SD established from $n = 4$ wells per experiment from three independent experiments.

4.4. Annexin V/PI Apoptosis Assay

The externalization of phosphatidylserine (PS) and membrane integrity were quantified using an annexin V-FITC staining kit [26]. In brief, 10^6 cells were grown in 35 mm diameter plates and were labeled with annexin V-FITC (10 µg/mL) and PI (20 µg/mL) prior to harvesting. After labeling, all plates were washed with a binding buffer and harvested. Cells were resuspended in the binding buffer at a concentration of 2×10^5 cells/mL before assessment on a FACS-Calibur flow cytometer (Beckman Coulter, Taipei, Taiwan) and analysis with CellQuest software. Approximately 10,000 cells were counted for each determination.

4.5. Determination of ROS Generation, and MMP Disruption

These assays were performed as described previously[26]. MMP disruption and ROS generation were detected with JC-1 cationic dye (5 µg/mL) and the carboxy derivative of fluorescein (carboxy-H_2DCFDA, 1.0 mM), respectively. In brief, the treated cells were labeled with a specific fluorescent dye for 30 min. After labeling, cells were washed with PBS and resuspended in PBS at a concentration of 1×10^6 cells/mL before analysis via flow cytometry.

4.6. Assay of Topoisomerase II Catalytic Inhibitors and Poisons

The assay was performed as described previously [25,26]. Standard relaxation reaction mixtures (20 µL) containing 50 mM Tris–HCl (pH 8.0), 10 mM $MgCl_2$, 200 mM potassium glutamate, 10 mM dithiothreitol, 50 µg/mL bovine serum albumin, 1 mM ATP, 0.3 µg of pHOT1 plasmid DNA, two units of human topoisomerase II (Topogen, Columbus, OH, USA), and the indicated concentrations of etoposide and 10AB were incubated at 37 °C for 30 min. Reactions were terminated by adding 2 µL of 10% SDS to facilitate trapping the enzyme in a cleavage complex, followed by the addition of 2.5 µL of proteinase K (50 µg/mL) to digest the bound protein (incubated at 37 °C for 15 min) and finally by adding 0.1 volume of the sample loading dye. The DNA products were analyzed via electrophoresis through vertical 2% agarose gels at 2 voltages/cm in 0.5× TAE buffer. Gels were stained with ethidium bromide and photographed using an Eagle Eye II system (Stratagene, La Jolla, CA, USA).

4.7. Co-Immunoprecipitaion and Western Blotting

Cell lysates were prepared by treating the cells for 30 min in RIPA lysis buffer, 1% Nonidet P-40, 0.5% sodium deoxycholate, 0.1% sodium dodecyl sulfate (SDS), 1 mM sodium orthovanadate, 100 µg/mL phenylmethylsulfonyl fluoride, and 30 µg/mL aprotinin (all chemicals were obtained from Sigma Aldrich). The lysates were centrifuged at 20,000×*g* for 30 min, and the protein concentration in the supernatant was determined using a BCA protein assay kit (Pierce, Rockford, IL, USA). Proteins were immunoprecipitated with the indicated antibodies. The precleared protein

A/G PLUS-agarose beads (Santa Cruz Biotechnology, Santa Cruz, CA, USA) were incubated with immunocomplexes and washed with the lysis buffer. Equal amounts of proteins were separated on 7.5%, 10% or 12% gels via SDS-polyacrylamide gel electrophoresis and were subsequently electrotransferred to a PVDF membrane. The membrane was blocked with a solution containing 5% non-fat dry milk TBST buffer (20 mM Tris-HCl, pH 7.4, 150 mM NaCl, and 0.1% Tween 20) for 1 h and washed with TBST buffer. Protein expression was monitored by immunoblotting assay using specific antibodies. These proteins were detected by an enhanced chemiluminescence kit (Pierce). Quantitation of protein expression was performed using Image J software (National Institutes of Health, Bethesda, MD, USA).

4.8. Immunofluorescence Analysis

After treatment with 10AB, cells were stained with 200 μM of Mitotracker for 30 min, fixed with 4% paraformaldehyde in 50 mM HEPES buffer (pH 7.3) for 30 min, and permeabilized for 20 min with 0.2% Trition X-100 in PBS (pH 7.4). To prevent non-specific protein binding, cells were incubated with 5% BSA in PBS containing 0.05% Trition X-100 (T-PBS) for 1 h at room temperature. The cells were then incubated with the primary cytochrome *c* antibodies (1:250) for 2 h and further with secondary antibodies (Alexa Fluor 586-conjugated goat anti-mouse IgG (H + L), Life Technologies, Carlsbad, CA, USA) diluted at 1:1000 for 1 h at room temperature. After washing with PBS, cells were observed under a FV1000 confocal laser scanning microscope (Olympus, Tokyo, Japan).

4.9. Statistics

The results were expressed as means ± standard deviation (SD). Comparison in each experiment was performed using an unpaired Student's *t*-test and a *p* value of less than 0.05 was considered to be statistically significant (* $p < 0.05$; ** $p < 0.01$; ** $p < 0.001$).

5. Conclusions

In the current study, we investigated the molecular targets of the cytotoxic furanoterpenoid derivative, 10AB, isolated from the marine sponge *Ircinia* sp. This furanoterpenoid derivative proved to be an interesting cytotoxic agent through its potent activity in several cancer cell lines with special selectivity for human acute myelocytic leukemia HL 60 cells [23,24]. Evaluation of the molecular targets of 10AB in HL 60 cells indicated that this compound suppressed topo IIαactivity and led to the accumulation of intracellular ROS followed by mitochondrial dysfunction. It also activated the expression of caspases and pro-apoptotic proteins. Moreover, it suppressed anti-apoptotic proteins, caspase inhibitors, XIAP, and survivin, which eventually led to apoptotic cell death. Scavenging ROS with NAC diminished the disruption of mitochondrial membrane potential and suppressed the apoptotic effect induced by 10AB treatment. Our results clearly suggested that the 10AB-induced mitochondrial apoptosis is directly mediated through ROS overproduction and mitochondrial dysfunction. These findings will provide opportunities for the future development of 10AB as a potential anti-cancer agent.

Acknowledgments

This research was partially supported by grants from the National Museum of Marine Biology and Aquarium (Grant No. 102200224) and the National Science Council (NSC 101-2320-B-259-001-MY3 & NSC 101-2325-B-291-001) awarded to Mei-Chin Lu and Ping-Jyun Sung. Other grants which supported this work include the NSC grants (NSC 103-2911-I-002-303 and NSC 101-2325-B-039-004), the grant from the National Health Research Institutes (NHRI-EX102-10241B1) and in part from the grant from Chinese Medicine Research Center, China Medical University (the Ministry of Education, the Aim for the Top University Plan) awarded to Yang-Chang Wu.

Author Contributions

Huei-Chuan Shih participated in evaluating the cytotoxic activity of 10AB and its effect on apoptotic proteins. Mohamed El-Shazly participated in the interpretation of the results and in writing the manuscript. Yung-Shun Juan participated in studying the effect of 10AB on mitochondrial membrane potential as well as mitochondrial metabolism-related proteins. Chao-Yuan Chang participated on studying the relation between 10AB and ROS generation. Jui-Hsin Su, Yu-Cheng Chen, Shou-Ping Shih participated in the collection of *Ircinia* sp. as well as isolation, purification and structural elucidation of 10AB. Huei-Mei Chen participated in studying the effect of 10AB on Topoisomerase IIα. Yang-Chang Wu and Mei-Chin Lu planned and guided the research as well as participated in the interpretation of results and writing the manuscript.

Conflicts of Interest

The authors declare no conflict of interest.

References

1. Cairns, R.A.; Harris, I.S.; Mak, T.W. Regulation of cancer cell metabolism. *Nat. Rev. Cancer* **2011**, *11*, 85–95.
2. Tatarkova, Z.; Kuka, S.; Petras, M.; Racay, P.; Lehotsky, J.; Dobrota, D.; Kaplan, P. Why mitochondria are excellent targets for cancer therapy. *Klin. Onkol.* **2012**, *25*, 421–426.
3. Gall, J.M.; Wong, V.; Pimental, D.R.; Havasi, A.; Wang, Z.; Pastorino, J.G.; Bonegio, R.G.; Schwartz, J.H.; Borkan, S.C. Hexokinase regulates Bax-mediated mitochondrial membrane injury following ischemic stress. *Kidney Int.* **2011**, *79*, 1207–1216.
4. Gogvadze, V.; Orrenius, S.; Zhivotovsky, B. Mitochondria as targets for chemotherapy. *Apoptosis* **2009**, *14*, 624–640.
5. Fogg, V.C.; Lanning, N.J.; Mackeigan, J.P. Mitochondria in cancer: At the crossroads of life and death. *Chin. J. Cancer* **2011**, *30*, 526–539.
6. Gasparre, G.; Porcelli, A.M.; Lenaz, G.; Romeo, G. Relevance of mitochondrial genetics and metabolism in cancer development. *Cold Spring Harb. Persp. Biol.* **2013**, *5*, doi:10.1101/cshperspect.a011411.

7. Patra, K.C.; Wang, Q.; Bhaskar, P.T.; Miller, L.; Wang, Z.; Wheaton, W.; Chandel, N.; Laakso, M.; Muller, W.J.; Allen, E.L.; *et al.* Hexokinase 2 is required for tumor initiation and maintenance and its systemic deletion is therapeutic in mouse models of cancer. *Cancer Cell* **2013**, *24*, 213–228.
8. Wenner, C.E. Cell signaling and cancer-possible targets for therapy. *J. Cell. Physiol.* **2010**, *223*, 299–308.
9. Arora, K.K.; Pedersen, P.L. Functional significance of mitochondrial bound hexokinase in tumor cell metabolism. Evidence for preferential phosphorylation of glucose by intramitochondrially generated ATP. *J. Biol. Chem.* **1988**, *263*, 17422–17428.
10. Shulga, N.; Wilson-Smith, R.; Pastorino, J.G. Hexokinase II detachment from the mitochondria potentiates cisplatin induced cytotoxicity through a caspase-2 dependent mechanism. *Cell Cycle* **2009**, *8*, 3355–3364.
11. Mathupala, S.P.; Ko, Y.H.; Pedersen, P.L. The pivotal roles of mitochondria in cancer: Warburg and beyond and encouraging prospects for effective therapies. *Biochim. Biophys. Acta* **2010**, *1797*, 1225–1230.
12. Murphy, M.P.; Holmgren, A.; Larsson, N.G.; Halliwell, B.; Chang, C.J.; Kalyanaraman, B.; Rhee, S.G.; Thornalley, P.J.; Partridge, L.; Gems, D.; *et al.* Unraveling the biological roles of reactive oxygen species. *Cell. Metab.* **2011**, *13*, 361–366.
13. Kim, K.Y.; Yu, S.N.; Lee, S.Y.; Chun, S.S.; Choi, Y.L.; Park, Y.M.; Song, C.S.; Chatterjee, B.; Ahn, S.C. Salinomycin-induced apoptosis of human prostate cancer cells due to accumulated reactive oxygen species and mitochondrial membrane depolarization. *Biochem. Biophys. Res. Commun.* **2011**, *413*, 80–86.
14. Circu, M.L.; Aw, T.Y. Reactive oxygen species, cellular redox systems, and apoptosis. *Free Radic. Biol. Med.* **2010**, *48*, 749–762.
15. Bauer, G. Tumor cell-protective catalase as a novel target for rational therapeutic approaches based on specific intercellular ROS signaling. *Anticancer Res.* **2012**, *32*, 2599–2624.
16. Martindale, J.L.; Holbrook, N.J. Cellular response to oxidative stress: Signaling for suicide and survival. *J. Cell. Physiol.* **2002**, *192*, 1–15.
17. Mates, J.M.; Segura, J.A.; Alonso, F.J.; Marquez, J. Oxidative stress in apoptosis and cancer: An update. *Arch. Toxicol* **2012**, *86*, 1649–1665.
18. Azad, N.; Iyer, A.; Vallyathan, V.; Wang, L.; Castranova, V.; Stehlik, C.; Rojanasakul, Y. Role of oxidative/nitrosative stress-mediated Bcl-2 regulation in apoptosis and malignant transformation. *Ann. N. Y. Acad. Sci.* **2010**, *1203*, 1–6.
19. Clement, M.V.; Hirpara, J.L.; Pervaiz, S. Decrease in intracellular superoxide sensitizes Bcl-2-overexpressing tumor cells to receptor and drug-induced apoptosis independent of the mitochondria. *Cell Death Differ.* **2003**, *10*, 1273–1285.
20. Macip, S.; Igarashi, M.; Berggren, P.; Yu, J.; Lee, S.W.; Aaronson, S.A. Influence of induced reactive oxygen species in p53-mediated cell fate decisions. *Mol. Cell. Biol.* **2003**, *23*, 8576–8585.

21. Llovet, J.M.; Di Bisceglie, A.M.; Bruix, J.; Kramer, B.S.; Lencioni, R.; Zhu, A.X.; Sherman, M.; Schwartz, M.; Lotze, M.; Talwalkar, J.; *et al.* Design and endpoints of clinical trials in hepatocellular carcinoma. *J. Natl. Cancer Inst.* **2008**, *100*, 698–711.
22. Yap, T.A.; Workman, P. Exploiting the cancer genome: Strategies for the discovery and clinical development of targeted molecular therapeutics. *Ann. Rev. Pharmacol. Toxicol.* **2012**, *52*, 549–573.
23. Su, J.H.; Tseng, S.W.; Lu, M.C.; Liu, L.L.; Chou, Y.; Sung, P.J. Cytotoxic C21 and C22 terpenoid-derived metabolites from the sponge *Ircinia* sp. *J. Nat. Prod.* **2011**, *74*, 2005–2009.
24. Su, J.H.; Chang, W.B.; Chen, H.M.; El-Shazly, M.; Du, Y.C.; Kung, T.H.; Chen, Y.C.; Sung, P.J.; Ho, Y.S.; Kuo, F.W.; *et al.* 10-Acetylirciformonin B, a sponge furanoterpenoid, induces DNA damage and apoptosis in leukemia cells. *Molecules* **2012**, *17*, 11839–11848.
25. Du, Y.C.; Chang, F.R.; Wu, T.Y.; Hsu, Y.M.; El-Shazly, M.; Chen, C.F.; Sung, P.J.; Lin, Y.Y.; Lin, Y.H.; Wu, Y.C.; *et al.* Antileukemia component, dehydroburicoic acid from *Antrodia camphorata* induces DNA damage and apoptosis *in vitro* and *in vivo* models. *Phytomedicine* **2012**, *19*, 788–796.
26. Su, J.H.; Chen, Y.C.; El-Shazly, M.; Du, Y.C.; Su, C.W.; Tsao, C.W.; Liu, L.L.; Chou, Y.; Chang, W.B.; Su, Y.D.; *et al.* Towards the Small and the Beautiful: A Small Dibromotyrosine Derivative from *Pseudoceratina* sp. Sponge Exhibits Potent Apoptotic Effect through Targeting IKK/NFkappaB Signaling Pathway. *Mar. Drugs* **2013**, *11*, 3168–3185.
27. Nitiss, J.L. Targeting DNA topoisomerase II in cancer chemotherapy. *Nat. Rev. Cancer* **2009**, *9*, 338–350.
28. Zheng, Y.; Yamaguchi, H.; Tian, C.; Lee, M.W.; Tang, H.; Wang, H.-G.; Chen, Q. Arsenic trioxide (As_2O_3) induces apoptosis through activation of Bax in hematopoietic cells. *Oncogene* **2005**, *24*, 3339–3347.
29. Gardai, S.J.; Hildeman, D.A.; Frankel, S.K.; Whitlock, B.B.; Frasch, S.C.; Borregaard, N.; Marrack, P.; Bratton, D.L.; Henson, P.M. Phosphorylation of Bax Ser184 by Akt regulates its activity and apoptosis in neutrophils. *J. Biol. Chem.* **2004**, *279*, 21085–21095.
30. Zhou, H.; Xu, M.; Gao, Y.; Deng, Z.; Cao, H.; Zhang, W.; Wang, Q.; Zhang, B.; Song, G.; Zhan, Y. Matrine induces caspase-independent program cell death in hepatocellular carcinoma through bid-mediated nuclear translocation of apoptosis inducing factor. *Mol. Cancer* **2014**, *13*, doi:10.1186/1476-4598-13-59.
31. Pang, B.; Qiao, X.; Janssen, L.; Velds, A.; Groothuis, T.; Kerkhoven, R.; Nieuwland, M.; Ovaa, H.; Rottenberg, S.; van Tellingen, O.; *et al.* Drug-induced histone eviction from open chromatin contributes to the chemotherapeutic effects of doxorubicin. *Nat. Commun.* **2013**, *4*, doi:10.1038/ncomms2921.
32. Wu, C.C.; Li, T.K.; Farh, L.; Lin, L.Y.; Lin, T.S.; Yu, Y.J.; Yen, T.J.; Chiang, C.W.; Chan, N.L. Structural basis of type II topoisomerase inhibition by the anticancer drug etoposide. *Science* **2011**, *333*, 459–462.
33. Ratain, M.J.; Rowley, J.D. Therapy-related acute myeloid leukemia secondary to inhibitors of topoisomerase II: From the bedside to the target genes. *Ann. Oncol.* **1992**, *3*, 107–111.

34. Roulston, D.; Anastasi, J.; Rudinsky, R.; Nucifora, G.; Zeleznik-Le, N.; Rowley, J.D.; McGavran, L.; Tsuchida, M.; Hayashi, Y. Therapy-related acute leukemia associated with t(11q23) after primary acute myeloid leukemia with t(8;21): A report of two cases. *Blood* **1995**, *86*, 3613–3614.
35. Kudo, K.; Yoshida, H.; Kiyoi, H.; Numata, S.; Horibe, K.; Naoe, T. Etoposide-related acute promyelocytic leukemia. *Leukemia* **1998**, *12*, 1171–1175.
36. Pedersen-Bjergaard, J.; Philip, P.; Larsen, S.O.; Andersson, M.; Daugaard, G.; Ersboll, J.; Hansen, S.W.; Hou-Jensen, K.; Nielsen, D.; Sigsgaard, T.C.; *et al.* Therapy-related myelodysplasia and acute myeloid leukemia. Cytogenetic characteristics of 115 consecutive cases and risk in seven cohorts of patients treated intensively for malignant diseases in the Copenhagen series. *Leukemia* **1993**, *7*, 1975–1986.
37. Chiara, A.D.; Pederzoli-Ribeil, M.; Burgel, P.R.; Danel, C.; Witko-Sarsat, V. Targeting cytosolic proliferating cell nuclear antigen in neutrophil-dominated inflammation. *Front. Immunol.* **2012**, *3*, doi:10.3389/fimmu.2012.00311.
38. Liebermann, D.A.; Hoffman, B. Gadd45 in the response of hematopoietic cells to genotoxic stress. *Blood Cells Mol. Dis.* **2007**, *39*, 329–335.
39. Liebermann, D.A.; Tront, J.S.; Sha, X.; Mukherjee, K.; Mohamed-Hadley, A.; Hoffman, B. Gadd45 stress sensors in malignancy and leukemia. *Crit. Rev. Oncog.* **2011**, *16*, 129–140.
40. Barreto, G.; Schafer, A.; Marhold, J.; Stach, D.; Swaminathan, S.K.; Handa, V.; Doderlein, G.; Maltry, N.; Wu, W.; Lyko, F.; *et al.* Gadd45a promotes epigenetic gene activation by repair-mediated DNA demethylation. *Nature* **2007**, *445*, 671–675.
41. Wadhwa, S.; Mumper, R.J. D-Penicillamine and other low molecular weight thiols: Review of anticancer effects and related mechanisms. *Cancer Lett.* **2013**, *337*, 8–21.
42. Gillies, L.A.; Kuwana, T. Apoptosis regulation at the mitochondrial outer membrane. *J. Cell. Biochem.* **2014**, *115*, 632–640.
43. Chiara, F.; Gambalunga, A.; Sciacovelli, M.; Nicolli, A.; Ronconi, L.; Fregona, D.; Bernardi, P.; Rasola, A.; Trevisan, A. Chemotherapeutic induction of mitochondrial oxidative stress activates GSK-3alpha/beta and Bax, leading to permeability transition pore opening and tumor cell death. *Cell Death Dis.* **2012**, *3*, e444.
44. Wang, Q.; Sun, S.-Y.; Khuri, F.; Curran, W.J.; Deng, X. Mono-or double-site phosphorylation distinctly regulates the proapoptotic function of Bax. *PLoS One* **2010**, *5*, e13393.
45. An, J.; Chen, Y.; Huang, Z. Critical upstream signals of cytochrome c release induced by a novel Bcl-2 inhibitor. *J. Biol. Chem.* **2004**, *279*, 19133–19140.
46. Steelman, L.S.; Franklin, R.A.; Abrams, S.L.; Chappell, W.; Kempf, C.R.; Basecke, J.; Stivala, F.; Donia, M.; Fagone, P.; Nicoletti, F.; *et al.* Roles of the Ras/Raf/MEK/ERK pathway in leukemia therapy. *Leukemia* **2011**, *25*, 1080–1094.
47. Palorini, R.; Simonetto, T.; Cirulli, C.; Chiaradonna, F. Mitochondrial complex I inhibitors and forced oxidative phosphorylation synergize in inducing cancer cell death. *Int. J. Cell. Biol.* **2013**, *2013*, doi: 10.1155/2013/243876.

48. Kim, J.S.; Ahn, K.J.; Kim, J.A.; Kim, H.M.; Lee, J.D.; Lee, J.M.; Kim, S.J.; Park, J.H. Role of reactive oxygen species-mediated mitochondrial dysregulation in 3-bromopyruvate induced cell death in hepatoma cells: ROS-mediated cell death by 3-BrPA. *J. Bioenerg. Biomembr.* **2008**, *40*, 607–618.
49. Wei, L.; Dai, Q.; Zhou, Y.; Zou, M.; Li, Z.; Lu, N.; Guo, Q. Oroxylin A sensitizes non-small cell lung cancer cells to anoikis via glucose-deprivation-like mechanisms: c-Src and hexokinase II. *Biochim. Biophys. Acta* **2013**, *1830*, 3835–3845.
50. Sebastian, S.; Kenkare, U.W. Expression of two type II-like tumor hexokinase RNA transcripts in cancer cell lines. *Tumor Biol*. **1998**, *19*, 253–260.
51. Marin-Hernandez, A.; Rodriguez-Enriquez, S.; Vital-Gonzalez, P.A.; Flores-Rodriguez, F.L.; Macias-Silva, M.; Sosa-Garrocho, M.; Moreno-Sanchez, R. Determining and understanding the control of glycolysis in fast-growth tumor cells. Flux control by an over-expressed but strongly product-inhibited hexokinase. *FEBS J*. **2006**, *273*, 1975–1988.
52. Liu, C.X.; Zhou, H.C.; Yin, Q.Q.; Wu, Y.L.; Chen, G.Q. Targeting peroxiredoxins against leukemia. *Exp. Cell Res*. **2013**, *319*, 170–176.

Zn-Driven Discovery of a Hydrothermal Vent Fungal Metabolite Clavatustide C, and an Experimental Study of the Anti-Cancer Mechanism of Clavatustide B

Panpan Ye, Ling Shen, Wei Jiang, Ying Ye, Chen-Tung Arthur Chen, Xiaodan Wu, Kuiwu Wang and Bin Wu

Abstract: A naturally new cyclopeptide, clavatustide C, was produced as a stress metabolite in response to abiotic stress elicitation by one of the hydrothermal vent fluid components Zn in the cultured mycelia of *Aspergillus clavatus* C2WU, which were isolated from *Xenograpsus testudinatus*. *X. testudinatus* lives at extreme, toxic habitat around the sulphur-rich hydrothermal vents in Taiwan Kueishantao. The known compound clavatustide B was also isolated and purified. This is the first example of a new hydrothermal vent microbial secondary metabolite produced in response to abiotic Zn treatment. The structures were established by spectroscopic means. The regulation of G1-S transition in hepatocellular carcinoma cell lines by clavatustide B was observed in our previous study. The purpose of the present study was to verify these results in other types of cancer cell lines and elucidate the possible molecular mechanism for the anti-cancer activities of clavatustide B. In different human cancer cell lines, including pancreatic cancer (Panc-1), gastric cancer (MGC-803), colorectal cancer (SW-480), retinoblastoma (WERI-Rb-1) and prostate cancer (PC3), clavatustide B efficiently suppressed cell proliferations in a dose-dependent manner. Although different cancer cell lines presented variety in Max effect dose and IC_{50} dose, all cancer cell lines showed a lower Max effect dose and IC_{50} dose compared with human fibroblasts (hFB) ($p < 0.05$). Moreover, significant accumulations in G1 phases and a reduction in S phases ($p < 0.05$) were observed under clavatustide B treatment. The expression levels of 2622 genes including 39 cell cycle-associated genes in HepG2 cells were significantly altered by the treatment with 15 μg/mL clavatustide B after 48 h. *CCNE2* (cyclin E2) was proved to be the key regulator of clavatustide B-induced G1-S transition blocking in several cancer cell lines by using real-time PCR.

Reprinted from *Mar. Drugs*. Cite as: Ye, P.; Shen, L.; Jiang, W.; Ye, Y.; Chen, C.-T.A.; Wu, X.; Wang, K.; Wu, B. Zn-Driven Discovery of a Hydrothermal Vent Fungal Metabolite Clavatustide C, and an Experimental Study of the Anti-Cancer Mechanism of Clavatustide B. *Mar. Drugs* **2014**, *12*, 3203–3217.

1. Introduction

Ocean hydrothermal vent microorganisms adapt and respond rapidly to changes in the concentrations and availability of metals within their environment [1]. In the previous study, we discovered two structurally interesting hepatocellular carcinoma cell inhibitory cyclodepsipeptides from a hydrothermal vent fungus [2], which we isolated from extreme, toxic habitat around the metal-rich hydrothermal vents in Taiwan Kueishantao [3]. The chemical diversity of the secondary metabolites from marine fungi is considerably high [4,5]. New strategies to discover the novel

bioactive compounds including biotic [6–8] and abiotic [4,9] stress elicitations have been applied. In this study, one naturally new cyclopeptide was produced as a stress metabolite in the cultured mycelia of hydrothermal fungus *Aspergillus clavatus* C2WU in response to abiotic Zn stress elicitation. Zn is one of the hydrothermal vent fluid components [10].

Cancer is a major public health problem and the leading cause of death worldwide. According to the data from the National Cancer Institute of United States [11], more than 1.6 million new cancer cases and a half million cancer deaths had been projected to occur in the United States in 2014 [11]. In China, there are 3.5 million newly diagnosed cancer patients and 2.5 million cancer deaths every year according to a recently released annual report from the National Cancer Prevention and Control Office. Comprehensive cancer therapy, including surgery, chemo- and radio-therapy and traditional Chinese Medicine has been advocated in recent years [12,13] in order to cure cancer or considerably prolong life while improving the quality of life. Some cancer types, including lung cancer, colorectal cancer, breast cancer, and prostate cancer have higher cure rates and declined death rates when detected early and treated with best practices. However, some other common cancer types, such as hepatobiliary and pancreatic cancer have higher death rates at similar detection time and treatment [11]. Therefore, the discovery of novel and potent anti-cancer drugs is desperately needed. We previously found that clavatustide B regulated G1-S transition in liver cancer cell lines [2]. In this study we presented the results obtained from other types of cancer cell lines. This study was also performed to elucidate the possible molecular mechanism of the anti-cancer activities of clavatustide B.

2. Results and Discussion

2.1. Structural Elucidation of the Stress Metabolite

The hydrothermal fungus *A. clavatus* C2WU isolated from *X. testudinatus*, was cultured in the absence and presence of the abiotic stress agent, $ZnSO_4$. Upon comparison of TLC plates of mycelia extracts from both conditions, an additional spot in the extract of $ZnSO_4$ treated culture was detected. The compound was putatively produced in response to abiotic stress. The stress metabolite clavatustide C was isolated by preparative TLC, and purified by Sephadex LH-20 column chromatography (Chart 1). Clavatustide B produced both in the normal and Zn treated culture condition was isolated using preparative HPLC (Chart 1).

Clavatustide C (**1**) was obtained as white powder. The HR-TOF-MS exhibited an ion peak at *m*/*z* 566.4279 $[M + H]^+$ (calcd. 566.4276), corresponding to the molecular formula, $C_{30}H_{55}N_5O_5$. The ^1H and ^{13}C NMR spectra for **1** exhibited resonances typical of a cyclic peptide (Table 1). In the ^{13}C NMR spectrum recorded in DMSO-d_6, five carbonyl resonances at δ_C 170.2, 172.6, 171.2, 171.2 and 172.0, respectively, were observed, suggestive of structural feature of pentapeptide. The peptide nature of the molecule was further supported by the presence of five NH protons in the ^1H NMR spectrum (δ_H 8.22, 8.35, 8.63, 7.87, 7.30, respectively) and five α-CH signals (δ_C 58.3, δ_H 4.04; δ_C 62.9, δ_H 3.34; δ_C 52.1, δ_H 4.31; δ_C 51.5, δ_H 4.31; δ_C 50.3, δ_H 4.41, respectively). Analysis of the 1D and 2D NMR data allowed the assignment of two isoleucine and three leucine residues in the molecule of **1**. The most common cyclic sequence of these five peptide units is

cyclo-(L-Leu-L-Ileu-L-Leu-L-Ile-L-Lue), viscumamide [14,15]. Two isoleucines are embedded among three leucines in the structure of viscumamide. However, the α-CH carbon resonance was observed to upshift about 4 ppm when compared the NMR data of **1** with those of viscumamide reported [14,15]. The diagnostic HMBC correction from the NH proton signal of one of the isoleucines at δ_H 8.22 (NH-7, d, J = 8.7 Hz) to the carbonyl carbon signal of the remaining isoleucine at δ_C 172.6 (C-8, s) linked two isoleucines by a peptide bond. Key long range correlations were shown in the Figure 1. Thus, the stress metabolite was elucidated as cyclo-(L-Ileu-L-Ile-L-Leu-L-Lue-L-Leu). The absolute configuration of L-isoleucine and L-leucine was determined by the analysis of acidic hydrolysates through a chiral HPLC column, when compared with the authentic L-isoleucine and L-leucine. Although this compound was synthesized by Sakurai and coworkers [15], this is the first time that the cyclic pentapeptide is isolated from a natural source. Since no trivial name has been given, it was, therefore, named as clavatustide C. This is also the first example of Zn-induced cyclic pentapeptide from marine fungi. Since the NMR data of compound **2** were in good agreement with previously reported, compound **2** was identified as the known compound clavatustide B [2].

Chart 1. Structures of clavatustides B and C.

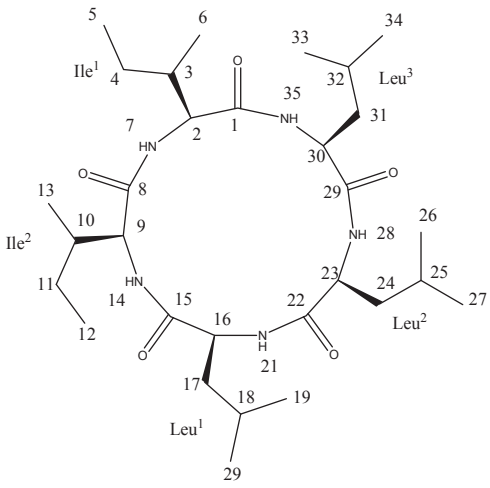

clavatustide C (**1**)

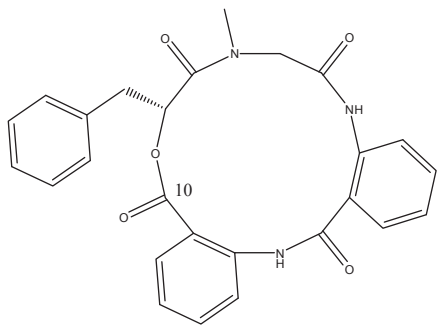

clavatustide B (**2**)

Table 1. NMR Data (500 MHz) for clavatustide C in DMSO-d_6.

Position	δ_C [a,b], multiplicities	δ_H [c], multiplicities (*J* in Hz)	Position	δ_C [a,b], multiplicities	δ_H [c], multiplicities (*J* in Hz)
Ile [1]			Leu[2]		
1	170.2, C		22	171.2, C	
2	58.3, CH	4.04, dd (8.2, 3.0)	23	51.5, CH	4.31, m
3	35.5, CH	1.88, m	24	41.5, CH_2	1.46, m
4	24.2, CH_2		25	24.3, CH [d]	1.48, overlap
5	11.3, CH_3	0,82, overlap	26	22.8, CH_3 [e]	0.87, overlap
6	15.6, CH_3	0.83, overlap	27	22.2, CH_3	0.87, overlap
7	NH	8.22, d (8.7)	28	NH	7.30, d (8.3)
Ile [2]			Leu[3]		
8	172.6, C		29	172.0, C	
9	62.9, CH	3.34, m	30	50.3, CH	4.41, m
10	33.2, CH	2.29, m	31	38.8, CH_2	1.46, m
11	25.1, CH_2	1.48, overlap	32	24.6, CH [d]	1.48, overlap
12	9.8, CH_3	0.79, t (7.5)	33	22.4, CH_3 [e]	0.87, overlap
13	15.4, CH_3	0.83, overlap	34	22.2, CH_3	0.87, overlap
14	NH	8.35, d (8.4)	35	NH	7.87, d (8.4)
Leu [1]					
15	171.2, C				
16	52.1, CH	4.31, m			
17	40.1, CH_2	1.51, m			
18	24.6, CH [d]	1.49, overlap			
19	22.4, CH_3 [e]	0.87, overlap			
20	22.2, CH_3	0.87, overlap			
21	NH	8.63, d (8.2)			

[a] Recorded at 125 MHz; [b] Multiplicities inferred from DEPT and HSQC experiments; [c] Recorded at 500 MHz; [d,e] Interchangeable.

Figure 1. Key 2D NMR correlations of **1**.

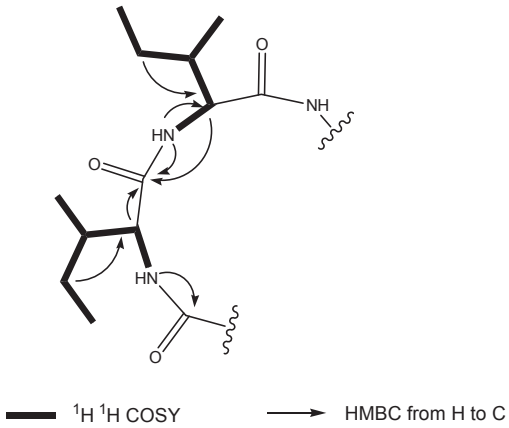

2.2. Clavatustide B Inhibits Growth of Cancer Cells

Our previous study showed that clavatustide B possessed a preliminary anti-proliferative effect on three hepatocellular cacinoma cell lines (HepG2, SMMC-7721 and Bel-7402) in a dose- and time-dependent manner [2]. This finding prompted us to further investigate the role of clavatustide B in other cancer cell lines, including human pancreatic cancer (Panc-1), gastric cancer (MGC-803), colorectal cancer (SW-480), retinoblastoma (WERI-Rb-1) and prostate cancer (PC3). The results showed that the clavatustide B treatment group exhibited an anti-proliferative effect in a dose-dependent manner in all five cell lines compared with the blank control (Figure 2). Viable cell number reduction became significant at 10–20 μg/mL and the Max effect dose was 40–50 μg/mL in the cancer cell lines after 24 h treatment. From 24 h to 72 h, viable cell number increased at low dose drug treatment (0–10 μg/mL) by comparison of OD values. In contrast, viable cell number at 40–50 μg/mL remained essentially identical between 24 h, 48 h and 72 h for each cell line. The OD values of MGC-803 cells increased from 0.7, 1.3 to 1.8 at zero drug treatment for 24 h, 48 h and 72 h, indicating that the cells continued to proliferate during the 72 h. However, the OD values at 40–50 μg/mL treatment during the same period remained fairly constant at 0.3, suggestive of an inhibition of cell proliferation. The predicted 50% inhibitory concentrations (IC_{50}) doses, which are determined as the midpoint between the zero cell killing and the maximal inhibitory effects, were all about essentially identical at 15–20 μg/mL for MGC-803 cell line at each time point. Similar observations were observed with the other four cell lines. The cell viabilities were reduced by 65%, 74%, 63%, 67% and 78% in Panc-1, MGC-803, SW-480, WERI-Rb-1 and PC3 cells, respectively, at a concentration of 40 μg/mL clavatustide B after 72 h treatments.

Figure 2. Clavatustide B inhibits growth of different cancer cells in a dose-dependent manner after 24 h (**A**); 48 h (**B**) and 72 h (**C**) treatments. * $p < 0.05$.

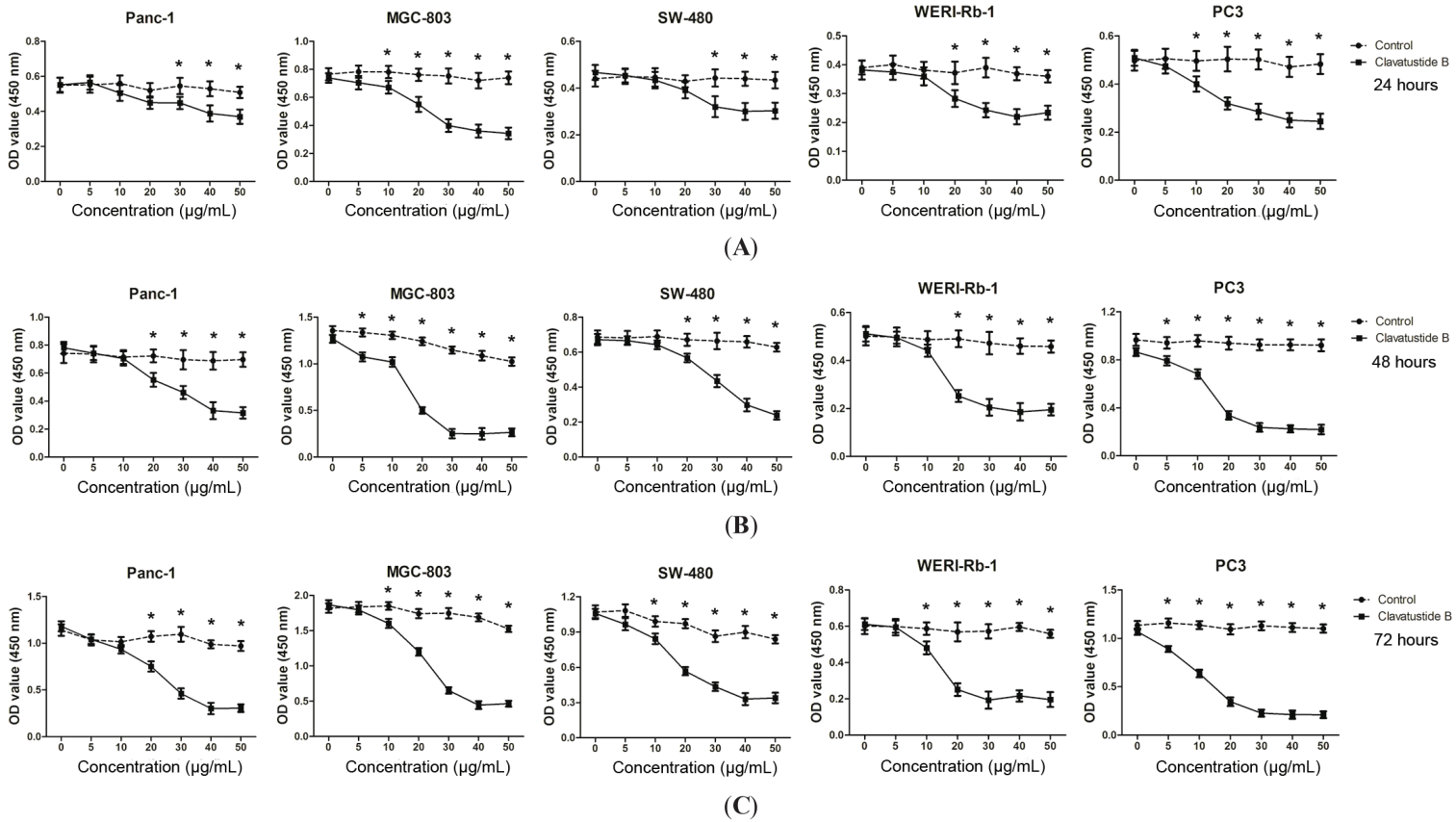

The results demonstrated that clavatustide B induced complete cessation of cell growth in various types of cancer cells in a short time at 40–50 μg/mL dose levels. The biological effect was dose-dependent but might not time-dependent. It should be noted that Panc-1 is one of the most frequently studied pancreatic cancer cell lines and is chemo- and radio-therapy resistant [16]. The prostate cancer cell line PC3 was also reported to be chemo-resistant [17]. A potent inhibition of cell growth of both cell lines was observed under the clavatustide B treatment. It is tentatively deduced that clavatustide B is a promising anti-cancer agent against chemo- and radio-therapy resistant cancers.

2.3. Evaluation of Cytotoxicity

The toxicity of clavatustide B was evaluated *in vitro* with normal human fibroblasts (hFB). The results showed that treatment of hFB with 0–50 μg/mL of clavatustide B for 24 h and 48 h did not induce an obvious suppression of cell proliferation. In contrast, the cancer cell line showed a significant inhibition of cell proliferation by clavatustide B (Figure 3A, Figure 3B). Viable cell number of hFB continued to increase during 48 h at 40–50 μg/mL of treatment by comparison of OD values, although a decrease in viable cell number was observed at 40–50 μg/mL compared with blank control at 72 h (Figure 3C). The results indicated that long-term treatment with clavatustide B (>72 h) with high concentration (>40 μg/mL) appeared to inhibit the growth of the normal human fibroblasts cells. However, since clavatustide B had hardly any effect on hFB cells even at Max effect dose for cancer cells with 48 h, it was inferred to be an anti-cancer agent with relatively low toxicity.

Figure 3. The evaluation of toxicity of clavatustide B by comparison of cell viability curves between normal human fibroblasts and cancer cell lines after 24 h (**A**); 48 h (**B**) and 72 h (**C**) treatments.

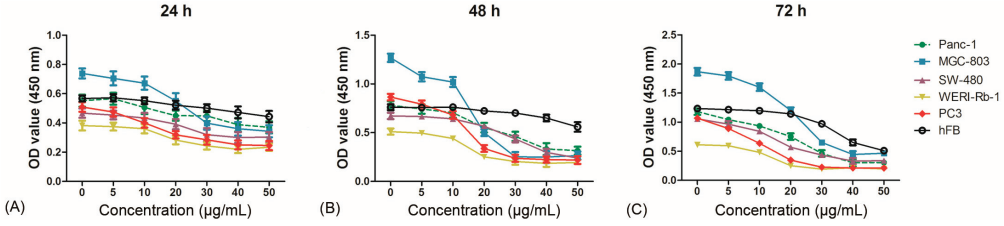

2.4. Clavatustide B Delays G1-S Cell Cycle Transition

Cell-cycle analysis was performed in HepG2 cells in our previous study, revealing an accumulation of HepG2 cells in G1 phase and reduction of cells in S phase induced by clavatustide B [2]. In the present study, the effect was confirmed in other cancer cell lines. The results showed that clavatustide B inhibited G1-S phase cell cycle transit in Panc-1, MGC-803, SW-480, WERI-Rb-1 and PC3 cells with the respective IC_{50} doses for 48 h (Figure 4).

The cell cycle can be divided into four phases, and the cellular decision to initiate mitosis or to become quiescent occurs during the G1 phase. Duration of G1 is highly variable and under the

control of a complex network [18]. This phase is marked by occurrence of proteins required in S phase, when DNA replication happens. Genetic alterations in genes that regulate progression through G1 phase, make a major contribution to the development of human cancers [18]. In this study, clavatustide B was proved to delay G1-S phase cell cycle transition, exhibiting significant anti-cancer potency (Figure 4).

Figure 4. Clavatustide B increases G1/S phase ratio in Panc-1, MGC-803, SW-480, WERI-Rb-1 and PC3 cells. * $p < 0.05$.

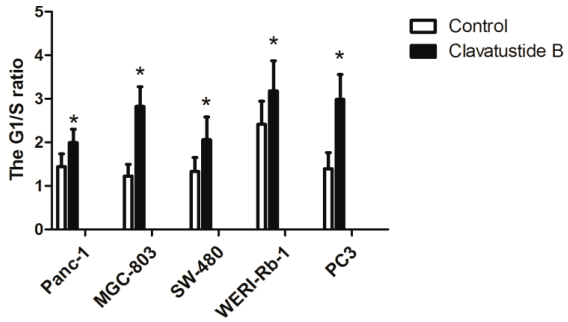

2.5. Clavatustide B Regulates G1-S Transition Genes

To further explore the mechanism of anti-proliferation effect, particularly the G1-S phase inhibition, Affymetrix GeneChip® Human Genome U133 Plus 2.0 Array was used to screen transcriptome differences between clavatustide B treated and untreated HepG2 cells. Expression levels of 2622 genes and 3648 long non-coding RNAs in HepG2 cells were significantly altered after treatment at a concentration of 25 μg/mL clavatustide B for 48 h (Figure 5A). Since we were still at the beginning of the exploration of lncRNAs and their functional roles, we focused on the regulation of mRNAs in the presented study. Among the 2622 genes, 39 cell cycle-associated genes were significantly regulated. Genes such as *GSPT2*, *USP2*, *TXNIP*, *FBXO31*, *CYLD* and *CCNE2* are believed to involve in G1-S transition [18]. *CCNE2* was significantly down-regulated by 1.91-fold. In contrast, *FBXO31* and *CYLD* were significantly up-regulated by 1.45- and 1.43-fold, respectively. These genes were finally enrolled into the next real-time PCR verification for other cancer cell lines. The results showed that the expression of *CCNE2* was significantly lower in the clavatustide B treated group than that in the control group in all five cancer cell lines (Figure 5). The *CYLD* had higher expression in the clavatustide B treated group than that in the control group. However, it is not statistically significant in Panc-1 cells. No significant difference between the clavatustide B treated group and the control group in the expression of *FBXO31* was observed.

The G1-S cell cycle checkpoint plays a key role in the progression of cell division, controlling the passage of cells from G1 into the S phase. Dozens of genes involved in the G1-S checkpoint signaling pathway have been discovered, including *P16*, *P21*, *P53*, *MDM2*, *CCND1*, *CHEK2*, *CDC2*, *CDC6*, *CDK4* and *CDK6* [18–20]. *CCNE2* (cyclin E2) activates cyclin-dependent kinase 2 and controls progression through the G1-S checkpoint [21]. *CYLD*, a tumor suppresser gene, negatively regulates cell proliferation via a significant delay in the G1-S transition [22]. In the

present study, down-regulation of *CCNE2* and up-regulation of *CYLD* by clavatustide B were observed, which would trap cancer cells at the G1-S checkpoint and prevent them from initiating DNA replication. These findings provided molecular evidence that clavatustide B reduced cancer cells growth and division, which might account for its anti-cancer potential.

Figure 5. The differentially expressed genes between clavatustide B treated group and the control group. (**A**) The Heat Map showing differentially expressed mRNAs and long non-coding RNAs between clavatustide B treated group and control group in HepG2 cells; (**B**) Real time PCR comparing the expression of *CCNE2*, *FBXO31* and *CYLD* between clavatustide B treated group and control group in Panc-1, MGC-803, SW-480, WERI-Rb-1 and PC3 cells. * $p < 0.05$.

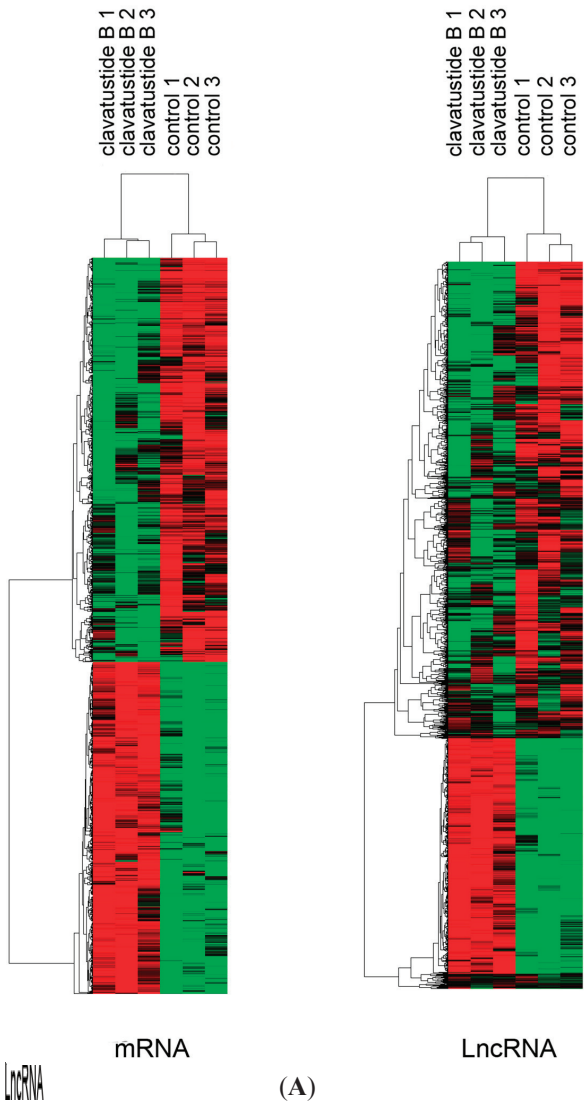

Figure 5. *Cont.*

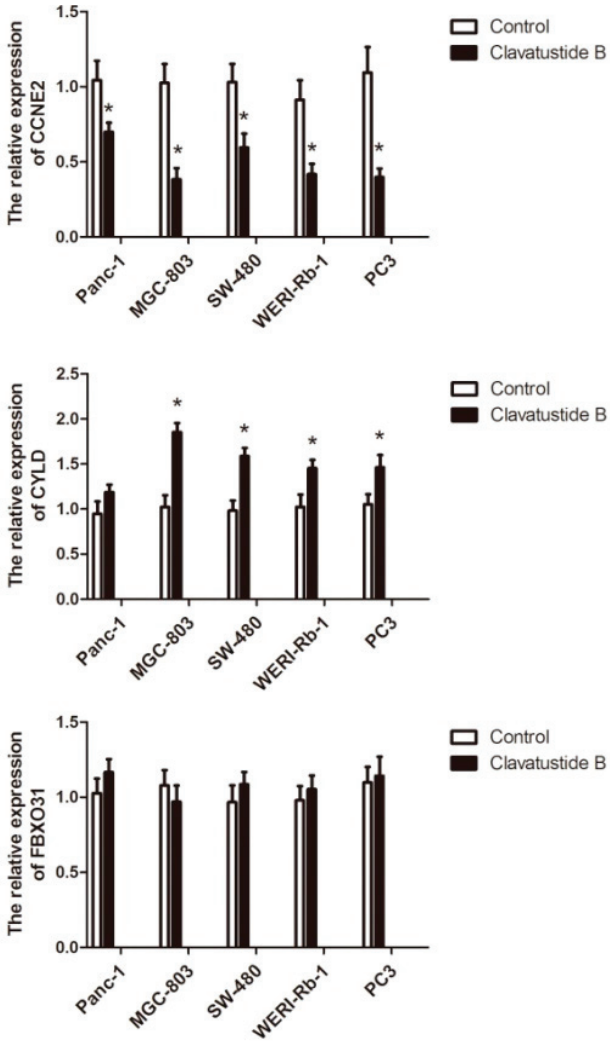

(**B**)

3. Experimental Section

3.1. General Experimental Procedures

Optical rotations were recorded on a Perkin-Elmer-341 polarimeter. The IR spectra ($CHCl_3$) were run on a NicoletAvatar-360FT-IR spectrometer. ^{1}H NMR (500 MHz) and ^{13}C NMR (125 MHz) spectra were measured at 25 °C on a Bruker AVANCE DMX 500 NMR spectrometer with TMS as internal standard. TOF-MS were recorded on a AB Sciex Triple TOF-MS spectrometer. ESIMS were recorded on an Agilent 6460 Triple Quad LC/MS. TLC was performed using Merck precoated plates (Silica gel 60 F254) of 0.25 mm thickness. Sephadex LH-20 (Amersham, Stockholm, Sweden) was used for column chromatography.

3.2. Fungal Cultivation and Stress Applications

The fungus *A. clavatus* C2WU was separated from the marine *X. testudinatus*, which was collected from Taiwan Kueishantao hydrothermal vent, and identified by its ITS-5.8s rDNA sequences. Subcultures of the organism are deposited at the Ocean College, Zhejiang University. Cultures were separated into control (5 L) and stressed groups (5 L). The control fungus was grown in the potato culture medium in sterilized and filtrated natural seawater. The stressed culture medium consisted of an additional 50 μmol/L $ZnSO_4$. The fermentations were carried out at 24 °C for 10 days.

3.3. Extraction and Isolation

The whole culture of the control and stressed broth of *A. clavatus* C2WU (5 L) were filtered. The air-dried mycelia of control (24 g) and the stressed group (20 g) were extracted at room temperature with MeOH (3 × 1 L), respectively. The extracts were evaporated *in vacuo* to afford a gummy residue for both Zn treated (1.8 g) and corresponding controls (2.0 g). The residues were partitioned in H_2O (500 mL) and extracted successively with EtOAc (3 × 500 mL) and *n*-butanol (3 × 500 mL). The EtOAc and *n*-butanol extracts of the treated and control cultures were subjected to TLC examination on aluminium sheets pre-coated with Silica gel 60 F254 (Merck, Darmstadt, Germany). The spots were applied in as equal amounts as possible. The plates were developed in the following developing solvent systems: benzene–acetone (7:1), benzene–EtOAc (5:1), petroleum ether–EtOAc (5:1) for the EtOAc extract; $CHCl_3$–MeOH (3:1), CH_2Cl_2–MeOH (4:1) and benzene–$CHCl_3$–MeOH (1:3:1) for the *n*-butanol extract. After development, the plates were examined under UV light (250 nm) to locate any additional spots in the different extracts of the treatments in comparison with those of the corresponding control extracts. The spots on the plates were also visualized by spraying with an EtOH-H_2SO_4 solution. One additional compound was detected on the plates developed in benzene–acetone (7:1) solvent system in the EtOAc extract of stress elicited mycelium. Several prep-TLC plates were prepared and the target compound was isolated by preparative TLC in the developing solvent systems of benzene–acetone (7:1). The crude compounds were applied to a Sephadex LH-20 column (1 × 80 cm, 38 g, Amersham), and eluted with acetone to yield pure compound **1** (5.3 mg). Compound **2** was prepared by the methods reported [2].

3.4. Cell Culture and Proliferation Assay

Human liver cancer (HepG2), pancreatic cancer (Panc-1), gastric cancer (MGC-803), colorectal cancer (SW-480), retinoblastoma (WERI-Rb-1), prostate cancer (PC3) and human fibroblasts (hFB) were purchased from the Cell Bank of the Chinese Academy of Sciences (Shanghai, China), and cultured in DMEM or RPMI-1640 with 10% fetal bovine serum at 37 °C in a humidified atmosphere containing 5% CO_2. Viable cell number was determined by cell counting kit-8 (Dojindo, Tokyo, Japan). Briefly, cells were plated in 96-well plate (2×10^3 cells per well) and incubated for 24 h. Then the cells were treated with clavatustide B for different time points and concentrations. After incubation, CCK-8 solution was added and the absorbance at 450 nm was

measured according to the manufacturer's instructions. The experiment was independently repeated three times.

3.5. Cell Cycle Assay

Cell cycle analysis was performed using flow cytometry as we described before [23]. Briefly, cells were washed and fixed in 70% cold ethanol overnight at 4 °C. Then cell was mixed with 0.5 mL DNA Prep LPR (Beckman Coulter, Fullerton, CA, USA) in the dark for 20 min. Cell cycle analysis was performed on the same flow cytometer (Cytomics FC 500, Beckman Coulter, Miami, USA). ModFit LT software (Verity Software House, Maine, USA) was used to calculate the percentage of cell population in S, G1 and G2 phase.

3.6. Microarray Assay

Cellular RNA from HepG2 cells was extracted using Trizol (Invitrogen, Carlsbad, CA, USA), and quality controlled as directed with the Affymetrix expression technical manual. RNA (25 ng) was used to produce biotin-labeled cRNA, which was hybridized to Affymetrix GeneChip® Human Transcriptome Array 2.0. Array washing, scanning and probe quantification protocols were carried out according to the manufacturer's instructions using Affymetrix GeneChip Operating Software (GCOS). For each array, GCOS output was imported as CEL files into Partek Genomic Suite software (Agilent, Palo Alto, CA, USA), and gene expression data quantified with the RMA (Robust Multichip Averaging) algorithm, normalized and corrected for multiple testing with random variance model (RVM) and Benjamin and Hochberg method for detection of differentially expressed genes and false discovery rate, respectively [23]. Fold change = Geom mean of intensities in clavatustide B group/Geom mean of intensities in control group.

3.7. Real-Time PCR

Cellular RNA was extracted from Panc-1, MGC-803, SW-480, WERI-Rb-1 and PC3 cells using Trizol (Invitrogen, Carlsbad, CA, USA) according to the manufacturer's instructions. Total RNA was reverse-transcribed using Superscript III reverse transcriptase and oligo (dT) primer. Real time PCR was performed and analyzed in ABI PRISM 7500 Sequence Detection System (Applied Biosystem, Carlsbad, CA, USA) with SYBR green ready mix (Applied Biosystem) and SDS 2.1 software (Applied Biosystems) as described before [24]. All reactions were measured in triplicates in a final volume of 10 μL. Cycling conditions were chosen according to the manufacturer's protocols. The relative level of mRNA was calculated against GAPDH (internal control) using the $2^{-\Delta\Delta Ct}$ method in each cell line, respectively.

3.8. Statistical Analysis

SPSS for Windows version 13.0 (SPSS Inc., Chicago, IL, USA) was used for statistical analysis. *P* values of less than 0.05 were considered statistically significant. Values in the present study were

reported as Mean ± SD from three independent experiments repeats. Two-sided student's unpaired test was used for comparison.

4. Conclusions

Marine hydrothermal vent microbial habitats are strongly influenced by elevated levels of metals. Hydrothermal microorganisms respond rapidly to changes in the concentrations and availability of metals within their environment, where geothermally heated water reacts with its host rock forming fluids that nourish a diverse array of geothermally dependent microorganisms [1]. In this study, small molecule clavatustide C was successfully induced by Zn. Clavatustide B, the product secreted both in the normal and metal spiked cultures of *A. clavatus* C2WU, exhibited a potent anti-cancer effect in various human cancers, including liver cancer, pancreatic cancer, gastric cancer, colorectal cancer, prostate cancer and retinoblastoma. Clavatustide B inhibited the proliferation of cancer cells via a remarkable delaying of G1-S cell cycle transition. The G1-S cell cycle checkpoint-associated molecules including Cyclin E2 played key roles in the clavatustide B-induced cell cycle blocking. The results showed that clavatustide B demonstrated a potent anti-proliferation effect in the chemo-resistant cell lines, such as Panc-1. Thus, clavatustide B was proved to be a promising anticancer candidate, particularly for the treatment of chemoradiotherapy resistant cancers.

Acknowledgments

This work was supported by National Science Foundation of China (81273386) and Zhejiang Provincial National Science Foundation of China (LQ14H120002).

Author Contributions

Panpan Ye and Ling Shen conducted the biological experiments. Wei Jiang isolated and purified the Clavatustide B. Ying Ye and Chen-Tung Arthur Chen collected the samples. Xiaodan Wu and Kuiwu Wang conducted the data analysis. Bin Wu conducted the Zn stress experiments and data analysis.

Conflicts of Interest

The authors have declared no conflict of interest.

References

1. Holden, J.F.; Adams, M.W.W. Microbe-metal interactions in marine hydrothermal environments. *Curr. Opin. Chem. Biol.* **2003**, *7*, 160–165.
2. Jiang, W.; Ye, P.; Chen, C.T.A.; Wang, K.; Liu, P.; He, S.; Wu, X.; Gan, L.; Wu, B. Two novel hepatocellular carcinoma cycle inhibitory cyclodepsipeptides from a hydrothermal vent crab-associated fungus *Aspergillus clavatus* C2WU. *Mar. Drugs* **2013**, *11*, 4761–4772.

3. Jeng, M.S.; Ng, N.K.; Ng, P.K.L. Hydrothermal vent crabs feast on sea "snow". *Nature* **2004**, *432*, doi:10.1038/432969a.
4. Wu, B.; Wu, X.; Sun, M.; Li, M. Two novel tyrosinase inhibitory sesquiterpenes induced by $CuCl_2$ from a marine-derived fungus *Pestalotiopsis* sp. Z233. *Mar. Drugs* **2013**, *11*, 2713–2721.
5. Wu, B.; Oesker, V.; Wiese, J.; Schmaljohann, R.; Imhoff, J.F. Two new antibiotic pyridones produced by a marine fungus *Trichoderma* sp. Strain MF106. *Mar. Drugs* **2014**, *12*, 1208–1219.
6. Jensen, P.R.; Fenical, W. Strategies for the discovery of secondary metabolites from marine bacteria: Ecological perspectives. *Annu. Rev. Microbiol.* **1994**, *48*, 559–584.
7. Cueto, M.; Jensen, P.R.; Kauffman, C.; Fenical, W.; Lobkovsky, E.; Clardy, K. Pestalone, a new antibiotic produced by a marine fungus in response to bacterial challenge. *J. Nat. Prod*. **2001**, *64*, 1444–1446.
8. Park, H.B.; Kwon, H.C.; Lee, C.-H.; Yang, H.O. Glionitrin A, an antibiotic-antitumor metabolite derived from competitive interaction between abandoned mine microbes. *J. Nat. Prod*. **2009**, *72*, 248–252.
9. Wu, F.; Jiang, W.; Wu, B. Methodological aspects about determination of plant defensive phenolics in response to stress. *Curr. Anal. Chem*. **2013**, *9*, 352–359.
10. Butterfield, D.A.; Jonasson, I.R.; Massoth, G.J.; Feely, R.A.; Roe, K.K.; Embley, R.E.; Holden, J.F.; McDuff, R.E.; Lilley, M.D.; Delaney, J.R. Seafloor eruptions and evolution of hydrothermal fluid chemistry. *Philos. Trans. R. Soc. Lond. A* **1997**, *355*, 369–386.
11. National Cancer Institute. Available online: http://seer.cancer.gov/statfacts/html/all.html (accessed on 5 April 2014).
12. Li, X.; Yang, G.; Zhang, Y.; Yang, J.; Chang, J.; Sun, X.; Zhou, X.; Guo, Y.; Xu, Y.; Liu, J.; *et al*. Traditional Chinese medicine in cancer care: A review of controlled clinical studies published in chinese. *PLoS One* **2013**, *8*, e60338.
13. Ling, Q.; Xu, X.; Wei, X.; Wang, W.; Zhou, B.; Wang, B.; Zheng, S. Oxymatrine induces human pancreatic cancer PANC-1 cells apoptosis via regulating expression of Bcl-2 and IAP families, and releasing of cytochrome c. *J. Exp. Clin. Cancer. Res.* **2011**, *30*, doi:10.1186/1756-9966-30-66.
14. Okumura, Y.; Sakurai, A. Chemical studies on the mistleteo. II. The structure of viscumamide, anew cyclic peptide isolated from *Viscum album* Linn. *var.* coloratum Ohwi. *Bull. Chem. Soc. Jpn.* **1973**, *46*, 2190–2193.
15. Sakurai, A.; Okumura, Y. Synthesis of viscumamide and its analogs. *Bull. Chem. Soc. Jpn.* **1979**, *52*, 540–543.
16. Ling, Q.; Xu, X.; Zheng, S.S.; Kalthoff, H. The diversity between pancreatic head and body/tail cancers: Clinical parameters and *in vitro* models. Hepatobiliary Pancreat. *Dis. Int.* **2013**, *12*, 480–487.
17. Mimeault, M.; Johansson, S.L.; Batra, S.K. Marked improvement of cytotoxic effects induced by docetaxel on highly metastatic and androgen-independent prostate cancer cells by downregulating macrophage inhibitory cytokine-1. *Br. J. Cancer* **2013**, *108*, 1079–1091.
18. Malumbres, M.; Barbacid, M. Cell cycle, CDKs and cancer: A changing paradigm. *Nat. Rev. Cancer* **2009**, *9*, 153–166.

19. Zhang, S.; Shao, Y.; Hou, G.; Bai, J.; Yuan, W.; Hu, L.; Cheng, T.; Zetterberg, A.; Zhang, J. QM-FISH analysis of the genes involved in the G1/S checkpoint signaling pathway in triple-negative breast cancer. *Tumour Biol.* **2014**, *35*, 1847–1854.
20. Musgrove, E.A.; Caldon, C.E.; Barraclough, J.; Stone, A.; Sutherland, R.L. Cyclin D as a therapeutic target in cancer. *Nat. Rev. Cancer* **2011**, *11*, 558–572.
21. Macdonald, F.H.; Yao, D.; Quinn, J.A.; Greenhalgh, D.A. PTEN ablation in Ras/Fos skin carcinogenesis invokes p53-dependent p21 to delay conversion while p53-independent p21 limits progression via cyclin D1/E2 inhibition. *Oncogene* **2013**, doi:10.1038/onc.2013.372.
22. Wickstrom, S.A.; Masoumi, K.C.; Khochbin, S.; Fassler, R.; Massoumi, R. CYLD negatively regulates cell-cycle progression by inactivating HDAC6 and increasing the levels of acetylated tubulin. *EMBO J.* **2010**, *29*, 131–144.
23. Wright, G.W.; Simon, R.M. A random variance model for detection of differential gene expression in small microarray experiments. *Bioinformatics* **2003**, *19*, 2448–2455.
24. Ye, P.; Liu, J.; He, F.; Xu, W.; Yao, K. Hypoxia-Induced deregulation of miR-126 and its regulative effect on VEGF and MMP-9 expression. *Int. J. Med. Sci.* **2013**, *11*, 17–23.

Profiling of Polar Lipids in Marine Oleaginous Diatom *Fistulifera solaris* JPCC DA0580: Prediction of the Potential Mechanism for Eicosapentaenoic Acid-Incorporation into Triacylglycerol

Yue Liang, Yoshiaki Maeda, Tomoko Yoshino, Mitsufumi Matsumoto and Tsuyoshi Tanaka

Abstract: The marine oleaginous diatom *Fistulifera solaris* JPCC DA0580 is a candidate for biodiesel production because of its high lipid productivity. However, the substantial eicosapentaenoic acid (EPA) content in this strain would affect the biodiesel quality. On the other hand, EPA is also known as the essential health supplement for humans. EPAs are mainly incorporated into glycerolipids in the microalgal cell instead of the presence as free fatty acids. Therefore, the understanding of the EPA biosynthesis including the incorporation of the EPA into glycerolipids especially triacylglycerol (TAG) is fundamental for regulating EPA content for different purposes. In this study, in order to identify the biosynthesis pathway for the EPA-containing TAG species, a lipidomic characterization of the EPA-enriched polar lipids was performed by using direct infusion electrospray ionization (ESI)-Q-TRAP-MS and MS/MS analyses. The determination of the fatty acid positional distribution showed that the *sn*-2 position of all the chloroplast lipids and part of phosphatidylcholine (PC) species was occupied by C16 fatty acids. This result suggested the critical role of the chloroplast on the lipid synthesis in *F. solaris*. Furthermore, the exclusive presence of C18 fatty acids in PC highly indicated the biosynthesis of EPA on PC. Finally, the PC-based acyl-editing and head group exchange processes were proposed to be essential for the incorporation of EPA into TAG and chloroplast lipids.

Reprinted from *Mar. Drugs*. Cite as: Liang, Y.; Maeda, Y.; Yoshino, T.; Matsumoto, M.; Tanaka, T. Profiling of Polar Lipids in Marine Oleaginous Diatom *Fistulifera solaris* JPCC DA0580: Prediction of the Potential Mechanism for Eicosapentaenoic Acid-Incorporation into Triacylglycerol. *Mar. Drugs* **2014**, *12*, 3218–3230.

1. Introduction

Over the past several decades, biofuel production has attracted much interest due to the approaching exhaustion of fossil fuels and their negative impacts on climate. Microalgae have been recognized as promising biofuel producers due to their advantages of higher biomass productivity and non-competition with foods [1–3]. Recent studies have discovered a number of microalgae possessing high content of lipids [4–9].

In addition to lipid content, the unsaturation degree of microalgal lipids, which directly determines the fuel quality, is another critical factor for biodiesel application [10]. High content of polyunsaturated fatty acid (PUFA) will result in low oxidative stability of the final product [11]. The PUFA (≥ 4 double bonds) content in biodiesel is limited to less than 1% by the EN 14214 standards in Europe. However, on the other hand, omega 3-long chain PUFAs (ω3-LCPUFAs), e.g., eicosapentaenoic acid (EPA, C20:5n3) and docosahexaenoic acid (DHA, C22:5n3) are essential

health supplements for humans [12]. The growing market of ω3-LCPUFAs has made it impossible to maintain a sustainable supply from the conventional source of fish oil. Therefore, the research in polyunsaturated lipid synthesis in microalgae thus receives much attention. Some microalgal strains, which were determined to produce high content of EPA and DHA [13], are the potential alternative source of ω3-LCPUFAs. The understanding of the biosynthesis pathway for ω3-LCPUFA and the assembly of ω3-LCPUFA into lipids is the essential task to control ω3-LCPUFA content in microalgae by means of metabolic engineering.

Among eukaryotic microalgae, a pennate diatom, *Phaeodactylum tricornutum* has been used as one of the model organisms for studies in ω3-LCPUFA synthesis [14,15] due to its high content of EPA [16], available genome information [17] and easy transformation [18,19]. In *P. tricornutum*, metabolic labeling analyses revealed that phosphatidylcholine (PC) was involved in the series of fatty acid-desaturation for EPA synthesis [15]. However, the mechanism how EPA is incorporated into triacylglycerol (TAG, a main source of biodiesel) has not yet thoroughly been discussed in any microalgae. Furthermore, the lipid content in *P. tricornutum* is moderate [5]; thus, this microalga may not be the best lipid producer for biodiesel production. In addition, the knowledge of polyunsatulated lipid synthesis in other diatoms is poorly accumulated.

In this study, we focused on another marine pennate diatom, *Fistulifera solaris* (formerly *Fistulifera* sp.) JPCC DA0580, which has been identified in our lab [20] as an oleaginous microalga and can accumulate oil up to nearly 60% of dried cell weight (DCW) [9,21]. *F. solaris* also maintains substantial amount of EPA [9,22]. Owing to the achievements on mass cultivation [9,23] genome sequencing (partially published [24]) and genetic transformation [25], we propose that this strain is one of the ideal candidates for either biofuel or EPA production. Recently, the lipidomic analysis targeting neutral lipids, and the desaturation process for EPA synthesis in *F. solaris* has been reported [22,26], while the exact substrates for desaturation and the process of EPA-incorporation into TAG have not yet been addressed. In this study, the fatty acid composition and positional distribution of major polar lipid species were determined. The distribution of EPA and its precursor fatty acids in polar lipids was analyzed with direct infusion electrospray ionization (ESI)-Q-TRAP-MS/MS in order to deeply understand the polyunsatulated lipid synthesis in *F. solaris*. The results suggest that EPA was desaturated on PC and the PC-based acyl-editing and head group exchange processes may contribute to the EPA-incorporation into TAG.

2. Results and Discussion

2.1. Polar Lipid Profile of Fistulifera solaris JPCC DA0580

In order to examine how EPA is synthesized and incorporated into TAGs in *F. solaris*, the polar lipid profile including the information of fatty acid composition and positional distribution was elucidated by direct infusion ESI-Q-TRAP-MS/MS, through which the intact molecular structures of lipids can be determined. In the phospholipid (PL) fraction, 14 types of lipids including 11 phosphatidylcholines (PCs), 2 phosphatidylglycerol (PGs), and 1 phosphatidylinositol (PI) were identified (Figure 1). Phosphatidylethanolamine (PE) was not detected in the PL fraction, indicating the absence of PE in *F. solaris*. In the glycolipid (GL) fraction, 16 types of lipids

including 8 monogalactosyldiacylglycerol (MGDGs), 5 digalactosyldiacylglycerol (DGDGs), and 3 sulfoquinovosyldiacylglycerol SQDGs were identified (Figure 2).

There are two distinct pathways for glycerolipid assembly in higher plants [27] and microalgae [28], *i.e.*, a prokaryotic pathway and a eukaryotic pathway. In diatoms, the chloroplast is enveloped with four membranes (outermost, second outermost, second innermost and innermost membranes, see also Figure 3). The innermost and second innermost membranes are actually corresponding to the two membranes of the primary chloroplast where glycerolipids are synthesized through the prokaryotic pathway. The space between the second outermost membrane and the outermost membrane represents the endoplasmic reticulum (ER, also known as chloroplast-ER; CER) where the eukaryotic pathway is responsible for the lipid synthesis. The lipids assembled through the prokaryotic pathway have a C16 fatty acid at the *sn*-2 position, while those through the eukaryotic pathway have a C18 or C20 fatty acid at the *sn*-2 position.

In *F. solaris*, the *sn*-2 position of major MGDGs, DGDGs, SQDGs, PGs and PI species was exclusively occupied by a C16 fatty acid. A part of PC species also possessed a C16 fatty acid at the *sn*-2 position (Figure 1A). In addition, the *sn*-2 position in most TAGs was also occupied by C16 fatty acids [22]. This specific distribution of C16 at the *sn*-2 position in large proportion of lipids was also reported in *P. tricornutum* [29,30]. These results indicate that the prokaryotic pathway in the chloroplast plays an essential role in the storage lipid TAG and chloroplast lipids including MGDG, DGDG, SQDG, and PG in diatoms. PC had both C16 and C18 (C20) fatty acids at the *sn*-2 position (Figure 1A), suggesting that both prokaryotic (in the chloroplast) and eukaryotic (in the ER) pathways could contribute to PC synthesis. This characteristic feature of PC has previously been confirmed only in *P. tricornutum* [30], and has not been found in higher plants and green algae, implying that this duplicated origin of PC could be a unique for diatoms. Furthermore, an *F. solaris*-specific feature was also found. The eukaryotic type of GLs which have been found in *P. tricornutum* [30] (e.g., MGDG 20:5/18:4, MGDG 20:5/20:5, MGDG 20:5/18:2, SQDG 20:5/18:4 and SQDG 22:6/18:1 (*sn*-1/*sn*-2)), were not detectable in this study.

2.2. Putative Pathways for the PUFA Synthesis in Fistulifera solaris

Another important finding of our analysis is that C18 fatty acids (e.g., C18:1, C18:2 and C18:3) were found only on PCs (Figure 1A). More specifically, C18 fatty acids are distributed only at the *sn*-2 position of PCs, indicating that these PCs are assembled through the eukaryotic pathway in ER. Since these C18 fatty acids are essential precursors for EPA synthesis [26], we propose that EPA synthesis in *F. solaris* was, at least partially, performed on PC in ER (Figure 3). EPA synthesis in ER is consistent with our previous study where most enzymes involved in the EPA synthesis are localized in the ER [26,31]. Furthermore, the involvement of PC in the EPA synthesis is also consistent with the previous metabolic labeling study on *P. tricornutum* [15], in which it was demonstrated that the C18:1 was desaturated on PC to C18:3 or C18:4, the subsequent elongation of the C18:3 and C18:4 to the C20:3 and C20:4 occurred on fatty acid-CoA, and finally, the C20:3 and C20:4 were desaturated to EPA on PC. These results suggest that diatoms may share the EPA synthesis mechanism in which PCs play a central role, although we have previously demonstrated that the EPA synthesis pathway in *F. solaris* was simpler than in *P. tricormutum* [26].

Figure 1. The representative MS spectra of phosphatidylcholine (PC) (**A**); phosphatidylglycerol (PG) (**B**), and phosphatidylinositol (PI) (**B**) profile of *Fistulifera* sp. Fatty acids in the *sn*-2 position are represented in bold and red.

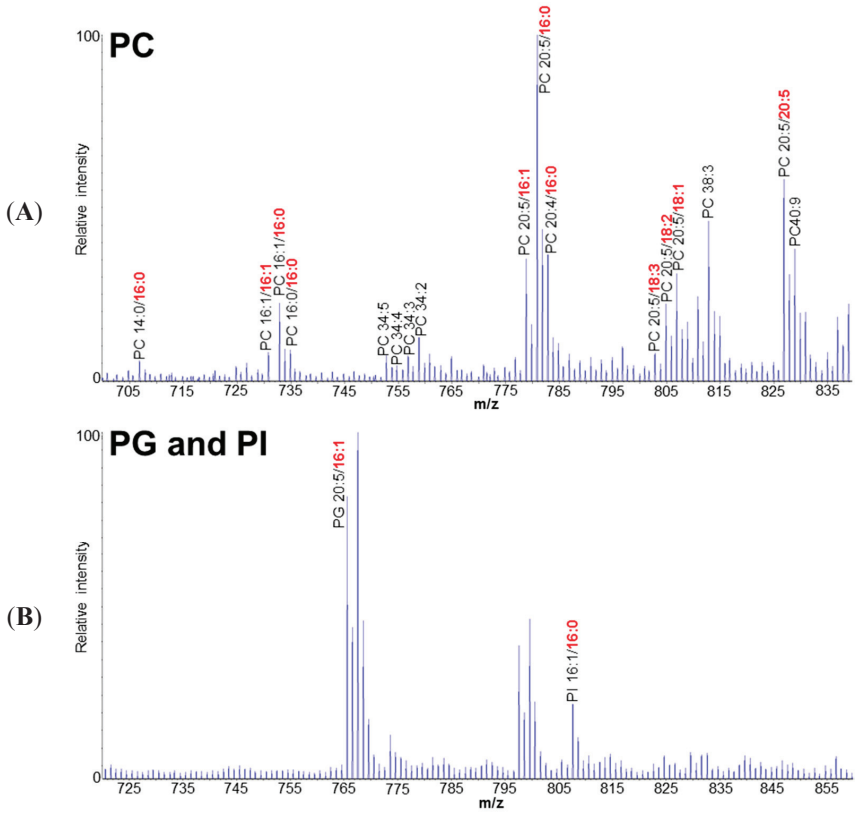

2.3. EPA Incorporation into TAG through the Acyl-Editing Process on PC

The EPA-containing TAGs in *F. solaris* mainly contain a C16 fatty acid at the *sn*-2 position which suggests the prokaryotic origination of those TAGs [22]. These TAGs can be theoretically synthesized by two pathways: the diacylglycerol acyltransferase (DGAT)-mediated *de novo* synthesis (the so called Kennedy pathway) and the phospholipid diacylglycerol acyltransferase (PDAT)-mediated membrane conversion. The DGAT catalyzes the acyltransfer reaction which incorporates the fatty acid at the fatty acid-CoA to the *sn*-3 or *sn*-1 position of the diacylglycerol (DAG) to generate TAG, while the PDAT catalyzes the acyltransfer reaction that incorporates the fatty acid at the *sn*-2 position of PC to the *sn*-3 or *sn*-1 position of DAG to generate TAG. For both enzymes, the substrate DAG is used as the backbone for TAG synthesis. In *F. solaris*, the exclusive existence of C14, C16 and C20:5 in the EPA-containing TAGs [22] strongly indicated that the major precursors for the synthesis of these specific TAGs could be DAG C16/C16 (*sn*-1/*sn*-2) (Figure 3; compound B) or DAG EPA/C16 (*sn*-1/*sn*-2) (Figure 3; compound C) because C14 fatty acid presented in a minor percentage in this strain.

Figure 2. The representative MS spectra of the monogalactosyldiacylglycerol (MGDG) (**A**); digalactosyldiacylglycerol (DGDG) (**B**); and sulfoquinovosyldiacylglycerol (SQDG) (**C**) profile of *Fistulifera* sp. Fatty acids in the *sn*-2 position are represented in bold and red.

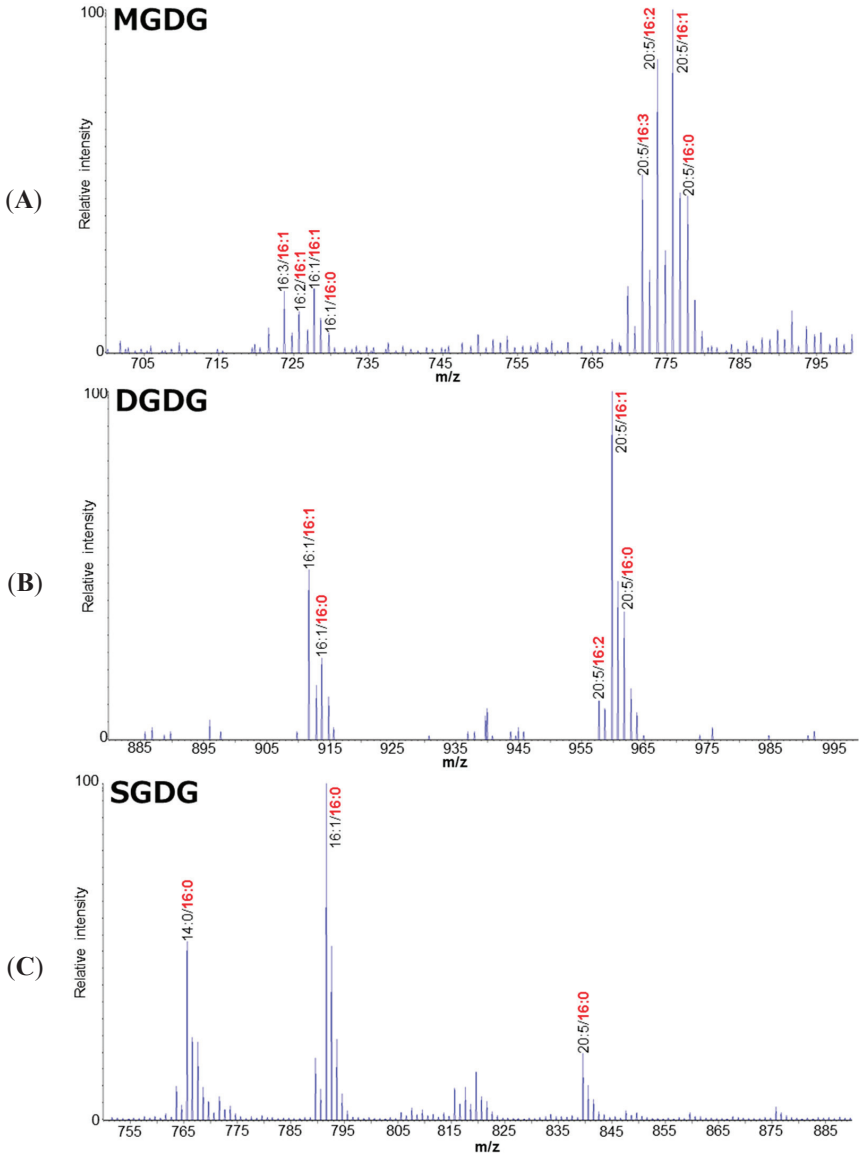

The most simple and reasonable pathway for the synthesis of EPA-containing prokaryotic TAG could be the PDAT-mediated acyltransfer with DAG C16/C16 (Figure 3; compound B) and PC EPA/EPA (Figure 3; compound A). Another possible pathway is DGAT-mediated acyltransfer with DAG EPA/C16 (*sn*-1/*sn*-2) (Figure 3; compound C) and fatty acid-CoA. We believe these two pathways are major contributors to incorporate EPA into TAG.

Figure 3. The scheme of the putative polar lipids and eicosapentaenoic acid (EPA) synthesis pathway in *Fistulifera solaris*. The plastid in this strain is considered to be surrounded by four membranes. Fatty acids and the prokaryotic lipids are *de novo* synthesized in the primary plastid. The eukaryotic lipids are *de novo* synthesized in the endoplasmic reticulum. The EPA was synthesized through the sequential desaturation of C18 fatty acid on PC. The acyl-editing and head group exchange processes on PC could not only provide EPA-CoA and EPA containing DAGs for the synthesis of other EPA-containing lipids but also promote the synthesis of the PC species maintain two C16 fatty acids. TAG in this figure is specified as the EPA-containing prokaryotic TAG. Arrow-headed lines represent synthesis, while dashed arrow-headed line represents transportation. OB, oil body; PS, periplastidal space; FAS, fatty acid synthesis; PLA, phospholipase A; LPCAT, acyl-CoA, lyso-phosphatidylcholine acyltransferase; PDCT, phosphatidylcholine diacylglycerol cholinephosphotransferase; FFA, free fatty acid; PDAT, phospholipid, diacylglycerol actyltransferase; DGAT, acyl-CoA, diacylglycerol acyltransferase; ELO, elongase.

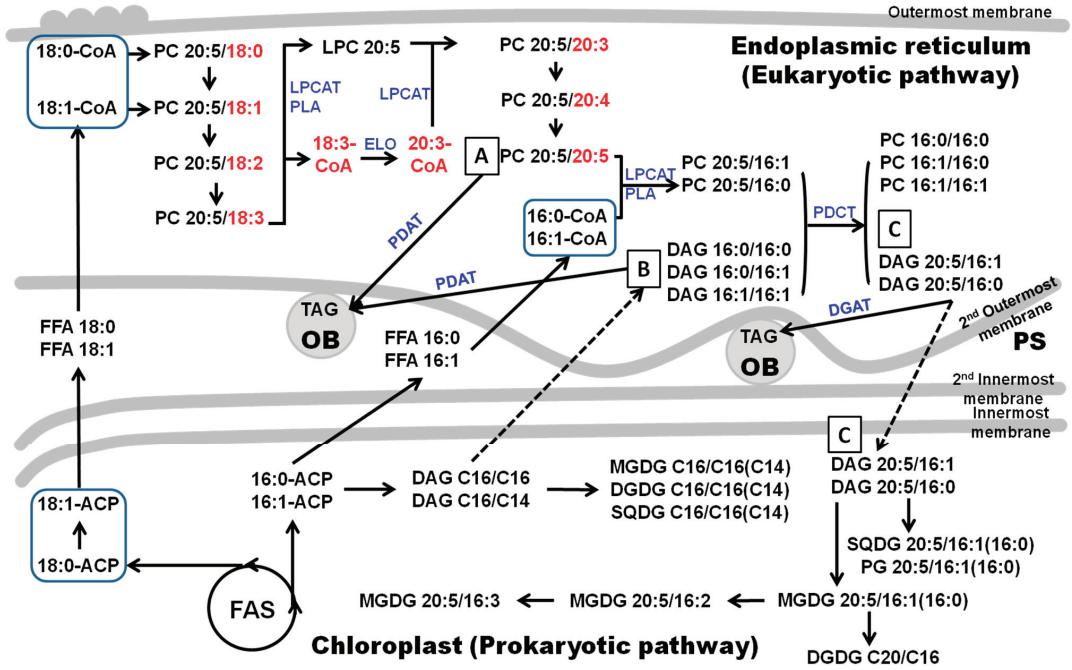

Thus far, the mechanism for the DAG EPA/C16 synthesis has never been discussed in any microalgae, but is important to be elucidated for controlling EPA-incorporation into TAG. One possibility is the *de novo* synthesis of DAG EPA/C16. In this mechanism, the EPA can be released from the PC in the ER to generate EPA-CoA. The generated EPA-CoA could then be transported into the chloroplast to generate EPA-ACP. Finally, the EPA on EPA-ACP is incorporated into DAG EPA/C16 in the chloroplast. However, this circuitous pathway can hardly be considered as reasonable. Therefore, we propose another pathway for the synthesis of DAG EPA/C16; *i.e.*, the

PC-based acyl-editing and head group exchange processes, which are recently demonstrated in higher plants to be essential for the incorporation of PUFA into TAG [32,33]. EPA-incorporation through this process is summarized in Figure 3. Three key enzymes are involved in these processese, the phospholipase A (PLA), acyl-CoA: lyso-phosphatidylcholine acyltransferase (LPCAT), and the phosphatidylcholine diacylglycerol cholinephosphotransferase (PDCT). The PLA catalyzes the reaction to degrade the PC into a lyso-PC (LPC) and the free fatty acid which was then converted to acyl-CoA by acyl-CoA synthetases. LPCAT catalyzes the esterification of the *sn*-2 position of a lyso-PC (LPC) to generate PC, as well as the reverse reaction [33]. PDCT catalyzes the transfer of the phosphocholine head group from PC to DAG to generate new species of PC and DAG. The eukaryotic type of PCs which maintain an EPA at the *sn*-1 position and a C18 or C20 fatty acid at the *sn*-2 position, which were abundantly detected (Figure 1A), can be served as the starting materials to produce DAG EPA/C16. The *sn*-2 positions of these EPA-containing eukaryotic PCs are then converted to the most abundant C16 through the PLA and LPCAT mediated acyl-editing process (Figure 4, Reaction I). The generated EPA-containing PCs could subsequently transfer their head group to the predominant DAG C16/C16 through the PDCT mediated head group exchange process to generate the DAG EPA/C16 (*sn*-1/*sn*-2) and PC C16/C16 (Figure 4, Reaction II). The DAG EPA/C16 (*sn*-1/*sn*-2) can be utilized for the generation of EPA-containing TAGs as well as the EPA-containing prokaryotic MGDG, DGDG, SQDG, PG, and PI (Figure 4).

Figure 4. The scheme of the proposed PC-based acyl-editing and head group exchange processes, which are catalyzed by PLA, LPCAT, and PDCT, for the synthesis of prokaryotic EPA-containing TAG, MGDG, DGDG, SQDG, PG and PI in *F. solaris*.

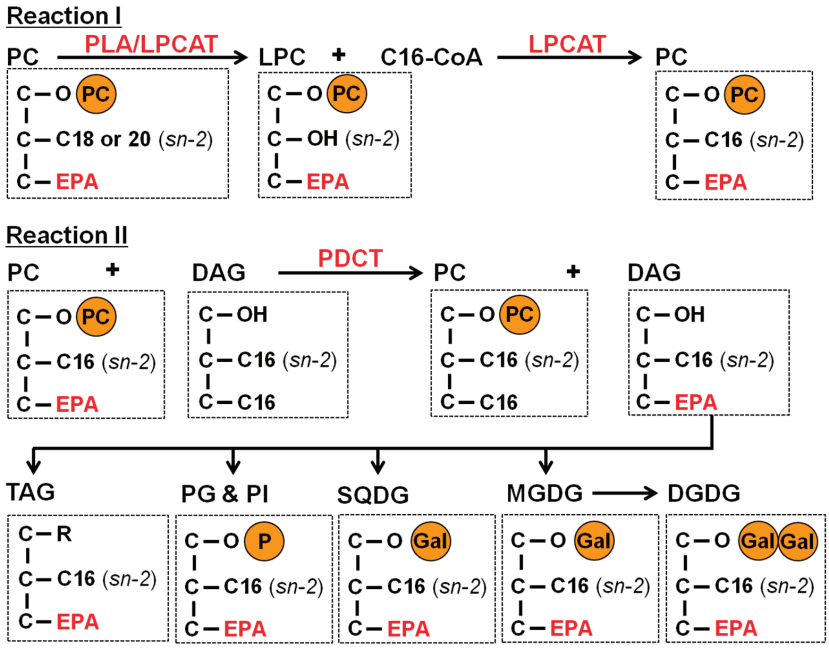

3. Experimental Section

3.1. Materials

The marine oleaginous diatom, *Fistulifera* sp. JPCC DA0580 was isolated by and identified in our group [21]. Silica gel 60 pre-coated thin-layer chromatography plates were from Merck (Darmstadt, Germany). The Supelclean™ LC-Si SPE Tube (100 mg, 1 mL) was purchased from Sigma Aldrich (Tokyo, Japan). LC-MS grade methanol, LC-MS grade formic acid, and HPLC grade chloroform were purchased from Wako (Tokyo, Japan). All other reagents were of the highest commercial grade available.

3.2. Strain and Culture Conditions

The cells were cultured as described previously [22]. In order to enhance the polar lipids recovery in *F. solaris* JPCC DA0580, the nutrition-rich 10f medium which contained 10-fold more nutrition components than f medium (150 mg $NaNO_3$, 12 mg $Na_2HPO_4 \cdot 2H_2O$, 1 μg vitamin B_{12}, 1 μg biotin, 200 μg thiamine HCl, 20 mg $Na_2SiO_3 \cdot 9H_2O$, 8.8 mg Na_2EDTA, 6.32 mg $FeCl_3 \cdot 6H_2O$, 24 μg $CoSO_4 \cdot 5H_2O$, 42 μg $ZnSO_4 \cdot 7H_2O$, 0.36 mg $MnCl_2 \cdot 4H_2O$, 140 μg $CuSO_4 \cdot 5H_2O$, and 14 μg $Na_2MoO_4 \cdot 2H_2O$ per liter of artificial seawater) [34] was selected to eliminate the intensive neutral lipid accumulation [22]. The cells were cultured with the initial cell concentration of 1.0×10^6 cells·mL^{-1} in flat-shape flasks (1.5 L). The growth curve was shown in Supplementary Figure S1. The temperature was maintained at 25 ± 1 °C, and continuous illumination was applied at 200 μmol·m^{-2}·s^{-1}. The cultures were bubbled with sterile air containing 2% CO_2 at a flow rate of 0.8 L/min. After 180 h of cultivation, the cells were harvested by centrifugation at 8500× *g* for 15 min and freeze-dried.

3.3. Lipid Extraction

Total lipids were extracted from the lyophilized cells by two-step chloroform/methanol extraction described by Ejsing *et al.* [35] with some modifications. In general, 25 mg of the lyophilized microalgal cells were re-suspended in 5 mL of chloroform/methanol (20:1 v/v) and disrupted by 15 min-sonication. Phase separation was induced by adding distillated water (1 mL). After centrifugation at 800× *g* for 10 min, the lower phase was collected. The remaining aqueous sample material was processed with the extraction procedure again with 5 mL chloroform/methanol (2:1, v/v). The lower organic phase was collected and combined with the formerly collected organic phase. The lipid extracts were dried under argon gas and stored at −30 °C.

3.4. Lipid Fractionation

In order to avoid the unwanted overlap of isotopic ion peaks in the direct infusion ESI-Q-TRAP MS analysis, the solid phase extraction (SPE) was carried out to separate the total lipid extract. The Supelclean™ LC-Si SPE Tube (100 mg, 1 mL) was used to fractionate the total lipids into neutral lipids (NLs), glycolipids (GLs), and phospholipids (PLs) according to the method of

Popovich *et al.* [36] with minor modifications. The columns were conditioned with 4 mL of hexane. The crude lipid extracts were dissolved in 200 μL of chloroform and loaded into the column. NLs were eluted with 4 mL of chloroform, and GLs were eluted with 4 mL of acetone/methanol (9:1 v/v), finally PLs were eluted with 4 mL of methanol. Each lipid fraction was collected into a glass vial and dried under argon gas. The efficiency of SPE separation was verified by thin-layer chromatography (TLC). Briefly, each lipid fraction was analyzed by TLC. The neutral lipids were developed by *n*-hexane:diethyl ether:acetic acid 70:30:1 (v/v/v), and the polar lipis were developed by chloroform:methanol:acetic acid:water 170:30:20:7 (v/v/v/v). Neutral lipids and polar lipids were stained with iodine, while glycolipids were stained with orcinol. No contaminate lipid bands were observed in the lane of each lipid fraction on the TLC plates (data not shown).

3.5. Direct Infusion Tandem MS/MS Analysis

PL and GL fractions were re-dissolved in chloroform/methanol (2:1 v/v). Adequate amount of lipid samples were added into the corresponding solvents according to the detecting ion mode. Chloroform/methanol (2:1 v/v with 1% of formic acid) was for the detection at positive ion mode, and chloroform/methanol (1:2 v/v) was for the detection at negative ion mode. Samples were introduced into ESI-Q-TRAP-MS (QTRAP4000, AB Sciex) with direct infusion at the flow rate of 10 μL/min. Sulfoquinovosyldiacylglycerols (SQDGs) were detected by Q1 scan at negative ion mode, while monogalactosyldiacylglycerols (MGDGs) and digalactosyldiacylglyerols (DGDGs) were detected by neutral loss scan at positive ion mode for the loss of *m*/*z* 162 which corresponding to the loss of a sugar group (galactose). Phosphatidylcholines (PCs) were detected by precursor ion scan for 184.07 (phosphocholine group) at positive ion modes, while other PLs including phosphatidylglycerols (PGs) and Phosphatidylinositos (PIs) were detected by Q1 scan at negative ion mode. Lipids were determined with their calculated *m*/*z*. The fatty acid composition and positional distribution [37,38] were identified with product ion scan of each lipid molecule. Generally, the center position of the glycerol backbone is referred to as *sn*-2 position, and other ends are *sn*-1 and sn-3 positions.

4. Conclusions

In conclusion, the polar lipid profile in *Fistulifera solaris* JPCC DA0580 was determined with direct infusion ESI-Q-TRAP-MS and MS/MS. Based on our analysis, the chloroplast was demonstrated to play an essential role in the lipid biosynthesis in *F. solaris*. EPA was synthesized on PC in *F. solaris*. In addition, we proposed that the PC-based acyl-editing and head group exchange processes may contribute to the incorporation of EPA into TAGs. To our best knowledge, this is the first report showing the possibility that the PC-based acyl-editing and head group exchange could contribute to the EPA-incorporation into TAG in diatoms. According to this study, the key enzymes in the acyl-editing and head group exchange processes, the PLA, LPCAT and PDCT, can be the future targets for metabolic engineering towards the regulation of EPA content for different purpose.

Acknowledgments

This study was supported by Japan Science and Technology Agency (JST), Core Research for Evolutionary Science and Technology (CREST).

Author Contributions

Tsuyoshi Tanaka designed overall experiments. Yue Liang performed experiments and analyzed data. All authors, including Yue Liang, Yoshiaki Maeda, Tomoko Yoshino, Mitsufumi Matsumoto, and Tsuyoshi Tanaka participated in discussions and preparation of the manuscript.

Conflicts of Interest

The authors declare no conflict of interest.

References

1. Hu, Q.; Sommerfeld, M.; Jarvis, E.; Ghirardi, M.; Posewitz, M.; Seibert, M.; Darzins, A. Microalgal triacylglycerols as feedstocks for biofuel production: Perspectives and advances. *Plant J.* **2008**, *54*, 621–639.
2. Li, Y.; Horsman, M.; Wu, N.; Lan, C.Q.; Dubois-Calero, N. Biofuels from microalgae. *Biotechnol. Prog.* **2008**, *24*, 815–820.
3. Lam, M.K.; Lee, K.T. Microalgae biofuels: A critical review of issues, problems and the way forward. *Biotechnol. Adv.* **2012**, *30*, 673–690.
4. Liang, Y.; Sarkany, N.; Cui, Y. Biomass and lipid productivities of *Chlorella vulgaris* under autotrophic, heterotrophic and mixotrophic growth conditions. *Biotechnol. Lett.* **2009**, *31*, 1043–1049.
5. Rodolfi, L.; Chini Zittelli, G.; Bassi, N.; Padovani, G.; Biondi, N.; Bonini, G.; Tredici, M.R. Microalgae for oil: Strain selection, induction of lipid synthesis and outdoor mass cultivation in a low-cost photobioreactor. *Biotechnol. Bioeng.* **2009**, *102*, 100–112.
6. Mata, T.M.; Martins, A.A.; Caetano, N.S. Microalgae for biodiesel production and other applications: A review. *Renew. Sustain. Energy Rev.* **2010**, *14*, 217–232.
7. Radakovits, R.; Jinkerson, R.E.; Fuerstenberg, S.I.; Tae, H.; Settlage, R.E.; Boore, J.L.; Posewitz, M.C. Draft genome sequence and genetic transformation of the oleaginous alga Nannochloropis gaditana. *Nat. Commun.* **2012**, *3*, doi:10.1038/ncomms1688.
8. Chiu, S.-Y.; Kao, C.-Y.; Tsai, M.-T.; Ong, S.-C.; Chen, C.-H.; Lin, C.-S. Lipid accumulation and CO_2 utilization of *Nannochloropsis oculata* in response to CO_2 aeration. *Bioresour. Technol.* **2009**, *100*, 833–838.
9. Satoh, A.; Ichii, K.; Matsumoto, M.; Kubota, C.; Nemoto, M.; Tanaka, M.; Yoshino, T.; Matsunaga, T.; Tanaka, T. A process design and productivity evaluation for oil production by indoor mass cultivation of a marine diatom, *Fistulifera* sp. JPCC DA0580. *Bioresour. Technol.* **2013**, *137*, 132–138.

10. Knothe, G. Dependence of biodiesel fuel properties on the structure of fatty acid alkyl esters. *Fuel Proc. Technol.* **2005**, *86*, 1059–1070.
11. Chisti, Y. Biodiesel from microalgae. *Biotechnol. Adv.* **2007**, *25*, 294–306.
12. Deckelbaum, R.J.; Torrejon, C. The omega-3 fatty acid nutritional landscape: Health benefits and sources. *J. Nutr.* **2012**, *142*, 587S–591S.
13. Arao, T.; Kawaguchi, A.; Yamada, M. Positional distribution of fatty acids in lipids of the marine diatom *Phaeodactylum tricornutum*. *Phytochemistry* **1987**, *26*, 2573–2576.
14. Arao, T.; Yamada, M. Biosynthesis of polyunsaturated fatty acids in the marine diatom, *Phaeodactylum tricornutum*. *Phytochemistry* **1994**, *35*, 1177–1181.
15. Arao, T.; Sakaki, T.; Yamada, M. Biosynthesis of polyunsaturated lipids in the diatom, *Phaeodactylum tricornutum*. *Phytochemistry* **1994**, *36*, 629–635.
16. Alonso, D.L.; Belarbi, E.-H.; Fernández-Sevilla, J.M.; Rodríguez-Ruiz, J.; Grima, E.M. Acyl lipid composition variation related to culture age and nitrogen concentration in continuous culture of the microalga *Phaeodactylum tricornutum*. *Phytochemistry* **2000**, *54*, 461–471.
17. Bowler, C.; Allen, A.E.; Badger, J.H.; Grimwood, J.; Jabbari, K.; Kuo, A.; Maheswari, U.; Martens, C.; Maumus, F.; Otillar, R.P.; *et al*. The Phaeodactylum genome reveals the evolutionary history of diatom genomes. *Nature* **2008**, *456*, 239–244.
18. Miyahara, M.; Aoi, M.; Inoue-Kashino, N.; Kashino, Y.; Ifuku, K. Highly efficient transformation of the diatom *Phaeodactylum tricornutum* by multi-pulse electroporation. *Biosci. Biotechnol. Biochem.* **2013**, *77*, 874–876.
19. Apt, K.E.; Kroth-Pancic, P.G.; Grossman, A.R. Stable nuclear transformation of the diatom *Phaeodactylum tricornutum*. *Mol. Gen. Genet.* **1996**, *252*, 572–579.
20. Matsumoto, M.; Mayama, S.; Nemoto, M.; Fukuda, Y.; Muto, M.; Yoshino, T.; Matsunaga, T.; Tanaka, T. Morphological and molecular phylogenetic analysis of the high triglyceride-producing marine diatom, *Fistulifera solaris* sp. nov. (Bacillariophyceae). *Phycol. Res.* **2014**, in press.
21. Matsumoto, M.; Sugiyama, H.; Maeda, Y.; Sato, R.; Tanaka, T.; Matsunaga, T. Marine diatom, *Navicula* sp. strain JPCC DA0580 and marine green alga, *Chlorella* sp. strain NKG400014 as potential sources for biodiesel production. *App. Biochem. Biotechnol.* **2010**, *161*, 483–490.
22. Liang, Y.; Maeda, Y.; Matsumoto, M.; Yoshino, T.; Tanaka, T. Profiling of fatty acid methyl esters from the oleaginous diatom *Fistulifera* sp. strain JPCC DA0580 under nutrition-sufficient and -deficient conditions. *J. Appl. Phycol.* **2014**, doi:10.1007/s10811-014-0265-y.
23. Sato, R.; Maeda, Y.; Yoshino, T.; Tanaka, T.; Matsumoto, M. Seasonal variation of biomass and oil production of the oleaginous diatom *Fistulifera* sp. in outdoor vertical bubble column and raceway-type bioreactors. *J. Biosci. Bioeng.* **2014**, *117*, 720–724.
24. Tanaka, T.; Fukuda, Y.; Yoshino, T.; Maeda, Y.; Muto, M.; Matsumoto, M.; Mayama, S.; Matsunaga, T. High-throughput pyrosequencing of the chloroplast genome of a highly neutral-lipid-producing marine pennate diatom, *Fistulifera* sp. strain JPCC DA0580. *Photosynth. Res.* **2011**, *109*, 223–229.

25. Muto, M.; Fukuda, Y.; Nemoto, M.; Yoshino, T.; Matsunaga, T.; Tanaka, T. Establishment of a genetic transformation system for the marine pennate diatom *Fistulifera* sp. strain JPCC DA0580—A high triglyceride producer. *Mar. Biotechnol.* **2013**, *15*, 48–55.
26. Liang, Y.; Maeda, Y.; Sunaga, Y.; Muto, M.; Matsumoto, M.; Yoshino, T.; Tanaka, T. Biosynthesis of polyunsaturated fatty acids in the oleaginous marine diatom *Fistulifera* sp. strain JPCC DA0580. *Mar. Drugs* **2013**, *11*, 5008–5023.
27. Somerville, C. Plant lipids: Metabolism, mutants, and membranes. *Science* **1991**, *252*, 80–87.
28. Fan, J.; Andre, C.; Xu, C. A chloroplast pathway for the *de novo* biosynthesis of triacylglycerol in *Chlamydomonas* reinhardtii. *FEBS Lett.* **2011**, *585*, 1985–1991.
29. Yongmanitchai, W.; Ward, O.P. Molecular species of triacylglycerols from the freshwater diatom, *Phaeodactylum tricor*. *Phytochemistry* **1993**, *32*, 1137–1139.
30. Yongmanitchai, W.; Ward, O.P. Positional distribution of fatty acids, and molecular species of polar lipids, in the diatom *Phaeodactylum tricornutum*. *J. Gen. Microbiol.* **1993**, *139*, 465–472.
31. Muto, M.; Kubota, C.; Tanaka, M.; Satoh, A.; Matsumoto, M.; Yoshino, T.; Tanaka, T. Identification and functional analysis of delta-9 desaturase, a key enzyme in PUFA synthesis, isolated from the oleaginous diatom *Fistulifera*. *PLoS One* **2013**, *8*, e73507.
32. Bates, P.D.; Browse, J. The significance of different diacylgycerol synthesis pathways on plant oil composition and bioengineering. *Front. Plant Sci.* **2012**, *3*, doi:10.3389/fpls.2012.00147.
33. Bates, P.D.; Fatihi, A.; Snapp, A.R.; Carlsson, A.S.; Lu, C. Acyl editing and headgroup exchange are the major mechanisms that direct polyunsaturated fatty acid flux into triacylglycerols. *Plant Physiol.* **2012**, *160*, 1530–1539.
34. Guillard, R.R.; Ryther, J.H. Studies of marine planktonic diatoms: I. *Cyclotella Nana* Hustedt, and *Detonula Confervacea* (Cleve) Gran. *Can. J. Microbiol.* **1962**, *8*, 229–239.
35. Ejsing, C.S.; Sampaio, J.L.; Surendranath, V.; Duchoslav, E.; Ekroos, K.; Klemm, R.W.; Simons, K.; Shevchenko, A. Global analysis of the yeast lipidome by quantitative shotgun mass spectrometry. *Proc. Natl. Acad. Sci. USA* **2009**, *106*, 2136–2141.
36. Popovich, C.A.; Damiani, C.; Constenla, D.; Leonardi, P.I. Lipid quality of the diatoms *Skeletonema costatum* and *Navicula gregaria* from the South Atlantic Coast (Argentina): Evaluation of its suitability as biodiesel feedstock. *J. Appl. Phycol.* **2012**, *24*, 1–10.
37. Malone, M.; Evans, J.J. Determining the relative amounts of positional isomers in complex mixtures of triglycerides using reversed-phase high-performance liquid chromatography-tandem mass spectrometry. *Lipids* **2004**, *39*, 273–284.
38. Xu, J.; Chen, D.; Yan, X.; Chen, J.; Zhou, C. Global characterization of the photosynthetic glycerolipids from a marine diatom *Stephanodiscus* sp. by ultra performance liquid chromatography coupled with electrospray ionization-quadrupole-time of flight mass spectrometry. *Anal. Chim. Acta* **2010**, *663*, 60–68.

Quorum Quenching Agents: Resources for Antivirulence Therapy

Kaihao Tang and Xiao-Hua Zhang

Abstract: The continuing emergence of antibiotic-resistant pathogens is a concern to human health and highlights the urgent need for the development of alternative therapeutic strategies. Quorum sensing (QS) regulates virulence in many bacterial pathogens, and thus, is a promising target for antivirulence therapy which may inhibit virulence instead of cell growth and division. This means that there is little selective pressure for the evolution of resistance. Many natural quorum quenching (QQ) agents have been identified. Moreover, it has been shown that many microorganisms are capable of producing small molecular QS inhibitors and/or macromolecular QQ enzymes, which could be regarded as a strategy for bacteria to gain benefits in competitive environments. More than 30 species of marine QQ bacteria have been identified thus far, but only a few of them have been intensively studied. Recent studies indicate that an enormous number of QQ microorganisms are undiscovered in the highly diverse marine environments, and these marine microorganism-derived QQ agents may be valuable resources for antivirulence therapy.

Reprinted from *Mar. Drugs*. Cite as: Tang, K.; Zhang, X.-H. Quorum Quenching Agents: Resources for Antivirulence Therapy. *Mar. Drugs* **2014**, *12*, 3245–3282.

Abbreviations

AHL, *N*-Acyl-homoserine lactonse; AI-2, Autoinducter-2; AI-3, Autoinducter-3; AIP, Autoinducing peptides; DSF, Diffusible signal factor; BDSF, *Burkholderia cenocepacia* diffusible signal factor; CAI-1, *Cholerae* autoinducer-1; Ea-C8-CAI-1, (*Z*)-3-Aminoundec-2-en-4-one; PQS, *Pseudomonas* quinolone signal; IQS, Integrating QS signal; *R*-THMF, (*2R*,*4S*)-2-Methyl-2,3,3,4-tetrahydroxytetrahydrofuran; *S*-THMF-borate, (*2S*,*4S*)-2-Methyl-2,3,3,4-tetrahydroxytetrahydrofuran-borate; DPD, 4,5-Dihydroxy-2,3-pentanedione.

1. Introduction

Antibiotics are recognized as effective antimicrobial agents for curing diseases caused by pathogenic bacteria. Traditional antibiotics are bactericidal or bacteriostatic by targeting essential processes for bacterial growth including cell wall synthesis, DNA replication, RNA transcription and protein synthesis [1]. However, because of the life-or-death selective pressure imposed on the targeted pathogens, antibiotic-resistant strains are constantly emerging. The inappropriate and excessive use of antibiotics accelerates the emergence of antibiotic resistance. Unfortunately, in contrast to the rising levels of antibiotic resistance, the pace of novel antibiotic development has severely slowed in the preceding few decades. This problem leads to the urgent need for the development of new antimicrobial agents targeting virulence (toxin function and delivery, regulation of virulence expression and bacterial adhesion) rather than the essential processes of

pathogenic microorganisms [1]. The so-called antivirulence therapy may impose less selective pressure on pathogenic microorganisms, and in theory, decrease resistance [1].

Quorum sensing (QS) is a process for bacteria to communicate, regulate gene expression and synchronize social behaviors, such as biofilm formation, bioluminescence and secretion of virulence factors [2,3]. Hitherto diverse molecular mechanisms of sophisticated QS have been unraveled [2]. In particular, it has been established that QS regulates the secretion of virulence factors in many pathogens, such as *Pseudomonas aeruginosa*, *Erwinia carotovora*, *Vibrio* spp. and *Burkholderia* spp. [2]. In addition, these pathogens use QS to regulate biofilm formation, which is a critical defense against antibacterial drugs or the immune system of a host. Because QS is not essential for the growth of bacteria, quenching QS (quorum quenching, QQ) in these pathogens would disarm virulence rather than kill the bacteria, which may considerably weaken the selective pressure imposed on the pathogens and delay the evolution of resistance to QQ drugs. All of these features make QS an ideal target for antivirulence therapy [1].

Here, we provide an overall summary of the uniformity and diversity of QS in microorganisms, as well as the QS circuits in some representative species. Two main QQ agents, *i.e.*, small molecular QS inhibitors and macromolecular QQ enzymes, are discussed. The current status and trends of antivirulence therapy utilizing QQ resources from the marine environment are considered. Based on this knowledge, a critical appraisal and perspective of the resource for antivirulence in the environment is presented.

2. The Distribution of QS Systems in Microorganisms

The term QS was first proposed to describe the phenomenon that marine bacteria, *i.e.*, *V. fischeri* and *V. harveyi*, use signaling molecules (autoinducers, AIs) as sensors of cell density so that the population as a whole may coordinate the social behavior of bioluminescence [4]. However, in addition to cell density, the concentration of AIs in the natural environment is determined by many other biotic and abiotic factors, such as the spatial distribution of cells and the diffusional characteristics of the environment [5–9]. Redfield [5] proposed a concept of diffusion sensing (DS) to challenge the previously assumed role of QS. She argued that cells employ AIs to assess diffusive properties of the environment, and thereby determine when to produce more costly secreted molecules, such as extracellular protease. This may be less effective in the environment with a high diffusion rate. Another concept of efficiency sensing (ES) was introduced in an attempt to unify both QS and DS [6]. In particular, it has been demonstrated that even a single cell may initiate QS-regulated behaviors by physical confinement [10,11], which provides support for the hypotheses of DS and ES. However, QS and DS are not diametrically opposed, and the utility of ES has been debated [8,12]. In addition, many other hypotheses emphasizing different factors have been suggested to compete or unite with QS [13]. However, Platt *et al.* [13] argued that the introduction of new hypotheses would lead to confusion rather than clarification. Therefore, it was suggested that the processes of QS could be viewed broadly with full awareness of the effects of environmental factors [13].

Despite the presence of distinct QS systems in different microorganisms, the fundamental processes are similar. Initially, AIs are synthesized by AI synthases and diffuse away. When the

concentrations of AIs increase to a threshold, AIs are detected by receptors. Subsequently, the AI-bound receptors activate the expression of relevant genes, including AI synthase-encoding genes. This results in a positive feed-back loop for biosynthesis of AIs, which may be able to promote the synchrony among a population.

Increasing evidence has revealed that QS is prevalent in bacteria, fungi and archaea (Figure 1, Table 1). For example, it is widely accepted that *N*-acylhomoserine lactones (AHLs) and autoinducing peptides (AIPs) are mainly used by Gram-negative and Gram-positive bacteria for intraspecies communication, respectively. Autoinducter-2 (AI-2) signals are hypothesized to be used for interspecies communication because AI-2 production and the synthase LuxS homologues are widespread among Gram-negative and Gram-positive bacteria [14,15]. However, many bacteria only produce AI-2, but lack cognate receptors. The two classes of AI-2 receptors, LuxPQ and Lsr-receptor, are restricted to Vibrionales representatives and pathogenic bacteria associated with endotherms, respectively [16,17]. Therefore, the QS role of LuxS protein is arguable. It may be only a metabolic enzyme involved in the activated methyl cycle (AMC) [18] in these bacteria that are devoid of a complete AI-2 signaling pathway [16]. In addition to AI-2, indole has been suggested as an interspecies signal molecule, because it is shared by 85 species of Gram-positive and Gram-negative bacteria [19] (Table 1). However, some exceptions have been discovered. One type of AHL, 3-oxo-octanoyl homoserine lactone (3OC8-HSL), is utilized by a Gram-positive bacterium, *Exiguobacterium* sp. MPO, as a QS signaling molecule to regulate biofilm formation and extracellular polymeric substance production [20]. In addition, peptide-based QS is also found in a hyperthermophilic Gram-negative bacterium, *Thermotoga maritima* [21], and additionally in the yeast *Cryptococcus neoformans* [22]. Furthermore, AHLs are not the only signal type employed by Gram-negative bacteria. The diffusible signal factor (DSF) family, *V. cholerae* autoinducer-1 (CAI-1) family and other particular signals, such as *Pseudomonas* quinolone signal (PQS), integrating QS signal (IQS) and pyrone signal are also employed by some Gram-negative bacteria (Table 1). Among these molecules, the CAI-1 family is found mainly in *Vibrio* spp. [23] whereas the DSF family commonly exists in some plant pathogens, such as *Xanthomonas* and *Burkholderia* spp. [24]. Likewise, social behaviors namely filamentation and biofilm formation by the opportunistic fungal pathogen *Candida albicans* are regulated by farnesol- and tyrosol-based QS [25,26]. Moreover, it is striking that AHLs are present in more microorganisms than originally expected. Recently, a novel type of AHL, *N*-carboxyl-acyl-homoserine lactones, was found in a methanogenic archaeum *Methanosaeta harundinacea* to regulate its filamentous growth [27]. Each of these signal families has different structures and is used by different microbial groups (Figure 1, Table 1). These diverse signals may allow microbial populations to differentiate themselves from others, so as to synchronize and coordinate social behaviors.

Table 1. Quorum sensing (QS) systems of microorganisms.

QS Signaling Type	Structure	Representative Microorganisms	Associated Phenomena	Reference
Intraspecies Communication Signals				
"Traditional" AHL	C4-C18, 3OC4-3OC18 and 3OHC4-3OHC18	Various Gram-negative bacteria; only one Gram-positive bacteria: *Exiguobacterium* sp. MPO	Virulence, biofilm, swarming and bioluminescence	[2,20]
"Noncanonical" AHL	*p*-Coumaroyl-HSL	*Rhodopseudomonas palustris* CGA009	Global gene expression	[28]
	Cinnamoyl-HSL	*Bradyrhizobium* spp.	Not identified	[29]
	Isovaleryl-HSL	*B. japonicum* USDA110	Not identified	[30]
	N-Carboxyl-acyl-HSL	Archaeum *Methanothrix harundinacea*	Filamentous growth	[27]
DSF family	*Cis*-unsaturated fatty acid	*Xanthomonas* spp., and *Burkholderia cenocepacia*	Virulence, biofilm and antibiotic tolerance	[24]
CAI-1 family	α-Hydroxyketones	*Vibrio* spp. and *Legionella pneumophila*	Virulence and biofilm	[23,31]
AIP family	Linear or cyclized oligopeptide	Many Gram-positive bacteria; only one Gram-negative bacterium: *Thermotoga maritima*	Virulence, biofilm, sporulation and exopolysaccharide production	[21,32]
PQS or IQS	Quinolone or thiazole compounds	*Pseudomonas aeruginosa*	Virulence and biofilm formation	[33,34]
Pyrones	α-Pyrones	*Photorhabdus luminescens*	Virulence	[35]
Interspecies and Interkingdom Communication Signals				
AI-2	*S*-THMF-borate *R*-THMF	Many Gram-negative and Gram-positives bacteria	Virulence and biofilm formation	[15]
AI-3	Unknown	Enterohemorrhagic *Escherichia coli* (EHEC)	Virulence	[36]
Indole	2,3-Benzopyrrole	Many Gram-negative and Gram-positives bacteria	Virulence and biofilm formation	[19]

Table 1. *Cont.*

QS Signals in Fungi				
Farnesol or Tyrosol	Sesquiterpene or phenylethanoid	*Candida albicans*	Inhibition or stimulation filamentation and biofilm formation	[25,26]
Peptide	NH_2-NFGAPGGAYPW-COOH	*Cryptococcus neoformans*	Colony formation in agar media	[22]

AHL: *N*-Acyl-homoserine lactonse; AI-2: Autoinducter-2; AI-3: Autoinducter-3; AIP: Autoinducing peptides; DSF: Diffusible signal factor; CAI-1: *Cholerae* autoinducer-1; PQS: *Pseudomonas* quinolone signal; IQS: Integrating QS signal.

Figure 1. Structures of representative quorum sensing (QS) signals.

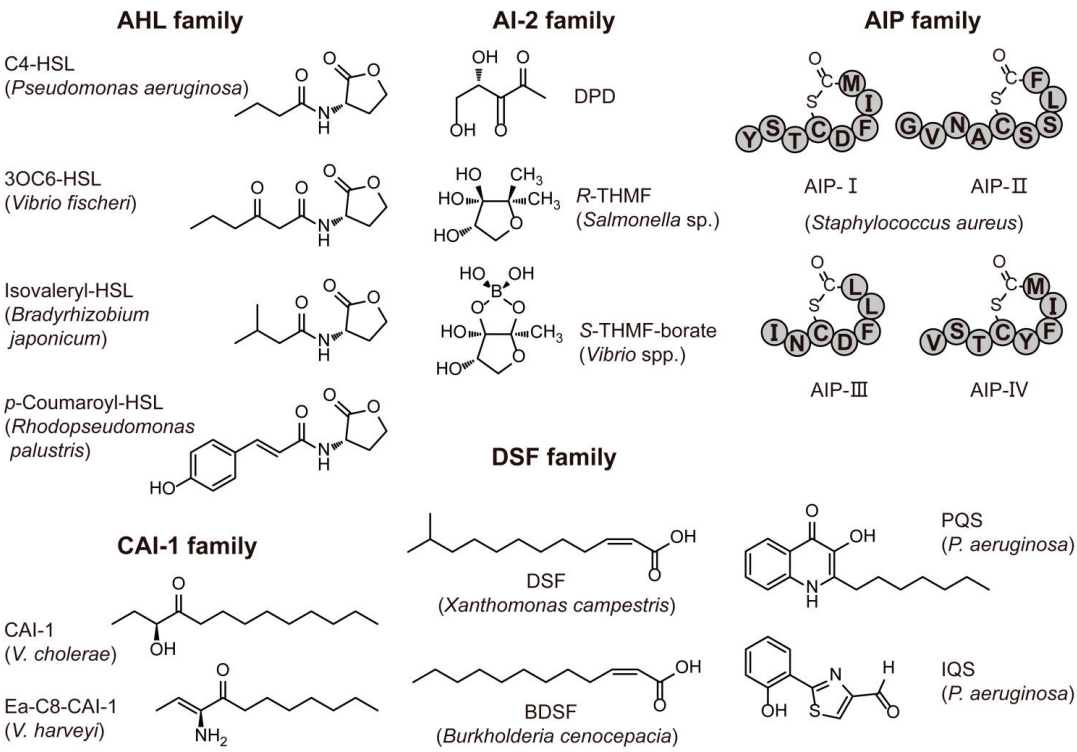

AHL: *N*-Acyl-homoserine lactonse; AI-2: Autoinducter-2; AIP: Autoinducing peptides; CAI-1: *Cholerae* autoinducer-1; Ea-C8-CAI-1: (*Z*)-3-Aminoundec-2-en-4-one; DSF: Diffusible signal factor; BDSF: *Burkholderia cenocepacia* diffusible signal factor; PQS: *Pseudomonas* quinolone signal; IQS: Integrating QS signal; *R*-THMF: (*2R*,*4S*)-2-Methyl-2,3,3,4-tetrahy droxytetrahydrofuran ; *S*-THMF-borate: (*2S*,*4S*)-2-Methyl-2,3,3,4-tetrahydroxytetrahydrofuran-borate; DPD: 4,5-Dihydroxy-2,3-pentanedione.

In most cases, one species usually employs a single type of QS. However, some species may harbor multiple QS systems. For example, *V. harveyi* utilizes a four-channel integrated QS system

(AHL-, CAI-1-, AI-2- and nitric oxide-dependent channels) [37,38], whereas *V. fischeri* possesses a multichannel system (C8-HSL- and AI-2-dependent channels) and an additionally LuxI/R circuit (3OC6-HSL) [37]. *P. aeruginosa* employs various QS systems, including two complete AHL-dependent QS circuits (RhlI/R and LasI/R circuits), a 3OC12-HSL-responsive orphan receptor QscR, a *Pseudomonas* quinolone signal (PQS)-dependent QS, and a recently identified IQS (integrating the QS network) signal, which together compose a hierarchical QS network to regulate virulence expression and respond to environmental stress [33,39].

2.1. Characteristics of AHL Molecules

AHL-dependent QS exists in many pathogenic bacteria. A typical AHL molecule consists of a homoserine lactone and an acyl chain with an even number of carbons (C4-C18) together with an occasional modification at the C3 position (hydroxy or olefinic double bond) [2]. The shortest and longest AHLs found in nature are C4-HSL and C18-HSL, respectively. Recently, some special AHLs with novel structures have been discovered in Gram-negative bacteria and archaea, and include aryl-homoserine lactone (*p*-coumaroyl-HSL and cinnamoyl-HSL) [28,29], branched-chain fatty acyl-homoserine lactone (isovaleryl-HSL) [30] and *N*-carboxyl-acyl-homoserine lactone [27] (Table 1).

The solubility, diffusibility and stabilization of AHLs are correlated with their structures. Generally, the solubility and diffusibility will be increased, and the stabilization decreased along with the shorter length of acyl chain of AHLs. For example, 3OC6-HSL used by *V. fischeri* shows higher solubility and diffusibility which enables diffusion inside and outside of cells [2]. Conversely, 3OC12-HSL in *P. aeruginosa* can only be transported through efflux pumps [2]. In addition, the modification at the C3 position (also termed the β position) may increase the solubility of AHLs. AHLs are susceptible to pH and temperature of the surrounding environment. In fact, alkaline pH and high temperatures will promote their abiotic hydrolysis [40]. Therefore, it seems appropriate that the hyperthermophilic Gram-negative bacterium *Thermotoga maritima* utilizes peptides as the QS signal rather than AHLs in its hydrothermal habitat [21]. Another case is that of the photosynthetic bacterium, *Rhodopseudomonas palustris*, which uses an AHL synthase to produce *p*-coumaroyl-HSL from environmental *p*-coumaric acid, which is a plant metabolite, rather than fatty acids from cellular pools. This indicates that *R. palustris* QS might have evolved to fit its surrounding [28].

2.2. The Diversity and Uniformity of QS Systems

The LuxI/R circuit in marine bioluminescent *V. fischeri* (Figure 2a) and the integrated QS of *V. harveyi* are good examples to explain how different QS circuits work in a similar way (Figure 2b). *V. harveyi* possesses a sophisticated QS system consisting of four parallel channels, *i.e.*, LuxM/N (AHL-dependent), LuxS/PQ (AI-2-dependent), CqsA/S (CAI-1-dependent) [2] and NO/H-NOX/HqsK (nitric oxide-dependent) [38]. In AHL-dependent QS, HAI-1 (3OHC4-HSL) is synthesized by the synthase LuxM. With AI-2-dependent QS, DPD (4,5-dihydroxy-2,3-pentanedione) is synthesized by LuxS, and is spontaneously cyclized and hydrated to form *R*-THMF and *S*-THMF (Figure 1).

R-THMF may be detected by *Salmonella enterica* serovar Typhimurium directly [41], whereas, in the presence of boron, *S*-THMF is further catalyzed to form *S*-THMF-borate that can be utilized by *Vibrio* species as the AI-2 signal. In CAI-1-dependent QS, Ea-C8-CAI-1 is synthesized by CqsA [42]. The cognate receptors LuxN, LuxPQ, and CqsS are bi-functional two-component enzymes that possess both kinase and phosphatase activities [2]. LuxP is a periplasmic protein in complex with LuxQ; the former detects signals, and the latter transfers phosphate [2]. In the NO-responsive QS, NO is sensed by H-NOX and the NO/H-NOX complex regulates kinase and phosphatase activities of HqsK [38]. LuxR and AphA are the primary and secondary master regulators of QS in *V. harveyi*, respectively. At low cell density (LCD) or low NO concentration, phosphates from unliganded receptors are transduced to a single phosphotransfer protein LuxU, and subsequently to LuxO. Phospho-LuxO, together with a sigma factor σ^{54}, activates the transcriptions of five small regulatory RNAs. Small RNAs repress the translation of LuxR and activate the translation of AphA [43,44]. At high cell density (HCD) or high NO concentration, phosphates are conversely transferred to the AI/NO-bound receptors and thereby the production of AphA is depressed whereas LuxR protein is maximally produced to regulate the expression of target genes [2]. Actually, LuxR is also present at LCD, whereas little or no AphA is present at HCD [45]. The two master regulators AphA and LuxR regulate 167 genes and 625 genes, respectively, and coregulate 77 genes, thereby generating a precise temporal pattern of gene expression [45].

Intriguingly, the biosynthesis pathways of AHLs, AI-2 and CAI-1 are related to each other and involved in the AMC, which is an important metabolic pathway responsible for the generation of the cell major methyl donor *S*-adenosylmethionine (SAM) and the recycling of methionine by detoxification of *S*-adenosyl-L-homocysteine (SAH) (Figure 2c). AHL is synthesized from SAM and acyl carrier protein (acyl-ACP) by LuxI-type synthase [2]. The structurally conserved homoserine lactone of AHL molecule is derived from SAM whereas the variable acyl tail is assembled from fatty acid. CAI-1 is synthesized from SAM and acyl-coenzyme A via a multistep reaction involving CsqA, pyridoxal phosphatase (PLP) and VC1059 [23]. CAI-1 and Ea-CAI-1 contain single three-carbon units, being derived from SAM and subsequently attached to an acyl tail. In AI-2 biosynthesis, the release of the activated methyl group from SAM to an acceptor molecule gives rise to a toxic intermediate, SAH, which is converted by 5′-methylthioadenosine/sadenosylhomocysteine nucleosidase (MTAN/Pfs) to *S*-ribosylhomocysteine (SRH) [46]. LuxS catalyzes the cleavage of SRH to homocysteine and DPD, which further undergoes spontaneously cyclization and hydration reactions to be mature AI-2 [46]. Unlike AHLs and CAI-1, all the carbons of DPD are derived from SAM.

All of the discovered QS circuits share three critical steps:

(1) production of signal molecules,
(2) release of signal molecules, and
(3) recognition of signal molecules by receptors.

In most cases, the LuxR-type transcriptional regulators are able to activate target genes, whereas the EsaR in *Pantoea stewartii* functions as a transcriptional repressor. Unliganded EsaR binds DNA and represses transcription. The binding of AI to EsaR promotes DNA release and thereby

promotes gene expression [47]. Also, QS in Gram-positive bacteria contains three steps. Unlike AHL-dependent QS, AIPs are secreted to the environment by specialized transporters and subjected to post-translation modification to become mature linear or cyclized AIPs during transport [32].

Figure 2. Representative QS circuits and autoinducer biosynthesis. (**a**) LuxI/R circuit of *Vibrio fischeri*. OM: outer membrane. IM: inner membrane; (**b**) QS circuit of *V. harveyi*; (**c**) Biosynthesis of *N*-acylhomoserine lactones (AHLs), *V. cholerae* autoinducer-1 (CAI-1) analogs and 4,5-dihydroxy-2,3-pentanedione (DPD). Differently colored carbons, nitrogens and oxygens show where they are derived. See details in the text.

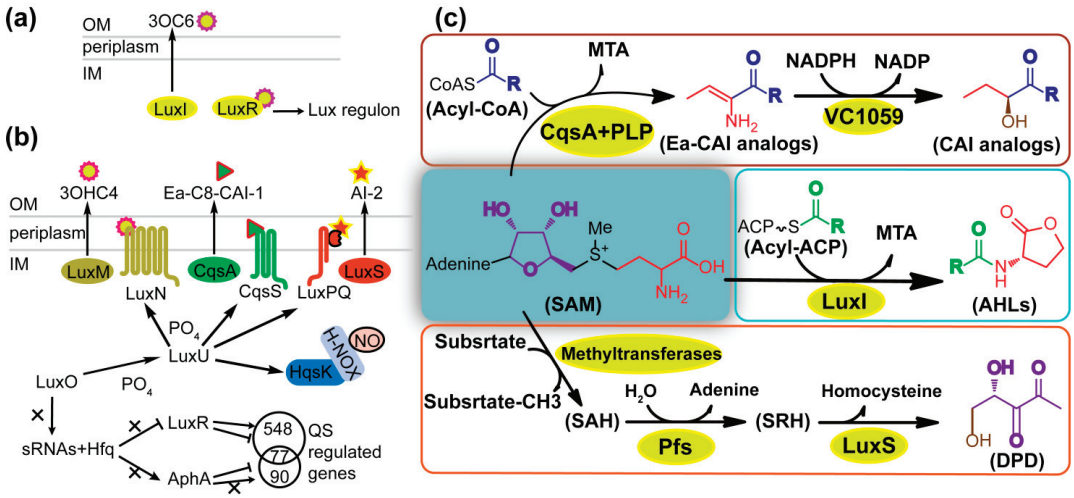

3. Natural Quorum Quenching Resources

Quorum quenching is now referred to as the interference with QS, and may reverse the QS regulated phenotypes, such as virulence. Because QS is not essential for the growth of bacteria, quenching QS has been recommended as a promising strategy for antivirulence therapy. In particular, diverse QQ agents have been identified from various sources and organisms. All of the QQ agents may be classified into two groups according to their molecular weight, *i.e.*, small molecular and macromolecular QQ agents, which are also referred to as QS inhibitors and QQ enzymes, respectively.

The words "quorum quenching" and "QS inhibitors" were first used to describe the enzymatic degradation of AHL signals [48] and inhibition of QS by small molecular antagonists [49], respectively. Here, in order to avoid a semantic quagmire, the word "quorum quenching" is used in its most extensive connotation to describe any forms of interference with QS, including QS inhibitors and QQ enzymes.

3.1. Small Molecular QQ Agents

There is abundant literature about the identification of novel and effective QS inhibitors from natural products and synthetic molecules. Multiple methods have been applied to identify QS inhibitors: purification from crude extracts of candidate organisms, random and high-throughput screening of QS inhibitors from compound libraries, and computer-aided screening from 3D structure libraries of known compounds. However, QS biosensors, which are genetically manufactured strains that express reporter genes (e.g., *lacZ*, *gfp* or *luxCDABEG*) in response to specific QS signals, are potent and indispensable tools for identifying QS inhibitors.

Natural QS inhibitors with highly diverse structures possess inhibitory activities against AHL, PQS, AI-2 and AIP-dependent QS (Table 2). It is notable that there are some unusual forms of interference with QS. Because the virulence factors of many pathogens are regulated positively by QS, it is reasonable to control pathogenicity by inhibiting QS. On the contrary, the orphan receptor QscR of *P. aeruginosa* [50] and CAI-1-dependent QS in *V. cholerae* [51] are negatively correlated with virulence, which means that these two particular pathways should be activated rather than inhibited for reducing virulence. Various synthetic agonists of each circuit have been identified [52–54]. However, natural compounds with this activity have not yet been found except for some corresponding AIs analogs, e.g., 3OC10-HSL for QscR and Ea-C8-CAI-1 for CqsS of *V. cholerae*. Therefore, specific screening work could be carried out to explore more natural QS inhibitors.

3.1.1. Marine-Derived Inhibitors against AHL-Dependent QS

AHL-dependent QS inhibitors account for the largest proportion of natural QS inhibitors (Table 2). Marine-derived QS inhibitors have been found in marine bacteria, fungi, algae, bryozoan, corals and sponges.

An increasing number of studies indicate that marine cyanobacteria have become one of the richest resources for biologically active and structurally unique natural products. Many AHL-dependent QS inhibitors with divergent structures have been discovered in several species of marine cyanobacteria (Table 2). The tumonoic acids (E, F, G and H), which have been isolated from *Blennothrix cantharidosmum*, inhibit the bioluminescence of *V. harveyi* BB120 without affecting bacterial growth. Here, tumonoic acid F is the most active moiety (IC_{50} of 62 μM) [55]. Moreover, *Lyngbya majuscula* produces four different compounds, including malyngolide (MAL), 8-epi-malyngamide C, lyngbic acid and lyngbyoic acid, which inhibit LasR of *P. aeruginosa* responding to exogenous 3OC12-HSL [56]. Interestingly, honaucins A–C [57], isolated from *Leptolyngbya crossbyana*, possess dual-inhibitory activity against both QS and inflammation, which may represent a new strategy for developing multi-functional drugs. It is noteworthy that marine cyanobacteria produce many different kinds of AHL-dependent QS inhibitors, and most likely have evolved mechanisms to control the associated microbial communities by interfering with their cell-to-cell communication.

Table 2. Natural QS inhibitors.

Category	Species	Inhibitor	Target	Reference
Marine-Derived Inhibitors against AHL-Dependent QS				
Actinobacteria	*Streptomyces* sp.	Piericidin A1	CviR	[58]
Bacteria	*Halobacillus salinus*	*N*-(2-Phenylethyl)-isobutyramide and 3-Methyl-*N*-(2-phenylethyl)-butyramide	LuxR, CviR and *Vibrio harveyi*	[59,60]
Bacteria	*Bacillus cereus* D28	Cyclo-L-proline-L-tyrosine	*Chromobacterium violaceum*	[60]
Bacteria	*Marinobacter* sp. SK-3	Diketopiperazines (dkps)	CviR and LuxR	[61]
Bryozoan	*Flustra foliacea*	Brominated alkaloids compounds	CepR and LuxR	[62]
Coral	*Pseudoplexaura flagellosa* and *Eunicea knighti*	Cembranoids	LuxR and *V. harveyi*	[63,64]
Cyanobacteria	*Blennothrix cantharidosmum*	Tumonoic acid F	*V. harveyi*	[55]
Cyanobacteria	*Lyngbya majuscula*	8-*Epi*-malyngamide C and lyngbic acid	LasR	[65]
Cyanobacteria	*L. majuscula*	Lyngbyoic acid	LasR	[66]
Cyanobacteria	*L. majuscula*	Malyngolide	CviR and LasR	[56]
Cyanobacteria	*Leptolyngbya crossbyana*	Honaucins A–C	LuxR	[57]
Cyanobacteria	*Lyngbya* sp.	Pitinoic acid A	LasR	[67]
Cyanobacteria	*Lyngbya* sp.	Pepitdes (microcolins A and B)	LuxR	[68]
Fungi	*Penicillium atramentosum*	Crude extracts	LasR	[69]
Red algae	*Ahnfeltiopsis flabelliformes*	Floridoside, betonicine and isethionic acid	TraR	[70]
Sponge	*Luffareilla variabilis*	Manoalide, manoalide monoacetate, and secomanoalide	LuxR and LasR	[71]
Sponge	*Hymeniacidon aldis*	Alkaloid (hymenialdisin)	LuxR and LasR	[68]
Terrestrial-Derived Inhibitors against AHL-Dependent QS				
Bacteria	*Staphylococcus delphini*	Yayurea A and B	LuxN	[72]
Bacteria	*Stenotrophomonas maltophilia* BJ01	*Cis*-9-octadecenoic acid	CviR	[73]
Bacteria	*Pseudomonas* spp.	Protoanemonin	LasR	[74]
Fungi	*Aspergillu*s spp.	Kojic acid	LuxR	[68]
Fungi	*Penicillium* spp.	Patulin and Penilillic acid	LasR and RhlR	[75]
Insect productions	Bee	Honey and propolis	*C. violaceum*, LasR and RhlR	[76,77]
Insect: fire ant	*Solenopis invicta*	Solenopsin A	*rhl* circuit	[78]

Table 2. *Cont.*

Plant	*Baccharis cassinaefolia*	Benzopyran	CviR, LuxR and LasR	[68]
Plant	*Syzygium aromaticum*	Eugenol	CviR, LasR and PQS	[79]
Plant: alfalfa	*Medicago sativa*	L-Canavanine	CviR and ExpR	[80]
Plant: *Combretaceae*	*Combretum albiflorum*	Catachin and naringenin	CviR and RhlR	[81,82]
Plant: *Compositae*	*Centratherum punctatum*	Sesquiterpene lactones	*Pseudomonas aeruginosa*	[83]
Plant: garlic	*Allium sativum*	Ajoene	LuxR family	[84]
Plant: horseradish	*Armoracia rusticana*	Iberin	LasR and RhlR	[85]
Plant: *Myristicaceae*	*Myristica cinnamomea*	Malabaricone C	CviR	[86]
Plant: tree	*Drimys winteri*	A drimane sesquiterpene	*C. violaceum*	[87]
Plant: turmeric	*Curcuma longa*	Curcumin	CviR	[88]
Plants	Various plants	*p*-Coumaric acid	PpuR, CviR and TraR	[89]
Plants and bacteria	*Conocarpus erectus*	Ellagitannins and urolithins	*P. aeruginosa* and *Yersinia enterocolitica*	[90,91]
Roundworm	*Caenorhabditis elegans*	Exudates	LuxR	[92]
Soil-freshwater alga	*Chlamydomonas reinhardtii*	Lumichrome	*Sinorhizobium meliloti*	[93,94]
TCMs *	Rhubarb	Emodin	*P. aeruginosa* and *S. maltophilia*	[95]
TCMs	*Scutellaria baicalensis*	Flavonoid (baicalein)	TraR and RhlR	[96]
Inhibitors against PQS System				
Fungi	*Candida albicans*	Farnesol (sesquiterpene)	PqsA	[97]
Inhibitors against AI-2 and AI-3 System				
Marine alga	*Delisea pulchra*	Furanone and its derivatives	LuxR and LuxS	[98,99]
Plant	Many plants	Cinnamaldehyde and its derivatives	LuxR and AI-2	[100–102]
Plant	Broccoli	Quercetin	AI-2 and AI-3	[103]
Plant	Grapefruit	Limonoids (obacunone)	EHEC	[104]
Inhibitors against AIP System				
Bacteria	*Lactobacillus reuteri*	Cyclic dipeptides: cyclo(L-Phe-L-Pro) and cyclo(L-Tyr-L-Pro)	*agr* system	[105]
Marine bacteria	*Photobacterium*	Cyclodepsipeptides (solonomide a, b)	*agr* system	[106]
Plant: witch hazel	*Hamamelis virginiana*	2,5-di-*O*-galloyl-D hamamelose	RNAIII	[107]

* TCMs: traditional Chinese medicines.

Other marine microorganisms also produce QS inhibitors (Table 2). The Gram-positive bacterium, *Halobacillus salinus*, produces two compounds, namely *N*-(2-phenylethyl)-isobutyramide and 3-methyl-*N*-(2-phenylethyl)-butyramide, which are capable of inhibiting violacein biosynthesis of C*hromobacterium violaceum* CV026 and GFP production of *Escherichia coli* JB525 in the presence of exogenous AHLs [59]. Both Gram-positive *Bacillus cereus* and Gram-negative *Marinobacter* sp. SK-3 produce diketopiperazines (DKPs) which inhibit

AHL-dependent QS [60,61]. Additionally, piericidin derived from marine actinobacteria inhibits violacein biosynthesis in *C. violaceum* CV026 [58,108].

Another source for QS inhibitors is marine algae. The red alga *Delisea pulchra* produces a number of halogenated furanones with antifouling and antimicrobial properties [98,109]. Furanones are supposed to bind AHL receptors due to the five-membered lactone scaffold structurally similar with AHLs. A series of synthetic derivatives of native furanones have been reported to interfere with AHL-mediated QS in many bacteria [99,110]. It was suggested that furanones may act to destabilize the AHL-dependent transcriptional activator LuxR of *V. fischeri* [111] and attenuate the DNA-binding activity of LuxR of *V. harveyi* [112]. Moreover, it has been found that furanones may affect the AI-2 circuit in Gram-negative and Gram-positive bacteria by covalently modifying and inactivating AI-2 synthase LuxS [113]. The protective effects of halogenated furanones in rotifers, brine shrimp and rainbow trout against pathogenic *Vibrio* species [114–116] and in mice against *P. aeruginosa* lung infection [117] have been demonstrated, though some furanones were found to be toxic to rainbow trout, rotifers and human fibroblasts [115,116]. Therefore, studies have focused on the synthesis of more effective and less toxic furanone derivatives that may promote their commercial or therapeutic use. Except for furanones, a mixture of floridoside, betonicine and isethionic acid, produced by the marine red alga, *Ahnfeltiopsis flabelliformes*, may also inhibit the reporter strain *A. tumefaciens* NTL4 (pCF218) (pCF372) responding to 3OC6-HSL [70]. In addition, extracts of several marine micro-algae are capable of inhibiting the QS-dependent responses of reporter strains *E. coli* JB523 and *V. harveyi* JMH612 [118].

3.1.2. Terrestrial-Derived Inhibitors against AHL-Dependent QS

Various natural products from a wide range of terrestrial organisms have been demonstrated to show inhibitory activity against AHL-dependent QS. Most of these bioactive substances are derived from plants, although some originate from bacteria, fungi and insects (Table 2). Many health-benefit food sources and traditional medicines, such as fruits, herbs and medicinal plants, have received special attention as potential sources of QS inhibitory compounds. However, only a few of the compounds have been isolated or structurally and biochemically identified. A variety of phenolic compounds showed inhibitory activity against AHL-dependent QS. Among them, the flavonoids comprise a well-studied group. Flavonoids are widely produced by plants and also exist in plant-related products, e.g., propolis and honey [119]. Flavonoids display many pharmacological activities and present structural divergence [119]. The flavan-3-ol catechin, isolated from *Combretum albiflorum* bark, is the first identified flavonoid compound and is capable of reducing the production of virulence factors in *P. aeruginosa* PAO1 by interfering with RhlR [81]. Several other flavonoids from citrus and traditional Chinese medicines inhibit QS in bacteria [82,106,120]. Additionally, honey and propolis are able to interfere with QS in *C. violaceum* and *P. aeruginosa*, respectively, which may be attributed to the high abundance of flavonoids in honey and propolis [119]. Hydrolysable tannins are another group of phenolic compounds; ellagitannins or tannin-rich fraction from various plants showed QS inhibitory activity against *C. violaceum* or *P. aeruginosa* [90,91].

3.1.3. Natural Inhibitors against Other QS Systems

Compared with the plentiful natural AHL-dependent QS inhibitors, natural inhibitors against other QS systems are rarely reported (Table 2). Peptide-based compounds and the phenolic compound hamamelitannin are capable of blocking *agr*-dependent QS of *Staphylococcus* spp. [105–107]. It is striking that farnesol (a common sesquiterpene), applied by the opportunistic pathogen *C. albicans* as a QS signal, inhibits the PQS circuit of *P. aeruginosa* by promoting non-productive interaction between PqsR and the *pqsA* promoter [97]. It was suggested that farnesol may play a role in interkingdom communications [97]. Besides farnesol, two other sesquiterpene derivatives, drimendiol from *Drimys winteri* and sesquiterpene lactones from *Centratherum punctatum* (Argentine herb), were identified as AHL-dependent QS inhibitors [83,87]. Referring to the AI-2 system, furanone, cinnamaldehyde and their derivatives may be the most effective inhibitors. Cinnamaldehyde (CA) is widely used as a flavoring substance in food chemistry [100]. Low concentrations of CA were previously found to be effective at inhibiting both AHL and AI-2 dependent QS in *V. harveyi* [101]. Subsequently, mobility shift assays revealed that CA could decrease the DNA-binding ability of LuxR of *V. harveyi*. CA and its analogs could increase significantly the survival of the nematode *Caenorhabditis elegans*, brine shrimp and giant freshwater prawn, *Macrobrachium rosenbergii*, infected with pathogenic *Vibrio* spp. [100,102,121].

3.1.4. Evaluation of Natural QS Inhibitors

Over the last decade, many natural substances have been evaluated for their ability to interfere with QS. QS inhibitors isolated from natural products are excellent resources for developing potent antivirulence drugs insofar as they may provide novel scaffolds for drug design. The natural *D. pulchra* furanone compounds are unable to inhibit the QS of *P. aeruginosa*, but modified furanone analogs enhance the inhibitory effectiveness against this organism [117]. Honaucin A from the cyanobacterium *Leptolyngbya* was recently identified as an inhibitor against QS of *V. harveyi* and *V. fischeri* [57], whereas two synthesized honaucin A derivates, 4'-bromohonaucin A and 4-iodohonaucin A, showed an increased QS inhibitory activity of nearly 30-fold compared to that of honaucin A [57]. Despite these remarkable discoveries, three factors hinder the development of novel antivirulence therapies based on these bioactive substances.

Firstly, there is an increasing requirement for standardization to verify the true QS inhibitory activity. In some cases, the QS inhibitory activities of bioactive substances have been challenged because of the lack of suitable methodologies. Several QS reporter strains are widely used to identify QS inhibitors. Recently, Defoirdt *et al.* [122] detailed the inherent drawbacks of these assays. In reporter strains, the QS-regulated phenotypes are often co-dependent on other factors and/or dependent on the metabolic activity of the cells, and may thus be directly interfered with by candidate compounds. Hence, the same biosensor strain with a QS-independent expression of reporter genes should be used for adequate control experiments to verify that there is no effect imposed by candidate compounds on the particular phenotype. Additionally, QS-regulated phenotypes may be affected if the candidate compounds are toxic against reporter strains. In most cases, toxicity is only assessed by evaluating the effect on growth in a complex growth medium,

which may cause false positives. For example, pyrogallol was found to be capable of inhibiting bioluminescence in a *V. harveyi luxN* mutant without affecting growth in a complex medium and therefore claimed as an AI-2 QS inhibitor [123]. However, it was subsequently found that pyrogallol inhibited bioluminescence when expressed constituently in an engineered strain, and the pyrogallol-related effect was abolished by the addition of catalase [124]. The apparent QS inhibitory activity of pyrogallol was demonstrated as a side effect of peroxide production [124]. Hence, more sensitive toxic assays towards bacterial cells are required [122].

Secondly, further studies on natural crude extracts with identified QS inhibitory activity are required. In many cases, the precise compounds of the bioactive molecules have not been elucidated. As mentioned above, natural inhibitors are resources for drug design to develop more potent antivirulence drugs, and purification of individual compounds is necessary to improve the likelihood of understanding the mechanisms of inhibition [39].

Moreover, the active mechanisms of these compounds are poorly understood. Successful drug design relies much on the knowledge of molecular mechanism of the connection between native signals or inhibitors and synthase or receptor, such as binding sites, conformational change and affinity change. Currently, the X-ray crystal structures of some AHL-bound LuxR-type receptors and computational protein docking methods provide powerful tools to determine the molecular mechanisms of interaction. However, the molecular mechanisms of only a few effective natural QS inhibitors have been studied in depth. The lack of information of binding interactions has thwarted the rational design of a more potent QS inhibitor.

3.2. Macromolecular QQ Agents

Various macromolecular agents have been found to possess the capability to quench QS. Unlike small molecular QS inhibitors, macromolecular QQ agents interfere with QS mostly through degrading signals rather than competitively binding to signal receptors. Most of the identified macromolecular QQ agents target the AHL-dependent QS, although enzymatic degradations of DSF, PQS and AI-2 have also been reported. *Bacillus*, *Staphylococcus* and *Pseudomonas* possess DSF inactivation activity [125]. The 2,4-dioxygenase, Hod, involved in quinaldine utilization pathway in *Arthrobacter nitroguajacolicus* is able to cleave PQS [126]. In the Lsr-type AI-2 system, cytoplasmic enzyme LsrK is responsible for phosphorylation of AI-2 and phospho-AI-2 is unstable [127]. When LsrK is artificially provided *in vitro*, the extracellular phosphor-AI-2 molecules cannot be transported into cells and are degraded overnight. LsrK-mediated degradation of AI-2 attenuates the QS response in *S. enterica* serovar Typhimurium and *V. harveyi* [127].

To date, many macromolecular QQ agents against AHL-dependent QS have been reported. Generally QQ enzymes are a major portion of the macromolecular agents, although a few antibodies have been generated to interfere with AHL-dependent QS through sequestration or hydrolyzation of AHLs [39]. Enzymatic degradation of AHLs has been extensively studied, and found in many organisms including mammals, plants, fungi, achaea and bacteria [39,128], although the genes responsible for AHL-degrading activity in plants and fungi have not been identified. A comprehensive summary of AHL-degrading bacteria with marine or terrestrial origin was provided in our previous publication [129].

AHL-degrading enzymes may be classified into three major types according to their enzymatic mechanisms: AHL lactonase (lactone hydrolysis), AHL acylase (amidohydrolysis) and AHL oxidase and reductase (oxidoreduction). AHL lactonase hydrolyzes the ester bond of AHL yielding the corresponding *N*-acyl-homoserine. This hydrolyzation may also occur spontaneously at alkaline pH, and may be reversed under acid pH [40]. AHL acylase hydrolyzes the amide bond of AHL to yield a homoserine lactone and the corresponding fatty acid chain, whereas AHL oxidase and reductase usually catalyzes a modification of AHLs. In most cases, AHL lactonases require metal ions (except AiiM and QsdH) and target both short and long acyl chain AHLs. Unlike lactonases, acylases exhibit substrate specificity based on the length of the acyl chain and the substitution on the β position of the AHL chain.

3.2.1. AHL Lactonases

To date, approximately 30 types of AHL lactonases have been identified (except for predicted AHL lactonases or highly similar enzymes in one genus). According to the amino acid sequences, these lactonases belong to the metallo-β-lactamase superfamily, the phosphotriesterase (PTE) family and other particular families (Figure 3a). Among them, the AHL lactonases of the metallo-β-lactamase superfamily have been most extensively studied, and are widespread in various bacterial species. The metallo-β-lactamase group may be further classified into several clusters, *i.e.*, AiiA, AidC and a novel marine AHL lactonase cluster [130] (discussed in depth later on) according to the phylogenetic tree (Figure 3a).

The first identified AHL lactonase AiiA (autoinducer inactivation) from *Bacillus* sp. 240B1 belongs to the metallo-β-lactamase family. AiiA was initially thought to hydrolyze the amide linkage between homoserine lactone and acyl side chain because metallo-β-lactamase can cleave the amide bond of the penicillin β-lactam ring. However, it was demonstrated later that AiiA degraded the ester rather than amide bond [131]. The *aiia* homogenous genes are widespread in *Bacillus* species. The molecular mechanism of AHL degradation has been revealed. AiiA amino acid sequence contains a "^{104}HXHXDH^{109}~60aa~H^{169}" motif, which is common in metallo-β-lactamases. Single-residue mutagenesis has shown that His 106, Asp 108, His 109 and His 169 are necessary for AiiA activity [131]. AiiA is a metalloprotein binding two equivalents of zinc, which is necessary for its activity [132]. Crystal studies of AiiA from *B. thuringiensis* showed the dinuclear zinc binding sites of AiiA: Zn 1 binds to His 104, His 106 and His 169, whereas Zn 2 binds to Asp 108, His 109 and His 235 [133]. These two Zn^{2+} ions, which are separated by a distance of 3.4 Å, are bridged by a hydroxide ion and the Oδ2 atom of Asp191 [133]. Additionally, Tyr 194 is essential for activity, and may be able to stabilize the substrate's carbonyl and/or a tetrahedral intermediate formed subsequent to hydroxide attack [133,134]. AiiA shows a broad substrate specificity and a preference for substrates with long acyl chain AHLs [135], however, C6-HSL is mostly used as substrate in crystal studies of AiiA [133,134]. Recently, another crystal study of a F107W mutation of *B. thuringiensis* AiiA revealed an unexpected interaction with the ring-opened product. Two aromatic residues, Phe 64 and Phe 68, form a hydrophobic clamp, centered around the seventh carbon of the decanoyl chain of ring-opened C10-HSL, making an interaction that would be available for longer substrates but not for shorter ones [136]. Although zinc was found in native

AiiA, dicobalt-, dimanganese- or dicadmium-substituted AiiA exhibits hyperactivity compared with that of dizinc-substituted enzyme [134,137]. Heterologous expression of *aiia* in numerous pathogenic bacteria, including *P. aeruginosa*, *B. thailandensis* and *E. carotovora*, may reduce AHL accumulation and decrease their virulence expression, which indicates the potential use of AiiA as a strategy for antivirulence therapy [131].

Figure 3. Neighbour-joining tree of *N*-acylhomoserine lactone (AHL) enzymes based on amino acid sequences. Each of these AHL lactonases was experimentally identified, except the members named with accession number in Genbank (bold). MomL, MomA and Murru 3261 were identified by us recently (blue colored). The dendrogram was constructed by neighbor-joining method with the MUSCLE program in the MEGA software package (1000 bootstrap replicates). Bootstrap coefficients below 50% were not shown. Scale bar, 0.1 substitutions per amino acid position. Marine clusters were colored in blue. (**a**) Tree of AHL lactonase; (**b**) tree of acylase. ND: not determined.

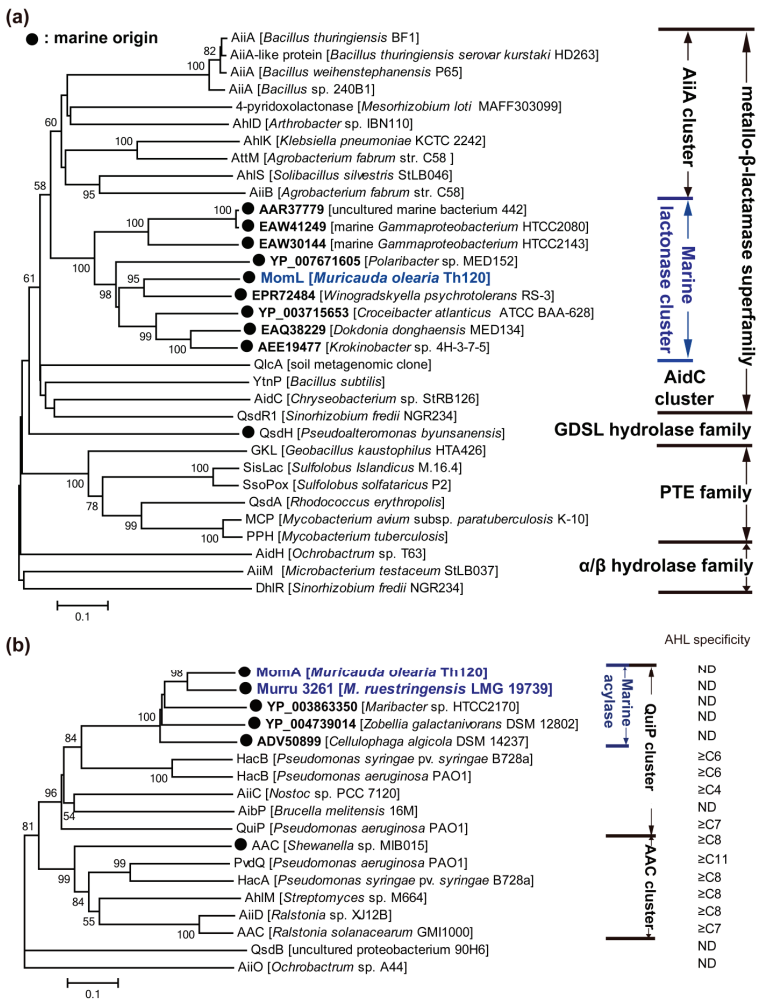

Two members of AiiA cluster, AttM and AiiB, showing 32% and 28% identity to AiiA$_{240B1}$, were found in the plant pathogen *A. tumefaciens* C58, and their corresponding coding genes *attm* and *aiib* (an *attm*-paralogous gene) located on the pAt plasmid and the pTi plasmid [138], respectively. Both AttM and AiiB have the "HXHXDH" motif and AiiB appears to be a metal-dependent AHL lactonase with broad substrate specificity [139]. *A. tumefaciens* infects a broad range of dicotyledonous plants and may transfer an oncogenic DNA fragment, the T-DNA, from its tumor-inducing plasmid to the nuclear genome of the plant hosts. These processes are regulated by TraI/R QS circuit, lactonases AttM and AiiB [140,141]. During the early process of *A. tumefaciens* infection in wounded plant hosts, the expression of *attm* is promoted by γ-aminobutyric acid, a molecule synthesized for defense by plants, and thereby the 3OC8-HSL-dependent virulence expression is attenuated. However, in the growing tumor, the high synthesis rate of 3OC8-HSL and the moderated expression of *attm* caused by plant produced L-proline permit the expression of QS-regulated functions including the transfer of Ti plasmid by conjugation [141].

The AidC cluster contains AidC and QsdR1 encoded by *Chryseobacterium* sp. StRB126 and *Sinorhizobium fredii* NGR234, respectively, and additionally includes YtnP, another AHL lactonase from *Bacillus* species [142–144]. Interestingly, the expression of *ytnP* in *B. subtilis* may be induced by streptomycin, and YtnP may conversely inhibit the production of streptomycin and the development of aerial mycelium in *Streptomyces griseus*. *B. subtilis* may activate *ytnP* expression in response to the presence of certain antimicrobial compounds as a defensive strategy against threatening bacteria since it would allow *B. subtilis* to selectively inhibit the QS-regulated behaviors of harmful microbial communities [144]. Furthermore, most of the AHL lactonases (both in the AiiA cluster and the AidC cluster) belonging to metallo-β-lactamase family are soil-derived. In this connection, we recently identified many marine bacteria with AHL-degrading activity [129], and one of these organisms, *Muricauda olearia* Th120, possesses a gene encoding a novel AHL lactonase which represents a new cluster of AHL lactonase in the metallo-β-lactamase family [130] (Figure 3a).

Apart from members of the metallo-β-lactamase family, another group of AHL lactonases shares key sequence and active site features with phosphotriesterases (PTEs), and these lactonases are termed PTE-like lactonases (PLLs). PLLs exist in both bacteria and archaea. Afriat *et al.* [145] discovered three PLLs, *M. tuberculosis* PPH, *R. erythropolis* AhlA and *Sulfolobus solfataricus* SsoPox. Although no significant sequence identities are shared with AiiA, PLLs show a wide range of AHL-degrading capability and require metal ions for their activities [145]. Crystal studies have revealed that the hyperthermophilic SsoPox shows a high level of similarity with the structure of AiiA [146]. Significantly, the production of AHLs and virulence factors of *P. aeruginosa* PAO1 may be greatly reduced in the presence of SsoPox-immobilized membranes [147]. The thermostability of SsoPox [147], as well as GKL of *Geobacillus kaustophilus* [148] and SisLac of *S. islandicus* [149], is an advantage for their biomedical applications. However, most PLLs showed relatively lower AHL-degrading activities than AiiA [147–149]. Curiously, all the identified PLLs exhibit promiscuous phosphotriesterase activities [147–149]. Bacterial PTEs belong to the amidohydrolase superfamily, a highly diverse superfamily with many different hydrolytic activities. They harbor a degrading rate approaching the diffusion limit ($k_{cat}/K_M \geq 4 \times 10^7$) for their

best substrate paraoxon, which is a widely used pesticide introduced in the 20th century. PTEs could have therefore evolved from a member of the PLL family, utilizing its latent promiscuous paraoxonase activity as an essential starting point [145]. Additionally, DhlR, AidH and AiiM can be temporarily sorted into one group because they belong to the alpha/beta hydrolase family (Figure 3a). Both AidH and AiiM are capable of degrading short- and long-chain AHLs in an unknown and metal-independent mechanism [150,151]. There is another non-bacteria-derived group of AHL lactonases, paraoxonases 1, 2, and 3, which are prevalent in mammalian cells [128]. They all catalyze lactone hydrolysis, but differ in their substrate specificity [128].

3.2.2. AHL Acylases

AHL acylases have been found in bacteria including *Pseudomonas*, *Ochrobactrum*, *Arthrobacter*, *Streptomyces*, *Nostoc* and *Brucella* (Figure 3b). The AiiD of *Ralstonia* sp. XJ12B isolated from a biofilm in an experimental water treatment system is the first identified AHL acylase [152], although an AHL acylase-like activity was previously detected in *Variovorax paradoxus* VAI-C which degrades and utilizes multiple AHLs as the sole source of carbon, nitrogen and energy [153]. AiiD belongs to the Ntn (*N*-terminal nucleophile) hydrolase superfamily, and shares 22%–24% identities with several cephalosporin and penicillin acylases [152]. Actually, AiiD degrades several AHLs, rather than penicillin G or ampicillin, indicating that AHLs are its unique substrates. In comparison, AhlM from *Streptomyces* sp. which shows 35% identity with AiiD in the deduced amino acid sequence, was capable of degrading penicillin G and long-chain AHLs [154]. The gene responsible for AHL-acylase activity in *V. paradoxus* was not identified until whole genomic sequencing of *V. paradoxus* revealed recently a putative AHL acylase gene (Vapar_3883 of *V. paradoxus* S110) [155]. However, biochemical studies are required to confirm its activity. Like AHL lactonase, AHL acylase is considered to have the potential to interfere with QS of bacterial pathogens. Expression of *aiiD* in *P. aeruginosa* PAO1 weakened its ability to swarm, to produce elastase and pyocyanin, and to paralyse nematodes [152]. The addition of AhlM to the growth medium for *P. aeruginosa* also reduced the accumulation of AHLs, and decreased the production of virulence factors including elastase, total protease and LasA [154].

P. aeruginosa PAO1 was previously found to utilize AHLs for growth, so far three proteins (PvdQ, QuiP, and HacB) belonging to the Ntn hydrolase have been characterized biochemically [156]. Among them, PvdQ (PA2385) is the most extensively studied AHL acylase. PvdQ is expressed as a proenzyme that is auto-proteolytically activated by post-translational cleavage resulting in the excision of a 23-residue prosegment and the formation of an 18 kDa α-chain and a 60 kDa β-chain [156]. The mature PvdQ can hydrolyze the amide bond of AHLs, and demonstrates substrate specificity for long-chain AHLs [156]. However, it is the gene *quiP* (*pa1032*) rather than *pvdQ* that is responsible for the ability of *P. aeruginosa* PAO1 to utilize AHLs as a sole carbon and energy source for growth [156,157]. Additionally, another AHL acylase HacB (PA0305) can degrade AHLs with acyl chains ranging in length from 6 to 14 carbons [158]. The physiological function of each of the three acylases in *P. aeruginosa* PAO1 is intriguing. PvdQ was found to be expressed only when iron is present at very low concentrations [159]. Mutation of *pvdQ* did not affect the growth of *P. aeruginosa* but abrogated pyoverdine production and greatly

affected swarming motility and biofilm formation at low iron concentrations [159]. Moreover, the virulence of *pvdQ* mutant against *C. elegans* was reduced. All of these data indicate that PvdQ plays an essential role in siderophore biosynthesis, on which *P. aeruginosa* depends for growth in iron-limited environments [159]. Therefore, PvdQ is a target for antivirulence therapy and different synthetic inhibitors are able to block its activity [160]. Nevertheless, the physiological functions of QuiP and HacB are still unknown.

To date, most of the identified AHL acylases belong to the Ntn hydrolase superfamily, except QsdB and AiiO which belong to the amidase family and α/β hydrolase fold family, respectively [161,162]. AHL acylases belonging to the Ntn hydrolase superfamily may also be classified into two clusters according to the phylogenetic tree (Figure 3c). These are referred to as AAC and QuiP clusters, respectively. The substrate specificity of each acylase cluster was also summarized, and it was speculated that the QuiP cluster might degrade a broader range of AHLs than the AAC cluster because some members of the QuiP cluster degrades C6-HSL even C4-HSL whereas those of AAC cluster could only degrade AHLs longer than C8-HSL. Additionally, most of these AHL acylases are located in the periplasmic space, whereas AhlM and HacB are secretory.

3.2.3. AHL Oxidoreductases

Compared to the abundant data of AHL lactonases and acylases, there are fewer reports about inactivation of AHLs by the modification of chemical structure of AHLs; only a few AHL oxidoreductases have been identified thus far. Because signal receptors usually respond to specific AHLs, the modification might affect the signal recognition, and thereby interfere with QS-regulated functions. Bacteria-derived AHL reduction activity was first discovered in *Rhodococcus erythropolis* in which AHLs with 3-oxo substituents were rapidly degraded by reduction of the keto group at the β position, yielding the corresponding 3-hydroxy derivative AHLs [163]. However, the gene responsible for this activity has not yet been identified. CYP102A1 from *Bacillus megaterium*, a widely studied cytochrome P450, is the second identified AHL oxidoreductases that oxidizes AHL at the ω-1, ω-2, and ω-3 carbons of the acyl chain [164]. Furthermore, this oxidation activity is very efficient towards ring-opened AHLs and fatty acid chains which are the corresponding products of AHL lactonase and acylase, respectively [164]. The third oxidoreductase, the NADH-dependent enzyme BpiB09, was identified by metagenomic analysis. Expression of *bpiB09* in *P. aeruginosa* reduced its swimming motilities, pyocyanin production, biofilm formation and thereby the pathogenicity to *C. elegans* [165]. Moreover, *Burkholderia* sp. GG4, isolated from ginger rhizosphere, was previously found to possess a unique AHL-modifying activity that reduces 3-oxo-AHLs to 3-hydroxy-AHLs [166] although the responsible gene has not been identified. The complete genome of this strain reported recently might reveal its responsible gene [167]. AHL can also be enzymatically inactivated by haloperoxidases from *D. pulchra* [168], *Laminaria digitata* [169] and *Nitzschia cf pellucida* [170] via a H_2O_2-dependent mechanism.

4. Microorganisms May Produce QQ Agents to Gain Benefits in a Competitive Environment

Microorganisms exist in a multi-species and competitive environment, and have developed many survival strategies to gain benefits and compete for space, nutrition and ecological niches. QS is possibly one critical strategy used for competition by microorganisms to synchronize and coordinate social behaviors. Many of these behaviors (e.g., the production of antimicrobial compounds) are primarily advantageous when expressed by a group of bacteria but seemingly futile if performed by a single bacterium [171], though QS-regulated processes can also be induced in single cells in a confined environment [10,11]. Whereas, for other microorganisms exposed to QS-regulated competitive determinants, the selective pressure may drive the evolution of defensive mechanisms of fighting with competing species. It may be assumed that one microbial species may evolve two possible strategies to fight with another species that produces an antimicrobial compound in a QS-regulated mechanism. One strategy is to develop antimicrobial compound-degrading enzymes or other antimicrobial compound-resistant mechanisms. Another conceivable strategy is to interrupt the QS of competing species [171]. The hypothesis of QS interruption is straightforward because QQ-agent-producing bacteria can inhibit the QS-regulated behaviors of competing species and therefore gain benefits or avoid being killed. In this situation, small molecular QS inhibitors should be secreted outside of cells since their targets (e.g., signal synthases or receptors) are located in the membranes or cytoplasm of competing cells, whereas QQ enzymes could be either secreted or cytoplasmic because the signal molecules are diffusible. However, the cellular localization of QQ compounds has been little investigated.

The discovery of co-existence of QS and QQ bacteria in various environments might provide supports for this hypothesis [166,172,173]. However, conclusive empirical evidence has not been demonstrated regarding the relationship between QQ agents and the benefits gained in the natural environment. Additionally, some laboratory co-cultures of QS and QQ bacteria may provide evidence. The pyocyanin, which is a QS-regulated product of *P. aeruginosa*, is toxic to *S. delphini* [174] that produces two AHL-dependent QS inhibitors (yayurea A and B) and protects itself from killing by *P. aeruginosa* via suppressing the production of pyocyanin [72]. Likewise, pyocyanin is toxic to *C. albicans* [175]. With the production of farnesol, *C. albicans* blocks the PQS circuit and thus the pyocyanin biosynthesis of *P. aeruginosa* [97]. Farnesol-like molecules are ubiquitous in the natural environment, and are able to interrupt the PQS circuit, which suggests that other organisms may have the potential to moderate *P. aeruginosa* virulence [97]. It seems likely that the benefits outweigh the costs for these microorganisms to produce compounds to prevent harmful QS-regulated activities of other bacteria and thereby gain space and other resources within microbial communities.

The interference of QS exists not only between different species but also between different strains of the same species. In Gram-negative bacteria, the native AHL utilized by *C. violaceum* ATCC 31532 is C6-HSL but the QS-regulated violacein production can be inhibited by long-chain AHLs produced by *C. violaceum* ATCC 12472 or other bacteria [176,177]. Gram-positive *S. aureus* utilizes four different groups of AIPs. Each can specifically activate its cognate AgrC receptor, but inhibit all others by competitive binding to the non-cognate receptors [178–181]. This

form of QS inhibition was suggested as a strategy for microorganisms to occupy specific niches during infection.

The physiological function of QQ enzyme has been discussed repeatedly but is still unclear [182–184]. PvdQ of *P. aeruginosa* participates in siderophore biosynthesis [159]. The major role of AttM in *A. tumefaciens* is for the degradation of γ-butyrolactone rather than regulation of AHL accumulation, and the AHL-degrading activity might be only a side effect [185]. *V. paradoxus* and *Arthrobacter* sp. utilize AHLs as a source of nitrogen or/and carbon for growth depending on their AHL-degrading enzymes [153,186]. AiiA is essential for rhizosphere colonization of *B. thuringensis* [187]. However, these results are insufficient to explain the physiological functions of QQ enzymes in these QQ bacteria that do not harbor the AHL-dependent QS and cannot utilize AHL to grow. Recently, Schneider *et al.* [144] reported that the expression of YtnP in *B. subtilis* was induced by streptomycin, an antibiotic produced by the *Streptomyces* species. Conversely, YtnP inhibits the production of streptomycin in *S. griseus* probably by degrading its QS signaling molecule γ-butyrolactone [144]. The streptomycin-induced expression of YtnP may allow *B. subtilis* to response to certain antimicrobial compounds and selectively inhibit the QS of harmful microorganisms before being killed. It seems likely that QQ enzyme could allow its producers to obtain competitive advantages over competitors in natural ecosystems.

The hypothesis that microorganisms produce QQ agents in order to gain competitive advantage is not sufficient to explain all of these discoveries. Although several examples showed that the QQ agent producers could survive or even gain benefit through inhibiting QS-regulated harmful behaviors of their competitors, the possibility of "accidental" QQ activity of some QQ agents still exists.

5. QQ in the Marine Environment: A Tremendous Resource to Be Developed

QQ may be a strategy used by microorganisms to gain benefit in a competitive environment. Also, it is believed that in the highly diverse marine ecosystem, microorganisms with capabilities of producing small QS inhibitors and QQ enzymes remain to be discovered. Romero *et al.* [184] proposed that QQ is likely to be a common activity in marine bacteria because a high abundance of QQ bacteria was found among marine cultivable bacteria [188] and a high frequency of QQ genes was discovered in marine metagenomes. In our previous study, 25 marine QQ strains belonging to 14 bacterial species were obtained and it is noteworthy that the QQ activities in 12 species had not been reported previously [129]. Although only a few studies have been carried out to assay the AHL-degrading activity of marine bacteria, more than 30 species of QQ bacteria belonging to *Alphaproteobacteria*, *Gammaproteobacteria Actinobacteria*, *Flavobacteriia* and *Firmicutes* have been identified thus far (Table 3). Additionally, some QQ strains have revealed degradative activity only against long-chain AHLs. Because AHL lactonases normally present broad AHL inactivating activities while many acylases are specific to long-chain AHLs, we assumed that AHL acylases might be more common than lactonases in the ocean. This is consistent with the distribution of acylase and lactonase coding sequences in metagenome collections [184]. Therefore, many marine QQ bacteria may be still undiscovered, and the prevalence of QQ enzymes in marine bacteria may be higher than expected.

The high diversity and abundance of marine QQ bacteria may lead to the discovery of new QQ enzymes and AHL-degrading mechanisms. However, few responsible genes in these bacteria have been identified (Table 3). One of our identified QQ bacteria, *M. olearia* Th120, showed strong AHL-degrading activity, and further studies revealed a novel AHL lactonase and a novel AHL acylase [130] (Figure 3). The identities of the amino acid sequence of AHL lactonase MomL (*Muricauda olearia* marine AHL lactonase) to known lactonases are below 30%, and the top eight strains (with identity higher than 39%) using BLASTP against the NR protein database are also typical marine bacteria. Therefore, MomL was believed to represent a new class of AHL lactonase, which may be widespread in the marine environment. Likewise, AHL acylase MomA (*Muricauda olearia* marine AHL acylase) may represent a marine-derived AHL acylase. It is even more astounding that the ethyl acetate extracts of Th120 culture showed inhibitory activity in *A. tumefaciens* A136 plate assay [130]. All of these findings indicate that marine microorganisms may be important resources for the discovery of new antivirulence strategies. Therefore, an increasing effort is needed in the discovery of new natural QQ agents from marine microorganisms.

Table 3. Marine quorum quenching bacteria.

Strain	AHL-Degrading Ability *	Activity **	Origin	Reference
Actinobacteria				
Rhodococcus erythropolis strains	C4, C6, C10 and 3OC12	Lactonase	*Fucus vesiculosus* and sediment	[188]
Alphaproteobacteria				
Hyphomonas sp. USC2	C4, C6, C10 and 3OC12	Lactonase	*Fucus vesiculosus*	[188]
Marivita sp. Th30	C6, C12 and C14	ND	Flounder	[129]
Novosphingobium sp. Th20	C6-C14 and 3OC6-3OC14	ND	Flounder	[129]
Paracoccus sp. PP2-663	C4-C12	ND	Manila clam	[189]
Phaeobacter sp. USC177	C4, C6, C10 and 3OC12	ND	*Fucus vesiculosus*	[188]
Rhodobacter sp. Th15	C8-C14 and 3OC14	ND	Flounder	[129]
Roseovarius aestuarii USC61	C4, C6, C10 and 3OC12	Lactonase	Water tank	[188]
Sphingopyxis flavimaris T51	C6-C14 and 3OC10-3OC14	ND	Flounder	[129]
Sphingopyxis litoris th8	C6-C14 and 3OC6-3OC14	ND	Flounder	[129]
Stappia sp. USC176	C4, C6, C10 and 3OC12	Lactonase	*Fucus vesiculosus*	[188]
Stappia sp. USC5	C4, C6, C10 and 3OC12	Lactonase	*Fucus vesiculosus*	[188]

Table 3. *Cont.*

Firmicutes				
Bacillus circulans USC24	C4, C6, C10 and 3OC12	Lactonase	Sediment	[188]
Bacillus sp. KT7	C6-C14, 3OC8-3OC12 and 3OHC8-3OHC12	ND	Intertidal rocks colonized by *Ulva*	[190]
Bacillus spp.	C6	ND	Shrimp and bass	[191]
Oceanobacillus spp.	C4, C6, C10 and 3OC12	Lactonase	*Fucus vesiculosus*	[188]
Flavobacteria				
Flaviramulus ichthyoenteri Th78	C6-C14 and 3OC6-3OC14	Lactonase	Flounder	[129]
Maribacter sp. 139	C4, C6, C10 and 3OC12	Lactonase	Ocean water	[184]
Muricauda olearia Th120	C6-C14 and 3OC6-3OC14	Latonase and acylase	Flounder	[129]
Olleya marilimosa 138E	C4, C6, C10 and 3OC12	Lactonase	Ocean water	[184]
O. marilimosa t168	C6-C14 and 3OC6-3OC14	Lactonase	Marine	[129]
Tenacibaculum discolor 20J	C4, C6, C10 and 3OC12	Lactonase	Sediment	[188]
T. discolor t84	C6-C14 and 3OC6-3OC14	ND	Gill of flounder	[129]
T. maritimum 2154^{t}	C10	Acylase	Fish farm disease	[192]
T. soleae strains	C6-C14 and 3OC6-3OC14	Lactonase	Gill of flounder	[129]
Gammaproteobacteria				
Alteromonas marina PP2-67	C4-C12	ND	Pod razor clam	[189]
Alteromonas sp. USC168	C4, C6, C10 and 3OC12	ND	*Fucus vesiculosus*	[188]
A. stellipolaris pp2-644	C4-C12	ND	Carpet-shell clam	[189]
Colwellia aestuarii T171	C8-C14 and 3OC10-3OC14	ND	Gill of flounder	[129]
Glaciecola sp. B20	C10-C14, 3OC10-, 3OHC10, 3OC12 and 3OHC12	ND	Intertidal rocks	[190]
Halomonas taeanensis USC33	C4, C6, C10 and 3OC12	Lactonase	Sediment	[188]
Marinobacterium sp. B2	3OC10, C12, 3OC12, 3OHC12 and C14	ND	Intertidal rocks	[190]
Pseudoalteromonas byunsanensis 1A01261	C4-C14 and 3OC4-3OC12	Lactonase	Marine	[193]
P. rydzensis Th125	C10-C14 and 3OC10-3OC14	ND	Flounder	[129]
Salinimonas sp. T194	C8-C14 and 3OC10-3OC14	ND	Gill of flounder	[129]
Salinicola salarius 131	C4, C6, C10 and 3OC12	Lactonase	Ocean water	[184]
Shewanella sp. B21	C8-C14, 3OC8-3OC12 and 3OHC8-3OHC12	ND	Intertidal rocks	[190]
Thalassomonas sp. PP2-459	C4-C12	ND	Carpet-shell clam	[189]
Thalassomonas sp. T202	C8-C14 and 3OC10-3OC14	ND	Gill of flounder	[129]

* All of AHLs contain even number of carbons; ** AHL-degrading activities were identified in bacterial cultures but not purified enzymes, except for *P. byunsanensis* 1A01261 and *M. olearia* Th120; ND: not determined.

6. Further Issues of Concern for the Application of QQ Agents

The antivirulence activities of small molecular QS inhibitors and QQ enzymes have been demonstrated *in vitro* and *in vivo*. However, both have advantages and drawbacks due to their entirely distinct molecular structures and functional mechanisms.

QS inhibitors may target one specific signal receptor or some homogenous receptors, such as the LuxR-like family. For example, compounds 4606–4327, CTL, CL and mBTL are synthetic AHL analogs with similar structures [194]. Each is the antagonist of CviR of *C. violaceum* and LuxN of *V. harveyi*. However, only mBTL is capable of inhibiting the pyocyanin production of *P. aeruginosa* PA14 whereas CL and CTL show non-inhibitory activity [195]. This may contribute to developing drugs that are capable of preventing virulence expression in specific pathogens. However, microbial infection is often caused by multiple pathogenic species, and one drug may be insufficient in this situation. In contrast, QQ enzymes, especially AHL lactonase, are capable of degrading a wide range of AHLs, and are likely to be more efficient for antivirulence by treating multi-microbial infection. Nevertheless, this capability of AHL-degrading enzymes could cause unintended consequences if a beneficial activity of a probiotic in the intestine of animals or human is positively regulated by its AHL-dependent QS [196].

Compared with QQ enzymes, the structures of QS inhibitors are relatively simple and can be easily modified through synthetic methods. Moreover, small QS inhibitors allow for temporal control of a biological system, and this control is often rapid, depending on the diffusibility of compounds. For example, the low molecular weight of QS inhibitors facilitates their absorption by animals; they may be administered orally or intravenously like other drugs. Furthermore, the nonproteinaceous nature as well as low molecular weight of QS inhibitors can effectively prevent an antibody-based immune response unlike that of QQ enzymes.

Stability is another important issue that should be taken into account for both of these two agents. QQ enzymes could be easily proteolyzed and most of them are sensitive to heat. Likewise, QS inhibitors may be degraded by abiotic or biotic elements. This is of concern especially for some QS inhibitors possessing similar structures with native AHLs. This type of QS inhibitor is suspected to be degraded by AHL-degrading enzymes because AiiA can degrade AHL analogs [135,137], and SisLac harbors AHL lactonase activity, esterase activity and phosphotriesterase activity [149]. Many of the identified QS inhibitors have similar structures to AHLs, especially of the synthetic AHL analogs. If this type of QS inhibitor was used to inhibit QS-dependent virulence in a multi-microbial community, it may be degraded by QQ enzymes produced by other microorganisms to obtain a competitive benefit in the environment. However, the QQ enzyme-mediated degradation of QS inhibitors has been ignored to date. It is advised that whether QS inhibitors can be degraded by QQ enzymes should be determined in the criteria proposed by Defoirdt *et al.* [122] for the scientific evaluation of QS inhibitory activity.

The emergence of resistance to QQ compounds has raised doubts about whether QS is an ideal target for antivirulence therapy. Defoirdt *et al.* [197] proposed that bacteria might evolve resistance to QQ compounds because QS disruption could indeed affect bacterial growth under certain conditions (e.g., during infection of a host). Subsequently, growth inhibition was observed by

cultivating *P. aeruginosa* PA14 on minimal medium using adenosine as the sole carbon source and with the simultaneous exposure to the synthetic QS inhibitor furanone C-30 [198]. Further studies revealed a QQ resistance mechanism through an increased efflux of C-30 from the cells by mutations in the *mexR* and *nalC* genes, both of which encode negative regulators of the MexAB-OprM multidrug resistance efflux pump [198]. Moreover, *mexR* and *nalC* mutations were found in several clinical *P. aeruginosa* isolates. However, unlike QS inhibitors, application of QQ lactonase would be less likely to induce QQ resistance [197,199]. The degradation activity of QQ enzyme targeting signals is extracellular rather than entering cells and targeting receptors, which would be hardly influenced by an increased efflux of compounds from cells. Despite the possible ways in which bacteria develop resistance to AHL-degrading enzymes, such as increasing production of autoinducers, synthesis of modified autoinducers and evolution of mutations with higher-affinity receptors [199], the high AHL-degrading activity and broad range of substrate specificity of QQ enzymes would reduce the possibility of evolving QQ resistance.

The potential for the development of antivirulence drugs has been emphasized for years, and a number of QQ agents have been discovered or synthesized, but none have been marketed. Certainly, the lack of appropriate delivery systems is one challenge. The corresponding QQ agents should be introduced into the hosts against different pathogens by controlling the rate, time, and place of release. The novel biological nanofactories engineered by Fernandes and colleagues would provide a promising specific delivery of QQ agents [200]. Another self-regulating system designed to release QQ agents dependent on the titer of bacteria surrounding medical devices has potential [201]. It is likely to be more difficult to develop formulations for delivering macromolecular QQ agents due to the extremely low bioavailability of protein drugs [202]. Although oral administration of AiiA homogenous protein and preparation dry powder of PvdQ have been attempted, there are concerns about the stability of QQ enzymes. Clatworthy *et al.* [1] argued that the greatest challenge for commercialization of antivirulence drugs is not technological but economic. Since antivirulence drugs are narrow-spectrum, their effectiveness is dependent on the precise diagnosis of the pathogens to achieve an appropriate choice of compounds. Therefore, appropriate tools need to be developed to allow decisions to be made [1]. Thus, the technological and economic obstacles for the commercialization of QQ drugs to be overcome in the future become more urgent than the discovery of novel QQ agents [1].

7. Concluding Remarks

In summary, the utilization of quorum quenching as a promising strategy of antivirulence therapy has been demonstrated *in vitro* and *in vivo*. The natural QQ agents, especially those derived from marine microorganisms, are great resources for developing antivirulence therapy. Recently, several studies have revealed a wide spread of QQ activities in marine microorganisms, however, these QQ resources need to be explored more deeply. Therefore, further research on QQ resources and mechanisms would provide more alternatives for developing antivirulence therapy.

Acknowledgments

We are very grateful to Brian Austin (University of Stirling, Scotland, UK) for careful English editing and critical reading of the manuscript. This work was supported by the International Science and Technology Cooperation Programme of China (no. 2012DFG31990).

Conflicts of Interest

The authors declare no conflict of interest.

References

1. Clatworthy, A.E.; Pierson, E.; Hung, D.T. Targeting virulence: A new paradigm for antimicrobial therapy. *Nat. Chem. Biol.* **2007**, *3*, 541–548.
2. Ng, W.L.; Bassler, B.L. Bacterial quorum-sensing network architectures. *Annu. Rev. Genet.* **2009**, *43*, 197–222.
3. Waters, C.M.; Bassler, B.L. Quorum sensing: Cell-to-cell communication in bacteria. *Annu. Rev. Cell. Dev. Biol.* **2005**, *21*, 319–346.
4. Fuqua, W.C.; Winans, S.C.; Greenberg, E.P. Quorum sensing in bacteria: The LuxR-LuxI family of cell density-responsive transcriptional regulators. *J. Bacteriol.* **1994**, *176*, 269–275.
5. Redfield, R.J. Is quorum sensing a side effect of diffusion sensing? *Trends Microbiol.* **2002**, *10*, 365–370.
6. Hense, B.A.; Kuttler, C.; Muller, J.; Rothballer, M.; Hartmann, A.; Kreft, J.U. Does efficiency sensing unify diffusion and quorum sensing? *Nat. Rev. Microbiol.* **2007**, *5*, 230–239.
7. Boyer, M.; Wisniewski-Dye, F. Cell-cell signalling in bacteria: Not simply a matter of quorum. *FEMS Microbiol. Ecol.* **2009**, *70*, 1–19.
8. West, S.A.; Winzer, K.; Gardner, A.; Diggle, S.P. Quorum sensing and the confusion about diffusion. *Trends Microbiol.* **2012**, *20*, 586–594.
9. Decho, A.W.; Norman, R.S.; Visscher, P.T. Quorum sensing in natural environments: Emerging views from microbial mats. *Trends Microbiol.* **2010**, *18*, 73–80.
10. Boedicker, J.Q.; Vincent, M.E.; Ismagilov, R.F. Microfluidic confinement of single cells of bacteria in small volumes initiates high-density behavior of quorum sensing and growth and reveals its variability. *Angew. Chem. Int. Ed.* **2009**, *48*, 5908–5911.
11. Carnes, E.C.; Lopez, D.M.; Donegan, N.P.; Cheung, A.; Gresham, H.; Timmins, G.S.; Brinker, C.J. Confinement-induced quorum sensing of individual *Staphylococcus aureus* bacteria. *Nat. Chem. Biol.* **2010**, *6*, 41–45.
12. Schuster, M.; Sexton, D.J.; Diggle, S.P.; Greenberg, E.P. Acyl-homoserine lactone quorum sensing: From evolution to application. *Annu. Rev. Microbiol.* **2013**, *67*, 43–63.
13. Platt, T.G.; Fuqua, C. What's in a name? The semantics of quorum sensing. *Trends Microbiol.* **2010**, *18*, 383–387.

14. Surette, M.G.; Miller, M.B.; Bassler, B.L. Quorum sensing in *Escherichia coli*, *Salmonella typhimurium*, and *Vibrio harveyi*: A new family of genes responsible for autoinducer production. *Proc. Natl. Acad. Sci. USA* **1999**, *96*, 1639–1644.
15. Pereira, C.S.; Thompson, J.A.; Xavier, K.B. AI-2-mediated signalling in bacteria. *FEMS Microbiol. Rev.* **2013**, *37*, 156–181.
16. Rezzonico, F.; Duffy, B. Lack of genomic evidence of AI-2 receptors suggests a non-quorum sensing role for *luxS* in most bacteria. *BMC Microbiol.* **2008**, *8*, 154.
17. Pereira, C.S.; de Regt, A.K.; Brito, P.H.; Miller, S.T.; Xavier, K.B. Identification of functional LsrB-like autoinducer-2 receptors. *J. Bacteriol.* **2009**, *191*, 6975–6987.
18. Winzer, K.; Hardie, K.R.; Burgess, N.; Doherty, N.; Kirke, D.; Holden, M.T.; Linforth, R.; Cornell, K.A.; Taylor, A.J.; Hill, P.J.; *et al.* LuxS: Its role in central metabolism and the *in vitro* synthesis of 4-hydroxy-5-methyl-3(2H)-furanone. *Microbiology* **2002**, *148*, 909–922.
19. Lee, J.H.; Lee, J. Indole as an intercellular signal in microbial communities. *FEMS Microbiol. Rev.* **2010**, *34*, 426–444.
20. Biswa, P.; Doble, M. Production of acylated homoserine lactone by Gram-positive bacteria isolated from marine water. *FEMS Microbiol. Lett.* **2013**, *343*, 34–41.
21. Johnson, M.R.; Montero, C.I.; Conners, S.B.; Shockley, K.R.; Bridger, S.L.; Kelly, R.M. Population density-dependent regulation of exopolysaccharide formation in the hyperthermophilic bacterium *Thermotoga maritima*. *Mol. Microbiol.* **2005**, *55*, 664–674.
22. Lee, H.; Chang, Y.C.; Nardone, G.; Kwon-Chung, K.J. TUP1 disruption in *Cryptococcus neoformans* uncovers a peptide-mediated density-dependent growth phenomenon that mimics quorum sensing. *Mol. Microbiol.* **2007**, *64*, 591–601.
23. Kelly, R.C.; Bolitho, M.E.; Higgins, D.A.; Lu, W.; Ng, W.-L.; Jeffrey, P.D.; Rabinowitz, J.D.; Semmelhack, M.F.; Hughson, F.M.; Bassler, B.L. The *Vibrio cholerae* quorum-sensing autoinducer CAI-1: Analysis of the biosynthetic enzyme CqsA. *Nat. Chem. Biol.* **2009**, *5*, 891–895.
24. Deng, Y.; Wu, J.; Tao, F.; Zhang, L.H. Listening to a new language: DSF-based quorum sensing in Gram-negative bacteria. *Chem. Rev.* **2011**, *111*, 160–173.
25. Chen, H.; Fujita, M.; Feng, Q.; Clardy, J.; Fink, G.R. Tyrosol is a quorum-sensing molecule in *Candida albicans*. *Proc. Natl. Acad. Sci. USA* **2004**, *101*, 5048–5052.
26. Hornby, J.M.; Jensen, E.C.; Lisec, A.D.; Tasto, J.J.; Jahnke, B.; Shoemaker, R.; Dussault, P.; Nickerson, K.W. Quorum sensing in the dimorphic fungus *Candida albicans* is mediated by farnesol. *Appl. Environ. Microbiol.* **2001**, *67*, 2982–2992.
27. Zhang, G.; Zhang, F.; Ding, G.; Li, J.; Guo, X.; Zhu, J.; Zhou, L.; Cai, S.; Liu, X.; Luo, Y.; *et al.* Acyl homoserine lactone-based quorum sensing in a methanogenic archaeon. *ISME J.* **2012**, *6*, 1336–1344.
28. Schaefer, A.L.; Greenberg, E.P.; Oliver, C.M.; Oda, Y.; Huang, J.J.; Bittan-Banin, G.; Peres, C.M.; Schmidt, S.; Juhaszova, K.; Sufrin, J.R.; *et al.* A new class of homoserine lactone quorum-sensing signals. *Nature* **2008**, *454*, 595–599.

29. Ahlgren, N.A.; Harwood, C.S.; Schaefer, A.L.; Giraud, E.; Greenberg, E.P. Aryl-homoserine lactone quorum sensing in stem-nodulating photosynthetic bradyrhizobia. *Proc. Natl. Acad. Sci. USA* **2011**, *108*, 7183–7188.
30. Lindemann, A.; Pessi, G.; Schaefer, A.L.; Mattmann, M.E.; Christensen, Q.H.; Kessler, A.; Hennecke, H.; Blackwell, H.E.; Greenberg, E.P.; Harwood, C.S. Isovaleryl-homoserine lactone, an unusual branched-chain quorum-sensing signal from the soybean symbiont *Bradyrhizobium japonicum*. *Proc. Natl. Acad. Sci. USA* **2011**, *108*, 16765–16770.
31. Gooding, J.R.; May, A.L.; Hilliard, K.R.; Campagna, S.R. Establishing a quantitative definition of quorum sensing provides insight into the information content of the autoinducer signals in *Vibrio harveyi* and *Escherichia coli*. *Biochemistry* **2010**, *49*, 5621–5623.
32. Saenz, H.L.; Augsburger, V.; Vuong, C.; Jack, R.W.; Gotz, F.; Otto, M. Inducible expression and cellular location of AgrB, a protein involved in the maturation of the staphylococcal quorum-sensing pheromone. *Arch. Microbiol.* **2000**, *174*, 452–455.
33. Lee, J.; Wu, J.; Deng, Y.; Wang, J.; Wang, C.; Wang, J.; Chang, C.; Dong, Y.; Williams, P.; Zhang, L.H. A cell-cell communication signal integrates quorum sensing and stress response. *Nat. Chem. Biol.* **2013**, *9*, 339–343.
34. Pesci, E.C.; Milbank, J.B.; Pearson, J.P.; McKnight, S.; Kende, A.S.; Greenberg, E.P.; Iglewski, B.H. Quinolone signaling in the cell-to-cell communication system of *Pseudomonas aeruginosa*. *Proc. Natl. Acad. Sci. USA* **1999**, *96*, 11229–11234.
35. Brachmann, A.O.; Brameyer, S.; Kresovic, D.; Hitkova, I.; Kopp, Y.; Manske, C.; Schubert, K.; Bode, H.B.; Heermann, R. Pyrones as bacterial signaling molecules. *Nat. Chem. Biol.* **2013**, *9*, 573–578.
36. Walters, M.; Sperandio, V. Autoinducer 3 and epinephrine signaling in the kinetics of locus of enterocyte effacement gene expression in enterohemorrhagic *Escherichia coli*. *Infect. Immun.* **2006**, *74*, 5445–5455.
37. Milton, D.L. Quorum sensing in vibrios: Complexity for diversification. *Int. J. Med. Microbiol.* **2006**, *296*, 61–71.
38. Henares, B.M.; Higgins, K.E.; Boon, E.M. Discovery of a nitric oxide responsive quorum sensing circuit in *Vibrio harveyi*. *ACS Chem. Biol.* **2012**, *7*, 1331–1336.
39. Lasarre, B.; Federle, M.J. Exploiting quorum sensing to confuse bacterial pathogens. *Microbiol. Mol. Biol. Rev.* **2013**, *77*, 73–111.
40. Yates, E.A.; Philipp, B.; Buckley, C.; Atkinson, S.; Chhabra, S.R.; Sockett, R.E.; Goldner, M.; Dessaux, Y.; Camara, M.; Smith, H.; *et al. N*-Acylhomoserine lactones undergo lactonolysis in a pH-, temperature-, and acyl chain length-dependent manner during growth of *Yersinia pseudotuberculosis* and *Pseudomonas aeruginosa*. *Infect. Immun.* **2002**, *70*, 5635–5646.
41. Taga, M.E.; Miller, S.T.; Bassler, B.L. Lsr-mediated transport and processing of AI-2 in *Salmonella typhimurium*. *Mol. Microbiol.* **2003**, *50*, 1411–1427.
42. Ng, W.L.; Perez, L.J.; Wei, Y.; Kraml, C.; Semmelhack, M.F.; Bassler, B.L. Signal production and detection specificity in *Vibrio* CqsA/CqsS quorum-sensing systems. *Mol. Microbiol.* **2011**, *79*, 1407–1417.

43. Tu, K.C.; Bassler, B.L. Multiple small RNAs act additively to integrate sensory information and control quorum sensing in *Vibrio harveyi*. *Genes Dev.* **2007**, *21*, 221–233.
44. Rutherford, S.T.; van Kessel, J.C.; Shao, Y.; Bassler, B.L. AphA and LuxR/HapR reciprocally control quorum sensing in vibrios. *Genes Dev.* **2011**, *25*, 397–408.
45. Van Kessel, J.C.; Rutherford, S.T.; Shao, Y.; Utria, A.F.; Bassler, B.L. Individual and combined roles of the master regulators AphA and LuxR in control of the *Vibrio harveyi* quorum-sensing regulon. *J. Bacteriol.* **2013**, *195*, 436–443.
46. Schauder, S.; Shokat, K.; Surette, M.G.; Bassler, B.L. The LuxS family of bacterial autoinducers: Biosynthesis of a novel quorum-sensing signal molecule. *Mol. Microbiol.* **2001**, *41*, 463–476.
47. Minogue, T.D.; Wehland-von Trebra, M.; Bernhard, F.; von Bodman, S.B. The autoregulatory role of EsaR, a quorum-sensing regulator in *Pantoea stewartii* ssp. *stewartii*: Evidence for a repressor function. *Mol. Microbiol.* **2002**, *44*, 1625–1635.
48. Dong, Y.H.; Wang, L.H.; Xu, J.L.; Zhang, H.B.; Zhang, X.F.; Zhang, L.H. Quenching quorum-sensing-dependent bacterial infection by an *N*-acyl homoserine lactonase. *Nature* **2001**, *411*, 813–817.
49. Eberhard, A.; Widrig, C.A.; McBath, P.; Schineller, J.B. Analogs of the autoinducer of bioluminescence in *Vibrio fischeri*. *Arch. Microbiol.* **1986**, *146*, 35–40.
50. Fuqua, C. The QscR quorum-sensing regulon of *Pseudomonas aeruginosa*: An orphan claims its identity. *J. Bacteriol.* **2006**, *188*, 3169–3171.
51. Kovacikova, G.; Skorupski, K. Regulation of virulence gene expression in *Vibrio cholerae* by quorum sensing: HapR functions at the aphA promoter. *Mol. Microbiol.* **2002**, *46*, 1135–1147.
52. Mattmann, M.E.; Shipway, P.M.; Heth, N.J.; Blackwell, H.E. Potent and selective synthetic modulators of a quorum sensing repressor in *Pseudomonas aeruginosa* identified from second-generation libraries of *N*-acylated *L*-homoserine lactones. *ChemBioChem* **2011**, *12*, 942–949.
53. Ng, W.L.; Perez, L.; Cong, J.; Semmelhack, M.F.; Bassler, B.L. Broad spectrum pro-quorum-sensing molecules as inhibitors of virulence in vibrios. *PLoS Pathog.* **2012**, *8*, e1002767.
54. Perez, L.J.; Karagounis, T.K.; Hurley, A.; Bassler, B.L.; Semmelhack, M.F. Highly potent, chemically stable quorum sensing agonists for *Vibrio cholerae*. *Chem. Sci.* **2014**, *5*, 151–155.
55. Clark, B.R.; Engene, N.; Teasdale, M.E.; Rowley, D.C.; Matainaho, T.; Valeriote, F.A.; Gerwick, W.H. Natural products chemistry and taxonomy of the marine cyanobacterium *Blennothrix cantharidosmum*. *J. Nat. Prod.* **2008**, *71*, 1530–1537.
56. Dobretsov, S.; Teplitski, M.; Alagely, A.; Gunasekera, S.P.; Paul, V.J. Malyngolide from the cyanobacterium *Lyngbya majuscula* interferes with quorum sensing circuitry. *Environ. Microbiol. Rep.* **2010**, *2*, 739–744.

57. Choi, H.; Mascuch, S.J.; Villa, F.A.; Byrum, T.; Teasdale, M.E.; Smith, J.E.; Preskitt, L.B.; Rowley, D.C.; Gerwick, L.; Gerwick, W.H. Honaucins A–C, potent inhibitors of inflammation and bacterial quorum sensing: Synthetic derivatives and structure-activity relationships. *Chem. Biol.* **2012**, *19*, 589–598.
58. Ooka, K.; Fukumoto, A.; Yamanaka, T.; Shimada, K.; Ishihara, R.; Anzai, Y.; Kato, F. Piericidins, novel quorum-sensing inhibitors against *Chromobacterium violaceum* CV026, from *Streptomyces* sp. TOHO-Y209 and TOHO-O348. *Open J. Med. Chem.* **2013**, *3*, 93–99.
59. Teasdale, M.E.; Liu, J.Y.; Wallace, J.; Akhlaghi, F.; Rowley, D.C. Secondary metabolites produced by the marine bacterium *Halobacillus salinus* that inhibit quorum sensing-controlled phenotypes in Gram-negative bacteria. *Appl. Environ. Microbiol.* **2009**, *75*, 567–572.
60. Teasdale, M.E.; Donovan, K.A.; Forschner-Dancause, S.R.; Rowley, D.C. Gram-positive marine bacteria as a potential resource for the discovery of quorum sensing inhibitors. *Mar. Biotechnol.* **2011**, *13*, 722–732.
61. Abed, R.M.; Dobretsov, S.; Al-Fori, M.; Gunasekera, S.P.; Sudesh, K.; Paul, V.J. Quorum-sensing inhibitory compounds from extremophilic microorganisms isolated from a hypersaline cyanobacterial mat. *J. Ind. Microbiol. Biotechnol.* **2013**, *40*, 759–772.
62. Peters, L.; König, G.M.; Wright, A.D.; Pukall, R.; Stackebrandt, E.; Eberl, L.; Riedel, K. Secondary metabolites of *Flustra foliacea* and their influence on bacteria. *Appl. Environ. Microbiol.* **2003**, *69*, 3469–3475.
63. Tello, E.; Castellanos, L.; Arevalo-Ferro, C.; Rodríguez, J.; Jiménez, C.; Duque, C. Absolute stereochemistry of antifouling cembranoid epimers at C-8 from the Caribbean octocoral *Pseudoplexaura flagellosa*. Revised structures of plexaurolones. *Tetrahedron* **2011**, *67*, 9112–9121.
64. Tello, E.; Castellanos, L.; Arevalo-Ferro, C.; Duque, C. Disruption in quorum-sensing systems and bacterial biofilm inhibition by cembranoid diterpenes isolated from the octocoral *Eunicea knighti*. *J. Nat. Prod.* **2012**, *75*, 1637–1642.
65. Kwan, J.C.; Teplitski, M.; Gunasekera, S.P.; Paul, V.J.; Luesch, H. Isolation and biological evaluation of 8-epi-malyngamide C from the Floridian marine cyanobacterium *Lyngbya majuscula*. *J. Nat. Prod.* **2010**, *73*, 463–466.
66. Kwan, J.C.; Meickle, T.; Ladwa, D.; Teplitski, M.; Paul, V.; Luesch, H. Lyngbyoic acid, a "tagged" fatty acid from a marine cyanobacterium, disrupts quorum sensing in *Pseudomonas aeruginosa*. *Mol. Biosyst.* **2011**, *7*, 1205–1216.
67. Montaser, R.; Paul, V.J.; Luesch, H. Modular strategies for structure and function employed by marine cyanobacteria: Characterization and synthesis of pitinoic acids. *Org. Lett.* **2013**, *15*, 4050–4053.
68. Dobretsov, S.; Teplitski, M.; Bayer, M.; Gunasekera, S.; Proksch, P.; Paul, V.J. Inhibition of marine biofouling by bacterial quorum sensing inhibitors. *Biofouling* **2011**, *27*, 893–905.
69. Wang, L.; Zou, S.; Yin, S.; Liu, H.; Yu, W.; Gong, Q. Construction of an effective screening system for detection of *Pseudomonas aeruginosa* quorum sensing inhibitors and its application in bioautographic thin-layer chromatography. *Biotechnol. Lett.* **2011**, *33*, 1381–1387.

70. Liu, H.B.; Koh, K.P.; Kim, J.S.; Seo, Y.; Park, S. The effects of betonicine, floridoside, and isethionic acid from the red alga *Ahnfeltiopsis flabelliformis* on quorum-sensing activity. *Biotechnol. Bioprocess Eng.* **2008**, *13*, 458–463.
71. Skindersoe, M.E.; Ettinger-Epstein, P.; Rasmussen, T.B.; Bjarnsholt, T.; de Nys, R.; Givskov, M. Quorum sensing antagonism from marine organisms. *Mar. Biotechnol. (N. Y.)* **2008**, *10*, 56–63.
72. Chu, Y.Y.; Nega, M.; Wolfle, M.; Plener, L.; Grond, S.; Jung, K.; Gotz, F. A new class of quorum quenching molecules from *Staphylococcus* species affects communication and growth of Gram-negative bacteria. *PLoS Pathog.* **2013**, *9*, e1003654.
73. Singh, V.K.; Kavita, K.; Prabhakaran, R.; Jha, B. *Cis*-9-octadecenoic acid from the rhizospheric bacterium *Stenotrophomonas maltophilia* BJ01 shows quorum quenching and anti-biofilm activities. *Biofouling* **2013**, *29*, 855–867.
74. Bobadilla Fazzini, R.A.; Skindersoe, M.E.; Bielecki, P.; Puchalka, J.; Givskov, M.; Martins sos Santos, V.A. Protoanemonin: A natural quorum sensing inhibitor that selectively activates iron starvation response. *Environ. Microbiol.* **2013**, *15*, 111–120.
75. HjelmgaardRasmussen, T.B.; Skindersoe, M.E.; Bjarnsholt, T.; Phipps, R.K.; Christensen, K.B.; Jensen, P.O.; Andersen, J.B.; Koch, B.; Larsen, T.O.; Hentzer, M.; *et al.* Identity and effects of quorum-sensing inhibitors produced by *Penicillium species*. *Microbiology* **2005**, *151*, 1325–1340.
76. Truchado, P.; Lopez-Galvez, F.; Gil, M.I.; Tomas-Barberan, F.A.; Allende, A. Quorum sensing inhibitory and antimicrobial activities of honeys and the relationship with individual phenolics. *Food Chem.* **2009**, *115*, 1337–1344.
77. Bulman, Z.; Le, P.; Hudson, A.O.; Savka, M.A. A novel property of propolis (bee glue): Anti-pathogenic activity by inhibition of *N*-acyl-homoserine lactone mediated signaling in bacteria. *J. Ethnopharmacol.* **2011**, *138*, 788–797.
78. Park, J.; Kaufmann, G.F.; Bowen, J.P.; Arbiser, J.L.; Janda, K.D. Solenopsin A, a venom alkaloid from the fire ant *Solenopsis invicta*, inhibits quorum-sensing signaling in *Pseudomonas aeruginosa*. *J. Infect. Dis.* **2008**, *198*, 1198–1201.
79. Zhou, L.; Zheng, H.; Tang, Y.; Yu, W.; Gong, Q. Eugenol inhibits quorum sensing at sub-inhibitory concentrations. *Biotechnol. Lett.* **2013**, *35*, 631–637.
80. Keshavan, N.D.; Chowdhary, P.K.; Haines, D.C.; Gonzalez, J.E. L-canavanine made by *Medicago sativa* interferes with quorum sensing in *Sinorhizobium meliloti*. *J. Bacteriol.* **2005**, *187*, 8427–8436.
81. Vandeputte, O.M.; Kiendrebeogo, M.; Rajaonson, S.; Diallo, B.; Mol, A.; El Jaziri, M.; Baucher, M. Identification of catechin as one of the flavonoids from *Combretum albiflorum* bark extract that reduces the production of quorum-sensing-controlled virulence factors in *Pseudomonas aeruginosa* PAO1. *Appl. Environ. Microbiol.* **2010**, *76*, 243–253.
82. Vandeputte, O.M.; Kiendrebeogo, M.; Rasamiravaka, T.; Stevigny, C.; Duez, P.; Rajaonson, S.; Diallo, B.; Mol, A.; Baucher, M.; El Jaziri, M. The flavanone naringenin reduces the production of quorum sensing-controlled virulence factors in *Pseudomonas aeruginosa* PAO1. *Microbiology* **2011**, *157*, 2120–2132.

83. Amaya, S.; Pereira, J.A.; Borkosky, S.A.; Valdez, J.C.; Bardon, A.; Arena, M.E. Inhibition of quorum sensing in *Pseudomonas aeruginosa* by sesquiterpene lactones. *Phytomedicine* **2012**, *19*, 1173–1177.
84. Jakobsen, T.H.; van Gennip, M.; Phipps, R.K.; Shanmugham, M.S.; Christensen, L.D.; Alhede, M.; Skindersoe, M.E.; Rasmussen, T.B.; Friedrich, K.; Uthe, F.; *et al.* Ajoene, a sulfur-rich molecule from garlic, inhibits genes controlled by quorum sensing. *Antimicrob. Agents Chemother.* **2012**, *56*, 2314–2325.
85. Jakobsen, T.H.; Bragason, S.K.; Phipps, R.K.; Christensen, L.D.; van Gennip, M.; Alhede, M.; Skindersoe, M.; Larsen, T.O.; Hoiby, N.; Bjarnsholt, T.; *et al.* Food as a source for quorum sensing inhibitors: Iberin from horseradish revealed as a quorum sensing inhibitor of *Pseudomonas aeruginosa*. *Appl. Environ. Microbiol.* **2012**, *78*, 2410–2421.
86. Chong, Y.M.; Yin, W.F.; Ho, C.Y.; Mustafa, M.R.; Hadi, A.H.A.; Awang, K.; Narrima, P.; Koh, C.L.; Appleton, D.R.; Chan, K.G. Malabaricone C from *Myristica cinnamomea* exhibits anti-quorum sensing activity. *J. Nat. Prod.* **2011**, *74*, 2261–2264.
87. Paza, C.; Carcamo, G.; Silva, M.; Becerra, J.; Urrutia, H.; Sossa, K. Drimendiol, a drimane sesquiterpene with quorum sensing inhibition activity. *Nat. Prod. Commun.* **2013**, *8*, 147–148.
88. Packiavathy, I.A.; Priya, S.; Pandian, S.K.; Ravi, A.V. Inhibition of biofilm development of uropathogens by curcumin-an anti-quorum sensing agent from *Curcuma longa*. *Food Chem.* **2014**, *148*, 453–460.
89. Bodini, S.F.; Manfredini, S.; Epp, M.; Valentini, S.; Santori, F. Quorum sensing inhibition activity of garlic extract and *p*-coumaric acid. *Lett. Appl. Microbiol.* **2009**, *49*, 551–555.
90. Giménez-Bastida, J.A.; Truchado, P.; Larrosa, M.; Espín, J.C.; Tomás-Barberán, F.A.; Allende, A.; García-Conesa, M.T. Urolithins, ellagitannin metabolites produced by colon microbiota, inhibit quorum sensing in *Yersinia enterocolitica*: Phenotypic response and associated molecular changes. *Food Chem.* **2012**, *132*, 1465–1474.
91. Adonizio, A.; Dawlaty, J.; Ausubel, F.M.; Clardy, J.; Mathee, K. Ellagitannins from *Conocarpus erectus* exhibit anti-quorum sensing activity against *Pseudomonas aeruginosa*. *Planta Med.* **2008**, *74*, 1035–1035.
92. Kaplan, F.; Badri, D.V.; Zachariah, C.; Ajredini, R.; Sandoval, F.J.; Roje, S.; Levine, L.H.; Zhang, F.L.; Robinette, S.L.; Alborn, H.T.; *et al.* Bacterial attraction and quorum sensing inhibition in *Caenorhabditis elegans* exudates. *J. Chem. Ecol.* **2009**, *35*, 878–892.
93. Teplitski, M.; Chen, H.; Rajamani, S.; Gao, M.; Merighi, M.; Sayre, R.T.; Robinson, J.B.; Rolfe, B.G.; Bauer, W.D. *Chlamydomonas reinhardtii* secretes compounds that mimic bacterial signals and interfere with quorum sensing regulation in bacteria. *Plant Physiol.* **2004**, *134*, 137–146.
94. Rajamani, S.; Bauer, W.D.; Robinson, J.B.; Farrow, J.M.; Pesci, E.C.; Teplitski, M.; Gao, M.S.; Sayre, R.T.; Phillips, D.A. The vitamin riboflavin and its derivative lumichrome activate the LasR bacterial quorum-sensing receptor. *Mol. Plant-Microbe Interact.* **2008**, *21*, 1184–1192.

95. Ding, X.; Yin, B.; Qian, L.; Zeng, Z.R.; Yang, Z.L.; Li, H.X.; Lu, Y.J.; Zhou, S.N. Screening for novel quorum-sensing inhibitors to interfere with the formation of *Pseudomonas aeruginosa* biofilm. *J. Med. Microbiol.* **2011**, *60*, 1827–1834.
96. Zeng, Z.; Qian, L.; Cao, L.; Tan, H.; Huang, Y.; Xue, X.; Shen, Y.; Zhou, S. Virtual screening for novel quorum sensing inhibitors to eradicate biofilm formation of *Pseudomonas aeruginosa*. *Appl. Microbiol. Biotechnol.* **2008**, *79*, 119–126.
97. Cugini, C.; Calfee, M.W.; Farrow, J.M., 3rd.; Morales, D.K.; Pesci, E.C.; Hogan, D.A. Farnesol, a common sesquiterpene, inhibits PQS production in *Pseudomonas aeruginosa*. *Mol. Microbiol.* **2007**, *65*, 896–906.
98. De Nys, R.; Wright, A.D.; König, G.M.; Sticher, O. New halogenated furanones from the marine alga *Delisea pulchra* (*cf. fimbriata*). *Tetrahedron* **1993**, *49*, 11213–11220.
99. Hentzer, M.; Riedel, K.; Rasmussen, T.B.; Heydorn, A.; Andersen, J.B.; Parsek, M.R.; Rice, S.A.; Eberl, L.; Molin, S.; Hoiby, N.; *et al.* Inhibition of quorum sensing in *Pseudomonas aeruginosa* biofilm bacteria by a halogenated furanone compound. *Microbiology* **2002**, *148*, 87–102.
100. Brackman, G.; Celen, S.; Hillaert, U.; van Calenbergh, S.; Cos, P.; Maes, L.; Nelis, H.J.; Coenye, T. Structure-activity relationship of cinnamaldehyde analogs as inhibitors of AI-2 based quorum sensing and their effect on virulence of *Vibrio* spp. *PLoS One* **2011**, *6*, e16084.
101. Niu, C.; Afre, S.; Gilbert, E.S. Subinhibitory concentrations of cinnamaldehyde interfere with quorum sensing. *Lett. Appl. Microbiol.* **2006**, *43*, 489–494.
102. Brackman, G.; Defoirdt, T.; Miyamoto, C.; Bossier, P.; van Calenbergh, S.; Nelis, H.; Coenye, T. Cinnamaldehyde and cinnamaldehyde derivatives reduce virulence in *Vibrio* spp. by decreasing the DNA-binding activity of the quorum sensing response regulator LuxR. *BMC Microbiol.* **2008**, *8*, 149.
103. Lee, K.M.; Lim, J.; Nam, S.; Yoon, M.Y.; Kwon, Y.K.; Jung, B.Y.; Park, Y.; Park, S.; Yoon, S.S. Inhibitory effects of broccoli extract on *Escherichia coli* O157:H7 quorum sensing and *in vivo* virulence. *FEMS Microbiol. Lett.* **2011**, *321*, 67–74.
104. Vikram, A.; Jesudhasan, P.R.; Jayaprakasha, G.K.; Pillai, B.S.; Patil, B.S. Grapefruit bioactive limonoids modulate E. coli O157:H7 TTSS and biofilm. *Int. J. Food Microbiol.* **2010**, *140*, 109–116.
105. Li, J.; Wang, W.; Xu, S.X.; Magarvey, N.A.; McCormick, J.K. *Lactobacillus reuteri*-produced cyclic dipeptides quench *agr*-mediated expression of toxic shock syndrome toxin-1 in staphylococci. *Proc. Natl. Acad. Sci. USA* **2011**, *108*, 3360–3365.
106. Mansson, M.; Nielsen, A.; Kjaerulff, L.; Gotfredsen, C.H.; Wietz, M.; Ingmer, H.; Gram, L.; Larsen, T.O. Inhibition of virulence gene expression in *Staphylococcus aureus* by novel depsipeptides from a marine *Photobacterium*. *Mar. Drugs* **2011**, *9*, 2537–2552.
107. Kiran, M.D.; Adikesavan, N.V.; Cirioni, O.; Giacometti, A.; Silvestri, C.; Scalise, G.; Ghiselli, R.; Saba, V.; Orlando, F.; Shoham, M.; *et al.* Discovery of a quorum-sensing inhibitor of drug-resistant staphylococcal infections by structure-based virtual screening. *Mol. Pharmacol.* **2008**, *73*, 1578–1586.

108. Duncan, M.C.; Wong, W.R.; Dupzyk, A.J.; Bray, W.M.; Linington, R.G.; Auerbuch, V. An NF-kappaB-based high-throughput screen identifies piericidins as inhibitors of the *Yersinia pseudotuberculosis* type III secretion system. *Antimicrob. Agents Chemother.* **2014**, *58*, 1118–1126.
109. De Nys, R.; Steinberg, P.; Willemsen, P.; Dworjanyn, S.; Gabelish, C.; King, R. Broad spectrum effects of secondary metabolites from the red alga *Delisea pulchra* in antifouling assays. *Biofouling* **1995**, *8*, 259–271.
110. Martinelli, D.; Grossmann, G.; Sequin, U.; Brandl, H.; Bachofen, R. Effects of natural and chemically synthesized furanones on quorum sensing in *Chromobacterium violaceum*. *BMC Microbiol.* **2004**, *4*, 25.
111. Manefield, M.; Rasmussen, T.B.; Henzter, M.; Andersen, J.B.; Steinberg, P.; Kjelleberg, S.; Givskov, M. Halogenated furanones inhibit quorum sensing through accelerated LuxR turnover. *Microbiology* **2002**, *148*, 1119–1127.
112. Defoirdt, T.; Miyamoto, C.M.; Wood, T.K.; Meighen, E.A.; Sorgeloos, P.; Verstraete, W.; Bossier, P. The natural furanone (*5Z*)-4-bromo-5-(bromomethylene)-3-butyl-2(*5H*)-furanone disrupts quorum sensing-regulated gene expression in *Vibrio harveyi* by decreasing the DNA-binding activity of the transcriptional regulator protein luxR. *Environ. Microbiol.* **2007**, *9*, 2486–2495.
113. Zang, T.; Lee, B.W.; Cannon, L.M.; Ritter, K.A.; Dai, S.; Ren, D.; Wood, T.K.; Zhou, Z.S. A naturally occurring brominated furanone covalently modifies and inactivates LuxS. *Bioorg. Med. Chem. Lett.* **2009**, *19*, 6200–6204.
114. Defoirdt, T.; Crab, R.; Wood, T.K.; Sorgeloos, P.; Verstraete, W.; Bossier, P. Quorum sensing-disrupting brominated furanones protect the gnotobiotic brine shrimp *Artemia franciscana* from pathogenic *Vibrio harveyi*, *Vibrio campbellii*, and *Vibrio parahaemolyticus* isolates. *Appl. Environ. Microbiol.* **2006**, *72*, 6419–6423.
115. Rasch, M.; Buch, C.; Austin, B.; Slierendrecht, W.J.; Ekmann, K.S.; Larsen, J.L.; Johansen, C.; Riedel, K.; Eberl, L.; Givskov, M.; *et al.* An inhibitor of bacterial quorum sensing reduces mortalities caused by vibriosis in rainbow trout (*Oncorhynchus mykiss*, *Walbaum*). *Syst. Appl. Microbiol.* **2004**, *27*, 350–359.
116. Tinh, N.T.N.; Linh, N.D.; Wood, T.K.; Dierckens, K.; Sorgeloos, P.; Bossier, P. Interference with the quorum sensing systems in a *Vibrio harveyi* strain alters the growth rate of gnotobiotically cultured rotifer *Brachionus plicatilis*. *J. Appl. Microbiol.* **2007**, *103*, 194–203.
117. Wu, H.; Song, Z.; Hentzer, M.; Andersen, J.B.; Molin, S.; Givskov, M.; Hoiby, N. Synthetic furanones inhibit quorum-sensing and enhance bacterial clearance in *Pseudomonas aeruginosa* lung infection in mice. *J. Antimicrob. Chemother.* **2004**, *53*, 1054–1061.
118. Natrah, F.M.I.; Kenmegne, M.M.; Wiyoto, W.; Sorgeloos, P.; Bossier, P.; Defoirdt, T. Effects of micro-algae commonly used in aquaculture on acyl-homoserine lactone quorum sensing. *Aquaculture* **2011**, *317*, 53–57.
119. Havsteen, B.H. The biochemistry and medical significance of the flavonoids. *Pharmacol. Ther.* **2002**, *96*, 67–202.

120. Vikram, A.; Jayaprakasha, G.K.; Jesudhasan, P.R.; Pillai, S.D.; Patil, B.S. Suppression of bacterial cell-cell signalling, biofilm formation and type III secretion system by citrus flavonoids. *J. Appl. Microbiol.* **2010**, *109*, 515–527.
121. Pande, G.S.J.; Scheie, A.A.; Benneche, T.; Wille, M.; Sorgeloos, P.; Bossier, P.; Defoirdt, T. Quorum sensing-disrupting compounds protect larvae of the giant freshwater prawn *Macrobrachium rosenbergii* from *Vibrio harveyi* infection. *Aquaculture* **2013**, *406–407*, 121–124.
122. Defoirdt, T.; Brackman, G.; Coenye, T. Quorum sensing inhibitors: How strong is the evidence? *Trends Microbiol.* **2013**, *21*, 619–624.
123. Ni, N.; Choudhary, G.; Li, M.; Wang, B. Pyrogallol and its analogs can antagonize bacterial quorum sensing in *Vibrio harveyi*. *Bioorg. Med. Chem. Lett.* **2008**, *18*, 1567–1572.
124. Defoirdt, T.; Pande, G.S.; Baruah, K.; Bossier, P. The apparent quorum-sensing inhibitory activity of pyrogallol is a side effect of peroxide production. *Antimicrob. Agents Chemother.* **2013**, *57*, 2870–2873.
125. Newman, K.L.; Chatterjee, S.; Ho, K.A.; Lindow, S.E. Virulence of plant pathogenic bacteria attenuated by degradation of fatty acid cell-to-cell signaling factors. *Mol. Plant Microbe Interact.* **2008**, *21*, 326–334.
126. Pustelny, C.; Albers, A.; Buldt-Karentzopoulos, K.; Parschat, K.; Chhabra, S.R.; Camara, M.; Williams, P.; Fetzner, S. Dioxygenase-mediated quenching of quinolone-dependent quorum sensing in *Pseudomonas aeruginosa*. *Chem. Biol.* **2009**, *16*, 1259–1267.
127. Roy, V.; Fernandes, R.; Tsao, C.Y.; Bentley, W.E. Cross species quorum quenching using a native AI-2 processing enzyme. *ACS Chem. Biol.* **2010**, *5*, 223–232.
128. Draganov, D.I.; Teiber, J.F.; Speelman, A.; Osawa, Y.; Sunahara, R.; La Du, B.N. Human paraoxonases (PON1, PON2, and PON3) are lactonases with overlapping and distinct substrate specificities. *J. Lipid Res.* **2005**, *46*, 1239–1247.
129. Tang, K.; Zhang, Y.; Yu, M.; Shi, X.; Coenye, T.; Bossier, P.; Zhang, X.H. Evaluation of a new high-throughput method for identifying quorum quenching bacteria. *Sci. Rep.* **2013**, *3*, 2935.
130. Zhang, X.H. Ocean University of China, Qingdao, China. MomL, a novel marine-derived *N*-acyl homeserine lactonase in *Muricauda olearia*. 2014, Unpublished work.
131. Dong, Y.H.; Xu, J.L.; Li, X.Z.; Zhang, L.H. AiiA, an enzyme that inactivates the acylhomoserine lactone quorum-sensing signal and attenuates the virulence of *Erwinia carotovora*. *Proc. Natl. Acad. Sci. USA* **2000**, *97*, 3526–3531.
132. Thomas, P.W.; Stone, E.M.; Costello, A.L.; Tierney, D.L.; Fast, W. The quorum-quenching lactonase from *Bacillus thuringiensis* is a metalloprotein. *Biochemistry* **2005**, *44*, 7559–7569.
133. Kim, M.H.; Choi, W.C.; Kang, H.O.; Lee, J.S.; Kang, B.S.; Kim, K.J.; Derewenda, Z.S.; Oh, T.K.; Lee, C.H.; Lee, J.K. The molecular structure and catalytic mechanism of a quorum-quenching *N*-acyl-L-homoserine lactone hydrolase. *Proc. Natl. Acad. Sci. USA* **2005**, *102*, 17606–17611.
134. Liu, D.; Momb, J.; Thomas, P.W.; Moulin, A.; Petsko, G.A.; Fast, W.; Ringe, D. Mechanism of the quorum-quenching lactonase (AiiA) from *Bacillus thuringiensis*. 1. product-bound structures. *Biochemistry* **2008**, *47*, 7706–7714.

135. Momb, J.; Wang, C.; Liu, D.; Thomas, P.W.; Petsko, G.A.; Guo, H.; Ringe, D.; Fast, W. Mechanism of the quorum-quenching lactonase (AiiA) from *Bacillus thuringiensis*. 2. substrate modeling and active site mutations. *Biochemistry* **2008**, *47*, 7715–7725.
136. Liu, C.F.; Liu, D.; Momb, J.; Thomas, P.W.; Lajoie, A.; Petsko, G.A.; Fast, W.; Ringe, D. A phenylalanine clamp controls substrate specificity in the quorum-quenching metallo-gamma-lactonase from *Bacillus thuringiensis*. *Biochemistry* **2013**, *52*, 1603–1610.
137. Momb, J.; Thomas, P.W.; Breece, R.M.; Tierney, D.L.; Fast, W. The quorum-quenching metallo-gamma-lactonase from *Bacillus thuringiensis* exhibits a leaving group thio effect. *Biochemistry* **2006**, *45*, 13385–13393.
138. Carlier, A.; Uroz, S.; Smadja, B.; Fray, R.; Latour, X.; Dessaux, Y.; Faure, D. The Ti plasmid of *Agrobacterium tumefaciens* harbors an *attM*-paralogous gene, *aiiB*, also encoding *N*-acyl homoserine lactonase activity. *Appl. Environ. Microbiol.* **2003**, *69*, 4989–4993.
139. Liu, D.; Thomas, P.W.; Momb, J.; Hoang, Q.Q.; Petsko, G.A.; Ringe, D.; Fast, W. Structure and specificity of a quorum-quenching lactonase (AiiB) from *Agrobacterium tumefaciens*. *Biochemistry* **2007**, *46*, 11789–11799.
140. Piper, K.R.; Beck von Bodman, S.; Farrand, S.K. Conjugation factor of *Agrobacterium tumefaciens* regulates Ti plasmid transfer by autoinduction. *Nature* **1993**, *362*, 448–450.
141. Haudecoeur, E.; Planamente, S.; Cirou, A.; Tannieres, M.; Shelp, B.J.; Morera, S.; Faure, D. Proline antagonizes GABA-induced quenching of quorum-sensing in *Agrobacterium tumefaciens*. *Proc. Natl. Acad. Sci. USA* **2009**, *106*, 14587–14592.
142. Wang, W.Z.; Morohoshi, T.; Someya, N.; Ikeda, T. AidC, a novel *N*-acylhomoserine lactonase from the potato root-associated *cytophaga-flavobacteria-bacteroides* (CFB) group bacterium *Chryseobacterium* sp. strain StRB126. *Appl. Environ. Microbiol.* **2012**, *78*, 7985–7992.
143. Krysciak, D.; Schmeisser, C.; Preuss, S.; Riethausen, J.; Quitschau, M.; Grond, S.; Streit, W.R. Involvement of multiple loci in quorum quenching of autoinducer I molecules in the nitrogen-fixing symbiont *Rhizobium* (*Sinorhizobium*) sp. strain NGR234. *Appl. Environ. Microbiol.* **2011**, *77*, 5089–5099.
144. Schneider, J.; Yepes, A.; Garcia-Betancur, J.C.; Westedt, I.; Mielich, B.; Lopez, D. Streptomycin-induced expression in *Bacillus subtilis* of YtnP, a lactonase-homologous protein that inhibits development and streptomycin production in *Streptomyces griseus*. *Appl. Environ. Microbiol.* **2012**, *78*, 599–603.
145. Afriat, L.; Roodveldt, C.; Manco, G.; Tawfik, D.S. The latent promiscuity of newly identified microbial lactonases is linked to a recently diverged phosphotriesterase. *Biochemistry* **2006**, *45*, 13677–13686.
146. Elias, M.; Dupuy, J.; Merone, L.; Mandrich, L.; Porzio, E.; Moniot, S.; Rochu, D.; Lecomte, C.; Rossi, M.; Masson, P.; *et al.* Structural basis for natural lactonase and promiscuous phosphotriesterase activities. *J. Mol. Biol.* **2008**, *379*, 1017–1028.
147. Ng, F.S.; Wright, D.M.; Seah, S.Y. Characterization of a phosphotriesterase-like lactonase from *Sulfolobus solfataricus* and its immobilization for disruption of quorum sensing. *Appl. Environ. Microbiol.* **2011**, *77*, 1181–1186.

148. Xue, B.; Chow, J.Y.; Baldansuren, A.; Yap, L.L.; Gan, Y.H.; Dikanov, S.A.; Robinson, R.C.; Yew, W.S. Structural evidence of a productive active site architecture for an evolved quorum-quenching GKL lactonase. *Biochemistry* **2013**, *52*, 2359–2370.
149. Hiblot, J.; Gotthard, G.; Chabriere, E.; Elias, M. Structural and enzymatic characterization of the lactonase SisLac from *Sulfolobus islandicus*. *PLoS One* **2012**, *7*, e47028.
150. Mei, G.Y.; Yan, X.X.; Turak, A.; Luo, Z.Q.; Zhang, L.Q. AidH, an alpha/beta-hydrolase fold family member from an *Ochrobactrum* sp. strain, is a novel *N*-acylhomoserine lactonase. *Appl. Environ. Microbiol.* **2010**, *76*, 4933–4942.
151. Wang, W.Z.; Morohoshi, T.; Ikenoya, M.; Someya, N.; Ikeda, T. AiiM, a novel class of *N*-acylhomoserine lactonase from the leaf-associated bacterium *Microbacterium testaceum*. *Appl. Environ. Microbiol.* **2010**, *76*, 2524–2530.
152. Lin, Y.H.; Xu, J.L.; Hu, J.; Wang, L.H.; Ong, S.L.; Leadbetter, J.R.; Zhang, L.H. Acyl-homoserine lactone acylase from *Ralstonia* strain XJ12B represents a novel and potent class of quorum-quenching enzymes. *Mol. Microbiol.* **2003**, *47*, 849–860.
153. Leadbetter, J.R.; Greenberg, E.P. Metabolism of acyl-homoserine lactone quorum-sensing signals by *Variovorax paradoxus*. *J. Bacteriol.* **2000**, *182*, 6921–6926.
154. Park, S.Y.; Kang, H.O.; Jang, H.S.; Lee, J.K.; Koo, B.T.; Yum, D.Y. Identification of extracellular *N*-acylhomoserine lactone acylase from a *Streptomyces* sp. and its application to quorum quenching. *Appl. Environ. Microbiol.* **2005**, *71*, 2632–2641.
155. Han, J.I.; Choi, H.K.; Lee, S.W.; Orwin, P.M.; Kim, J.; Laroe, S.L.; Kim, T.G.; O'Neil, J.; Leadbetter, J.R.; Lee, S.Y.; *et al.* Complete genome sequence of the metabolically versatile plant growth-promoting endophyte *Variovorax paradoxus* S110. *J. Bacteriol.* **2011**, *193*, 1183–1190.
156. Sio, C.F.; Otten, L.G.; Cool, R.H.; Diggle, S.P.; Braun, P.G.; Bos, R.; Daykin, M.; Cámara, M.; Williams, P.; Quax, W.J. Quorum quenching by an *N*-acyl-homoserine lactone acylase from *Pseudomonas aeruginosa* PAO1. *Infect. Immun.* **2006**, *74*, 1673–1682.
157. Huang, J.J.; Petersen, A.; Whiteley, M.; Leadbetter, J.R. Identification of QuiP, the product of gene PA1032, as the second acyl-homoserine lactone acylase of *Pseudomonas aeruginosa* PAO1. *Appl. Environ. Microbiol.* **2006**, *72*, 1190–1197.
158. Wahjudi, M.; Papaioannou, E.; Hendrawati, O.; van Assen, A.H.G.; van Merkerk, R.; Cool, R.H.; Poelarends, G.J.; Quax, W.J. PA0305 of *Pseudomonas aeruginosa* is a quorum quenching acylhomoserine lactone acylase belonging to the Ntn hydrolase superfamily. *Microbiology* **2011**, *157*, 2042–2055.
159. Nadal Jimenez, P.; Koch, G.; Papaioannou, E.; Wahjudi, M.; Krzeslak, J.; Coenye, T.; Cool, R.H.; Quax, W.J. Role of PvdQ in *Pseudomonas aeruginosa* virulence under iron-limiting conditions. *Microbiology* **2010**, *156*, 49–59.
160. Clevenger, K.D.; Wu, R.; Er, J.A.; Liu, D.; Fast, W. Rational design of a transition state analogue with picomolar affinity for *Pseudomonas aeruginosa* PvdQ, a siderophore biosynthetic enzyme. *ACS Chem. Biol.* **2013**, *8*, 2192–2200.

161. Czajkowski, R.; Krzyżanowska, D.; Karczewska, J.; Atkinson, S.; Przysowa, J.; Lojkowska, E.; Williams, P.; Jafra, S. Inactivation of AHLs by *Ochrobactrum* sp. A44 depends on the activity of a novel class of AHL acylase. *Environ. Microbiol. Rep.* **2011**, *3*, 59–68.
162. Tannieres, M.; Beury-Cirou, A.; Vigouroux, A.; Mondy, S.; Pellissier, F.; Dessaux, Y.; Faure, D. A metagenomic study highlights phylogenetic proximity of quorum-quenching and xenobiotic-degrading amidases of the AS-family. *PLoS One* **2013**, *8*, e65473.
163. Uroz, S.; Chhabra, S.R.; Camara, M.; Williams, P.; Oger, P.; Dessaux, Y. *N*-Acylhomoserine lactone quorum-sensing molecules are modified and degraded by *Rhodococcus erythropolis* W2 by both amidolytic and novel oxidoreductase activities. *Microbiology* **2005**, *151*, 3313–3322.
164. Chowdhary, P.K.; Keshavan, N.; Nguyen, H.Q.; Peterson, J.A.; Gonzalez, J.E.; Haines, D.C. *Bacillus megaterium* CYP102A1 oxidation of acyl homoserine lactones and acyl homoserines. *Biochemistry* **2007**, *46*, 14429–14437.
165. Bijtenhoorn, P.; Mayerhofer, H.; Muller-Dieckmann, J.; Utpatel, C.; Schipper, C.; Hornung, C.; Szesny, M.; Grond, S.; Thurmer, A.; Brzuszkiewicz, E.; *et al.* A novel metagenomic short-chain dehydrogenase/reductase attenuates *Pseudomonas aeruginosa* biofilm formation and virulence on *Caenorhabditis elegans*. *PLoS One* **2011**, *6*, e26278.
166. Chan, K.G.; Atkinson, S.; Mathee, K.; Sam, C.K.; Chhabra, S.R.; Camara, M.; Koh, C.L.; Williams, P. Characterization of *N*-acylhomoserine lactone-degrading bacteria associated with the *Zingiber officinale* (ginger) rhizosphere: Co-existence of quorum quenching and quorum sensing in *Acinetobacter* and *Burkholderia*. *BMC Microbiol.* **2011**, *11*, 51; doi:10.1186/1471-2180-11-51.
167. Hong, K.-W.; Koh, C.-L.; Sam, C.-K.; Yin, W.-F.; Chan, K.-G. Complete genome sequence of *Burkholderia* sp. strain GG4, a Betaproteobacterium that reduces 3-oxo-*N*-acylhomoserine lactones and produces different *N*-acylhomoserine lactones. *J. Bacteriol.* **2012**, *194*, 6317; doi:10.1128/JB.01578-12.
168. Sandy, M.; Carter-Franklin, J.N.; Martin, J.D.; Butler, A. Vanadium bromoperoxidase from *Delisea pulchra*: Enzyme-catalyzed formation of bromofuranone and attendant disruption of quorum sensing. *Chem. Commun.* **2011**, *47*, 12086–12088.
169. Borchardt, S.A.; Allain, E.J.; Michels, J.J.; Stearns, G.W.; Kelly, R.F.; McCoy, W.F. Reaction of acylated homoserine lactone bacterial signaling molecules with oxidized halogen antimicrobials. *Appl. Environ. Microbiol.* **2001**, *67*, 3174–3179.
170. Syrpas, M.; Ruysbergh, E.; Blommaert, L.; Vanelslander, B.; Sabbe, K.; Vyverman, W.; de Kimpe, N.; Mangelinckx, S. Haloperoxidase mediated quorum quenching by *Nitzschia cf pellucida*: Study of the metabolization of *N*-acyl homoserine lactones by a benthic diatom. *Mar. Drugs* **2014**, *12*, 352–367.
171. Hibbing, M.E.; Fuqua, C.; Parsek, M.R.; Peterson, S.B. Bacterial competition: Surviving and thriving in the microbial jungle. *Nat. Rev. Microbiol.* **2010**, *8*, 15–25.
172. D'Angelo-Picard, C.; Faure, D.; Penot, I.; Dessaux, Y. Diversity of *N*-acyl homoserine lactone-producing and -degrading bacteria in soil and tobacco rhizosphere. *Environ. Microbiol.* **2005**, *7*, 1796–1808.

173. Chemistry, A.; July, R.; Sepetember, A.; Shewanella, I. *N*-acyl homoserine lactone-producing or -degrading bacteria Isolated from the intestinal microbial flora of Ayu fish (*Plecoglossus altivelis*). *ASM News* **2005**, *20*, 264–268.
174. Biswas, L.; Biswas, R.; Schlag, M.; Bertram, R.; Götz, F. Small-colony variant selection as a survival strategy for *Staphylococcus aureus* in the presence of *Pseudomonas aeruginosa*. *Appl. Environ. Microbiol.* **2009**, *75*, 6910–6912.
175. Kerr, J.; Taylor, G.; Rutman, A.; Høiby, N.; Cole, P.; Wilson, R. *Pseudomonas aeruginosa* pyocyanin and 1-hydroxyphenazine inhibit fungal growth. *J. Clin. Pathol.* **1999**, *52*, 385–387.
176. McClean, K.H.; Winson, M.K.; Fish, L.; Taylor, A.; Chhabra, S.R.; Camara, M.; Daykin, M.; Lamb, J.H.; Swift, S.; Bycroft, B.W.; *et al.* Quorum sensing and *Chromobacterium violaceum*: Exploitation of violacein production and inhibition for the detection of *N*-acylhomoserine lactones. *Microbiology* **1997**, *143*, 3703–3711.
177. Morohoshi, T.; Kato, M.; Fukamachi, K.; Kato, N.; Ikeda, T. *N*-acylhomoserine lactone regulates violacein production in *Chromobacterium violaceum* type strain ATCC 12472. *FEMS Microbiol. Lett.* **2008**, *279*, 124–130.
178. Lyon, G.J.; Wright, J.S.; Muir, T.W.; Novick, R.P. Key determinants of receptor activation in the agr autoinducing peptides of *Staphylococcus aureus*. *Biochemistry* **2002**, *41*, 10095–10104.
179. Dufour, P.; Jarraud, S.; Vandenesch, F.; Greenland, T.; Novick, R.P.; Bes, M.; Etienne, J.; Lina, G. High genetic variability of the agr locus in *Staphylococcus* species. *J. Bacteriol.* **2002**, *184*, 1180–1186.
180. Jarraud, S.; Lyon, G.J.; Figueiredo, A.M.; Lina, G.; Vandenesch, F.; Etienne, J.; Muir, T.W.; Novick, R.P. Exfoliatin-producing strains define a fourth agr specificity group in *Staphylococcus aureus*. *J. Bacteriol.* **2000**, *182*, 6517–6522.
181. Ji, G.; Beavis, R.; Novick, R.P. Bacterial interference caused by autoinducing peptide variants. *Science* **1997**, *276*, 2027–2030.
182. Hong, K.W.; Koh, C.L.; Sam, C.K.; Yin, W.F.; Chan, K.G. Quorum quenching revisited-from signal decays to signalling confusion. *Sensors (Basel)* **2012**, *12*, 4661–4696.
183. Czajkowski, R.; Jafra, S. Quenching of acyl-homoserine lactone-dependent quorum sensing by enzymatic disruption of signal molecules. *Acta Biochim. Pol.* **2009**, *56*, 1–16.
184. Romero, M.; Martin-Cuadrado, A.B.; Otero, A. Determination of whether quorum quenching is a common activity in marine bacteria by analysis of cultivable bacteria and metagenomic sequences. *Appl. Environ. Microbiol.* **2012**, *78*, 6345–6348.
185. Khan, S.R.; Farrand, S.K. The BlcC (AttM) lactonase of *Agrobacterium tumefaciens* does not quench the quorum-sensing system that regulates Ti plasmid conjugative transfer. *J. Bacteriol.* **2009**, *191*, 1320–1329.
186. Flagan, S.; Ching, W.K.; Leadbetter, J.R. *Arthrobacter* strain VAI-A utilizes acyl-homoserine lactone inactivation products and stimulates quorum signal biodegradation by *Variovorax paradoxus*. *Appl. Environ. Microbiol.* **2003**, *69*, 909–916.
187. Park, S.J.; Park, S.Y.; Ryu, C.M.; Park, S.H.; Lee, J.K. The role of AiiA, a quorum-quenching enzyme from *Bacillus thuringiensis*, on the rhizosphere competence. *J. Microbiol. Biotechnol.* **2008**, *18*, 1518–1521.

188. Romero, M.; Martin-Cuadrado, A.B.; Roca-Rivada, A.; Cabello, A.M.; Otero, A. Quorum quenching in cultivable bacteria from dense marine coastal microbial communities. *FEMS Microbiol. Ecol.* **2011**, *75*, 205–217.
189. Torres, M.; Romero, M.; Prado, S.; Dubert, J.; Tahrioui, A.; Otero, A.; Llamas, I. *N*-acylhomoserine lactone-degrading bacteria isolated from hatchery bivalve larval cultures. *Microbiol. Res.* **2013**, *168*, 547–554.
190. Tait, K.; Williamson, H.; Atkinson, S.; Williams, P.; Camara, M.; Joint, I. Turnover of quorum sensing signal molecules modulates cross-kingdom signalling. *Environ. Microbiol.* **2009**, *11*, 1792–1802.
191. Defoirdt, T.; Thanh, L.D.; Van Delsen, B.; De Schryver, P.; Sorgeloos, P.; Boon, N.; Bossier, P. *N*-acylhomoserine lactone-degrading *Bacillu*s strains isolated from aquaculture animals. *Aquaculture* **2011**, *311*, 258–260.
192. Romero, M.; Avendaño-Herrera, R.; Magariños, B.; Cámara, M.; Otero, A. Acylhomoserine lactone production and degradation by the fish pathogen *Tenacibaculum maritimum*, a member of the *Cytophaga–Flavobacterium–Bacteroides* (CFB) group. *FEMS Microbiol. Lett.* **2010**, *304*, 131–139.
193. Huang, W.; Lin, Y.; Yi, S.; Liu, P.; Shen, J.; Shao, Z.; Liu, Z. QsdH, a novel AHL lactonase in the RND-type inner membrane of marine *Pseudoalteromonas byunsanensis* strain 1A01261. *PLoS One* **2012**, *7*, e46587.
194. Swem, L.R.; Swem, D.L.; O'Loughlin, C.T.; Gatmaitan, R.; Zhao, B.X.; Ulrich, S.M.; Bassler, B.L. A quorum-sensing antagonist targets both membrane-bound and cytoplasmic receptors and controls bacterial pathogenicity. *Mol. Cell* **2009**, *35*, 143–153.
195. O'Loughlin, C.T.; Miller, L.C.; Siryaporn, A.; Drescher, K.; Semmelhack, M.F.; Bassler, B.L. A quorum-sensing inhibitor blocks *Pseudomonas aeruginosa* virulence and biofilm formation. *Proc. Natl. Acad. Sci. USA* **2013**, *110*, 17981–17986.
196. Whitehead, N.A.; Welch, M.; Salmond, G.P. Silencing the majority. *Nat. Biotechnol.* **2001**, *19*, 735–736.
197. Defoirdt, T.; Boon, N.; Bossier, P. Can bacteria evolve resistance to quorum sensing disruption? *PLoS Pathog.* **2010**, *6*, e1000989.
198. Maeda, T.; Garcia-Contreras, R.; Pu, M.; Sheng, L.; Garcia, L.R.; Tomas, M.; Wood, T.K. Quorum quenching quandary: Resistance to antivirulence compounds. *ISME J.* **2012**, *6*, 493–501.
199. Garcia-Contreras, R.; Maeda, T.; Wood, T.K. Resistance to quorum-quenching compounds. *Appl. Environ. Microbiol.* **2013**, *79*, 6840–6846.
200. Fernandes, R.; Roy, V.; Wu, H.-C.; Bentley, W.E. Engineered biological nanofactories trigger quorum sensing response in targeted bacteria. *Nat. Nano* **2010**, *5*, 213–217.
201. Komnatnyy, V.V.; Chiang, W.C.; Tolker-Nielsen, T.; Givskov, M.; Nielsen, T.E. Bacteria-triggered release of antimicrobial agents. *Angew. Chem. Int. Ed. Engl.* **2014**, *53*, 439–441.
202. Park, K.; Kwon, I.C.; Park, K. Oral protein delivery: Current status and future prospect. *React. Funct. Polym.* **2011**, *71*, 280–287.

The Protective Effect of Fucoidan in Rats with Streptozotocin-Induced Diabetic Nephropathy

Jing Wang, Huaide Liu, Ning Li, Quanbin Zhang and Hong Zhang

Abstract: Diabetic nephropathy (DN) has long been recognized as the leading cause of end-stage renal disease, but the efficacy of available strategies for the prevention of DN remains poor. The aim of this study was to investigate the possible beneficial effects of fucoidan (FPS) in streptozotocin (STZ)-induced diabetes in rats. Wistar rats were made diabetic by injection of STZ after removal of the right kidney. FPS was administered to these diabetic rats for 10 weeks. Body weight, physical activity, renal function, and renal morphometry were measured after 10 weeks of treatment. In the FPS-treated group, the levels of blood glucose, BUN, Ccr and Ucr decreased significantly, and microalbumin, serum insulin and the β2-MG content increased significantly. Moreover, the FPS-treated group showed improvements in renal morphometry. In summary, FPS can ameliorate the metabolic abnormalities of diabetic rats and delay the progression of diabetic renal complications.

Reprinted from *Mar. Drugs*. Cite as: Wang, J.; Liu, H.; Li, N.; Zhang, Q.; Zhang, H. The Protective Effect of Fucoidan in Rats with Streptozotocin-Induced Diabetic Nephropathy. *Mar. Drugs* **2014**, *12*, 3292–3306.

1. Introduction

Diabetic nephropathy (DN) is a major complication of diabetes and a leading cause of end-stage renal failure throughout much of the world [1]. DN is characterized by changes in both glomerular and tubular structure and function. The pathogenesis of DN includes genetic, hemodynamic and metabolic factors, and oxidative stress as well as renal hypertrophy, but the exact mechanism is not clear [2]. Most studies have focused on alterations in the glomerulus, including abnormalities in glomerular permeability and capillary pressure, glomerular hyperplasia or hypertrophy and increases in mesangial volume [3,4]. To prevent and treat diabetic nephropathy, current methods using agents such as angiotensin-converting enzyme inhibitors, angiotensin-receptor blockers and antihypertensive drugs have been tried in clinical practice [5]. Unfortunately, currently available medical interventions are unable to effectively reverse or even delay the progression of DN [6].

Polysaccharides can reduce blood glucose levels in normal rats, streptozotocin (STZ)-induced diabetic rats and alloxan-induced diabetic rats [7]. He *et al.* found that *Ganoderma lucidum* polysaccharide could ameliorate the metabolic abnormalities of diabetic mice and prevent or delay the progression of diabetic renal complications [8]. Zhang *et al.* found that *Astragalus* polysaccharide improved early diabetic nephropathy and affected the mRNA expression of NF-κB and IκB in the renal cortex of STZ-induced diabetic rats [9].

Sulfated polysaccharides are considered to be an attractive class of compounds as drug candidates [10,11]. Fucoidans are highly sulfated cell-wall polysaccharides found mainly in various species of brown seaweeds such as *Saccharina japonica*, *Undaria pinnatifida*, and *Sargassum* C.

Ag., and variant forms of fucoidans have also been found in animal species, including the sea cucumber [12]. Fucoidan has been reported to possess diverse biological activities of potential medicinal value, such as anticoagulant, antitumor, anti-inflammatory, antiviral and antioxidant activities [13].

The brown seaweed, *Saccharina japonica*, is a common seafood in China and many other countries, and has been documented as a drug in traditional Chinese medicine for over a thousand years. In the past thousand years and more, Chinese people have been using it as a traditional medicine to cure edema disease, a symptom of kidney disease [14]. FPS extracted from *Saccharina japonica* is an acidic sulfated polysaccharide, mainly made of fucose, galactose and sulfate, with smaller amounts of mannoses, glucuronic acid, glucose, rhamnose, arabinose and xylose. Recent studies have corroborated a renoprotective role for fucoidan in animal models of kidney injury. Our previous studies have found that FPS and its derivatives extracted from *Saccharina japonica* are effective in ameliorating abnormal biochemical changes in experimental chronic renal failure (CRF) [15]. The mechanism of action of FPS derivatives in CRF rats is related to the antioxidant activities, the substituted group and the molecular weight of FPS [16]. Zhang *et al.* also found that FPS could inhibit the development of proteinuria associated with Heymann nephritis [17,18]. Furthermore, we found that FPS exhibited a considerable hypoglycemic effect, possibly by stimulating the pancreatic release of insulin and/or by reducing insulin metabolism [19]. Diabetic retinopathy (DR) is one of the severe complications of diabetes. Our study found that low molecular weight fucoidan could alleviate diabetic retinal neovascularization and damage, likely through lowering HIF-1α and VEGF expressions [20]. Diabetic patients are at high risk of endothelial and vascular dysfunction, we also demonstrated that fucoidan could protect vasoendothelial function and reduce basal blood pressure in type 2 diabetes rats via, at least in part, preservation of endothelial NO synthase (eNOS) function [21].

Oxidative stress has been considered to be a common pathogenic factor in DM and its complications including nephropathy. In DN, free radicals have been shown to decrease *de novo* synthesis of heparin sulfate proteoglycans, which correlates with proteinuria seen in this condition [22]. Ha *et al.* demonstrated increased 8-hydroxydeoxyguanosine (8-OHdG) in STZ-induced diabetic kidneys and suggest that formation of 8-OHdG and, therefore, oxidative damage are closely related in the process of diabetic nephropathy [23]. Brezniceanu *et al.* demonstrated that renal catalase overexpression in db/db mice attenuated reactive oxygen species (ROS) generation, angiotensinogen, proapoptotic gene expression and apoptosis in the kidneys of diabetic mice *in vivo*. This study points to an important role of ROS in the pathophysiology of diabetic nephropathy [24]. Combination of strategies to prevent overproduction of ROS and to increase the removal of performed ROS may prove to be effective in preventing the development and progression of diabetic nephropathy [25]. Zhang *et al.* found that *Astragalus membranaceus* (root) as a free radical scavenger implies its effect against oxidative stress in the early stages of DN [6]. Bhatia *et al.* evaluate the oxidative stress status in Asian Indian patients suffering from type 2 diabetes mellitus (DM) with nephropathy. Results of their study indicate that oxidative stress is increased and antioxidant defenses are compromised in type 2 DM. These derangements are of a higher magnitude in patients of type 2 DM with nephropathy [26].

Our previous study found that FPS had antioxidant activity, renoprotective and hypoglycemic activity *in vivo* and *in vitro* [15,19,27]. Thus there is a need to study whether FPS has renal protective effects in STZ-induced diabetic rats.

2. Results and Discussion

2.1. Results

2.1.1. Chemical Analysis

The chemical composition of the FPS was analyzed in this study. The results showed that the principal chemical components of the FPS were fucose and sulfate along with uronic acid and a small amount of protein. The fucose and sulfate content was 29.12% and 33.01%, respectively. The constituents of the neutral monosaccharide of the FPS were analyzed with high performance liquid chromatography (HPLC). The results showed that fucose was the main form of sugar, representing 62.08% of the total neutral sugar in the FPS. In addition to fucose and galactose, mannose, glucose, xylose, and arabinose were also observed in the FPS. The molecular weight of FPS was 87,000 Da. These results show that the chemical properties of FPS may substantially influence its activity, as demonstrated in this study.

2.1.2. Effects of FPS on Physical Activity

All the rats in the normal control group (NC) group survived and exhibited normal physical appearance and behavior during the experiments, showing smooth fur and weight gain (Figure 1). However, two rats died in the other groups. The surviving rats in the DN group exhibited unresponsive behavior and rough fur and were significantly thinner during the experiments. Their eyes showed a 7/20 ratio of cataracts. The surviving rats in the high fucoidan (HF), medium fucoidan (MF) and PC groups exhibited significantly better behavior with little rough fur and a ratio of cataracts of 3/20, 4/20 and 4/20, respectively. However, the surviving rats in the low fucoidan (LF) group exhibited no significant changes compared with the DN group. The ratio of cataracts in the LF group was 3/20. The weight of the rats in all groups except the NC group showed no significant changes compared with the DN group.

2.1.3. Effects of FPS on Blood Glucose

The effects of FPS on blood glucose in the rats with STZ-induced DN are shown in Figure 2. The blood glucose level increased significantly in the DN and other treatment groups relative to the NC group at week 0 and at the 2nd, 4th, 6th, 8th and 10th weeks (Figure 2). The HF group showed a significantly decreased blood glucose level after 8 weeks compared with the DN group. The blood glucose level decreased significantly in the PC group at 4, 6, 8 and 10 weeks. The MF and LF treatment group showed no significant effect on blood glucose.

Figure 1. Effects of fucoidan (FPS) on the weight of streptozotocin (STZ)-induced diabetic nephropathy rat. NC: Normal control group; DN: Diabetic nephropathy group; LF: FPS, 75 mg/kg body wt; MF: FPS, 150 mg/kg body wt; HF: FPS, 300 mg/kg body wt; * $p < 0.05$, ** $p < 0.01$, compared with the DN group. Statistical analysis was performed using ANOVA. Data are presented as mean ± S.D.

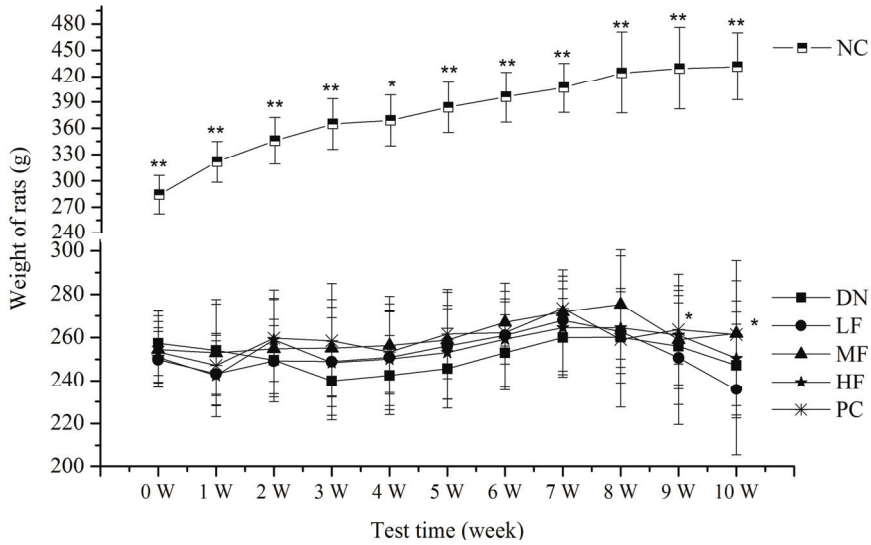

2.1.4. Effects of FPS on Renal Function

Figure 3 shows the effects of FPS on urine volume and urine protein in the rats with STZ-induced DN. Compared with the NC group, the 24 h urine volume and urine protein increased significantly in the other groups at 2, 4, 6, 8 and 10 weeks. The HF group showed a significant decrease in 24 h urine volume and urine protein at 6, 8 and 10 weeks compared with the DN group.

The effects of FPS on the ratio of kidney weight to body weight, renal function, serum insulin, glycosylated hemoglobin, microalbumin and β2-MG in the rats with STZ-induced DN are shown in Table 1. Compared with the NC group, the rats in the DN group and treatment group showed renal hypertrophy and a significant increase in relative kidney weight. However, the HF and PC groups showed a significant decrease in the ratio of kidney weight to body weight.

BUN increased significantly in the DN group compared with the NC group and decreased significantly in the MF and HF groups. However, the treatment group had no significant effect on Scr. The HF and PC groups showed higher effects on urinary creatinine excretion (Ucr) and creatinine clearance (Ccr). Serum insulin, glycosylated hemoglobin and β2-MG decreased significantly in the DN group compared with the NC group. The HF group showed an increased insulin and microalbumin level compared with the DN group. All treatment groups showed an increased level of β2-MG.

Figure 2. Effects of FPS on the weight of STZ-induced diabetic nephropathy rat. NC: Normal control group; DN: Diabetic nephropathy group; LF: FPS, 75 mg/kg body wt; MF: FPS, 150 mg/kg body wt; HF: FPS, 300 mg/kg body wt; * $p < 0.05$, ** $p < 0.01$, compared with the DN group. Statistical analysis was performed using ANOVA. Data are presented as mean ± S.D.

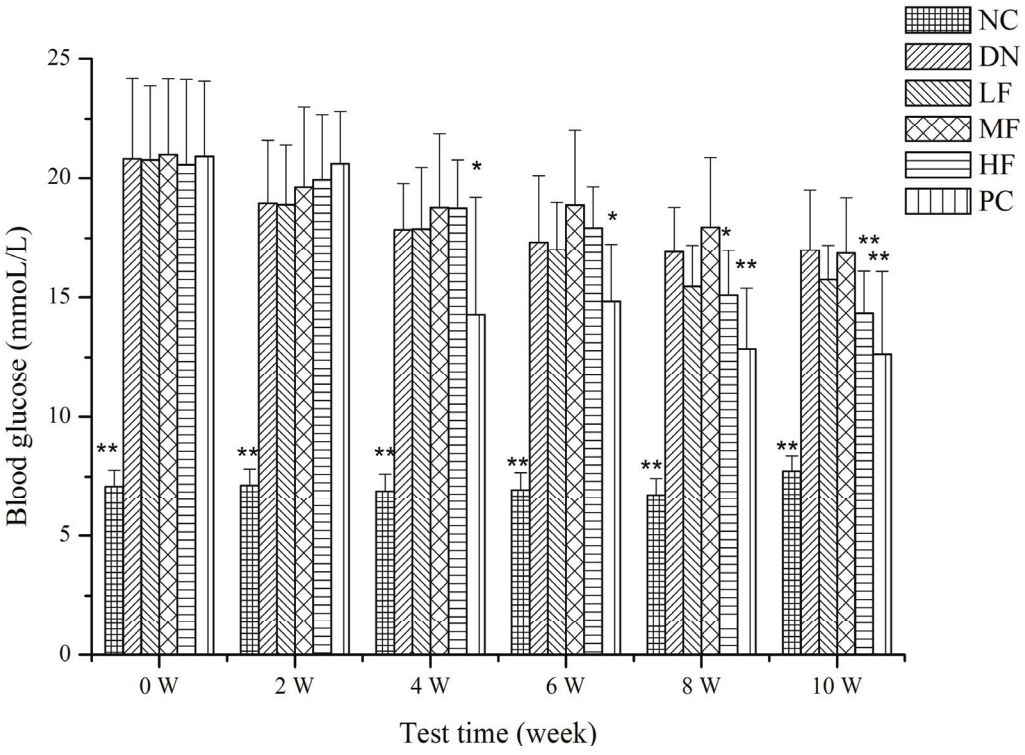

2.1.5. Effects of FPS on Renal Morphological Changes

The NC group showed no changes in kidney tissue morphology, whereas the DN group showed significant changes in kidney tissue morphology (Figures 4 and 5). The glomerular volume and the number of cells increased, reflecting the dilation of glomerular capillaries and the tubular epithelial cell degeneration in the rats of the DN group. The morphological changes occurring in the kidney varied among treatment groups. Compared with the DN group, the MF and HF groups showed significantly decreased glomerular capsule perimeters, cross-sectional areas and cell numbers.

Figure 3. Effects of FPS on the weight of STZ-induced diabetic nephropathy rat. NC: Normal control group; DN: Diabetic nephropathy group; LF: FPS, 75 mg/kg body wt; MF: FPS, 150 mg/kg body wt; HF: FPS, 300 mg/kg body wt; * $p < 0.05$, ** $p < 0.01$, compared with the DN group. Statistical analysis was performed using ANOVA. Data are presented as mean ± S.D.

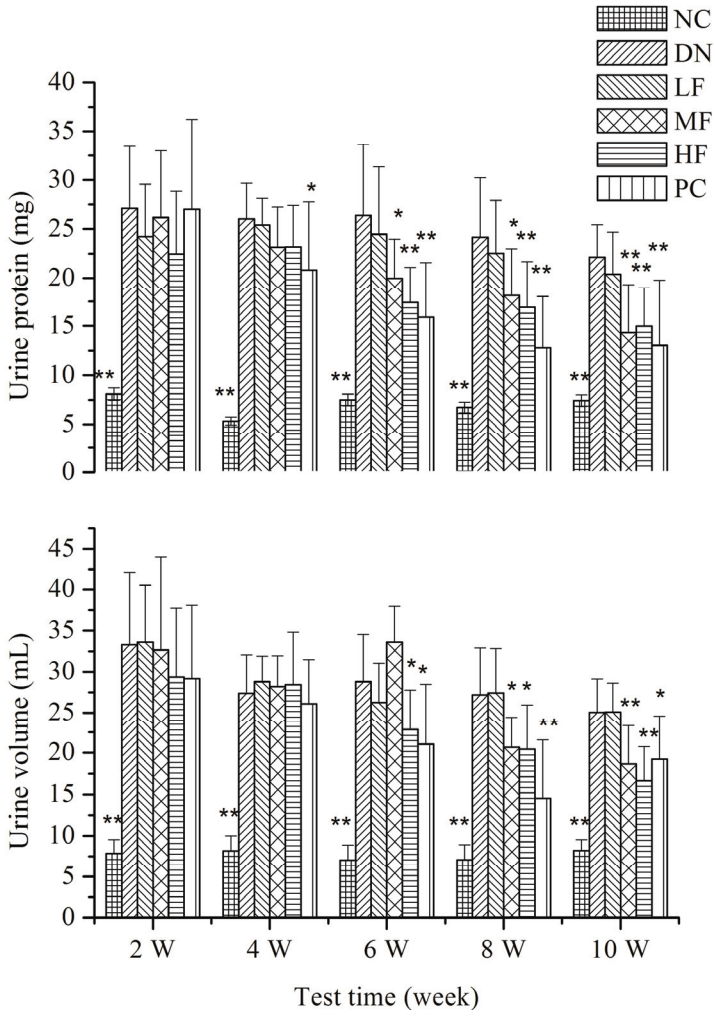

Table 1. Effect of FPS on the ratio of the weight of the kidney to body weight, renal function, serum insulin, glycosylated hemoglobin, microalbumin and β2-microglobulin in the STZ-induced diabetic nephropathy rats.

Group	Relative kidney weight (%)	BUN (μg/mL)	Scr (μmol/L)	Ucr (μmol/L)	Ccr (mL/min)	Serum insulin (μIU/mL)	Glycosylated hemoglobin (%)	Microalbumin (μg/mL)	β2-MG (μg/mL)
NC	0.31 ± 0.05 **	6.44 ± 0.65 **	42.69 ± 3.54	11,968.4 ± 978.7 **	1.61 ± 0.32 **	10.83 ± 2.92 **	21.16 ± 6.41 **	1.42 ± 0.15 *	0.12 ± 0.04 **
DN	0.82 ± 0.12	25.40 ± 7.90	40.18 ± 4.81	2359.5 ± 490.4	1.00 ± 0.15	5.74 ± 1.43	18.28 ± 1.66	1.25 ± 0.15	0.07 ± 0.05
LF	0.78 ± 0.11	21.55 ± 6.29	39.87 ± 3.33	2703.4 ± 312.4	1.19 ± 0.25	5.87 ± 1.33	19.52 ± 2.08	1.33 ± 0.18	0.11 ± 0.03 *
MF	0.73 ± 0.13	18.48 ± 6.99 *	42.27 ± 5.42	4476.5 ± 1238.1 **	1.35 ± 0.41	6.67 ± 1.38 *	17.29 ± 2.59	1.47 ± 0.29	0.08 ± 0.03
HF	0.70 ± 0.06 *	18.42 ± 5.13 *	44.11 ± 5.05	5289.1 ± 1607.1 **	1.40 ± 0.42 *	6.18 ± 1.34 *	18.78 ± 2.89	1.42 ± 0.18 *	0.11 ± 0.04 *
PC	0.70 ± 0.10 *	18.56 ± 5.49 *	41.40 ± 4.90	4671.0 ± 1274.4 **	1.46 ± 0.43 *	6.61 ± 1.53 *	17.32 ± 4.53	1.45 ± 0.18 *	0.09 ± 0.04

NC: Normal control group; DN: Diabetic nephropathy group; LF: FPS, 75 mg/kg body wt; MF: FPS, 150 mg/kg body wt; HF: FPS, 300 mg/kg body wt; BUN: blood urea nitrogen; Scr: serum creatinine; Ucr: urine creatinine; Ccr: creatinine clearance; β2-MG: β2-microglobulin; * $p < 0.05$, ** $p < 0.01$, compared with the DN group. Statistical analysis was performed using ANOVA. Data are presented as mean ± S.D.

Figure 4. Effects of FPS on the weight of STZ-induced diabetic nephropathy rat. NC: Normal control group; DN: Diabetic nephropathy group; LF: FPS, 75 mg/kg body wt; MF: FPS, 150 mg/kg body wt; HF: FPS, 300 mg/kg body wt; * $p < 0.05$, ** $p < 0.01$, compared with the DN group. Statistical analysis was performed using ANOVA. Data are presented as mean ± S.D.

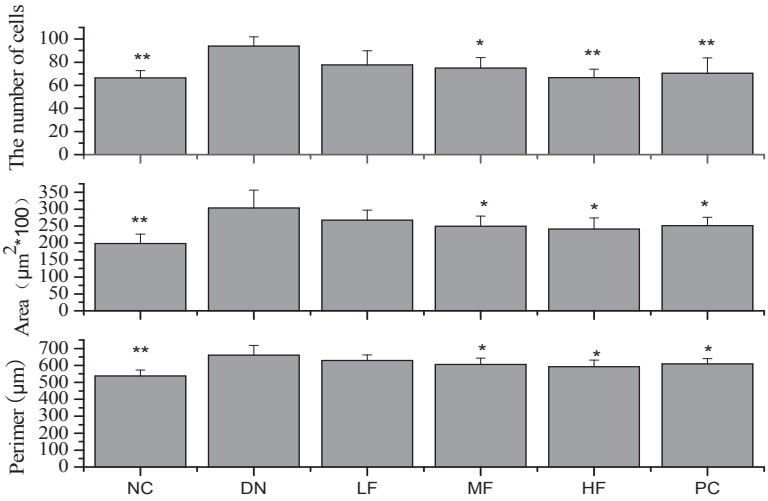

Figure 5. Effects of FPS on the weight of STZ-induced diabetic nephropathy rat. NC: Normal control group; DN: Diabetic nephropathy group; LF: FPS, 75 mg/kg body wt; MF: FPS, 150 mg/kg body wt; HF: FPS, 300 mg/kg body wt; * $p < 0.05$, ** $p < 0.01$, compared with the DN group. Statistical analysis was performed using ANOVA. Data are presented as mean ± S.D.

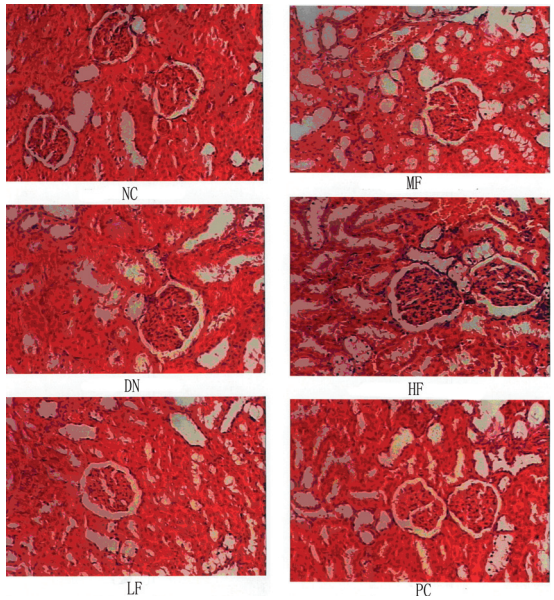

2.2. Discussion

The kidneys are vital for removing toxic waste products from the body and for maintaining fluids, minerals, and electrolytes at physiological levels. Elevated blood glucose can damage the cells and microblood vessels of the kidney [28]. Our previous study found that FPS affected chronic renal failure and diabetic complications [15,22]. However, very little is known about the preventive or therapeutic effect of FPS against diabetic complications, including nephropathy. It is important to examine the effectiveness of herbal drugs on these diseases from the standpoint of the development of new bioactive resources. STZ can selectively damage insulin-producing pancreatic endocrine cells and induce experimental hyperglycemia. These effects are stable and long lasting. The extraction of one kidney can increase the burden on the contralateral kidney and accelerate the progression of the disease, accelerating the development of DN.

Both decreases and gains in body weight were observed in conjunction with the progression of diabetes. The inhibition of these decreases in body weight has been viewed as evidence of the successful treatment of diabetes and diabetic complications [29]. In this study, the FPS dose-dependently inhibited the loss and/or gain in body weight relative to the DN group.

High blood glucose is known to be an important cause of DN. The control of glucose can prevent the occurrence and development of DN. Specifically, the control of blood glucose is one of the important measures used for the prevention and treatment of DN [30]. The results of the current study showed that the blood glucose in the rats of the DN group increased significantly and that this increase persisted for 10 weeks. The HF group showed a marked hypoglycemic effect after the administration of FPS for 8 and 10 weeks. We hypothesize that HF can prevent and treat DN by reducing the blood glucose level.

During the progression of diabetes, an increase in kidney weight, the elevation of the BUN and Scr levels due to interstitial atrophy and vasodilated atrophic changes in the glomeruli and tubules, including epithelial necrosis and ballooning with focal fibrosis, known as diabetic nephropathies, are generally observed [31]. In addition, these indices have been used to observe the occurrence and progression of DN [32]. An improvement in these abnormal changes is considered direct evidence of an improvement in DN [33]. In this study, the 24 h urine protein and urine volume increased significantly two weeks after the initiation of the disease model. Ten weeks after the initiation of the disease model, renal hypertrophy was observed, renal function was abnormal and BUN increased significantly. These observations showed that the model of DN had been successfully established. The DN rats showed damage to the kidney and renal insufficiency. As a result of these effects, BUN increased and Ucr and Ccr decreased significantly. Accordingly, many toxic substances accumulated in the body and aggravated the DN. The experimental results reported in this study showed that FPS could significantly decrease the BUN content and increase Ucr and Ccr levels, producing significant improvements in renal function. This outcome means that FPS effectively controls DN.

Renal hypertrophy is an important pathological feature of early DN, and the control of kidney hypertrophy is an important sign of the effectiveness of drugs used to treat DN. The experimental results reported in this study showed that FPS could significantly decrease the kidney coefficient of

DN rats and inhibit renal hypertrophy. These results also showed that FPS could diminish glomerular damage in diabetic rats.

Recent studies strongly support the concept that the primary cause of DN involves a metabolic disorder. In particular, the importance of hyperglycemia as a risk factor for DN is supported by several observations and pieces of experimental evidence [34]. In this study, all treatment groups showed an elevated β2-MG level and certain treatment groups showed increased levels of serum insulin and glycosylated hemoglobin. These results suggest that the mechanism of renal protection by FPS is, most likely, the modulation of metabolic abnormalities in the hyperglycemic state. Additionally, FPS had obvious hypoglycemic effects, as previously demonstrated. In this study, hypoglycemic effects were also identified as a possible reason for the improvement of nephropathy. Therefore, further studies are planned to determine the mechanisms of action of FPS on diabetes and DN.

Increasing evidence in both experimental and clinical studies suggests that oxidative stress plays a major role in the pathogenesis of both types of diabetes mellitus. Oxidative stress is increased in diabetes, and the overproduction of ROS in diabetes is a direct consequence of hyperglycemia. Abnormally high levels of free radicals and the simultaneous decline of antioxidant defense mechanisms can lead to damage of cellular organelles and enzymes, increased lipid peroxidation, and development of insulin resistance [19]. Many researchers suggest that antioxidants may be helpful in the treatment of DN [25]. *Lycium barbarum* polysaccharide (LBP) has been shown to have hypoglycemic and diabetic nephropathy properties in a streptozotocin-induced diabetic rat model. Diabetic rats treated with LBP-4 (10 mg/kg) for 8 weeks showed increased activity of antioxidant enzymes and increased scavenging of oxygen radicals, while the activity of protein kinase C (PKC) in the renal cortex was maintained at a physiological level [34]. *Ganoderma lucidum* polysaccharides (GL-PS) can positively influence the metabolic abnormalities of diabetic mice and prevent or delay the progression of diabetic renal complications, and the mechanism is related to its antioxidant activity [35]. Our previous study found that fucoidan and its fractions had strong antioxidant activity *in vitro* and *in vivo*, the mechanism of fucoidan on chronic kidney disease (CKD) rats was related to their antioxidant activities, the samples of which could enhance the activity of antioxidant enzymes and reduce the LPO level, which alleviated the symptom of CKD complications [15,31]. We suppose the mechanism of fucoidan on the DN rats also was related with its antioxidant activity.

Diabetic nephropathy (DN) is the major life-threatening complication of diabetes. Abnormal permselectivity of the glomerular basement membrane (GBM) plays an important role in DN pathogenesis. Heparanase is the predominant enzyme that degrades heparan sulfate (HS), the main polysaccharide of the GBM. Gil *et al.* found the crucial role of heparanase in the pathogenesis of DN and its potential as a highly relevant target for interventions in patients with DN [36]. The chemical characteristics of fucoidan and HS are that both of them have sulfated group, a carbohydrate chain and a negative charge, we suppose fucoidan could react with heparanase in DN rats in order to reduce the lack of HS. However, the exact mechanism needs further study.

3. Experimental Section

3.1. Materials

Saccharina japonica, cultured in Rongcheng, China, was collected in July 2012. The fresh algae were promptly washed, sun dried, and kept in plastic bags at room temperature for use.

3.2. Preparation of Natural Polysaccharides

FPS was extracted according to the modified method of Wang *et al.* [27]. Generally, 100 g dry algae were cut roughly and autoclaved in water at 115–125 °C for 3 h. The hot aqueous solution was separated, concentrated, dialyzed, precipitated, and then dried to give polysaccharide, named FPS (yield 2.3%).

3.3. Animals

One hundred thirty male wistar rats were obtained from the Institute of Zoology, Chinese Academy of Medical Sciences. The feeding and care of the animals followed the Guiding Principles for Care and Use of Laboratory Animals of China. The animals were housed in a controlled environment (at a temperature of 24 ± 1 °C and under a 12 L:12 D lighting cycle with the light turned on at 7 a.m.) and were given free access to standard rat food and water but were not treated with insulin or any other anti-diabetic drugs. This project was approved by Chinese Academy of Medical Sciences on January 2013. The project identification code was 20130106.

3.4. Experimental Protocols

Two steps were used to develop the DN model. First, the rats received intraperitoneal anesthesia with 40 mg/kg sodium pentobarbital. An incision was made in the skin of the back. The muscle was separated, the right kidney was removed and the muscle and skin were sutured. The rats then received conventional care for 2 weeks. Ten additional rats were assigned to a sham operation group. The operation was performed without removal of the right kidney. This group served as the control group (NC group). Second, the experimental rats received 50 mg/kg of STZ (freshly dissolved in 0.1 mmol/L citrate buffer, pH 4.5) intraperitoneally after fasting for 12 h [9]. The NC group received only the same volume of citrate buffer. Two days after the STZ treatment, the development of diabetes in the experimental rats was confirmed by measuring the levels of glucose in the blood (sampled from the tail vein) and urine. Rats with blood glucose levels of 17 mmol/L or higher and strongly positive urine glucose levels were considered diabetic. The blood glucose levels in the NC group remained normal for the duration of the study. A total of 60 rats that developed DN was randomly assigned to five groups of 12 rats each: the DN model group (DN group); the DN rats treated with FPS (*i.e.*, the HF, MF and LF groups); and the DN positive control group (PC group). The rats were gavaged as follows: 10 mL/kg/day 0.5% CMC for the NC and DN groups; 300 mg/kg, 150 mg/kg and 75 mg/kg FPS for the HF, MF and LF groups, respectively; and

15 mg/kg gliguidone and 1.5 mg/kg lotensin for the PC group. All groups were gavaged once daily at the same time for 10 weeks.

3.5. Biochemical Analysis

The total sugar content of FPS was determined according to the method of Dubois *et al.* using L-fucose as the standard [37]. Sulfate content was analyzed with the barium chloride-gelatin method of Kawai *et al.* [38]. Uronic acid was estimated in a modified carbazole method using D-glucuronic acid as the standard [39]. Neutral sugar composition was determined with HPLC chromatography [40]. The molecular weight of the sample was assayed by a high performance—gel permeation chromatography (HP-GPC) system at 40 °C, where 2.84% Na_2SO_4 solution was used as mobile phase with a flow rate of 0.5 mL/min. TSK G300 column (300 mm × 7.8 mm) and 2140 refractive index detector was used. A series of different molecular weight dextrans purchased from the National Institute for the control of Pharmaceutical and Biological Products (Beijing, China) were used as standard. The changes in body weight of the various groups were recorded once a week. The rats were individually housed in metabolic cages for 24 h for urine collection at the end of the 2nd, 4th, 6th, 8th and 10th weeks. Urine protein levels were analyzed using kits from Nanjing Jiancheng (NanJing JianCheng Bio Inst, Nanjing, China). Blood glucose levels were determined after fasting for 4 h by collecting 50 μL blood from the rat's eye socket at the end of the 2nd, 4th, 6th, 8th and 10th weeks. The blood glucose levels were determined using an enzymatic colorimetric assay [41]. At the end of the experiment, the rats were fasted overnight for 12 h, blood samples were collected from the aorta abdominalis and the serum was separated for measurement of the biochemical parameters. Scr (serum creatinine) and BUN (blood urea nitrogen) were analyzed with an Olympus Au640 (Tianjin, China) automatic biochemical analyzer. A radioimmunoassay was used to assay microalbumin, β2-microglobulin (β2-MG), serum insulin and glycosylated hemoglobin.

3.6. Histopathological Procedures

After blood was collected, the rats were killed, the left kidneys rapidly removed and weighed, and tissue fragments fixed in 10% neutral buffered formalin solution, embedded in paraffin and then stained with hematoxylin and eosin (H&E). Renal pathological changes were observed under an optical microscope, and the glomerular diameter and the area were calculated.

3.7. Data Statistical Analysis

The data are presented as mean values ± 1 SD (n = 8–10). The data were analyzed with a one-way ANOVA, a Duncan's multiple-range test and an LSD test at a significance level of $p < 0.05$. SPSS 17.0 software was used for the analysis.

4. Conclusions

In summary, our study demonstrated that FPS showed protective properties in DN rats. The most likely mechanism of renal protection by FPS is that FPS modulates metabolic abnormalities and reduces blood glucose levels. The results suggest that FPS can be considered as a potential candidate for developing a new anti-diabetic agent.

Acknowledgments

This study was supported by Natural Science Foundation of China (41376166), Applied Research Projects of Nantong Municipal (BK2013011), Jiangsu Science and Technology Project (BE2012687), and the Ocean Public Welfare Scientific Research Project, State Oceanic Administration of China (No. 201005024 and No. 201405040).

Author Contributions

Jing Wang designed of the study, provided most of the data and wrote the article; Huaide Liu co-authored the article; Hong Zhang provided some data; Ning Li co-designed the study.

Conflicts of Interest

The authors declare no conflict of interest.

References

1. Ritz, E.; Rychlík, I.; Locatelli, F.; Halimi, S. End-stage renal failure in type 2 diabetes: A medical catastrophe of worldwide dimensions. *Am. J. Kidney Dis.* **1999**, *34*, 795–808.
2. Chuang, L.Y.; Guh, J.Y. Extracellular signals and intracellular pathways in diabetic nephropathy. *Nephrology* **2001**, *6*, 165–172.
3. Kanter, M. Protective effects of thymoquinone on streptozotocin-induced diabetic nephropathy. *J. Mol. Histol.* **2009**, *40*, 107–115.
4. Ihm, C.-G.; Lee, G.S.; Nast, C.C.; Artishevsky, A.; Guillermo, R.; Levin, P.S.; Glassock, R.J.; Adler, S.G. Early increased renal procollagen α1 (IV) mRNA levels in streptozotocin induced diabetes. *Kidney Int.* **1992**, *41*, 768–777.
5. Brenner, B.M.; Cooper, M.E.; de Zeeuw, D.; Keane, W.F.; Mitch, W.E.; Parving, H.H.; Remuzzi, G.; Snapinn, S.M.; Zhang, Z.; Shahinfar, S.; *et al.* Effects of losartan on renal and cardiovascular outcomes in patients with type 2 diabetes and nephropathy. *N. Engl. J. Med.* **2001**, *345*, 861–869.
6. Zhang, J.Q.; Xie, X.; Li, C.; Fu, P. Systematic review of the renal protective effect of *Astragalus membranaceus* (root) on diabetic nephropathy in animal models. *J. Ethnopharmacol.* **2009**, *126*, 189–196.
7. Li, S.P.; Zhang, G.H.; Zeng, Q.; Huang, Z.G.; Wang, Y.T.; Dong, T.T.; Tsim, K.W. Hypoglycemic activity of polysaccharide, with antioxidation, isolated from cultured *Cordyceps mycelia*. *Phytomedicine* **2006**, *13*, 428–433.

8. He, C.Y.; Li, W.D.; Guo, S.X.; Lin, S.Q.; Lin, Z.B. Effect of polysaccharides from *Ganoderma lucidum* on streptozotocin-induced diabetic nephropathy in mice. *J. Asian Nat. Prod. Res.* **2006**, *8*, 705–711.
9. Zhang, Y.W.; Wu, C.Y.; Cheng, J.T. Merit of *Astragalus* polysaccharide in the improvement of early diabetic nephropathy with an effect on mRNA expressions of NF-κB and IκB in renal cortex of streptozotoxin-induced diabetic rats. *J. Ethnopharmacol.* **2007**, *114*, 387–392.
10. Witvrouw, M.; de Clercq, E. Sulfated Polysaccharides Extracted from Sea Algae as Potential Antiviral Drugs. *Gen. Pharmacol.* **1997**, *29*, 497–511.
11. Baba, M.; de Clercq, E.; Schols, D.; Pauwels, R.; Snoeck, R.; van Boeckel, C.; van Dedem, G.; Kraaijeveld, N.; Hobbelen, P.; Ottenheijm, H.; *et al.* Novel sulfated polysaccharides: Dissociation of anti-human immunodeficiency virus activity from antithrombin activity. *J. Infect. Dis.* **1990**, *161*, 208–213.
12. Bilan, M.I.; Usov, A.I. Structural Analysis of Fucoidans. *Nat. Prod. Commun.* **2008**, *3*, 1639–1648.
13. Feldman, S.C.; Reynaldi, S.; Stortz, C.A.; Cerezo, A.S.; Damont, E.B. Antiviral properties of fucoidan fractions from *Leathesia difformis*. *Phytomedicine* **1999**, *6*, 335–340.
14. Jia, Y.H. Laminaria japonica *Aresch in Chinese Pharmaceutics of Maine Lakes and Marshes*; Xueyuan Press: Beijing, China, 1996; pp. 321–322.
15. Wang, J.; Zhang, Q.; Jin, W.; Niu, X.; Zhang, H. Effects and mechanism of low molecular weight fucoidan in mitigating the peroxidative and renal damage induced by adenine. *Carbohydr. Polym.* **2011**, *84*, 417–423.
16. Wang, J.; Wang, F.; Yun, H.; Zhang, H.; Zhang, Q. Effect and mechanism of fucoidan derivatives from *Laminaria japonica* in experimental adenine-induced chronic kidney disease. *J. Ethnopharmacol.* **2012**, *139*, 807–813.
17. Zhang, Q.B.; Li, Z.; Xu, Z.; Niu, X.; Zhang, H. Effects of fucoidan on chronic renal failure in rats. *Planta Med.***2003**, *69*, 537–541.
18. Zhang, Q.B.; Li, N.; Zhao, T.; Qi, H.; Xu, Z.; Li, Z. Fucoidan inhibits the development of proteinuria in active *Heymann nephritis*. *Phytother. Res.* **2005**, *19*, 50–53.
19. Wang, J.; Jin, W.; Zhang, W.; Hou, Y.; Zhang, H.; Zhang, Q. Hypoglycemic property of acidic polysaccharide extracted from *Saccharina japonica* and its potential mechanism. *Carbohydr. Polym.* **2013**, *95*, 143–147.
20. Yang, W.; Yu, X.; Zhang, Q.; Lu, Q.; Wang, J.; Cui, W.; Zheng, Y.; Wang, X.; Luo, D. Attenuation of streptozotocin-induced diabetic retinopathy with low molecular weight fucoidan via inhibition of vascular endothelial growth factor. *Exp. Eye Res.* **2013**, *115*, 96–105.
21. Cui, W.; Zheng, Y.; Zhang, Q.; Wang, J.; Wang, L.; Yang, W.; Guo, C.; Gao, W.; Wang, X.; Luo, D. Low-molecular-weight fucoidan protects endothelial function and ameliorates basal hypertension in diabetic Goto-Kakizaki rats. *Lab. Invest.* **2014**, *94*, 382–393.
22. Kashihara, N.; Watanabe, Y.; Makino, H.; Wallner, E.I.; Kanwar, Y.S. Selective decreased *de novo* synthesis of glomerular proteoglycans under the influence of reactive oxygen species. *Proc. Natl. Acad. Sci. USA* **1992**, *89*, 6309–6313.

23. Ha, H.; Kim, C.; Son, Y.; Chung, M.H.; Kim, K.H. DNA damage in the kidneys of diabetic rats exhibiting microalbuminuria. *Free Rad. Biol. Med.* **1994**, *16*, 271–274.
24. Brezniceanu, M.; Liu, F.; Wei, C.C.; Tran, S.; Sachetelli, S.; Zhang, S.L.; Guo, D.F.; Filep, J.G.; Ingelfinger, J.R.; Chan, J.S. Catalase overexpression attenuates angiotensinogen expression and apoptosis in diabetic mice. *Kidney Int.* **2007**, *71*, 912–923.
25. Ha, H.; Hwang, I.A.; Park, J.H.; Lee, H.B. Role of reactive oxygen species in the pathogenesis of diabetic nephropathy. *Diabetes Res. Clin. Pract.* **2008**, *82*, S42–S45.
26. Bhatia, S.; Shukla, R.; Venkata Madhu, S.; Kaur Gambhir, J.; Madhava Prabhu, K. Antioxidant status, lipid peroxidation and nitric oxide end products in patients of type 2 diabetes mellitus with nephropathy. *Clin. Biochem.* **2003**, *36*, 557–562.
27. Wang, J.; Zhang, Q.; Zhang, Z.; Li, Z. Antioxidant activity of sulfated polysaccharide fractions extracted from *Laminaria japonica*. *Int. J. Biol. Macromol.* **2008**, *42*, 127–132.
28. Suzuki, R.; Okada, Y.; Okuyama, T. The favorable effect of style of *Zea mays* L. on streptozotocin induced diabetic nephropathy. *Biol. Pharm. Bull.* **2005**, *28*, 919–920.
29. Guerrero-Analco, J.A.; Hersch-Martínez, P.; Pedraza-Chaverri, J.; Navarrete, A.; Mata, R. Antihyperglycemic effect of constituents from *Hintonia standleyana* in streptozotocin-induced diabetic rats. *Planta Med.* **2005**, *71*, 1099–1105.
30. Xu, J.; Li, Z.; Cao, M.; Zhang, H.; Sun, J.; Zhao, J.; Zhou, Q.; Wu, Z.; Yang, L. Synergetic effect of *Andrographis paniculata* polysaccharide on diabetic nephropathy with andrographolide. *Int. J. Biol. Macromol.* **2012**, *51*, 738–742.
31. Cohen, M.P.; Clements, R.S.; Cohen, J.A.; Shearman, C.W. Prevention of decline in renal function in the diabetic db/db mouse. *Diabetologia* **1996**, *39*, 270–274.
32. Montilla, P.; Barcos, M.; Munoz, M.C.; Bujalance, I.; Munoz-Castaneda, J.R.; Tunez, I. Red wine prevents brain oxidative stress and nephropathy in streptozotocin-induced diabetic rats. *J. Biochem. Mol. Biol.* **2005**, *38*, 539–544.
33. Clark, T.A.; Heyliger, C.E.; Edel, A.L.; Goel, D.P.; Pierce, G.N. Codelivery of a tea extract prevents morbidity and mortality associated with oral vanadate therapy in streptozotocin-induced diabetic rats. *Metabolism* **2004**, *53*, 1145–1151.
34. Larkins, R.G.; Dunlop, M.E. The link between hyperglycemia and diabetic nephropathy. *Diabetologia* **1992**, *35*, 499–504.
35. Zhao, R.; Li, Q.W.; Li, J.; Zhang, T. Protective effect of *Lycium barbarum* polysaccharide 4 on kidneys in streptozotocin-induced diabetic rats. *Can. J. Physiol. Pharmacol.* **2009**, *87*, 711–719.
36. Gil, N.; Goldberg, R.; Neuman, T.; Garsen, M.; Zcharia, E.; Rubinstein, A.M.; van Kuppevelt, T.; Meirovitz, A.; Pisano, C.; Li, J.P.; *et al.* Heparanase is essential for the development of diabetic nephropathy in mice. *Diabetes* **2012**, *61*, 208–216.
37. Dubois, M.; Gilles, K.A.; Hamilton, J.K.; Rebers, P.A.; Smith, F. Colorimetric Method for Determination of Sugars and Related Substabces. *Anal. Chem.* **1956**, *28*, 350–357.
38. Kawai, Y.; Seno, N.; Anno, K. A modified method for chondrosulfatase assay. *Anal. Biochem.* **1969**, *32*, 314–321.

39. Bitter, T.; Muir, H.M. A modified uronic acid carbazole reaction. *Anal. Biochem.* **1962**, *4*, 330–334.
40. Honda, S.; Akao, E.; Suzuki, S.; Okuda, M.; Kakehi, K.; Nakamura, J. High-performance liquid chromatography of reducing carbohydrates as strongly ultraviolet-absorbing and electrochemically sensitive 1-phenyl-3-methyl5-pyrazolone derivatives. *Anal. Biochem.* **1989**, *180*, 351–357.
41. Barham, D.; Trinder, P. An improved colour reagent for the determination of blood glucose by the oxidase system. *Analyst* **1972**, *97*, 142–145.

Chromomycins A_2 and A_3 from Marine Actinomycetes with TRAIL Resistance-Overcoming and Wnt Signal Inhibitory Activities

Kazufumi Toume, Kentaro Tsukahara, Hanako Ito, Midori A. Arai and Masami Ishibashi

Abstract: A biological screening study of an actinomycetes strain assembly was conducted using a cell-based cytotoxicity assay. The CKK1019 strain was isolated from a sea sand sample. Cytotoxicity-guided fractionation of the CKK1019 strain culture broth, which exhibited cytotoxicity, led to the isolation of chromomycins A_2 (**1**) and A_3 (**2**). **1** and **2** showed potent cytotoxicity against the human gastric adenocarcinoma (AGS) cell line (IC_{50} **1**; 1.7 and **2**; 22.1 nM), as well as strong inhibitory effects against TCF/β-catenin transcription (IC_{50} **1**; 1.8 and **2**; 15.9 nM). **2** showed the ability to overcome tumor necrosis factor (TNF)-related apoptosis-inducing ligand (TRAIL) resistance. To the best of our knowledge, the effects of chromomycins A_2 (**1**) and A_3 (**2**) on TRAIL resistance-overcoming activity, and on the Wnt signaling pathway, have not been reported previously. Thus, **1** and **2** warrant potential drug lead studies in relation to TRAIL-resistant and Wnt signal-related diseases and offer potentially useful chemical probes for investigating TRAIL resistance and the Wnt signaling pathway.

Reprinted from *Mar. Drugs*. Cite as: Toume, K.; Tsukahara, K.; Ito, H.; Arai, M.A.; Ishibashi, M. Chromomycins A_2 and A_3 from Marine Actinomycetes with TRAIL Resistance-Overcoming and Wnt Signal Inhibitory Activities. *Mar. Drugs* **2014**, *12*, 3466–3476.

1. Introduction

Natural small molecules from actinomycetes provide a number of antimicrobials and anticancer agents with original and ingenious structures, as well as strong biological activities [1]. As a result, they are widely recognized as a promising resource that can potentially supply new drug discovery lead or seed compounds. We have previously isolated actinomycetes from soil, sea sand and seawater samples collected around Japan in order to investigate the bioactive metabolites obtained from these actinomycetes. Using these assembled actinomycetes, we examined the bioactive metabolites of actinomycetes strains and isolated a rare phenazine [2], its glycosides [3], nonactin derivatives [4], cyclic hydroxamates [5], azaquinone-phenylhydrazone [6] and naphthopyridazone alkaloid [7] from *Streptomyces* sp. Of these compounds, several showed the ability to abrogate tumor necrosis factor (TNF)-related apoptosis-inducing ligand (TRAIL) resistance [6–8], along with inhibitory effects on the Wnt signal pathway [4,5].

In our screening program for obtaining bioactive natural products from our actinomycetes assembly, which consists of more than 1200 strains, we detected several strains that showed potent cytotoxicity. Of these strains, we recently examined the active constituents in the fermented broth of the actinomycetes strain, CKK1019, which led to the isolation of chromomycins A_2 (**1**) and A_3 (**2**) as bioactive compounds. Chromomycins, members of the aureolic acid family, are known to

have antitumor activity and were isolated from soil- and marine-derived actinomycetes [9]. Herein, we will describe the activity-guided isolation and identification of those active compounds.

2. Results and Discussion

*2.1. Isolation and Identification of **1** and **2***

Using a cell-based cytotoxicity assay system, we examined the extracts of actinomycetes isolated and cultivated in our laboratory and detected the cytotoxic effects against the human gastric adenocarcinoma (AGS) cell line (34% viability of the control at 10 μg/mL) of the MeOH extract of the CKK1019 actinomycetes strain, which was isolated from a sea sand sample collected at Okinoshima Island, Tateyama City, Chiba Prefecture, Japan. The culture conditions of this strain were then investigated. The strain was cultivated in 4%, 2% and 0% artificial seawater containing liquid Waksman media. After the extraction of culture broth, these extracts exhibited the same retention factor (Rf) value spots, the same pattern on TLC and similar cytotoxicities.

Next, large-scale cultivation was conducted using seawater-free liquid Waksman media. EtOAc was used to extract the supernatant of the culture broth (6.2 L). Cytotoxicity-guided fractionation of the EtOAc extract, which showed cytotoxicity, was conducted using silica gel and ODS column chromatography, as well as preparative ODS HPLC. These processes yielded chromomycins A_2 (**1**, 50 mg) [10,11] and A_3 (**2**, 86.3 mg) [10] (Figure 1), which were identified on the basis of spectroscopic data, including NMR, MS and optical rotation with references to the literature [10,11].

Figure 1. Structures of isolated Compounds **1** and **2**.

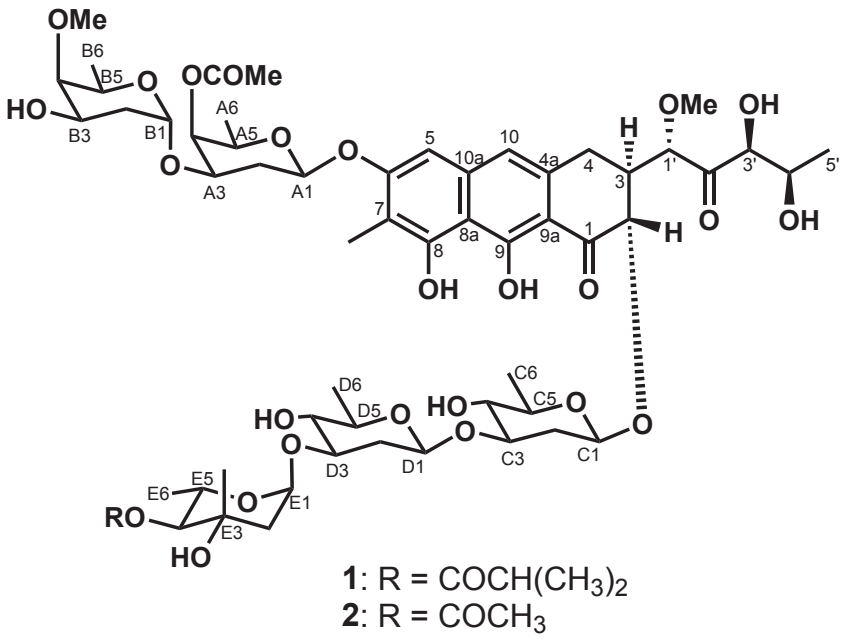

*2.2. Biological Activities of **1** and **2***

Chromomycins A_2 (**1**) and A_3 (**2**) exhibited potent cytotoxicity against the AGS cell line, with IC_{50} values of 1.7 and 22.1 nM, respectively (Figure 2).

Figure 2. Cytotoxicities of chromomycins A_2 (**1**) and A_3 (**2**) against human gastric adenocarcinoma (AGS) cells. AGS cells were treated at the indicated concentration of test samples for 24 h. Cell viability was determined after 24 h by the fluorometric microculture cytotoxicity assay (FMCA). The bars represent the means ± SD (n = 3) with significance determined with Tukey's test. ** $p < 0.01$ *vs.* the control (blank containing 0.1% DMSO without compound).

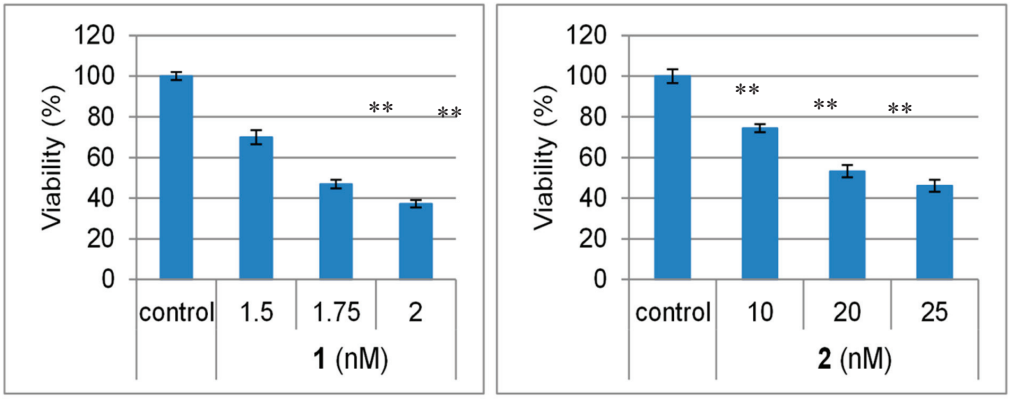

The AGS cell line is known to be resistant against the tumor necrosis factor (TNF)-related apoptosis-inducing ligand (TRAIL) [12]. TRAIL, a member of the TNF superfamily, is considered to be a promising anti-cancer agent, due to its ability to cause tumor selective apoptosis. TRAIL binds to death receptors, such as death receptor 5 (DR5) and/or death receptor 4 (DR4), which allows the formation of a death-inducing signaling complex (DISC), resulting in the activation of caspase-signaling pathways and, ultimately, apoptosis [13]. However, large numbers of cancer cells, especially highly malignant tumors, are resistant to TRAIL. Therefore, identifying compounds that can overcome TRAIL-resistance has become an important strategy in the development of new anticancer drugs. The ability of chromomycin A_3 (**2**) to overcome TRAIL resistance was evaluated using the previously described method [14,15]. As shown in Figure 3, the treatment of AGS cells with 100 ng/mL TRAIL for 24 h resulted in only a slight decrease in cell viability (20%), while luteolin [16] at 17.5 μM, which was used as a positive control, was 35% more potent when administered in combination with TRAIL than when the compound was administrated alone. The treatment of AGS cells with **2** (10 nM) in the presence of TRAIL (100 ng/mL) led to cell viability being 52% lower than that of treatment with the compound alone (without TRAIL), which confirmed the potent abilities of these compounds to overcome TRAIL resistance.

Figure 3. TNF-related apoptosis-inducing ligand (TRAIL) resistance-overcoming activity of chromomycin A_3 (**2**) in AGS cells. AGS cells were treated at the indicated concentration of test samples and/or 100 ng/mL of TRAIL for 24 h. Cell viability was determined after 24 h by a FMCA assay. The bars represent means ± SD (n = 3) with significance determined with Tukey's test. ** $p < 0.01$ *vs.* the control (blank containing 0.1% DMSO without compound).

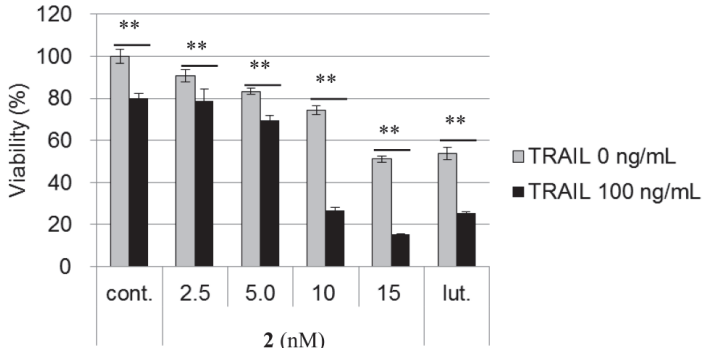

Next, we examined the effects of chromomycins A_2 (**1**) and A_3 (**2**) on the Wnt signaling pathway. To the best of our knowledge, the effects of chromomycins on Wnt signaling have not been reported. The Wnt signaling pathway has been highly conserved throughout evolution from metazoans to humans and plays an important role in the regulation of numerous cellular processes, including embryonic development, differentiation, proliferation, survival, polarity, migration and the specification of cell fate in various cells [17]. However, the strong activation of Wnt signaling is a pivotal factor for oncogenesis in various types of cancer [18,19], particularly in human colon cancer. Therefore, Wnt signaling is considered to be an attractive therapeutic target for colon cancer. Furthermore, recent studies revealed that this signaling pathway might play significant roles in supporting differentiation, as well as the formation and maintenance of stem cells [20]. On the other hand, the deregulation of this pathway has also been associated with various human diseases, including diabetes, osteoporosis and Alzheimer's disease [18]. Therefore, small molecules that have the ability to modulate the Wnt signaling pathway can be useful biological study agents and have the potential to become lead compounds for drug discovery. Using the luciferase reporter gene assay system [21,22], the inhibitory activities of these compounds on TCF/β-catenin transcription were evaluated.

Wnt signaling activates gene transcription by forming a complex between the DNA-binding proteins of the TCF/LEF family and β-catenin, and that, under this condition, SuperTOP-Flash, a β-catenin-responsive reporter plasmid with seven copies of TCF-binding sites (CCTTTGATC), is activated. STF/293 cells, 293 cells stably expressing the SuperTOP-Flash reporter construct, were used for the TOP-Flash assay. Together with the TOP-Flash assay, the cell viability of STF/293 cells was also tested. Because a decrease in cell number may contribute to the false positive inhibition of TCF/β-catenin transcriptional activity, an inhibitor of TCF/β-catenin transcription may inhibit SuperTOP-Flash activity, but it will not be able to inhibit transcription in

SuperFOP-Flash-transfected cells because SuperFOP-Flash has six copies of the mutated TCF-binding sites (CCTTTGGCC). The FOP-Flash assay was conducted using 293 T cells transiently transfected with the SuperFOP-Flash reporter construct. As shown in Figure 4, chromomycins A_2 (**1**) and A_3 (**2**) strongly inhibited TCF/β-catenin transcription, with IC_{50} values of 1.8 and 15.9 nM, high viability (>69%) and no significant decrease in SuperFOP-Flash activity. These results indicate that chromomycins A_2 (**1**) and A_3 (**2**) are potent TCF/β-catenin transcription inhibitors.

Figure 4. The inhibitory activity of chromomycins A_2 (**1**) and A_3 (**2**) on TCF/β-catenin transcription. The TOP-Flash (TOP) and FOP-Flash (FOP) assays were evaluated luciferase assay system using STF (SuperTOP-Flash)/293 and 293 T cells, respectively. Cells were treated with compounds and LiCl (15 mM) for 24 h, then the luciferase activity was measured. The cell viability of STF/293 cells of each treatment (24 h) was also evaluated by the FMCA assay. Data are presented as the mean ± SD. ** $p < 0.01$ *vs.* the control (blank containing 0.1% DMSO without compound).

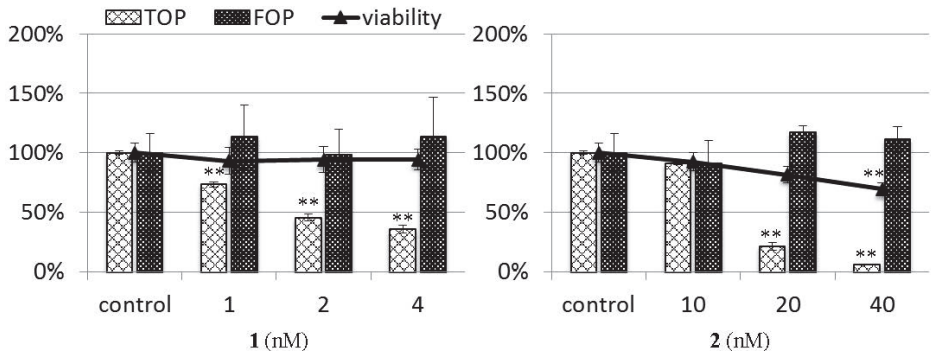

3. Experimental Section

3.1. General Experimental Procedures

Optical rotations were measured with a JASCO P-1020 polarimeter. NMR spectra were recorded on JEOL ECA600 and ECP400 spectrometers with a deuterated solvent, the chemical shifts of which were used as an internal standard. Electrospray ionization mass spectra (ESIMS) were obtained on a Shimadzu LCMS-2020 spectrometer. Column chromatography was performed using silica gel PSQ100B and Chromatorex ODS (Fuji Silysia Chemical Ltd., Kasugai, Japan). Preparative HPLC was performed using Develosil ODS HG-5 (Nomura Chemical Co., Ltd., Seto, Japan).

3.2. Microbial Strain and Fermentation

CKK1019 was separated on humic acid-vitamin (HV) agar [23], a medium for the selective isolation of actinomycetes, from a sea sand sample collected at Okinoshima Island, Tateyama City, Chiba Prefecture, Japan, as described previously [24]. Briefly, the sea sand sample was shaken in water, filtrated using a nitrocellulose membrane filter (pore size: 0.22 μm; GSWP, Merck Millipore

Billerica, MA, USA), after which the filter was overlaid on a plate of HV agar. After a three-or four-day incubation, the filter was removed from the agar, and the plate was reincubated until growth was observed. The spores of this strain were kept in a freezer in a 15% glycerol solution, grown on solid Waksman medium containing agar for 3–5 days, transferred to a flask (500 mL) and inoculated into 100 mL of a Waksman medium consisting of glucose (2 g/100 mL), meat extract (0.5 g/100 mL), peptone (0.5 g/100 mL), dried yeast (0.3 g/100 mL), NaCl (0.5 g/100 mL) and $CaCO_3$ (0.3 g/100 mL). The mixture was then cultured at 28 °C for three days on a reciprocating shaker. The seed culture (20 mL) was then transferred into a flask (3 L) containing 700 mL of the Waksman medium and cultured at 28 °C for seven days on the reciprocating shaker.

3.3. Extraction and Isolation

The culture broth (6.2 L in total) of CKK1019 was harvested and centrifuged (6000 rpm, 15 min) to separate mycelia and the supernatant. The supernatant was concentrated under reduced pressure to approximately 500 mL and partitioned between EtOAc (500 mL × 3) to obtain the EtOAc-soluble fraction (2.4 g). The EtOAc-soluble fractions of the supernatant were subjected to silica gel column chromatography (28 × 250 mm) eluted stepwise ($CHCl_3$:MeOH = 100:0, 95:5, 90:10, 85:15, 80:20, 70:30, 60:40, 0:100) to obtain eleven fractions, 1A to 1K. Fractions 1E and 1F eluted with $CHCl_3$:MeOH = 95:5 were combined (1043 mg), then subjected to the ODS column (28 × 205 mm), which was eluted with MeOH:H_2O = 6/4, 65/35, 7/3, 8/2, 1/0 to obtain 13 fractions. Fraction 2G (86.3 mg), which was eluted with MeOH:H_2O = 7:3, was identified as chromomycin A_3 (**2**). A portion (67 mg) of Fraction 2J (231 mg), eluted with MeOH:H_2O = 7:3, was further separated by preparative HPLC (CAPCELL PACK C18 MG-2, 10 × 250 mm; eluent, 55% MeCN in H_2O; flow rate, 2.0 mL/min; UV detection at 254 nm and Refractive Index (RI) detection) to obtain chromomycin A_2 (**1**, 50 mg, t_R 31 min).

Chromomycin A_2 (**1**): $[\alpha]_D^{25}$ −12 (*c* 1.2 EtOH); ^1H and ^{13}C NMR data, see Table 1; ESIMS *m*/*z* 1233 $[M + Na]^+$.

Chromomycin A_3 (**2**): $[\alpha]_D^{25}$ −42 (*c* 1.0 EtOH); ^1H and ^{13}C NMR data, see Table 1; ESIMS *m*/*z* 1205 $[M + Na]^+$.

3.4. Viability Assay (FMCA Assay [25])

AGS cells were seeded in a 96-well culture plate (6×10^3 cells per well) in 200 µL of Roswell Park Memorial Institute (RPMI) medium containing 10% fetal bovine serum (FBS). STF/293 cells (3×10^4) were split into 96-well plates and incubated for 24 h. They were then incubated at 37 °C in a 5% CO_2 incubator for 24 h. Test samples at different doses with or without TRAIL (100 ng/mL) were added to each well and incubated for 24 h. They were then treated with fluorescein diacetate (Wako, Osaka, Japan) in PBS buffer (10 µg/mL), and fluorescence was detected after a 1-h incubation. Assays were performed in triplicate at least. The sample was prepared as outlined above. Data are shown as the mean ± SD. The significance of differences between the data sets was determined with Tukey's test (** $p < 0.01$ was regarded as significant). IC_{50} values were calculated by probit analysis.

Table 1. ^{1}H and ^{13}C NMR spectroscopic data for chromomycins A_2 (**1**) and A_3 (**2**).

Position	1			2	
	δ_H (*J* in Hz) [a]	δ_H (*J* in Hz) [b]	δ_C [c]	δ_H (*J* in Hz) [b]	δ_C [c]
1			202.1		202.1
2	4.64, d (11.2)	4.71, d (11.4)	75.9	4.71, d (11.6)	75.9
3	2.58, m	2.58, m	43.7	2.67, m	43.7
4	3.00, d (15.2)	3.06, d (13.1)	26.9	3.13, m	26.9
	2.58, m	2.58, m		2.67, m	
5	6.58, s	6.54, s	100.8	6.60, s	100.7
6			159.6		159.6
7			111.6		111.6
8			156.1		156.1
9			165.3		165.2
10	6.70, s	6.66, s	117.0	6.72, s	117.0
4a			134.6		134.5
8a			108.1		108
9a			108.1		108
10a			138.4		138.3
7-CH_3	2.10, s	2.16, s	8.2	2.16, s	8.2
8-OH		9.74		9.78, s	
9-OH		15.67		15.68, s	
1′	4.67, s	4.69, br s	81.8	4.70, d (1.6)	81.9
2′			211.2		211.2
3′	4.11, d (1.5)	4.20, br s	78.2	4.21, d (2.0)	78.2
4′	4.21, qd (6.4, 1.5)	4.36, q (6.0)	67.9	4.37, qd (6.4, 2.0)	67.8
5′	1.25 d (6.4)	1.35, d (6.0)	20.5	1.37, d (6.4)	20.5
1′-OCH_3	3.40, s	3.49, s	59.6	3.50, s	59.6
Sugar A					
A1	5.18, d (8.4)	5.19, d (10.0, 2.0)	97.3	5.21, dd (9.8, 2.1)	97.3
A2	2.16, m	2.20, m	32.9	2.26, m	32.9
	2.00, m	2.02, m		2.26, m	
A3	3.96, m	3.93, m	69.9	4.00, m	69.8
A4	5.10, d (1.7)	5.15, d (2.6)	67.2	5.16, d (3.0)	67.2
A5	3.76, m	3.80, q (6.4)	69.7	3.82, q (6.4)	69.7
A6	1.19, d (6.0)	1.27, d (6.4)	16.8	1.28, d (6.4)	16.8
$\underline{CH_3}$-CO	2.09, s	2.15, s	20.8	2.15, s	20.8
CH_3-$\underline{CO}$			170.9		170.9
Sugar B					
B1	5.05, d (2.8)	5.10, br s	95.2	5.10, d (2.4)	95.1
B2	1.78, m	1.63–1.74, m	33.5	1.63–1.75, m	33.4
	1.64, m	1.63–1.74, m		1.63–1.75, m	
B3	3.89, dd (7.8, 2.8)	3.93, m	65.9	3.93, m	65.8
B4	3.14, d (2.8)	3.21, d (3.2)	81.5	3.21, d (3.2)	81.5
B5	3.82, q (6.5)	3.93, m	66.7	3.89, q (6.4)	66.7
B6	1.14, d (6.5)	1.27, d (6.5)	17.2	1.29, d (6.4)	17.2
B4-OCH_3	3.51, s	3.57, s	62.3	3.58, s	62.3

Table 1. *Cont.*

Position	1			2	
	δ_H (*J* in Hz) [a]	δ_H (*J* in Hz) [b]	δ_C [c]	δ_H (*J* in Hz) [b]	δ_C [c]
Sugar C					
C1	5.01, d (9.2)	5.07, br d (9.7)	100.3	5.08, dd (9.7, 1.6)	100.3
C2	2.46, dd (12.2, 4.6)	2.49, dd (11.4, 5.2)	37.4	2.49, ddd (12.8, 5.1, 1.6)	37.4
	1.64, m	1.63, m		1.75, m	
C3	3.59, m	3.57, m	82.3	3.59, m	82.3
C4	3.06, d (8.8)	3.13, d (9.0)	75.1	3.08, m	75.1
C5	3.27, m	3.38, dq (9.0, 5.5)	72.1	3.32, dq (9.1, 5.5)	72.1
C6	1.28, d (5.6)	1.34, d (5.5)	18.0	1.34, d (5.5)	18.0
Sugar D					
D1	4.55, d (9.6)	4.59, d (9.0)	99.7	4.60, d (9.6, 2.0)	99.7
D2	2.22, dd (11.9, 4.2)	2.27, dd (13.1, 4.8)	37.1	2.29, dd (5.9, 2.0)	37.0
	1.56, d (11.9)	1.63, m		1.75, m	
D3	3.49, m	3.49, m	80.7	3.47, m	80.5
D4	3.03, d (8.0)	3.10, d (8.5)	75.2	3.08, m	75.2
D5	3.27, m	3.30, qd (9.0, 6.0)	72.3	3.40, dq (9.1, 6.0)	72.2
D6	1.31, d (6.0)	1.37, d (6.0)	17.8	1.38, d (6.0)	17.8
Sugar E					
E1	4.96 (t, 2.8)	4.99, dd (3.9, 2.0)	97.1	5.01, dd (4.0, 2.2)	97.0
E2	1.92, m	2.00, m	43.8	2.00, dd (13.8, 4.0)	43.6
E3			70.6	2.06, dd (13.8, 2.2)	70.6
E4	4.55, d (9.6)	4.59, d (9.0)	79.4	4.61, d (9.3)	79.5
E5	3.98, m	3.88, q (6.7)	67.0	4.00, m	67.0
E6	1.22, d (5.2)	1.21, d (7.4)	17.8	1.23, d (6.4)	17.8
E3-CH_3	1.28, s	1.33, s	22.9		
($\underline{CH_3}$)$_2$CH-CO	1.13, d (6.8)	1.19, d (7.4)	19.0		
(CH_3)$_2\underline{CH}$-CO	2.58, m	2.56, m	34.2		
(CH_3)$_2$CH-$\underline{CO}$			177.5		
$\underline{CH_3}CO$				2.12, s	20.9
$CH_3\underline{CO}$					171.4

[a] Measured at 400 MHz in $CDCl_3$:CD_3OD (10:1); [b] measured at 400 MHz in $CDCl_3$; [c] measured at 150 MHz in $CDCl_3$.

3.5. Luciferase Assay

SuperTOP-Flash assay: Stable reporter cells, STF/293 cells (3×10^4), were split into 96-well plates and grown in DMEM with 10% FBS for 24 h. Cells were treated with compounds and LiCl (final concentration: 15 mM). After the 24 h incubation, the cells were lysed with CCLR (20 μL/well cell culture lysis reagent; 20 μL/well, Promega, Madison, WI, USA), and luciferase activity was measured with a Luciferase 1000 Assay System (Promega, Madison, WI, USA).

SuperFOP-Flash assay: Transient transfection was performed using Lipofectamine 2000 (Invitrogen, Carlsbad, CA, USA). 293T cells (1×10^5) were split into 24-well plates and grown in DMEM with 10% FBS for 24 h. After 24 h, cells were transfected with 1 μg of the luciferase

reporter construct (SuperFOP-Flash) and 0.05 μg of pRL-CMV (Promega, USA) for normalization. Three hours after the transfection, compounds were added to the medium containing FBS. 293 T cells were treated with compounds in an FBS-containing medium combined with 15 mM of LiCl. Cells incubated for 24 h were lysed in passive lysis buffer (Promega , Madison, WI, USA, 50 μL/well), and luciferase activity was measured with a Dual-Glo Luciferase Assay System (Promega, Madison, WI, USA).

Luciferase chemiluminescence was measured using a Luminoskan Ascent (Thermo, Waltham, MA, USA). The assay sample was stored as a 10-mM solution in DMSO, then diluted to the indicated concentrations with medium. The final concentration of DMSO was less than 0.1% (v/v). Assays were performed in triplicate at least. Data are shown as the mean ± SD. The significance of differences was determined with Tukey's test (** $p < 0.01$ *vs.* control). IC_{50} values were calculated by probit analysis.

4. Conclusions

In our research into the bioactive natural products in actinomycetes, we demonstrated the abilities of chromomycins A_2 (**1**) and A_3 (**2**) to overcome TRAIL resistance and inhibit TCF/β-catenin transcription. Chromomycin A_3 has been shown to exhibit antitumor activity [9] and inhibit DNA synthesis by inhibiting DNA gyrase [26]. However, to the best of our knowledge, the effects of chromomycins on TRAIL resistance and Wnt signaling have not been reported. Therefore, these compounds may be potential drug leads for TRAIL-resistant and Wnt signal-related diseases and will be useful chemical tools for use in investigating TRAIL and the Wnt signaling pathway.

Acknowledgments

We would like to thank Jeremy Nathans (John Hopkins University School of Medicine) for the STF/293 cells and Ronald T. Moon (University of Washington) for the SuperFOP-Flash plasmid. This study was supported by Grants-in-Aid for Scientific Research from the Japan Society for the Promotion of Science (JSPS), a Grant-in-Aid for Scientific Research on Innovative Areas "Chemical Biology of Natural Products" from The Ministry of Education, Culture, Sports, Science and Technology (MEXT), Japan, the Cosmetology Research Foundation, the Hamaguchi Foundation for the Advancement of Biochemistry and the Uehara Memorial Foundation, AstraZeneca R&D Grant, Japan Antibiotics Research Association, and Sekisui Chemical Innovations Inspired by the Nature Research Support Program.

Author Contributions

Kazufumi Toume, Midori A. Arai, and Masami Ishibashi designed the project, analyzed the results, organized and wrote the manuscript. Kentaro Tsukahara achieved screening isolation, identification of compounds. Kentaro Tsukahara and Hanako Ito evaluated the biological activity of compounds.

Conflicts of Interest

The authors declare no conflict of interest.

References

1. Takahashi, Y.; Omura, S. Isolation of new actinomycetes strains for the screening of new bioactive compounds. *J. Gen. Appl. Microbiol.* **2003**, *49*, 141–154.
2. Abdelfattah, M.S.; Kazufumi, T.; Ishibashi, M. Izumiphenazines A–C: Isolation and structure elucidation of phenazine derivatives from *Streptomyces* sp. IFM 11204. *J. Nat. Prod.* **2010**, *73*, 1999–2002.
3. Abdelfattah, M.S.; Toume, K.; Ishibashi, M. Isolation and structure elucidation of izuminosides A–C: A rare phenazine glycosides from *Streptomyces* sp. IFM 11260. *J. Antibiot.* **2011**, *64*, 271–275.
4. Tamai, Y.; Toume, K.; Arai, M.A.; Hayashida, A.; Kato, H.; Shizuri, Y.; Tsukamoto, S.; Ishibashi, M. Nonactin and related compounds found in a screening program for Wnt signal inhibitory activity. *Heterocycles* **2012**, *84*, 1245–1250.
5. Tamai, Y.; Toume, K.; Arai, M.A.; Ishibashi, M. Griseoviridin and cyclic hydroxamates found in a screening program for Wnt signal inhibitor. *Heterocycles* **2012**, *86*, 1517–1524.
6. Abdelfattah, M.S.; Toume, K.; Arai, M.A.; Masu, H.; Ishibashi, M. Katorazone, a new yellow pigment with a 2-azaquinone-phenylhydrazone structure produced by *Streptomyces* sp. IFM 11299. *Tetrahedron Lett.* **2012**, *53*, 3346–3348.
7. Abdelfattah, M.S.; Toume, K.; Ishibashi, M. Yoropyrazone, a new naphthopyridazone alkaloid isolated from *Streptomyces* sp. IFM 11307 and evaluation of its TRAIL resistance-overcoming activity. *J. Antibiot.* **2012**, *65*, 245–248.
8. Abdelfattah, M.S.; Kazufumi, T.; Ishibashi, M. New pyranonaphthoquinones and a phenazine alkaloid isolated from *Streptomyces* sp. IFM 11307 with TRAIL resistance-overcoming activity. *J. Antibiot.* **2011**, *64*, 729–734.
9. Lombo, F.; Menendez, N.; Salas, J.A.; Mendez, C. The aureolic acid family of antitumor compounds: Structure, mode of action, biosynthesis, and novel derivatives. *Appl. Microbiol. Biotechnol.* **2006**, *73*, 1–14.
10. Yoshimura, Y.; Koenuma, M.; Matsumoto, K.; Tori, K.; Terui, Y. NMR studies of chromomycins, olivomycins, and their derivatives. *J. Antibiot.* **1988**, *41*, 53–67.
11. Hu, Y.; Espindola, A.P.D.M.; Stewart, N.A.; Wei, S.; Posner, B.A.; MacMillan, J.B. Chromomycin SA analogs from a marine-derived *Streptomyces* sp. *Bioorg. Med. Chem.* **2011**, *19*, 5183–5189.
12. Jin, C.Y.; Park, C.; Cheong, J.; Choi, B.T.; Lee, T.H.; Lee, J.D.; Lee, W.H.; Kim, G.Y.; Ryu, C.H.; Choi, Y.H. Genistein sensitizes TRAIL-resistant human gastric adenocarcinoma AGS cells through activation of caspase-3. *Cancer Lett.* **2007**, *257*, 56–64.
13. Mellier, G.; Huang, S.; Shenoy, K.; Pervaiz, S. TRAILing death in cancer. *Mol. Aspects Med.* **2010**, *31*, 93–112.

14. Minakawa, T.; Toume, K.; Arai, M.A.; Koyano, T.; Kowithayakorn, T.; Ishibashi, M. Prenylflavonoids isolated from *Artocarpus champeden* with TRAIL-resistance overcoming activity. *Phytochemistry* **2013**, *96*, 299–304.
15. Ahmed, F.; Toume, K.; Sadhu, S.K.; Ohtsuki, T.; Arai, M.A.; Ishibashi, M. Constituents of *Amoora cucullata* with TRAIL resistance-overcoming activity. *Org. Biomol. Chem.* **2010**, *8*, 3696–3703.
16. Horinaka, M.; Yoshida, T.; Shiraishi, T.; Nakata, S.; Wakada, M.; Nakanishi, R.; Nishino, H.; Matsui, H.; Sakai, T. Luteolin induces apoptosis via death receptor 5 upregulation in human malignant tumor cells. *Oncogene* **2005**, *24*, 7180–7189.
17. Clevers, H.; Nusse, R. Wnt/β-catenin signaling and disease. *Cell* **2012**, *149*, 1192–1205.
18. Baron, R.; Kneissel, M. WNT signaling in bone homeostasis and disease: From human mutations to treatments. *Nat. Med.* **2013**, *19*, 179–192.
19. Anastas, J.N.; Moon, R.T. WNT signalling pathways as therapeutic targets in cancer. *Nat. Rev. Cancer* **2013**, *13*, 11–26.
20. Takebe, N.; Harris, P.J.; Warren, R.Q.; Ivy, S.P. Targeting cancer stem cells by inhibiting Wnt, Notch, and Hedgehog pathways. *Nat. Rev. Clin. Oncol.* **2011**, *8*, 97–106.
21. Toume, K.; Kamiya, K.; Arai, M.A.; Mori, N.; Sadhu, S.K.; Ahmed, F.; Ishibashi, M. Xylogranin B: A potent Wnt signal inhibitory limonoid from *Xylocarpus granatum*. *Org. Lett.* **2013**, *15*, 6106–6109.
22. Li, X.; Ohtsuki, T.; Koyano, T.; Kowithayakorn, T.; Ishibashi, M. New Wnt/β-catenin signaling inhibitors isolated from *Eleutherine palmifolia*. *Chem. Asian J.* **2009**, *4*, 540–547.
23. Hayakawa, M.; Nonomura, H. Humic acid-vitamin agar, a new medium for the selective isolation of soil actinomycetes. *J. Ferment. Technol.* **1987**, *65*, 501–509.
24. Hirsch, C.F.; Christensen, D.L. Novel method for selective isolation of actinomycetes. *Appl. Environ. Microbiol.* **1983**, *46*, 925–929.
25. Lindhagen, E.; Nygren, P.; Larsson, R. The fluorometric microculture cytotoxicity assay. *Nat. Protoc.* **2008**, *3*, 1364–1369.
26. Simon, H.; Wittig, B.; Zimmer, C. Effect of netropsin, distamycin-A and chromomycin-A (3) on the binding and cleavage reaction of DNA gyrase. *FEBS Lett.* **1994**, *353*, 79–83.

Emerging Strategies and Integrated Systems Microbiology Technologies for Biodiscovery of Marine Bioactive Compounds

Javier Rocha-Martin, Catriona Harrington, Alan D.W. Dobson and Fergal O'Gara

Abstract: Marine microorganisms continue to be a source of structurally and biologically novel compounds with potential use in the biotechnology industry. The unique physiochemical properties of the marine environment (such as pH, pressure, temperature, osmolarity) and uncommon functional groups (such as isonitrile, dichloroimine, isocyanate, and halogenated functional groups) are frequently found in marine metabolites. These facts have resulted in the production of bioactive substances with different properties than those found in terrestrial habitats. In fact, the marine environment contains a relatively untapped reservoir of bioactivity. Recent advances in genomics, metagenomics, proteomics, combinatorial biosynthesis, synthetic biology, screening methods, expression systems, bioinformatics, and the ever increasing availability of sequenced genomes provides us with more opportunities than ever in the discovery of novel bioactive compounds and biocatalysts. The combination of these advanced techniques with traditional techniques, together with the use of dereplication strategies to eliminate known compounds, provides a powerful tool in the discovery of novel marine bioactive compounds. This review outlines and discusses the emerging strategies for the biodiscovery of these bioactive compounds.

Reprinted from *Mar. Drugs*. Cite as: Rocha-Martin, J.; Harrington, C.; Dobson, A.D.W.; O'Gara, F. Emerging Strategies and Integrated Systems Microbiology Technologies for Biodiscovery of Marine Bioactive Compounds. *Mar. Drugs* **2014**, *12*, 3516–3559.

1. Introduction

The marine habitat continues to be a source of unique natural products used for pharmaceutical and biotechnological applications [1]. In fact, the Roman philosopher Plinius first described the use of marine natural organisms such as sponges in medicinal applications, such as for the treatment of wounds, sunstroke and infections, around 2000 years ago [2]. More than 20,000 structurally diverse marine natural products have been isolated from ocean life forms such as sponges, ascidians, aplysia, algae, corals, bryozoan, worms, sea-hares, sea-cucumbers, fish species and microorganisms (Tables 1 and 2) [3,4]. Marine microorganisms continue to be a major focus of many natural product research efforts, with a 10% increase in the number of compounds reported from 2011 to 2012 [4]. More than 70% of the Earth's surface is covered by the ocean which contains a vast collection of diverse microbial communities, all interacting with each other and with the environment around them. In fact, it is estimated that the ocean contains the highest percentage of prokaryotic cells on Earth, with a reported 3.67×10^{30} cells [5]. It is believed that specific physiochemical properties of the marine environment, such as pressure, temperature, pH, osmolarity, and uncommon functional groups (such as isonitrile, dichloroimine, isocyanate, and

halogenated functional groups) may result in the production of bioactive substances with different properties from those found in terrestrial habitats (Tables 1 and 2) [3,6,7].

Table 1. Examples of marine bioactive compounds or derivatives approved by U.S. Food and Drug Administration (FDA) or in clinical trial with a bacterium predicted biosynthetic cluster. Sources: [3,8,9].

Compounds	Natural Product or Derivative	Collected Source Organism	Activity	Clinical Status
Salinosporamide A (Marizomib)	Natural product	Bacterium	Antitumor	Phase I
Plitidepsin (Aplidin)	Natural product	Tunicate	Antitumor	Phase III
Bryostatin 1	Natural product	Bacterium	Antitumor/ Anti-Alzheimer	Phase II
Cytarabine	Derivative	Sponge	Antitumor	Approved
Vidarabine	Derivative	Sponge	Antiviral	Approved
Eribulin Mesylate	Derivative	Sponge	Antitumor	Approved
Trabectidin (ET-743)	Natural product	Tunicate	Antitumor	EU approved

The marine environment can also be considered relatively unexplored in relation to the presence of enzymatic activities which can be found. Moreover, a marine enzyme may carry more novel chemical and stereochemical properties than those found in terrestrial environments [7]. Marine microorganisms are considered to be the primary source of marine enzymes. In particular, there is a huge interest in extremophiles, as the robustness of their biocatalysts have allowed them to adapt in order to survive and indeed thrive in extreme ecological niches such as in high or low temperatures, extremes of pH, high salt concentrations and high pressure. These characteristics, along with substrate specificity, are evolved properties that are linked to the metabolic functions of the enzymes and to the ecological asset related to natural sources [7]. This biodiversity has greatly increased interest in this field.

Sponges are the dominant source of novel natural products in the marine environment. In fact, more novel compounds are identified per year from marine sponges than from any other invertebrate phylum [10]. In a recent review by Hu *et al.* [11], approx. 3500 (out of 12,000) novel marine natural products were identified from marine sponges (such as novel anti-inflammatory agents, anticancer agents and antibiotics) between 1985 and 2008, which further emphasizes their importance in drug discovery and bio-prospecting [11]. Sponges are believed to be highly complex selective feeders that house a dense and diverse arsenal of symbiotic bacteria (bacterial phyla such as Actinobacteria, Acidobacteria, Chloroflexi, Planctomycetes, Proteobacteria, Nitrospira, Cyanobacteria, Bacteriodetes, Verrucomicrobia and Poribacteria), archea and unicellular Eukaryotes within their mesohyl tissue [12]. Fungi and microalgae are also known to inhabit and form symbiotic relationships with marine sponges [13]. These symbiotic microorganisms can represent approximately 35%–40% of the total sponge volume, densities which are much higher than the surrounding sea water [14]. As sessile organisms, sponges rely on a barrage of chemical entities,

generally produced by their associated microorganisms, to defend against disease and to gain a competitive advantage within the marine ecosystem [12].

Table 2. Examples of recently identified biocatalysts from marine environment.

Enzyme	Source	Screening Technologies	Reference
Laccase	Metagenome	Sequence-based	[15]
Esterase	Metagenome	Function-based	[16]
Fumarase	Metagenome	Sequence-based	[17]
α-amilase	*Bacillus subtilis* S8–18	Function-based	[18]
Glycoside hydrolase	Metagenome	Function-based	[19]
Baeyer-Villiger monooxigenase	*Stenotrophomonas maltophila* PML168	Function-based	[20]
Cellulase	*Marinimicrobium* sp.	Function-based	[21]
Dehalogenase	*Pseudomonas stutzeri* DEH130	Function-based	[22]
Aldehyde reductase	*Oceanospirillum* sp.	Genome-based	[23]
Lipase	*Bacillus smithii* BTMS11	Function-based	[24]
Dehalogenase	*Psycromonas ingrahamii*	Genome-based	[25]
Xylanase	*Streptomyces viridochromogenes*	Function-based	[26]

In this review, strategies for the discovery of novel marine bioactive compounds are discussed, in particular, how modern molecular biology approaches ("omic" approaches) can be integrated with microbiology techniques to provide new and better options for the mining of novel bioactive compounds and enzymes from marine bacteria.

2. Culture Dependent and Independent Isolation of Marine Microorganisms

2.1. Culture Dependent Analysis of Structure and Function of Marine Microbial Communities

Isolation and cultivation of a novel marine microorganism presents a bottleneck in the discovery of new marine natural products. In many natural environments, including the marine environment, bacterial numbers estimated by direct counts using microscopic techniques are generally several orders of magnitude higher than estimations by Colony-Forming Units (CFUs) using standard culture techniques. Only between 0.001% and 2% of bacterial cells can form colonies by conventional plate cultivation due to the large number of "Viable But Not Culturable" (VBNC) strains [27]. This is therefore the major limitation of culture dependent techniques [28].

In recent years, however, huge improvements have been made in the production of both culture media and cultivation procedures. These have been devised to mimic natural environments in terms of nutrients (composition and concentration), pressure, pH, oxygen gradient, *etc.* to maximize the cultivable fraction of microbial communities [29–34]. With these improvements, some previously VBNC species can now be grown by the refinement of classical approaches or by the use of advanced techniques (e.g., High Throughput Screening (HTS), diffusion chamber system, encapsulation method, soil substrate membrane system, filtration method, density-gradient

centrifugation, extinction dilution and Fluorescence-Activated Cell Sorting (FACS)), which are discussed in detail in several published reviews, focused on this topic [35–38].

2.2. Culture Independent Analysis of Structure and Function of Marine Microbial Communities

In the past, the identification of the number of bacteria within a sample was completed using standard microscopy. However, recent advances in DNA/RNA-based techniques and sequence technologies have allowed for the identification and characterization of the diversity and function of bacteria within a microbial community without the use of laborious microscopy techniques [39]. Thanks to these advances, over the last few decades, tremendous progress has been made in the field of microbial ecology. These techniques have been classified into two major categories: partial community analysis approaches and whole community analysis approaches (Figure 1) [39].

2.2.1. Partial Community Analysis Approaches

Partial community analysis approaches generally involve polymerase chain reaction (PCR)-based methods where total DNA/RNA extracted from an environmental sample is used in the characterization of microorganisms. Clone library construction is the most widely used method to analyze PCR products amplified from an environmental sample [40–43]. Using this technique, the bacterial communities in three sponges—namely *Hymeniacidon perlevis*, *Ophlitaspongia papilla* and *Polymastia penicillus*—from the Atlantic coast of Portugal were characterized, confirming a unique and diverse microbial community from 10 different bacterial phyla [42]. Likewise, this method was used in the seasonal characterization of the bacterial community of the Irish coastal water sponge *Hymeniacidon perlevis*, with three bacterial phyla detected in summer, and four detected in spring [44].

Genetic fingerprinting—another technique commonly used in partial community analysis—generates a profile of a microbial community based on the direct analysis of PCR products amplified from environmental DNA, generally using 16S rRNA gene analysis [45]. These techniques include DGGE (denaturing-gradient gel electrophoresis)/TTGE (temperature-gradient gel electrophoresis) [46], SSCP (Single-Strand Conformation Polymorphism), RAPD (Random Amplified Polymorphic DNA) [47,48], ARDRA (Amplified Ribosomal DNA Restriction Analysis) [49], T-RFLP (Terminal Restriction Fragment Length Polymorphism) [50], LH-PCR (Length Heterogeneity PCR) and RISA (Ribosomal Intergenic Spacer Analysis) (Figure 1) [51,52].

To increase the throughput of the detection of microorganisms within complex samples, DNA microarrays can be used in parallel for the detection of multiple species. DNA microarrays used in microbial ecology can be classified into two groups depending on the probes used: (1) 16S rRNA gene microarrays [40,53,54]; and (2) functional gene arrays (FGA) to detect specific metabolic groups of bacteria [54,55].

RT-PCR (Real Time-PCR) (also known as qPCR (Quantitative-PCR)) has also been applied to quantify functional genes within the environment [56,57].

Figure 1. Culture independent analysis of structure and function of marine microbial communities.

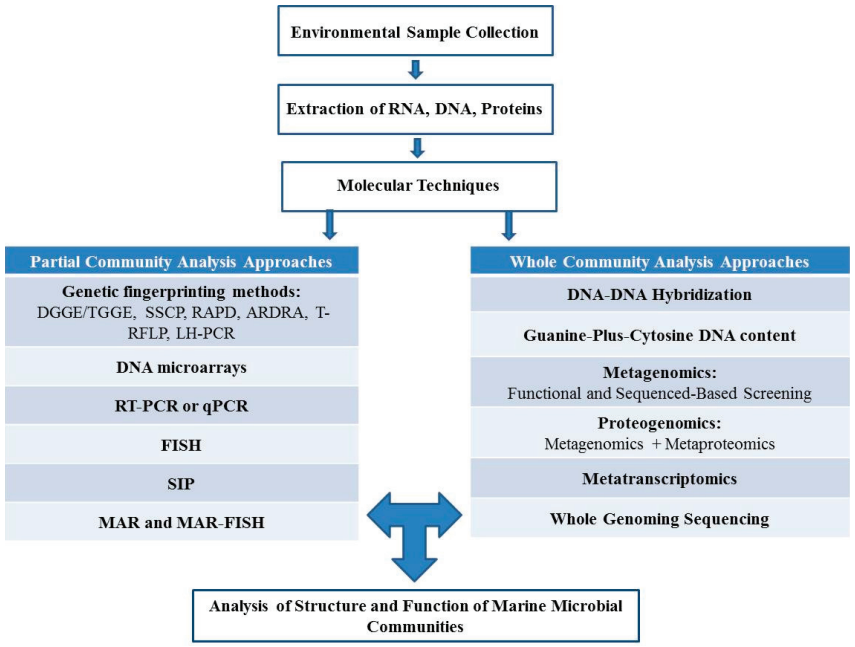

Fluorescence *in situ* hybridization (FISH) has enabled the identification of bacterial taxa and their spatial distribution [58–60]. In FISH analysis, probes are designed to target a particular 16S rRNA gene within a sample. Sequence analysis of 16S rRNA genes is commonly used in microbial ecological studies. However, despite its highly conserved nature, the 16S rRNA gene does not provide sufficient resolution at species and strain level [61]. Another drawback of FISH analysis is that, although bacterial cell numbers can be estimated using this approach, non-viable cells are still included and hence results can be misleading [62].

RNA extracted from environmental samples provides more valuable information than DNA in revealing active microbial communities *versus* dormant microbial communities [63]. This is due to the fact that rRNA and mRNA are considered to be indicators of functionally active microbial populations. The amount of rRNA in a cell is approximately correlated with the growth activity of bacteria, and the mRNA of functional genes allows the detection and identification of bacteria expressing key enzymatic activities under determined conditions [64]. The comparative and quantitative analysis of expressed rRNA and key enzymatic genes can be useful in obtaining information about bacterial groups responsible for processes such as methane oxidation, denitrification and nitrification [63].

More advanced partial community analysis approaches include stable isotope probing (SIP) [65,66], where active microbial communities that utilize the labeled biomolecules (e.g., DNA, RNA, phospholipid fatty acids) during growth incorporate isotopes within their biomass. Subsequently, the labeled biomolecules are separated from their biomass by different biochemical methods, and the phylogenetic identity of microorganisms metabolizing the substrate can be established using molecular techniques. SIP can be combined with microarray technology for monitoring the

substrate uptake profiles and establishing the taxonomic identities of active microbial communities [67]. Other techniques, such as microautoradiography (MAR) rely on the fact that metabolically active cells utilizing radiolabeled substrate can be visualized by exposure to radiation-sensitive silver halide emulsion [60]. The combination of MAR with FISH (MAR–FISH) allows the simultaneous phylogenetic identification of active cells that consume the radioactive substrate [68].

2.2.2. Whole Community Analysis Approaches

Whole community analysis approaches offer a more comprehensive view of the genetic diversity within a community compared to PCR-based molecular approaches, which target only a single or a few genes [39]. These approaches attempt to analyze all the genetic information present in total DNA extracted from an environmental sample or pure culture. The techniques in question include DNA-DNA hybridization kinetics, guanine-plus-cytosine (G + C) DNA content, metagenomics and whole-microbial genome sequencing as well as emerging "omics" technologies which will be discussed later.

In DNA–DNA hybridization, the total DNA extracted from an environmental sample (eDNA) is denatured and subsequently incubated under conditions that allow hybridization to occur. The rate of DNA hybridization is correlated with the genomic diversity present in the sample [69].

Another technique known as guanine-plus-cytosine (G + C) is based on the separation of bacterial groups based on the varying G + C content of their DNA [70]. Total community DNA is physically separated (by density-gradient centrifugation) into highly purified fractions, each representing a specific percentage G + C content that can be analyzed by additional molecular techniques such as DGGE/ARDRA to better assess total community diversity [71].

Through metagenomic tools, we can analyze the microbial diversity of an environmental sample, bypassing the need for a culture based approach and thus allowing the study of VBNC in the laboratory [72]. Metagenomic library construction involves the following steps: isolation of eDNA, shotgun cloning of random DNA fragments into a suitable vector, transformation of the clones into a host bacterium and screening for positive clones. Metagenomic libraries can be screened either by sequence-driven metagenomic analysis that involves massive high-throughput sequencing, or by functional screening of expressed phenotypes. High throughput screening (HTS) of large libraries enables the identification of individual clones containing regions of DNA encoding potentially novel genetic clusters. PCR amplification of the DNA segment within a specific clone then allows for the identification of the gene responsible for the observed phenotype. In depth analyses of the bacterial populations associated with marine sponges have been completed using metagenomic analysis. These studies have identified a large amount of species diversity within marine samples [73,74]. More recently, the emergence and development of the Next Generation Sequencing (NGS) platforms (454 from Roche, SoLiD from ABI or Solexa from Illumina) has helped to improve the quality and speed of the processor DNA [75]. This technology, for example, has facilitated the generation of an exponential number of sequencing reads from metagenomic DNA samples and has enabled the identification of members of the "rare-biosphere" [76]. As the major drawback to the metagenomic approach is the lack of reference genomes and sequences, the

vast increase in data and tools now becoming available should gradually minimize this problem [77]. Another problem frequently encountered in metagenomic studies is the availability of suitable hosts for the heterologous expression of these unknown DNA sequences in order to ascertain the maximum information from functional metagenomic analyses [77]. Once the sequences are obtained, they are aligned and assembled into finished sequences using specialized computer programs such as MEGAN (MEtaGenome ANalyzer) [78]. These sequences can be annotated into open reading frames (ORFs) to predict the encoded proteins (functions), using web-based programs such as Rapid Annotation using Subsystem Technology (RAST) [79,80]. The assignment of the taxonomic status to these sequences requires the use of softwares such as Metagenomic And rDNA Taxonomy Assigner (MARTA) [81] which is available at the MARTA web site [82], or Genomic Signature based Taxonomic Classifier (GSTaxClassifier) [83] which is available at GSTaxClassifier web site [84]. The exploration of microbial communities through whole-microbial genomes is an exhaustive and integrated approach to understand microbial ecology and function. The enormous amount of data gathered from genome sequencing programs is deposited in searchable databases that could be mined using various powerful bioinformatic tools available, such as Integrated Microbial Genomes with Microbiome Samples (IMG/M) web server [85,86] for evolutionary studies, comparative genomics, and proteomics, CAMERA (Community CyberInfrastructure for Advanced Marine Microbial Ecology Research and Analysis) [87,88], MG-RAST for phylogenetic and functional analysis of metagenomes [89,90]. For example, Microbial Genomes Resources at the National Center for Biotechnology Information (NCBI) [91] is a public database for prokaryotic genome sequencing projects. The Genome Online Database (GOLD) [92] is another database resource for comprehensive information regarding complete and ongoing genome projects, metagenomes and metadata. As of 22 February 2014, the GOLD database held 3012 completed and published genomes, 2690 bacterial and 171 archaeal genomes, and 17,564 bacterial genomes in progress [93].

2.2.3. Emerging “Omics” Technologies to Analyze the Structure and Function of Marine Microbial Communities

The emerging “omics” technologies, such as metaproteomics, proteogenomics and metatranscriptomics, have potential applications in microbial ecology in the identification of novel functional genes, new catalytic enzymes or metabolic pathways, and in the use of biomarkers to monitor the changes in a microbial community over time. Therefore, these technologies allow us to link the structure and function in microbial communities.

Metaproteomics allow us to determine which proteins were synthesized by microorganisms at the time of sample collection. This allows the reconstruction of the most important metabolic pathways and microbial processes in the configuration of an ecosystem [94]. In metaproteomics, the correct bioinformatic assignment of spectrometrically determined peptide masses of environmental origin is highly dependent on the available genomes of closely related species in the database [95]. This approach has been performed on the microbial population of the world’s oceans [96–98]. For example, Cavicchioli *et al.* [98] have examined the proteome of microbial communities in coastal Antarctic waters for differences in functional processes (transport, metabolism and energy

generation processes) occurring between summer and winter. Recently, Steen *et al.* [99] used a proteomic approach to study anaerobic methanotrophic archaea and sulfate-reducing bacteria in cold marine sediments, investigating expressed functions of the community in combination with assembled sequences from the metagenome.

In metaproteomics, protein sequences can be identified with confidence only if they have significant homology to existing proteins in available databases. However, in most environmental proteomic surveys, proteins are only distantly related to known database sequences. These limitations have been overcome by combining metaproteomic and metagenomic approaches together under the name of proteogenomics [100]. Christie-Oleza *et al.* [101] used whole-cell, Matrix-Assisted Laser Desorption/Ionization Time-Of-Flight Mass Spectrometry (MALDI-TOF MS) for the screening of natural marine isolates obtained from the coastal waters of the Western Mediterranean Sea. In order to make this technique accessible for environmental studies, they proposed to (1) define biomarkers that will always show up with an intense m/z (mass number/charge number ratio) signal in the MALDI-TOF spectra (HU, a DNA binding protein, and the ribosomal proteins, L29 and L30, were proposed as the most robust biomarkers within the Roseobacter clade) and (2) create a database with all the possible *m/z* values that these biomarkers can generate to screen new isolates. The molecular weights of the three proposed biomarkers, as for other conserved homologous proteins, vary due to sequence variation above the genus level. Therefore, the expected m/z values were calculated for each one of the known *Roseobacter* genera and tested *versus* standard sequencing methods (such as 16S rDNA sequencing). Another interesting approach, although the samples are not from marine source, is described by Singer *et al.* [102]. Here, the authors carried out metagenomic and proteogenomic analyses of a compost-derived bacterial consortium adapted to switchgrass at elevated temperatures with high levels of glycoside hydrolase activities. Singer *et al.* identified genes for lignocellulose processing and metabolic reconstructions, and suggested *Rhodothermus*, *Paenibacillus* and *Gemmatimonadetes* as key groups for degrading biomass. *Thermus* was identified as a group that may especially metabolize low molecular weight compounds. Partial genomes were also reconstructed for a number of lower abundance thermophilic *Chloroflexi* populations. These studies indicate that there are unexplored proteins (potential source of thermophilic enzymes) with important roles in bacterial lignocellulose deconstruction. A similar approach can be used in the marine environment to discover interesting biocatalysts.

Metatranscriptomics enables us to identify activities and investigate gene regulation in complex microbial communities, both for experimental studies of genetically manipulated systems and for descriptive studies of gene expression, without the necessity of presupposing which genes should be targeted [103–105]. Thus, metatranscriptomics is particularly suitable for measuring changes in gene expression and regulation with respect to changing environmental conditions. Oruga *et al.* [103] constructed two libraries from samples of marine microorganisms taken from Hiroshima bay in Japan. Functional analysis of genes revealed that a small number of gene groups, namely ribosomal RNA genes and chloroplast genes, were dominant in both libraries. Taxonomic distribution analysis of the libraries suggests that Stramenopiles form a major taxon that includes diatoms. The combination of metagenomic and metatranscriptomic approaches has proven to be an effective

strategy in deciphering the phylogenetic composition, and metabolic approaches have proven efficacious in deciphering the phylogenetic composition, and the metabolic pathways of marine microbial communities [105–107]. Here, the metagenomic approach provides information on the metabolic potential of a microbial community and the taxonomic composition, while the metatranscriptomic approach provides information about the actual metabolic activities of the community at a concrete place and time, and how those activities change in response to biotic interactions or environmental forces. For example, in a recent study, using coupled metagenomic and metatranscriptomic analysis of the microbial communities in the deep-sea water of the North Pacific Ocean [107], it was determined that, within the prokaryotic community, bacteria are dominant over archaea in both metagenomic and metatranscriptomic data pools. On one hand, the main compositional change in prokaryotic communities in the deep-sea water, compared with the reference Global Ocean Sampling Expedition (GOS) surface water, was the emergence of the archaeal phyla Crenarchaeota, Euryarchaeota, Thaumarchaeota, bacterial phyla Actinobacteria, Firmicutes, and bacterial sub-phyla Betaproteobacteria, Deltaproteobacteria, and Gammaproteobacteria. On the other hand, decreased levels of the bacterial phyla Alphaproteobacteria and Bacteroidetes were observed. Photosynthetic Cyanobacteria were present in all four metagenomic libraries and two metatranscriptomic libraries studied. Functional analysis indicated that the groups with adaptive advantages against high pressure, low nutrient concentration and multidrug resistance to antimicrobials increase their presence in the deep-sea water. All these adaptations are indicative of a defensive lifestyle [107].

2.3. Culture Dependent and Independent Analysis. Combined or Separately?

The limitations of both strategies are well known (involving the isolation and cultivation of a novel microorganism in the case of culture methods, and the DNA extraction and PCR efficiency in the case of independent analysis), however, numerous studies in the literature have overcome this by combining the use of both culture dependent and independent approaches in order to strengthen their results [108–112]. For example, the microbiota of the marine demosponge *Crambe crambe* was examined using these combined cultivation-dependent and cultivation-independent molecular approaches [109]. Authors found a low microbial diversity, which is dominated by a thus far uncharacterized bacterium belonging to a betaproteobacterial clade that is specific to sponges and corals. The most frequently isolated genus of 107 isolated from three *C. crambe* individuals was *Pseudovibrio*, followed by *Microbulbifer*, *Bacillus* and *Ruegeri*. Phylogenetic analysis based on 16S rRNA gene sequence was then used to determine the relative abundance of these isolates to avoid cultivation bias. These analyses showed that *Pseudovibrio* spp., *Microbulbifer* spp., *Ruegeria* spp. isolated were closely related to microorganisms previously isolated from marine sponges and other marine invertebrates by cultivation dependent and independent methods. Each 16S rRNA gene sequence obtained from the isolates was compared to pyrosequencing libraries generated. This comparison revealed that only a low number of the isolates (around 0.4% of the total microbiota) were also detected in the 16S rRNA gene pyrosequencing libraries, while others were absent. One exception was *Microbulbifer* spp. isolates, which were present in a high number of pyrosequencing reads only in one *C. crambe* individual and absent in the other individual. The fact

that they were found in relatively high numbers in the individual from which it was isolated shows a certain degree of overlap between cultivation dependent and independent approaches. *Pseudovibrio*, which was the most frequently isolated genus, was detected in only very low numbers in both 16S rRNA gene sequence datasets. Öztürk *et al.* suggested that the potential production of antibacterial compounds by *Pseudovibrio* spp. might be one of the reasons why they overgrow in enrichment cultures.

On the other hand, a study of hydrocarbonoclastic bacteria in various oily habitats in Kuwait by Al-Awadhi *et al.* [108] showed that bacterial identities varied dramatically depending on the analytical approach used. In this work, the results obtained by molecular analysis were compared with the results obtained by culture-dependent analysis of a previous study [113]. In contrast to the culture-dependent technique, primers used in the molecular analysis preferentially amplified the 16S rDNA of hydrocarbonoclastic bacteria in the total environmental genomic DNA of all the studied samples. On the other hand, molecular analysis failed to reveal members of the phylum *Actinobacteria*, which conversely were identified via the culture-based approach. In view of these results, the authors recommended that the two analytical approaches should be used simultaneously because their combined results would reflect the bacterial community composition more precisely than either of them could do alone.

Moreover, even genomic analysis has been used to guide cultivation efforts. For example, in a study performed by Tripp *et al.*, the genomic analysis of the SAR11 α-proteobacterial clade showed that the clade was deficient in assimilatory sulphate reduction genes [114]. Therefore, the complementary use of cultivation-dependent and cultivation-independent approaches would provide a more robust screening strategy. Molecular techniques that allow us to bypass the need for isolation and cultivation are highly desirable for in depth characterization of environmental microbial communities. However, culture dependent techniques provide more information about the physiological and metabolic characteristics of bacteria and their communities, and their responses to environmental changes.

3. Strategies for Marine Natural Compounds Discovery from Marine Microbial Communities

Different screenings approaches have been exploited in the identification of novel natural compounds including conventional screening, genomics, metagenomics, combinatorial biosynthesis and synthetic biology.

3.1. Conventional Screening Methods: Bioactivity-Guided Screening

Bioactivity screening is based on the direct detection of the activity (e.g., antibacterial, antifungal, antitumor, antiviral activity) using the culture supernatant or extract of cell pellet [115–119]. In one particular study, Tong *et al.* [115] collected 38 microbial extracts from Hawaiian coastal waters, which were then evaluated for their antiviral activity against four mammalian viruses, namely herpes simplex virus type one (HSV-1), vesicular stomatitis virus (VSV), vaccinia virus and poliovirus type one (poliovirus-1) using an *in vitro* cell culture assay. Nine of these microbial extracts showed antiviral activity, and three of the nine showed significant activity against the

enveloped viruses. In this manner, the secosteroid 5α(*H*),17α(*H*),(20*R*)-beta-acetoxyergost-8(14)-ene was identified as a novel bioactive compound in these extracts.

Dalisay and coworkers [120] investigated marine sediments collected in the temperate cold waters of British Columbia, Canada, as a valuable source of novel groups of marine-derived *Streptomyces* with antimicrobial activities. They performed culture dependent isolation from 49 marine sediments samples and obtained 186 *Streptomyces* isolates. Twenty-five percent of these isolates exhibited antimicrobial activity. Phylogenetic analyses of these isolates revealed four different clusters, with one in particular representing a novel species. Chemical analyses revealed structurally diverse secondary metabolites produced by marine-derived *Streptomyces*, including four new antibacterial novobiocin analogues. They conducted structure-activity relationship studies of these novobiocin analogues against methicillin-resistant *Staphylococcus aureus* (MRSA). This study revealed the importance of carbamoyl and OMe moieties at positions 3′ and 4′ of novobiose as well as the hydrogen substituent at position 5 of hydroxybenzoate ring for the anti-MRSA activity. In another interesting approach, Sanchez *et al.* [119] examined six species of fish through a combination of dissection and culture-dependent evaluation of intestinal microbial communities. Using a specific enrichment medium designed to isolate marine *Actinobacteria*, Sanchez and coworkers found three main clades that showed taxonomic divergence from known strains. Furthermore, several of these strains have been previously described as nonculturable. Microbial extracts from these strains exhibited a wide range of activities against Gram-negative, Gram-positive human pathogens, and several fish pathogens. Exploration of these extracts has identified the novel bioactive lipid sebastenoic acid as an anti-microbial agent, with activity against *S. aureus*, *Enterococcus faecium*, *Bacillus subtilis*, and *Vibrio mimicus*.

The repeated discovery of known compounds is a major limitation of existing assay methods, hence it is necessary not only to increase the availability of novel techniques to maximize the discovery of new compounds, but also to utilize dereplication strategies to avoid the discovery of known compounds. These strategies include the generation of antibiotic resistance markers and chemical profile analysis based on LC-NMR, LC-MS and HPLC-UV [121].

3.2. Genome-Guided Bioprospecting

Genomic sequencing of microorganisms in recent years has unveiled unprecedented insights into the biosynthetic potential of microorganisms, and thus the discovery of bioactive compounds has entered into the new postgenomic era. In recent years, the sequence data of microorganisms has been compiled into online databases such as Genomes On Line Database [92]. The development of the Microbial Genome Sequencing Project resulted in the sequence, assembly and annotation of 182 marine bacterial genomes, which are available at [122]. Due to these advances in bioinformatics, it is now possible to rapidly identify the gene clusters of bioactive compounds and predict their chemical structure *in silico* based on genomic information. For example, the genome sequencing of *Streptomyces griseus* IFO 13350 revealed 34 biosynthetic gene clusters involved in the biosynthesis of unknown or known secondary metabolites [123].

Figure 2. How AntiSMASH works. AntiSMASH is used for the detection of secondary metabolites. Abbreviations: pHMMs library: profile hidden Markov models composed of protein sequences of experimentally characterized biosynthetic enzymes; smCOGs: secondary metabolite-specific clusters of orthologous groups.

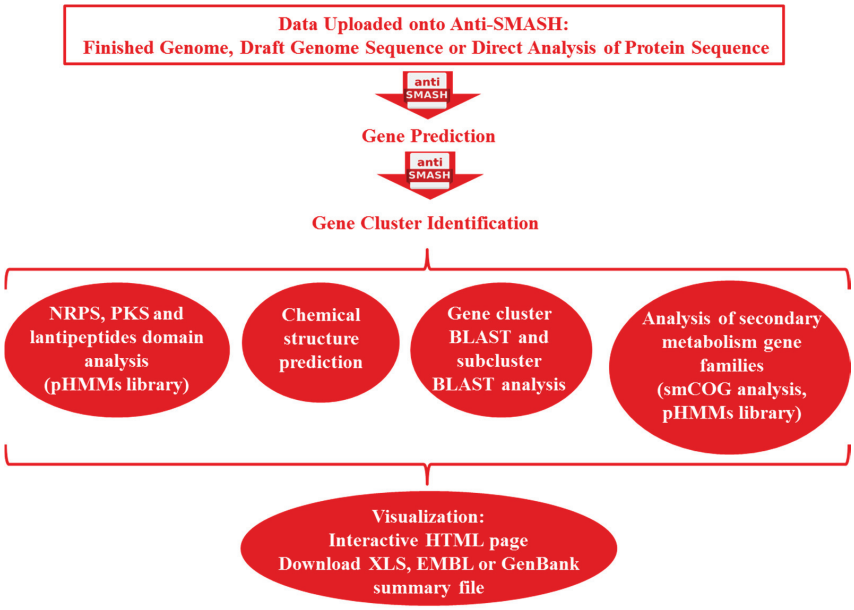

Along with advances in bioinformatics, genome sequencing has made it possible to rapidly identify the gene cluster of bioactive compounds and *in silico* predict their chemical structure based on genomics information. Development of software such as Antibiotics & Secondary Metabolite Analysis SHell (antiSMASH) (Figure 2), which allows the user to efficiently detect secondary metabolite gene clusters in the genomes of bacteria and fungi, has been a significant help to researchers [124,125]. AntiSMASH allows for the detection of biosynthetic gene clusters of secondary metabolites such as type I, II and III PolyKetides (PKs), Non-Ribosomal Peptides (NRPs), phosphoglycolipids, oligosaccharide antibiotics, phenazines, thiopeptides, homoserine lactones, phosphanates, furans, terpenes, ectoines, bacteriocins, lantibiotics, nucleosides, aminoglucosydes, aminocumarins amongst others. AntiSMASH also has the ability to partially predict types of compounds that can be produced if the gene cluster is completely functional [125].

Other useful bioinformatics tools for analyzing sequence data include: Bacteriocin Genome Mining Tool 3 (BAGEL3) for the detection and annotation of bacteriocin and ribosomally synthesized and posttranslationally modified peptides gene clusters [126,127]; Natural Product Domain Seeker (NaPDoS) for phylogenetic analysis of PoliKetyde Synthase (PKS) ketoreductases and Non-Ribosomal Peptides Synthase (NRPS) domains from DNA or amino acid sequence data [128]; NP searcher for the detection and annotation of PKS and NRPS gene clusters [129,130]; PKSIIIpred for the prediction of PKS and NRPS structures [131,132]; Structure-Based Sequence Analysis of PKS (SBSPKS) for detection and annotation of PKS and NRPS gene clusters and

prediction of substrate specificity, identification of key PKS/NRPS amino acid residues, and 3D modelling of PKS modules [133,134].

Genome-guided strategies have been applied to the discovery of secondary metabolites such as PKs, NRPs and PK-NRP hybrids. These secondary metabolites are biosynthesized by large multisynthase complexes [135,136]. The genome sequence of the marine actinomycete, *Salinispora tropica*, reported by Udwary *et al.* [137] revealed a complex secondary metabolome. Bioinformatics analysis showed that a large percentage of its genome (almost 10%) was responsible for the biosynthesis of natural products, such as genes encoding for PKS and/or NRPS. Particularly, *S. tropica* was shown to produce a potent anticancer PK-NRP hybrid, salinosporamide A. After bioinformatic analysis predicted the structure of this PK-derived natural product, a polyene macrolactam with the predicted structure was isolated. A detailed overview of the biochemistry of PK pathways is referred to in other reviews [128,138,139]. In a publication by Zhang *et al.*, several secondary metabolite gene clusters were identified from the sequenced genome of *Streptomyces* sp. W007 [140]. One of these gene clusters indicated that *Streptomyces* sp. W007 may produce aromatic PK of angucyclinone antibiotics. In this way, 3-hydroxy-1-keto-3-methyl-8-methoxy-1,2,3,4-tetrahydro-benz[α]anthracene and kiamycin were isolated from fermentation extracts of *Streptomyces* sp. W007. Both secondary metabolites showed potent cytotoxicity against human cancer cell lines [140].

The cryptic or silent pathways, in which the putative natural product are overlooked under standard culture methods and detection conditions, are attracting the attention of the researchers as they present new opportunities for the discovery of novel bioactive compounds [141]. Genome sequencing has allowed the identification of cryptic genes in *Streptomycetes* and other microorganisms [141]. By using different strategies, it has been possible to determine the structures and bioactivities of the encoded molecules. This includes the selection for mutations in genes that enhance transcription and translation, overexpression or disruption of regulatory genes, modification of the culture medium, and overexpression of an entire biosynthetic gene cluster, gene cassettes or single cryptic genes in heterologous hosts [142]. Some examples are the biosynthesis of antibiotics, such as polyeneoic acid amide, 4-*Z*-annimycin, 4-*E*-annimycin by *S.calvus* [142], and enediynes by *Streptomyces coelicolor* and *Streptomyces avermitilis* [141].

3.3. Gene-Guided Bioprospecting

Gene-guided screening has been developed towards target genes associated with the biosynthetic pathways of bioactive compounds, such as those associated with the production of PKS [117,118], NRPS [117,118], bacteriocins [143] and dTDP-glucose-4,6-dehydratase [144]. For example, Wu *et al.* [144] reported the isolation, structure, and biological activities of two new 6-deoxyglycosidic elaiophylin antibiotics. PCR-based genetic screening targeting the dTDP-glucose-4,6-dehydratase gene revealed that a marine sediment derived strain, *Streptomyces* sp. 7-145, had the potential to produce glycosidic antibiotics. Guided by the PCR results, chemical investigation of one of the strains, *Streptomyces* sp. 7-145, led to the isolation and characterization of 11′,12′-dehydroelaiophylin and 11,11′-*O*-dimethyl-14′-deethyl-14′-methylelaiophylin. The

former showed antibacterial activities against a number of drug-resistant pathogens, including methicillin-resistant *S. aureus* (MRSA) and vancomycin-resistant enterococci (VRE) strains.

Ansamycins are a family of macrolactams that are synthesized by type I PKS using 3-amino-5-hydroxybenzoic acid (AHBA) as the starter unit. Most members of the family have strong antimicrobial, antifungal, anticancer and/or antiviral activities. Wang and coworkers [145], through PCR screening of AHBA synthase gene, identified 26 of these genes. A similar strategy was performed by Kalan *et al.* to identify polyether epoxidase genes, a critical tailoring enzyme involved in the biosynthesis of polyether ionophores. A total of 44 putative polyether epoxidase gene-positive strains were obtained by the PCR-based screening of 1068 actinomycetes isolated from eight different habitats [146]. Hornung *et al.* [147] used PCR screening to identify 103 novel putative halogenase genes involved in the synthesis of halometabolites from 550 randomly selected actinomycetes strains.

The screening of bacterial genome databases for genes encoding enzymes with potentially novel biochemical characteristics offers an increasingly attractive option in enzyme discovery. The most common approaches that are employed to identify enzymes in a genome are based on sequence similarity with homologs whose function is known. This is routinely performed by using either sequence–sequence comparison methods such as FASTA [148], BLAST [149], MetaGene [150], GeneMark [151] or by using profile-sequence comparison methods like PSI-BLAST [152]. This approach has been used to identified epoxide hydrolases [153], ω-transaminases [154], and nitrilases [155] among others.

The combined strategy of gene and bioactivity based screens creates a more powerful tool which allows us to obtain valuable strains with the potential to synthesize new bioactive compounds. As previously discussed, marine sponge associated bacteria have been shown to produce a cocktail of secondary metabolites [6,156]. With this in mind, a combined gene and bioactivity-based approach was used by Zhang *et al.* [157] in the identification of 15 NRPS genes from 109 bacteria obtained from four separate marine sponges. Most of the NRPS fragments identified in the study were highly diverse and potentially novel, as they displayed less than 70% sequence identity to their closest known neighbor.

3.4. Metagenomics

Metagenomics is the study of DNA from a mixed population of organisms and initially involves the cloning of either total or enriched DNA directly from the environment (eDNA) into a host that can be easily cultivated [158]. Currently, function driven analysis and sequence-driven analysis are the two main approaches used for eDNA library screening (Figure 3) [77,159]. More recently, advances in NGS technologies have allowed isolated eDNA to be sequenced and analyzed directly from environmental samples (via direct eDNA sequencing or shotgun metagenomics) (Figure 3) [160,161]. This is an effective strategy to access bioactive compounds encoded by the genomes of previously uncultured microbes through introduction of eDNA into a suitable host, bypassing the laborious step of library construction. This strategy has been used in human genome project and has also aided in the identification of novel biomass-degrading enzymes from cow rumen and compost [161].

Figure 3. Metagenomic approaches for the discovery of novel biocatalysts or small molecules. (**1**) Sequence-based screening; (**2**) Functional-based screening; (**3**) Shotgun metagenomics and (**4**) Single cell genomics.

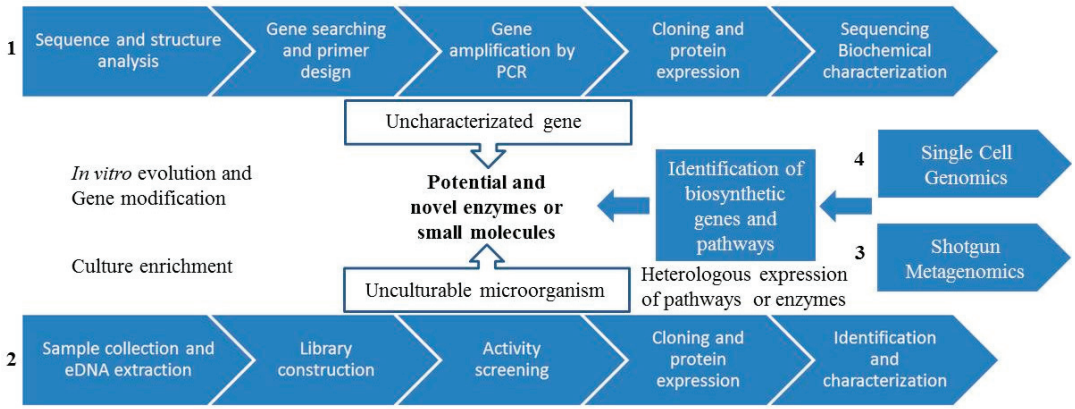

3.4.1. Metagenomics: Functional Screening

Functional screening has allowed for the identification of a large number of bioactive compounds and biosynthetic pathways including industrially important enzymes such as cellulases [21], proteases [162,163], lipases [164,165], esterases [166–168], glycoside hydrolases [19]. For example, the isolation of clone-specific metabolites produced by eDNA clones identified from bacterial top agar overlay assays has led to the characterization of a wide variety of bioactive compounds. Among these compounds can be found long-chain *N*-acyl amino acid antibiotics, a novel isonitrile functionalized indole antibiotic, antibacterial active pigments such as violacein, indigo and turbomycin [169], terragines [170], fatty acid derivatives [171], and aromatic poliketydes [172], all of which have been recovered from soil libraries. The cyclic peptides nocarmide and patellamide D have also been isolated in this manner from soil and marine sponge libraries, respectively [173,174]. Functional screening was used by Selvin *et al.* [164] for the discovery of novel lipases. In this manner, a marine metagenomic library was built from the DNA extracted of the sponge *Haliclona simulans*. This library of 48,000 clones was screened by plates supplemented with tributyrin. Using this approach, a novel lipase was identified, heterologously expressed and characterized. In another study, Robertson *et al.* [175] collected 651 environmental samples from terrestrial and aquatic microenvironments. Fragments of these samples 1–10 kb in size were cloned into genomic eDNA libraries. Authors primarily isolated inserted DNA fragments containing target genes using a culture dependent assay with adiponitrile or (*R*,*S*)-4-chloro-3-hydroxyglutaronitrile as the sole nitrogen source. Growth resulted from a clone's ability to hydrolyze the nitrile substrate, generating ammonia, which enabled the clone's growth. Positive clones were isolated and sequenced for subcloning. Finally, 137 unique nitrilase genes were expressed and characterized. A similar approach was used by Bayer *et al.* [176] to select nitrilases from metagenomic libraries (one from oil contaminated soil, two from forest soils and one from gravel from an experimentally

constructed wetland for wastewater treatment from a refinery) resulting in the isolation of *Nit1*, an aliphatic nitrilase which catalyzes dinitriles.

3.4.2. Metagenomics: Sequenced-Based Screening

Sequenced-based screening using homologous PCR or clone hybridization allows the identification of essential genetic components for cluster assembly. Sequenced-based screening has been used together with NGS technologies in the identification of PKS and NRPS clusters from a number of cultured strains [177]. Further to this, sequence-based analysis of marine metagenomic libraries has to date revealed the presence of a number of enzymes including peptidases [178], alkane hydroxylases [179], laccase [15], and a fumarase [17]. In the case of the peptidases, the Sargasso Sea Whole Genome Sequence (WGS) dataset, involving a total of 1.045 billion base pairs of metagenomic DNA sequence, with over 1.2 million protein encoding ORFs [180], was analyzed by Cotrell and coworkers [178] by using BLAST, in the identification of potential hydrolases. Following cloning and expression in the heterologous *E. coli* host, an abundance of peptidase was detected. Bayer *et al.* [181] designed degenerate PCR primers to identify $FADH_2$-dependent halogenase genes from several Caribbean and Mediterranean sponges. By sequence-based screening, three novel phylogenetically and functionally distinct halogenase gene clusters were discovered. Another example of this approach appears in a recent report on the isolation of a novel laccase from a marine microbial metagenome of the South China Sea [15]. Here, researchers used PCR primers based on the conserved copper binding sites to identify putative laccases in metagenomic DNA. Subsequently, the gene encoding the putative laccase was heterologously expressed in *E. coli*, yielding a recombinant protein that exhibited alkalescence-dependent and chloride- tolerant laccase activity.

Another interesting approach involves the *in silico* screening of NCBI sequence databases, for example, using bioinformatics, and the subsequent identification of putative genes of interest. Genes identified using this approach are usually uncharacterized, annotated as being either putative or hypothetical, or are from either environmental metagenomes or unknown organism sources. These genes are then computationally optimized for expression in suitable hosts, and the DNA is chemically synthesized, cloned into expression vectors and functionally screened in heterologous systems, such as *E. coli* or *Saccharomyces cerevisiae*. Such an approach has been successfully employed in the identification of methyl halidetransferases (MHT), with potential applications in the production of methyl halides from different biomass sources, thereby transforming renewable carbon sources into products such chemicals and liquid fuels [182]. Vergne-Vaxelaire *et al.* [155] collected sequences coding for experimentally characterized nitrilases and used these for similarity sequence analyses using UniprotKB and Genoscope databases. Candidate nitrilases were then selected according to their genome availability in the Genoscope strain collection and from a wastewater treatment plant metagenomic library. From the 290 selected candidates, 163 genes were successfully cloned and overexpressed in *Escherichia coli* BL21. While only 9.6% of these enzymes were previously annotated as predicted nitrilases, 17% were misannotated as amidohydrolases and the majority of the remainder of enzymes were only annotated as putative carbon-nitrogen hydrolases. These putative enzymes were screened against 25 nitriles chosen to

represent a wide structural diversity (such as β-hydroxylated, α-hydroxylated, β-aminated, arylaceto-, saturated and unsaturated nitriles). Out of the 125 studied nitrilases, 31 were purified and characterized for substrate specificity. With a selection of these nitrilases, the authors performed the synthesis of three building blocks (such as 4-methoxy-4-oxo-3-phenylbutanoic, 3-oxocyclopentanecarboxylic acid and 2-((cyanomethyl)aminoacetic acid)) which are difficult to synthesize using conventional organic methods. The availability of these enzymes with nitrilase activity opens the way for the improvement of their catalytic properties by genetic engineering. This collection of nitrilases could be very useful in the production of nitrile derivatives as building blocks.

3.4.3. Novel Metagenomics Approaches

In contrast with the conventional metagenomic approach, single cell genomics (Figure 3) begins with the isolation of the microbial cell fraction from an environmental sample and the separation of an individual prokaryotic cell through microfluidics, cytometry, or micromanipulation. Single cell genomics is dependent on multiple displacement amplification (MDA), which allows the generation of genomic DNA suitable for shotgun sequencing from unique microbial cells. Thereby, the entire biochemical potential of a single uncultured microbe can be evaluated from within a complex microbial community [183]. Using this approach, microbial cells are firstly singularized by FACS, sorted, and individual microbial cells are then subjected to Whole Genomic Amplification (WGA). The amplified genome can then be sequenced, and the catalytic and metabolic potential of the genome analyzed. This approach has recently been employed by the Hentschel group, who used single cell genomics to characterize Poribacteria that form part of the microbial consortia of the Mediterranean sponge *Aplysina aerophoba* [184]. Using this approach, nearly 1.6 Mb of DNA sequence was obtained from the poriobacterial genome that, following the annotation, allowed the identification of several enzymes, including several sulfatases and peptidases.

Recently, there has been a huge increase in the development of novel screening methods based on metagenomic tools. For example, Substrate-Induced Gene-Expression screening (SIGEX), metabolite-regulated screening (METREX) and a technique based on subtractive hybridization magnetic bead capture. METREX involves the introduction of metagenomic DNA into a suitable host cell containing a biosensor plasmid to detect compounds of interest, for example, compounds that induce bacterial quorum sensing. Thereby, a sensor such as green fluorescent protein (GFP) is expressed by the cell either when gene (or genes) is introduced into the cell or when an exogenous quorum-sensing inducer is applied leading to the synthesis of an inducer. This can be identified using FACS or by fluorescence microscopy [185]. SIGEX has been developed to isolate novel catabolic genes from metagenomes which are particularly difficult to obtain using traditional gene cloning methods [186]. In SIGEX, digested metagenome fragments are ligated into an operon-trap vector containing a reporter protein such as GFP, and a metagenomic library is constructed in a liquid medium by transforming a suitable cloning host. This library is screened by a SIGEX assay, and positive clones are selected by detecting the activity of a co-expressed marker, in this case, the GFP fluorescence. [187]. Another interesting approach that has been described is based on

substrate hybridization capture involving the use of magnetic beads [188]. This involves the amplification of the internal portion of the gene of interest using degenerate primers, and the subsequent immobilization of the partial gene amplicons on streptavidin-covered magnetic beads. These beads are then used as hybridization probes to target full-length genes from metagenomic DNA. This method has been used to clone novel bacterial multicopper oxidases from soil but would clearly also have use in marine metagenomic samples [189]. Another example has been described by Margassery *et al.* [190], where HTS was used to identify calcineurin inhibitors in large libraries of chemical compounds, microbial extracts and metagenomic libraries. Calcineurin is a eukaryotic calmodulin-dependent serine/threonine phosphatase type 3CA involved in several neurodegenerative diseases. There is a large amount of interest in identifying novel calcineurin inhibitors due to side-effects that occur with the long-term use of those currently available. This HTS-directed approach is based on the detection of activity of a *CDRE::lacZ* gene fusion in pMRK212 plasmid introduced into *S. cerevisiae*. A cytoplasmic calcium concentration is triggered by alkaline pH, which activates calmodulin, calcineurin and Crz1p (the main target of calcineurin in yeast). Dephosphorylation by calcineurin causes Crz1p translocation to the nucleus, where it activates transcription of target genes by binding to a promoter sequence known as the CDRE element. Expression of the *CDRE::lacZ* gene fusion can be detected using a modified enzymatic assay for the β-galactosidase. The validation of this method was carried out by the HTS of extracts of marine sponge-associated bacteria. In this way, Margassery and coworkers identified three candidate extracts with potential calcineurin inhibitor [190]. To demonstrate that calcineurin prevents the translocation of Crz1p to the nucleus, the construct *GFP::CRZ1* gene fusion was used. By fluorescence microscopy, GFP fluorescence was observed throughout the cell. This, therefore, supported the theory that calcineurin prevents the Crz1p translocation to the nucleus. Thereby, this novel HTS approach proved successful in the identification of potential calcineurin inhibitors.

3.5. Combinatorial Biosynthesis

Combinatorial biosynthesis is a technology based on the genetic manipulation of biosynthetic clusters encoding bioactive compounds. Genetic manipulation techniques used include amino acid substitution, deletion or inactivation, swapping or borrowing of genes within a module, gene fusions, and assembly of these components, with the aim of producing novel structures in order to obtain new or altered structures that would be difficult to synthesize using other methods [191]. This approach has been used mainly in multi-modular enzymes such as PKS, NRPS and hybrid PKS-NRPS. The rapid advances in microbial genome analysis have not only enabled the identification of these gene clusters, but have also provided the necessary tools for engineering the biosynthesis of novel compounds by combinatorial biosynthesis [139,191–193].

For example, Kim *et al.* obtained a barbamide biosynthetic gene cluster from the marine cyanobacterium *Moorea producen*, and subsequently heterologously expressed it in a genetically engineered strain of *S. venezuelae* DHS 2001 where the pikromycin PKS gene cluster was deleted. This approach resulted in the production of the marine natural products, 4-*O*-demethylbarbamide, a barbamide derivative [194]. Another example has been described by Doekel and coworkers for

the production of analogues of the antibiotic daptomycin [195]. The lipopeptide backbone of daptomycin is produced by three NRPS multi-synthases encoded by *dptA*, *dptBC* and *dptD* genes, which are interconnected by peptide linkers. Authors introduced mutations such as amino acid substitutions, insertions and deletions in the inter-module linkers with no negative effects on the lipopeptide production. dptD enzyme consists in two modules—one of the modules incorporates 3-methylglutamic acid ($3mGlu_{12}$) and the other incorporate kynurenine (kyn_{13}) to the daptomycin. Daptomycin was redirected to incorporate Trp and Ile/Val, in place of Kyn_{13}, as position 13 has been described as crucial for determining the antimicrobial activity of the antibiotic. In this way, hybrids dptD were constructed by fusion of $3mGlu_{12}$ to the terminal modules for Trp_{11} and Ile_{13} from CDA (Calcium Dependent Antibiotic) and A54145 NRPSs, respectively. Lipopeptide biosynthesis was restored in strain *S. roseosporus* UA378 with dptD deleted in these hybrid subunits, resulting in similar efficiency to those recombinants reconstructed to produce daptomycin. These hybrid recombinant cells produced daptomycin analogues with Trp_{13} or Ile_{13} at high efficiencies. Moreover, a recombinant dptD strain with a hybrid Kyn_{13} module synthesized a novel daptomycin analogue containing Asn_{13}.

This approach has also been used for the production of antimycins (ANTs). ANTs differ in their alkylation at C7 and acylation at C8, however, the effects of these functionalities on biological activities and associated modes of action remain unclear [196]. The *antB* gene was deleted in the ANT-producing strain *Streptomyces* sp. NRRL 2288, aiming at the construction of an engineered biosynthetic apparatus for diversity-oriented production of dilactone scaffolds *in vivo* [197]. The resulting mutant strain AL2110 failed to produce mature ANTs, but accumulated a series of C8-deacylated ANTs that vary in the alkylation at C7. Three carboxylates, chloropentanoate, cyclohexanepropanoate, and 10-undecynoate, were then fed to AL2110 strain, to examine whether naturally unavailable units could be incorporated into ANTs to increase the diversity at C7. As a result, all feedings produced new C8-deacylated ANTs [197]. Another example is the production of the fluorinated analog fluorosalinosporamide by engineering the bacterium *Salinispora tropica*. *S. tropica* has been modified by replacing the chlorinase gene *salL* by the fluorinase gene *flA* from *Streptomyces catteleya* [198]. Thereby, $salL^{-}flA^{+}$ mutant strain in the presence of inorganic fluoride induced the production of fluorosalinosporamide.

Despite the many successes of combinatorial biosynthesis, engineered biosynthetic clusters often show lower catalytic efficiency (and hence lower productivity) than the original cluster [191].

3.6. Synthetic Biology

Synthetic biology is a promising strategy to improve the production of known marine compounds or activate silent gene clusters by genetic manipulation of the biosynthetic machinery (natural or artificial) involved in the assembly of bioactive compounds [199]. This approach is based on the development of genome manipulation techniques such as hierarchical Conjugative Assembly Genome Engineering (CAGE) [200] and Multiplex Automated Genome Engineering (MAGE) [201], as well as functional characterization of abundant genetic materials (e.g., controllable regulatory elements, synthetic RNA/protein scaffolds) [202]. In addition to the efficient genome handling and transfer technologies, compatibilities between microbial hosts and

all the necessary machinery to obtain the targeted product are very important for the choice of the most suitable host. This includes the proper expression of the genes responsible for the production of the target compound, compatibility with the enzyme activity and the availability of precursors. Nowadays, synthetic biology is used for the development of microbial cell factories for bioactive compound production [203] or to synthesize gene clusters enabling *in situ* therapeutic delivery [202]. In recent years, many successful examples of bioactive compounds production with therapeutic interest through synthetic biology have been reported. Antibiotics such as aminoglycosides derivatives, which include neomycin, kanamycin and gentamicin [204], as well as other natural products like PKS [205–207] and NRPS [207] have been produced. In addition, the enzymes responsible for the production of these chemical compounds can be isolated and used as biocatalysts to synthesize bioactive compounds, their intermediates, and derivate compounds.

An interesting approach is the retrobiosynthetic method, which is based on the backward search for biosynthetic routes to a target a compound such as a bioactive compound or an enzyme. Through the implementation of a defined set of biochemical transformation rules (namely retrosynthesis algorithms, such as pathway length, favorable thermodynamic, estimate gene compatibility, estimate enzyme performance, and compound toxicity) efficient heterologous biosynthetic metabolic pathways are designed and inserted in host organisms [208]. A retrosynthetic map containing the entire metabolic network, including annotated and putative enzymatic reactions catalyzed by identified enzymes, and alternative metabolic pathways to reach the target compound can then be designed. All the necessary information to build a retrosynthetic map can be found in various databases, such as Kyoto Encyclopedia of Genes and Genomes (KEGG) which gives information about enzyme sequences and annotated reactions, and BRaunschweig ENzyme Database (BRENDA) which provides experimental enzymatic kinetic constants. All this information provides a full biosynthetic automated network for the design and production of bioactive compounds and enzymes, considering the insertion cost of each metabolic pathway based on different criteria such as gene insertion cost, expression levels and catalytic efficiency [208]. This novel approach is attracting the attention of biocatalysis [209] and is allowing the identification of previously unknown biosynthetic routes, such as some antimicrobial peptide biosynthetic routes [207].

Another novel approach that allows the transfer of a complete biosynthetic pathway into a different bacterium has been reported recently by Loeschcke and coworkers [210]. The TRansfer and EXpression system (TREX) involves the transfer an entire biosynthetic pathway to a suitable host. TREX employs conjugation for DNA transfer, randomized transposition for its chromosomal insertion, and T7 RNA polymerase for unhindered bidirectional gene expression. The TREX system consists of two cassettes, designated left and right (L-TREX and R-TREX), which contain all functional elements needed for establishing a novel biosynthetic pathway in a bacterial host. In addition, L-TREX and R-TREX cassette contain selection markers, namely tetracycline resistance gene and gentamicin resistance gene, respectively. The target gene cluster (which can be located on BAC, plasmid or cosmid) is labeled by the two TREX cassettes. The transfer of metabolic pathways can be achieved by restriction endonuclease-based cloning or more advanced techniques such as restriction enzyme-independent cloning, and recombineering techniques based on λ phage

or yeast recombinases that enable a better handling of large DNA fragments [210]. In the second step, the TREX-labeled gene cluster is transferred to a bacterial host. The origin of transfer, located into L-TREX, enables the conjugational transfer of large DNA fragments. This fact allows the efficient release of recombinant DNA molecules. In the next step, the gene cluster is inserted into the chromosomal DNA of the expression host by transposition. Finally, two T7 RNA polymerase-dependent promoters, located within the L- and R-TREX cassettes in opposite directions, allow the bidirectional expression of cluster genes regardless of their orientation. The authors constructed a TREX module, namely <L-TREX-R> to simplify the TREX labeling. This module—provided on plasmid pIC20H-RL, GenBank Accession Number: JX668229—includes both TREX cassettes where the two T7 promoters point outwards. This system has been applied to the transfer and expression in bacteria of two biosynthetic pathways responsible for the production of two secondary metabolites, prodigiosin and zeaxanthin [210]. In this way, TREX can help to identify and synthesize novel bioactive compounds.

Therefore, synthetic biology permits the user manipulate the cell biosynthetic machinery to produce unnatural metabolites, to improve the production of known compounds and to activate silent gene clusters of biosynthetic pathways. Synthetic biology is an emerging discipline that, upon further development, will play an important role in the production of marine bioactive compounds [211].

3.7. Heterologous Production of Bioactive Compounds

In order to achieve the heterologous production of novel bioactive compounds, the development of marine-derived hosts such as cyanobacteria, actinomycete, and symbiotic fungi is key. Moreover, heterologous expression of genes or entire biosynthetic gene clusters involved in the synthesis of bioactive compounds is an important strategy in the identification of the function of these genes or genes clusters [212]. Techniques such as natural product screening, compound chemical characterization, host isolation, gene cluster identification, sequencing analysis or synthesis, and metabolic and process engineering are necessary in the optimization of heterologous production [213].

Through heterologous production, compounds such as PKs in *E. coli* (6-methylsalicylic acid and 6-deoxyerythronolide B) [213,214], granaticin, epothilones A, 6-deoxyerthronolide B, medermycin, 6-methylsalicylic acid, novobiocin and several type II PK products in *Streptomyces coelicolor* [215–222], and 6-methylsalicylic acid in *S. lividans* [223] have been obtained. Also, heterologous production of NRPs and hybrid NRP-PKs compounds has been performed in *Streptomyces* spp (daptomycin and capreomycin) [224], in *E. coli* (echinomycin, yersiniabactin, tyrocidine intermediates) [225–228], *Bacillus subtilis* [213], and *Pseudomonas putida* [229]. As well as this, the heterologous production of isoprenoids (such as artemisin and taxol) has been described in *E. coli* and *S. cerivisiae*, respectively [193,213].

3.8. "Omic" Integrated Approaches to Characterize Bioactive Compounds Biosynthetic Gene Clusters and Pathways

"Omics" approaches utilize genomic, proteomic, metabolomic, and transcriptomic tools to bypass cultivation limitations by studying the collective material of organisms from environmental samples, thus enabling powerful new approaches to gene, genome, protein and metabolic pathway discovery [161]. Access to NGS and the development of bioinformatics tools is essential for the resolution of the tremendous databases generated from these technology applications. Below, we will discuss in detail case studies where integrated "omic" approaches were used successfully in the discovery and characterization of biosynthetic gene clusters and pathways.

3.8.1. Integrated Approach to Investigate the ET-743 Biosynthetic Pathway

An integrated "omic" approach was used by Rath *et al.* [230] to identify and characterize the ET-743 or trabectedin (Yondelis®) biosynthetic pathway from invertebrate-derived microbial consortia. A summary of this approach taken by Sherman *et al.* can be seen in Figure 4. ET-743 is a tetrahydroisoquinoline with strong anticancer activity isolated from the tunicate *Ecteinascidia turbinata.* This compound has been clinically approved in Europe against sarcoma and ovarian neoplasms. In this study, ET-743 was produced semi-synthetically for clinical application from fermentation-derived cyanosafracin B. Raw reads from the shotgun sequencing were assembled and subsequently filtered using BLASTX and TBLASTN to measure the relatedness of translated protein sequences to safracin and saframycin NRPS. Twenty-five presumed ET-743 biosynthetic genes were identified and annotated with proposed functions that account for all of the core NRPS genes of ET-743 using the BLASTX tool against the NCBI NR database. These results suggested that individual genes appear to be of bacterial origin (for example, lacking introns and polycistronic) and hence the gene cluster is not derived from the tunicate genome. The presence of the predicted enzymes from the sequence analysis involved in the ET-743 biosynthetic pathway was used to mine the metaproteome by mass spectrometry. ET-743 biosynthetic pathway enzymes predicted via gene cluster analysis were then searched for in the metaproteome using mass spectrometry.

16S rRNA gene amplicon library and a random shotgun fragment library for 454 pyrosequencing were prepared using this DNA. Additionally, MG-RAST was used to perform the taxonomic classification of the raw reads and of the total assembly. Results showed that ~40% of the classified sequences were of eukaryotic origin (mainly *Ciona*), and 60% were of proteobacterial origin, within which the two major populations were γ-proteobacterial and α-proteobacterial. Sequence analysis based on codon usage of two large unlinked contigs suggested that *Candidatus Endoecteinascidia frumentensis* produces the ET-743 metabolite. Finally, the expression of three key biosynthetic proteins, along with the functional analysis of these enzymes, confirmed their assigned catalytic activity in the biosynthetic pathway, enabling the direct correlation between bioactive compound, the *Etu* gene cluster, and predicted biosynthetic enzymes. Therefore, these three biosynthetic pathway enzymes were identified, and comparisons with standards suggested that ET-743 biosynthetic genes expressed in the tunicate-microbial community. These *in vitro*

findings will drive future efforts to engineer the production (via heterologous expression and synthetic biology) of the ET-743 drug and its related analogues. Moreover, this strategy provided a general approach to characterize bioactive compound biosynthetic systems from complex marine consortia.

Figure 4. An integrated approach to investigate the ET-743 biosynthetic pathway.

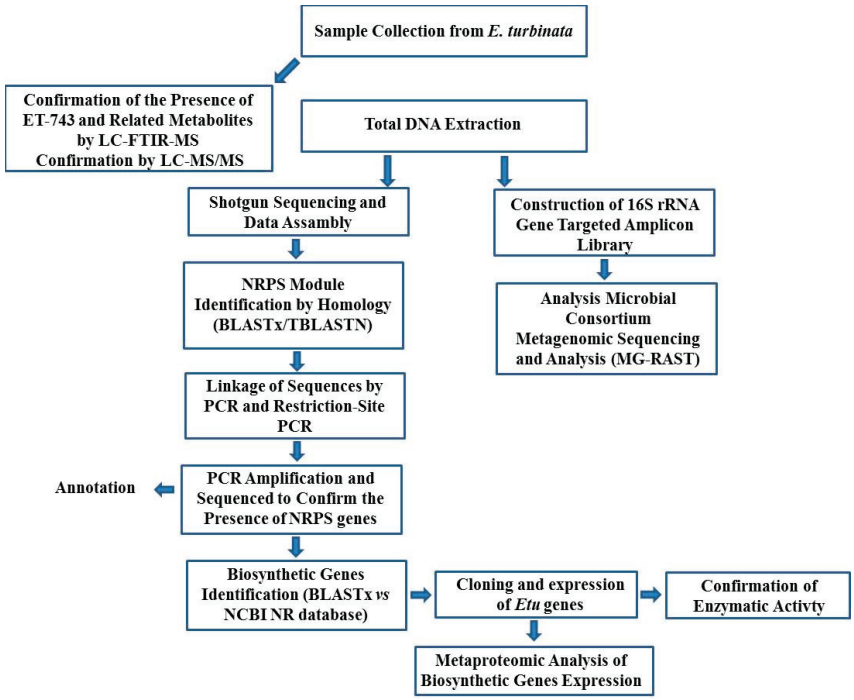

3.8.2. An Integrated Approach in the Discovery a Novel Lantibiotic from *B. subtilis* Strain Isolated from a Marine Sponge

An interesting approach has been recently used in the discovery of subtilomycin, the novel lantibiotic from *B. subtilis* MMA7 isolated from the marine sponge *Haliclona simulans* (Figure 5). This approach combined traditional analysis with modern genomic technologies [231]. Antimicrobial assays were performed with a colony overlay assay, which demonstrated activity against several bacterial strains such as marine associated Gram-negative bacteria and pathogenic strains. Conventional PCR was used to test for the presence of genes encoding bacteriocins such as subtilin, subtilosin and sublancin in *B. subtilis* MMA7. Only the presence of subtilosin was detected by PCR. However, Phelan and coworkers did not observe any differences in antimicrobial activity between the wild type and MMA7 strain after inserting a mutation in the subtilosin biosynthetic gene cluster. This result suggested that other antimicrobial compounds were being produced by this strain. In order to purify this unknown compound, the active microbial crude extract was purified by Reverse Phase High Performance Liquid Chromatography (RP-HPLC). The active fractions collected from RP-HPLC were subjected to MALDI-TOF MS, which revealed a

unique peak corresponding to a mass of 3235 Da. After a search of different antimicrobial databases, no matches were found with this molecular mass. When tested, the compound retained antimicrobial activity against indicator strains used in the initial antimicrobial assays. Primary amino acid sequence was obtained using trypsin digestion and alkylation of this peptide, followed by MALDI MS and tandem mass spectrometry analysis (MS^2). The obtained amino acid sequence was used in BLASTP and BLASTN searches against the genome of *B. subtilis* MMA7 to look for genes involved in the synthesis of this peptide. In this manner, the gene encoding the novel class I lantibiotic subtilomycin was identified by coupling functional based screening assays with an integrated "omic" approach.

Figure 5. Bioprospecting of novel natural compounds. A combined approach of traditional assays and modern genomic technologies were utilized by Phelan *et al.* to unlock the biotechnological potential of the marine sponge associated endospore-formers.

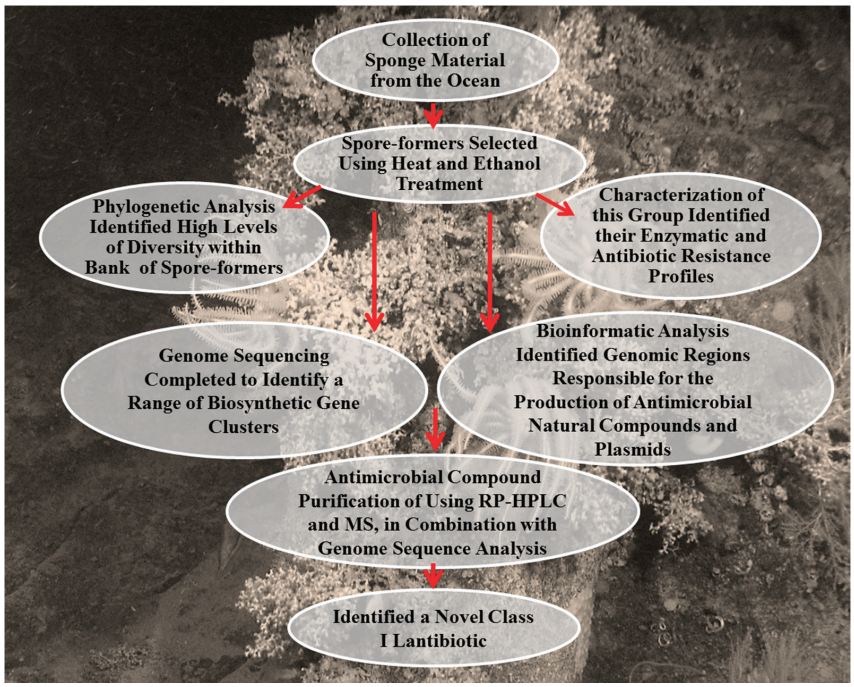

3.8.3. Integrated Approaches in the Investigation of the Biosynthetic Pathways and the Characterization of Glycosylated Bioactive Compounds

Glycosylated natural products (GNPs) are a structurally different class of molecules with important agrochemical and pharmaceutical applications [232]. Kersten and coworkers characterized the *O*- and *N*-glycosyl groups in their sugar monomers by MS^n analysis and connected the groups to their corresponding genes in secondary metabolic pathways through an MS-glycogenetic code [232]. Firstly, the extract of sequenced bacteria was analyzed by LC-MS^n to

detect the presence of GNPs. The candidate GNPs were then identified according to the peaks of extracted ion chromatograms (sugar-specific B/C-ion masses or Y/Z-ion neutral losses) in the chromatogram data. These putative GNPs were confirmed by characterization of the MS^n spectra. Subsequently, the putative GNP molecules were connected with the corresponding glycosylation genes in the microbial genome by genome mining, based on the observed sugar fragments. On the other hand, the glycogenomic approach was used to test the presence of new glycosylated compounds in *Salinispora arenicola* CNB-527 and *Streptomyces* sp. SPB74. The genome sequences of these bacteria were analyzed by antiSMASH. All the secondary metabolic gene clusters were predicted and analyzed for the presence of specific and widespread glycosylation genes, in addition to a functional prediction of glycosylation genes by BLAST. In this manner, the presence of glycosylation genes was tested in each observed MS^n candidate sugars, and the positive matches were analyzed by BLAST. The structure of these positive matches was elucidated from MS^n and genetic data. Finally, a further characterization of the purified compounds was carried out by NMR. This approach led to the rapid characterization of the anticancer agent cinerubin B and its gene cluster from *Streptomyces* sp. SPB74, and the discovery of the antibiotic arenimycin B, and its biosynthetic gene cluster from *S. arenicola* CNB-527.

Therefore, MS^n can be used in the analysis of microbial metabolic extract to identify biosynthetic building blocks. Used together with genome mining, MS^n can be aimed at a number of expressed biosynthetic pathways in one assay. In addition, combined with automated platforms like liquid chromatography-tandem mass spectrometry (LC-MS), MS^n analysis has the potential to be automated.

3.8.4. Integrated Approaches using Orthogonal Active Site Identification System (OASIS) and Proteomic Interrogation of Secondary Metabolism (PrISM)

The Orthogonal Active Site Identification System (OASIS) and Proteomic Interrogation of Secondary Metabolism (PrISM) have had a significant impact on the application of proteomic to natural products research [161].

PrISM allows for the screening of the expressed enzymes related to natural product biosynthesis [233]. In a PrISM, microbes are cultured under various conditions, and their proteomes are analyzed by MS. Expressed proteins for secondary metabolite biosynthesis are detected, which enables the biosynthetic gene cluster and the associated secondary metabolite to be discovered simultaneously. The PrISM approach was used to screen expressed NRPSs and PKSs from *Streptomyces* spp. and to identify an orphan NRPS gene cluster from *Streptomyces* sp. NRRL F-6652. Through bioinformatics analysis of the gene cluster and metabolomics analysis using MS, a new class of peptide aldehyde natural products called flavopeptins was discovered and identified as the products of the orphan gene cluster [234]. These flavopeptins are synthesized through an NRPS and contain a terminal NAD(P)H dependent reductase domain probably used for the reductive release of the peptide with a C-terminal aldehyde. Similar to other peptide aldehydes, flavopeptins showed inhibitory activities against cysteine proteases and anti-proliferative activity against multiple myeloma and lymphoma cell lines [234]. Another example of this strategy is the discovery of koramine (an NP associated with *Bacillus* species) through the PrISM method [235]

described by Evans *et al.* [235]. Evans and coworkers cloned the complete gene cluster and elucidated the biosynthesis of the novel compound, which is produced by a non-sequenced *Bacillus* sp. strain isolated from soil. The original discovery of the compound began with a proteome strategy, where microbial proteomes were scanned for expressed gene clusters. 23 unsequenced environmental isolates were cultured under nine different sets of conditions and analyzed by SDS-PAGE. Of the 23 strains, 20 showed some evidence of proteins over 150 kDa in size. These tend to be large NRPS or PKS enzymes, which often are >1300 amino acids in length. A MS analysis of direct peptide sequencing by MS^2 gave the amino acid subsequences that guided the design of PCR primers for amplification of DNA corresponding to the region between the identified peptides and the conserved core regions of NRPS adenylation domains. Eventual DNA sequencing of this >30 kb gene cluster and prediction of its functional elements led to the prediction and the detection of a new peptide natural product named koranimine. The structure of koranimine was determined using multistage MS^2, stable isotope incorporation, NMR spectroscopy, and *in vitro* enzyme reconstitution [235].

OASIS uses chemical probes that bind the active sites of NRPS and PKS enzymes allowing the enrichment of complex proteomic samples before being applied to MS^2 [236]. These enzymes utilize a small carrier protein (CP) to covalently bond activated monomers and intermediates directly to the enzymes throughout the biosynthetic process domain. The site of this covalent attachment is at the terminal thiol of the 4′-phosphopantetheine (PPant) prosthetic group. The PPant posttranslational modification has only been observed within PKS, NRPS and related enzymes, and their activities can be detected through labeling approaches (e.g., enzyme inhibitors labeled with fluorescence) or observation of a unique fragmentation during MS^2. This approach has been used to obtain a profile of PKS and NRPS enzymes present in *Bacillus subtilis* [237].

4. Dereplication Strategies

It is of the utmost importance that studies in the discovery of novel marine bioactive compounds, such as antimicrobial compounds, should be performed in parallel with a defined dereplication strategy to screen for previously known bioactive compounds. Dereplication itself is the process of screening samples for the presence of active compounds which have already been studied, thereby eliminating them from consideration. The identification of known molecules early in the marine bioactive compound discovery process minimizes time, effort and cost (Figure 6) [121,238]. Dereplication processes are generally achieved through morphological comparison of obtained colonies on different solid media, and/or using molecular methods such as 16S-Internal Transcribed Spacer (ITS) RFLP, partial 16S rDNA sequencing, and repetitive extragenic palindromic-PCR of the BOX DNA element (BOX-PCR). While these approaches have proven to be of great utility, more modern systematics-guided methods of bioprocessing and dereplication have been developed. At present, dereplication strategies include High Performance Liquid Chromatography-Mass Spectrometry (HPLC-MS), HPLC-Nuclear Magnetic Resonance (NMR), HPLC-NMR-MS, HPLC-Solid Phase Extraction (SPE)-NMR, and Ultra High Performance Liquid Chromatography (UHPLC)-MS, or bioactivity fingerprints, such as cytological profiling or BioMAP are commonly in use [238,239]. The development of high quality libraries, composed of

marine microorganisms, provide a diverse collection of structurally distinct molecules to enhance the discovery of novel bioactive compounds, thereby improving the results of dereplication strategies [90]. MS can be used to confirm the size of different natural compounds, and their subsequent molecular weights can be compared against natural product databases. Nowadays, multiple databases are available, such as AntiBase, MarinLit, AntiMarin (which contains the combination of the compound data from AntiBase and MarinLit), Beilstein Dictionary of Natural Products, FastGroupII (available on [240]), SciFinder and BACTIBASE (available on [241]), a data repository of bacteriocin natural antimicrobial peptides [238,242–244]. Another useful tool, COMET, has been developed by Microbial Screening Technologies. COMET is a metabolite recognition software that compiles and analyzes co-metabolite patterns in natural product mixtures [245]. These resources are used to determine the novelty and proposed structure of a specific sample, thereby helping to identify the compound and ensure dereplication of previously known compounds. Despite these alternatives, the creation of an open access database of the MS spectra of known compounds would prove invaluable for researchers.

Figure 6. Example of general dereplication workflow. For example, the obtained MS spectra can be compared against natural products databases.

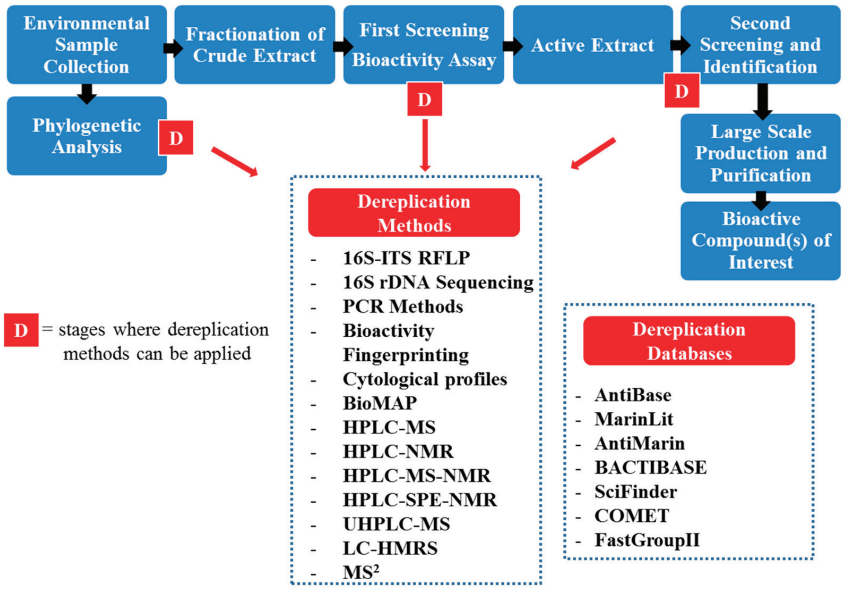

Recently, Yang *et al.* [238] and Forner *et al.* [239] used a dereplication approach involving Liquid Chromatography–High Resolution Mass Spectrometry (LC–HRMS). Only small-scale fermentation extracts are necessary to capture novel secondary metabolite production in a rapid and robust process, while minimizing the detection of undesired media components. In this way, a chemical barcode of the fermentation extract is generated. Therefore, the preprocessing of LC–HRMS data is a critical step in this study. For example, cluster analysis applied to barcoded LC–HRMS data was shown to be a sensitive and reproducible technique for the grouping of

Streptomyces isolates according to their chemical fingerprints [239]. In this study, a large library of 120 isolates of Actinomycetes was collected from three sites off the coast of Canada. Twenty-two *Streptomyces* isolates of these 120 were selected due to their close genetic relationship despite their different geographic location. These isolates were characterized using 16S rDNA sequencing combined with BOX-PCR, and 16S-ITS RFLP. Using these molecular techniques, groups were created and compared by LC-HRMS dereplication methodology. A second group of 120 isolates was submitted to the same molecular dereplication methodology and chemically dereplicated into 35 clades to further validate this approach, and using these techniques some groups showed putative novel chemistry, as barcodes showed metabolites with unique *m/z* ratios. Forner and coworkers demonstrated that the chemical diversity of produced metabolites was reproducible and provided an enhanced resolution for the discrimination of redundant microbial strains compared to present molecular dereplication techniques. Moreover, this method provides us with the ability to identify putative novel chemical compounds.

5. Conclusions

The blue technology sector is a rapidly growing area, with the market projected to exceed €3.11 billion by 2015 [246], and the global market of enzymes projected to reach $4.4 billion by 2015 [246]. The discovery of novel bioactive compounds and biocatalysts is thereby hugely important and is still presenting a major challenge to researchers. As this review has shown, there is a growing arsenal of methodologies available in the field of marine biodiscovery. In the coming years, the development of emerging "omics" strategies such direct sequencing of eDNA, single cell technologies, metaproteomic and synthetic biology (such co-selection-MAGE strategy [247]) will improve the discovery and production of these compounds. With the development of model microbial systems for heterologous expression, NGS technologies (which are becoming increasingly accessible) and bioinformatic tools, the rapid exploitation of biosynthetic gene clusters will continue to be facilitated. These emerging strategies in many cases allow us to study the biosynthetic pathway systems of organisms previously inaccessible to us by traditional methods. The combination of conventional and innovative approaches, along with the use of novel dereplication strategies will continue to provide us with essential tools in the discovery of novel marine bioactive compounds with potential applications in both medicine and industry.

Acknowledgments

This work was supported in part by grants awarded by the Science Foundation of Ireland (SSPC2 12/RC/2275, 13-TIDA-B2625, 07/IN.1/B948, 12/TIDA/B2411, 12/TIDA/B2405, 09/RFP/BMT 2350); the Department of Agriculture, Fisheries and Food (DAFF11/F/009 MabS, FIRM/RSF/CoFoRD; FIRM 08/RDC/629); the Environmental Protection Agency (EPA 2008-PhD/S-2), the Irish Research Council for Science, Engineering and Technology (PD/2011/2414; RS/2010/2413), the European Commission (FP7-PEOPLE-2013-ITN, 607786; OCEAN2012, 287589; FP7-KBBE-2012-6, CP-TP 311975; FP7-KBBE-2012-6, CP-TP-312184;

Marie Curie 256596); and the Marine Institute (Beaufort award C2CRA 2007/082); Teagasc (Walsh Fellowship 2013) and the Health Research Board (HRA/2009/146).

Conflicts of Interest

The authors declare no conflict of interest.

References

1. Houssen, W.; Jaspars, M. Isolation of marine natural products. In *Natural Products Isolation: Methods and Protocols*, 3rd ed.; Sarker, S.D., Nahar, L., Eds.; Humana Press: Clifton, NJ, USA, 2012; Volume 864, pp. 367–392.
2. Sipkema, D.; Franssen, M.R.; Osinga, R.; Tramper, J.; Wijffels, R. Marine sponges as pharmacy. *Mar. Biotechnol.* **2005**, *7*, 142–162.
3. Bharate, S.B.; Sawant, S.D.; Singh, P.P.; Vishwakarma, R.A. Kinase inhibitors of marine origin. *Chem. Rev.* **2013**, *113*, 6761–6815.
4. Blunt, J.W.; Copp, B.R.; Keyzers, R.A.; Munro, M.H.G.; Prinsep, M.R. Marine natural products. *Nat. Prod. Rep.* **2012**, *29*, 144–222.
5. Whitman, W.B.; Coleman, D.C.; Wiebe, W.J. Prokaryotes: The unseen majority. *Proc. Natl. Acad. Sci. USA* **1998**, *95*, 6578–6583.
6. Bhatnagar, I.; Kim, S.-K. Immense essence of excellence: Marine microbial bioactive compounds. *Mar. Drugs* **2010**, *8*, 2673–2701.
7. Trincone, A. Marine biocatalysts: Enzymatic features and applications. *Mar. Drugs* **2011**, *9*, 478–499.
8. Giddings, L.-A.; Newman, D. Microbial natural products: Molecular blueprints for antitumor drugs. *J. Ind. Microbiol. Biotechnol.* **2013**, *40*, 1181–1210.
9. ClinicalTrials.gov. A Service of the U.S. National Institutes of Health. Available online: http://clinicaltrials.gov/ct2/home (accessed on 21 January 2014).
10. Blunt, J.W.; Copp, B.R.; Keyzers, R.A.; Munro, M.H.G.; Prinsep, M.R. Marine natural products. *Nat. Prod. Rep.* **2014**, *31*, 160–258.
11. Hu, G.-P.; Yuan, J.; Sun, L.; She, Z.-G.; Wu, J.-H.; Lan, X.-J.; Zhu, X.; Lin, Y.-C.; Chen, S.-P. Statistical research on marine natural products based on data obtained between 1985 and 2008. *Mar. Drugs* **2011**, *9*, 514–525.
12. Taylor, M.W.; Radax, R.; Steger, D.; Wagner, M. Sponge-associated microorganisms: Evolution, ecology, and biotechnological potential. *Microbiol. Mol. Biol. Rev.* **2007**, *71*, 295–347.
13. Webster, N.S.; Taylor, M.W. Marine sponges and their microbial symbionts: Love and other relationships. *Environ. Microbiol.* **2012**, *14*, 335–346.
14. Li, J.W.-H.; Vederas, J.C. Drug discovery and natural products: End of an era or an endless frontier? *Science* **2009**, *325*, 161–165.

15. Fang, Z.; Li, T.; Wang, Q.; Zhang, X.; Peng, H.; Fang, W.; Hong, Y.; Ge, H.; Xiao, Y. A bacterial laccase from marine microbial metagenome exhibiting chloride tolerance and dye decolorization ability. *Appl. Microbiol. Biotechnol.* **2011**, *89*, 1103–1110.
16. Fu, C.; Hu, Y.; Xie, F.; Guo, H.; Ashforth, E.J.; Polyak, S.W.; Zhu, B.; Zhang, L. Molecular cloning and characterization of a new cold-active esterase from a deep-sea metagenomic library. *Appl. Microbiol. Biotechnol.* **2011**, *90*, 961–970.
17. Jiang, C.; Wu, L.-L.; Zhao, G.-C.; Shen, P.-H.; Jin, K.; Hao, Z.-Y.; Li, S.-X.; Ma, G.-F.; Luo, F.-F.; Hu, G.-Q.; *et al.* Identification and characterization of a novel fumarase gene by metagenome expression cloning from marine microorganisms. *Microb. Cell Fact.* **2010**, *9*, 1–9.
18. Kalpana, B.J.; Sindhulakshmi, M.; Pandian, S.K. Amylase enzyme from *Bacillus subtilis* S8-18: A potential desizing agent from the marine environment. *Biotechnol. Appl. Biochem.* **2014**, *61*, 134–144.
19. Wierzbicka-Wos, A.; Bartasun, P.; Cieslinski, H.; Kur, J. Cloning and characterization of a novel cold-active glycoside hydrolase family 1 enzyme with beta-glucosidase, beta-fucosidase and beta-galactosidase activities. *BMC Biotechnol.* **2013**, *13*, 22.
20. Willetts, A.; Joint, I.; Gilbert, J.A.; Trimble, W.; Mühling, M. Isolation and initial characterization of a novel type of Baeyer-Villiger monooxygenase activity from a marine microorganism. *Microb. Biotechnol.* **2012**, *5*, 549–559.
21. Zhao, K.; Guo, L.Z.; Lu, W.D. Extracellular production of novel halotolerant, thermostable, and alkali-stable carboxymethyl cellulase by marine bacterium *Marinimicrobium* sp. LS-A18. *Appl. Biochem. Biotechnol.* **2012**, *168*, 550–567.
22. Zhang, J.; Cao, X.; Xin, Y.; Xue, S.; Zhang, W. Purification and characterization of a dehalogenase from *Pseudomonas stutzeri* DEH130 isolated from the marine sponge *Hymeniacidon perlevis*. *World J. Microb. Biotechnol.* **2013**, *29*, 1791–1799.
23. Li, G.; Ren, J.; Wu, Q.; Feng, J.; Zhu, D.; Ma, Y. Identification of a marine NADPH-dependent aldehyde reductase for chemoselective reduction of aldehydes. *J. Mol. Catal. B-Enzym.* **2013**, *90*, 17–22.
24. Lailaja, V.P.; Chandrasekaran, M. Detergent compatible alkaline lipase produced by marine *Bacillus smithii* BTMS 11. *World J. Microb. Biotechnol.* **2013**, *29*, 1349–1360.
25. Novak, H.; Sayer, C.; Panning, J.; Littlechild, J. Characterisation of an l-haloacid dehalogenase from the marine psychrophile *Psychromonas ingrahamii* with potential industrial application. *Mar. Biotechnol.* **2013**, *15*, 695–705.
26. Liu, Z.; Zhao, X.; Bai, F. Production of xylanase by an alkaline-tolerant marine-derived *Streptomyces viridochromogenes* strain and improvement by ribosome engineering. *Appl. Microbiol. Biotechnol.* **2013**, *97*, 4361–4368.
27. Bernard, L.; Schäfer, H.; Joux, F.; Courties, C.; Muyzer, G.; Lebaron, P. Genetic diversity of total, active and culturable marine bacteria in coastal seawater. *Aquat. Microb. Ecol.* **2000**, *23*, 1–11.
28. Hugenholtz, P. Exploring prokaryotic diversity in the genomic era. *Genome Biol.* **2002**, *3*, 0003.0001–0003.0008.

29. Ferrari, B.C.; Winsley, T.; Gillings, M.; Binnerup, S. Cultivating previously uncultured soil bacteria using a soil substrate membrane system. *Nat. Protoc.* **2008**, *3*, 1261–1269.
30. Schut, F.; de Vries, E.J.; Gottschal, J.C.; Robertson, B.R.; Harder, W.; Prins, R.A.; Button, D.K. Isolation of typical marine bacteria by dilution culture: Growth, maintenance, and characteristics of isolates under laboratory conditions. *Appl. Environ. Microbiol.* **1993**, *59*, 2150–2160.
31. Shigematsu, T.; Hayashi, M.; Kikuchi, I.; Ueno, S.; Masaki, H.; Fujii, T. A culture-dependent bacterial community structure analysis based on liquid cultivation and its application to a marine environment. *FEMS Microbiol. Lett.* **2009**, *293*, 240–247.
32. Simu, K.; Holmfeldt, K.; Zweifel, U.L.; Hagström, Å. Culturability and coexistence of colony-forming and single-cell marine bacterioplankton. *Appl. Environ. Microbiol.* **2005**, *71*, 4793–4800.
33. Rappé, M.S.; Connon, S.A.; Vergin, K.L.; Giovannoni, S.J. Cultivation of the ubiquitous SAR11 marine bacterioplankton clade. *Nature* **2002**, *418*, 630–633.
34. Connon, S.A.; Giovannoni, S.J. High-throughput methods for culturing microorganisms in very-low-nutrient media yield diverse new marine isolates. *Appl. Environ. Microbiol.* **2002**, *68*, 3878–3885.
35. Vartoukian, S.R.; Palmer, R.M.; Wade, W.G. Strategies for culture of "unculturable" bacteria. *FEMS Microbiol. Lett.* **2010**, *309*, 1–7.
36. Stewart, E.J. Growing unculturable bacteria. *J. Bacteriol.* **2012**, *194*, 4151–4160.
37. Kaeberlein, T.; Lewis, K.; Epstein, S.S. Isolating "uncultivable" microorganisms in pure culture in a simulated natural environment. *Science* **2002**, *296*, 1127–1129.
38. Zengler, K.; Toledo, G.; Rappé, M.; Elkins, J.; Mathur, E.J.; Short, J.M.; Keller, M. Cultivating the uncultured. *Proc. Natl. Acad. Sci. USA* **2002**, *99*, 15681–15686.
39. Rastogi, G.; Sani, R. Molecular techniques to assess microbial community structure, function, and dynamics in the environment. In *Microbes and Microbial Technology*; Ahmad, I., Ahmad, F., Pichtel, J., Eds.; Springer: New York, NY, USA, 2011; pp. 29–57.
40. DeSantis, T.; Brodie, E.; Moberg, J.; Zubieta, I.; Piceno, Y.; Andersen, G. High-density universal 16S rRNA microarray analysis reveals broader diversity than typical clone library when sampling the environment. *Microb. Ecol.* **2007**, *53*, 371–383.
41. Cottrell, M.T.; Kirchman, D.L. Community composition of marine bacterioplankton determined by 16S rRNA gene clone libraries and fluorescence *in situ* hybridization. *Appl. Environ. Microbiol.* **2000**, *66*, 5116–5122.
42. Alex, A.; Silva, V.; Vasconcelos, V.; Antunes, A. Evidence of unique and generalist microbes in distantly related sympatric intertidal marine sponges (Porifera: Demospongiae). *PLoS One* **2013**, *8*, e80653.
43. Urakawa, H.; Kita-Tsukamoto, K.; Ohwada, K. Microbial diversity in marine sediments from Sagami Bay and Tokyo Bay, Japan, as determined by 16S rRNA gene analysis. *Microbiology* **1999**, *145*, 3305–3315.

44. Harrington, C.; Del Casale, A.; Kennedy, J.; Neve, H.; Picton, B.E.; Mooij, M.J.; O'Gara, F.; Kulakov, L.A.; Larkin, M.J.; Dobson, A.D.W. Evidence of bacteriophage-mediated horizontal transfer of bacterial 16S rRNA genes in the viral metagenome of the marine sponge *Hymeniacidon perlevis*. *Microbiology* **2012**, *158*, 2789–2795.
45. Nübel, U.; Garcia-Pichel, F.; Kühl, M.; Muyzer, G. Quantifying microbial diversity: Morphotypes, 16S rRNA genes, and carotenoids of oxygenic phototrophs in microbial mats. *Appl. Environ. Microbiol.* **1999**, *65*, 422–430.
46. Muyzer, G.; Smalla, K. Application of denaturing gradient gel electrophoresis (DGGE) and temperature gradient gel electrophoresis (TGGE) in microbial ecology. *Antonie van Leeuwenhoek* **1998**, *73*, 127–141.
47. Neilan, B.A. Identification and phylogenetic analysis of toxigenic cyanobacteria by multiplex randomly amplified polymorphic DNA PCR. *Appl. Environ. Microbiol.* **1995**, *61*, 2286–2291.
48. Roberts, M.A.; Crawford, D.L. Use of randomly amplified polymorphic DNA as a means of developing genus- and strain-specific *Streptomyces* DNA probes. *Appl. Environ. Microbiol.* **2000**, *66*, 2555–2564.
49. Heyndrickx, M.; Vauterin, L.; Vandamme, P.; Kersters, K.; de Vos, P. Applicability of combined amplified ribosomal DNA restriction analysis (ARDRA) patterns in bacterial phylogeny and taxonomy. *J. Microbiol. Methods* **1996**, *26*, 247–259.
50. Moeseneder, M.M.; Arrieta, J.M.; Muyzer, G.; Winter, C.; Herndl, G.J. Optimization of terminal-restriction fragment length polymorphism analysis for complex marine bacterioplankton communities and comparison with denaturing gradient gel electrophoresis. *Appl. Environ. Microbiol.* **1999**, *65*, 3518–3525.
51. Fuhrman, J.A.; Steele, J.A.; Hewson, I.; Schwalbach, M.S.; Brown, M.V.; Green, J.L.; Brown, J.H. A latitudinal diversity gradient in planktonic marine bacteria. *Proc. Natl. Acad. Sci. USA* **2008**, *105*, 7774–7778.
52. Brown, M.V.; Schwalbach, M.S.; Hewson, I.; Fuhrman, J.A. Coupling 16S-ITS rDNA clone libraries and automated ribosomal intergenic spacer analysis to show marine microbial diversity: Development and application to a time series. *Environ. Microbiol.* **2005**, *7*, 1466–1479.
53. Peplies, J.; Lau, S.C.K.; Pernthaler, J.; Amann, R.; Glöckner, F.O. Application and validation of DNA microarrays for the 16S rRNA-based analysis of marine bacterioplankton. *Environ. Microbiol.* **2004**, *6*, 638–645.
54. Zhou, J. Microarrays for bacterial detection and microbial community analysis. *Curr. Opin. Microbiol.* **2003**, *6*, 288–294.
55. Wu, L.; Kellogg, L.; Devol, A.H.; Tiedje, J.M.; Zhou, J. Microarray-based characterization of microbial community functional structure and heterogeneity in marine sediments from the Gulf of Mexico. *Appl. Environ. Microbiol.* **2008**, *74*, 4516–4529.
56. Smith, C.J.; Osborn, A.M. Advantages and limitations of quantitative PCR (Q-PCR)-based approaches in microbial ecology. *FEMS Microbiol. Ecol.* **2009**, *67*, 6–20.

57. Cassler, M.; Peterson, C.L.; Ledger, A.; Pomponi, S.A.; Wright, A.E.; Winegar, R.; McCarthy, P.J.; Lopez, J.V. Use of real-time qPCR to quantify members of the unculturable heterotrophic bacterial community in a deep sea marine sponge, *Vetulina* sp. *Microb. Ecol.* **2008**, *55*, 384–394.
58. Glöckner, F.O.; Fuchs, B.M.; Amann, R. Bacterioplankton compositions of lakes and oceans: A first comparison based on fluorescence *in situ* hybridization. *Appl. Environ. Microbiol.* **1999**, *65*, 3721–3726.
59. Moter, A.; Göbel, U.B. Fluorescence *in situ* hybridization (FISH) for direct visualization of microorganisms. *J. Microbiol. Methods* **2000**, *41*, 85–112.
60. Kindaichi, T.; Ito, T.; Okabe, S. Ecophysiological interaction between nitrifying bacteria and heterotrophic bacteria in autotrophic nitrifying biofilms as determined by microautoradiography-fluorescence *in situ* hybridization. *Appl. Environ. Microbiol.* **2004**, *70*, 1641–1650.
61. Konstantinidis, K.T.; Tiedje, J.M. Prokaryotic taxonomy and phylogeny in the genomic era: Advancements and challenges ahead. *Curr. Opin. Microbiol.* **2007**, *10*, 504–509.
62. Colwell, R.R. Viable but nonculturable bacteria: A survival strategy. *J. Infect. Chemother.* **2000**, *6*, 121–125.
63. Torsvik, V.; Øvreås, L. Microbial diversity and function in soil: From genes to ecosystems. *Curr. Opin. Microbiol.* **2002**, *5*, 240–245.
64. Wellington, E.M.H.; Berry, A.; Krsek, M. Resolving functional diversity in relation to microbial community structure in soil: Exploiting genomics and stable isotope probing. *Curr. Opin. Microbiol.* **2003**, *6*, 295–301.
65. Webster, G.; Watt, L.C.; Rinna, J.; Fry, J.C.; Evershed, R.P.; Parkes, R.J.; Weightman, A.J. A comparison of stable-isotope probing of DNA and phospholipid fatty acids to study prokaryotic functional diversity in sulfate-reducing marine sediment enrichment slurries. *Environ. Microbiol.* **2006**, *8*, 1575–1589.
66. Radajewski, S.; McDonald, I.R.; Murrell, J.C. Stable-isotope probing of nucleic acids: A window to the function of uncultured microorganisms. *Curr. Opin. Biotechnol.* **2003**, *14*, 296–302.
67. Adamczyk, J.; Hesselsoe, M.; Iversen, N.; Horn, M.; Lehner, A.; Nielsen, P.H.; Schloter, M.; Roslev, P.; Wagner, M. The isotope array, a new tool that employs substrate-mediated labeling of rRNA for determination of microbial community structure and function. *Appl. Environ. Microbiol.* **2003**, *69*, 6875–6887.
68. Nielsen, J.L.; Nielsen, P.H. Combined microautoradiography and fluorescence *in situ* hybridization (MAR-FISH) for the identification of metabolically active microorganisms. In *Handbook of Hydrocarbon and Lipid Microbiology*; Timmis, K., Ed.; Springer Berlin Heidelberg: Berlin, Germany, 2010; pp. 4093–4102.
69. Pinhassi, J.; Zweifel, U.L.; Hagström, A. Dominant marine bacterioplankton species found among colony-forming bacteria. *Appl. Environ. Microbiol.* **1997**, *63*, 3359–3366.

70. Nüsslein, K.; Tiedje, J.M. Characterization of the dominant and rare members of a young Hawaiian soil bacterial community with small-subunit ribosomal DNA amplified from DNA fractionated on the basis of its guanine and cytosine composition. *Appl. Environ. Microbiol.* **1998**, *64*, 1283–1289.
71. Holben, W.E.; Feris, K.P.; Kettunen, A.; Apajalahti, J.H.A. GC fractionation enhances microbial community diversity assessment and detection of minority populations of bacteria by denaturing gradient gel electrophoresis. *Appl. Environ. Microbiol.* **2004**, *70*, 2263–2270.
72. Riesenfeld, C.S.; Schloss, P.D.; Handelsman, J. Metagenomics: Genomic analysis of microbial communities. *Annu. Rev. Genet.* **2004**, *38*, 525–552.
73. Kennedy, J.; Codling, C.E.; Jones, B.V.; Dobson, A.D.W.; Marchesi, J.R. Diversity of microbes associated with the marine sponge, *Haliclona simulans*, isolated from Irish waters and identification of polyketide synthase genes from the sponge metagenome. *Environ. Microbiol.* **2008**, *10*, 1888–1902.
74. Kisand, V.; Valente, A.; Lahm, A.; Tanet, G.; Lettieri, T. Phylogenetic and functional metagenomic profiling for assessing microbial biodiversity in environmental monitoring. *PLoS One* **2012**, *7*, e43630.
75. Webster, N.S.; Taylor, M.W.; Behnam, F.; Lücker, S.; Rattei, T.; Whalan, S.; Horn, M.; Wagner, M. Deep sequencing reveals exceptional diversity and modes of transmission for bacterial sponge symbionts. *Environ. Microbiol.* **2010**, *12*, 2070–2082.
76. Sogin, M.L.; Morrison, H.G.; Huber, J.A.; Welch, D.M.; Huse, S.M.; Neal, P.R.; Arrieta, J.M.; Herndl, G.J. Microbial diversity in the deep sea and the underexplored "rare biosphere". *Proc. Natl. Acad. Sci. USA* **2006**, *103*, 12115–12120.
77. Kennedy, J.; Flemer, B.; Jackson, S.A.; Lejon, D.P.H.; Morrissey, J.P.; O'Gara, F.; Dobson, A.D.W. Marine metagenomics: New tools for the study and exploitation of marine microbial metabolism. *Mar. Drugs* **2010**, *8*, 608–628.
78. Huson, D.H.; Auch, A.F.; Qi, J.; Schuster, S.C. MEGAN analysis of metagenomic data. *Genome Res.* **2007**, *17*, 377–386.
79. Aziz, R.; Bartels, D.; Best, A.; DeJongh, M.; Disz, T.; Edwards, R.; Formsma, K.; Gerdes, S.; Glass, E.; Kubal, M.; *et al.* The RAST Server: Rapid annotations using subsystems technology. *BMC Genomics* **2008**, *9*, 75.
80. Rapid Annotation using Subsystem Technology. Available online: http://rast.nmpdr.org/ (accessed on 21 January 2014).
81. Horton, M.; Bodenhausen, N.; Bergelson, J. MARTA: A suite of Java-based tools for assigning taxonomic status to DNA sequences. *Bioinformatics* **2010**, *26*, 568–569.
82. Metagenomic And rDNA Taxonomy Assigner. Available online: http://bergelson.uchicago.edu/software/marta (accessed on 21 January 2014).
83. Yu, F.; Sun, Y.; Liu, L.; Farmerie, W. GSTaxClassifier: A genomic signature based taxonomic classifier for metagenomic data analysis. *Bioinformation* **2010**, *4*, 46–49.
84. Genomic Signature based Taxonomic Classifier. Available online: http://helix2.biotech.ufl.edu:26878/metagenomics/ (accessed on 21 January 2014).

85. Markowitz, V.M.; Chen, I.-M.A.; Palaniappan, K.; Chu, K.; Szeto, E.; Pillay, M.; Ratner, A.; Huang, J.; Woyke, T.; Huntemann, M.; *et al.* IMG 4 version of the integrated microbial genomes comparative analysis system. *Nucleic Acids Res.* **2014**, *42*, D560–D567.
86. Integrated Microbial Genomes with Microbiome Samples. Available online: https://img.jgi.doe.gov/cgi-bin/m/main.cgi (accessed on 21 January 2014).
87. Seshadri, R.; Kravitz, S.A.; Smarr, L.; Gilna, P.; Frazier, M. CAMERA: A community resource for metagenomics. *PLoS Biol.* **2007**, *5*, e75.
88. Community CyberInfrastructure for Advanced Marine Microbial Ecology Research and Analysis. Available online: http://camera.calit2.net/ (accessed on 21 January 2014).
89. Meyer, F.; Paarmann, D.; D'Souza, M.; Olson, R.; Glass, E.; Kubal, M.; Paczian, T.; Rodriguez, A.; Stevens, R.; Wilke, A.; *et al.* The metagenomics RAST server—A public resource for the automatic phylogenetic and functional analysis of metagenomes. *BMC Bioinform.* **2008**, *9*, 386.
90. MG-RAST: Metagenomics Analysis Server. Available online: http://metagenomics.anl.gov/ (accessed on 22 January 2014).
91. NCBI: National Center for Biotechnology Information. Available online: http://www.ncbi.nlm.nih.gov/genome (accessed on 22 January 2014).
92. Bernal, A.; Ear, U.; Kyrpides, N. Genomes OnLine Database (GOLD): A monitor of genome projects world-wide. *Nucleic Acids Res.* **2001**, *29*, 126–127.
93. GOLD: Genomes Online Database. Available online: http://www.genomesonline.org (accessed on 22 February 2014).
94. Wilmes, P.; Bond, P.L. Metaproteomics: Studying functional gene expression in microbial ecosystems. *Trends Microbiol.* **2006**, *14*, 92–97.
95. Slattery, M.; Ankisetty, S.; Corrales, J.; Marsh-Hunkin, K.E.; Gochfeld, D.J.; Willett, K.L.; Rimoldi, J.M. Marine proteomics: A critical assessment of an emerging technology. *J. Nat. Prod.* **2012**, *75*, 1833–1877.
96. Sowell, S.M.; Wilhelm, L.J.; Norbeck, A.D.; Lipton, M.S.; Nicora, C.D.; Barofsky, D.F.; Carlson, C.A.; Smith, R.D.; Giovanonni, S.J. Transport functions dominate the SAR11 metaproteome at low-nutrient extremes in the Sargasso Sea. *ISME J.* **2009**, *3*, 93–105.
97. Morris, R.M.; Nunn, B.L.; Frazar, C.; Goodlett, D.R.; Ting, Y.S.; Rocap, G. Comparative metaproteomics reveals ocean-scale shifts in microbial nutrient utilization and energy transduction. *ISME J.* **2010**, *4*, 673–685.
98. Williams, T.J.; Long, E.; Evans, F.; Demaere, M.Z.; Lauro, F.M.; Raftery, M.J.; Ducklow, H.; Grzymski, J.J.; Murray, A.E.; Cavicchioli, R. A metaproteomic assessment of winter and summer bacterioplankton from Antarctic Peninsula coastal surface waters. *ISME J.* **2012**, *6*, 1883–1900.
99. Stokke, R.; Roalkvam, I.; Lanzen, A.; Haflidason, H.; Steen, I.H. Integrated metagenomic and metaproteomic analyses of an ANME-1-dominated community in marine cold seep sediments. *Environ. Microbiol.* **2012**, *14*, 1333–1346.
100. Banfield, J.F.; Verberkmoes, N.C.; Hettich, R.L.; Thelen, M.P. Proteogenomic approaches for the molecular characterization of natural microbial communities. *OMICS* **2005**, *9*, 301–333.

101. Christie-Oleza, J.A.; Miotello, G.; Armengaud, J. Proteogenomic definition of biomarkers for the large *Roseobacter* clade and application for a quick screening of new environmental isolates. *J. Proteome Res.* **2013**, *12*, 5331–5339.
102. D'Haeseleer, P.; Gladden, J.M.; Allgaier, M.; Chain, P.S.G.; Tringe, S.G.; Malfatti, S.A.; Aldrich, J.T.; Nicora, C.D.; Robinson, E.W.; Paša-Tolić, L.; *et al.* Proteogenomic analysis of a thermophilic bacterial consortium adapted to deconstruct switchgrass. *PLoS One* **2013**, *8*, e68465.
103. Ogura, A.; Lin, M.; Shigenobu, Y.; Fujiwara, A.; Ikeo, K.; Nagai, S. Effective gene collection from the metatranscriptome of marine microorganisms. *BMC Genomics* **2011**, *12*, S15.
104. Coll-Lladó, M.; Acinas, S.G.; Pujades, C.; Pedrós-Alió, C. Transcriptome fingerprinting analysis: An approach to explore gene expression patterns in marine microbial communities. *PLoS One* **2011**, *6*, e22950.
105. Shi, Y.; McCarren, J.; DeLong, E.F. Transcriptional responses of surface water marine microbial assemblages to deep-sea water amendment. *Environ. Microbiol.* **2012**, *14*, 191–206.
106. Martinez, A.; Ventouras, L.A.; Wilson, S.T.; Karl, D.M.; DeLong, E.F. Metatranscriptomic and functional metagenomic analysis of methylphosphonate utilization by marine bacteria. *Front. Microbiol.* **2013**, *4*, 340.
107. Wu, J.; Gao, W.; Johnson, R.; Zhang, W.; Meldrum, D. Integrated metagenomic and metatranscriptomic analyses of microbial communities in the meso- and bathypelagic realm of North Pacific Ocean. *Mar. Drugs* **2013**, *11*, 3777–3801.
108. Al-Awadhi, H.; Dashti, N.; Khanafer, M.; Al-Mailem, D.; Ali, N.; Radwan, S. Bias problems in culture-independent analysis of environmental bacterial communities: A representative study on hydrocarbonoclastic bacteria. *SpringerPlus* **2013**, *2*, 369.
109. Öztürk, B.; De Jaeger, L.; Smidt, H.; Sipkema, D. Culture-dependent and independent approaches for identifying novel halogenases encoded by *Crambe crambe* (marine sponge) microbiota. *Sci. Rep.* **2013**, *3*, 2780.
110. Zeng, Y.; Zou, Y.; Grebmeier, J.; He, J.; Zheng, T. Culture-independent and -dependent methods to investigate the diversity of planktonic bacteria in the northern Bering Sea. *Polar Biol.* **2012**, *35*, 117–129.
111. Hirayama, H.; Sunamura, M.; Takai, K.; Nunoura, T.; Noguchi, T.; Oida, H.; Furushima, Y.; Yamamoto, H.; Oomori, T.; Horikoshi, K. Culture-dependent and -independent characterization of microbial communities associated with a shallow submarine hydrothermal system occurring within a coral reef off Taketomi Island, Japan. *Appl. Environ. Microbiol.* **2007**, *73*, 7642–7656.
112. Besaury, L.; Marty, F.; Buquet, S.; Mesnage, V.; Muyzer, G.; Quillet, L. Culture-dependent and independent studies of microbial diversity in highly copper-contaminated chilean marine sediments. *Microb. Ecol.* **2013**, *65*, 311–324.
113. Al-Awadhi, H.; Al-Mailem, D.; Dashti, N.; Khanafer, M.; Radwan, S. Indigenous hydrocarbon-utilizing bacterioflora in oil-polluted habitats in Kuwait, two decades after the greatest man-made oil spill. *Arch. Microbiol.* **2012**, *194*, 689–705.

114. Tripp, H.J.; Kitner, J.B.; Schwalbach, M.S.; Dacey, J.W.H.; Wilhelm, L.J.; Giovannoni, S.J. SAR11 marine bacteria require exogenous reduced sulphur for growth. *Nature* **2008**, *452*, 741–744.
115. Tong, J.; Trapido-Rosenthal, H.; Wang, J.; Wang, Y.; Li, Q.X.; Lu, Y. Antiviral activities and putative identification of compounds in microbial extracts from the Hawaiian coastal waters. *Mar. Drugs* **2012**, *10*, 521–538.
116. Cheng, Z.-B.; Xiao, H.; Fan, C.-Q.; Lu, Y.-N.; Zhang, G.; Yin, S. Bioactive polyhydroxylated sterols from the marine sponge *Haliclona crassiloba*. *Steroids* **2013**, *78*, 1353–1358.
117. Engelhardt, K.; Degnes, K.F.; Kemmler, M.; Bredholt, H.; Fjærvik, E.; Klinkenberg, G.; Sletta, H.; Ellingsen, T.E.; Zotchev, S.B. Production of a new thiopeptide antibiotic, TP-1161, by a marine *Nocardiopsis* species. *Appl. Environ. Microbiol.* **2010**, *76*, 4969–4976.
118. Graça, A.P.; Bondoso, J.; Gaspar, H.; Xavier, J.R.; Monteiro, M.C.; de la Cruz, M.; Oves-Costales, D.; Vicente, F.; Lage, O.M. Antimicrobial activity of heterotrophic bacterial communities from the marine sponge *Erylus discophorus* (Astrophorida, Geodiidae). *PLoS One* **2013**, *8*, e78992.
119. Sanchez, L.M.; Wong, W.R.; Riener, R.M.; Schulze, C.J.; Linington, R.G. Examining the fish microbiome: Vertebrate-derived bacteria as an environmental niche for the discovery of unique marine natural products. *PLoS One* **2012**, *7*, e35398.
120. Dalisay, D.S.; Williams, D.E.; Wang, X.L.; Centko, R.; Chen, J.; Andersen, R.J. Marine sediment-derived *Streptomyces* bacteria from British Columbia, Canada are a promising microbiota resource for the discovery of antimicrobial natural products. *PLoS One* **2013**, *8*, e77078.
121. Liu, X.; Bolla, K.; Ashforth, E.; Zhuo, Y.; Gao, H.; Huang, P.; Stanley, S.; Hung, D.; Zhang, L. Systematics-guided bioprospecting for bioactive microbial natural products. *Antonie van Leeuwenhoek* **2012**, *101*, 55–66.
122. CAMERA: Community CyberInfrastructure for Advanced Marine Microbial Ecology Research and Analysis. Available online: https://portal.camera.calit2.net/gridsphere/gridsphere?cid=microgenome (accessed on 22 January 2014).
123. Ohnishi, Y.; Ishikawa, J.; Hara, H.; Suzuki, H.; Ikenoya, M.; Ikeda, H.; Yamashita, A.; Hattori, M.; Horinouchi, S. Genome sequence of the streptomycin-producing microorganism *Streptomyces griseus* IFO 13350. *J. Bacteriol.* **2008**, *190*, 4050–4060.
124. Medema, M.H.; Blin, K.; Cimermancic, P.; de Jager, V.; Zakrzewski, P.; Fischbach, M.A.; Weber, T.; Takano, E.; Breitling, R. antiSMASH: Rapid identification, annotation and analysis of secondary metabolite biosynthesis gene clusters in bacterial and fungal genome sequences. *Nucleic Acids Res.* **2011**, *39*, W339–W346.
125. Blin, K.; Medema, M.H.; Kazempour, D.; Fischbach, M.A.; Breitling, R.; Takano, E.; Weber, T. antiSMASH 2.0—A versatile platform for genome mining of secondary metabolite producers. *Nucleic Acids Res.* **2013**, *41*, W204–W212.
126. van Heel, A.J.; de Jong, A.; Montalbán-López, M.; Kok, J.; Kuipers, O.P. BAGEL3: Automated identification of genes encoding bacteriocins and (non-)bactericidal posttranslationally modified peptides. *Nucleic Acids Res.* **2013**, *41*, W448–W453.

127. Bacteriocin Genome Mining Tool 3. Available online: http://bagel2.molgenrug.nl/index.php/bagel3 (accessed on 22 February 2014).
128. Meier, J.L.; Burkart, M.D. The chemical biology of modular biosynthetic enzymes. *Chem. Soc. Rev.* **2009**, *38*, 2012–2045.
129. Li, M.; Ung, P.; Zajkowski, J.; Garneau-Tsodikova, S.; Sherman, D. Automated genome mining for natural products. *BMC Bioinform.* **2009**, *10*, 185.
130. NP searcher. Available online: http://dna.sherman.lsi.umich.edu/ (accessed on 22 January 2014).
131. Mallika, V.; Sivakumar, K.C.; Jaichand, S.; Soniya, E.V. Kernel based machine learning algorithm for the efficient prediction of type III polyketide synthase family of proteins. *J. Integr. Bioinform.* **2010**, *7*, 143:1–143:8.
132. PSIPRED Protein Sequence Analysis Workbench. Available online: http://bioinf.cs.ucl.ac.uk/psipred/ (accessed on 22 February 2014).
133. Anand, S.; Prasad, M.V.R.; Yadav, G.; Kumar, N.; Shehara, J.; Ansari, M.Z.; Mohanty, D. SBSPKS: Structure based sequence analysis of polyketide synthases. *Nucleic Acids Res.* **2010**, *38*, W487–W496.
134. Structure-Based Sequence Analysis of PKS (SBSPKS). Available online: http://www.nii.ac.in/~pksdb/sbspks/master.html (accessed on 22 January 2014).
135. Hertweck, C. The biosynthetic logic of polyketide diversity. *Angew. Chem. Int. Ed.* **2009**, *48*, 4688–4716.
136. Fischbach, M.A.; Walsh, C.T. Assembly-line enzymology for nolyketide and nonribosomal peptide antibiotics: Logic, machinery, and mechanisms. *Chem. Rev.* **2006**, *106*, 3468–3496.
137. Udwary, D.W.; Zeigler, L.; Asolkar, R.N.; Singan, V.; Lapidus, A.; Fenical, W.; Jensen, P.R.; Moore, B.S. Genome sequencing reveals complex secondary metabolome in the marine actinomycete *Salinispora tropica*. *Proc. Natl. Acad. Sci. USA* **2007**, *104*, 10376–10381.
138. Lai, J.R.; Koglin, A.; Walsh, C.T. Carrier protein structure and recognition in polyketide and nonribosomal peptide biosynthesis. *Biochemistry* **2006**, *45*, 14869–14879.
139. Walsh, C.T. Polyketide and nonribosomal peptide antibiotics: Modularity and versatility. *Science* **2004**, *303*, 1805–1810.
140. Zhang, H.; Wang, H.; Wang, Y.; Cui, H.; Xie, Z.; Pu, Y.; Pei, S.; Li, F.; Qin, S. Genomic sequence-based discovery of novel angucyclinone antibiotics from marine *Streptomyces* sp. W007. *FEMS Microbiol. Lett.* **2012**, *332*, 105–112.
141. Zazopoulos, E.; Huang, K.; Staffa, A.; Liu, W.; Bachmann, B.O.; Nonaka, K.; Ahlert, J.; Thorson, J.S.; Shen, B.; Farnet, C.M. A genomics-guided approach for discovering and expressing cryptic metabolic pathways. *Nat. Biotechnol.* **2003**, *21*, 187–190.
142. Kalan, L.; Gessner, A.; Thaker, M.N.; Waglechner, N.; Zhu, X.; Szawiola, A.; Bechthold, A.; Wright, G.D.; Zechel, D.L. A cryptic polyene biosynthetic gene cluster in *Streptomyces calvus* is expressed upon complementation with a functional *blda* gene. *Chem. Biol.* **2013**, *20*, 1214–1224.

143. Prieto, M.L.; O'Sullivan, L.; Tan, S.P.; McLoughlin, P.; Hughes, H.; O'Connor, P.M.; Cotter, P.D.; Lawlor, P.G.; Gardiner, G.E. Assessment of the bacteriocinogenic potential of marine bacteria reveals lichenicidin production by seaweed-derived *Bacillus* spp. *Mar. Drugs* **2012**, *10*, 2280–2299.
144. Wu, C.; Tan, Y.; Gan, M.; Wang, Y.; Guan, Y.; Hu, X.; Zhou, H.; Shang, X.; You, X.; Yang, Z.; *et al.* Identification of elaiophylin derivatives from the marine-derived actinomycete *Streptomyces* sp. 7-145 using PCR-based screening. *J. Nat. Prod.* **2013**, *76*, 2153–2157.
145. Wang, H.X.; Chen, Y.Y.; Ge, L.; Fang, T.T.; Meng, J.; Liu, Z.; Fang, X.Y.; Ni, S.; Lin, C.; Wu, Y.Y.; *et al.* PCR screening reveals considerable unexploited biosynthetic potential of ansamycins and a mysterious family of AHBA-containing natural products in actinomycetes. *J. Appl. Microbiol.* **2013**, *115*, 77–85.
146. Wang, H.; Liu, N.; Xi, L.; Rong, X.; Ruan, J.; Huang, Y. Genetic screening strategy for rapid access to polyether ionophore producers and products in actinomycetes. *Appl. Environ. Microbiol.* **2011**, *77*, 3433–3442.
147. Hornung, A.; Bertazzo, M.; Dziarnowski, A.; Schneider, K.; Welzel, K.; Wohlert, S.-E.; Holzenkämpfer, M.; Nicholson, G.J.; Bechthold, A.; Süssmuth, R.D.; *et al.* A genomic screening approach to the structure-guided identification of drug candidates from natural sources. *ChemBioChem* **2007**, *8*, 757–766.
148. Pearson, W.R.; Lipman, D.J. Improved tools for biological sequence comparison. *Proc. Natl. Acad. Sci. USA* **1988**, *85*, 2444–2448.
149. Altschul, S.F.; Gish, W.; Miller, W.; Myers, E.W.; Lipman, D.J. Basic local alignment search tool. *J. Mol. Biol.* **1990**, *215*, 403–410.
150. Noguchi, H.; Park, J.; Takagi, T. MetaGene: Prokaryotic gene finding from environmental genome shotgun sequences. *Nucleic Acids Res.* **2006**, *34*, 5623–5630.
151. Lukashin, A.V.; Borodovsky, M. GeneMark: New solutions for gene finding. *Nucleic Acids Res.* **1998**, *26*, 1107–1115.
152. Altschul, S.F.; Madden, T.L.; Schäffer, A.A.; Zhang, J.; Zhang, Z.; Miller, W.; Lipman, D.J. Gapped BLAST and PSI-BLAST: A new generation of protein database search programs. *Nucleic Acids Res.* **1997**, *25*, 3389–3402.
153. van Loo, B.; Kingma, J.; Arand, M.; Wubbolts, M.G.; Janssen, D.B. Diversity and biocatalytic potential of epoxide hydrolases identified by genome analysis. *Appl. Environ. Microbiol.* **2006**, *72*, 2905–2917.
154. Kwon, Y.-C.; Lee, K.-H.; Kim, H.-C.; Han, K.; Seo, J.-H.; Kim, B.-G.; Kim, D.-M. Cloning-independent expression and analysis of ω-transaminases by use of a cell-free protein synthesis system. *Appl. Environ. Microbiol.* **2010**, *76*, 6295–6298.
155. Vergne-Vaxelaire, C.; Bordier, F.; Fossey, A.; Besnard-Gonnet, M.; Debard, A.; Mariage, A.; Pellouin, V.; Perret, A.; Petit, J.-L.; Stam, M.; *et al.* Nitrilase activity screening on structurally diverse substrates: Providing biocatalytic tools for organic synthesis. *Adv. Synth. Catal.* **2013**, *355*, 1763–1779.
156. Mondol, M.; Shin, H.; Islam, M. Diversity of secondary metabolites from marine *Bacillus* species: Chemistry and biological activity. *Mar. Drugs* **2013**, *11*, 2846–2872.

157. Zhang, W.; Li, Z.; Miao, X.; Zhang, F. The screening of antimicrobial bacteria with diverse novel nonribosomal peptide synthetase (NRPS) genes from South China Sea sponges. *Mar. Biotechnol.* **2009**, *11*, 346–355.
158. Handelsman, J. Metagenomics: Application of genomics to uncultured microorganisms. *Microbiol. Mol. Biol. Rev.* **2004**, *68*, 669–685.
159. Lee, H.S.; Kwon, K.K.; Kang, S.G.; Cha, S.-S.; Kim, S.-J.; Lee, J.-H. Approaches for novel enzyme discovery from marine environments. *Curr. Opin. Biotechnol.* **2010**, *21*, 353–357.
160. Shokralla, S.; Spall, J.L.; Gibson, J.F.; Hajibabaei, M. Next-generation sequencing technologies for environmental DNA research. *Mol. Ecol.* **2012**, *21*, 1794–1805.
161. Schofield, M.M.; Sherman, D.H. Meta-omic characterization of prokaryotic gene clusters for natural product biosynthesis. *Curr. Opin. Biotechnol.* **2013**, *24*, 1151–1158.
162. Biver, S.; Portetelle, D.; Vandenbol, M. Characterization of a new oxidant-stable serine protease isolated by functional metagenomics. *SpringerPlus* **2013**, *2*, 410.
163. Waschkowitz, T.; Rockstroh, S.; Daniel, R. Isolation and characterization of metalloproteases with a novel domain structure by construction and screening of metagenomic libraries. *Appl. Environ. Microbiol.* **2009**, *75*, 2506–2516.
164. Selvin, J.; Kennedy, J.; Lejon, D.P.H.; Kiran, G.S.; Dobson, A.D.W. Isolation identification and biochemical characterization of a novel halo-tolerant lipase from the metagenome of the marine sponge *Haliclona simulans*. *Microb. Cell Fact.* **2012**, *11*, 72.
165. Hårdeman, F.; Sjöling, S. Metagenomic approach for the isolation of a novel low-temperature-active lipase from uncultured bacteria of marine sediment. *FEMS Microbiol. Ecol.* **2007**, *59*, 524–534.
166. Jiang, X.; Xu, X.; Huo, Y.; Wu, Y.; Zhu, X.; Zhang, X.; Wu, M. Identification and characterization of novel esterases from a deep-sea sediment metagenome. *Arch. Microbiol.* **2012**, *194*, 207–214.
167. Jeon, J.H.; Lee, H.S.; Kim, J.T.; Kim, S.J.; Choi, S.H.; Kang, S.G.; Lee, J.H. Identification of a new subfamily of salt-tolerant esterases from a metagenomic library of tidal flat sediment. *Appl. Microbiol. Biotechnol.* **2012**, *93*, 623–631.
168. Chu, X.; He, H.; Guo, C.; Sun, B. Identification of two novel esterases from a marine metagenomic library derived from South China Sea. *Appl. Microbiol. Biotechnol.* **2008**, *80*, 615–625.
169. Gillespie, D.E.; Brady, S.F.; Bettermann, A.D.; Cianciotto, N.P.; Liles, M.R.; Rondon, M.R.; Clardy, J.; Goodman, R.M.; Handelsman, J. Isolation of antibiotics turbomycin A and B from a metagenomic library of soil microbial DNA. *Appl. Environ. Microbiol.* **2002**, *68*, 4301–4306.
170. Wang, G.-Y.-S.; Graziani, E.; Waters, B.; Pan, W.; Li, X.; McDermott, J.; Meurer, G.; Saxena, G.; Andersen, R.J.; Davies, J. Novel natural products from soil DNA libraries in a streptomycete host. *Org. Lett.* **2000**, *2*, 2401–2404.
171. Brady, S.F.; Clardy, J. Synthesis of long-chain fatty acid enol esters isolated from an environmental DNA clone. *Org. Lett.* **2002**, *5*, 121–124.

172. Feng, Z.; Kallifidas, D.; Brady, S.F. Functional analysis of environmental DNA-derived type II polyketide synthases reveals structurally diverse secondary metabolites. *Proc. Natl. Acad. Sci. USA* **2011**, *108*, 12629–12634.
173. Brady, S.F.; Simmons, L.; Kim, J.H.; Schmidt, E.W. Metagenomic approaches to natural products from free-living and symbiotic organisms. *Nat. Prod. Rep.* **2009**, *26*, 1488–1503.
174. Banik, J.J.; Brady, S.F. Recent application of metagenomic approaches toward the discovery of antimicrobials and other bioactive small molecules. *Curr. Opin. Microbiol.* **2010**, *13*, 603–609.
175. Robertson, D.E.; Chaplin, J.A.; DeSantis, G.; Podar, M.; Madden, M.; Chi, E.; Richardson, T.; Milan, A.; Miller, M.; Weiner, D.P.; *et al.* Exploring nitrilase sequence space for enantioselective catalysis. *Appl. Environ. Microbiol.* **2004**, *70*, 2429–2436.
176. Bayer, S.; Birkemeyer, C.; Ballschmiter, M. A nitrilase from a metagenomic library acts regioselectively on aliphatic dinitriles. *Appl. Microbiol. Biotechnol.* **2011**, *89*, 91–98.
177. Johnston, C.; Ibrahim, A.; Magarvey, N. Informatic strategies for the discovery of polyketides and nonribosomal peptides. *MedChemComm* **2012**, *3*, 932–937.
178. Cottrell, M.T.; Yu, L.; Kirchman, D.L. Sequence and expression analyses of Cytophaga-like hydrolases in a Western Arctic metagenomic library and the Sargasso Sea. *Appl. Environ. Microbiol.* **2005**, *71*, 8506–8513.
179. Xu, M.; Xiao, X.; Wang, F. Isolation and characterization of alkane hydroxylases from a metagenomic library of Pacific deep-sea sediment. *Extremophiles* **2008**, *12*, 255–262.
180. Venter, J.C.; Remington, K.; Heidelberg, J.F.; Halpern, A.L.; Rusch, D.; Eisen, J.A.; Wu, D.; Paulsen, I.; Nelson, K.E.; Nelson, W.; *et al.* Environmental Genome Shotgun Sequencing of the Sargasso Sea. *Science* **2004**, *304*, 66–74.
181. Bayer, K.; Scheuermayer, M.; Fieseler, L.; Hentschel, U. Genomic mining for novel $FADH_2$-dependent halogenases in marine sponge-associated microbial consortia. *Mar. Biotechnol.* **2013**, *15*, 63–72.
182. Bayer, T.S.; Widmaier, D.M.; Temme, K.; Mirsky, E.A.; Santi, D.V.; Voigt, C.A. Synthesis of methyl halides from biomass using engineered microbes. *J. Am. Chem. Soc.* **2009**, *131*, 6508–6515.
183. Stepanauskas, R.; Sieracki, M.E. Matching phylogeny and metabolism in the uncultured marine bacteria, one cell at a time. *Proc. Natl. Acad. Sci. USA* **2007**, *104*, 9052–9057.
184. Siegl, A.; Kamke, J.; Hochmuth, T.; Piel, J.; Richter, M.; Liang, C.; Dandekar, T.; Hentschel, U. Single-cell genomics reveals the lifestyle of Poribacteria, a candidate phylum symbiotically associated with marine sponges. *ISME J.* **2011**, *5*, 61–70.
185. Williamson, L.L.; Borlee, B.R.; Schloss, P.D.; Guan, C.; Allen, H.K.; Handelsman, J. Intracellular screen to identify metagenomic clones that induce or inhibit a quorum-sensing biosensor. *Appl. Environ. Microbiol.* **2005**, *71*, 6335–6344.
186. Uchiyama, T.; Miyazaki, K. Substrate-induced gene expression screening: A method for high-throughput screening of metagenome libraries. In *Metagenomics: Methods and Protocols*; Humana Press: Clifton, NJ, USA, 2010; Volume 668, pp. 153–168.

187. Uchiyama, T.; Watanabe, K. Substrate-induced gene expression (SIGEX) screening of metagenome libraries. *Nat. Protoc.* **2008**, *3*, 1202–1212.
188. Meiring, T.; Mulako, I.; Tuffin, M.; Meyer, Q.; Cowan, D. Retrieval of full-length functional genes using subtractive hybridization magnetic bead capture. In *Metagenomics: Methods and Protocols*; Streit, W.R., Daniel, R., Eds.; Humana Press: Clifton, NJ, USA, 2010; Volume 668, pp. 287–297.
189. Meyer, Q.C.; Burton, S.G.; Cowan, D.A. Subtractive hybridization magnetic bead capture: A new technique for the recovery of full-length ORFs from the metagenome. *Biotechnol. J.* **2007**, *2*, 36–40.
190. Margassery, L.M.; Kennedy, J.; O'Gara, F.; Dobson, A.D.; Morrissey, J.P. A high-throughput screen to identify novel calcineurin inhibitors. *J. Microbiol. Methods* **2012**, *88*, 63–66.
191. Menzella, H.G.; Reeves, C.D. Combinatorial biosynthesis for drug development. *Curr. Opin. Microbiol.* **2007**, *10*, 238–245.
192. Wong, F.T.; Khosla, C. Combinatorial biosynthesis of polyketides-a perspective. *Curr. Opin. Chem. Biol.* **2012**, *16*, 117–123.
193. Fisch, K.M. Biosynthesis of natural products by microbial iterative hybrid PKS-NRPS. *RSC Adv.* **2013**, *3*, 18228–18247.
194. Kim, E.J.; Lee, J.H.; Choi, H.; Pereira, A.R.; Ban, Y.H.; Yoo, Y.J.; Kim, E.; Park, J.W.; Sherman, D.H.; Gerwick, W.H.; *et al.* Heterologous production of 4-*O*-demethylbarbamide, a marine cyanobacterial natural product. *Org. Lett.* **2012**, *14*, 5824–5827.
195. Doekel, S.; Coëffet-Le Gal, M.-F.; Gu, J.-Q.; Chu, M.; Baltz, R.H.; Brian, P. Non-ribosomal peptide synthetase module fusions to produce derivatives of daptomycin in *Streptomyces roseosporus*. *Microbiology* **2008**, *154*, 2872–2880.
196. Seipke, R.F.; Hutchings, M.I. The regulation and biosynthesis of antimycins. *Beilstein J. Org. Chem.* **2013**, *9*, 2556–2563.
197. Yan, Y.; Chen, J.; Zhang, L.; Zheng, Q.; Han, Y.; Zhang, H.; Zhang, D.; Awakawa, T.; Abe, I.; Liu, W. Multiplexing of combinatorial chemistry in antimycin biosynthesis: Expansion of molecular diversity and utility. *Angew. Chem. Int. Ed.* **2013**, *52*, 12308–12312.
198. Eustáquio, A.S.; O'Hagan, D.; Moore, B.S. Engineering fluorometabolite production: Fluorinase expression in *Salinispora tropica* yields fluorosalinosporamide. *J. Nat. Prod.* **2010**, *73*, 378–382.
199. Winter, J.M.; Tang, Y. Synthetic biological approaches to natural product biosynthesis. *Curr. Opin. Biotechnol.* **2012**, *23*, 736–743.
200. Isaacs, F.J.; Carr, P.A.; Wang, H.H.; Lajoie, M.J.; Sterling, B.; Kraal, L.; Tolonen, A.C.; Gianoulis, T.A.; Goodman, D.B.; Reppas, N.B.; *et al.* Precise manipulation of chromosomes *in vivo* enables genome-wide codon replacement. *Science* **2011**, *333*, 348–353.
201. Wang, H.H.; Isaacs, F.J.; Carr, P.A.; Sun, Z.Z.; Xu, G.; Forest, C.R.; Church, G.M. Programming cells by multiplex genome engineering and accelerated evolution. *Nature* **2009**, *460*, 894–898.
202. Khalil, A.S.; Collins, J.J. Synthetic biology: Applications come of age. *Nat. Rev. Genet.* **2010**, *11*, 367–379.

203. Keasling, J.D. Manufacturing molecules through metabolic engineering. *Science* **2010**, *330*, 1355–1358.
204. Park, S.R.; Park, J.W.; Ban, Y.H.; Sohng, J.K.; Yoon, Y.J. 2-Deoxystreptamine-containing aminoglycoside antibiotics: Recent advances in the characterization and manipulation of their biosynthetic pathways. *Nat. Prod. Rep.* **2013**, *30*, 11–20.
205. Yuzawa, S.; Kim, W.; Katz, L.; Keasling, J.D. Heterologous production of polyketides by modular type I polyketide synthases in *Escherichia coli*. *Curr. Opin. Biotechnol.* **2012**, *23*, 727–735.
206. Gao, X.; Wang, P.; Tang, Y. Engineered polyketide biosynthesis and biocatalysis in *Escherichia coli*. *Appl. Microbiol. Biotechnol.* **2010**, *88*, 1233–1242.
207. Zakeri, B.; Lu, T.K. Synthetic biology of antimicrobial discovery. *ACS Synth. Biol.* **2013**, *2*, 358–372.
208. Carbonell, P.; Planson, A.-G.; Faulon, J.-L. Retrosynthetic design of heterologous pathways. In *Systems Metabolic Engineering: Methods and Protocols*; Alper, H.S., Ed.; Humana Press: Clifton, NJ, USA, 2013; Volume 985, pp. 149–173.
209. Turner, N.J.; O'Reilly, E. Biocatalytic retrosynthesis. *Nat. Chem. Biol.* **2013**, *9*, 285–288.
210. Loeschcke, A.; Markert, A.; Wilhelm, S.; Wirtz, A.; Rosenau, F.; Jaeger, K.-E.; Drepper, T. TREX: A universal tool for the transfer and expression of biosynthetic pathways in bacteria. *ACS Synth. Biol.* **2012**, *2*, 22–33.
211. Wang, J.; Xiong, Z.; Meng, H.; Wang, Y.; Wang, Y. Synthetic biology triggers new era of antibiotics development. In *Reprogramming Microbial Metabolic Pathways*; Wang, X., Chen, J., Quinn, P., Eds.; Springer: Dordrecht, The Netherlands, 2012; Volume 64, pp. 95–114.
212. Gomez-Escribano, J.; Bibb, M. Heterologous expression of natural product biosynthetic gene clusters in *Streptomyces coelicolor*: From genome mining to manipulation of biosynthetic pathways. *J. Ind. Microbiol. Biotechnol.* **2014**, *41*, 425–431.
213. Zhang, H.; Boghigian, B.A.; Armando, J.; Pfeifer, B.A. Methods and options for the heterologous production of complex natural products. *Nat. Prod. Rep.* **2011**, *28*, 125–151.
214. Pfeifer, B.A.; Admiraal, S.J.; Gramajo, H.; Cane, D.E.; Khosla, C. Biosynthesis of complex polyketides in a metabolically engineered strain of *E. coli*. *Science* **2001**, *291*, 1790–1792.
215. Kao, C.; Katz, L.; Khosla, C. Engineered biosynthesis of a complete macrolactone in a heterologous host. *Science* **1994**, *265*, 509–512.
216. Ichinose, K.; Bedford, D.J.; Tornus, D.; Bechthold, A.; Bibb, M.J.; Peter Revill, W.; Floss, H.G.; Hopwood, D.A. The granaticin biosynthetic gene cluster of *Streptomyces violaceoruber* Tü22: Sequence analysis and expression in a heterologous host. *Chem. Biol.* **1998**, *5*, 647–659.
217. Ichinose, K.; Ozawa, M.; Itou, K.; Kunieda, K.; Ebizuka, Y. Cloning, sequencing and heterologous expression of the medermycin biosynthetic gene cluster of *Streptomyces* sp. AM-7161: Towards comparative analysis of the benzoisochromanequinone gene clusters. *Microbiology* **2003**, *149*, 1633–1645.
218. Tang, L.S. Cloning and heterologous expression of the epothilone gene cluster. *Science* **2000**, *287*, 640.

219. Bedford, D.J.; Schweizer, E.; Hopwood, D.A.; Khosla, C. Expression of a functional fungal polyketide synthase in the bacterium *Streptomyces coelicolor* A3(2). *J. Bacteriol.* **1995**, *177*, 4544–4548.
220. Eustáquio, A.S.; Gust, B.; Galm, U.; Li, S.-M.; Chater, K.F.; Heide, L. Heterologous expression of novobiocin and clorobiocin biosynthetic gene clusters. *Appl. Environ. Microbiol.* **2005**, *71*, 2452–2459.
221. Zhang, W.; Ames, B.D.; Tsai, S.-C.; Tang, Y. Engineered biosynthesis of a novel amidated polyketide, using the malonamyl-specific initiation module from the oxytetracycline polyketide synthase. *Appl. Environ. Microbiol.* **2006**, *72*, 2573–2580.
222. Winter, J.M.; Moffitt, M.C.; Zazopoulos, E.; McAlpine, J.B.; Dorrestein, P.C.; Moore, B.S. Molecular basis for chloronium-mediated meroterpene cyclization: Cloning, sequencing, and heterologous expression of the napyradiomycin biosynthetic gene cluster. *J. Biol. Chem.* **2007**, *282*, 16362–16368.
223. Ito, T.; Roongsawang, N.; Shirasaka, N.; Lu, W.; Flatt, P.M.; Kasanah, N.; Miranda, C.; Mahmud, T. Deciphering pactamycin biosynthesis and engineered production of new pactamycin analogues. *ChemBioChem* **2009**, *10*, 2253–2265.
224. Penn, J.; Li, X.; Whiting, A.; Latif, M.; Gibson, T.; Silva, C.; Brian, P.; Davies, J.; Miao, V.; Wrigley, S.; *et al.* Heterologous production of daptomycin in *Streptomyces lividans*. *J. Ind. Microbiol. Biotechnol.* **2006**, *33*, 121–128.
225. Pfeifer, B.A.; Wang, C.C.C.; Walsh, C.T.; Khosla, C. Biosynthesis of yersiniabactin, a complex polyketide-nonribosomal peptide, using *Escherichia coli* as a heterologous host. *Appl. Environ. Microbiol.* **2003**, *69*, 6698–6702.
226. Mutka, S.C.; Carney, J.R.; Liu, Y.; Kennedy, J. Heterologous production of epothilone C and D in *Escherichia coli*. *Biochemistry* **2006**, *45*, 1321–1330.
227. Gruenewald, S.; Mootz, H.D.; Stehmeier, P.; Stachelhaus, T. *In vivo* production of artificial nonribosomal peptide products in the heterologous host *Escherichia coli*. *Appl. Environ. Microbiol.* **2004**, *70*, 3282–3291.
228. Watanabe, K.; Hotta, K.; Praseuth, A.P.; Koketsu, K.; Migita, A.; Boddy, C.N.; Wang, C.C.C.; Oguri, H.; Oikawa, H. Total biosynthesis of antitumor nonribosomal peptides in *Escherichia coli*. *Nat. Chem. Biol.* **2006**, *2*, 423–428.
229. Fu, J.; Wenzel, S.C.; Perlova, O.; Wang, J.; Gross, F.; Tang, Z.; Yin, Y.; Stewart, A.F.; Müller, R.; Zhang, Y. Efficient transfer of two large secondary metabolite pathway gene clusters into heterologous hosts by transposition. *Nucleic Acids Res.* **2008**, *36*, e113.
230. Rath, C.M.; Janto, B.; Earl, J.; Ahmed, A.; Hu, F.Z.; Hiller, L.; Dahlgren, M.; Kreft, R.; Yu, F.; Wolff, J.J.; *et al.* Meta-omic characterization of the marine invertebrate microbial consortium that produces the chemotherapeutic natural product ET-743. *ACS Chem. Biol.* **2011**, *6*, 1244–1256.
231. Phelan, R.; Barret, M.; Cotter, P.; Connor, P.; Chen, R.; Morrissey, J.; Dobson, A.; Gara, F.; Barbosa, T. Subtilomycin: A new lantibiotic from *Bacillus subtilis* strain MMA7 isolated from the marine sponge *Haliclona simulans*. *Mar. Drugs* **2013**, *11*, 1878–1898.

232. Kersten, R.D.; Ziemert, N.; Gonzalez, D.J.; Duggan, B.M.; Nizet, V.; Dorrestein, P.C.; Moore, B.S. Glycogenomics as a mass spectrometry-guided genome-mining method for microbial glycosylated molecules. *Proc. Natl. Acad. Sci. USA* **2013**, *110*, E4407–E4416.
233. Bumpus, S.B.; Evans, B.S.; Thomas, P.M.; Ntai, I.; Kelleher, N.L. A proteomics approach to discovering natural products and their biosynthetic pathways. *Nat. Biotechnol.* **2009**, *27*, 951–956.
234. Chen, Y.; McClure, R.A.; Zheng, Y.; Thomson, R.J.; Kelleher, N.L. Proteomics guided discovery of flavopeptins: Anti-proliferative aldehydes synthesized by a reductase domain-containing non-ribosomal peptide synthetase. *J. Am. Chem. Soc.* **2013**, *135*, 10449–10456.
235. Evans, B.S.; Ntai, I.; Chen, Y.; Robinson, S.J.; Kelleher, N.L. Proteomics-based discovery of koranimine, a cyclic imine natural product. *J. Am. Chem. Soc.* **2011**, *133*, 7316–7319.
236. Meier, J.L.; Burkart, M.D. Proteomic analysis of polyketide and nonribosomal peptide biosynthesis. *Curr. Opin. Chem. Biol.* **2011**, *15*, 48–56.
237. Meier, J.L.; Niessen, S.; Hoover, H.S.; Foley, T.L.; Cravatt, B.F.; Burkart, M.D. An orthogonal active site identification system (OASIS) for proteomic profiling of natural product biosynthesis. *ACS Chem. Biol.* **2009**, *4*, 948–957.
238. Yang, J.Y.; Sanchez, L.M.; Rath, C.M.; Liu, X.; Boudreau, P.D.; Bruns, N.; Glukhov, E.; Wodtke, A.; de Felicio, R.; Fenner, A.; *et al.* Molecular networking as a dereplication strategy. *J. Nat. Prod.* **2013**, *76*, 1686–1699.
239. Forner, D.; Berrué, F.; Correa, H.; Duncan, K.; Kerr, R.G. Chemical dereplication of marine actinomycetes by liquid chromatography–high resolution mass spectrometry profiling and statistical analysis. *Anal. Chim. Acta* **2013**, *805*, 70–79.
240. FastGroupII. Available online: http://fastgroup.sdsu.edu/ (accessed on 22 February 2014).
241. BACTIBASE. Available online: http://bactibase.pfba-lab-tun.org/main.php (accessed on 22 February 2014).
242. Laatsch, H. *Antibase Version 4.0*; Wiley-VCH Verlag GmbH & Co: Weinheim, Germany, 2012.
243. Hammami, R.; Zouhir, A.; Le Lay, C.; Ben Hamida, J.; Fliss, I. BACTIBASE second release: A database and tool platform for bacteriocin characterization. *BMC Microbiol.* **2010**, *10*, 22.
244. Yu, Y.; Breitbart, M.; McNairnie, P.; Rohwer, F. FastGroupII: A web-based bioinformatics platform for analyses of large 16S rDNA libraries. *BMC Bioinform.* **2006**, *7*, 57.
245. Microbial Screening Technologies. Available online: http://www.microbialscreening.com/dereplication.htm (accessed on 23 February 2014).
246. Murray, P.M.; Moane, S.; Collins, C.; Beletskaya, T.; Thomas, O.P.; Duarte, A.W.F.; Nobre, F.S.; Owoyemi, I.O.; Pagnocca, F.C.; Sette, L.D.; *et al.* Sustainable production of biologically active molecules of marine based origin. *N. Biotechnol.* **2013**, *30*, 839–850.
247. Carr, P.A.; Wang, H.H.; Sterling, B.; Isaacs, F.J.; Lajoie, M.J.; Xu, G.; Church, G.M.; Jacobson, J.M. Enhanced multiplex genome engineering through co-operative oligonucleotide co-selection. *Nucleic Acids Res.* **2012**, *40*, e132.

Bis(2,3-dibromo-4,5-dihydroxybenzyl) Ether, a Marine Algae Derived Bromophenol, Inhibits the Growth of *Botrytis cinerea* and Interacts with DNA Molecules

Ming Liu, Genzhu Wang, Lin Xiao, Xuanli Xu, Xiaohui Liu, Pingxiang Xu and Xiukun Lin

Abstract: Bis(2,3-dibromo-4,5-dihydroxybenzyl) ether (BDDE) is a bromophenol isolated from marine algae. Previous reports have shown that BDDE possesses cytotoxic and antibacterial activity. In the present study, we demonstrate that BDDE displays broad-spectrum antifungal activities, especially on *Botrytis cinerea*. BDDE inhibits the growth of *B. cinerea* cultured on a solid medium of potato dextrose agar (PDA) as well as on the potato dextrose broth (PDB) medium. Moreover, BDDE decreases the incidence of fruit decay and severity of strawberries infected with *B. cinerea*. Further studies have revealed that BDDE decreases the germination rate and inhibits the mycelial growth of *B. cinerea*. The inhibition mechanisms are related to the disruption of the cell membrane integrity in *B. cinerea* spores and newly formed germ tubes. This study also suggests that BDDE possibly interacts with DNA via intercalation and minor groove binding. The studies provide evidence that BDDE has potential application in the control of gray mold after fruit harvest and the compound could serve as a candidate or lead template for rational drug design and for the development of antifungal agents.

Reprinted from *Mar. Drugs*. Cite as: Liu, M.; Wang, G.; Xiao, L.; Xu, X.; Liu, X.; Xu, P.; Lin, X. Bis(2,3-dibromo-4,5-dihydroxybenzyl) Ether, a Marine Algae Derived Bromophenol, Inhibits the Growth of *Botrytis cinerea* and Interacts with DNA Molecules. *Mar. Drugs* **2014**, *12*, 3838–3851.

1. Introduction

Phytopathogenic fungi, one type of major parasitic organisms, constitute a main threat to plants, and usually induce serious diseases and yield losses in crops [1]. Currently, infection by phytopathogenic fungi on plants, such as gray mold, is generally treated with synthetic fungicides to control susceptible pathogens [2]. Although the synthetic fungicides are effective and used widely, continuous application of these fungicides has resulted in loss of biological control and has led to drug resistance and environmental problems [3]. Moreover, synthetic fungicides often induce concern in food safety. To overcome these problems, continuous efforts to find safer, more effective control options with minimal risk to human health and the environment is urgent.

Marine bromophenols, usually existing in marine sponges and algae, have attracted much attention in the field of antimicrobial agents [4]. Accumulated evidence indicates that marine bromophenols possess promising antibacterial activity [5–7] and antiviral activities [8,9]. For example, a synthesized bromophenol compound, 2,4,6,2′,4′,6′-hexabromodiorcinol, shows potent antibacterial activity against several pathogenic bacteria with MIC values ranging from 0.556 to 1.11 μM [7]. In addition, symphyocladin G, a new bromophenol adduct derived from marine red alga *Symphyocladia latiuscula*, is found to possess antifungal activity against *Candida albicans* [10].

Several bromophenols isolated from red alga *Odonthalia corymbifera* have been reported to be promising candidates for antifungal agents in crop protection. These bromophenols could inhibit the pathogenicity of fungus *Magnaporthe grisea* and reduce the appressorium formation on rice plants [11].

Bis(2,3-dibromo-4,5-dihydroxybenzyl) ether (BDDE, Figure 1A), isolated from the marine algae *Leathesia nana*, *Rhodomela confervoides*, and *Rhodomela confervoides*, possesses a variety of bioactivities, such as cytotoxicity to cancer cells [12,13], inhibition of protein tyrosine phosphatase 1B [14], and α-gulcosidase [15–18]. BDDE also exhibits antibacterial activity against several strains of Gram positive and Gram negative bacteria [6]. In this study, we demonstrate that BDDE displays antifungal activities on several strains of fungal pathogens, and has the potential to control gray mold in fruit caused by *Botrytis cinerea*. We find that BDDE inhibits the spore germination and germ tube elongation of *B. cinerea*, and the mechanisms are related to the disruption of cell membranes in *B. cinerea* and the interaction with DNA.

Figure 1. Chemical structure of bis(2,3-dibromo-4,5-dihydroxybenzyl) ether (BDDE).

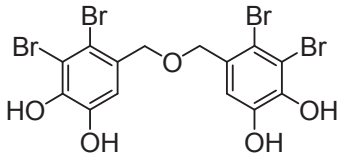

2. Results

2.1. BDDE Inhibits the Mycelial Growth of Fungal Pathogens

To evaluate the antifungal activities of BDDE *in vitro*, we examined its inhibition on mycelial growth to seven fungal pathogens. As shown in Table 1 and Figure 2A, BDDE (100 μg/mL) displayed broad and potent inhibition on the mycelial growth of *B. cinerea* (a), *Valsa mali* (b), *Fusarium graminearum* (c), *Coniothyrium diplodiella* (d), and *Colletotrichum gloeosporioides* (e), but no inhibition on *Alternaria mali Roberts* and *Alternaria porri* (Table 1). Among these pathogens, *B. cinerea* was relatively more sensitive to BDDE with an inhibition rate of about 83.3% (Table 1). BDDE caused obvious decreases in the colony expansion cultured on PDA medium plate (Figure 2Aa). In addition, BDDE could also inhibit the mycelial growth of *B. cinerea* in PDB medium (Figure 2B). Therefore, *B. cinerea* was selected for further analysis.

2.2. BDDE Inhibits the Growth of Gray Mold on Strawberries

To further confirm the antifungal activities of BDDE, fruit decay tests were carried out on freshly harvested strawberries. As shown in Figure 3A, the fruits infected with *B. cinerea* for 5 days showed serious decay in the control group. However, the formation of gray mold was delayed and the decay incidence decreased to 83%, 57%, and 39% when treated with BDDE at a concentration of 25, 50, 100 μg/mL, respectively (Figure 3B). These results confirmed that BDDE could inhibit the formation of gray mold on strawberries induced by *B. cinerea*.

Figure 2. BDDE inhibits the mycelial growth of fungal pathogens. (**A**) The inhibitory effect of BDDE on the mycelial growth of fungal pathogens. The fungal pathogens including *B. Cinerea* (**a**); *Valsa mali* (**b**); *Fusarium graminearum* (**c**); *Coniothyrium diplodiella* (**d**); *Colletotrichum gloeosporioides* (**e**) were cultured on potato dextrose agar (PDA) medium and treated with BDDE for 4, 2, 3, 2, 3 days, respectively. Three replicates were performed for each fungus; (**B**) BDDE inhibits the mycelial growth of *B. cinerea* cultured in potato dextrose broth (PDB) liquid medium. Fungal spores were pre-germinated in PDB medium for 24 h. Then the spores with germ tube were incubated for another 24 h in the absence (**a**) and presence (**b**) of 100 μg/mL BDDE.

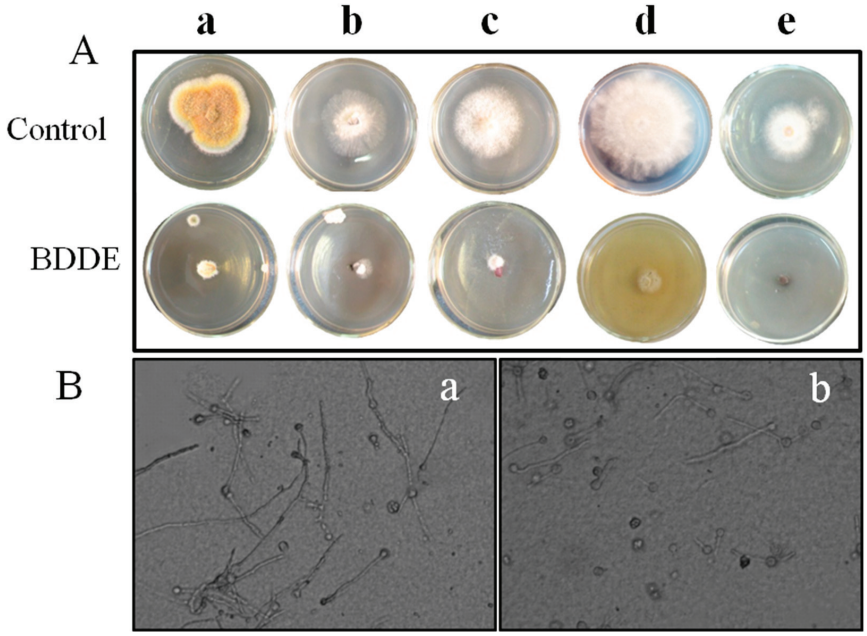

Table 1. Antifungal activities of BDDE against seven fungal pathogens on PDA medium plate containing 100 μg/mL BDDE. Three replicates were used for each fungus.

Pathogenic Fungi	Inhibition Rate (%)
Botrytis cinerea	83.3 ± 6.8
Valsa mali	80.0 ± 7.2
Fusarium graminearum	77.1 ± 5.3
Coniothyrium diplodiella	75.0 ± 8.5
Colletotrichum gloeosporioides	67.7 ± 5.9
Alternaria mali Roberts	0
Alternaria porri	0

Figure 3. Inhibitory effect of BDDE on strawberry gray mold caused by *B. cinerea*. (**A**) Representative pictures of strawberries treated with (100 μg/mL) or without BDDE for 5 days at 23 °C; (**B**) Histogram shows the decay incidence in the absence or presence of BDDE. The experiment was repeated three times. Values are expressed as means ± SD. * $p < 0.05$, ** $p < 0.01$ *versus* control indicates significant difference according to Student's *t*-test.

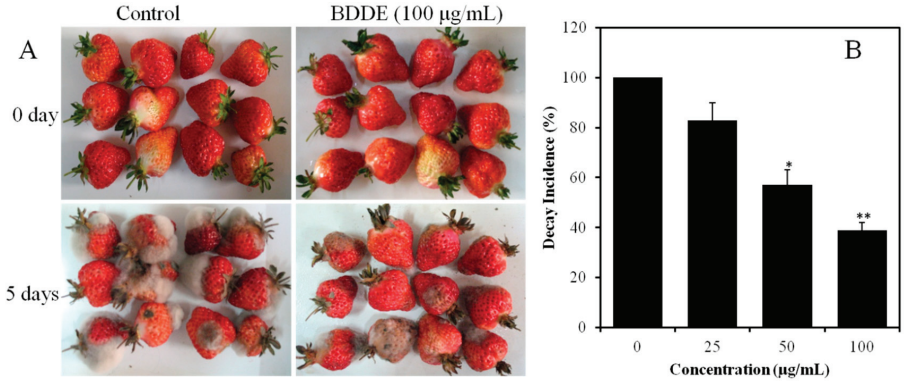

2.3. BDDE Inhibits Spore Germination and Germ Tube Elongation of B. cinerea

The effect of BDDE on spore germination and germ tube elongation in PDB medium was investigated. As shown in Figure 4A, the spore germination of *B. cinerea* was significantly inhibited by BDDE in a concentration dependent manner. The germination rate was 87% in the control group. However, the rate was decreased significantly when the spores were treated with BDDE; the germination rate decreased to 74%, 45%, 39%, and 6%, when treated the spores with 12.5, 25, 50, and 100 μg/mL BDDE, respectively (Figure 4B). The IC_{50} value of BDDE on *B. cinerea* germination is about 31 μg/mL. In addition, BDDE also suppressed the elongation of germ tube. Germ tube elongation decreased with the increasing concentration of BDDE, and was almost completely inhibited by BDDE at 100 μg/mL (Figure 4A). These results indicated that both spore germination and germ tube elongation were inhibited by BDDE.

2.4. BDDE Destroys the Membrane Integrity of B. cinerea

In order to illustrate the mechanisms underlying the BDDE inhibition against *B. cinerea*, we first detected the membrane integrity of *B. cinerea* using the propidium iodide (PI) staining assay. The PI stained cells from more than 100 spores were counted under a fluorescence microscope. As shown in Table 2, compared with the control group, more spores were stained by PI and the percentage of stained cells increased in a concentration dependent manner; in the absence of BDDE, the percentage of PI stained spores was only 5.6%. However, it increased to 11%, 16%, and 23% when treated with BDDE at a concentration of 25, 50 and 100 μg/mL, respectively. These results suggested that BDDE enhanced the membrane permeabilization of *B. cinerea*.

Figure 4. Effect of BDDE on spore germination and germ tube elongation of *B. cinerea* in PDB. (**A**) Spores were treated without (**a**) or with BDDE at a concentration of 25 (**b**), 50 (**c**), and 100 μg/mL (**d**). The germination rate and germ tube elongation were observed using a microscope; (**B**) Histogram shows the germination inhibition rate in the absence or presence of BDDE. Values are expressed as means ± SD. * $p < 0.05$, ** $p < 0.01$ *versus* control indicates significant difference according to Student's *t*-test.

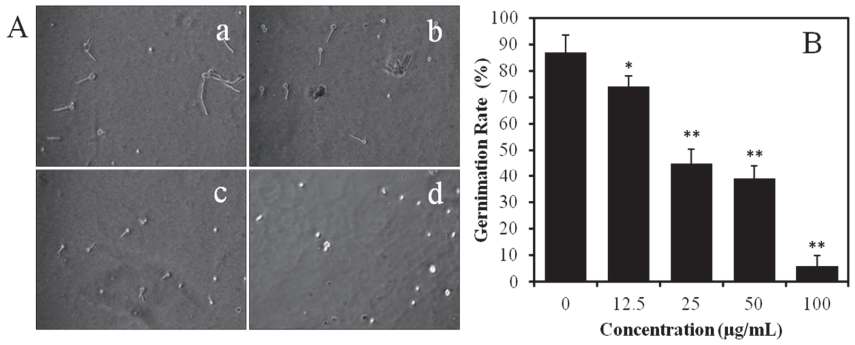

Table 2. Number of total spores and PI stained spores untreated or treated with 25, 50, and 100 μg/mL of BDDE for 24 h, respectively.

BDDE (μg/mL)	Total Number of Spores	Number of PI Stained Spores	Percentage of PI Stained Spores (%)
0	123	7	5.6
25	116	12	11
50	106	17	16
100	108	25	23

2.5. BDDE Interacts with DNA

It is well established that many antifungal agents can interact with DNA molecules [19]. To investigate if BDDE could interact with DNA, a series of spectroscopic analyses was performed using calf thymus DNA (ctDNA), which is widely used to study the interaction between small molecules and DNA. As shown in Figure 5A, the UV-VIS spectrum of ctDNA displayed an obvious absorption at 260 nm, while BDDE alone only present a relatively low absorption. However, a significant suppression was found when adding BDDE to the ctDNA solution and a red shift of the maximum peak was found, indicating that an interaction happens between BDDE and ctDNA. DAPI can interact with DNA molecules by binding in the minor groove and the major groove [20]. To further confirm the interaction between DNA and BDDE, a DAPI displacement fluorescence assay was employed. The results showed that, in the absence of the BDDE, the peak fluorescent intensity of DNA and DAPI was 265 ± 16. However, the intensity decreased to 235 ± 14 and 222 ± 13, when treated with 15 and 30 μM BDDE, respectively. As shown in Figure 5B, the representative fluorescence emission spectra showed that a significant reduction in fluorescence

was observed upon treatment with BDDE. The results suggested that BDDE displaced the DAPI from DNA, and there was an interaction between BDDE and DNA.

Figure 5. BDDE interacts with calf thymus DNA (ctDNA). (**A**) BDDE changes the absorption spectrum of ctDNA. The UV absorption spectra of ctDNA (50 μM) at 260 nm were analyzed in the presence (100 μM) and absence of BDDE using a Beckman DU 650 UV-VIS spectrophotometer (Kleve, Germany); (**B**) DAPI is displaced by BDDE as determined by fluorescence emission spectra. ctDNA (50 μM) was incubated with DAPI (1.5 μM) or concentrations of BDDE (15, 30 μM) for 30 min at 37 °C, respectively. Fluorescence emission spectra (λ_{max} = 488 nm, λ_{exc} = 340 nm) were determined using a Hitachi F-4500 fluorescence spectrophotometer (Tokyo, Japan). The experiment was repeated more than three times.

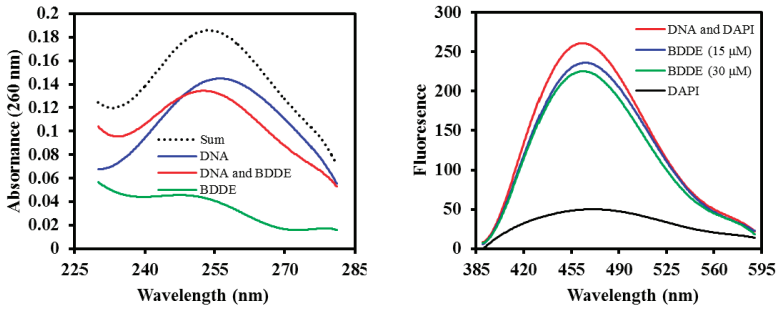

2.6. BDDE Intercalates ctDNA and Binds with the Minor Groove of ctDNA

Acridine orange (AO), a DNA probe agent, can intercalate into DNA molecules [21], and Hoechst33258 is a DNA binding agent, which can interact with the minor groove of DNA [22]. To further study the interaction between BDDE and DNA, displacement experiments were performed. The results showed that both AO and Hoechst33258 could be displaced from ctDNA (Figure 6A,B), indicating that the interaction between BDDE and DNA includes both intercalation mode and minor groove binding mode. The result was consistent with our previous study in that BDDE molecule fitted well into the minor groove of the DNA fragment consisting of sequential A-T base pairs [13].

Analysis of the CD spectrum also confirmed the interaction; a distinct change was found in the UV region of the CD spectrum of ctDNA when treated with BDDE, and there was a significant decrease in the positive DNA diachronic signal and a reduction in molar ellipticity in the negative band (Figure 6C). To determine if BDDE can cleave DNA directly, we incubated BDDE and pBR322 DNA together, and then checked if cleaved fragments were produced. As shown in Figure 6D, no cleaved fragments were observed, even when treated with high concentration of BDDE. These results suggested that there was interaction between DNA and BDDE *in vitro*; the interaction might include DNA binding as well as intercalation.

Figure 6. Interaction mode between BDDE and DNA. (**A**) BDDE displaces AO from DNA. AO (0.5 μM) was incubated with ctDNA (50 μM) in the absence or presence of BDDE at a concentration of 15, 30 μM for 30 min at 37 °C, respectively. Fluorescence emission spectra (λ_{exc} = 502 nm) were determined using a Hitachi F-4500 fluorescence spectrophotometer (Tokyo, Japan); (**B**) BDDE displaces Hoechst33258 from DNA. Hoechst33258 (1.5 μM) was incubated with ctDNA (50 μM) in the absence or presence of BDDE at a concentration of 7.5, 15.0 μM for 30 min at 37 °C, respectively. Fluorescence emission spectra (λ_{exc} = 352 nm) were analyzed using a Hitachi F-4500 fluorescence spectrophotometer (Tokyo, Japan); (**C**) Intrinsic CD spectra of ctDNA affected by BDDE. CD spectra of ctDNA alone (1.5 mM) or ctDNA treated with BDDE (12.5 μM) were measured with a JASCO 715 spectropolarimeter (Tokyo, Japan); (**D**) BDDE does not cleave DNA as detected by the agarose gel electrophoresis. Supercoiled plasmid pBR322 DNA was treated without (lane 1) or with 15.5 (lane 2), 31.3 (lane 3), 62.5 (lane 4), 125 (lane 5), 250 (lane 6), 500 (lane 7), and 1000 μM (lane 8) BDDE for 30 min at 37 °C, respectively. The DNA samples were resolved on 1% agarose, stained with ethidium bromide (1 μg/mL) and photographed under UV light.

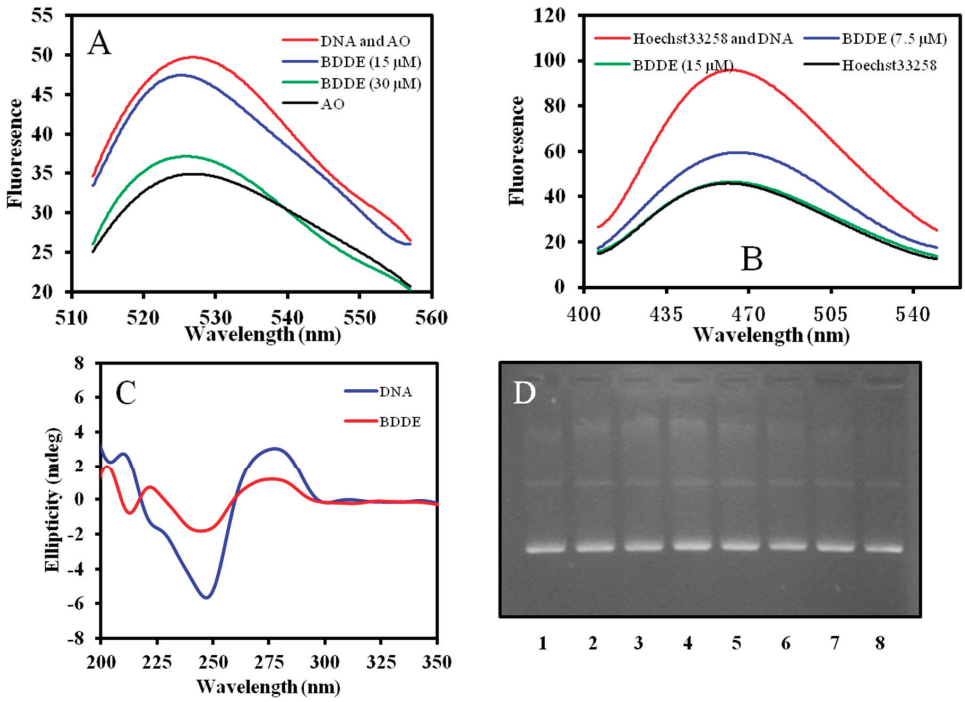

3. Discussion

In the present study, we demonstrate that BDDE can inhibit several fungal pathogens, including *B. cinerea*, *Valsa mali*, *Fusarium graminearum*, *Coniothyrium diplodiella*, and *Colletotrichum gloeosporioides*. BDDE inhibits the growth of *B. cinerea* most clearly, and prevents the gray mold

on strawberries induced by the *B. cinerea*. BDDE can suppress the spore germination and mycelial growth; treatment of the spores with BDDE results in the disruption of the integrity of the cell membrane in *B. cinerea* spores and newly formed germ tubes. Many antifungal agents inhibit the fungal growth by affecting cell membrane permeability. For example, boron decreases gray mold decay by breakdown of the cell membrane and the loss of the cytoplasmic materials [23]; dill oil shows antifungal activities by disrupting the permeability of the plasma membrane [24]. In the present experiments, BDDE induced membrane damage is observed. Loss of membrane integrity in *B. cinerea* has also been reported in several antifungal agents, including *Streptomyces globisporus* JK-1 and quinoa (*Chenopodium quinoa* Willd) alkali. These kinds of compounds usually lead to the leakage of cellular constituents, such as soluble proteins and carbohydrates from hyphae of *B. cinerea* [25,26]. Our study provides more evidence that affecting the integrity of the cell membrane is one of the main mechanisms for antifungal agents.

The results from this study reveal that BDDE can increase the cell permeability. However, compared with the inhibition rate (85%) on the mycelia growth, the percentage of PI stained spores is very low (23%), suggesting a lot of dead spores keep membrane integrity and other mechanisms may play some roles in BDDE induced fungal inhibition. Additionally, these two experiments are performed by different approaches. In the analysis of mycelia growth inhibition, the treatment time of BDDE is 2–4 days. However, in the cell membrane permeabilization experiment, the exposure time of BDDE is only 24 h before PI staining. Some antifungal agents usually result in mitochondrial dysfunction and intracellular ROS accumulation on fungal pathogens [27]. The effects of BDDE on the mitochondria and ROS need to be addressed further. Also, we have observed that on exposure of strawberries to BDDE for 10 days the antifungal effects are still present (data not shown). These primary results indicated the high stability of the compounds. However, a more systemic study is needed to address if the compound is effective for longer term preservation of strawberries or other fruits.

In our previous report, we found that BDDE could displace EB from the DNA molecule [13]. In the present study, we show that BDDE can interact with DNA by binding in the minor groove as well as by intercalation; BDDE can also displace DAPI, AO and Hoechst33258. The data provide primary evidence that identification of compounds interacting with DNA molecules is an important strategy for finding novel antifungal agents. However, more studies are needed to address whether BDDE can interact with DNA *in vivo*; more experiments like co-localization should be performed to document the *in vivo* interaction between DNA and BDDE.

Currently gray mold on fresh fruits is primarily controlled by application of fungicides in the pre-harvest and sulfur dioxide fumigation in the post-harvest periods, and application of these kinds of compounds usually results in problems of safety in the food supply and in the environment. Marine natural compounds, like BDDE, provide an alternate resource for the development of antifungal agents. Considering the wide antifungal spectrum of BDDE, the compound may be used in the prevention of fungal infections in different plants. Additionally, since marine bromophenols are widely distributed in marine algae and sponges, its application as anticancer, as antioxidant agents or when used as antifungal agent is worthy of further study. However, the safety of application of BDDE in agriculture needs consideration. Our previous study has shown that BDDE

possess a relatively low toxicity on a non-tumorigenic epithelial cell line MCF 10A and human vascular endothelium cells (HUVEC) [13]. However, there are reports to show that some bromophenol compounds are suspected of displaying negative impact on human and animal health, acting as endocrine disruptor and moderate toxic agent on mammalian cell [4]. More studies are needed to evaluate the safety of BDDE used as an antifungal agent.

4. Experimental Section

4.1. Drugs, Reagents, and Fruits

BDDE was synthesized as described previously [18]. Propidium iodide (PI), acridine orange (AO), 4′,6-diamidino-2-phenylindole (DAPI), and Hoechst33258 were the products of Beyond, Shanghai, China. Freshly harvested strawberries with no infection or physical injuries were bought from Tianshan orchard, Qingdao, China.

4.2. Fungal Pathogens

The fungal pathogens, *B. cinerea*, *Valsa mali*, *Fusarium graminearum*, *Coniothyrium diplodiella*, *Colletotrichum gloeosporioides*, *Alternaria mali Roberts*, and *Alternaria porri* were kindly provided by College of Chemistry and Pharmaceutical Sciences, Qingdao Agricultural University, Qingdao, China. All of these fungi were cultured on potato dextrose agar (PDA) plates at 23 °C. Spores of *B. cinerea* were obtained from 14 day old cultures by washing with sterile distilled water containing 0.05% (*v/v*) Tween 80 and filtered by sterile cheesecloth. The concentration of the spores was determined using hemocytometer.

4.3. Effect of BDDE on Mycelial Growth of Fungal Pathogens on PDA Plates

The effect of BDDE on mycelial growth of seven fungal pathogens was analyzed in PDA as described previously [28]. Briefly, the fungal pathogens including *B. cinerea*, *Valsa mali*, *Fusarium graminearum*, *Coniothyrium diplodiella*, *Colletotrichum gloeosporioides*, *Alternaria mali Roberts*, and *Altenaria porri* were cultured on PDA plates. After incubation for 7 days, the mycelial agar (5 mm) was cut and placed in the center of a 6-cm-diameter Petri dish containing PDA without and with 100 μg/mL of BDDE. Radial growth of each fungi was observed after incubation for 2–4 days at 23 °C and the inhibition rate of mycelial growth was calculated using the following formula: Inhibition rate of mycelial growth (%) = (1 − diameter of mycelia in the BDDE-treated medium/diameter of mycelia in the no-treatment medium) × 100.

4.4. Effect of BDDE on Mycelial Growth of B. cinerea in Liquid Medium

The effect of BDDE on mycelial growth in liquid medium of *B. cinerea* was analyzed. Briefly, *B. cinerea* spores were pre-germinated in PDB medium for 24 h at 23 °C to form a germ tube. The germ tube and mycelial growth was observed using a microscope after treatment with BDDE (0–100 μg/mL) for another 24 h.

4.5. Inhibition of Fruit Decay by BDDE

Effect of BDDE on fruit decay was tested using the methods described previously with little modification [29]. Briefly, freshly harvested healthy strawberries were surface-sterilized in 70% ethanol for 30 s, and washed with sterile water. All of the fruits were inoculated with a *B. cinerea* spore suspension. Inocula (1.0×10^6 spores/mL, 3 mL) were sprayed on about 48 berries with an air-brush sprayer. Berries were dried in air for 1 h, randomized into 4 groups (12/group), and then soaked in certain concentrations of BDDE (25, 50, 100 μg/mL) or sterile water for 10 s. After the treatment, fruits were kept in trays covered with plastic film and incubated for 5 days at 23 °C. Damage severity was observed and the decay incidence was calculated using the following formula: Disease incidence (%) = (Number of decayed berries/Total number of treated berries) × 100.

4.6. Effect of BDDE on Spore Germination and Germ Tube Elongation of B. cinerea

Inhibition of BDDE on spore germination and germ tube elongation of *B. cinerea* was measured as described previously with little modifications [30]. In brief, *B. cinerea* spores (final concentration of 5×10^5 spores/mL) were added in PDB medium containing certain concentrations of BDDE (0–100 μg/mL) and incubated at 23 °C on a rotary shaker at 100 rpm for 12 h. Spores were considered germinated if the germ tube was equal to or greater than the diameter of the spore and a minimum of 100 spores were counted in each replicate under a microscope using a micrometer. The percentage of spore germination was calculated using the following formula: Germinated rate (%) = (Number of germinated spores/Total number of spores) × 100.

4.7. Analysis of Membrane Integrity Using Propidium Iodide (PI) Staining

Membrane integrity was detected using PI staining as reported previously [23]. Spores of *B. cinerea* were treated with BDDE (0–100 μg/mL) in PDB medium. After incubation at 23 °C for 24 h, spores were collected by centrifugation and stained with 10 μg/mL propidium iodide (PI) for 10 min at 30 °C. The spores were washed twice with PBS, and spread onto slides. A minimum of 100 spores were counted under the fluorescence microscopy (Zeiss, Germany). The percentage of PI-stained spores and germ tubes was calculated using the following formula: Percentage of PI negative staining (%) = (Number of PI negative stained spores/Total number of spores) × 100.

4.8. UV Absorption Spectroscopy

BDDE (100 μM) and DNA (50 μM) were dissolved in 50 mM phosphate buffer (pH 7.0). The absorption spectra were recorded in the presence or absence of BDDE (100 μM) using a Beckman DU 650 UV-VIS spectrometer (Kleve, Germany), respectively.

4.9. Circular Dichroism Spectroscopy for Secondary Structure of ctDNA

CD spectra (220–300 nm) of ctDNA (1.5 mM) treated with BDDE (12.5 μM) were measured with a JASCO 715 spectropolarimeter (JASCO, Tokyo, Japan). The spectra were collected and corrected by reduction of noise and smoothing using the program JWSSE (JASCO, Tokyo, Japan).

4.10. DAPI, AO, and Hoechst33258 Displacement Fluorescence Assay

DAPI, AO, and Hoechst33258 displacement fluorescence assay were employed to determine the interaction and interaction mode between BDDE and DNA. ctDNA (50 μM) was dissolved in 50 mM phosphate buffer (pH 7.0) and incubated with DAPI (1.5 μM), AO (0.5 μM), and Hoechst33258 (1.5 μM), respectively. Certain concentrations of BDDE were added and incubated for 30 min at 37 °C. Fluorescence emission spectra of DAPI, AO, and Hoechst33258 were determined using a Hitachi F-4500 fluorescence spectrophotometer (JASCO, Tokyo, Japan).

4.11. Agarose Gel Electrophoresis

Supercoiled plasmid pBR322 DNA (0.25 μg) was dissolved in the reaction buffer (35 mM Tris-HCl, 72 mM KCl, 5 mM $MgCl_2$, 5 mM DTT, 5 mM spermidine and 0.1% BSA). Certain concentrations of BDDE (0–1000 μM) were added in the reaction buffer and incubated for 30 min at 37 °C. The reaction was terminated by lyophilizing at −80 °C and DNA samples were resolved on 1% agarose, stained with ethidium bromide (1 μg/mL) and photographed under UV light.

4.12. Data Analysis

Student's *t*-test was used for statistical analysis of the data, and values were expressed as mean ± SD. Differences of $p < 0.05$ were considered statistically significant.

5. Conclusions

In conclusion, the present study reveals that the bromophenol BDDE displays inhibition against several fungal pathogens. BDDE decreases the germination rate, inhibits the mycelial growth of *B. cinerea*, and destroys the integrity of the fungal cell membrane. BDDE interacts with DNA via intercalation and minor groove binding, and both the membrane disruption effect and the DNA-binding activities may contribute to the antifungal effects in BDDE-induced inhibition of fungal pathogens. With the unique chemical structure different from the current fungicides, BDDE may serve as a novel antifungal candidate or parent compound for rational drug design.

Acknowledgments

This work was supported by the National Natural Science Foundation of China (No. 81001396 and No. 81273550) and State Innovative Drugs Development Program of China (No. 2013ZX09103003019). We are also grateful to Fred Bogott at the Minnesota University and Poul Erik Hansen in Roskilde University for their careful editing of the manuscript.

Author Contributions

Ming Liu, Lin Xiao, and Xiukun Lin contributed to the study concept and design, and the manuscript preparation. Ming Liu, Lin Xiao and Genzhu Wang performed the experimental studies and analyzed the data. Xuanli Xu, Xiaohui Liu, and Pingxiang Xu helped acquire data and

statistical analysis. Ming Liu, Genzhu Wang., and Xiukun Lin revised the article critically for intellectual content.

Conflicts of Interest

The authors declare no conflict of interest.

References

1. Gonzalez-Fernandez, R.; Jorrin-Novo, J.V. Contribution of proteomics to the study of plant pathogenic fungi. *J. Proteome Res.* **2012**, *11*, 3–16.
2. Elad, Y.; Gullino, M.L.; Shtienberg, D.; Aloi, C. Managing *Botrytis cinerea* on tomatoes in greenhouses in the Mediterranean. *Crop Prot.* **1995**, *14*, 105–109.
3. Soylu, E.M.; Kurt, Ş.; Soylu, S. *In vitro* and *in vivo* antifungal activities of the essential oils of various plants against tomato grey mould disease agent *Botrytis cinerea*. *Int. J. Food Microbiol.* **2010**, *143*, 183–189.
4. Liu, M.; Hansen, P.E.; Lin, X. Bromophenols in marine algae and their bioactivities. *Mar. Drugs* **2011**, *9*, 1273–1292.
5. Popplewell, W.L.; Northcote, P.T. Colensolide A: A new nitrogenous bromophenol from the New Zealand marine red alga *Osmundaria colensoi*. *Tetrahedron Lett.* **2009**, *50*, 6814–6817.
6. Xu, N.; Fan, X.; Yan, X.; Li, X.; Niu, R.; Tseng, C.K. Antibacterial bromophenols from the marine red alga *Rhodomela confervoides*. *Phytochemistry* **2003**, *62*, 1221–1224.
7. Chen, M.; Shao, C.L.; Fu, X.M.; Xu, R.F.; Zheng, J.J.; Zhao, D.L.; She, Z.G.; Wang, C.Y. Bioactive indole alkaloids and phenyl ether derivatives from a marine-derived *Aspergillus* sp. Fungus. *J. Nat. Prod.* **2013**, *76*, 547–553.
8. Park, H.J.; Kurokawa, M.; Shiraki, K.; Nakamura, N.; Choi, J.S.; Hattori, M. Antiviral activity of the marine alga *Symphyocladia latiuscula* against herpes simplex virus (HSV-1) *in vitro* and its therapeutic efficacy against HSV-1 infection in mice. *Biol. Pharm. Bull.* **2005**, *28*, 2258–2262.
9. Kim, S.Y.; Kim, S.; Oh, M.J.; Jung, S.J.; Kang, S. *In Vitro* antiviral activity of red alga, *Polysiphonia morrowii* extract and its bromophenols against fish pathogenic infectious hematopoietic necrosis virus and infectious pancreatic necrosis virus. *J. Microbiol.* **2011**, *49*, 102–106.
10. Xu, X.; Piggott, A.M.; Yin, L.; Capon, R.J.; Song, F. Symphyocladins A–G: Bromophenol adducts from a Chinese marine red alga, *Symphyocladia latiuscula*. *Tetrahedron Lett.* **2012**, *53*, 2103–2106.
11. Lee, H.S.; Lee, T.H.; Lee, J.H.; Chae, C.S.; Chung, S.C.; Shin, D.S.; Shin, J.; Oh, K.B. Inhibition of the pathogenicity of magnaporthe grisea by bromophenols, isocitrate lyase inhibitors, from the red alga *Odonthalia corymbifera*. *J. Agric. Food Chem.* **2007**, *55*, 6923–6928.

12. Xu, X.; Song, F.; Wang, S.; Li, S.; Xiao, F.; Zhao, J.; Yang, Y.; Shang, S.; Yang, L.; Shi, J. Dibenzyl bromophenols with diverse dimerization patterns from the brown alga *Leathesia nana*. *J. Nat. Prod.* **2004**, *67*, 1661–1666.
13. Liu, M.; Zhang, W.; Wei, J.; Qiu, L.; Lin, X. Marine bromophenol bis(2,3-dibromo-4, 5-dihydroxybenzyl) ether, induces mitochondrial apoptosis in K562 cells and inhibits topoisomerase I *in vitro*. *Toxicol. Lett.* **2012**, *211*, 126–134.
14. Shi, D.; Xu, F.; He, J.; Li, J.; Fan, X.; Han, L. Inhibition of bromophenols against PTP1B and anti-hyperglycemic effect of *Rhodomela confervoides* extract in diabetic rats. *Chin. Sci. Bull.* **2008**, *53*, 2476–2479.
15. Kurihara, H.; Mitani, T.; Kawabata, J.; Takahashi, K. Inhibitory potencies of bromophenols from Rhodomelaceae algae against α-glucosidase activity. *Fish Sci.* **1999**, *65*, 300–303.
16. Kurihara, H.; Mitani, T.; Kawabata, J.; Takahashi, K. Two new bromophenols from the red alga *Odonthalia corymbifera*. *J. Nat. Prod.* **1999**, *62*, 882–884.
17. Kim, K.Y.; Nguyen, T.H.; Kurihara, H.; Kim, S.M. Alpha-glucosidase inhibitory activity of bromophenol purified from the red alga *Polyopes lancifolia*. *J. Food Sci.* **2010**, *75*, H145–H150.
18. Liu, M.; Zhang, W.; Wei, J.; Lin, X. Synthesis and α-glucosidase inhibitory mechanisms of bis(2,3-dibromo-4,5-dihydroxybenzyl) ether, a potential marine bromophenol α-glucosidase inhibitor. *Mar. Drugs* **2011**, *9*, 1554–1565.
19. Lou, L.; Velligan, M.; Roberts, C.; Stevens, D.A.; Clemons, K.V. DNA binding compounds targeting fungal pathogens: An emerging concept in the discovery of novel antifungal agents. *Curr. Opin. Investig. Drugs* **2002**, *3*, 1437–1445.
20. Banerjee, D.; Pal, S.K. Dynamics in the DNA recognition by DAPI: Exploration of the various binding modes. *J. Phys. Chem. B* **2008**, *112*, 1016–1021.
21. Nafisi, S.; Saboury, A.A.; Keramat, N.; Neault, J.F.; Tajmir-Riahi, H.A. Stability and structural features of DNA intercalation with ethidium bromide, acridine orange and methylene blue. *J. Mol. Struct.* **2007**, *827*, 35–43.
22. Palchaudhuri, R.; Hergenrother, P.J. DNA as a target for anticancer compounds: methods to determine the mode of binding and the mechanism of action. *Curr. Opin. Biotechnol.* **2007**, *18*, 497–503.
23. Qin, G.; Zong, Y.; Chen, Q.; Hua, D.; Tian, S. Inhibitory effect of boron against *Botrytis cinerea* on table grapes and its possible mechanisms of action. *Int. J. Food Microbiol.* **2010**, *138*, 145–150.
24. Tian, J.; Ban, X.; Zeng, H.; He, J.; Chen, Y.; Wang, Y. The mechanism of antifungal action of essential oil from dill on *Aspergillus flavus*. *PLoS One* **2012**, *7*, e30147.
25. Li, Q.; Ning, P.; Zheng, L.; Huang, J.; Li, G.; Hsiang, T. Effects of volatile substances of Streptomyces globisporus JK-1 on control of *Botrytis cinerea* on tomato fruit. *Biol. Control* **2012**, *61*, 113–120.
26. Stuardo, M.; San Martín, R. Antifungal properties of quinoa (*Chenopodium quinoa* Willd) alkali treated saponins against *Botrytis cinerea*. *Ind. Crop. Prod.* **2008**, *27*, 296–302.

27. Helmerhorst, E.J.; Troxler, R.F.; Oppenheim, F.G. The human salivary peptide histatin 5 exerts its antifungal activity through the formation of reactive oxygen species. *Proc. Natl. Acad. Sci. USA* **2001**, *98*, 14637–14642.
28. Droby, S.; Wisniewski, M.; El Ghaouth, A.; Wilson, C. Influence of food additives on the control of postharvest rots of apple and peach and efficacy of the yeast-based biocontrol product aspire. *Postharvest Biol. Technol.* **2003**, *27*, 127–135.
29. Huang, R.; Che, H.J.; Zhang, J.; Yang, L.; Jiang, D.H.; Li, G.Q. Evaluation of *Sporidiobolus pararoseus* strain YCXT3 as biocontrol agent of *Botrytis cinerea* on post-harvest strawberry fruits. *Biol. Control* **2012**, *62*, 53–63.
30. Qin, G.Z.; Tian, S.P.; Xu, Y.; Wan, Y.K. Enhancement of biocontrol efficacy of antagonistic yeasts by salicylic acid in sweet cherry fruit. *Physiol. Mol. Plant Pathol.* **2003**, *62*, 147–154.

Oleosome-Associated Protein of the Oleaginous Diatom *Fistulifera solaris* Contains an Endoplasmic Reticulum-Targeting Signal Sequence

Yoshiaki Maeda, Yoshihiko Sunaga, Tomoko Yoshino and Tsuyoshi Tanaka

Abstract: Microalgae tend to accumulate lipids as an energy storage material in the specific organelle, oleosomes. Current studies have demonstrated that lipids derived from microalgal oleosomes are a promising source of biofuels, while the oleosome formation mechanism has not been fully elucidated. Oleosome-associated proteins have been identified from several microalgae to elucidate the fundamental mechanisms of oleosome formation, although understanding their functions is still in infancy. Recently, we discovered a diatom-oleosome-associated-protein 1 (DOAP1) from the oleaginous diatom, *Fistulifera solaris* JPCC DA0580. The DOAP1 sequence implied that this protein might be transported into the endoplasmic reticulum (ER) due to the signal sequence. To ensure this, we fused the signal sequence to green fluorescence protein. The fusion protein distributed around the chloroplast as like a meshwork membrane structure, indicating the ER localization. This result suggests that DOAP1 could firstly localize at the ER, then move to the oleosomes. This study also demonstrated that the DOAP1 signal sequence allowed recombinant proteins to be specifically expressed in the ER of the oleaginous diatom. It would be a useful technique for engineering the lipid synthesis pathways existing in the ER, and finally controlling the biofuel quality.

Reprinted from *Mar. Drugs*. Cite as: Maeda, Y.; Sunaga, Y.; Yoshino, T.; Tanaka, T. Oleosome-Associated Protein of the Oleaginous Diatom *Fistulifera solaris* Contains an Endoplasmic Reticulum-Targeting Signal Sequence. *Mar. Drugs* **2014**, *12*, 3892–3903.

1. Introduction

With an increased demand for a sustainable energy supply, biofuel production has attracted much attention. Microalgal biodiesel production has been researched to meet such demand due to its advantageous features (e.g., global carbon dioxide fixation, no competition for food, much higher biomass yield than higher plants, and oil accumulation at a high level inside the cells) [1]. Several oleaginous microalgae can accumulate triacylglycerol (TAG) in high level as a form of the oleosome (also known as oil body), and such promising oil producers have been intensively studied to understand the TAG biosynthesis [2–6].

A current trend in this field is genome and transcriptome analyses to determine the active synthesis pathways for fatty acids and TAG in the target oil-producing organisms [7–11], while proteome analysis has also been launched to identify the proteins closely attached around the oleosomes. The proteomic approach is expected to identify the novel protein machineries directly participating in the oleosome formation, which conventional pathway analysis can hardly address. It leads to the elucidation of the biological mechanism for oleosome development, and can provide

promising targets of genetic engineering for the purpose of oil production improvements. However, the oleosome-associated proteins have been studied in only a few microalgae [12–19].

Among such rare examples, we have focused on *Fistulifera solaris* JPCC DA0580, an oleaginous marine diatom screened from our marine microalgal culture collection [17]. Beneficial features of this strain for practical biodiesel production include a high growth rate, high lipid content (up to 60%, *w*/*w*), a low unsaturation degree of the accumulated lipids, as well as ease of mass cultivation [20–23]. Recently, the proteome analysis for this diatom identified two oleosome-associated proteins, G12504 and G16188 (formerly g4301 and g6574, respectively) [17]. The GFP-fusion experiment demonstrated that G16118 (tentative potassium channel) showed a broad subcellular distribution including the oleosome. In contrast, G12504 (containing a quinonprotein alcohol dehydrogenase-like domain) exhibited a strict localization only on the oleosomes, implying that this protein could play a role for oleosome formation, and contain a specific signal sequence directing the proteins onto the oleosomes. This notion led us to further research the sequence features of this diatom-oleosome-associated protein, G12504 (referred to as DOAP1 in this study) in detail, and encouraged us to estimate the routing mechanism of this protein into oleosome-targeting. Particularly we focused on the *N*-terminal signal sequence which primarily governs the localization of the nuclear-encoded polypeptides within the cell organelles [24].

In this study, we carefully determined the *N*-terminal signal sequence of DOAP1, and fused it with GFP in order to examine the initial localization of this oleosome-associated protein. Fluorescent microscopy of the fusion protein revealed that the signal sequence of DOAP1 could transport proteins into endoplasmic reticulum (ER) of *F. solaris*, implying the initial localization of DOAP1 at the ER and subsequent transportation to the oleosomes. Additionally, this study also means the success in specific expression of the recombinant protein into the oleaginous microalgal ER where important lipid synthesis reactions occur [25]. It would be useful for future metabolic engineering for improvement of biofuel quality.

2. Results

2.1. Characterization of Doap1 Gene Structure

Comparison between the genomic and cDNA sequences revealed that *doap1* gene includes one internal intron. RNA-seq data (partially published [25,26]) supported the transcribed region with 1977 bp (Supplementary Figure S1). TATA-box candidate sequences were found upstream of the transcribed region, indicating the presence of a promoter for *doap1* gene. It would be reasonable to consider that translation of DOAP1 starts from the most forward start codon in the RNA-seq supporting region, thus the start codon was predicted to locate 93 bp-downstream from the transcription initiation site (Supplementary Figure S1).

The coding region is estimated to produce a polypeptide with 562 amino acid residues (~59.0 kDa, Supplementary Figure S2). Sequence features of DOAP1 were examined with the SignalP [27] and InterProScan algorisms, and it was predicted that DOAP1 contains an *N*-terminal signal sequence (ranging from M1 to A19), as well as quinonprotein alcohol dehydrogenase-like superfamily (IPR011047, ranging from Q18 to P184). Subcellular localization of DOAP1 was

predicted with a series of bioinformatics tools we have utilized [17,25], and as a result ER-localization was assumed. A proline knot motif was found in the plant oleosome-associated proteins, and demonstrated to work as a specific signal for oleosome-targeting in plants (oleosins) [28,29]. In the case of microalgal oleosome-associated proteins found to date, the proline knot motif is not present, but proline-rich hydrophobic domain is contained [19]. Similarly, DOAP1 is less likely to have the proline knot-like motif, while a proline-rich region (Supplementary Figure S2) and a highly hydrophobic region [17] individually exist at the *C*-terminus. BLAST screening revealed that *Phaeodactylum tricornutum*, a pennate diatom same with *F. solaris*, is the only organism which has an ortholog of this protein according to the present national center for biotechnology information (NCBI) database, while its function remains unknown.

2.2. GFP Expression in the Transformants

To confirm the initial subcellular localization of DOAP1, we attempted to express the fusion protein of DOAP1 signal sequence and GFP (S_{DOAP1}-GFP). Although the DOAP1-coding region was assumed as mentioned above, we determined to fuse the DNA fragment ranging from the tentative promoter region to the predicted coding region of the *N*-terminal 57 amino acid of DOAP1 (including the signal sequence and a part of mature DOAP1, see also Supplementary Figures S1 and S2) with *green fluorescence protein* (*gfp*) gene in order to ensure the actual native signal sequence can be expressed. It should be noted that our previous study also utilized the same DNA region to express the full length of DOAP1 fused with GFP [17]. The constructed expression vector was introduced into *F. solaris* cells. As-prepared transformants were subjected to Western blotting to confirm whether the fusion protein S_{DOAP1}-GFP was produced in the cells. A specific band was visualized in the transformant sample using anti-GFP antibody (Figure 1). The detected protein was larger than the neat GFP produced in the *F. solaris* transformants (Supplementary Figure S3), suggesting the successful expression of the target fusion protein. Furthermore, its size was smaller than the intact protein corded (approximately 33 kDa); this could be caused by the cleavage of the signal peptide after transportation [30]. As a negative control experiment, wild type cells were also examined, and no signal was detected.

2.3. ER-Targeting of S_{DOAP1}-GFP

To examine whether the DOAP1 signal sequence directs proteins to specific organelles, the cells expressing S_{DOAP1}-GFP were observed using a fluorescent microscope. The intense fluorescence was observed around the chloroplast, as well as central cellular region (Figure 2). This fluorescence distribution was obviously different from that of the fusion protein consisted of full length of DOAP1 and GFP, which strictly localized at the oleosomes [17]. When GFP and chlorophyll distribution was spatially profiled, it was demonstrated that the peak of GFP fluorescence was outside of the chlorophyll (Figure 3a). This feature was reproducibly confirmed in several cells (Supplementary Figure S4), suggesting that S_{DOAP1}-GFP localizes outside the chloroplast. In the case of the transformants expressing the neat GFP, only the central cellular region emitted significant fluorescence, suggesting the expression at the cytoplasm (Figure 3b). When the cells

were stained with the Hoechst dye, the nucleus was demonstrated to localize at the center of the cell, and surrounded by the GFP emission (Supplementary Figure S5).

Figure 1. Green fluorescence protein (GFP) detection with Western blotting from *F. solaris* JPCC DA0580 transformants expressing neat GFP (**Lane 1**); SDOAP1-GFP (**Lane 2**); and wild-type cells (**Lane 3**). Lane M represents molecular marker.

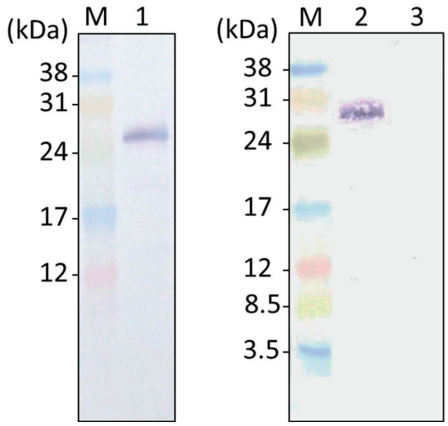

Figure 2. Microscopy studies on *F. solaris* JPCC DA0580 transformants expressing SDOAP1-GFP. (**a**) Bright field and fluorescent images of the transformants; (**b**) Magnified images of the square regions in (**a**). Black arrows represent oleosomes. (scale bar = 2 μm).

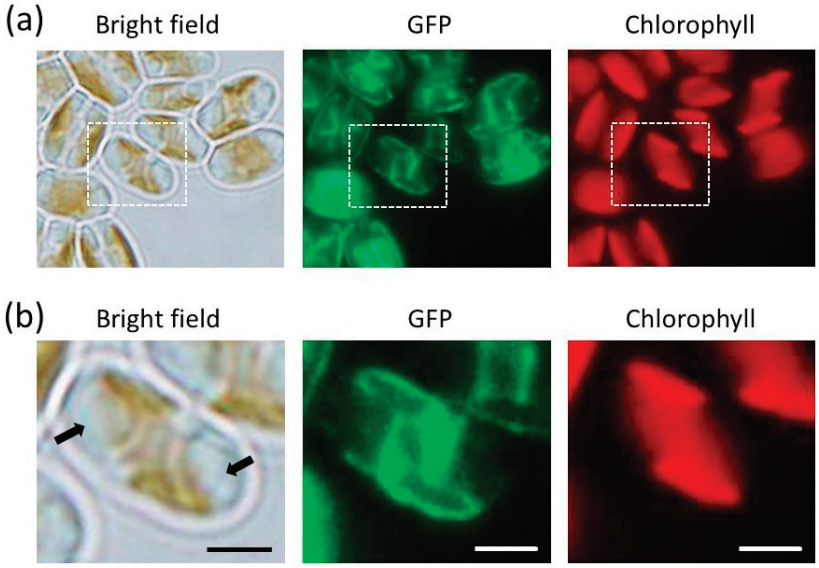

Confocal microscopy reconstituted three-dimensional (3D) arrangement of SDOAP1-GFP in the cells. GFP fluorescence delineated the network of membranes thought to represent the ER

(Figure 4 and Supplementary Figure S6). The fluorescent network extended through the cell, and surrounded the chloroplast. This 3D arrangement closely resembles that observed in *P. tricornutum* expressing GFP at the ER [24]. When *F. solaris* was stained with an ER-specific dye, a similar feature was observed (Supplementary Figure S7).

Figure 3. Fluorescence profiling on the microscopic images of *F. solaris* JPCC DA0580 expressing S_{DOAP1}-GFP (**a**) and neat GFP (**b**). Fluorescent signals of GFP and chlorophyll along the white arrows in the images are shown in green and red lines, respectively. Fluorescent peaks of GFP outside of the chlorophyll fluorescent region are shown with the black arrows. (scale bar = 5 μm).

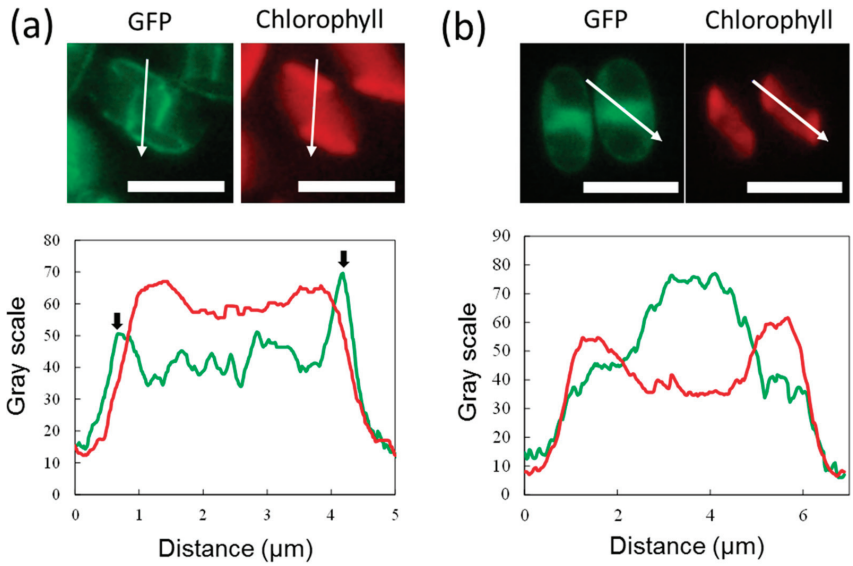

Figure 4. Confocal microscopic images of *F. solaris* JPCC DA0580 transformant expressing S_{DOAP1}-GFP.

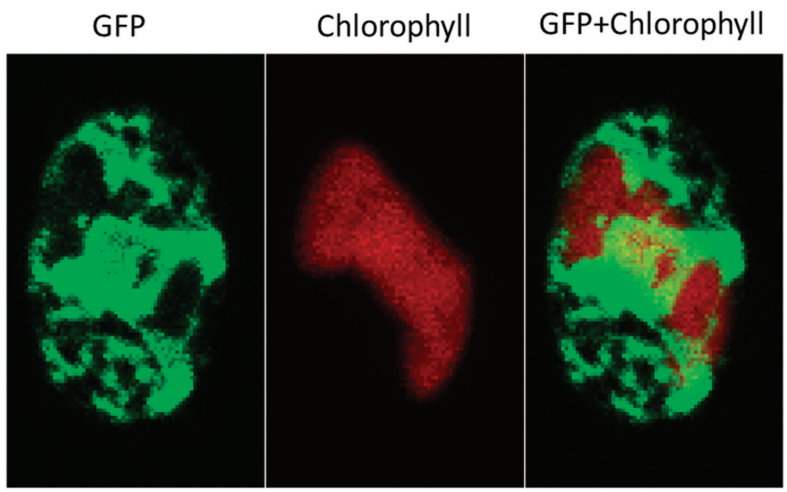

3. Discussion

DOAP1 has been identified an oleosome-associated protein through our proteomic research. It was predicted to have 506 amino acids in length previously [17]. However, recently obtained RNA-seq data allowed us to find the *N*-terminal extension, which we have fortunately introduced in the expression vector in the previous study [17] but did not consider that this extra sequence may be a part of the coding region. By SignalP algorism, this sequence is predicted to be an ER-targeting signal sequence which can be recognized by a Sec61 complex for transition across the ER membrane [31].

Next, to test whether this tentative signal sequence can route proteins into the ER of *F. solaris*, we constructed the expression vector of S_{DOAP1}-GFP, where the signal sequence and a part of mature DOAP1 (M1–M57 in the Supplementary Figure S2) were together fused at the *N*-terminus of GFP. Western blotting for the *F. solaris* transformants harboring the S_{DOAP1}-GFP expression gene confirmed substantial expression of the target protein, as well as the cleavage of the signal sequence. Although the cleavage site is likely to be the point between A19 and Q20 according to the SignalP algorism, actual cleavage site still remains unclear, and can be elucidated with *N*-terminal sequencing of the cleaved protein [24]. *In vivo* localization of S_{DOAP1}-GFP in *F. solaris* was observed with fluorescent microscopy. As a result, intensive green fluorescence was detected surrounding the chloroplast and nucleus (Figures 2 and 3, and Supplementary Figures S4 and S5). Confocal microscopic analysis further revealed the meshwork-like structure showing GFP fluorescence around the chloroplast, suggesting that the target fusion protein was transported into the ER. It has been widely accepted that diatoms have complex chloroplasts which are surrounded by four membranes owing to their evolutional history with secondary symbiosis [32]. The innermost and second innermost membranes are actually corresponding to the two membranes of the primary chloroplast. The space between the second outermost membrane and the outermost membrane represents the ER (also known as chloroplast-ER; CER). Organelle-specific targeting by recombinant proteins in diatoms has been studied in a pennate diatom, *P. tricornutum* [24,30,33,34]. ER-targeting has been achieved by fusing the specific signal presequence at the *N*-terminus of proteins, while the inner chloroplast-targeting needed an extra transit sequence-like domain following the ER signal. In the case of ER-targeting by GFP, meshwork of green fluorescence was observed around the chloroplast as well as the nucleus in *P. tricornutum* [24,30]; the GFP distribution was similar with that observed in this study. These previous studies also support that the GFP distribution in this study represented the ER-targeting of S_{DOAP1}-GFP. ER-staining with the specific dye further supported this notion.

When DOAP1 with its full length was labeled with GFP, fluorescence was only observed on the oleosomes [17]. In contrast, the truncated DOAP1 including the signal sequence and the following partial mature protein sequence (Supplementary Figure S2) directed the GFP into the ER, and little fluorescence was observed from the oleosomes (usually two oleosomes exist in a *F. solaris* cell at the polar position). These results suggest that DOAP1 could localize in the ER at first due to the *N*-terminal signal sequence, then it is transported onto the oleosomes. Specific signals for targeting oleosome (e.g., proline knot) is not yet identified in DOAP1, thus the transportation mechanism

from the ER to oleosomes still remains unknown. We assume that the proline-rich region at the *C*-terminus of DOAP1 might be a possible candidate of oleosome-targeting signal because similar feature was found in lipid droplet surface protein (LDSP) in other microalga, *Nannochloropsis* sp. [19]. Incidentally SignalP did not detect ER-signal sequence from LDSP. In order to specify the oleosome-targeting sequence in DOAP1, the GFP fusion experiment with various truncated forms of DOAP1 will be performed in the near future. The protein transportation from the ER to oleosomes also implies the direct interaction between these two organelles, otherwise DOAP1 cannot eventually move to the oleosomes. This notion is consistent with our previous study, in which the oleosome membrane was hypothesized to be derived from the ER membrane [17].

Another significance of this study is establishment of the method for ER-specific recombinant protein expression in the oleaginous microalga. At the ER, many critical reactions with regard to the biofuel productivity and quality take place. For instance, acyl-chain desaturation and elongation would be performed at ER [25], and the acyl-chain length and desaturation degree directly affects the resultant biodiesel fuel quality [35]. Engineering these metabolic pathways by transporting heterogeneous enzymes could be a promising approach to control the fuel quality derived from *F. solaris*, and the DOAP1 signal sequence could achieve the transportation by just fusing it at the *N*-terminus of the target proteins.

4. Experimental Section

4.1. Culture Conditions

The marine diatom, *F. solaris* JPCC DA0580, was isolated from the junction of the Sumiyo and Yakugachi Rivers, in Kagoshima, Japan (28°15'N, 129°24'E) [21]. *F. solaris* was cultured in the f/2 medium [36] (75 mg $NaNO_3$, 6 mg $Na_2HPO_4 \cdot 2H_2O$, 0.5 μg vitamin B12, 0.5 μg biotin, 100 μg Thiamine HCl, 10 mg $Na_2SiO_3 \cdot 9H_2O$, 4.4 mg Na_2-EDTA, 3.16 mg $FeCl_3 \cdot 6H_2O$, 12 μg $CoSO_4 \cdot 5H_2O$, 21 μg $ZnSO_4 \cdot 7H_2O$, 0.18 mg $MnCl_2 \cdot 4H_2O$, 70 μg $CuSO_4 \cdot 5H_2O$, and 7 μg $Na_2MoO_4 \cdot 2H_2O$) dissolved per liter of artificial seawater. Transformant cells were incubated in the f/2 medium with antibiotics G418 (500 μg/mL). Cultures were aerated with sterile air at 25°C under 140 μmol/m^2/s of continuous illumination.

4.2. Characterization of Nucleotide and Protein Sequences

DNA sequence neighboring the tentative *doap1* (*g12504*) gene was retrieved from our domestic database of *F. solaris* whole genome sequence (Supplementary Figure S1) [37]. cDNA sequence and RNA-seq data regarding *doap1* gene has already been obtained in our previous studies [17,25]. TATA-boxes upstream of *doap1* gene were predicted with the polymerase II promoter function of GENETYX ver.10. Protein features were analyzed with SignalP [27], InterProScan and BLAST.

4.3. Vector Construction and Transformation

The expression vector, pSP-DOAP1GFP/GAPDH, for full length of DOAP1 (formerly g4301) fused with GFP, was constructed in our previous study [17], in which the predicted coding region

(without intron) and its up-stream sequence (638 bp) were synthesized (Integrated DNA Technologies, Inc., Coraville, IA, USA), and inserted between the glyceraldehyde 3-phosphate dehydrogenase (GAPDH) promoter derived from *F. solaris* and *gfp* gene. Transcription is terminated by the fucoxanthin chlorophyll a/c-binding protein A (fcpA) terminator derived from *P. tricornutum* [38]. In this study, the DNA fragment including a part of *doap1* gene was amplified by polymerase chain reaction (PCR) using the primer pair (5′-ATGTTCCCTGGGCATTCGTG-3′ and 5′-CTTGTCTCCCGACAACAAGATG-3′) and pSP-DOAP1GFP/GAPDH as a template. The amplified fragment was inserted between the same promoter and GFP gene. The constructed plasmid was referred to as pSP-S_{DOAP1}GFP/GAPDH.

Transformation of *F. solaris* was performed by microparticle bombardment using the Biolistic PDS-1000/He Particle Delivery System (Bio-Rad Laboratories, Inc., Hercules, CA, USA) as described previously [17,38].

4.4. Western Blotting

F. solaris transformants (1×10^7 cells) were collected by centrifugation, washed with water, suspended in 100 µL of 1% (*w*/*v*) sodium dodecyl sulfate (SDS) in aqueous solution and boiled for 10 min. After centrifugation, supernatant was collected, and SDS sample buffer was added (final concentration of 62.5 mM Tris-HCl, pH 6.8, 5% 2-mercaptoethanol, 2% SDS, 5% sucrose, and 0.002% bromophenol blue). Denatured proteins were separated by SDS-polyacrylamide gel electrophoresis (SDS-PAGE) using a 12.5% (*w*/*v*) gel, and transferred to a polyvinylidene difluoride membrane. GFP was then detected using alkaline phosphatase (ALP)-labeled anti-GFP antibody (Rockland immunochemicals Inc., Gilbertsville, PA, USA, 1/5000 dilution from stock in PBS containing 0.05% Tween 20). BCIP/NBT-Blue (Sigma, St. Louis, MO, USA) was used as the ALP substrate for visualization.

4.5. Fluorescent Microscopy and Image Analysis

Transformant cells were observed using a fluorescent microscope BX51 (Olympus Corporation, Tokyo, Japan); a NIBA filter set for GFP, a WIG filter set for chlorophyll and a WU filter set for Hoechst 33342 fluorescence, respectively. Confocal microscopy was performed with Fluoview FV1000 (Olympus Corporation, Tokyo, Japan). Hoechst staining was conducted by adding Hoechst 33342 (Invitrogen, Eugene, OR, USA) to the cell culture at 1:50 volume ratio (final concentration = 200 µg/mL). The images obtained were analyzed with Image J program. In order to display the grayscale of the GFP and chlorophyll fluorescence, the fluorescence images obtained were converted into 8-bit black-and-white images, and then plot profiling was performed.

5. Conclusions

The fusion experiment with GFP and the signal sequence of the oleosome-associated protein DOAP1 revealed that DOAP1 contains the signal sequence targeting the ER. This result suggests that DOAP1 could initially be transported into the ER with the aid of its signal sequence, and subsequently transported onto the oleosomes. This new finding implies the interaction between the

ER membrane and oleosome. Protein targeting to the ER achieved in this study is also useful for engineering the lipid synthesis pathway in *F. solaris* because key reactions for lipid synthesis including elongation and desaturation of acyl chains occur in the ER. This could contribute to improvement of biodiesel quality derived from *F. solaris*.

Acknowledgments

This study was supported by the Japan Science and Technology Agency (JST) and CREST.

Author Contributions

T.T. designed overall experiments. Y. M. and Y. S. performed experiments and analyzed data. All authors, including Y.M., Y. S., T.Y., and T.T. participated in discussions and preparation of the manuscript.

Conflicts of Interest

The authors declare no conflicts of interest.

References

1. Smith, V.H.; Sturm, B.S.; Denoyelles, F.J.; Billings, S.A. The ecology of algal biodiesel production. *Trends Ecol. Evol.* **2010**, *25*, 301–309.
2. Liang, Y.; Sarkany, N.; Cui, Y. Biomass and lipid productivities of *Chlorella vulgaris* under autotrophic, heterotrophic and mixotrophic growth conditions. *Biotechnol. Lett.* **2009**, *31*, 1043–1049.
3. Mahapatra, D.M.; Chanakya, H.; Ramachandra, T. *Euglena* sp. as a suitable source of lipids for potential use as biofuel and sustainable wastewater treatment. *J. Appl. Phycol.* **2013**, *25*, 855–865.
4. Matsunaga, T.; Matsumoto, M.; Maeda, Y.; Sugiyama, H.; Sato, R.; Tanaka, T. Characterization of marine microalga, *Scenedesmus* sp. strain JPCC GA0024 toward biofuel production. *Biotechnol. Lett.* **2009**, *31*, 1367–1372.
5. Oh, S.H.; Han, J.G.; Kim, Y.; Ha, J.H.; Kim, S.S.; Jeong, M.H.; Jeong, H.S.; Kim, N.Y.; Cho, J.S.; Yoon, W.B.; *et al*. Lipid production in *Porphyridium cruentum* grown under different culture conditions. *J. Biosci. Bioeng.* **2009**, *108*, 429–434.
6. Rodolfi, L.; Chini Zittelli, G.; Bassi, N.; Padovani, G.; Biondi, N.; Bonini, G.; Tredici, M.R. Microalgae for oil: Strain selection, induction of lipid synthesis and outdoor mass cultivation in a low-cost photobioreactor. *Biotechnol. Bioeng.* **2009**, *102*, 100–112.
7. Corteggiani Carpinelli, E.; Telatin, A.; Vitulo, N.; Forcato, C.; D'Angelo, M.; Schiavon, R.; Vezzi, A.; Giacometti, G.M.; Morosinotto, T.; Valle, G. Chromosome scale genome assembly and transcriptome profiling of *Nannochloropsis gaditana* in nitrogen depletion. *Mol. Plant* **2014**, *7*, 323–325.

8. Guarnieri, M.T.; Nag, A.; Smolinski, S.L.; Darzins, A.; Seibert, M.; Pienkos, P.T. Examination of triacylglycerol biosynthetic pathways via *de novo* transcriptomic and proteomic analyses in an unsequenced microalga. *PLoS One* **2011**, *6*, e25851.
9. Radakovits, R.; Jinkerson, R.E.; Fuerstenberg, S.I.; Tae, H.; Settlage, R.E.; Boore, J.L.; Posewitz, M.C. Draft genome sequence and genetic transformation of the oleaginous alga *Nannochloropis gaditana*. *Nat. Commun.* **2012**, *3*, 686; doi:10.1038/ncomms1688.
10. Rismani-Yazdi, H.; Haznedaroglu, B.Z.; Hsin, C.; Peccia, J. Transcriptomic analysis of the oleaginous microalga *Neochloris oleoabundans* reveals metabolic insights into triacylglyceride accumulation. *Biotechnol. Biofuels* **2012**, *5*, 74; doi:10.1186/1754-6834-5-74.
11. Wang, H.; Alvarez, S.; Hicks, L.M. Comprehensive comparison of iTRAQ and label-free LC-based quantitative proteomics approaches using two Chlamydomonas reinhardtii strains of interest for biofuels engineering. *J. Proteome Res.* **2012**, *11*, 487–501.
12. Davidi, L.; Katz, A.; Pick, U. Characterization of major lipid droplet proteins from *Dunaliella*. *Planta* **2012**, *236*, 19–33.
13. Frandsen, G.I.; Mundy, J.; Tzen, J.T. Oil bodies and their associated proteins, oleosin and caleosin. *Physiol. Plant.* **2001**, *112*, 301–307.
14. Lin, I.; Jiang, P.-L.; Chen, C.-S.; Tzen, J.T. A unique caleosin serving as the major integral protein in oil bodies isolated from *Chlorella* sp. cells cultured with limited nitrogen. *Plant Physiol. Biochem.* **2012**, *61*, 80–87.
15. Moellering, E.R.; Benning, C. RNA interference silencing of a major lipid droplet protein affects lipid droplet size in *Chlamydomonas reinhardtii*. *Eukaryot. Cell* **2010**, *9*, 97–106.
16. Nguyen, H.M.; Baudet, M.; Cuiné, S.; Adriano, J.M.; Barthe, D.; Billon, E.; Bruley, C.; Beisson, F.; Peltier, G.; Ferro, M. Proteomic profiling of oil bodies isolated from the unicellular green microalga *Chlamydomonas reinhardtii*: With focus on proteins involved in lipid metabolism. *Proteomics* **2011**, *11*, 4266–4273.
17. Nojima, D.; Yoshino, T.; Maeda, Y.; Tanaka, M.; Nemoto, M.; Tanaka, T. Proteomics analysis of oil body-associated proteins in the oleaginous diatom. *J. Proteome Res.* **2013**, *12*, 5293–5301.
18. Peled, E.; Leu, S.; Zarka, A.; Weiss, M.; Pick, U.; Khozin-Goldberg, I.; Boussiba, S. Isolation of a novel oil globule protein from the green alga *Haematococcus pluvialis* (Chlorophyceae). *Lipids* **2011**, *46*, 851–861.
19. Vieler, A.; Brubaker, S.B.; Vick, B.; Benning, C. A lipid droplet protein of *Nannochloropsis* with functions partially analogous to plant oleosins. *Plant Physiol.* **2012**, *158*, 1562–1569.
20. Liang, Y.; Maeda, Y.; Yoshino, T.; Matsumoto, M.; Tanaka, T. Profiling of fatty acid methyl esters from the oleaginous diatom *Fistulifera* sp. strain JPCC DA0580 under nutrition-sufficient and -deficient conditions. *J. Appl. Phycol.* **2014**, doi:10.1007/s10811-014-0265-y.
21. Matsumoto, M.; Sugiyama, H.; Maeda, Y.; Sato, R.; Tanaka, T.; Matsunaga, T. Marine diatom, *Navicula* sp. strain JPCC DA0580 and marine green alga, *Chlorella* sp. strain NKG400014 as potential sources for biodiesel production. *Appl. Biochem. Biotechnol.* **2010**, *161*, 483–490.

22. Sato, R.; Maeda, Y.; Yoshino, T.; Tanaka, T.; Matsumoto, M. Seasonal variation of biomass and oil production of the oleaginous diatom *Fistulifera* sp. in outdoor vertical bubble column and raceway-type bioreactors. *J. Biosci. Bioeng.* **2014**, *117*, 720–724.
23. Satoh, A.; Ichii, K.; Matsumoto, M.; Kubota, C.; Nemoto, M.; Tanaka, M.; Yoshino, T.; Matsunaga, T.; Tanaka, T. A process design and productivity evaluation for oil production by indoor mass cultivation of a marine diatom, *Fistulifera* sp. JPCC DA0580. *Bioresour. Technol.* **2013**, *137*, 132–138.
24. Apt, K.E.; Zaslavkaia, L.; Lippmeier, J.C.; Lang, M.; Kilian, O.; Wetherbee, R.; Grossman, A.R.; Kroth, P.G. *In vivo* characterization of diatom multipartite plastid targeting signals. *J. Cell Sci.* **2002**, *115*, 4061–4069.
25. Liang, Y.; Maeda, Y.; Sunaga, Y.; Muto, M.; Matsumoto, M.; Yoshino, T.; Tanaka, T. Biosynthesis of polyunsaturated fatty acids in the oleaginous marine diatom *Fistulifera* sp. strain JPCC DA0580. *Mar. Drugs* **2013**, *11*, 5008–5023.
26. Nemoto, M.; Maeda, Y.; Muto, M.; Tanaka, M.; Yoshino, T.; Mayama, S.; Tanaka, T. Identification of a frustule-associated protein of the marine pennate diatom *Fistulifera* sp. strain JPCC DA0580. *Mar. Genomics* **2014**, doi:10.1016/j.margen.2014.01.006.
27. Bendtsen, J.D.; Nielsen, H.; von Heijne, G.; Brunak, S. Improved prediction of signal peptides: SignalP 3.0. *J. Mol. Biol.* **2004**, *340*, 783–795.
28. Abell, B.M.; Holbrook, L.A.; Abenes, M.; Murphy, D.J.; Hills, M.J.; Moloney, M.M. Role of the proline knot motif in oleosin endoplasmic reticulum topology and oil body targeting. *Plant Cell* **1997**, *9*, 1481–1493.
29. Huang, A.H. Oleosins and oil bodies in seeds and other organs. *Plant Physiol.* **1996**, *110*, 1055–1061.
30. Kilian, O.; Kroth, P.G. Identification and characterization of a new conserved motif within the presequence of proteins targeted into complex diatom plastids. *Plant J.* **2005**, *41*, 175–183.
31. Stork, S.; Lau, J.; Moog, D.; Maier, U.G. Three old and one new: Protein import into red algal-derived plastids surrounded by four membranes. *Protoplasma* **2013**, *250*, 1013–1023.
32. Gibbs, S.P. The chloroplast endoplasmic reticulum: Structure, function, and evolutionary significance. *Int. Rev. Cytol.* **1981**, *72*, 49–99.
33. Gruber, A.; Vugrinec, S.; Hempel, F.; Gould, S.B.; Maier, U.G.; Kroth, P.G. Protein targeting into complex diatom plastids: Functional characterisation of a specific targeting motif. *Plant Mol. Biol.* **2007**, *64*, 519–530.
34. Peschke, M.; Moog, D.; Klingl, A.; Maier, U.G.; Hempel, F. Evidence for glycoprotein transport into complex plastids. *Proc. Natl. Acad. Sci. USA* **2013**, *110*, 10860–10865.
35. Knothe, G. Dependence of biodiesel fuel properties on the structure of fatty acid alkyl esters. *Fuel Process. Technol.* **2005**, *86*, 1059–1070.
36. Guillard, R.R.; Ryther, J.H. Studies of marine planktonic diatoms. I. *Cyclotella nana* Hustedt, and *Detonula confervacea* (cleve) Gran. *Can. J. Microbiol.* **1962**, *8*, 229–239.

37. Tanaka, T.; Maeda, Y.; Veluchamy, A.; Tanaka, M.; Bowler, C.; Muto, M.; Sunaga, Y.; Tanaka, M.; Yoshino, T.; Taniguchi, T.; *et al*. Genome and transcriptome analyses of theoleaginous diatom *Fistulifera* sp. reveals the oil accumulation mechanism. 2014, to be submitted for publication.
38. Muto, M.; Fukuda, Y.; Nemoto, M.; Yoshino, T.; Matsunaga, T.; Tanaka, T. Establishment of a genetic transformation system for the marine pennate diatom *Fistulifera* sp. strain JPCC DA0580—A high triglyceride producer. *Mar. Biotechnol.* **2013**, *15*, 48–55.

Marine Microorganism-Invertebrate Assemblages: Perspectives to Solve the "Supply Problem" in the Initial Steps of Drug Discovery

Miguel Costa Leal, Christopher Sheridan, Ronald Osinga, Gisela Dionísio, Rui Jorge Miranda Rocha, Bruna Silva, Rui Rosa and Ricardo Calado

Abstract: The chemical diversity associated with marine natural products (MNP) is unanimously acknowledged as the "blue gold" in the urgent quest for new drugs. Consequently, a significant increase in the discovery of MNP published in the literature has been observed in the past decades, particularly from marine invertebrates. However, it remains unclear whether target metabolites originate from the marine invertebrates themselves or from their microbial symbionts. This issue underlines critical challenges associated with the lack of biomass required to supply the early stages of the drug discovery pipeline. The present review discusses potential solutions for such challenges, with particular emphasis on innovative approaches to culture invertebrate holobionts (microorganism-invertebrate assemblages) through *in toto* aquaculture, together with methods for the discovery and initial production of bioactive compounds from these microbial symbionts.

Reprinted from *Mar. Drugs*. Cite as: Leal, M.C.; Sheridan, C.; Osinga, R.; Dionísio, G.; Rocha, R.J.M.; Silva, B.; Rosa, R.; Calado, R. Marine Microorganism-Invertebrate Assemblages: Perspectives to Solve the "Supply Problem" in the Initial Steps of Drug Discovery. *Mar. Drugs* **2014**, *12*, 3929–3952.

1. Introduction

Marine ecosystems harbor a substantial fraction of Earth's biodiversity and provide a wide range of goods and services [1]. Among these, marine natural products (MNP) have received special attention in recent years. The main driver for this particular focus on MNP was the urgent need for new chemical diversity to fuel the drug discovery pipeline. This impulse led to a major increase in the discovery of MNP in the past decades [2,3], with over 20,000 new compounds described since the 1950s [4]. A large fraction of these new metabolites were obtained from marine invertebrate species [2], which make up about 50% of all extant non-microbial marine biodiversity in the oceans [5]. Although success stories of marine derived-drugs are already a reality [6], the true potential of MNP from invertebrates as future drug candidates is yet to be unraveled [7,8]. However, one critical issue usually associated with the initial steps of marine drug discovery from invertebrates is the lack of a constant and reliable supply of animal biomass [9]. Relevant to this supply problem is the realization that symbiotic microorganisms, including protists, may, in fact, synthesize a large number of metabolites once considered to be produced by marine invertebrates [9–12].

The present review addresses the potential of MNP derived from microorganisms-invertebrate assemblages and the production of the target metabolites for the initial steps of drug discovery. This work focuses on *in toto* aquaculture of invertebrate holobionts, *i.e.*, the invertebrate host and

the associated community of microorganisms, as well as on culture-dependent and independent strategies for the isolation of bioactive compounds from microbial symbionts for drug discovery. Although aquaculture for drug discovery is still an emerging field, particular emphasis is also given to the manipulation of culture conditions that may contribute toward maximizing the production of microbial symbionts and their secondary metabolites.

2. Marine Microorganism-Invertebrate Assemblages

Marine invertebrates are a source of high microbial abundance and diversity (e.g., [13–15]). For instance, the number of bacteria in sponges may exceed bacterial concentrations in seawater by two to four orders of magnitude [16]. Cnidarians, especially corals, also harbor an impressive number of microbial organisms; for example, the coral mucus may reach microbial concentrations 100- to 1000-fold higher than those observed in seawater [17]. Invertebrate microbial symbionts are also highly diverse [18]. The abundant and unique symbiotic microbial diversity hosted by marine invertebrates [18,19] plays a very important role in their biology and ecology, particularly in its nutrition [20–22], disease-resistance [13,17] and response to environmental perturbations [23,24]. Symbiotic microorganisms are also known to be active players in the chemical mediation of interactions among marine organisms [25].

Marine microbial symbionts have been recognized for their active role in chemical defenses of marine invertebrates against both predators and competitors [25–27]. The symbionts produce chemically diverse and biologically active secondary metabolites, such as anti-inflammatory, antibiotic, antitumor, anticancer, antibacterial and antifungal compounds, whose properties are particularly interesting for drug discovery [6,11,28]. The microbiome of marine invertebrates may represent a remarkable proportion of the holobiont biomass. In sponges, for instance, the microbial community may contribute up to 60% of the holobiont biomass [29]. Contrastingly, in other invertebrates, such as scleractinian corals, symbiotic microorganisms are highly abundant in the soft tissue of the host, but represent a minor fraction of the total biomass, due to the weight that their hard calcium carbonate skeleton represents [30]. However, regardless of microbial abundance, the compounds produced by symbiotic microorganisms of marine invertebrates with potential for drug discovery are usually secondary metabolites. As such, these compounds are naturally produced in low quantities. This imposes critical challenges to the drug discovery pipeline, particularly during the early phases of discovery and the selection of which leads should advance to the next step [31–33].

3. The Supply Problem in Marine Drug Discovery

While in the past, the search for new MNP heavily relied on the harvesting of wild specimens and large quantities of animal biomass were needed to screen for new chemical diversity, nowadays, small amounts of tissue from a single individual can be enough for an initial screening [32,34]. Nonetheless, this dependence on natural samples may still entail replicability issues [32]. Wild marine organisms collected for bioprospecting are exposed to environmental variability, as well as changes at the community level, which may significantly affect their chemical ecology [35].

Individuals of the same species sampled in different areas, or time frames, may not display the same chemical composition [36] and, therefore, fail to guarantee the supply of a target metabolite (a pitfall commonly termed "loss of the source"). This may also be a potential caveat for the initial detection of bioactive metabolites, as environmental and individual variability in the chemical composition of target organisms may bias bioprospecting [32]. Also associated with replicability issues is the potential loss of the source through extinction of target species. This issue is particularly relevant in the oceans of today and tomorrow, as vulnerability to extinction in marine ecosystems is predicted to be higher on tropical coral reefs [37,38], which have been bioprospecting hotspots since the 1990s [2].

The relatively low natural abundance of bioactive metabolites that is often recorded in marine invertebrates [39] is not a constraint for the initial steps of the drug discovery pipeline, as only small amounts of biomass are currently required. However, while the amount of pure compound required for screening an isolate is usually lower than 1 mg, an increase in several orders of magnitude of target compound quantity (e.g., a few g) is needed to progress satisfactorily towards preclinical trials [34]. Once the compound proceeds through clinical trials and is commercialized as a pharmaceutical, kilograms of the pure compound are required to supply drug production, which may correspond to an annual capture or production of several tones of the invertebrate holobiont [33,34]. Overall, the challenges associated with the harvest/culture of target organisms to yield either milligrams, grams or kilograms of a given pure compound inevitably triggers supply issues that only escalate as the compound progresses into later development stages of the drug discovery pipeline [40]. Therefore, the production of these compounds at a scale large, enough to fulfill the needs of drug discovery and potential commercial applications, has been a major issue [6,40] that has prompted innovative solutions. To overcome the "supply problem", current R&D strategies of the pharmaceutical industry are largely associated with the development of synthetic or hemisynthetic analogues and the use of heterologous gene expression techniques [41], as well as with the design of molecules displaying a lower complexity and a similar bioactive function that can be synthesized using standardized techniques [33,42]. However, there are several constraints associated with these approaches. The remarkable complexity of certain natural molecules (most are chiral and display intricate structures) makes it very difficult, and often impossible, to replicate the natural molecule in the laboratory [40,43]. Furthermore, the large number of steps often required to produce such synthetic analogues, together with the notable number of misassigned products, commonly represent an extreme financial burden that most drug discovery companies are unable to support [44]. Hypothetically, even if chemical synthesis was a technically feasible option, the production of the target metabolite at the kilogram scale would probably not be affordable for commercial applications [45]. While heterologous gene expression is a very useful and promising technique for drug discovery from symbiotic microorganisms [31], it is important to note that target genes from source organisms might not be expressed in all hosts, and therefore, developing such an assay for new species requires considerable efforts. Moreover, the target gene from the symbiotic microorganism may need a cue to trigger its expression, such as the influence of other community members, or share a metabolic pathway with its invertebrate host [46].

It is therefore undeniable that the "supply problem" is at the center of the main constraints impairing drug discovery from the marine environment and is usually strongest at the early stages of drug development [6,32,40]. This issue becomes even more relevant when target compounds are produced by symbiotic microbes due to the low levels at which these metabolites are produced, along with the smaller proportion that microbial biomass commonly represents when compared to the majority of their invertebrate hosts [10,11,31]. Nevertheless, the interest in the remarkable properties of MNP remains appealing enough to inspire innovative solutions to the supply problem [6]. The *in toto* aquaculture of the holobiont [47] and the culture of symbiotic microorganisms present in the microbiome of invertebrates [48] are certainly promising approaches to find potential solutions for such bottlenecks.

4. Aquaculture of Marine Invertebrates

Current aquaculture practices can be broadly classified as *in situ* or *ex situ*. This terminology is mostly associated with the production site. *In situ* aquaculture, also known as mariculture, is the culture of organisms in the marine environment using natural conditions. *Ex situ* aquaculture is the process of producing organisms in a controlled environment. Both have advantages and disadvantages (Figure 1). *In situ* aquaculture entirely relies on natural conditions (water physical and chemical parameters, water flow, current and hydrodynamics, light and nutrients) required for the propagation and growth of the target species and requires no adaption to an artificial propagation system. However, cultured species can be potentially exposed to several deleterious factors present in the natural environment, such as sedimentation, unfavorable meteorological conditions, predators, parasites, competitors and other natural hazards, which can reduce survival and growth [49]. Human resources play a major role in the assemblage and maintenance of infrastructures, with the most manpower being necessary to kick-off the culture process and to harvest cultured specimens at the end of production cycles. The ability to manipulate culture conditions is, however, fairly limited, as the largest allowed flexibility is the selection of the location where production structures are implemented. This decision is extremely important, as different areas may display contrasting environmental conditions and thus affect the success of *in situ* aquaculture [50]. In contrast, *ex situ* aquaculture requires a more skilled work force and has higher costs associated with the building and operation of culture facilities. Nonetheless, the ability to manipulate biotic and abiotic factors to maximize animal biomass and metabolite production is incomparably higher than that for *in situ* aquaculture. *Ex situ* aquaculture allows the use of optimized husbandry methodologies specifically designed for the target species being produced. Additionally, and unlike *in situ* aquaculture, *ex situ* production prevents the risks of genetic pollution of natural populations associated with the mass culture of single genotypes in the wild [51]. Nonetheless, *ex situ* aquaculture techniques may also have impacts on the natural environment, which should be prevented or minimized through proper regulation of effluents that may be loaded with nutrients and chemicals used for therapeutic purposes and water-quality management [52]. However, it should be noted that *ex situ* aquaculture of invertebrates for non-food purposes often uses recirculation techniques specifically designed to minimize the discharge of waste water.

Despite the technological simplicity of production *in situ* and the correspondingly expected low production costs, this approach has proven to be more technically challenging and expensive than previously assumed for supporting drug discovery [53]. While incurring higher production costs and requiring skilled workers for the implementation and maintenance of production systems, *ex situ* aquaculture can be implemented in privileged locations, such as in the vicinity of pharmaceutical laboratories; this physical location can ensure a more rigorous processing after the harvesting of produced specimens and, thus, avoid costs associated with paperwork, handling, packaging, shipping and spoilage during the transport of produced biomass.

The drawbacks associated with *in situ* aquaculture (Figure 1) may be overcome through *ex situ* aquaculture in controlled environments, which may eliminate problems commonly faced by researchers, such as the loss of the source and reproducibility. Additionally, in *ex situ* cultures, environmental conditions can be manipulated, optimized and stabilized to: (i) accelerate the growth of cultured species; (ii) ensure the presence of symbiotic taxa in the invertebrate host that are known to be important producers of the target compound (e.g., *Aspergillus* spp. in sponges) [54–57]; (iii) increase or decrease the number of symbionts according to their relevance in metabolite production; and (iv) adjust the biotic and/or abiotic settings that ensure the maximum yield of the target bioactive compounds [58]. *Ex situ* aquaculture further allows better control of the genetic selection of the target species, which ultimately leads to the optimization of culture conditions for particular genotypes that may yield higher metabolite production. Specific genotypes may also hold contrasting microbial communities with different metabolite production.

The use of aquaculture for drug discovery is still in its infancy, and *in toto* production of marine organisms is a process that deserves greater attention from researchers aiming to produce the biomass of secondary metabolites [47]. The use of controlled environments *ex situ* can minimize environmental variability that affects the chemical ecology of the holobiont and, consequently, contributes to achieving a higher degree of replicability. This feature is of paramount importance to maintain a stable community of bioactive metabolite-producing symbiotic microorganisms in the invertebrate host. Furthermore, as previously mentioned, culture protocols may also be optimized to continuously provide animal/microbial biomass and maximize target metabolite production [58].

The following sections focus on aquaculture practices of different invertebrate groups and the optimization of culture protocols that can maximize symbiont biomass and metabolite production, with emphasis on successful case studies. The invertebrate groups emphasized here are sponges, cnidarians, mollusks, as well as a few other taxa relevant for drug discovery (e.g., bryozoans, tunicates and worms). This selection is based on the importance of these groups in MNP discovery [2], as well as on ongoing efforts to address the aquaculture of these marine invertebrate groups [59–62].

Figure 1. SWOT analysis (strengths, weaknesses, opportunities and threats) of the *in situ* and *ex situ* aquaculture of marine invertebrates for marine drug discovery and development.

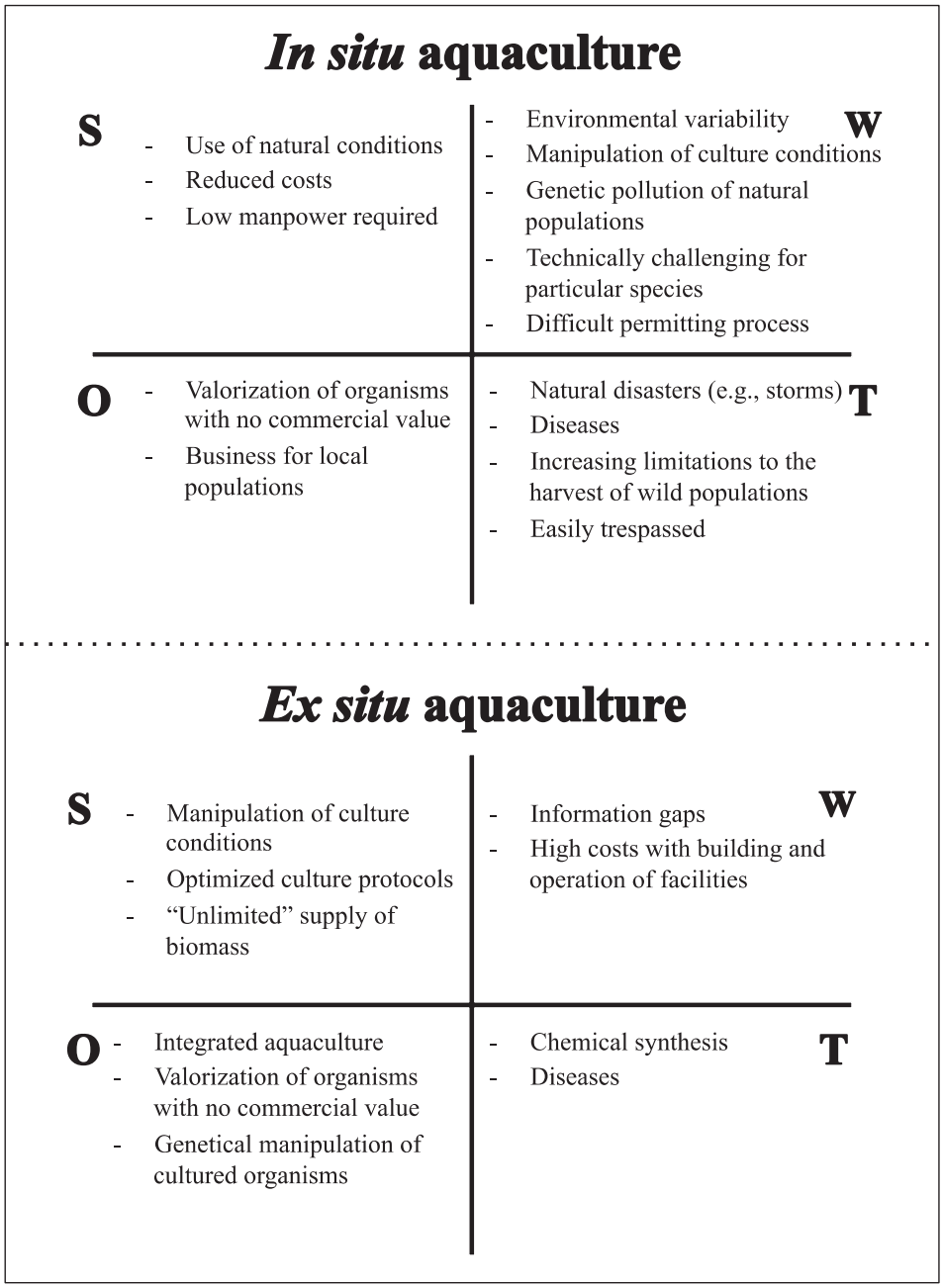

4.1. Sponges

For many years, sponges (Porifera) have been regarded as the primary target for MNP discovery [2]. Sponges illustrate the supply issue at its best, as their MNP are biochemically complex (*i.e.*, difficult targets for chemical synthesis) and are often present only in minute quantities in animal tissues. Sponges are also known to host a large and diverse community of microorganisms [63], which can compose a notable fraction of the sponge tissue volume [16]. Such symbiotic microorganisms may display interesting bioactivities as new drug leads. For instance, marine-derived fungi, such as *Aspergillus ustus* and *Petriella* sp., were isolated from the sponge, *Suberites domuncula*, and yielded cytotoxic sesquiterpenoids that have anticancer applications [64,65]. Moreover, bacteria within the genera, *Aquamarina*, *Pseudovibrio* and *Streptomyces*, displaying anti-fungal and anti-bacterial activity, were isolated from the sponges, *Amphilectus fucorum* and *Haliclona simulans* [66].

Many sponge species with the potential for drug discovery are not available in large quantities in nature, and sponges are notoriously difficult to culture [67]. A well-known example is the anticancer compound, halichondrin B, isolated from *Halichondria okadai*, which is now a drug (Halaven®) and was based on a synthesis of the active end following an initial biomass supply from New Zealand, with the original compound being present in quantities lower than 1 $mg \cdot kg^{-1}$ of wet sponge biomass [41]. This example clearly shows that reliable methods for the production of sponge materials are desired to fully explore the possibilities that sponge MNP have to offer.

Scientists have substantially increased their efforts to develop culture techniques for marine sponges, which include *in situ* aquaculture (reviewed by [68]) and *ex situ* culture approaches, such as aquarium culture, primmorphs and cell cultures (reviewed by [67,69]). While sea-based culture techniques (Figure 2) have proven to be feasible for products, such as halichondrin [70], avarol [61] and discodermolide [71], *ex situ* approaches have not yet been very successful, mostly due to the lack of scientific knowledge on sponge biology. Sponges have a high potential for growth, but release most of their productivity through the shedding of cellular materials into the environment [72–76].

Apart from general methodological issues, such as choices of culture materials, site selection, cutting methods and explant sizes, recent studies have also included more advanced aspects, such as heredity [68]. A clear genotype-associated difference in performance (*i.e.*, growth and metabolite production) was observed for *Discodermia dissoluta* [71]. Such genotypic differences suggest that broodstock optimization through genotypic selection can help increase sponge mariculture productivity. Notwithstanding this, negative effects of repetitive cloning have been reported [49], which may counteract the benefits of genotypic selection. Future studies are therefore required to further elaborate on this aspect.

Most sponges in mariculture retain their ability to produce the compound of interest [49,50,71,77–79]. Cultured explants of *Discodermia dissoluta* even contained higher amounts of discodermolide than their wild conspecifics [71]. Attempts to enhance secondary metabolism in mariculture included stress treatments, which were successfully applied to increase the production of avarol [80] and latrunculin B [81]. Other factors reported to influence metabolite concentration include location, depth and seasonality [82,83].

Figure 2. Examples of Mediterranean sponges in sea-based aquacultures. (**A**) Culture frame with spike-cultures of *Dysidea avara*, as described in Osinga *et al.* [78]. In addition, many sponges primarily feed on dissolved organic carbon (DOC) rather than being particle feeders [72–75], which has altered the view on designing feeding regimes for sponges in aquaria; (**B**) Detail of *D. avara* growing on spikes; (**C**) Culture of *Chondrilla nucula* on vertical plates. Images by M. Gokalp and R. Osinga.

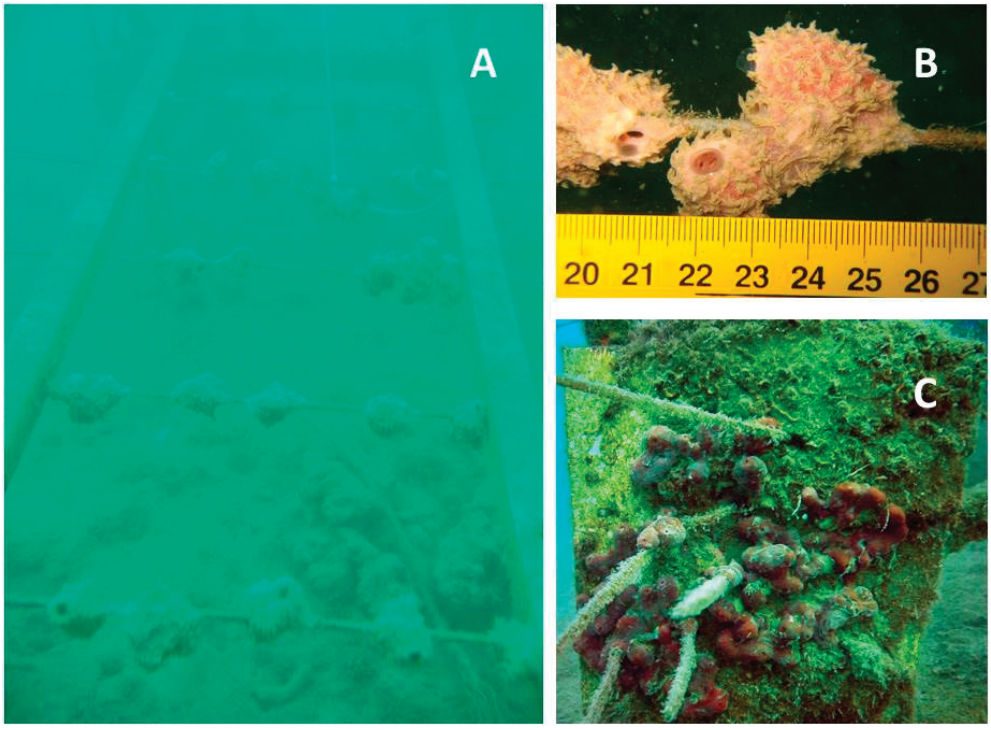

4.2. Cnidarians

Cnidarians have become the second most bioprospected group of marine invertebrates [2]. Besides the bioactive metabolites associated with cnidarians [7], there are also important metabolites produced by symbiotic microorganisms associated with corals, such as the fungi, *Nodulisporium* sp. and *Zygosporium* sp., associated with unidentified corals (reviewed by [84]), *Vibrio* species isolated from the soft coral, *Sinularia polydactyla* [85], *Chondrostereum* sp. isolated from the soft coral, *Sarcophyton tortuosum*, and *Aspergillus versicolor* from the soft coral, *Cladiella* sp. (reviewed by [86]), among others. Despite the remarkable chemical diversity and potential for drug discovery displayed by this group of invertebrates, to the best of our knowledge, no metabolite from cnidarians has yet reached the pharmaceutical clinical pipeline, *i.e.*, entered clinical trials or obtained approval for commercialization.

Most efforts on cnidarian aquaculture have been focused on corals (e.g., [87,88]) and sea anemones (e.g., [89]). Studies on *in situ* production methods have primarily focused on asexual propagation through fragmentation [90] and the selection of the area for the grow-out of coral

fragments [91–93]. The *ex situ* culture of cnidarians is usually performed in tanks with controlled environmental settings: physico-chemical parameters, water flow, light spectra and intensity, as well as feeding. All of these parameters are critical to maximize survival, nutritional/physiological condition and growth [62,89,94–99]. Micropropagation techniques have also been developed and create progeny from tissue explants derived from a single polyp of colonial corals [100]. Sexual reproduction of cnidarians is becoming increasingly popular as a method for the production of a large number of organisms, particularly corals [101]. However, research efforts on coral sexual reproduction have been targeting reef restoration and management of captive populations [102,103].

Environmental factors, such as light [58], are important drivers of metabolite production in cnidarians. To our knowledge, only a single study assessed the effect of light intensity on metabolite production (flexibilide) by the soft coral, *Sinularia flexibilis* [58]. The use of herbivorous fishes in the production tanks may also contribute to the production of secondary metabolites that cnidarians use as chemical defense mechanisms [104]. Furthermore, the polyculture of different cnidarian species within the same tank may also induce metabolite production. For instance, chemical extracts from the stony coral *Tubastraea faulkneri* kill larvae of other coral species [105]. Thus, the combination of different coral species, either stony or soft corals, is likely to trigger the production of bioactive metabolites, but may also induce coral mortality [106].

Specimen selection is also an important factor to consider, as the production of secondary metabolites may show sex-specific and inter-clonal variability [106]. Genotypic differences may also affect the composition of the associated microbiota. Symbiotic microorganisms are mainly present in the soft tissue and/or mucus produced by cnidarians, and therefore the increase of the proportion of soft tissue and mucus to the total holobiont biomass may represent a significant increase in the yield of the target metabolite for drug discovery. Although the drivers of coral tissue growth are still poorly investigated, it is known that heterotrophic feeding maximizes coral tissue growth [96,107] and that mucus production is associated with protection from UV, desiccation and increased sediment loading [108].

While cnidarian aquaculture is already an established technology that allows the production of monoclonal organisms [89,99], it has hardly been applied for drug discovery research. Nevertheless, production costs are likely to be affordable to pharmaceutical companies [99] and may even decrease with the use of new technologies, such as LED illumination, that have a lower energetic consumption [96]. *Ex situ* culture systems may also be used to either keep a live library of cnidarians and its associated microbial community or to produce the target organism synthetizing the desired metabolite.

4.3. Mollusks

Approximately 1100 distinct compounds have been isolated from less than 300 species of mollusks, and most of them have been isolated from gastropods [4]. The origin of their NP has been attributed to their ability to bio-accumulate or biotransform molecules acquired through feeding [109], *de novo* synthesis [110] and bacterial symbionts [33]. While some mollusk species are protected by shells and an arsenal of peptide toxins, they also host symbiotic bacteria that

contribute to their chemical defenses, a feature that holds great interest for marine drug discovery [111]. Shell-less mollusks, such as the sacoglossans, *Elysia* spp., also associate with a number of bacteria that provide chemical defense, which are usually found in their gut and mucus [112,113]. Such mollusks have also been an important source of a very potent class of cytotoxic peptides—the kahalalides [114,115]. For example, cyanobacteria of genera *Symploca* and *Lyngbya* associated with the aplysiid *Dolabella auriculata* produce Dolastatin 10, an antimicrobial peptide [116,117] that is currently in phase II clinical trials as an anticancer agent [118]. Bacteria, such as *Mycoplasma* spp. and *Vibrio* spp., that are known to associate with the sacoglossan, *Elysia rufescens*, produce elisidepsin (Irvalec©), another cyclic peptide belonging to the kahalalide family that is currently under phase II development [43]. Actinomycetes represent another example of biochemically interesting symbionts from mollusks. Actinomycetes living in close association with cone snails (*Conus* spp.) contribute to the production of conotoxins, which are peptide-based neurological toxins with analgesic properties [119–122]. Ziconotide (Prialt®), the synthetic equivalent of a naturally occurring 25-amino acid peptide (ω-conotoxin MVIIA) derived from the venom of a predatory cone snail, was the first marine drug to be approved for clinical use [122] to treat chronic pain. Kurasoins, soraphinol C and other molecules with important neuroactive biological properties have also been isolated from three different species of cone snail (*Conus rolani*, *C. pulicarius* and *C. tribblei*) [123,124].

Although the supply problems of these success stories have been mostly overcome through the chemical synthesis of target molecules, many more metabolites from mollusks and their symbiotic microbiota could be on a more advanced stage of the drug discovery pipeline if the supply issue were solved, particularly at the initial steps of drug discovery.

In situ aquaculture of mollusks has been widely applied to bivalves for food production [125]. Although there were a few NP discovered in marine bivalves [2], there are still no endeavors developing the *in situ* aquaculture of bivalves for drug discovery. As opposed to bivalves and in contrast to other invertebrate groups, such as sponges and cnidarians, most efforts toward the aquaculture of gastropods have been undertaken *ex situ*. While new advances have been achieved in the last decades in the larviculture and grow-out of marine snails for human consumption and restocking purposes (e.g., [126,127]), large-scale production for biotechnological applications is yet to be addressed. Sea slug production is still restricted to *Aplysia californica*, which is a widely used model organism in neurosciences research [128]. Nonetheless, recent data using small-scale recirculating culture systems opens good perspectives for the production of several other sea slug species and their associated microbiota [60]. The most important environmental parameters to successfully culture sea slugs are associated with water physico-chemical parameters (e.g., temperature, pH, light cycle) and nutrition [129–131].

4.4. Other Invertebrates

Bioprospecting efforts targeting marine invertebrates have clearly been biased towards sponges and cnidarians [2]. Nonetheless, other groups of marine invertebrates, such as bryozoans, tunicates and nemertine worms, have also yielded promising compounds to fuel drug discovery programs. For example, one pharmaceutical already being commercialized (Yondelis®) was inspired from

trabectedin, a secondary metabolite from the tunicate, *Ecteinascidia turbinata*, whereas the NP plitidepsin (Aplidin®), described as being from the ascidian (tunicate) *Aplidium albicans*, is now under clinical evaluation [132]. Moreover, 3-(2,4-Dimethoxybenzylidene)-Anabaseine (DMXBA; also called GTS-21) is an anabaseine derivative from the hoplonemertine worm, *Amphiporus lactifloreus*, that is in clinical development to treat Alzheimer's and schizophrenia [133]. It is also worth highlighting that both tunicates and bryozoans have already been targeted by aquaculture efforts aiming to supply drug discovery [134].

The bryozoan *Bugula neritina* has been the focus of pharmaceutical companies due to its NP bryostatin 1, an antineoplastic agent [135]. The first aquaculture efforts for this species employing an *ex situ* approach failed, due to the lack of adequate food provisioning and a constant larval supply [53]. The latter prompted the collection of mature wild organisms to spawn in the laboratory [136] and the improvement of culture protocols [137]. Asexual reproduction of bryozoans through fragmentation, as previously described for corals, has also been described [138]. Issues associated with constant and reliable *ex situ* production promoted the development of *in situ* culture approaches [53,136], which were successfully employed to produce this bryozoan and yield bryostatin 1 within the normal range for ocean populations (average 7.5 μg/g dry weight) [136]. It is further important to note the important role played by symbionts in the biosynthesis of other bioactive metabolites in bryozoans. *B. neritina* is one of the best-documented examples of bioactive metabolite symbiosis, and other bryostatins discovered in this bryozoan species are, in fact, biosynthesized by its bacterial symbionts (reviewed by [139]).

The tunicate, *E. turbinata*, also represents an interesting case study for aquaculture. Its most potent NP, trabectedin, is present at very low yields (0.0001%), resulting in nearly 1 ton of animal biomass being required to isolate 1 gram of this compound [39,140]. Initial aquaculture efforts were performed both *in situ* (using PVC structures with ropes where lab-settled colonies were attached) and *ex situ* (in tanks) [136]. During the development of Yondelis®, the developing enterprise addressed the supply problem with both *in situ* and *ex situ* aquaculture. This approach allowed them to pursue the clinical development of the drug, but aquaculture was revealed to be unfeasible for commercialization due to high production costs and low metabolite yield [140].

These two case studies highlight the importance that aquaculture may play in the production of metabolite biomass from bryozoans and tunicates for drug discovery, at least in the early steps of the discovery pipeline. Although these NP (bryostatin 1 and trabectedin) are produced by the invertebrate host, aquaculture practices may also be used to yield metabolites produced by symbiotic organisms [31]. It is also important to note that the aquaculture of *B. neritina* and *E. turbinata* has mostly been focused on the maximization of biomass production, without any effort to manipulate culture conditions that may increase the production of target metabolites. Stress experiments may contribute toward understanding the drivers of secondary metabolite production and optimizing aquaculture protocols to magnify the yield of target molecules [53,58].

5. Discovery of Bioactive Compounds from Marine Invertebrate-Associated Microorganisms and Their Production

The isolation of a pure culture of target microorganisms can be extremely challenging and is often a necessary step in the drug discovery pipeline [141]. Traditionally, microorganisms can be cultivated through serial plating on selective growth media. However, when using these techniques, only 0.001%–1% of the total microbial diversity can be successfully cultivated [142]. These numbers are certainly far from providing an acceptable overview of the microbial landscape of the source environment [143]. When comparing marine and terrestrial environments, the first is highly unstable, heterogeneous and oligotrophic. These conditions make the marine environment particularly difficult to mimic for the cultivation of marine microbes. Some of the constraints that researchers have to face when addressing this issue include: (i) the inability to reproduce highly complex nutritional and environmental conditions, as well as complex networks of cell-cell interactions (e.g., metabolites exchange and signaling); (ii) the overgrowth of slow- by fast-growing microorganisms; (iii) viral infections; and (iv) insufficient time allowed for growth [47,142,143].

Recent breakthroughs have allowed the cultivation of microorganisms previously labeled as unculturable [144]. Initial attempts consisted in optimizing traditional cultivation methods through modifications of culture media (e.g., carbon sources, electron acceptors, nutrient concentration) and growth conditions (e.g., inoculation size, temperature, pH, incubation time) [144,145]. For example, the use of low substrate/nutrient concentrations combined with extended growth time has allowed the cultivation of formerly unculturable bacteria from the taxa Verrucobacteria, Actinobacteria, Acidobacteria and Proteobacteria [146]. Such optimizations of culture conditions and media have allowed significant increases in the propagation of microbial colonies of the culturable fraction of bacteria [147]. However, successful microbial development generally requires interactions between microbes and their environment (*i.e.*, their invertebrate host for microorganism-invertebrate assemblages), as well as with other members of the community. Such interactions include the exchange of metabolites and signals (chemical cues), which is incompatible with traditional pure culture isolation methods [148]. New techniques developed to overcome this issue consist of simulating the conditions of the source environment, either through co-culture (simulating microbial interactions) or *in situ* cultivation (simulating both environmental conditions and microbial interactions).

The co-culture approach, which allows the development of colonies of microorganisms generally able to grow only in combination with other microbes, has led to the successful isolation and/or enrichment of several previously unculturable microorganisms (e.g., [149,150]). However, while these techniques allow interactions between different members of the cultured communities, they do not simulate/provide other variables of the source environment. A variety of *in situ* cultivation techniques based on diffusion chambers and encapsulation have been proposed in order to fill this gap (see [143,144,147] for a review). Systems based on diffusion chambers have been developed in diverse varieties (e.g., [151–153]) and allow communication between the cultured organisms and their environment. Although initial model systems [153] were labor-intensive and low-throughput, the methods developed subsequently were much more efficient and allowed the

simultaneous *in situ* cultivation of micro-colonies in up to 96 [152] or 384 [151] diffusion chambers. This approach resulted in the culture of a significantly higher microbial diversity than that commonly achieved using "traditional" techniques [154].

An alternative technique, initially developed by Zengler *et al.* [141], involves the high-throughput cultivation of microorganisms individually encapsulated in agar gel microdroplets (GMDs). While this method was particularly appropriate for the cultivation of slow-growing organisms, as they were protected from overgrowth by fast-growing organisms, the lack of protection from the environment prevented its use for incubation *in situ* [48]. Ben-Dov *et al.* [48] proposed an improvement on GMDs by encapsulating similar agar spheres in a polysulfonic polymeric membrane permeable to nutrients and cues from the environment. This "double encapsulation" technique allows for cell-to-cell interactions and exchanges between the microorganisms and their environment and resulted in the successful *in situ* isolation of previously unidentified microorganisms, including bacteria, fungi and stramenopiles [48].

Whereas the *in situ* cultivation techniques described above are extremely promising, much of the microbial diversity remains to be explored, leaving untapped a huge array of secondary metabolites potentially useful for the development of new drugs. Culture-independent methods may help fill this gap in a variety of ways. Metagenomics can be used to express genes from environmental DNA samples in appropriate vectors, which can then be screened for new compounds of interest through sequence mining or functional expression [155]. Such heterologous gene expression has been successfully used to produce bioactive compounds of pharmaceutical interest from marine organism-associated microbial symbionts, thereby proving the potential of this technique for culture-independent production of bioactive compounds. For example, patellamides A and C, promising compounds for their moderate cytotoxicity and potential to reverse multidrug resistance produced by *Prochloron didemni*, a cyanobacterial symbiont of the marine ascidian, *Lissoclinum patella*, have been produced through expression in *Escherichia coli* [156,157]. Furthermore, techniques, such as immunofluorescent viability screening and micromanipulation, may improve the efficiency of microbial cultivation [144]. Finally, with the development and increasing affordability of new sequencing technologies, whole genomes/transcriptomes and proteomes from microorganisms may be sequenced and subsequently mined for new bioactive metabolites or to provide relevant information for the development of successful culture methods [155].

The range of both culture-dependent and independent approaches available for the discovery and high-throughput production of new bioactive compounds from symbiotic microorganisms provides excellent prospects that the true potential of these metabolites for drug discovery may soon be unveiled. Together, these methods may allow marine invertebrate symbionts to provide a steady and sustainable supply of bioactive secondary metabolites to fuel the next generation of MNP.

6. Future Prospects

The production of biomass of marine invertebrate-microorganisms assemblages through *in toto* aquaculture is a potential solution to some of the critical challenges that the pharmaceutical industry has been facing in order to find a constant and reliable supply of biomass to fuel the marine drug discovery pipeline. *Ex situ* aquaculture provides a stable environment and allows the

application of specific stressors/effects that may trigger metabolic reactions in the microbiota associated with marine invertebrates and promote higher yields of target metabolites. It is important to stress that although aquaculture is not the final solution to solve the "supply issue" in marine drug discovery (from bioprospecting to drug commercialization), it may certainly be a suitable approach for the initial steps of the drug discovery pipeline, namely, while synthetic or semisynthetic alternatives are still being technically and financially optimized. Furthermore, the combination of aquaculture practices with a variety of techniques to cultivate symbiotic microorganisms appears to be a highly promising approach for the discovery of new bioactive compounds from invertebrate-microorganisms assemblages. Culture independent methods may also contribute significantly to marine drug discovery [39], either by helping to improve microbial cultivation techniques or by producing the target metabolite by transgenic organisms able to express the gene responsible for its synthesis.

Acknowledgments

M.C.L. was supported by a PhD scholarship (SFRH/BD/63783/2009) funded by the Fundação para a Ciência e Tecnologia (QREN-POPH-Type 4.1: Advanced training, subsidized by the European Social Fund and national funds, MEC). C.S. was supported by a research fellowship from the National Fund for Scientific Research (FNRS; F3/5/5-A2/5-MCF/DM-A115). R.O. has received funding from the EU 7th FWP (FP7/2007-2013) under grant agreement No. KBBE-2010-266033. This work was supported by European Funds through COMPETE and by National Funds through the Portuguese Science Foundation (FCT) within project PEst-C/MAR/LA0017/2013. We also thank two anonymous reviewers for their important comments and suggestion to improve the manuscript.

Conflicts of Interest

The authors declare no conflict of interest.

References

1. Halpern, B.S.; Longo, C.; Hardy, D.; McLeod, K.L.; Samhouri, J.F.; Katona, S.K.; Kleisner, K.; Lester, S.E.; O'Leary, J.; Ranelletti, M.; *et al.* An index to assess the health and benefits of the global ocean. *Nature* **2012**, *488*, 615–620.
2. Leal, M.C.; Puga, J.; Serôdio, J.; Gomes, N.C.M.; Calado, R. Trends in the discovery of new marine natural products from invertebrates over the last two decades—Where and what are we bioprospecting? *PLoS One* **2012**, *7*, e30580.
3. Leal, M.C.; Munro, M.H.G.; Blunt, J.W.; Puga, J.; Jesus, B.; Calado, R.; Rosa, R.; Madeira, C. Biogeography and biodiscovery hotspots of macroalgal marine natural products. *Nat. Prod. Rep.* **2013**, *30*, 1380–1390.
4. Blunt, J.W.; Munro, M.H.G. MarinLit database 2013, Department of Chemistry, University of Canterbury. Available online: http://www.chem.canterbury.ac.nz/marinlit/marinlit.shtml (accessed on 1 August 2013).

5. Appeltans, W.; Bouchet, P.; Boxshall, G.A.; de Broyer, C.; de Voogd, N.J.; Gordon, D.P.; Hoeksema, B.W.; Horton, T.; Kennedy, M.; Mees, J.; *et al.* World Register of Marine Species. Accessed online: http://www.marinespecies.org (accessed on 28 February 2014).
6. Molinski, T.F.; Dalisay, D.S.; Lievens, S.L.; Saludes, J.P. Drug development from marine natural products. *Nat. Rev. Drug Discov.* **2009**, *8*, 69–85.
7. Rocha, J.; Peixe, L.; Gomes, N.C.M.; Calado, R. Cnidarians as a source of new marine bioactive compounds—An overview of the last decade and future steps for bioprospecting. *Mar. Drugs* **2011**, *9*, 1860–1886.
8. Leal, M.C.; Madeira, C.; Brandão, C.A.; Puga, J.; Calado, R. Bioprospecting of marine invertebrates for new natural products—A zoogeographical and chemical perspective. *Molecules* **2012**, *17*, 9842–9854.
9. Hill, R.T.; Fenical, W. Pharmaceuticals from marine natural products: Surge or ebb? *Curr. Opin. Biotechnol.* **2010**, *21*, 777–779.
10. Haygood, M.G.; Schmidt, E.W.; Davidson, S.K.; Faulkner, D.J. Microbial symbionts of marine invertebrates: Opportunities for microbial biotechnology. *J. Mol. Microbiol. Biotechnol.* **1999**, *1*, 33–43.
11. Piel, J. Metabolites from symbiotic bacteria. *Nat. Prod. Rep.* **2004**, *21*, 519–538.
12. Harel, M.; Ben-Dov, E.; Rasoulouniriana, D.; Siboni, N.; Kramarsky-Winter, E.; Loya, Y.; Barak, Z.; Wiesman, Z.; Kushmaro, A. A new Thraustochytrid, strain *Fng1*, isolated from the surface of the hermatypic coral *Fungia granulosa*. *FEMS Microbiol. Ecol.* **2008**, *64*, 378–387.
13. Shnit-Orland, M.; Kushmaro, A. Coral mucus-associated bacteria: A possible first line of defense. *FEMS Microbiol. Ecol.* **2009**, *67*, 371–380.
14. Olson, J.B.; Kellogg, C.A. Microbial ecology of corals, sponges, and algae in mesophotic coral environments. *FEMS Microbiol. Ecol.* **2010**, 1–14.
15. Sweet, M.J.; Croquer, A.; Bythell, J.C. Bacterial assemblages differ between compartments within the coral holobiont. *Coral Reefs* **2010**, *30*, 39–52.
16. Hentschel, U.; Usher, K.M.; Taylor, M.W. Marine sponges as microbial fermenters. *FEMS Microbiol. Ecol.* **2006**, *55*, 167–177.
17. Rosenberg, E.; Koren, O.; Reshef, L.; Efrony, R.; Zilber-Rosenberg, I. The role of microorganisms in coral health, disease and evolution. *Nat. Rev. Microbiol.* **2007**, *5*, 355–362.
18. Rohwer, F.; Seguritan, V.; Azam, F.; Knowlton, N. Diversity and distribution of coral-associated bacteria. *Mar. Ecol. Prog. Ser.* **2002**, *243*, 1–10.
19. Knowlton, N.; Rohwer, F. Multispecies microbial mutualisms on coral reefs: The host as a habitat. *Am. Nat.* **2003**, *162*, S51–S62.
20. Agostini, S.; Suzuki, Y.; Higuchi, T.; Casareto, B.E.; Yoshinaga, K.; Nakano, Y.; Fujimura, H. Biological and chemical characteristics of the coral gastric cavity. *Coral Reefs* **2011**, *31*, 147–156.

21. Leal, M.C.; Nejstgaard, J.C.; Calado, R.; Thompson, M.E.; Frischer, M.E. Molecular assessment of heterotrophy and prey digeston in zooxanthellate cnidarians. *Mol. Ecol.* **2013**, doi:10.1111/mec.12496.
22. Webster, N.S.; Taylor, M.W. Marine sponges and their microbial symbionts: Love and other relationships. *Environ. Microbiol.* **2012**, *14*, 335–346.
23. Ainsworth, T.; Thurber, R.; Gates, R. The future of coral reefs: A microbial perspective. *Trends Ecol. Evol.* **2010**, *25*, 233–240.
24. Ainsworth, T.; Hoegh-Guldberg, O. Bacterial communities closely associated with coral tissues vary under experimental and natural reef conditions and thermal stress. *Aquat. Biol.* **2009**, *4*, 289–296.
25. Paul, V.J.; Puglisi, M.P. Chemical mediation of interactions among marine organisms. *Nat. Prod. Rep.* **2004**, *21*, 189–209.
26. Paul, V.J.; Ritson-Williams, R.; Sharp, K. Marine chemical ecology in benthic environments. *Nat. Prod. Rep.* **2011**, *28*, 345–388.
27. Hay, M.E. Marine Chemical Ecology: Chemical Signals and Cues Structure Marine Populations, Communities, and Ecosystems. *Annu. Rev. Mar. Sci.* **2009**, *1*, 193–212.
28. Kobayashi, J.; Ishibashi, M. Bioactive metabolites of symbiotic marine microorganisms. *Chem. Rev.* **1993**, *93*, 1753–1769.
29. Hentschel, U.; Hopke, J.; Horn, M.; Friedrich, A.B.; Wagner, M.; Hacker, J.; Moore, B.S. Molecular evidence for a uniform microbial community in sponges from different oceans. *Appl. Environ. Microbiol.* **2002**, *68*, 4431–4440.
30. Davies, P. Effect of daylight variations on the energy budgets of shallow-water corals. *Mar. Biol.* **1991**, *108*, 137–144.
31. Piel, J. Bacterial symbionts: Prospects for the sustainable production of invertebrate-derived pharmaceuticals. *Curr. Med. Chem.* **2006**, *13*, 39–50.
32. Li, J.W.-H.; Vederas, J.C. Drug Discovery and Natural Products: End of an Era or an Endless Frontier? *Science* **2009**, *325*, 161–165.
33. Radjasa, O.K.; Vaske, Y.M.; Navarro, G.; Vervoort, H.C.; Tenney, K.; Linington, R.G.; Crews, P. Highlights of marine invertebrate-derived biosynthetic products: Their biomedical potential and possible production by microbial associants. *Bioorg. Med. Chem.* **2011**, *19*, 6658–6674.
34. Munro, M.; Blunt, J.W.; Dumdei, E.; Hickford, S.; Lill, R.; Li, S.; Battershill, C.; Duckworth, A. The discovery and development of marine compounds with pharmaceutical potential. *J. Biotechnol.* **1999**, *70*, 15–25.
35. Hay, M. Marine chemical ecology: What's known and what's next? *J. Exp. Mar. Biol. Ecol.* **1996**, *200*, 103–134.
36. Aratake, S.; Tomura, T.; Saitoh, S.; Yokokura, R.; Kawanishi, Y.; Shinjo, R.; Reimer, J.D.; Tanaka, J.; Maekawa, H. Soft Coral *Sarcophyton* (Cnidaria: Anthozoa: Octocorallia) Species Diversity and Chemotypes. *PLoS One* **2012**, *7*, e30410.

37. Roberts, C.M.; McClean, C.J.; Veron, J.E.; Hawkins, J.P.; Allen, G.R.; McAllister, D.E.; Mittermeier, C.G.; Schueler, F.W.; Spalding, M.; Wells, F.; *et al.* Marine biodiversity hotspots and conservation priorities for tropical reefs. *Science* **2002**, *295*, 1280–1284.
38. Cheung, W.W.L.; Lam, V.W.Y.; Sarmiento, J.L.; Kearney, K.; Watson, R.; Pauly, D. Projecting global marine biodiversity impacts under climate change scenarios. *Fish Fish.* **2009**, *10*, 235–251.
39. Gerwick, W.H.; Moore, B.S. Lessons from the past and charting the future of marine natural products drug discovery and chemical biology. *Chem. Biol.* **2012**, *19*, 85–98.
40. Glaser, K.B.; Mayer, A. A renaissance in marine pharmacology: From preclinical curiosity to clinical reality. *Biochem. Pharmacol.* **2009**, *78*, 440–448.
41. Martins, A.; Vieira, H.; Gaspar, H.; Santos, S. Marketed marine natural products in the pharmaceutical and cosmoceutical industries: Tips for success. *Mar. Drugs* **2014**, *12*, 1066–1101.
42. Piel, J. Approaches to capturing and designing biologically-active small molecules produced by uncultured microbes. *Annu. Rev. Microbiol.* **2011**, *65*, 431–453.
43. Mayer, A.M.; Glaser, K.B.; Cuevas, C.; Jacobs, R.S.; Kem, W.; Little, R.D.; McIntosh, J.M.; Newman, D.J.; Potts, B.C.; Shuster, D.E. The odyssey of marine pharmaceuticals: A current pipeline perspective. *Trends Pharmacol. Sci.* **2010**, *31*, 255–265.
44. Suyama, T.L.; Gerwick, W.H.; McPhail, K.L. Survey of marine natural product structure revisions: A synergy of spectroscopy and chemical synthesis. *Bioorg. Med. Chem.* **2011**, *19*, 6675–6701.
45. Qian, P.-Y.; Xu, Y.; Fusetani, N. Natural products as antifouling compounds: Recent progress and future perspectives. *Biofouling* **2010**, *26*, 223–234.
46. Wilkinson, B.; Micklefield, J. Mining and engineering natural-product biosynthetic pathways. *Nat. Chem. Biol.* **2007**, *3*, 379–386.
47. Leal, M.C.; Calado, R.; Sheridan, C.; Alimonti, A.; Osinga, R. Coral aquaculture to support drug discovery. *Trends Biotechnol.* **2013**, *31*, 555–561.
48. Ben-Dov, E.; Kramarsky-Winter, E.; Kushmaro, A. An *in situ* method for cultivating microorganisms using a double encapsulation technique. *FEMS Microbiol. Ecol.* **2009**, *68*, 363–371.
49. Page, M.J.; Handley, S.J.; Northcote, P.T.; Cairney, D.; Willan, R.C. Successes and pitfalls of the aquaculture of the sponge *Mycale hentscheli*. *Aquaculture* **2011**, *312*, 52–61.
50. Page, M.J.; Northcote, P.T.; Webb, V.L.; Mackey, S.; Handley, S.J. Aquaculture trials for the production of biologically active metabolites in the New Zealand sponge *Mycale hentscheli* (Demospongiae: Poecilosclerida). *Aquaculture* **2005**, *250*, 256–269.
51. Cognetti, G.; Maltagliati, F.; Saroglia, M. The risk of "genetic pollution" in Mediterranean fish populations related to aquaculture activities. *Mar. Pollut. Bull.* **2006**, *52*, 1321–1323.
52. Garren, M.; Smriga, S.; Azam, F. Gradients of coastal fish farm effluents and their effect on coral reef microbes. *Environ. Microbiol.* **2008**, *10*, 2299–2312.
53. Mendola, D. Aquaculture of three phyla of marine invertebrates to yield bioactive metabolites: Process developments and economics. *Biomol. Eng.* **2003**, *20*, 441–458.

54. Thomas, T.R.A.; Kavlekar, D.P.; LokaBharathi, P.A. Marine Drugs from Sponge-Microbe Association—A Review. *Mar. Drugs* **2010**, *8*, 1417–1468.
55. Kooperman, N.; Ben-Dov, E.; Kramarsky-Winter, E.; Barak, Z.; Kushmaro, A. Coral mucus-associated bacterial communities from natural and aquarium environments. *FEMS Microbiol. Lett.* **2007**, *276*, 106–113.
56. Isaacs, L.; Kan, J.; Nguyen, L.; Videau, P.; Anderson, M.; Wright, T.; Hill, R. Comparison of the Bacterial Communities of Wild and Captive Sponge Clathria prolifera from the Chesapeake Bay. *Mar. Biotechnol.* **2009**, *11*, 758–770.
57. Sweet, M.; Jones, R.; Bythell, J. Coral diseases in aquaria and in nature. *J. Mar. Biol. Assoc. UK* **2011**, 1–11.
58. Khalesi, M.K.; Beeftink, H.H.; Wijffels, R.H. Light-Dependency of Growth and Secondary Metabolite Production in the Captive Zooxanthellate Soft Coral Sinularia flexibilis. *Mar. Biotechnol.* **2009**, *11*, 488–494.
59. Olivotto, I.; Planas, M.; Simões, N.; Holt, G.; Avella, M.; Calado, R. Advances in breeding and rearing marine ornamentals. *J. World Aquac. Soc.* **2011**, *42*, 135–166.
60. Dionísio, G.; Rosa, R.; Leal, M.C.; Cruz, S.; Brandão, C.; Calado, G.; Serôdio, J.; Calado, R. Beauties and beasts: A protrait of sea slugs aquaculture. *Aquaculture* **2013**, *408–409*, 1–14.
61. Sipkema, D.; Osinga, R.; Schatton, W.; Mendola, D.; Tramper, J.; Wijffels, R.H. Large-scale production of pharmaceuticals by marine sponges: Sea, cell, or synthesis? *Biotechnol. Bioeng.* **2005**, *90*, 201–222.
62. Sheridan, C.; Kramarsky-Winter, E.; Sweet, M.; Kushmaro, A.; Leal, M.C. Diseases in coral aquaculture: Causes, implications and preventions. *Aquaculture* **2013**, *396–399*, 124–135.
63. Hooper, J.N.A.; van Soest, R.W.M. *Systema Porifera: A Guide do the Classification of Sponges*; Kluwer Academic/Plenum Publishers: New York, NY, USA, 2002.
64. Proksch, P.; Putz, A.; Ortlepp, S.; Kjer, J.; Bayer, M. Bioactive natural products from marine sponges and fungal endophytes. *Phytochem. Rev.* **2010**, *9*, 475–489.
65. Proksch, P.; Ebel, R.; Edrada-Ebel, R.A.; Riebe, F.; Liu, H.; Diesel, A.; Bayer, M.; Li, X.; Li, W.H.; Grebenyuk, V.; *et al.* Sponge-associated fungi and their bioactive compounds: The *Suberites* case. *Bot. Mar.* **2008**, *51*, 209–218.
66. Margassery, L.M. Biodiscovery of Natural Products from Microbes Associated with Irish Coastal Sponges. Ph.D. Thesis, University College Cork, Cork, Ireland, April 2013.
67. Schippers, K.J.; Sipkema, D.; Osinga, R.; Smidt, H.; Pomponi, S.A.; Martens, D.E.; Wijffels, R.H. Cultivation of sponges, sponge cells and symbionts: Achievements and future prospects. *Adv. Mar. Biol.* **2012**, *62*, 273–337.
68. Duckworth, A. Farming Sponges to Supply Bioactive Metabolites and Bath Sponges: A Review. *Mar. Biotechnol.* **2009**, *11*, 669–679.
69. Grasela, J.J.; Pomponi, S.A.; Rinkevich, B.; Grima, J. Efforts to develop a cultured sponge cell line: Revisiting an intractable problem. *In Vitro Cell. Dev. Biol.-Anim.* **2012**, *48*, 12–20.

70. Dumdei, E.J.; Blunt, J.W.; Munro, M.H.G.; Battershill, C.N.; Page, M.J. The whys and whats of sponge chemistry: Why chemists extract sponges and what problems does this cause? In *Sponge Sciences, Multidisciplinary Perspectives*; Watanabe, Y., Fusetani, N., Eds.; Springer: Tokyo, Japan, 1998.
71. Ruiz, C.; Valderrama, K.; Zea, S.; Castellanos, L. Mariculture and Natural Production of the Antitumoural (+)-Discodermolide by the Caribbean Marine Sponge *Discodermia dissoluta*. *Mar. Biotechnol.* **2013**, *15*, 571–583.
72. De Goeij, J.; Moodley, L.; Houtekamer, M.; Carballeira, N.; Duyl, F. Tracing ^{13}C-enriched dissolved and particulate organic carbon in the bacteria-containing coral reef sponge Halisarca caerulea: Evidence for DOM feeding. *Limnol. Oceanogr.* **2008**, *53*, 1376–1386.
73. De Goeij, J.M.; van den Berg, H.; van Oostveen, M.M.; Epping, E.H.G.; van Duyl, F.C. Major bulk dissolved organic carbon (DOC) removal by encrusting coral reef cavity sponges. *Mar. Ecol. Prog. Ser.* **2008**, *357*, 139–151.
74. De Goeij, J.M.; van Oevelen, D.; Vermeij, M.J.A.; Osinga, R.; Middelburg, J.J.; Admiraal, W. Surviving in a marine desert: The sponge loop retains resources within coral reefs. *Science* **2013**, *342*, 108–110.
75. Yahel, G.; Sharp, J.H.; Marie, D.; Haese, C.; Genin, A. *In situ* feeding and element removal in the symbiont-bearing sponge *Theonella swinhoei*: Bulk DOC is the major source for carbon. *Limnol. Oceanogr.* **2003**, *48*, 141–149.
76. De Goeij, J.M.; de Kluijver, A.; van Duyl, F.C.; Vacelet, J.; Wijffels, R.H.; de Goeij, A.F.P.M.; Cleutjens, J.P.M.; Schutte, B. Cell kinetics of the marine sponge *Halisarca caerulea* reveal rapid cell turnover and shedding. *J. Exp. Biol.* **2009**, *212*, 3892–3900.
77. Muller, W.E.G.; Wimmer, W.; Schatton, W.; Bohm, M.; Batel, R.; Filic, Z. Initiation of an aquaculture of sponges for the sustainable production of bioactive metabolites in open systems: Example, *Geodia cydonium*. *Mar. Biotechnol.* **1999**, *1*, 569–579.
78. Osinga, R.; Sidri, M.; Cerig, E.; Gokalp, S.Z.; Gokalp, M. Sponge aquaculture in the East Mediterranean Sea: New approaches to earlier ideas. *Open Mar. Biol. J.* **2010**, *4*, 74–81.
79. Bergman, O.; Mayzel, B.; Anderson, M.A.; Shpigel, M.; Hill, R.T.; Ilan, M. Examination of Marine-Based Cultivation of Three Demosponges for Acquiring Bioactive Marine Natural Products. *Mar. Drugs* **2011**, *9*, 2201–2219.
80. De Caralt, S.; Sánchez-Fontenla, J.; Uriz, M.J.; Wijffels, R.H. *In situ* aquaculture methods of *Dysidea avara* (Demospongiae, Porifera) in the northwestern Mediterranean. *Mar. Drugs* **2010**, *8*, 1731–1742.
81. Hadas, E.; Shpigel, M.; Ilan, M. Sea ranching of the marine sponge *Negombata magnifica* (Demospongiae, Latruncullidae) as a first step for Latrunculin B mass production. *Aquaculture* **2005**, *244*, 159–169.
82. Duckworth, A.R.; Battershill, C.N.; Schiel, D.R. Effects of depth and water flow on growth, survival and bioactivity of two temperate sponges cultured in different seasons. *Aquaculture* **2004**, *242*, 237–250.

83. Domenicotti, C. Growth dynamics and bioactivity variation of the Mediterranean demosponges *Agelas oroides* (Agelasida, Agelasidae) and *Petrosia ficiformis* (Haplosclerida, Petrosiidae). *Mar. Ecol.* **2009**, *30*, 327–336.
84. Blunt, J.W.; Copp, B.R.; Munro, M.H.G.; Northcote, P.T.; Prinsep, M.R. Marine natural products. *Nat. Prod. Rep.* **2010**, *27*, 165–237.
85. Al-Zereini, W.; Yao, C.B.F.F.; Laatsch, H.; Anke, H.J. Aqabamycins A–G: Novel nitro maleimides from a marine Vibrio species. I. Taxonomy, ferentation, isolation and biological activities. *J. Antibiot.* **2010**, *63*, 297–301.
86. Blunt, J.W.; Copp, B.R.; Keyzers, R.A.; Munro, M.H.G.; Prinsep, M.R. Marine natural products. *Nat. Prod. Rep.* **2013**, *30*, 237–323.
87. Pomeroy, R.; Parks, J.; Balboa, C. Farming the reef: Is aquaculture a solution for reducing fishing pressure on coral reefs? *Mar. Policy* **2006**, *30*, 111–130.
88. Shafir, S.; van Rijn, J.; Rinkevich, B. Coral nubbins as source material for coral biological research: A prospectus. *Aquaculture* **2006**, *259*, 444–448.
89. Leal, M.C.; Nunes, C.; Engrola, S.; Dinis, M.; Calado, R. Optimization of monoclonal production of the glass anemone *Aiptasia pallida* (Agassiz in Verrill, 1864). *Aquaculture* **2012**, *354–355*, 91–96.
90. Jaap, W.C. Coral reef restoration. *Ecol. Eng.* **2000**, *15*, 345–364.
91. Delbeek, J. Coral farming: Past, present and future trends. *Aquar. Sci. Conserv.* **2001**, *3*, 171–181.
92. Ellis, S. *Farming Soft Corals for the Marine Aquarium Trade*; Center for Tropical and Subtropical Aquaculture: Pohnpei, Federal States of Micronesia, 1999.
93. Shafir, S.; van Rijn, J.; Rinkevich, B. Steps in the construction of underwater coral nursery, an essential component in reef restoration acts. *Mar. Biol.* **2006**, *149*, 679–687.
94. Rocha, R.J.M.; Serôdio, J.; Leal, M.C.; Cartaxana, P.; Calado, R. Effect of light intensity on post-fragmentation photobiological performance of the soft coral *Sinularia flexibilis*. *Aquaculture* **2013**, *388–391*, 24–29.
95. Leal, M.C.; Nunes, C.; Kempf, S.C.; Reis, A.; Silva, T.L.; Serôdio, J.; Cleary, D.F.R.; Calado, R. Effect of light, temperature and diet on the fatty acid profile of the tropical sea anemone *Aiptasia pallida*. *Aquac. Nutr.* **2013**, *19*, 818–826.
96. Rocha, R.J.M.; Pimentel, T.; Serôdio, J.; Rosa, R.; Calado, R. Comparative performance of light emitting plastma (LEP) and light emitting diode (LED) in *ex situ* aquaculture of scleractinian corals. *Aquaculture* **2013**, *402–403*, 38–45.
97. Rocha, R.J.M.; Calado, R.; Cartaxana, P.; Furtado, J.; Serôdio, J. Photobiology and growth of leather coral *Sarcophyton* cf. *glaucum* fragments stocked under low light in a recirculated system. *Aquaculture* **2013**, *414–415*, 235–242.
98. Wijgerde, T.; Henkemans, P.; Osinga, R. Effects of irradiance and light spectrum on growth of the scleractinian coral *Galaxea fascicularis*—Applicability of LEP and LED lighting to coral aquaculture. *Aquaculture* **2012**, *344–349*, 188–193.

99. Osinga, R.; Schutter, M.; Griffioen, B.; Wijffels, R.H.; Verreth, J.A.J.; Shafir, S.; Henard, S.; Taruffi, M.; Gili, C.; Lavorano, S. The Biology and Economics of Coral Growth. *Mar. Biotechnol.* **2011**, *13*, 658–671.
100. Vizel, M.; Loya, Y.; Downs, C.A.; Kramarsky-Winter, E. A novel method for coral explant culture and micropropagation. *Mar. Biotechnol.* **2011**, *13*, 423–432.
101. Petersen, D.; Laterveer, M.; van Bergen, D.; Hatta, M.; Hebbinghaus, R.; Janse, M.; Jones, R.; Richter, U.; Ziegler, T.; Visser, G.; *et al*. The application of sexual coral recruits for the sustainable management ofex situ populations in public aquariums to promote coral reef conservation—SECORE Project. *Aquat. Conserv.: Mar. Freshw. Ecosyst.* **2006**, *16*, 167–179.
102. Petersen, D.; Falcato, J.; Gilles, P.; Jones, R. Sexual coral reproduction in live coral exhibits—Current status and future perspectives. *Int. Zoo Yearb.* **2007**, *41*, 122–137.
103. Baums, I.B. A restoration genetics guide for coral reef conservation. *Mol. Ecol.* **2008**, *17*, 2796–2811.
104. Fleury, B.G.; Lages, B.G.; Barbosa, J.P.; Kaiser, C.R.; Pinto, Â.C. New hemiketal steroid from the introduced soft coral *Chromonephthea braziliensis* is a chemical defense against predatory fishes. *J. Chem. Ecol.* **2008**, *34*, 987–993.
105. Koh, E.; Sweatman, H. Chemical warfare among scleractinians: Bioactive natural products from Tubastraea faulkneri Wells kill larvae of potential competitors. *J. Exp. Mar. Biol. Ecol.* **2000**, *251*, 141–160.
106. Fleury, B.; Cool, J.; Sammarco, P. Complementary (secondary) metabolites in a soft coral: Sex-specific variability, inter-clonal variability, and competition. *Mar. Ecol.* **2006**, *27*, 204–218.
107. Houlbrèque, F.; Ferrier-Pagès, C. Heterotrophy in Tropical Scleractinian Corals. *Biol. Rev.* **2009**, *84*, 1–17.
108. Brown, B.; Bythell, J. Perspectives on mucus secretion in reef corals. *Mar. Ecol. Prog. Ser.* **2005**, *296*, 291–309.
109. Avila, C. Natural products of opisthobranch molluscs: A biological review. *Oceanogr. Mar. Biol. Annu. Rev.* **1995**, *33*, 487–559.
110. Cimino, G.; Ghiselin, M.T. Chemical defense and the evolution of opisthobranch gastropods. *Proc. Calif. Acad. Sci.* **2009**, *60*, 175–422.
111. Olivera, B.M.; Teichert, R.W. Diversity of the Neurotoxic Conus Peptides. *Mol. Interv.* **2007**, *7*, 251–260.
112. Devine, S.P. Characterization of Bacteria Associated with the Kleptoplastic Sea Slug Elysia chlorotica and Its Algal Prey Vaucheria litorea Using Metagenomics. Electronic Theses and Dissertations, University of Maine, 2012. Available online: http://digitalcommons.library.umaine.edu/etd/1757 (accessed on 1 August 2013).
113. Davis, J.; Fricke, W.F.; Hamann, M.T.; Esquenazi, E.; Dorrestein, P.C.; Hill, R.T. Characterization of the Bacterial Community of the Chemically Defended Hawaiian Sacoglossan Elysia rufescens. *Appl. Environ. Microbiol.* **2013**, *79*, 7073–7081.

114. Hamann, M.T.; Otto, C.S.; Scheuer, P.J.; Dunbar, D.C. Kahalalides: Bioactive Peptides from a Marine Mollusk Elysia rufescens and Its Algal Diet *Bryopsis* sp.1. *J. Org. Chem.* **1996**, *61*, 6594–6600.
115. Pardo, B.; Paz-Ares, L.; Tabernero, J.; Ciruelos, E.; García, M.; Salazar, R.; López, A.; Blanco, M.; Nieto, A.; Jimeno, J. Phase I clinical and pharmacokinetic study of kahalalide F administered weekly as a 1-hour infusion to patients with advanced solid tumors. *Clin. Cancer Res.* **2008**, *14*, 1116–1123.
116. Luesch, H.; Moore, R.E.; Paul, V.J.; Mooberry, S.L.; Corbett, T.H. Isolation of dolastatin 10 from the marine cyanobacterium Symploca species VP642 and total stereochemistry and biological evaluation of its analogue symplostatin 1. *J. Nat. Prod.* **2001**, *64*, 907–910.
117. Harrigan, G.G.; Luesch, H.; Yoshida, W.Y.; Moore, R.E.; Nagle, D.G.; Paul, V.J.; Mooberry, S.L.; Corbett, T.H.; Valeriote, F.A. Symplostatin 1: A dolastatin 10 analogue from marine cyanobacterium *Symploca hydnoides*. *J. Nat. Prod.* **1998**, *61*, 1075–1077.
118. Kamiya, H.; Sakai, R.; Jimbo, M. Bioactive molecules from sea hares. *Prog. Mol. Subcell. Biol.* **2006**, *43*, 215–239.
119. Myers, R.A.; Cruz, L.J.; Rivier, J.E.; Olivera, B.M. Conus peptides as chemical probes for receptors and ion channels. *Chem. Rev.* **1993**, *93*, 1923–1936.
120. Olivera, B.M. E.E. Just Lecture, 1996: Conus Venom Peptides, Receptor and Ion Channel Targets, and Drug Design: 50 Million Years of Neuropharmacology. *Mol. Biol. Cell* **1997**, *8*, 2101–2109.
121. Buczek, O.; Bulaj, G.; Olivera, B.M. Conotoxins and the posttranslational modification of secreted gene products. *Cell. Mol. Life Sci.* **2005**, *62*, 3067–3079.
122. Prommer, E. Zinconotide: A new option for refractory pain. *Drugs Today* **2006**, *24*, 369–378.
123. Lin, Z.; Marett, L.; Hughen, R.W.; Flores, M.; Forteza, I.; Ammon, M.A.; Concepcion, G.P.; Espino, S.; Olivera, B.M.; Rosenberg, G.; *et al.* Neuroactive diol and acyloin metabolites from cone snail-associated bacteria. *Bioorg. Med. Chem. Lett.* **2013**, *23*, 4867–4869.
124. Peraud, O.; Biggs, J.S.; Hughen, R.W.; Light, A.R.; Concepcion, G.P.; Olivera, B.M.; Schmidt, E.W. Microhabitats within Venomous Cone Snails Contain Diverse Actinobacteria. *Appl. Environ. Microbiol.* **2009**, *75*, 6820–6826.
125. O'Brien, F.X.; McKindsey, C.H.; Landry, T.; Costa-Pierce, B.A. Methods of sustainable shelfish aquaculture. In *Sustainable Food Production*; Christou, P., Savin, R., Costa-Pierce, B.A., Misztal, I., Whitelaw, B.A., Eds.; Springer Science+Business Media: New York, NY, USA, 2013; pp. 1436–1548.
126. Shawl, A.L.; Davis, M. Captive breeding behaviour of four strombidae conch. *J. Shellfish Res.* **2004**, *23*, 157–164.
127. Dolorosa, R.G.; Grant, A.; Gill, J.A.; Avillanosa, A.L.; Gonzales, B.J. Indoor and Deep Sub-Tidal Intermediate Culture of *Trochus niloticus* for Restocking. *Rev. Fish. Sci.* **2013**, *21*, 414–423.
128. Capo, T.; Bardales, A.; Gillette, P.; Lara, M.; Schmale, M.; Serafy, J. Larval growth, development, and survival of laboratory-reared *Aplysia californica*: Effects of diet and veliger density. *Comp. Biochem. Phys. C* **2008**, *149*, 215–223.

129. Leal, M.C.; Nunes, C.; Alexandre, D.; Silva, T.L.; Reis, A.; Dinis, M.T.; Calado, R. Parental diets determine the embryonic fatty acid profile of the tropical nudibranch *Aeolidiella stephanieae*: The effect of eating bleached anemones. *Mar. Biol.* **2012**, *159*, 1745–1751.
130. Cruz, S.; Calado, R.; Serôdio, J.; Cartaxana, P. Crawling leaves: Photosynthesis in sacoglossan sea slugs. *J. Exp. Bot.* **2013**, *64*, 3999–4009.
131. Carroll, D.; Kempf, S. Laboratory culture of the aeolid nudibranch *Berghia verrucicornis* (Mollusca, Opisthobranchia): Some aspects of its development and life history. *Biol. Bull.* **1990**, *179*, 243–253.
132. Mayer, A.M.S.; Glaser, K.B. Marine pharmacology and the marine pharmaceuticals pipeline. *FASEB J.* **2013**, *27*, 1167.7.
133. Haefner, B. Drugs from the deep: Marine natural products as drug candidates. *Drug Discov. Today* **2003**, *8*, 536–544.
134. Fusetani, N. *Drugs from the Sea*; Krager: Basel, Switzerland, 2000; p. 164.
135. Lilly, M.; Brown, C.; Pettit, G.; Kraft, A. Bryostatin 1: A potential anti-leukemic agent for chronic myelomonocytic leukemia. *Leukemia* **1991**, *5*, 283–287.
136. Mendola, D. Aquaculture production of bryostatin 1 and ecteinascidin 743. In *Drugs from the Sea*; Fusetani, N., Ed.; Krager: Basel, Switzerland, 2000; pp. 120–133.
137. Dahms, H.-W.; Gao, Q.-F.; Hwang, J.-S. Optimized maintenance and larval production of the bryozoan *Bugula neritina* (Bugulidae: Gymnolaemata) in the laboratory. *Aquaculture* **2007**, *265*, 169–175.
138. Kahle, J.; Liebezeit, G.; Gerdes, G. Growth aspects of Flustra foliacea (Bryozoa, Cheilostomata) in laboratory. In *Migrations and Dispersal of Marine Organisms*; Jones, M.B., Infólfsson, A., Ólafsson, E., Helgason, G.V., Gunnarsson, K., Svavarsson, J., Eds.; Springer Science+Business Media B.V.: Dordrecht, The Netherlands, 2003; Volume 174, pp. 237–244.
139. Trindade-Silva, A.E.; Lim-fong, G.E.; Sharp, K.H.; Haygood, M.G. Bryostatins: Biological context and biotechnological prospects. *Curr. Opin. Biotechnol.* **2010**, *21*, 834–842.
140. Cuevas, C.; Francesch, A. Development of Yondelis (R) (trabectedin, ET-743). A semisynthetic process solves the supply problem. *Nat. Prod. Rep.* **2009**, *26*, 322–337.
141. Zengler, K.; Toledo, G.; Rappé, M.; Elkins, J.; Mathur, E.J.; Short, J.M.; Keller, M. Cultivating the uncultured. *Proc. Natl. Acad. Sci. USA* **2002**, *99*, 15681–15686.
142. Amann, R.I.; Ludwig, W.; Schleifer, K.H. Phylogenetic identification and *in situ* detection of individual microbial cells without cultivation. *Microbiol. Rev.* **1995**, *59*, 143–169.
143. Joint, I.; Mühling, M.; Querellou, J. Culturing marine bacteria—An essential prerequisite for biodiscovery. *Microb. Biotechnol.* **2010**, *3*, 564–575.
144. Pham, V.H.T.; Kim, J. Cultivation of unculturable soil bacteria. *Trends Biotechnol.* **2012**, *30*, 475–484.
145. Alain, K.; Querellou, J. Cultivating the uncultured: Limits, advances and future challenges. *Extremophiles* **2009**, *13*, 583–594.

146. Janssen, P.H.; Yates, P.S.; Grinton, B.E.; Taylor, P.M.; Sait, M. Improved Culturability of Soil Bacteria and Isolation in Pure Culture of Novel Members of the Divisions Acidobacteria, Actinobacteria, Proteobacteria, and Verrucomicrobia. *Appl. Environ. Microbiol.* **2002**, *68*, 2391–2396.
147. Stewart, E.J. Growing Unculturable Bacteria. *J. Bacteriol.* **2012**, *194*, 4151–4160.
148. Straight, P.D.; Kolter, R. Interspecies Chemical Communication in Bacterial Development. *Annu. Rev. Microbiol.* **2009**, *63*, 99–118.
149. Ohno, M.; Shiratori, H.; Park, M.J.; Saitoh, Y.; Kumon, Y.; Yamashita, N.; Hirata, A.; Nishida, H.; Ueda, K.; Beppu, T. Symbiobacterium thermophilum gen. nov. sp. nov. a symbiotic thermophile that depends on co-culture with a Bacillus strain for growth. *Int. J. Syst. Evol. Microbiol.* **2000**, *50*, 1829–1832.
150. Pagnier, I.; Raoult, D.; La Scola, B. Isolation and identification of amoeba-resisting bacteria from water in human environment by using an Acanthamoeba polyphaga co-culture procedure. *Environ. Microbiol.* **2008**, *10*, 1135–1144.
151. Nichols, D.; Cahoon, N.; Trakhtenberg, E.M.; Pham, L.; Mehta, A.; Belanger, A.; Kanigan, T.; Lewis, K.; Epstein, S.S. Use of Ichip for High-Throughput In Situ Cultivation of "Uncultivable" Microbial Species. *Appl. Environ. Microbiol.* **2010**, *76*, 2445–2450.
152. Aoi, Y.; Kinoshita, T.; Hata, T.; Ohta, H.; Obokata, H.; Tsuneda, S. Hollow-Fiber Membrane Chamber as a Device for In Situ Environmental Cultivation. *Appl. Environ. Microbiol.* **2009**, *75*, 3826–3833.
153. Kaeberlein, T.; Lewis, K.; Epstein, S.S. Isolating "Uncultivable" Microorganisms in Pure Culture in a Simulated Natural Environment. *Science* **2002**, *296*, 1127–1129.
154. Bollmann, A.; Lewis, K.; Epstein, S.S. Incubation of Environmental Samples in a Diffusion Chamber Increases the Diversity of Recovered Isolates. *Appl. Environ. Microbiol.* **2007**, *73*, 6386–6390.
155. Singh, B.K.; Macdonald, C.A. Drug discovery from uncultivable microorganisms. *Drug Discov. Today* **2010**, *15*, 792–799.
156. Schmidt, E.W.; Nelson, J.T.; Rasko, D.A.; Sudek, S.; Eisen, J.A.; Haygood, M.G.; Ravel, J. Patellamide A and C biosynthesis by a microcin-like pathway in *Prochloron didemni*, the cyanobacterial symbiont of *Lissoclinum patella*. *Proc. Natl. Acad. Sci. USA* **2005**, *102*, 7315–7320.
157. Long, P.F.; Dunlap, W.C.; Battershill, C.N.; Jaspars, M. Shotgun Cloning and Heterologous Expression of the Patellamide Gene Cluster as a Strategy to Achieving Sustained Metabolite Production. *ChemBioChem* **2005**, *6*, 1760–1765.

Nocapyrones: α- and γ-Pyrones from a Marine-Derived *Nocardiopsis* sp

Youngju Kim, Hiromu Ogura, Kazuaki Akasaka, Tsutomu Oikawa, Nobuyasu Matsuura, Chiaki Imada, Hisato Yasuda and Yasuhiro Igarashi

Abstract: One new α-pyrone (nocapyrone R (**1**)), and three known γ-pyrones (nocapyrones B, H and L (**2**–**4**)) were isolated from the culture extract of a *Nocardiopsis* strain collected from marine sediment. Structures of these compounds were determined on the basis of spectroscopic data including NMR and MS. γ-Pyrones **2**–**4** were found to induce adiponectin production in murine ST-13 preadipocyte cells but the α-pyrone **1** had no activity. The absolute configuration of the *anteiso*-methyl branching in **4** was determined by HPLC comparison of a degraded product of **4** with standard samples as a 2:3 enantiomeric mixture of (*R*)- and (*S*)-isomers.

Reprinted from *Mar. Drugs*. Cite as: Kim, Y.; Ogura, H.; Akasaka, K.; Oikawa, T.; Matsuura, N.; Imada, C.; Yasuda, H.; Igarashi, Y. Nocapyrones: α- and γ-Pyrones from a Marine-Derived *Nocardiopsis* sp. *Mar. Drugs* **2014**, *12*, 4110–4125.

1. Introduction

Natural products have been playing an important role for the development of novel therapeutics owing to their enormous and unpredictable structural diversity [1]. Specifically, actinomycetes are continuously providing structurally diverse secondary metabolites possessing pharmaceutically useful bioactivities. More than 70% of microbial antibiotics have been discovered from actinomycetes [2]. In recent years, in addition to the terrestrial species, actinomycetes from marine environments are attracting a substantial attention as a new resource of novel drug candidates [3]. The differences between the marine and terrestrial environments are likely reflected in the genetic divergences. Marine-derived actinomycetes are recognized to actually produce a range of chemically distinctive secondary metabolites that terrestrial actinomycetes are not able to produce [4]. Consequently, the number of novel metabolites from marine actinomycetes has been increasing in recent years.

The increasing incidents of type 2 insulin-resistant diabetes, as a result of growing obesity rates, are causing a serious social and economic problem [5]. Adipose tissue secretes various types of biologically active adipokines, such as free fatty acids, tumor necrosis factor-α, adiposin, resistin, and leptin, to regulate energy homeostasis [6]. Adiponectin is one of such adipokines secreted exclusively by mature adipocytes [7] and this proteineous substance functions to regulate the glucose and lipid metabolism [8]. Recent research revealed that the mRNA expression of adiponectin is reduced in obese diabetic murine model [9] and type 2 diabetic patients [10–12], and also plasma level of adiponcetin is significantly lower in obese diabetic mice and humans [13–15]. Therefore, the replenishment of adiponectin by transcriptional induction in adipocytes is believed to provide a new effective therapeutic approach to insulin resistance, type 2 diabetes, and related diseases. Thiazolidinediones represented by rosiglitazone (Avandia) and pioglitazone (Actos) are

widely-used orally available drugs for type 2 diabetes. These synthetic compounds activate transcription by PPARγ (peroxisome proliferator activated receptor γ) primarily in adipose tissues and induce the elevation of adiponectin plasma level. Meanwhile, several research groups have demonstrated that serious side effects are caused by rosiglitazone; the use of this drug is associated with a 43% increase in myocardial infraction and 64% increase in the risk of death from cardiovascular causes [16]. Thus, the development of side effect-free new agents for type 2 diabetes is desperately desired. In our screening program for discovering new lead scaffolds for adiponectin inducers from natural products [17–19], a marine-derived *Nocardiopsis* strain was found to produce a new α-pyrone (**1**) along with three known γ-pyrones, nocapyrones B, H, and L (**2**–**4**, Figure 1). Interestingly, nocapyrone L (**4**) was isolated as an enantiomeric mixture, which is noticeable in marine natural products. Herein, we describe isolation, structure determination, and biological activities of these compounds.

Figure 1. Structures of nocapyrones R (**1**), B (**2**), H (**3**), and L (**4**).

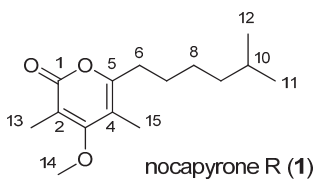

nocapyrone R (**1**)

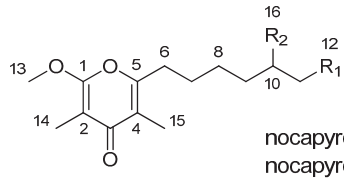

nocapyrone B (**2**) : R_1=H, R_2=CH_3
nocapyrone H (**3**) : R_1=CH_3, R_2=H
nocapyrone L (**4**) : R_1=R_2=CH_3 (10*R*:10*S*=2:3)

2. Results and Discussion

2.1. Structure Analysis and Characterization

2.1.1. Isolation

The producing strain TP-A0876 was isolated from a sediment sample collected at −775 m in Ishikari gulf, Hokkaido, Japan. On the basis of the result of 16S rRNA gene sequence similarity, the isolate was identified as *Nocardiopsis* sp. The strain TP-A0876 was cultured in A-3M medium at 30 °C for 6 days and the whole culture broth was extracted with 1-butanol. The crude extract was subjected to silica gel and ODS column chromatographies, followed by HPLC purification, to yield nocapyrone R (**1**) along with nocapyrones B, H, and L (**2**–**4**), three known compounds previously isolated from marine *Nocardiopsis* strains by other groups [20,21].

2.1.2. Nocapyrone R (**1**)

Nocapyrone R (**1**) was isolated as colorless amorphous. The molecular formula of **1** was determined as $C_{15}H_{24}O_3$ by high resolution ESITOFMS (Electrospray Ionization Time Of Flight Mass Spectrometry) analysis that showed a pseudomolecular ion at *m*/*z* 275.1619 $[M + Na]^+$ (calcd for $C_{15}H_{24}O_3Na$, 275.1623), which was corroborated by the ^1H and ^{13}C NMR data. The IR spectrum indicated the presence of alkene (2944 cm^{-1}) and carbonyl (1660 cm^{-1}) groups. ^1H and ^{13}C NMR data in combination with the HSQC (Heteronuclear Single Quantum Coherence) analysis revealed

the presence of 15 carbons assignable to one carbonyl carbon, four sp^2 quaternary carbons, four sp^3 methylenes, one sp^3 methine, and five methyl groups (one is oxygenated) (Table 1, Supplementary Figures S1, S2 and S4). The NMR spectra of nocapyrone R (**1**) showed the resonances for a pyrone unit as well as two methyl (C-13 and C-15) and one methoxy (C-14) substituents (Table 1, Supplementary Figures S1 and S2): however, the UV spectrum showing absorption maximum at λ_{max} 290 nm was different from that for γ-pyrone (**2**–**4**: UV λ_{max} 252 nm). Furthermore, the ester carbonyl absorption of IR spectrum and the ester carbonyl signal of ^{13}C NMR suggested the presence of an ester/lactone functionality. Protons of two olefinic methyl groups (H_3-13 and H_3-15) had HMBC correlations with C-3, to which was correlated the methoxy protons (H_3-14), establishing the α-pyrone substructure with a methoxy group at C-3 flanked by two olefinic methyl groups (Supplementary Figure S5). The ^1H-^1H COSY spectrum provided two fragments, H_2-6/H_2-7/H_2-8/H_2-9 and H_3-11/H-10/H_3-12. These two fragments were assembled into an alkyl chain bearing an isopropyl terminus by HMBC correlations from H_3-12 to C-9, C-10, and C-11. This was consistent with the presence of two doublet methyl proton signals for H_3-11 and H_3-12 (Supplementary Figures S3 and S5). The alkyl side chain was attached to C-5 by HMBC correlations from H_2-6 to C-4 and C-5, completing the structure of **1** (Figure 2).

Table 1. ^1H and ^{13}C NMR data for nocapyrone R (**1**) in $CDCl_3$.

Position	δ_C [a]	δ_H mult (*J* in Hz) [b]	COSY [b]	HMBC [b,c]
1	166.3, qC			
2	109.3, qC			
3	168.4, qC			
4	109.0, qC			
5	159.3, qC			
6	31.1, CH_2	2.49, t (7.8)	7	4, 5, 7
7	27.7, CH_2	1.61, m	6, 8	5
8	27.1, CH_2	1.31, m	7, 9	10
9	38.7, CH_2	1.18, m	8	7, 11, 12
10	27.9, CH	1.52, m		11, 12
11	22.6, CH_3	0.86, d (6.5)	10, 12	9, 10, 12
12	22.6, CH_3	0.86, d (6.5)	10, 11	9, 10, 11
13	10.2, CH_3	2.03, s		1, 2, 3
14	60.2, CH_3	3.80, s		3
15	10.1, CH_3	1.92, s		3, 4, 5

[a] recorded at 100 MHz; [b] recorded at 500 MHz; [c] HMBC correlations are from proton(s) stated to the indicated carbon.

Figure 2. 2D-NMR correlations for nocapyrone R (**1**).

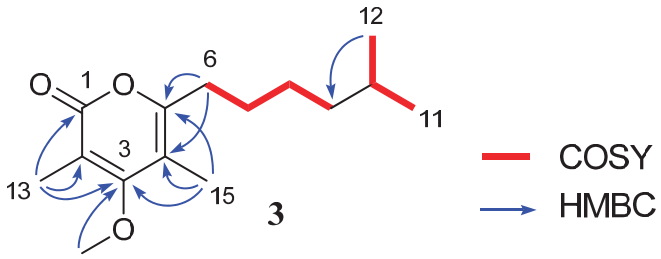

2.1.3. Absolute Configuration of Nocapyrone L (**4**)

Nocapyrone L (**4**) has been reported as a secondary metabolite of *Nocadiopsis* sp. isolated from a mollusk as a symbiotic bacterium [21]. Due to the remoteness of the branched methyl chiral center (C-10) from the modifiable functional groups, the absolute configuration of **4** had not been assigned. From the structural analogy of **4** to germicidin A, we hypothesized that **4** could be biosynthesized through condensation of an amino acid-derived starter with malonate extenders [22]. Consequently, the *anteiso*-subunit known to be originated from L-isoleucine is assumed to have *S* configuration. Interestingly, the specific rotation of **4** we isolated showed $[\alpha]_D^{25} = -2.2$ (c = 0.1, $CHCl_3$), while that of reported one is $[\alpha]_D^{25} = +9.0$ (c = 0.1, $CHCl_3$) [21]. In order to clarify the absolute configuration of **4**, Ohrui-Akasaka method was applied (Scheme 1) [23]. The pyrone unit of **4** was oxidatively degraded by the treatment with a catalytic amount of ruthenium (III) chloride and sodium periodate in a biphasic solvent system (CCl_4–MeCN–H_2O) to give 6-methyloctanoic acid **5** [24]. This *anteiso*-fatty acid was then esterified with a chiral anthracene reagent, (*R*)-2-(anthracene-2,3-dicarboximido)propanol [(*R*)-2A1P], to yield *nat*-**5**-(*R*)-2A1P (Supplementary Figure S6). HPLC analysis of this derivative was performed on Develosil ODS-HG-3 column (4.6 mm × 150 mm, column temp. −58.5 °C) with the eluent of MeOH/MeCN/THF (4:3:1) at a flow rate of 0.2 mL/min. (*S*)-6-Methyloctanoic acid [(*S*)-5], which was prepared from commercially available (*S*)-6-methyloctanol, was labeled with (*R*)-2A1P or (*S*)-2A1P to give reference samples, (*S*)-**5**-(*R*)-2A1P and (*S*)-**5**-(*S*)-2A1P (Supplementary Figures S7 and S8). Retention times of reference samples were 130.5 min for (*S*)-**5**-(*S*)-2A1P (corresponding to (*R*)-**5**-(*R*)-2A1P diastereomer) and 139.3 min for (*S*)-**5**-(*R*)-2A1P (Figure 3a). Surprisingly, *nat*-**5**-(*R*)-2A1P derived from **4** showed two peaks for (*R*)-**5**-(*R*)-2A1P and (*S*)-**5**-(*R*)-2A1P in a ratio of 2:3 (Figure 3b). Consequently, nocapyrone L (**4**) was confirmed as an enantiomeric mixture of (*R*)- and (*S*)-isomers in a ratio of 2:3. This was supported by the ^{1}H NMR signal for C-6 methyl protons of *nat*-**5**-(*R*)-2A1P, which showed overlapped signals for those of (*S*)-**5**-(*S*)-2A1P and (*S*)-**5**-(*R*)-2A1P (Figure 4).

Scheme 1. Degradation of **4** to **5** and labeling with (*R*)-2A1P.

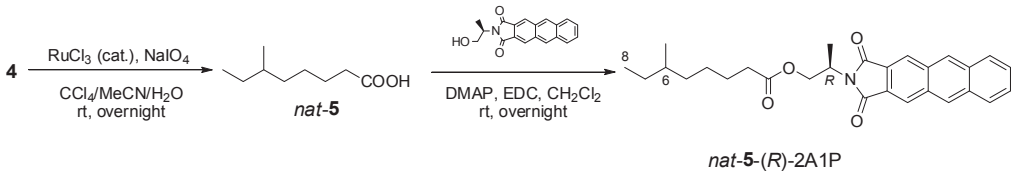

Figure 3. Determination of absolute configuration of *anteiso*-methyl group by HPLC. (**a**) HPLC chromatogram of standard (*S*)-**5**-(*S*)-2A1P (right graph) and (*S*)-**5**-(*R*)-2A1P (left graph); (**b**) HPLC chromatogram of *nat*-**5**-(*R*)-2A1P.

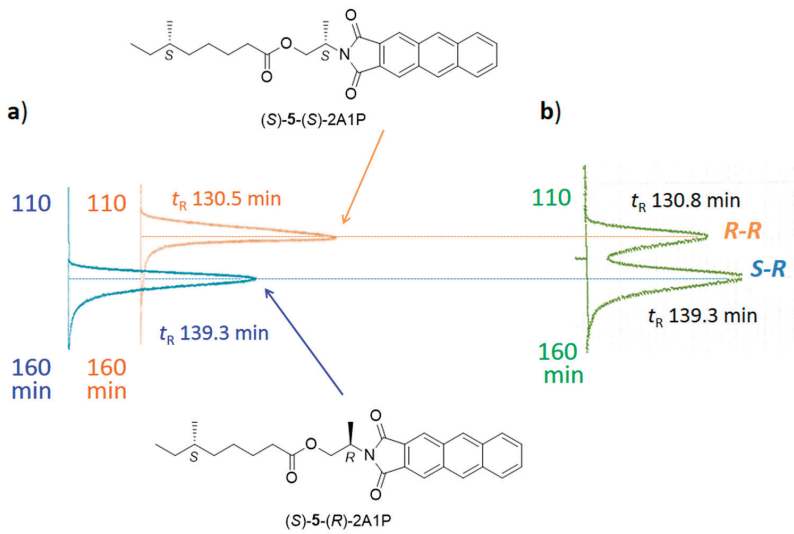

2.2. Biological Activities

Activity of compounds **1**–**4** to promote adiponectin-production in adipocyte cells was assessed by measuring the mRNA expression level of adiponectin-coding gene [25]. After the treatment of murine ST-13 preadipocyte cells with the compounds for 11 days, the total mRNA was subjected to quantitative real-time PCR analysis. All the γ-pyrones (**2**–**4**) enhanced the expression of adiponectin mRNA in a concentration-dependent manner while the α-pyrone (**1**) showed no such effect (Figure 5). Especially, **2** and **4** more strongly induced adiponectin production at 8 μM and at the same concentration the accumulation of lipid droplets were observed (Figure 6, oil red O staining) that indicates the differentiation to mature adipocyte cells. Compound **2** was further examined for the transcriptional activation of PPARγ that is the main target of the antidiabetic drug, thiazolidinediones. In the luciferase reporter assay, troglitazone activated the transcription through PPARγ but **2** did not (Figure 7), confirming that **2** is not a ligand for PPARγ and its mode of action

is different from thiazolidinediones. These effects on adipocytes or adiponectin-inducing activity have not been described for nocapyrones and other related pyrone compounds.

Figure 4. Expanded ^{1}H NMR spectra of *nat*-**5**-(*R*)-2A1P, standard (*S*)-**5**-(*S*)-2A1P and (*S*)-**5**-(*R*)-2A1P. (**a**) comparison of *nat*-**5**-(*R*)-2A1P (bottom) with standard (*S*)-**5**-(*S*)-2A1P (top) and (*S*)-**5**-(*R*)-2A1P (middle); (**b**) analysis of ^{1}H NMR signal of *nat*-**5**-(*R*)-2A1P.

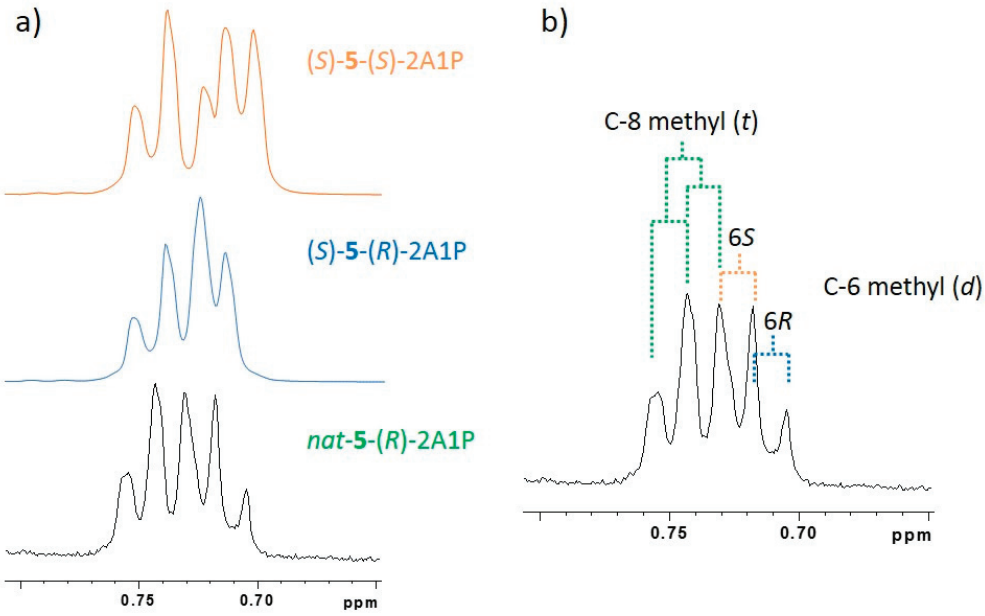

Figure 5. Effect of nocapyrones on expression of adiponectin mRNA (ROS = rosiglitazone, 20 nM).

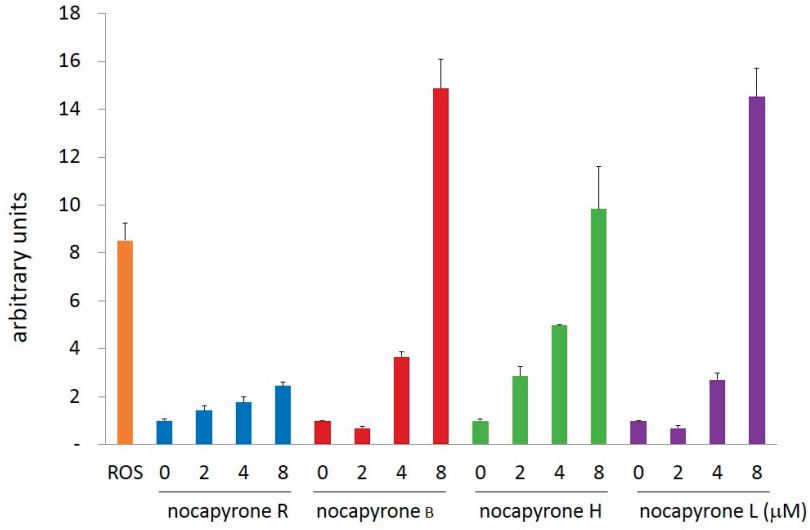

Figure 6. Adipocyte differentiation induced by nocapyrones B and L.

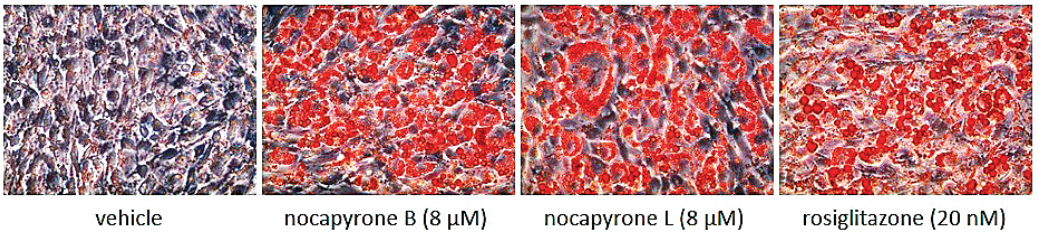

Figure 7. Effect of nocapyrone B on activation of PPARγ in luciferase ligand assay system.

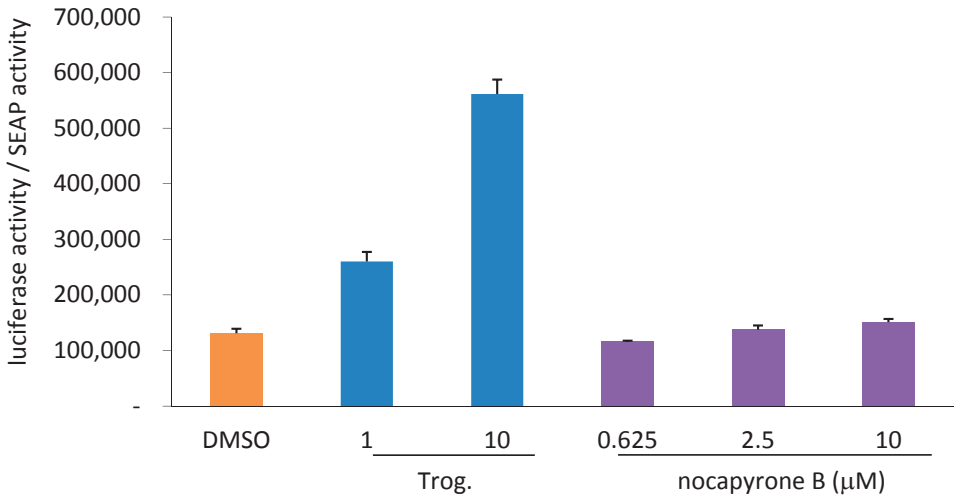

3. Experimental Section

3.1. General Experimental Procedures

Optical rotation was measured using a JASCO DIP-3000 polarimeter (JASCO Corporation, Hachioji, Japan). UV spectra were recorded on a Hitachi U-3210 spectrophotometer (Hitachi High-Technologies Corporation, Tokyo, Japan). IR spectra were measured on a Perkin-Elmer Spectrum 100 (Perkin-Elmer Japan Co. Ltd., Yokohama, Japan). NMR spectra were obtained on a Bruker AVANCE 400 (Bruker BioSpin K.K., Yokohama, Japan) or a Bruker AVANCE 500 spectrometer (Bruker BioSpin K.K., Yokohama, Japan). HR-ESI-TOFMS were recorded on a Bruker microTOF focus (Bruker Daltonics K.K., Yokohama, Japan). Cosmosil 75C18-PREP (Nakalai Tesque, Inc., Kyoto, Japan, 75 μm) was used for ODS column chromatography.

3.2. Microorganism

Strain TP-A0876 was isolated from a sediment sample collected at a depth of 775 m off the island of Hokkaido (N 42°56′80″, E 140°06′32″), Japan in 2006 (August), using a piston corer. The

strain was identified as a member of the genus *Nocardiopsis* on the basis of 100% 16S rRNA gene sequence (1455 nucleotides; GenBank accession number AB488799) similarity to *Nocardiopsis* sp. 123 (accession number AY036002).

3.3. Fermentation

Strain TP-A0876 cultured on a Bn-2 agar plate soluble starch 0.5%, glucose 0.5%, meat extract (Kyokuto Pharmaceutical Industrial Co., Ltd., Tokyo, Japan) 0.1%, yeast extract (Difco Laboratories, Surrey, United Kingdom) 0.1%, NZ-case (Wako Pure Chemical Industries, Ltd., Osaka, Japan) 0.2%, NaCl 0.2%, $CaCO_3$ 0.1% and agar 1.5%] was inoculated into 500-mL K-1 flasks each containing 100 mL of the V-22 seed medium consisting of soluble starch 1%, glucose 0.5%, NZ-case 0.3%, yeast extract 0.2%, Tryptone (Difco Laboratories) 0.5%, K_2HPO_4 0.1%, $MgSO_4 \cdot 7H_2O$ 0.05%, and $CaCO_3$ 0.3% (pH 7.0). The flasks were placed on a rotary shaker (200 rpm) at 30 °C for 4 days. The seed culture (3 mL) was transferred into 500-mL K-1 flasks each containing 100 mL of the A-3M production medium consisting of glucose 0.5%, soluble starch 2.0%, glycerol 2.0%, yeast extract 0.3%, Pharmamedia (Trader's Protein) 1.5%, and Diaion HP-20 (Mitsubishi Chemical Holdings Corporation, Tokyo, Japan) 1%. The pH of the medium was adjusted to 7.0 before sterilization. The inoculated flasks were placed on a rotary shaker (200 rpm) at 30 °C for 7 days.

3.4. Extraction and Isolation

At the end of the fermentation period, 100 mL of 1-butanol was added to each flask, and they were allowed to shake for one hour. The mixture was centrifuged at 5000 rpm for 10 min and the organic layer was separated from the aqueous layer containing the mycelium. Evaporation of the solvent gave 7.8 g of extract from 2 L of culture. The crude extract (7.8 g) was subjected to silica gel column chromatography with a step gradient of $CHCl_3$/MeOH (1:0, 20:1, 10:1, 4:1, 2:1, 1:1, and 0:1 *v/v*). Fractions 2 (20:1) and 3 (10:1) were combined and concentrated *in vacuo* to give brown oil (0.97 g) which was further fractionated by reverse-phase ODS column chromatography with a gradient of MeCN/distilled water (2:8, 3:7, 4:6, 5:5, 6:4, 7:3, and 8:2 *v/v*). Fractions 4 (5:5) and 5 (6:4) were combined and evaporated and the remaining aqueous solution was extracted with EtOAc. The organic layer was washed with brine, dried over anhydrous Na_2SO_4, filtered, and evaporated to dryness. The residual brown solid (0.28 g) was then subjected to HPLC purification using an ODS column (Cosmosil ARII, 10 mm × 250 mm) with 55% MeCN in distilled water at 3.0 mL/min to give nocapyrone B (**2**, t_R 28.1 min, 10 mg), nocapyrone H (**3**, t_R 31.3 min, 2.3 mg) and a mixture of nocapyrones R and L (**1** and **4**, t_R 41.2 min, 3.8 mg). **1** and **4** were separated by using a cholesterol-bonded reverse-phase column (Cosmosil Cholester, 10 mm × 250 mm) with 55% MeCN in distilled water at 3.0 mL/min to give **4** (t_R 29.9 min, 2.1 mg) and **1** (t_R 35.0 min, 0.8 mg).

Nocapyrone R (**1**): colorless amorphous solid; UV (MeOH) λ_{max} (log ε) 290 (4.04) nm; IR (ATR) ν_{max} 2944, 1660 cm^{-1}; ^1H and ^{13}C-NMR data, see Table 1; HRESITOFMS *m/z* 275.1619 $[M + Na]^+$ (calcd for $C_{15}H_{24}O_3Na$, 275.1623).

*3.5. Determination of the Absolute Configuration of the Anteiso-Methyl Group in **4** by Ohrui-Akasaka Method*

Oxidative Degradation of **4** to Yield **5**: A solution of nocapyrone L (**4**, 4 mg, 15 μmol) in a mixture of MeCN (320 μL) and H_2O (240 μL) was stirred with $NaIO_4$ (19.2 mg, 89 μmol) until the salt was dissolved. To this solution were added CCl_4 (320 μL) and 1 mg/mL solution of $RuCl_3$ hydrate in 0.1 M sodium phosphate buffer (240 μL, pH 7.6) and the biphasic mixture was vigorously stirred at room temperature for 17 h. The reaction mixture was passed through Celite and the filter cake was washed with MeCN. After evaporation of the organic solvent from the filtrate, the aqueous solution was acidified with 2 M HCl and extracted with EtOAc. The EtOAc layer was concentrated and the remaining material was dissolved in MeOH (1 mL) and THF (1 mL). To this solution was added 1 M NaOH (1 mL) and the mixture was stirred at room temperature for 12 h. The reaction mixture was then acidified with 2 M HCl and extracted with EtOAc. The EtOAc layer was washed with water and brine, dried over anhydrous Na_2SO_4, and concentrated *in vacuo* to give 6-methyloctanoic acid (**5**, 1.2 mg) which was used for the next reaction without further purification:^{1}H NMR ($CDCl_3$, 500 MHz) δ 0.84 (3H, d, J = 6.0 Hz), 0.85 (3H, t, J = 7.6 Hz), 1.12 (2H, m), 1.28–1.35 (5H, m), 1.62 (2H, m), 2.36 (1H, t, J = 7.5 Hz).

Preparation of *nat*-**5**-(*R*)-2A1P: 6-Methyloctanoic acid (**5**) obtained by degradation of nocapyrone L (**4**) was reacted with (*R*)-2-(anthracene-2,3-dicarboximido)propanol [(*R*)-2A1P] (2 mg, 6.6 μmol) in dry CH_2Cl_2 (1 mL) in the presence of EDAC (2 mg, 10 μmol) and DMAP (trace amount) at room temperature for 17 h. The reaction mixture was diluted with ice-water and extracted with EtOAc. The organic layer was concentrated under reduced pressure and the residue was chromatographed over a silica gel column (*n*-hexane–EtOAc = 1:0~1:1) to give (*R*)-2A1P ester derivative of naturally occurring 6-methyloctanoic acid [*nat*-**5**-(*R*)-2A1P, 0.8 mg].

Preparation of standard (*S*)-6-methyloctanoic acid: To a solution of (*S*)-6-methyl-1-octanol (10 mg, 69 μmol, Wako Pure Chemical Industries, Ltd., Osaka, Japan) in acetone (1 mL) was added Jones reagent (0.4 mL, 80 μmol) dropwise. After stirring for 3 h at room temperature, the reaction mixture was extracted with EtOAc and the organic layer was concentrated *in vacuo* to give (*S*)-6-methyloctanoic acid (7.0 mg): ^{1}H NMR ($CDCl_3$, 500 MHz) δ 0.85 (3H, t, J = 5.5 Hz), 0.87 (3H, d, J = 7.0 Hz), 1.25–1.35 (5H, m), 1.33 (2H, m), 1.62 (2H, m), 2.36 (3H, t, J = 7.5 Hz).

Preparation of standard (*S*)-**5**-(*R*)-2A1P and (*S*)-**5**-(*S*)-2A1P: In the same manner as described for the preparation of *nat*-**5**-(*R*)-2A1P, (*S*)-**5**-(*R*)-2A1P and (*S*)-**5**-(*S*)-2A1P were prepared by the reaction of (*S*)-6-methyloctanoic acid with (*R*)- and (*S*)-2A1P, respectively.

(*S*)-**5**-(*R*)-2A1P: ^{1}H NMR ($CDCl_3$, 500 MHz) δ 0.72 (3H, d, J = 5.2 Hz), 0.74 (3H, t, J = 6.7 Hz), 0.97 (2H, m), 1.11–1.25 (5H, m), 1.49 (2H, m), 1.57 (2H, d, J = 7.1 Hz), 2.22 (2H, t, J = 7.7 Hz), 4.61 (1H, t, J = 6.1 Hz), 4.43 and 4.73 (2H, m), 7.62 (1H, dd, J = 6.5, 2.9 Hz), 8.07 (1H, dd, J = 6.3, 2.8 Hz), 8.48 (1H, s), 8.60 (1H, s).

(*S*)-**5**-(*S*)-2A1P: ^{1}H NMR ($CDCl_3$, 500 MHz) δ 0.71 (3H, d, J = 5.9 Hz), 0.74 (3H, t, J = 6.8 Hz), 0.96 (2H, m), 1.13–1.25 (5H, m), 1.48 (2H, m), 1.57 (2H, d, J = 7.1 Hz), 2.23 (2H, t, J = 7.7 Hz),

4.62 (1H, t, *J* = 6.1 Hz), 4.44 and 4.74 (2H, m), 7.62 (1H, dd, *J* = 7.0, 3.1 Hz), 8.07 (1H, dd, *J* = 6.3, 2.8 Hz), 8.48 (1H, s), 8.60 (1H, s).

HPLC analysis: *nat*-**5**-(*R*)-2A1P derived from nocapyrone L (**4**) and synthetic (*S*)-**5**-(*R*)-2A1P and (*S*)-**5**-(*S*)-2A1P were analyzed by HPLC under the following conditions. Column: Develosil ODS-HG-3 (4.6 mm × 150 mm, Nomura Chemical); mobile phase: MeOH/MeCN/THF=4:3:1; column temperature: −58.5 °C; flow rate: 0.2 mL/min. The column was cooled by using Cryocool CC-100 (Neslab Instruments Inc., Portsmouth, NH, USA). HPLC peaks were detected by monitoring fluorescence intensity at 460 nm with the excitation at 362 nm by using an FP-920 fluorescence detector (JASCO Corporation, Hachioji, Japan). Retention times were 130.5 min for (*S*)-**5**-(*S*)-2A1P and 139.3 min for (*S*)-**5**-(*R*)-2A1P. Natural product-derived *nat*-**5**-(*R*)-2A1P gave peaks at 130.8 min and 139.3 min in a ratio of 2:3.

3.6. Biological Activity Study

Adipocyte differentiation assay was carried out according to the procedure previously described [25].

3.6.1. Real-Time Quantitative PCR Analysis

The total RNA (1 μg) was reverse-transcribed to cDNA using a Super Script TM II RT (Invitrogen, Tokyo, Japan). To quantitatively estimate the mRNA levels of several genes, PCR amplification was performed using a Light Cycler system (Roche Diagnostic Co., Tokyo, Japan). Real-time PCR was carried out in a total volume of 20 μL containing 500 nM each of gene-specific primers, cDNA, and SYBRP remix Ex Tag (Takara, Kyoto, Japan). Expression was normalized to glyceraldehyde-3-phosphate dehydrogenase (GAPDH). Thermal cycling conditions for the PCR were 95 °C for 5 min, followed by 45 cycles of 95 °C for 5 s, 60 °C for 15 s, and 72 °C for 10 s, then a melting curve analysis from 65 °C to 95 °C, every 0.1 °C. The primer sequences used were: adiponectin, 5′-GAAGCCGCTTATATGTATCG-3′ (forward) and 5′-GCCGTCATAATGATTCTGT-3′ (reverse); GAPDH, 5′-CCAGAACATCATCCCTGC-3′ (forward) and 5′-CCACGACGGACACATT-3′ (reverse); fatty acid-binding protein (aP2), 5′-GAAATCACCGCAGACG-3′ (forward) and 5′-ACATTCCACCACCAGC-3′ (reverse); PPARγ2, 5′-CTGTTGACCCAGAGCA-3′ (forward) and 5′-GCGAGTGGTCTTCCAT-3′ (reverse).

3.6.2. Oil Red O Staining

ST-13 cells treated with nocapyrones B and L for 11 days were washed three times with phosphate-buffered saline (PBS), fixed with 10% formalin neutral buffer solution (Wako Pure Chemical, Osaka, Japan) at room temperature for 10 min, and then washed with distilled water to remove formalin solution. Furthermore, the cells were rinsed with 60% 2-propanol for 5 min, stained with 0.24% oil red O at room temperature for 20 min, and then were photographed under a phase contrast microscope (×100 magnification) equipped with a CCD camera (Leica Microsystems Japan, Tokyo, Japan).

3.6.3. Luciferase Reporter Assay

An expression plasmid containing the ligand binding domain of human PPARγ fused to the GAL4 DNA binding domain (pPPARγ-GAL4), and the luciferase reporter plasmid, 17m2G TATA Luc (p17m2G), were kindly donated by Dr. S. Kato (University of Tokyo, Tokyo, Japan). We transiently transfected COS-1 cells (6×10^5 cells) with pPPARγ-GAL4 (0.25 μg) and p17m2G (1 μg) using Effectene Transfection Reagent (QIAGEN, Tokyo, Japan). Transfections were performed in triplicate in 24-well plates according to the manufacture's instructions. After 16 h, the transfected cells received the indicated concentrations of nocapyrones B (or troglitazone), and were cultured for additional 24 h at 37 °C in a 5% CO_2 incubator. Then cells were harvested and luciferase activities were measured by a Steady-Glo® Luciferase Assay System (Promega, Madison, WI, USA) according to manufacturer's instructions.

4. Conclusions

In this study, a marine-derived actinomycete *Nocardiopsis* sp. TP-A0876 was isolated from a sediment sample and its secondary metabolites were investigated. Purification from the 1-butanol extract of the culture broth resulted in isolation of one α-pyrone and three γ-pyrones. Based on the spectroscopic analysis, the α-pyrone was confirmed as a new compound, whereas other three γ-pyrones were identified as nocapyrones B (**2**), H (**3**), and L (**4**). Biological testing in a set of assays proved that γ-pyrone compounds (**2**–**4**) have ability to induce preadipocyte differentiation and adiponectin production in murine ST13 preadipocyte cells. Since the α-pyrone compound **1** showed no activity, the γ-pyrone structure is proposed to play a key role in this activity.

A large number of pyrone–containing marine natural products are known [26–32]. Specifically, a series of nocapyrones (A–Q) have been continuously reported from marine-derived *Nocardiopsis* strains with a wide range of bioactivity (Figure 8). Nocapyrones B (**2**) and H (**3**) modulate nerve cell depolarization, activate or inhibit Ca^{2+} flux into a panel of human cells overexpressing various transient receptor potential (TRP) channels depending upon the agent and channel subtype, together with cytotoxicity against human breast adenocarcinoma, but have no antibacterial activity [21]. Nocapyrones E–G are described to have modest antibacterial activity against *Bacillus subtilis* [30]. Nocapyrone H* inhibits NO production in LPS-stimulated BV-2 microglial cells and neuro-protective effect [31], and nocapyrones H*, I*, and M* were shown to suppress gene expression in quorum sensing [32]. However, there is no report on the activity of these pyrones for preadipocyte differentiation or adiponectin production. Although the effectiveness is lower than thiazolidinediones, different mode of action of the γ-pyrones may provide an opportunity of drug development from this new therapeutic scaffold for insulin resistance type 2 diabetes. The concise synthetic strategies [33–36] and interesting bioactivities of structurally related compounds have been reported [37,38]. On the base of these studies, further synthetic and biological studies of nocapyrone families could be inspiring.

Figure 8. Nocapyrones isolated from marine-derived *Nocardiopsis*.

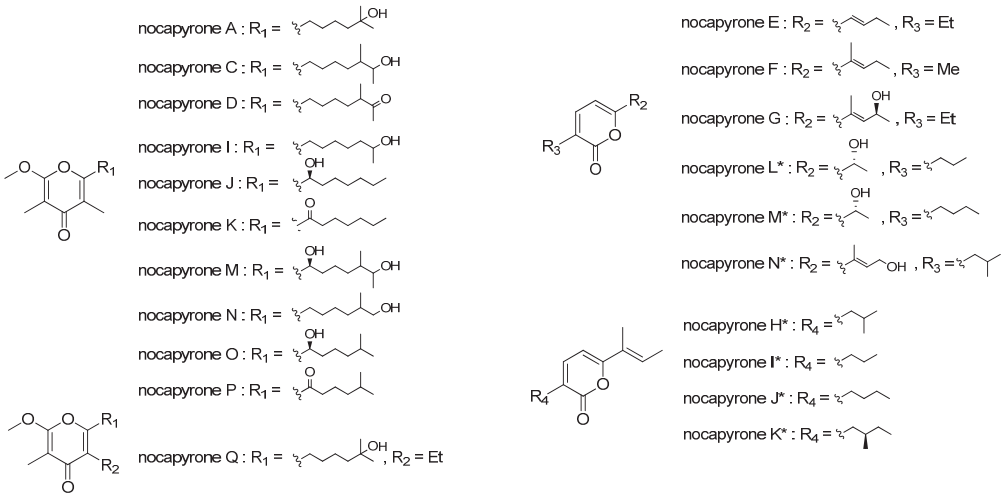

***** Overlapped nomenclatures.

The absolute configuration of *anteiso*-methyl group is known and believed to be *S* in most cases because it is derived from L-isoleucine. However, the *anteiso*-methyl branching in **4** was confirmed as a mixture of (*R*)- and (*S*)-configurations in a ratio of 2:3. Along with the advances in synthetic and analytical techniques, several enantiomeric mixtures have been discovered in natural products (Figure 9) [39–41]. Many of them are marine-derived: trichodenone A, an antitumor metabolite of *Trichoderma harzianum* isolated from marine sponge (*Halichondria okadai*), is an (*R*)- and (*S*)-enantiomeric mixture [39]; pericosines B and C, metabolites of *Periconia byssoide* isolated from sea hare *Aplysia kurodai*, bearing four chiral centers are also enantiomeric mixtures [40]. Recently, the enantiomeric mixture regarding to the *anteiso*-methyl asymmetry was found in the insect pheromone. 4,8-Dimethyldecanal, the male aggregation pheromone of the red flour beetle (*Tribolium castaneum*), consists of four diastereomers, (4*R*, 8*R*)-, (4*R*, 8*S*)-, (4*S*, 8*R*)-, and (4*S*, 8*S*)-forms in a ratio of 4:4:1:1 [41]. To the best of our knowledge, nocapyrone L (**4**) is the first microbial metabolite proved to comprise an enantiomeric pair of *R*- and *S*-configurations at the *anteiso*-methyl substituent. The *sec*-methyl group at C-10 of nocapyrones C [20] and M [21] are reported to be an *R*/*S*-mixture but these compounds have a hydroxyl group on the neighboring carbon [21]. Biosynthetic origin of their *anteiso*-methyl portion should be clarified. Further investigation, focused on the biosynthetic precursors and gene analysis with our nocapyrone H (**4**), are under way to identify the enzymatic reactions responsible for the formation of enantiomeric mixture [42].

Figure 9. Natural products existing as mixtures of enantiomers.

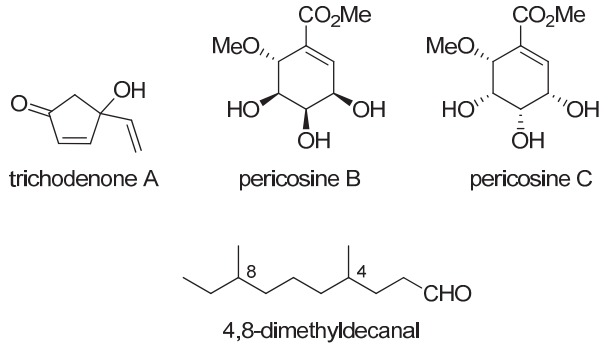

Author Contributions

Conceived and designed the experiments: Yasuhiro Igarashi. Extraction, isolation and characterization: Youngju Kim (nocapyrones R and H) and Hiromu Ogura (nocapyrones B and L). Determination of absolute configuration of nocapyrone L: Hiromu Ogura and Kazuaki Akasaka. Evaluation of biological activities: Tsutomu Oikawa and Nobuyasu Matsuura. Isolation of microorganism: Chiaki Imada and Hisato Yasuda. Wrote the manuscript: Youngju Kim and Yasuhiro Igarashi. Read and approved the final manuscript: Youngju Kim and Yasuhiro Igarashi.

Conflicts of Interest

The authors declare no conflict of interest.

References

1. Harvey, A.L. Natural products in drug discovery. *Drug Discov. Today* **2008**, *13*, 894–901.
2. Bérdy, J. Bioactive microbial metabolites. *J. Antibiot*. **2005**, *58*, 1–26.
3. Lam, K.S. Discovery of novel metabolites from marine actinomycetes. *Curr. Opin. Microbiol.* **2006**, *9*, 245–251.
4. Haefner, B. Drugs from the deep: Marine natural products as drug candidates. *Drug Discov. Today* **2003**, *8*, 536–544.
5. Candib, L.M. Obesity and diabetes in vulnerable populations: Reflection on proximal and distal causes. *Ann. Fam. Med.* **2007**, *5*, 547–556.
6. Trayhurn, P.; Wood, I.S. Signalling role of adipose tissue: Adipokines and inflammation in obesity. *Biochem. Soc. Trans.* **2005**, *33*, 1078–1081.
7. Simons, P.J.; van den Pangaart, P.S.; van Roomen, C.P.; Aerts, J.M.; Boon, L. Cytokine-mediated modulation of leptin and adiponectin secretion during *in vitro* adipogenesis: Evidence that tumor necrosis factor-alpha- and interleukin-1beta-treated human preadipocytes are potent leptin producers. *Cytokine* **2005**, *32*, 94–103.
8. Tsao, T.S.; Lodish, H.F.; Fruebis, J. ACRP30, a new hormone controlling fat and glucose metabolism. *Eur. J. Pharmacol.* **2002**, *440*, 213–221.

9. Hu, E.; Liang, P.; Spiegelman, B.M. AdipoQ is a novel adipose-specific gene dysregulated in obesity. *J. Biol. Chem.* **1996**, *271*, 10697–10703.
10. Hotta, K.; Funahashi, T.; Arita, Y.; Takahashi, M.; Matsuda, M.; Okamoto, Y.; Iwahashi, H.; Kuriyama, H.; Ouchi, N.; Maeda, K.; *et al.* Plasma concentrations of a novel, adipose-specific protein, adiponectin, in type 2 diabetic patients. *Arterioscler. Thromb. Vasc. Biol*. **2000**, *20*, 1595–1599.
11. Lihn, A.S.; Østergard, T.; Nyholm, B.; Pedersen, S.B.; Richelsen, B.; Schmitz, O. Adiponectin expression in adipose tissue is reduced in first-degree relatives of type 2 diabetic patients. *Am. J. Physiol. Endocrinol. Metab.* **2003**, *284*, 443–448.
12. Tiikkainen, M.; Häkkinen, A.M.; Korsheninnikova, E.; Nyman, T.; Mäkimattila, S.; Yki-Järvinen, H. Effects of rosiglitazone and metformin on liver fat content, hepatic insulin resistance, insulin clearance, and gene expression in adipose tissue in patients with type 2 diabetes. *Diabetes* **2004**, *53*, 2169–2176.
13. Yang, W.S.; Jeng, C.Y.; Wu, T.J.; Tanaka, S.; Funahashi, T.; Matsuzawa, Y.; Wang, J.P.; Chen, C.L.; Tai, T.Y.; Chuang, L.M. Synthetic peroxisome proliferator-activated receptor-gamma agonist, rosiglitazone, increases plasma levels of adiponectin in type 2 diabetic patients. *Diabetes Care* **2002**, *25*, 376–380.
14. Yamauchi, T.; Kamon, J.; Waki, H.; Terauchi, Y.; Kubota, N.; Hara, K.; Mori, Y.; Ide, T.; Murakami, K.; Tsuboyama-Kasaoka, N.; *et al.* The fat-derived hormone adiponectin reverses insulin resistance associated with both lipoatrophy and obesity. *Nat. Med*. **2001**, *7*, 941–946.
15. Kadowaki, T.; Yamauchi, T. Adiponectin and adiponectin receptors. *Endocr. Rev*. **2005**, *26*, 439–451.
16. Nissen, S.E.; Wolski, K. Effect of rosiglitazone on the risk of myocardial infarction and death from cardiovascular causes. *N. Engl. J. Med.* **2007**, *356*, 2457–2471.
17. Igarashi, Y.; Tanaka, Y.; Ikeda, M.; Oikawa, T.; Kitani, S.; Nihira, T.; Mongkol, P.; Janhom, M.; Panbangred, W. Prajinamide, a new modified peptide from a soil-derived *Streptomyces*. *J. Antibiot.* **2012**, *65*, 157–159.
18. Igarashi, Y.; Yu, L.; Ikeda, M.; Oikawa, T.; Kitani, S.; Nihira, T.; Bayanmunkh, B.; Panbangred, W. Jomthonic acid, a modified amino acid from a soil-derived *Streptomyces*. *J. Nat. Prod*. **2012**, *75*, 986–990.
19. Indananda, C.; Igarashi, Y.; Ikeda, M.; Oikawa, T.; Thamchaipenet, A. Linfuranone A, a new polyketide from plant-derived *Microbispora* sp. GMKU 363. *J. Antibiot*. **2013**, *66*, 675–677.
20. Schneemann, I.; Ohlendorf, B.; Zinecker, H.; Nagel, K.; Wiese, J.; Imhoff, J.F. Nocapyrones A–D, γ-pyrones from a *Nocardiopsis* strain isolated from the marine sponge *Halichondria panicea*. *J. Nat. Prod*. **2010**, *73*, 1444–1447.
21. Lin, Z.; Torres, J.P.; Ammon, M.A.; Marett, L.; Teichert, R.W.; Reilly, C.A.; Kwan, J.C.; Hughen, R.W.; Flores, M.; Tianero, M.D.; *et al.* A bacterial source for mollusk pyrone polyketides. *Chem. Biol*. **2013**, *24*, 73–81.
22. Gregory, L.C. Mining microbial genomes for new natural products and biosynthetic pathways. *Microbiology* **2008**, *154*, 1555–1569.

23. Akasaka, K.; Imizumi, K.; Ohrui, H. Enantiomeric separation of branched fatty acids having chiral centers remote from the carboxyl group by labelling with chiral fluorescent derivatization reagents. *Enantiomer* **1998**, *3*, 169–174.
24. Nunez, M.T.; Martin, V.S. Efficient oxidation of phenyl groups to carboxylic acids with ruthenium tetraoxide. A simple synthesis of (*R*)-γ-caprolactone, the pheromone of *Trogoderma granarium*. *J. Org. Chem*. **1990**, *55*, 1928–1932.
25. Ikeda, M.; Kurotobi, Y.; Namikawa, A.; Kuranuki, S.; Matsuura, N.; Sato, M.; Igarashi, Y.; Nakamura, T.; Oikawa, T. Norlichexanthone isolated from fungus P16 promotes the secretion and expression of adiponectin in cultured ST-13 adipocytes. *Med. Chem*. **2011**, *7*, 250–256.
26. Singh, M.P.; Kong, F.; Janso, J.E.; Arias, D.A.; Suarez, P.A.; Bernan, V.S.; Petersen, P.J.; Weiss, W.J.; Carter, G.; Greenstein, M. Novel α-pyrones produced by a marine *Pseudomonas* sp. F92S91: Taxonomy and biological activities. *J. Antibiot*. **2003**, *56*, 1033–1044.
27. Trisuwan, K.; Rukachaisirikul, V.; Sukpondma, Y.; Preedanon, S.; Phongpaichit, S.; Rungjindamai, N.; Sakayaroj, J. Epoxydons and a pyrone from the marine-derived fungus *Nigrospora* sp. PSU-F5. *J. Nat. Prod.* **2008**, *71*, 1323–1326.
28. Yu, K.; Ren, B.; Wei, J.; Chen, C.; Sun, J.; Song, F.; Dai, H.; Zhang, L. Verrucisidinol and Verrucosidinol Acetate, Two pyrone-type polyketides isolated from a marine derived fungus, *Penicillium aurantiogriseum*. *Mar. Drugs* **2010**, *8*, 2744–2754.
29. Carbone, M.; Ciavatta, M.L.; Wang, J.R.; Cirillo, I.; Mathieu, V.; Kiss, R.; Mollo, E.; Guo, Y.W.; Gavagnin M. Extending the record of polypropionates from marine pulmonate mollusks. *J. Nat. Prod*. **2013**, *76*, 2065–2073.
30. Fu, P.; Liu, P.; Qu, H.; Wang, Y.; Chen, D.; Wang, H.; Li, J.; Zhu, W. A-pyrones and diketopiperazine derivatives from the marine-derived actinomycete *Nocardiopsis dassonvillei* HR10–5. *J. Nat. Prod*. **2011**, *74*, 2219–2223.
31. Kim, M.C.; Kwon, O.W.; Park, J.S.; Kim, S.Y.; Kwon, H.C. Nocapyrones H–J, 3,6-disubstituted α-pyrones from the marine actinomycete *Nocardiopsis* sp. KMF-001. *Chem. Pharm. Bull*. **2013**, *61*, 511–515.
32. Fu, P.; Liu, P.; Gong, Q.; Wang, Y.; Wanga, P.; Zhu, W. α-Pyrones from the marine-derived actinomycete *Nocardiopsis dassonvillei* subsp. *dassonvillei* XG-8–1. *RSC Adv*. **2013**, *3*, 20726–20731.
33. Shimamura, H.; Sunazuka, T.; Hizoura, T.; Hirose, T.; Shiomi, K.; Omura, S. Total synthesis and biological evaluation of verticipyrone and analogues. *Org. Lett*. **2007**, *9*, 65–67.
34. Lipshutz, B.H.; Amorelli, B. Carboalumination/Ni-catalyzed couplings. A short synthesis of verticipyrone. *Tetrahedron Lett*. **2009**, *50*, 2144–2146.
35. De Paolis, M.; Rosso, H.; Henrot, M.; Prandi, C.; d'Herouville, F.; Maddaluno, J. A concise route to α′-methoxy-γ-pyrones and verticipyrone based upon the desymmetrization of α,α′-dimethoxy-γ-pyrone. *Chem. Eur. J*. **2010**, *16*, 11229−11232.
36. Rosso, H.; de Paolis, M.; Collin, V.C.; Dey, S.; Hecht, S.M.; Prandi, C.; Richard, V.; Maddaluno, J. One-pot regio- and stereoselective synthesis of α′-methoxy-γ-pyrones: Biological evaluation as mitochondrial respiratory complex inhibitors. *J. Org. Chem*. **2011**, *76*, 9429–9437.

37. Sharma, P.; Powell, K.J.; Burnley, J.; Awaad, A.S.; Moses, J.E. Total Synthesis of polypropionate-derived γ-pyrone natural products. *Synthesis* **2011**, *2011*, 2865−2892.
38. Wilk, W.; Waldmann, H.; Kaiser, M. Gamma-pyrone natural products—A privileged compound class provided by nature. *Bioorg. Med. Chem*. **2009**, *17*, 2304–2309.
39. Usami, Y.; Ikura, T.; Amagata, T.; Numata, A. First total synthesesand configurational assignments of cytotoxic trichodenones A–C. *Tetrahedron Asymmetry* **2000**, *11*, 3711–3725.
40. Usami, Y.; Okada, Y.; Yamada, T. Natural pericosines B and C as enantiomeric mixtures: direct evidence by chiral HPLC analysis. *Chirality* **2001**, *23*, E7–E11.
41. Akasaka, K.; Tamogami, S.; Beeman,R.W.; Mori, K. Pheromone synthesis. Part 245: Synthesis and chromatographic analysis of the four stereoisomers of 4,8-dimethyldecanal, the male aggregation pheromone of the red flour beetle, *Tribolium castaneum*. *Tetrahedron* **2011**, *67*, 201–209.
42. Komaki, H.; Ichikawa, N.; Hosoyama, A.; Fujita, N.; Igarashi, Y. Draft genome sequence of marine-derived actinomycete *Nocardiopsis* sp. TP-A0876, a producer of polyketide pyrones. *Genome Announc.* **2014**, in press.

Marine Sponge Derived Natural Products between 2001 and 2010: Trends and Opportunities for Discovery of Bioactives

Mohammad Ferdous Mehbub, Jie Lei, Christopher Franco and Wei Zhang

Abstract: Marine sponges belonging to the phylum Porifera (Metazoa), evolutionarily the oldest animals are the single best source of marine natural products. The present review presents a comprehensive overview of the source, taxonomy, country of origin or geographical position, chemical class, and biological activity of sponge-derived new natural products discovered between 2001 and 2010. The data has been analyzed with a view to gaining an outlook on the future trends and opportunities in the search for new compounds and their sources from marine sponges.

Reprinted from *Mar. Drugs*. Cite as: Mehbub, M.F.; Lei, J.; Franco, C.; Zhang, W. Marine Sponge Derived Natural Products between 2001 and 2010: Trends and Opportunities for Discovery of Bioactives. *Mar. Drugs* **2014**, *12*, 4539–4577.

1. Introduction

Discovery of marine derived natural products is a promising, but comparatively new field, which started with the discovery of unusual nucleoside derivatives in the sponge *Tethya crypta* in the 1950s by Bergmann and Feeney [1,2]. In the early 1960s, research on marine natural products was driven by chemical studies and few compounds were tested for any relevant bioactivity [3] such as production of a pyrrole antibiotic by a marine bacterium *Pseudomonas bromoutilis [4]*. However, utilization of marine organisms as sources of bioactive metabolites started seriously at the end of 1960s [5] with the isolation of prostaglandin derivatives from the Caribbean Gorgonian *Plexaura homomalla* [6]. In the 1980s effective collaborations were established between marine chemists and pharmacologists and the investigations were focused on central nervous system membrane active toxins, ion channel effectors, anticancer and anti-viral agents, tumor promoters and anti-inflammatory agents [7]. In the 1990s pharmaceutical and biotechnological industries focused their screens on chemical libraries of both natural products, as well as synthetic compounds produced by combinatorial methods [8]. Invertebrates, mainly sponges, tunicates, bryozoans or molluscs provided the majority of the marine natural products involved in clinical or preclinical trials [9].

The discovery of marine natural products has accelerated over the last two decades with the number of new compounds discovered annually increasing from 20 to more than 200 [10]. It has been estimated that by 2010 more than 15,000 new marine natural products (NMNP) had been discovered [11–13] with 8368 new compounds recorded for the decade between 2001 and 2010. This constitutes over half of all the compounds discovered since 1951.

Among all the marine organisms investigated, marine sponges (Porifera) are recognized as the richest sources of NMNP, with about 4851 compounds to date, contributing to nearly 30% of all marine natural products discovered so far. It should be noted that of these, 1499 new compounds were isolated in the five years from 2008 to 2012 [14–18]. This makes sponges the most prolific marine producers of compounds with more than 200 new compounds reported each year for the last

decade [19]. With this myriad of NMNP available, numerous studies have revealed a broad spectrum of biological activities for these compounds, including anticancer, antiviral, antibacterial, antifungal, antiprotozoal, anthelmintic, anti-inflammatory, immunosuppressive, neurosuppressive, neuroprotective, antifouling and a range of other bioactivities [20]. In addition, as infectious microorganisms evolve and develop resistance to existing pharmaceuticals, marine sponges provide novel leads against bacterial, fungal and viral diseases [19,21]. Figure 1a shows the almost linear growth of new compounds over the last three decades. It is predicted that if this rate can be sustained, the discovery of marine natural products from sponges, in particular, and as well as other major marine organisms will bring about new and effective therapies against human diseases [22–24].

Figure 1b shows the trends of novel marine natural products discovered from different phyla of marine organisms during 2001–2010. The annual discovery of marine natural products remained at a constant level of about 500 products in the late 1990s [10] but this number has increased from 600 to over 1000 compounds from 2008 to 2010, a significant increase which was partly driven by new developments in modern analytical technology and instruments, especially the development of the high resolution nuclear magnetic resonance spectrometer (NMR) and mass spectrometry (MS) coupled with high-performance LC and GC [10].

Although sponges have shown the highest potential for natural product discovery, no comprehensive reviews have been published that focus only on compounds from sponges in terms of their source areas, modes of action, chemical class and taxonomy. Two review papers written by Hu *et al*. 2011 and Leal *et al.* 2012 [10,25] described the overall trends in marine natural products, including those from Porifera, during the last two decades. Therefore, we prepared this manuscript based on sponge-derived new natural products from 2001 to 2010 and all the graphs and tables generated for this paper are based on the data reviewed by Blunt *et al.* from the *Natural Product Reports* of 2003–2012 [13–16,20,26–30]. Information was collected from each individual published paper during this time period and data was generated and analyzed accordingly.

Sponges are exclusively aquatic animals that dominate in many benthic habitats. They are sessile and do not have tissues or sensory organs but have different types of cells which conduct all forms of bodily function. They consume food and excrete waste products within cells without a body cavity [31].

Numerous ecological studies have shown that secondary metabolites produced by sponges often serve defensive purposes to protect them from threats such as predator attacks, microbial infections, biofouling, and overgrowth by other sessile organisms [32,33]. For this reason Porifera are attractive subjects for natural product chemists due to the sheer number of metabolites produced, the novelty of structure encountered, and the therapeutic potential of these compounds in the treatment of human diseases [7]. There is evidence that some compounds originally found in sponge cells are synthesized by microorganisms associated with sponges, since the mesohyl of sponges is often inhabited by microbes and many poriferan natural products resemble metabolites produced by marine microbes [34].

However, these natural products have interesting biomedical potential, pharmaceutical relevance and diverse biotechnological applications [5,35–39]. Moreover, sponge-derived antifouling molecules have been found to be less toxic, environmentally friendly biocides that are often very effective [40].

Figure 1. (**a**) Number of new compounds isolated from marine organisms per decade from 1970 to 2010; (**b**) Total number of new compounds isolated from different marine organisms from 2001 to 2010.

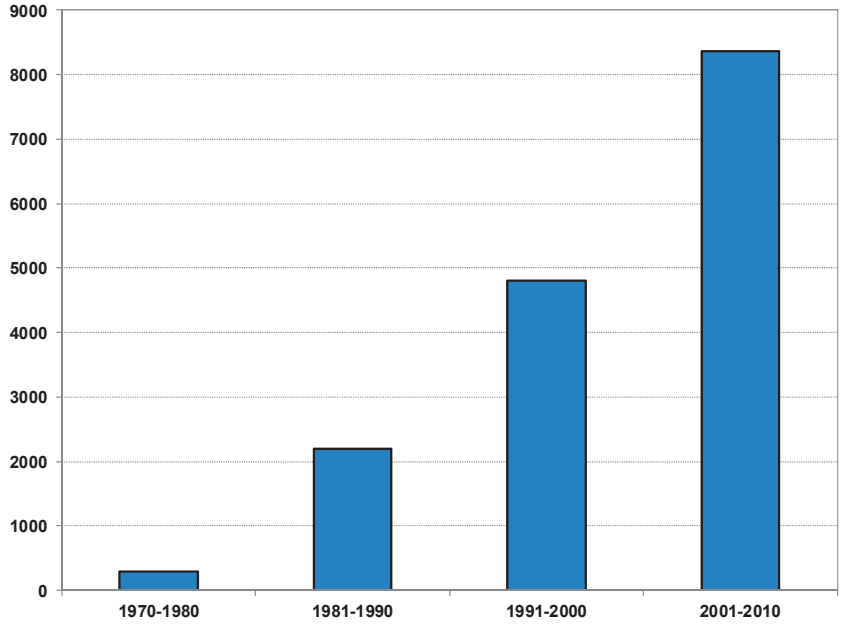

(**a**)

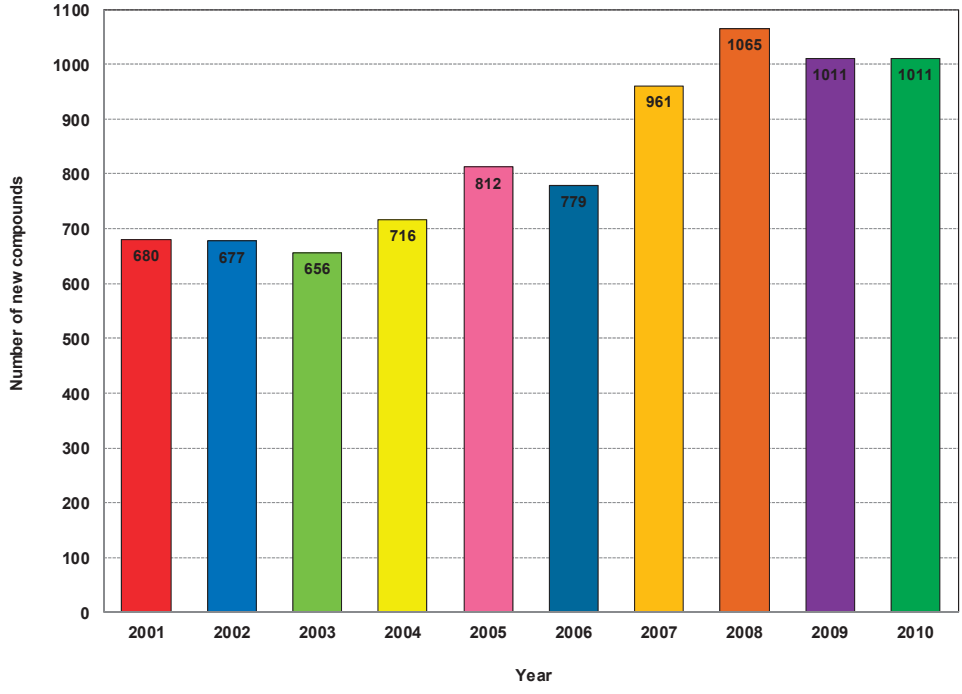

(**b**)

It is of both scientific and industrial interest as to why and how marine sponges possess such a high diversity of novel marine natural products. As the oldest metazoan, sponges have survived in the ocean for over 600 million years [41] throughout the vast changes experienced by the ocean. The fact that sponges still exist in all waters from fresh to saline, from intertidal to deep-sea, from tropical to frozen waters indicates the tremendous ability of sponges to respond and adapt to the varied environmental conditions over this period. In addition, sponges are one of the most efficient sessile filter feeders: they can filter up to 24 $m^3 \cdot kg^{-1}$ day^{-1} [42]. Bacterial numbers in sponge tissue often exceed those of the surrounding seawater by two to three orders of magnitude as the sponge mesohyl provides a unique ecological niche for particular bacterial species. In many cases, sponge mesohyl harbours the bacterial symbionts (30%–60%) [43]. Bacteria provide their hosts with products of their metabolism, thereby granting the sponge access to bacteria-specific traits such as autotrophy, nitrogen fixation and nitrification [44]. Other examples show that sponge-associated bacteria can process metabolic waste compounds, stabilize the sponge skeleton and provide protection against UV radiation [35,45,46]. The most prominent example of sponge bacterial symbiosis, however, is the involvement of bacteria in the production of bioactive metabolites [47] that have a role in defense [48].

These highly intensive, constant interactions with the environment have given sponges a unique biochemistry to produce the high diversity of metabolites that can either help them survive or prompt them to evolve. Being attached to a solid surface, a sponge is unable to escape when confronted with a predator, and so, when threatened they release stored secondary metabolites that have cytotoxic, antibiotic and feeding deterrent properties [48]. Some chemicals prevent settlement of fouling organisms on the sponge surface and restrict competition for space with neighbors. The sponge bacterial associations and interactions have been widely studied, with evidence that the sponge-associated bacteria can help the sponges to produce secondary metabolites to protect them against their predators [49]. In an ecological context, sponges have developed special mechanisms to protect themselves from pathogenic bacteria, viruses, parasites, fungus and other predators that include both chemical defense mechanisms and physiological responses. Chemical defense mechanisms help to protect sponges against certain deleterious bacteria [33,50,51]. In this way, *sponges* provide novel leads against *viral*, *fungal* and parasitic diseases [52]. By producing different types of toxins or malevolent tastes and odors, sponges protect themselves against predators or inhibit coral overgrowth that could threaten the sponge osculum or other systems. As a physical defense they have spicules and collagen. Sponges may also succumb to microbial and fungal infections which could result in the disintegration of the sponge fibers/tissue and ultimately lead to sponge death [53]. The fact that sponges are susceptible to microbial infection suggests that they should also possess mechanisms to prevent these types of diseases [54]. Maldonado and co-workers [55] showed how sponges recover from a bacterial infection: their ultrastructural study revealed that the sponges secrete successive collagen barriers at the diseased area and abandon decaying body parts external to the barrier.

Recently, the ubiquitous defense enzyme, phospholipase A2 (PLA2) detected in a sponge associated bacterium envisaged the possible functional role in the ecological succession of the host sponge against predatory/fouling pressure in the habitat [56]. In response to predators and pathogens, sponges have engineered complex secondary metabolites from a diverse set of biological precursors.

Secondary metabolites are organic compounds that are not directly involved in the normal growth, development or reproduction of organisms. These metabolites produced by sponges and their associated microflora can be classified chemically as alkaloids, terpenoids, glycosides, phenols, phenazines, polyketides, fatty acid products and peptides, amino acid analogues, nucleosides, porphyrins, aliphatic cyclic peroxides and sterols [57,58]. Many of these compounds are very potent because the diluting effect of the ocean drives the construction of molecules that are highly active and stable in saline conditions [59].

Given the significance of sponges in marine natural product discovery, the aim of this review is to present a comprehensive overview of sponge-derived natural product discovery during the recent decade from 2001 to 2010, in order to understand the defining trends and provide insights into avenues for further compound discovery. The temporal trends of the discovery of sponge-derived marine natural products and their biological activities, the sources of discovery in terms of sponge taxonomy, the chemical classes of these natural products, and the countries of collection have been categorized. Our analysis also includes a short description of the relative distribution and contribution of these discoveries with reference to governmental funding, policies and known national priorities given to marine natural products. Finally, the opportunities and challenges have been identified for future R and D in this fast growing field.

The new compounds isolated during the last decade were classified into 18 chemical classes including acid, alkaloid, ester, fatty acid, glycoside, ketone, lipid, macrolide, alcohol, peptide, peroxide, polyketide, quinone, steroid, sterol, terpene, terpenoid and unclassified, based on the data reviewed by Blunt *et al.* from *Natural Product Reports* of 2003 to 2012 [13–16,20,26–30]. The World Porifera Database [60] was used for the taxonomic classification of the sponges mentioned in the Natural Product Reports [13–16,20,26–30]. The World Register of Marine Species (WoRMS) database [60] was also used to cross check detailed taxonomical information (order and family) for each surveyed species and to validate and/or update their scientific names [61].

During the recent decade the sponges collected were from 19 known orders as well as 12 sponges of unknown identity which provided new compounds. These included Agelasida, Astrophorida, Axinellida, Chondrosida, Choristida, Clathrinida, Dendroceratida, Dictyoceratida, Hadromerida, Halichondrida, Haplosclerida, Homosclerophorida, Leucosolenida, Lithistida, Lyssacinosida, Ocilosclerida, Poecilosclerida, Spirophorida and Verongida. Sixty two countries (with Antarctica labeled as a country for reporting purposes) were the sources for the sponge samples studied. The bioactivities were mainly classified as anti-Alzheimer's, antibacterial, antituberculosis, anticancer, antifungal, anti-inflammatory, antimalarial, antiviral and anti-HIV.

2. New Compounds and Their Distribution 2001–2010

2.1. Yearly Distribution of Phyla that Produce Natural Products Discovered from 2001 to 2010

To investigate the distribution of sources of NMNP, 12 different categories including a separate group comprising marine microorganisms and phytoplankton were used for this review (Figure 2). Invertebrates comprise approximately 60% of all marine animal diversity [62]. Most belong to the phyla Porifera (sponges), Annelida, Arthropoda, Bryozoa, Cnidaria, Echinodermata, Mollusca and

Chordata. Several studies addressing marine invertebrates also include these groups of organisms [32,33,63].

Figure 2. Total number of new compounds isolated from different types of marine sources, 2001–2010.

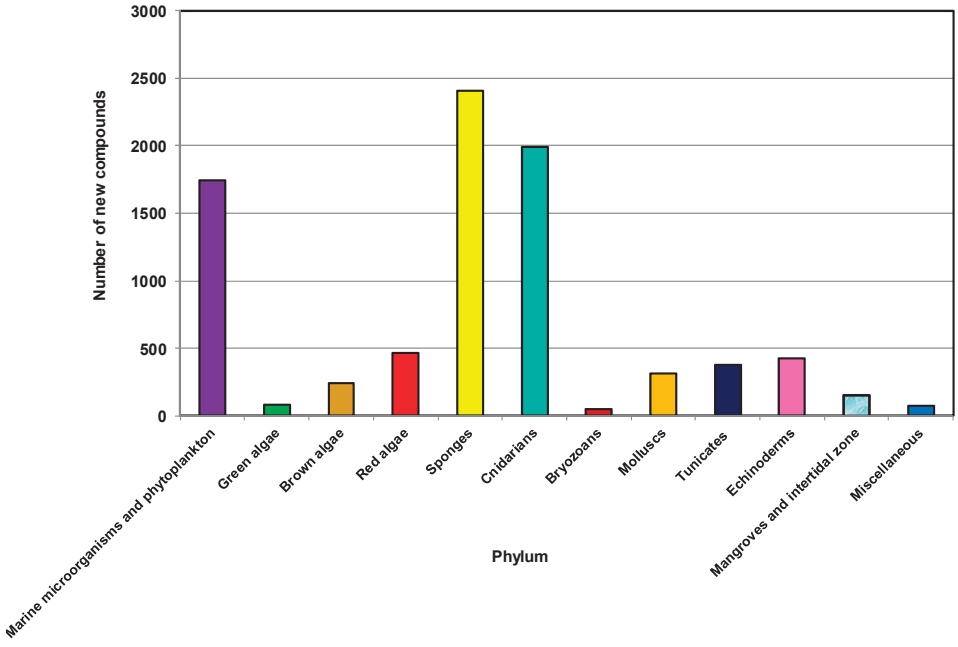

As highlighted in other reviews [10,64], the phyla Porifera and Cnidaria have been the two main sources of NMNP. During the last 10 years from 2001 to 2010, more than 2400 new natural products have been discovered from 542 genera and 671 species of sponges. These sponges belong to 19 known orders and 74 families, contributing about 29% of the marine natural products discovered during this decade, making it the largest source among all marine organisms [48,65].

2.2. Sponges (Porifera) as a Source of New Natural Products and Drugs for the Future

A review in 2003 collected the most important marine natural compounds which were undergoing preclinical and clinical trials (I, II, III) for anticancer activity. Among those, compounds from sponges were the following: Discodermolide, Hemiasterlins A & B, modified Halichondrin B, KRN-7000, Alipkinidine (alkaloid), Fascaphysins (alkaloid), Isohomohalichondrin B, Halichondrin B, Laulimalide/Fijianolide, 5-Methoxyamphimedine (alkaloid) and Variolin (alkaloid) [66]. A review paper was published by Sipkema *et al.* 2004 about the drugs from marine sponges [67].

Marine natural sources as potential anticancer agents were reviewed in 2011 which mentioned 39 marine-derived potential anticancer agents and among them 18 compounds from sponges with different mechanisms of action [68]. Interestingly, from the 16 marine natural products that are currently under preclinical trials as new drug candidates, most are derived from invertebrates. Of

these, Porifera remain the most important phylum, with six of the 16 compounds [69–71]. A review paper published in 2013 classified anticancer molecules according to their current status in the clinical phase trials (approved/phase IV/phase III/phase II/phase I) and updated the data to April 2012 [72]. A very recent review, published in 2014, showed the compounds derived from marine sources currently in clinical trials against cancer with more updated information on clinical and late preclinical developments [73]. This paper also mentioned that although many compounds showed potential against cancer and entered clinical trials in cancer, to date, only Cytarabine, Yondelis® (ET743), Eribulin (a synthetic derivative based on the structure of Halichondrin B), and the Dolastatin 10 derivative, monomethylauristatin E (MMAE or vedotin) as a warhead, have been approved for use in humans (Adcetris®) [73].

Although a number of compounds from sponges showed promising activity to be potential drug candidates over the last few decades they are generally not ready for further development due to the challenge of obtaining continuous and larger supplies of the compounds, unless they can be chemically synthesized. Considerable quantities of a drug candidate are vital for clinical trials, but only a few milligrams of most natural products can be isolated from marine samples [74]. One solution is farming sponges to source bioactive metabolites [75]. On the other hand, sponge compounds that are produced by sponge-associated microorganisms can be scaled up as the microorganisms are able to flourish independently of the sponge. Another way to ensure supply is using sponge cell culture, although this is still a growing area. Muller *et al.* in 2000 described the production of bioactive compounds by sponge cell culture [76] and Zhang *et al.* in 2003 and Cao *et al.* in 2007 showed improved cell proliferation and spiculogenesis from primmorphs of sponges and dynamics of spicule production in *in vitro* sponge cell culture systems [77]. The sustainable production of bioactive compounds from sponges was reviewed in 2004 [78] and again in 2009 where the advantage and disadvantage of sponge cell culture was discussed, with the conclusion that the understanding of the metabolic pathways is one of the potential advantages of sponge cell culture systems [79]. However, the most promising solution was answered by Wilson *et al.* in 2014; his findings illuminated two promising approaches for addressing the supply problem [80]: firstly, large-scale cultivation of the microorganisms that produce interesting metabolites, and secondly, expressing the biosynthetic pathway of interest in an easily cultivable surrogate host. The discovery of Wilson and Piel and their colleagues identified *Entotheonella* and members of the newly proposed phylum Tectomicrobia as a "biochemically talented" phylum on a par with the actinomycetes [80–82]. Thus, these results could facilitate a new era of drug discovery.

2.3. The Distribution of New Marine Natural Products from Sponges

To date, about 11,000 species of sponges have been formally described of which approximately 8500 are considered valid, but as many as twice those numbers are thought to exist [83]. Well known sponge fauna in the Caribbean, Mediterranean, and the British Isles each contain 500–800 species, whereas less well characterized sponge fauna in Australia, Papua New Guinea and Indonesia possess a high biodiversity [84]. Sponges are currently divided into four distinct classes, 25 orders, 128 families and 680 genera [59,60].

The sponges reported to produce new compounds in the last ten years were from 19 known orders although a number of sponges were not identified. A careful analysis of the trends of the discovery of new bioactive compounds from different orders of sponges is presented here to guide scientists in future discoveries.

As shown in Figure 3a, 504, 355, 337, 274 and 201 new compounds were found from the five orders Dictyoceratida, Haplosclerida, Poecilosclerida, Halichondrida and Astrophorida, respectively. Notably, these five orders contributed more than 70% of the new compounds. The highest numbers of new compounds were found from Dictyoceratida with 72 found in 2008, 66 in 2004, 63 in 2009, 58 in 2001 and 51 in 2005.

Table 1 shows that some orders have been found to be productive sources of NMNP, many with a large chemical diversity. Astrophorida, Dictyoceratida, Halichondrida, Haplosclerida and Poecilosclerida are the orders from which more than 50 species were studied [83].

Dictyoceratida contributed at least 16% of new compounds each year except in 2010 (11.9%), reaching a peak of 28.5% in 2005 (Figure 3b). Haplosclerida contributed at least 13.58% of new compounds each year except 2004 and 2008 with values of 9.4% and 7.7% respectively. This order yielded the highest number of compounds in 2001 at 24.6%. In the case of Poecilosclerida, a gradual increase was observed until 2004 and reached a peak in 2009 at 22.1%. From 2004 to 2008 Halichondrida contributed at least 11.4% new compounds each year.

This corresponds with a recent review on clinically active compounds from sponges which had Astrophorida, Chondrosida, Dendroceratida, Dictyoceratida, Hadromerida, Halichondrida, Haplosclerida, Lithistida, Poecilosclerida, Spirophorida and Verongida as the main orders from which clinically active compounds were found [85]. Leal *et al.* 2012, covering 1990–2009, found that NMNP were recorded in 17 orders of Demospongiae, and about 89% of the natural products were derived from only eight of those orders, namely Astrophorida, Dictyoceratida, Halichondrida, Haplosclerida, Homosclerophorida, Lithistida, Poecilosclerida and Verongida [25].

All NMNP discovered since 1990 were recorded in 64 families belonging to the phylum Porifera. However, about 51% of these products were derived from only nine families: Spongiidae, Dysideidae and Thorectidae in the order Dictyoceratida; Chalinidae and Petrosiidae in the order Haplosclerida; Halichondriidae in the order Halichondrida; Ancorinidae belonging to the order Astrophorida; Plakinidae belonging to the order Homosclerophorida and Theonellidae of the order Lithistida. Here, the highest increase in the number of NMNP annually discovered was recorded for the families Chalinidae and Spongiidae. The family Theonellidae has yielded a number of unique compounds [86] with a broad spectrum of biological activities, including antifungal [87] and cancer cell growth inhibitors [88,89].

Figure 4 shows that between 9 and 16 genera were found to produce new molecules each year from the order Dictyoceratida which revealed a high availability of different genera from this particular order, with the highest number found in 2009. This order will be examined in greater detail in a subsequent review covering 2001–2010. Genera belonging to the orders Haplosclerida, Halichondrida, Poecilosclerida, and Astrophorida also showed more than five productive genera for most of the last decade. The number of new compounds correlated with the high diversity of sponges because the higher the diversity the higher the possibility of getting more novel compounds. Another

possible reason that makes Dictyoceratida the most prolific producers of NMNP as well as Astrophorida, Haplosclerida, Homosclerophorida and Halichondrida is because these orders harbor high densities of microorganisms [25,85].

Figure 3. (**a**) Total number of new compounds isolated from different orders of marine sponges 2001–2010; (**b**) Distribution of new compounds isolated from different orders of marine sponges as a percentage found within the year, 2001–2010.

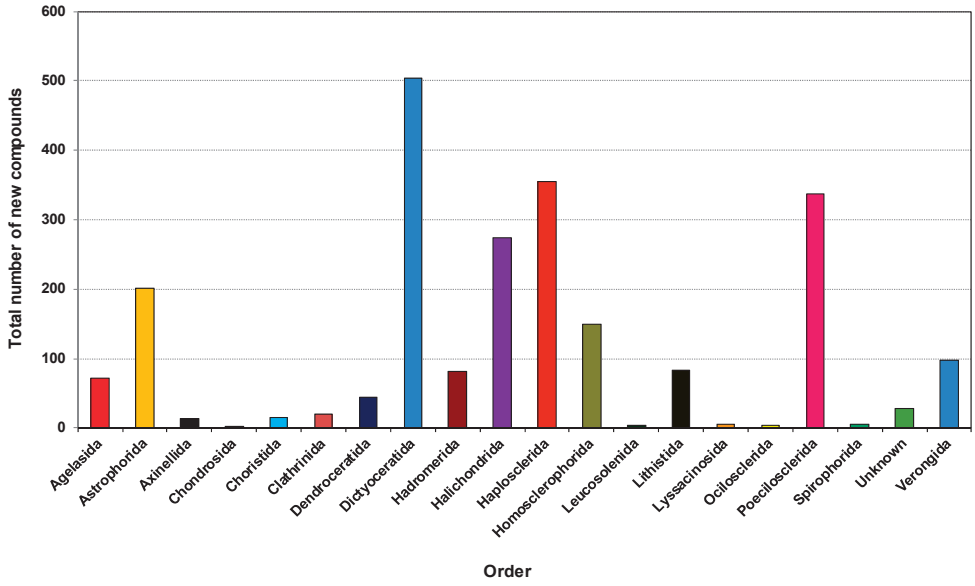

(**a**)

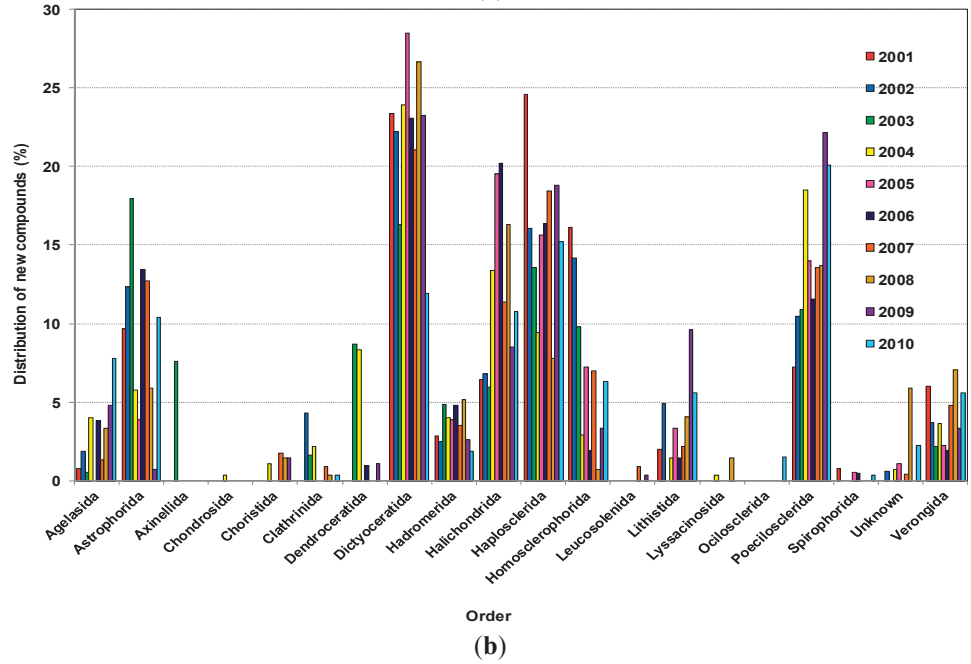

(**b**)

Table 1. Total number of new compounds isolated from different orders of marine sponges with number of families, genera, species and number of references published from 2001 to 2010.

Order	Number of Families	Number of Genera	Number of Species	Number of References
Agelasida	9	9	21	24
Astrophorida	26	58	63	62
Axinellida	2	2	2	2
Chondrosida	1	1	1	1
Choristida	3	3	3	3
Clathrinida	5	5	7	7
Dendroceratida	7	10	11	13
Dictyoceratida	40	117	145	161
Hadromerida	24	31	32	33
Halichondrida	31	69	86	84
Haplosclerida	52	80	100	120
Homosclerophorida	10	20	39	50
Leucosolenida	1	1	1	1
Lithistida	14	20	23	32
Lyssacinosida	2	2	2	2
Ocilosclerida	1	1	1	2
Poecilosclerida	67	68	81	83
Spirophorida	4	4	4	5
Unknown	8	12	12	10
Verongida	27	29	37	46
Total	334	542	671	741

Figure 4. Number of different types of genera used for isolation of new compounds from different orders of marine sponges from 2001 to 2010.

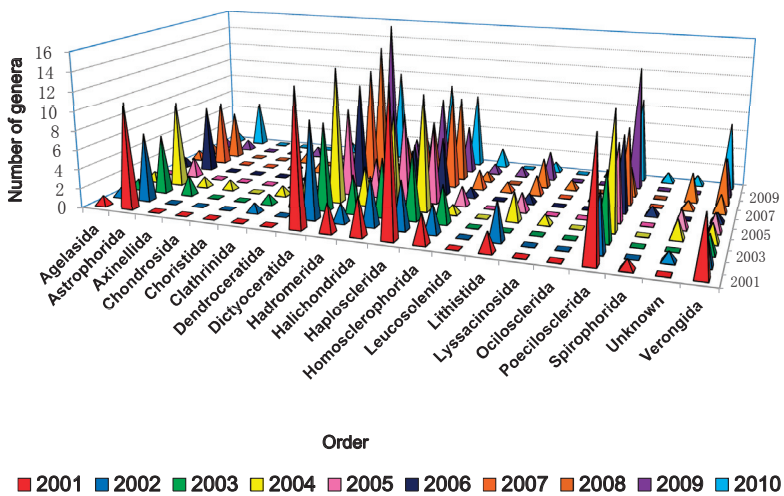

2.4. Distribution of New Compounds per Species from Different Orders

During the last decade each individual species from different sponges contributed on an average four new compounds under different orders (Figure S1, Supplementary Information). Although very few species have been studied from the orders Axinellida and Choristida, on an average they also produce almost the same number of compounds. This finding permits the inference that each individual species has the potential for contributing similar numbers of new compounds regardless of the order.

2.5. Symbiotic Relationships: Sponge Associated Microorganisms

Hentchel *et al.* 2002 reported that although it is generally believed that symbiotic interactions exist between sponges and specific microorganisms, consideration of alternative explanations such as the selective enrichment of ubiquitous seawater bacteria is also important [42]. Moreover, they stated that very specific type of selective pressures, perhaps the hostility to digestion, must exist to establish the uniform composition arrangements of the microbial communities existing in sponges that have otherwise few commonalities [42].

However, it was consequently observed that marine sponges host abundant and diverse communities of symbiotic microorganisms [90]. Webster *et al.* 2012 mentioned that microbial symbionts are undoubtedly important to sponge health, and therefore it is likely that interruptions to symbiosis as a result of climate change/environmental stress will influence sponge health, growth rates or their ability to defend themselves from predation, fouling and disease [91]. Symbiotic interactions between sponges and microorganisms could contribute to sponge nutrition as well [92]. Important roles of the symbionts include photosynthetic carbon fixation [93], nitrification [94,95], nitrogen fixation [44,96,97], and anaerobic metabolism [98]. Another important role of sponge-associated bacteria is the production of potential secondary metabolites, such as antibiotics, antifungal compounds and anti-predation or antifouling compounds [39]. Whilst the microbes associated with the sponges produce the secondary metabolites, possibly all of these sponges have particular microbial associations [99]. More research is necessary to explore the relationship between microorganisms and phytoplankton associated with sponges because it has been suggested that (at least) some of the bioactive secondary metabolites isolated from sponges are produced by functional enzyme clusters which originated from these microorganisms. The role of these microorganisms in sponge biology varies from source of nutrition to mutualistic symbiosis with the sponge [100].

It has been recognized that metabolites synthesized by marine microorganisms associated with sponges could become a major source for the discovery of new drugs, not only because the biological diversity in marine ecosystems like coral reefs or deep sea floors is probably higher than in the rainforest, but because marine microorganisms offer a renewable resource for the scale-up and development of potentially new drugs [101,102].

A number of examples of the functions of the sponge-associated microorganisms are provided to signify the diversity of functions. Dudler and Eberl 2006 conducted a study on interactions between bacteria and eukaryotes which showed increasing evidence to support the hypothesis that secondary metabolites produced by symbiotic bacteria are a result of bacterial cell-to-cell signaling [103].

In a similar vein, Schmidt *et al.* 2008 looked at how organisms cooperate in the synthesis of natural products. They found that partners may exchange and modify the natural products produced by each other and also explained how these secondary metabolites are utilized by the host organisms [104].

Many sponge-derived metabolites resemble bacterial natural products or belong to substance classes typical for these microorganisms [82]. In a recent paper, the Piel group demonstrated beyond doubt that almost all bioactive polyketides and peptides known from the marine sponge *Theonella swinhoei* were attributed to a single phylotype, *Entotheonella* spp. and are extensively distributed in sponges [80].

The diversity in the locations (Okinawa, the Philippines, Indonesia, the Red Sea, Italy, South Africa, and Papua New Guinea) and genera of sponges (*Amphimedon* sp. and *Acanthostrongylophora*) responsible for the production of manzamine alkaloids are widely believed to be a result of a symbiotic relationship between these sponges with common or closely related microorganism(s), which may account for the generation of manzamine enantiomers [105].

Crambe crambe (Schmidt, 1862) (Poecilosclerida) is a red incrusting marine sponge present in the Mediterranean Sea and reported to produce diverse PGAs, namely crambescidins 800, 816, 830, 844, as well as isocrambescidin [106,107]. Using 16S rRNA gene pyrosequencing it has been found that the associated bacterial community of *C. crambe* is dominated by a single bacterial species affiliated to the Betaproteobacteria [108].

2.6. The Distribution of Chemical Classes

Although acid, ester, ketone, peroxide do not directly fall into chemical classes, we considered these as chemical classes just to show the distribution as such described in the original paper as well as mentioned by Blunt *et al.* [13–16,20,26–30] in their annual review of marine natural products that were used in preparing this manuscript. In fact, classes of natural products should be classified based on their biosynthesis. However, it is important to remember that a macrolide is often a polyketide and a sterol a steroid and fatty acid belongs to lipid.

A wide range of chemical and functional diversity has been observed among new compounds during the last decade. The analyzed data (Figure 5a) has shown that in the last ten years 450, 331, 188 and 155 new compounds were classified as alkaloids, terpenes, terpenoids and peptides, respectively, and these four classes make up approximately 50% of compounds discovered. While alkaloids contributed 20% of the new molecules the terpene/terpenoid classification which are often not readily distinguishable, together made up 23% of the total within the decade.

The chemical diversity of bioactive compounds reportedly produced by sponge-microbe associations showed that certain chemical classes such as quinones, steroids, fatty acids, diketopiperazines, alkaloids, terpenes, terpenoids, trichoverroids and prodigiosin derivatives, diglucosyl-glycerol, polyketides, cyclopeptides, glycoglycerolipid, benzoic acid derivatives are responsible for anticancer or antitumor activity; quinolone derivatives for anti HIV activity; fatty acid esters and fatty acids for anti-inflammatory activity; alkaloids and quinolone derivatives for antimalarial activity; polyketides glycopeptides, α-pyrone derivatives, peptides, proteins, antimycin, lipopeptides, polybrominated biphenyl ether, cyclic depsipetide, terpenes, pentaketides, furan carboxylic acid, alkaloid, diketopiperazine, anthraquinone, chromones, steroid, lactone, quinolone derivative, trisindole derivative, macrolactam,

ethers, phenol derivative for antimicrobial activity; and dihydropyridine for neuroprotective activity [85]. In this review it was also evident that anticancer, antimicrobial, anti-HIV, antiflammatory, antimalarial, and neuroprotective disease and antituberculosis were the main classes activity exhibited by most of the new compounds during the recent decade. Terpenoid quinones and hydroquinones, the chemical classes found mainly from Dictyoceratid sponges [11,12,20], have been continuously reviewed and updated. Sesquiterpenoid quinones and hydroquinones showed versatile activities and even a hydro-quinone displays multiple activities [109].

Figure 5. (**a**) Chemical classes of new compounds isolated from marine sponges from 2001 to 2010; (**b**) The distribution of different chemical classes of new compounds isolated from marine sponges from 2001 to 2010.

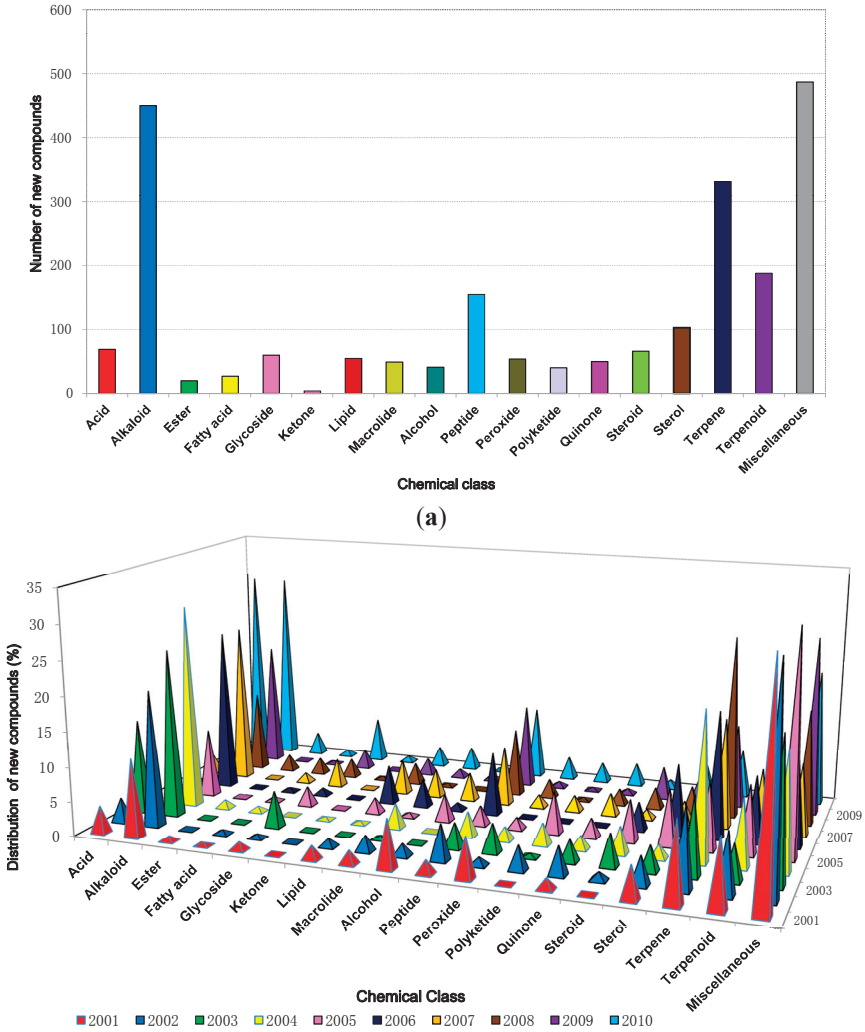

The reason that most sponges produce alkaloids could be for protection from predators such as fish as alkaloids act as good toxicants against predators. Assman *et al*. 2000 presented data suggesting that bromopyrrole alkaloids fulfill multiple ecological functions in the defense mechanisms of the common and diverse genus *Agelas* [110]. A striking example of the significance of marine alkaloids for chemical defense against fish is provided by the red coloured sponge *Latrunculia magnificea* (order Poecilosclerida) from the Red Sea. Even though *L. magnificea* growth is exposed, it is apparently avoided by fish, whereas other sponges from the same habitat that are cryptic are readily consumed by fish when artificially exposed [111].

Further information on the different classes of secondary metabolites of marine sponges and their bioactivities are the subject of previous reviews [14,93,112,113].

2.7. The Distribution of Bioactive Compounds

Table 2 shows that during the decade until 2010, 332, 229, 227, 173 and 149 new bioactive compounds were found from Dictyoceratida, Haplosclerida, Poecilosclerida, Halichondrida and Astrophorida, respectively, the highest number of new bioactive compounds isolated from different orders of sponges in this period. Dictyoceratida alone contributed 20.6% of all bioactives, Haplosclerida and Poecilosclerida both contributed 14%, whereas Halichondrida and Astrophorida contributed 10.8% and 9.3% respectively. The detail of yearly distribution is presented in Figure 6. Therefore, these five orders contributed 69% of bioactive compounds among all the different orders of sponges.

In sponges the role of the chemical constituents is clouded by the complexity of the sponge-symbiont relationship [114]. The current body of evidence is too limited to make broad generalizations, but it suggests complex chemical and biological interactions that have not yet been resolved [115]. This knowledge will feed into strategies to relieve a major bottleneck for sponge metabolite production, namely: understanding metabolites production in the sponge [79].

Table 2. Total number of new compounds isolated from different orders of marine sponges with different bioactivities from 2001 to 2010.

Orders of Sponges	Anti-Alzheimer's	Antibacterial	Antituberculosis	Anticancer/ Cytotoxicity	Antifungal	Anti-inflammatory	Antimalarial	Anti-HIV	Antiviral	Miscellaneous	Total
Agelasida	0	17	0	11	6	0	6	0	0	14	54
Astrophorida	0	8	6	97	7	0	1	5	3	22	149
Axinellida	0	0	0	0	0	0	0	0	0	8	8
Chondrosida	0	0	0	3	3	0	0	0	0	0	6
Choristida	0	0	0	12	0	0	0	0	0	12	24
Clathrinida	0	4	3	3	2	0	0	0	0	0	12
Dendroceratida	0	4	0	14	3	3	0	0	0	14	38
Dictyoceratida	0	38	3	182	11	2	1	5	0	90	332
Hadromerida	0	2	3	45	1	0	0	5	0	18	74
Halichondrida	1	18	4	99	16	1	2	1	0	31	173
Haplosclerida	8	15	2	100	20	0	7	4	0	73	229
Homosclerophorida	0	2	3	55	10	0	9	1	0	34	114
Leucosolenida	0	1	0	2	0	0	0	0	0	0	3
Lithistida	0	5	2	38	9	2	0	16	0	16	88
Lyssacinosida	0	0	0	1	0	0	0	0	0	0	1
Ocilosclerida	0	0	0	0	0	0	0	0	0	0	0
Poecilosclerida	0	17	5	143	21	1	1	4	1	34	227
Spirophorida	0	0	0	4	0	0	0	0	0	0	4
Unknown	0	0	0	2	0	0	0	0	0	7	9
Verongida	0	14	0	17	5	0	0	0	0	34	70
Total	9	145	31	828	114	9	27	41	4	407	1615

The origin and role of a number of compounds such as bioactive peptides within the sponges have yet to be clarified, as many of these compounds have potent activities not always clearly related to their *in situ* role [116]. However, it was subsequently found that antimicrobial peptides (AMPs) are components of innate immunity, forming the first-line of defense used by any organisms against the invading pathogens [117]. Pasupuleti *et al.* 2012 termed AMPs as the key component of the innate immune system [118]. Two good examples of AMPs produced by Porifera are Stylisin and Discodermin A [119,120], although many AMPs have been produced since the first production of Discodermin from sponges [121]. In 2013 a review paper was published on antimicrobial peptides with versatile biological activities which included a few sponges producing AMPs [122].

There is a sign that the quick evolution of molecules related to cell adhesion and pathogen killing (AMP precursors) has been acute in the successful alteration of sponges [123]. In their 2010 review Otero-González *et al.* discussed the new frontier for microbial infection control by antimicrobial peptides including Porifera [121]. A review published by Brogden *et al.* 2005 commented that translocated peptides can modify cytoplasmic membrane septum creation, hinder cell-wall synthesis, constrain nucleic-acid synthesis, inhibit protein synthesis, or obstruct enzymatic activity [124].

Figure 6. Distribution of bioactive compounds isolated from various marine sponge orders 2001–2010.

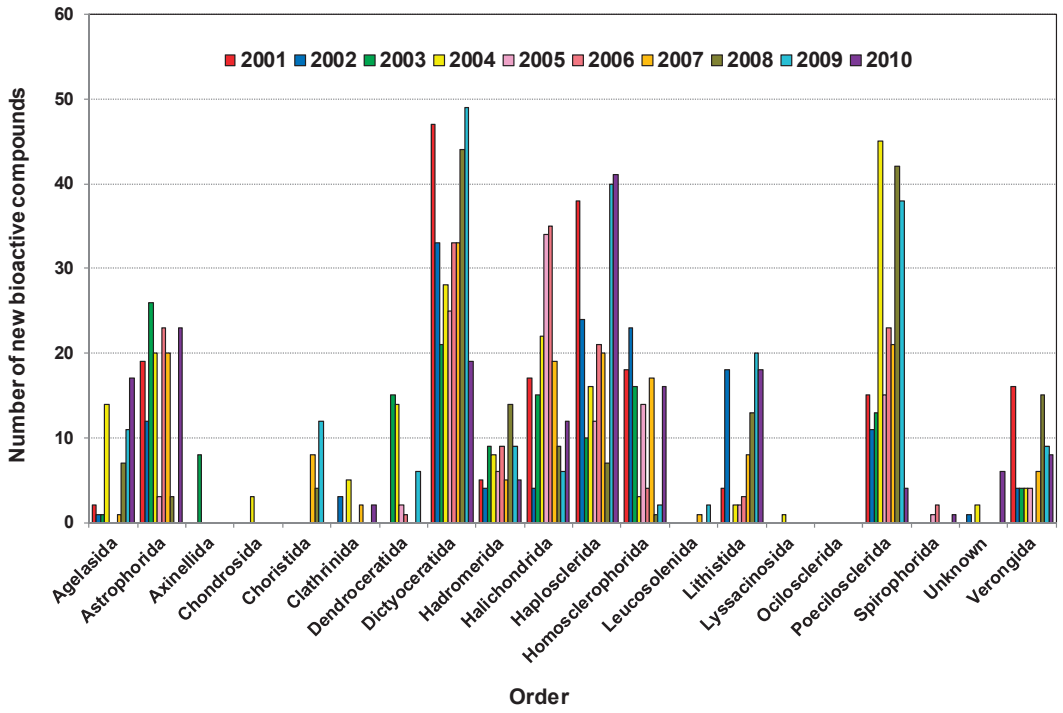

Some external activities of these peptides are as antitumorals, antivirals, immunosuppressive and antimicrobial agents, as well as neurotoxins, hepatotoxin, and cardiac stimulants. The various functional roles of some terpenoids are considered as hormones (gibberellins), photosynthetic

pigments (phytol, carotenoids), electron carriers (ubiquinone, plastoquinone), and mediators of polysaccharide assembly, as well as communication and defense mechanisms [125]. Terpenes may also act as safeguard for a variety of organisms in the marine world, including algae, sponges, corals, mollusks and fish [33].

It is important to note that most of the orders showed cytotoxicity or anticancer activity although only a few have been tested for *in vivo* antitumor activity. In the five year period from 1986 to 1991, more than 400 novel marine natural products with cytotoxic activity were reported in the literature [126] with the majority of compounds only tested for cytotoxicity in cell culture assays. Although cytotoxic activity is regarded as the first indicator in identifying anticancer drugs [127], we have considered these compounds to be cytotoxic unless further experimentation indicates their potential role as an anticancer drug. Increasing evidence has shown that cell death can be induced via three different mechanisms: apoptosis, autophagy and oncosis [128]. Most of these sponge-derived novel compounds have been screened for cytotoxic activity but not for apoptosis [129–131], although analysis should focus on a number of cancer relevant targets associated with the cell cycle, signal transduction, angiogenesis or apoptosis [132–135]. A recent overview (2011) retrieved scientific papers identifying 39 compounds from marine sponges with apoptosis-inducing anticancer properties [136]. In another example that distinguishes cytotoxicity from antitumor activity, a recent study used a novel *in vitro* assay to screen 2036 extracts from 683 individual sponges that led to the identification of bioactive compounds (which were prepared in pure form and in sufficient quantities) that could treat solid tumors [137].

Figure 7a,b show that the number of compounds with reported inhibition of cancer cell lines (or cytotoxicity) was highest with the number of 825, antibacterial activity at 145, and antifungal and anti-HIV activities at 111 and 41, respectively. Thus, cytotoxicity or anticancer activity contributed at least half of the reported activity. Progress towards marine anticancer drugs dominates, with the prime source phylum being sponges, followed by microorganisms, tunicates and mollusks [22]. Antiviral and anti-HIV activities have been observed from samples of Astrophorida*,* Lithistida and Poecilosclerida. The most promising antiviral substances from sponges appear to be 4-methylaaptamine, manzamines [19], besides Papuamides C and D [138], haplosamates A and B [139] and avarol [140] which are examples of HIV-inhibiting compounds from different sponges.

In a recent overview of 132 natural products from marine sources obtained during the period 2002–2011, which exhibited anti-HIV activity, it was reported that sponges contributed more than half of all anti-HIV natural products from marine organisms. These were mainly alkaloids and cyclic depsipeptides [141], such as Cortistatin A (CA), a recently discovered natural steroidal alkaloid isolated from the marine sponge *Corticium simplex* [142]. It has been reported to display anti-proliferative properties towards human umbilical vein endothelial cells (HUVECs) with an average half-maximal inhibitory concentration (IC_{50}) of 0.35 μM [142,143]. A recent study showed that Cortistatin A potently suppresses Tat-dependent HIV transcription [144]. Further reading on the structural characteristics of sponge derived cyclodepsipeptides can be found in a recent review [145]. It is important to note that Halichondrida and Haplosclerida are the only orders from which anti-Alzheimer's activity was reported during the last decade.

There have been many interesting compounds with unusual structures with potential activity which have been observed during the last decade. Some of the compounds are illustrated in Table 3.

Figure 7. (**a**) Total number of new compounds isolated from different marine sponges with various bioactivities from 2001 to 2010; (**b**) The distribution of new compounds isolated from different orders of marine sponges with various bioactivities from 2001 to 2010.

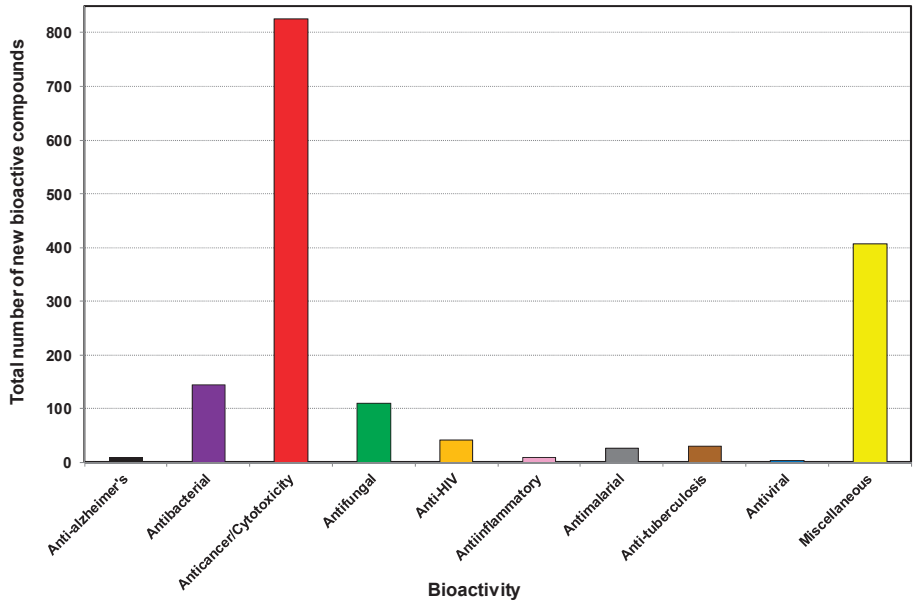

(**a**)

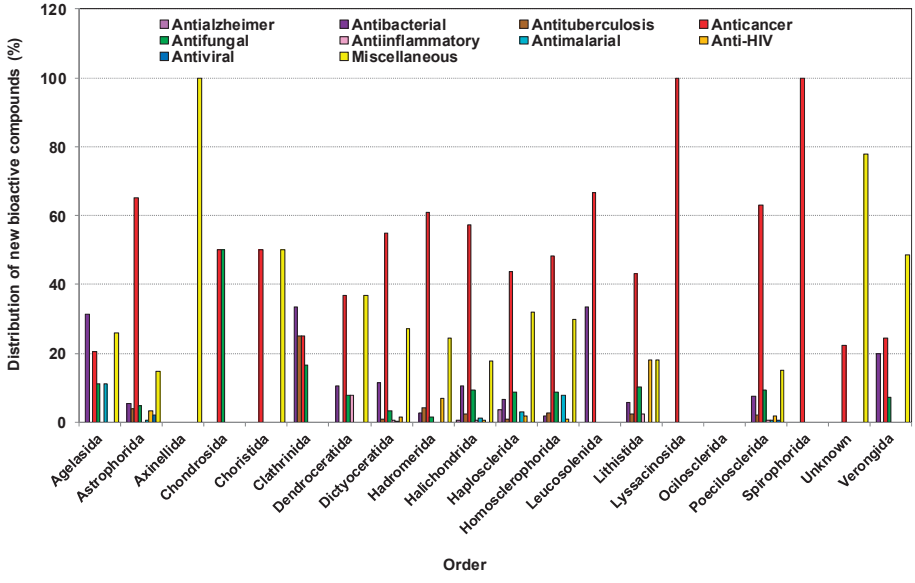

(**b**)

Table 3. Selected compounds with unusual structure and significant activity from sponges.

Organism	Order	Compound Name	Chemical Class	Special Feature/Activity	Source, Country, Year,/Depth	Reference
Sarcotragus sp.	Dictyoceratida	Sarcotragin A, & B	Trisnorsesterterpenoid lactam	Showed moderate cytotoxicity (LC_{50} 207 μg/mL) toward the leukemia cell-line K562	Seoguipo, Jaeju Island, Korea, 2001	[146]
Polymastia tenax	Hadromerida	5α,6α-epoxy-24*R**-ethylcholest-8(14)-en-3β,7α-diol and 5α,6α-epoxy-24*R**-ethylcholest-8-en-3β, 7α-diol	Sterol	Exhibited significant cytotoxic activity *vs.* human lung carcinoma (A-549), human colon carcinomas (HT-29 and H-116), and human prostate carcinoma (PC-3) cell lines with the LC_{50} (μg/mL) value of 5–10, 1–5, 1–5, 0.5–1 and 1–5	Punta de Betín, Bahía de Santa Marta, in the Colombian Caribbean, Colombia, 2002	[147]
Crella spinulata	Poecilosclerida	Benzylthiocrellidone	Bis-dimedone thioether	First report of a natural product containing a dimedone moiety. No activity reported	Davies and Bowden Reefs Australia, 2002	[148]
Ectyoplasia ferox	Poecilosclerida	Ectyoceramide	Galactofuranosylceramide (GSL)	The first example of a monohexofuranosylceramide and the first natural GSL with its first sugar in the furanose form. No activity reported	Island of Rum Cay, Bahamas, 2000	[149]
Cribrochalina olemda	Haplosclerida	Kapakahine E	Peptide (cyclic)	Kapakahine E showed moderate cytotoxicity against P388 murine leukemia cells at IC_{50} of 5.0 μg/mL	Pohnpei, Micronesia, 2003	[150]
Haliclona Viscosa	Haplosclerida	Viscosamine	Trimeric 3-alkyl pyridinium alkaloid	First trimeric 3-alkyl pyridinium compound from a marine environment. No activity reported	Coast of Blomstrandhalvøya, near Hansneset, Kongsfjorden, Arctic Ocean, 2003	[151]
Phakellia fusca	Axinellida	Compound **1**, **2**, **3**	5-Fluorouracil alkaloid	First report of fluorine containing natural products from a marine source. No activity reported	Yongxiong Island of the Xisha Islands, South China Sea, China 2003	[152]

Table 3. *Cont.*

Agelas clathrodes	Agelasida	Clarhamnoside	Rhamnosylated *R*-Galactosylceramide	The first Rhamnosylated *R*-Galactosylceramide, a glycolipid containing an unusual L-rhamnose unit. No activity reported	Grand Bahamas Island (Sweetings Cay), Bahamas, 2004	[153]
Psammocinia sp.	Dictyoceratida	Psymberin	Cytotoxin (distantly related to the Pederin family)	Several melanoma, breast, and colon cancer cell lines demonstrated high sensitivity ($LC_{50} < 2.5 \times 10^{-9}$ M) to psymberin, and all six leukemia cell lines proved comparably insensitive	Papua New Guinea, 2004	[154]
Callyspongia abnormis	Haploscerida	Callynormine A	Cyclic Peptide	Represents a new class of heterodetic cyclic peptides (designated endiamino peptides). This compound possessing an α-amido-β-aminoacrylamide cyclization functionality	Shimoni reef, Kenya, 2004	[155]
Axinella infundibula	Halichondrida	Axinelloside A	Lipopolysaccharide (Sulfated)	Axinelloside A, a complex polysulfated glycolipid, which strongly inhibited the activity of human telomerase with an IC_{50} value of 0.4 μM	Shikine-jima Island, the Izu Islands, Japan, 2005	[156]
Theonella swinhoei	Lithistida	Plytheonamide A, B	Polypeptide	Showed cytotoxicity against P388 murine leukemia cells with IC_{50} values of 78 and 68 pg/mL, respectively. Linear polypeptides with unprecedented structural features	Hachijo-jima Island, Japan, 2005	[157]
Neopetrosia sp.	Haplosclerida	Neopetrosiamide A, B	Peptide (diastereomeric tricyclic)	Active in inhibiting the amoeboid invasion by human tumor cells	Near Milne Bay, Papua New Guinea, 2005	[158]
Prianos osiros	Haplosclerida	(3*R*,3′*R*,5*S*)-3,3′,5,19′-tetrahydroxy-7′,8′-didehydro-γ,ε-carotene-8-one	Acetylenic carotenoid	Contains an unusual cytotoxic carotenoid	Pohnpei, Micronesia, 2005	[159]

Table 3. *Cont.*

Ircinia sp.	Dictyoceratida	Irciniasulfonic acid B	Fatty acid derivative (taurine conjugated)	Reversed the multi-drug resistance to vincristine in KB/VJ300 cells at the concentration of 100 μM	Tsuzumi Island, Fukuoka Prefecture, Japan, 2006	[160]
Suberites japonicus	Hadromerida	Seragamide A–F	Depsipeptide (actin targeting)	Caused multinuclei formation in cells at 0.01–0.02 μg/mL	Seragaki, Okinawa, Japan, 2006	[161]
Theonella swinhoei	Lithistida	Hurghadolide A	Macrolide	Caused disruption of the actin cytoskeleton at concentrations of 7.3 nM. Active against *Candida albicans* (MIC 31.3 μg/mL)	Red Sea, Egypt, 2006	[89]
Theonella swinhoei	Lithistida	Swinholide I	Macrolide	as above	Red Sea, Egypt, 2006	[89]
Coelocarteria cfr. *singaporensis*	Poecilosclerida	Coelodiol and Coelic acid	Diterpene (ent-isocopalane)	Inhibit the *in vitro* growth of MKN-45 cell line (human gastric adenocarcinoma) at 20 and 40 μg/mL respectively	Bunaken, Marine Park (North Sulawesi), Indonesia, 2006	[162]
Lendenfeldia sp.	Dictyoceratida	(*S*)-2,2′-Dimethoxy-1, 1′-binaphthyl-5,5′,6,6′-tetraol	Naphthalene dimer	Significantly inhibited both hypoxia-induced (IC_{50} values 4.3 μM) and iron chelator (1, 10-phenanthroline)-induced HIF-1 activation in T47D breast tumor cells. This compound inhibited HIF-1 activation at concentrations that were significantly lower than those that suppressed tumor cell viability	Collected at 2 m depth on May 22, 1993 (sample C011337), from a sea grass bed, Indonesia, 2007	[163]
Erylus formosus	Astrophorida	Eryloside F1–F4	Triterpene glycoside	At a concentration of 100 μg/mL were found to activate Ca2 influx into mouse spleenocytes. biosides having aglycons related to penasterol with additional oxidation patterns in their side chains	Puerto Morelos (the Caribbean Sea), Mexico 2007	[164]

Table 3. *Cont.*

Erylus formosus	Astrophorida	Eryloside M–Q	Triterpene glycoside	As above, contain new variants of carbohydrate chains with three, four and six sugar units. Contain 14-carboxy-24-methylenelanost-8(9)-en-3β-ol	Puerto Morelos (the Caribbean Sea), Mexico, 2007	[164]
Cacospongia mycofijiensis	Dictyoceratida	CTP-431	Thiopyrone	Showed only mild cytotoxicity (IC_{50}: 18 μM) against human colon carcinoma HCT-116. This compound has no previous precedent in natural products chemistry. Its structure including absolute configuration as 8*R*,9*R*,10*S*,13*S*	Beqa Lagoon, Fiji, 2008	[165]
Homophymia sp.	Lithistida	Homophymine A	Cyclodepsipeptide	Exhibited cytoprotective activity against HIV-1 infection with a IC_{50} of 75 nM	Coast of New Caledonia, 2008	[166]
Ianthella sp.	Verongida	Petrosterol-3,6-dione and 5α,6α-epoxy-petrosterol	C29 sterol	Showed growth-inhibitory effects with IC_{50} values of 8.4, 19.9, 17.8, 16.2 and 22.1 μM against lung (A549), colon (HT-29), breast (MCF-7), ovary (SK-OV-3), and two types of leukemia (HL-60 and U937) human cancer cell lines	Namyet Island, Khanh Hoa province, Vietnam, 2009	[167]
Topsentia sp.	Halichondrida	Geodisterol-3-*O*-sulfite and 29-demethylgeodisterol-3-*O*-sulfite	Sterol (sulphated)	Reverses efflux pump mediated fluconazole resistance. Also enhances fluconazole activity in a *Saccharomyces cerevisiae* strain overexpressing the *Candida albicans* efflux pump MDR1, as well as in a fluconazole-resistant *Candida albicans* clinical isolate known to overexpress MDR1	Chuuk, Micronesia, 2009	[168]

Table 3. *Cont.*

Spongia (*Heterofibria*) sp.	Dictyoceratida	Heterofibrin A1–A3 and B1–B3	Fatty acid	Possess a diyne-ene moiety, while the monolactyl and dilactyl moiety featured in selected heterofibrins is unprecedented in the natural products literature. Inhibited lipid droplet formation in A431 fibroblast cells (up to 60% at 10 μM)	Great Australian Bight, Australia, 2010	[169]
Xestospongia sp.	Haplosclerida	Xestosaprol F–M	Xestosaprol (pentacyclic compound)	Showed moderate inhibition of the aspartic protease BACE1 (memapsin-2), which has a central role in the etiology of Alzheimer's disease with the IC_{50} value of 135 ± 11 μM. First examples of a monooxygenated A-ring	Coral reef at Sangalaki, Indonesia, 2010	[170]
Theonella swinhoei	Lithistida	Paltolides A–C	Peptides (Anabaenopeptin like)	Closely related to a group of anabaenopeptins that are submicromolar inhibitors of carboxypeptidase U with greater than 50 fold selectivity over other carboxypeptidases	Uchelbeluu Reef, Palau, 2010	[171]
Neopetrosia proxima	Haplosclerida	Neopetrosiamine A	Alkaloid (tetracyclic bis-piperidine)	Exhibited strong inhibitory activity against MALME-3M melanoma cancer, CCRF-CEM leukemia, and MCF7 breast cancer with IC_{50} values of 1.5, 2.0, and 3.5 μM, respectively. *In vitro* activity *vs.* pathogenic strain of *Mycobacterium tuberculosis* (H37Rv) and *Plasmodium falciparum*	Mona Island, Puerto Rico, 2010	[172]
Iotrochota baculifera	Poecilosclerida	Baculiferins A–O	*O*-sulfated pyrrole alkaloids	Baculiferins C, E–H, and K–N (4, 6–9, 12–15) are potent inhibitors of HIV-1 IIIB virus in both MT4 and MAGI cells. Additionally could bind to the HIV-1 target proteins Vif, APOBEC3G, and gp41	Inner coral reef, Hainan Island, China, 2010	[173]

2.8. Distribution of New Compounds Based on Country/Geographical Area

One important aspect of sponges is their geographical location. A high percentage of bioactive sponge species were reported from different geographical regions [174–176].

Figure 8 shows that the new compounds were mainly isolated from sponges collected from 61 countries. Of these, sponges from Japan had the highest number of compounds (332) followed by Indonesia (235), Korea (211). Sponge samples from Australia and China contributed 187 and 146 compounds, respectively, during the last decade. The Bahamas, Mexico, Palau, Papua New Guinea, Philippines and Vanuatu are the other countries which were the source of more than 50 new compounds found in the last ten years. The obvious question is why do some regions show a high diversity of compounds as well as an abundance of sponges? Studies showed that the highest concentration of toxic or antioxidant sponge metabolites are found in habitats such as coral reefs that are characterized by intense competition and feeding pressure from carnivorous fish [177]. The adaptive significance of the chemical defenses of sponges are that they are highly effective against most species of fish and a group of shell-less gastropods, the nudibranchs that feed on sponges and sequester their chemical armory [177]. An excellent paper on the global diversity of sponges includes global sponge diversity information which was collected from different regional projects and resources and also reviewed was information on invasive sponges that might well have some influence on distribution patterns in the future [83].

Figure 8. Total number of new compounds isolated from different marine sponges and their source locations from 2001 to 2010.

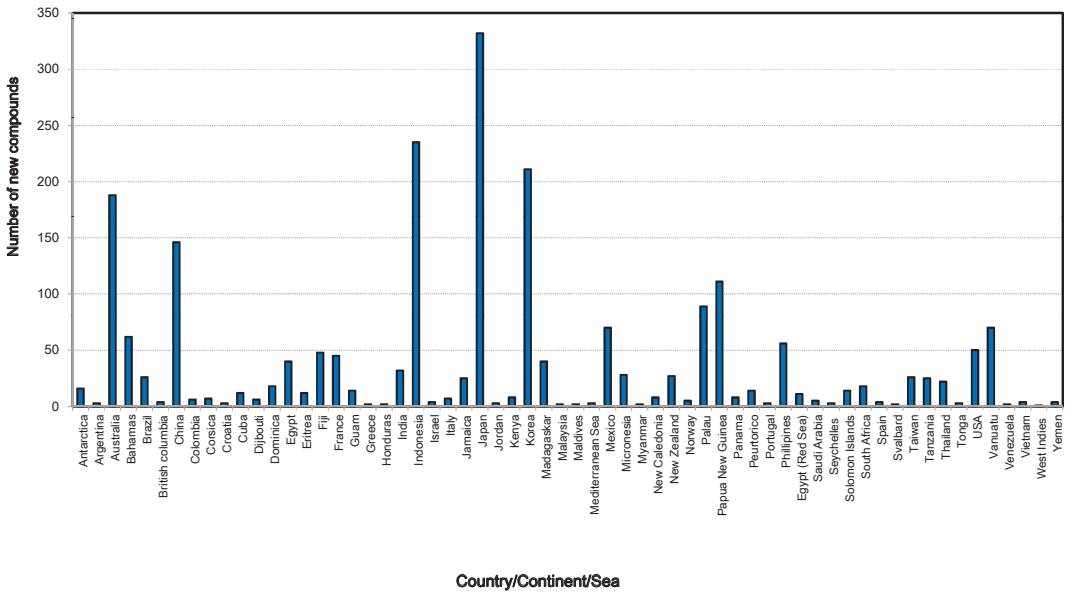

Figure 9 shows the total number of new compounds isolated from the top ten countries. It has been found that each year from 2001 to 2010 at least 20 new compounds were isolated from Japanese sponge samples, with the highest output occurring in 2004 and 2005 with 46 new compounds (Figure S2, Supplementary Information). From 2006 to 2009 at least 20 compounds were found each year in Indonesia. Marine invertebrates, which are plentiful in the Indo-Pacific regions including Indonesia, are rich in secondary metabolites and are becoming targets for the continuing search for bioactive compounds [178].

Figure 9. Total number of new compounds isolated from marine sponges from the top 10 source countries from 2001 to 2010.

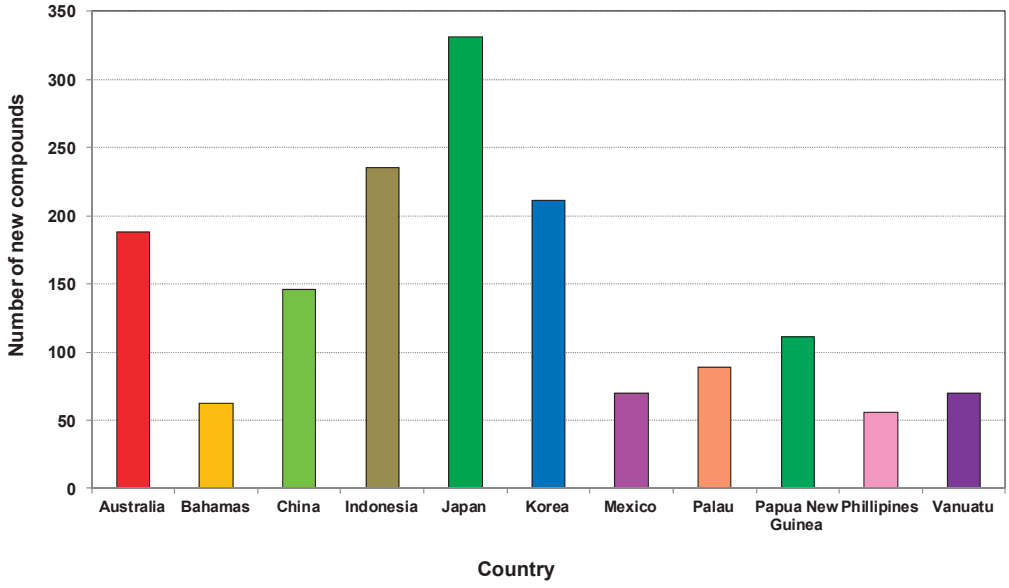

Although in 2001 the highest contributors of new compounds derived from sponges were from Japan, Korea and Australia at 22.9%, 18.9% and 14.3%, respectively, the scenario changed during 2010 where the highest contributions of new compounds came from China, Australia and Indonesia at 23.9%, 21.3%, and 21%, respectively [179]. China started its marine high-tech program since 1996, and after 15 years it emerged as one of the highest contributors to marine sponge natural products discovery in 2010. This achievement demonstrates how significant the government science and technology funding policy can impact the development of marine biotechnology. Australia is one of only 17 recognised megabiodiverse countries primarily based on its highly biodiverse and endemic terrestrial flora and fauna [180,181]. While the full extent of Australian marine biodiversity remains relatively unexplored [182], several marine biodiversity hotspots including centers of endemicity have been recognized, especially in coral reefs [183,184], the temperate coastline [185] and the Great Australian Bight off the coast of South Australia [186]. There have been reports on the high species diversity of sponges in the north west [187–190], in the deep sea off the south west [191,192] of the Bight, and the Great Barrier Reef [189]. Therefore, there is urgent need to explore those potential locations in order to obtain new compounds and drugs for the future.

The Australian Institute of Marine Science (AIMS) conducted a study based on the Australian marine habitat and identified biogeographic bioactivity hotspots that correlated with biodiversity hotspots. AIMS found that high-level phylogeny, and therefore the metabolic machinery available to an organism, is a major basis of bioactivity, while habitat diversity and ecological circumstance are possible drivers in the stimulation of this machinery and bioactive secondary metabolism [193]. Therefore, in near future, knowledge of metabolomics coupled with genomics tool and bioinformatics could be a high level device for the exploration of target specific bioactive compounds from sponges.

In addition, microbes associated with marine sponges could vary with the geographical area, so, if these associated bacteria are responsible for producing compounds, then it is possible that the same sponge species in different geographical locations could produce different secondary metabolites [194,195]. However, a recent study showed the stability of bacterial communities in two temperate sponges exposed to environmental variation, which is consistent with previous research on other temperate sponges. This study used next generation sequencing and revealed how different components of bacterial communities associated with *Ecionemia alata* and *Tethya bergquistae* responded to environmental variation *in situ* [196]. The similarity observed in bacterial communities among specimens occupying different habitats suggests that environmental variation occurring in those habitats does not affect the stability of the community, and hence, most likely does not radically alter the metabolism of these sponges. The study recommends further study to improve the understanding of the role of microbial symbiont communities which may affect the physiology and ecology of sponges on temperate rocky reefs [196].

A recent pyrosequencing analysis of 32 sponge species from eight locations around the world identified few bacterial species that are common to more than a handful of sponge species [177]. They stated that different sponges were found to contain different bacterial species (species-specific community) but share only very few bacterial species (core community) [197]. However, the bacterial species in different sponges are still more closely related to each other than, for example, to seawater bacteria (indicated by Plus-OTUs and sponge-specific clusters), consistent with previous studies suggesting at least partially overlapping communities among different sponges. Sponges therefore contain a uniform, sponge-specific bacterial community although each sponge species contains different bacterial species [197]. Perhaps, this is one of the main reasons for getting new compounds in species level regardless of the genera and order. Although we commented on this, based on our study of sponges of the last decade, further study to prove this hypothesis would be worthwhile.

3. Conclusions

In the decade 2001–2010 marine sponges continued to be the most promising source of marine natural products. Marine microorganisms and phytoplankton grew rapidly to become the third largest source by increasing their contribution from 9% to 39% during the decade. Sponges are a reservoir of marine microorganisms with up to 40%–60% as microbial biomass. In the coming decade sponge associated microorganisms promise to be an outstanding source of the NMNP.

From the current trend of discovery it could be predicted that China, Australia and Indonesia will be the source of more new compounds in the future competing with Japan and Korea. However,

although Indonesia is an excellent source of sponges, most of their studies were conducted by scientists in other countries. Certainly, exploration of new compounds from marine sponges is dependent on government funding and policy, industrial interest and investment, research facilities, the expertise of scientists, infrastructure and laboratory facilities, equipment, machinery and institutional support.

Astrophorida, Dictyoceratida, Halichondrida, Haplosclerida and Poecilosclerida were the key orders of sponges studied during the first decade of the 21st century. The examination of the contribution from an individual species revealed that regardless of the order each species contributed on average 3–5 compounds. The high number of new compounds was the result of the high diversity of species from these particular orders. Alkaloids (20%), terpenes (14.7%) or terpenoids (8.3%) and peptides (6.8%) represented the three main chemical classes of compounds discovered from sponges in this period, and together with the other chemical classes showed a range of biological activities. Of all the biological activities investigated cytotoxicity or anticancer activity against different cancer cell lines was most frequently reported at 53.6%. Antibacterial and antifungal activity were two other areas where new compounds showed potential activity at 9.4% and 7.2%, respectively. Anti-Alzheimer's, antibacterial, antituberculosis, anticancer, antifungal, anti-inflammatory, antimalarial, antiviral, anti-HIV were the other activities exhibited by the new compounds from sponges. Because sponge extracts showed potent cytotoxic activity, which is often reported as anticancer activity, it is very important to study the mode of action of these extracts by isolating pure compounds rather than only testing cytotoxicity.

The order Dictyoceratida was found to be the most prolific producer of new compounds among all the sponge orders studied. *Dysidea* sp. and *Ircinia* sp. were found to be the most promising genera because of their capacity for producing new bioactive compounds.

In any event, the discovery of marine natural products from sponges relies particularly on finding new genera and species from the most prolific to the least abundant orders, which is still achievable. In order to overcome the problem of production of sponge-derived compounds, synthesis of bioactive, low molecular weight compounds by cloning biosynthetic gene clusters using recombinant techniques could be applied. Most importantly, sponge derived compounds should be utilized with a combination of innovative technologies which could develop new fields of application that will impact significantly on biotechnology.

Acknowledgments

Financial support from Centre for Marine Bioproducts Development, Flinders University; Flinders University for their IPRS scholarship to Mohammad Mehbub.

Author Contribution

Mohammad Ferdous Mehbub did the coordination for collecting all the information to prepare a comprehensive database for writing this manuscript, proof read the database, wrote a major part of the manuscript and generates the graphs and tables, proof reading the manuscript as well and made necessary correction.

Jie Lei helped to collect the information to develop the database for preparing this manuscript.

Christopher Franco wrote a significant part of the manuscript, decided on the format and figures to be included and did the final proofreading and corrections.

Wei Zhang has the original idea, structure and plan for this manuscript, and planned and refined the graphs and tables with Mohammad Ferdous Mehbub, and wrote the abstract, and wrote a significant portion for the introduction.

Conflicts of Interest

The authors declare no conflict of interest.

References

1. Bergmann, W.; Feeney, R.J. Contributions to the study of marine products. XXXII. The nucleosides of sponges I. *J. Org. Chem.* **1951**, *16*, 981–987.
2. Bergmann, W.; Feeney, R.J. The isolation of a new thymine pentoside from sponges 1. *J. Am. Chem. Soc.* **1950**, *72*, 2809–2810.
3. Carte, B.K. Biomedical potential of marine natural products. *Bioscience* **1996**, *46*, 271–287.
4. Burkholder, P.R.; Pfister, R.M.; Leitz, F.H. Production of a pyrrole antibiotic by a marine bacterium. *Appl. Microbiol.* **1966**, *14*, 649–653.
5. Proksch, P.; Edrada, R.; Ebel, R. Drugs from the seas—Current status and microbiological implications. *Appl. Microbiol. Biotechnol.* **2002**, *59*, 125–134.
6. Weinheimer, A.J.; Spraggins, R.L. The occurrence of two new prostaglandin derivatives (15-*epi*-PGA and its acetate, methyl ester) in the Gorgonian *Plexaura homomalla* chemistry of Coelenterates. XV. *Tetrahedron Lett.* **1969**, *10*, 5185–5188.
7. Ireland, C.M.; Copp, B.R.; Foster, M.P.; McDonald, L.A.; Radisky, D.C.; Swersey, J.C. Biomedical potential of marine natural products. In *Pharmaceutical and Bioactive Natural Products*; Springer: Berlin/Heidelberg, Germany, 1993; pp. 1–43.
8. Gordon, E.M.; Barrett, R.W.; Dower, W.J.; Fodor, S.P.; Gallop, M.A. Applications of combinatorial technologies to drug discovery. 2. Combinatorial organic synthesis, library screening strategies, and future directions. *J. Med. Chem.* **1994**, *37*, 1385–1401.
9. Alonso, D.; Khalil, Z.; Satkunanthan, N.; Livett, B. Drugs from the sea: Conotoxins as drug leads for neuropathic pain and other neurological conditions. *Mini Rev. Med. Chem.* **2003**, *3*, 785–787.
10. Hu, G.P.; Yuan, J.; Sun, L.; She, Z.G.; Wu, J.H.; Lan, X.J.; Zhu, X.; Lin, Y.C.; Chen, S.P. Statistical research on marine natural products based on data obtained between 1985 and 2008. *Mar. Drugs* **2011**, *9*, 514–525.
11. Faulkner, D.J. Marine natural products. *Nat. Prod. Rep.* **2000**, *17*, 7–55.
12. Faulkner, D.J. Marine natural products. *Nat. Prod. Rep.* **2002**, *19*, 1–48.
13. Blunt, J.W.; Copp, B.R.; Munro, M.H.G.; Northcote, P.T.; Prinsep, M.R. Marine natural products. *Nat. Prod. Rep.* **2006**, *23*, 26–78.

14. Blunt, J.W.; Copp, B.R.; Munro, M.H.G.; Northcote, P.T.; Prinsep, M.R. Marine natural products. *Nat. Prod. Rep.* **2010**, *27*, 165–237.
15. Blunt, J.W.; Copp, B.R.; Munro, M.H.G.; Northcote, P.T.; Prinsep, M.R. Marine natural products. *Nat. Prod. Rep.* **2011**, *28*, 196–268.
16. Blunt, J.W.; Copp, B.R.; Keyzers, R.A.; Munro, M.H.G.; Prinsep, M.R. Marine natural products. *Nat. Prod. Rep.* **2012**, *29*, 144–222.
17. Blunt, J.W.; Copp, B.R.; Keyzers, R.A.; Munro, M.H.G.; Prinsep, M.R. Marine natural products. *Nat. Prod. Rep.* **2013**, *30*, 237–323.
18. Blunt, J.W.; Copp, B.R.; Keyzers, R.A.; Munro, M.H.G.; Prinsep, M.R. Marine natural products. *Nat. Prod. Rep.* **2014**, *31*, 160–258.
19. Laport, M.; Santos, O.; Muricy, G. Marine sponges: Potential sources of new antimicrobial drugs. *Curr. Pharma. Biotechnol.* **2009**, *10*, 86–105.
20. Blunt, J.W.; Copp, B.R.; Munro, M.H. G.; Northcote, P.T.; Prinsep, M.R. Marine natural products. *Nat. Prod. Rep.* **2005**, *22*, 15–61.
21. Sagar, S.; Kaur, M.; Minneman, K.P. Antiviral lead compounds from marine sponges. *Mar. Drugs* **2010**, *8*, 2619–2638.
22. Paul, V.J.; Ritson-Williams, R.; Sharp, K. Marine chemical ecology in benthic environments. *Nat. Prod. Rep.* **2011**, *28*, 345–387.
23. Molinski, T.F.; Dalisay, D.S.; Lievens, S.L.; Saludes, J.P. Drug development from marine natural products. *Nat. Rev. Drug Discov.* **2009**, *8*, 69–85.
24. Wijffels, R.H. Potential of sponges and microalgae for marine biotechnology. *Trends Biotechnol.* **2008**, *26*, 26–31.
25. Leal, M.C.; Puga, J.; Serôdio, J.; Gomes, N.C.; Calado, R. Trends in the discovery of new marine natural products from invertebrates over the last two decades—Where and what are we bioprospecting? *PLoS One* **2012**, *7*, e30580.
26. Blunt, J.W.; Copp, B.R.; Munro, M.H. G.; Northcote, P.T.; Prinsep, M.R. Marine natural products. *Nat. Prod. Rep.* **2003**, *20*, 1–48.
27. Blunt, J.W.; Copp, B.R.; Munro, M.H. G.; Northcote, P.T.; Prinsep, M.R. Marine natural products. *Nat. Prod. Rep.* **2004**, *21*, 1–49.
28. Blunt, J.W.; Copp, B.R.; Hu, W.-P.; Munro, M.H.G.; Northcote, P.T.; Prinsep, M.R. Marine natural products. *Nat. Prod. Rep.* **2008**, *25*, 35–94.
29. Blunt, J.W.; Copp, B.R.; Hu, W.-P.; Munro, M.H.G.; Northcote, P.T.; Prinsep, M.R. Marine natural products. *Nat. Prod. Rep.* **2009**, *26*, 170–244.
30. Blunt, J.W.; Copp, B.R.; Hu, W.-P.; Munro, M.H. G.; Northcote, P.T.; Prinsep, M.R. Marine natural products. *Nat. Prod. Rep.* **2007**, *24*, 31–86.
31. Hooper, J.N. *Sponguide. Guide to Sponge Collection and Identification*; Queensland Museum: Queensland, Australia, 2000.
32. Paul, V.J.; Puglisi, M.P. Chemical mediation of interactions among marine organisms. *Nat. Prod. Rep.* **2004**, *21*, 189–209.
33. Paul, V.J.; Puglisi, M.P.; Ritson-Williams, R. Marine chemical ecology. *Nat. Prod. Rep.* **2006**, *23*, 153–180.

34. McClintock, J.B.; Baker, B.J. *Marine Chemical Ecology*; CRC Press: Boca Raton, FL, USA, 2010; pp. 1–624.
35. Lee, Y.K.; Lee, J.-H.; Lee, H.K. Microbial symbiosis in marine sponges. *J. Microbiol.* **2001**, *39*, 254–264.
36. Jensen, P.R.; Fenical, W. Strategies for the discovery of secondary metabolites from marine bacteria: Ecological perspectives. *Ann. Rev. Microbiol.* **1994**, *48*, 559–584.
37. Bernan, V.; Greenstein, M.; Maiese, W. Marine microorganisms as a source of new natural products. *Adv. Appl. Microbiol.* **1997**, *43*, 57–90.
38. Haygood, M.G.; Schmidt, E.W.; Davidson, S.K.; Faulkner, D.J. Microbial symbionts of marine invertebrates: Opportunities for microbial biotechnology. *J. Mol. Microbiol. Biotechnol.* **1999**, *1*, 33–43.
39. Osinga, R.; Armstrong, E.; Burgess, J.G.; Hoffmann, F.; Reitner, J.; Schumann-Kindel, G. Sponge—Microbe associations and their importance for sponge bioprocess engineering. *Hydrobiologia* **2001**, *461*, 55–62.
40. Fusetani, N. Biofouling and antifouling. *Nat. Prod. Rep.* **2004**, *21*, 94–104.
41. Li, C.-W.; Chen, J.-Y.; Hua, T.-E. Precambrian sponges with cellular structures. *Science* **1998**, *279*, 879–882.
42. Hentschel, U.; Hopke, J.; Horn, M.; Friedrich, A.B.; Wagner, M.; Hacker, J.; Moore, B.S. Molecular evidence for a uniform microbial community in sponges from different oceans. *Appl. Environ. Microbiol.* **2002**, *68*, 4431–4440.
43. Selvin, J.; Shanmugha Priya, S.; Seghal Kiran, G.; Thangavelu, T.; Sapna Bai, N. Sponge-associated marine bacteria as indicators of heavy metal pollution. *Microbiol. Res.* **2009**, *164*, 352–363.
44. Wilkinson, C.; Fay, P. Nitrogen fixation in coral reef sponges with symbiotic cyanobacteria. *Nature* **1979**, *279*, 527–529.
45. Diaz, M.C.; Rutzler, K. Sponges: An essential component of Caribbean coral reefs. *Bull. Mar. Sci.* **2001**, *69*, 535–546.
46. Thoms, C.; Horn, M.; Wagner, M.; Hentschel, U.; Proksch, P. Monitoring microbial diversity and natural product profiles of the sponge *Aplysina cavernicola* following transplantation. *Mar. Biol.* **2003**, *142*, 685–692.
47. Thoms, C.; Schupp, P. Biotechnological potential of marine sponges and their associated bacteria as producers of new pharmaceuticals (Part II). *J. Int. Biotechnol. Law* **2005**, *2*, 257–264.
48. Proksch, P. Defensive roles for secondary metabolites from marine sponges and sponge-feeding nudibranchs. *Toxicon* **1994**, *32*, 639–655.
49. Pawlik, J.R.; McFall, G.; Zea, S. Does the odor from sponges of the genus *Ircinia* protect them from fish predators? *J. Chem. Ecol.* **2002**, *28*, 1103–1115.
50. Mahon, A.R.; Amsler, C.D.; McClintock, J.B.; Amsler, M.O.; Baker, B.J. Tissue-specific palatability and chemical defenses against macropredators and pathogens in the common articulate brachiopod *Liothyrella uva* from the Antarct*. Penins*. *J. Exp. Mar. Biol. Ecol.* **2003**, *290*, 197–210.

51. Paul, V.; Cruz-Rivera, E.; Thacker, R. Chemical mediation of macroalgal-herbivore interactions: Ecological and evolutionary perspectives. In *Marine Chemical Ecology*; CRC Press: Boca Raton, FL, USA, 2001; pp. 227–265.
52. Unson, M.D.; Holland, N.D.; Faulkner, D.J. A brominated secondary metabolite synthesized by the cyanobacterial symbiont of a marine sponge and accumulation of the crystalline metabolite in the sponge tissue. *Mar. Biol.* **1994**, *119*, 1–11.
53. Vacelet, J.; Vacelet, E.; Gaino, E.; Gallissian, M. Bacterial attack of spongin skeleton during the 1986–1990 Mediterranean sponge disease. In *Sponges in Time and Space*; Balkema: Rotterdam, The Netherlands, 1994; pp. 355–362.
54. Boehm, M.; Hentschel, U.; Friedrich, A.; Fieseler, L.; Steffen, R.; Gamulin, V.; Mueller, I.; Müller, W. Molecular response of the sponge *Suberites domuncula* to bacterial infection. *Mar. Biol.* **2001**, *139*, 1037–1045.
55. Maldonado, M.; Sánchez-Tocino, L.; Navarro, C. Recurrent disease outbreaks in corneous demosponges of the genus *Ircinia*: Epidemic incidence and defense mechanisms. *Mar. Biol.* **2010**, *157*, 1577–1590.
56. Selvin, J.; Ninawe, A.; Seghal Kiran, G.; Lipton, A. Sponge-microbial interactions: Ecological implications and bioprospecting avenues. *Crit. Rev. Microbiol.* **2010**, *36*, 82–90.
57. Thakur, N.L.; Müller, W.E. Biotechnological potential of marine sponges. *Curr. Sci.* **2004**, *86*, 1506–1512.
58. Tilvi, S.; Rodrigues, C.; Naik, C.; Parameswaran, P.; Wahidhulla, S. New bromotyrosine alkaloids from the marine sponge *Psammaplysilla purpurea*. *Tetrahedron* **2004**, *60*, 10207–10215.
59. Abad, M.; Bedoya, L.; Bermejo, P. Marine compounds and their antimicrobial activities. In *Science Against Microbial Pathogens: Communicating Current Research and Technological Advances*; Formatex Research Center: Badajoz, Spain, 2011.
60. Van Soest, R.; Boury-Esnault, N.; Hooper, J.; Rützler, K.; de Voogd, N.; Alvarez de Glasby, B.; Hajdu, E.; Pisera, A.; Manconi, R.; Schoenberg, C. World Porifera Database. The World Register of Marine Species (WoRMS). Available online: http://www.marinespecies.org/porifera (accessed on 25 October 2012).
61. Appeltans, W.; Decock, W.; Vanhoorne, B.; Hernandez, F.; Bouchet, P.; Boxshall, G.; Fauchald, K.; Gordon, D.P.; Poore, G.C.B.; van Soest, R.; *et al*. The World Register of Marine Species. In Proceedings of the future of the 21st century ocean: Marine Sciences and European Research Infrastructures, Brest, France, 28 June–1 July 2011; p. 30.
62. Ausubel, J.; Trew Christ, D.; Waggoner, P. First Census of Marine Life 2010: Highlights of A Decade of Discovery. Available online: http://www.coml.org/pressreleases/census2010/PDF/Highlights-2010-Report-Low-Res.pdf (accessed on 11 January 2014).
63. Valerie, P.; Raphael, R.-W. Marine chemical ecology. *Nat. Prod. Rep.* **2008**, *25*, 662–695.
64. Skropeta, D. Deep-sea natural products. *Nat. Prod. Rep.* **2008**, *25*, 1131–1166.
65. Faulkner, D.J. Marine natural products. *Nat. Prod. Rep.* **1998**, *15*, 113–158.

66. Crews, P.; Gerwick, W.; Schmitz, F.; France, D.; Bair, K.; Wright, A.; Hallock, Y. Molecular approaches to discover marine natural product anticancer leads-an update from a drug discovery group collaboration. *Pharm. Biol.* **2003**, *41*, 39–52.
67. Sipkema, D.; Franssen, M.C.; Osinga, R.; Tramper, J.; Wijffels, R.H. Marine sponges as pharmacy. *Mar. Biotechnol.* **2005**, *7*, 142–162.
68. Bhanot, A.; Sharma, R.; Noolvi, M.N. Natural sources as potential anti-cancer agents: A review. *Int. J. Phytomed.* **2011**, *3*, 9–26.
69. Newman, D.J.; Cragg, G.M. Marine natural products and related compounds in clinical and advanced preclinical trials. *J. Nat. Prod.* **2004**, *67*, 1216–1238.
70. Thakur, A.N.; Thakur, N.L.; Indap, M.M.; Pandit, R.A.; Datar, V.V.; Müller, W.E. Antiangiogenic, antimicrobial, and cytotoxic potential of sponge-associated bacteria. *Mar. Biotechnol.* **2005**, *7*, 245–252.
71. Cragg, G.M.; Newman, D.J.; Snader, K.M. Natural products in drug discovery and development. *J. Nat. Prod.* **1997**, *60*, 52–60.
72. Petit, K.; Biard, J.-F. Marine natural products and related compounds as anticancer agents: An overview of their clinical status. *Anti-Cancer Agents Med. Chem.* **2013**, *13*, 603–631.
73. Newman, D.J.; Cragg, G.M. Marine-sourced anti-cancer and cancer pain control agents in clinical and late preclinical development. *Mar. Drugs* **2014**, *12*, 255–278.
74. Kinghorn, A.D.; Chin, Y.-W.; Swanson, S.M. Discovery of natural product anticancer agents from biodiverse organisms. *Curr. Opin. Drug Discov. Dev.* **2009**, *12*, 189–196.
75. Duckworth, A. Farming sponges to supply bioactive metabolites and bath sponges: A review. *Mar. Biotechnol.* **2009**, *11*, 669–679.
76. Müller, W.E.G.; Böhm, M.; Batel, R.; de Rosa, S.; Tommonaro, G.; Müller, I.M.; Schröder, H.C. Application of cell culture for the production of bioactive compounds from sponges: Synthesis of Avarol by primmorphs from *Dysidea avara*. *J. Nat. Prod.* **2000**, *63*, 1077–1081.
77. Zhang, X.; Cao, X.; Zhang, W.; Yu, X.; Jin, M. Primmorphs from archaeocytes-dominant cell population of the sponge *Hymeniacidon perleve*: Improved cell proliferation and spiculogenesis. *Biotechnol. Bioeng.* **2003**, *84*, 583–590.
78. Müller, W.E.; Grebenjuk, V.A.; le Pennec, G.; Schröder, H.-C.; Brümmer, F.; Hentschel, U.; Müller, I.M.; Breter, H.-J. Sustainable production of bioactive compounds by sponges—Cell culture and gene cluster approach: A review. *Mar. Biotechnol.* **2004**, *6*, 105–117.
79. Koopmans, M.; Martens, D.; Wijffels, R.H. Towards commercial production of sponge medicines. *Mar. Drugs* **2009**, *7*, 787–802.
80. Wilson, M.C.; Mori, T.; Rückert, C.; Uria, A.R.; Helf, M.J.; Takada, K.; Gernert, C.; Steffens, U.A.; Heycke, N.; Schmitt, S. An environmental bacterial taxon with a large and distinct metabolic repertoire. *Nature* **2014**, *506*, 58–62.
81. Jaspars, M.; Challis, G. Microbiology: A talented genus. *Nature* **2014**, *506*, 38–39.
82. Piel, J. Metabolites from symbiotic bacteria. *Nat. Prod. Rep.* **2004**, *21*, 519–538.
83. Van Soest, R.W.; Boury-Esnault, N.; Vacelet, J.; Dohrmann, M.; Erpenbeck, D.; de Voogd, N.J.; Santodomingo, N.; Vanhoorne, B.; Kelly, M.; Hooper, J.N. Global diversity of sponges (Porifera). *PLoS One* **2012**, *7*, e35105.

84. Kalaitzis, J.A. 2005. Chemical Investigations of Australian Marine Sponges. Available online: https://www120.secure.griffith.edu.au/rch/file/786c6d3d-925a-dea0-3864-2db686e40950/1/02Chapter1.pdf (accessed on 29 April 2014).
85. Thomas, T.R.A.; Kavlekar, D.P.; LokaBharathi, P.A. Marine drugs from sponge-microbe association—A review. *Mar. Drugs* **2010**, *8*, 1417–1468.
86. Matsunaga, S.; Fusetani, N. Nonribosomal peptides from marine sponges. *Curr. Org. Chem.* **2003**, *7*, 945–966.
87. Matsunaga, S.; Fusetani, N.; Kato, Y.; Hirota, H. Aurantosides A and B: Cytotoxic tetramic acid glycosides from the marine sponge *Theonella* sp. *J. Am. Chem. Soc.* **1991**, *113*, 9690–9692.
88. Carmely, S.; Kashman, Y. Structure of swinholide-a, a new macrolide from the marine sponge *Theonella swinhoei*. *Tetrahedron Lett.* **1985**, *26*, 511–514.
89. Youssef, D.T.; Mooberry, S.L. Hurghadolide A and Swinholide I, potent actin-microfilament disrupters from the Red Sea sponge *Theonella swinhoei*. *J. Nat. Prod.* **2006**, *69*, 154–157.
90. Webster, N.S.; Blackall, L.L. What do we really know about sponge-microbial symbioses? *Int. Soc. Micobial. Ecol. J.* **2009**, *3*, 1–3.
91. Webster, N.S.; Taylor, M.W. Marine sponges and their microbial symbionts: Love and other relationships. *Environ. Microbiol.* **2012**, *14*, 335–346.
92. Mohamed, N.M.; Rao, V.; Hamann, M.T.; Kelly, M.; Hill, R.T. Monitoring bacterial diversity of the marine sponge *Ircinia strobilina* upon transfer into aquaculture. *Appl. Environ. Microbiol.* **2008**, *74*, 4133–4143.
93. Wilkinson, C.R. Net primary productivity in coral reef sponges. *Science* **1983**, *219*, 410–412.
94. Corredor, J.E.; Wilkinson, C.R.; Vicente, V.P.; Morell, J.M.; Otero, E. Nitrate release by Caribbean reef sponges. *Limnol. Oceanogr.* **1988**, *33*, 114–120.
95. Diaz, M.C.; Ward, B.B. Sponge-mediated nitrification in tropical benthic communities. *Mar. Ecol. Prog. Ser.* **1997**, *156*, 97–107.
96. Shieh, W.Y.; Lin, Y.M. Association of heterotrophic nitrogen-fixing bacteria with a marine sponge of *Halichondria* sp. *Bull. Mar. Sci.* **1994**, *54*, 557–564.
97. Wilkinson, C.C.; Summons, R.R.; Evans, E. Nitrogen fixation in symbiotic marine sponges: Ecological significance and difficulties in detection. *Mem. Qld. Mus.* **1999**, *44*, 667–673.
98. Hoffmann, F.; Larsen, O.; Thiel, V.; Rapp, H.T.; Pape, T.; Michaelis, W.; Reitner, J. An anaerobic world in sponges. *Geomicrobiol. J.* **2005**, *22*, 1–10.
99. Hentschel, U.; Fieseler, L.; Wehrl, M.; Gernert, C.; Steinert, M.; Hacker, J.; Horn, M. Microbial diversity of marine sponges. In *Sponges (Porifera)*; Springer: Berlin/Heidelberg, Germany, 2003; pp. 59–88.
100. Kennedy, J.; Baker, P.; Piper, C.; Cotter, P.D.; Walsh, M.; Mooij, M.J.; Bourke, M.B.; Rea, M.C.; O'Connor, P.M.; Ross, R.P. Isolation and analysis of bacteria with antimicrobial activities from the marine sponge *Haliclona simulans* collected from Irish waters. *Mar. Biotechnol.* **2009**, *11*, 384–396.

101. Rahman, H.; Austin, B.; Mitchell, W.J.; Morris, P.C.; Jamieson, D.J.; Adams, D.R.; Spragg, A.M.; Schweizer, M. Novel anti-infective compounds from marine bacteria. *Mar. Drugs* **2010**, *8*, 498–518.
102. Lu, X.; Cao, X.; Liu, X.; Jiao, B. Marine microbes-derived anti-bacterial agents. *Mini Rev. Med. Chem.* **2010**, *10*, 1077–1090.
103. Dudler, R.; Eberl, L. Interactions between bacteria and eukaryotes via small molecules. *Curr. Opin. Biotechnol.* **2006**, *17*, 268–273.
104. Schmidt, E.W. Trading molecules and tracking targets in symbiotic interactions. *Nat. Chem. Biol.* **2008**, *4*, 466–473.
105. Hu, J.-F.; Hamann, M.T.; Hill, R.; Kelly, M. The manzamine alkaloids. *Alkaloids Chem. Biol.* **2003**, *60*, 207–285.
106. Jares-Erijman, E.A.; Sakai, R.; Rinehart, K.L. Crambescidins: New antiviral and cytotoxic compounds from the sponge *Crambe crambe*. *J. Org. Chem.* **1991**, *56*, 5712–5715.
107. Berlinck, R.; Braekman, J.C.; Daloze, D.; Bruno, I.; Riccio, R.; Ferri, S.; Spampinato, S.; Speroni, E. Polycyclic guanidine alkaloids from the marine sponge *Crambe crambe* and Ca++ channel blocker activity of crambescidin 816. *J. Nat. Prod.* **1993**, *56*, 1007–1015.
108. Croué, J.; West, N.J.; Escande, M.-L.; Intertaglia, L.; Lebaron, P.; Suzuki, M.T. A single betaproteobacterium dominates the microbial community of the crambescidine-containing sponge *Crambe crambe*. *Sci. Rep.* **2013**, *3*, 1–8.
109. Sladic, D.; Gasic, M.J. Reactivity and biological activity of the marine sesquiterpene hydroquinone avarol and related compounds from sponges of the order Dictyoceratida. *Molecules* **2006**, *11*, 1–33.
110. Assmann, M.; Lichte, E.; Pawlik, J.R.; Köck, M. Chemical defenses of the Caribbean sponges *Agelas wiedenmayeri* and *Agelas conifera*. *Mar. Ecol. Prog. Ser.* **2000**, *207*, 255–262.
111. Neeman, I.; Fishelson, L.; Kashman, Y. Isolation of a new toxin from the sponge *Latrunculia magnifica* in the Gulf of Aquaba (Red Sea). *Mar. Biol.* **1975**, *30*, 293–296.
112. Keyzers, R.A.; Davies-Coleman, M.T. Anti-inflammatory metabolites from marine sponges. *Chem. Soc. Rev.* **2005**, *34*, 355–365.
113. Taylor, M.W.; Radax, R.; Steger, D.; Wagner, M. Sponge-associated microorganisms: Evolution, ecology, and biotechnological potential. *Microbiol. Mol. Biol. Rev.* **2007**, *71*, 295–347.
114. Dumdei, E.J.; Blunt, J.W.; Munro, M.H.G.; Battershill, C.N.; Page, M.J. The whys and whats of sponge chemistry: Why chemists extract sponges and what problems does this cause? In *Sponge Sciences. Multidiscipinary Perspectives*; Watanabe, Y., Fusetani, N., Eds.; Springer-Verlag: Tokyo, Japan, 1998; pp. 353–364.
115. Sacristán-Soriano, O.; Banaigs, B.; Casamayor, E.O.; Becerro, M.A. Exploring the links between natural products and bacterial assemblages in the sponge *Aplysina aerophoba*. *Appl. Environ. Microbiol.* **2011**, *77*, 862–870.
116. Rinehart, K.L. Secondary metabolites from marine organisms. *Ciba Found. Symp.* **1992**, *171*, 236–249.

117. Jenssen, H.; Hamill, P.; Hancock, R.E. Peptide antimicrobial agents. *Clin. Microbiol. Rev.* **2006**, *19*, 491–511.
118. Pasupuleti, M.; Schmidtchen, A.; Malmsten, M. Antimicrobial peptides: Key components of the innate immune system. *Crit. Rev. Biotechnol.* **2012**, *32*, 143–171.
119. Mohammed, R.; Peng, J.; Kelly, M.; Hamann, M.T. Cyclic heptapeptides from the Jamaican sponge *Stylissa caribica*. *J. Nat. Prod.* **2006**, *69*, 1739–1744.
120. Matsunaga, S.; Fusetani, N.; Konosu, S. Bioactive marine metabolites, IV. Isolation and the amino acid composition of discodermin A, an antimicrobial peptide, from the marine sponge *Discodermia kiiensis*. *J. Nat. Prod.* **1985**, *48*, 236–241.
121. Otero-González, A.J.; Magalhães, B.S.; Garcia-Villarino, M.; López-Abarrategui, C.; Sousa, D.A.; Dias, S.C.; Franco, O.L. Antimicrobial peptides from marine invertebrates as a new frontier for microbial infection control. *FASEB J.* **2010**, *24*, 1320–1334.
122. Pushpanathan, M.; Gunasekaran, P.; Rajendhran, J. Antimicrobial peptides: Versatile biological properties. *Int. J. Pept.* **2013**, *2013*, doi:10.1155/2013/675391.
123. Cooper, E.L. Comparative immunology. *Integr. Comp. Biol.* **2003**, *43*, 278–280.
124. Brogden, K.A. Antimicrobial peptides: Pore formers or metabolic inhibitors in bacteria? *Nat. Rev. Microbiol.* **2005**, *3*, 238–250.
125. Langenheim, J.H. Higher plant terpenoids: A phytocentric overview of their ecological roles. *J. Chem. Ecol.* **1994**, *20*, 1223–1280.
126. Schmitz, F.J.; Bowden, B.F.; Toth, S.I. Antitumor and cytotoxic compounds from marine organisms. In *Pharmaceutical and Bioactive Natural Products*; Springer: Berlin/Heidelberg, Germany, 1993; pp. 197–308.
127. Zheng, L.; Yan, X.; Han, X.; Chen, H.; Lin, W.; Lee, F.S.; Wang, X. Identification of norharman as the cytotoxic compound produced by the sponge (*Hymeniacidon perleve*)-associated marine bacterium *Pseudoalteromonas* piscicida and its apoptotic effect on cancer cells. *Biotechnol. Appl. Biochem.* **2006**, *44*, 135–142.
128. Folmer, F.; Jaspars, M.; Dicato, M.; Diederich, M. Marine cytotoxins: Callers for the various dances of death. *Gastroenterol. Hepatol. Bed Bench* **2009**, *2*, S34–S50.
129. Bao, B.; Sun, Q.; Yao, X.; Hong, J.; Lee, C.-O.; Cho, H.Y.; Jung, J.H. Bisindole alkaloids of the topsentin and hamacanthin classes from a marine sponge *Spongosorites* sp. *J. Nat. Prod.* **2007**, *70*, 2–8.
130. Luo, X.; Li, F.; Hong, J.; Lee, C.-O.; Sim, C.J.; Im, K.S.; Jung, J.H. Cytotoxic oxylipins from a marine sponge *Topsentia* sp. *J. Nat. Prod.* **2006**, *69*, 567–571.
131. Mansoor, T.A.; Lee, Y.M.; Hong, J.; Lee, C.-O.; Im, K.S.; Jung, J.H. 5,6:8,9-Diepoxy and other cytotoxic sterols from the marine sponge *Homaxinella* sp. *J. Nat. Prod.* **2006**, *69*, 131–134.
132. Nagle, D.G.; Zhou, Y.-D.; Mora, F.D.; Mohammed, K.A.; Kim, Y.-P. Mechanism targeted discovery of antitumor marine natural products. *Curr. Med. Chem.* **2004**, *11*, 1725.
133. Aoki, S.; Cho, S.-H.; Ono, M.; Kuwano, T.; Nakao, S.; Kuwano, M.; Nakagawa, S.; Gao, J.-Q.; Mayumi, T.; Shibuya, M. Bastadin 6, a spongean brominated tyrosine derivative, inhibits tumor angiogenesis by inducing selective apoptosis to endothelial cells. *Anti-Cancer Drugs* **2006**, *17*, 269–278.

134. Singh, R.; Sharma, M.; Joshi, P.; Rawat, D.S. Clinical status of anti-cancer agents derived from marine sources. *Anti-Cancer Agents Med. Chem.* **2008**, *8*, 603–617.
135. Gong, H.; Zuliani, P.; Komuravelli, A.; Faeder, J.R.; Clarke, E.M. Analysis and verification of the HMGB1 signaling pathway. *BMC Bioinform.* **2010**, *11*, S10.
136. Essack, M.; Bajic, V.B.; Archer, J.A. Recently confirmed apoptosis-inducing lead compounds isolated from marine sponge of potential relevance in cancer treatment. *Mar. Drugs* **2011**, *9*, 1580–1606.
137. Valeriote, F.A.; Tenney, K.; Pietraszkiewicz, H.; Edelstein, M.; Johnson, T.A.; Amagata, T.; Crews, P. Discovery and development of anticancer agents from marine sponges: Perspectives based on a chemistry-experimental therapeutics collaborative program. *J. Exp. Ther. Oncol.* **2012**, *10*, 119–134.
138. Ford, P.W.; Gustafson, K.R.; McKee, T.C.; Shigematsu, N.; Maurizi, L.K.; Pannell, L.K.; Williams, D.E.; Dilip de Silva, E.; Lassota, P.; Allen, T.M. Papuamides AD, HIV-inhibitory and cytotoxic depsipeptides from the sponges *Theonella mirabilis* and *Theonella swinhoei* collected in Papua New Guinea. *J. Am. Chem. Soc.* **1999**, *121*, 5899–5909.
139. Qureshi, A.; Faulkner, D.J. Haplosamates A and B: New steroidal sulfamate esters from two haplosclerid sponges. *Tetrahedron* **1999**, *55*, 8323–8330.
140. Müller, W.E.; Sobel, C.; Diehl-Seifert, B.; Maidhof, A.; Schröder, H.C. Influence of the antileukemic and anti-human immunodeficiency virus agent avarol on selected immune responses *in vitro* and *in vivo*. *Biochem. Pharmacol.* **1987**, *36*, 1489–1494.
141. Zhou, X.; Liu, J.; Yang, B.; Lin, X.; Yang, X.-W.; Liu, Y. Marine natural products with anti-HIV activities in the last decade. *Curr. Med. Chem.* **2013**, *20*, 953–973.
142. Aoki, S.; Watanabe, Y.; Sanagawa, M.; Setiawan, A.; Kotoku, N.; Kobayashi, M. Cortistatins A, B, C, and D, anti-angiogenic steroidal alkaloids, from the marine sponge *Corticium simplex*. *J. Am. Chem. Soc.* **2006**, *128*, 3148–3149.
143. Aoki, S.; Watanabe, Y.; Tanabe, D.; Arai, M.; Suna, H.; Miyamoto, K.; Tsujibo, H.; Tsujikawa, K.; Yamamoto, H.; Kobayashi, M. Structure-activity relationship and biological property of cortistatins, anti-angiogenic spongean steroidal alkaloids. *Bioorg. Med. Chem.* **2007**, *15*, 6758–6762.
144. Mousseau, G.; Clementz, M.A.; Bakeman, W.N.; Nagarsheth, N.; Cameron, M.; Shi, J.; Baran, P.; Fromentin, R.; Chomont, N.; Valente, S.T. An analog of the natural steroidal alkaloid cortistatin a potently suppresses tat-dependent hiv transcription. *Cell Host Microbe* **2012**, *12*, 97–108.
145. Andavan, G.S.B.; Lemmens-Gruber, R. Cyclodepsipeptides from marine sponges: Natural agents for drug research. *Mar. Drugs* **2010**, *8*, 810–834.
146. Shin, J.; Rho, J.R.; Seo, Y.; Lee, H.S.; Cho, K.W.; Sim, C.J. Sarcotragins A and B, new sesterterpenoid alkaloids from the sponge *Sarcotragus* sp. *Tetrahedron Lett.* **2001**, *42*, 3005–3007.
147. Santafé, G.; Paz, V.; Rodríguez, J.; Jiménez, C. Novel cytotoxic oxygenated C29 Sterols from the Colombian marine sponge *Polymastia tenax*. *J. Nat. Prod.* **2002**, *65*, 1161–1164.

148. Pattenden, G.; Wickramasinghe, W.A.; Bandaranayake, W.M. Benzylthiocrellidone, a novel thioether with strong UV A and B absorption from the Great Barrier Reef sponge Crella spinulata, (Poecilosclerida: Crellidae). *Trends Comp. Biochem. Physiol.* **2002**, *9*, 205–216.
149. Costantino, V.; Fattorusso, E.; Imperatore, C.; Mangoni, A. Ectyoceramide, the first natural hexofuranosylceramide from the marine sponge *Ectyoplasia ferox*. *Eur. J. Org. Chem.* **2003**, *2003*, 1433–1437.
150. Nakao, Y.; Kuo, J.; Yoshida, W.Y.; Kelly, M.; Scheuer, P.J. More Kapakahines from the marine Sponge *Cribrochalina olemda*. *Org. Lett.* **2003**, *5*, 1387–1390.
151. Volk, C.A.; Kŏck, M. Viscosamine: The first naturally occurring trimeric 3-alkyl pyridinium alkaloid. *Org. Lett.* **2003**, *5*, 3567–3569.
152. Xu, X.-H.; Yao, G.-M.; Li, Y.-M.; Lu, J.-H.; Lin, C.-J.; Wang, X.; Kong, C.-H. 5-Fluorouracil derivatives from the sponge *Phakellia fusca*. *J. Nat. Prod.* **2003**, *66*, 285–288.
153. Costantino, V.; Fattorusso, E.; Imperatore, C.; Mangoni, A. Glycolipids from sponges. 13.1 Clarhamnoside, the first rhamnosylated α-galactosylceramide from *Agelas clathrodes*. Improving spectral strategies for glycoconjugate structure determination. *J. Org. Chem.* **2004**, *69*, 1174–1179.
154. Cichewicz, R.H.; Valeriote, F.A.; Crews, P. Psymberin, a potent sponge-derived cytotoxin from *Psammocinia* distantly related to the pederin family. *Org. Lett.* **2004**, *6*, 1951–1954.
155. Berer, N.; Rudi, A.; Goldberg, I.; Benayahu, Y.; Kashman, Y. Callynormine A, a new marine cyclic peptide of a novel class. *Org. Lett.* **2004**, *6*, 2543–2545.
156. Warabi, K.; Hamada, T.; Nakao, Y.; Matsunaga, S.; Hirota, H.; van Soest, R.W.M.; Fusetani, N. Axinelloside A, an unprecedented highly sulfated lipopolysaccharide inhibiting telomerase, from the marine sponge, *Axinella infundibula*. *J. Am. Chem. Soc.* **2005**, *127*, 13262–13270.
157. Hamada, T.; Matsunaga, S.; Yano, G.; Fusetani, N. Polytheonamides A and B, highly cytotoxic, linear polypeptides with unprecedented structural features, from the marine sponge, *Theonella swinhoei*. *J. Am. Chem. Soc.* **2005**, *127*, 110–118.
158. Williams, D.E.; Austin, P.; Diaz-Marrero, A.R.; Soest, R.V.; Matainaho, T.; Roskelley, C.D.; Roberge, M.; Andersen, R.J. Neopetrosiamides, peptides from the marine sponge *Neopetrosia* sp. that inhibit amoeboid invasion by human tumor cells. *Org. Lett.* **2005**, *7*, 4173–4176.
159. Rogers, E.W.; Molinski, T.F. A cytotoxic carotenoid from the marine sponge *Prianos osiros*. *J. Nat. Prod.* **2005**, *68*, 450–452.
160. Emura, C.; Higuchi, R.; Miyamoto, T. Irciniasulfonic acid B, a novel taurine conjugated fatty acid derivative from a Japanese marine sponge, *Ircinia* sp. *Tetrahedron* **2006**, *62*, 5682–5685.
161. Tanaka, C.; Tanaka, J.; Bolland, R.F.; Marriott, G.; Higa, T. Seragamides A–F, new actin-targeting depsipeptides from the sponge *Suberites japonicus* Thiele. *Tetrahedron* **2006**, *62*, 3536–3542.
162. Fattorusso, E.; Romano, A.; Taglialatela-Scafati, O.; Bavestrello, G.; Bonelli, P.; Calcinai, B. Coelodiol and coeloic acid, ent-isocopalane diterpenes from the Indonesian sponge *Coelocarteria* cfr. *singaporensis*. *Tetrahedron Lett.* **2006**, *47*, 2197–2200.
163. Dai, J.; Liu, Y.; Zhou, Y.-D.; Nagle, D.G. Cytotoxic metabolites from an Indonesian sponge *Lendenfeldia* sp. *J. Nat. Prod.* **2007**, *70*, 1824–1826.

164. Antonov, A.S.; Kalinovsky, A.I.; Stonik, V.A.; Afiyatullov, S.S.; Aminin, D.L.; Dmitrenok, P.S.; Mollo, E.; Cimino, G. Isolation and structures of Erylosides from the Carribean sponge *Erylus formosus*. *J. Nat. Prod.* **2007**, *70*, 169–178.
165. Johnson, T.A.; Amagata, T.; Oliver, A.G.; Tenney, K.; Valeriote, F.A.; Crews, P. The unexpected isolation of CTP-431, a novel thiopyrone from the sponge *Cacospongia mycofijiensis*. *J. Org. Chem.* **2008**, *73*, 7255–7259.
166. Zampella, A.; Sepe, V.; Luciano, P.; Bellotta, F.; Monti, M.C.; D'Auria, M.V.; Jepsen, T.; Petek, S.; Adeline, M.-T.R.S.; Laprévôte, O. Homophymine A, an anti-HIV cyclodepsipeptide from the sponge *Homophymia* sp. *J. Org. Chem.* **2008**, *73*, 5319–5327.
167. Tung, N.H.; Minh, C.V.; Ha, T.T.; Kiem, P.V.; Huong, H.T.; Dat, N.T.; Nhiem, N.X.; Tai, B.H.; Hyun, J.-H.; Kang, H.-K.; *et al*. C29 sterols with a cyclopropane ring at C-25 and 26 from the Vietnamese marine sponge *Ianthella* sp. and their anticancer properties. *Bioorg. Med. Chem. Lett.* **2009**, *19*, 4584–4588.
168. DiGirolamo, J.A.; Li, X.-C.; Jacob, M.R.; Clark, A.M.; Ferreira, D. Reversal of fluconazole resistance by sulfated sterols from the marine sponge *Topsentia* sp. *J. Nat. Prod.* **2009**, *72*, 1524–1528.
169. Salim, A.A.; Rae, J.; Fontaine, F.; Conte, M.M.; Khalil, Z.; Martin, S.; Parton, R.G.; Capon, R.J. Heterofibrins: Inhibitors of lipid droplet formation from a deep-water southern Australian marine sponge, *Spongia* (Heterofibria) sp. *Org. Biomol. Chem.* **2010**, *8*, 3188–3194.
170. Dai, J.; Sorribas, A.; Yoshida, W.Y.; Kelly, M.; Williams, P.G. Xestosaprols from the Indonesian marine sponge *Xestospongia* sp. *J. Nat. Prod.* **2010**, *73*, 1188–1191.
171. Plaza, A.; Keffer, J.L.; Lloyd, J.R.; Colin, P.L.; Bewley, C.A. Paltolides A–C, Anabaenopeptin-type peptides from the Palau sponge *Theonella swinhoei*. *J. Nat. Prod.* **2010**, *73*, 485–488.
172. Wei, X.; Nieves, K.; Rodríguez, A.D. Neopetrosiamine A, biologically active bis-piperidine alkaloid from the Caribbean sea sponge *Neopetrosia proxima*. *Bioorg. Med. Chem. Lett.* **2010**, *20*, 5905–5908.
173. Fan, G.; Li, Z.; Shen, S.; Zeng, Y.; Yang, Y.; Xu, M.; Bruhn, T.; Bruhn, H.; Morschhäuser, J.; Bringmann, G.; Lin, W. Baculiferins A–O, *O*-sulfated pyrrole alkaloids with anti-HIV-1 activity, from the Chinese marine sponge *Iotrochota baculifera*. *Bioorg. Med. Chem.* **2010**, *18*, 5466–5474.
174. Schmitt, S.; Hentschel, U.; Taylor, M.W. Deep sequencing reveals diversity and community structure of complex microbiota in five Mediterranean sponges. *Hydrobiologia* **2012**, *687*, 341–351.
175. Erwin, P.M.; López-Legentil, S.; González-Pech, R.; Turon, X. A specific mix of generalists: Bacterial symbionts in Mediterranean *Ircinia* spp. *FEMS Microbiol. Ecol.* **2012**, *79*, 619–637.
176. Thiel, V.; Leininger, S.; Schmaljohann, R.; Brümmer, F.; Imhoff, J.F. Sponge-specific bacterial associations of the Mediterranean sponge *Chondrilla nucula* (Demospongiae, Tetractinomorpha). *Microb. Ecol.* **2007**, *54*, 101–111.

177. Perdicaris, S.; Vlachogianni, T.; Valavanidis, A. Bioactive natural substances from marine sponges: New developments and prospects for future pharmaceuticals. *Nat. Prod. Chem. Res.* **2013**, *1*, 1–8.
178. Sabdono, A. Microbial symbionts in marine sponges: Marine natural product factory. *J. Coast. Dev.* **2011**, *11*, 57–61.
179. Laird, S.; Monagle, C.; Johnston, S. Queensland biodiscovery collaboration: The Griffith University AstraZeneca Partnership for natural product discovery: An access and benefit sharing case study. In *An Access and Benefit Sharing Case Study*; United Nations University, Institute of Advanced Studies: Yokohama, Japan, 2008.
180. Mittermeier, R.A.; Goettsch Mittermeier, C. *Megadiversity: Earth's Biologically Wealthiest Nations. Megadiversity: Most Biological Rich Countries of the World*; Cemex: San Pedro Garza García, Mexico, 1997.
181. Tolley, M. *UNEP-WCMC World Conservation Monitoring Centre Website*; UNEP: Cambridge, UK, 2011.
182. Butler, A.J.; Rees, T.; Beesley, P.; Bax, N.J. Marine biodiversity in the Australian region. *PLoS One* **2010**, *5*, e11831.
183. Hughes, T.P.; Bellwood, D.R.; Connolly, S.R. Biodiversity hotspots, centres of endemicity, and the conservation of coral reefs. *Ecol. Lett.* **2002**, *5*, 775–784.
184. Roberts, C.M.; McClean, C.J.; Veron, J.E.; Hawkins, J.P.; Allen, G.R.; McAllister, D.E.; Mittermeier, C.G.; Schueler, F.W.; Spalding, M.; Wells, F. Marine biodiversity hotspots and conservation priorities for tropical reefs. *Science* **2002**, *295*, 1280–1284.
185. Wernberg, T.; Russell, B.D.; Moore, P.J.; Ling, S.D.; Smale, D.A.; Campbell, A.; Coleman, M.A.; Steinberg, P.D.; Kendrick, G.A.; Connell, S.D. Impacts of climate change in a global hotspot for temperate marine biodiversity and ocean warming. *J. Exp. Mar. Biol. Ecol.* **2011**, *400*, 7–16.
186. Ward, T.M.; Sorokin, S.J.; Currie, D.R.; Rogers, P.J.; McLeay, L.J. Epifaunal assemblages of the eastern Great Australian Bight: Effectiveness of a benthic protection zone in representing regional biodiversity. *Cont. Shelf Res.* **2006**, *26*, 25–40.
187. Fromont, J.; Vanderklift, M.A.; Kendrick, G.A. *Marine Sponges of the Dampier Archipelago, Western Australia: Patterns of Species Distributions, Abundance and Diversity*; Springer: Berlin/Heidelberg, Germany, 2006; Volume 15, pp. 3731–3750.
188. Hooper, J.; Kennedy, J.A. Small-scale patterns of sponge biodiversity (Porifera) from the Sunshine Coast reefs, eastern Australia. *Invertebr. Syst.* **2002**, *16*, 637–653.
189. Hooper, J.N.; Kennedy, J.A.; Quinn, R.J. Biodiversity "hotspots", patterns of richness and endemism, and taxonomic affinities of tropical Australian sponges (Porifera). *Biodivers. Conserv.* **2002**, *11*, 851–885.
190. Heyward, A.A.; Fromont, J.J.; Schoenberg, C.C.; Colquhoun, J.J.; Radford, B.B.; Gomez, O.O. The sponge gardens of Ningaloo Reef, Western Australia. *Open Mar. Biol.* **2010**, *4*, 3–11.
191. Fromont, J.; Althaus, F.; McEnnulty, F.R.; Williams, A.; Salotti, M.; Gomez, O.; Gowlett-Holmes, K. Living on the edge: The sponge fauna of Australia's southwestern and northwestern deep continental margin. *Hydrobiologia* **2012**, *687*, 127–142.

192. Williams, A.; Althaus, F.; Dunstan, P.K.; Poore, G.C.; Bax, N.J.; Kloser, R.J.; McEnnulty, F.R. Scales of habitat heterogeneity and megabenthos biodiversity on an extensive Australian continental margin (100–1100 m depths). *Mar. Ecol.* **2010**, *31*, 222–236.
193. Evans-Illidge, E.A.; Logan, M.; Doyle, J.; Fromont, J.; Battershill, C.N.; Ericson, G.; Wolff, C.W.; Muirhead, A.; Kearns, P.; Abdo, D. Phylogeny drives large scale patterns in australian marine bioactivity and provides a new chemical ecology rationale for future biodiscovery. *PLoS One* **2013**, *8*, e73800.
194. Dayton, P.K.; Robilliard, G.A.; Paine, R.T.; Dayton, L.B. Biological accommodation in the benthic community at McMurdo Sound, Antarctica. *Ecol. Monogr.* **1974**, *44*, 105–128.
195. Haefner, B. Drugs from the deep: Marine natural products as drug candidates. *Drug Discov. Today* **2003**, *8*, 536–544.
196. Cárdenas, C.A.; Bell, J.J.; Davy, S.K.; Hoggard, M.; Taylor, M.W. Influence of environmental variation on symbiotic bacterial communities of two temperate sponges. *FEMS Microbiol. Ecol.* **2014**, *88*, 516–527.
197. Schmitt, S.; Tsai, P.; Bell, J.; Fromont, J.; Ilan, M.; Lindquist, N.; Perez, T.; Rodrigo, A.; Schupp, P.J.; Vacelet, J. Assessing the complex sponge microbiota: Core, variable and species-specific bacterial communities in marine sponges. *Int. Soc. Micob. Ecol. J.* **2012**, *6*, 564–576.

Production of Avaroferrin and Putrebactin by Heterologous Expression of a Deep-Sea Metagenomic DNA

Masaki J. Fujita and Ryuichi Sakai

Abstract: The siderophore avaroferrin (**1**), an inhibitor of *Vibrio* swarming that was recently identified in *Shewanella algae* B516, was produced by heterologous expression of the biosynthetic gene cluster cloned from a deep-sea sediment metagenomic DNA, together with two analogues, bisucaberin (**2**) and putrebactin (**3**). Avaroferrin (**1**) is a macrocyclic heterodimer of *N*-hydroxy-*N*-succinyl cadaverine (**4**) and *N*-hydroxy-*N*-succinyl-putrescine (**5**), whereas analogues **2** and **3** are homodimers of **4** and **5**, respectively. Heterologous expression of two other related genes from culturable marine bacteria resulted in production of compounds **1**–**3**, but in quite different proportions compared with production through expression of the metagenomic DNA.

Reprinted from *Mar. Drugs*. Cite as: Fujita, M.J.; Sakai, R. Production of Avaroferrin and Putrebactin by Heterologous Expression of a Deep-Sea Metagenomic DNA. *Mar. Drugs* **2014**, *12*, 4799–4809.

1. Introduction

Metagenomics enables genomic DNA to be obtained directly from environmental samples without any microbial isolation and cultivation steps [1]. This method facilitates the isolation of biosynthetic genes from previously unreachable genetic pools, such as uncultivated environmental microorganisms or symbionts of marine invertebrates, which are difficult to culture in most cases [2].

Currently, two major metagenomic approaches are used in the field of marine natural product chemistry: sequence-based and function-based methods (Figure 1). The sequence-based approach targets conserved biosynthetic genes and searches for homologous sequences within a large set of sequence data or mines for genes from a random DNA pool using PCR amplification. This method is highly advantageous for searches involving well-studied gene classes, such as those encoding biosynthetic machineries of polyketides, non-ribosomal peptides, and post-translationally modified ribosomal peptides. Remarkable advances in targeting such genes have been made recently following the development of next-generation sequencing techniques [3–6]. The sequence-based approach has thus become the standard method for mining the enormous biosynthetic gene clusters of marine symbiotic bacteria, which are thought to be responsible for the production of various secondary metabolites of marine invertebrates.

The function-based metagenomic approach involves the isolation of biosynthetic genes from a random metagenomic library using specific selection methods (e.g., biological assays) [2]. The function-based approach relies on the ability of a heterologous host microorganism (*E. coli* in most cases) to produce functional molecules that are detectable by the selection method employed. Therefore, only genes that can produce the final product are selected. To date, several marine metagenomic products have been heterologously produced using this approach, such as halichrome

A and indole-porphyrin hybrids from the marine sponges *Halichondria okadai* [7] and *Discodermia calyx* [8], respectively.

Figure 1. General scheme of metagenomic studies in the field of marine natural product chemistry.

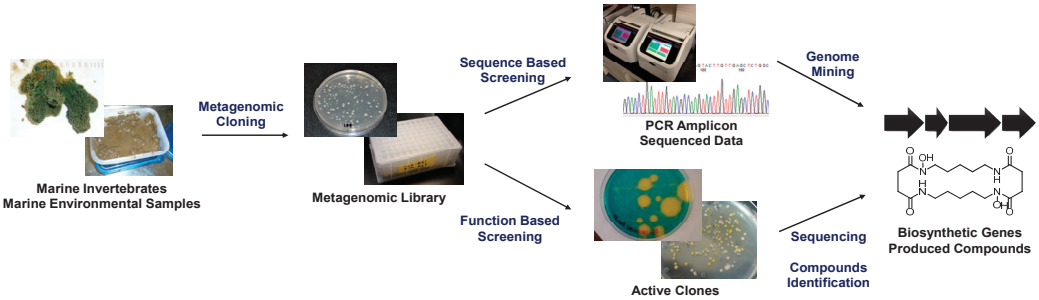

Figure 2. Structures of *N*-hydroxy-*N*-succinyl diamine (HSD)-based siderophores.

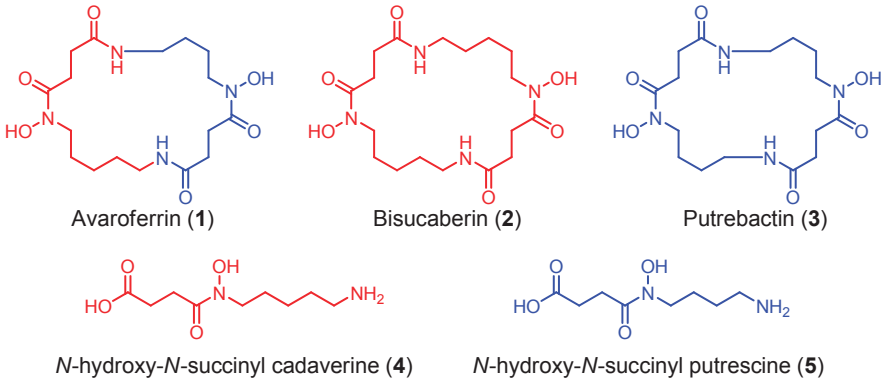

Using a functional metagenomic approach and marine samples, we previously produced several siderophores, including the polycarboxylate-type siderophore vibrioferrin [9] and the hydroxamate-type siderophore bisucaberin (**2**) [10,11], the latter of which is a macrocyclic dimer of *N*-hydroxy-*N*-succinyl cadaverine (**4**, HSC, Figure 2). Recently, we found that the substrate selectivity of the bisucaberin (**2**) biosynthesis enzymes MbsA, B, and C encoded in the cloned metagenomic DNA is broader than would be expected, because both the bisucaberin (**2**) precursor HSC (**4**) and another potential precursor, *N*-hydroxy-*N*-succinyl putrescine (HSP, **5**), were detected in the culture broth of the *mbsA-C* clone [12], suggesting the presence of additional products. We were thus interested in the expandable nature of the marine metagenome, which enables the production of a diverse array of molecules from a single set of genes. Here, we report the results of our detailed analysis of the metabolites from a metagenomic clone and a comparison of the catalytic features of the enzymes with related biosynthetic enzymes from other marine bacteria. Our results demonstrate the potential diversity of the marine metagenome and the usefulness of the function-based approach to analyze genes with unknown functions.

2. Results and Discussion

A gene cluster (*mbsA-D*) encoding enzymes for the biosynthesis of the siderophore bisucaberin (**2**) was cloned from a metagenomic library derived from a deep-sea sediment sample collected off the Tokara Islands [11]. In a previous study, we reported the isolation of **2**, an HSC (**4**) dimer, as the sole product from the cultured clone. We later realized, however, that MbsA, B, and C are capable of supplying not only HSC (**4**) but also HSP (**5**) [12]. This result suggested to us that other macrocyclic products containing HSP (**5**) as a precursor can be biosynthesized from the same gene set. To examine this possibility, the biosynthetic gene cluster *mbsA-D* was again expressed in *E. coli* and the culture broth was analyzed using LC-MS (Figure 3a). We not only found the expected major product, **2**, but also putrebactin (**3**; *m/z* 373) [13], avaroferrin (**1**; *m/z* 387; a heterodimer of HSC (**4**) and HSP (**5**)), bisucaberin B (**7**; *m/z* 419) [14], and three other putative linear intermediates (**6a**, **6b** [*m/z* 405], and **8** [*m/z* 391]). Isolation of macrocyclic compounds **2** and **3** from several marine bacteria was reported decades ago [10,13], whereas compound **1** was isolated from a cultured marine bacterium, *Shewanella algae* B516, only recently during preparation of this manuscript [15]. Compounds **1** and **3** were purified by HPLC and their structures confirmed unambiguously by spectral analysis. This is the first report of the heterologous production of **1** and **3**, and the deep-sea metagenomic clone encoding *MbsA-D* represents the first cluster of avaroferrin (**1**) biosynthetic enzymes thus far experimentally confirmed.

Avaroferrin (**1**) was reported to inhibit the swarming of *Vibrio alginolyticus* B522 [15]. In our previous study, we reported the isolation of **2** as the sole product of the same metagenomic cluster. Our present results, however, clearly show that this gene set can produce more than one siderophore. Differences in the results between those studies are largely due to difference in the isolation and detection method, that is; we purified **2** simply by recrystallization in the previous study, but this time we thoroughly investigated the gene product by utilizing LC-MS, to characterize the versatile nature of the enzymes. The ferric ion-chelating activities of compounds **1**–**3** as determined by a chrome azurol S titration assay [16] were similar (EC_{50} values: 4.0, 3.5, and 4.8 μM, respectively, see Supplementary Information), suggesting that all three compounds function as ferric ion acquisition agents for the original producer.

The present results provide some insights into the functions of the enzymes involved in the biosynthesis of *N*-hydroxy-*N*-succinyl diamine (HSD)-based siderophores. In the previously proposed HSD-based siderophore biosynthesis pathway, the first three enzymes A–C catalyze successive reactions leading from lysine and ornithine to the HSDs [17]. Subsequently, the fourth enzyme D catalyzes both the oligomerization of the HSDs and final macrocyclization. The fact that the MbsA-D enzyme set cloned into *E. coli* produced the cyclic products **1**–**3** and the linear intermediates **6**–**8** simultaneously strongly suggests that MbsD can utilize both **4** and **5** as immediate precursors and condense them in both a homo- and hetero-meric manner. To test this hypothesis, we constructed two fused gene sets, comprising *mbsA-C* plus either $bibC^{C}$ or *pubC*, both of which encode condensation enzymes corresponding to *mbsD* from the biosynthetic systems of **2** [18] and **3** [19] from the siderophore-producing marine bacteria *Aliivibrio salmonicida* LFI1238 and *Shewanella* sp. MR-4, respectively. These chimeric gene clusters allowed for

functional testing of the fourth enzymes, as the metagenomic MbsA-C enzymes would supply the common monomers **4** and **5**, whereas the fourth enzymes would catalyze the oligomerization and macrocyclization of the monomers when expressed in the heterologous host.

Figure 3. Selected ion current LC-MS chromatograms of the culture broths of the marine metagenome-derived *mbsA-D* clone (**a**); fusion gene cluster clones (**b**,**c**); and *Shewanella algae* NBRC103173 (**d**).

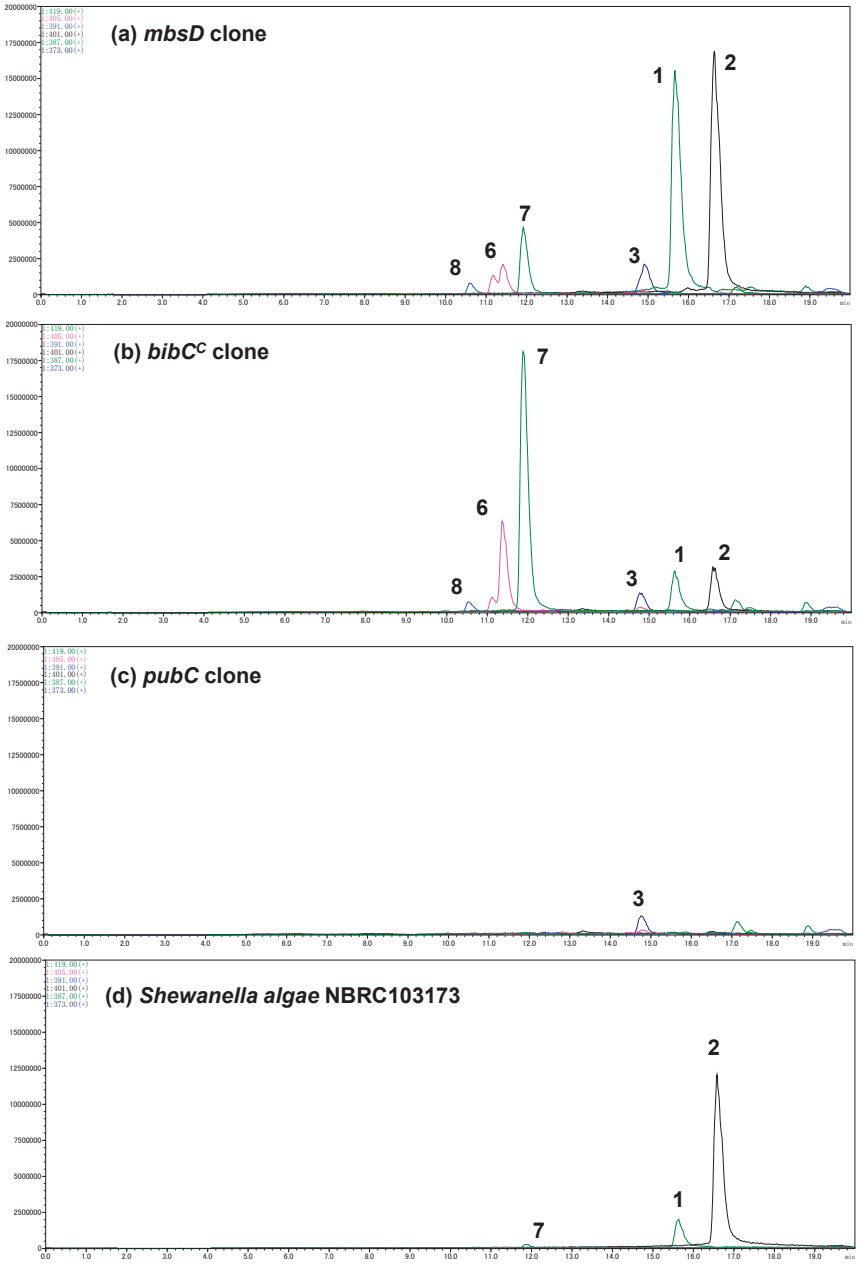

Figure 4. Proposed general scheme for the biosynthesis of HSD-based siderophores (**a**) and composition of their biosynthetic gene clusters (**b**); The fusion gene cluster system involving metagenome-derived *mbsA-C* and *genes D* of other origin is also shown (**c**).

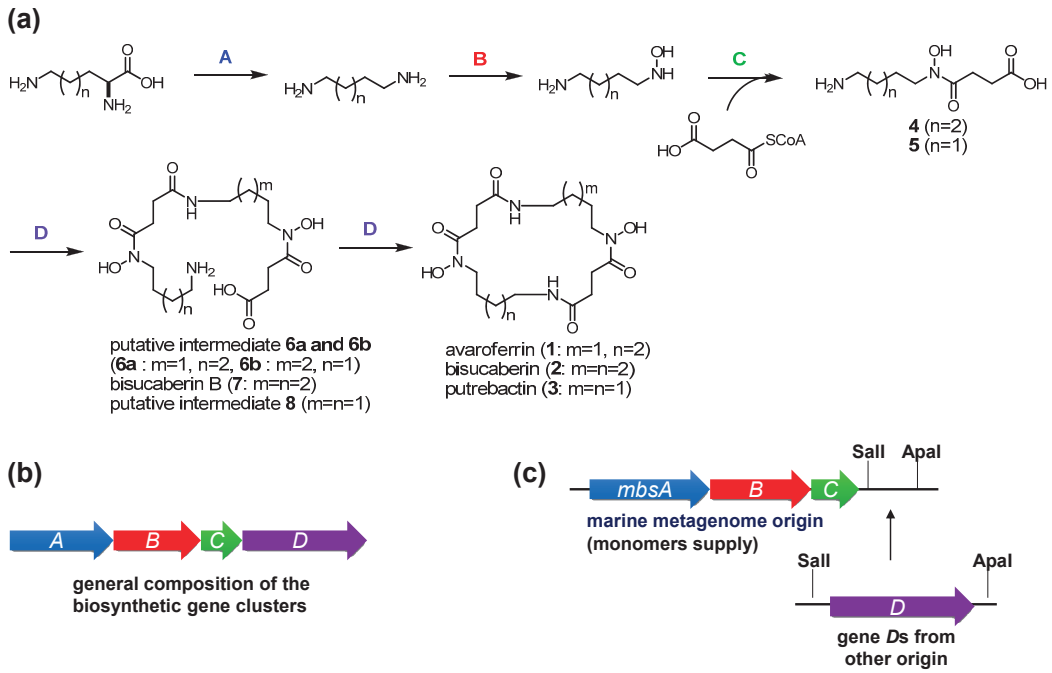

The codon-optimized *bibC*^{C} and *pubC* genes were chemically synthesized and inserted downstream of *mbsC* using the cassette method (Figure 4c). Transformants of these fusion gene clusters were cultured and the supernatants were subjected to LC-MS analysis (Figure 3b,c). The clone containing *bibC*^{C} produced compounds **1** and **2**, together with a small amount of **3**, in a 2:2:1 ratio. However, the major metabolites of this clone were acyclic intermediates (compounds **6**–**8**). Of note, the accumulation of bisucaberin B (**7**) was six-times that of the macrocyclic counterpart **2**. These results suggested that BibC^{C} is also capable of producing avaroferrin (**1**) and putrebactin (**3**), but its macrocyclization activity is not as potent as that of MbsD, at least in the heterologous host *E. coli*. In the case of the *pubC* clone, the most abundant siderophore produced was putrebactin (**3**), and aside from unknown background peaks, no detectable amounts of other metabolites were observed in the LC-MS chromatogram. Overall siderophore production in this case was around 3% compared with that of the *mbsD* and *bibC*^{C} clones, suggesting that the inherent functionality of PubC was not expressed in the heterologous host.

We also analyzed the siderophores from *Shewanella algae* NBRC103173, which is another strain of avaroferrin (**1**)-producing bacterium (Figure 3d). Interestingly, this *S. algae* strain produced mainly bisucaberin (**2**) and a small amount of avaroferrin (**1**) but did not produce detectable amounts of **3**. This production pattern was quite different from that reported for *S. algae* strain B516, which produced compounds **1**–**3** at a 1:2:1 ratio [15]. Although the culture conditions

were not completely the same, one can suggest, judging from the large difference of the production profiles, that these enzyme sets can be one of the keys to add metabolic diversity even within the same species.

The amino acid sequence identity for the three condensation enzymes examined, MbsD, BibC^{C}, and PubC, is around 60%, but it is unclear which amino acid residues are responsible for the differences in enzyme function. In addition, the molecular mechanisms of the enzymatic oligomerization and macrocyclization reactions are still largely unknown. Structural-biological analyses of these enzymes as well as other related biosynthetic pathways are in progress.

The results of the present study demonstrating the production of multiple siderophores by one enzyme system reveal the remarkable versatility of the biosynthetic enzymes of HSD-based siderophores. The unique property of these enzymes might be advantageous to producers in competitive microbial communities. For example, some *Vibrio* species are known to utilize exogenous siderophores produced by other bacteria in the community by expressing siderophore-specific receptors [20]. This phenomenon, termed *siderophore piracy*, may explain discrete differences in the ecological functions of the structurally related siderophores **1**–**3**, and is illustrated by *V. alginolyticus* B522, which is capable of "stealing" **2** and **3** (but not **1**) using specific receptors (siderophore uptake system) [15]. Thus, the ability to produce multiple siderophores could represent a strategy to avoid siderophore piracy. Our study demonstrates that a slight change in the sequence of a siderophore biosynthesis gene can significantly modify the enzyme's properties and thus have a large impact on siderophore production.

The *mbsA-D* metagenomic siderophore biosynthesis gene cluster may have a common ancestor with that of *Shewanella* sp. or related strains, based on sequence similarity with the putative avaroferrin (**1**) biosynthesis gene cluster from *S. algae* B516 [15]. However, the apparent differences in catalytic function of the *mbsA-D* cluster compared with other related enzymes thus far isolated from culturable bacteria demonstrate the power of the function-based metagenomic approach, which may result in the discovery of completely unexpected functions of environmental genomes.

3. Experimental Section

3.1. General Experimental Procedures

Low- and high-resolution ESI mass spectra were measured on an Exactive mass spectrometer (Thermo Scientific, Waltham, MA, USA). NMR spectra were recorded on an ECP-400 NMR spectrometer (JEOL, Tokyo, Japan) at 400 MHz for ^{1}H and 100 MHz for ^{13}C in CD_3OD and DMSO-d_6 (1:1) as a solvent. Chemical shifts of ^{1}H and ^{13}C in NMR spectra were referenced to the solvent peaks: δ_H 3.30 and δ_C 49.0 for CD_3OD. UV absorption in the CAS assay was measured on a SpectraMax M2 microplate reader (Molecular Devices, Sunnyvale, CA, USA). Preparative HPLC was done with a Prominence HPLC system equipped with a photodiode array detector (Shimadzu, Kyoto, Japan). LC-MS analyses were done with an LCMS-8040 LC-MS system equipped with a Prominence HPLC system (Shimadzu). DNA sequences were determined with a BigDye terminator cycle sequencing kit (Thermo Fisher Scientific) and a 3130*xl* Genetic Analyzer (Thermo Fisher Scientific). For DNA cloning, NEB 10-beta-competent *E. coli* cells (New England BioLabs,

Ipswich, MA, USA) were used. Electroporation was done with a MicroPulser electroporator (Bio-Rad, Hercules, CA, USA). Oligo DNAs for cloning and DNA sequencing were purchased from Hokkaido System Science (Sapporo, Japan). A GeneAtlas thermal cycler (Astec, Fukuoka, Japan) and a KOD Plus Neo PCR kit (Toyobo, Osaka, Japan) were used to amplify DNA fragments. All chemicals were purchased from Wako Pure Chemical Industries (Osaka, Japan), Nacalai Tesque (Kyoto, Japan), or Takara Bio (Shiga, Japan) except for those specifically mentioned.

3.2. Construction and Screening of a Metagenomic Library

Detailed methods for construction of a deep sea sediment metagenomic library and cloning of *mbs* gene cluster have been reported in the previous paper [11]. Briefly, deep sea sediment samples were collected by dredging (150–1000 m) and directly poured into flasks containing sterilized sea water, and then vigorously shaken to wash out bacteria cells. The suspension was fractionated by stepwise centrifugation to afford cell pellet. It was washed with TES buffer (20 mM Tris-HCl (pH 8.0), 100 mM EDTA (pH 8.0), 50 mM NaCl, 25% sucrose) and centrifuged, then re-suspended in TES buffer. Cells were lysed with SDS and proteinase K, and then treated with 5 M NaCl aqueous solution and 10% cetyltrimethylammonium bromide (CTAB). The resulting DNA solution was cleaned up by phenol-chloroform treatment, followed by precipitation by addition of isopropanol to afford crude metagenomic DNA. It was size fractionated by agarose gel electrophoresis. The recovered large molecular weight DNA was blunt-ended and ligated into fosmid vector. This was transformed into *E. coli* and plated on the LB agar containing chloramphenicol to construct a metagenomic library. The *mbs* cluster containing clone (*mbsA-D*, DNA Data Bank of Japan; AB643578) was obtained based on the siderophore production activity using chrome azurol S assay [16].

3.3. Artificial Genes

Two artificial genes whose sequence was optimized for *E. coli* expression were chemically synthesized by FASMAC (Kanagawa, Japan). Recognition sites for restriction enzymes SalI and ApaI were added at the 5′ and the 3′ ends, respectively (for sequence, see Supplemental Information).

pubC: 1887 bp DNA fragment encoding 629 amino acids of the putrebactin biosynthetic enzyme PubC (*Shewanella* sp. MR-4; NCBI referenced sequence: YP_733587).

bibC^{C}: 1857 bp DNA fragment encoding 619 amino acids of the C-terminal portion of the biosynthetic enzyme BibC (*Aliivibrio salmonicida* LFI1238; NCBI referenced sequence: YP_002261686).

3.4. Preparation of Siderophore Producing Fusion Gene Cluster Clones

A DNA fragment encoding metagenomic bisucaberin biosynthetic enzymes, MbsA-C, was amplified from the bisucaberin biosynthetic gene cluster from a deep sea metagenome (accession number: AB643578) by PCR using a following primer set: forward, 5′-ACGTCTAGATDGATCGCTCTCAACTCAGCC-3′ and reverse, 5′-TTTGTCGACTCATTGTGTGGCTCCTGTTGC-3′ (underlined sequences show XbaI and SalI

recognition sites, respectively). Polymerase chain reaction was done following the protocol provided by the manufacturer, initial denaturation at 95 °C for 2 min, followed by 30 cycles 30 s at 92 °C, 30 s at 60 °C, and 2.5 min at 72 °C. The amplicon was cut by XbaI and SalI, purified, and ligated into pBCSK+ phagemid vector (Agilent Technologies, Santa Clara, CA, USA) to form a monomers supply clone. Purchased artificial genes, *pubC* and $bibC^{C}$, were digested by SalI and ApaI, then ligated into monomer supply clone downstream of *mbsA-C* with T4 DNA ligase (Takara Bio) to produce the fusion gene clusters. They were transformed into NEB 10-beta-competent *E. coli* cells by electroporation, and then spread onto LB agar plates supplemented with chloramphenicol to obtain the fusion cluster clones (*mbsA-C* + *pubC*, *mbsA-C* + $bibC^{C}$).

3.5. Production and Identification of Avaroferrin and Putrebactin

The metagenome derived *mbsA-D* cluster clone was pre-cultured overnight in LB medium containing chloramphenicol and then inoculated into four 1-L flasks containing 400 mL of LB medium supplemented with 30 μg/mL chloramphenicol and 0.1 mM isopropyl β-thiogalactopyranoside (IPTG). They were incubated at 37 °C for 3 day with shaking at 225 rpm. After centrifugation, the siderophore active molecules in the supernatant were adsorbed onto C18 resin, then eluted with stepwise aqueous-MeOH gradient system (0%–100% MeOH). Fractions eluted with 20%–50% MeOH were combined and fractionated with Sephadex G-10 gel filtration with water. The fraction containing the mixture of siderophores was further separated by Sephadex LH-20 column chromatography with 50% aqueous MeOH to afford siderophore concentrated fraction. A part of the fraction (600 mL culture equivalent) was purified by repetitive C18 reversed phase HPLC (Inertsil ODS-3, GL Sciences, Tokyo) with an aqueous MeOH linear gradient (first HPLC: 20%–60% MeOH, second HPLC: 30%–44% over 30 min) to yield pure avaroferrin (**2**, 6.9 mg from 600 mL).

Putrebactin (**3**) was also isolated in a similar manner to that described above. Total 8.0 L of cultured medium was solid phase extracted with C18 resin, then subjected to the two steps of C18 column chromatography with aqueous MeOH. Compound **3** containing fractions (eluted with 10%–20% MeOH) were combined and subsequently fractionated by a Sephadex G-10 column with water containing 0.2% acetic acid, then C18 HPLC (20%–60% MeOH) to yield putrebactin (**3**, 9.5 mg from 8.0 L)

Avaroferrin (**1**): white amorphous; HR-ESIMS, 409.20543 (calcd. for $C_{17}H_{30}O_6N_4Na$, −0.8 ppm); NMR data (CD_3OD: DMSO-d_6 = 1:1) δ_H 3.65 (t, J = 6.4 Hz, 2H), 3.64 (t, J = 6.4 Hz, 2H), 3.19 (t, J = 6.4 Hz, 4H), 2.77 (t, J = 6.4 Hz, 4H), 2.47 (t, J = 6.4 Hz, 4H), 1.67(quint., J = 7.2 Hz, 4H), 1.52 (m, 4H), 1.34 (m, 2H); δ_C 173.8 (4C), 47.4 (1C)[a], 47.0 (1C), 38.6 (2C)[a], 30.6 (2C), 28.3 (1C), 28.0 (2C), 26.3 (1C), 25.6 (1C), 24.0 (1C), 22.8 (1C) (a: carbon chemical shifts were determined from the HSQC spectrum due to peak overlapping on solvent signals).

Putrebactin (**3**): colorless residue; HR-ESIMS, 395.19011 (calcd. for $C_{16}H_{28}O_6N_4Na$, −0.01 ppm); NMR data (CD_3OD: DMSO-d_6 = 1:1) δ_H 3.63 (t, J = 6.8 Hz, 4H), 3.19 (t, J = 6.8 Hz, 4H), 2.77 (t, J = 6.4 Hz, 4H), 2.46 (t, J = 6.4 Hz, 4H), 1.65 (broad t., J = 6.8 Hz, 4H), 1.52 (m, 4H), (carbon NMR signals were not detected due to too low solubility in any solvents tested).

3.6. LC-MS Analysis

Siderophore producing clones were cultured at 30 °C for 3 day with shaking at 225 rpm in LB medium, containing 30 μg/mL of chloramphenicol and 0.1 mM IPTG. The resulting culture medium was mixed with an equal volume of MeOH, then centrifuged to remove insoluble materials. A portion of the supernatant was analyzed by LC-MS (column, Inertsil ODS-3, 2 × 100 mm; solvents, 0%–60% aqueous-MeOH linear gradient system with 0.2% AcOH; flow rate, 0.2 mL/min; detection, SIM at *m/z* 419, 405, 401, 391, 387, and 373. Marine bacterium *Shewanella algae* NBRC103173 was cultured in the sea water based medium (0.5 g trypton, 0.05 g yeast extract in 1.0 L sea water)) at 30 °C for 3 day with shaking at 225 rpm. Culture broth was subjected to the LC-MS analysis with the same method. Peak area of the mass chromatogram was quantitated using LC-MS solution software (Shimadzu, Kyoto, Japan).

3.7. Chrome Azurol S Assay

Test sample solutions (100 μL) were mixed with equal volume of CAS assay solution (0.6 mM cetyltrimethylammonium bromide, 15 μM $FeCl_3$, 150 mM CAS, 0.5 M anhydrous piperazine, 0.75 M HCl) in a 96 well microplate, and kept at room temperature for 4 h, and then the absorption at 630 nm was measured by microplate reader. Experiments were performed in triplicate.

4. Conclusions

Two additional siderophores, avaroferrin (**1**) and putrebactin (**3**), were heterologously produced together with previously reported bisucaberin (**2**) using a marine metagenome-derived siderophore biosynthesis gene cluster. Compound **1** was only recently identified in a marine bacterium, *Shewanella algae* B516, and was shown to inhibit the swarming behavior of *Vibrio parahaemolyticus* B522. LC-MS analyses of the fusion gene cluster clones revealed that other homologous enzymes can catalyze the production of compound **1**, but the production ratio of compounds **1**–**3** was quite different. These results suggest that a metagenomic approach is a practical way to isolate enzymes with characteristic catalytic properties and that it might be possible to isolate previously unidentified biosynthetic enzymes from uncultivated bacteria.

Acknowledgments

This project was financially supported by JST Special Coordination Funds for Promoting Science and Technology, and JSPS Grant-in-Aid for Scientific Research on Innovative Areas (Biosynthetic Machinery) 25108701.

Author Contributions

Conceived and designed the experiments: MJF, RS. Performed the experiments: MJF. Analyzed the data: MJF, RS. Wrote the paper: MJF, RS.

Conflicts of Interest

The authors declare no conflict of interest.

References

1. Rondon, M.R.; August, P.R.; Bettermann, A.D.; Brady, S.F.; Grossman, T.H.; Liles, M.R.; Loiacono, K.A.; Lynch, B.A.; MacNeil, I.A.; Minor, C.; *et al.* Cloning the soil metagenome: A strategy for accessing the genetic and functional diversity of uncultured microorganisms. *Appl. Environ. Microbiol.* **2000**, *66*, 2541–2547.
2. Kennedy, J.; Flemer, B.; Jackson, S.A.; Lejon, D.P.H.; Morrissey, J.P.; O'Gara, F.; Dobson, A.D.W. Marine metagenomics: New tools for the study and exploitation of marine microbial metabolism. *Mar. Drugs* **2010**, *8*, 608–628.
3. Piel, J.; Hui, D.; Wen, G.; Butzke, D.; Platzer, M.; Fusetani, N.; Matsunaga, S. Antitumor polyketide biosynthesis by an uncultivated bacterial symbiont of the marine sponge theonella swinhoei. *Proc. Natl. Acad. Sci. USA* **2004**, *101*, 16222–16227.
4. Freeman, M.F.; Gurgui, C.; Helf, M.J.; Morinaka, B.I.; Uria, A.R.; Oldham, N.J.; Sahl, H.-G.; Matsunaga, S.; Piel, J. Metagenome mining reveals polytheonamides as posttranslationally modified ribosomal peptides. *Science (Wash.)* **2012**, *338*, 387–390.
5. Wilson, M.C.; Mori, T.; Rueckert, C.; Uria, A.R.; Helf, M.J.; Takada, K.; Gernert, C.; Steffens, U.A.E.; Heycke, N.; Schmitt, S.; *et al.* An environmental bacterial taxon with a large and distinct metabolic repertoire. *Nature (Lond.)* **2014**, *506*, 58–62.
6. Sudek, S.; Lopanik, N.B.; Waggoner, L.E.; Hildebrand, M.; Anderson, C.; Liu, H.; Patel, A.; Sherman, D.H.; Haygood, M.G. Identification of the putative bryostatin polyketide synthase gene cluster from "Candidatus endobugula sertula", the uncultivated microbial symbiont of the marine bryozoan bugula neritina. *J. Nat. Prod.* **2007**, *70*, 67–74.
7. Abe, T.; Kukita, A.; Akiyama, K.; Naito, T.; Uemura, D. Isolation and structure of a novel biindole pigment substituted with an ethyl group from a metagenomic library derived from the marine sponge halichondria okadai. *Chem. Lett.* **2012**, *41*, 728–729.
8. Yang, X.-L.; Wakimoto, T.; Takeshige, Y.; He, R.; Egami, Y.; Awakawa, T.; Abe, I. Indole-porphyrin hybrids produced by metagenomics. *Bioorg. Med. Chem. Lett.* **2013**, *23*, 3810–3813.
9. Fujita, M.J.; Kimura, N.; Sakai, A.; Ichikawa, Y.; Hanyu, T.; Otsuka, M. Cloning and heterologous expression of the vibrioferrin biosynthetic gene cluster from a marine metagenomic library. *Biosci. Biotechnol. Biochem.* **2011**, *75*, 2283–2287.
10. Kameyama, T. Bisucaberin, a new siderophore, sensitizing tumor cells to macrophage-mediated cytolysis. I. Taxonomy of the producing organism, isolation and biological properties. *J. Antibiot.* **1987**, *40*, 1664–1670.
11. Fujita, M.J.; Kimura, N.; Yokose, H.; Otsuka, M. Heterologous production of bisucaberin using a biosynthetic gene cluster cloned from a deep sea metagenome. *Mol. Biosyst.* **2012**, *8*, 482–485.

12. Fujita, M.J.; Sakai, R. Heterologous production of desferrioxamines with a fusion biosynthetic gene cluster. *Biosci. Biotechnol. Biochem.* **2013**, *77*, 2467–2472.
13. Ledyard, K.M.; Butler, A. Structure of putrebactin, a new dihydroxamate siderophore produced by shewanella putrefaciens. *JBIC J. Biol. Inorg. Chem.* **1997**, *2*, 93–97.
14. Fujita, M.J.; Nakano, K.; Sakai, R. Bisucaberin b, a linear hydroxamate class siderophore from the marine bacterium tenacibaculum mesophilum. *Molecules* **2013**, *18*, 3917–3926.
15. Boettcher, T.; Clardy, J. A chimeric siderophore halts swarming vibrio. *Angew. Chem. Int. Ed.* **2014**, *53*, 3510–3513.
16. Schwyn, B.; Neilands, J.B. Universal chemical assay for the detection and determination of siderophores. *Anal. Biochem.* **1987**, *160*, 47–56.
17. Kadi, N.; Oves-Costales, D.; Barona-Gomez, F.; Challis, G.L. A new family of atp-dependent oligomerization-macrocyclization biocatalysts. *Nat. Chem. Biol.* **2007**, *3*, 652–656.
18. Kadi, N.; Song, L.; Challis, G.L. Bisucaberin biosynthesis: An adenylating domain of the bibc multi-enzyme catalyzes cyclodimerization of n-hydroxy-n-succinylcadaverine. *Chem. Commun. (Cambridge, UK)* **2008**, 5119–5121.
19. Kadi, N.; Arbache, S.; Song, L.; Oves-Costales, D.; Challis, G.L. Identification of a gene cluster that directs putrebactin biosynthesis in shewanella species: Pubc catalyzes cyclodimerization of n-hydroxy-n-succinylputrescine. *J. Am. Chem. Soc.* **2008**, *130*, 10458–10459.
20. Kim, C.-M.; Park, Y.-J.; Shin, S.-H. A widespread deferoxamine-mediated iron-uptake system in vibrio vulnificus. *J. Infect. Dis.* **2007**, *196*, 1537–1545.

Additional Evidence of the Trypanocidal Action of (−)-Elatol on Amastigote Forms through the Involvement of Reactive Oxygen Species

Vânia Cristina Desoti, Danielle Lazarin-Bidóia, Daniela Bueno Sudatti, Renato Crespo Pereira, Tania Ueda-Nakamura, Celso Vataru Nakamura and Sueli de Oliveira Silva

Abstract: Chagas' disease, a vector-transmitted infectious disease, is caused by the protozoa parasite *Trypanosoma cruzi*. Drugs that are currently available for the treatment of this disease are unsatisfactory, making the search for new chemotherapeutic agents a priority. We recently described the trypanocidal action of (−)-elatol, extracted from the macroalga *Laurencia dendroidea*. However, nothing has been described about the mechanism of action of this compound on amastigotes that are involved in the chronic phase of Chagas' disease. The goal of the present study was to evaluate the effect of (−)-elatol on the formation of superoxide anions ($O_2^{\bullet-}$), DNA fragmentation, and autophagy in amastigotes of *T. cruzi* to elucidate the possible mechanism of the trypanocidal action of (−)-elatol. Treatment of the amastigotes with (−)-elatol increased the formation of $O_2^{\bullet-}$ at all concentrations of (−)-elatol assayed compared with untreated parasites. Increased fluorescence was observed in parasites treated with (−)-elatol, indicating DNA fragmentation and the formation of autophagic compartments. The results suggest that the trypanocidal action of (−)-elatol might involve the induction of the autophagic and apoptotic death pathways triggered by an imbalance of the parasite's redox metabolism.

Reprinted from *Mar. Drugs*. Cite as: Desoti, V.C.; Lazarin-Bidóia, D.; Sudatti, D.B.; Pereira, R.C.; Ueda-Nakamura, T.; Nakamura, C.V.; de Oliveira Silva, S. Additional Evidence of the Trypanocidal Action of (−)-Elatol on Amastigote Forms through the Involvement of Reactive Oxygen Species. *Mar. Drugs* **2014**, *12*, 4973–4983.

1. Introduction

Chagas' disease is a vector-transmitted infectious disease that is caused by the protozoa parasite *Trypanosoma cruzi*. It affects approximately 10 million individuals in worldwide [1]. This disease is appearing in non-endemic areas, because of immigration, through non-vectorial transmission mechanisms, such as congenital, blood transfusion and organs donation [2]. In turn, it is appearing in endemic countries mainly through of foodborne transmission, which have attracted great attention [3]. The available therapies for this infection are based on two nitroheterocyclics, nifurtimox and benznidazole, that are unsatisfactory because they present low efficacy, with cure rates of 60% in the acute phase and only 10%–20% in the chronic phase of the disease [4]. Additionally, serious toxic side effects are associated with nifurtimox and benznidazole [4,5] with prolonged treatment [6]. Thus, the search for new chemotherapeutic agents is a priority.

Numerous compounds have been studied for the treatment of Chagas' disease [7]. For example, the literature presents studies of extracts and pure compounds obtained from marine algae with

trypanocidal activity [8–10], but little is known about the biochemical alterations induced by them. We recently described the trypanocidal mechanism of action of (−)-elatol, a halogenated sesquiterpene extracted from the red macroalga *Laurencia dendroidea* (Figure 1), collected on the Brazilian coast, on trypomastigote forms of *T. cruzi* [11]. However, nothing has been described about the mechanism of action of this compound on amastigote forms that are involved in the chronic phase of Chagas' disease. Both forms, trypomastigotes (nonreplicative) and amastigotes (replicative), are infective forms found in the vertebrate host [12].

Figure 1. Chemical structure of (−)-elatol (**A**), the halogenated sesquiterpene extracted from the red macroalga *Laurencia dendroidea* (**B**).

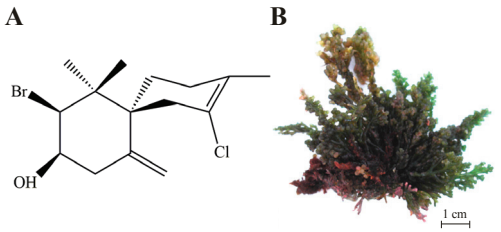

Considering the trypanocidal activity of (−)-elatol and lack of information on the mechanism of action in amastigote forms of *T. cruzi*, the present study provides data on the probable mode of trypanocidal action. Based on the ultrastructural alterations observed in intracellular amastigotes treated with (−)-elatol [10] and autophagic compartments and DNA fragmentation observed herein, we conclude that amastigotes treated with (−)-elatol died through autophagic and apoptotic processes. Our results provide further insights into the mechanism of action of (−)-elatol, strongly suggesting that (−)-elatol may be an effective treatment for Chagas' disease with remarkable trypanocidal action against the amastigote forms of *T. cruzi*.

2. Results and Discussion

Natural products have proven to be valuable sources of new therapeutic agents that act against infectious and noninfectious diseases by providing an alternative to conventional treatments [7]. However, few studies of marine natural products have been conducted, despite the fact that marine algae have been used in traditional remedies in many Asian countries [13]. These natural products hold great promise. For example, bioactive compounds [14–16], such as the halogenated sesquiterpene (−)-elatol from *Laurencia dendroidea*, have significant biological activities. Some studies have demonstrated the chemotherapeutic properties of this compound, including antibacterial [17–19] and antiprotozoal activity [10,20], especially in the amastigote forms of *T. cruzi* [10]. Therefore, we sought to delineate the putative mechanism of action of (−)-elatol in amastigote forms.

Based on our previous results obtained with trypomastigotes treated with (−)-elatol [11], we evaluated the production of superoxide anions ($O_2^{\bullet-}$), a reactive species of oxygen (ROS). The production of this radical was measured using a highly sensitive fluorimetric assay in mitochondria of the amastigote forms of *T. cruzi* treated with (−)-elatol. As shown in Figure 2, (−)-elatol

significantly increased $O_2^{\bullet-}$ production at all concentrations of (−)-elatol tested over 3 h compared with untreated cells. A 60% increase was observed in higher concentration compared with the negative control. The positive control with antimicyn A also increased mitochondrial $O_2^{\bullet-}$ production (data not shown).

Figure 2. Mitochondrial $O_2^{\bullet-}$ production in amastigote forms of *Trypanosoma cruzi* treated with 3, 15, and 30 μM (−)-elatol for up to 3 h using the fluorescent probe MitoSOX. At the indicated times, amastigotes were used to fluorimetrically measure oxidized MitoSOX (oxMitoSOX). The results are expressed in arbitrary units (mean ± SD of at least three independent experiments). * $p \leq 0.05$, significant differences relative to the negative control (untreated cells; two-way analysis of variance followed by Tukey *post hoc* test).

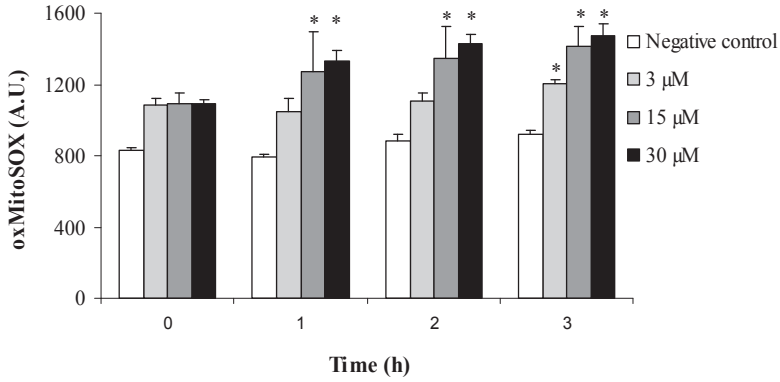

The increase in $O_2^{\bullet-}$ production, induced by (−)-elatol, might induce radical reactions triggering a cascade of damage, such as a break in DNA that is a hallmark of apoptotic death [21]. The apoptotic process is associated with signaling cascades involving mitochondria (intrinsic pathway) or death receptors (extrinsic pathway) [22]. In both pathways ROS can act as signaling molecules [23]. As shown in Figure 3, bright fluorescence, indicating DNA fragmentation, was observed in amastigote forms treated with 1.5 and 3 μM (−)-elatol for 24 h and subjected to the TUNEL assay (Figure 3D,F, respectively). The untreated control was TUNEL-negative (Figure 3B). Additionally, bright fluorescence was observed with actinomycin D, a known inducer of apoptosis (data not shown).

Based on our previous work that showed extensive vacuolization in the amastigote and trypomastigote forms of *T. cruzi* treated with (−)-elatol, demonstrated by transmission electron microscopy and fluorescence microscopy, respectively [10,11], we assessed whether autophagy is an alternative pathway to cell death induced by (−)-elatol in amastigote forms. Autophagy is a mechanism that involves degradation of unnecessary or dysfunctional cellular molecules through the actions of lysosomes/vacuole [24]. The cellular damage might be result from the high levels of ROS that can oxidize macromolecules [25]. Thus, we evaluated autophagy in amastigotes treated with (−)-elatol and stained with monodansylcadaverine, a fluorescent marker that accumulates in autophagic vacuoles [26]. Figure 4 shows the presence of fluorescent, rounded structures in cells treated with (−)-elatol, indicating the formation of autophagic compartments (Figure 4D,F), in

contrast to untreated cells (Figure 4B). This effect could be partially prevented in amastigotes that were pretreated with wortmannin (Figure 4H).

Figure 3. DNA fragmentation in amastigote forms of *Trypanosoma cruzi* treated with (−)-elatol for 24 h using TUNEL assay. The gray column is differential interference contrast (DIC), and the black column is fluorescence. Untreated amastigote forms (**A** and **B**). Amastigote forms treated with 1.5 μM (−)-elatol (**C** and **D**). Amastigote forms treated with 3 μM (−)-elatol (**E** and **F**). Scale bar = 10 μM.

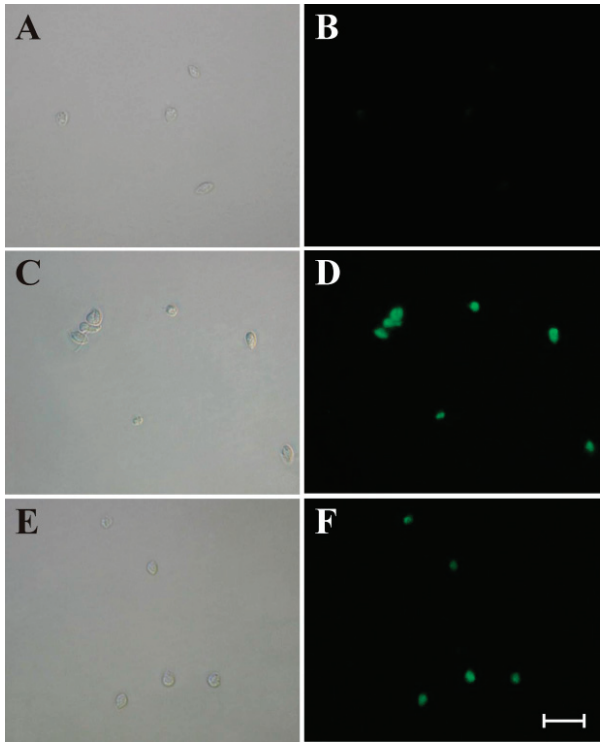

The results presented above indicate that (−)-elatol induces alterations that might be responsible for two types of cell death, apoptosis (demonstrated by DNA fragmentation; type I programmed cell death [PCD]) [27,28] and autophagy (demonstrated by the formation of autophagic vacuoles; type II PCD) [28], in amastigote forms of *T. cruzi*. Apoptosis has several classic characteristics, such as DNA fragmentation, which is one of the final steps in the apoptotic process [21,23]. Autophagy is characterized by an increase in cytoplasmic vacuolization [29,30]. Both cell death pathways have been well described for trypanosomatids, with significant mitochondrion and ROS participation [31,32]. However, independent of the pathway, (−)-elatol affected mitochondrial function by increasing mitochondrial $O_2^{\bullet-}$ production. Reactive oxygen species might trigger biochemical alterations that lead to cell death. Interestingly, the evidence suggests that the transition from apoptosis or autophagy is associated with excessive mitochondrial ROS production [33,34].

Figure 4. Autophagic compartments in amastigote forms of *Trypanosoma cruzi* treated with (−)-elatol for 24 h and stained with monodansylcadaverine. The gray column is differential interference contrast (DIC), and the black column is fluorescence. Untreated amastigote forms (**A** and **B**). Amastigote forms treated with 1.5 μM (−)-elatol (**C** and **D**). Amastigote forms treated with 3 μM (−)-elatol (**E** and **F**). Amastigote forms treated with 3 μM (−)-elatol + 500 nM wortmannin (**G** and **H**). Scale bar = 10 μM.

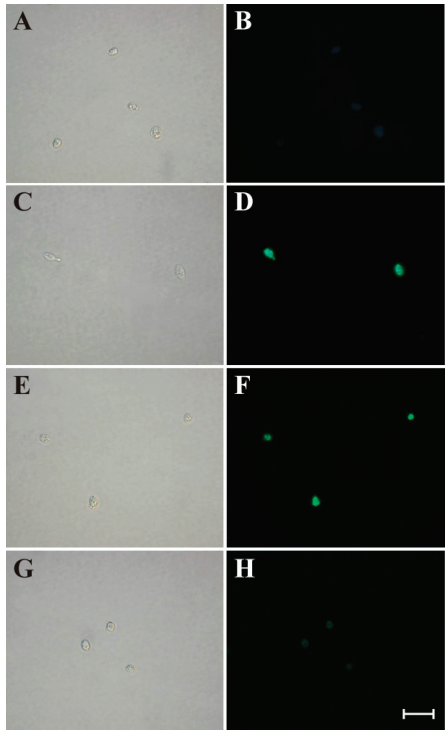

3. Experimental Section

3.1. Chemicals and Materials

Actinomycin D, antimycin A, dimethylsulfoxide, monodansylcadaverine, and wortmannin were purchased from Sigma-Aldrich (St. Louis, MO, USA). Dulbecco's modified Eagle's medium (DMEM) and fetal bovine serum (FBS) were obtained from Invitrogen (Grand Island, NY, USA). The MitoSOX and TUNEL kits were obtained from Invitrogen (Eugene, OR, USA). All of the other reagents were analytical-grade.

3.2. Isolation of (−)-Elatol from L. dendroidea

The halogenated sesquiterpene (−)-elatol was isolated from specimens of the red macroalga *L. dendroidea* collected by hand during low tide in the midlittoral zone on the rocky coast of Cabo Frio Island (22°59′ S, 42°59′ W), Rio de Janeiro State, Brazil. The seaweed was transported to the laboratory between moist paper sheets inside individual plastic bags that were placed in coolers.

These specimens were dried in the dark at room temperature to avoid photolysis and thermal degradation. Dr. Mutue Toyota Fujii identified the specimens of *L. dendroidea* used in this study, and voucher specimens were deposited in the herbaria SP, Instituto de Botânica, São Paulo State, Brazil (SP no. 399789).

The freeze-dried algal material (300 g) yielded 50 mg (−)-elatol through successive and exhaustively extraction in *n*-hexane at room temperature for 15 days. The solvent was eliminated in a rotary evaporator at low temperature (<50 °C), yielding 3.64 g of a dark green extract that contained the sesquiterpene (−)-elatol, which was detected as a blue spot on TLC plates after spraying with a solution of ceric sulfate and sulfuric acid (2.1 g $Ce_2[SO_4]_3 \cdot 4H_2O$, 21 mL H_2SO_4, and 300 mL H_2O), followed by heating at 100 °C for 3 min. An aliquot of the extract (0.35 g) was subjected to preparative thin-layer chromatography (PTLC; Merck; silica gel 60 F_{254}, 20 × 20 cm, mobile phase: *n*-hexane:ethyl acetate [8:2]), to yield a yellowish oil (50 mg) that was identified as the sesquiterpene (−)-elatol. The purity was confirmed by TLC (R_f = 0.45) using *n*-hexane:AcOEt (8:2) as the mobile phase and ^{1}H-NMR spectroscopy (300 MHz), and comparisons were made with the literature [35].

(−)-Elatol stock solutions (1 mg/mL) were prepared in dimethylsulfoxide (DMSO). All of the groups (including controls) were tested at final concentrations of less than 1% DMSO, which has no effect on amastigotes (data not shown). The concentrations of (−)-elatol used in the assays were equal to and above 50% inhibitory concentration (IC_{50}) value [10].

3.3. Parasites and Cells

All of the experiments were performed using the Y strain of *T. cruzi*. Amastigote forms were obtained from the supernatants of previously infected monolayers of $LLCMK_2$ cells (epithelial cells of monkey kidney [*Macaca mulatta*]; CCL-7; American Type Culture Collection, Rockville, MD, USA) in DMEM supplemented with 2 mM L-glutamine, 10% FBS, and 50 mg/L gentamicin and buffered with sodium bicarbonate in a 5% CO_2 air mixture at 37 °C.

3.4. Fluorimetric Detection of Mitochondrion-Derived $O_2^{\bullet-}$

The mitochondrial production of $O_2^{\bullet-}$ was evaluated during exposure of the amastigotes to 3, 15 and 30 μM of (−)-elatol using the fluorescent $O_2^{\bullet-}$-sensitive, mitochondrial-targeted probe MitoSOX (3,8-phenanthridinediamine,5-[6-triphenylphosphoniumhexyl]-5,6-dihydro-6-phenyl). Amastigotes (2×10^7 cells/mL) were preloaded with 5 μM MitoSOX for 10 min at room temperature and then washed with Krebs-Henseleit buffer (pH 7.3) that contained 15 mM $NaHCO_3$, 5 mM KCl, 120 mM NaCl, 0.7 mM Na_2HPO_4, and 1.5 mM NaH_2PO_4 before the assays. Loaded cells were exposed to different concentrations of (–)-elatol. After different times (0–3 h), fluorescence was measured in a fluorescence microplate reader (Victor X3, PerkinElmer) at λ_{ex} = 510 nm and λ_{em} = 580 nm. Oxidized MitoSOX becomes highly fluorescent upon binding to nucleic acids. In some of the experiments, the cells were exposed to 10 μM antimycin A, which is known to induce mitochondrial $O_2^{\bullet-}$ production [36].

3.5. Evaluation of DNA Fragmentation

DNA fragmentation was evaluated *in situ* using terminal deoxynucleotide transferase dUTP nick-end labeling (TUNEL). Amastigote forms (1×10^7 cells/mL) were treated with 1.5 and 3 μM (−)-elatol for 24 h at 37 °C after the cells were subjected to the TUNEL assay according to the manufacturer's instructions. The compound actinomycin D (20 mM) was used as a positive control. Cells that undergo DNA double-strand ruptures should fluoresce brightly, unlike untreated cells. Fluorescence was observed in a fluorescence microscope Olympus BX51 (Olympus®, Tokyo, Japan) at λ_{ex} = 495 nm and λ_{em} = 519 nm, and images were captured with a UC30 camera (Olympus®).

3.6. Evaluation of Autophagic Compartments

Autophagic compartments were evaluated using monodansylcadaverine labeling [37]. Amastigote forms (1×10^7 cells/mL) were treated with 1.5 and 3 μM (−)-elatol for 24 h at 37 °C. The cells were then incubated with 0.05 mM monodansylcadaverine in phosphate-buffered saline (PBS) for 15 min at 37 °C. After incubation, the cells were washed in PBS two times. Monodansylcadaverine staining was analyzed using a fluorescence microscope Olympus BX51 (Olympus®) at λ_{ex} = 380 nm and λ_{em} = 525 nm, and images were captured with a UC30 camera (Olympus®). In some of the experiments, the cells were pretreated with 500 nM wortmannin before the induction of autophagy. The compound is a potent phosphatidylinositol 3-kinase (PI3K) inhibitor, an enzyme that is involved in autophagy regulation [38].

3.7. Statistical Analysis

The data shown in the graphs are expressed as the mean ± standard deviation of at least three independent experiments. The data were analyzed using two-way analysis of variance (ANOVA), and significant differences among means were identified using the Tukey *post hoc* test. Values of $p \leq 0.05$ were considered statistically significant. The statistical analyses were performed using Statistica software.

4. Conclusions

In summary, the present study provided further insights into the effects of (–)-elatol on amastigote forms of *T. cruzi* in an attempt to find new and specific therapies for Chagas' disease. (–)-Elatol might be an effective compound for further *in vivo* analysis and may be a prototypical compound for the development of synthetic derivatives that may be used to treat this infection that affects millions of people in Latin America.

Acknowledgments

This work was supported by grants from the Conselho Nacional de Desenvolvimento Científico e Tecnológico (CNPq), Capacitação de Aperfeiçoamento de Pessoal de Nível Superior (CAPES), Financiadora de Estudos e Projetos (FINEP), Programa de Núcleos de Excelência (PRONEX/Fundação Araucária), Programa de Pós-Graduação em Ciências Farmacêuticas da

Universidade Estadual de Maringá, Complexo de Centrais de Apoio a Pesquisa (COMCAP-UEM), and Fundação de Amparo à Pesquisa do Estado do Rio de Janeiro (FAPERJ).

Author Contributions

Conceived and designed the experiments: V.C.D., D.L.-B., D.B.S, R.C.P and S.O.S. Performed the experiments: V.C.D., D.L.-B. and D.B.S. Analyzed the data: V.C.D., D.L.-B., D.B.S, R.C.P., C.V.N. and S.O.S. Contributed reagents/materials/analysis tools: R.C.P., T.U.-N., C.V.N and S.O.S. Collected the macroalga: D.B.S and R.C.P. Wrote the paper: V.C.D., D.L.-B., D.B.S, R.C.P., C.V.N. and S.O.S.

Conflicts of Interest

The authors declare no conflict of interest.

References

1. World Health Organization (WHO). *First WHO Report on Neglected Tropical Diseases: Working to Overcome the Global Impact of Neglected Tropical Diseases*; WHO: Geneva, Switzerland, 2010. Available online: http://whqlibdoc.who.int/publications/2010/9789241564090_eng.pdf (accessed on 10 December 2013).
2. Rassi, A., Jr.; Rassi, A.; Marin-Neto, J.A. Chagas' disease. *Lancet* **2010**, *375*, 1388–1402.
3. Pereira, K.S.; Schmidt, F.L.; Guaraldo, A.M.A.; Franco, R.M.B.; Dias, V.L.; Passos, L.A.C. Chagas' disease as a foodborne illness. *J. Food Prot.* **2009**, *72*, 441–446.
4. Coura, J.R.; Castro, S.L. A critical review on Chagas' disease chemotherapy. *Mem. Inst. Oswaldo Cruz* **2002**, *97*, 3–24.
5. Coura, J.R. Present situation and new strategies for Chagas' disease chemotherapy: A proposal. *Mem. Inst. Oswaldo Cruz* **2009**, *104*, 549–554.
6. Izumi, E.; Morello, L.G.; Ueda-Nakamura, T.U.; Yamada-Ogatta, S.F.; Dias Filho, B.P.; Cortez, D.A.G.; Ferreira, I.C.P.; Morgado-Díaz, J.A.; Nakamura, C.V. *Trypanosoma cruzi*: Antiprotozoal activity of parthenolide obtained from *Tanacetum parthenium* (L.) Schultz Bip. (Asteraceae, Compositae) against epimastigote and amastigote forms. *Exp. Parasitol.* **2008**, *118*, 324–330.
7. Izumi, E.; Ueda-Nakamura, T.; Dias Filho, B.P.; Veiga-Júnior, V.F.; Nakamura, C.V. Natural products and Chagas' disease: A review of plant compounds studied for activity against *Trypanosoma cruzi*. *Nat. Prod. Rep.* **2011**, *28*, 809–823.
8. Nara, T.; Kamei, Y.; Tsubouchi, A.; Annoura, T.; Hirota, K.; Iizumi, K.; Dohmoto, Y.; Ono, T.; Aoki, T. Inhibitory action of marine algae extracts on the *Trypanosoma cruzi* dihydroorotate dehydrogenase activity and on the protozoan growth in mammalian cells. *Parasitol. Int.* **2005**, *54*, 59–64.

9. Spavieri, J.; Allmendinger, A.; Kaiser, M.; Casey, R.; Hingley-Wilson, S.; Lalvani, A.; Guiry, M.D.; Blunden, G.; Tasdemir, D. Antimycobacterial, antiprotozoal and cytotoxic potential of twenty-one brown algae (Phaeophyceae) from British and Irish waters. *Phytother. Res.* **2010**, *24*, 1724–1729.
10. Veiga-Santos, P.; Pelizzaro-Rocha, K.J.; Santos, A.O.; Ueda-Nakamura, T.; Dias Filho, B.P.; Silva, S.O.; Sudatti, D.B.; Bianco, E.M.; Pereira, R.C.; Nakamura, C.V. *In vitro* antitrypanosomal activity of elatol isolated from red seaweed *Laurencia dendroidea*. *Parasitology* **2010**, *137*, 1661–1670.
11. Desoti, V.C.; Lazarin-Bidóia, D.; Sudatti, D.B.; Pereira, R.C.; Alonso, A.; Ueda-Nakamura, T.; Dias Filho, B.P.; Nakamura, C.V.; Silva, S.O. Trypanocidal action of (−)-elatol involves an oxidative stress triggered by mitochondria dysfunction. *Mar. Drugs* **2012**, *10*, 1631–1646.
12. De Souza, W.; de Carvalho, T.M.; Barrias, E.S. Review on *Trypanosoma cruzi*: Host cell interaction. *Int. J. Cell Biol.* **2010**, *2010*, 1–18.
13. Wang, B.-G.; Zhang, W.-W.; Duan, X.-J.; Li, X.-M. *In vitro* antioxidative activities of extract and semi-purified fractions of the marine red alga, *Rhodomela confervoides* (Rhodomelaceae). *Food Chem.* **2009**, *113*, 1101–1105.
14. Chatter, R.; Othman, R.B.; Rabhi, S.; Kladi, M.; Tarhouni, S.; Vagias, C.; Roussis, V.; Guizani-Tabbane, L.; Kharrat, R. *In vivo* and *in vitro* anti-inflammatory activity of neorogioltriol, a new diterpene extracted from the red algae *Laurencia glandulifera*. *Mar. Drugs* **2011**, *9*, 1293–1306.
15. Pacheco, F.C.; Villa-Pulgarin, J.A.; Mollinedo, F.; Martín, M.N.; Fernández, J.J.; Daranas, A.H. New polyether triterpenoids from *Laurencia viridis* and their biological evaluation. *Mar. Drugs* **2011**, *9*, 2220–2235.
16. Liang, Y.; Li, X.-M.; Cui, C.-M.; Li, C.-S.; Sun, H.; Wang, B.-G. Sesquiterpene and acetogenin derivatives from the marine red alga *Laurencia okamurai*. *Mar. Drugs* **2012**, *10*, 2817–2825.
17. Vairappan, C.S.; Daitoh, M.; Suzuki, M.; Abe, T.; Masuda, M. Antibacterial halogenated metabolites from the Malaysian *Laurencia* species. *Phytochemistry* **2001**, *58*, 291–297.
18. Vairappan, C.S. Potent antibacterial activity of halogenated metabolites from Malaysian red algae, *Laurencia majuscule* (Rhodomelaceae, Ceramiales). *Biomol. Eng.* **2003**, *20*, 255–259.
19. Paradas, W.C.; Salgado, L.T.; Sudatti, D.B.; Crapez, M.A.; Fujii, M.T.; Coutinho, R.; Pereira, R.C.; Amado Filho, G.M. Induction of halogenated vesicle transport in cells of the red seaweed *Laurencia obtusa*. *Biofouling* **2010**, *26*, 277–286.
20. Santos, A.O.; Veiga-Santos, P.; Ueda-Nakamura, T.; Dias Filho, B.P.; Sudatti, D.B.; Bianco, E.M.; Pereira, R.C.; Nakamura, C.V. Effect of elatol, isolated from red seaweed *Laurencia dendroidea* on *Leishmania amazonensis*. *Mar. Drugs* **2010**, *8*, 2733–2743.
21. Kroemer, G.; Galluzzi, L.; Vandenabeele, P.; Abrams, J.; Alnemri, E.S.; Baehrecke, E.H.; Blagosklonny, M.V.; El-Deiry, W.S.; Golstein, P.; Green, D.R.; *et al.* Classification of cell death recommendations of the Nomenclature Committee on Cell Death 2009. *Cell Death Differ*. **2009**, *16*, 3–11.

22. Igney, F.H.; Krammer, P.H. Death and anti-death: Tumour resistance to apoptosis. *Nat. Rev. Cancer* **2002**, *2*, 277–288.
23. Mignotte, B.; Vayssiere, J.-L. Mitochondria and apoptosis. *Eur. J. Biochem.* **1998**, *252*, 1–15.
24. Klionsky, D.J.; Emr, S.D. Autophagy as a regulated pathway of cellular degradation. *Science* **2000**, *290*, 1717–1721.
25. Ba, X.; Gupta, S.; Davidson, M.; Garg, N.J. *Trypanosoma cruzi* induces the reactive oxygen species-PARP-1-RelA pathway for up-regulation of cytokine expression in cardiomyocytes. *J. Biol. Chem.* **2010**, *285*, 11596–11606.
26. Biederbick, A.; Kern, H.F.; Elsasser, H.P. Monodansylcadaverine (MDC) is a specific *in vivo* marker for autophagic vacuoles. *Eur. J. Cell Biol.* **1995**, *66*, 3–14.
27. Samuilov, V.D.; Oleskin, A.V.; Lagunova, E.M. Programmed cell death. *Biochemistry Mosc.* **2000**, *65*, 873–887.
28. Kanzawa, T.; Kondo, Y.; Ito, H.; Kondo, S.; Germano, I. Induction of autophagic cell death in malignant glioma cells by arsenic trioxide. *Cancer Res.* **2003**, *63*, 2103–2108.
29. Tsujimoto, Y.; Shimizu, S. Another way to die: Autophagic programmed cell death. *Cell Death Differ.* **2005**, *12*, 1528–1534.
30. Jiménez-Ruiz, A.; Alzate, J.F.; MacLeod, E.T.; Lüder, C.G.; Fasel, N.; Hurd, H. Apoptotic markers in protozoan parasites. *Parasit. Vectors* **2010**, *3*, 1–15.
31. Menna-Barreto, R.F.S.; Salomão, K.; Dantas, A.P.; Santa-Rita, R.M.; Soares, M.J.; Barbosa, H.S.; de Castro, S.L. Different cell death pathways induced by drugs in *Trypanosoma cruzi*: An ultrastructural study. *Micron* **2009**, *40*, 157–168.
32. Smirlis, D.; Duszenko, M.; Jiménez-Ruiz, A.; Scoulica, E.; Bastien, P.; Fasel, N.; Soteriadou, K. Targeting essential pathways in trypanosomatids gives insights into protozoan mechanisms of cell death. *Parasit. Vectors* **2010**, *3*, 1–15.
33. Addabbo, F.; Montagnani, M.; Goligorsky, M.S. Mitochondria and reactive oxygen species. *Hypertension* **2009**, *53*, 885–892.
34. Kaminskyy, V.O.; Zhivotovsky, B. Free radicals in cross talk between autophagy and apoptosis. *Antioxid. Redox Signal.* **2014**, in press.
35. Konig, G.M.; Wright, A.D. Sesquiterpene content of the antibacterial dichlormethane extract of the red alga *Laurencia obtusa*. *Planta Med.* **1997**, *63*, 186–187.
36. Piacenza, L.; Irigoin, F.; Alvarez, M.N.; Peluffo, G.; Taylor, M.C.; Kelly, J.M.; Wilkinson, S.R.; Radi, R. Mitochondrial superoxide radicals mediate programmed cell death in *Trypanosoma cruzi*: Cytoprotective action of mitochondrial iron superoxide dismutase overexpression. *Biochem. J.* **2007**, *403*, 323–334.
37. Munafó, D.B.; Colombo, M.I. A novel assay to study autophagy: Regulation of autophagosome vacuole size by amino acid deprivation. *J. Cell Sci.* **2001**, *114*, 3619–3629.
38. Wymann, M.P.; Bulgarelli-Leva, G.; Zvelebil, M.J.; Pirola, L.; Vanhaesebroeck, B.; Waterfield, M.D.; Panayotou, G. Wortmannin inactivates phosphoinositide 3-kinase by covalent modification of Lys-802, a residue involved in the phosphate transfer reaction. *Mol. Cell Biol.* **1996**, *16*, 1722–1733.

MDPI AG
Klybeckstrasse 64
4057 Basel, Switzerland
Tel. +41 61 683 77 34
Fax +41 61 302 89 18
http://www.mdpi.com/

Marine Drugs Editorial Office
E-mail: marinedrugs@mdpi.com
http://www.mdpi.com/journal/marinedrugs

MDPI • Basel • Beijing • Wuhan • Barcelona
ISBN 978-3-03842-108-5 Volume 1-2
ISBN 978-3-03842-110-8 Volume 2
www.mdpi.com